Synthesis and Characterization of Uniform Macromolecules and Data Storage in Small Compounds

Zur Erlangung des akademischen Grades eines

DOKTORS DER NATURWISSENSCHAFTEN

(Dr. rer. nat.)

von der KIT-Fakultät für Chemie und Biowissenschaften

des Karlsruher Instituts für Technologie (KIT)

genehmigte

DISSERTATION

von

M. Sc. Philipp Bohn

aus Gernsbach

Dekan: Prof. Dr. Hans-Achim Wagenknecht

Referent: Prof. Dr. Michael A. R. Meier

Korreferent: Prof. Dr. Joachim Podlech

Tag der mündlichen Prüfung: 20.07.2022

Meiner Familie

“Just because something works doesn’t mean that it cannot be improved.”

Shuri (Letitia Wright), Black Panther

Declaration of Authorship

Die vorliegende Arbeit wurde von März 2018 bis Juni 2022 unter Anleitung von Prof. Dr. Michael A. R. Meier am Institut für Organische Chemie (IOC) des Karlsruher Instituts für Technologie (KIT) angefertigt.

Erklärung

Hiermit versichere ich, dass ich die Arbeit selbstständig angefertigt, nur die angegebenen Quellen und Hilfsmittel benutzt und mich keiner unzulässigen Hilfe Dritter bedient habe. Insbesondere habe ich wörtlich oder sinngemäß aus anderen Werken übernommene Inhalte als solche kenntlich gemacht. Die Satzung des Karlsruher Instituts für Technologie (KIT) zur Sicherung wissenschaftlicher Praxis habe ich beachtet. Des Weiteren erkläre ich, dass ich mich derzeit in keinem laufenden Promotionsverfahren befinde, und auch keine vorausgegangenen Promotionsversuche unternommen habe. Die elektronische Version der Arbeit stimmt mit der schriftlichen Version überein und die Primärdaten sind gemäß Abs. A (6) der Regeln zur Sicherung guter wissenschaftlicher Praxis des KIT beim Institut abgegeben und archiviert.

Karlsruhe, den 27. Februar 2023.

_____

Philipp Bohn

ACKNOWLEDGEMENTS

Eine unerwartete Reise

„Sie werden Ihr Praktikum bei Maike Unverferth aus dem Arbeitskreis Professor Meier im Erdgeschoss Raum 011 durchführen.“

Ich erinnere mich als wäre es gestern gewesen, als Andreas Rapp mir diese Nachricht nach der Vorbesprechung für das OCF Praktikum überbrachte. Die Reaktion in meinem Kopf war darauf erst einmal: „Maike wie? Professor wer? – Oh Gott, was kommt da denn auf mich zu?“

Damals hätte ich mir nicht träumen lassen, dass damit eine lange Reise in deinem Arbeitskreis beginnt, die nun hier mit der Promotion zu Ende geht.

Für diese gemeinsame Zeit in deiner Gruppe möchte ich mich bei dir, Mike, von ganzem Herzen bedanken. Auch wenn wir uns beide bei der Themenstellung nie ausgemalt hätten, dass es so ein langwieriger Weg wird, bin ich an dieser Arbeit gewachsen und würde mich der Herausforderung immer wieder stellen. Deine Tür stand wortwörtlich immer offen und du gabst mir das Gefühl, dass ich mit egal welchem Problem zu dir kommen konnte. Auch wenn es manchmal etwas Überzeugungsarbeit gekostet hat, hast du mir die Freiheit gegeben, über den Tellerrand hinauszuschauen und ich konnte stets mit deiner Unterstützung rechnen.

Vielen Dank für die Betreuung meiner Doktorarbeit und die vielen gemeinsamen Jahre. Das Labor ist für mich wie ein zweites Zuhause geworden. Aber auch an die Gruppenaktivitäten, Ausflüge, Weihnachtsfeiern und Konferenzen erinnere ich mich gerne zurück. Ich wünsche dir für die Zukunft nur das Beste.

Anschließend möchte ich mich bei der Deutschen Forschungsgemeinschaft (DFG) für die finanzielle Unterstützung im Rahmen des Sonderforschungsbereichs (SFB 1176, „Strukturierung weicher Materie“) bedanken, was auch die Ermöglichung verschiedener Konferenzen und Tagungen, sowie das Besuchen von Unternehmen

beinhaltete. Darin einbezogen meinen Kollaborationskollegen des Projektes C3 „Optimized Polymer-Based Alignment Media for NMR Spectroscopy“, Dr. Thomas Gloge aus der Arbeitsgruppe von Prof. Dr. Burkhard Luy sowie Dr. Diego Estupinan Mendez aus der Arbeitsgruppe von Prof. Dr. Leonie Barner. Danke auch an alle weiteren SFB-Kollegen für die gute Zusammenarbeit und den Austausch bei Workshops, wobei der Spaß auch nicht zu kurz kam.

Vielen Dank an meine Kollaborationspartner: Dr. Valerian Hirschberg aus der Arbeitsgruppe von Prof. Dr. Manfred Wilhelm (ITCP, KIT) und Simon Buchheiser aus der Arbeitsgruppe von Prof. Dr. Hermann Nirschl (MVM, KIT) für die SAXS Messungen. Janne Wiedmann aus der Gruppe von Prof. Dr. Pavel Levkin (IBCS, IOC, KIT) für das Drucken meiner Moleküle. Dr. Quiqin Zhou und Dr. Stefan Schmidt aus der Arbeitsgruppe von Prof. Dr. Carsten Hopf (Center for Mass Spectrometry and Optical Spectroscopy (CeMOS), HS Mannheim) für die MALDI-MS/MS Messungen. Maximilian Weisel für die Programmierarbeiten.

Furthermore, I would like to thank current employees and alumni that I had the pleasure of meeting during my time at KIT. Namely: Dr. Hatice Mutlu, Dr. Matthias Winkler, Dr. Ansgar Sehlinger, Dr. Baptiste Monney, Dr. Susanne Solleder, Dr. Audrey Llevot, Dr. Charlotte Over, Dr. Barbara Ridder, Dr. Maike Unverferth, Dr. Zafer Söyler, Dr. Marc von Czapiewski, Dr. Andreas Boukis, Dr. Patrick Dannecker, Dr. Stefan Oelmann, Dr. Rebekka Schneider, Dr. Gregor Klein, Dr. Kelechukwu (Kenny) Onwukamike, Dr. Philip Scholten, Dr. Benjamin Bitterer, Dr. Yasmin Raupp, Dr. Katharina Wetzel, Dr. Eren Esen, Dr. Maximiliane Frölich, Dr. Pia Löser, Dr. Kevin Waibel, Dr. Julian Windbiel, Dr. Daniel Hahn, Dr. Luca Filippi, Ann-Kathrin Werther, Cornelia Weber, Pinar Sancar, Stefano Sechi, Jonas Wenzel, Larissa Bihr, Rebecca Seim, Fabienne Urbanek, Rieke Schulte, Elena Foitzik, Marie Gabrielsen, Lisa Wanner, Michelle Karsten, Luis Correa, Francesca Chiara Destaso, Federico Ferrari, Andreas Ganzbuhl, Dennis Barther, Anja Kirchberg, Jiangling (Caitlyn) Liu, Roman Nickisch, Michael Rhein, Clara Scheelje, Sarah Schmidt, Jonas Wolfs and of course also Dr. Dafni Moatsou.

I was warmly welcomed into the group by all of you and over time colleagues have also become friends. You were like a family to me and created a very pleasant working

atmosphere. Even outside the lab, you were always enthusiastic about one or the other activity, whether it was a barbecue, cooking together or a nice bike ride. Overall, I think we had a great time together and without you, the doctorate would not have been nearly as much fun.

Ein großes Dankeschön an die analytische Abteilung des organischen Instituts am KIT. Pia Lang, Tanja Ohmer, Despina Savvidou sowie Andreas Rapp, die die NMR-Geräte Tag und Nacht am Laufen gehalten und mit meinen Molekülen befeuert haben. Ihr habt keine Mühen gescheut, auch wenn ich mal wieder mit einem Blumenstrauß an Proben an der Tür geklopft habe. Auch für sehr spontane Messungen konntet ihr immer noch die ein oder andere freie Minute freischaufeln. Zudem danke an Angelika Mösle und Lara Hirsch für die Geduld, meine weiß Gott wie viele Masseproben zu messen. Ich hatte zeitweise ein schlechtes Gewissen und weiß eure Arbeit sehr zu schätzen, ohne euch würde der Laden nicht laufen. Im Zuge dessen ein Dank an Richard von Budberg für die herausragende Arbeit, was die Reparatur etlicher Glasapparaturen sowie die Maßanfertigung von Säulen angeht. Danke an Sina Zimmermann für vollen Einsatz in der Institutswerkstatt sowie Christoph Götz in der Chemikalien- und Lösungsmittelausgabe.

Für die SEC-ESI-MS Messungen möchte ich Dr. Janin Offenloch, Dr. Charlotte Petit, Dr. David Marschner und Dr. Martina Nardi von der Arbeitsgruppe von Prof. Dr. Christopher Barner-Kowollik danken.

Vielen Dank an die fleißigen Korrekturleser Fabienne, Clara, Jonas, Katharina, Yasmin, Luis, Conni, Kevin, Luca, Andreas, Anja, Dafni, Bodo, Francesca, Julian und Valerian.

Während meiner Zeit haben mir folgende Personen unter die Arme gegriffen und mich synthetisch unterstützt: Lisa Gramespacher, Fabienne Urbanek, Helene Nies, Ninon Möhl, Thomas Sattelberger, Rebecca Seim, Rieke Schulte, Maximilian Knab, Manuel Schorer, Lisa Wanner, Maya Ludwig und Peter Conen. Danke für eure großartige Motivation. Ich hoffe, ihr hattet trotz der tagelangen Säulen auch etwas Spaß und euch

hat der kleine Einblick in meine Promotion gefallen. Auch ein Dankeschön an Jan Hobich, Tobias Volkmann, Peter Gödtel, Stefano Sechi, Qianyu Cai und Tamara Meyer, dass ihr mir euer Vertrauen geschenkt habt, eure Abschlussarbeiten zu betreuen. Ich hoffe, ich konnte euch für euren weiteren Weg hilfreiche Ratschläge und Tipps mitgeben. Ohne euch wäre die Arbeit so nicht zustande gekommen, dafür Danke.

Auch möchte ich mich bei der Arbeitsgruppe von Prof. Dr. Hans-Achim Wagenknecht bedanken. Ich war in eurer Küche immer herzlich willkommen und konnte so auch das ein oder andere leckere Essen bei einer Einstandsfeier abstauben. Danke dass ihr Vertrauen in mich hattet, die Fotos für eure Homepage zu machen. Es hat mir immer viel Spaß gemacht und ich habe einiges dazugelernt.

Des Weiteren möchte ich mich von ganzem Herzen bedanken bei:

- ♥ Edu. Für alles, was ich von dir gelernt habe. Angefangen bei einer Brombrezel bis hin zu Fleischwurst mit Marshmallow Creme. Für deine Freundschaft, das Dummgeschwätz und die gemeinsamen Partys. Für die Tee- und Foodora-Abende in der MZE-Küche. Für das Assi-Frühstück und die Einführung des Black Fridays. Für all die schönen Erinnerungen und einfach deine Anwesenheit im Nachbarlabor. *Life isch a Rennbahn* und ich hoffe, wir treffen uns mal wieder im McDonalds zum GNTM schauen.
- ♥ Abenteurer Daniel. Für deine angenehme und ruhige Art und gleichzeitig deinen extrem trockenen Humor „That's what she said". Für das ein oder andere Abenteuer - sei es zu Fuß, auf dem Fahrrad oder mit dem Kanu. Für die geile Zeit auf Kreta „Had to have high, high hopes for a living" und für die Zimmergenossenschaft bei SFB Workshops. Dafür, dass du uns des Öfteren mit deinen Backkünsten beglückt hast und für die Freundschaft, die sich während der Promotion entwickelt hat. Irgendwann hört man aber auch mal auf, Daniel zu heißen.

- ♥ Anja. Für deine immer gute Laune und positive Ausstrahlung, die du an jeden Tag gelegt hast. Für die vielen Tee-Pausen und Schneespaziergänge mit interessanten und schönen Gesprächen. Für die Grillabende und gemeinsamen Kochdates. Für die eine schöne Rennradtour, auf die hoffentlich noch viele weitere folgen werden.
- ♥ Unserem Feel-Good-Manager Herrn Doktorand Jonas Wolfs. Für die Digitalisierung des Arbeitskreises und dafür, dass der Schnuckelschrank immer prall gefüllt war. Für die gemeinsamen, oft nicht direkten, Heimfahrten mit dem Fahrrad. Für die oft spontanen kulinarischen Highlights, die mir den ein oder anderen langen Arbeitstag retteten. Dafür, dass du einen gewöhnlichen Samstagmorgen in einen Urlaubstag verwandelt hast. Für deinen absolut trockenen Mainzer Humor. Durch deine vielen Stromberg Zitate weiß ich heute, dass man aus Mettwurst eben kein Marzipan machen kann. Für die vielen geistreichen und hitzigen Diskussionen und dass wir Clara mit unseren Sprüchen oftmals zur Weißglut getrieben haben.
- ♥ Conni. Für die Koch- und Cake-Dates, deine leckere Donauwelle und den Jahresvorrat an Marmelade. Für die ein oder andere überragende Party bis in die frühen Morgenstunden, sei es ACF, OCF, Marktlücke oder eine WG-Party. Dafür, dass du immer da warst und ein offenes Ohr hattest, wenn ich jemanden zum Quatschen gebraucht habe. Für deine herrlichen Lachflashes. Für die mega lustigen Gin-Partys mit Klavierunterricht. Und vor allem für die unvergessliche Zeit in Dublin. Auch wenn wir bis auf die Knochen nass wurden, hat sich die Wanderung in Glendalough zweifellos gelohnt. Auch der Abend im Merchants Arch mit überragender Livemusik wird mir immer in Erinnerung bleiben. „Good times never seemed so good“. Danke dafür!
- ♥ Laserfrosch Dave. Für die langen Lab Abende in 204, die oft mit Pizza in der Küche endeten. Für dein dickes Gehirn und deine unfassbare Begeisterung, nicht nur für Wissenschaft. Für deine Verplantheit und dafür, dass du dir aber trotzdem für jedes Problem Zeit nimmst. Für deine extrem ansteckend gute Laune, Feiereieieien in der Marktlücke oder zahlreiche Aufzugpartys. Für die vielen lustigen, aber auch ernsten Gespräche sowie deine Motivationsspritzen. Nie in meinem ganzen Leben werde ich unsere Backstreet Boys Einlage am Kronenplatz oder die spontanen Koaleszenz- und Kinetikmessungen

vergessen. Irgendwann komme ich dich in Zürich besuchen – versprochen! Dein Johannes.

- ♥ Lisa. Für die schöne Zeit mit dir nebenan in 407, aber auch außerhalb des Labors. Dafür, dass du als Gegenpol zu Edu und mir uns immer wieder auf den Boden zurückgebracht hast. Für die stundenlangen, sehr lustigen Telefonate während des Lockdowns und dass du immer ein offenes Ohr für mich hattest. Dafür, dass ich in der Kaiser-WG immer herzlichst willkommen war, für die ein oder andere Partynacht oder auch GoT-Abende. Auch wenn es bei dir mit der Chemie nicht sein sollte, wünsche ich dir in deinem neuen Beruf viel Erfolg und nur das Beste.
- ♥ Fabienne. Für deine unermüdliche Geduld mit mir. Für unsere Dream-Team Zeiten in den gemeinsamen Praktika. Für die vielen lustigen Kaffee- und Mittagspausen. Dafür, dass ich immer zu dir kommen konnte, wenn ich ein Problem hatte, und du dir immer Zeit genommen hast mir zuzuhören. Dafür, dass du mich motiviert und mir zurecht manchmal in den Allerwertesten getreten hast. Für deine ganze Unterstützung und dass du immer an mich geglaubt hast, auch was die Fotoshootings anging. Ohne dich wäre ich nicht da, wo ich heute stehe. Danke für deine Freundschaft und die schöne Zeit in, aber vor allem auch außerhalb der Uni.
- ♥ Frau Dr. Rebekka Valerie Schneider. Isch des Jungle? Dafür, dass ich während meiner Bacherlorarbeit dachte, dass ich dir auf die Nerven gehe, haben wir uns echt gut verstanden. Danke für die schönen und interessanten Gespräche und die ewig langen Chatverläufe.
- ♥ Roman. Für die Montag-Asia Dates in der Küche mit überragenden Gesprächen. Für die schöne Zeit mit dir als Labornachbar und unzähligen Zitaten aus dem Brückner. Für deine enorme Hilfsbereitschaft und dass du für jedes Problem eine Lösung findest. Dafür, dass du mit Michi jede Party auf ein ganz anderes Level gebracht hast. Für deine ansteckende Leidenschaft für Chemie und natürlich Renates vorzügliche Kuchen – da hat sie sich echt nicht lumpen lassen. Ich bin mir sicher, dass du deinen Weg erfolgreich gehen wirst, und ich würde mich hiermit schonmal unverbindlich beim AK Nickisch bewerben.

♥ Michi. Danke für die ein oder andere schöne Ausfahrt auf dem Moped. Für die Ausflüge nach Fribourg und Lüttich, bei denen wir uns ein Zimmer geteilt haben. Seitdem wissen wir, dass eben nur ein Johnny gelbe Felgen hat. Für deine Initiative, die des Öfteren in feuchtfröhlichen Abenden in der Küche endeten. Auch wenn ich nicht viel Schlaf abbekommen habe und die Betten viel zu klein für uns beide waren, würde ich mir immer wieder ein Bett mit dir teilen.

♥ Maxi. Für die Zeit, die wir zusammen an der ESI verbracht haben und verzweifelt nach meinen Molekülfragmenten gesucht habe. Für die schönen Gespräche auf dem Heimweg, bei denen wir immer an der Haltestelle versackt sind. Für die lustigen Koch-, Back- und Spielabende, bei denen ich gelernt habe, dass man keine Straßen würfelt, man rechtsrum die Backe na schlägt und jedes Spiel eigentlich wie Binokel ist. Für die Zeit in Berlin inklusive Touri-Tour.

♥ Katha. Für die schöne Zeit in Gent, Lüttich und vor allem auf Kreta. Für die vielen Stunden, die wir zusammen versucht haben, die Varian GPC zum Laufen zu bringen. Für die ein oder andere Wanderung im Schwarzwald/ Pfälzer Wald und die Fotoausflüge.

♥ Larissa. Dafür, dass ich dich deine komplette Masterarbeit nerven durfte, ob wir zusammen Rennrad fahren. Für deine motivierend gute Laune, deinen herrlich schwäbischen Dialekt und die schönen Gespräche während der Wartezeit am Druckreaktor.

♥ Clara. Für die schöne Zeit mit dir im Labor mit den Ohren schmeichelnder Musik. Freut mich, dass ich dich von Deichkind und Alligatoah weg hin zu niederländischem Après-Ski und Eko Fresh führen konnte. Dafür, dass du mir ab heute mal die Fischstäbchen bringen kannst. Für die tiefgründigen, aber auch oftmals lustigen Gespräche und viele weitere, die mit „Spaß“ beendet wurden. Deinen unberechenbaren Arbeitsbeginn und deine Verplantheit. Ich hoffe, wir führen unseren alphabetischen Playlists noch fort, bis wir bei X angekommen sind.

♥ Dafni. ευχαριστώ for your unique humor. For the great cooperation, your help and support, especially in the last weeks. For the nice discussions, your helpful input and the motivation. I have learned a lot from you and wish you only the best for the future.

♥ Federico. Mille grazie for all the helpful discussions. For your unconditional help with every analytical instrument and your dedication to keep them running. You are one of the most helpful people I know – please do not lose that.

♥ Sarah. Für die sehr spontanen Messungen am 500er NMR, wenn bei uns alle im Urlaub waren. Für deine permanente Hilfsbereitschaft und die immer netten Gespräche auf dem Gang. Für das lustige Fotoshooting, bei dem wir fast die Bilder löschen mussten, und die mega leckeren Cookies.

♥ Iuliana. Thanks Luli for the nice eight weeks having you in our group. It was amazing - exactly? Next time we see each other in Stockholm.

♥ Pinar, Anni, Conny. Für die Unterstützung und Bewerkstelligung aller organisatorischen Angelegenheiten. Ihr habt mir damit viel Arbeit abgenommen, bei der ich allein völlig aufgeschmissen gewesen wäre.

♥ Labor 408. All diejenigen, mit denen ich über die Jahre hinweg in einem Labor arbeiten durfte. Namentlich: Rebekka, Yasmin, Patrick, Kevin, Katharina, Roman, Clara, Caitlyn, Becci und Michelle. Ihr habt die Promotion zu einer ganz besonderen gemacht. Auch wenn euch mein wilder Musikgeschmack wohl ab und zu auf die Palme gebracht hat, hatten wir Seite an Seite eine sehr schöne Zeit.

♥ Labor 407. Danke auch an unseren lieben Nachbarn Edu, Conni, Yannick, Ossi, Julian, Moritz und Clara. Als direkte Schnittstelle zum Arbeitskreis Prof. Dr. Stefan Bräse wart ihr durch den direkten Laborzugang strategisch in bester Lage, was den Austausch von Wissen, aber auch Chemikalien und Glasgeräten anging. Auch wenn ich nie verstanden habe, wieso ihr euch ab und zu meine überragende Musik entgehen lassen konntet, haben wir doch in Symbiose und Einklang gelebt und sind der beste Beweis, dass Zusammenarbeit auch innerhalb unterschiedlicher Arbeitsgruppen funktioniert.

♥ Gernsbacher Lausbuben und FC Kurpark. Auch wenn persönliche Treffen mit Beginn der Promotion exponentiell abgenommen haben, ist der Kontakt dank modernster Technik nie wirklich abgebrochen. Ich bin euch für die gesamten gemeinsamen Jahre und die vielen Abenteuer, die wir zusammen erlebt haben, sehr dankbar.

♥ Meiner Familie. Insbesondere meinen Eltern und meinem Bruder für die jahrelange Unterstützung und den unendlichen Rückhalt. Danke, dass ihr mich immer aufgemuntert und motiviert habt, wenn ich es allein nicht mehr konnte oder es gerade mal nicht so gut lief. Auch wenn ich es nicht so oft wahrgenommen habe, weiß ich, dass ich bei euch als Anlaufstelle immer mit offenen Armen empfangen werde, und blicke mit Zuversicht in eine Zukunft, in der wir mehr Zeit miteinander verbringen werden. Der fachliche Austausch hat sich zwar ab und zu etwas schwierig gestaltet, aber nichtsdestotrotz habt ihr mir immer zugehört und interessiert eure Aufmerksamkeit geschenkt. Ich weiß, dass ihr immer hinter mir steht, ich mich immer auf euch verlassen kann, und ich bin genauso stolz auf euch, wie ihr es auf mich seid. Ich weiß, ihr konntet manchmal nicht verstehen, wieso ich Tag und Nacht in der Uni verbracht habe, und habt euch wahrscheinlich des Öfteren gefragt, was ich den ganzen lieben langen Tag im Labor zusammenmische. Die Antwort darauf haltet ihr hier in euren Händen.

ABSTRACT

Inspired by the highly complex and sequence defined structure of biomacromolecules, such as deoxynucleic acid (DNA), a new field of research has developed with the synthesis and study of uniform, sequence defined non-natural macromolecules. Since conventional polymer chemistry has always been characterized by molecular weight and composition distribution, the synthesis of uniform sequence-defined structures has long time been limited to biopolymers.

In this work, uniform poly(ethylene glycol)-*block*-poly(ε-caprolactone) (PEG-*b*-PCL) block copolymers (BCP)s were synthesized and investigations of the effect of the dispersity on the structure-property relationship were performed. Furthermore, the application of highly complex small organic molecules as potential data storage media on a surface was studied.

Three uniform BCPs varying in the length of the hydrophobic PCL block were prepared *via* coupling of the uniform PEG and PCL homopolymers, which were prepared *via* an iterative exponential growth strategy. Ring-opening polymerization of ε-caprolactone using a methoxy-PEG as initiator provided reference molecules with similar M_n and a narrow molar mass distribution ($Đ$ = 1.06). The thermal properties were investigated by differential scanning calorimetry (DSC) and the phase separation behavior of the BCPs was studied *via* small-angle X-ray scattering (SAXS). The results show a clear constitution and dispersity dependent structure-property relationship based on the crystallization temperature T_c and a difference in self-assembly of the smallest BCP as a function of dispersity.

In the second part of the work, small complex organic molecules were investigated for application as potential data storage media on a surface. The respective compounds were synthesized in a one-step protocol, using a Passerini three-component reaction (P-3CR) in combination with a hetero-Michael addition. Using an exemplary database of 708 commercially available components and considering all permutations, 2.63 M unique structures are potentially accessible with the described approach. This number of permutations corresponds to a data storage capacity of 21 bits per molecule. The

molecules were printed on a glass surface using a liquid dispenser and encoded *via* the unique respective fragment patterns obtained with high-resolution matrix-assisted laser desorption/ionization tandem mass spectrometry (MALDI-MS/MS).

In another approach, a rapid and efficient method for storing information in commercially available compounds was demonstrated. Molecular mixtures were used to store a 625 bits QR code, which was decoded with 100% accuracy using gas chromatography (GC) for read-out, supported by a custom programmed computer script.

KURZZUSAMMENFASSUNG

Inspiriert durch die hoch komplexe und sequenzdefinierte Struktur von Biomakromolekülen, wie zum Beispiel Desoxynukleinsäure (DNS), hat sich mit der Synthese und Untersuchung uniformer, sequenzdefinierter Makromoleküle nicht-natürlichen Ursprungs ein neues Forschungsgebiet entwickelt. Da klassische Polymerchemie durch Dispersität und Strukturverteilung geprägt ist, beschränkte sich die Synthese von uniformen, sequenzdefinierten Strukturen lange Zeit auf Biopolymere.

In dieser Arbeit wird die Synthese von uniformen poly(ethylenglycol)-*block*-poly(ε-caprolacton) (PEG-*b*-PCL) Blockcopolymeren (BCP) beschrieben, die zur Untersuchung der dispersitätsabhängigen Struktur-Eigenschafts-Beziehungen verwendet werden. Des Weiteren wurde die Anwendung von komplexen kleinen organischen Molekülen als potenzielle Medien für Datenspeicherung auf Oberflächen untersucht.

Drei uniforme BCP, die in der Länge des hydrophoben PCL-Blocks variieren, wurden über die Kopplung von uniformen PEG- und PCL-Homopolymeren gebildet, welche über ein iteratives exponentielles Wachstum hergestellt wurden. Ringöffnende Polymerisation von ε-Caprolacton mit Methoxy-OEG als Makroinitiator lieferte Vergleichsmoleküle mit identischem M_n und einer engen Molmassenverteilung ($Đ$ = 1.06). Die thermischen Eigenschaften wurde mittels dynamischer Differenzkalorimetrie (DSC) und das Phasenseparationsverhalten der BCP über Kleinwinkel-Röntgenstreuung (*engl. small-angle X-ray scattering,* SAXS) untersucht. Die Ergebnisse zeigen eine eindeutige konstitutions- und dispersitätsabhängige Struktur-Eigenschaftsbeziehung anhand der Kristallisationstemperatur T_c sowie ein unterschiedliches Phasenseparationsverhalten des kleinsten BCP in Abhängigkeit von der Dispersität.

In dem zweiten Teil der Arbeit wurden kleine komplexe organische Moleküle für die Anwendung als potenzielle Datenspeichermedien auf einer Oberfläche untersucht. Die jeweiligen Verbindungen wurden in einer einstufigen Synthese unter Verwendung der

Passerini-Dreikomponenten-Reaktion (P-3KR) in Kombination mit einer Hetero-Michael-Addition synthetisiert. Unter Verwendung einer Datenbank aus 708 kommerziell erhältlichen Komponenten, sind mit dem beschriebenen Ansatz 2.63 Mio einzigartige Strukturen potenziell zugänglich. Diese Anzahl an Permutationen entspricht einer Datenspeicherkapazität von 21 Bit pro Molekül. Die Moleküle wurden mit einem Pipettierroboter auf eine Glasoberfläche gedruckt und mittels hochauflösender Matrix-assistierter Laser-Desorption-Ionisation (MALDI) Tandem Massenspektrometie (MS/MS) anhand des resultierenden Fragmentmusters eindeutig identifiziert.

In einem weiteren Ansatz wurde eine schnelle und effiziente Methode zur Speicherung von Informationen in kommerziell erhältlichen Verbindungen demonstriert. In mehreren Molekülmischungen wurde ein 625 bit QR-code gespeichert und mittels Gaschromatographie (GC) ausgelesen und, unterstützt durch ein eigens programmiertes Computerskript, mit 100%iger Genauigkeit entschlüsselt.

TABLE OF CONTENTS

1. INTRODUCTION

HERMANN STAUDINGER's macromolecular hypothesis 100 years ago, for which he was awarded the 1953 Nobel prize, set a milestone for the world of synthetic polymers.[1,2] In the early 20th century, WALLACE H. CAROTHERS laid the foundation for the emerging field of polymer chemistry with his pioneering work in the field of polycondensation reactions.[3] From then on, scientists strived for ever more highly defined macromolecular structures to achieve a distinct insight into the structure-property relationship of synthetic macromolecules. A breakthrough in the synthesis of well-defined polymers was achieved *via* the development of living[4] and controlled polymerization techniques, such as cationic,[5] and anionic,[4] and reversible deactivation radical polymerization (RDRP) techniques.[6–8] The study of MICHAEL SZWARC on the anionic polymerization of styrene in 1956 set the basis for the term *living polymerization*,[4,9] which was already described earlier by MELVILLE[10] and FLORY[11] and realized by ZIEGLER[12] in 1936 and PERRY and HIBBERT in 1940.[13] The foundation for the development of the atom transfer radical polymerization (ATRP)[14–16] and other RDRPs,[6–8] such as reversible addition-fragmentation chain transfer (RAFT) polymerization[17–19] and nitroxide-mediated polymerization (NMP)[20–25] was set by KHARASCH *et al.*, who investigated the addition of radicals to unsaturated hydrocarbons.[26] First investigations on the living ring-opening polymerization (ROP) of lactones were performed by TEYSSIE,[27] PENCZEK,[28] and BOILEAU[29] in the 1970s, and the living ring-opening metathesis polymerization (ROMP) was developed in the 1980s.[30,31] Furthermore, the pioneering progress of analytical tools, such as nuclear magnetic resonance (NMR) spectroscopy[32] and mass spectrometry (MS)[33] enabled a more precise characterization of macromolecules. In particular, the development of size exclusion chromatography (SEC) in the 1960s enabled the monitoring of the polymerization process *via* the hydrodynamic volume of the respective macromolecule and was one of the most important inventions for modern polymer chemistry.[34] The

ability to adjust the dispersity *via* controlled and living polymerization approaches permitted the opportunity to tune the properties of a polymer and the synthesis of tailor-made materials for a vast range of applications became an emerging research field.[35–38] Within this context, the term *sequence-controlled copolymers*[39–46] was defined as *"…macromolecules in which monomer units of different chemical nature are arranged in an ordered fashion*" by LUTZ, OUCHI, and SAWAMOTO in 2013.[39] Especially block copolymers (BCP)s are of interest, due to their self-assembly (SA) behavior,[47–50] which is the basis for several applications, such as drug delivery,[51] organic optoelectronics,[52] or as supramolecular materials for membranes.[53] The experimental SA of copolymers, supported by theoretical studies such as the Flory-Huggins theory[54,55] or the self-consistent mean field theory (SCMFT),[56] has been extensively investigated since the 1960s for the SA in bulk,[57–61] and from 1995 on also for the SA in solution.[62–64] In particular, the tuneability and predictability of the formed morphologies, dependent on the dispersity[65–76] and the shape of the molecular weight distribution[77–79] have emerged as hot topics in modern polymer chemistry and nanotechnology.

However, since the field of polymer chemistry has always been the science of distribution and dispersity, the synthesis of perfectly defined structures, as present in biopolymers by nature, remained an unreached goal for a long time.[43] Based on the sequence-defined primary structure, where all molecules exhibit a similar monomer arrangement and molecular weight (*i.e.* $Đ = 1.00$)[80] the formation of secondary or tertiary architectures, such as the DNA double helix by Watson-Crick base-pairing[81] enables unique and complex biochemical processes. With the transfer of the uniform structure to synthetic polymers, insights into the distinct structure-property relationship of macromolecules were accessible and made a significant contributions to material and life science.[82–88]

Pioneering work in the field of synthetic uniform biopolymers has been done by ROBERT B. MERRIFIELD with the development of the Solid-Phase-Peptide-Synthesis (SPPS) in 1963,[89] for which he was awarded the 1984 Nobel Prize.[90] The concept was transferred to other classes of polymers, such as peptoids,[91] glycopeptides,[92] or oligonucleotides,[93,94] and has set the foundation for an enormous variety of synthetic sequence-defined polymers.[83,95] Different approaches, including solid-[96–98] and liquid phase,[99,100] or solid supported synthesis,[101] single unit monomer insertion (SUMI),[102] or template assisted synthesis were investigated.[103,104] In this context, the iterative

exponential growth (IEG) strategy, which was developed by WHITING *et al.* in 1982,[105,106] and the bidirectional growth strategy[107–110] allows a fast build-up of uniform macromolecules, while being limited in the degree of definition. In contrast, stepwise iterative approaches enable the highest possible definition, while suffering from a slow build-up.[83]

With digitization, the global amount of data is increasing exponentially[111] and sequence-defined molecules have gained interest as alternative data storages.[84,86] DNA and RNA as natural information carriers were considered as an inspiration and the decoding of the human genome and protein sequencing were among the biggest scientific achievements of the 20th century.[112–115] Pioneering work in the field of information-containing synthetic sequence-defined macromolecules has been done by LUTZ *et al*.[116–147] which has become one of the hot topics in modern polymer chemistry.[84,86,110,148–163] In this context, multicomponent reactions (MCR) such as the Passerini-three component reaction (P-3CR)[164] or the Ugi-four component reaction (U-4CR)[165] emerged as powerful tools to achieve sequence definition in a macromolecule.[149–151,153,166–170] In order to read the encoded information, tandem mass spectrometry (MS/MS), which was developed by JEAN FUTRELL und DEAN MILLER in 1966[171] in combination with electrospray ionization (ESI, since 1968)[172,173] or matrix-assisted laser desorption/ionization (MALDI, since 1985)[174,175] has been established as a powerful tool.

In this thesis, uniform block copolymers are prepared *via* an iterative exponential growth strategy aiming for investigations on the distinct structure-property relationships. Furthermore, small defined organic compounds were studied as potential molecular data storages.

2. THEORETICAL BACKGROUND

2.1. Sequence-definition in polymer chemistry

Inspired by the highly defined structure of biomacromolecules, such as DNA, which carries the genetic information for the functioning of evolution, growth and reproduction of all known organisms and many viruses,[81,176–180] a new branch of research has been established: *The synthesis and characterization of uniform, sequence-defined macromolecules*. Over time, synthesis and purification methods have been developed, the structure-property relationships were investigated, and the application in areas such as data storage were demonstrated.[82–88] Within this chapter, the different synthetic approaches as well as selected examples for research on purification methods are described.

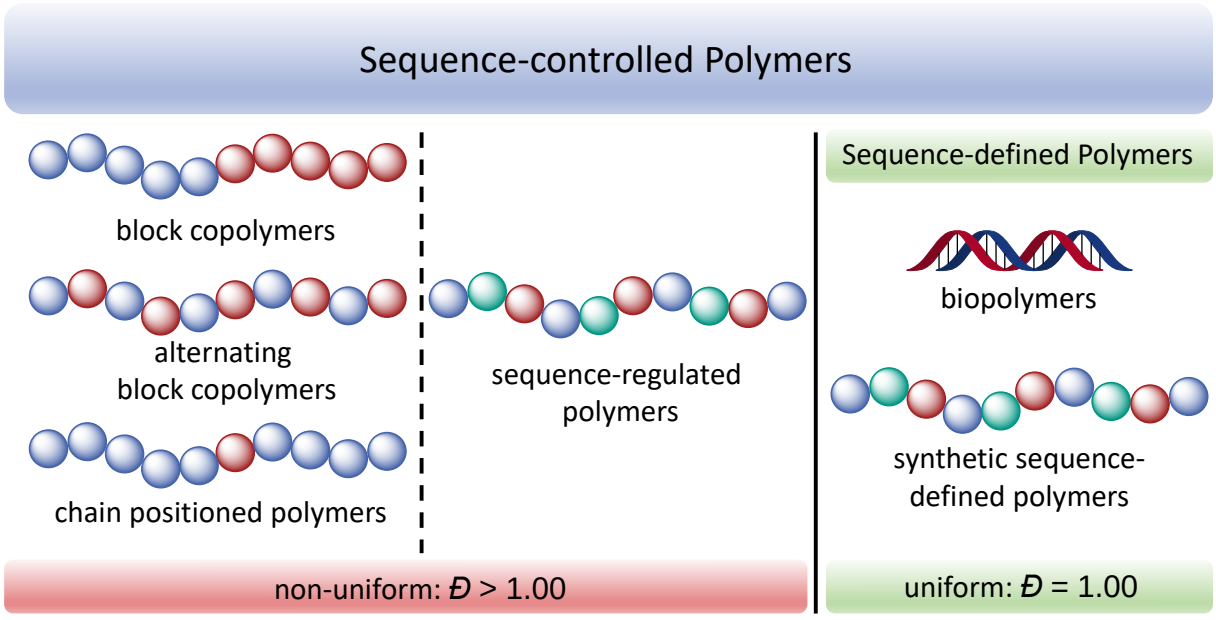

Figure 1: Classification of polymers depending on the degree of control. Adapted from the literature.[45,181]

The class of uniform polymers is defined by the International Union of Pure and Applied Chemistry (IUPAC) as a "*A polymer composed of molecules uniform with respect to*

relative molecular mass and constitution".[80],[I] It is a subgroup of sequence-controlled polymers, which was defined for the first time in 2013 by LUTZ, OUCHI and SAWAMOTO as *"…macromolecules in which monomer units of different chemical nature are arranged in an ordered fashion*" (Figure 1).[39]

Block, alternating, and periodic copolymers, chain positioned polymers or sequence-regulated polymers are examples for synthetic sequence-controlled polymers. The simplest representatives consist of two different monomer units (A and B), which are arranged in a specific order. The reaction protocols rely on well-known polymerization techniques, such as chain and step growth polymerization. Yet, since traditional polymer chemistry has always been the science of dispersity and distribution, new strategies, such as living anionic[4,12,182,183] or controlled radical polymerizations (ATRP,[14,184] NMP,[22] and RAFT[17,18])[185,186] were developed to achieve a higher control over the sequence. However, these polymers exhibit chain-to-chain distributions in their composition and molecular weight, and thus a dispersity $Đ$ >1.00. Several examples for sequence-regulated approaches were reported in the literature, which are not further described within the scope of this thesis.[39,42,45,187,188] In contrast, sequence-defined, uniform macromolecules are compounds of one single molecular weight, with a perfectly defined monomer sequence and show a dispersity of $Đ$ = 1.00. These include biomacromolecules known from living organisms, *e.g.*, proteins, DNA and RNA, which are synthesized *via* biological procedures, such as ribosomal protein synthesis or DNA replication. Their perfectly defined structure is crucial for the formation of secondary and tertiary structures. These complex architectures enable their essential properties for biochemical processes, such as self-replication, biocatalysis, self-assembly, and molecular recognition.[179,189–191] Thanks to the development of solid phase peptide synthesis (SPPS)[89] and the phosphoramidite synthesis,[93,94] manmade DNA and peptides are accessible. However, they are limited to the building blocks provided by nature, the five different nucleobases adenine (A), cytosine (C), guanine (G), thymine (T), and uracil (U) and the 22 proteinogenic amino acids. The advantage of non-natural synthetic sequence-defined polymers is the possibility to design more complex sequences due to the access to a plethora of building blocks' structures.

[I] The terms "monodisperse" and "polydisperse" are deeply rooted in the literature and still frequently used by the community.[80]

To achieve uniformity, several synthetic approaches, based on solid-,[96–98] liquid-,[99,100] and fluorous-supported synthesis,[192–195] as well as polymer-tethered protocols,[101,144,196,197] were investigated,[83] which are further divided into four different concepts, as shown in Figure 2.

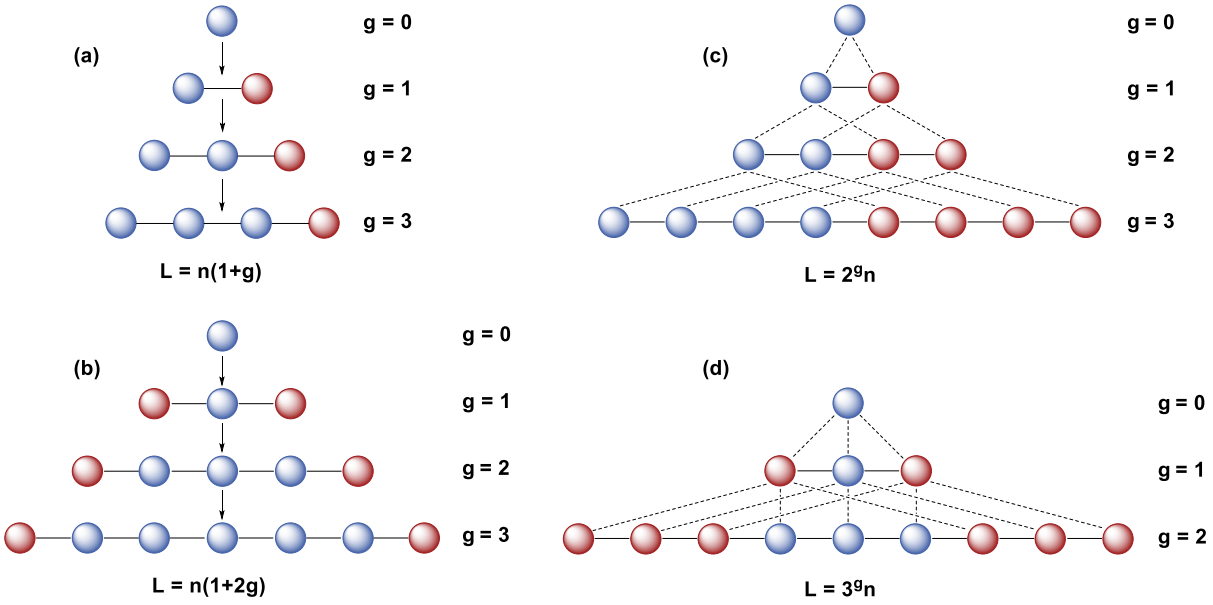

Figure 2: (a) unidirectional iterative coupling, L = n(1+g); (b) bidirectional iterative coupling L = n(1+2g); (c) chain doubling (IEG), L = 2^gn; (d) chain tripling, L = 3^gn, where L = length of the oligomer/polymer, g = number of couplings, n = monomer units in the starting material.[83,198]

The stepwise addition of one monomer unit per coupling step “g” to either one end of the growing chain in the unidirectional chain growth (a), or both ends of a difunctional molecule in the bidirectional growth (b) is time-consuming to obtain long-chain macromolecules. More rapid strategies are the iterative exponential growth (IEG) (c) and the chain tripling approach (d). However, they offer the least control over the sequence and thus the IEG is mostly applied for the synthesis of uniform homopolymers and alternating copolymers (examples are described in chapter 2.2 and 2.3), whereas chain tripling is not commonly used. The advantage of methods (a) and (c) is the possibility to achieve monofunctionalized products, whereas for concepts (b) and (d) often a large excess of the building block is necessary to prevent the formation of side products *via* monofunctionalization.

The most prominent example of an unidirectional chain growth concept was developed by ROBERT BRUCE MERRIFIELD in 1963, who did pioneering work on the solid phase peptide synthesis (SPPS),[89] for which he was awarded the Nobel prize in 1884.[90] The synthesis consists of a two-step iterative chain elongation cycle including an amide

coupling and a deprotection step. In this concept, the peptide is built from the C to the N-terminus. Thus, in the first step, a *tert*-butyloxycarbonyl- (boc) or 9-fluorenyl methoxy carbonyl (Fmoc) -protected amino acid is attached *via* the C-terminus to the linker of the resin (highly crosslinked copolymers of styrene and 1,4-divinyl benzene or poly(acrylamide)). Afterwards, the amine protecting group is cleaved, followed by the coupling with another protected amino acid. In the final step, the peptide is cleaved from the solid support and the protecting group is cleaved to obtain the sequence-defined molecule.[89]

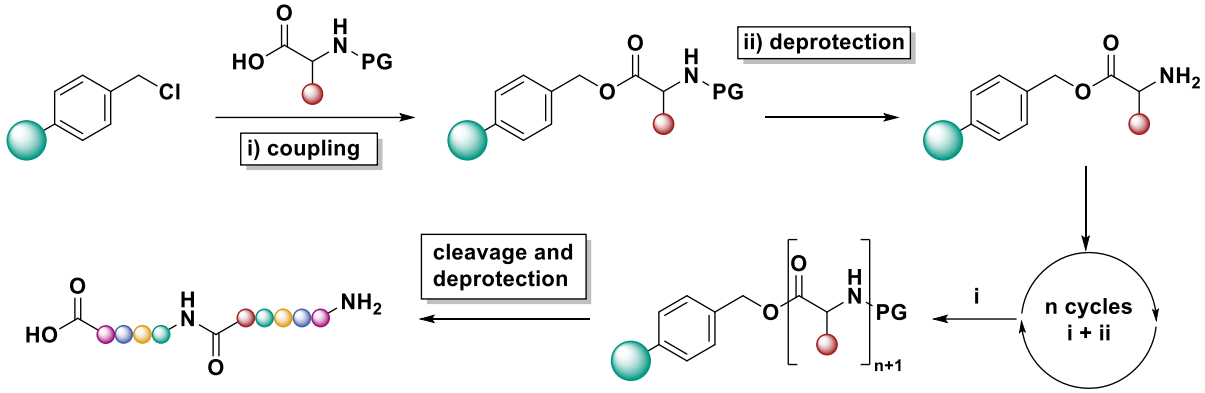

Scheme 1: General reaction scheme for the SPPS developed by MERRIFIELD.[89,199]

The advantage of a simple workup procedure *via* filtration and washing steps allows the use of large excess of the reactant to achieve quantitative yields in each step[200] and the automatization of the complete process, which was already reported three years after its development, in 1966. This way, the rapid preparation of long chain peptides with a minimum of effort is accessible and the syntheses of bovine insulin containing 52 amino acids and ribonuclease A containing 124 amino acids were demonstrated.[201–203]

Besides the initial use of the SPPS to synthesize sequence-defined peptides, the solid phase chemistry was transferred to peptoid and nucleotide sequences[42,91,93,94,204–206] as well as non-natural molecules (so called solid phase organic synthesis, SPOS).[207]

A recent example for the synthesis of thiolactone-based sequence-defined macromolecules *via* a unidirectional growth strategy (Figure 2 (a)) employing solid phase chemistry was demonstrated by the group of DU PREZ in 2013 and is still continuously investigated. In the initial approach, a thiolactone building block, equipped with a Michael acceptor, was used. A ring-opening of the thiolactone was conducted using an amine as nucleophile as well as for the introduction of the side chain definition. The resulting thiol was reacted in a thia-Michael addition with a second

thiolactone building block to complete the reaction cycle. By repetition of the two-step iterative chain elongation cycle, sequence-defined tetramers were successfully prepared.[208] Based on this study, the initial building block was replaced by α-isocyanato-γ-thiolactone and two different strategies were investigated, shown in Scheme 2. In the first one (upper reaction cycle) the thiolactone motif was incorporated as a thioether into the backbone structure of the growing chain. An amine was employed for a nucleophilic ring-opening of the α-isocyanato-γ-thiolactone and the introduction of a sidegroup.

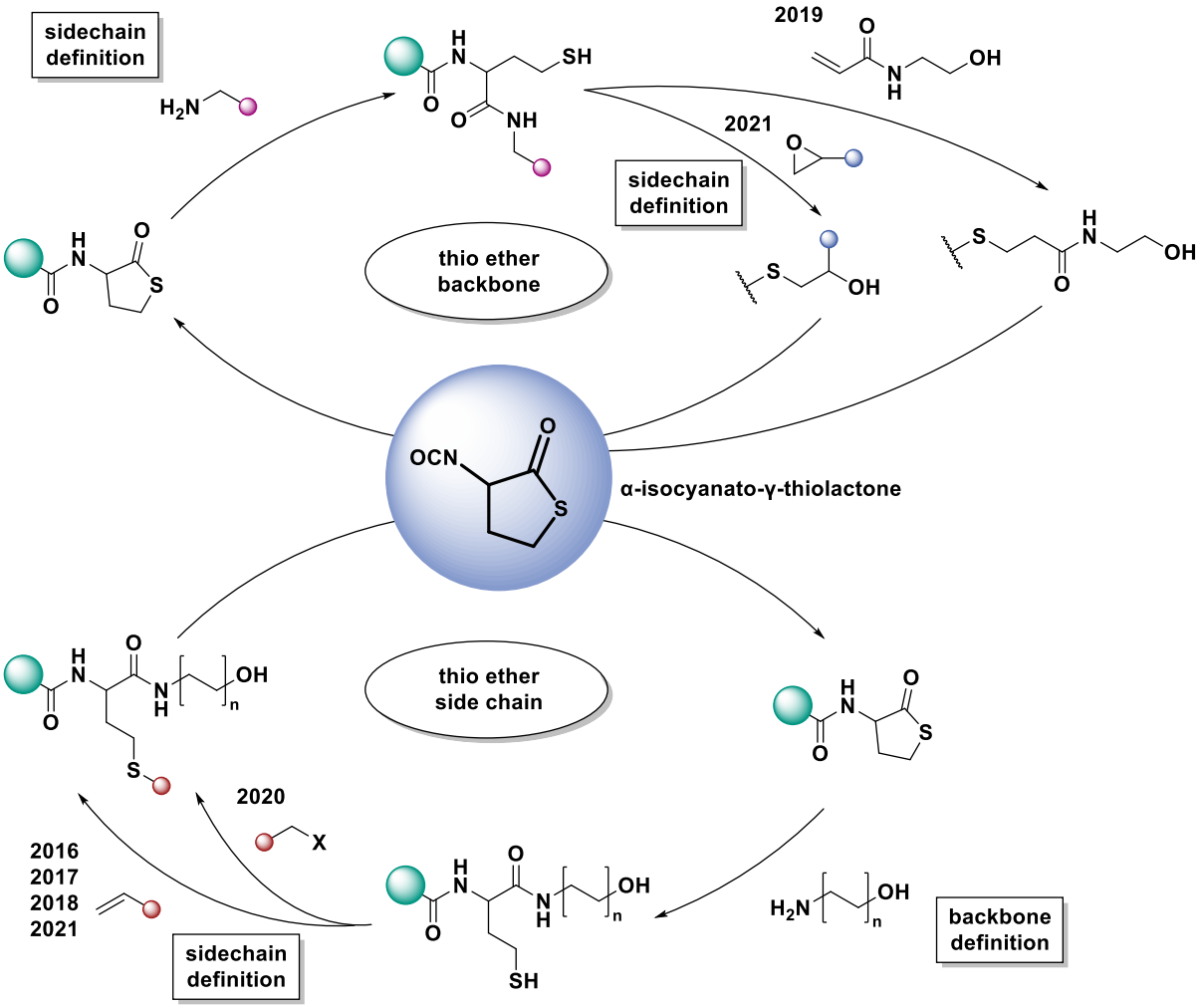

Scheme 2: Overview of the different approaches for the synthesis of sequence-defined macromolecules *via* thiolactone chemistry. In the upper reaction cycle, the thiolactone motif is incorporated into the backbone structure.[209],[152] In the lower reaction cycle, an amino alcohol was employed for the nucleophilic ring opening of the thiolactone. Sidechain definition was achieved *via* modification of the resulting thiol.[98],[210],[211],[155,212]

Subsequently, an alcohol function was introduced either *via* a thia-Michael addition (2019),[209] or with another nucleophilic ring-opening of an epoxide (2021),[152]

introducing a second sidechain. In the next step, the alcohol was reacted with the isocyanate of the thiolactone to complete the reaction cycle.

As illustrated in the lower reaction cycle, an amino alcohol was employed for the ring-opening of the thiolactone and sidechain definition was achieved *via* modification of the thiol either *via* thiol-ene reactions (2016,[98] 2017,[210] 2018,[155] 2021[211]) or *via* nucleophilic substitution (2020).[212] As described in the first example, the alcohol moiety was reacted with the isocyanate of the thiolactone to complete the reaction cycle. All approaches were conducted using solid phase chemistry. Furthermore the group has demonstrated the automatization of this concept[209,212] and the application of these sequences as information-containing molecules, which is described in detail in chapter 2.5.8.1.[152,155] Sequence-defined polyampholytes were obtained, which show UCST behavior and could be of interest as cryoprotectants.[211] In another approach, the sequence-defined pentamers were conjugated to PEG, which might show potentials for biomedical applications.[213]

A concept based on the use of multicomponent reactions to achieve sequence-defined macromolecules *via* a unidirectional growth strategy was described by our group. Two different concepts were demonstrated, which are shown in Scheme 3. In the left reaction cycle, a combination of the Passerini three-component reaction (P-3CR) or the Ugi four-component reaction (U-4CR) and a thiol-ene was employed in an iterative mode. These multicomponent reactions are explained in detail in chapter 2.6.2. In the P-3CR, an isocyanide, an aldehyde, and a carboxylic acid react in a one-pot manner to a single product, which was used as starting unit of the macromolecule. For the aldehyde component, 10-undecenal was employed to introduce a terminal double bond for the subsequent thiol-ene reaction with 3-mercaptopropionic acid. This way, the carboxylic acid moiety was introduced to complete the reaction cycle and allowed the implementation of a further P-3CR. Sidechain definition was achieved by varying the isocyanide component.[166] In the Ugi approach, an amine is used as additional fourth component. Thus dual side chain definition was achieved, employing unique amines.[167] In the right reaction cycle (Scheme 3), an iterative chain elongation, consisting of a P-3CR and a subsequent reductive hydrogenation of a benzyl ester was conducted. Since toluene is the only side product, which was easily removed *via* evaporation under reduced pressure, an efficient strategy for the synthesis of sequence-defined macromolecules was described. Several aldehydes were used to introduce sidechain definition, whereas the benzyl ester was implemented *via* the

isocyanide component.[168] The sequence-defined pentamer and tetramer used in the joint project for determination of the impurity quantity in a uniform macromolecule were prepared according to this procedure.[I] The corresponding part of the discussion is provided in the respective publication.[214] Furthermore, backbone and sidechain definition was achieved by varying the isocyano benzyl ester.[150]

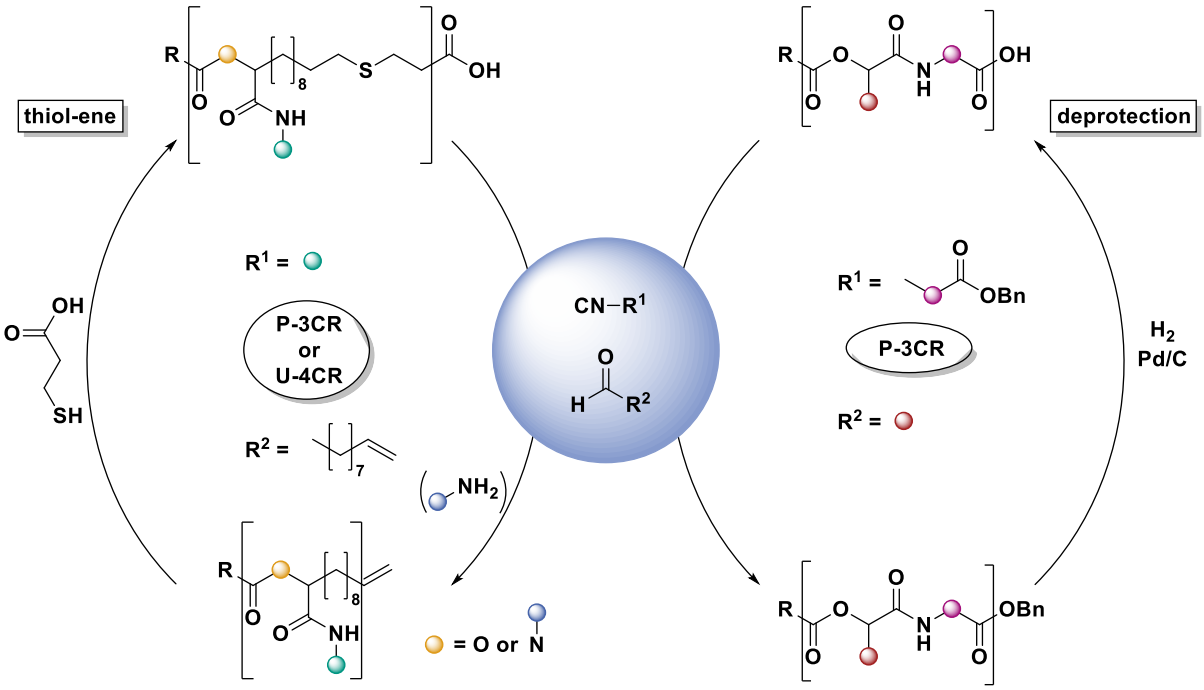

Scheme 3: Overview of the synthesis of sequence-defined macromolecules *via* multicomponent reactions. The left reaction cycle includes either a P-3CR or a U-4CR in combination with a subsequent thiol-ene reaction to introduce a carboxylic acid to complete the reaction cycle. Sidechain definition was achieved by varying the isocyanide component (P-3CR, 2014)[166] or both, the isocyanide and the amine component, when using an Ugi reaction (dual sidechain definition, 2015).[167] In the right reaction cycle, repetitive P-3CR and subsequent reductive hydrogenation of a benzyl ester were performed for chain elongation. Sidechain definition was achieved by employing different aldehydes (2016).[149,168] By using unique isocyano benzyl esters, additional backbone definition was accomplished (2020).[150]

Just recently, the application of these sequence-defined molecules as information-containing molecules was demonstrated for the backbone and sidechain dual sequence definition approach,[150] as well as for molecular mixtures (see chapter 2.5.8).[149]

[I] The synthesis as well as the implementation of the purity study for the respective Passerini sequences were carried out by MAXIMILIANE FRÖLICH in scope of her dissertation "*Increasing the data storage capacity of sequence-defined macromolecules*".[214]

Approaches for the synthesis of uniform PEGs and sequence defined information-containing macromolecules based on a unidirectional or bidirectional growth strategy (Figure 2 (a) and (b)) are described in detail in chapters 2.2 and 2.5. Further protocols for the preparation of non-conjugated, sequence-defined macromolecules described by different working groups, are not explained in detail within the scope of this work. However, they are not less important for this research area.[82,83,169,215–220]

Another interesting class of materials are conjugated polymers, where the investigations of uniform representatives should give more insight into the structure property relationship in terms of their optical and electronical properties. Two different approaches for the synthesis of oligo(1,4-phenylene ethynylene)s (OPE)s based on a unidirectional growth strategy (Figure 2 (a)) were studied by our group (Scheme 4). A two-step iterative reaction cycle, consisting of either a decarboxylative coupling and subsequent saponifation of an ethyl ester, or a Sonogashira cross-coupling followed by a TMS deprotection, were presented. For the latter approach, TMS-protected 4-iodophenylacetylenes equipped with different side chains were employed to achieve sequence definition.[221] The sequence-defined tetramer and trimer used in the joint project for determination of the impurity quantity in a uniform macromolecule were prepared according to this procedure.[I] The corresponding part of the discussion is provided in the respective publication.[223] In contrast, for the protocol based on the decarboxylative coupling, a 4-bromophenylacetylenes derivates equipped with an ethyl ester at the terminal alkyne was employed. This way, a more practical and efficient approach, in terms of reaction time and purification effort was presented.[224]

[I] The synthesis of the respective OPE sequences was carried out by REBEKKA SCHNEIDER in scope of her dissertation "*Synthesis and Characterization of Sequence-Defined Stiff Oligomers Using the Sonogashira Reaction*".[222] The corresponding purity study was carried out by DANIEL HAHN in scope of his dissertation "*Improved Strategies towards Conjugated Oligo Phenylene Ethynylenes*".[223]

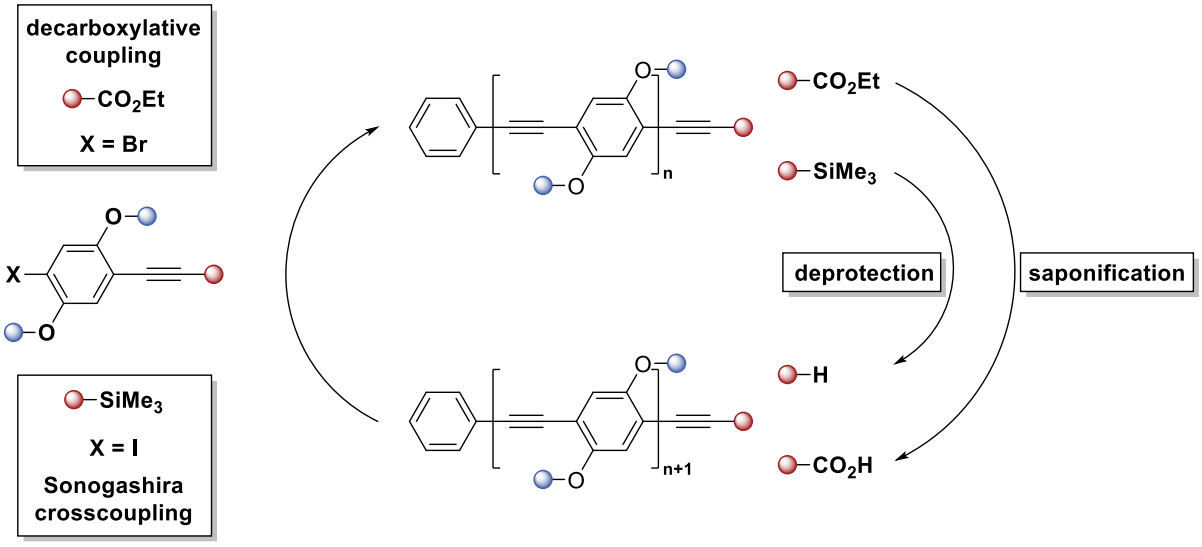

Scheme 4: General reaction scheme for the synthesis of OPEs based on a two-step iterative reaction cycle consisting either of a decarboxylative coupling and a saponification or a Sonogashira crosscoupling in combination with a deprotection.[221,224]

Further protocols for the preparation of conjugated, sequence-defined macromolecules based on a unidirectional or bidirectional growth strategy (Figure 2 (a) and (b)) described by different working groups, *e.g.,* oligo(phenylene vinylene)s (OPV)s,[225–230] oligo(arylene ethynylene)s (OAE)s,[231] or oligo(1,4-phenylene ethynylene)s (OPE)s,[232,233] are not explained in detail within the scope of this work.

For the fast synthesis of large sequence-defined macromolecules, the iterative exponential growth (IEG) (also known as divergent/convergent approach) strategy is the method of choice. Typically, orthogonal protecting groups are employed. The resulting building blocks are splitted into two parts, are separately orthogonally deprotected, and coupled in a convergent step. This way, monomers are coupled to dimers, dimers to tetramers, tetramers to octamers, and so on, and an exponential growth is achieved. However, the introduction of sidechain definition is challenging and thus the synthesis is limited to uniform homopolymers or palindromic sequences.[83]

The first iterative exponential growth was reported in 1982 by WHITING *et al*., who described the synthesis of linear long-chain aliphatic compounds *via* "*molecular doubling*". A C_{12}-bromoacetal monomer was employed in a three-step iterative cycle consisting of a transformation of the bromine to a phosphine of half of the monomer and an acetal deprotection of the second half, followed by the coupling of the phosphine and the aldehyde. After repetition of this chain elongation cycle, an octamer was obtained.[105,106]

An improved strategy based on the IEG, the so called IEG+, was reported by JOHNSON *et al.* in 2015, which is shown in Scheme 5. A monomer building block equipped with an epoxide at the one end and a TBS-protected alkyne on the other end was employed in a three-step iterative cycle, consisting of the deprotection of the TBS and the ring opening of the epoxide with sodium azide. The simultaneously formed secondary alcohol was further modified with different electrophiles, thus sidechain definition was achieved. Afterwards a CuAAC of the azide and the alkyne towards the corresponding tetrazole dimer allows chain-elongation. By repetition of this reaction cycle, uniform macromolecules defined in their sequence and stereoconfiguration, containing up to 32 monomer units, were obtained.[234]

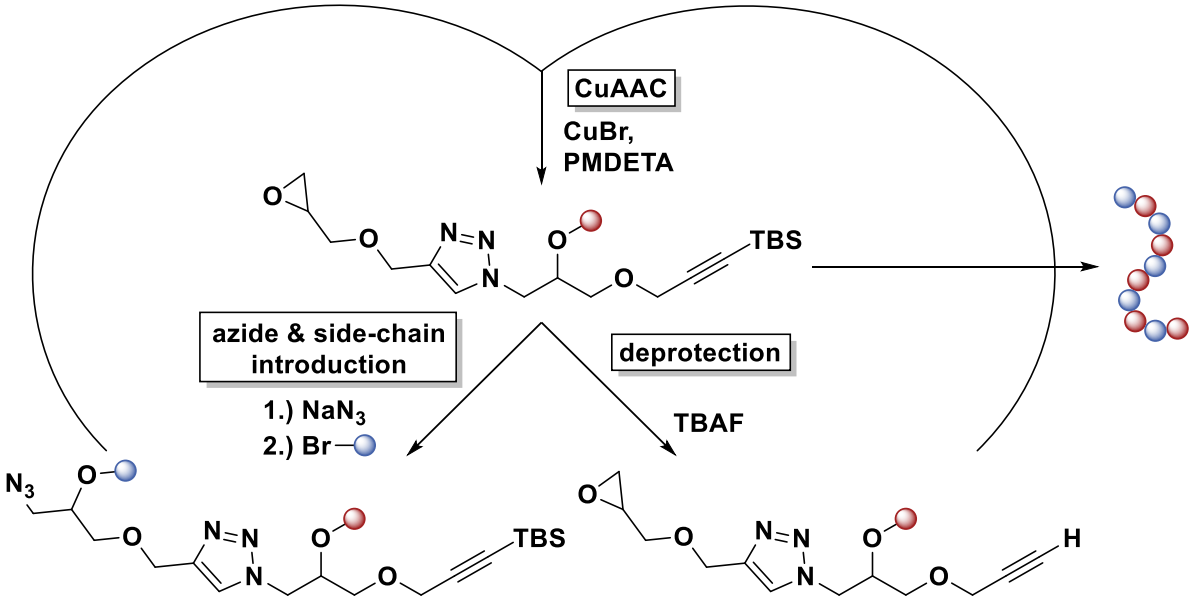

Scheme 5: Synthesis of uniform sequence- and stereo-defined macromolecules *via* IEG+.[234]

Approaches for the synthesis of uniform polyesters and sequence defined information-containing macromolecules based on an IEG strategy (Figure 2 (c)) are described in detail in chapters 2.2,[235–238] 2.3,[239–244] 2.4.3,[73,74] and 2.5.8.[148,245] Further protocols for the preparation of sequence defined macromolecules described by different working groups,[246–262] are not explained in detail within the scope of this work. However, they are not less important for this research area.

Besides synthetic approaches to prepare sequence-defined macromolecules, also investigations on purification methods and automated techniques have been made to achieve uniformity. One example is the fluorous solid phase extraction (FSPE). Thereby, the substrate is equipped with an fluorous-tag (F-Tag) and the reaction

mixture is purified depending on the fluorophilic/-phobic interactions with a fluorous stationary phase. First, the non-F-tagged organic compounds are eluted with fluorophobic solvents (*e.g.*, 70-80% MeOH/H_2O, 50-60% MeCN/H_2O, 80-90% DMF/H_2O, or pure DMSO). Afterwards, the F-tagged substrate of interest is eluted employing fluorophilic elution (*e.g.*, pure MeOH, MeCN, or THF).[263] Similar to the SPPS, reactants can be used in excess to achieve quantitative conversion to the desired product and removed afterwards effortlessly *via* simple FSPE. Examples are reported by TOUR *et al*.,[192] ALABI and POREL,[193] ANDERSON *et al*.,[194] and JIANG *et al*.[195]

Increasingly, automated synthesis and automated purification methods are significantly improving the efficiency of the reaction and purification times of the compounds. Examples of this are approaches carried out using flow chemistry.[261,262,264,265] Automated silica column chromatography and/or preparative SEC are used for the purification of the respective products. Since SEC separates the substrates according to their hydrodynamic volume, this method is restricted by the resolution limit of the separation columns, of the respective chromatograph, to IEG approaches. Due to the exponential growth, the difference in the hydrodynamic volume of the reactants and product, above a certain chain length, is sufficient to separate them easily by preparative SEC as shown in the example of KIM *et al*.[148,239,245] For the low molecular weight products automated silica column chromatography was used.

A different approach, the isolation of individual chain length of a narrow-distributed product sample on a multigram scale (2 to >10 g), was described by the group of HAWKER.[75,266–269] The strategy is based on the separation of polystyrene-*b*-polyisoprene (PS-*b*-PI)[270,271] and polystyrene-*b*-poly(methyl methacrylate) (PS-*b*-PMMA),[272] with a low dispersity and an average molecular weight of 20-80 kDa, into samples with $Đ$ <1.01 using high-performance liquid chromatography (HPLC), reported by CHANG *et al*. However, the loading quantity for preparative purification methods is mostly limited to milligram scales.[95] Making use of the advantages of automated chromatography systems, the scalability challenge was addressed for different polymer structures, such as oligoacrylates, oligostryrenics, and oDMS,[266] oligovinylacetates, conjugated oligomers and block copolymers, such as poly(dodecyl acrylate)-*block*-poly(lactide) (PDDA-*b*-PLA).[75,95] In this way, a broadly applicable and efficient method to obtain uniform structures (also vinyl-based polymers that are not accessible *via* a step-by-step synthesis) was demonstrated. Furthermore,

time-consuming repetitive multi step synthesis was avoided, since the narrow-distributed polymer samples were prepared *via* conventional controlled polymerization techniques in a single step. As an example, automated fractionation of 2.5 g PDDA-*b*-PLA yielded 20 well-defined samples, varying in their chain-length, within one hour of purification. Such compound libraries are of great interest for investigations on the effect of the dispersity as well as the domain composition on the block copolymer self-assembly and the structure property relationship in general (see chapter **2.4.3**).[75,76] However, the separation decreases with increasing degree of polymerization (DP), thus only oligomers up to a chain length of 15 repeating units were described yet.[95]

Within this work, the IEG approach according to the report of HAWKER *et al*.[240] and BRUCE *et al*.[273] were used for the preparation of uniform PCL and uniform PEG homopolymers, respectively (see chapter 2.2 and 2.3 for the description of the methods and 0 and 4.2 for the discussion of the results observed within this work).

2.2. Uniform polyether

2.2.1. Ethylene glycol-based uniform polyethers

Parts of this chapter and the associated supplementary information have already been published:

Bohn, P., Meier, M.A.R. Uniform poly(ethylene glycol): a comparative study. *Polym. J.* **52,** 165–178 (2020). https://doi.org/10.1038/s41428-019-0277-1.[274]

In 1859, LOURENÇO and WURZT independently reported the synthesis of PEG for the first time.[275] Today, the standard protocol for the preparation of PEGs is *via* anionic ring-opening polymerization (aROP) of ethylene oxide, which was already studied by PAUL FLORY in the 1940s.[276] Due to the living character of the aROP, a control of the molecular weight and its distribution is possible, therefore providing access to tailor-made PEGs.[277]

Poly(ethylene glycol)s (PEGs) are versatile,[278–280] biocompatible,[281,282] chemically stable,[283,284] flexible,[285–287] relatively non-toxic,[288,289] and water-soluble polymers.[290] These polymers are most frequently used in biopharmaceutical research as well as for everyday detergent applications. PEG-ylation[291–299] of biomacromolecules, such as proteins and peptides, or small therapeutic molecules has been shown to improve the pharmacological properties of these compounds, for instance by increasing their solubility[300] and stability, and influencing their pharmacokinetics and mode of action (for instance, the oral bioavailability is enhanced).[291,301–303] PEG also increases the size of the conjugate and acts as a steric shield to protect counterpart active ingredients against recognition by the immune system.[304] By increasing the half-life of drugs *in vivo*, the dosing frequency can be reduced.[305–309] Furthermore, PEGs are applied in many other fields, such as bionanoparticles,[310] electrolytes,[311] nanocomposite films,[312] and organic–inorganic hybrid materials.[313] Particularly in medicine, where heterogeneity influences the biological activity of PEG-ylated drugs (*e.g.*, their toxicity and efficacy), it is essential to use uniform PEGs to obtain distinct structure–property relationships and to precisely adjust the aforementioned functions.

PEGs with very low dispersity and more than four EG units, *i.e.*, tetra(ethylene glycol), are commercially not readily available and are rather expensive (111 EUR/g for $PEG_8 \geq 95\%$[314]). Separation *via* either distillation or preparative size exclusion

chromatography (SEC) of a nonuniform (polydisperse) polymer mixture would be a Sisyphean task, due to the similar physical properties of the different chain length. Thus, over recent decades, several working groups have developed different methods to synthesize uniform PEGs (Figure 3).[13,107,108,195,198,236–238,273,315–322]

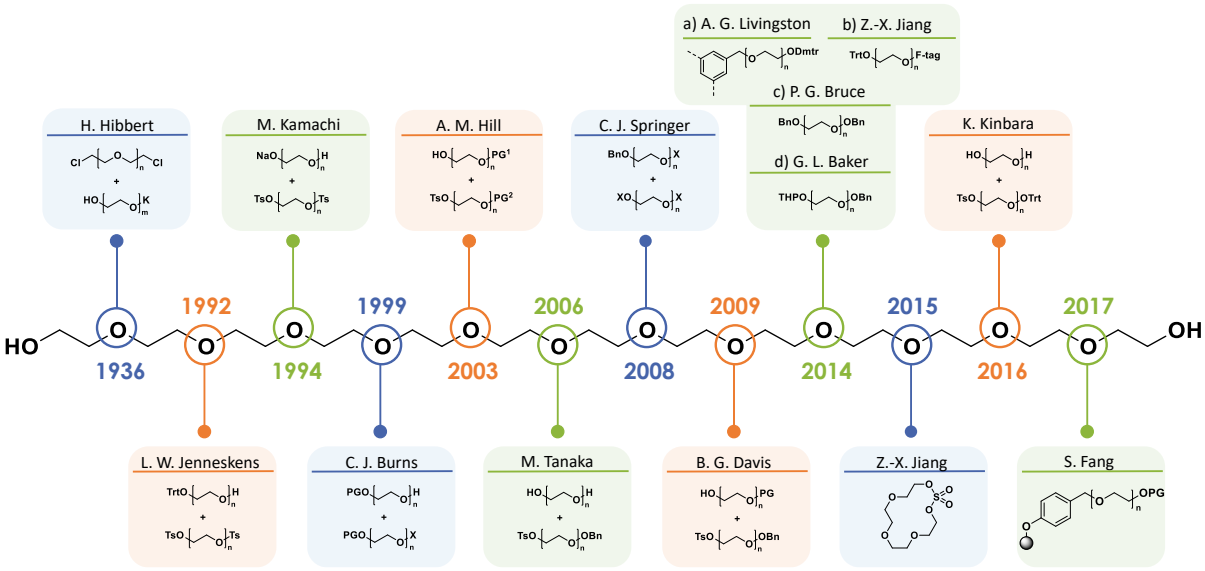

Figure 3: Previous work on the synthesis of uniform PEGs; 1936: first reported PEG obtained by reacting dichloro- and mono-alkali ethylene glycol alkoxides;[13,321] 1992: bidirectional growth using a PEG-ditosylate and a mono-tritylated ethylene glycol[107] or a mono-alkali ethylene glycol alkoxide (1994);[315] 1999: reaction of a protected ethylene glycol with another EG unit, bearing a protecting group and a leaving group;[238] 2003: synthesis of asymmetric PEGs *via* iterative exponential growth using orthogonal protecting groups;[236] 2006: bidirectional growth applying a monobenzyl ethylene glycol tosylate and a diol;[108] 2008: synthesis of symmetric PEGs using monobenzyl ethylene glycol blocks;[316] 2009: improvement of the IEG strategy reported by HILL *et al.*;[237] 2014: iterative unidirectional growth **a** by using a benzyl hub[198,322] and **b** *via* fluorous synthesis.[195] **c** Improvement of the ether synthesis reported by TANAKA *et al*. and DAVIS *et al*.[273] **d** Practical and scalable chromatography-free method using a protection/deprotection strategy;[317] 2015: preparation of asymmetrical and uniform PEGs *via* nucleophilic ring opening of macrocyclic sulfates;[318] 2016: chromatography-free synthesis *via* iterative monofunctionalization of tetra(ethylene glycol);[319] 2017: unidirectional growth using a Wang resin as a solid support.[320] Adapted from the literature.[274]

These approaches to synthesize uniform macromolecules are based on iterative methods. Hence, the preparation of high molecular weight macromolecules that retain their uniform nature requires particular synthetic effort, including the use of protecting groups and an excess of starting materials to achieve maximum yield for monofunctionalization. Here, the Williamson ether synthesis [I] is the reaction mechanism of choice.[323] However, due to the often employed harsh conditions (*i.e.*, >100 °C for several hours), where elimination is the most significant side reaction, tedious purification after each step to achieve highly pure products is crucial.[324]

In 1936, HIBBERT and coworkers reported a dodeca(ethylene glycol) by reacting a dichloro- and a mono-deprotonated ethylene glycol, and an oligo(ethylene glycol) with 42 repeat units was reported in 1939.[13,321] KAMACHI *et al*. adopted this approach in 1994 by replacing the dichloro compound with a ditosylate to obtain a PEG_{28}.[315] In the last three decades, four different concepts (unidirectional and bidirectional growth, IEG, and chain tripling) to obtain uniform structures were developed, which were already mentioned in chapter 2.1 in Figure 2.

JENNESKENS and coworkers described the synthesis of a dodeca(ethylene glycol) *via* bidirectional growth of a mono-protected and a ditosylated tetra(ethylene glycol).[107] The product was obtained in 95% yield over two steps on a multigram scale. By reacting two equivalents of a monobenzyl tetra(ethylene glycol) tosylate with a PEG_{36} diol, a uniform PEG_{44} was prepared by TANAKA and AHMED with an overall yield of 17% in nine steps on a 1.6 g scale.[108] In 2008, SPRINGER *et al*. obtained a 29-mer in an overall yield of 36% (490 mg) in six steps *via* bidirectional growth starting from hexa(ethylene glycol).[316] Based on the procedure of TANAKA and AHMED, the group of BRUCE achieved a bis-methyl-protected 24-mer on a multigram scale with the highest purity reported to date, as determined by MALDI-MS (>98% after one ether coupling and >95% after three couplings).[273] More recently, JIANG and coworkers described a new strategy for the synthesis of uniform PEGs, taking advantage of a macrocyclic sulfate (MCS), which circumvents the protection and activation steps.[318] An overview

[I] The Williamson ether synthesis was developed by ALEXANDER W. WILLIAMSON in 1850 and describes the reaction of an alkoxide ion and a primary alkyl halide *via* a conventional S_N2 mechanism after initial deprotonation of the alcohol, resulting in the desired ether.

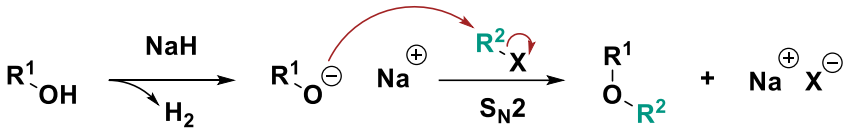

of the synthesis protocol is shown in Figure 4. In the initial step, the diol is converted into a macrocyclic sulfite using thionyl chloride, which is oxidized *in situ* to the MCS in a one-pot reaction. A bidirectional growth was performed by using tetra(ethylene glycol) for the ring-opening of the cyclic sulfate. This way, a 36-mer was prepared in four steps with an overall yield of 50%. A PEG_{64} mono methyl ether was synthesized in eight steps and an overall yield of 15% using sodium methoxide as a nucleophile and the macrocyclic octamer for the iterative ring-opening. The macrocycles are not limited to OEG-diols, thus eight examples of macrocyclic sulfites containing either longer aliphatic diols, thioethers or double- and triple bonds in the backbone were presented. Furthermore, 19 different nucleophiles were successfully employed for the ring-opening, thus providing a powerful reaction protocol for the mono functionalization of diols.

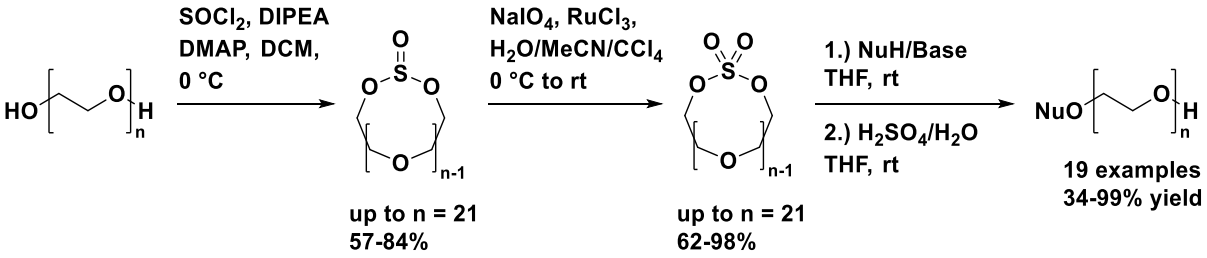

Figure 4: Overview of the reaction protocol reported by JIANG *et al*. The macrocyclic sulfates are prepared in a one-port reaction of the diols with thionyl chloride and subsequent oxidation with $NaIO_4$. Mono functionalized PEGs are obtained *via* nucleophilic ring-opening of the MCS.[318]

The disadvantage of the bidirectional concept and chain tripling (Figure 2 (b) and (d)) relates to the fact that only symmetric products are achieved *via* bidirectional growth. Since single post-functionalization of PEGs longer than 12 repeating units is challenging due to the lack of selectivity,[107] unidirectional approaches (Figure 2 (a) and (c)) describe a more versatile approach. Furthermore, full conversion *via* approaches (b) and (d) (Figure 2) is difficult to achieve. For example, chain tripling of PEG_{16} with α-benzyl-ω-tosyl hexadeca(ethylene glycol) yielded a mixture containing 31% monobenzyl PEG_{32} and 8% bis-dibenzyl PEG_{48}.[237] In the iterative exponential growth strategy (Scheme 6), orthogonal protecting groups are necessary. Repetition of a coupling reaction and subsequent selective deprotection leads to the elongation of the PEG chain. In 1999, BURNS *et al*. prepared hexa(ethylene glycol) on a 17.0 g scale in 80% yield.[238] Uniform dodeca(ethylene glycol)s were synthesized by HILL *et al*. on multigram scales with overall yields between 49 and 55%, starting from hexa(ethylene glycol) building blocks. Furthermore, 1.65 g of a PEG_{24} was obtained in

an overall yield of 43%.[236] DAVIS and coworkers described the syntheses of PEG_{32} and PEG_{48} in purities >98%, determined *via* MALDI-MS. In addition, hydroxyl-, azido-, and amino hexadeca(ethylene glycol) monomethyl ethers were prepared on gram scales with purities >99.8%.[237]

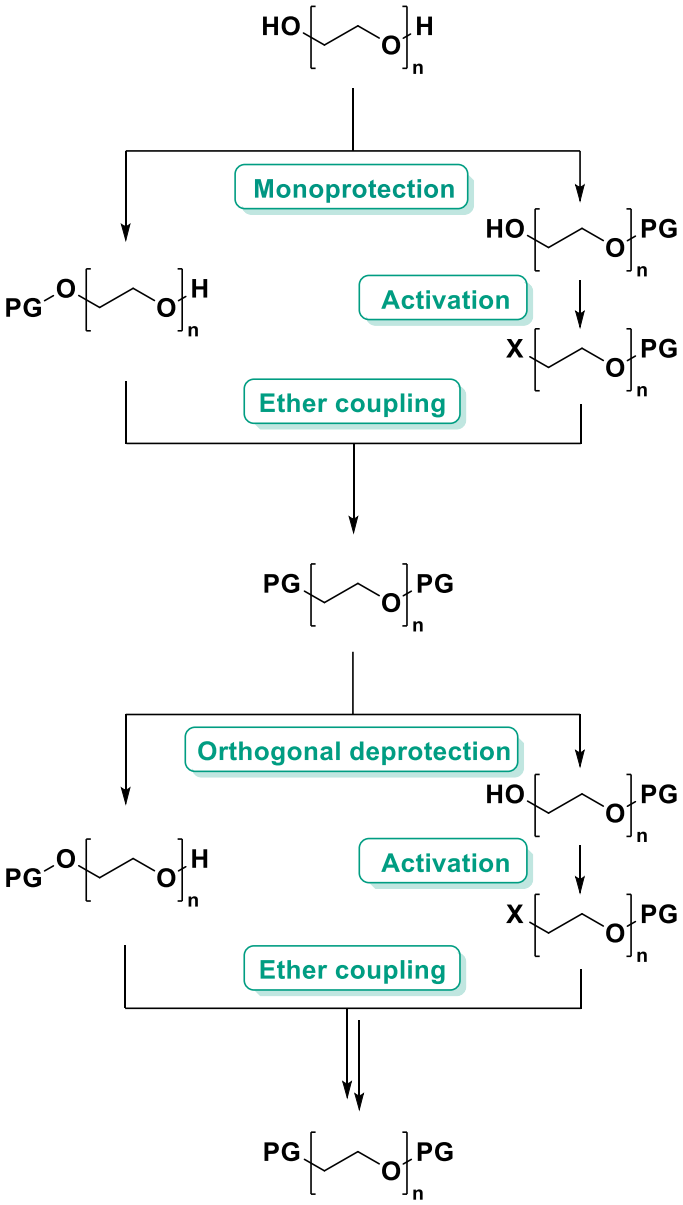

Scheme 6: General reaction scheme for the synthesis of uniform PEGs *via* an IEG strategy using orthogonal protection groups. PG = protecting group, X = leaving group.

To avoid tedious purification steps, BAKER *et al*. reported a chromatography-free synthesis using tetrahydropyranyl (THP) and benzyl protecting groups and taking advantage of selective extraction. A practical and scalable method for the preparation of asymmetric and well-defined PEGs was developed. In this way, benzyl octa(ethylene glycol) was obtained on a 100 g scale.[317]

LIVINGSTON, GAFFNEY and coworkers applied unidirectional synthesis (Figure 2 (a)) towards heterofunctional uniform oligo(ethylene glycol)s by using a three-armed "benzyl hub" (Figure 8). Iterative chain extension with mono-protected octa(ethylene glycol) in combination with simplified purification, end-group functionalization, and cleavage from the core unit, in the final step, was conducted. In this way, PEG_{24} monomethyl ether (yield 37%) and PEG_{56}-acetoxy-monomethyl ether in an overall yield of 13% were obtained on a milligram scale.[198,322] Furthermore, combining this method with a molecular sieving strategy, a highly efficient approach was demonstrated for the synthesis of sequence-defined polyether. Site-selective post polymerization allows a huge variety of tailor-made products, suitable for applications in nanotechnology, healthcare and information storage.[325]

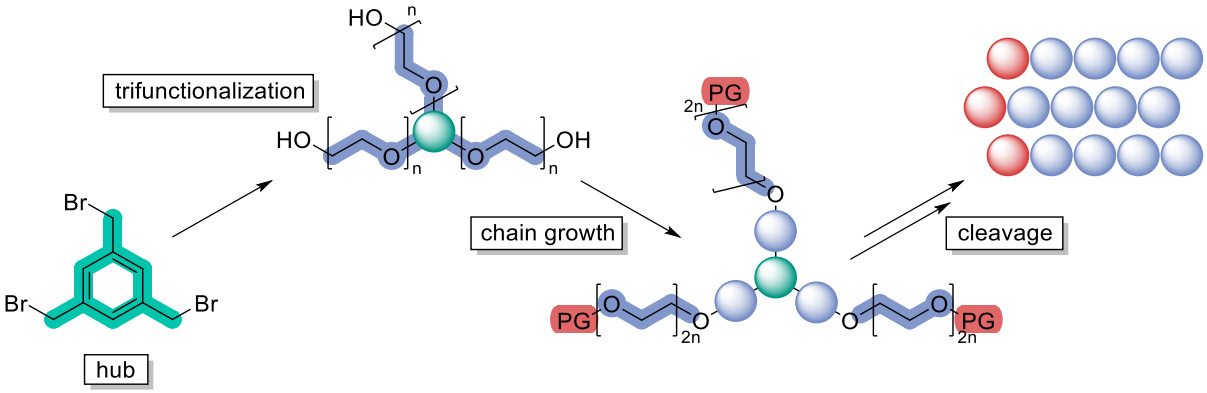

Figure 5: Schematic overview of the synthesis of uniform PEG reported by LIVINGSTON *et al*. The PEG chain is extended using a benzyl hub as core molecule and cleaved after reaching the desired chain length.[198,325] PG = protecting group.

In addition, JIANG *et al*. prepared well-defined oligo(ethylene glycol)s in a step-by-step manner on a fluorous tag, which allows simple purification *via* fluorous solid-phase extraction (FSPE) and solid-phase extraction (SPE). PEG_{20} was obtained in an overall yield of 13% in 13 steps on a gram scale.[195]

Recently, FANG *et al.* reported the synthesis of PEG_{12} on a 36 mg scale with an overall yield of 81% in five steps *via* the stepwise addition of a dimethoxytrityl tetra(ethylene glycol) tosylate on a Wang resin and monobenzyl PEG_{12} on a gram scale with an overall yield of 80% in five steps using benzyl-protected building blocks. By applying this approach, column chromatography was completely avoided, milder reaction conditions were applied, and post-functionalization after cleavage was possible. The purity of the products was determined with ESI and MALDI-TOF MS and was described

as "close to monodispersity". Further attempts for chain elongation to PEG_{16} and PEG_{20} led however to mixtures with different chain lengths.[320]

It is worth mentioning that, in the literature, purification methods are not always reported and product characterization by multiple techniques, including at least one chromatographic analysis, is often neglected. As the importance of complete characterization, especially for sequence-defined compounds is inevitable to ensure a uniform structure, chapter 4.1.1.3 will focus on the thorough discussion of uniformity confirmation by the major analytic techniques including SEC, NMR, and MS.

2.2.2. Non-ethylene glycol based uniform polyethers

In 1983, CHIELLINI and coworkers reported the preparation of uniform (S)-1,2-propanediol dimers and trimers *via* iterative Williamson-type etherification of the sodium salt of the mono benzyl- or mono trityl protected monomer and the orthogonally THP protected (S)-1,2-propanediol tosylate.[326]
PECEC and ASANDEI presented the synthesis of an uniform liquid crystalline polyether based on 1-(4-hydroxy-4′-biphenylyl)-2-(4-hydroxyphenyl)butane (TPB) monomer units linked *via* an aliphatic C_{10} spacer in 1997. Starting from the dimer, a three-step iterative cycle, consisting of separate activation of the alcohol *via* mesylatation and deprotection of the benzyl ether through reductive hydrogenation, followed by a subsequent coupling *via* etherification, was performed. Thus, a chain doubling was achieved per iteration and the successful preparation of a 16-mer was reported. A general reaction scheme of the reported iterative reaction cycle is shown in Figure 6. The obtained 16-mer was further employed in a final bidirectional growth with a monomer diol, resulting in a doubly benzyl protected 33-mer. Investigations on the phase behavior of the oligomers dependent on the chain length and the end groups, were performed using DSC.[235]

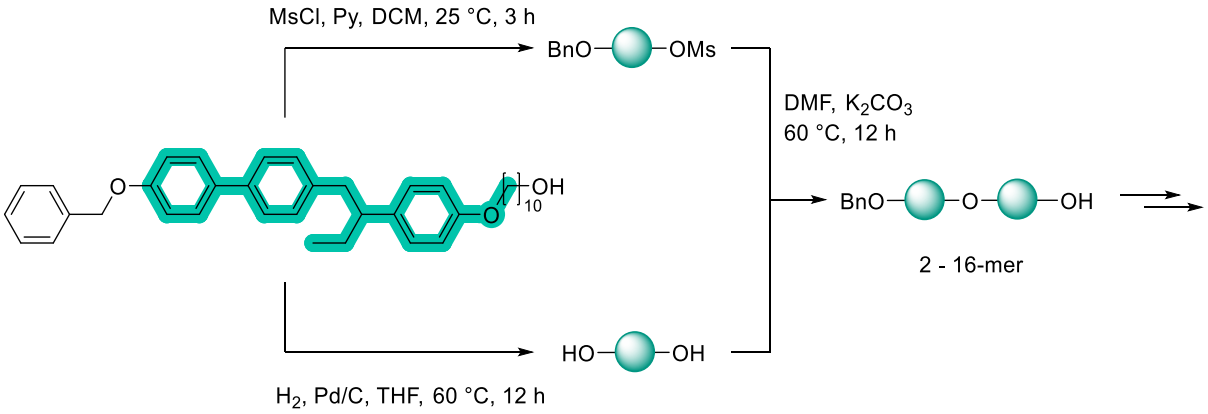

Figure 6 General reaction scheme for the three-step iterative chain elongation cycles of TPB connected with an aliphatic C_{10} spacer.[235]

The preparation of uniform oligo(butylene glycol) and oligo(propylene glycol) was described by GIN *et. al*. in 2003. Two different synthetic protocols were demonstrated. The first involves an iterative cycle of an IBX-mediated oxidation, the formation of an acetal, and a reductive ring opening. This way, a penta(1,4-butylene glycol) was prepared. The second iterative approach for the formation of hexa(1,3-propylene glycol) involves a phase-transfer etherification and subsequent reductive hydrogenation of the benzyl ether.[327]

In addition to the ROP of ethylene oxide resulting in disperse PEGs and the mentioned iterative approaches to achieve uniformity, a novel approach for the synthesis of uniform PEGs *via* a $GaBr_3$-catalyzed reduction was investigated within this work. A general introduction is provided in the next chapter.

2.2.3. $GaBr_3$-catalyzed ester-to-ether reduction as synthetic tool

In addition to the classical Williamson ether synthesis,[323] other approaches for the preparation of ethers have been developed over time, *e.g.* the Mitsunobu reaction,[328] the copper-mediated Ullmann-type[329–331] and Chan-Lam couplings,[329,332,333] the palladium-catalyzed Buchwald-Hartwig arylation,[334,335] the direct acid-mediated etherification of alcohols,[336–339] the addition of an alcohol to an olefin or alkyne (hydroetherification),[340–343] but also several reductive approaches, which are summarized in the review of CABRERO-ANTONINO *et al*.[344]

In 2007, SAKAI *et al*. reported the first Lewis acid-catalyzed ester reduction towards the corresponding ether, using $InBr_3$ as catalyst and Et_3SiH (TES) as reductant. The reaction was optimized on phenylethyl acetate as substrate and 5 mol% catalyst, 4 equiv. of TES, chloroform as solvent, and a reaction temperature of 60 °C gave the best results with 99% yield after one hour of reaction time (Scheme 7). Employing $PhMe_2SiH$ as reducing agent resulted in a comparable yield of 94%, whereas with $(EtO)_3SiH$, no conversion was observed. Further Lewis acids, *e.g.*, $InCl_3$, $In(OTf)_3$, or $In(OAc)_3$ showed no catalytic activity in that reaction. Apolar solvents, such as toluene and benzene, gave also high yields of >85%, while low conversions were observed for more polar representatives like THF or MeCN. A large substrate scope of 20 examples, including lactones and substrates bearing a bromide, a nitro group or a thiophene moiety, demonstrated a substantial functional group tolerance of the reduction. The corresponding ethers were obtained in yields of 10 – 99%.[345]

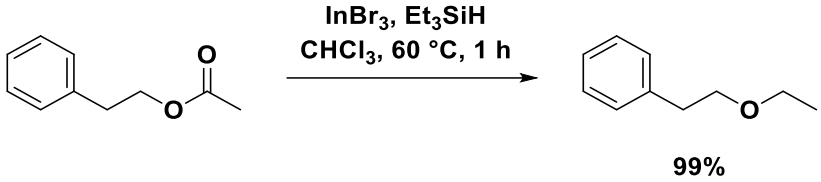

Scheme 7: Ester reduction using $InBr_3$ as catalyst and Et_3SiH as reductant, according to the procedure of SAKAI *et al*.[345]

Furthermore, SAKAI *et al*. proposed a possible reaction mechanism of the $InBr_3$-catalyzed reduction of esters to ethers *via* a radical pathway, which is depicted in Figure 7.[345]

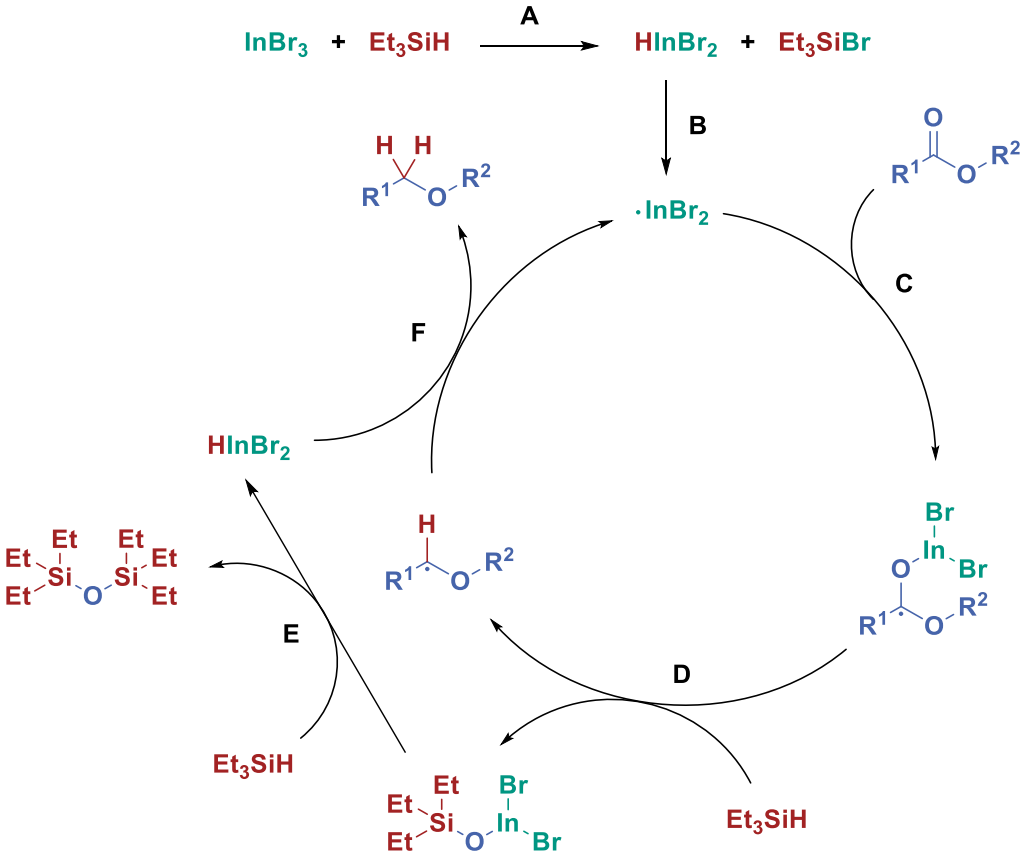

Figure 7: Proposed reaction mechanism of the $InBr_3$-catalyzed reduction of esters to ethers, reported in 2007 by SAKAI *et al*.[345]

In the first, initial step (A), a transmetalation between $InBr_3$ and Et_3SiH occurs, followed by the radical formation of the catalyst *via* hydrogen abstraction (B). Afterwards, an acetal radical is formed from the respective ester (C), which is subsequently reduced by Et_3SiH (D). The indium siloxane species is then transformed into the dibromo indium hydride and the byproduct of the reaction, hexaethylenedisiloxane (E). In the final step, the desired ether is formed *via* a hydrogen abstraction of the radical intermediate under regeneration of the indium dibromide radical species (F). Due to the similar electronic configuration, the reduction with $GaBr_3$ and TMDS most likely follows the same mechanism.

Since 2014, the application of $GaBr_3$ and TMDS as suitable reactants for the reduction of esters to ethers was presented on different substrates, which are summarized Figure 8.[346–349]

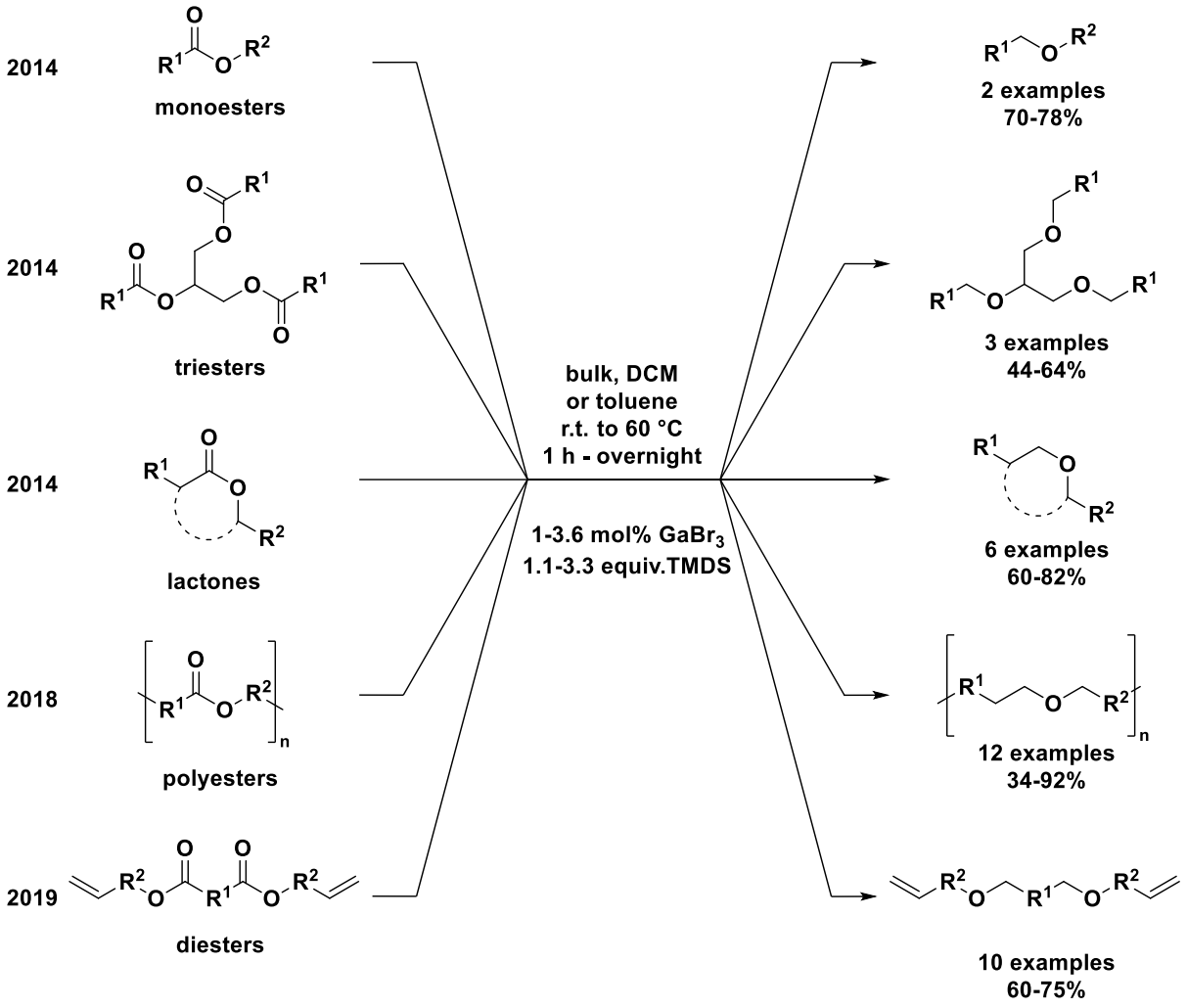

Figure 8: Overview of the $GaBr_3$-catalyzed reduction with TMDS of different substrates, ranging from monoesters to polyesters, as well as lactones.[346–349]

METZGER and BIERMANN published investigations of the $GaBr_3$-catalyzed reduction of high oleic sunflower oil to the corresponding trioleyl ether using TMDS as reductant. Compared to the reaction protocols of SAKAI *et al.*, in which 5 mol% $InBr_3$ and TES were employed at 60 °C in chloroform, and BELLER *et al.*, using 10 mol% $Fe_3(CO)_{12}$ and TMDS at 100 °C in toluene, several improvements were reported. In general, the reaction was performed under milder conditions, considerably lowering the temperature to room temperature, decreasing the quantity of catalyst to 0.5 – 1 mol% per ester functionality, while performing the reaction in bulk. Additionally, when applying $GaBr_3$ instead of $InBr_3$, a significant decrease from 20 to 7% of the ester cleavage to the corresponding oleyl alcohol *via* overreduction was observed in the ^{13}C NMR spectrum, leading to the conclusion of $GaBr_3$ being the more efficient and milder catalyst. Full conversion of the ester was achieved already after one hour of reaction time. The reaction scope was further expanded by the same group to mono

methyl esters, triglycerides, and γ- and δ-lactones. Using substoichiometric quantities of TMDS and the preference of the lactone group compared to the linear ester was shown. The proposed synthesis protocol was employed for the preparation of 11 ethers, with yields ranging from 44-82%.[346,347]

The sustainability aspect of the $GaBr_3$-catalyzed reduction compared to other methods was used by our group as a novel synthesis protocol of polyethers from renewable polyesters in 2018.[348] The experimental procedure was adjusted to the reduction of polymers, thus DCM was applied as solvent leading to conversions >99%, as indicated by NMR, while suppressing the ester cleavage side-reaction to a minimum. This way, the preparation of uncommon and previously unavailable polyethers was achieved. Seven different polyethers were obtained in high yields between 83 and 92%, whereas a decrease in yield to 34% was observed for more polar polyesters (five examples).

In 2019, the same protocol was applied to synthesize fatty acid-based ω,ω'-unsaturated diene diether monomers *via* reduction of the respective diester precursors. Six dienes were obtained in moderate yields between 60-84% and were subsequently polymerized *via* ADMET or thiol-ene polymerization. Afterwards, the isolated polymers were further functionalized by oxidation or hydrogenation and the thermal properties were investigated.[349]

In addition, the reduction with silanes is not strictly limited to ester functionalities. HUANG *et al*. reported the successful reduction of amides with TMDS and tris(pentafluorophenyl)boron as catalyst in a one-pot reaction. This way, a substrate scope of 24 different secondary amines was prepared in yields between 56 and 98% (Scheme 8).[350] Using the same combination of catalyst and reductant, the reductions of different amides were reported by ADRONOV *et al.*[351] and CANTAT *et al*.[352] Further reductions of amides to amines using silanes are summarized in a review by NAGASHIMA.[353]

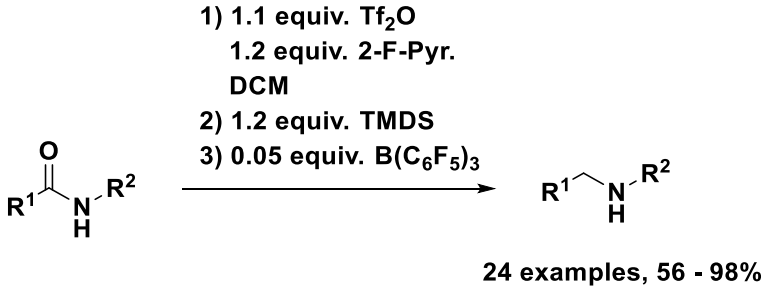

Scheme 8: One-pot reduction of amides to the corresponding secondary amines using tris(pentafluorophenyl)boron ($B(C_6F_5)_3$) as catalyst and TMDS as reductant. Tf_2O = triflic anhydride, 2-F-Pyr. = 2-fluoropyridine.[350]

Conclusively, the reduction of esters employing $GaBr_3$ as catalyst and silanes as reductants was shown to be a more sustainable and efficient method, compared to further (metal-) catalyzed approaches, and especially compared to the Williamson ether synthesis, to convert polyesters and small molecule esters into ethers.

The advantages of milder reaction conditions and the less purification effort, compared to classic etherification protocols, was investigated within this work for the synthesis of uniform PEGs, which is discussed in detail in chapter 4.1.2.

2.3. Uniform polyester

The common strategies for the synthesis of polyesters are based on a polycondensation of (functionalized) alcohols and (functionalized) carboxylic acids, or alternatively the ring opening polymerization of (functionalized) lactones. In the first approach, AA + BB-type monomers or AB + BA-type monomers are employed in a condensation reaction and small molecules *e.g.*, water, methanol or HCl are formed as byproducts. To maximize conversion, often high temperatures and/or vacuum are applied, thus removing the byproduct, and shifting the equilibrium to the product side. Typically, according to the Carothers equation, a dispersity of $Đ = 2$ is obtained at full conversion and stoichiometric ratio of the functional groups.[354] In contrast, the ring-opening polymerization (ROP) of cyclic esters allows a certain control of the dispersity and thus the physical and chemical properties, due to the living character of the reaction.[277]

Polyesters are an important class of materials, which are widely used in many fields. Since this work focuses on uniform PCL and the corresponding PCL-*b*-PEG BCP, the properties and the synthesis *via* ROP (chapter 2.4.1) are explained in detail.

PCL is one of the earliest polymers synthesized by CAROTHERS *et al.* in 1934.[355] It is prepared either *via* polycondensation[356] of 6-hydroxyhexanoic acid or metal-, organo- or enzyme-catalyzed ROP of ε-caprolactone.[357–361] Depending on the used approach, the ROP proceeds according to four different mechanisms, including cationic, anionic, monomer-activated and coordination-inserted ROP.[356] The hydrophobic and semicrystalline polymer[362] is highly soluble in various solvents at room temperature, *e.g*. THF, DCM, DMC, or toluene,[363] and furthermore miscible with many other polymers, *e.g*. poly(vinyl chloride) (PVC), poly(styrene–acrylonitrile) (SAN), poly(acrylonitrile butadiene styrene) (ABS).[356] Due to its interesting properties such as controlled biodegradability,[364] biocompatibility,[365] and possible renewability,[356] it is used in various fields of application, *e.g.* as packaging material,[366,367] as adhesives,[368,369] in microelectronics,[370] as well as in biomedicine, where it is employed as scaffolds in tissue engineering[371–377] or as long-term drug delivery systems.[377–379] Especially for the latter applications, the knowledge about the distinct structure property-relationship is crucial, thus synthesis protocols for the preparation of uniform PCL (and polyester in general) based on an IEG were reported in the last two decades.[240,242,243,380]

The synthesis of a uniform polyester was reported in 1995 by HUANG and HERMES. Sequence-defined alternating (L-lactic acid)-*co*-(glycolic acid) oligomers were prepared *via* an iterative exponential growth strategy. Therefore, orthogonal protection groups were essential, thus the hydroxy group was functionalized as a methoxyethoxymethyl (MEM) ether, whereas the carboxylic acid was capped with a benzyl ester. Starting from the (L-lactic acid)-*co*-(glycolic acid) dimer, the hexadecamer was prepared by repetition of the convergent/divergent chain elongation cycle, consisting of separate orthogonal deprotection and a subsequent coupling reaction. The MEM protection group was cleaved in the presence of TMSCl and NaI and the benzyl ester *via* palladium-catalyzed reductive hydrogenation. For the coupling reaction, a Steglich esterification[I] was conducted, using DCC and DMAP.[242]

One year later, in 1996, SEEBACH *et al*. made use of a similar reaction protocol for the synthesis of uniform (R)-3-hydroxybutanoic acid oligomers (OHB). The carboxylic acid was protected with a benzyl ester, whereas the alcohol was transferred into a *tert*-butyldiphenylsilyl (TBDPS) ether, which was deprotected with HF in pyridine. For the coupling reaction, the carboxyl-terminated building block was converted into the corresponding acid chloride derivative. After seven iterations of the convergent/divergent reaction cycle, a uniform 128-mer was obtained.[380] Furthermore, uniform cyclic polyesters were prepared from the hydroxy acid precursors, with 8 – 32 repeating units, applying thiopyridine and $CuBr_2$, which were studied as Ca^{2+}-ion carriers through phospholipids bilayers of artificial vesicles.[381] In addition, the linear uniform OHBs were coupled to amino acids, carbohydrates,

[I] The Steglich esterification was described by WOLFGANG STEGLICH in 1978. DMAP is used as catalyst and DCC as an activation reagent. In the initial step, the carboxylic acid reacts with DCC to an *O*-acylurea, which forms a *N*-acylpyridiniumion in a reaction with DMAP. A nucleophilic attack of the alcohol to the carbonyl takes place resulting in the corresponding ester under release of DMAP and DCU.

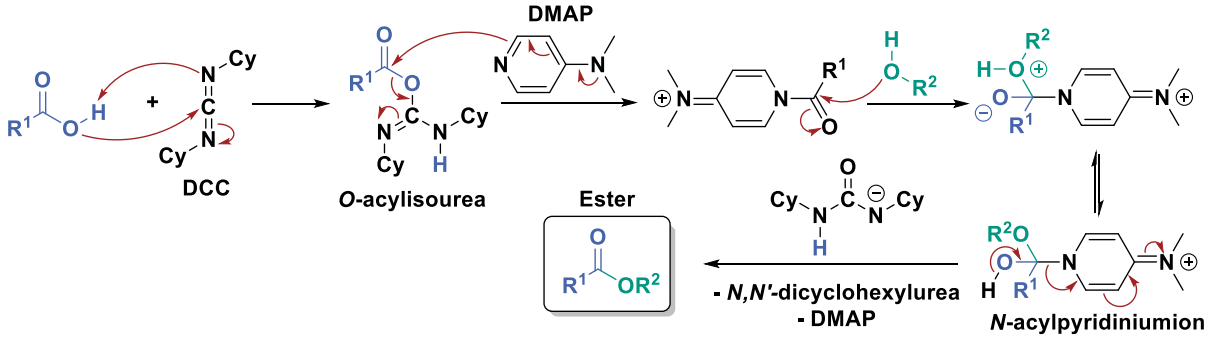

coumarin and biotin to increase their water solubility and offer the possibility for biochemical investigations.[382]

Uniform alternating poly(butylene glutarate) oligomers with chain length up to 64 repeating units were reported by CHAPMAN *et al*. in 2003. Starting from butane diol and glutaric anhydride, an iterative exponential growth strategy was performed using 9-fluorenylmethoxycarbonyl (Fmoc) chloride and *p*-methoxybenzyl (PMB) alcohol as protecting agents, and EDC/DMAP for the coupling reaction. A careful characterization was reported confirming the high purity of the products, as well as yields above 70%. However, traces of impurities ranging from the 62 – 66-mer were observed *via* MALDI-TOF for the 64-mer.[243]

In 2008, HAWKER *et al*. reported the synthesis of uniform ε-caprolactone oligomers *via* an iterative exponential growth strategy. The reaction scheme of the investigated synthesis protocol is shown in Scheme 9. As starting material, ε-caprolactone was used, which was transferred into the monomer, 6-hydroxyhexanoic acid, in the initial step *via* a base-catalyzed nucleophilic ring-opening with aqueous sodium hydroxide solution. The product was obtained in quantitative yield, employing a continuous extraction. A careful study for the selection of the orthogonal protection groups was conducted and the alcohol was protected with a *tert*-butyldimethylsilyl (TBDMS) ether and the carboxylic acid with a benzyl ester. Since acyl halides or active ester derivatives, used in the subsequent convergent coupling reaction, resulted in low yields or minor deprotection of the TBDMS protection group, DCC and *N,N'*-4-dimethylaminopyridine (DMAP) provided the best results up to the tetramer. Occurring side reactions, *e.g.* the formation of unreactive *N*-acylureas, were suppressed using 4-(dimethylamino)pyridinium *p*-toluenesulfonate (DPTS) for the coupling reaction of the larger oligomers. For the separate orthogonal deprotection steps, the silyl ether was treated with tetra-*n*-butyl ammonium fluoride (TBAF) under acidic conditions, whereas the benzyl ester was cleaved *via* palladium-catalyzed reductive hydrogenation. By repetition of the chain elongation cycle, consisting of the convergent Steglich esterification and the divergent orthogonal deprotection, a doubly protected 64-mer was obtained in a purity of >95%. Yields above 90% were obtained for the deprotection steps and >65% for the coupling reactions. All molecules were carefully characterized with ^{1}H, ^{13}C NMR spectroscopy, SEC and MALDI or ESI-MS. Furthermore, the thermal properties were investigated by DSC and the decomposition

temperatures *via* TGA, both showing increasing values with increasing chain length.[240]

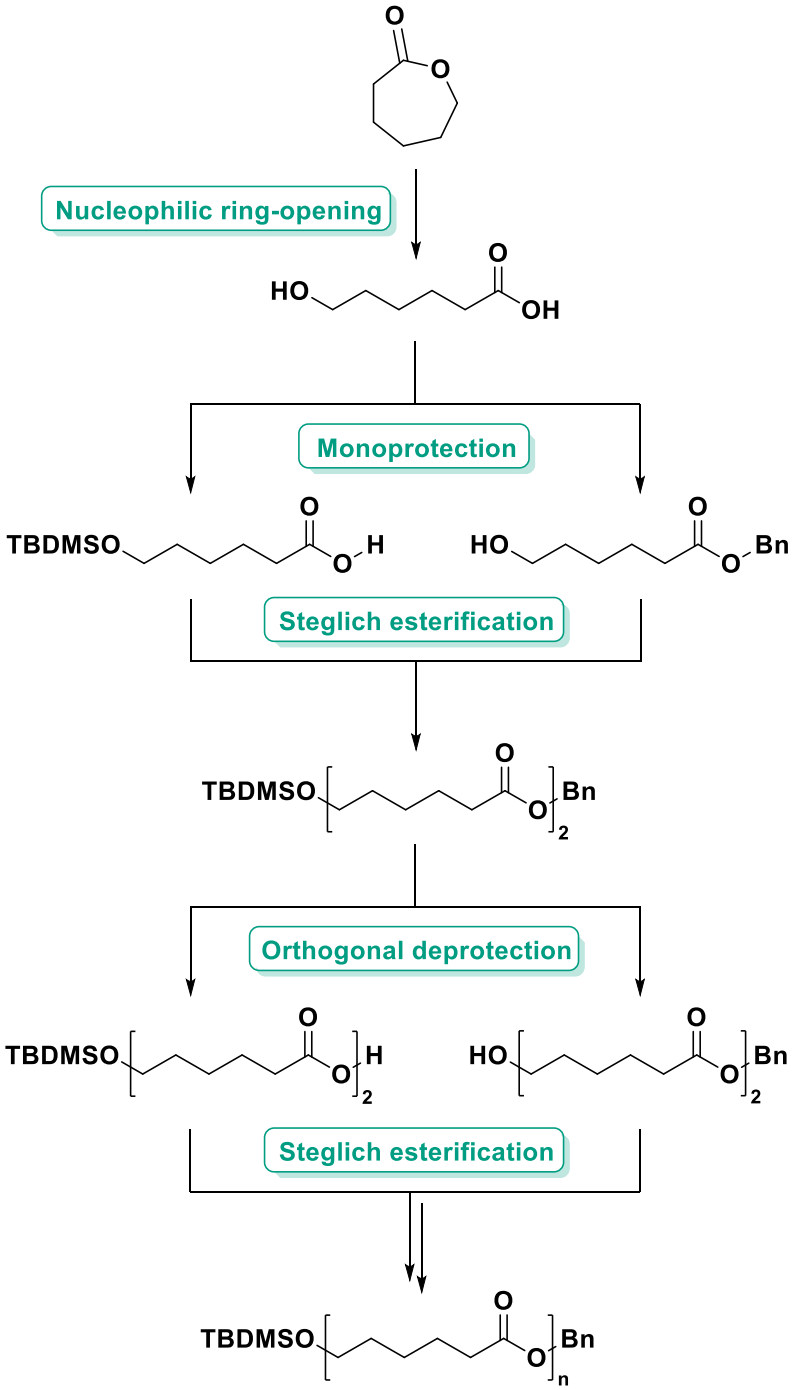

Scheme 9: Overview of the iterative exponential growth strategy towards uniform poly(ε-caprolactone) according to the procedure of HAWKER *et al*. The monomer 6-hydroxyhexanoic acid was prepared *via* nucleophilic ring opening of ε-caprolactone followed by the separate protection of the alcohol and the carboxylic acid with TBDMS-Cl or benzyl bromide, respectively. Afterwards an iterative chain elongation cycle consisting of a Steglich esterification and separate deprotection was employed, yielding the doubly protected 64-mer.[240]

Interestingly, two melting points were observed in the DSC starting from the hexadecamer, indicating the presence of either two crystallite sizes, a crystal-to-crystal transition, or two coexisting crystalline structures. Furthermore, a lamellar crystalline structure was observed *via* SAXS from the octamer on, indicating chain-folding for the larger oligomers.[240]

In the same year, the synthesis and characterization of uniform (L)-lactic acid oligomers, based on a similar reaction protocol, was reported by HAWKER *et. al*. As for the uniform ε-caprolactone oligomers, high yields of 70 – 100% were observed for the separate deprotection steps as well as for the coupling reaction using DCC or EDC (3-(ethyliminomethylidenamino)-*N*,*N*-dimethyl-propan-1-amine). All products were carefully characterized and the stereogenic sequence was confirmed *via* ^{1}H NMR spectroscopy and single crystal diffraction. Furthermore, the crystallinity behavior and the thermal properties were investigated and a distinct structure-property relationship was observed, *e.g.* a higher thermal stability of the uniform structures and compared to commercial PLA.[241]

In 2009, KLOK *et al*. presented the synthesis of uniform hydrophilic/hydrophobic patterned α-hydroxy acid oligomers using (2S)-2-hydroxy-4-methylpentanoic acid and (2S)-2-hydroxypent-4-enoic acid as starting materials. Tetrahydropyran (THP) ether and allyl ester were selected as orthogonal protection groups, which were cleaved separately in the iterative chain elongation cycle with catalytic amounts of *p*-TsOH and *via* Pd^{0}-catalyzed allyl transfer to morpholine with tetrakis(triphenylphosphane) palladium(0) [$Pd(PPh_3)_4$]. A Steglich esterification utilizing DCC and DMAP was employed for the esterification. This way, a doubly protected octamer was prepared bearing allyl side chains, which were then post functionalized in a thiol-ene click reaction with various thiols, thus resulting in hydrophilic/hydrophobic patterned oligomers, which tend to form foldamer secondary structures.[244]

Recently, in 2020, KIM and coworkers reported the synthesis of uniform, sequence-defined aperiodic copolyester. *rac*-Phenyllactic acid and *rac*-lactic acid were used as starting materials for the preparation of four doubly protected dyads of all combinations. Similar to the group of Hawker, the alcohol was protected with a TBDMS ether and the carboxylic acid with a benzyl ester. In contrast, EDC was used as activation agent in the coupling reaction and the deprotection was performed with boron trifluoride etherate (BF_3•Et_2O). Yields >95% for the orthogonal deprotection

steps and >70% for the esterification were reported. By repetition of the cross-convergent chain elongation cycle, the chain length increased in an exponential fashion. Thus, a sequence-defined alternating 128-mer and a 256-mer were successfully prepared and a high purity was confirmed by a careful characterization, including ^{1}H and ^{13}C spectroscopy, SEC and MALDI-TOF. Since the difference in the hydrodynamic volume increases with every other coupling step, the sequences greater than 16 repeating units were easily purified *via* fast and efficient recycling preparative size-exclusion chromatography in 1-gram scales. Furthermore, the application of these compounds as information-containing molecules was demonstrated, which is described in chapter 2.5.8.[245]

In the same year, the group of KIM presented the intramolecular cyclization of uniform PLA. Linear precursors up to 1024 repeating units were prepared using the same synthesis and purification protocol as mentioned above on gram scales. A decrease of the yield in the individual coupling steps from 92% for the 64-mer to 62% for the 512-mer and a massive reduction of yield to <5% for the 1024-mer was described. By increasing the concentration of the alcohol precursor and elongating the reaction time, the yield was significantly increased to 59%. However, a trend for the limits in terms of chain length was observed for the preparation of sequence-defined macromolecules. The functional end-groups were converted to an acetylene and an azide group, respectively, resulting in a doubly functionalized macromolecule suitable for an intramolecular cyclization *via* CuBr-catalyzed azide-alkyne click reaction. Due to the decrease of the hydrodynamic volume, separation from linear species was successfully conducted with preparative SEC. This way, five examples of sequence defined macrocycles ranging from 32 to 512 repeating units were prepared. Furthermore, a uniform cyclic block copolymer was synthesized from a LA_{64}-*b*-PL_{64} block copolymer precursor, which is described in chapter 2.4.3.[239]

In 2022, KIM *et al.* presented investigations to further increase the efficiency of the protocol for the synthesis of uniform polymers. A semi-automated synthesis of sequence-defined poly(L-lactic-*co*-glycolic acid)s (PLGAs) applying continuous flow chemistry was demonstrated for the preparation of 16 macromolecules containing 64 repeating units. The compounds were also used as digital polymers for the storage of information, which is further described in chapter 2.5.8.[148]

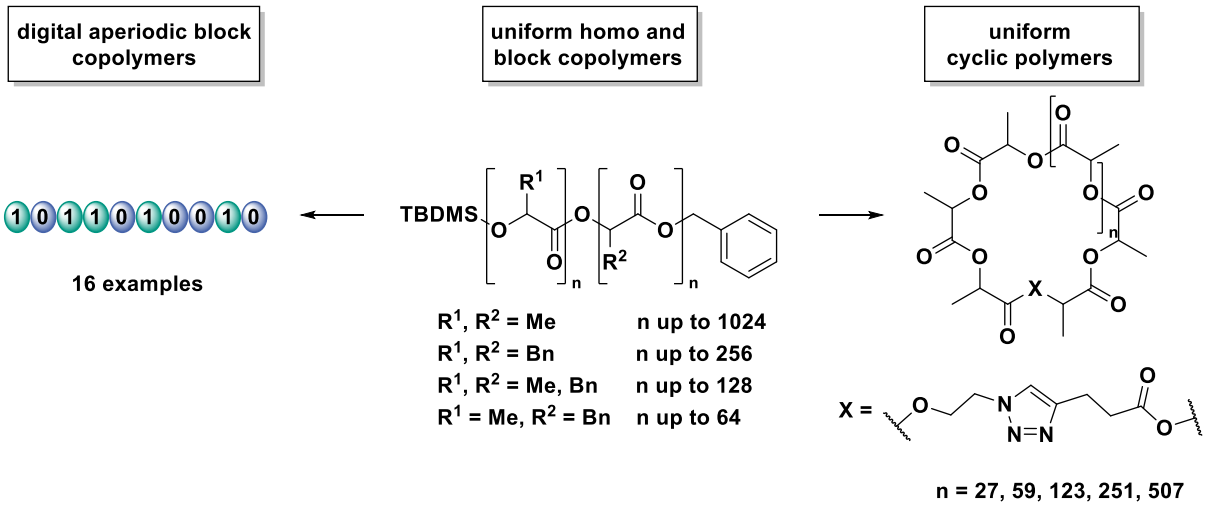

Figure 9: Schematic overview of uniform homo and block copolymers prepared *via* repetitive Steglich esterification in an IEG strategy, which were either used as digital polymers or transferred into uniform cyclic polymers.[148,239,245]

In a comparative study of ZHANG and coworkers in 2021, the above-mentioned approaches were evaluated and further optimized, resulting in a highly versatile, scalable approach with a large functional group tolerance. For the orthogonal protection groups, TBDPS ether and *tert*-butyl ester provided the best results and were cleaved with TBAF and *p*-toluene sulfonic acid/silica gel, respectively. DCC and DPTS were used for the convergent coupling reaction. Nine different uniform oligo- and polyesters including oligo(lactic acid) (oLA), oligo(glycolide acid) (oGA), oligo(*p*-diocanone) (oPDO), oligo(γ-butyrolactone) (oBL), poly(ε-caprolactone) (PCL), oligo(ε-caprolactone-co-γ-butyrolactone) (oCLBL), copolymers of itaconic acid and lactic acid (oITALA), copolymers based on 2-butenoic acid and lactic acid (oFULA) and oligo(4-hydroxy-2-butynoic acid) (oALKY), up to 256 repeating units, were prepared, underlining the highly versatile approach.[383]

2.4. Block copolymers

2.4.1. General introduction and synthetic approaches

Block copolymers (BCP) together with random, graft, alternating, periodic,[384] aperiodic,[181] and gradient copolymers,[385] belong to the general class of copolymers (Figure 10),[386] which are polymers obtained from more than one monomer species. The properties of copolymers are based on the structure of the used monomers, their distribution within the copolymer and the polymer architecture. Block copolymers are further divided into different architectures, such as linear, comb, cyclic and star BCP.[387] Linear diblock copolymers consist of exactly two different homopolymers, covalently linked to each other on one end and represent the simplest block copolymer.[388]

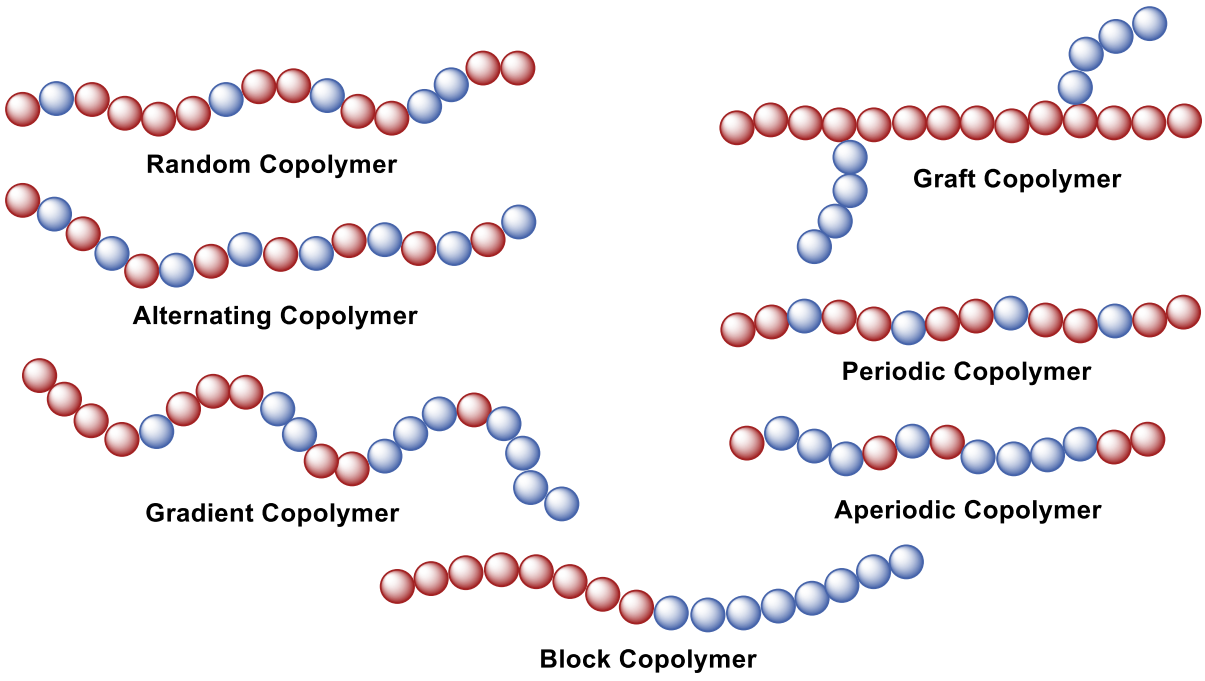

Figure 10: Different types of copolymers, depending on the monomer distribution.[386]

Practically, to obtain a diblock copolymer, the homopolymerization of monomer A is commonly performed, followed by the addition of monomer B. Controlled and living polymerization techniques, such as reversible deactivation radical polymerizations (RDRPs), *e.g.,* ATRP,[385,389] RAFT polymerization,[390] and NMP,[391] or living anionic polymerization,[4,186] are the most important methods for the synthesis of precisely controlled block copolymers.[58,392–395] After a fast initiation and formation of an active center (*e.g.,* carbocation, carbanion, or radical), the propagation of the

homopolymerization of monomer A occurs until depletion of the monomer in the mixture. The active center is still “alive” after complete consumption of the reactants and the polymer can either be extended by further addition of monomer or functionalized *via* a terminating agent. For a typical diblock copolymer, monomer B is added, and its living/controlled polymerization takes place resulting in chain elongation. The term living polymerization was defined by MICHAEL SZWARC in 1956 for the anionic polymerization of styrene.[4,186] The key characteristic of a living reaction process is the absence of side reactions, such as chain termination of chain transfer,[35,396,397] whereas in RDRP, the termination is suppressed, but not eliminated. Furthermore, living/ controlled polymerizations show constant propagation rate due to the controlled and fast initiation, which results in polymers with defined molecular weight distributions with a low dispersity ($Đ < 1.05$).[398,399] In this way, tailor-made BCPs are accessible for many fields of application, such as drug delivery systems,[400] surface patterning,[401] advanced materials (*e.g.*, thermoplastic elastomers[402]) and many others.[403]

Another approach for the synthesis of diblock copolymers, which was employed within the scope of this thesis is the ROP of lactones (ε-caprolactone), using a macroinitiator (mPEG) to obtain the desired block copolymer (mPEG-*b*-PCL).

The chain elongation of a ROP can proceed in four different main mechanisms: anionic,[404,405] cationic,[404,405] monomer-activated,[406,407] and coordination-inserted ROP.[404,405] The respective reaction mechanisms are shown in Scheme 10 on the basis of the ring opening of ε-caprolactone. In the anionic ROP (**a**), an anionic species attacks the carbonyl carbon of the lactone, and the cycle is opened at the acyl-oxygen, resulting in an alkoxide, enabling the ring-opening of another monomer.[404,405] The cationic ROP (**b**) consists of the formation of a cationic species, followed by a nucleophilic attack of the carbonyl oxygen of a second monomer in a bimolecular nucleophilic substitution (S_N2) reaction.[404,405] In the third mechanism (**c**), the monomer is activated by the catalyst and is subsequently attacked by the activated initiator or polymer chain.[406,407] The coordination-insertion ROP is the most common mechanism (**d**). The monomer coordinates to the catalyst and inserts into the metal-oxygen bond. The growing chain is attached *via* an alkoxide bond to the metal during the propagation.[404,405]

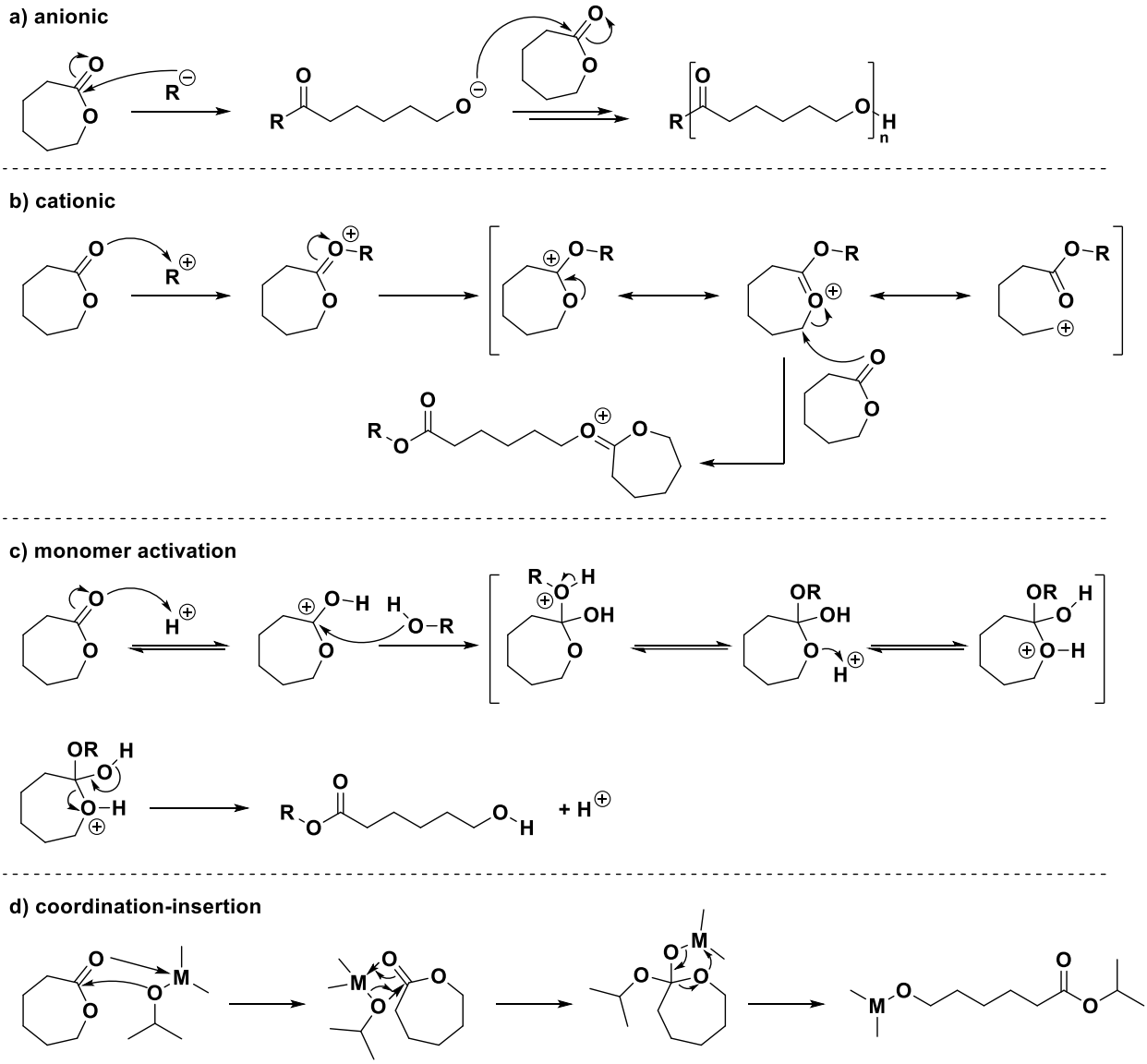

Scheme 10: Main mechanisms of the ROP of ε-caprolactone depending on the employed catalyst. (a) anionic;[405] (b) cationic;[404,405] (c) monomer activation;[406,407] (d) coordination-insertion.[404,405]

Within this work, 1,5,7-triazabicyclo[4.4.0]dec-5-ene (TBD) was used as organo-catalyst for the ROP of ε-caprolactone (results are discussed in chapter 4.4). Compared to 1,8-diazabicyclo[5.4.0]undec-7-ene (DBU) or *N*-methyl-1,5,7-triazabicyclo[4.4.0]dec-1-ene (MTBD), TBD shows the advantage of simultaneously activating both the ε-caprolactone monomer and the alcohol (initiator or polymer chain). Thus, no co-catalyst, such as thiourea is required. The activation *via* TBD and ring-opening of ε-caprolactone is depicted in Scheme 11.[356,408]

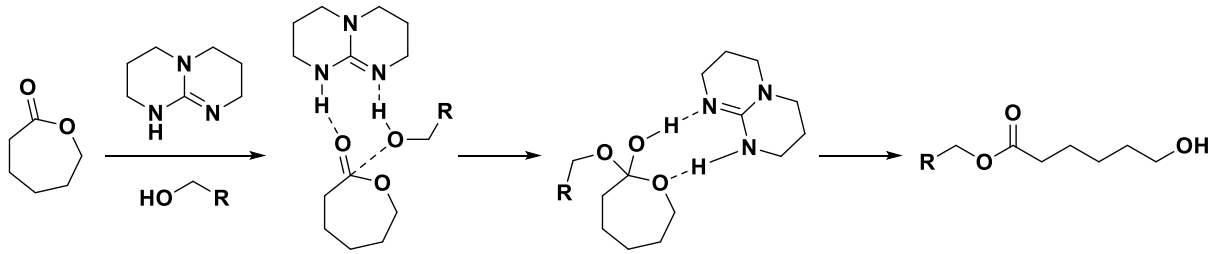

Scheme 11: TBD-catalyzed ROP of ε-caprolactone.[356,408]

Due to the controlled character of ROPs,[409] it is a prevalent method for the synthesis of narrowly distributed block copolymers with versatile characteristics, such as polarity, which in turn results in immiscible compartments within the macromolecule. Thus, several nanostructures are accessible *via* self-assembly of the BCPs, making them interesting for a large field of applications, such as drug and gene delivery,[410,411] or nanoporous materials.[412–416] An introduction to the microphase separation of BCPs is provided in the next chapter.

2.4.2. Microphase separation of block copolymers

2.4.2.1. Self-assembly in bulk

Block copolymers are of great interest for many areas of application,[57,403,417] because of their ability to form nanoscopic architectures, including spheres, cylinders, bicontinuous gyroids, lamellae, etc., *via* self-assembly (SA).[59–61,418] The SA in bulk has been extensively studied theoretically and experimentally since the 1960s and is well understood.[57–61] The driving force of this microphase separation (MPS) is an unfavorable mixing enthalpy ΔH_{mix} of the different polymer blocks coupled with a small mixing entropy ΔS_{mix}, which is described by the Gibbs-Helmholtz equation (1), where T is the temperature. The SA is based on the incompatibility of the block segments that prefer to segregate as individual polymer chains, which is not possible due to their covalent linkage. As a result, stretching of the polymer segments and MPS occurs to minimize the interface between the different blocks. If the Gibbs energy ΔG_{mix} is negative, there is miscibility, whereas phase separation occurs with positive values for ΔG_{mix}.

$$\Delta G_{mix} = \Delta H_{mix} - T\Delta S_{mix} \quad (1)$$

The mixing enthalpy ΔH_{mix} and the mixing entropy ΔS_{mix} for a BCP can be described *via* the Flory-Huggins theory:

$$\Delta H_{mix} = RT\chi_{AB}\Phi_A\Phi_B$$

$$\Delta S_{mix} = -R\left(\frac{\Phi_A}{N_A} ln\,\Phi_A + \frac{\Phi_B}{N_b} ln\,\Phi_B\right)$$

where N_A and N_B are the degree of polymerization of the blocks A and B, Φ_A and Φ_B are the volume fractions of corresponding blocks, R is the gas constant, T the absolute temperature and (χ_{AB}) the Flory-Huggins interaction parameter.[54,55],[I] Thus, the higher the degree of polymerization N, the more likely MPS occurs, since the mixing entropy ΔS_{mix} has less influence as the chain length increases. Thus the MPS of a diblock copolymer depends on: (i) the total volumetric degree of polymerization ($N = N_A + N_B$), (ii) the relative block volume fractions of block A and B ($\Phi_A + \Phi_B = 1$), and (iii) the Flory-Huggins interaction parameter (χ_{AB}),[54,55] and thus the temperature T.[419–424] Increasing the system temperature results in an increase of the entropy term and thus an increase of the miscibility of the blocks. The temperature at which a homogeneous phase is obtained is the so-called *order-disorder transition* (T_{ODT}).[424]

The resulting morphologies of the MPS include various sphere phases, gyroids, lamellae, and hexagonal packed cylinders.[425–427] However, owing to the aforementioned parameters, the self-assembly morphology is very sensitive to small changes in the composition and dispersity of the copolymer.[48,65,428] For instance, HILLMEYER and LYND described an increase in the domain spacing of the lamellar phase of poly(ethylene-co-propylene)-*block*-poly(lactide) due to an increase of the dispersity, while keeping M_n constant for a high interaction parameter. In contrast, for a low interaction parameter, the formation of different morphologies depending on a change in dispersity were observed.[65] Not only the dispersity of the polymer sample has an influence on their morphologies, but also the shape of the molecular weight distribution itself. FORS *et al*. performed investigations on the impact of the asymmetry of the molecular weight distribution on the self-assembly behavior of a copolymer. By

[I] The Flory–Huggins parameter χ was developed by PAUL JOHN FLORY and MAURICE LOYAL HUGGINS and describes the excess free energy of mixing and determines the phase behavior for block copolymers and polymer blends.[54,55]

altering the shape, the morphological phase diagram as well as the polymer properties can be manipulated.[77–79]

The calculated phase diagram of a linear diblock copolymer based on the self-consistent mean field theory (SCMFT),[56] as a function of the volume fraction Φ (f) and χN is shown in Figure 11 a.[429] For a BCP with equal volume fractions of A and B ($\Phi_A = \Phi_B = 0.5$) and a value of $\chi N > \sim 10.5$, order-to-disorder transition (ODT) occurs. Above the ODT, SA takes place with increasing Φ (f) starting from closely packed spheres (CPS) to body-centered cubic spheres (S), to hexagonally packed cylinders (C), to bicontinuous gyroids (G), and to lamellae (L). With an inverted BCP composition, an inverted morphology course is described (L → G' → C' → S' → CPS') (Figure 11).[418]

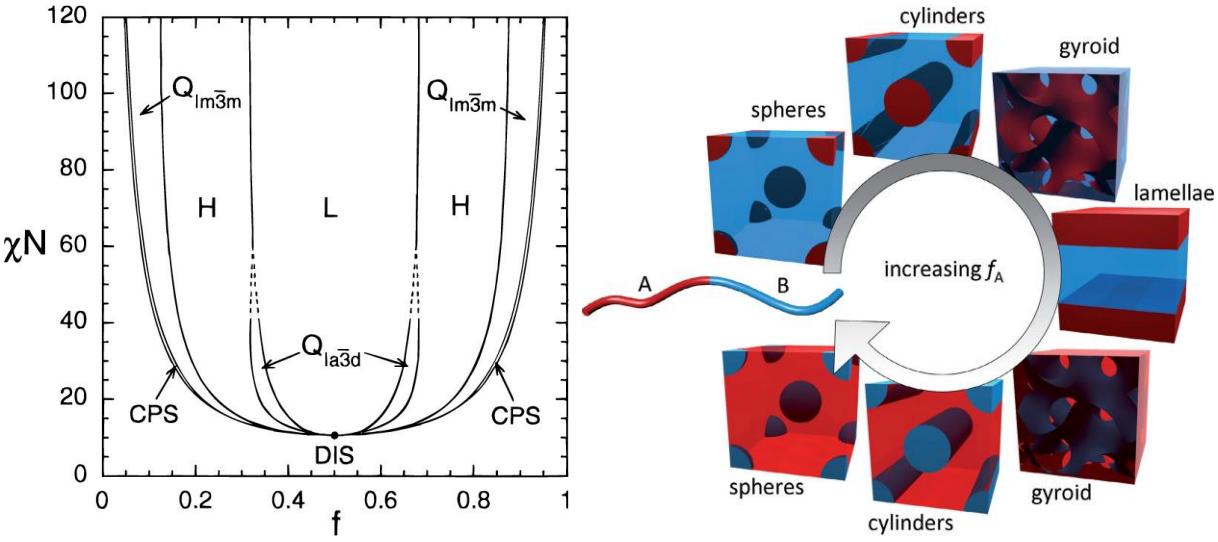

Figure 11: (a) phase diagram of a diblock copolymer calculated using SCMFT; where f = volume fraction; χ = Flory-Huggins interaction parameter; N = degree of polymerization; L = lamellae; H = hexagonally packed cylinders; $Q_{Im\bar{3}m}$ = body-centered spheres; $Q_{Ia\bar{3}d}$ = doubly-gyroid phase; CPS = closed-packed spheres, DIS = discorded;[430] Reprinted (adapted) with permission from Matsen, M. W.; Bates, F. S., Unifying Weak- and Strong-Segregation Block Copolymer Theories. *Macromolecules* **1996**, 29 (4), 1091–1098. DOI: 10.1021/ma951138i. Copyright 1996 American Chemical Society (b) different morphologies resulted from the SA of diblock polymers.[431] Reprinted from materialstoday, 13/ 5, I. Botiz, S. B. Darling, Optoelectronics using block copolymers, 42-51, Copyright 2010, with permission from Elsevier.

2.4.2.2 Self-assembly in solution

Amphiphilic BCPs are also widely applied in the field of biomedicine, pharmaceutics, and nanotechnology due to their ability to form designed morphologies *via* microphase separation in solution.[49,432,433] The complexity of the self-assembly of BCPs in solution has been actively studied since 1995.[62–64] The driving force is the minimization of free energy between each block (A and B) and the surrounding solvent (S) (χ_{AS} *and* χ_{BS}) and between the two blocks in solution (χ_{AB}).[434] This is dictated by the solvophibicity, the degree of polymerization of each block, N, and the relative volume fractions, f. Furthermore, the SA in solution is primarily determined by the packing parameter p ($p = v/a_0 l_c$), where l_c is the length and v the volume of the hydrophobic tail, and a_0 the optimal area of the head group.[435] The packing parameter can be controlled by the BCP composition and concentration, additives, water content and the chosen solvent. Changing these parameters results the BCP adopting a different interfacial curvature and thus to the formation of different morphologies, such as spheres ($p \leq ⅓$), cylindrical micelles ($⅓ \leq p \leq ½$), and polymersomes ($½ \leq p \leq 1$) etc. (Figure 12).[436] A BCP solution below the critical micelle concentration results in disassembled structures. Specific morphologies can be targeted by controlling the volume fraction *via* aforementioned controlled/ living polymerization techniques. By increasing the molecular weight distribution, different polymers within the same sample will prefer to adopt different interfacial curvatures and thus different morphologies can be formed if the copolymer ratio is close to a phase boundary.[66]

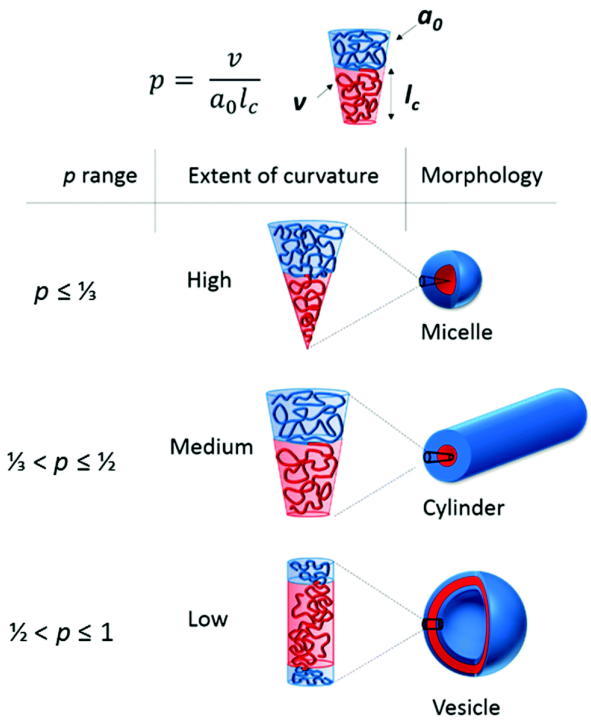

Figure 12: Morphologies obtained *via* microphase separation of amphiphilic block copolymers in solution. The type of structure depends on the inherent curvature of the molecule, which can be estimated *via* calculations of the packing parameter *p*, where l_c is the length and *v* the volume of the hydrophobic tail, and a_0 the optimal area of the head group. Reproduced from Ref 66 (Doncom, Kay E. B.; Blackman, Lewis D.; Wright, Daniel B.; Gibson, Matthew I.; O'Reilly, Rachel K. *Dispersity effects in polymer self-assemblies: a matter of hierarchical control*, *Chem. Soc. Rev*. **2017**, *46*, 4119-4134.) with permission from the Royal Society of Chemistry.[66]

EISENBERG *et al*. investigated the effect of the molecular weight distribution of polystyrene-*block*-poly(acrylic acid) (PS-*b*-PAA) BCPs on their self-assembly behavior in selected solvents. An increase of the PAA dispersity resulted in decrease in size of the formed vesicles, which is explained by the length segregation of the PAA chains, that smaller chains segregate to the inner surface while larger chains to the outer surface of the vesicle.[67]

Further studies on the impact of dispersity on the phase segregation of block copolymers in solution were performed by CHUNNINGHAM *et al*.,[68] SAWAMOTO *et al*.[69] and more.[66] Furthermore, interesting results: the formation of increasingly well-defined particles with an increasing dispersity of the core forming block in the BCP and a *vice versa* trend, were reported by JUNKERS and coworkers.[70] Therefore, the self-assembly of a copolymer in bulk and in solution relies on several parameters and a molecular weight dispersity within the copolymer is not solely confined to size distribution of the self-assembled structures.

However, the formation of nanostructures *via* self-assembly in solution is commonly conducted in dilution in a post-polymerization process,[63,437–441] which is a significant limitation for potential commercial applications. To challenge this problem, polymer-induced self-assembly (PISA) offers a promising solution. PISA is based on the principle of growing an insoluble block onto a soluble precursor block, in a chosen solvent. At a critical degree of polymerization (DP), the second block becomes insoluble and self-assembly of the BCP occurs.[442–450] Further advantages, such as a very high monomer conversion within a short reaction time, broad tolerance to various solvents, high reproducibility, access to several morphologies while using different living polymerization techniques, make PISA an emerging field in modern polymer chemistry.[451–453]

In order to investigate the morphology of a copolymer, transmission electron microscopy (TEM),[454–456] scanning electron microscopy (SEM),[5] atomic force microscopy (AFM),[457] and small-angle X-ray scattering (SAXS),[454,455,458] are the most common analytical tools.

In general, the control of the formation of the different morphologies enables a vast application area for BCP, for example in micellar catalysis[459] or drug delivery agents,[460] in nanolithography,[461,462] organic photovoltaics (OPVs),[463] or in light emitting diodes (OLEDs).[52]

In summary, experimental studies,[65,464,465] supported by theoretical reports,[466–469] suggest that an increase in dispersity results in a shifting of the phase boundaries and an increase of the domain spacing, which is based in a lower stretching energy due to existence of different chain length. However, the complete understanding of the influence of dispersity on the formation of morphologies is one of the hot topics in polymer chemistry. An improved understanding of the structure-property relationship could be provided by the study of uniform block copolymers. This research area is still in its infancy, due to the challenge of producing uniform BCPs, which is addressed in this work on PEG-*b*-PCL BCPs.

2.4.3. Dispersity effect on the self-assembly of BCPs

Within this work, PEG-*b*-PCL BCPs were synthesized and studied. Such block copolymers are widely used in the literature as their low toxicity, biocompatibility as well as their biodegradability is of great interest for applications in nanotechnology, medicine, or biotechnology, *e.g.*, as drug delivery systems, particularly considering their micellar formation in aqueous media.[470–472] Hydrophobic drugs are entrapped into the PCL core surrounded by the PEG corona that disperses the system in water. Thus, drug concentrations that exceed their intrinsic water solubility are facilitated by the micellar formations. Furthermore, the PEG shell protects the drug against hydrolysis and enzymatic degradation, and increases the blood circulation times.[51] The formation of uniform microspheres is crucial to predict their properties, such as the delivery of precise drug amounts per micelle to different organs or tissues, optimized release kinetics, and the maximum protection of the drug from degradation.[473] These parameters can be addressed by fine-tuning the polymer structure, which requires the preparation of uniform BCP structures.[387]

There are many reports investigating the self-assembly and the morphologies of PEG-*b*-PCL diblock copolymers in bulk,[474–476] as well as in solution,[477–480] mainly focusing on the influence of the BCP composition of the MPS. In 2016, the group of Meier described the effect of the BCP dispersity on the self-assembly and the resulting morphologies of PEG-*b*-PCL.[71] They addressed the fact that the formation of meso- and nanoscale structures depends on the method of SA preparation, the block length as well as the composition.[479,481–484] In general, mixed morphologies[485] and a broadening of the size distribution of the formed aggregates[486] were observed with increasing dispersity. For instance, for the SA *via* film rehydration of a PEG(2k)-*b*-PCL(9.5k) with a dispersity of $Đ$ = 1.14, mainly the formation of mesoscale polymersomes was observed,[479] whereas increasing the dispersity to $Đ$ = 1.42 for a PEG(2k)-*b*-PCL(9k) resulted in mostly mesoscale worm-like structures.[482] The group of Meier *et al*. controlled the molecular weight distribution of the $SnOct_2$-catalyzed ROP of ε-caprolactone *via* the reaction time of the homopolymerization. In this way, PEG(2k)-*b*-PCL(16-17.4k) with dispersities, $Đ$, ranging from 1.08 to 1.55 were obtained. For the most defined BCP ($Đ$ = 1.08) polymersomes with a diameter of 1.6±0.5 µm were obtained, whereas an increase of the dispersity to $Đ$ = 1.23 led to an increase in the diameter (4.1±2.5 µm). The BCP with $Đ$ = 1.55 formed different types

of polymersomes (elongated and multicompartment) as well as aggregates.[71] They further point out the importance of uniform BCP for the preparation of distinct and uniform 3D structures, which was addressed within the scope of this work.

However, since BCPs obtained *via* living polymerization techniques still exhibit a molecular weight distribution (*e.g., Đ* < 1.05 for living anionic polymerization), further approaches were necessary to synthesize uniform BCP with a dispersity of *Đ* = 1.00.

Uniform block copolymers

Pioneering work for the synthesis and investigations on the crystallization and self-assembly behavior of macromolecules has been performed by the group of ZUCKERMANN on sequence-defined peptoid diblock copolymers.[487–489] This also includes the publications of MEIJER and coworkers on the phase separation of oligo(dimethylsiloxane)-*b*-oligo(lactic acid) (oDMS-*b*-oLA) diblock copolymers.[490,491] In a comparative study of the phase behavior of oDMS-*b*-oLA ranging from a dispersity of *Đ* = 1.00 to 1.09, an increase of the self-organization, a decrease of the stability of the microphase-separated state, and a decrease of the domain spacing with a decreasing dispersity was observed.[72]

JOHNSON *et al*. presented the synthesis of uniform diblock copolymers *via* an IEG+[234] strategy, which was already described in chapter 2.1.[73] The complete reaction cycle of the synthesis of the uniform homopolymers **II** containing up to 16 monomer units, the subsequent side-chain modification and the formation of the uniform BCP is shown in Scheme 12. In the approach reported in 2016, only (*R*)-glycidyl propargyl ether **I** ((*R*)-GPE) was used, resulting in corresponding L-configurated allyl-homopolymers **II**. Half of the product was post-modified *via* a thiol-ene reaction with 1-decanthiol. Separately, the other half was deprotected and the uniform BCP was formed *via* a CuAAC.

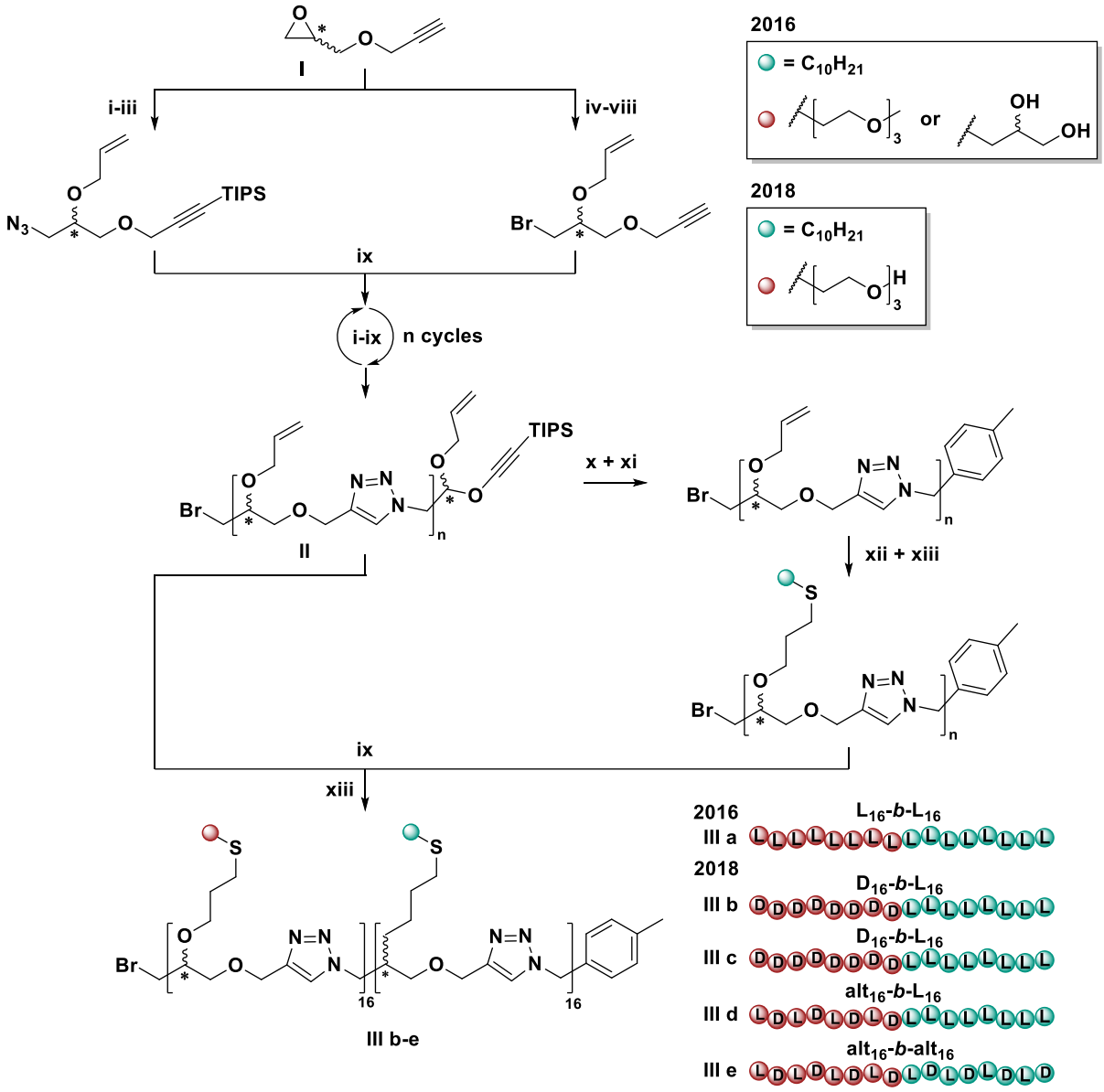

Scheme 12: Reaction scheme of the synthesis of uniform BCP reported by JOHNSON *et al*. (i) *n*-BuLi, TIPSCl, THF, −78 °C to rt; (ii) NaN_3, AcOH, DMF, 65 °C; (iii) allyl bromide, NaH, DMF, rt; (iv) *t*-BuOH, $Mg(ClO_4)_2$, rt; (v) allyl bromide, NaH, DMF, rt; (vi) H_3PO_4, rt; (vii) TsCl, 4-DMAP, TEA, DCM, rt; (viii) LiBr, DMF, 45 °C; (ix) CuBr, PMDETA, DMF, 50 °C; (x) TBAF, THF, rt; (xi) 1-(azidomethyl)-4-methylbenzene, CuBr, PMDETA, DMF, 50 °C; (xii) NaN_3, DMF, 35 °C; (xiii) **R**SH, DMPA, DMF, hν (365 nm). The different moieties of the thiol in step (xiii) are depicted in the scheme for the approaches of 2016 and 2018, respectively.[73,74]

In the final step, the remaining allyl side groups were reacted with either 1-mercapto-triethyleneglycol monomethyl ether (TEG-SH) or thioglycerol (TG-SH) providing the final uniform BCP **III a**. Investigations on the bulk self-assembly of the BCP according to the study of Zuckermann,[489] were performed *via* DSC, SAXS, AFM and TEM. No melting transitions were observed with DSC, indicating that the BCP are amorphous. Thermal annealing of both BCPs resulted in a well-ordered hexagonal cylinder (HC)

morphology, which was observed by SAXS and supported by TEM, and, for the BCP containing the TG sidechains, also *via* AFM. In addition, polymer backbone distances determined by WAXS closely matched the calculated ones.[73] In the report of JOHNSON *et al*. from 2018, stereo definition was implemented into the described BCP by using ((*S*)-GPE) and ((*R*)-GPE) as starting materials, resulting in L-*b*-L, D-*b*-L, alt-*b*-L, alt-*b*-alt configurated BCP **III b-e**. Instead of the mTEG side group, a TEG side group was used. The results show how the stereo definition in the BCP led to interesting changes in the self-assembly, which is explained in detail in the respective literature.[74]

An acid-orthogonal IEG protocol to obtain stereo- and sequence-defined block copolymers with a thioetheramide backbone was described by the group of TAO in 2022.[492]

Linear and cyclic uniform block copolymers were reported by the group of KIM in 2020. As already mentioned in chapter 2.3, an iterative exponential growth protocol was conducted for the synthesis of the two uniform homo block copolymers: poly(lactic acid) (PLA) and poly(phenyllactic acid) (PPL) (Scheme 13).[239] A TBDMS ether and a benzyl ester were introduced as orthogonal protection groups for the alcohol and carboxylic acid, respectively, of the monomer building block. In the subsequent divergent step, the orthogonal protecting groups were separately cleaved, the silyl ether *via* treatment with BF_3 and the benzyl ester under reductive conditions using triethylsilane and Pd/C. The subsequent chain doubling was achieved *via* an esterification of the two monofunctionalized building blocks, applying EDC and DTPS. By repetition of this three-step iterative chain elongation cycle, a uniform PLA containing up to 1,024 monomer units, and a PPL, containing up to 64 building blocks, were obtained. The uniform PLA_{64}-*b*-PPL_{64} block copolymer was obtained *via* an esterification of the respective 64-mer homopolymers. The linear block copolymer PLA_{64}-*b*-PPL_{64} was transformed into a cyclic block copolymer *c*-PLA_{64}-*b*-PPL_{64} *via* an intramolecular CuAAC. To achieve this, the protecting groups were orthogonally removed, and the alcohol was esterified with 4-pentynoic acid to yield the terminal triple bond. The carboxylic acid, on the other hand, was reacted with 2-azidoethanol to install the azide functionality. All products from the 64-mer homopolymers on were purified on a 1 g scale *via* preparative SEC, to ensure the absence of low molecular precursor molecules. Uniformity of the linear and cyclic block copolymer was confirmed with NMR, GPC, and MALDI-TOF analysis. Investigations of the self-assembly behavior depended on their topology[493] were performed *via* self-assembly of the linear and

cyclic BCP in solution (methanol). The formation of nanoaggregates with a diameter of 783 nm (polydispersity (PD) = 0.145) for the linear BCP and a diameter of 117 nm (polydispersity (PD) = 0.083) for the cyclic BCP were observed *via* DLS. Further TEM and cryo-TEM results showed spherical morphologies and supported the aggregate particle sizes obtained with DLS.[239] Thus the topological impact (linear compared to cyclic BCP) on the self-assembly behavior was demonstrated, resulting in a distinct insights of the structure property relationships.

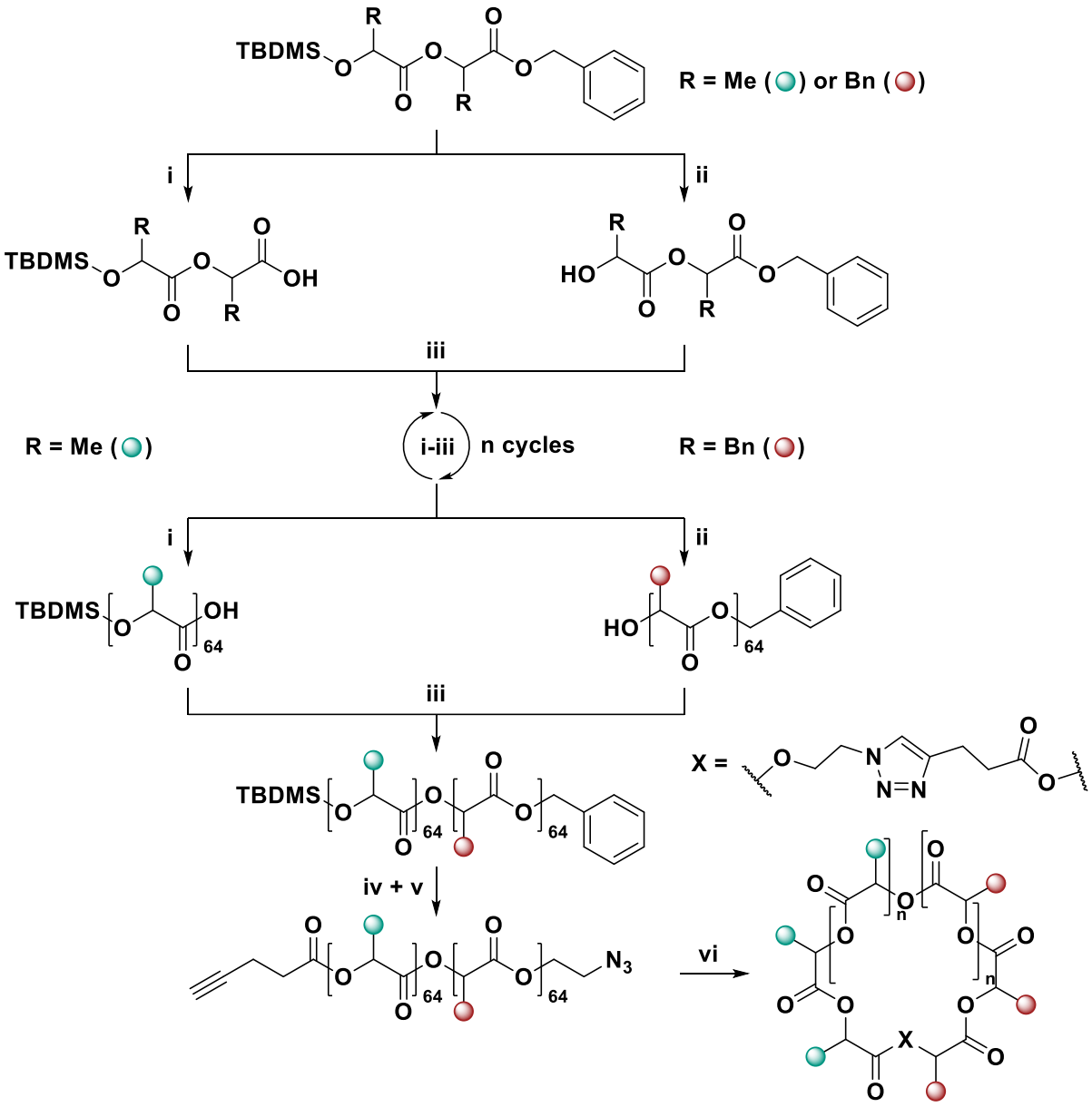

Scheme 13: Reaction scheme of the synthesis of linear and cyclic uniform PLA-*b*-PPL block copolymers reported by KIM *et al*. (i) Et_3SiH, Pd/C; (ii) BF_3 Et_2O; (iii) EDC, DPTS; (iv) Et_3SiH, Pd/C; 2-azidoethanol, EDC, DPTS; (v) BF_3 Et_2O; 4-pentynoic acid, EDC, DPTS; (vi) CuBr, PMDETA.[239]

In contrast to the aforementioned synthetic procedures, the group of HAWKER reported a strategy for the rapid generation of uniform BCP libraries based on automated chromatography separation of a narrowly distributed BCP. The operating principle is depicted in Figure 13. The reported method presented not only a versatile, scalable, and highly efficient method to obtain uniform block copolymers, varying in their block volume composition f_A, but also provided insights into the structure-property relationship of the BCP. The influence of the dispersity on the phase behavior is presented on different BCP examples, such as PDDA-*b*-PLA, PDMS-*b*-PLA, PTFEA-*b*-PDDA, PTFEA-*b*-PDMOA, and PTFEA-*b*-P(±)MnA.[75]

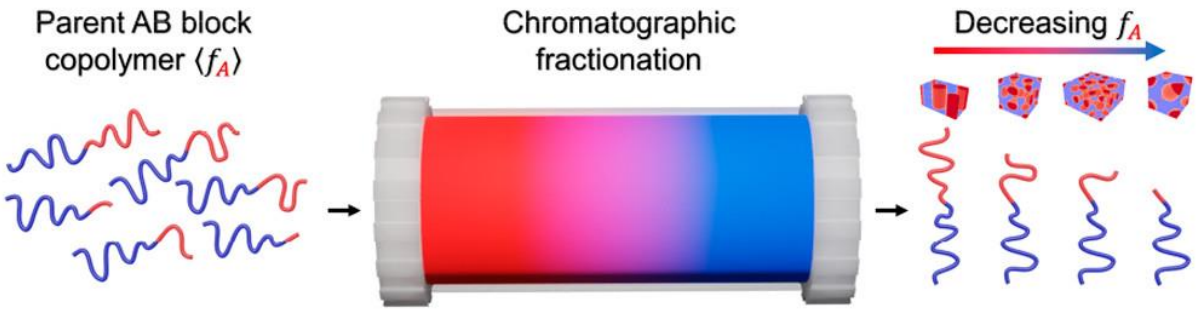

Figure 13 Overview of the fractionating strategy, reported by HAWKER *et al*. for the rapid generation of uniform BCP libraries.[75] Reprinted with permission from C. M. Bates, A. K. Whittaker, C. J. Hawker, *et al*. *Rapid Generation of Block Copolymer Libraries Using Automated Chromatographic Separation*, *J. Am. Chem. Soc*. **2020**, *142*, 21, 9843-9849.

In another example by HAWKER, BATES and coworkers, the dispersity effect on the self-assembly behavior of dimethylsiloxane-*b*-methyl methacrylate (DMS-*b*-MMA) BCP was investigated. A decrease in domain spacing, sharper scattering reflections (SAXS) as well as an increase in the T_{ODT} was observed for the uniform samples compared to the disperse BCP.[76] In this way, a library of well-defined BCPs, varying in their composition was obtained *via* chromatographic fractionation of a narrowly distributed sample. Several morphologies were obtained for the individual fraction, which were not formed and detected in the parent BCP. This underlines the crucial need of uniform molecules for the investigation of the structure-property relationship.

In conclusion, the copolymer composition is a key parameter in the determination of the morphology resulting from the SA both in bulk and in solution. However, the complete absence of dispersity has drawn significant attention from the polymer chemistry community who have sought to study the SA of copolymers with high dispersity and skewed molecular weight distribution. Nonetheless, as uniformity

remains challenging, this chapter points out the two different strategies for the preparation of uniform BCP: (i) an iterative synthesis of the homopolymers and a subsequent coupling reaction and (ii) purification of a narrowly molecular weight-distributed BCP prepared by controlled/living polymerization techniques. With the second method, many different BCP compositions can be obtained within a short amount of time, thus obtaining a large amount of information about the phase separation behavior of the samples. However, it is limited to milligram scales due to the purification methods, whereas by iterative synthesis protocols a desired BCP can be prepared in multigram scales.

The microphase separation depends on three parameters: (i) the total volumetric degree of polymerization ($N = N_A + N_B$), (ii) the relative block volume fractions of block A and B ($\Phi_A + \Phi_B = 1$), and (iii) the Flory-Huggins interaction parameter (χ_{AB}),[54,55] Selected literature examples were used to illustrate the importance of uniform structures for the study of structure-property relationships in relation to self-assembly.[73–76,239,492] This thesis is a further contribution to this research area and the corresponding results on the self-assembly behavior of uniform PEG-*b*-PCL block copolymers is discussed in chapter 4.5.

2.5. Molecular data storage in defined structures

2.5.1. General introduction

Parts of this chapter and the associated supplementary information have already been published:

Bohn, P., Weisel, M.P., Wolfs, J., Meier, M. A R. Molecular data storage with zero synthetic effort and simple read-out. *Sci Rep* **12**, 13878 (2022). https://doi.org/10.1038/s41598-022-18108-9.[494]

The demand for non-conventional data storage solutions is increasing due to digitization and the enormous growth in data volumes worldwide. While the total amount of data globally was around 5 ZB in 2011, it reached 79 ZB in 2021 and is growing exponentially, expected to reach 181 ZB in 2025.[111] As the data carrier of life, DNA has come increasingly into focus as a possible alternative data storage medium in recent years.[495–499] The data density of DNA is higher than in magnetic tapes, the read-out is well investigated *via* sequencing approaches[500] and it can store information for thousands of years.[501]

Inspired by DNA, an increasing and continuing focus on methods for the preparation of synthetic sequence-defined molecules over the last ten years is observed.[83,84,86,100,159,167–169,193,208,216,217,220,325,492,502,503] Such unique macromolecules have lately gained interest in life and material science, *e.g.* as data storage devices.[86] DNA is limited to the four information-containing nucleobases provided by nature (adenine (A), cytosine (C), guanine (G), thymine (T)), and thus long sequences are necessary to store large amounts of information. In contrast, the building blocks for coding in synthetic molecules can be more diverse, resulting in an increase of the permutations per repeating unit, and thus a higher storage density. The data storage capacity “n” in bit of a sequence-defined macromolecule is calculated *via* equation (1), where “P” is the number of permutations in the respective molecule. Since one bit in a binary code requires two different states (permutations) “0” and “1”, “n” is to the power of the base 2. “P” is equal to the number of permutations per repeating unit (P_{RP}) to the power of the degree of polymerization (DP).

$$P = 2^n \tag{1}$$

$$n = \frac{\log(P)}{\log(2)}$$

$$P = (P_{RP})^{DP} \quad (2)$$

As an example, *i.e.*, for the storage of 8 bits in DNA, 256 permutations and thus a sequence of four repeating units (tetramer) is required. If the number of permutations per repeating unit is doubled, this results in 4096 permutations in a tetramer and an increase of the data storage capacity to 12 bits is achieved.

In this context, pioneering work was performed by LUTZ *et al.*, who presented the potential of sequence-defined binary encoded poly(phosphodiester)s,[97,122–126,135,504] oligo(triazole amide)s,[145,146,505] oligo(alkoxyamine amide)s,[139–144] oligourethanes,[127–134,506] and oligo(alkoxyamine phosphodiester)s[136–138] as so-called digital polymers.

2.5.2. Oligo(triazole amide)s

In 2014, the group of LUTZ reported the synthesis of encoded oligo(triazole amide)s *via* a chemoselective iterative synthesis of two difunctional building blocks AB and CD. The first building unit contained an acid (A) and an alkyne (B) and the second contained an amine (C) and an azide function (D). The chain elongation cycle, consisting of an amidification of A with C and the subsequent CuAAC of B and D, was conducted on a non-modified Wang resin (Scheme 14).

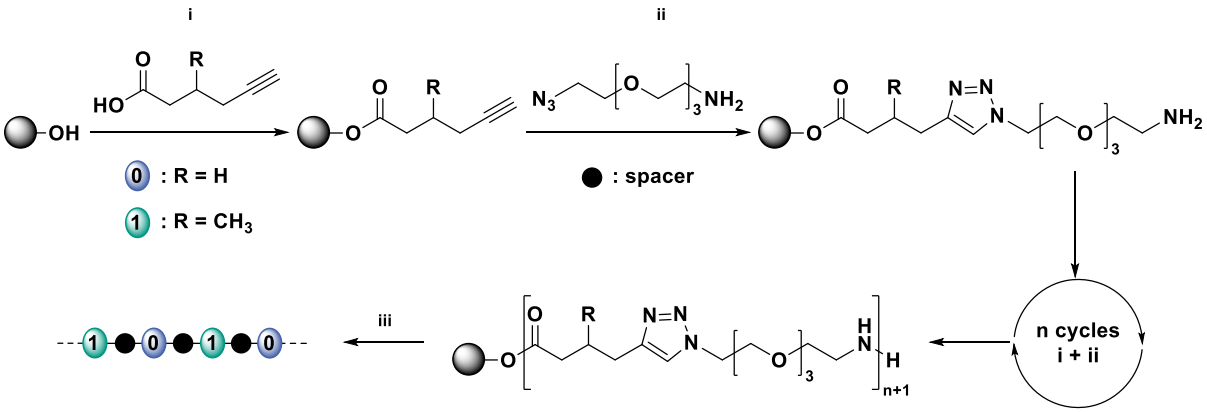

Scheme 14: General reaction scheme of the preparation of encoded oligo(triazole amide)s *via* a two-step iterative chain elongation cycle. i: PyBOP, DIPEA; DCM; ii: CuBr, dNbipy, THF; iii: TFA, DCM (9:1).[505]

Incorporation of a binary code, consisting of “0”s and “1”s into the growing sequence was achieved by placing two different AB building blocks in a precise order. 4-Pentynoic acid, bearing a proton in α-position to the ester, was used to write a “0” and 2-methyl-4-pentynoic acid, which carried a methyl group in α-position to the ester, was used to write a “1”, respectively. In this way, all eight possible triads were

synthesized and characterized by ^{1}H NMR spectroscopy, MALDI-TOF MS, and SEC.[505]

One year later, in 2015, an improved protocol was presented by the same group. Employing a library of four coded AB dyads of all combinations of 5-hexynoic acid (“0”) and 3-methyl-5-hexynoic acid (“1”). An 8-bit octamer sequence was prepared in seven coupling steps (successive CuAAC and amidification), instead of 15 coupling steps, when using AB monomers.[146]

The successful read-out of information-containing oligo(triazole amide)s *via* ESI tandem MS was demonstrated in 2016, with a sequence-defined heptamer. The fragments resulting from the cleavage of the amide function as well as the ether next to the amide (The fragmentation pathway is shown in Figure 14 at the end of this chapter) of the protonated parent ion were observed. The complete fragmentation pattern was deciphered with 100% accuracy, confirming the structure of the sequence.[145]

2.5.3. Poly(phosphodiester)s

Making use of phosphoramidite chemistry, the group of LUTZ reported the synthesis of non-natural sequence-encoded polyphosphates. For this purpose, three unique (dimethoxytrityl) DMT-protected phosphoramidite coding units were used. Thus, a propyl group motif was translated into a “0”, a dimethyl-propyl motif into a “1”, and a dipropagyl-propyl group into a “1’”. The introduction of the propagyl moieties allowed postfunctionalization *via* CuAAC, and thus control of the stored information encoded in the sequence of the sidechains.[126] Repetition of a three-step chain elongation cycle, consisting of a phosphoramidite coupling, a phosphite oxidation and subsequent DMT deprotection under acidic conditions yielded in information-containing macromolecules (Scheme 15). Since this is a well-studied approach for the synthesis of, *e.g.,* DNA, and has been optimized over the years for biochemical purposes,[93] the synthesis of long chain sequence defined polymers, with more than hundred repeating units was accessible in a short amount of time.[507] This way, a binary coded 24-mer[504] and later a 104-mer[97] were prepared *via* solid phase automated synthesis.

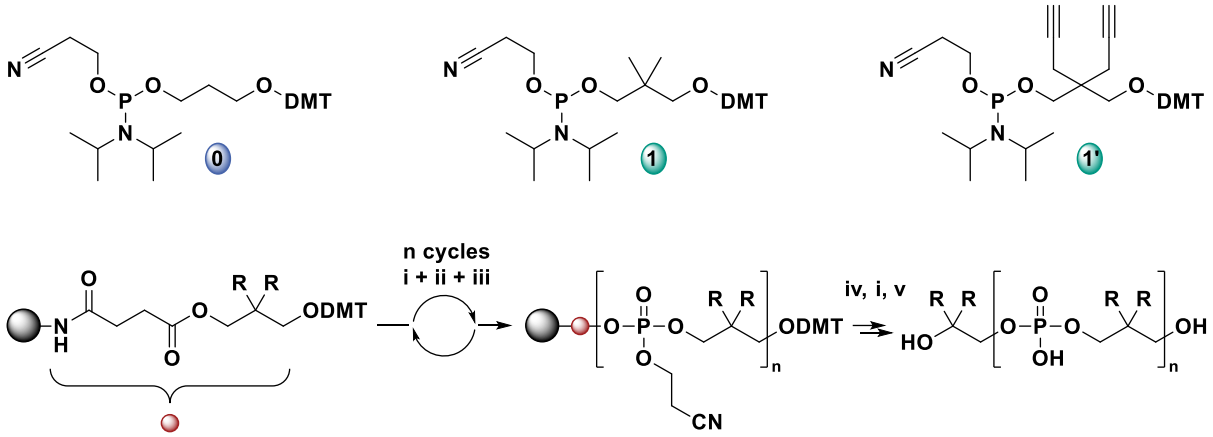

Scheme 15 General reaction scheme of the preparation of encoded poly(phosphodiester)s *via* a three-step iterative chain elongation cycle. i: DMT deprotection: trichloroacetic acid (TCA), DCM; ii: coupling step: rt, AcCN, tetrazole; iii: oxidation: rt, I_2, H_2O/pyridine/THF; iv: cyanoethyl deprotection: piperidine, AcCN; v: cleavage: NH_3, H_2O, dioxane.[504]

Employing four different monomers for the phosphoramidite synthesis, bearing light sensitive *o*-nitrobenzyl ether or light-inert *p*-nitrobenzyl ether sidechains, offered the possibility to either erase or manipulate the stored information in the sequence after irradiation (λ = 365 nm). Furthermore, this approach was used to write a secret message, which could not be deciphered by tandem MS upon irradiation with light to reveal the initial code. The concept is illustrated in Scheme 16. In the first example (Scheme 16a), two *o*-nitrobenzyl ether motifs, different in mass, were used to write a binary code of “0”s and “1”s into the sequence. After irradiation, the different *o*-nitrobenzyl ether were cleaved, resulting in identical and indistinguishable monomer units bearing an alcohol function. In the second example (Scheme 16b), *o*- and *p*-nitrobenzyl ether (“1”), and unprotected building blocks (“0”) were used to store the initial data. Since only the *o*-nitrobenzyl ether was affected by the irradiation and thus converted from a “1” to a “0”, a change of the code was obtained. In the last example (Scheme 16c), a sequence containing only *o*- and *p*-nitrobenzyl ether was prepared. Since both building units exhibit the same mass, the individual monomer units are indistinguishable. However, similar to the second example, the *o*-nitrobenzyl was deprotected after irradiation, resulting in an alcohol function and revealing a hidden code.[124]

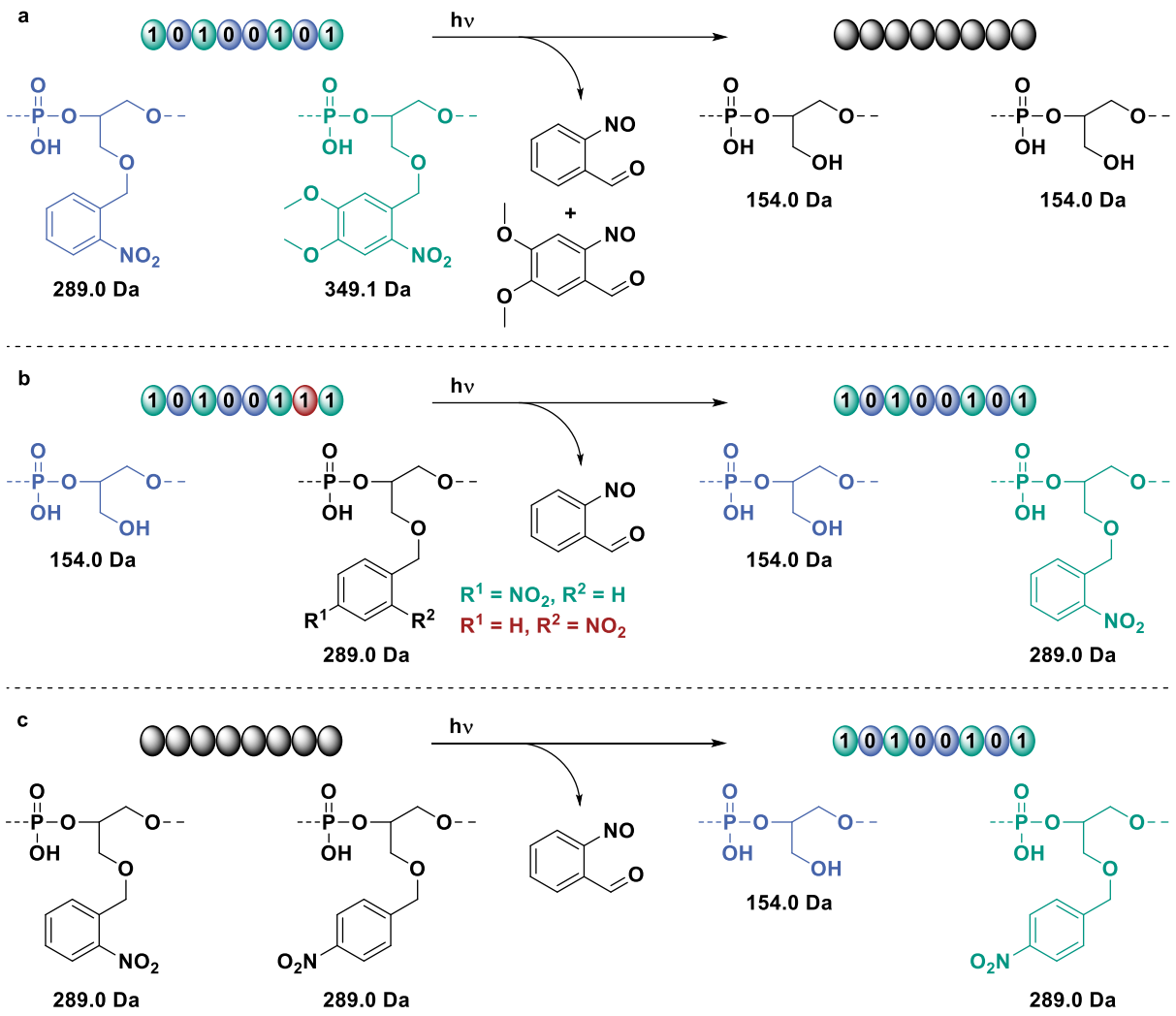

Scheme 16: Reaction schemes of encoded sequence-defined macromolecules, prepared *via* phosphoramidite synthesis bearing partially photolabile *o*-nitrobenzyl ether motifs. After irradiation (λ = 365 nm), the initial information was either **a** cleaved, **b** manipulated, or **c** revealed.[124]

The read-out of poly(phosphodiester)s *via* fragmenting negative mode ESI-MS/MS was investigated. Cleavage of all phosphate bonds enabled the complete read-out of the poly(phosphodiester) sequences. However, starting from a chain length of more than 50 repeating units, the data interpretation was challenging due to the formation of multiple charged ions and their uncontrolled dissociation into many fragments, leading to complex mass spectra.[125]

2.5.4. Oligo(alkoxyamine phosphodiester)s

In order to overcome the issue of the uncontrolled dissociation, an alkoxyamine was introduced alternately to the phosphodiester, which acted as a predetermined breaking point, due to the low dissociation energy of the C-ON bond.[508] The applied reaction protocol relied on a three-step iteration cycle. First, the phosphoramidite coupling of

an alcohol and the respective phosphoramidite building block equipped with a tertiary alkyl bromide, followed by *in situ* oxidation of the phosphite ester to the corresponding phosphate. Afterwards, the radical-radical coupling of the carbon radical resulting from activation of the alkyl bromide with copper bromide and a hydroxy-functionalized nitroxide is performed. By repetition of the repetitive chain elongation cycle, shown in Scheme 17, a sequence-defined octamer, containing 3 bits per repeating unit, was obtained and successfully deciphered with ESI-MS/MS.[125,137]

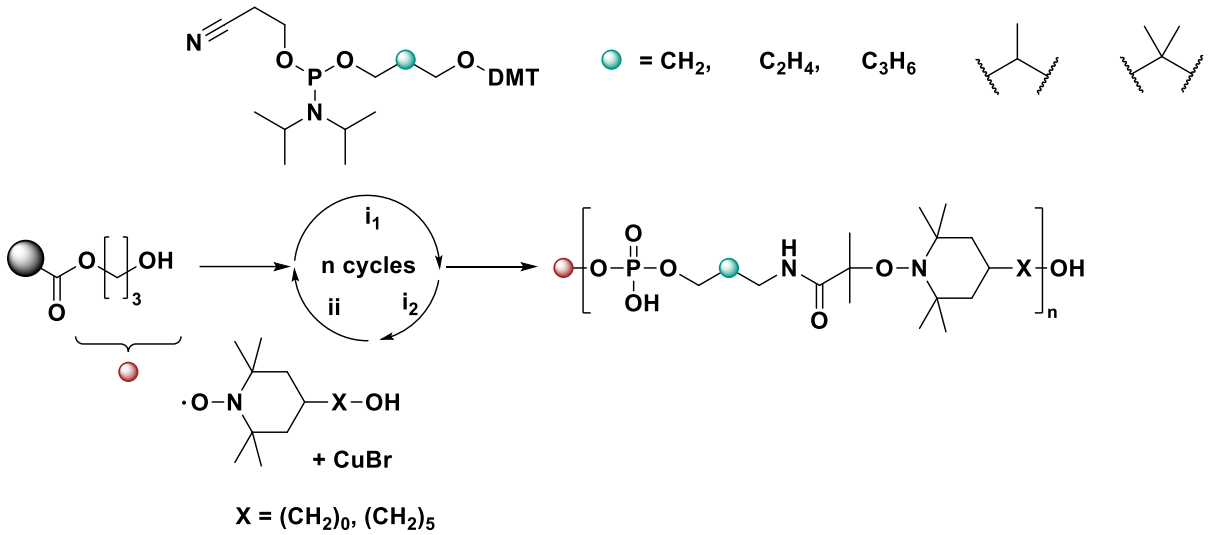

Scheme 17 General reaction scheme of the synthesis of sequence-defined oligo(alkoxyamine phosphodiester)s. i_1: phosphoramidite coupling: rt, AcCN, tetrazole; i_2: oxidation: rt, I_2, 2,6-lutidine, THF/H_2O; radical-radical coupling: CuBr, Me_6TREN, DMSO; ii cleavage: piperidine, AcCN, rt, then $MeNH_2$, NH_4OH, H_2O, rt.[137,138]

Although the readout was more predictable, due to the predetermined breaking point of the C-ON bond, the readout of larger oligomers would still be challenging.[125] Therefore, further investigations on the synthesis protocol were conducted by inserting coded dyads between two alkoxyamine motifs, in order to simplify the extraction of the information.[138] Additionally, employing an alkoxyamine-containing linker molecule, polymers of up to 18 one-byte polyphosphodiester sequences connected *via* alkoxyamine motifs were prepared *via* fully automated phosphoramidite synthesis. For this purpose, a library of up to 8 phosphoramidite monomers, and thus 3 bits per monomer (triads) was used, resulting in 144 bits per polymer chain.[123]

The alkoxyamine bonds were selectively cleaved and the polymer decomposed into a library of predicable fragments, when subjected to CID (interbyte fragmentation). Since these segments could be of the same mass, specific nucleosidic phosphoramidites were installed to each segment in the initial sequence as an identification tag. By

increasing the cone voltage of the mass spectrometer, the individual segments were fragmented in a so-called pseudo-MS^3 experiment and the manual read-out of the complete sequence was successfully demonstrated.[119,123] In order to encrypt the fragmentation pattern *via* a computer-assisted software (MS-DECODER), the aliphatic alkoxyamine-containing C_3 linker was exchanged with an aromatic linker to prevent unwanted mass signals resulting from a rearrangement reaction.[121,135] In this way, the en- and decoding of a 440 bits portrait of ANTOINE DE LAVOISIER was demonstrated in a single molecule.[120]

2.5.5. Oligo(alkoxyamine amide)s

The labile C-ON alkoxyamine linkages in poly(alkoxyamine amide)s acts as a predetermined breaking point, rendering this compound class a suitable candidate for the use of information-containing molecules. Since there is no competitive low-energy bong cleavage in tandem MS, the fragmentation pattern as well as the read-out is straightforward. Using three coding units (0 or 1 bit) and two spacer molecules, eight pentamers containing all possible binary triads were prepared on a glycine-loaded Wang resin in five steps by LUTZ *et al*.[144] The synthesis is based on an iterative strategy consisting of two chemoselective reactions using two AB-type monomers. 2-Bromopropionic acid anhydride and 2-bromo-isobutyric anhydride were used as noncoding (0-bit) and coding (1-bit) building blocks and 4-amino-TEMPO as a spacer. The first reaction is a nucleophilic substitution of the TEMPO primary amine with an anhydride, yielding an *N*-substituted amide. The second step is based on a radical-radical coupling of the nitroxide with a carbon-centered radical obtained by copper activation of the bromo species. Poly(alkoxyamine amide)s, containing a nitroxide spacer bearing a carboxymethyl group as α- and a bromine as ω-chain end, were obtained with different chain length by repetition of this synthetic cycle (Scheme 18). Since no protecting groups were needed and fast reactions were selected, poly(alkoxyamine amide)s were accessible in a facile and straightforward fashion. Moreover, the synthesis on a glycine-loaded polystyrene-based soluble support as well as on a non-cleavable polystyrene support, which was obtained *via* ATRP polymerization, was shown, and offered comparable results.[509]

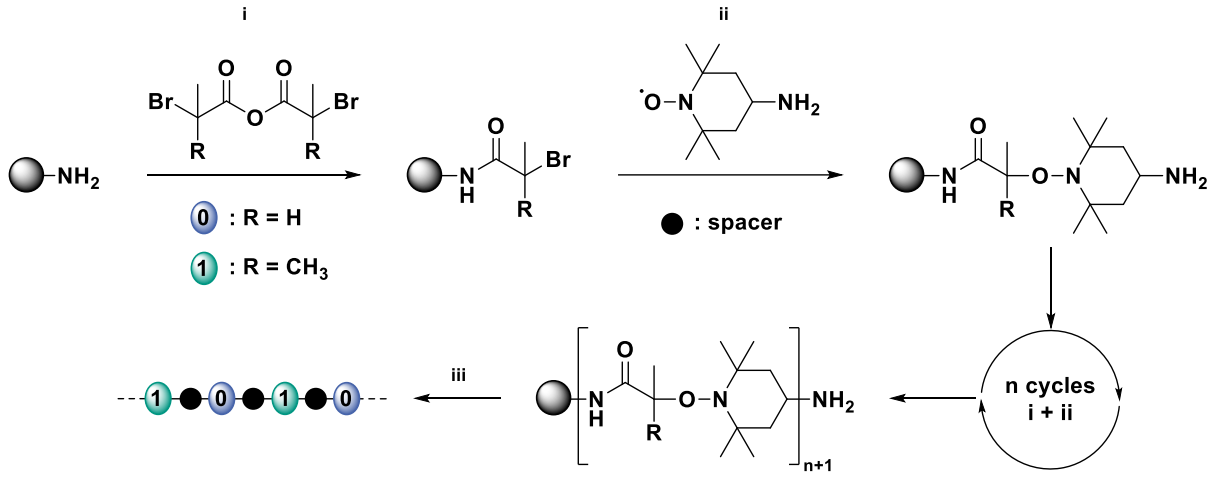

Scheme 18 General reaction scheme of the preparation of oligo(alkoxyamine amide)s *via* solid phase chemistry. i: amidation *via* nucleophilic substitution: THF, DIPEA or K_2CO_3; ii: radical-radical coupling: CuBr, Me_6TREN, DMSO; iii: cleavage of the solid support: TFA, DCM.[144]

Uniformity was confirmed with SEC and soft ionization ESI-MS, whereas the conditions in MALDI-MS were too harsh for the fragile molecule.[142] The sequence was easy to decipher in positive and negative[140] mode ESI-MS/MS, because the homolysis of C-ON bonds between a coding and a TEMPO unit occured as the only cleavage. Three triads were applied to CID to further investigate the dissociation behavior.[142] The observed fragments were completely identified, and reading from the α- or ω-end was possible.

As for the above-mentioned approaches, the synthetic protocol was improved by employing binary-encoded dyads resulting in a fast and efficient strategy for the synthesis of information-containing macromolecules *via* solid phase chemistry. Thus, only half of the synthetic steps were necessary to prepare a uniform octamer, which was successfully deciphered by ESI-MS/MS analysis.[143]

Furthermore, since alkoxyamines are known as thermolabile materials, which tend to dissociate above 60 °C, thermal stability studies were conducted. Therefore, controlled degradation of the poly(alkoxyamine amide)s in solid or solution was performed at 120 °C in presence of a large excess of TEMPO to trap the intermediate radicals and clarify the degradation process. This property offers the possibility to erase the stored information by increasing the temperature, which is interesting for the application in the field of data storage.[144]

2.5.6. Oligourethanes

The potential of oligourethanes as information-containing macromolecules was demonstrated by the group of LUTZ in 2016.[134] A general reaction scheme, as well as the investigated monomer structures, are shown in Scheme 19. The chemoselective two-step iterative approach consists of the reaction of an alcohol and *N*,*N*'-disuccinimidyl carbonate (DSC), resulting in an activated carbonate (i). In the second step, a carbamate was selectively formed by employing different amino alcohols (ii). In the final step, the sequence was cleaved from the polystyrene resin under acidic conditions (iii). Quantitative yields were reported for both iterative reactions, providing uniform structures. The binary code of "1"s and "0"s was implemented into the sequence by using amino alcohols with or without a methyl side chain.[134]

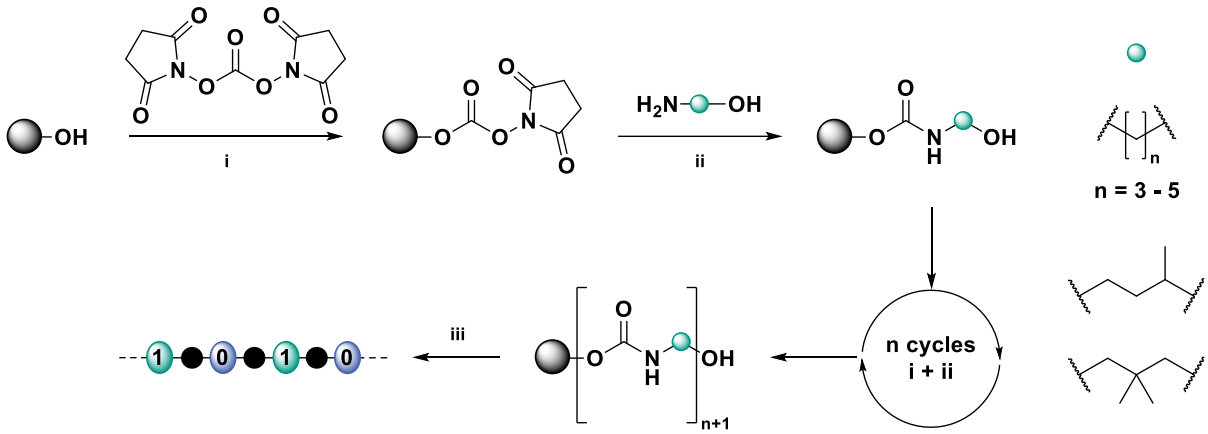

Scheme 19 General reaction scheme of the solid phase synthesis of sequence defined encoded oligourethanes *via* a chemoselective two-step iterative cycle. i: ACN, TEA, microwave, 60 °C; ii: DMS, TEA, rt; iii: TFA/DCM, rt. Solid phase = crosslinked hydroxy functionalized polystyrene resin beads.[134]

Repetition of the two-step chain elongation cycle yielded a sequence-defined pentamer, which was fragmented and easily deciphered *via* negative-mode ESI-MS/MS. On the other hand, applying positive-mode tandem MS, a complicated fragment pattern was obtained, due to C-O and C-N fragmentation of the protonated oligourethanes, which was completely suppressed by a proton/sodium exchange.[129] A detailed study of the fragmentation mechanisms in negative-mode ESI-MS/MS was reported in 2017.[132] Although three different fragmentation pathways were observed, they did not introduce additional complexity for long chain oligomers with 16 repeating units. However, a drastic decrease of the ionization ability *via* deprotonation with increasing chain length of the polyurethanes was observed, which was addressed by

the insertion of a second acidic end-group.[132] Furthermore, the application of binary encoded oligourethanes as anticouterfeiting agents was demonstrated by processing them with different materials and successfully deciphering the complete sequence after extraction from the product. In relation to this, sequence-defined oligourethanes were employed as macroinitiators in the ATRP of styrene resulting in a binary code-tagged polymer.[506]

In 2019, LUTZ *et al.* presented the preparation of poly(*N*-substituted urethane)s up to 28 repeating units by implementing secondary instead of primary amino alcohols in the same synthesis protocol as shown in Scheme 19. Four unique monomer building blocks were used, thus containing 2 bits of information each (dyads). Several advantages were observed compared to the sequence-defined oligourethanes, *e.g*. reduced synthesis time, access of longer chains, and better solubility and processing in common organic solvents, while a simple read-out *via* ESI-MS/MS was still ensured.[130] A detailed study about the fragmentation mechanism was reported by the same group in 2020. Complementary to the N-H oligourethanes, CH_2-O cleavage was observed for the N-R oligourethanes instead of O-(CO) bond cleavage, in both positive- and negative-mode ESI-MS/MS. Different rearrangements, produced up to four product ions per carbamate, thus resulting in a complex fragment pattern. Similar to the N-H oligourethanes these rearrangements were suppressed by a simple H/Na exchange of the carboxylic end-group. Furthermore, the procedure could be further simplified by formation of the methyl ester of the end group, resulting in only one fragment per repeating unit.[127]

2.5.7. Further approaches for the storage of data in molecular structures

Information-containing oligomers, obtained by a thia-maleimide Michael coupling, followed by a read-out using MALDI-TOF-MS/MS, were reported by ZHANG and coworkers.[157,158] In this example, an IEG strategy was applied using a difunctional precursor bearing a furan-protected maleimide and an acetyl-protected thiol. After separation and orthogonal deprotection, a thiol-maleimide Michael coupling was performed yielding the corresponding succinimide thioether dimer (Scheme 20). After repetition of the three-step chain elongation cycle for seven times, a 128-mer was obtained in an overall yield of 13% on a multi-gram scale.

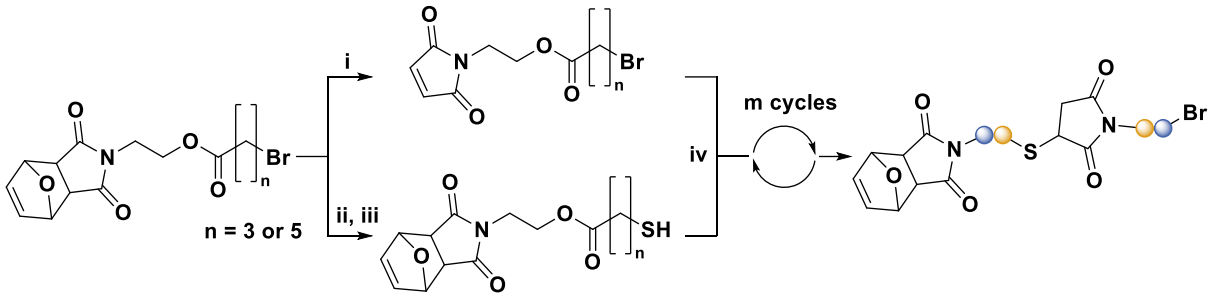

Scheme 20: Reaction scheme of the IEG strategy for the synthesis of sequence-coded succinimide thioether. i: toluene, 110 °C; ii: thiourea, EtOH, 65 °C; iii: $Na_2S_2O_5$, 18-crown-6, DCM/H_2O, 50 °C; iv: TEA, $CHCl_3$, 25 °C.[157]

Furthermore, by using different starting materials, backbone definition was achieved, and a sequence-defined dodecamer was obtained and fully characterized by MALDI-MS/MS. By reducing the succinimide thioether to the corresponding vinylic double bond, a second thiol-maleimide Michael coupling was performed resulting in dithiosuccinimide (DTS) motifs. Thus, a branching point was generated, and a sequence-defined dendron was prepared *via* a double exponential dendrimer growth (DEDG).[159] In a further study by the same group, various DTS building blocks were prepared in order to synthesize a side-chain defined uniform sequence. These molecules were used to store information in form of a binary code. For this, a non-functionalized succinimide thioether was translated into a “0”, whereas with the installation of a DTS unit a ”1” was written. The read-out was performed *via* MALDI-MS/MS and the fragmenting mechanism was uncovered assisted by computer simulations. This way, an information-containing dodecamer bearing three different side chain motifs, and 12 bits of data, was successfully decoded.[158] An improved protocol of this approach was reported just recently in 2020. First, a bromine precursor molecule was used, which offers a higher structural diversity and acts as an isotopic marker in the later read-out *via* tandem MS analysis. Prior to the thiol-maleimide Michael addition, the bromine was converted into the desired thiol *via* thiourea/bromine substitution. Furthermore, the thioether was oxidized to the sulfoxide, thus decreasing the C-S bond dissociation energy from 57.2 to 32.2 kcal/mol and increasing the possibility of a controlled and selective fragmentation. Additionally, an ester functionality was incorporated into the backbone structure, which tends to form easy detectable sodium adducts in mass analysis. By repetition of this four-step chain elongation cycle, a 64-mer was prepared in 24 steps in an overall yield of 5%. Products ranging from the 4-mer to the 32-mer were obtained in purities >95% and the SEC traces showed narrow distributions with dispersities of $Đ$ = 1.01. Peak broadening

($Đ$ = 1.03) and a decrease in the purity (>92%) was observed for the 64-mer. The binary code was written into the backbone sequence, by varying the aliphatic spacer of the bromine precursors. A C_3 spacer was translated into a “0” and a C5 chain into a “1”, respectively. The decoding *via* MALDI-MS/MS analysis was presented using an octamer containing 8-bits of information.[157]

In 2020, KÉKI focused on an alcohol-isocyanate click approach for the synthesis of encoded polyethylene glycol. Various uniform monomethoxy polyethylene glycols with 5 to 8 repeating units were coupled with uniform linear aliphatic isocyanates, ranging from the butyl to the octyl derivative, resulting in 20 different defined products. MALDI-TOF-MS was used for the read-out of the information and due to their structural similarity, an equal ionization efficiency was obtained. An alphabet based on a five-bit code was employed, thus four characters (20 bits) could be stored in one spot on the MALDI target. The absence or the presence of a certain compound was used to en- and decode a binary code of “0”s and “1”s, whereby the chain length of the PEG part was indicated the order of the characters. In this way, a text file consisting of 476 characters and in total 297.5 byte, a picture with 952 byte, and a Musical Instrumental Digital Interface (MIDI) were recovered with 100% accuracy.[510]

Most of the shown concepts are based on using two monomer units, resulting in a binary code along the sequence. In order to store larger amounts of data, long sequences have to be synthesized, which is time-consuming and bears difficulties in terms of the read-out *via* tandem MS. Addressing the first point, automatic synthesis was used, reducing the reaction time and allowing an easy parallelization.[98,155,156,209,212]

2.5.8. Increasing the data density

A recent example was demonstrated by ANSLYN and coworkers in 2021, using self-immolative chiral, abiotic sequence-defined urethanes as potential information-containing compounds, for the first time. A library of 16 unique amino alcohols were obtained from the respective amino acids *via* reduction, further converted into the Fmoc-protected and activated carbonates using 4-nitrophenylchloroformate. The chain elongation was performed on a 2-chlorotrityl chloride polystyrene *via* sequential addition of one monomer at a time following a coupling/deprotection protocol (Scheme 21). This approach shows a robust and efficient character, allowing a high throughput synthesis of 18 oligomers in parallel. The information of a text file consisting of

158 characters was translated into a hexadecimal code and encoded into 17 decamers (containing 9 hex symbols and an index for the start of the sequence) and a hexamer. The sequencing of the urethanes *via* self-immolation (5-*exo*-*trig* cyclization elimination) was performed under basic conditions at 70 °C and was monitored with LC-MS. All used 158 information-containing monomers were deciphered with 100% accuracy using a computer-assisted read-out of the mass spectra.[156]

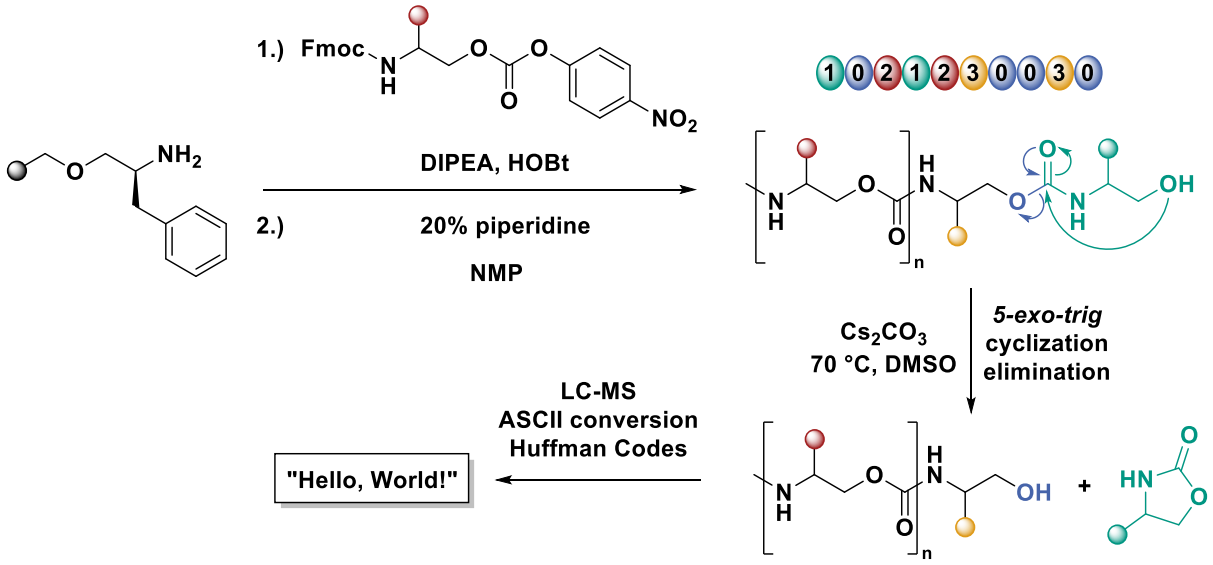

Scheme 21: General reaction scheme for the synthesis of sequence-coded self-immolative polyurethanes.[156]

KIM *et al*. described the semiautomated synthesis of poly(L-lactic-*co*-glycolic acid)s (PLGAs) and the storage of 896 bits in 14 compounds (64-mers). The general synthesis protocol, using a three-step IEG consisting of divergent separate deprotection and the coupling *via* esterification, was already mentioned in chapter 2.4.3. Following a convergent approach, 16 double-protected tetramers of all combinations of the two starting monomer units (lactic acid and glycolic acid) were prepared *via* continuous flow chemistry. The 64-mers were subsequently synthesized *via* cross-convergent coupling of the tetrads. The total process time for one 64-mer PLGA from tetrads was eight hours, including the final purification *via* preparative SEC. Each of the 64-mers was used to store 56 bit of information and an 8 bit chain identifier at the start of every sequence. The successful read-out was demonstrated with MALDI-MS/MS.[148]

Another approach is the shortening of the chain length by increasing the data density per monomer unit. Research in the direction of multifunctional sidechains has been reported by DING *et al.* for sequence-defined oligotriazoles. A two-step unidirectional

growth strategy was employed, consisting of an azidation of an alcohol tosylate, and a subsequent iridium-catalyzed azide alkyne cycloaddition (IrAAC). The alkynes were easily accessible and a library of six examples, bearing different side chains was prepared. A general reaction scheme of the applied synthesis protocol is shown in Scheme 22. By repetition of this approach, a sequence-defined hexamer, equipped with six different side chains at the C4 position of the triazole function, was obtained after 12 steps, containing 15.6 bits of information. The constituent cleavage of the C(sp^3)-S and the S(sp^3)-N bonds generated a distinct fragment pattern *via* MALDI tandem MS analysis, which was deciphered with 100% accuracy.[162]

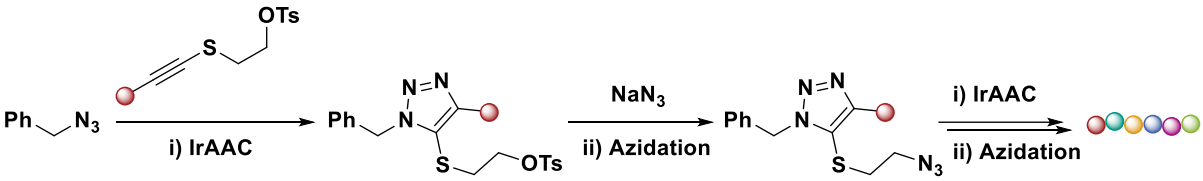

Scheme 22: General reaction scheme of the synthesis of sequence-coded oligotriazoles *via* repetitive IrAAC and azidation.[162]

In 2021, YAO *et al.* published the storage of data in peptide sequences. Eight out of the 20 natural amino acids, and thus 3 bits per repeating unit, were selected for the synthesis of short peptide sequences. Mixtures of 40 18-mers and 511 18-mers were prepared for the storage of a 848-bit textfile or a 13.8 kbits MIDI, respectively. For the text file, a data storage density of 1.7×10^{10} bits g^{-1} and an accuracy of 100% was achieved for the read-out of the information *via* LC-MS/MS, whereas a 10% error was observed for the MIDI (2.6×10^9 bits g^{-1}).[511]

Furthermore, a similar approach was shown by the same group for the synthesis of stereocontrolled sequence-defined oligotriazoles, by employing a chiral L-prolinol-derived azide. The reaction of the azide with a functionalized 3-thiopropagyl alcohol resulted in different chiral triazole monomer units. A three-step iterative chain elongation cycle, consisting of a separate deprotection step of the Boc-protected proline, the halogenation of the alcohol unit, and a subsequent coupling step v*ia* a substitution reaction was employed. With this reaction protocol, an IEG towards an 8-mer bearing similar side chains, and an iterative sequential growth (ISG) towards a tetramer with four different side chains, were conducted. The sequence-defined tetramer with four different side chains was chain doubled in a final step leading to an overall yield of 27% in 9 steps. A variety of four different sidechain-containing building blocks resulted in a storage capacity of 16 bit for the presented octamers. Two

fragmenting pathways were described, including the Csp^3-N bond cleavages on the triazole ring and in *β*-position to the triazole function. Based on this, a successful read-out was demonstrated *via* MALDI-TOF-MS/MS analysis.[160,162]

Different monomers containing a photoreactive benzaldehyde, which reacts as a diene from its *o*-quinodimethane state obtained under UV irradiation (so-called 'photo-caged dienes'[512]), and a furan-protected maleimide were used for the preparation of information containing macromolecules by the group of BARNER-KOWOLLIK in 2016. Starting from a dimaleimide core, a bidirectional growth, consisting of the successive photo ligation of the benzaldehyde species with the maleimide and subsequent deprotection of the furan protecting group, was conducted (Scheme 23). Several sequence-defined homopolymers, alternating copolymers, and block copolymer up to decamers were obtained. A library of six different monomer building blocks was presented, allowing side chain or backbone definition, thus resulting in 26 bits per decamer, which were successfully deciphered *via* MALDI tandem MS.[110]

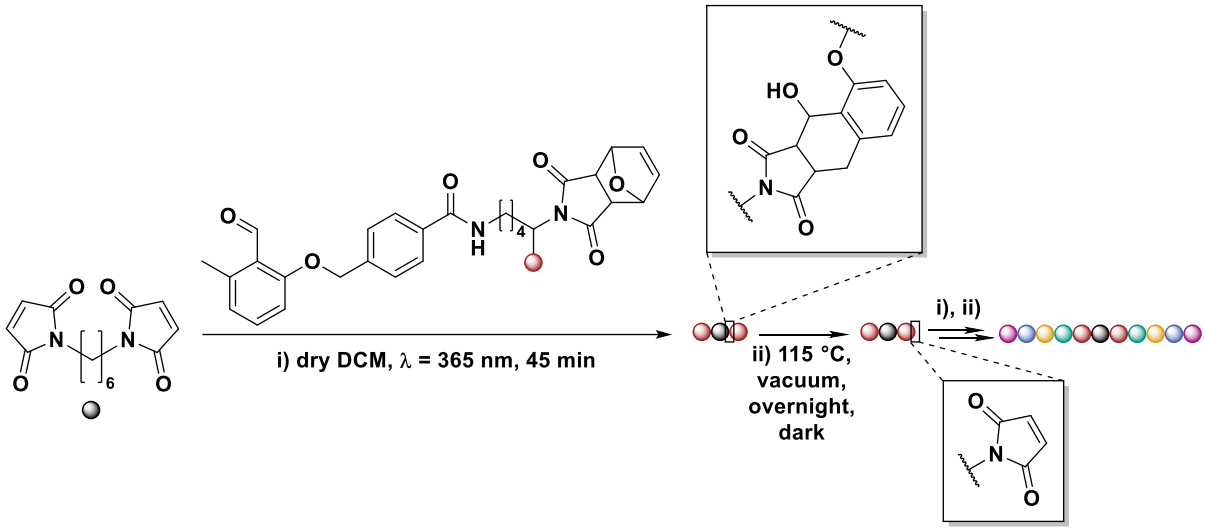

Scheme 23: General reaction scheme of the synthesis of information-containing macromolecules *via* photoligation.[110]

Another approach for data storage in sequence-defined structures, based on the well investigated thiolactone chemistry described in chapter 2.1, was presented by DU PREZ and coworkers in 2018. Applying the reaction protocol shown in Scheme 2 (2018, chapter 2.1), 71 short defined oligomers (1 monomer, 11 pentamers and 59 hexamers) were prepared *via* simultaneous automated synthesis. In order to accomplish sidechain definition, a library of 15 different acrylates were used. Thus, a total data capacity of 1,089 bits was achieved and the successful en- and the computer-assisted decoding of a 33×33-pixel QR code was demonstrated *via*

MALDI-MS/MS. The controlled and characteristic fragmentation of the carbamate backbone allowed a reading from left to right and *vice versa*.[155]

2.5.8.1. Dual side chain control

Further methods to increase the complexity of the repeating units, and thus the storage capacity, rely on dual side chain control, as demonstrated by DU PREZ and coworkers *via* an *in situ* successive nucleophilic ring opening of thiolactones and epoxides. This way, two different side chains were installed in a two-step cycle. Using a library containing 12 different amines, and seven unique epoxides, three pentamers bearing ten different side chains, and thus containing 32 bits of information each, were prepared and fragmented *via* MALDI-MS/MS.[152] Also the group of DING *et al*. has recently reported an improved approach for the synthesis of sequence-defined tetrazole implementing dual side chain control. By using a difunctional instead of a monofunctional alkyne for the IrAAC described above, two different side chains were implemented in one reaction step. This way uniform tetramers containing 16 bits each were prepared and fragmented *via* MALDI-MS/MS.[161]

2.5.8.2. Backbone and sidechain control

Backbone and sidechain control was presented by our group using an iterative chain elongation protocol consisting of a Passerini reaction and a reductive hydrogenation of a benzyl ester, which was already mentioned in chapter 2.1. Employing nine unique isocyanide building blocks bearing a benzyl ester, backbone definition was achieved, whereas a library of eleven aldehydes was used to achieve sidechain definition. In this way, a sequence-defined pentamer containing 33 bits of information was fragmentated by ESI-MS/MS and deciphered successfully with 100% accuracy.[150] Another approach using a combination of a hydroxyl-yne and thiol-ene click reaction was published by the group of TANG. A pentamer was obtained in eleven steps in an overall yield of 54% on gram scale. A 4 × 4 monomer library was employed and thus a storage capacity of 20 bits was achieved. Further description of this approach is given in chapter 4.6.1.[163]

2.5.8.3. Dual sidechain and backbone control

To further increase the storage capacity per repeating unit, a dual side chain and single backbone-controlled protocol was presented by DU PREZ *et al*. By combining the P-3CR with an addition of 1,2,4-triazoline-3,5-diones (TAD) to indoles, a sequence-defined tetramer, containing 12 variable functions was prepared. In this way, a similar storage capacity of 20 bits compared to the pentamer of TANG *et al.* was achieved in eight reaction steps. Furthermore, a potential application of this “macromolecular pin code” for anti-counterfeiting purpose was demonstrated.[153]

2.5.8.4. Triple sidechain and triple backbone control

The combination of two multicomponent reactions (the Passerini and the Biginelli reaction) for the synthesis sequence-defined macromolecules, showing high complexity per repeating unit, was demonstrated by our group. Six different components (three side chain and three backbone functionalities) were varied per chain elongation cycle using a library of in total 33 unique components, and thus adding 13 bits of information per repeating unit to the growing chain. The fragmentation pathways and the successful read-out were demonstrated *via* ESI-MS/MS analysis.[151]

General structures of the information-containing (macro)molecules prepared *via* the approaches described within this chapter are shown in Figure 14. The storage capacity per repeating unit, as well as the maximal deciphered chain length is provided. If reported, the preferred cleavage, when subjected to tandem MS, is marked with dashed lines in the molecule structure.

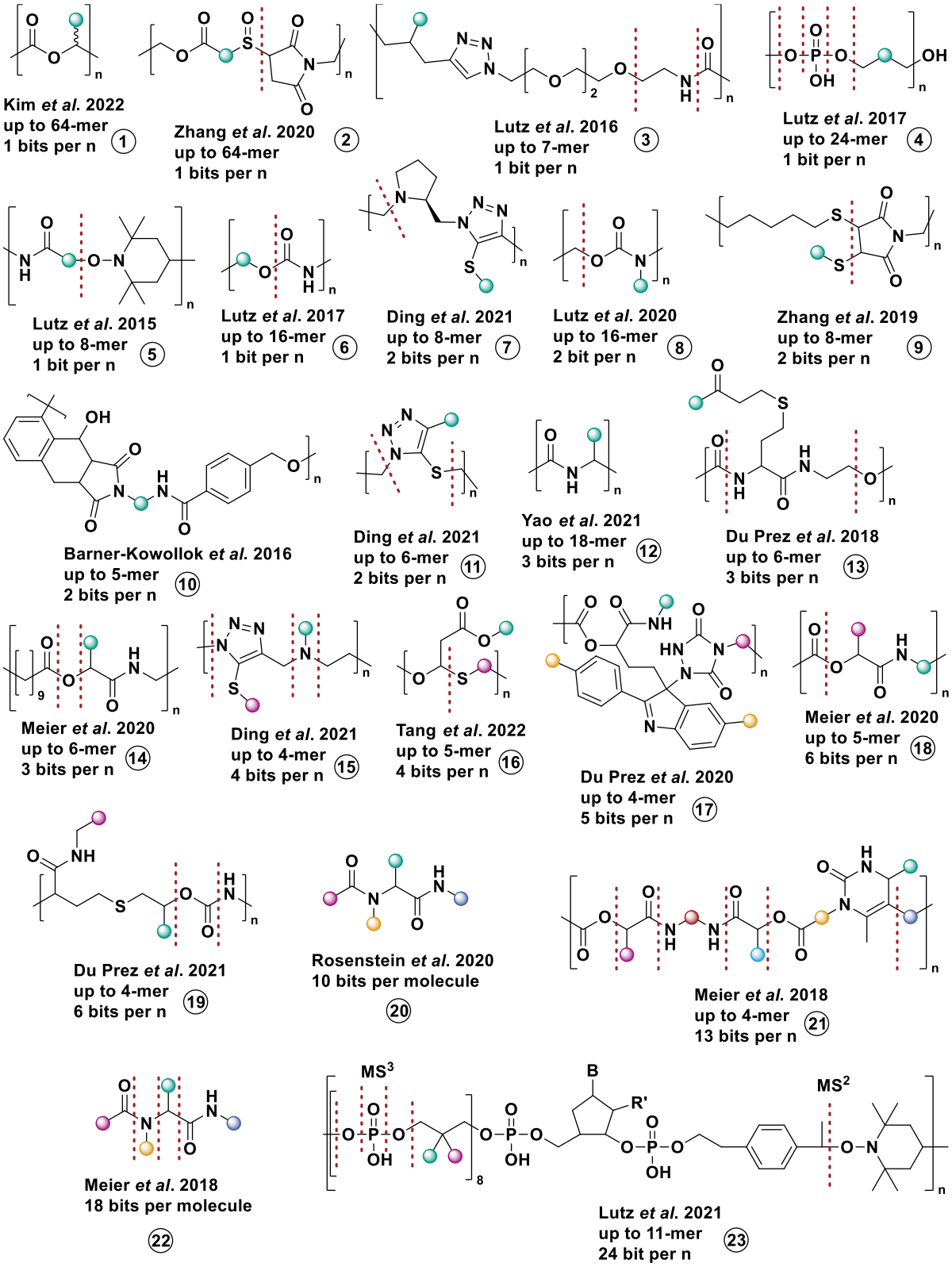

Figure 14: Overview of information-containing molecules and corresponding fragmentation pathways (if reported) described in chapter 2.5. 1. KIM *et al*. 2022[148]; 2. ZHANG *et al*. 2020[157]; 3. LUTZ *et al*. 2016[145]; 4. LUTZ *et al*. 2017[125]; 5. LUTZ *et al*.[143]; 6. LUTZ *et al*.[132]; 7. DING *et al*. 2021[160]; 8. LUTZ *et al*.[127]; 9. ZHANG *et al*. 2019[158]; 10. BARNER-KOWOLLIK *et al*. 2016[110]; 11. DING *et al*. 2021[162] 12. YAO *et al*. 2021[511]; 13. DU PREZ *et al*. 2018[155]; 14. MEIER *et al*. 2020[149]; 15. DING *et al*. 2021[161] 16. TANG *et al*. 2022[163]; 17. DU PREZ *et al*. 2020[153]; 18. MEIER *et al*. 2020[150]; 19. DU PREZ *et al*. 2021[152]; 20. ROSENSTEIN *et al*.[513]; 21. MEIER *et al*. 2018[151]; 22. MEIER *et. al*. 2018[514]; 23. LUTZ *et al*. 2021[120].

2.5.8.5. Data storage in molecular mixtures

The read-out of mixtures of sequence-defined oligomers (three hexamers, up to 64 bits in total), thus avoiding the synthesis of longer sequences, was recently reported by our group using the iterative synthesis protocol containing a Passerini reaction and subsequent reductive hydrogenation (see Scheme 3, chapter 2.1).[149]

To further simplify the procedures, small molecules can be used for the storage of data as well. Highly complex small molecules, *i.e.,* made by multicomponent reactions, exhibit a high data storage density as shown in an example by our group in 2018. Using a library of 130 commercially available compounds in an Ugi reaction, providing 500,000 permutations and thus a storage capacity of 18 bits of information per molecule, was achieved.[514]

Whereas all methods described so far are based on the read-out *via* fragmenting mass analysis, in the now discussed approaches only the presence or absence of the molecular mass within the corresponding mixture was decisive for the transmission of information. Thus, each molecule represented one bit of information. The writing and read-out of a 0.88 megapixel drawing of Pablo Picasso has been demonstrated by ROSENSTEIN *et al*. using up to 1536 unique molecular mixtures of up to 575 different Ugi-compounds with an accuracy of 97.57% (Figure 14, 20).[513]

The same strategy was used by WHITESIDES using mixtures of commercially available small oligopeptides analyzed by MALDI-MS.[515] In total, 400 kbit of information were written in mixtures of up to 32 compounds with 8 bits/s on a gold surface and retranslated with 20 bit/s with >99% accuracy. The "*Principles of Information Storage in Small-Molecule Mixtures*" is explained in detail by ROSENSTEIN *et al*.[516] They theoretically point out the immense storage capacity and density of small-molecule mixtures, underlined by experimental demonstrations.[513] It is also addressed that the read-out is not mandatorily restricted to MS or tandem MS, but can also be performed utilizing spectroscopic or chromatographic analysis.[513] Mixtures of fluorescent dyes for writing approximately 400 kbits of data in a binary code at a rate of 128 bits/s on a surface, and decoding these at a rate of 469 bits/s with >99% accuracy *via* a confocal microscope, were demonstrated.[517] Another example in this context using Raman scattering of alkynes was described by GAO and coworkers.[518] Data storage in a single molecule, which was used for secret communication and deciphered *via* fluorescence spectroscopy was reported by MARGULIES *et al*.[519] A binary code was encoded in

mixtures of up to 22 aromatic compounds by KEINAN *et al.* using their own coding language and making use of specific chemical shifts and concentration-dependent integral values in ^{1}H NMR spectroscopy.[520] A similar approach is used in NMR photography to draw images with molecules based on their chemical shifts.[521]

The ever-increasing amount of information encoded in either sequence defined macromolecules or molecular mixtures entails the handling of ever-larger data sets. Thus, writing the data and the subsequent manual decoding reach their limits. For writing, increasingly automated synthesis and chemical printers are used, and software is being developed for processing the amount of data and reading out the original information.[121],[155],[149,156]

In chapter 4.6.1 investigations on an alternative approach for the synthesis of sequence-defined macromolecules suitable for the application as information-containing molecules are discussed. For this purpose, a chemoselective two-step iterative chain elongation cycle, consisting of a Passerini reaction and a phenyl-yne Michael addition was studied.

Furthermore, the fast and efficient data storage in mixtures of common, commercially available chemicals and the subsequent decoding *via* basic and commonly available analytical tools (^{1}H NMR spectroscopy and gas chromatography (GC)) with zero synthetic effort is shown. We made use of a simple comparison approach, where the absence and the presence of a molecule, and its position in the respective spectrum or chromatogram, are used as binary information to carry either the information of an ASCII code or the black and white pixel of a bitmap. We further demonstrate a smart solution for the ordering issue, when handling more than one coding sample, by making use of the linear dependence of the integral on the peak concentration (GC). Furthermore, a software for decoding information from the compound mixtures analyzed by GC is introduced and showed a reliable readout for two 25×25-pixel bitmaps.

2.6. Multicomponent reactions

2.6.1. General introduction

Since the discovery of the amino acid synthesis by ADOLPH STRECKER in 1850,[522] multicomponent reactions (MCRs) have received an increasing interest in organic[523] and polymer chemistry,[524–532] as well as material science.[533] In a MCR, three or more starting materials react in a one-pot reaction to a single product, incorporating most of the atoms of the reactants.[534] Because of the high atom efficiency and their convergent character, highly complex architectures are accessible in a single reaction step. Thus, they show an advantage over conventional multistep synthesis strategies concerning working time and experimental simplicity, since isolation or purification of intermediates is not necessary. Furthermore, often high yields are achieved, and the mostly environmentally friendly starting materials are commercially available making MCRs suitable and versatile tools in combinatorial chemistry[535,536] and drug discovery,[537,538] but also in the context of synthesis of highly defined sequences[150,167] or polymeric structures.[526,528–530,532,539] Due to the mentioned features of MCR, they can be considered as “ideal reactions” according to the concept of an ideal synthesis described by WRIGHT *et al.*[540] In general, MCRs can be classified into three different types depending on their reaction mechanism, as shown in Scheme 24.[541]

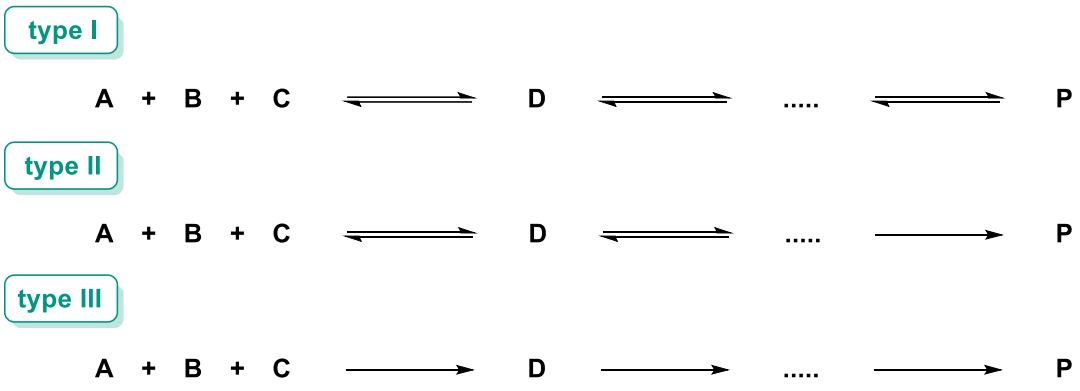

Scheme 24: Categorization of MCRs into three different types, established by DÖMLING and UGI in 2000. Type I: all reaction steps are reversible; type II: only the last step is irreversible; type III: each reaction step is irreversible, where A, B and C are starting materials, D is the intermediate and P the product.[541]

In a type I MCR, all reactions steps are reversible. Thus, the starting materials, intermediates and the product are in equilibrium, leading to theoretical yields between 0 and 100% depending on the individual equilibrium constants. Furthermore, side reactions can occur due to incomplete conversion, which additionally complicate the

isolation of the desired product. In contrast, the last step in type II MCR is irreversible. Therefore, based on *The Equilibrium Law* described by HENRY LOUIS LE CHATELIER,[542,543] the equilibrium in type II MCR is strongly shifted to the product side. The reason for the chemical driving force is the formation of a thermodynamically stable compounds and can be of many natures: *e.g.*, formation of stable products, irreversible ring closure, aromatization, or the oxidation of the isocyanide ($C^{II} \rightarrow C^{III}$) in the P-3CR and U-4CR. The ideal type III MCR consist only of irreversible reaction steps and are rarely encountered in synthetic chemistry but can be often found in enzymatic biochemical processes. It must be noted that this is an ideal schematic overview, and an exact classification is not always possible.

Additionally, MCRs can be divided into non-isocyanide based, isocyanide based (IMCR) and metal-catalyzed MCRs. A chronologic overview of the most common MCRs is given in the following section.

In 1850, ADOLPH STRECKER described the three-component reaction of an aldehyde, hydrogen cyanide and ammonia.[522] Subsequent acidic hydrolysis of the formed α-aminonitrile yielded a racemic mixture of the respective amino acid (Scheme 25). The Strecker synthesis is known to be the first MCR and a milestone has been set for further reactions of this class. In 1882, ARTHUR HANTZSCH developed a four-component reaction towards 1,4-dihydropyridines (DHP) *via* the condensation of an aldehyde, two equivalents of an β-ketoester and ammonia.[544] DHPs can be easily oxidized to the corresponding pyridines and are of special interest in the pharmaceutical area due to their biological activity.[545] The most important example is the drug Nifedipin, a calcium channel blocker, which is employed in treatment of angina and cardiovascular diseases.[546] Another important MCR was published by HANTZSCH in 1890. It includes the condensation reaction of an β-ketoester, α-halo ketone and ammonia forming a pyrrole structure.[547] The aza-analogue of the Hantzsch DHP synthesis was discovered by PIETRO BIGINELLI 1891.[548] The product, a 3,4-dihydropyrimidin-2(1*H*)-one (DHMP), proceeds *via* the reaction of an aldehyde, urea, and acetoacetate. The Mannich reaction, which was reported by CARL MANNICH in 1912, describes an aminomethylation of an oxo-component (aldehyde or ketone) using an amine and formaldehyde.[549] In 1934, the reaction of an aldehyde, a carboxylic acid, hydrogen cyanide and ammonia towards a hydantoins was published by HANS THEODOR BUCHERER[550] and HERMANN BERGS.[551] MARTIN ISRAILEWITSCH KABACHNIK and ELLIS K. FIELDS independently discovered a three-component reaction of an amine, an oxo-

component (aldehyde or ketone) and a dialkylphophate yielding aminophosphonates in 1952.[552–554]

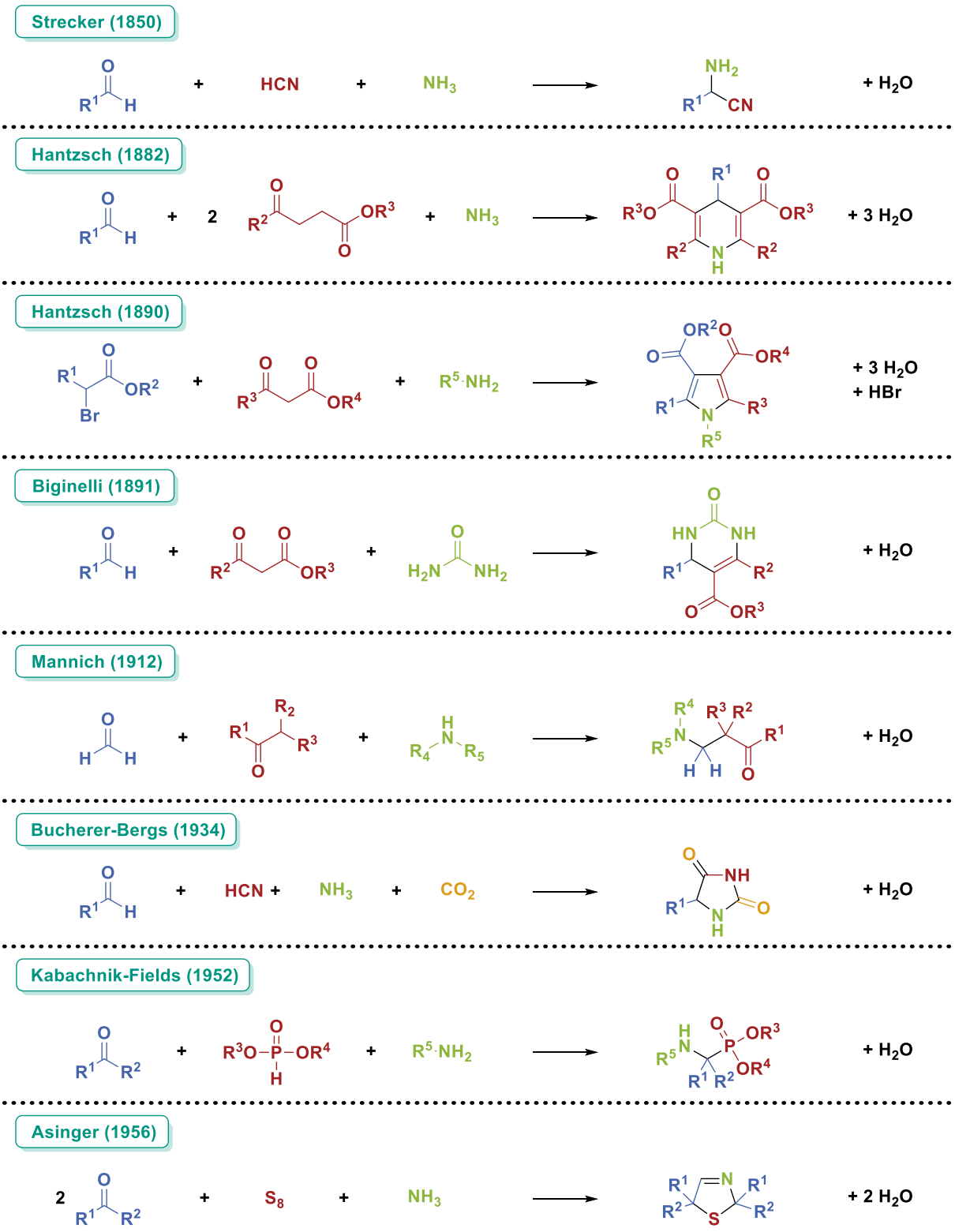

Scheme 25: Chronologic overview of non-isocyanide based MCR.[522,544,547,549,555]

Another MCR for the synthesis of thiazoline derivatives using elemental sulfur, two equivalents of a ketone, and ammonia, was described a few years later in 1956 by FRIEDRICH ASINGER.[556]

From an industrial point of view, cobalt-catalyzed carbon monoxide containing MCRs are of special interest, *e.g.* the hydroformylation of alkenes, which was described 1938 by OTTO ROELEN[557] or the hydrocarboxylation of alkynes by WALTER REPPE in 1949.[558] Furthermore, PETER LUDWIG PAUSON and IHSAN ULLAH KHAND reported the [2+2+1]-cycloaddition using an alkyne, an alkene and carbon monoxide to form a α,β-cyclopentenone derivatives.[559]

2.6.2. Isocyanide-based multicomponent reactions

IMCRs are a special class of MCR,[526,560] which were applied in the second part of this thesis for the synthesis of information-containing molecules (chapter 4.6.2).

The most known examples are the Passerini three-component reaction (P-3CR)[164] and the Ugi four-component reaction (U-4CR),[165] which will be discussed in detail in the following chapter. Before, synthetic strategies for the preparation of isocyanides and their extraordinary reactivity will be briefly introduced.

2.6.2.1. Isocyanides

In 1859, LIEKE intended to synthesize allyl cyanide by reacting allyl iodide and silver cyanide.[561] Instead, he obtained the corresponding isocyanide by accident. The actual presence of the isocyanide was confirmed ten years later (Scheme 26) in 1869, by ARMAND GAUTIER[562] and can be explained with Kornblum's rule.[563,564] Another synthesis protocol was reported by AUGUST WILHELM VON HOFMANN in 1867,[565] by reacting a primary amine with chloroform in the presence of potassium hydroxide. It took around 100 years, until further approaches were reported by IVAR UGI in 1958 and 1960.[566,567] He developed the preparation of isocyanides *via* a dehydration of *N*-formamides under basic condition. First, highly toxic phosgene was used as dehydration agent, which is still applied in industry nowadays. However, other compounds, such as di- or triphosgene, phosphorous oxychloride, the *Burgess reagent*, trifluoromethanesulfonic anhydride or recently *p*-toluenesulfonyl chloride have proven to be suitable dehydration agents.[568,569] Ugis approach was a milestone in the synthesis of isocyanides and since then IMCR became more and more attractive for organic chemistry.[570] Recently, ALEXANDER DÖMLING is performing pioneer work, in

terms of efficient, varied, and fast synthesis of isocyanides.[571] In 2015, he discovered the Leuckart-Wallach reaction as valuable tool for the preparation of *N*-formamides.[572]

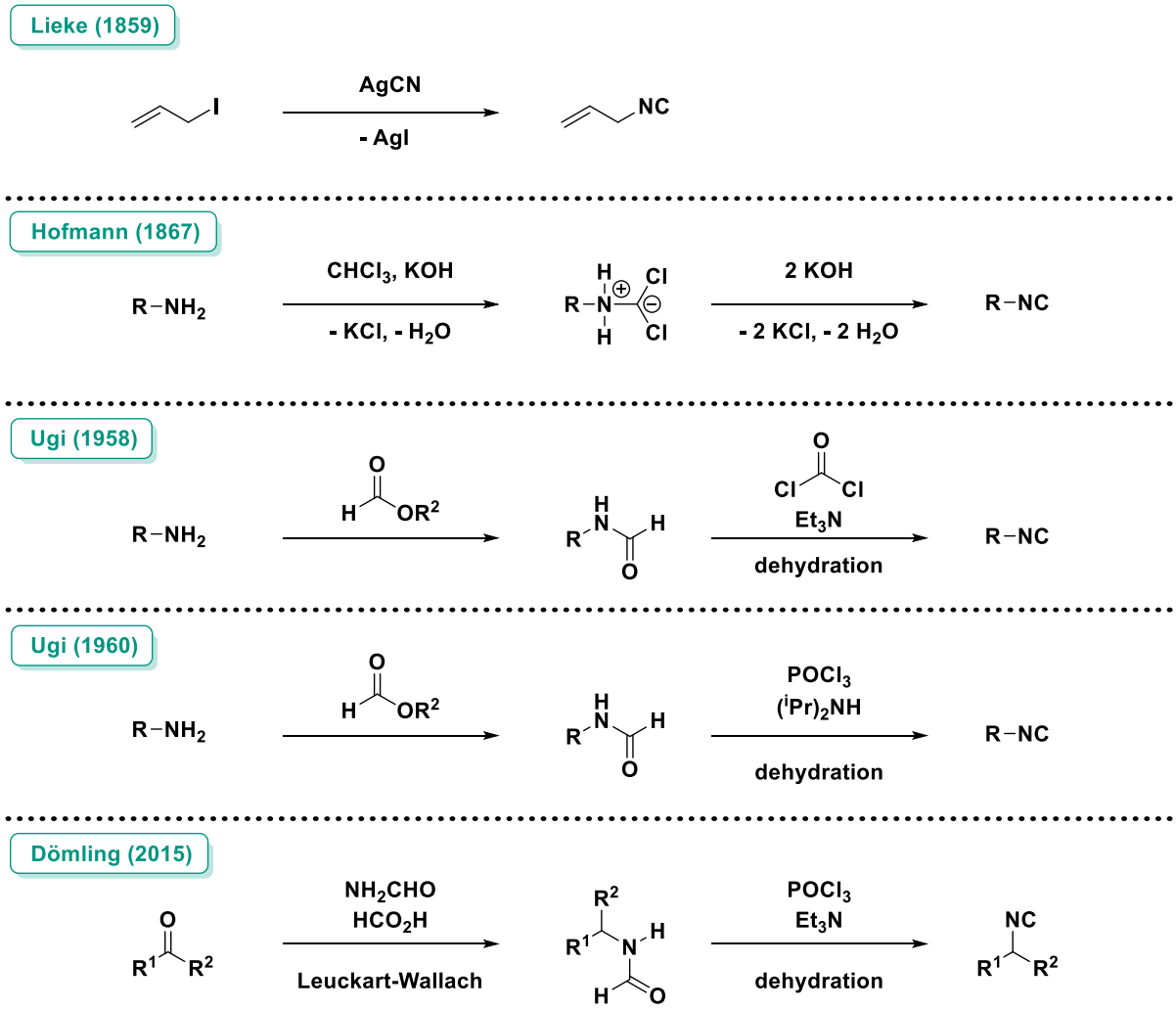

Scheme 26: Selected approaches for the isocyanide synthesis in chronological order.[561,565–567,572]

The characteristic reactivity of isocyanides is based on the formally stable divalent carbon atom. Only carbon monoxide and carbenes share the same special property. In Scheme 27, the mesomeric resonance structure of isocyanides is depicted. Besides the carbene structure, a zwitterionic configuration can be formed, explaining the ambident character of the carbon atom.[573] Thus, isocyanides react usually in an α-addition, which is one key-steps in the mechanism of the P-3CR and the U-4CR. Here, the carbon atom is transformed into an electrophile after it reacts as a nucleophile, allowing a nucleophilic attack at the same position. Furthermore, their diverse reactivity can be explained by their α-acidity, which can be increased by electron-withdrawing groups (EWG) attached at the α-position, or the ability to form radicals. The latter feature could lead to polymerization or cyclization. Isocyanides are

highly stable under basic conditions, but very sensitive towards acids and hydrolyze to the corresponding *N*-formamides.[570]

Scheme 27: Resonance structure of the isocyanide functional group.

2.6.2.2. Passerini three-component reaction

The P-3CR describes the reaction of an aldehyde, a carboxylic acid, and an isocyanide towards an α-acyloxy amide. It is the first mentioned IMCR and was discovered by the italian chemist MARIO PASSERINI in 1921.[164] Typically for a MCR, the P-3CR is characterized by its simple execution under ambient conditions. Usually aprotic solvents, such as DCM are used and up to quantitative yields can be achieved,[570] also since the last reaction step is irreversible, rendering the P-3CR a type II MCR reaction (Scheme 24).[570] The Passerini reaction exhibits an atom economy of 100%, as no side product is formed and thus every atom of the starting materials is incorporated in the product structure.

Last year, in 2021, the Passerini reaction had its 100th anniversary. Nevertheless, the reaction mechanism has not yet been completely clarified. The net reaction as well as one proposed mechanism,[164] which is commonly accepted, is shown in Scheme 28. It starts with the activation of the oxo-component (here an aldehyde) by the carboxylic acid *via* hydrogen-bonding. In the next step, the isocyanide reacts in an α-addition with the hydrogen-bonded adduct **I**. Hereby, the isocyanide first reacts as a nucleophile with the carbonyl center of the activated aldehyde and subsequently gets attacked by the carboxylic acid at the formed electrophilic carbon atom resulting the cyclic transition state **II**. In the final irreversible rearrangement, an intramolecular transacylation takes place and an α-acyloxy amide is formed as the product. This mechanism was proposed by MARIO PASSERINI[164] himself and was supported by kinetic investigations by IVAR UGI and RAYMOND H. BAKER in 1959 and 1961, respectively.[574,575]

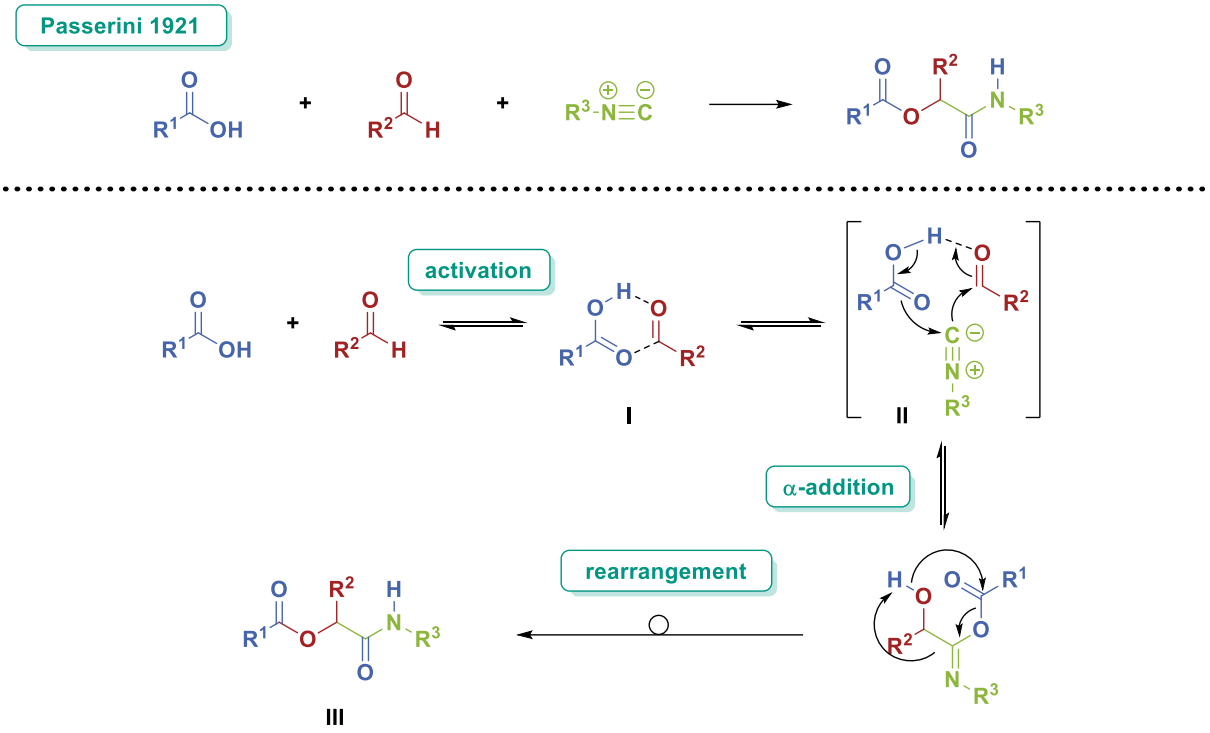

Scheme 28: Reaction equation and commonly accepted mechanism of the Passerini reaction.[164]

However, HAGEDORN and EHOLZER proposed a controversial mechanism in 1965, describing a *N*-protonation of the isocyanide in presence of catalytical amounts of mineral acid as a first step.[576] These results are in conformity with a publication of MICHAEL P. PIRRUNG, that the P-3CR and U-4CR are accelerated in aqueous solution,[577] which, however, is in contradictory to the statement of UGI, who described the acceleration in non-polar, aprotic solvents.[578] In 2011, another mechanism was postulated by MAEDA *et al.* based on quantum-chemical calculations in the gas phase. They specified the Passerini reaction as a four-component reaction with an additional carboxylic acid, which acts as an organo catalyst and lowers the energy of the transition state (TS).[579] However, this would be in contrast with the mechanism of HAGEDORN and EHOLZER, but was confirmed by MOROKUMA with further DFT studies.[580] The mechanism is shown in Scheme 29 and the reaction steps including the α-addition are identical with the previously discussed mechanism of PASSERINI. Afterwards, a cyclic intermediate **II** is formed *via* a four-component cyclic TS **I**, which rearranges *via* another four-component TS **III** to the product.

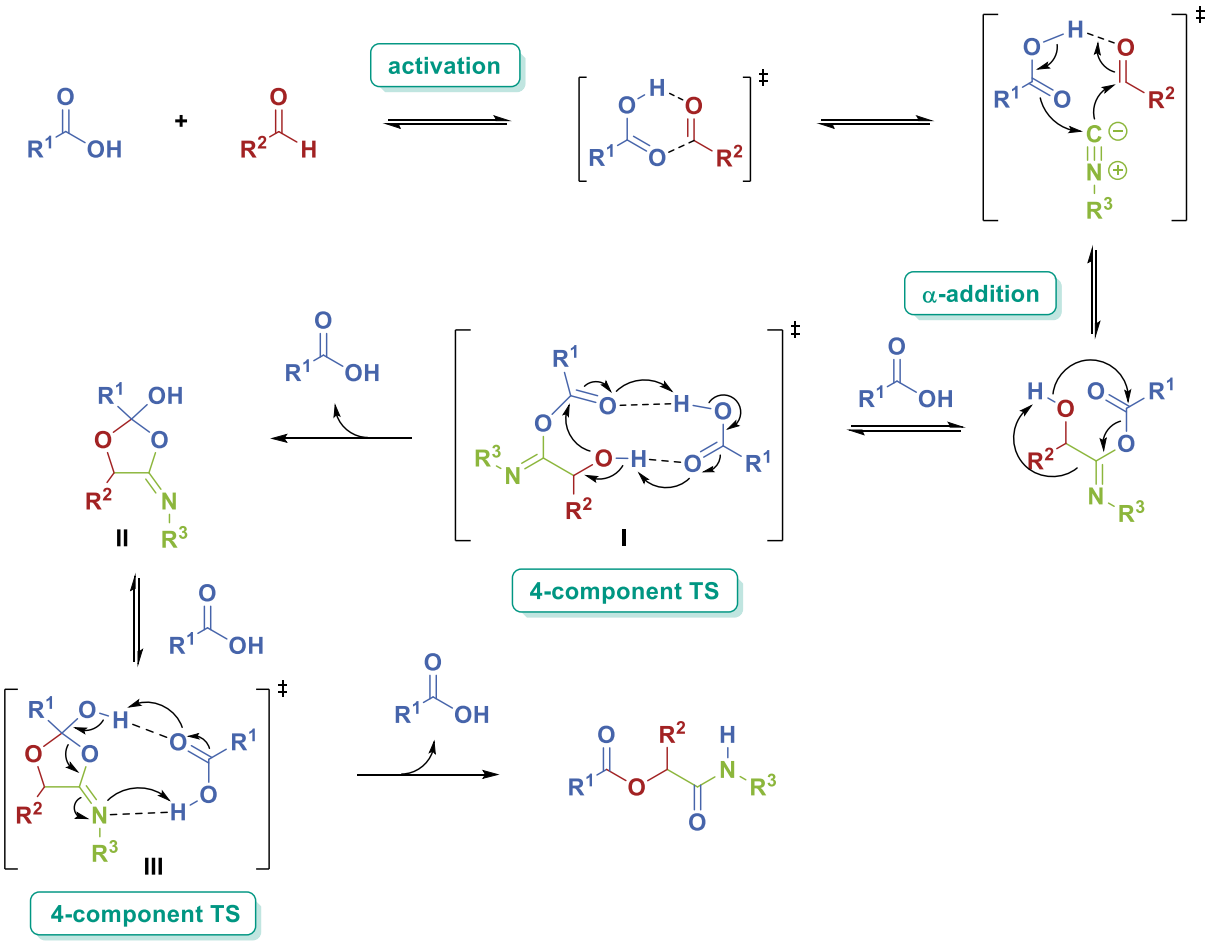

Scheme 29: Alternative reaction mechanism of the Passerini reaction proposed by MAEDA *et. al*. involving a second carboxylic acid component. TS = transition state.[579]

The following scheme shows the many different variations of the P-3CR and clearly illustrates the versatile scope and significant role in the field of combinatorial chemistry of the reaction (Scheme 30). By replacing either the carboxylic acid or the oxo-component, diverse structural motifs are accessible *via* this MCR. In addition to the already explained main variant, carbonic ester amides can be achieved by applying an alcohol in presence of CO_2 instead of the carboxylic acid, resulting in a Passerini four-component reaction (**b**).[581] The straightforward synthesis of *O*-arylamides *via* a Smiles rearrangement in the Passerini reaction with electron-deficient phenols is depicted in reaction (**c**).[582,583] Furthermore, the carboxylic acid can be substituted by hydrazoic acid or trimethylsilyl azide in the type (**d**) reaction leading to tetrazole derivatives.[584–586] By exchanging the acid component with mineral acids, α-hydroxyamides are obtained (**e**).[587] Moreover the carboxylic acid can be replaced by 1,1,1,3,3,3-hexafluoro-propan-2-ol (HFIP),[588] suppressing the Mumm- or Smiles rearrangement, or an alcohol and 2-iodoxybenzoic acid (IBX) as *in situ* oxidizing agent,[589] leading either to α-hydroxyamines or the common Passerini product. The latter approach is a

practical alternative, since aldehydes are air-sensitive and tend to oxidize to the corresponding carboxylic acid, which leads to the formation of side products. Further, alcohols are commercially more available than aldehydes. Other than replacing the carboxylic acid, the oxo-component can be substituted by acyl isocyanates (**f**) or ketenes (**g**), yielding in *N*,*N*-diacyloxamides[590] and α,γ-diketo-carboxamides,[591] respectively.

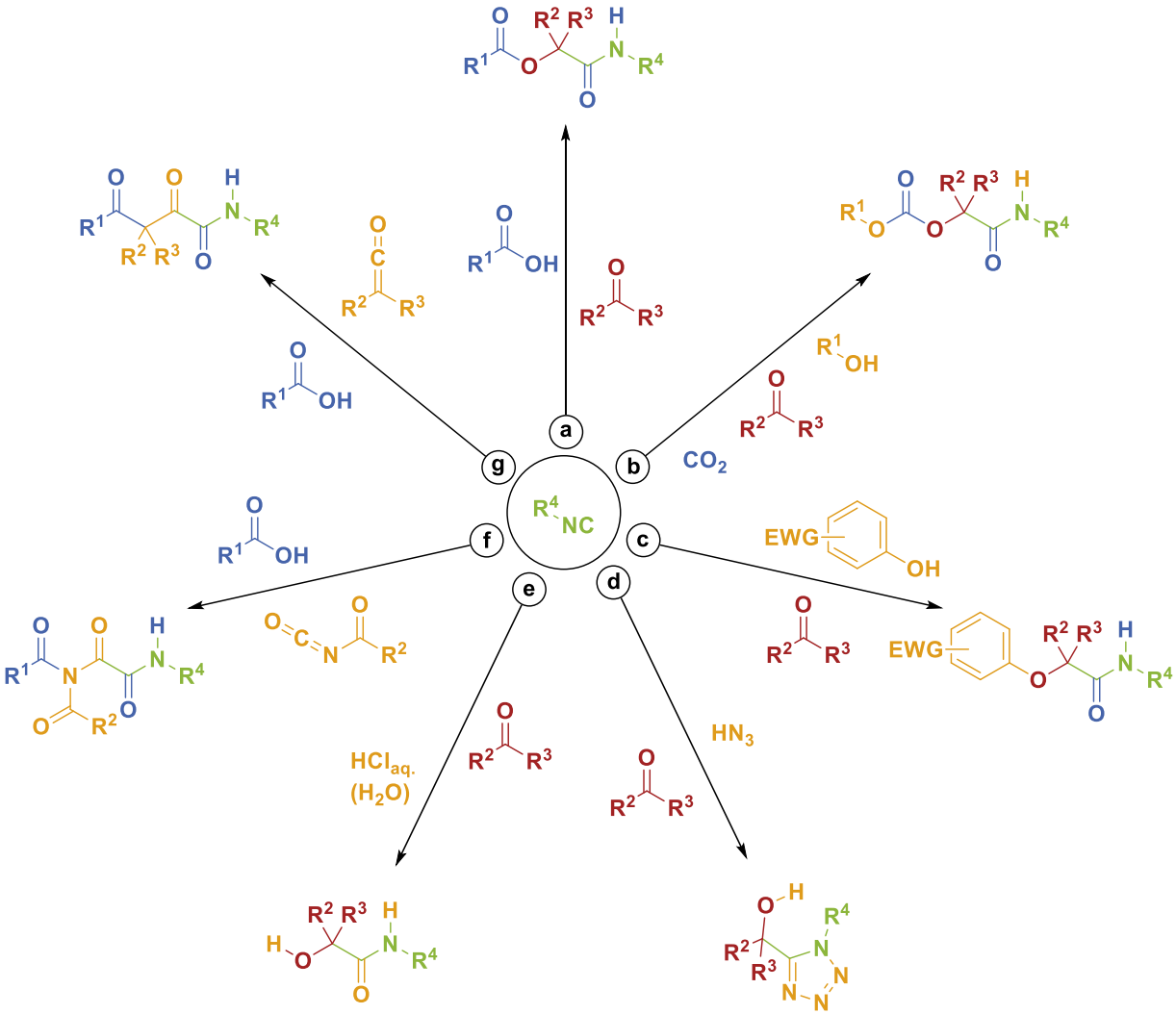

Scheme 30: Overview of the different variants of the Passerini reaction. Besides the main approach (**a**) the carboxylic acid (**b**-**e**) or the oxo-component (**f**,**g**) can be substituted resulting in a variety of structure motifs.[581–591] Adapted from.[592]

In the context of this work, the versatility of the reaction was used to synthesize a compound library for molecular data storage application. However, it was limited to the common variant of the Passerini reaction in combination with a subsequent hetero-Michael addition of different nucleophiles, which will be introduced in chapter 2.6.3. Recently, the successful application of the reaction has been used for

the synthesis of sequence-defined macromolecules[83,168,169,216,217,593] and the preparation of polymers.[532,594,595]

2.6.2.3. Ugi four-component reaction

The Ugi four-component reaction was developed by IVAR KARL UGI in 1959. Additional to the aldehyde, isocyanide and carboxylic acid used in the Passerini reaction, an amine component is employed in the U-4CR.[165,574,596,597] The reaction equation and the commonly accepted mechanism is shown in Scheme 31. In the first step, an imine condensation of the oxo-component and an amine takes place. The resulting imine is activated *via* protonation of the carboxylic acid followed either by the direct α-addition of the isocyanide forming a nitrilium intermediate **I** with subsequent addition of the carboxylic acid (ionic pathway), or the α-addition *via* a hemiaminal **II** in the non-ionic mechanism (isocyanide-insertion). After a final irreversible Mumm rearrangement, the Ugi product, an α-aminoacylamide is formed.

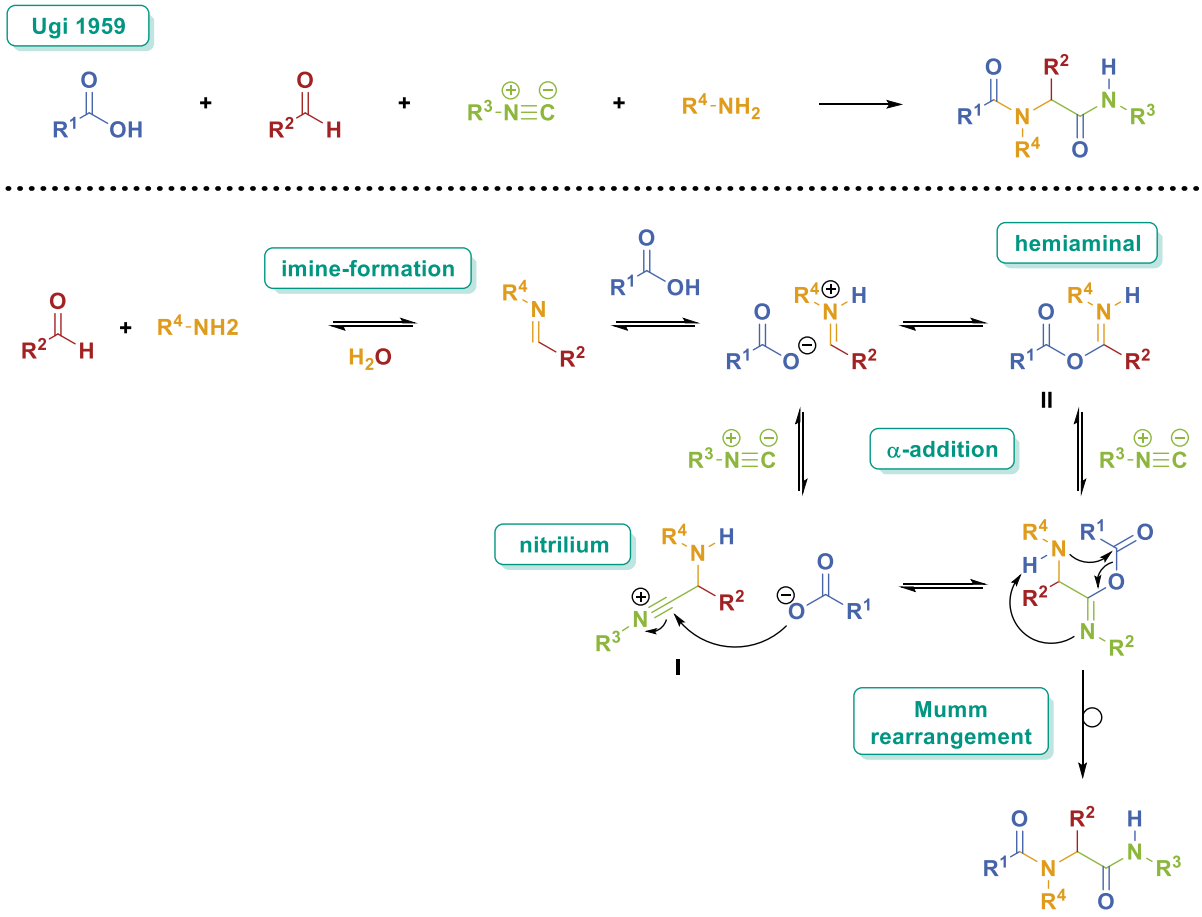

Scheme 31: Reaction equation and commonly accepted mechanism of the Ugi reaction.

Due to the additional amine component, compared to the Passerini reaction, even more complex molecules are easily accessible in a one-pot reaction. Thus, the U-4CR

is a powerful synthesis tool in many fields of application, e.g. pharmaceutical,[538,598,599] combinatorial,[535,536] and polymer chemistry,[524–532,539] synthesis of sequence-defined macromolecules[167,170,218] and recently as molecular data storage devices.[513,514]

Similar to the Passerini reaction, several variants of the Ugi reaction were investigated over the last years, which are not further described within this work.[600–605]

2.6.3. Combination of MCR with Michael addition

If one of the employed components of the P-3CR or U-4CR is equipped with a Michael acceptor, a subsequent post-functionalization with several nucleophiles or an intramolecular cyclization is possible in a one-pot manner. Thus, complex molecular architectures are easily accessible. A vast variety of post-functionalization of Ugi products based on propiolates were reported by MAHDAVI *et al.*[606] and SHAKERI *et al*.[607]

The classic Michael addition was published in 1887 by ARTHUR MICHAEL and describes the 1,4-conjugate addition of a nucleophile (Michael donor) to an α,β-unsaturated carbonyl compound (Michael acceptor).[608] The mechanism for the carbon-Michael addition is shown in Scheme 32. In the initial step, the C-H-acidic compound is deprotonated by the base catalyst. Since the resulting enolate is a soft nucleophile according to the HSAB concept, it attacks the β-position of the acrylate. After protonation of the carbanion, the catalyst is regenerated, and the Michael adduct is formed.[609]

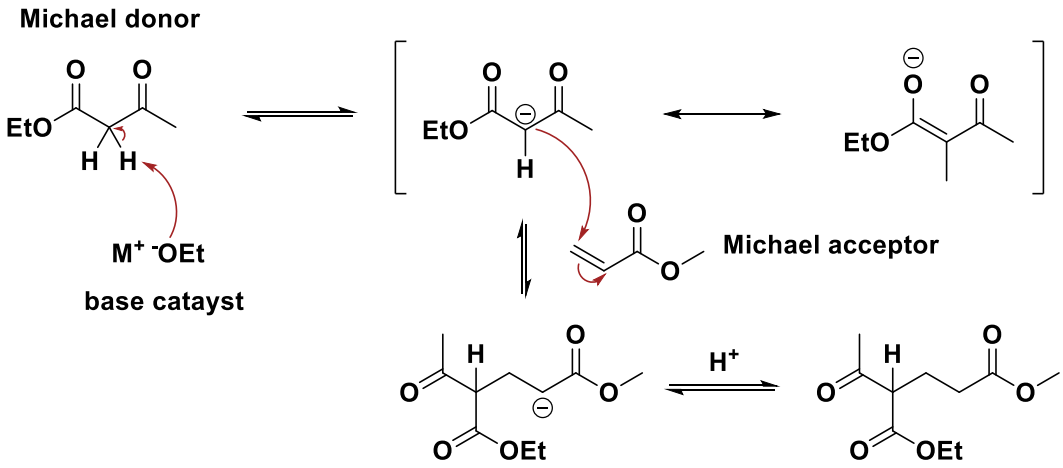

Scheme 32: General reaction mechanism for the carbon-Michael addition.[609]

The nucleophilic conjugate addition of thiols, amines, and alcohols to activated alkynes was recently reviewed in detail by DOVE *et al*. in terms of substrate, solvent, and

catalyst effects, reactivity and the different applications in fields of organic, polymer, and biochemistry.[610] Furthermore, a detailed study of the reaction mechanism assisted with density functional theory (DFT) calculations of the aza-Michael addition was published by the group of TANG, confirming the experimental regio- and stereoselectivity of the reaction towards the *E*-configurated anti-Markovnikov product.[611]

The combination of the U-4CR reaction and an aza-Michael reaction was reported by the group of BIJANZADEH, which is shown in Scheme 33. Different primary amines, isocyanides and aldehydes were reacted with propiolic acid in an Ugi reaction. To avoid the formation of unwanted side products, the five components were added to the reaction mixture in predetermined order. First the primary amine and the aldehyde were added to produce the imine followed by the addition of the propiolic acid and the isocyanide component. After full conversion towards the Ugi product, the secondary amine was added. Since amines act as both nucleophile and base, no additional catalyst was needed. Thus, a spontaneous reaction with the propiolate without isolation of the Ugi intermediate resulted in regio- and stereo-selective 1,4-disubstituted piperazines with yields greater than 88%.[612,613] The reaction is considered as click reaction according to the guidelines of SHARPLESS, since it possesses an atom efficiency of 100% and no formation of side products is witnessed. Further, the reaction exhibits fast reaction kinetics, simple reaction conditions and product isolation in high yields leading to a wide field of applications.[614]

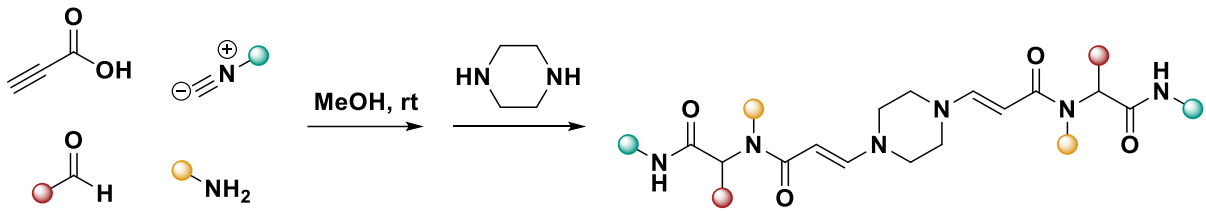

Scheme 33: Stereoselective preparation of enaminonen *via* successive U-4CR/aza-Michael addition one-pot reaction.[612]

In 2014, the same group reported the combination of the U-4CR with an oxa-Michael addition towards the corresponding enols. Deprotonation of the alcohol was necessary, due to the low nucleophilicity. The solvent (methanol) was replaced by EA prior the oxa-Michael addition to avoid the formation of unwanted side product.[615] Alternatively to addition of a catalyst, the acceptor system can be activated by introducing a Brønsted acid.[616]

Although thiols in general are more nucleophilic than amines and alcohols, due to their higher acidity, bases are used as catalyst for the deprotonation.[609] Just recently, the group of DU PREZ reported the use of the thiol-yne and the subsequent reversible thiol-ene reaction for the design of covalent adaptable networks (CAN). Several electron-withdrawing groups for activation of the triple bond were investigated for this purpose. A simple procedure was described, and quantitative yield were observed after 10 min of reaction time. Furthermore, the formation of either the thioenol or the thioacetal was controlled by the equivalents of the added thiol.[617]

Since alcohols, amines, and thiols are the most common commercially available nucleophiles, they are of special interest for the scope of this work to increase the number of permutations for the final product and thus the data storage capacity per molecule (see chapter 2.5.1 for the correlation of permutations and data storage capacity, and chapter 4.6.2 for the data storage capacity of a P-3CR in combination with a hetero-Michael addition). Propiolic acid is readily commercially available and can be directly used in the P-3CR and U-4CR to implement an electron-deficient triple bond, which is highly reactive towards additions of several nucleophiles (schematic overview in chapter 4.6.2, Scheme 49).

3. AIMS OF THE THESIS

In the first part of this thesis, the aim was to investigate possible structure-property relationships and the influence of the dispersity on the self-assembly of a PEG-*b*-PCL diblock copolymer. The to be used synthesis protocols are based on an iterative exponential growth strategy, which were already investigated for the build-up of uniform structures reported in the literature (chapter 0 and 4.2). Due to preliminary results obtained during my master thesis,[618] the main focus is on the careful purification of each compound to ensure their high purity, which is of utmost importance for the investigations of the structure-property relationship of a uniform molecule. The obtained structures are to be compared regarding their thermal properties and their morphologies obtained *via* self-assembly through thermal and solvent-vapor annealing with narrowly distributed BCPs (chapter 4.5). These can be obtained *via* organo-catalyzed ROP of ε-caprolactone using a disperse mPEG initiator.

In connection to this, the determination of the resolution limits of common analytical tools used for purity determination (NMR, SEC, ESI-MS, chapter 4.1.1.3) is a crucial study to identify possible impurities, which might influence the further course of the synthesis or the result of the structure-property study.

Additionally, a novel strategy for the synthesis of uniform PEGs, based on the $GaBr_3$-catalyzed reduction of esters, should be developed (chapter 4.1.2). In order to simplify the purification, the focus is on the optimization of the reduction step. The aim is to achieve full conversion of the ester to the corresponding ether while keeping the overreduction to the alcohol at a minimum. Due to milder reaction conditions and an easier purification protocol, this method presents an alternative to conventional ether syntheses.

The objective of the second part of this thesis is the application of multicomponent reactions in combination with a hetero-Michael addition for the synthesis of molecular data storage devices. The chemoselectivity of both reactions allows an efficient and protection group-free synthesis of the sequence-defined macromolecules, where sidechain definition is introduced in each synthetic step (chapter 4.6.1). To improve the

efficiency of storing digital information in a molecular structure, in terms of a higher writing rate and data density, the synthesis of highly complex small molecules is described (chapter 4.6.2). The resulting molecules can be printed on a surface for an application as write-once, read-often data storage device. The evaluation of their storage capacity and read-out of the information *via* a unique fragment pattern, can be performed *via* MALDI-MS/MS.

In the last part of this thesis, the goal was the molecular data storage with zero synthetic effort and read-out *via* non-fragmenting analysis. For this purpose, commercially available compounds can be used, and the simple read-out is carried out *via* computer assisted GC analysis (chapter 4.6.3).

4. RESULTS AND DISCUSSION

4.1. Uniform PEGs

Parts of this chapter and the associated supplementary information were published before:

Bohn, P., Meier, M.A.R. Uniform poly(ethylene glycol): a comparative study. *Polym J* **52,** 165–178 (2020). https://doi.org/10.1038/s41428-019-0277-1.[274]

Experiments were partly carried out by students under the co-supervision of Philipp Bohn, which are marked with footnotes accordingly.

Abstract

Poly(ethylene glycol) (PEG) is a biocompatible, flexible, and hydrophilic polymer that is widely applied in numerous fields. Especially in pharmaceutical research, PEG is used as a bioconjugate agent for PEG-ylated drugs. A well-defined structure is crucial, since dispersity affects biological activity (e.g., toxicity and efficacy). Thus, intensive efforts to develop synthetic protocols approaching uniformity have been made in recent decades. Different approaches utilizing iterative step-by-step synthesis procedures have yielded promising results, and improvement is still ongoing. In this comparative study, we adopted several procedures for the preparation of uniform PEGs in combination with careful characterization, including size exclusion chromatography (SEC) analysis, which has yet to be reported. Oligo(ethylene glycol)s up to the dodecamer were synthesized. The results obtained were compared in terms of yield and purity with those previously reported in the literature. We clearly show the importance of SEC analysis with high separation capacity in the oligomer range for the synthesis of short-chain oligo(ethylene glycol)s.

4.1.1. Uniform poly(ethylene glycol): a comparative study

Within this chapter, different literature known approaches for the monofunctionalization of oligo(ethylene glycols) (chapter 4.1.1.1) and their subsequent chain elongation *via* ether synthesis (chapter 4.1.1.2) were investigated. The results were compared in terms of yield and purity. In relation to this, a purity study was carried out using different analytical methods, which is presented in chapter 4.1.1.3. Further approaches, such as a chromatography-free method and the synthesis of uniform PEGs *via* macrocyclic sulfates are described in chapters 4.1.1.4 and 4.1.1.5. Afterwards the separate deprotection of the orthogonal protecting groups (chapter 4.1.1.6) and the chain elongation to the hexadeca(ethylene glycol) is demonstrated (chapter 4.1.1.7).

Introduction

PEGs with a low dispersity of $Đ \leq 1.04$ are prepared *via* well-controlled anionic polymerization of 2-(benzyloxy)ethanol, potassium hydride, and ethylene oxide.[619,620] To achieve uniformity (i.e., $Đ = 1.00$), an iterative synthesis approach must be followed. Therefore, desymmetrization by introduction of protecting groups is indispensable, representing a synthetic bottleneck due to the formation of double-protected ethylene glycols as side products. HILL *et al*. reported the synthesis of monofunctionalized PEGs by adopting the BOUZIDE procedure of using stoichiometric amounts of the protecting group and silver(I) oxide (Ag_2O).[236,621] In this way, monobenzyl-, monotrityl-, mono-*p*-methoxybenzyl-, and monotosyl ethylene glycols with three or six repeating units were prepared in yields between 43 and 92%. To avoid stoichiometric amounts of Ag_2O, an excess of less expensive tri- or tetra(ethylene glycol) can be used, which can be easily removed by washing with water. The combination with a slow addition of the protecting group statistically favors monofunctionalization, resulting in yields comparable with those of the silver(I) oxide approach. We therefore started our investigations by adopting different reported procedures for the synthesis of THP-, trityl (Trt)-, and benzyl-protected tri- or tetra(ethylene glycol), as summarized in Scheme 34.

4.1.1.1. Monofunctionalization of PEG-diols

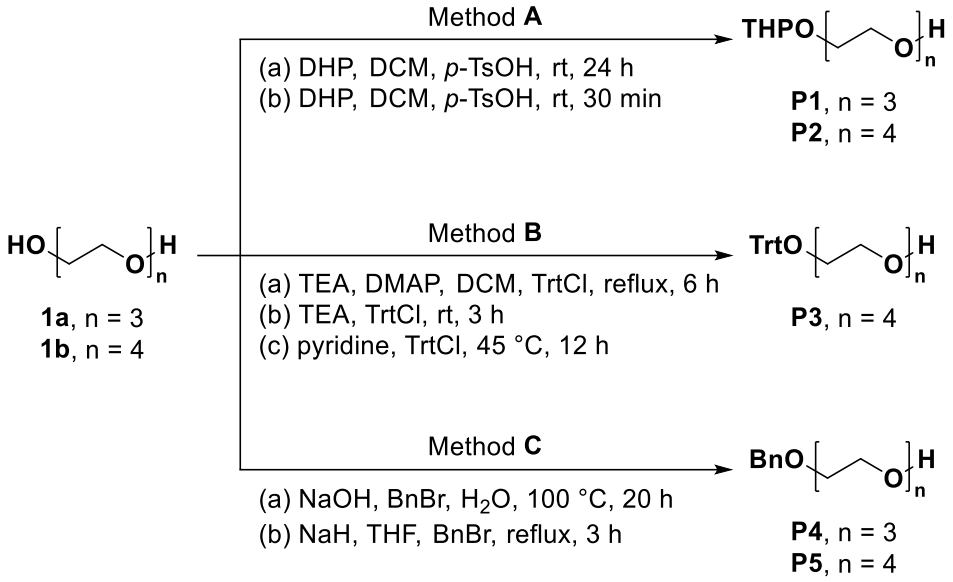

Scheme 34: Desymmetrization of PEG-diols; method **A**: synthesis of mono(tetrahydropyranyl) (ethylene glycol)s **P1** and **P2**; method **B**: different approaches for the preparation of monotrityl tetra(ethylene glycol) **P3** using trityl chloride; method **C**: synthesis of monobenzyl (ethylene glycol)s **P4** and **P5**.

Thus, we were able to compare yields and purity directly for the different approaches. SEC analysis using columns that offer high resolution in the oligomer range proved to be the most important technique for assessing the efficiency of the different approaches in terms of uniformity, especially that of the crude reaction mixtures. The investigated protecting groups were chosen due to the simple purification required after the deprotection step *via* filtration, solvent evaporation, and/or extraction.

The THP protecting group was introduced by applying the chromatography-free reaction protocol of BAKER *et al*.[317] under acidic conditions using *p*-toluenesulfonic acid (0.10 eq.) in anhydrous dichloromethane (Scheme 34, method A). Tri(ethylene glycol) **1a** was used in an excess of five equivalents. Although traces of doubly protected ethylene glycol ($THP_2(EG)_3$) would not influence the subsequent reaction steps, product **P1a** was purified *via* column chromatography, affording a yield of 60.9%. The same reaction was conducted with tetra(ethylene glycol) **1b**, affording the crude mono(THP)-protected PEG_4 **P2a** in a yield of 2.30 g (74.4%). In addition, a procedure for the synthesis of **P2b** described by AHMED and TANAKA was performed.[108] Here, the reaction time was decreased considerably to 30 min. Product **P2b** was obtained in 51.0% yield after purification *via* column chromatography.

Figure 15 shows the SEC traces of the THP-protected ethylene glycols. A significant shift towards a lower retention time was observed for **P2a** and **P2b** compared with tetra(ethylene glycol) **1b**. Interestingly, the crude product **P2a** obtained *via* method **A(i)** exhibits tailing towards higher hydrodynamic volumes, which was ascribed to the doubly protected ethylene glycol *via* NMR analysis. For the purified products **P1a** and **P2b**, symmetric and narrow SEC traces with dispersity indices of $Đ = 1.00$ were obtained, indicating high purity.

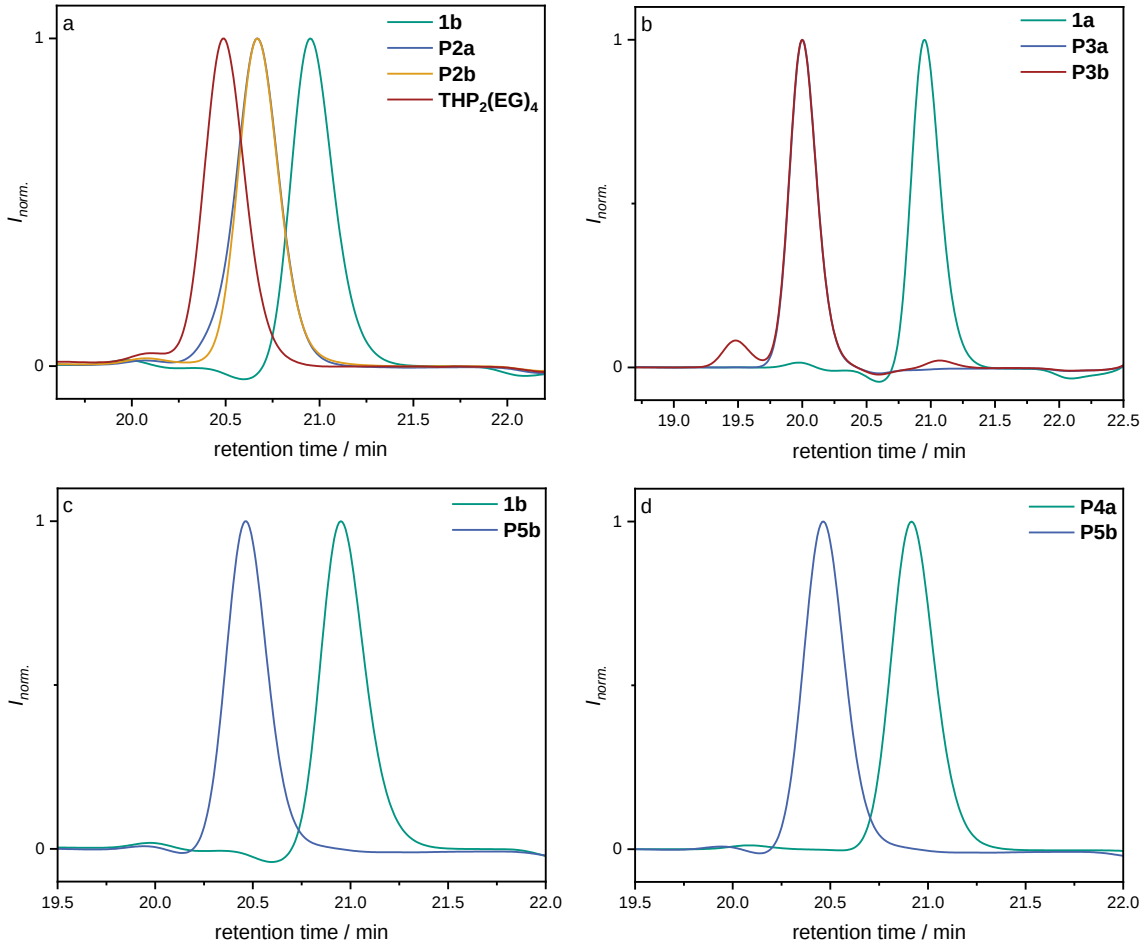

Figure 15: Comparison of the SEC chromatograms of **a** the monotetrahydropyranyl tetra(ethylene glycol) **P2** with tetra(ethylene glycol) **1b** and the doubly protected product ($THP_2(EG)_4$); **b** the crude monotrityl tetra(ethylene glycol) **P3b** and after purification *via* column chromatography **P3a** with tetra(ethylene glycol) **1b**; **c** the monobenzyl tetra(ethylene glycol) **P5b** with tetra(ethylene glycol) **1b**; **d** monobenzyl tri- (**P4a**) and tetra(ethylene glycol) **P5b**.

Monotrityl tetra(ethylene glycol) **P3a** (Scheme 34, method B) was prepared from **1b** using triethylamine, 4-dimethylaminopyridine (DMAP), and trityl chloride.[318] The reaction was refluxed for 6 h, and purification of the product *via* column chromatography afforded **P3a** in 64.6% yield. In another chromatography-free

approach adopted from KINBARA *et al.*, the reaction was performed using DMAP without any additional solvent. The reaction time and temperature were decreased to 3 h and room temperature, respectively.[319] SEC analysis showed a contamination of 8% with symmetric tetra(ethylene glycol) bis-trityl ether and 3% of the starting material, even after several additional washing steps (Figure 15b, **P3b**). The yield of the pure product **P3b** was calculated *via* SEC (88.4%, product not separated). The mixture was used for the next step without any further purification. In a third approach, an increase of 28.6 percentage points in yield compared with that of **P3a** was obtained when following the procedure of DAVIS *et al*.[237] Here, pyridine was used as the base, the reaction was conducted at 45 °C for 12 h, and toluene was used for the extraction instead of DCM. The narrow and monomodal SEC trace of **P3a** (Figure 15b) and **P3c** with a dispersity of $Đ = 1.00$ confirms the uniformity.

Benzyl ether was chosen as an orthogonal protecting group for a trityl- or THP functionality (Scheme 34, method **C**). It was introduced *via* a nucleophilic substitution of an alkali alkoxide and benzyl bromide. Deprotonation was accomplished either with sodium hydroxide under aqueous conditions (Scheme 34, **P4a**, **P5a**)[316] or with sodium hydride in anhydrous tetrahydrofuran (THF)[273] (Scheme 34, **P5b**). The monobenzylated tetra(ethylene glycol)s **P5a** and **P5b** were obtained in comparable yields of 77–83% after purification *via* column chromatography. Hence, our initial comparative study revealed that method **C(a)** is preferred because of its more practicable performance and the avoidance of hydrogen formation. In this way, tri(ethylene glycol) monobenzyl ether **P4a** was synthesized in 72.9% yield. The products were again analyzed with SEC (Figure 15c) in addition to NMR spectroscopy and MS to confirm their purity. A comparison of the monobenzyl tri- (**P4a**) and tetra(ethylene glycol) (**P5a**) is shown in Figure 15d. A difference of 0.45 min in the retention times was observed.

In the literature, the electrophilicity of the mono-protected ethylene glycol is shown to be improved by chlorination with thionyl chloride, which unfortunately leads to bond cleavage (depolymerization) affording a mixture of different chain lengths.[238,324] Therefore, sulfonate esters (mesylate and tosylate) are more suitable for the activation of alcohol functions.[13,321,622] Although the mesylate shows marginally better results in ether coupling than the tosylate, AHMED and TANAKA showed that the tosylation in aqueous THF is more reasonable than the introduction of mesylate in pyridine. In addition, mono-tosylation with subsequent protection is not appropriate because traces

of the formed bis-tosylate must be carefully removed to prevent undesired side products in the subsequent reaction process. Elimination of the mono(THP)- and monotrityl-protecting groups was observed under the tosylation conditions.[108] Here, we adopted the reaction procedure of BRUCE *et al.* (Scheme 35). Bifunctionalized tri- and tetra(ethylene glycol)s (**P6** and **P7**) were obtained after reacting **P4** or **P5** for 15 h in basic aqueous THF with *p*-tosyl chloride. Purification *via* column chromatography afforded the monobenzyl ethylene glycol tosylates in 55.7% (**P6**) and 96.2% (**P7**) yield, respectively. Careful characterization *via* NMR spectroscopy, SEC (Figure 16) and MS revealed the purity of the products. To prevent the degradation of the tosylates, they were stored under argon and shielded from light.

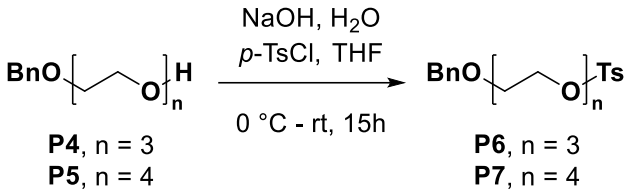

Scheme 35: Tosylation of monobenzyl ethylene glycols **P4** and **P5** according to the procedure of BRUCE *et al*.[273]

A comparison of the SEC traces of the monobenzyl ethylene glycols **P4** and **P5** with the corresponding tosylated products **P6** and **P7** is shown in Figure 16. Narrow peaks with a dispersity of $Đ = 1.00$ and a shift towards lower retention times and thus a higher hydrodynamic volume was observed.

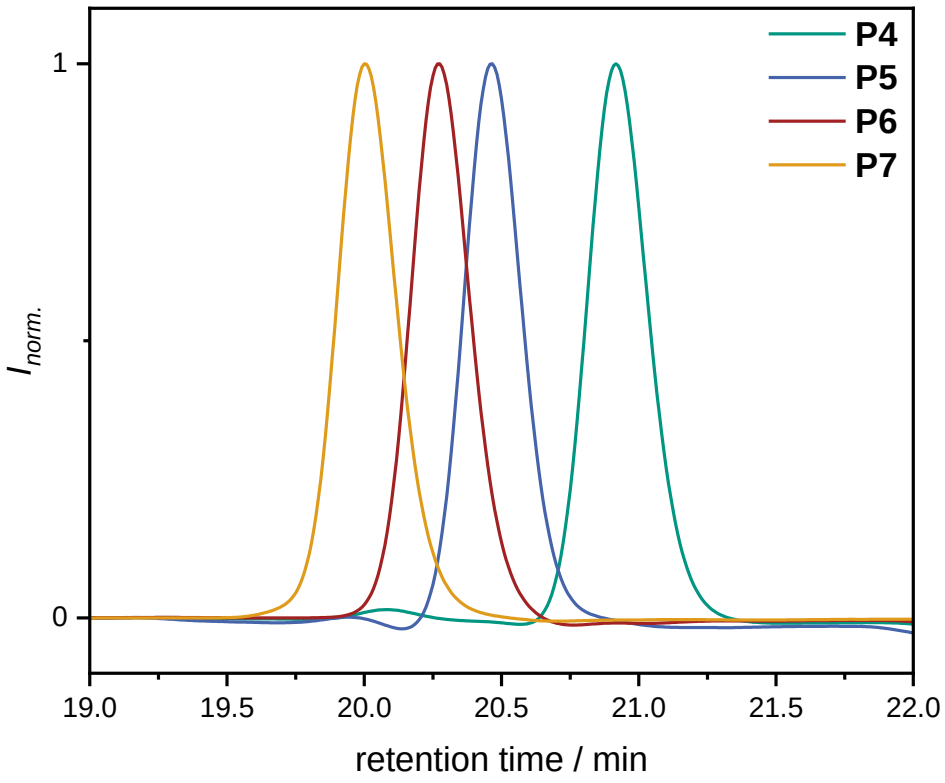

Figure 16: SEC chromatograms of the monobenzyl ethylene glycols **P4** and **P5** and the corresponding tosylates **P6** and **P7**

Chain elongation for the synthesis of uniform PEGs is conducted *via* iterative Williamson's ether synthesis, where elimination under harsh reaction conditions constitutes the most significant side reaction and is thus related directly to the purity of the product.[323] TANAKA *et al*. described the synthesis of PEG_{44} by applying sodium hydride in THF. Unfortunately, chain degradation was observed, induced by the formation of PEG-alkoxides under basic conditions.[108] BAKER *et al*. adopted the TANAKA procedure and added sodium iodide as a catalyst, which undergoes tosylate–iodide exchange in a Finkelstein-type reaction to improve the reactivity of the alkylating agent. Well-defined PEGs were obtained by a chromatography-free method, affording the products of ether coupling in quantitative yields.[317] Substitution of NaH in THF with KO^{t}Bu in DMF and 18-crown-6 was investigated by DAVIS *et al*. The base was added slowly to the reactants to keep the alkoxide concentration as low as possible and thus to prevent chain scission. To simplify the purification by column chromatography, orthogonal protecting groups (Bn, *tert*-butyl, and trityl) were used. Since the trityl- and benzyl ether protecting groups are both cleavable *via* reductive hydrogenolysis, the yields using these protecting groups were significantly lower than those with *tert*-butyl ether. Nevertheless, PEG_{32} and PEG_{48} derivatives were obtained with 98.9 and 98.0%

purity, as indicated by MALDI-MS, which allowed the first exceptional insight into the 3D-PEG morphology and an extended helical secondary structure by X-ray crystallography.[237] Further optimization studies were performed by BRUCE *et al*. with the aim of avoiding the addition of 18-crown-6 to improve the solubility of KO*t*Bu in DMF, as this additive was difficult to separate. To overcome the solubility issue, DMF was replaced by less toxic THF, which is also easier to evaporate. In addition, the reaction temperature was decreased, and the addition of the base was changed due to crystallization issues. In this way, PEGs with a purity >95% after three coupling steps, as indicated by MALDI-MS, were prepared on a multigram scale.[273]

We adopted the above-discussed procedures for the synthesis of uniform PEG oligomers, which were all carried out under an argon atmosphere. Bis-benzyl dodeca(ethylene glycol) **P8** was prepared according to the procedure of BAKER *et al*. (Scheme 36 **P8a**) using sodium iodide as a catalyst.[317] In a second approach, the reaction was performed with KO*t*Bu instead of NaH (Scheme 36 **P8b**), according to the synthesis protocol of BRUCE *et al*.[273]

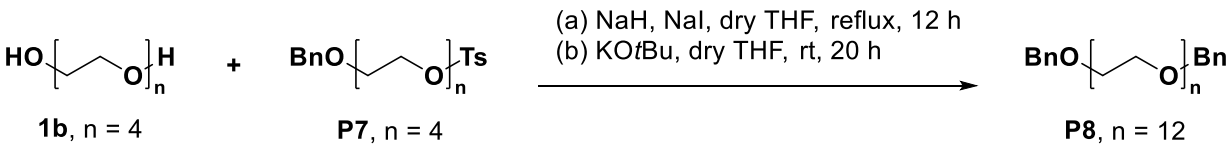

Scheme 36: Symmetrical bis-benzyl dodeca(ethylene glycol) **P8** *via* chain tripling/bidirectional growth.

Based on the findings of TANAKA *et al*., tetra(ethylene glycol) **1b** and monobenzyl tetra(ethylene glycol) tosylate **P7** were used as coupling reagents instead of bis-tosylate and monobenzyl tetra(ethylene glycol), since the elimination product of the monosubstituted intermediate is more difficult to separate from **P8**. Unfortunately, we observed various byproducts by SEC measurements of the crude reaction mixtures (Figure 17a). The SEC traces of **P8a** and **P8b** show the formation of the bis-benzyl dodeca(ethylene glycol) **P8**, as indicated by a significant shift towards a lower retention time of 18.8 min compared with that of the starting materials. Additional peaks beside the product peak were successfully assigned *via* SEC coupled to electrospray ionization-mass spectrometry (SEC-ESI-MS) analysis for **P8b** and are summarized in Supplementary Table 1. Several mono- and bifunctionalized oligo(ethylene glycol)s ranging from monobenzyl octa(ethylene glycol) to bis-benzyl icosa(ethylene glycol), as well as the elimination product of **P7**, were observed. Due to the structural similarity of the formed compound mixture, separation *via* column chromatography was

challenging, and the products were obtained in rather low yields of 12.6% (**P8a**) and 36.5% (**P8b**) with a purity of ≥98% determined by SEC (Figure 17b). These results demonstrate the importance of SEC analysis and clearly show that this synthetic approach leads to unfavorable results.

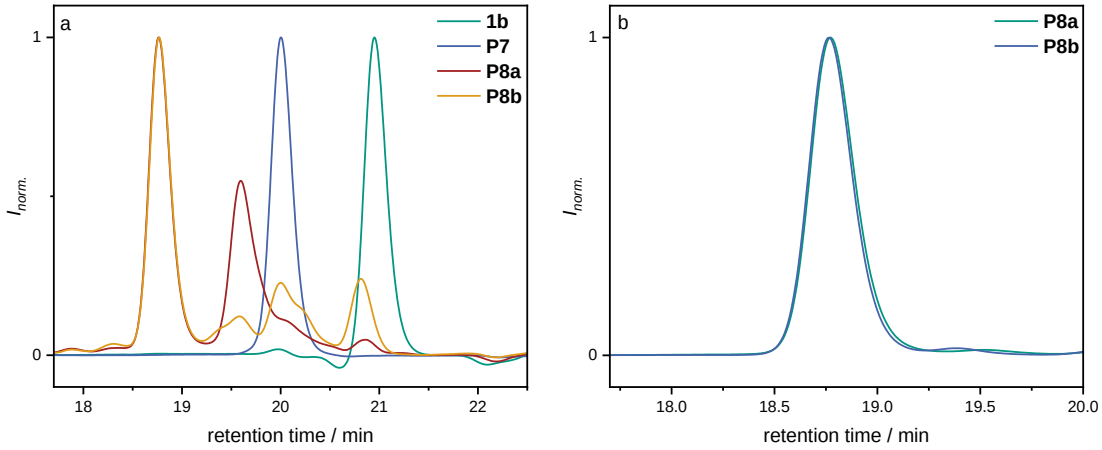

Figure 17 Comparison of the SEC chromatograms of the crude products **P8a** and **P8b** obtained from the starting materials tetra(ethylene glycol) **1b** and monobenzyl tetra(ethylene glycol) tosylate **P7** (**a**); SEC chromatograms of **P8a** and **P8b** after purification *via* column chromatography (**b**).

4.1.1.2. Orthogonally protected PEGs *via* IEG

Although the chain growth for the first two ether couplings is faster in the case of chain tripling/bidirectional growth when compared with the iterative exponential growth, we could not obtain the dodeca(ethylene glycol) **P8** in reasonable yields *via* bidirectional growth (Scheme 36, approaches (a) and (b)). This might be related to improved analytical protocols (*i.e.*, SEC with high resolution). Therefore, attempts to prepare orthogonally protected oligo(ethylene glycol)s by applying iterative exponential growth were conducted. The monobenzyl oligo(ethylene glycol) tosylate **P6** or **P7** was coupled with either mono(THP)- (**P1**, **P2**) or monotrityl tetra(ethylene glycol) **P5**, affording bifunctionalized hepta- and octa(ethylene glycol)s **P9**, **P10**, and **P11**. The reaction conditions were adopted from BAKER *et al*. (Scheme 37 (a))[317] and BRUCE *et al*. (Scheme 37 (b)),[273] which were already applied for the chain-tripling approach.

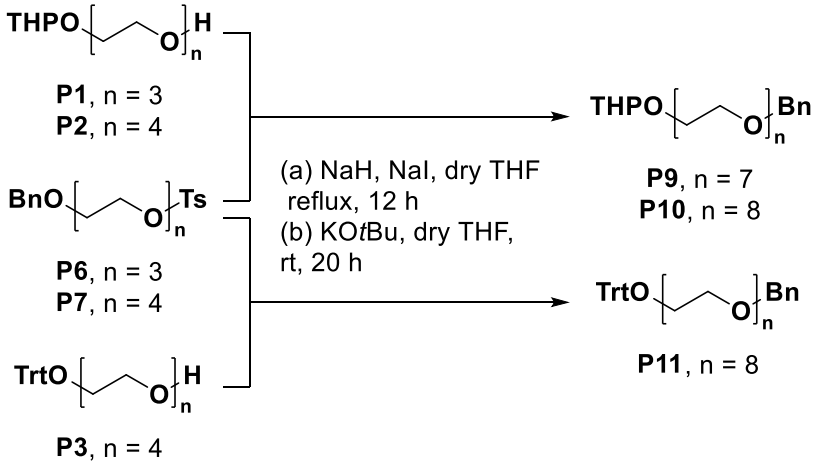

Scheme 37: Ether coupling of monobenzyl oligo(ethylene glycol) tosylate **P6** or **P7** with mono(tetrahydropyranyl)- (**P1**, **P2**) and monotrityl tetra(ethylene glycol) **P3** yielding the corresponding bifunctionalized products **P9**, **P10**, and **P11**

SEC traces of the coupling products before and after purification *via* column chromatography are shown in Figure 18a-c. A peak corresponding to **P7** was observed at a retention time of 20 min in the SEC of method (b), since it was used in an excess of 1.30 equivalents (Figure 18a, b). However, both reaction methods proceeded in a similar fashion. A clear shift to a lower retention time was observed for the formation of products **P9**, **P10**, and **P11**. Smaller impurities were found at a higher hydrodynamic volume and at a retention time of 20.8 min in the case of method (a) (Figure 18a, b). Several masses of byproducts up to the mono-protected hexadecamers were observed by SEC–ESI–MS analysis for the synthesis of **P10b**, which are summarized in Supplementary Table 4. Different solvent systems (DCM:MeOH, DCM:acetone, pure ethyl acetate) were tested, but the separation of the products *via* normal phase column chromatography was difficult, resulting in a decrease in yield. Interestingly, BAKER *et al*. claimed a quantitative yield for the synthesis of **P10a** after drying under high vacuum.[317] In contrast, we obtained a yield of 68.4% for **P10a** and 34.5% for **P9a** after purification *via* column chromatography. Furthermore, the yields of the products prepared *via* method (b) were not constant in repeated trials but were 37.0-47.6% for the octamer and 71.3% for the heptamer. Since the THP protecting group is unstable under acidic conditions, we changed the reported purification protocol and used water instead of 1 M HCl for the washing step. Unfortunately, no considerable increase in yield was observed. Using monotrityl tetra(ethylene glycol) **P3** in the ether coupling (method b), we obtained α-benzyl-ω-trityl octa(ethylene glycol) **P11** (Figure 18c) in 49.6% yield, which is lower than that described in the

literature.[237] However, the high purity of the bifunctionalized ethylene glycols was indicated by NMR spectroscopy, MS, and SEC analysis. In summary, we can reveal that it is possible to distinguish PEG_7 and PEG_8 *via* SEC (Figure 18d), again pointing out the necessity to report SEC traces when working with uniform macromolecules, which is also described in detail in the following chapter.

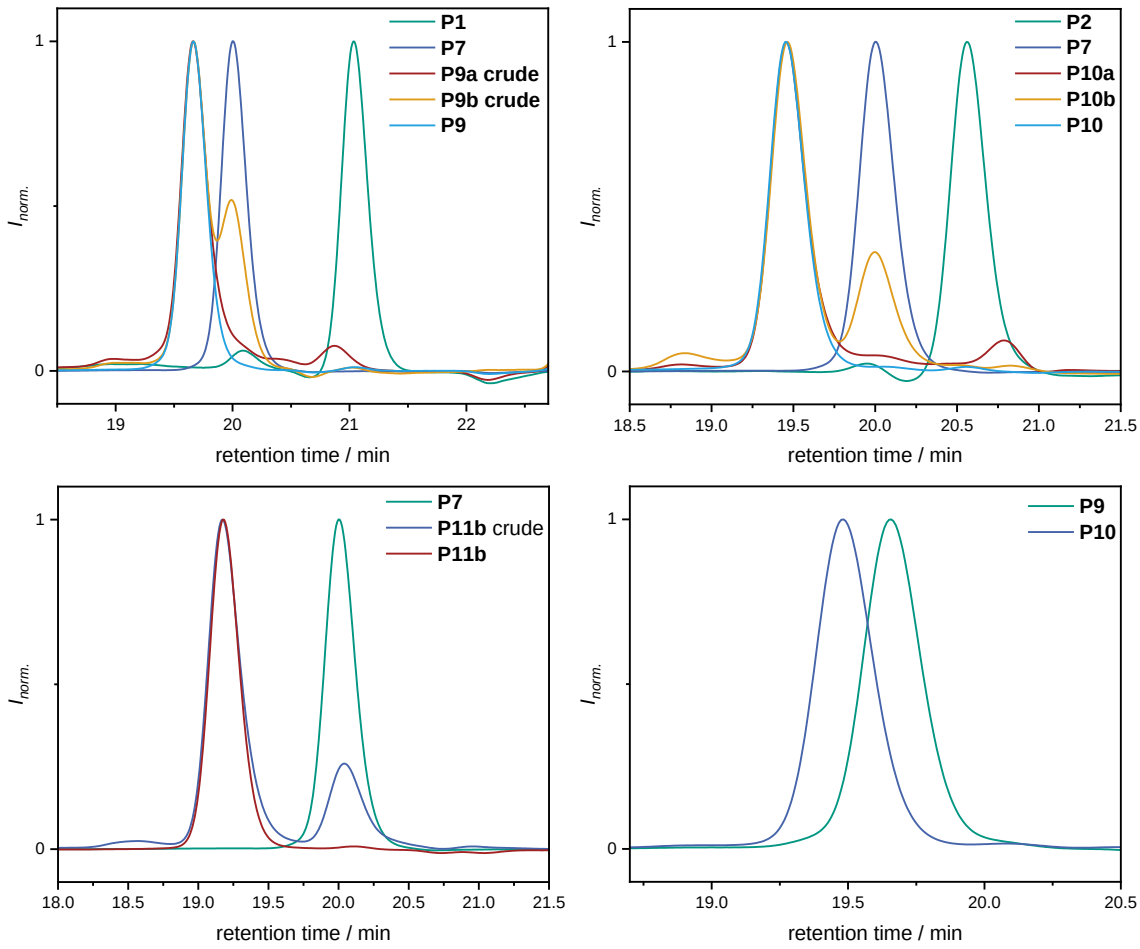

Figure 18: Comparison of the SEC chromatograms the α-benzyl-ω-tetrahydropyranyl (ethylene glycol)s **P9** and **P10** with the mono(tetrahydropyranyl) (ethylene glycol)s **P1** and **P2**, and the monobenzyl tetra(ethylene glycol) **P7** before and after purification; **c** the α-benzyl-ω-trityl octa(ethylene glycol) **P11** with **P7** before and after purification; **d** the doubly protected heptamer **P9** with the octamer **P10**.

4.1.1.3. Insertion: Purity study of PEGs

Where is the limit of purity?

Within the framework of the project “Uniform poly(ethylene glycol)s: a comparative study”, our main focus was on the separation protocols, and the purity determination of PEGs *via* SEC analysis, in addition to NMR and MS of several reported procedures.[274]

Investigations of different samples of the doubly protected octamer **P10** contaminated with varying amounts of the corresponding heptamer **P9**, ranging from 1 to 10wt%, were analyzed by SEC. A broadening in the peaks in the chromatograms was observed with increasing amount of the impurity (Figure 19 a and b). Using a simple peak symmetry analysis, contaminations of 2wt% and more could be clearly observed, thus setting the resolution limit of our SEC instrument to 98%, which is shown in Figure 19 c.[274] Since a careful high-resolution analysis is crucial for the synthesis and characterization of uniform macromolecules, the questions arose, whether these observations also count for further molecular systems and what the resolution limit of other standard analytical tools is.

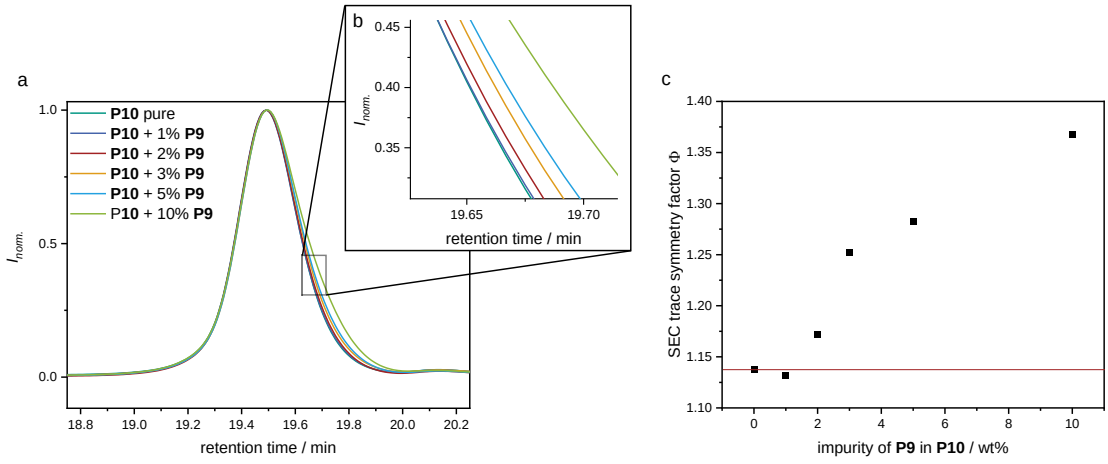

Figure 19: SEC analysis of purity study. **a** Comparison of the SEC traces of α-benzyl-ω-tetrahydropyranyl octa(ethylene glycol) **P10** containing different amounts (wt%) of impurity of α-benzyl-ω-tetrahydropyranyl hepta(ethylene glycol) **P9**. **b** Enlarged detail of the SEC traces. Broadening of the peaks dependending on the amount of **P9** was observed. **c** Analysis of the peak symmetry as a measure for purity of the SEC traces depicted in **a**. The plot indicates that an impurity of 2wt% can be clearly observed by SEC. Φ describes the ratio of integrals of one half of the SEC peak to the other (peak was divided vertically through the peak maximum; the baseline for integration was set to a value of 0.1 to exclude the baseline noise in the calculation of the factor).[274]

For this purpose, three different compound sets, consisting of uniform PEGs, sequence-defined oligo(phenylene ethynylene) (OPEs) and uniform Passerini oligomers were investigated on their purity *via* SEC, ^{1}H NMR spectroscopy and ESI-MS. Therefore, pure oligomers of a certain structure and chain length "n" were contaminated with the corresponding "n-1" oligomer. Ten different samples with an impurity ranging from 1-15wt% were prepared and analyzed. The study was performed in a joint project with DR. MAXIMILIANE FRÖLICH and DR. DANIEL HAHN.[214,223] The synthesis and evaluation of the results shown within the scope of this thesis were performed by PHILIPP BOHN and are discussed in the following section.

To ensure the highest possible purity of the used products, the heptamer **P9** and the octamer **P10** were purified by silica column chromatography for two times, respectively. The corresponding SEC chromatograms and a comparison of the crude and the purified product are shown in the experimental section (Supplementary Figure 19 and Supplementary Figure 20 for **P9** and Supplementary Figure 23 - Supplementary Figure 25 for **P10**). The product fraction **P9 cc2 F13** for the heptamer and **P10 cc3 F2** for the octamer, respectively, showing the narrowest peaks, were further characterized with NMR, IR, and ESI-MS, confirming the high product purity. These samples were then used for the impurity study. As for the other two sequence-defined macromolecule pairs, an amount ranging between 1-15wt% of the (n-1) oligomer (here heptamer **P9**) was added as an impurity to the oligomer with n repeating units (here octamer **P10**).[214,223] For the ^{1}H NMR analysis, the different samples were prepared in a concentration of 20 mg mL^{-1} and were recorded on a 500 MHz instrument with 64 scans at room temperature. The same samples were used in the subsequent characterization *via* SEC and MS. A detailed instrument information and the preparation of the samples is provided in the experimental section 6.2.

A comparison of the ^{1}H NMR spectra and the peak assignment of the pure products **P9** and **P10**, in addition to the mixture samples with 1wt% and 15wt% impurity, are shown in Figure 20. Since the two molecules only differ in one ethylene glycol unit and thus in four protons in the PEG structure, the only distinction is the integral of the backbone signal **5**. As observed from the integral values, the number of protons did neither match with the molecular structure, nor correlate with the added amount of impurity.

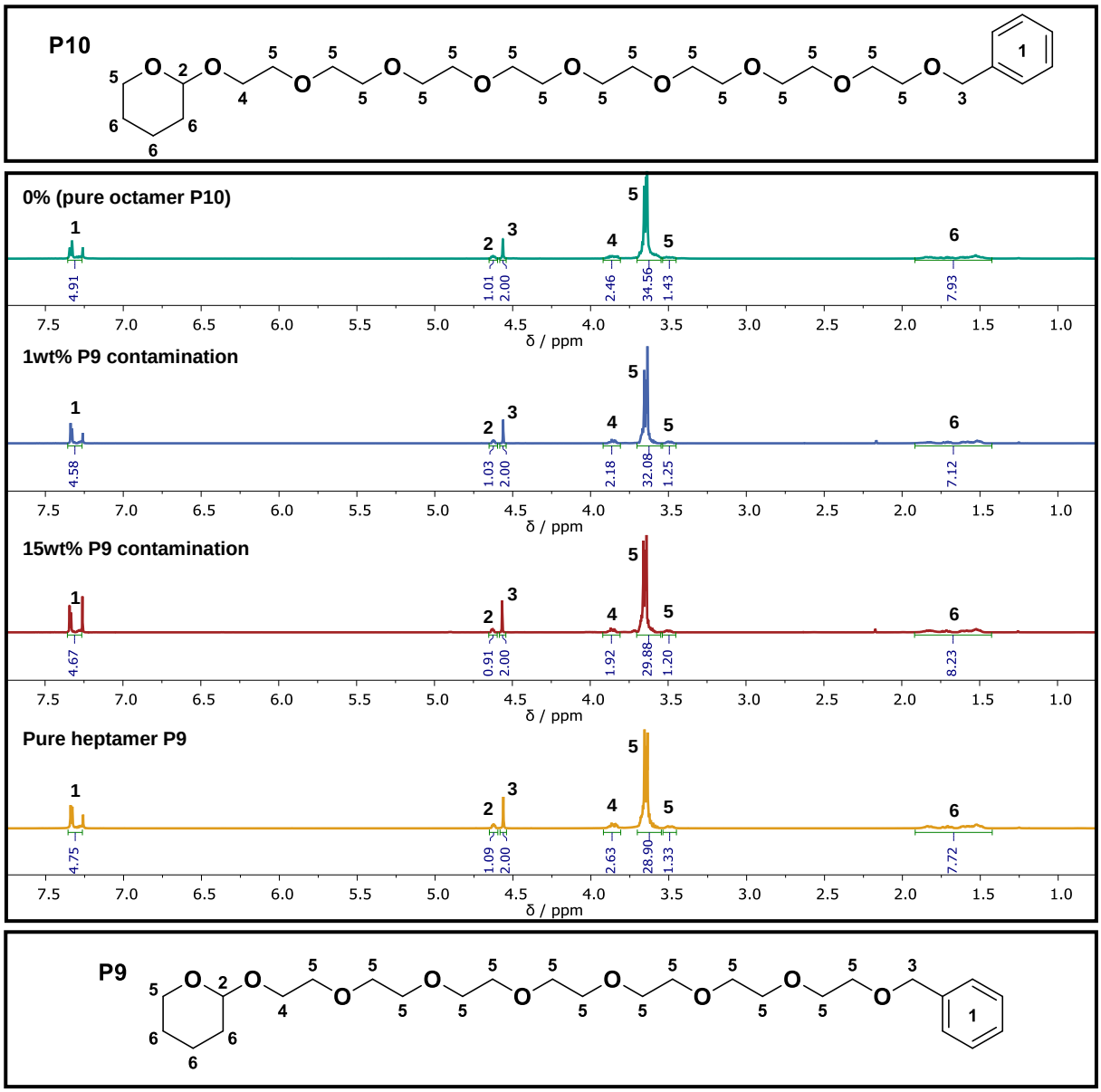

Figure 20: Comparison of the ^{1}H NMR spectra of the doubly protected octamer **P10** and the corresponding heptamer **P9**, and mixtures containing 1wt% and 15wt% impurity, respectively.

The resonance of the aromatic protons was assigned to signal **1**, whereas the CH_2-group of the benzyl ester showed a peak at 4.56 ppm (signal **3**). Signals at 4.63 ppm and in the range of 1.92-1.42 ppm were assigned to the CH- and the methylene protons of the THP protecting group (**2** and **6**). The ethylene backbone signals and the CH_2-group of the THP moiety next to the oxygen were assigned to the signals ranging from 3.92-3.45 ppm (signals **4** and **5**), which were used for the evaluation of the individual mixtures, in reference to the benzyl methylene peak. Since the sum of the protons of signals **4** and **5** for the doubly protected octamer **P10** is 34, and for the corresponding heptamer **P9** 30, the integral value should in principle decrease with an increasing amount of heptamer impurity. The calculated data up to

the octamer sample containing 15 wt% heptamer **P9**, show the expected negative linear trend and are compared with the experimental results depicted in Figure 21. Since the start and end point of the integral immensely influences the result, six volunteer colleagues with experience in NMR evaluation were asked to integrate signals **3** and **4**+**5** independently from each other, without giving advice on how to integrate. This resulted in two trends, which are highlighted in green and red (Figure 21). The red highlights in Figure 21 were evaluated by persons 2, 3 and 4, showing a constant decrease of the number of protons depending on the increase of the impurity. The average values and the linear fit are depicted in blue. Interestingly, the lines are concurrent to each other, intersecting in x = 0, y = 34, which leads to an increasing deviation with increasing wt% of impurity. Compared to the calculated values (black squares), the slope of -0.1 protons per added wt% of impurity is too steep, as the extrapolation would result in a value of 29 protons for a mixture of 1:1, which is below the theoretical minimum of 30 protons for the pure heptamer. On the other hand, the results of the integrations made by persons 1, 5 and 6 showed a quasi-exponential decay for a small degree of contamination but might change to a more linear progression for a higher amount of impurity, depicted by the green straights in Figure 21, which run parallel to the calculated fit. To further confirm this, mixtures containing a higher percentage of heptamer impurity must be prepared and analyzed. However, in each evaluation, the integral values for 1wt%, and partially 2wt% of impurity, are above the maximum number of theoretical protons, and from a value of 3wt% onwards, a trend could be observed, thus setting the resolution limit of the NMR instrument to 97%. The measured values for 5wt% impurity are clearly off the trends and could be caused by pipetting errors. Due to the large deviation, it was not considered for the linear fit.

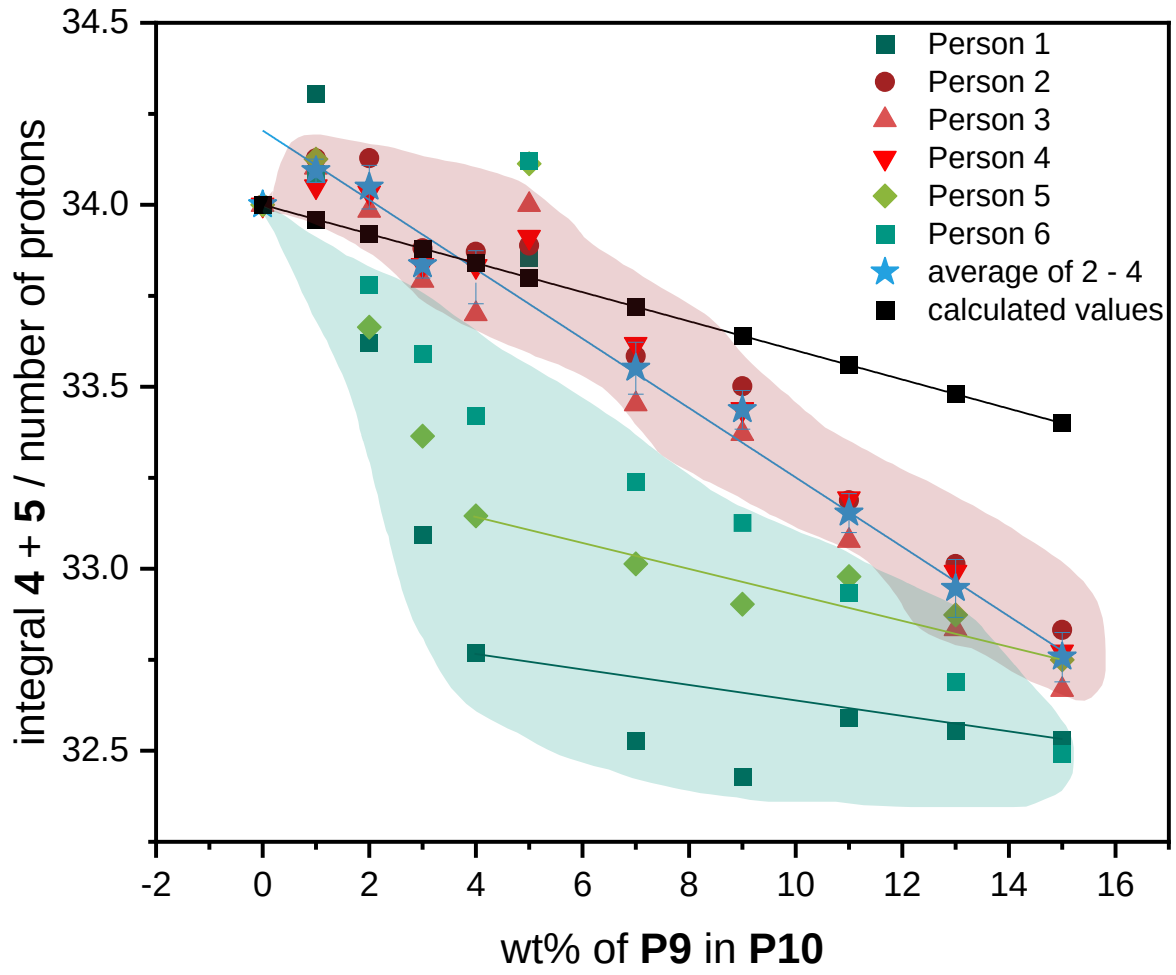

Figure 21: Plot of the observed integrals against the contamination of heptamer **P9** in wt% in the octamer **P10**. The black squares and the linear fit are the calculated values. The integral values highlighted in red obtained from person 2, 3 and 4 follow a linear trend. The corresponding average values and the linear trend are plotted in blue. The integral values highlighted in green, obtained from person 1, 5 and 6, showed a quasi-exponential decay for a small degree of contamination but might change to a linear progression for a higher amount of impurity depicted by the green straights.

In summary, NMR spectroscopy is a powerful tool to determine the purity of a certain compound, if the impurity peak pattern is known and is not overlapping with that of the analyte. Since the main impurities in sequence-defined oligomers are unreacted precursor compounds, they are of the same kind of structure, only varying in the chain length. Thus, the chemical shifts are identical and purity determination *via* NMR becomes challenging, as demonstrated for the doubly protected octamer **P10** containing different amounts of heptamer **P9** impurities. Similar challenges were observed for the uniform OPEs and the sequence-defined Passerini products, as described by FRÖLICH and HAHN.[214,223] For the latter compounds, a pentamer was contaminated with the corresponding tetramer and it was possible to successfully

identify the impurity level from 5wt% onwards *via* end-group analysis.[214] In contrast, even with an impurity of 15wt% of an OPE trimer mixed into the corresponding tetramer, no significant difference was observed compared to the pure tetramer.[223] This clearly shows that the NMR itself is not sufficient to confirm the purity of the compound pairs presented here. Furthermore, it demonstrates the importance of a multidimensional analysis for the characterization of molecules in general.

SEC analysis was performed in a concentration of 2 mg mL^{-1} and the measurements were recorded in THF on a Shimadzu instrument at 30°C for all of the molecule pairs. The system was equipped with two separation columns with a high resolution for oligomer structures. Three measurements were taken of each sample directly one after another and the average chromatograms are shown in Figure 22 a. Because of the little mass difference of only 44 g mol^{-1}, the hydrodynamic radii of the structures were very similar. Therefore, these measurements are close to the resolution limit of the instrument and thus the detection of the impurity percentage was the most challenging for the SEC. The peaks were superimposed at 19.6 min and a y-value of 0.1. In the magnitude, the trend of the peak broadening with an increasing amount of impurity is clearly visible (Figure 22 b). In contrast to the previous study, where the purity level was determined *via* the peak symmetry,[274] within this study, we calculated and compared the peak width at a threshold of y = 0.1. The peak width Ω, determined by a three-fold determination, is plotted against the wt% of the contamination of the doubly protected heptamer **P9** in the octamer **P10** (Figure 22 c). A linear trend was observed and even a sample containing an impurity of only 1wt% was successfully distinguishable from the pure octamer. The samples of the 4 and 5wt% impurity exhibit approximately the same peak width, which is in accordance with the observed overlap of the yellow and orange trace in Figure 22 b.

Compared to the Passerini molecules and the OPEs, where the difference in the hydrodynamic volume of the compared oligomers is higher than for the uniform PEGs, 1wt% of impurity was clearly observed, as a separate signal, already in the raw chromatograms, thus no further calculations of the peak width or peak symmetry were performed.[214,223] In contrast, as already mentioned above, the change in the hydrodynamic volume of a doubly protected octa(ethylene glycol) and the corresponding heptamer is not that significant, resulting in a peak broadening instead of the formation of a separate signal. Therefore, individual calculations were performed to determine the purity of the samples. Furthermore, a reference of the pure substance

is needed to evaluate the difference in the peak shape of a certain sample. Until now, we reported the identification of a 2wt% impurity with analysis of our SEC system.[274] Within this study, we demonstrated the successful determination of 1wt% impurity for three different compound sets (PEGs, OPEs[223] and Passerini oligomers[214]), and thus the importance of SEC analysis for the confirmation of uniformity of oligomeric structures.

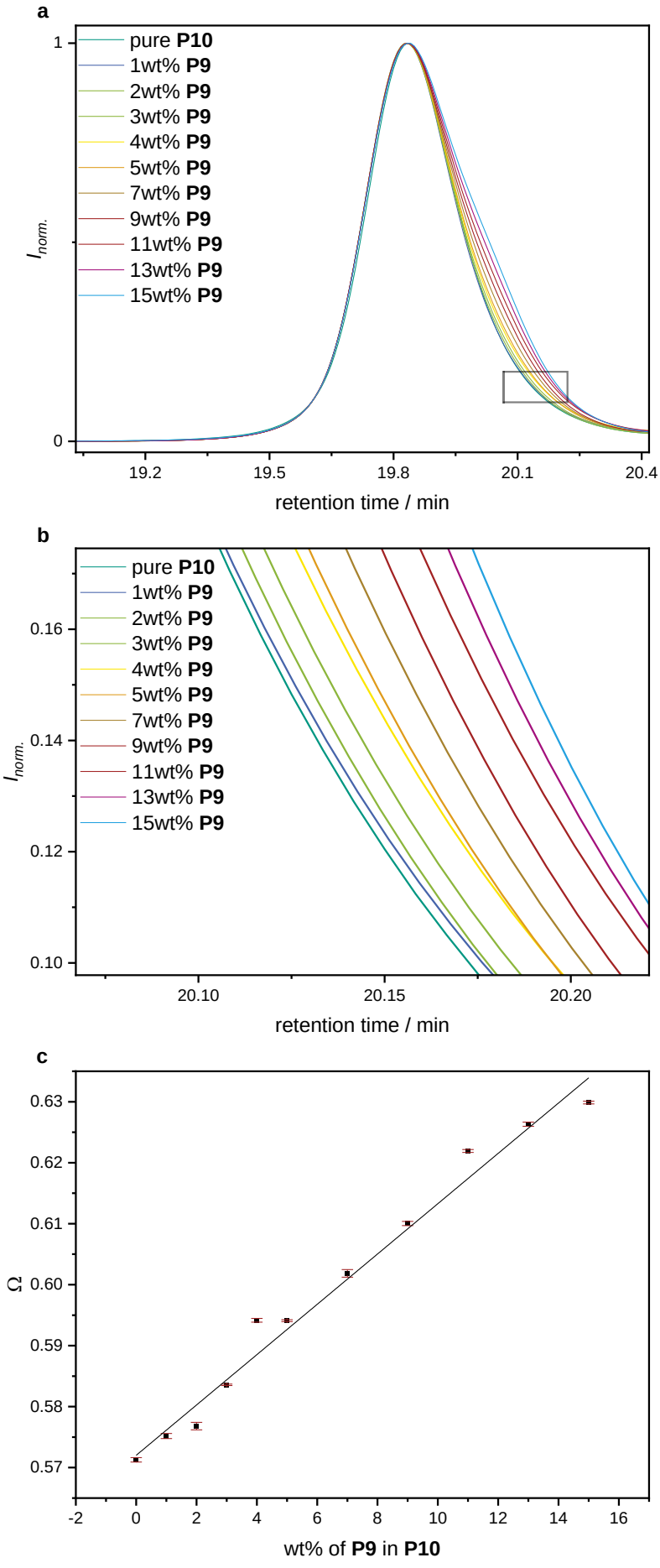

Figure 22: (a) SEC chromatograms of the octamer **P10** contaminated with different quantities of the heptamer **P9** (1-15wt%). The individual chromatograms were superimposed at a retention time of 19.6 min. and a y-value of 0.1. The averaged chromatograms calculated from the three-fold determination was plotted; (b) detailed section to highlight the trend of the peak broadening with an increasing amount of impurity; (c) plot of the peak width Ω at a threshold of y = 0.1 against the wt% of the contamination of the double protected heptamer **P9** in the octamer **P10**.

To complete the standard analysis protocol, ESI-MS of the different samples was performed. The mass spectrum of the uniform doubly protected octamer **P10**, which was purified three times *via* column chromatography, is shown in Figure 23 a. The masses of the ammonium adduct ($[M+NH_4]^+$ = 562.3591 Da), the sodium adduct ($[M+Na]^+$ = 567.3141 Da) and the potassium adduct ($[M+K]^+$ = 583.2878 Da) were observed. In the area highlighted in green, the mass of the corresponding heptamer was expected. The signals were only visible in a zoomed in view of this section at low intensities of <0.06 in relation to the sodium adduct of the octamer, which was normalized to a value of 100. Similar to the detected mass of the octamer, also of the heptamer **P9** the ammonium adduct ($[M+NH_4]^+$ = 518.3327 Da), the sodium adduct ($[M+Na]^+$ = 523.2882 Da) and the potassium adduct ($[M+K]^+$ = 539.2623 Da) were observed. According to the official definition of a “uniform polymer” by the IUPAC, this molecule must be stated as uniform compound related to SEC analysis. Although, this was the highest purity we were able to achieve according to the given purification methods, the analysis *via* ESI-MS of the samples containing impurities of the heptamer ranging from 1-7 and 15wt% was performed. The mass spectrum for the sample with 1wt% impurity is shown in Figure 23 a, and the slight traces of the heptamer were already observed without magnification, underlining the high sensitivity and resolution of the analysis tool. The detailed mass area of the sodium adduct of the heptamer ($[M+Na]^+$ = 523.2882 Da) is shown in Figure 23 b and the increase of the signal intensity with increasing wt% of heptamer in the sample was clearly observed. ESI-MS is suitable for quantitative analysis, since the ion signal is proportional to the analyte concentration, under certain circumstances, *e.g.,* concentration limit of the detector or ionization efficiency of the compound. Typically, an internal standard, similar to the structure of the analyte, is required. Since all samples contained the analytes in a known concentration, we have not added an additional internal standard. Due to the structural similarity of the compared products, the ionization efficiency, which is strongly compound dependent, was neglected. The relative peak intensity of the sodium adducts of the heptamer relative to sodium adducts of the octamer in relation to the wt% of the impurity are shown in the experimental section in Supplementary Figure 27. A linear trend up to an impurity content of 7wt% was observed. However, since the quantitative MS analysis was not the aim within this study, the use of an internal standard was renounced and thus the results are not as accurate as when using an internal standard.

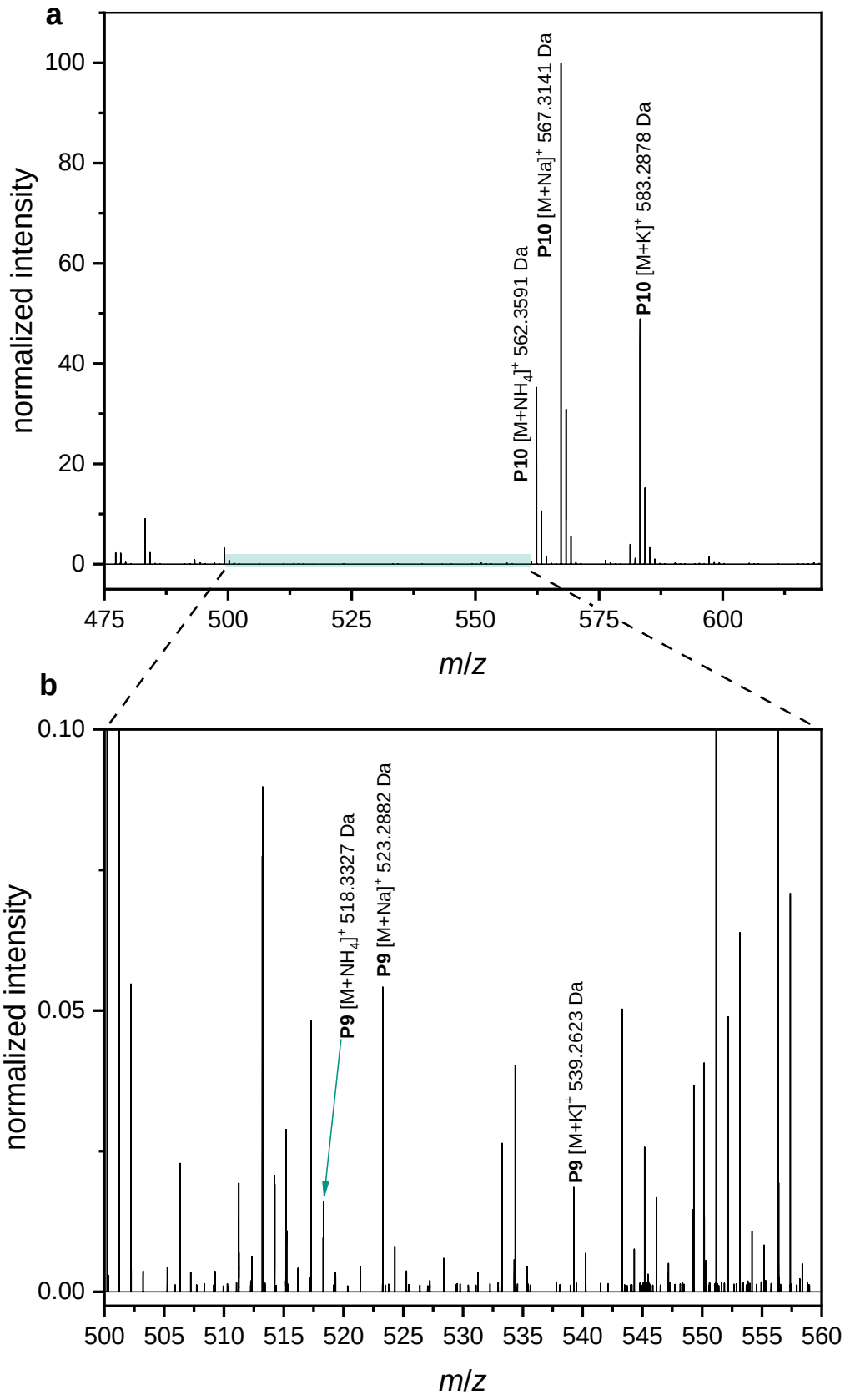

Figure 23: ESI-MS spectrum of the octamer **P10**. **a** The mass of the NH_4, Na, and K adducts of the product were found. **b** The detailed section of the area highlighted in green revealed, that product **P10** already contained traces of the heptamer **P9**, even after further purification. The corresponing masses of the NH_4, Na, and K adducts were observed with a low relative intensity of <0.06.

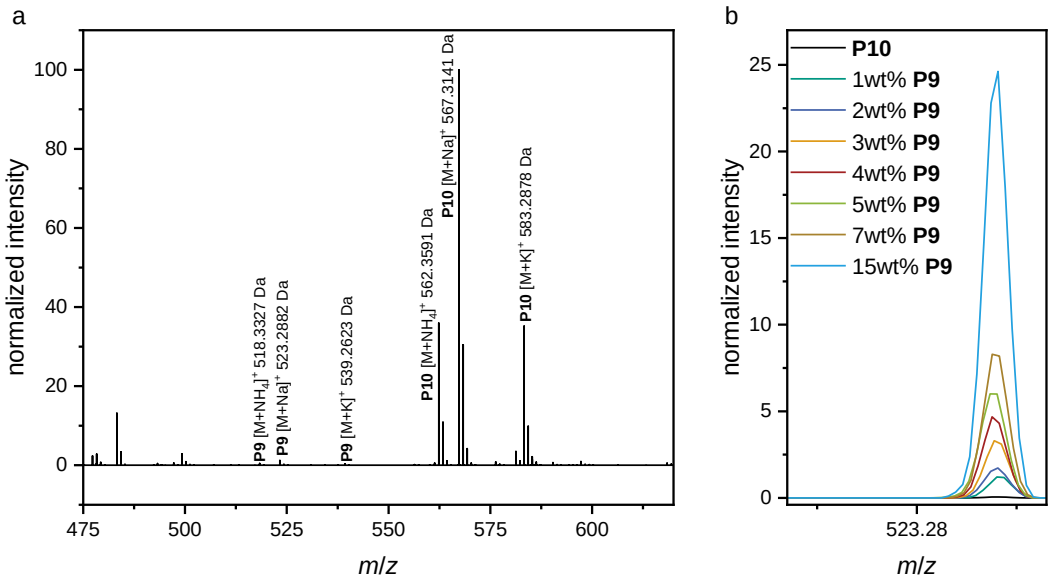

Figure 24: **a** ESI-MS spectrum of the doubly protected octamer **P10** contaminated with 1wt% of the doubly protected heptamer **P9**. **b** detailed section where the signal of the sodium adduct of the doubly protected heptamer ($[M+Na]^+$ = 523.2882 Da) is expected. Various samples containing different wt% of heptamer impurity are compared.

In summary, this study showed the challenges in analysis and determination of the purity of uniform PEGs, contaminated with different wt% of the (n-1)-oligomer. ^{1}H NMR spectroscopy, SEC and ESI-MS were used, and their individual resolution limit was rigorously proven, regarding structural similarity and small mass difference of the analytes. ^{1}H NMR analysis provided the most ambiguous results. However, from 3wt% impurity on, a trend in the experimental results was observed, nevertheless leaving a great challenge for practical determination of impurities by ^{1}H NMR. On the other hand, SEC allowed the determination of 1wt% impurity and with ESI-MS, even in the pure substance, low amounts of impurity were detected. In summary, there is not one standalone analytical method for determining the purity of a compound. Each of the mentioned tools has its strengths and weaknesses in a certain field of application, and therefore the combination of several analytical instruments is inevitable for both the characterization of a substance and the determination of purity.

4.1.1.4. Chromatography-free approach

To avoid tedious purification *via* column chromatography, KINBARA *et al*. established a chromatography-free approach for the synthesis of well-defined asymmetric PEGs. Making use of the functionalization-dependent distribution of PEGs between the organic and aqueous phases, an iterative monofunctionalization of tetra(ethylene

glycol) is described (Scheme 38).[319] A trityl protecting group was used as a hydrophobic tag, as well as a *p*-toluenesulfonyl moiety, which also acted as a leaving group in Williamson ether coupling. Bis-trityl-protected PEG byproducts, which did not interfere in further reactions, were transferred to the subsequent step, and could be easily removed after the final deprotection step *via* liquid–liquid extraction. Since products that differ in one ethylene glycol unit, resulting either from the base-induced depolymerization or from impurities in the starting material, cannot be separated during the extraction step, a suitable analytical method was crucial to verify uniformity. Taking advantage of the *p*-toluenesulfonyl group as a chromophore for UV detection, reverse-phase HPLC (RP-HPLC) previously showed a higher resolution in comparison with MALDI measurements, demonstrating that MS is not a suitable method for quantitative dispersity analysis.[623]

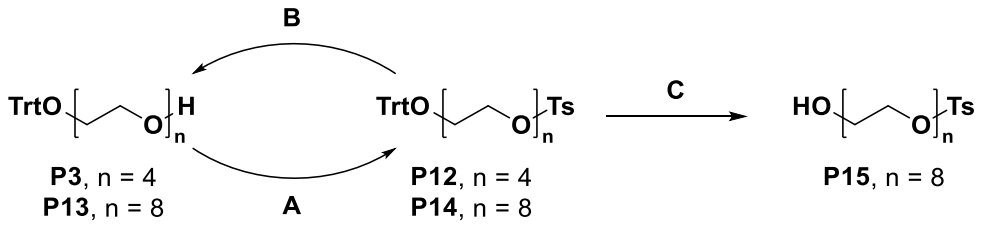

Scheme 38: Chromatography-free approach for the synthesis of monotrityl oligo(ethylene glycol)s. **A**: tosylation of the monotrityl ethylene glycol. **B**: monofunctionalization of tetra(ethylene glycol) with NaH. **C**: deprotection of the trityl ether with *p*-toluenesulfonic acid.

In this way, PEG_8-Ts (72% yield over five steps, 98.7% RP-HPLC purity), PEG_{12}-Ts (63% over seven steps, 98.2% RP-HPLC purity), and PEG_{16}-Ts (62% yield over nine steps, 97.0% RP-HPLC purity) were prepared on multigram scales. The limitation of this procedure was investigated, since PEG tosylate with a certain chain length prefers the aqueous phase during the extraction step, but even the PEG_{24}-tosylate remained quantitatively in the organic layer, as indicated by HPLC analysis. Here, monotrityl tetra(ethylene glycol) **P3b** (contaminated with 8% of bis-trityl tetra(ethylene glycol), as indicated by SEC analysis) was activated *via* tosylation, and **P12** was obtained in quantitative yield, still contaminated with 8% bis-trityl tetra(ethylene glycol), which was used in the subsequent step without further purification. In the coupling step, NaH was used as the base, and tetra(ethylene glycol) **1b** was added in an excess of 7.32 equivalents, leading to monotrityl octa(ethylene glycol) **P13** in quantitative yield. Another tosylation was performed, affording **P14** in 95.9% yield. In the last two steps, an additional impurity of bis-trityl dodeca(ethylene glycol) (2%) was observed in the

SEC chromatogram. In the final reaction step, the trityl protecting group was cleaved under acidic conditions, affording the crude octa(ethylene glycol) monotosylate **P15** in an overall yield of 66.3% in five steps, which is 5–10% lower than that reported in the literature.[319] However, SEC indicated a contamination with 12% impurities at a lower retention time (Figure 25 a); thus, purification of product **P15** *via* column chromatography was necessary after the final step, resulting in a 2.5% loss of the product (63.8% final yield). The crude and isolated yields are summarized in Table 1. The results demonstrate that a chromatography-free approach with an optional final purification step is a practical synthetic option.

Table 1 Comparison of crude and isolated yields for the chromatography-free approach

#	Scale / mmol*	m_{crude} / g[a]	$yield_{crude}$ / %	$yield_{Lit}$ / %	$purity_{Lit}$ / %[319]	$purity_{crude}$ / %[c,319]	$yield_{isolated}$ / %	$purity_{isolated}$ / %
P3b	44.8	17.3	88.4	*ca.* 87	93	92	-	-
P12a	39.6	24.5	quant.	*ca.* 99	93	92	-	-
P13	39.6	22.3	99.2	*ca.* 90	88	90	48.2	≥98
P14	31.7	23.3	95.9	*ca.* 99	88	90	49.5	≥98
P15	28.2	11.7	78.8	*ca.* 99	97.7[b]	88	75.9	≥98

* Indicates approximately half of the literature scales; [a] not considering impurities indicated by SEC analysis; [b] determined by RP-HPLC; [c] determined by SEC.

SEC chromatograms of each step are shown in Figure 25 (before (a) and after purification *via* column chromatography (b)). The contamination of the bis-trityl tetra(ethylene glycol) at 19.5 min is no longer visible in **P12a**, since the retention time is similar. Narrow and monomodal peaks with a dispersity of $Đ = 1.00$ were obtained for the single products after purification.

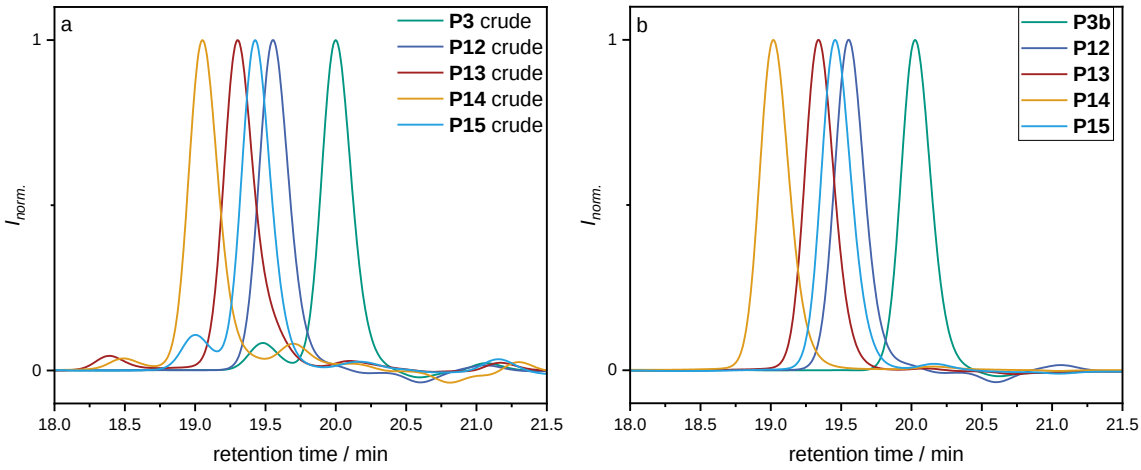

Figure 25: **a** SEC chromatograms of the monotrityl tetra(ethylene glycol) **P3**, the corresponding tosylate **P12**, monotrityl octa(ethylene glycol) **P13**, the corresponding tosylate **P14**, and octa(ethylene glycol) monotosylate **P15** before purification; **b** after purification *via* column chromatography.

4.1.1.5. Macrocyclization of ethylene glycols

Recently, JIANG *et al*. reported the synthesis of uniform PEG derivatives *via* nucleophilic ring opening of an MCS. Macrocyclization was performed with several diols and thionyl chloride at a rather high concentration of 0.04 M, followed by in situ oxidation of the cyclic sulfite with ruthenium tetroxide (RuO_4) (Scheme 39). A variety of different nucleophiles were used for the nucleophilic ring opening, giving PEG derivatives in yields of 34–99%.[318] Since this method avoids the use of protection and activation steps, it is an adequate alternative to previously described procedures. Furthermore, JIANG *et al*. reported the scalability and versatility of this method, *e.g*., for the synthesis of dual-functional PEGs,[624] as well as the preparation of an α-amino-ω-methoxyl dodeca(ethylene glycol) on a 53-g scale, high purity determined by ^{1}H NMR and an overall yield of 61% in eight steps.[625]

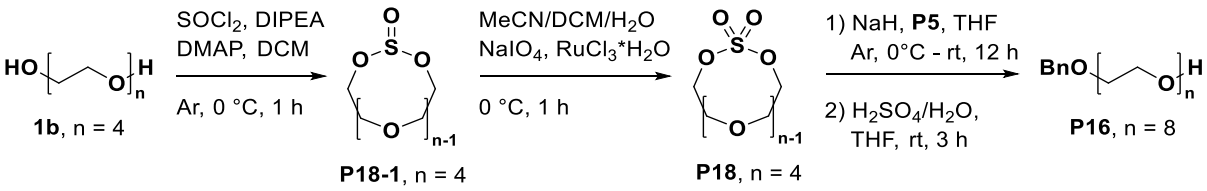

Scheme 39: Macrocyclization of tetra(ethylene glycol) **1b** with thionyl chloride towards the macrocyclic sulfite **P18-1**, in situ oxidation with RuO_4 affording the macrocyclic sulfate **P18** and subsequent nucleophilic ring opening using monobenzyl tetra(ethylene glycol) **P5** yielding the monobenzyl octa(ethylene glycol) **P16.**

Unfortunately, even at lower concentrations of 0.01 M, we observed the formation of larger macrocycles in SEC traces for the macrocyclization of tetra(ethylene glycol) **1b**, up to the cyclic pentamer (Figure 26), which was further confirmed by SEC-ESI-MS analysis (Supplementary Table 7 and Supplementary Table 8). Interestingly, the approach at a concentration of 0.02 M showed the lowest side product formation and was therefore used for in situ oxidation (Figure 26a). The MCS was purified *via* column chromatography, affording product **P18** in 59.7% yield, which was used in a nucleophilic ring opening with monobenzyl-protected tetra(ethylene glycol) **P5**, leading to the monobenzyl octa(ethylene glycol) **P16**. Due to ring formation, the hydrodynamic volume decreases, resulting in a shift of the product peak of **P18-1** towards a higher retention time, whereas cyclic oligomers were observed at a lower retention time compared with tetra(ethylene glycol) **1b** (Figure 26). As a result of the nucleophilic ring opening with monobenzyl tetra(ethylene glycol) **P5**, a clear shift towards a lower retention time was observed. Unfortunately, we were not able to reproduce the results described by JIANG *et al*. ESI–MS analysis confirmed the formation of the desired product **P16**, but we also observed a side product at a lower retention time in SEC, which we could not assign to products of the ring opening of larger macrocycles.

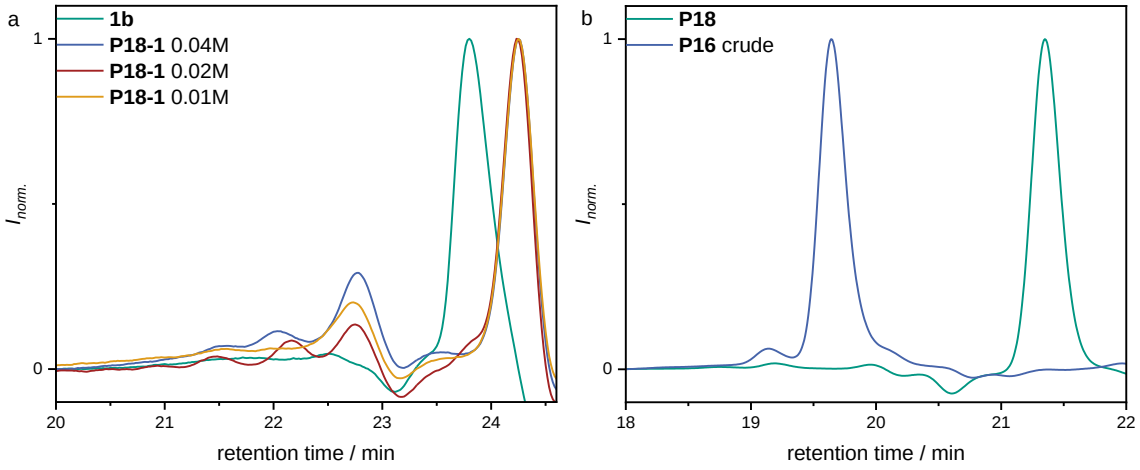

Figure 26: Comparison of SEC chromatograms for the macrocyclization of tetra(ethylene glycol) 1b towards the macrocyclic sulfite **P18-1** at different concentrations (**a**). Nucleophilic ring opening of the macrocyclic sulfate **P18** yielding the benzyl octa(ethylene glycol) **P16** (**b**).

4.1.1.6. Separate deprotection of the α-benzyl-ω-tetrahydropyranyl octa(ethylene glycol)

Nevertheless, to complete the IEG, orthogonal deprotection of α-benzyl-ω-tetrahydropyranyl octa(ethylene glycol) **P10** was performed separately (Scheme 40). The THP-ether was deprotected under acidic conditions according to the procedure of BAKER *et al*.,[317] affording the monobenzyl octa(ethylene glycol) **P16** in 97.7% yield.

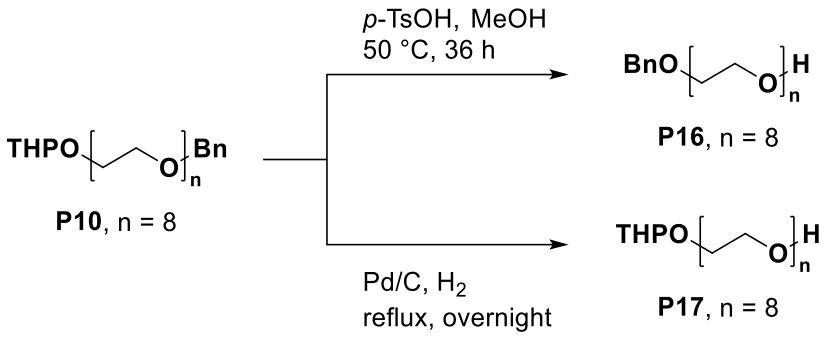

Scheme 40: Separate deprotection of α-benzyl-ω-tetrahydropyranyl octa(ethylene glycol) **P10**.

Reductive hydrogenation under reflux conditions was conducted to cleave the benzyl protecting group, resulting in mono(THP) octa(ethylene glycol) **P17** in 98.9% yield. A comparison of SEC chromatograms of products **P16** and **P17** with starting material **P10** is shown in Figure 27. Significant shifts towards higher retention times were observed due to a decrease in the hydrodynamic volume. A narrow peak was observed for product **P17**, whereas peak broadening occurred after benzyl deprotection, which could be the result of complete deprotection towards the octa(ethylene glycol), since the mass was determined from the ESI-MS spectra as well. Furthermore, the mass of bis-benzyl octa(ethylene glycol) was found in product **P16** and the mass of bis-tetra(hydropyranyl) octa(ethylene glycol) in product **P17**.

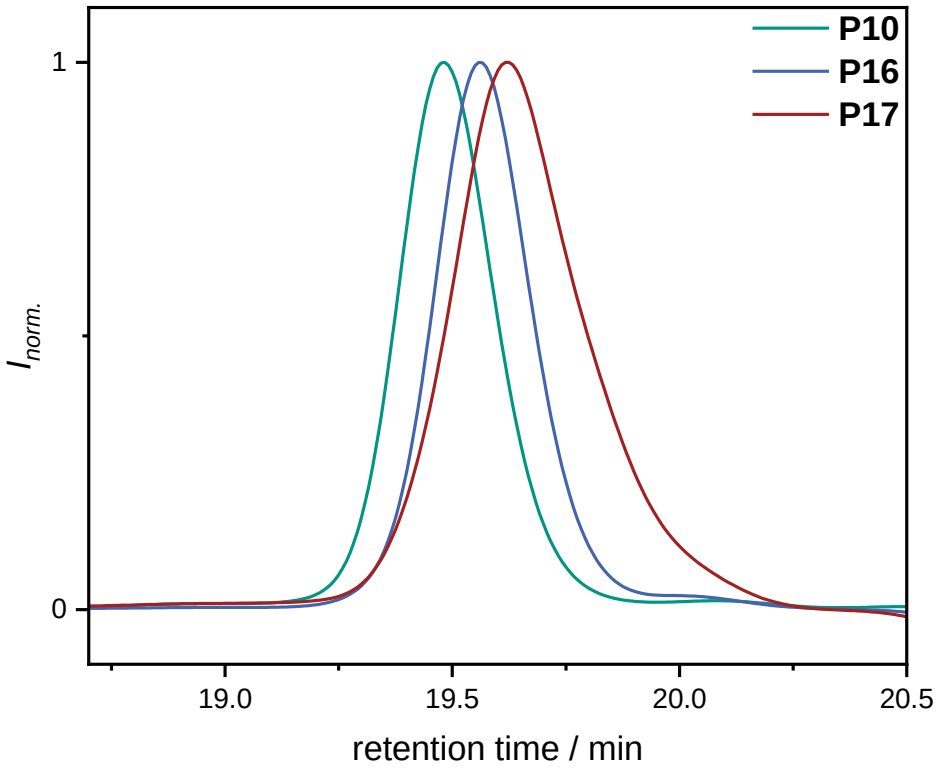

Figure 27: Comparison of SEC chromatograms for the separate deprotection of α-benzyl-ω-tetrahydropyranyl octa(ethylene glycol) **P10** yielding monobenzyl- (**P16**) and mono(tetrahydropyranyl) octa(ethylene glycol) **P17**.

Conclusion

We find that SEC measurements using columns optimized for separation in the oligomer range reveal currently unreported selectivity issues and allow comparison and optimization of the reported routes. SEC, compared with other chromatographic methods such as HPLC, offers the advantage of running isocratically and typically using RI instead of UV detectors, thus allowing a straightforward routine analysis without the necessary gradient optimization and allowing all present species (contaminations) to be detected. The purity values are based on a simple peak symmetry analysis (Figure 19). The chapters objectively compare reported synthetic routes towards uniform PEGs by using a set of characterization methods that allow the establishment of an unbiased data set for comparison. It is important to clarify that we compare different synthetic methods and approaches to highlight advantages and disadvantages, whereas it was not our intention to exactly reproduce the procedures described in the literature, since this is often not possible practically (*i.e.*, availability of different grades of reagent, same type of silica, and so on).

In summary, different synthetic strategies to achieve mono-protected octa(ethylene glycol)s were investigated according to described literature procedures.[108,237,273,317–319] Most importantly, all reactions were analyzed using an SEC system with high resolution in the oligomer range, thus allowing an unambiguous comparison of the different procedures in terms of practicality, selectivity, purity of the final product, and yield. In contrast, the literature indicates that SEC is not suitable for verifying the purity of PEGs.[273] Nonetheless, it is quite possible to distinguish oligomers with only one additional repeat unit for the described oligo(ethylene glycol)s, as monodisperse species should be observed as highly symmetric peaks in SEC. As shown in Figure 19, contamination of a PEG_8 **P10** with only 2wt% PEG_7 **P9** can be clearly identified by SEC using a simple symmetry peak analysis, and even 1wt% was detectable *via* comparison of the peak width (Figure 22). Furthermore, for most side products, we observed a difference of at least four repeating units, thus supporting our hypothesis that SEC is a powerful analytical tool to monitor the reaction process. The results obtained in chapters 4.1.1.1, 4.1.1.2 and 4.1.1.4 are summarized in Table 2 and Table 3 and compared with the values described in the respective reference. They reveal that there is no difficulty in mono- and difunctionalization (Table 2: entries 1-7,Table 3: entries 1–3), but the yields are often lower than those reported if SEC is used to measure the purity.

Table 2: Summery of the results of the different reproduced literature approaches compared and investigated herein.

entry	#	Author, Reference	$Scale_{Lit}$ / mmol	$yield_{Lit}$ / %	$purity_{Lit}$ / %	Scale / mmol[319]	yield / %	purity[b] / %
1	**P2a**	BAKER *et al.*[317]	8000	96.3[c]	89[d]	11.1	74.4[c]	88[d]
2	**P2b**	TANAKA *et al.*[108]	2.00	80[c]	*n.a.*	2.00	51.0	≥98
3	**P3a**	JIANG *et al.*[626]	90.0	85[a]	*n.a.*	10.0	64.4	≥98
4	**P3c**	DAVIS *et al.*[237]	257	68[e]	99.7	10.0	93.2	≥98
5	**P5a**	DAVIS *et al.*[237]	259	*n.a.*	99.7	11.7	76.9	93
6	**P5b**	BRUCE *et al.*[273]	100	90.5[e]	>99[d,f]	100	83.4	≥98
7	**P7**	BRUCE *et al.*[273]	88.6	99.6[c]	>99[d,f]	7.03	96.2	≥98
8	**P8b**	BRUCE *et al.*[273]	15.0	69.4[e]	>98[f]	2.57	36.6	≥98
9	**P10a**	BAKER *et al.*[317]	250	99.3[c]	*n.a.*	1.80	68.4	≥98
10	**P16**	BAKER *et al.*[317]	267	90[c]	*n.a.*	7.34	97.7[c]	≥98

[a] Purification was performed by column chromatography; [b] purity determined *via* SEC based on simple peak symmetry analysis; [c] non-purified products; [d] purification by automated column chromatography; [f] purity estimated by MALDI-MS; purity estimated by ESI-MS.

Table 3: Summery of the results of PEG derivatives synthesized in this work according to literature procedures.

entry	#	Author, Reference	Scale / mmol	Yield / %[a]	Purity / %[b]
1	**P2a**	BAKER *et al*.[317]	34.0	60.9	≥98
2	**P4a**	DAVIS *et al*.[237]	120	72.9	≥98
3	**P6**	BRUCE *et al*.[273]	60.8	55.7	≥98
4	**P8a**	BAKER *et al*.[317]	2.57	12.6	98
5	**P9a**	BAKER *et al*.[317]	2.13	34.5	≥98
6	**P9b**	BRUCE *et al*.[273]	0.88	71.3	≥98
7	**P10b**	BRUCE *et al*.[273]	0.94	47.6	≥98
8	**P11b**	BRUCE *et al*.[273]	0.93	49.6	≥98
9	**P12b**	BRUCE *et al*.[273]	1.15	83.5	≥98
10	**P17**	DAVIS *et al*.[237]	7.34	98.9[c]	≥98

[a] Purification was performed by column chromatography; [b] purity was determined *via* SEC based on simple peak symmetry analysis; [c] non-purified products

This also accounts for the separate deprotection of oligo(ethylene glycol)s **P16** and **P17**, while problems reproducing the ether coupling described in the literature arose (Table 2: entries 8 and 9,Table 3: entries 4–9). The purities calculated *via* SEC analysis are comparable with those reported, which were estimated mostly just by MS analysis. Chromatography, which detects all species and does not have a bias towards ionization of different species, is a better choice and gives more trustworthy data. The best yield was obtained for the synthesis of the double-protected heptamer **P9b** according to the procedure of BRUCE *et al*.,[273] whereas the results for the chain tripling method did not match those described in the literature (**P8a** and **P8b**). Due to the formation of several side products, identified *via* SEC-ESI–MS (Supplementary Table 1), the isolation of the products *via* normal phase column chromatography was rather challenging, resulting in low and nonconsistent yields. Such side products were not identified before, suggesting that the previously reported samples were contaminated. The results described herein provide a generalized overview of previously reported procedures as well as their limitations.

The iterative cycle, consisting of the activation of **P16** with *p*-toluenesulfonyl chloride, the coupling of two orthogonal protected octa(ethylene glycol)s **P16** and **P17** according to the procedure of BRUCE *et al*.,[273] and the subsequent THP deprotection, was continued to obtain the corresponding monobenzyl hexadeca(ethylene glycol) **P21**.

4.1.1.7. Chain elongation – synthesis of PEG_{16} derivatives

Compared to the tosylation of **P5**, a yield of only 51% was achieved for **P19** after purification *via* column chromatography, which was used directly in the coupling reaction prior to degradation. Unfortunately, similar side reactions as for the octamer **P10** were observed for the ether synthesis of the hexadecamer **P20** by SEC. Thus, the isolation of **P20** was rather challenging and time-consuming, and two chromatographic purification steps were necessary to achieve the uniform product. The column chromatography separations took approximately one week, each. The product was collected as 58 fractions of various purity. The amounts of each fraction, the SEC results, and the corresponding purities are shown in Supplementary Figure 48 and Supplementary Table 10. The purities, determined by SEC of the product-containing fractions, varies from 5 to >99% with dispersities ranging from 1.00 to 1.01. The fractions highlighted in red were discarded, the ones in yellow were purified *via* a second column chromatography and the ones highlighted in green were used for further synthesis.

An overview of all so far synthesized PEG derivatives is shown in Figure 28, ranging from the starting material tetra(ethylene glycol) **1b** at the highest retention time of 21.0 min (light green trace) to the α-benzyl-ω-tetrahydropyranyl hexadeca(ethylene glycol) **P20** at a retention time of 18.3 min (dark green trace). All SEC traces show a narrow and monomodal shape. Additional characterization by NMR spectroscopy and MS indicated the uniformity of the products (see experimental section, chapters 6.3.1 and 6.3.2).

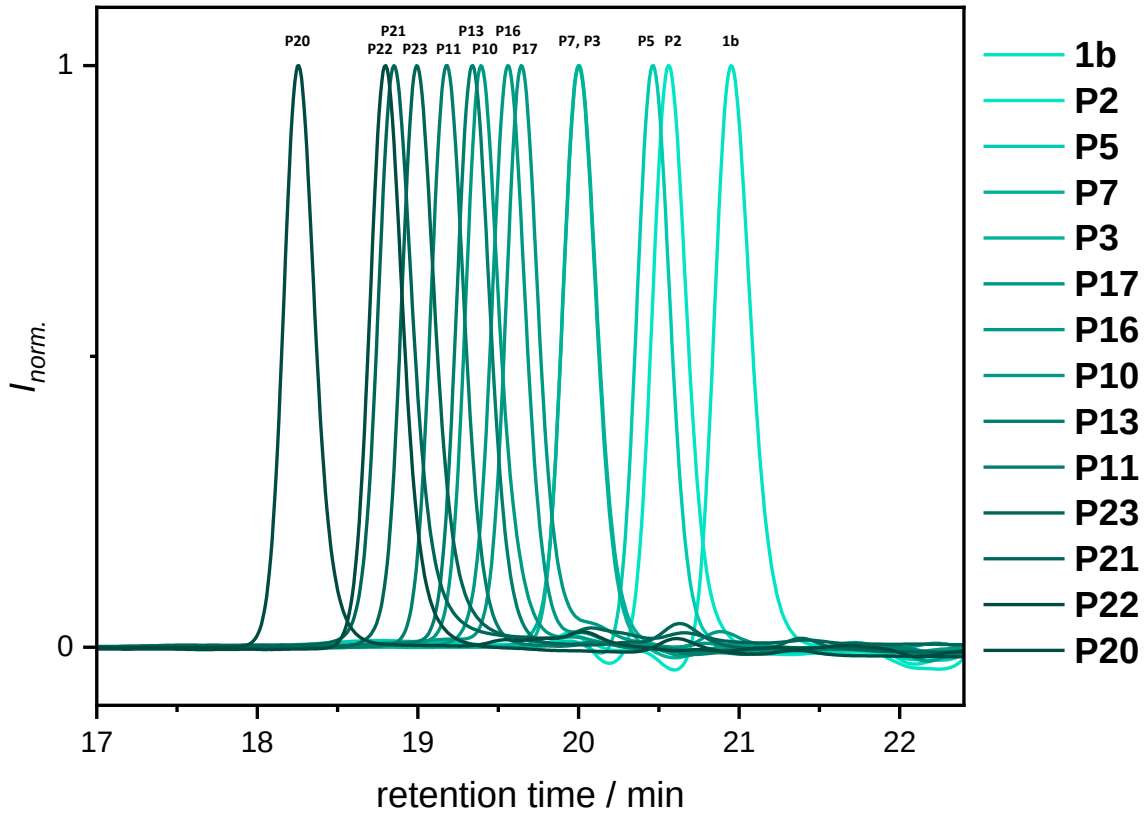

Figure 28: SEC overview of the synthesized PEGs. The SEC traces range from the starting material tetra(ethylene glycol) 1b at a retention time of 21.0 min in light green to the doubly protected hexadeca(ethylene glycol) P20 at 18.3 min in dark green. All traces show a narrow and monomodal shape indicating the high purity of the products.

The THP-protecting group was then cleaved under acidic conditions and the monobenzyl hexadeca(ethylene glycol) **P21** was obtained in quantitative yield without further purification. Afterwards, the protection group had to be exchanged (Figure 26) in order to obtain an identical structure for the uniform block copolymers (described in chapter 4.2) as for the disperse ones (described in chapter 4.4.1).

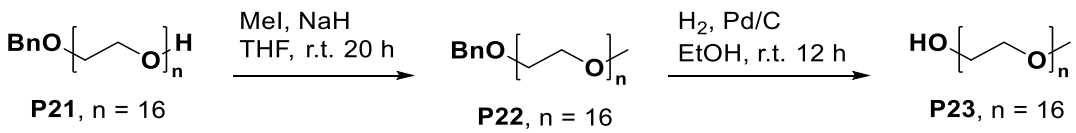

Scheme 41 Schematic overview of the exchange of protection group for PEG_{16}. Monobenzyl hexadeca(ethylene glycol) **P21** was methylated yielding the doubly protected PEG_{16} **P22**. Then, the benzyl protection group was cleaved *via* reductive hydrogenation to obtain the desired $mPEG_{16}$ **P23**.

Therefore, the alcohol moiety of compound **P21** was methylated in a nucleophilic substitution using a ten-fold excess of methyl iodide as electrophile and NaH as deprotonating agent. TLC indicated full conversion after stirring the reaction over night at room temperature. After purification *via* column chromatography, 30% of pure

product **P22** and 70% with a purity of 93 - 98% were obtained. In the final step, the benzyl protection group was cleaved *via* reductive hydrogenation. Compared to the procedure described in Scheme 40, here, the reaction was performed in EtOH and at room temperature, according to the procedure described by HAAG *et al.*,[627] instead of ethyl acetate and reflux. Using this milder reaction conditions, the side reaction was avoided, and the product **P23** was obtained in 97.6% yield and was utilized without further purification steps.

The corresponding ^{1}H NMR spectra of the exchange of the protecting group are shown in Figure 29. The spectrum of the monobenzyl hexadeca(ethylene glycol) **P21** is shown in green on top. The characteristic multiplet (7.35 - 7.26 ppm) as well as the methylene singlet (4.56 ppm) of the benzyl protection group are highlighted in orange.

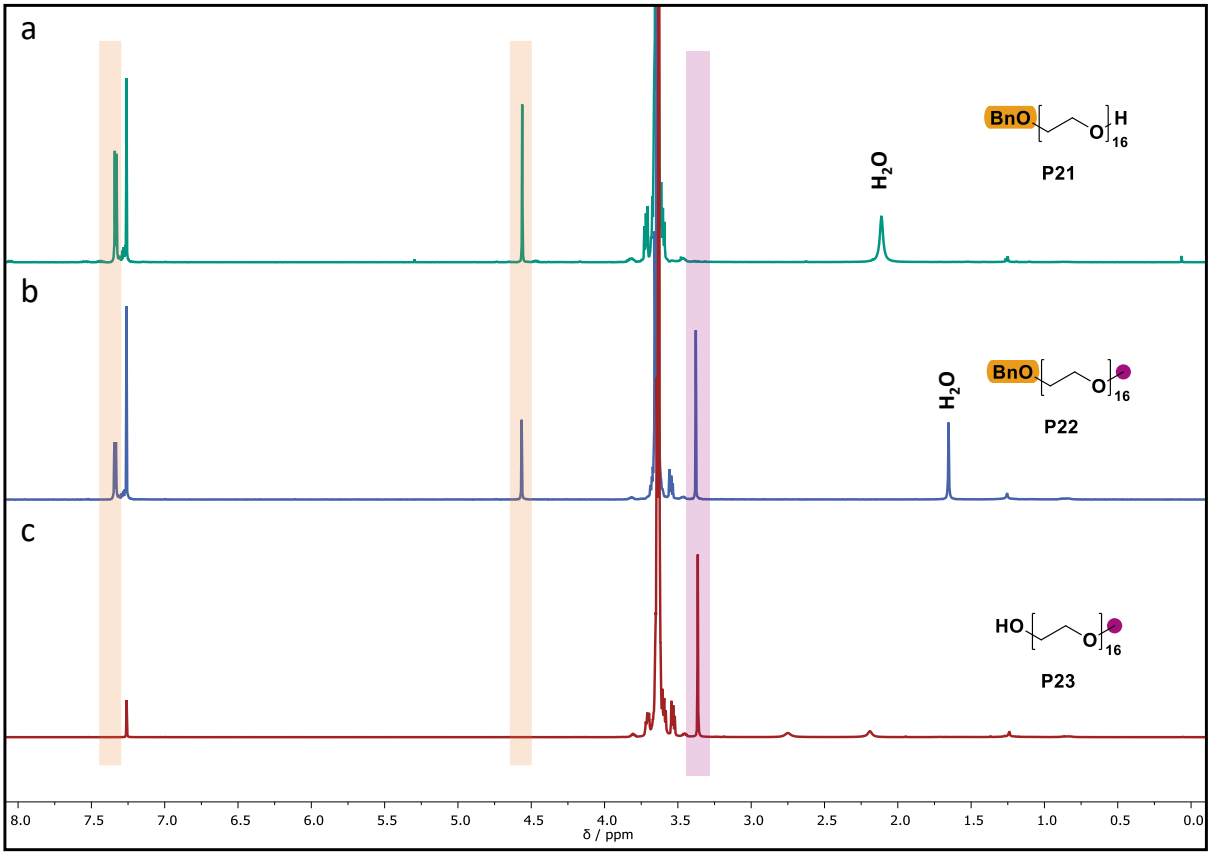

Figure 29: ^{1}H NMR spectra of the exchange of the protection group of PEG_{16}. The green spectrum on top shows the chemical shifts of the monobenzyl hexadeca(ethylene glycol) **P21**. The aromatic and methylene signals at 7.35 - 7.26 and 4.56 ppm of the benzyl moiety are highlighted in orange. The spectrum for the doubly protected PEG_{16} **P22** is shown in the middle (blue). The characteristic singlet signal of the methyl capping group appears at 3.38 ppm (highlighted in purple). The ^{1}H NMR spectrum after the reductive hydrogenation (**P23**) is shown in red on the bottom. The signals according to the benzyl protection group vanished completely, whereas the methyl group is still intact.

After methylation of the alcohol moiety, a singlet at a chemical shift of 3.38 ppm appeared (**P22**, blue spectrum, middle), which was identified as the methoxy protons highlighted in blue. In the red spectrum on the bottom (**P23**), the specific signals of the benzyl protecting group completely vanished, confirming full conversion during the reductive cleavage. The most intense signal around 3.65 ppm belongs to the PEG backbone.

Figure 30 shows the SEC traces of the protection group exchange process of PEG_{16}. Product **P21** exhibits a retention time of 18.9 min in the SEC. After capping the free alcohol with a methyl group, the signal shifts to a lower retention time of 18.8 min, due to the increase in the hydrodynamic volume (blue trace, product **P22**). On the other hand, a higher retention time of 19.0 min was observed after the reductive hydrogenation of the benzyl ether, yielding product **P23** (red trace). All curves show a narrow and monomodal shape, indicating uniformity. Further data of the full characterization consisting of ^{1}H, ^{13}C NMR and IR spectroscopy, MS, and SEC of the purification of **P22** *via* columns chromatography are provided in the experimental part and confirmed the high purity of the compounds (chapter 6.3.2). Product **P23** was used without further purification in chapter 4.2 for the synthesis of uniform block copolymers (**uBCPs**).

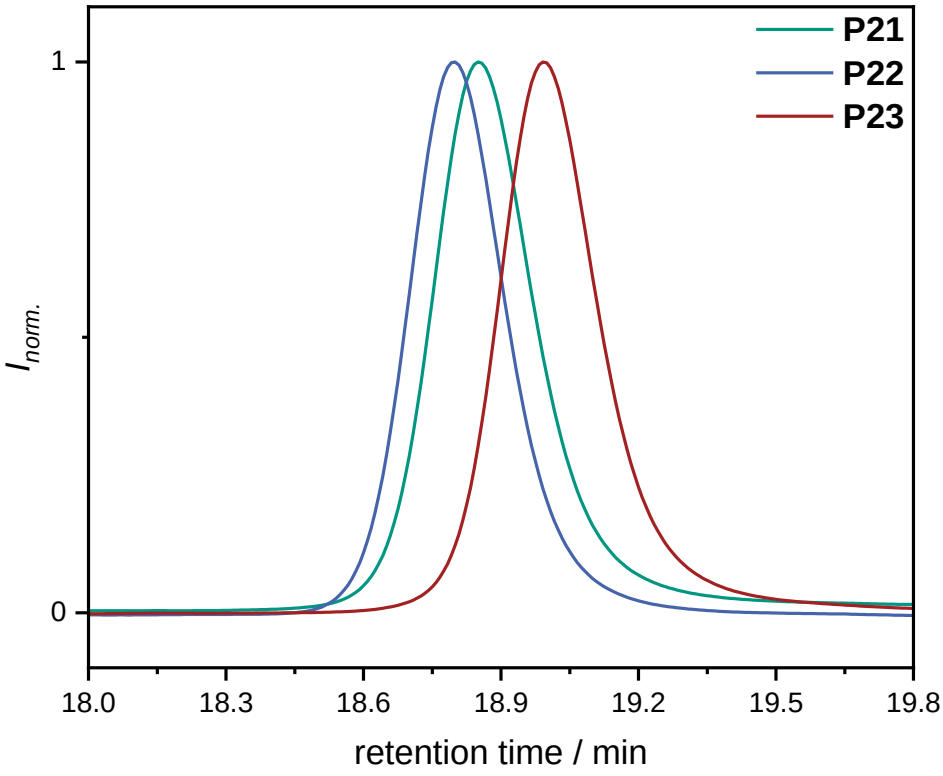

Figure 30: SEC chromatograms of the exchange of the protection group of PEG_{16}. The green curve at a retention time of 18.9 min belongs to the crude monobenzyl hexadeca(ethylene glycol) **P21**. After methylation, the signal shifts to a lower retention time of 18.8 min due to the higher hydrodynamic radius (blue curve, product **P22**, after purification *via* column chromatography. The red curve shows the chromatogram of the crude product **P23**. The retention time decreased to 19.0 min after the cleavage of the benzyl group.

Due to the described challenges in the synthesis and purification of PEGs to achieve uniformity, there is still an ongoing interest to develop alternative approaches. In 2019, LIVINGSTON *et. al*. reported a strategy for the synthesis of sequence-defined multifunctional polyethers based on purification *via* molecular sieving (Nanostar Sieving Technology).[325] The strategy is used in industry for the synthesis of defined oligonucleotides, peptides, homopolymers and sequence-defined polymers.[628] Another approach follows the purification of PEGs *via* Sample Displacement Chromatography (SDC).[629]

These approaches focus more on the purification of PEGs to achieve uniformity. In the next chapter an alternative route for the direct synthesis of highly defined PEGs is presented, based on the $GaBr_3$-catalyzed reduction of an ester with silanes.

4.1.2. Uniform PEG *via* $GaBr_3$-catalyzed reduction of esters

From a synthetic point of view, the synthesis of uniform PEGs is based on the iterative ether coupling of (orthogonally) protected building blocks (Scheme 42 a),[107,108,236–238,273,316,317,319,623] or step by step addition on a hub unit (Scheme 42 b).[198,322,325] The nucleophilic ring opening of macrocyclic sulfates was reported in 2015 as a novel route to achieve defined PEGs (Scheme 42 c).[318] Within the scope of this work, investigations towards an alternative preparation of uniform PEGs, based on the $GaBr_3$-catalyzed reduction of esters with silanes, were carried out (Scheme 42 d).

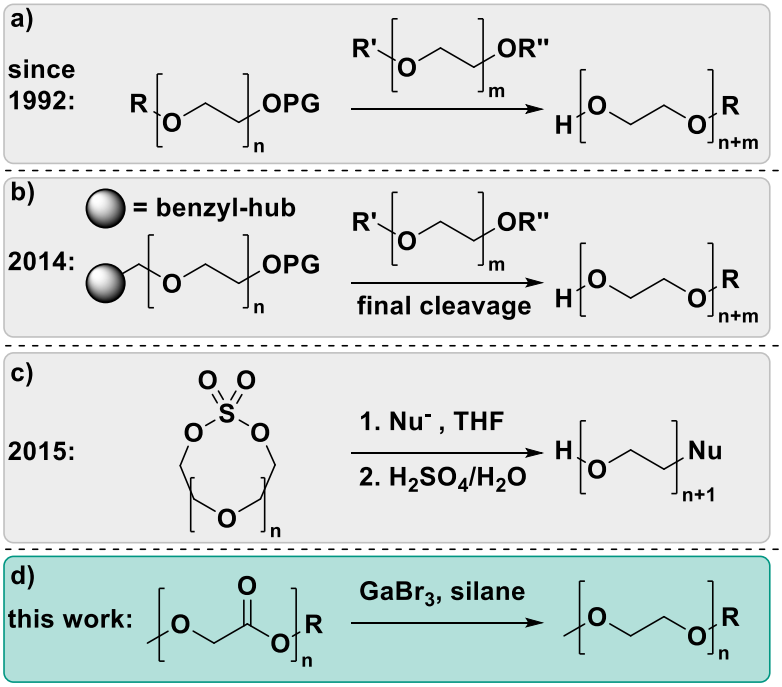

Scheme 42: Summary of the synthetic approaches for the preparation of uniform PEGs since 1992. A detailed overview is shown in Figure 3 (chapter 2.2.1).

Applications of such ester reductions have been presented in the literature by BIERMANN and METZGER for lactones, methyl oleate[346] and high oleic sunflower oil,[347] and in a collaboration with our group for renewable polyesters (see chapter 2.2.3).[348] The overreduction and thus the cleavage of the ester function was reported and is the major challenge to achieve uniform products.

The first examinations of this project were carried out by QIANYU CAI in her study "*Synthesis of uniform PEGs via $GaBr_3$-catalyzed reduction*"[630] and were continued by research assistants PETER CONEN and MAYA EYLEEN LUDWIG under lab-supervision and major data interpretation of PHILIPP BOHN. A schematic overview of the iterative reaction cycle is shown in Scheme 43. The reaction protocol includes the monomer

synthesis and the subsequent iterative chain elongation of the PEGs, consisting of a transesterification, a reduction, and a final deprotection step, which are explained in detail in the following.

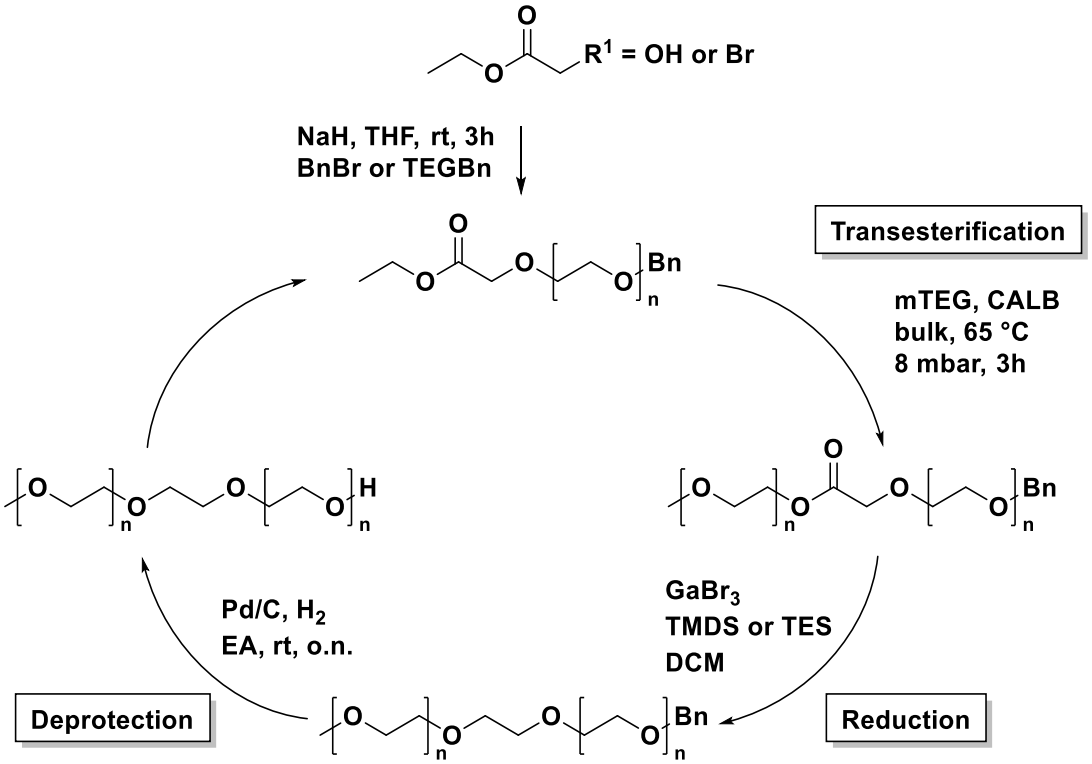

Scheme 43: Schematic overview of the synthesis of uniform PEGs *via* $GaBr_3$-catalyzed reduction of ester functions. The approach includes the synthesis of the monomer units as well as the iterative reaction cycle, consisting of CALB catalyzed transesterification, a $GaBr_3$-catalyzed reduction and a deprotection step *via* reductive hydrogenation.

In the first step of the reaction cycle, the alcohol function of ethyl glycolate was protected with benzyl bromide using the same procedure as described above for the tetra(ethylene glycol).[273] The product **P24** was obtained in a yield of 94% after purification *via* column chromatography.[I]

Afterwards, a CALB (*Candida antarctica* Lipase B)-catalyzed transesterification (Scheme 43) with monomethyl tetra(ethylene glycol) was conducted in bulk. The reaction was (simply) performed in a flask connected to a rotary evaporator, according to a procedure presented by PUSKAS *et al*.[631] The temperature was set to 65 °C and vacuum (8 mbar) was applied to remove ethanol and thus shift the equilibrium towards the product side. Quantitative yields were reported in the literature, whereas within this

[I] The synthesis was carried out by B. Sc. QIANYU CAI under the lab-supervision of PHILIPP BOHN.

work, a moderate yield of 79% was obtained after column chromatography.[I] The reaction was followed by GC-FID analysis and showed full conversion of the starting material after the respective reaction time. Therefore, the purification process needs to be further improved, since a high yield in the first steps is essential to achieve uniform high molecular weight PEGs in large quantities.

Since $GaBr_3$ is highly water sensitive and the PEG-ester precursors are hydrophilic and tend to draw water easily, they were dried carefully *via* azeotropic distillation with toluene and further dried overnight under high vacuum and stored under argon atmosphere until usage in the subsequent reduction. The reduction of the ester function to the corresponding ether, which is the key step of the reaction cycle, was optimized in terms of reducing agent and its quantity, catalyst loading and reaction time.[II] Either the disilane TMDS (1,1,3,3-tetramethyldisiloxane) or the monosilane TES (triethylsilane) were used as reducing compound. For a better comparison of the individual approaches, two equiv. of TES were used related to one equiv. of TMDS. The conversion was monitored *via* NMR and IR spectroscopy and the results are summarized in Table 4.

Using a similar quantity of catalyst (1.00 mol%) as described in the literature, almost no conversion was observed when using 1.10 or 2.20 equiv. of TMDS (entries 1 and 2). Full conversion was achieved with 3.30 equiv. of TMDS, but on the other hand 28% of the alcohol side product were formed due to overreduction (entry 3). Increasing the amount of catalyst to 2.00 mol% or higher, the conversion increased to >80% for all approaches and the ester cleavage was decreased. In comparison, the alcohol formation was significantly lower when using TES (4-7%) instead of TMDS (6-28%). Furthermore, ^{1}H NMR analysis showed additional side products for the reduction of the ester with TMDS, which is shown in Supplementary Figure 64 in the experimental section 6.3.3. Thus, the most promising results were achieved using 5.00 mol% of catalyst and 4.40 or 6.60 equiv. TES per ester function. After 67 or 44 h, respectively, quantitative conversion of the ester and only 7% side product formation in both cases were observed (entries 9 and 10). To further optimize the reaction conditions in terms of decreasing the reaction time and overreduction, online monitoring would be a powerful tool to gain important insight into the reaction process.

[I] The synthesis was carried out by B. Sc. QIANYU CAI under the lab-supervision of PHILIPP BOHN.
[II] All reduction steps were performed by B. Sc. PETER CONEN under the lab-supervision of PHILIPP BOHN.

Table 4: Optimization study of the $GaBr_3$-catatyzed reduction of **P25**

#	$GaBr_3$ / mol%	TMDS / equiv.[1]	t / h	conv.[3,4] / %	alc.[5] / %	TES[2] / equiv.[1]	t / h	conv.[3,4] / %	alc.[5] / %
1	1.00	1.10	140	14 / 4	(9)	2.20	-	-	-
2	1.00	2.20	66	9 / 7	(6)	4.40	-	-	-
3	1.00	3.30	93	>99 / >99	28	6.60	-	-	-
4	2.00	1.10	67	82 / 86	12	2.20	144	83 / 87	5
5	2.00	2.20	67	>99 / >99	7	4.40	144	94 / 96	6
6	2.00	3.30	20	>99 / >99	17	6.60	144	85 / 89	5
7	3.00	1.10	73	86 / 87	13	2.20	73	86 /87	4
8	5.00	1.10	-	-	-	2.20	144	96 / 97	7
9	5.00	2.20	-	-	-	4.40	67	>99 / >99	7
10	5.00	3.30	-	-	-	6.60	44	98 / >99	7

[1] equivalents per ester function; [2] for a better comparison, double the amount of the monosilane (TES) were used related to one equiv. of the disilane (TMDS); [3] determined by ^{1}H NMR spectroscopy *via* integration of the ethylene signals **3** and **4** (Figure 31) related to the aromatic protons (signal **1**) / [4]determined by IR spectroscopy *via* the peak height of the carbonyl (C=O) vibration at 1752 cm^{-1} normalized, to the methoxy stretching (O-CH_3) vibration at 2869 cm^{-1}; [5] determined by IR spectroscopy *via* the peak height of the alcohol (O-H) vibration at 3500 cm^{-1}, normalized to the methoxy stretching (O-CH_3) vibration at 2869 cm^{-1}; Complete evaluation of the reaction monitoring *via* NMR and IR spectroscopy is provided in the experimental section.

The monitoring with ^{1}H NMR spectroscopy of the entries 9 and 10 of Table 4 and a comparison with the starting material **P25** and the purified product is shown in Figure 31. During this reduction, the ^{1}H NMR signals of the CH_2 unit next to the ester at 4.21 ppm (signal 3) is shifted high field and overlaps with the broad signal of the OEG backbone at 3.51 ppm (signal 4 in the product). The benzyl methylene peak at 4.54 ppm (signal 2) is shifted to the high field (4.49 ppm) as well, due to the loss of the deshielding effect of the carbonyl group.

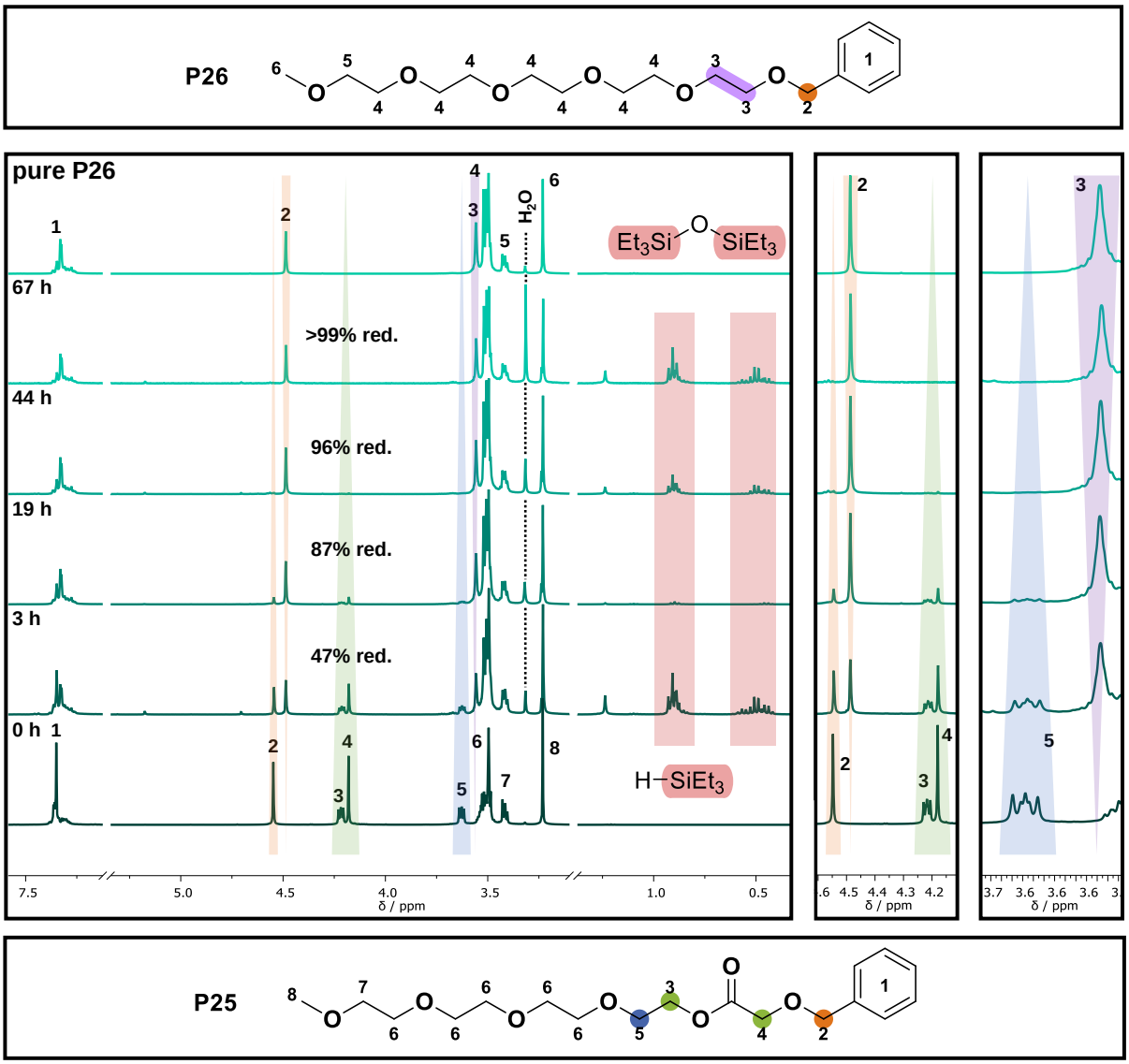

Figure 31: Reaction monitoring of the reduction of **P25** *via* ^{1}H NMR spectroscopy using 5 mol% of $GaBr_3$ and 4.40 equiv. of TES. All NMR spectra were measured in DMSO-d_6. The starting material **P25** (botton spectrum) is compared to the corresponding product **P26** (top spectrum) and the shifts of the ^{1}H signals are monitored over the reaction time and highlighted in a color code.

Furthermore, the singlet signal 4 of the methylene group, in α-position to the ester, at 4.18 ppm is shifted to 3.56 ppm and overlaps with the CH_2 group next to it, which arises due to the reduction of the carbonyl function. In addition to the signals in the aliphatic region, highlighted in red, which belong to the ethyl groups of the reducing agent (TES) and the corresponding side product hexamethyldisiloxane, only small amounts of impurities were detected at 5.17, 4.70 and 1.24 ppm, which could be removed easily *via* column chromatography (Figure 31).

The overreduction of the ester to the corresponding alcohols *via* the $GaBr_3$-catalyzed approach was described in the literature as the main side reaction.[346–348] The possible side products are shown in Figure 32 c.

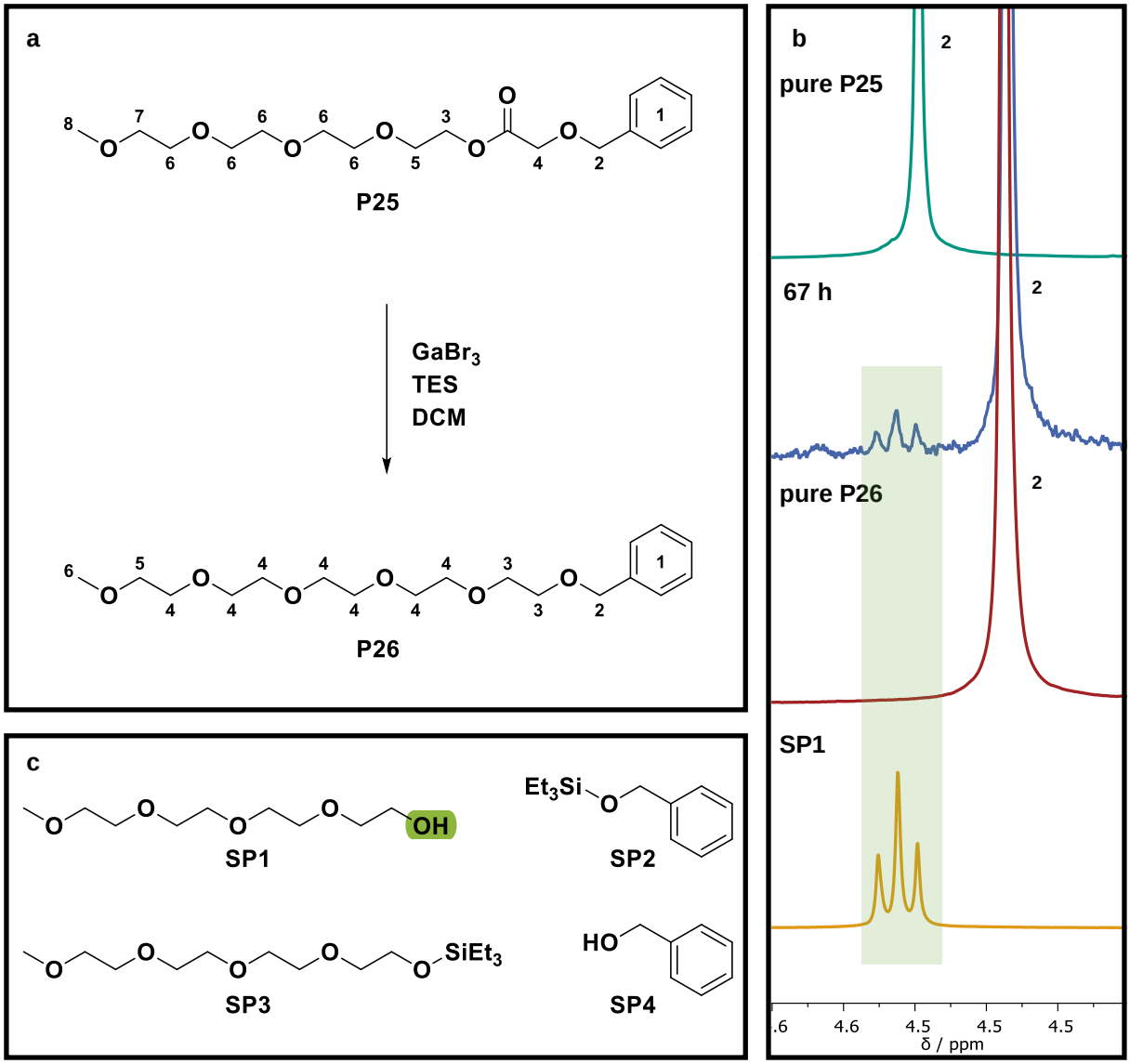

Figure 32: Investigation of the side product formation during the $GaBr_3$-catalyzed reduction of **P25** *via* ^{1}H NMR spectroscopy. **a** reaction scheme of the reduction of **P25** to the corresponding ether **P26**; **b** detailed ^{1}H NMR section (4.5-4.6 ppm), which shows the shift of the benzyl methylene signal **2** indicating complete reduction (green and red spectrum); **c** possible side products resulting from overreduction and thus ester cleavage. The yellow spectrum shows the alcohol signal of monomethyl tetra(ethylene glycol) **SP1** at 4.56 ppm, which is also observed in the reaction monitoring after 67 h in the blue spectrum.

Since the ^{1}H NMRs were measured in DMSO-d_6 the alcohol signals could be detected. The relevant spectra sections as well as the peak assignment are shown in Figure 32 a-c. Since the ^{1}H signal for the monomethyl tetra(ethylene glycol) **SP1** (yellow spectrum) occurs at 4.56 ppm and thus overlaps with signal **2** of the parent molecule

(green spectrum), the ester cleavage could only be quantified *via* ^{1}H NMR, if the ester was completely converted. For the approach shown in Figure 31 using 5 mol% of $GaBr_3$ and 4.40 equiv. of TES, full conversion was achieved after 44 h. At this point, approximately 9.5 % of alcohol were formed due to overreduction (please note a weak signal to noise ratio was observed (blue spectrum), thus the value might be erroneous). However, the signal completely vanished after the isolation of the product. For the purification, the reaction mixtures of entries 9 and 10 (Table 4) were combined and 39% of the desired product was obtained after column chromatography (please note: Since several samples were taken out of the reaction mixture for the monitoring *via* NMR and IR spectroscopy, the yield is significantly decreased and is lower than the observed conversion). In order to quantify the formation of the other possible side products, further investigations must be carried out, *e.g.*, by additional mass analysis.

Due to the characteristic carbonyl vibration band at 1752 cm^{-1}, which decreases in intensity during the reaction, IR spectroscopy provides another powerful tool to monitor the degree of ester reduction. Figure 33 shows the corresponding superimposed IR spectra for the reduction, using the same reaction conditions as for the ^{1}H NMR monitoring shown in Figure 31 (5.00 mol% $GaBr_3$, 4.40 equiv. TES). The spectra were normalized to the end group methyl ether (O-CH_3) stretching vibration at 2869 cm^{-1} and the conversion of the ester was observed by the decrease of the C=O vibration (Figure 33 b). A significant peak at a wavenumber around 3500 cm^{-1} was observed from a reaction time of 19 h on and can be assigned to the O-H stretching vibration of the formed alcohol side product *via* overreduction (Figure 33 c). 7% ester cleavage and quantitative reduction of the carbonyl were calculated after 67 h, which confirms the values determined by ^{1}H NMR spectroscopy.

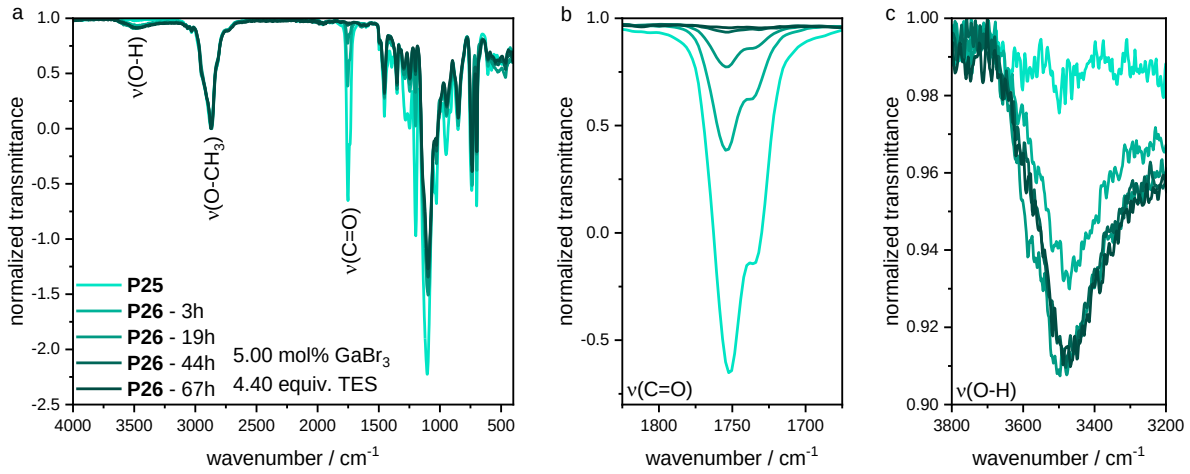

Figure 33: Superimposed IR spectra of $GaBr_3$-catalyzed reduction of **P25**. **a** complete IR spectra normalized to the methoxy -O-CH_3 stretching vibration at 2869 cm^{-1}; **b** detailed section of the carbonyl (C=O) vibration at 1752 cm^{-1}, which is decreasing due to the reduction; **c** detailed section of the arising O-H vibration at around 3500 cm^{-1} indication alcohol formation *via* overreduction.

In the last step of the reaction cycle, the benzyl ether **P26** was deprotected *via* palladium-catalyzed reductive hydrogenation (Figure 34). Full conversion was achieved after stirring the mixture at room temperature under hydrogen atmosphere (balloon) overnight, indicated by ^{1}H NMR analysis (Figure 34). The signals **1** and **2** corresponding to the benzyl group at 7.33 and 4.49 ppm completely vanished due to the cleavage, whereas a triplet at 4.56 ppm associated to the formed alcohol function was observed (product signal **1**). Furthermore, the ethylene signal **3** at 3.56 ppm was shifted high field to 3.45 and 3.42 ppm (product signal **3** and **4**).

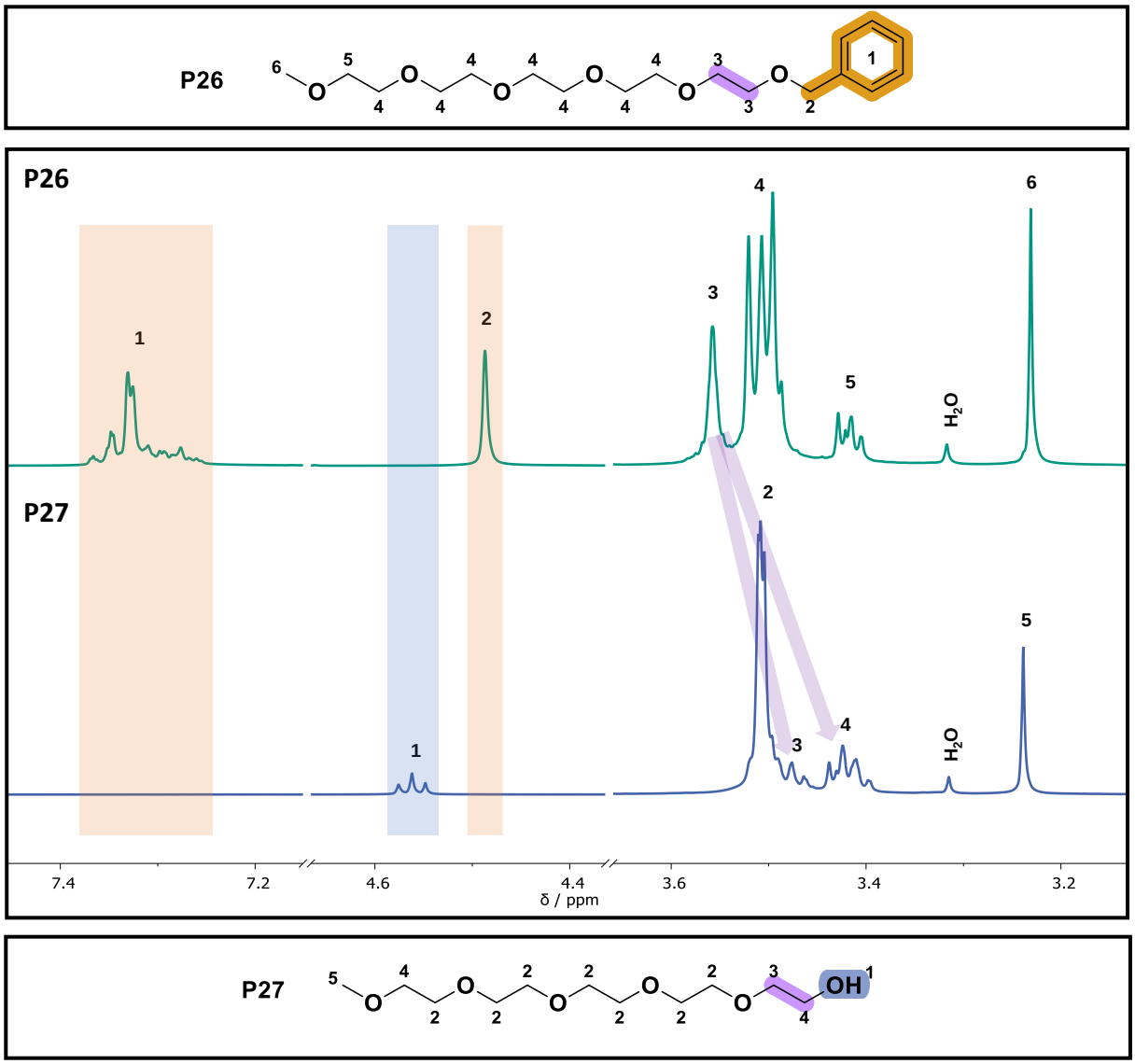

Figure 34: Reaction monitoring of the deprotection of **P26** *via* ^{1}H NMR in DMSO-d_6. Comparison of the ^{1}H NMR spectra of **P26** before and of **P27** after the deprotection. The signals associated to the benzyl protecting group at 7.33 and 4.49 ppm completely vanished, indicating full conversion. The signal at 4.56 ppm is assigned to the formed alcohol. The ethylene signal 3 in the starting material at 3.56 ppm is shifted high field to 3.45 and 3.42 ppm.

After filtering off the catalyst and evaporating the solvent and the side product toluene, the desired product **P27** was obtained in a quantitative yield.

Additionally, a comparison of the ^{13}C NMR spectra of the reduction and deprotection step is shown in Figure 35. Due to the reduction of the carbonyl function, the quaternary carbon signal **1** of the ester **P26** at 170.1 ppm completely vanished in the spectrum of the corresponding ether **P27** (highlighted in orange). Furthermore, the peaks associated to carbon **9**, **10** and **11** were shifted low field and partially overlap with the backbone signal (highlighted in yellow). Signal **8** of **P26** was assigned with the help of

2D HMBC analysis (highlighted in purple) due to the correlation to signal **5**. After the deprotection *via* reductive hydrogenation, the benzyl signals (highlighted in blue) completely vanished and the carbon peaks next to the formed alcohol function (signal **1** and **5**, highlighted in green) were shifted to 72.4 and 60.2 ppm, respectively.

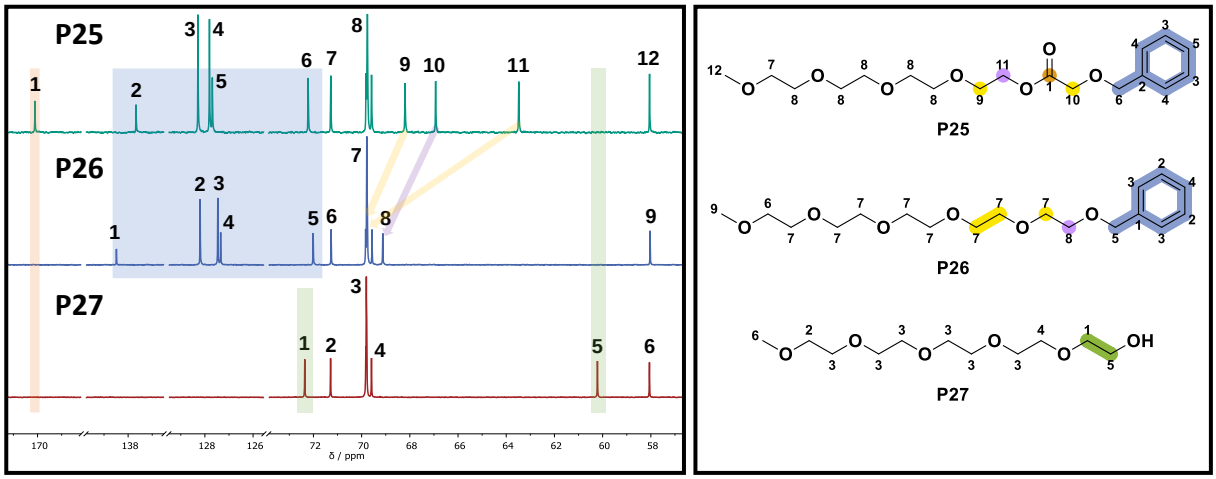

Figure 35: Comparison of ^{13}C NMR spectra of the reduction and deprotection step of iterative chain elongation cycle (Scheme 43). The corresponding molecular structures **P25** (top spectrum), **P26** (middle spectrum) and **P27** (bottom spectrum) are shown next to the spectra, as well as the peak assignment.

Figure 36 shows the SEC chromatograms of the product **P25** (red trace), the product **P26** crude (green trace) and after purification (yellow trace) and the alcohol **P27** (blue trace). In general, narrowly distributed signals were observed for the three compounds in the SEC analysis, but also impurities towards higher retention times and thus a lower molecular weights were present (please note that the products eluate barely at the lower resolution limit of the SEC instrument, thus overlapping with system peaks might occur). A complete analysis including ^{1}H, ^{13}C and IR spectroscopy as well as MS is provided in the experimental section 6.3.3. Furthermore, it should be highlighted that product **P26** was already obtained in a purity of 94% directly after the reduction, without further purification. Since the side products were easily separated *via* column chromatography, this first investigations of the presented approach shows that it is a promising alternative to the commonly used Williamson ether synthesis discussed in chapter 0.

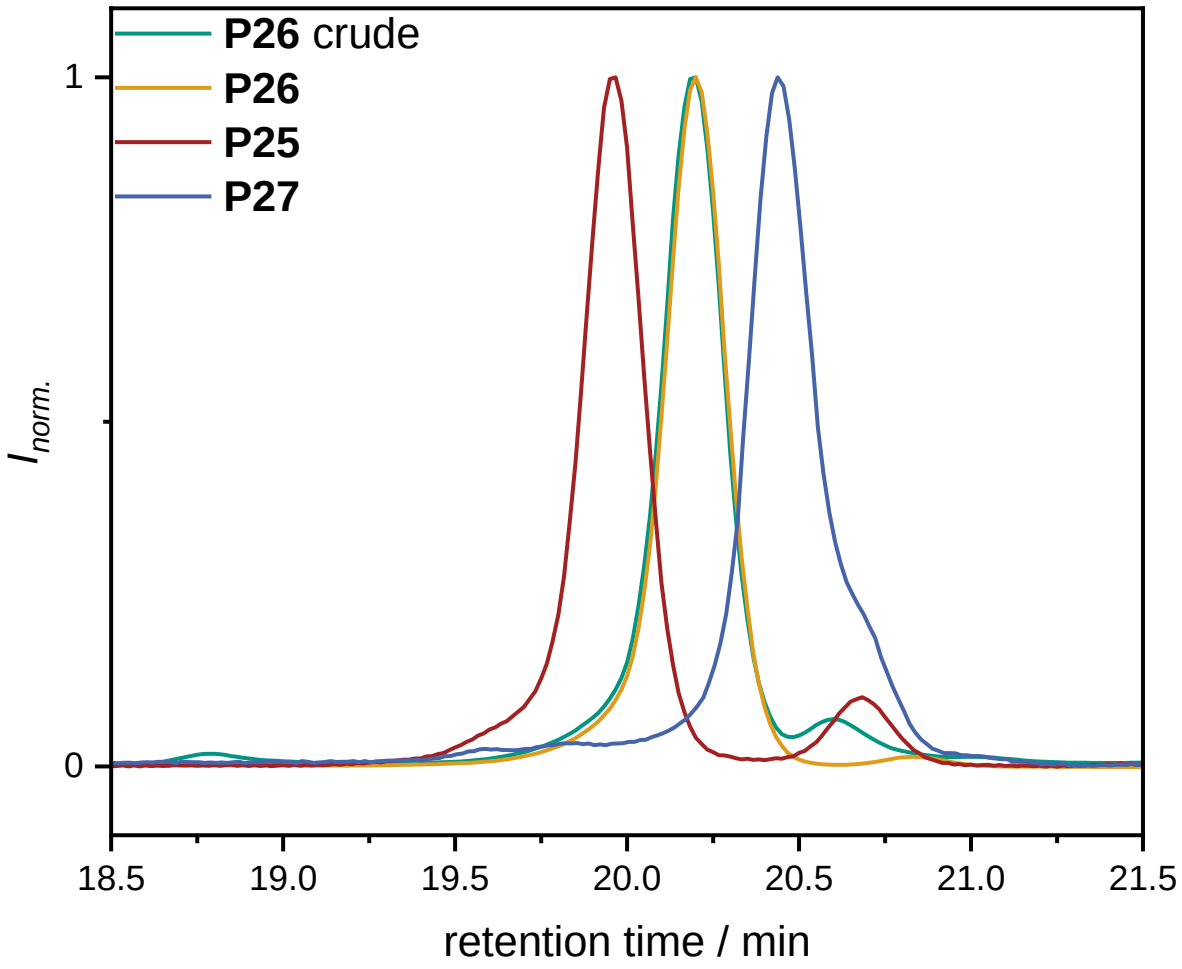

Figure 36: Comparison of SEC traces of products **P25** (red trace), **P26** crude (green trace) and after purification (yellow trace) and **P27** (blue trace).

The generated alcohol **P27** can be applied directly, without further purification, in a subsequent transesterification with **P24**. Thus, the PEG chain is elongated by one EG unit per reaction cycle consisting of a CALB-catalyzed transesterification, a $GaBr_3$-catalyzed reduction and a Pd/C-catalyzed deprotection.

With the presented results, a promising proof of principle for the synthesis of uniform PEGs was demonstrated. In order to synthesize high molecular weight uniform PEGs, the addition of one unit per three steps is not efficient and therefore not sufficient. Therefore, the ethyl ester **P24**, which is the iterative transesterification agent, can be easily substituted to increase the monomer addition per reaction cycle. Therefore, compound **P28** was prepared in a one-step ether synthesis using ethyl bromo acetate (EBA) and tetra(ethylene glycol) monobenzyl ether **P5**. The reaction was performed in a multi-gram scale according to the procedure of WANG *et al*.[632] and the product **P28** was obtained in 78% yield after purification *via* column chromatography.[I] The ester was then used in the transesterification with monomethyl tetra(ethylene glycol) according to the reaction protocol of PUSKAS *et al*.[631] and the desired product **P29** was obtained in a moderate yield of 65%.[II] The stacked ^{1}H NMR spectra of **P28** (green spectrum, top) and **P29** (blue spectrum, bottom) as well as the peak assignments are shown in Figure 37. The characteristic triplet at 1.28 ppm and the quartet at 4.21 ppm, both assigned to the ethyl ester, completely vanished (signal **3** and **6**, highlighted in orange) and new signals for the transesterification product **P29** were observed at 4.29, 3.45 and 3.37 ppm (color-coded). Further analysis, *e.g.,* SEC, must be carried out as well as the investigation of the subsequent reduction protocol.

[I] The synthesis was carried out by B. Sc. MAYA EYLEEN LUDWIG under the lab-supervision of PHILIPP BOHN.
[II] The synthesis was carried out by KIARA MAURER under the lab-supervision of PHILIPP BOHN.

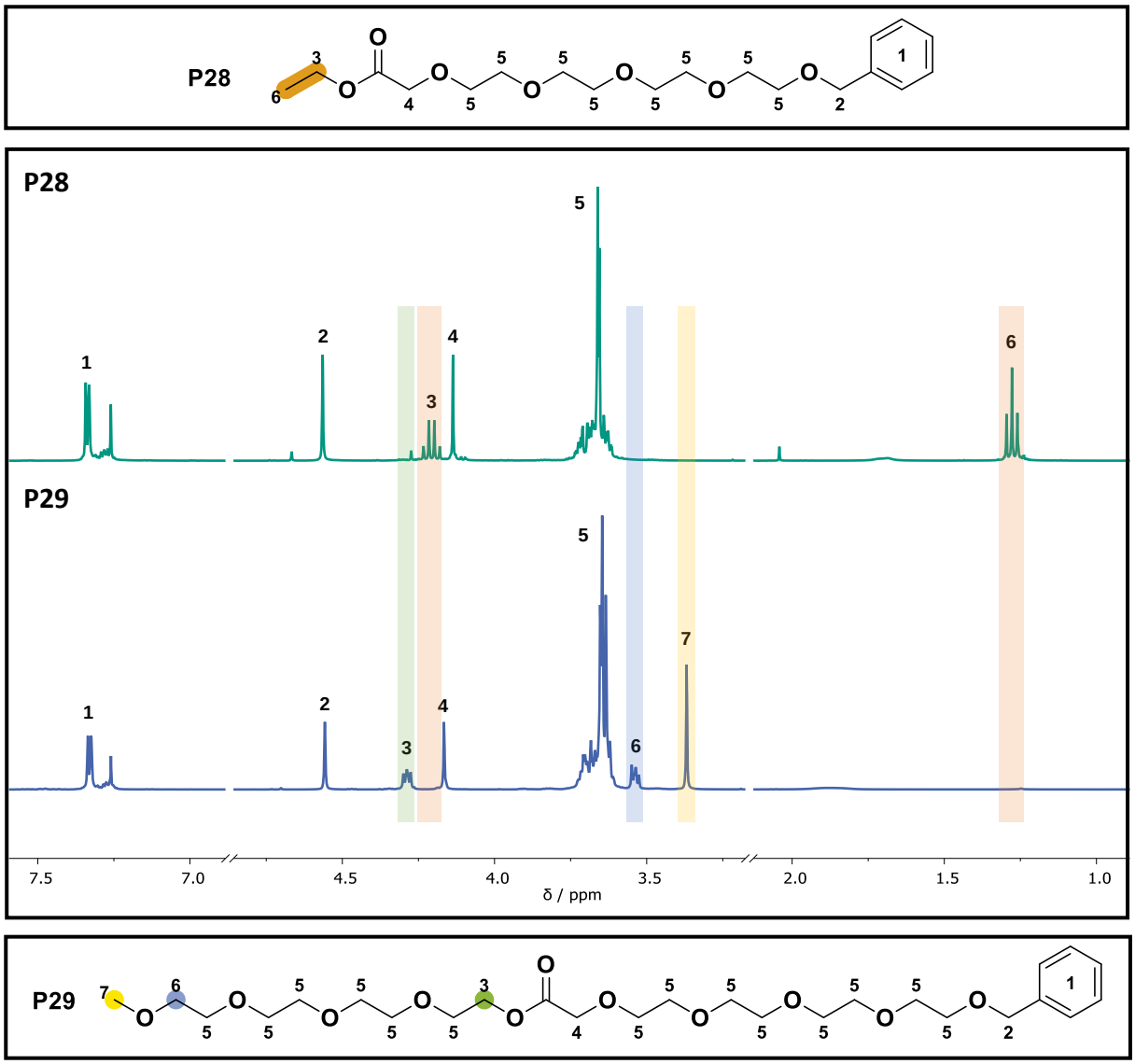

Figure 37: Comparison and assignment of ^{1}H NMR spectra of **P28** (green spectrum, top) and **P29** (blue spectrum, bottom). The signals of the ethyl ester in compound **P28** at 1.28 and 4.21 ppm (signal **3** and **6**, highlighted in orange) completely vanished after the transesterification with monomethyl tetra(ethylene glycol). Signals at 4.29, 3.45 and 3.37 ppm (highlighted in green, blue and yellow) arose due to the formation of product **P29**.

Within this study, the high potential of the $GaBr_3$-catalyzed reduction of esters was shown to be a competitive synthesis protocol to previously reported approaches in order to prepare uniform PEGs. Investigations of the reduction step, in terms of reducing agent and their used quantity, catalyst loading and reaction time, were carried out *via* NMR and IR monitoring. Full conversion was achieved while keeping the overreduction and the formation of the side products at an appropriate low level. In this way, the successful addition of one EG monomer unit *via* a three-step reaction cycle, as well as the potential of increasing the degree of elongation per cycle, was shown.

4.2. Synthesis and characterization of uniform PCLs

In this chapter, the synthesis of uniform oligo(ε-caprolactone) is presented and discussed. All procedures were performed according to the iterative exponential growth strategy reported by HAWKER *et al*.[240] A schematic overview of the synthesis protocol is shown in Scheme 44. Parts of the synthesis within this project were already examined in more detail during the master thesis of the author.[618] With these findings, the synthesis protocol for the preparation of uniform PCL was started again from the beginning on a larger scale. Footnotes in the experimental section mark the molecules, which were already synthesized and fully characterized during the master thesis.

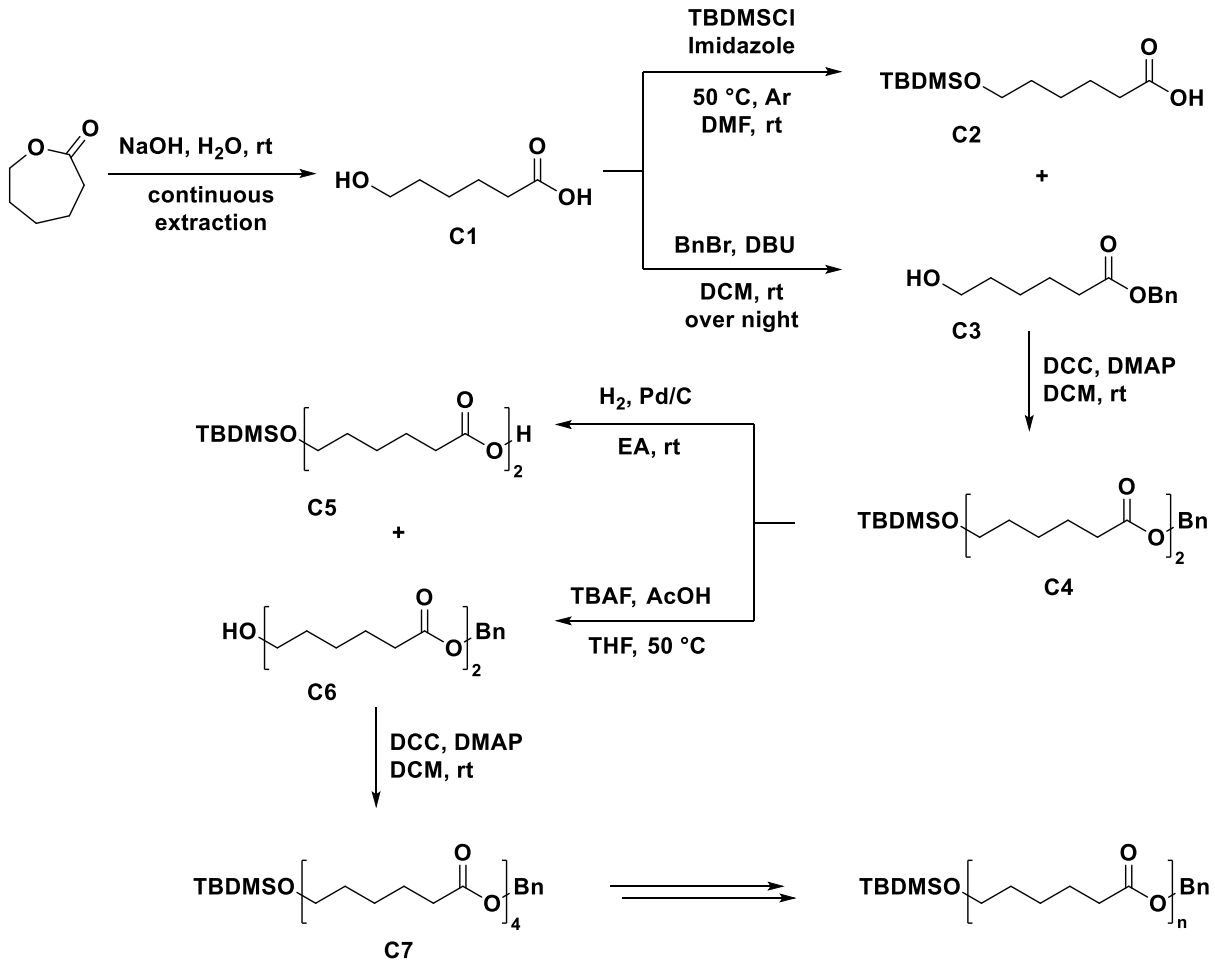

Scheme 44: Synthesis of uniform oligo(ε-caprolactone) *via* iterative exponential growth strategy according to the procedure of HAWKER *et al*.[240]

First, a base-catalyzed ring-opening of ε-caprolactone was performed on a multi-gram scale, and the monomer unit, 6-hydroxyhexanoic acid **C1**, was obtained in 94% yield *via* continuous extraction with diethyl ether over four days. In the next divergent step, the functional groups were protected separately using orthogonal protecting groups.

Therefore, the alcohol moiety of one batch of **C1** was protected with *t*-butyldimethylsilyl (TBDMS) ether, and the carboxylic acid of another batch of **C1** was transferred into a benzyl ester. The selection of the protecting groups was performed according to HAWKER *et al*. after a comparison of different protecting groups. This orthogonal pair was proven the most efficient and selective in consideration of the complete synthesis protocol.[240] The subsequent convergent coupling reaction of the monofunctionalized compounds **C2** and **C3** was performed *via* a Steglich esterification using DCC for activation of the carboxylic acid and DMAP as catalyst, also according to the procedure of HAWKER *et al*. As reported, activation *via* acyl halides or other active esters resulted in low yields or partial deprotection of the TBDMS group. The doubly protected dimer **C4** was obtained as the product of the esterification. Afterwards, the protecting groups were cleaved orthogonally under specific reaction conditions. The benzyl ester was deprotected *via* reductive hydrogenation and the silyl ether by treatment with tetra-*n*-butyl ammonium fluoride (TBAF) under acidic conditions, affording either the carboxyl- or the hydroxyl-terminated dimers **C5** and **C6** in quantitative yields. By repetition of the coupling step and the separate deprotection reactions, the caprolactone chain grows in an exponential manner. From the synthesis of the octamer on, 4-(dimethylamino)pyridinium *p*-toluenesulfonate (DPTS) was used instead of DMAP to suppress the formation of reported unreactive *N*-acyl ureas.[633,634] Using this IEG-strategy, a carboxyl-terminated PCL_{64} **C20** was obtained in 20 steps in an overall yield of 33.1%, considering always the lowest yield of the divergent steps. In total, 88 column chromatographic purification steps were performed during this synthesis. Each of the products was characterized with ^{1}H, ^{13}C, and IR spectroscopy, as well as MS and SEC to confirm the high purity. The complete characterization data of all products is provided in the experimental section. In Figure 38, representative ^{1}H NMR spectra for the products obtained from the Steglich esterification and both separate orthogonal deprotection steps are shown, using the octamer derivatives as an example. The spectrum of the doubly protected octamer **C10** is shown in green on top. All peaks were assigned to the molecular structure. The characteristic signals of the protection groups, as well as the methylene groups in α-position, respectively, are highlighted in yellow for the TBDMS group (signal 4 at 3.55 ppm, 10 at 0.85 ppm, and 11 at 0.01 ppm) and in green for the benzyl ester (signal 1 at 7.35 ppm, 2 at 5.08 ppm and 5 at 2.35 ppm). After deprotection of the benzyl ester *via* a reductive hydrogenation, where toluene is released and the carboxylic acid is formed (product **C11**, blue spectra

in the middle), the signals 1 and 2 have completely vanished and the signal at 12.05 ppm, belonging to the acid proton, was observed. In addition, the methylene group in α-position (signal 5) was shifted upfield. For the TBDMS deprotection, similar changes of the corresponding signals were observed. The ^{1}H NMR spectrum of product **C12** is shown on the bottom Figure 38 in red. The peaks of the TBDMS moiety at 0.85 and 0.01 ppm completely vanished and a signal belonging to the formed alcohol appeared at 4.36 ppm. As for the benzyl deprotection, the methylene group in α-position is shifted upfield (from 3.55 to 3.36 ppm).

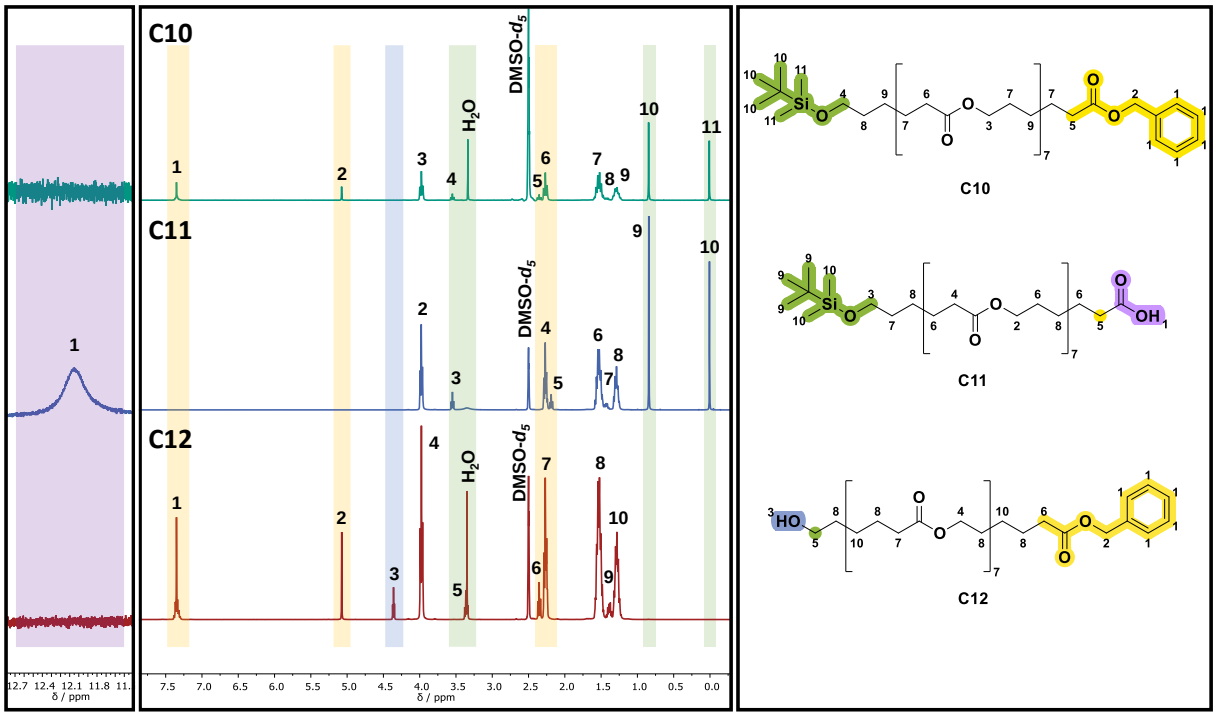

Figure 38: Comparison of ^{1}H NMR spectra of octa(ε-caprolactone) derivatives. The green spectrum on the top shows the characteristic signals of the doubly protected octamer **C10**. The specific peaks **10** and **11** for the TBDMS protecting group are highlighted in green at 0.01, 0.85 ppm, and for the α-methylene group **4** at 3.55 ppm, and for the benzyl ester in yellow, at 7.35 ppm for the aromatic protons (signal **1**), at 5.08 ppm for the benzyl methylene group (signal **2**) and the α-methylene group **5** at 2.35 ppm. After reductive hydrogenation of the benzyl ester, the corresponding peaks completely vanished and a signal at 12.1 ppm is observed for the carboxylic acid (signal highlighted in purple, blue spectrum in the middle of compound **C11**). The α-methylene group next to the carboxylic acid shifted to 2.19 ppm. In the case of TBDMS cleavage (red spectrum on the bottom of **C12**), the corresponding peaks highlighted in green completely vanished, and the α-methylene group next to the resulted alcohol (at 4.36 ppm) function shifted to 3.36 ppm. These spectra are representative for all coupling and deprotection products obtained during the IEG. A full characterization for each of them is provided in the experimental section.

In addition, Figure 39 shows the comparison of the corresponding ^{13}C NMR spectra of the octamer derivatives **C10** (green spectrum, top), **C11** (blue spectrum, middle) and **C12** (red spectrum, bottom) and the change of the peak pattern as a result of the separate orthogonal cleavage of the TBDMS- and the benzyl protecting group. The same color coding is used as in Figure 38. Thus, the carbon signals of the benzyl group (**2**-**6**, green spectrum, compound **C10**) are highlighted in yellow and vanish completely during the deprotection to the product **C11**. The carbonyl carbon **1** is shifted downfield to 174.4 ppm, whereas the signal corresponding to the methylene carbon in α-position to the ester, is shifted to 33.6 ppm and overlaps with another signal of the backbone.

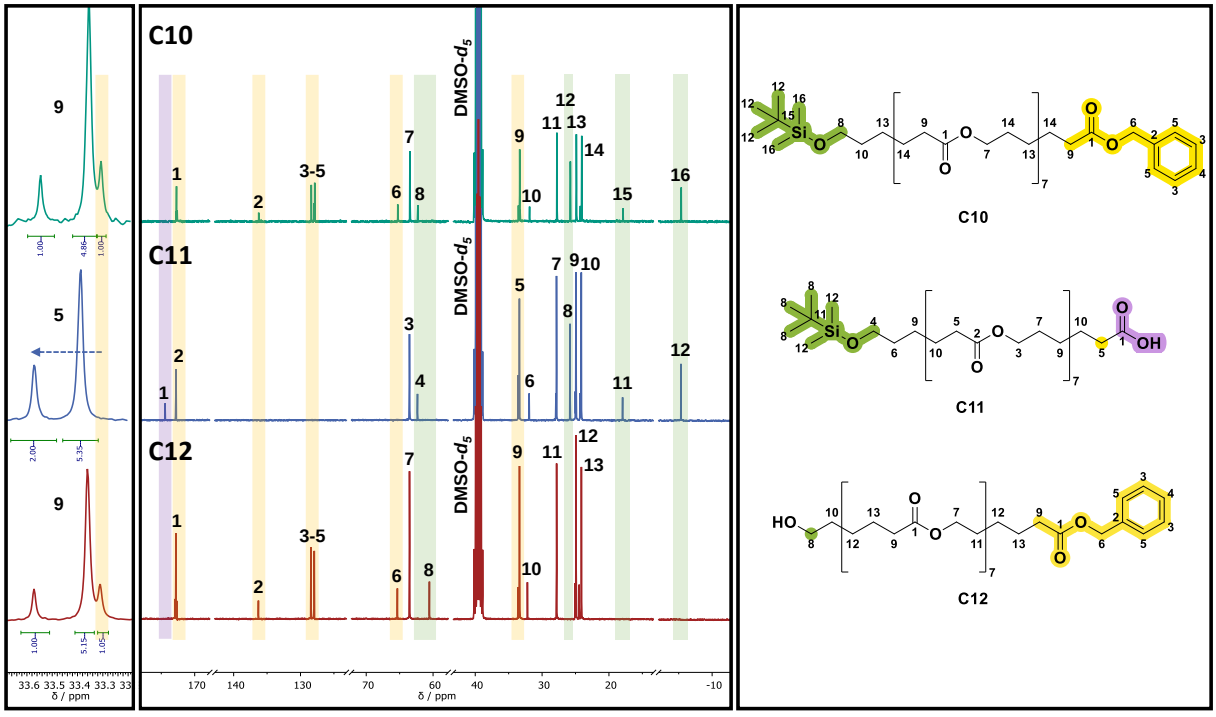

Figure 39: Comparison of ^{13}C NMR spectra of octa(ε-caprolactone) derivatives. The green spectrum on the top shows the characteristic signals of the doubly protected octamer **C10**. The specific peaks of the benzyl protection group highlighted in yellow are completely vanished after the reductive hydrogenation (compare blue spectrum of **C11**). Further, the CH_2-group in α-position to the ester and the quaternary carbon of the carboxylic acid is shifted downfield to 33.6 ppm and overlaps with another backbone signal (detailed section **a**), and 174.4 ppm (signal **1** of **C11**, highlighted in purple), respectively. In the case of the TBDMS cleavage (red spectrum on the bottom of **C12**), the corresponding peaks, highlighted in green, completely vanished and the α-methylene group next to the resulting alcohol is shifted upfield from 62.3 to 60.6 ppm. These spectra are representative for all coupling and deprotection products obtained during the IEG. A full characterization for each of them is provided in the experimental section.

This is an assumption based on the integral ratio shown in the spectrum cutout, but could not be confirmed by correlated 2D NMR, since the signals are too close to each other. On the other hand, the vanishing of the signals, which belong to the TBDSM protecting group (signal **12**, **15**+**16**, highlighted in green) confirmed the complete deprotection yielding the alcohol **C12** (red spectrum, bottom). Furthermore, the methylene carbon in α-position to the alcohol (signal **12**) is shifted upfield, when compared to the silyl ether.

Figure 38 and Figure 39 clearly point out that ^{1}H and ^{13}C NMR spectroscopy is a solid tool for monitoring the separate deprotection of the orthogonal protecting groups as well as the coupling reaction of the IEG growth strategy towards uniform PCLs. However, as described in section 4.1.1.3, one analytical method is not sufficient to determine the purity, and especially not the uniformity of a compound.

In accordance to the description of HAWKER *et al.*, from the synthesis of the hexadecamer on, a small impurity, that matches in terms of the retention time, to the precursor molecules, respectively, was observed. In the literature, they specified the products with purities >95%, which were used without further purification.[633] Here, a purity of 98.6% was determined by SEC analysis for the doubly protected hexadecamer **C13** after flash column chromatography (see Supplementary Figure 104). Strictly speaking, these compounds are to be declared as non-uniform molecules according to the official IUPAC definition of uniform polymers.[80] Therefore, we focused on the careful purification of compound **C13** *via* fractionating column chromatography. The crude product of a 15.5 mmol (31.8 g) batch was applied on a silica column and the mobile phase was chosen to allow the product to elute as slowly as possible. Thus, the separation from impurities of precursor molecules, which exhibit almost similar retention factors, is more likely. Three of these fractionating isolation steps were performed, and in total 46 fractions were collected, 31 of which contained the product in purities ranging from 50.2 to >99%. The SEC chromatograms are shown in Supplementary Figure 100 - Supplementary Figure 103 and the corresponding evaluated data sets in Supplementary Table 13 - Supplementary Table 16. The fractions highlighted in green exhibit a high purity of >99% and were selected for further synthesis. The samples with an insufficient purity were either further purified (highlighted in yellow) or discarded, if they only contained a few milligrams of the product or if no product was found (highlighted in red). Impurity signals ranging from 15 to 21 min in the SEC chromatogram were observed for the individual purification

steps. By comparison with the chromatograms of the starting materials, the according signals could be identified. The masses corresponding to the other signals could be obtained *via* SEC-ESI-MS and thus give more insight into formed side products. Initially, 1.4% of impurity were detected in a 31.8 g sample after purification *via* flash column chromatography (Supplementary Figure 100 - Supplementary Figure 103 and Supplementary Table 13 - Supplementary Table 16), which correlates to 446 mg. After performing the fractionated column chromatography, 1.20 g of impurities were obtained, which were not detected before (please note: this amount also contains impurities from the used solvents). In total, approximately 60 L of solvents were used for the purification. Each purification step required about one week of work, but in the end, the doubly protected hexadecamer **C13** was obtained in a yield of 97.1% and a high purity confirmed by SEC (>99%), NMR spectroscopy, and MS. At this point of the study, it should be pointed out once more, that not only a completely optimized synthesis strategy, but also a careful purification and characterization is inevitable when preparing uniform macromolecules. Furthermore, an improvement of analytical instruments in terms of resolution, and preparative purification methods, which are at the moment rather expensive for large scale demands, is crucial.

The same effort was performed for the isolation of the doubly protected PCL_{32} **C16**, resulting in 82.8% yield and a purity of >99% (SEC) after two consecutive fractionating column chromatography steps (see Supplementary Figure 111 and Supplementary Figure 112, and Supplementary Table 17 and Supplementary Table 18). Since the focus of this thesis was more on the high purity of the products than on the yield, the doubly protected PCL_{64} was purified only once (*i.e.,* impure fractions were discarded instead of performing additional column chromatography), resulting in a yield of 84.1% (7.34 g) and a purity of >99% (SEC). Thus, enough product was obtained for the remaining synthetic steps. Nevertheless, especially for long synthesis protocols, a high yield is essential. An overview of all steps, including the scale, yield, dispersity, and purity determined by SEC is shown in Table 5. A full characterization *via* NMR as well as IR spectroscopy and MS of each of the products is provided in the experimental section (chapter 4.2).

Table 5: Overview of scale, yield, dispersity, and purity of the synthesized PCL.				
product	scale / mmol	yield / %	$Đ^1$	purity[1] / %
C1	263	94.3	1.00	>99
C2	125	85.3	1.00	>99
C3	127	87.9	1.00	>99
C4	45.1	88.3	1.00	>99
C5	11.1	99.0	1.00	>99
C6	27.7	98.9	1.00	>99
C7	86.3	87.9	1.00	>99
C8	14.7	99.1	1.00	>99
C9	8.84	99.8	1.00	>99
C10	41.5	94.4	1.00	>99
C11	2.64	quant.	1.00	>99
C12	2.64	97.3	1.00	>99
C13	1.92	97.1	1.00	>99
C14	7.29	quant.	1.00	>99
C15	7.32	98.1	1.00	>99
C16	5.37	82.8	1.00	>99
C17	1.81	93.4	1.00	>99
C18	1.81	96.5	1.00	>99
C19	1.16	84.1	1.00	>99
C20	0.40	95.0	1.00	99
[1] determined *via* SEC (system II)				

The carboxyl-terminated PCL_{64} **C20** was obtained in an overall yield of 33.1% in 20 reaction steps. A minor impurity of 1% was observed in the SEC after the last reductive hydrogenation, thus a purity of 99% is reported, which was used without further purification in a coupling reaction with product **P23** (chapter 4.3). All precursor PCL derivatives from the monomer **C1** to the doubly protected PCL_{64} **C19** were obtained in a purity >99% (SEC) and can be declared as uniform. An overview of the corresponding SEC chromatograms is shown in Figure 40, ranging from the monomer unit 6-hydroxyhexanoic acid **C1** in light green at a retention time of 21.0 min to the doubly protected PCL_{64} **C19** in dark green at 13.8 min All traces show a monomodal

and narrow shape, indicating the high purity of the compounds. Only the final product **C20** shows a small impurity of 1% at 15.2 min.

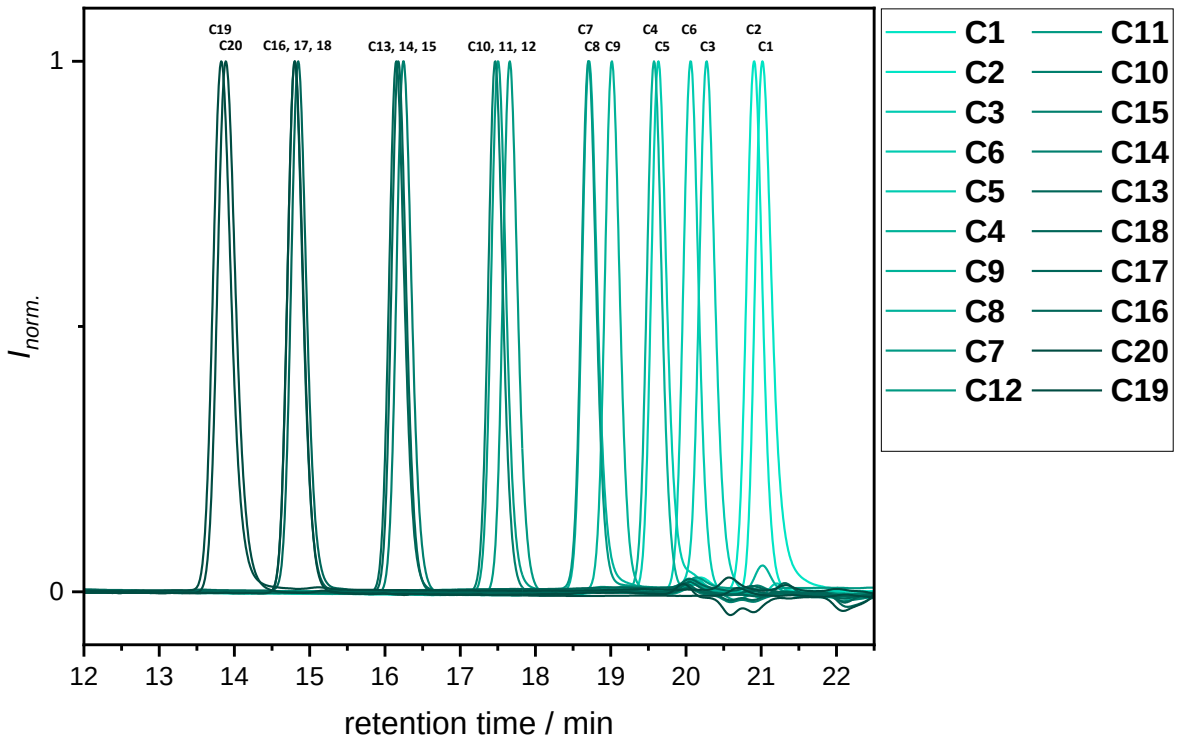

Figure 40: SEC overview of the synthesized PCLs. The SEC traces range from the monomer, 6-hydroxyhexanoic acid **C1** at a retention time of 21.0 min in light green to the doubly protected PCL_{64} **C19** at 13.8 min in dark green. All traces show a narrow and monomodal shape indicating the high purity of the products.

The exponential chain growth can also be monitored with NMR spectroscopy. Figure 41 shows the stacked ^{1}H NMR spectra of the individual doubly protected PCLs. A clear increase of the caprolactone backbone integrals is observed due to the chain doubling per iterative reaction cycle, which is highlighted in Figure 41 with the light blue triangles. Since the proton number of end groups for the doubly protected PCLs is constant during the complete synthesis protocol, the integrals of the orthogonal protecting groups are consistent.

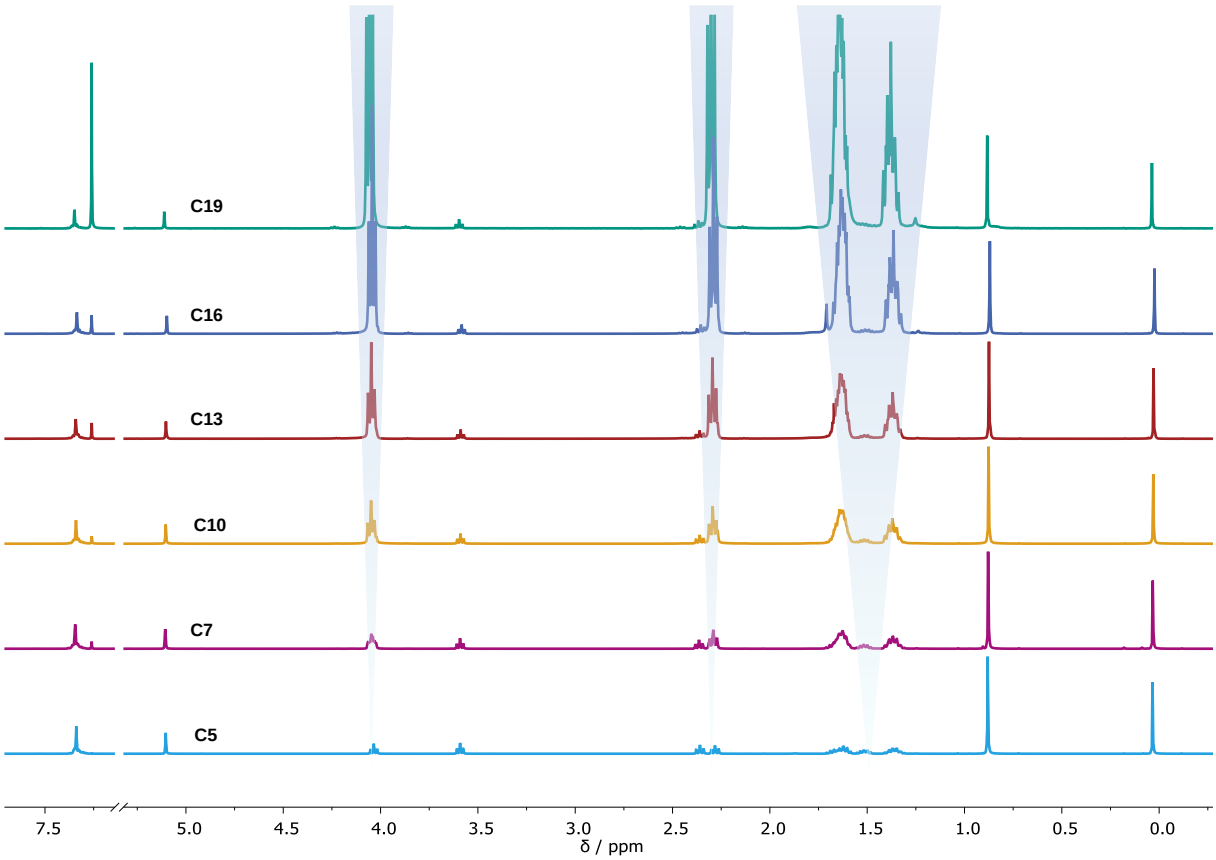

Figure 41: Stacked ^{1}H NMR spectra of the synthesized doubly protected oligo(ε-caprolactone)s from the dimer **C4** on the bottom (light blue spectrum) to the 64-mer **C19** on top (green spectrum). The increase of the backbone signals with increasing chain length is highlighted in blue.

4.3. Uniform PEG-*b*-PCL block copolymers

In order to synthesize uniform PEG-*b*-PCL block copolymers, the hydroxyl-terminated mPEG$_{16}$ **P23** was reacted in a Steglich esterification with the corresponding carboxyl-terminated oligo(ε-caprolactone) **C14**, **C17**, and **C20** of desired chain length (Scheme 45). Applying the same reaction conditions as for the oligo(ε-caprolactone) coupling reaction, only 16% product formation was observed after two days of stirring at room temperature, as determined *via* SEC. After further addition of 0.8 equiv. catalyst (DPTS) and 6.00 equiv. of DCC (in portion of 2.00 equiv.) 62% of product formation was observed after stirring for nine days. From the beginning, side reactions towards side products eluting at a lower retention time than the desired **uBCP-1** were observed. The reaction was stopped and purified *via* column chromatography twice, to afford the product **uBCP-1** in a moderate yield of 54%. Unfortunately, the side product at lower retention times could not be completely removed. The SEC chromatograms of the fractions obtained from the isolation steps are provided in the experimental part (Supplementary Figure 132 and Supplementary Figure 133). To identify the formed

side products with a higher hydrodynamic volume, further analysis, *e.g.,* SEC-ESI-MS needs to be performed.

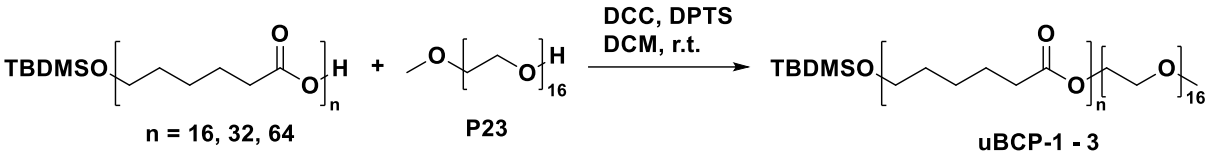

Scheme 45: Reaction scheme for the synthesis of uniform PEG-*b*-PCL BCPs. The hydroxyl-terminated mPEG$_{16}$ **P23** was coupled *via* a Steglich esterification with the corresponding carboxyl-terminated oligo(ε-caprolactone)s **C14**, **C17**, and **C20** to obtain three PEG-*b*-PCL BCPs varying in the length of the hydrophobic ε-caprolactone block.

Since further addition of DPTS and DCC to the reaction mixture increased the conversion, the catalyst was used in equimolar amounts and the carbodiimide in an excess of 6.00 equiv. in a second approach directly from the beginning. After stirring at room temperature overnight, almost full conversion was observed *via* SEC analysis. A comparison of the reaction control and the starting materials **P23** and **C14** is shown in (Figure 42 a). The formation of the desired product **uBCP-1** was confirmed by the appearance of a new signal at a retention time of 15.9 min. As already observed in the first approach, a side product at a lower retention time (14.9 min) was detected. However, remarkably less of the side product was observed if compared to the first test reaction. Furthermore, a slight tailing towards higher retention times and a small signal at 18.8 min were observed, which might be assigned to remaining starting material. In general, the reaction process was significantly improved by using these optimized conditions, which were thus also used for the synthesis of **uBCP-2** and **uBCP-3** as well.

Purification *via* column chromatography was challenging, since the elution behavior of the different substances were very similar and the substances were only slightly visible on a TLC plate, independent from the choice of staining solution (Seebach, vanillin or $KMnO_4$), resulting in loss of yield. The fractions obtained after the isolation of the product are shown in Figure 42 b. Fractions 1 and 3 contain mostly the product, but also either small impurities at a lower retention time (green trace) or a slight tailing towards higher retention times. Therefore, only 49% of product **uBCP-1** were obtained in a purity of >99%.

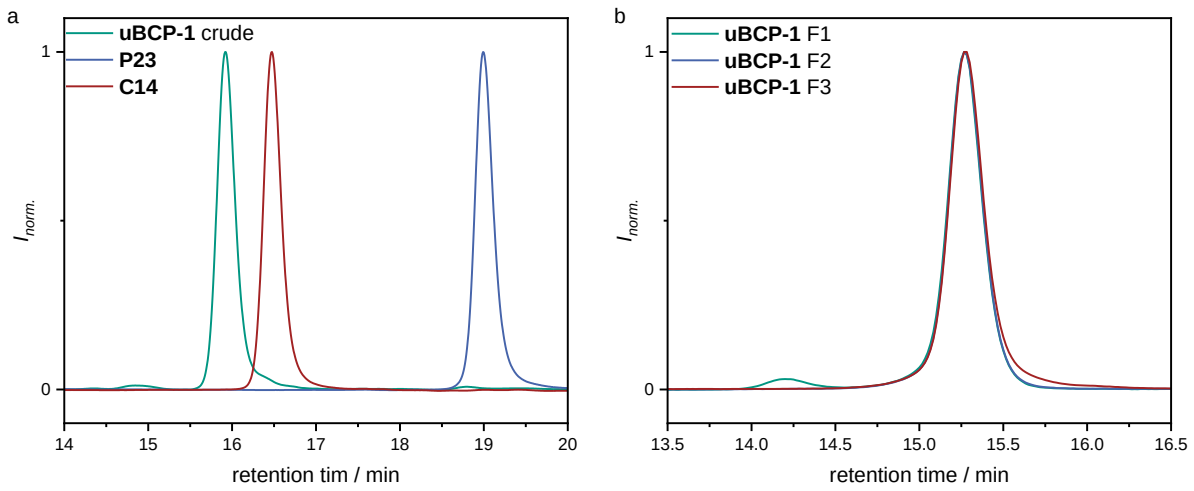

Figure 42: SEC analysis for the synthesis and purification of **uBCP-1**. a The uniform homopolymers are shown in the blue and the red trace. The green trace shows the chromatogram of the corresponding **uBCP-1** after the coupling reaction. Only small impurities were observed at a retention time of 14.9 min and 18.8 min, and a tailing towards higher retention time. b Different fractions (F1-F3) of the isolation process of **uBCP-1** *via* column chromatography. The blue traces (F2) shows a narrow and monomodal shape, indicating a high purity of the product, whereas the blue (F1) and the red (F3) chromatograms show small impurities at higher and lower retention times.

The coupling reaction of the mono functionalized homopolymers **P23** and **C14** could also be monitored *via* ^{1}H NMR spectroscopy, as shown in Figure 43. The green spectrum on top corresponds to the $mPEG_{16}$ homopolymer **P23**. During the esterification with the TBDMS protected PCL_{16} homopolymer **C14** (blue spectrum, middle), only the signal assigned to the methylene group next to the hydroxyl moiety (signal **3**, highlighted in blue, top spectrum) is shifted downfield from 3.59 to 4.22 ppm, due to a higher deshielding caused by the formed ester function in proximity. All other signals of the homopolymers **P23** and **C14** remain at the same chemical shifts in the resulting **uBCP-1**. Since signal **2** of the PCL homopolymer **C14** (highlighted in green, middle spectrum) exhibits a similar chemical shift as signal **3** of the PEG homopolymer **P23** (highlighted in blue, top spectrum), 2D NMR spectra (COSY and HMBC, see experimental section, Supplementary Figure 129 and Supplementary Figure 130) were recorded to confirm the presented peak assignment of the **uBCP-1**.

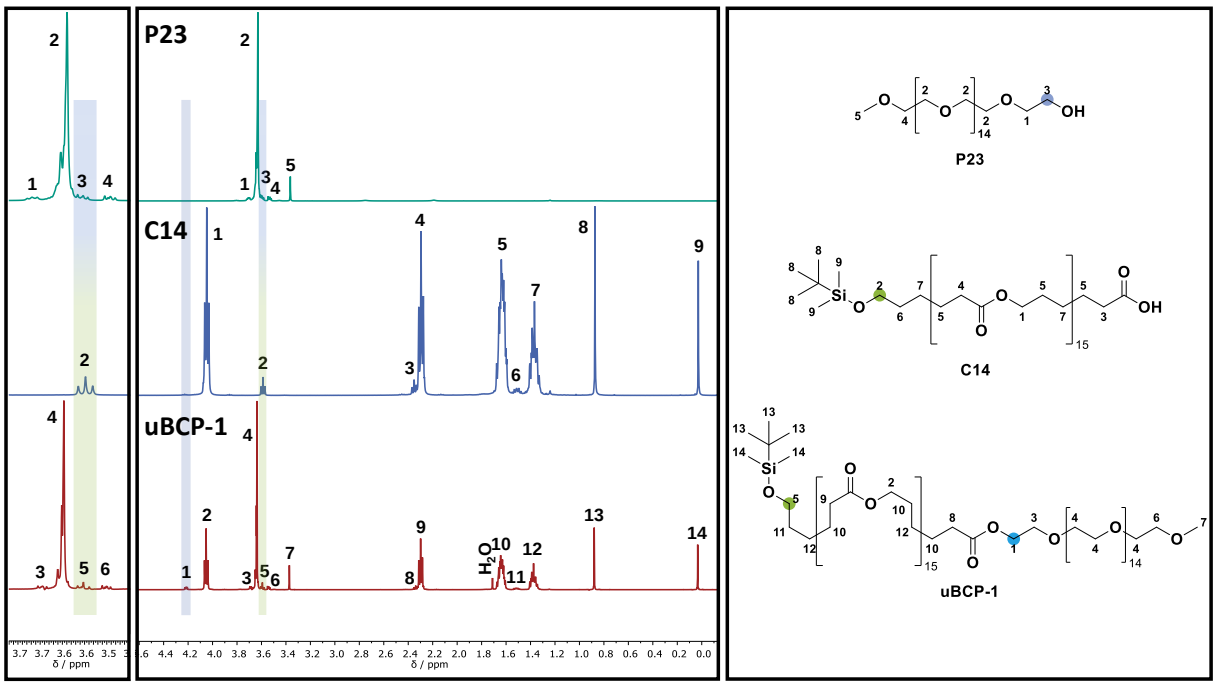

Figure 43: Comparison of ^{1}H NMR spectra of the monomethyl hexadeca(ethylene glycol) **P23**, the carboxyl-terminated hexadeca(ε-caprolactone) **C14** and the corresponding product **uBCP-1**. Signal **3** of the mPEG16 is shifted upfield from 3.59 to 4.22 ppm due to the esterification. All other signals remain at the same chemical shift. These spectra are representative for the synthesis of all three BCP. A full characterization for each of them is provided in the experimental section.

The comparison of the ^{13}C spectra of the PEG_{16} and PCL_{16} homoblocks **P23** and **C14** with the desired block copolymer **uBCP-1** is shown in Figure 44. The carbon signals next to the alcohol of **P23** or the carboxylic acid of **C14**, are shifted in the product spectrum (red spectrum middle) and highlighted in the respective color code. Signal **1** of the $mPEG_{16}$ is shifted upfield from 72.7 to 69.3 ppm (highlighted in orange), whereas signals **5** and **4** are shifted downfield due to the coupling reaction. The latter overlaps with the backbone ethylene peak **3** at 70.7 ppm in the product spectrum (highlighted in purple). Similar to that, the carbonyl signal **1** at 117.0 ppm (highlighted in green) and the CH_2-group in α-position to the ester of the PCL_{16} homoblock at 33.7 ppm (highlighted in blue) are shifted to 173.7 and 34.2 ppm, respectively and are overlapping with the backbone peaks.

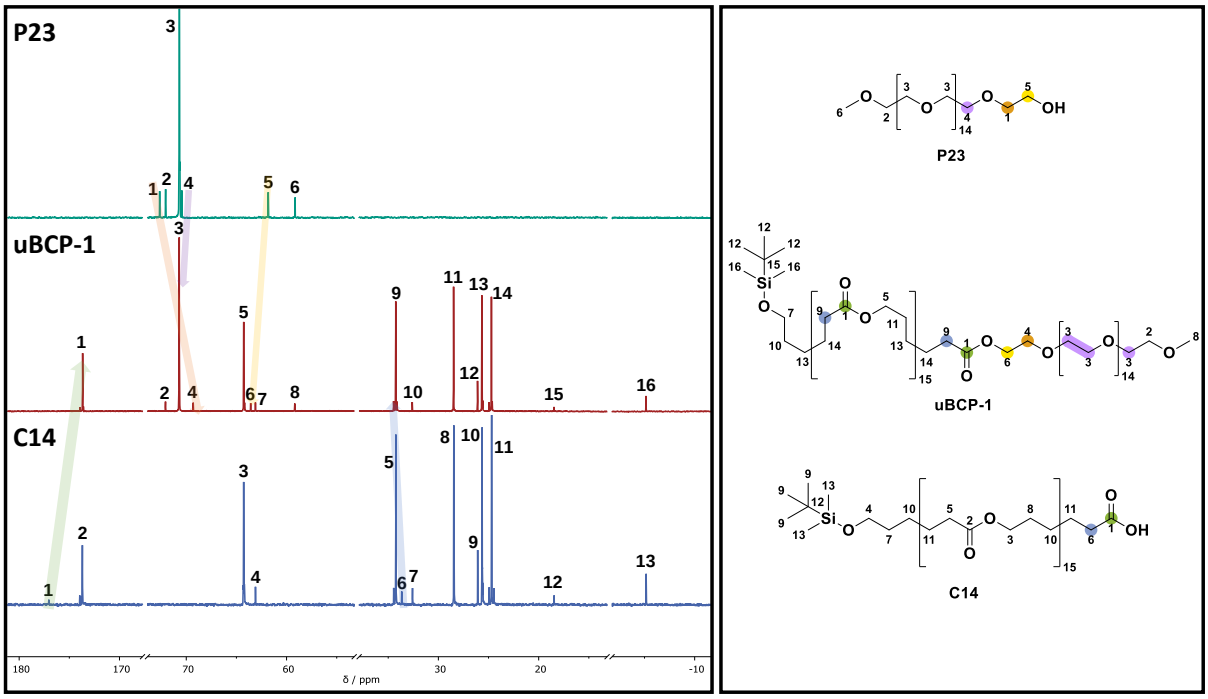

Figure 44: Comparison of ^{13}C NMR spectra of the monomethyl hexadeca(ethylene glycol) **P23**, the carboxyl-terminated hexadeca(ε-caprolactone) **C14**, and the corresponding product **uBCP-1**. The signals next to the alcohol of **P23** or the carboxylic acid of **C14**, are shifted in the product spectrum (red spectrum middle) and highlighted in the respective color code A full characterization for each of them is provided in the experimental section.

Additionally, ESI-MS and DOSY analyses were performed to further determine the purity of the product. The found mass and the experimental isotopic pattern of the single charged sodium adduct ($[M+Na]^+$ *m/z* found 2698.6143 matched with the calculated *m/z* values ($[M+Na]^+$ *m/z* calc. 2698.6106, Figure 45). The complete ESI-MS spectrum and the found masses are provided in the experimental section 6.3.5 in Supplementary Figure 127.

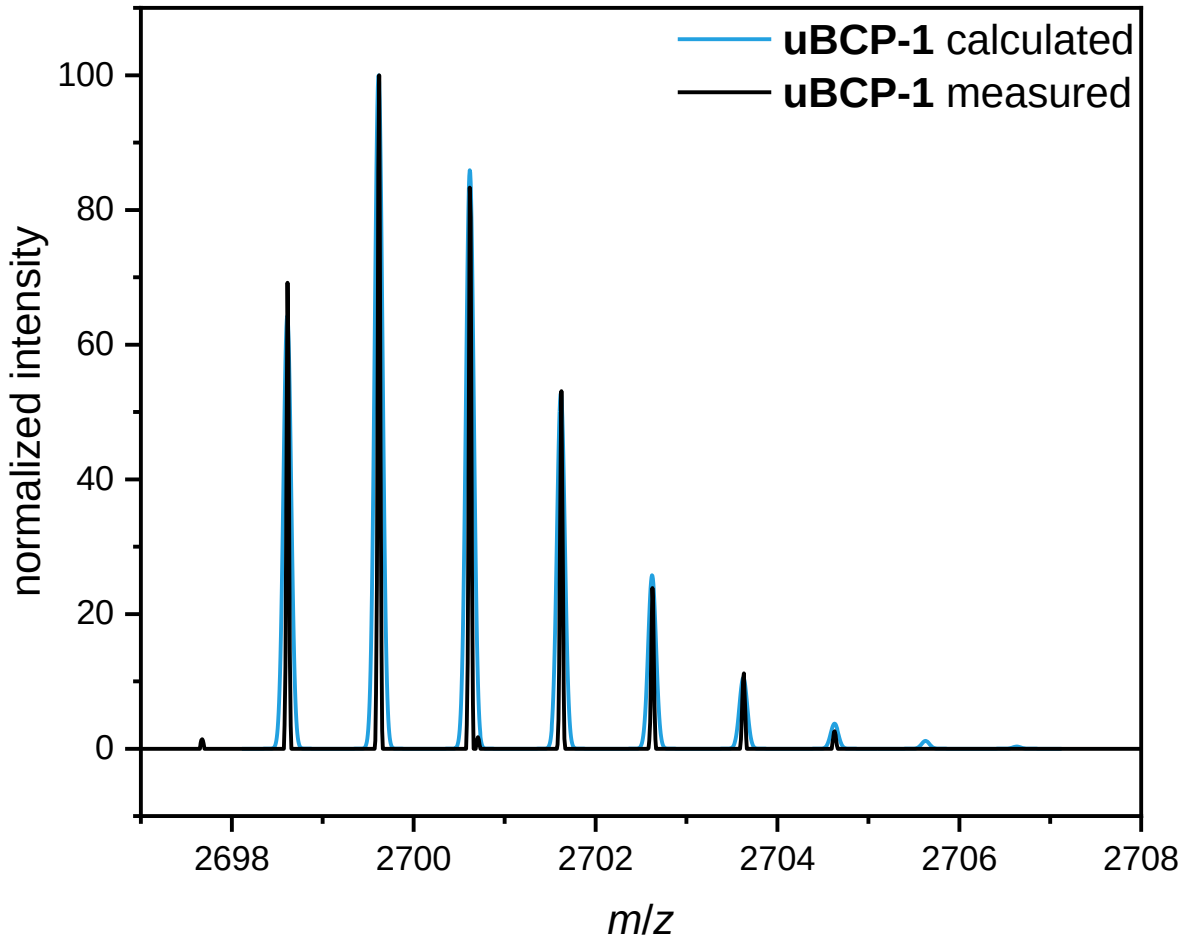

Figure 45: Comparison of the isotopic pattern of the single charged sodium adduct of the experimental **uBCP-1** (black spectrum) and the calculated values (blue spectrum).

We have recently demonstrated that the uniformity of a sequence-defined decamer, obtained *via* an iterative Passerini reaction and subsequent deprotection, was confirmed with DOSY experiments.[635] Therefore, the product **uBCP-1** was analyzed *via* DOSY at a concentration of 0.8wt% and except for a weak water signal with a diffusion coefficient of $D = 5.48 \times 10^{-9}$ m^2 s^{-1}, the desired product **uBCP-1** was the only detected signal with a diffusion coefficient of $D = 3.32 \times 10^{-10}$ m^2 s^{-1} and thus confirming the high purity (Figure 46). Surprisingly, in the DOSY spectrum of **uBCP-2** several peaks ranging from $D = 1.50 \times 10^{-10}$ - 6.48×10^{-10} m^2 s^{-1} were observed and were confirmed by repetition of the measurement (see experimental section Supplementary Figure 126). This is in contrast to the results observed from NMR, SEC, and MS analyses. Furthermore, the direct comparison to the DOSY results of the disperse block copolymer **dBCP-2** (see experimental section Supplementary Figure 137) is contradictory to these results, since a distinct signal with a diffusion coefficient

of $D = 2.14 \times 10^{-10}$ m^2 s^{-1} was observed. Further investigations need to be performed to explain the peak pattern observed for **uBCP-2**.

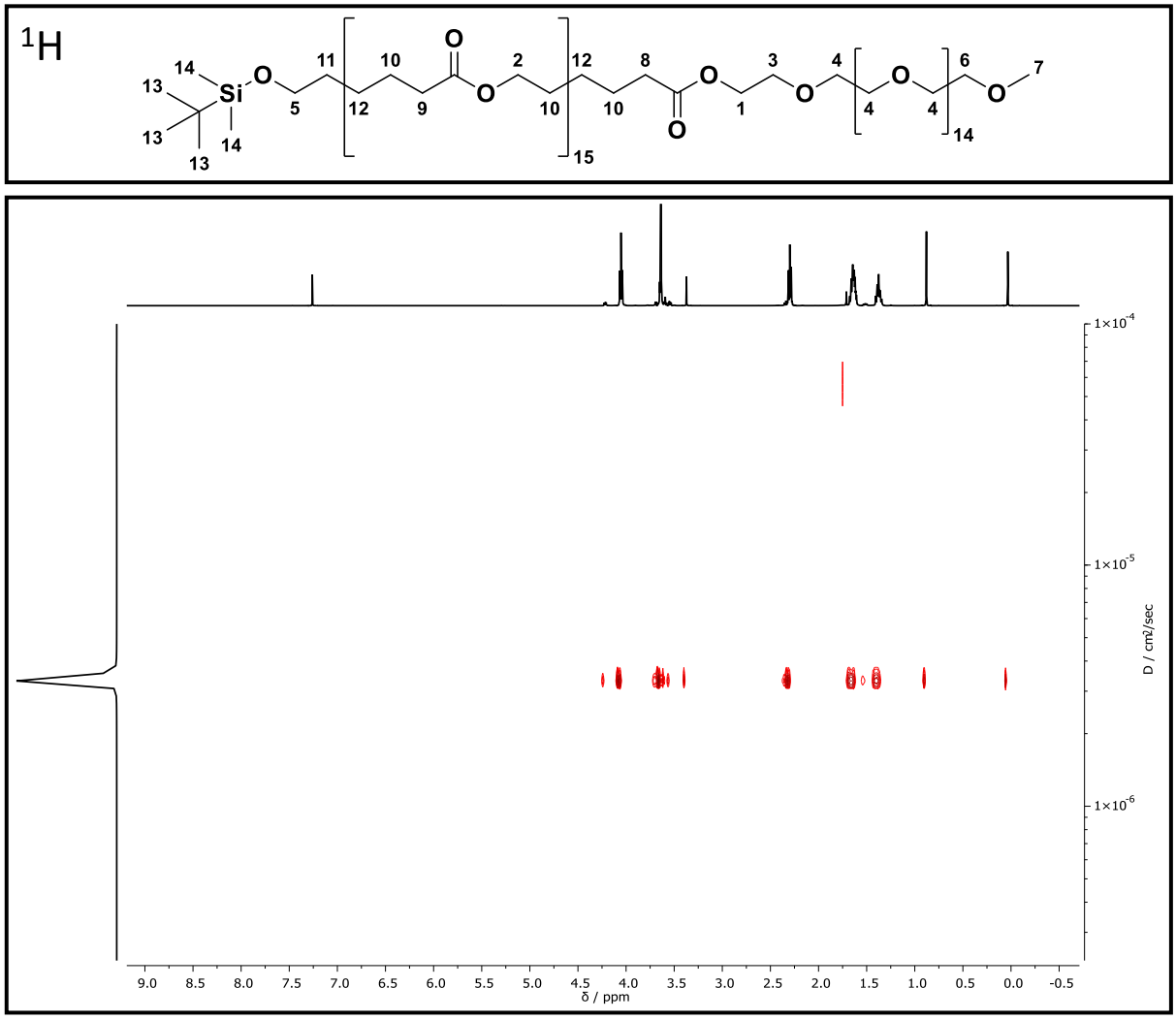

Figure 46: Spectrum of the DOSY experiment of the **uBCP-1**.

The same synthesis protocol as for **uBCP-1** was conducted using the carboxyl-terminated PCL homopolymers **C17** and **C20** with a chain length of 32 and 64 units, respectively yielding the corresponding **uBCP-2** and **uBCP-3**. Thus, a set of three block copolymers were synthesized varying in the domain length of their PCL block and therefore in the ratio of the hydrophilic to the hydrophobic part. After purification *via* column chromatography, product **uBCP-2** was obtained in a yield of 43.2% (four isolation steps) and **uBCP-3** in 18.4% (three isolation steps) in a high purity of >99% determined by SEC analysis. The SEC chromatograms of the individual purification steps and the evaluated data is provided in the experimental section 6.3.5. Only the fraction with the highest purity was included in the yield and used for the intended purpose of this thesis, resulting in a drastic loss of yield. For all the other fractions, also

excellent purities were obtained. The complete characterization of the block copolymers **uBCP-1** and **uBCP-2** including ^{1}H, ^{13}C, and diffusion-ordered NMR, and IR spectroscopy, SEC, and high-resolution ESI-MS was performed. Furthermore, DSC and SAXS analyses were conducted to investigate the structure-property-relationship, in terms of the self-assembly behavior of the presented block copolymers, depending on the dispersity (see section 4.5). Unfortunately, impurities of mPEG$_n$-*b*-PCL$_{m-1}$-TBDMS were observed in the ESI-MS spectra of the products **uBCP-2** and **uBCP-3**, which could not be quantified with an additional analysis tool. Therefore, only **uBCP-1** is considered uniform as indicated by the complete characterization, whereas **uBCP-2** and **uBCP-3** must be classified as “uniform with respect to SEC” according to the official IUPAC definition of a uniform polymer.[80] The SEC chromatograms of the three block copolymers are presented in Figure 47. All SEC traces show a narrow and monomodal shape, indicating uniform structures.

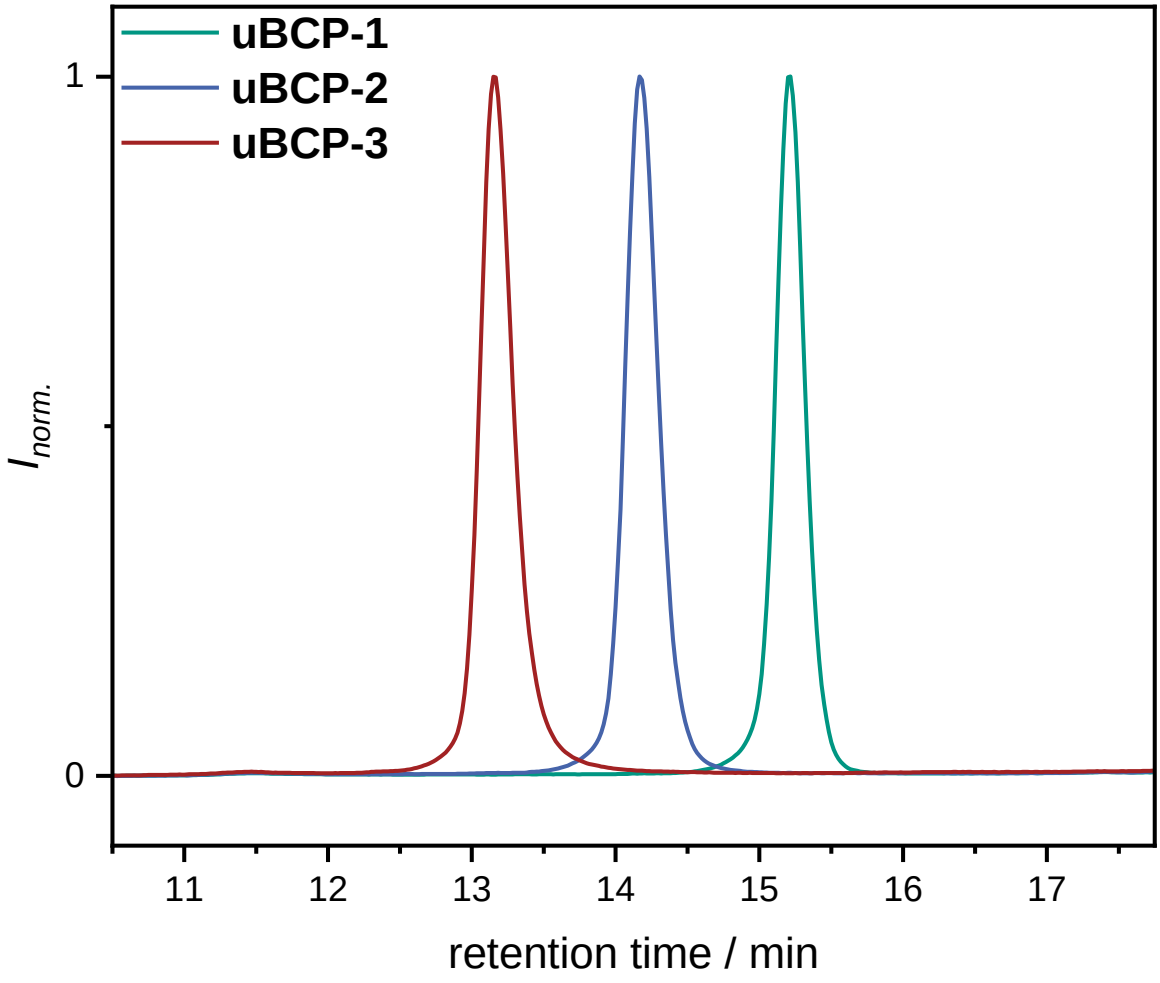

Figure 47: SEC chromatograms of the three synthesized uniform block copolymers **uBCP-1** (green), **uBCP-2** (blue), and **uBCP-3** (red).

In order to investigate the structure-property relationship in terms of the self-assembly behavior of the amphiphilic block copolymers, identical structures, similar in M_n with the uniform BCP, but exhibiting a slight molecular weight distribution, were prepared. The synthesis and characterization are explained in detail in the following chapter.

4.4. Disperse PEG-*b*-PCL block copolymers

The disperse PEG-*b*-PCL block copolymer analogs were prepared in a two-step synthesis. First, a base-catalyzed ring-opening polymerization of ε-caprolactone was conducted using a commercially available monomethyl poly(ethylene glycol) with a number average molecular weight of M_n = 750 Da as macroinitiator. The reaction was performed according to the procedure of HEDRICK, WAYMOUTH and coworkers, and TBD was utilized as organo-catalyst (Scheme 46).[408] Increasing the equivalents M of the monomer ε-caprolactone and thus the resulting ratio to the amount of used macroinitiator, increases the polymerization speed, and thus offers the possibility to have a control of the dispersity *Đ* of the desired block copolymer, since the probability of side reactions increases with the reaction time. A detailed study of the influence of several catalysts and different monomers on the conversion and the dispersity is presented in the literature.[408]

Scheme 46: Reaction scheme for the synthesis of PEG-*b*-PCL BCP. mPEG (M_n = 750 Da) was used as a macroinitiator for the TBD-organo-catalyzed ROP of ε-caprolactone. By variation of the equivalents (M) of the ε-caprolactone, the DP (n) was controlled (M > n). The reaction conditions were adopted from HEDRICK, WAYMOUTH and coworkers.[408]

The reaction was performed under water-free and inert conditions, since water could act as an initiation reagent or hydrolyzes the formed ester function under the used reactions conditions, which would lead to unwanted side products. Therefore, all chemicals were dried carefully prior to usage. A detailed description of the reaction procedure is provided in the experimental section 6.3.6. Since we were aiming for polymers with similar M_n, compared to the uniform analogs, and thus the same retention time in SEC (assuming a symmetrical peak shape), monitoring *via* SEC was performed. The resulting stacked chromatograms received from five different approaches, varying in their M/I ratios, ranging from M/I = 40-1226, and the

corresponding evaluated data sets are shown in the experimental section 6.3.6. A linear relationship of the molecular weight depending on the reaction time was observed in all reactions, whereas the dispersity remained constant up to a reaction time of three hours for all approaches. After four hours, a slight increase was recorded for the reactions with a M/I ratio of 40, 80, and 167. Correspondingly, high molecular mass shoulders at lower retention times occurred in the associated SEC chromatograms, respectively. For the reaction with the highest M/I ratio of 1226, a low-molecular tailing, increasing over the reaction time, was observed. Such effects are caused by side reactions *via* intramolecular (backbiting) or intermolecular (chain transfer) transesterification reactions and could be prevented to a certain degree by increasing the monomer concentration and thus decreasing the reaction time to obtain the desired degree of polymerization. Furthermore, quenching of the catalyst with benzoic acid prevented post-polymerization transesterification. To achieve the correct retention time of the block copolymers in SEC, *i.e.,* the same retention time as for the uniform system described above, several approaches were carried out and stopped at minutes intervals, based on the results of the kinetic study. The corresponding SEC chromatograms as well as for the individual purification steps *via* column chromatography are shown in the experimental section 6.3.6. All chromatograms were recorded in the same sequence directly one after each other, to avoid shifting caused by pressure and temperature fluctuations of the instrument. The SEC results for the most suitable approaches for the comparison study with the uniform analogs are depicted in Figure 48 in green, blue, and red. Since the subsequent end-group functionalization increases the hydrodynamic radii of the polymers, the reactions were deliberately stopped at that point, where the corresponding SEC traces show a slight shift towards higher retention times compared to the uniform BCP (black traces). With the purification process, it was possible to reduce the high-molecular shoulder and the tailing, but unfortunately not to remove it quantitatively (see experimental section chapter 6.3.6). Further analysis *via* ^{1}H and ^{13}C NMR was performed, which is provided in the experimental section (chapter 6.3.6).

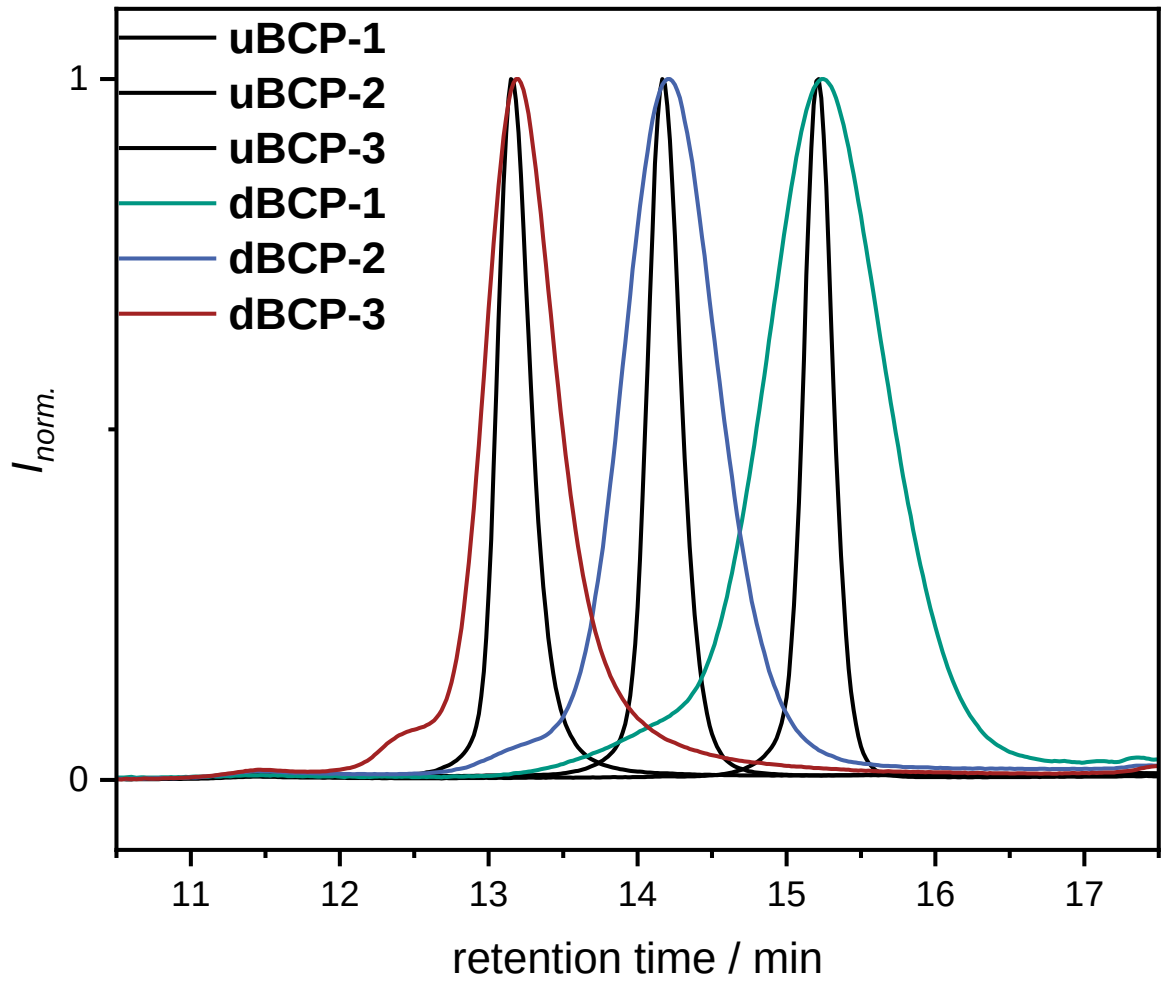

Figure 48: Comparison of the SEC chromatograms of the uniform **uBCP-1 – 3** (black traces) and the disperse alcohol-terminated block copolymers **dBCP-1** (green trace), **dBCP-2** (blue trace) and **dBCP-3** (red trace).

4.4.1. Protection of mPEG-*b*-PCL with TBDMS-Cl

In the final step, the hydroxyl end-group of the disperse block copolymers **dBCP-1 – 3** were capped in a post-polymerization protection with TBDMS-Cl (Figure 49 a). To ensure a quantitative functionalization, an excess of 30 equiv. of the silyl chloride and 1*H*-imidazole were used, respectively. The reaction was stirred overnight at 50 °C in DMF and the reaction process was monitored *via* NMR and IR spectroscopy and SEC to confirm complete conversion. ^{1}H NMR spectra were recorded in DMSO-d_6 in order to follow the conversion by the alcohol signal. The comparison or the relevant section of the spectra, before (**dBCP-1**, green) and after (**dBCP-4**, blue) the protection reaction is shown in Figure 49 b. Full conversion was observed due to the completed vanishing of the alcohol signal at 4.32 ppm (highlighted in yellow). However, since the products

dBCP-2 and **3** and the corresponding TBDMS-protected polymers were poorly soluble in DMSO, this approach was not suitable to determine the conversion of the reaction.

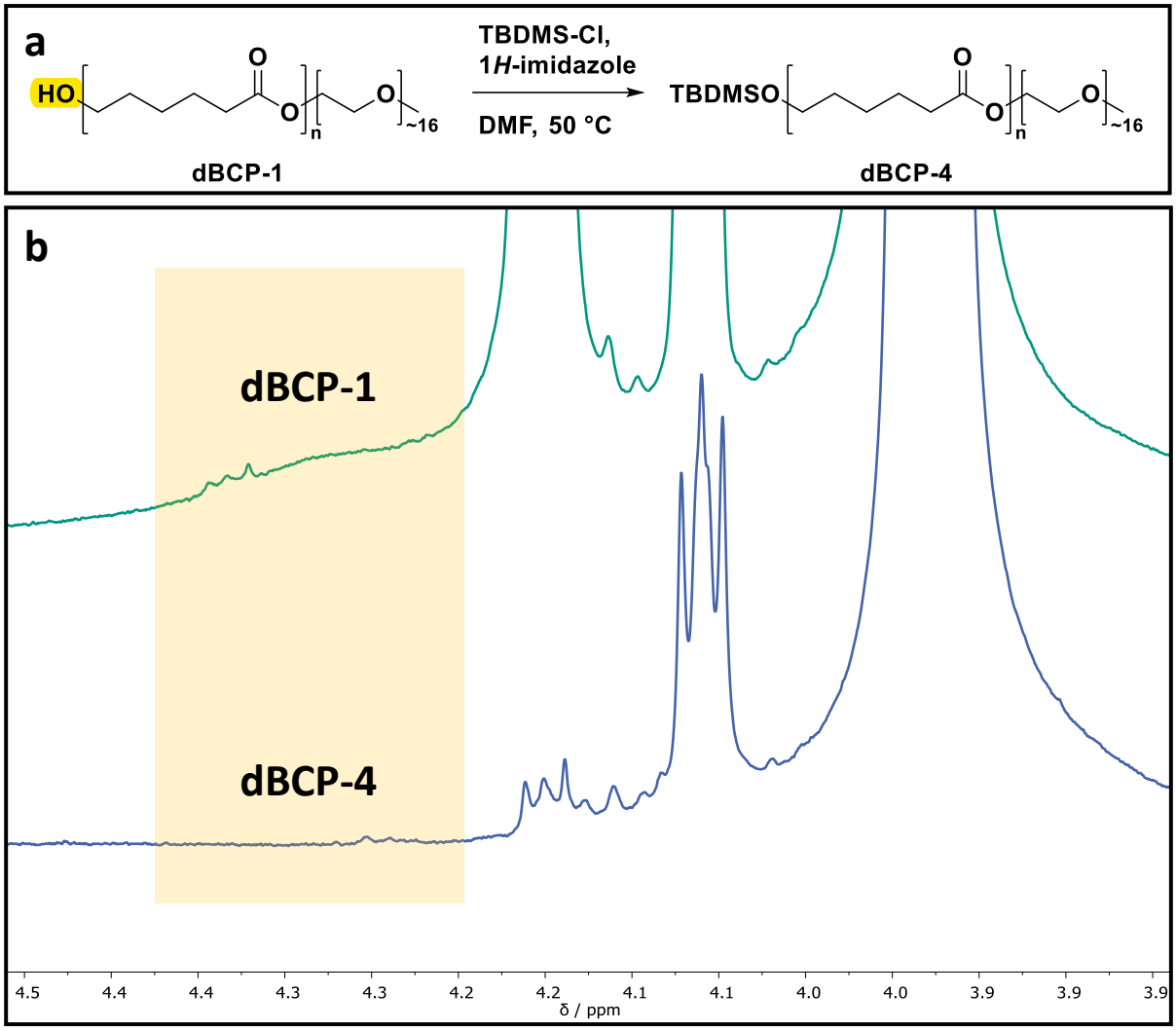

Figure 49: **a** Reaction scheme of the TBDMS protection of the alcohol function of the three disperse PEG-*b*-PCL block copolymers **dBCP-1 – 3**. **b** ^{1}H NMR recorded in DMSO-d_6 of dBCP-1 (green spectrum) compared to the desired protected compound **dBCP-4** (blue spectrum). The broad alcohol signal at 4.32 ppm is highlighted in yellow and is completely vanished after the protection.

Therefore, the NMR spectra were recorded in $CDCl_3$. The stacked spectra and the peak assignment of **dBCP-2** (green) and **dBCP-5** (blue) are presented in Figure 50. The two signals corresponding to the ethylene group next to the alcohol moiety were shifted slightly upfield (highlighted in green and orange) after the protection. However, since the initial chemical shifts of the alcohol were overlapping with backbone signals, it was challenging to quantify complete conversion. The determination of the converted alcohol *via* end group analysis of the appeared signals of the TBDMS protection group

at 0.88 and 0.03 ppm, respectively, was insufficient due to the challenges in terms of integration, which were mentioned in chapter 4.1.1.3.

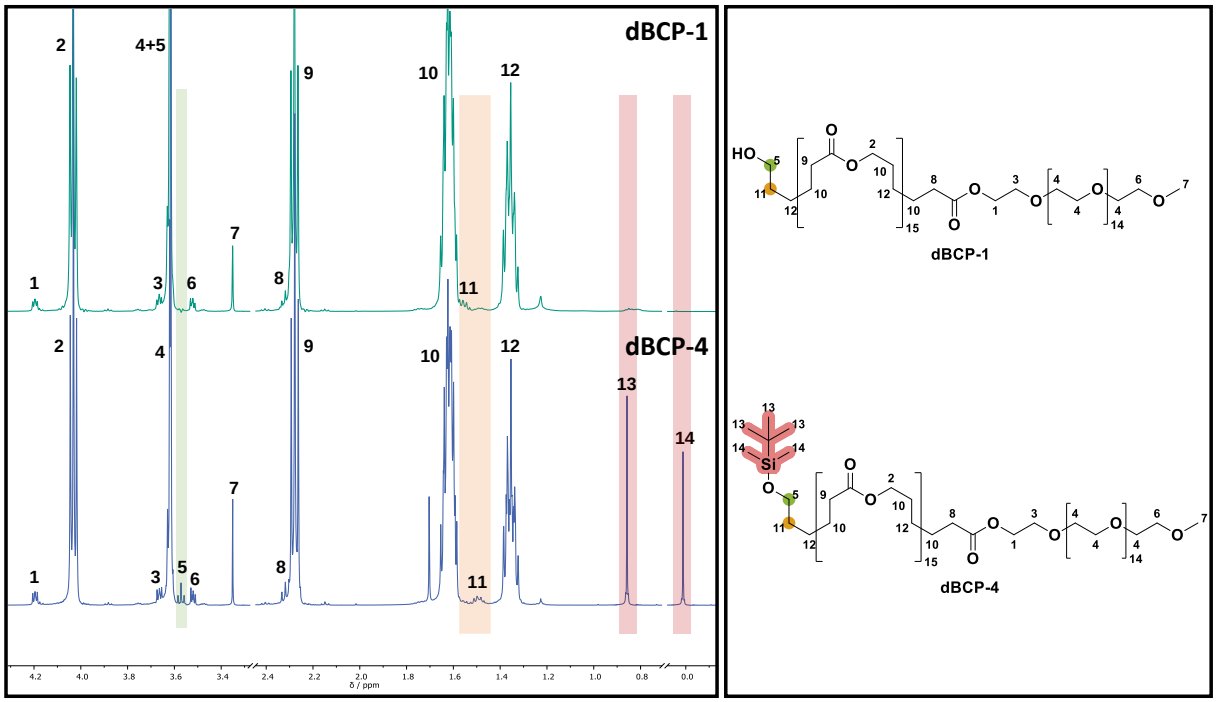

Figure 50 Stacked ^{1}H NMR spectra and peak assignment of **dBCP-2** (green) and **dBCP-5** (blue) recorded in $CDCl_3$. The shifts towards lower ppm of the signals according to the ethylene group **5** and **11** next to the alcohol are highlighted in green and orange. The peaks at 0.9 and 0.0 ppm were assigned to the TBDMS protecting group (highlighted in red).

On the other hand, under consideration of the carbon signals of the same ethylene group next to the alcohol, quantitative conversion was observed by a chemical shift of both signals towards higher ppm (downfield). A comparison of the ^{13}C spectra of compound **dBCP-2** (green) and **dBCP-5** (blue) is shown in Figure 51. Signal **7** was shifted from 62.7 to 63.1 ppm, whereas signal **10** was shifted from 32.4 to 32.6 ppm. Furthermore, the appearance of the quaternary carbon **15** at 18.5 ppm and the CH_3 signals **12** and **16** at 26.1 and -5.6 ppm of the protecting group indicated a successful reaction.

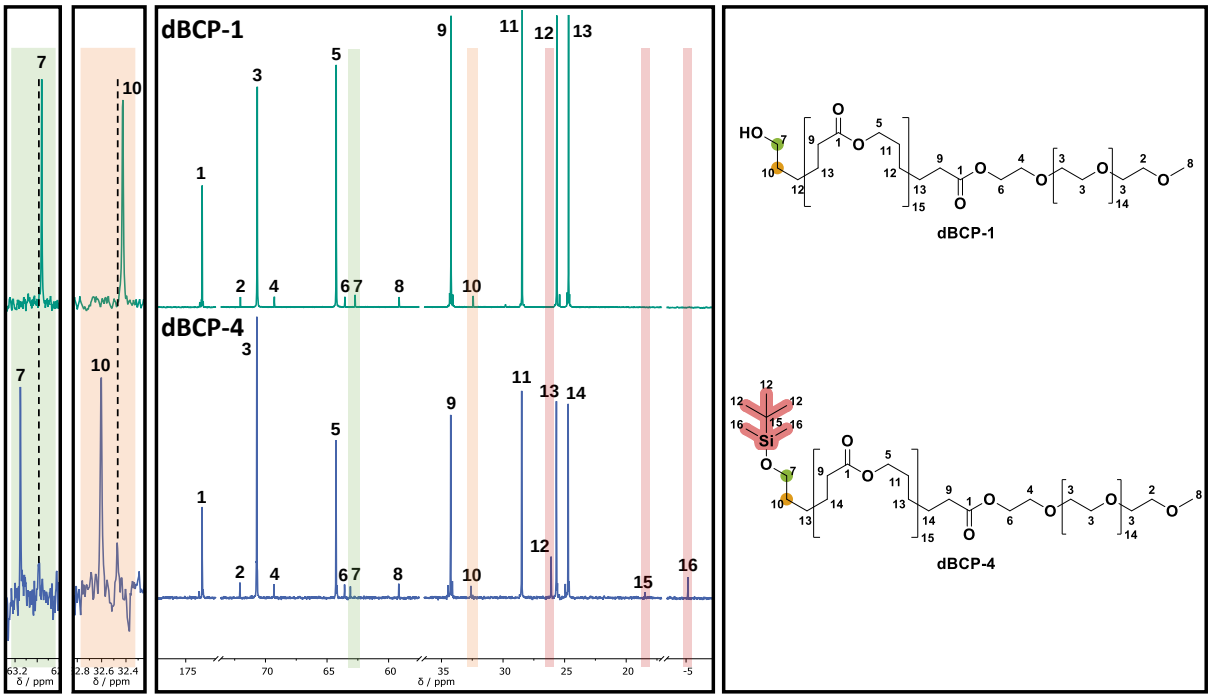

Figure 51: ^{13}C NMR spectra and peak assignment of **dBCP-2** (green) and **dBCP-5** (blue) recorded in $CDCl_3$. The shifts towards higher ppm of the signals according to the ethylene group **7** and **10** next to the alcohol are highlighted in green and orange. The peaks at 26.1, 18.5, and -5.6 ppm were assigned to the TBDMS protecting group (highlighted in red).

An increase of the hydrodynamic volume is expected as a result of the TBDMS-protection of the alcohol function of the products **dBCP-1 – 3**, which was already considered for the synthesis strategy, as mentioned above. The SEC chromatograms of the disperse block copolymers of different chain length before and after the transformation into the silyl ether is shown in Figure 52. A shift of the peak maximum of 0.05 min towards lower retention times and thus a higher hydrodynamic volume was observed for the products **dBCP-1** (dark green) and **dBCP-4** (light blue). In contrast a smaller shift of 0.02 min. was detected for the other two polymer pairs **dBCP-2** (dark blue) and **dBCP-5** (orange), and **dBCP-3** (red) and **dBCP-6** (light green). This observation is another indication for the successful functionalization of the alcohol.

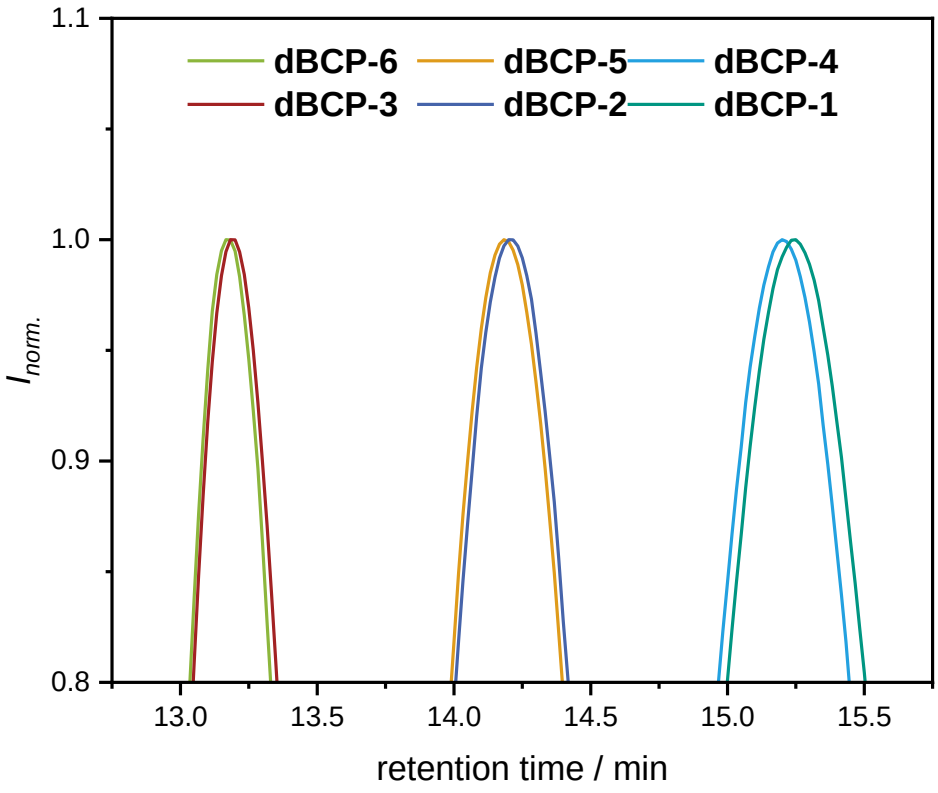

Figure 52: Comparison of the SEC chromatograms of the block copolymers before (**dBCP-1** (dark green), **dBCP-2** (dark blue) and **dBCP-3** (red)) and after (**dBCP-4** (light blue), **dBCP-5** (orange), and **dBCP-6** (light green)) the protection of the alcohol with TBDMS-Cl.

IR is another useful tool to monitor the protection of the alcohol with TBDMS-Cl. The IR spectra of the polymers before and after the protection are presented in Figure 53 a. Since the alcohol shows a characteristic broad vibration at around 3500 cm^{-1} a detailed view of the corresponding area is shown in Figure 53 b. Since the PEG block is very hydrophilic and tends to draw moisture easily, which shows a signal in the same region as the alcohol, the polymers were carefully dried before the measurements. Therefore, the individual samples were dissolved in DCM, dried over anhydrous sodium sulfate, filtered and the solvent was removed again under reduced pressure. Afterwards, an azeotropic distillation with toluene (3 ×) was performed and the samples were further dried overnight under high vacuum. The drying process was also crucial to protect the polymers from degradation *via* hydrolysis of the ester and was performed for the uniform BCP as well. For the compounds **dBCP-1** and **3**, a significant alcohol vibration was observed, whereas for **dBCP-2** the peak showed a weak intensity. However, after protection of the alcohol moiety, the broad signal decreased for each of the samples, but a slight peak remained, which might be caused by air humidity during the measurement.

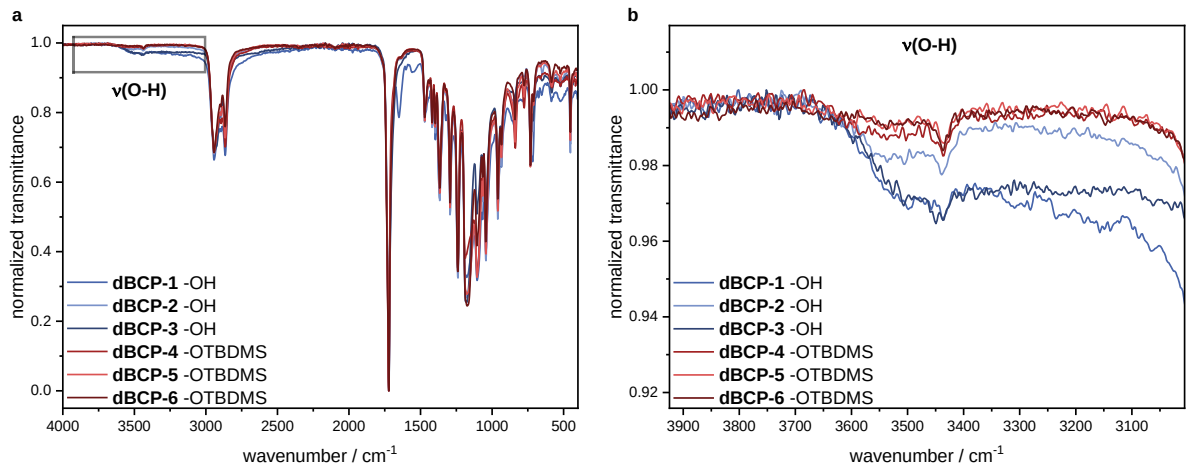

Figure 53: **a** Stacked IR spectra of the disperse block copolymers **dBCP-1 – 6** before and after the protection of the alcohol. **b** detailed area of the broad alcohol vibration around 3500 cm^{-1}.

The reaction process of the TBDMS-protection of the alcohol was carefully monitored with the given analytical methods, to ensure a quantitative end-group functionalization. As already discussed in chapter 4.1.1.3, the combination of different analysis tools is crucial for a meaningful result.

The compounds **dBCP-3 – 6** were purified *via* precipitation in *n*-hexane from DCM to remove the excess of TBDMS-Cl and washed with water and brine to remove the 1*H*-imidazole and residual DMF. Unfortunately, impurities were still present. Therefore, the polymers were purified twice by column chromatography, yielding narrow distributed $mPEG_{16}$-*b*-PCL_n-TBDMS block copolymers, varying in the domain size of the PCL block.

A comparison of the SEC traces of the uniform (**uBCP-1 – 3**, green) and the corresponding disperse block copolymers (**dBCP-4 – 6**, blue) is shown in Figure 54. A significant peak broadening was observed, as expected, due to the larger distribution in chain length with a dispersity of $Đ = 1.06$ for **dBCP-4 – 6** compared to $Đ = 1.01$ **uBCP-1 – 3**.

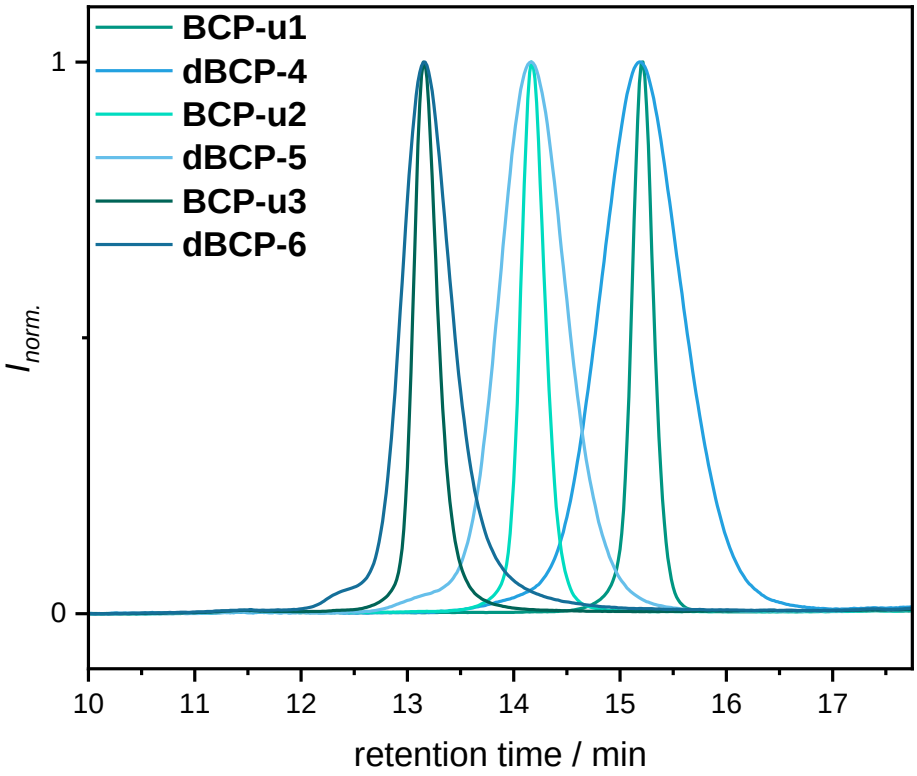

Figure 54: Comparison of the SEC traces of the uniform (**uBCP-1 – 3**, green) and the corresponding disperse (**dBCP-4 – 6**, blue) block copolymers.

In the next chapter, the differences in terms of self-assembly and thermal properties based on the small difference in the dispersity of the disperse and uniform block copolymers are investigated and discussed using DSC and SAXS analysis.

4.5. DSC and SAXS – comparison of uBCP and dBCP

To investigate the thermal properties and potential differences of the thermal transitions of the uniform and non-uniform BCP (**uBCP-1 – 3** and **dBCP-4 – 6**), DSC measurements were performed. The BCP pairs of similar size (uniform (green traces) and non-uniform (blue traces)) are individually compared in Figure 55 a – c. The BCP were analyzed with the following heating program with two identical cycles: heating from -15 °C to 70 °C in 20 K min^{-1} and subsequent cooling from 70 °C to -15 °C in -10 K min^{-1}. A general trend of an increase in both the melting temperature, T_m, and the crystallization temperature, T_c, with an increasing degree of polymerization, N, of the PCL block was observed, which are summarized in Table 6. For the samples with N_{PCL} = 16 (**uBCP-1** and **dBCP-4**), two melting points were observed for both polymer samples, with the non-uniform showing two distinct T_ms, whereas for the uniform sample a shoulder towards higher temperatures was observed. A clear trend of a

decrease in ΔT_m of the two melting points with increasing N_{PCL} was observed for the non-uniform samples. For **dBCP-4** a difference of ΔT_m = 6 °C and 3 °C for **dBCP-5**, whereas **dBCP-6** showed only one melting temperature at 54 °C. In comparison, for the uniform BCPs with N_{PCL} = 32 and N_{PCL} = 64 only one melting transition at 48 °C and 55 °C was observed, respectively. For the crystallization transition, a shift towards lower temperatures was observed with decreasing temperature for the samples **uBCP-1** and **uBCP-3** compared to the corresponding non-uniform BCPs (**dBCP-4** and **dBCP-6**).

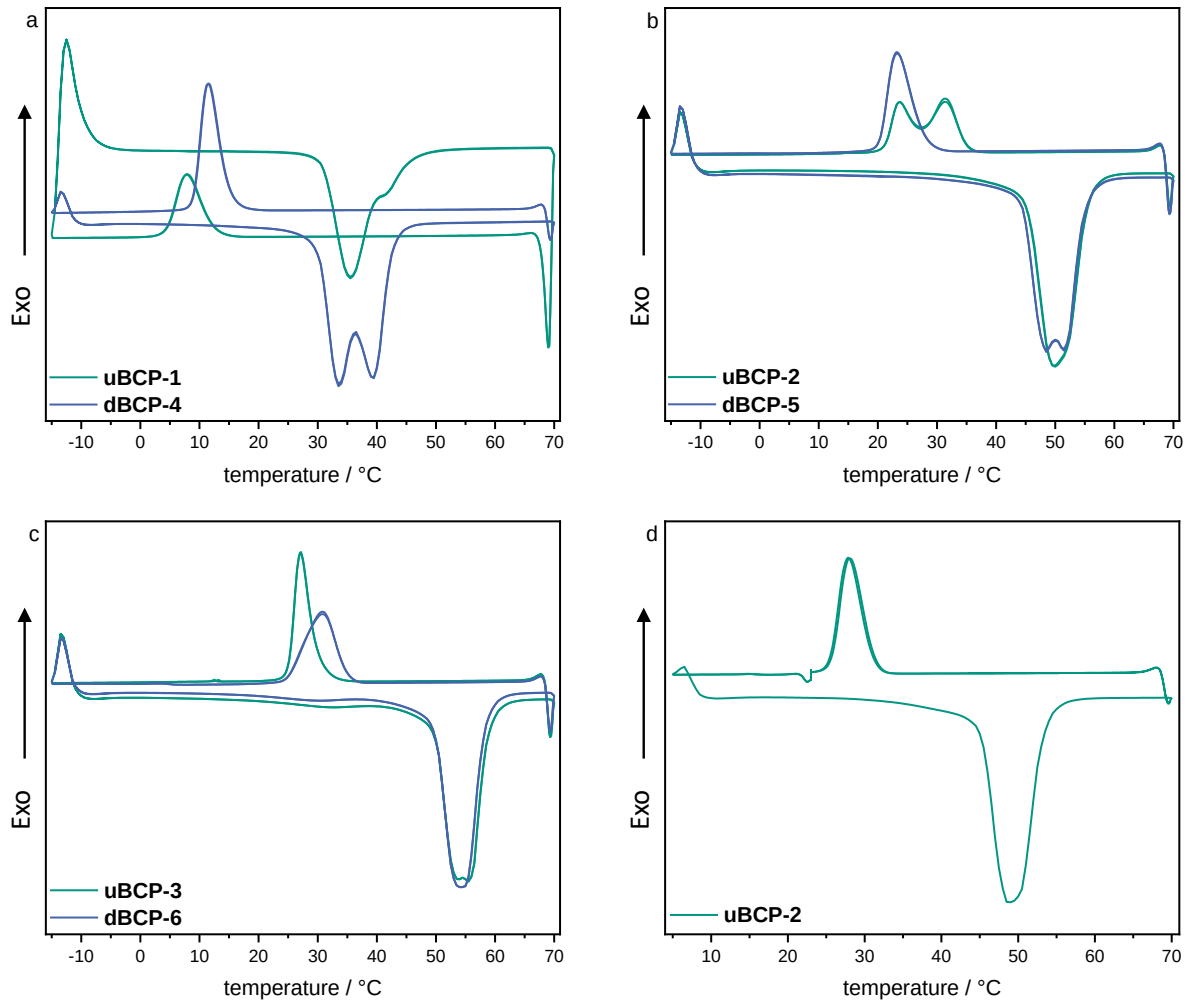

Figure 55: DSC traces of the individual uniform (green) and non-uniform (blue) BCP pairs (**a**, **b**, **c**) using a heating program with two identical cycles: heating from -15 °C to 70 °C in 20 K min^{-1} and subsequent cooling from 70 °C to -15 °C in -10 K min^{-1}. **d** DSC trace of uBCP-2 using a heating program as follows: 5 °C to 70 °C in 20 K min^{-1} and subsequent cooling from 70 °C to 23 °C in -10 K min^{-1}, keeping that temperature for 5 min; cooling from 23 °C to 5 °C in -10 K min^{-1}.

This behavior could be explained by larger macromolecules only present within the non-uniform samples, which could act as crystallization nuclei. Interestingly, the

uniform BCP with NPCL = 32 (**uBCP-2**) showed two crystallization transitions at T_c = 24 °C and T_c = 32 °C, whereas only one transition at T_c = 24 °C was observed for the corresponding non-uniform sample (**dBCP-5**). To slow down the crystallization process, the temperature program was adjusted by inserting an isotherm for 5 min at 23 °C (Figure 55 d). Thus, only a single crystallization transition was observed for **uBCP-2**, indicating the crystallization being slower than the initial cooling rate. Furthermore, glass transition temperatures, T_g, for the BCPs with N_{PCL} = 64 were observed at 25 °C (**uBCP-3**) and 22 °C (**dBCP-6**), respectively.

No noticeable difference in the comparison of the melting enthalpy, Δ_m, of the uniform and non-uniform samples with N_{PCL} = 32 and NPCL = 64 (see Table 6, please note: for **uBCP-1** an exothermic phase transition was observed at -13 °C in the heating cycle. Therefore, these results were not considered in the comparison).

Table 6: Comparison of DSC results of the uniform and non-uniform BCPs.

	m / mg	**T_c^{onset} / °C**	**T_c^{peak} / °C**	**ΔH_c / J g^{-1}**	**T_m^{onset} / °C**	**T_m^{peak} / °C**	**ΔH_m / J g^{-1}**
uBCP-1	5.3	13	8	36	31	35	-38
dBCP-4	5.3	15	12	56	30	34/40	-58
uBCP-2	6.5	28	24/32	60	44	48	-63
dBCP-5	6.5	30	24	60	45	49/52	-63
uBCP-3	5.5	30	28	58	49	55	-57
dBCP-6	5.5	35	31	57	49	54	-55

Further adjustments, such as a decrease of the cooling rate to decelerate the crystallization process could provide insights into the possible formation of structures with higher crystallinity for the uniform BCPs compares to the non-uniform BCPs.

However, further microscopic analysis (TEM and AFM) must be performed to investigate the crystalline structure of the PEG-*b*-PCL BCP dependent on their block composition and dispersity. The following investigates of the BCPs *via* SAXS result in first assumptions about the morphology and the long-range-order distance.

The uniform and non-uniform BCPs (**uBCP-1 – 3** and **dBCO-4 – 6**) were self-assembled directly on Kapton® foil *via* either thermal or solvent vapor annealing (SVA) with acetone. For thermal annealing, the sample was heated to 70 °C under vacuum, kept at that temperature for three hours and was subsequently cooled to room temperature overnight. To evaluate the long-range order distance (domain size, $L_0 = 2\pi/q_0$) in the uniform and non-uniform BCPs, SAXS was performed at room temperature. The 1D SAXS patterns for the thermally annealed samples are shown in Figure 56 a-c. In general, the samples showed SAXS reflection at $1q_0$ and $3q_0$ consistent with a symmetrical lamellar morphology, with the exception of **uBCP-1$_{\mathbf{therm}}$**. (Figure 56 a, green trace), which had an exact degree of polymerization of $N = 16$ for both the PEG and PCL block, that lacked the higher-order peak. Compared to the corresponding non-uniform BCP (**dBCP-4$_{\mathbf{therm}}$**., Figure 56 a, blue trace) a single broad peak at $q_0 = 0.42$ Å^{-1} was observed indicating a less ordered structure. These observations are inconsistent with the findings of MEIJER, PALMANS *et al*. and HAWKER, BATES and coworkers, who describe the opposite effect for uniform and non-uniform oligo(DMS-*b*-LA) BCPs[72] and oligo(DMS-*b*-MMA) BCPs,[76] respectively. With a decrease in dispersity, an increase in the (long-range) order was described.[72,76] On the other hand, note that the reported difference in dispersity of the compared BCPs is twice as large ($\Delta Đ \sim 0.13$)[76] as for the BCPs described within this thesis ($\Delta Đ = 0.05$). Since **uBCP-1** and **dBCP-4** are similar in their volume fraction of PCL ($\Phi_{PCL} = 0.71$), but differ in their degree of polymerization, N, the resulting difference in χN could be decisive for the effect in segregation.

Similar results for the degree of order, as described for the thermal annealing of **uBCP-1** and **dBCP-4**, were observed for the self-assembly *via* SVA in acetone (Figure 56 d). Here, however, due to less pronounced phase separation a broad peak, was observed at $q_0 = 0.59$ Å^{-1} compared to Figure 56 a, corresponding to a decrease in the long-range order distance of $\Delta L_0 = 3.1$ nm (L_0(**uBCP-1$_{\mathbf{SVA}}$**) = 10.5 nm) compared to the non-uniform dBCP-4 (L_0(**dBCP-4$_{\mathbf{SVA}}$**) = 13.6 nm) was observed. A comparison of L_0 of **uBCP-2$_{\mathbf{SVA}}$** ($L_0 = 13.6$ nm) and **dBCP-5$_{\mathbf{SVA}}$** ($L_0 = 13.8$ nm) showed the same trend ($\Delta L_0 = 0.2$ nm, Figure 56 e) as well as **uBCP-3$_{\mathbf{SVA}}$** ($L_0 = 12.6$ nm) and **dBCP-6$_{\mathbf{SVA}}$** ($L_0 = 13.0$ nm) with a difference of $L_0 = 0.4$ nm (Figure 56 f).

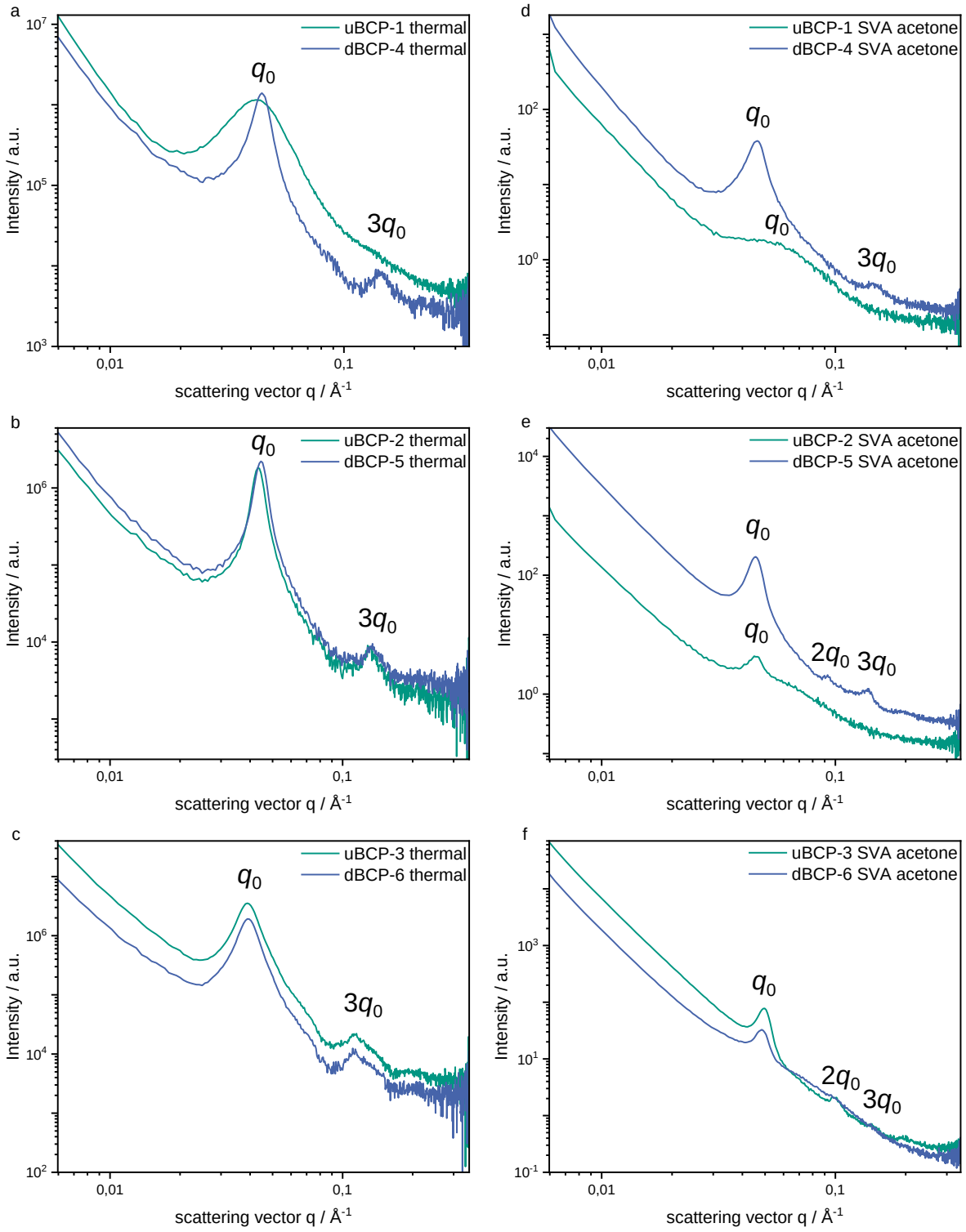

Figure 56: SAXS data for the uniform (**uBCP-1 – 3**, green traces) and non-uniform BCP (**dBCP-4 -6**, blue traces). Self-assembly *via* thermal (**a**-**c**) or solvent vapor (**d**-**f**) annealing on Kapton® foil.[I]

[I] The SAXS measurements were performed by SIMON BUCHHEISER (group of PROF. DR. HERMANN NIRSCHL) at the Institute of Mechanical Process Engineering and Mechanics (MVM) at the Karlsruhe Institute of Technology (KIT, Karlsruhe, Germany).

Thus, even small differences of $\Delta Đ = 0.05$ in relation to the uniform BCP affected the expansion of the lamellar period for the SVA, resulting in an increase of the primary Bragg reflection q_0, which is in agreement with the results of previous experimental reports and predictions by self-consistent field theory (SCFT).[65,72,76]

However, a contradictory trend was obtained for the samples self-assembled *via* thermal annealing (Figure 56 a-c). A decrease in the dispersity resulted in an increase of the L_0 up to 4% (0.5 nm for $N = 32$) compared to the non-uniform BCPs. Since the scattering vector, q_0, is proportional to the radius of gyration, R_g, which in turn is proportional to the square root of the average degree of polymerization, N, shorter chains in a non-uniform polymer have greater impact on the R_g. Thus, smaller values for q_0 are expected for a symmetrical widening of the molecular weight distribution, resulting in larger L_0 (Table 7, thermal). Similar results were reported by FORS *et al*. with polymers showing a positively and negatively skewed molecular weight distribution. Furthermore, an increase of Φ_{PCL} resulted in an expected increase in L_0 for the thermal annealing (excluding the less ordered **uBCP-1$_{therm}$**), where an inverted trend was observed for the SVA of the samples in acetone.

Table 7: Primary SAXS peak analysis for the uniform (**uBCP-1 - 3**) and non-uniform (**dBCP-4 – 6**) BCPs.

compound	N_{PEG}	N_{CL}	$Đ^a$	$\Phi_{PCL}{}^c$	$L_0{}^d$ / nm	$L_0{}^e$ / nm
uBCP-1	16	16	1.01	0.71	14.8	10.5
uBCP-2	16	32	1.01	0.83	14.6	13.6
uBCP-3	16	64	1.01	0.91	16.1	12.6
dBCP-4	17[a]	17[b]	1.06	0.71	14.1	13.6
dBCP-5	17[a]	34[b]	1.06	0.83	14.1	13.8
dBCP-6	17[a]	74[b]	1.06	0.92	15.8	13.0

[a]determined *via* SEC (system III); [b]determined *via* ^{1}H NMR; [c]PCL volume fraction using densities of 1.094 g mL^{-1} for mPEG (M_n = 750 Da) and 1.146 g mL^{-1} for PCL (average M_w ~ 14k; average M_n ~ 10k by GPC); [d]Long-range order distance calculated *via* $L_0 = 2\pi/q_0$ (thermal annealing); [e]Long-range order distance calculated *via* $L_0 = 2\pi/q_0$ (solvent vapor annealing).

In summary, a clear difference in the self-assembly behavior of the uniform and non-uniform PEG-*b*-PCL BCP with $\Phi_{PCL} = 0.71$ was demonstrated for thermal as well as solvent vapor annealing. Furthermore, an increase of the long-range order distance L_0 with increasing dispersity was obtained for all BCPs *via* SVA, which is in accordance

with the literature. However, contradictory results were obtained for both annealing processes and no expected narrowing of the signals was observed.

These findings should motivate the study of the effect of the molecular weight distribution on the self-assembly on BCPs to get a complete understanding of the structure-property relationship. Further investigations *via* AFM, TEM and SA in solution would be the first step in that direction.

4.6. Data storage in defined structures

4.6.1. Sequence-definition approach

As described in chapter 2.5.1, the interest of synthetic sequence-defined molecules for the application as data storage devices has strongly increased over the last decade.[84,86] Sequences obtained by iterative chain elongation cycles, consisting of chemoselective reactions, are of particular interest because they do not require intermediate steps,[152,163,216,217] *e.g.*, deprotection[148,150,151,159,168,215,504] or re-functionalization,[157,167,169] and thus no further purification steps. In addition, information can be written in each synthetic step into the growing chain. In order to develop a new protocol based on two orthogonal reactions, the combination of the Passerini three-component reaction and a subsequent hydroxy-yne reaction was investigated.

First, both reactions were tested independently. A general reaction scheme is shown in Scheme 47. For the hydroxyl-yne reaction (**a**), ethyl propiolate was used as starting material, and was converted with butanol to the desired enol ether. The reaction was performed according to a procedure of LIANG *et al.*, applying DABCO as catalyst.[636]

The Passerini test reaction was performed using 2-ethylbutyraldehyde, *tert*-butyl isocyanide and propiolic acid (Scheme 47 **b**). A propiolate is formed as the product, including the two variable moieties of the aldehyde and isocyanide, which can be applied in a subsequent functionalization with a nucleophile.

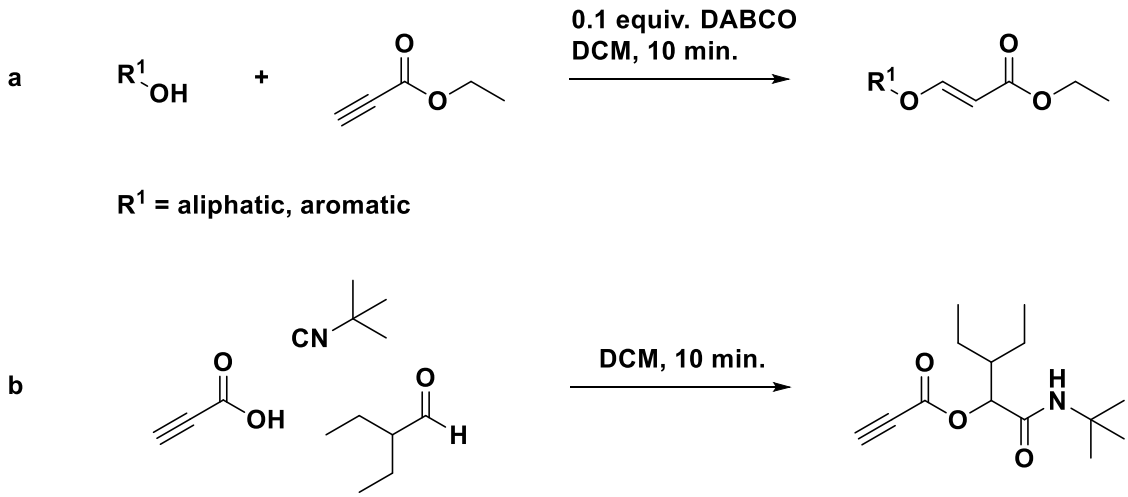

Scheme 47: Reaction schemes for the hydroxyl-yne reaction (**a**) and the Passerini three-component reaction (**b**).

Both reactions were conducted in DCM, and full conversion was indicated by ^{1}H NMR spectroscopy after 10 min of stirring at room temperature. The corresponding ^{1}H NMR spectra as well as the peak assignment of product **S1** and **S2** are shown in Figure 57. Since the starting materials were used in equimolar quantities, respectively, and only minor side reactions were observed, both products were obtained in almost quantitative yield without further purification, after removal of the solvent under reduced pressure.

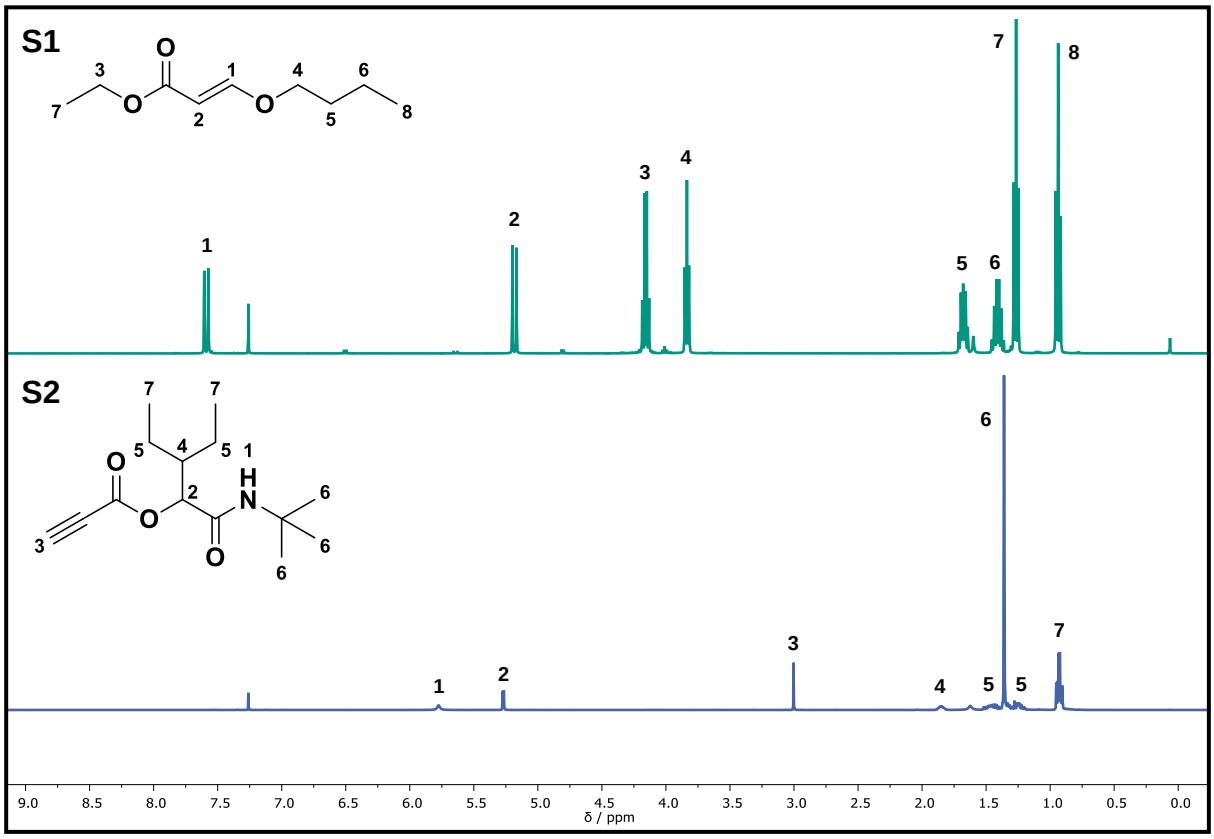

Figure 57: ^{1}H NMR spectra and the corresponding peak assignment of the enol ether **S1**, and the Passerini product **S2**.

In order to synthesize a sequence-defined macromolecule *via* an iterative reaction cycle, a bifunctional molecule bearing an alcohol moiety and one of the Passerini reactive groups is necessary, enabling an iterative reaction cycle. Therefore, aromatic hydroxy aldehydes were used, since alcohols containing an isocyanide functionality were commercially not available. A complete overview of the reaction protocol, including the preparation of a starting molecule and the subsequent chain elongation *via* repetitive phenol-yne[637] and Passerini reaction is shown in Figure 58.

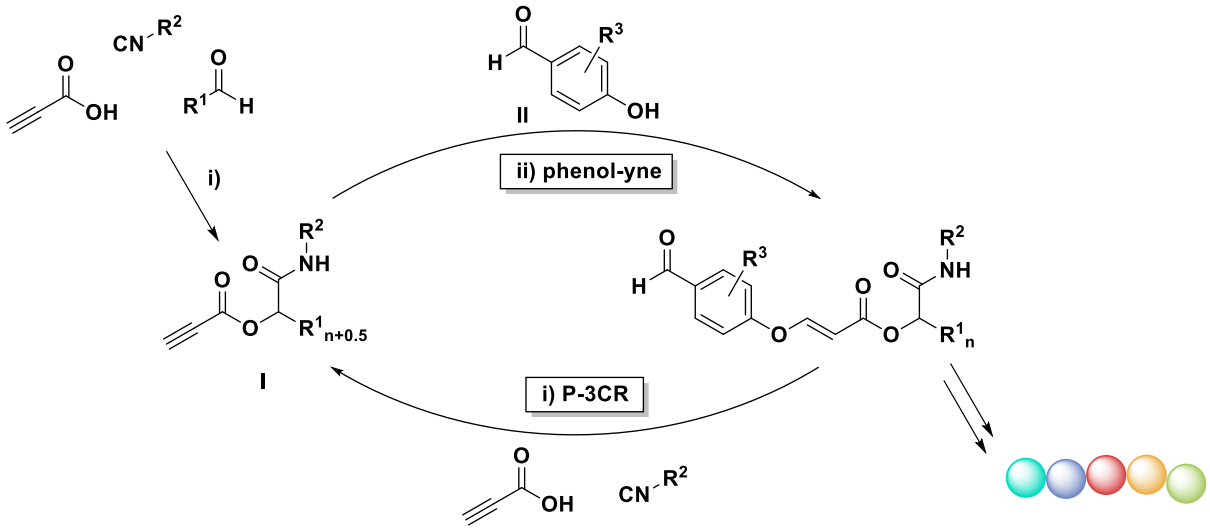

Figure 58: Overview of the general reaction scheme for the synthesis of sequence-defined macromolecules *via* repetitive phenol-yne and Passerini-reaction. i) DCM, rt; ii) 0.1 equiv. DABCO, DCM, rt.

The starting unit **I** was prepared *via* a Passerini reaction containing the electron-deficient triple bond of the propiolic acid component for the subsequent addition of the alcohol in the DABCO-catalyzed phenol-yne reaction.[637] Differently substituted aromatic hydroxy aldehydes **II** can be employed in this step to increase the structural variety of the sequence. In the second reaction of the cycle, the aldehyde endgroup is reacted with an isocyanide component and propiolic acid in another Passerini reaction under regeneration of the propiolate. By repetition of this two-step reaction cycle, a dual side chain definition per repeating unit is achieved by variation of the phenol and the isocyanide component.

The preparation of a sequence-defined dimer was successfully performed using the presented protocol.[l] A comparison of the ^{1}H NMR spectra of product **S2** -**S5** after purification *via* column chromatography is shown in Figure 59. For the starting unit, the same components were used as for the test reaction described above on a 12 mmol scale. The product was easily identified with the characteristic peaks of the amide NH proton **1**, with a broad signal at 5.78 ppm, and the CH proton **2**, with a doublet at 5.27 ppm, which are formed during the Passerini reaction (Figure 59, compound **S2**, orange spectrum). After full conversion, as indicated *via* GC analysis, 4-hydroxy

[l] The syntheses of the sequence-defined macromolecules *via* the phenol-yne P-3CR one-pot reaction were carried out by REBECCA SEIM under the lab-supervision of PHILIPP BOHN, who evaluated the obtained results.

benzaldehyde was directly added into the reaction mixture for the *in-situ* phenol-yne addition. The reaction was stirred overnight and the desired product **S3** was obtained in a yield of 65% after purification *via* column chromatography. The terminal alkyne signal completely vanished in the ^{1}H NMR spectrum, due to the functionalization with the alcohol.

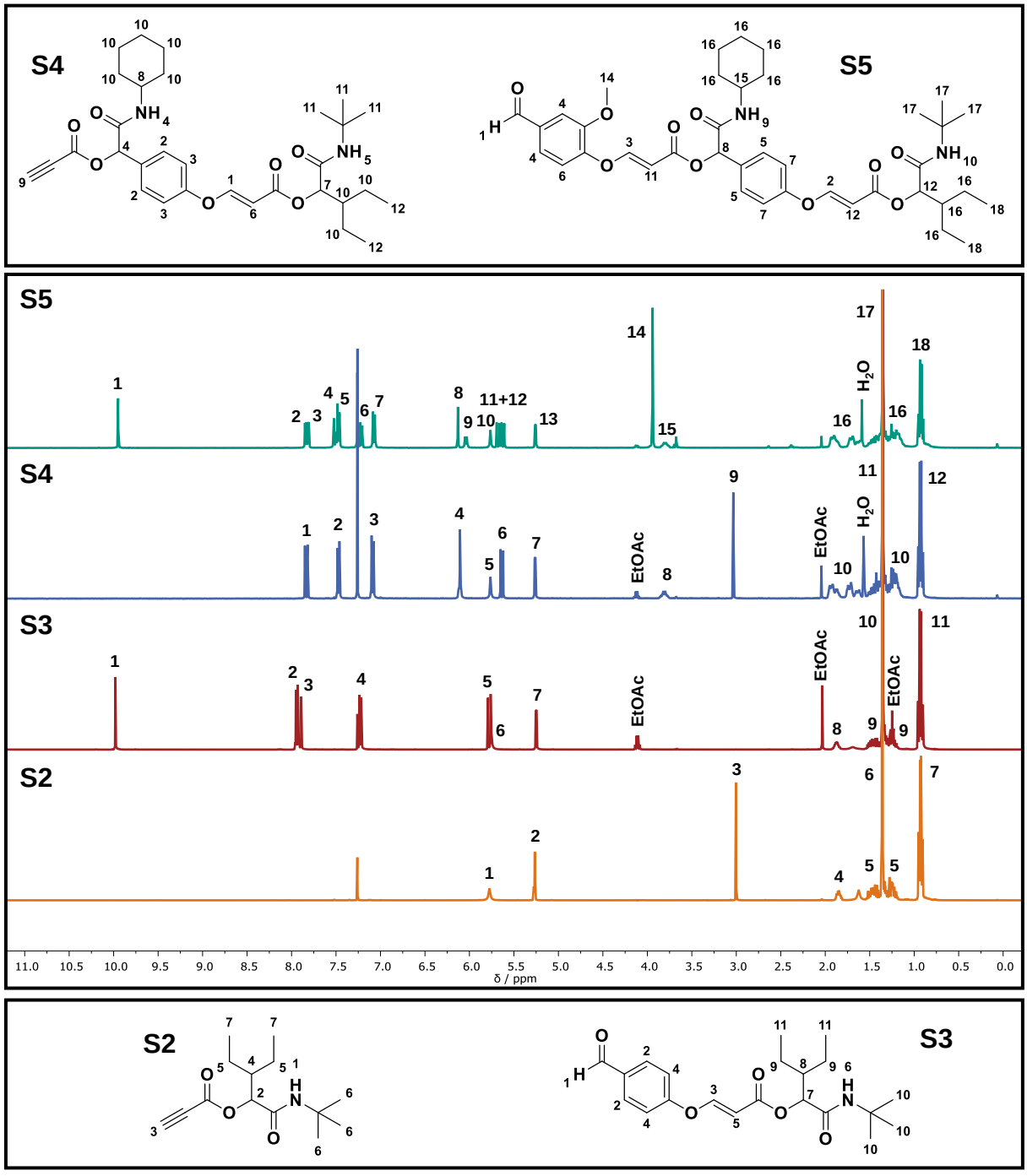

Figure 59: Comparison and peak assignment of the ^{1}H NMR spectra of products **S2** – **S5** after purification *via* column chromatography.

Two characteristic doublets at 7.91 and 5.78 ppm arose and were assigned to the formed double bond (Figure 59, compound **S3**, red spectrum, signals **2** and **5**). A coupling constant of J = 12.1 Hz was determined, indicating the selective formation of the *E* configuration. Furthermore, the characteristic signal of the aldehyde appeared at 9.98 ppm. The isocyanide component was varied in the following Passerini reaction, and thus cyclohexyl isocyanide was used. However, even after further addition of 0.2 equiv. of propiolic acid and isocyanide, only 72% conversion was achieved after two weeks of stirring at room temperature. After purification *via* column chromatography, a low yield of only 16% of pure product **S4** was obtained. Applying a higher reaction temperature might increase the conversion and thus simplify the purification of the product. In the ^{1}H NMR spectrum (Figure 59, compound **S4**, blue spectrum), the characteristic signal of the aldehyde completely vanished and peaks belonging to the formed CH and NH group (signal **4**, blue spectrum) were overlapping at 6.11 ppm. The terminal alkyne proton **9** and the CH proton of the cyclohexyl moiety **8** were assigned to the signals at 3.03 and 3.81 ppm, respectively, whereas the CH_2 protons of the cyclohexyl group **10** were found in the aliphatic region between 1.98 – 1.13 ppm. In the second phenol-yne reaction, a methoxy-substituted 4-hydroxy benzaldehyde (vanillin) was used as alcohol component, and thus side group definition was achieved at a different position of the structure. The reaction was monitored *via* SEC analysis and full conversion was indicated after stirring the mixture over night. Afterwards, the product was purified *via* column chromatography and obtained in a yield of 82%. As for the first phenol-yne reaction, the ^{1}H NMR signals of the terminal alkyne group completely vanished, whereas the peak at 9.95 ppm was assigned to the aldehyde function **1** (Figure 59, compound **S5**, green spectrum). Furthermore, two additional doublets **3** and **11** allocated to the formed double bond at 7.82 and 5.66 ppm with a coupling constant of J = 12.1 Hz appeared. Additionally, the methoxy singlet **14** was observed at 3.94 ppm.

The SEC chromatograms of the products **S3**, **S4** and **S5** are compared in Figure 60. A general trend towards lower retention times, and thus a higher hydrodynamic volume was observed due to the chain elongation in each reaction step. The green graph associated to product **S3** exhibits a narrow and monomodal shape, indicating a high purity of the product, whereas impurity signals at higher and lower retention times were observed for the products **S4** (blue trace) and **S5** (red trace), respectively.

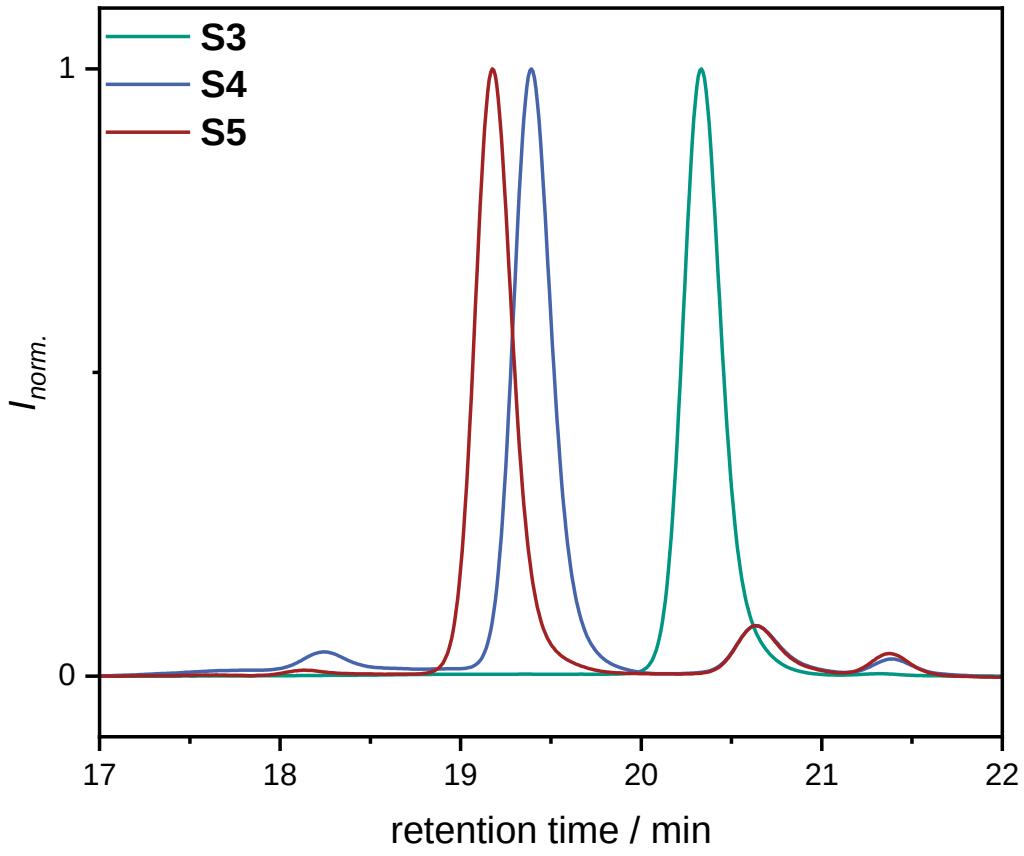

Figure 60: Comparison of the SEC chromatograms of product **S3** (green trace), **S4** (blue trace) and **S5** (red trace).

However, a further Passerini reaction was performed, using benzyl isocyanide and propiolic acid to obtain product **S6** (Figure 61). Unfortunately, an even lower conversion of 18%, compared to the Passerini reaction to obtain product **S4**, was observed after one week of reaction time. Further addition of 1.5 equivalents of the acid and isocyanide component and increasing the reaction temperature to 60 °C (solvent was changed to chloroform) had no improving effect on the conversion. Thus, no isolation steps or investigations on the fragmentation of the product were performed.

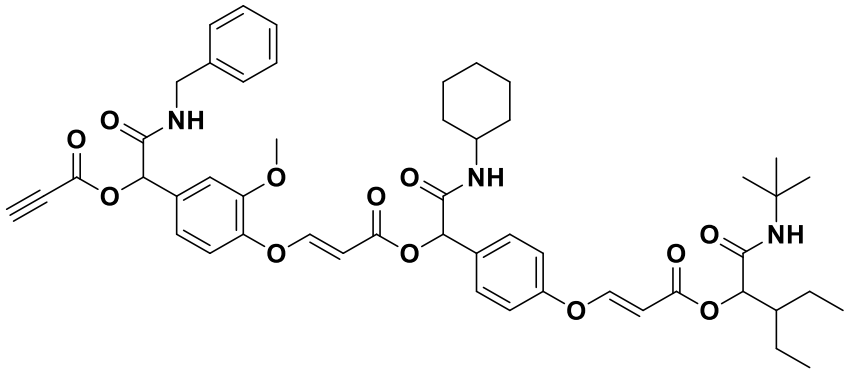

Figure 61 Desired product **S6** *via* a Passerini reaction of **S5** with benzyl isocyanide and propiolic acid.

Since the expected results of a simple and efficient approach for the synthesis of sequence-defined macromolecules using a two-step repetitive reaction cycle consisting of a P-3CR in combination with a phenol-yne reaction were not achieved, due to the lower reactivity of aromatic aldehydes in the Passerini reaction, the approach was not pursued further. On the other hand, an interesting study on sequence-defined macromolecules based on the high reactivity of propiolates in a Michael addition reaction as well as the application in the field of information storage was just recently reported by TANG and coworkers (Scheme 48 **a**).[163] In contrast to the approach discussed above, where the Passerini product as well as the Michael adduct were incorporated into the backbone structure, hydroxy thiols were reacted in a combination of a hydroxyl-yne and a subsequent thiol-ene reaction with the propiolate to build a monothioacetal backbone structure. By variation of the hydroxy thiols and the propiolic acid esters, dual sequence-definition (sidechain and backbone) was achieved by the authors per iteration cycle. Since the structural diversity in this approach is limited due to the rather low availability of different hydroxy thiols and propiolates, the combination with propiolates obtained *via* multi-component reactions would massively increase the number of permutations, and thus the data storage capacity per repeating unit. The facile and fast preparation of a library of such building blocks in a parallel operation is demonstrated in chapter 4.6.2. Thus, using the P-3CR in combination with the approach of TANG *et al*., a single backbone and dual side chain definition would be achieved, which could be further increased to a triple side chain definition applying propiolates prepared by the Ugi reaction (Scheme 48 **b**). However, investigations on the fragmentation of such highly complex structures need to be performed, to ensure the readability of the sequence and thus possible applications in molecular data storage.

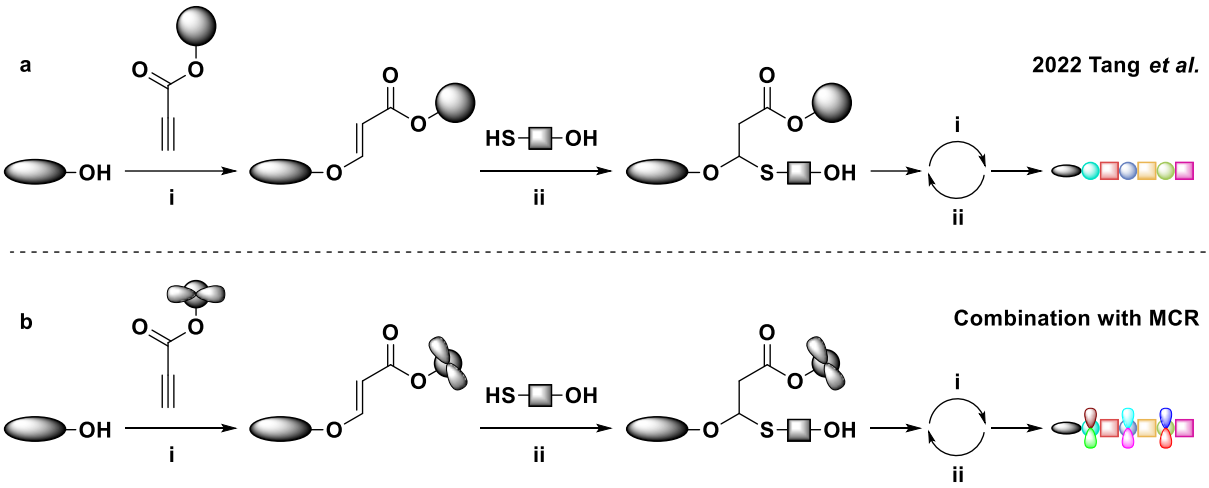

Scheme 48: **a** Schematic dual sequence-definition approach reported by TANG *et al*. *via* a combination of hydroxyl-yne and thiol-ene click reactions.[163] **b** Suggestion for an improvement of the protocol by TANG by using propiolates prepared *via* multi-component reactions, and thus increasing the data storage density per repeating unit immensely.

Even with an optimized reaction protocol, many iterative preparation steps are usually necessary to achieve a high data storage capacity, which is often associated with a time-consuming synthesis and several purification steps. To further simplify the molecular data storage, investigations on the storage of information into mixtures of small, highly complex molecules have been presented in last years by different groups (see chapter 2.5.8.5).[513–517,519] Since the electron-deficient triple bond of propiolates offers the possibility of various functionalizations with different nucleophiles, a large variety of highly complex structural motifs are easily accessible (Scheme 49), making this chemistry suitable for the synthesis of compound libraries for the application in the field of molecular data storage.

4.6.2. Data storage in small molecules

The first examinations of this project were carried out by STEFANO FLAVIO SECHI in his study about "*Digital Monomers via the Passerini-Amino-yne Cascade One-Pot-Reaction*"[638] and continued by TAMARA MEYER in her study about "*Data Storage in Small Molecules*"[639] under lab-supervision of PHILIPP BOHN. The calculations for the Design of Experiments (DoE) as well as the synthesis of the compound libraries were performed by PHILIPP BOHN, if not otherwise noted. The printing was performed by JANNE WIEDMANN (working group of PROF. DR. PAVEL LEVKIN) from the Institute of Biological and Chemical Systems – Functional Molecular Systems (IBCS-FMS) at the Karlsruhe Institute of Technology (KIT). The MALDI-MS/MS measurements were

performed by DR. QUIQIN ZHOU in a collaboration with DR. STEFAN SCHMIDT (working group of PROF. DR. CARSTEN HOPF) from the Center for Mass Spectrometry and Optical Spectroscopy (CeMOS) in Mannheim, Germany.

In Scheme 49, the variety of structural motifs accessible through the functionalization of propiolic acid esters with different nucleophiles is presented by a selection of literature-known reactions. The immense diversity is crucial to increase the number of permutations and thus the data storage capacity of a single highly complex molecule.

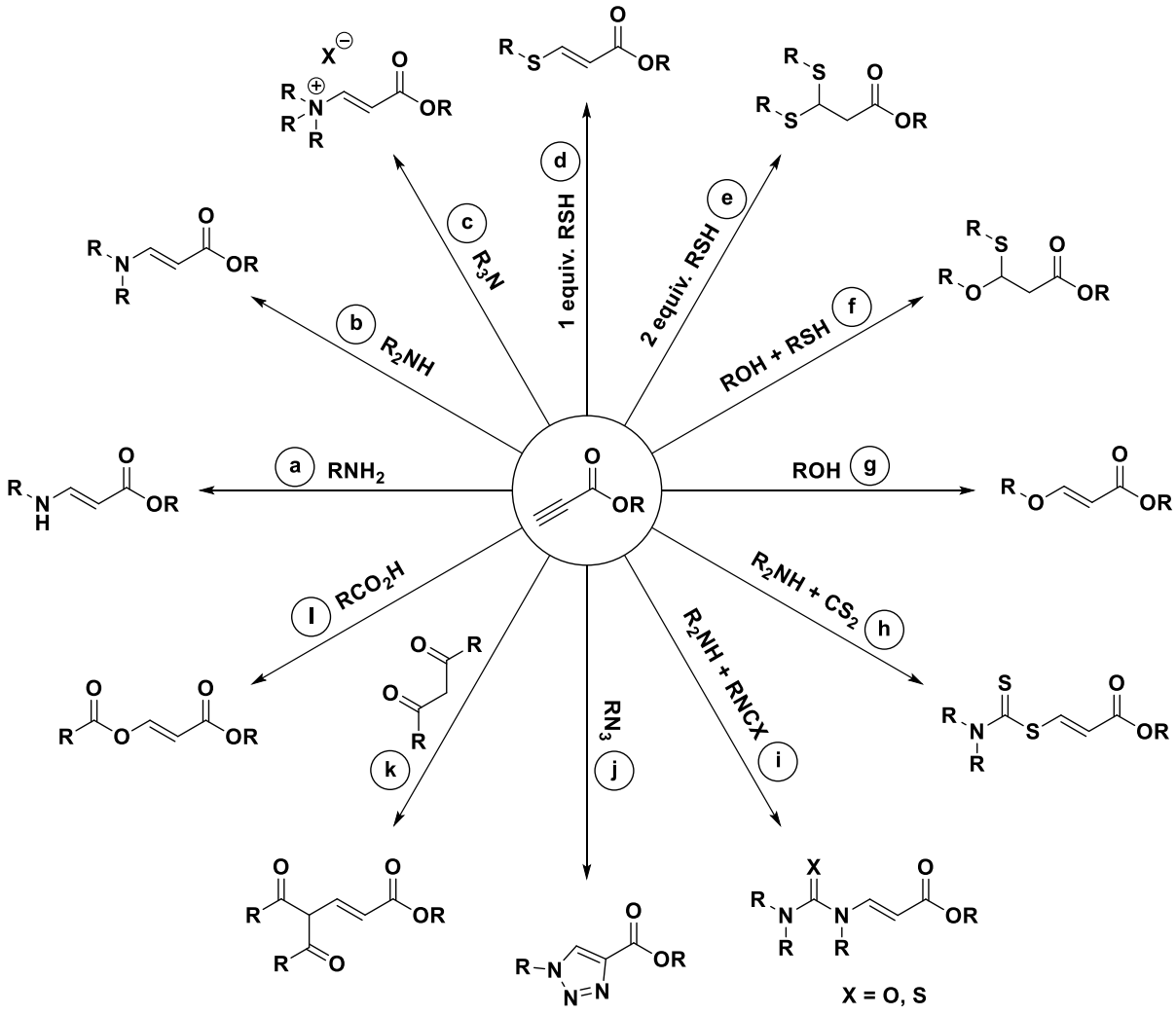

Scheme 49: A general selection of literature-known functionalization of propiolic acid esters with several nucleophiles.

The addition of primary (a), secondary (b) and tertiary amines (c) lead to the formation of the corresponding enamines. Especially the use of secondary amines is often described in the literature due to the spontaneous and quantitative formation of *E*-configured products as well as the fast reaction kinetics.[640,641] The base-catalyzed mono (d) and double addition (e) of thiols to the alkynone can be controlled by the

employed equivalents of the thiol component.[642] As already described above, a combination of a DABCO-catalyzed hydroxyl-yne and a subsequent NHC-catalyzed thiol-ene addition yield the monothioacetal (f).[163] The DABCO-catalyzed single addition of alcohols yields the corresponding enol structures (g). Aliphatic as well as phenolic alcohols can be applied for this reaction.[637] Dithiocarbamates are accessible *via* the combination of amines and CS_2 (h),[643] whereas the urea and thiourea derivatives are obtained from the isocyanate and isothiocyanate precursors in combination with an amine (i).[644,645] The well-known copper-catalyzed azide alkyne cycloaddition was also performed with propiolates yielding the desired 1,2,3-triazoles (j).[646] Furthermore, the addition of carbon nucleophiles were investigated e.g. on pentan-2,4-dione derivatives (k),[647] as well as carboxylic acids as nucleophilic component (l).[636]

Within the context of this work, the focus was on the most commonly commercially available classes of compounds (amines, alcohols, thiols, and carboxylic acids). A general reaction scheme of the Passerini reaction in combination with the Michael addition of different nucleophiles is shown in Scheme 50.

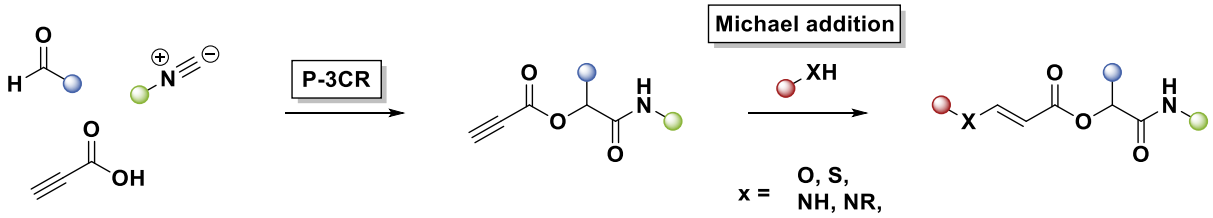

Scheme 50: General reaction scheme for the synthesis of highly functionalized molecules *via* a combination of the P-3CR and subsequent Michael addition of different nucleophiles.

As limitations for the compounds, suitable for this reaction, an upper prize limit of 50 € g^{-1} has been set, except for the isocyanide component. Furthermore, the nucleophiles must not contain a second nucleophilic group to prevent unwanted side reactions. Additionally, only one constitutional isomer of a compound is included in the molecule list to prevent issues in the later read-out *via* fragmentating mass spectrometry. This preselection resulted in 160 suitable aldehydes, 32 isocyanides, 229 primary and secondary amines, 54 thiols, and 231 alcohols, which were commercially available at Sigma Aldrich, and were appropriate candidates for this approach. Thus, 2.63 M different combinations for the preparation of the product were possible. Since the synthesis of all molecules would not be feasible and even be highly challenging using synthesis robots, a Design of Experiments (DoE) based on the logP

value per Connolly Molecular Area (CMA)[l] was conducted. The logP value indicates how lipophilic or hydrophilic the respective compound is and is therefore a relative measure of the polarity of a substance. The basic idea of a DoE approach is to gain the maximum knowledge with the minimum synthetic effort, to predict the outcome of an experiment dependent on a change of the variables (here logP per CMA of the components). Typically, such a design is used as a statistical approach for reaction and process optimization, by varying all parameters at the same time and thus to find the optimal conditions in a defined reaction space. In case of the reaction approach described above, the logP value per CMA of the three variable components (aldehyde, isocyanide, and nucleophile) are the adjustable parameters. Thus, the reaction space is a cube, where the corners are defined by all combinations of the most lipophilic and hydrophilic components. Performing a full factorial design, the experiments for the corner compound combinations, as well as the combination for the center of the cube were conducted. The premise is, that if these reactions are successful, all other combinations located in the reactions space should also be successful, considering polarity as the only reaction-determining parameter. If this is not the case, a new set of experiments needs to be performed, until the desired result is achieved. Thus, a smaller reaction space compared to the initial is defined. Within the scope of this project, 25 experiments were performed of the top and bottom surface of the reaction space, respectively, in order to better demonstrate the feasibility of the library synthesis. A graphical representation for the combination of a P-3CR and an amino-yne Michael addition is shown in Figure 62. An equal distribution of the component combinations (green and red spheres) of the top and bottom reaction surfaces (green and red area) was preselected. The used aldehydes and isocyanides are depicted along the x- and y-axis, whereas the amine structures are given within the cube. A list of the logP per CMA ratios of the complete compound libraries is provided as supplementary information on the CD.

All 51 P-3CR and subsequent amino-yne reactions employing the preselected component combinations were performed in one-pot reactions. After stirring the reactions over night at room temperature, the solvent was removed under reduced pressure and the products were analyzed *via* NMR spectroscopy and ESI-MS without further purification. Since a high conversion was achieved for every combination and

[l] The contact surface created when a spherical probe is rolled over the molecular model.

the similar core structure of the compounds, the peak assignment and identification of the products *via* ^{1}H NMR spectroscopy was straightforward. The desired masses were found for 47 out of the 51 products (see experimental section 6.3.8, Supplementary Table 24 and Supplementary Table 25) with ESI-MS analysis, confirming a successful reaction.

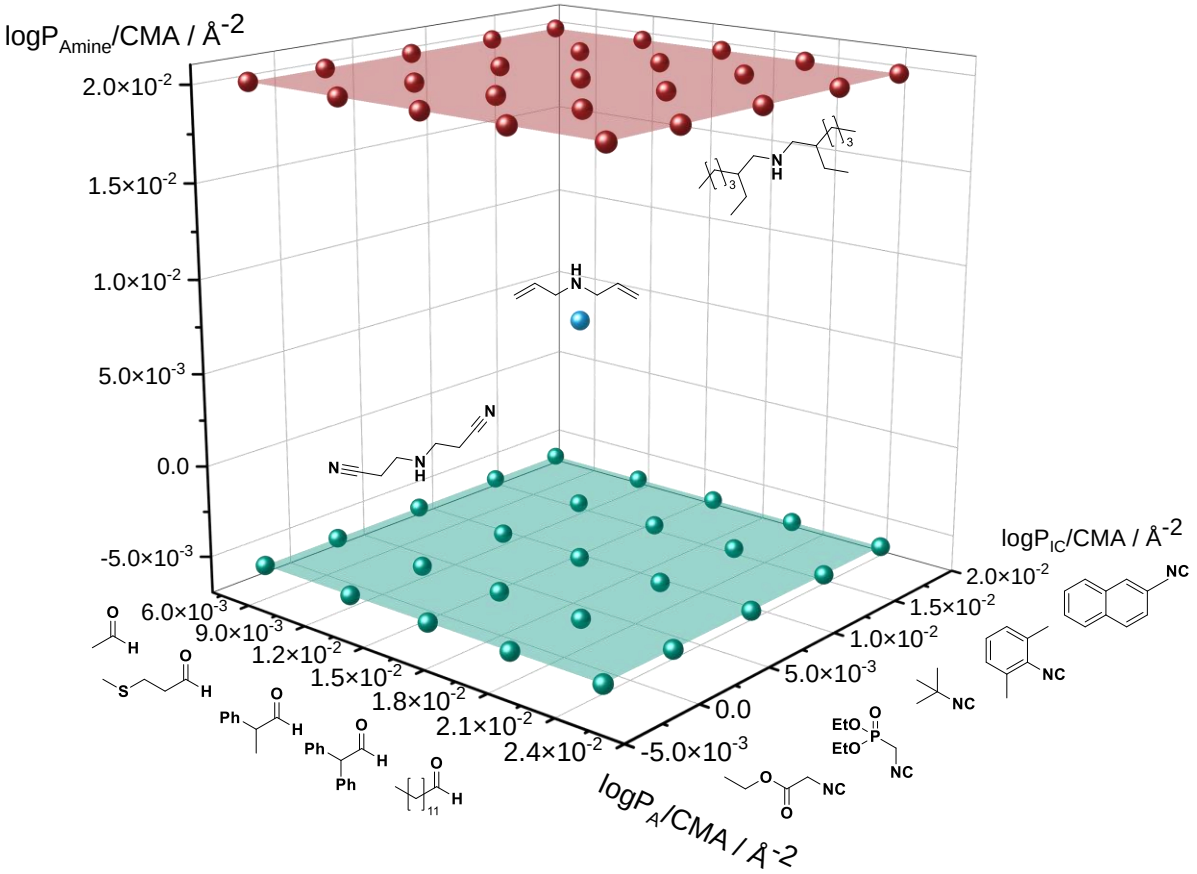

Figure 62 DoE based on the logP/CMA ratio of the components used for a Passerini reaction and subsequent amino-yne Michael addition shown in (Scheme 50).

Assuming, that all the 2.63 M compound combinations result in the formation of the desired product, this reaction protocol is suitable for the synthesis of small information-containing molecules. The storage capacity of one molecule was calculated with equation (3), where the number of permutations P is equal to the number of bits n to the base 2 (each bit is defined by 2 states “0” and “1”).

$$P = n_{aldehyde} * m_{isocyanide} * (w_{amine} + x_{thiol} + y_{alcohol}) \qquad (2)$$

$$P = 160 * 32 * (229 + 54 + 231)$$

$$P = 2\,631\,680$$

$$P = 2^n \tag{3}$$

$$n = \frac{\log(P)}{\log(2)}$$

$$n = \frac{\log(2\,631\,680)}{\log(2)}$$

$$n = \frac{\log(P)}{\log(2)}$$

$$n = 21\ bits$$

Thus, 2.63 M possible permutations resulted in 21 bits per molecule. Compared with the literature, where an 18 bits molecular key based on 0.5 M possible Ugi products was described and identified with ESI tandem MS,[514] here the five-fold number of permutations is achieved, representing an increase of 3 bits. In other studies, the presence or absence of a certain compound in a molecule mixture was translated into a “1”s and “0”s, respectively and were used for the en- and decoding of images up to 0.8 megapixel.[513,515] For the read-out of the information, non-fragmenting mass analysis was used, thus only compounds distinctly distinguishable by their parent ion could be applied.

To further improve this approach, tandem mass analysis was performed within this context. In this way, also constitutional isomers could be exactly identified by their characteristic fragmentation pattern, considering the limitations in the selection of the components, which has been proven in a previous study.[514]

Therefore, the synthesized compounds were printed on a glass slide using a liquid dispenser, which represents the writing process of the information to be stored. A schematic overview is presented in Figure 63. The individual spots exhibit a diameter of 900 µm and a distance of 225 µm to the neighbor molecule spot. Thus, in total 81 products could be printed per square centimeter on the target, resulting in a data storage density of 1701 (81 × 21) bits per cm^2. The matrix for the MALDI read-out was printed as a second layer on top of the compound spots. Four different matrices (α-cyano-4-hydroxycinnamic acid (HCCA), dihydroxybenzoic acid (DHB), sinapinic acid (SA), and 2-[(2*E*)-3-(4-*tert*-butylphenyl)-2-methylprop-2-enylidene]malonitrile (DCTB)), and three different analyte concentrations were tested (10, 50, 100 pmol/spot), where HCCA gave the most promising results regardless of the

analyte concentration. In order to read the stored information, tandem MS analysis was conducted, and the preselected proton adduct of the analyte was fragmented applying a collision energy of 15 eV.

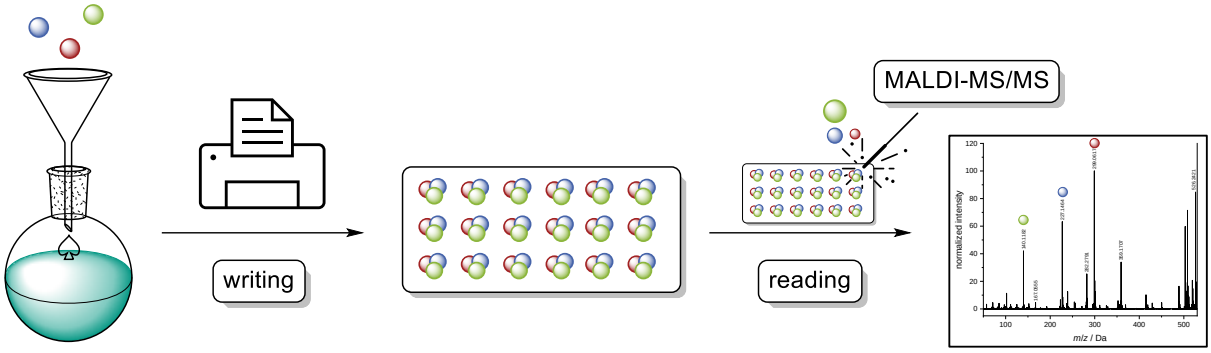

Figure 63: Schematic overview of the synthesis, printing, and analysis *via* MALDI-MS/MS for the information-containing small molecules prepared *via* a combination of P-3CR and Michael addition

The observed fragmentation pattern of product **D8c1** as well as the individual fragments for the peak assignment are shown in Figure 64. Most of the observed fragment masses were clearly identified, thus confirming the exact structure of the product, and offering the possibility of using also constitutional isomers for the data storage (limitations mentioned above). Furthermore, an error in the read-out process was reported in the literature with single MS analysis,[513,515] which could be reduced to a minimum applying a tandem MS approach for each molecule. A general scheme, presenting the most common fragmentation pathways of the product core structure is shown in Scheme 51 exemplarily for product **D8c1**.

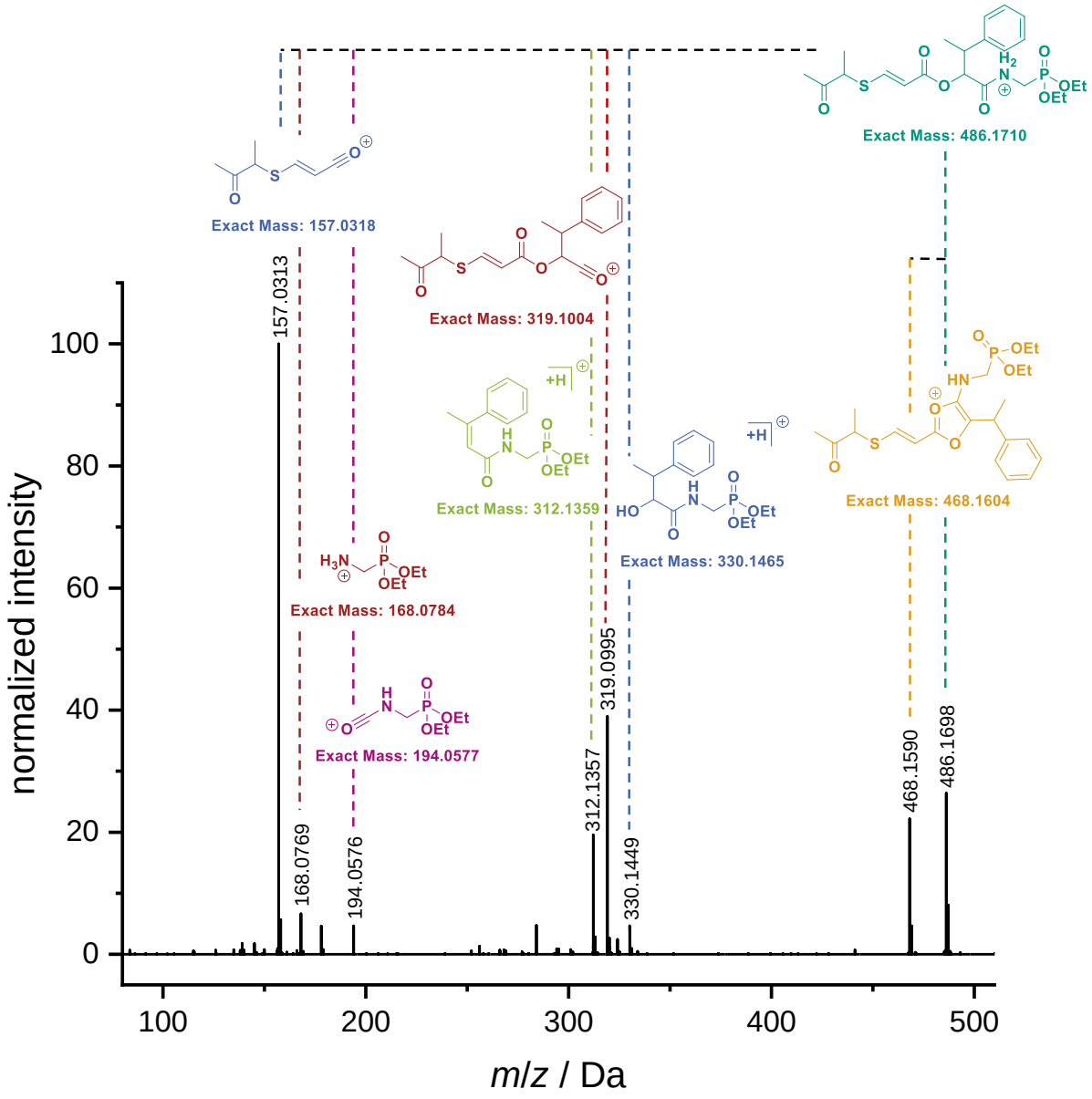

Figure 64: Fragmentation pattern of product **D8c1** observed *via* MALDI tandem MS of the proton adduct $[M+H]^+$ applying a collision energy of 15 eV.

The α-cleavages of the ester and amide function are literature-known and result in the formation of the acylium ions α_1 in case of ester cleavage and x_1 and b_1 *via* fragmentation of the amide bond (see Scheme 51). Furthermore, the protonated alcohol and ammonium adducts are obtained *via* the same cleavages. The respective mass for an elimination of water was found and an oxolium species was postulated as suitable fragment. A McLafferty-like rearrangement resulted in the formation of an α,β-unsaturated amide proton adduct 'McL' (Figure 64 green structure). To generalize these proposed fragments, further investigations on different substrates need to be performed.

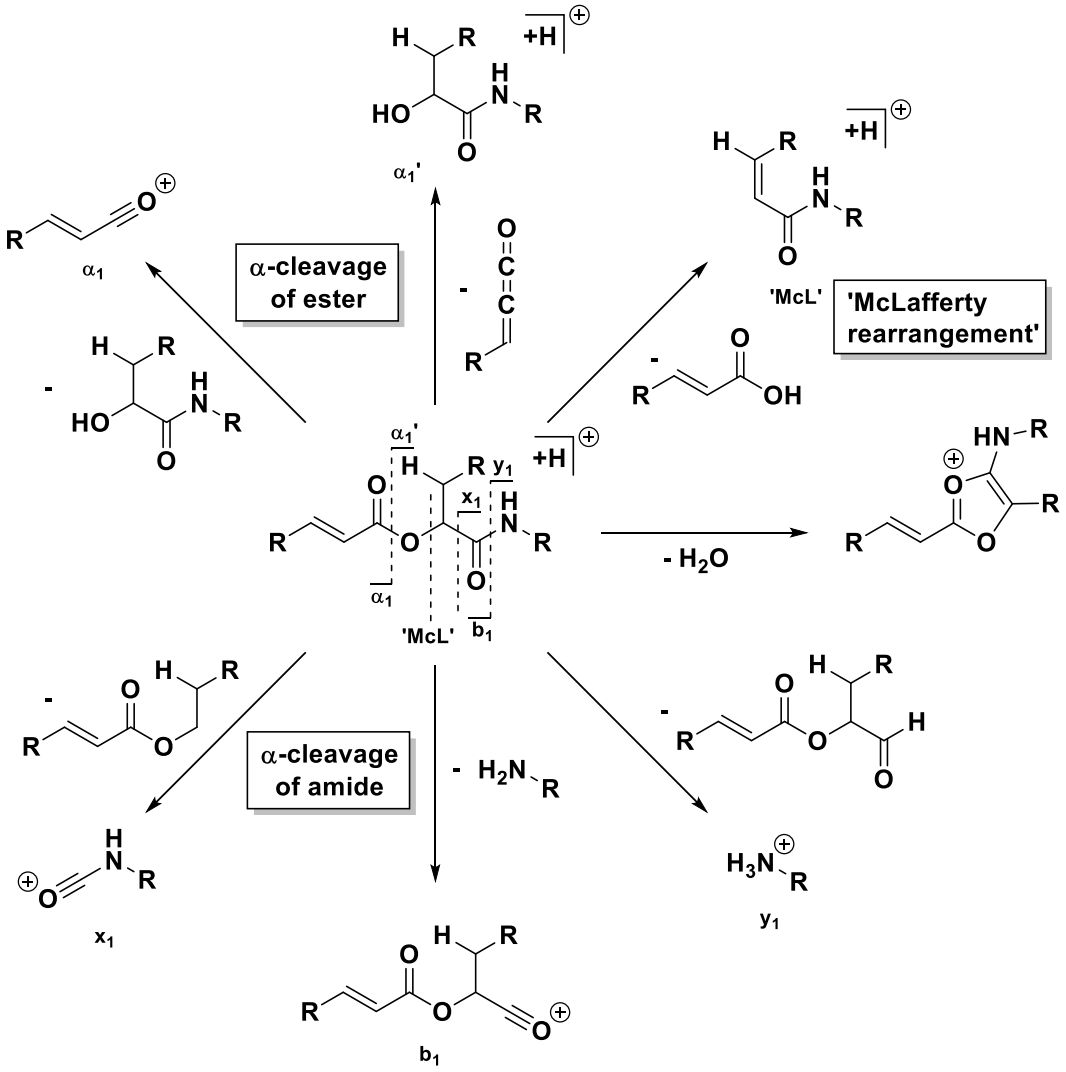

Scheme 51: Proposed fragmentation pathways based on the fragments observed *via* MALDI-MS/MS of product **D8c1**.

To increase the data storage density on the surface, more than one molecule can be printed on a single spot. For this purpose, the molecule mixtures could be directly synthesized in a one-pot fashion, by using equimolar quantities of different nucleophiles (in sum: one equivalent related to the triple bond). A series of up to five different secondary amines were applied in such an approach resulting in the formation of the desired products **M1** – **M5** (Scheme 52). The masses of each proton adduct were found in ESI-MS, but the read-out *via* tandem mass spectrometry was not performed yet. However, the principle of reading molecule mixtures was just recently successfully proven by our group by the example of a mixture containing three sequence-defined hexamers.[149]

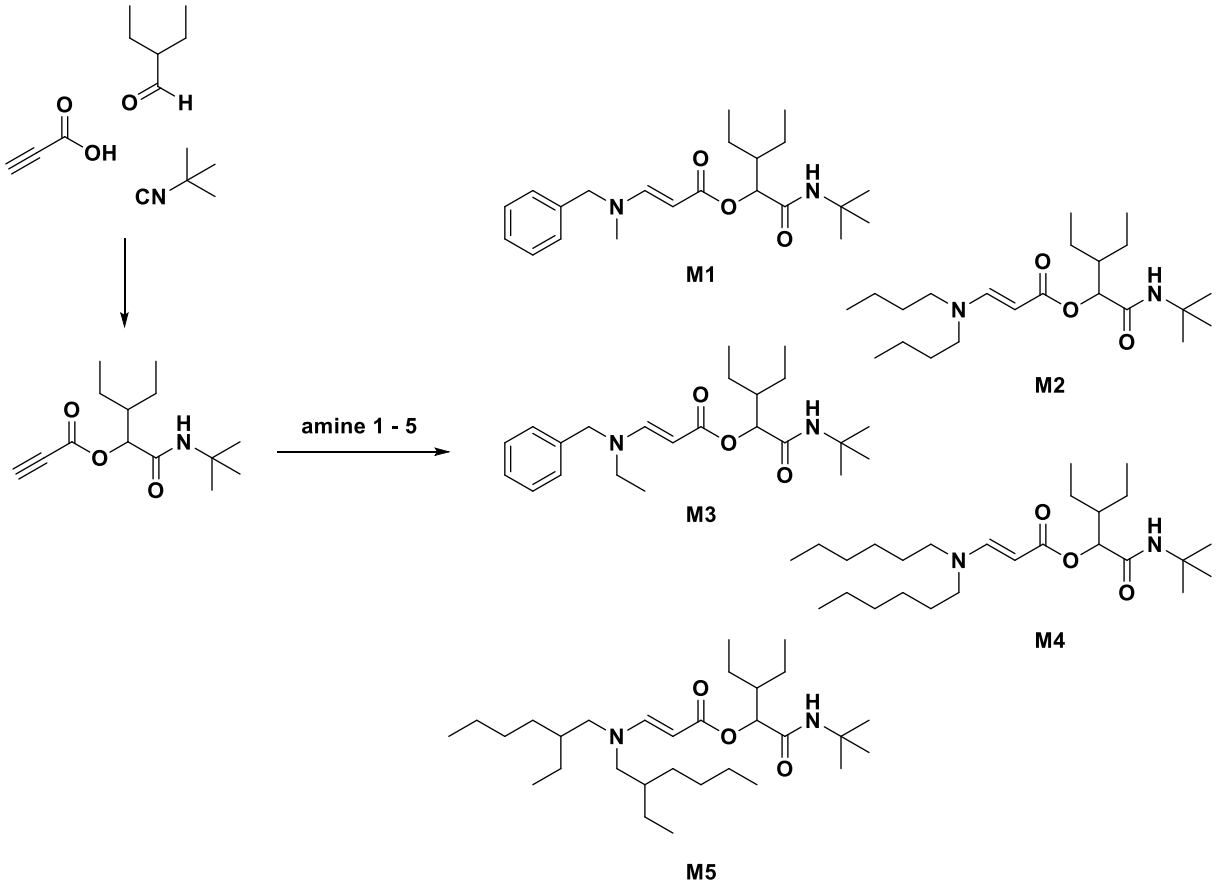

Scheme 52: Reaction scheme for the synthesis of molecular mixtures *via* a combination of the P-3CR and a subsequent amino-yne Michael addition of five different secondary amines, in a one-pot fashion.

In the example shown in Scheme 52, the Passerini reaction was performed using propiolic acid, 2-ethylbutyraldehyde and tert-butylisocyanide as components. After full conversion as indicated by GC analysis, a mixture of *N*-benzylmethyl amine (amine **1**), dibutylamine (amine **2**), *N*-benzylethyl amine (amine **3**), dihexylamine (amine **4**), and bis(2-ethylhexyl)-amine (amine **5**), 0.2 equivalents each, was added for the subsequent amino yne click reaction. A comparison of the ^{1}H NMR spectra as well as the peak assignment of reaction with one (green spectrum on bottom) to five (purple spectrum on top) nucleophiles is presented in Figure 65. In combination with the ESI-MS analysis, the formation of each desired structure was confirmed.

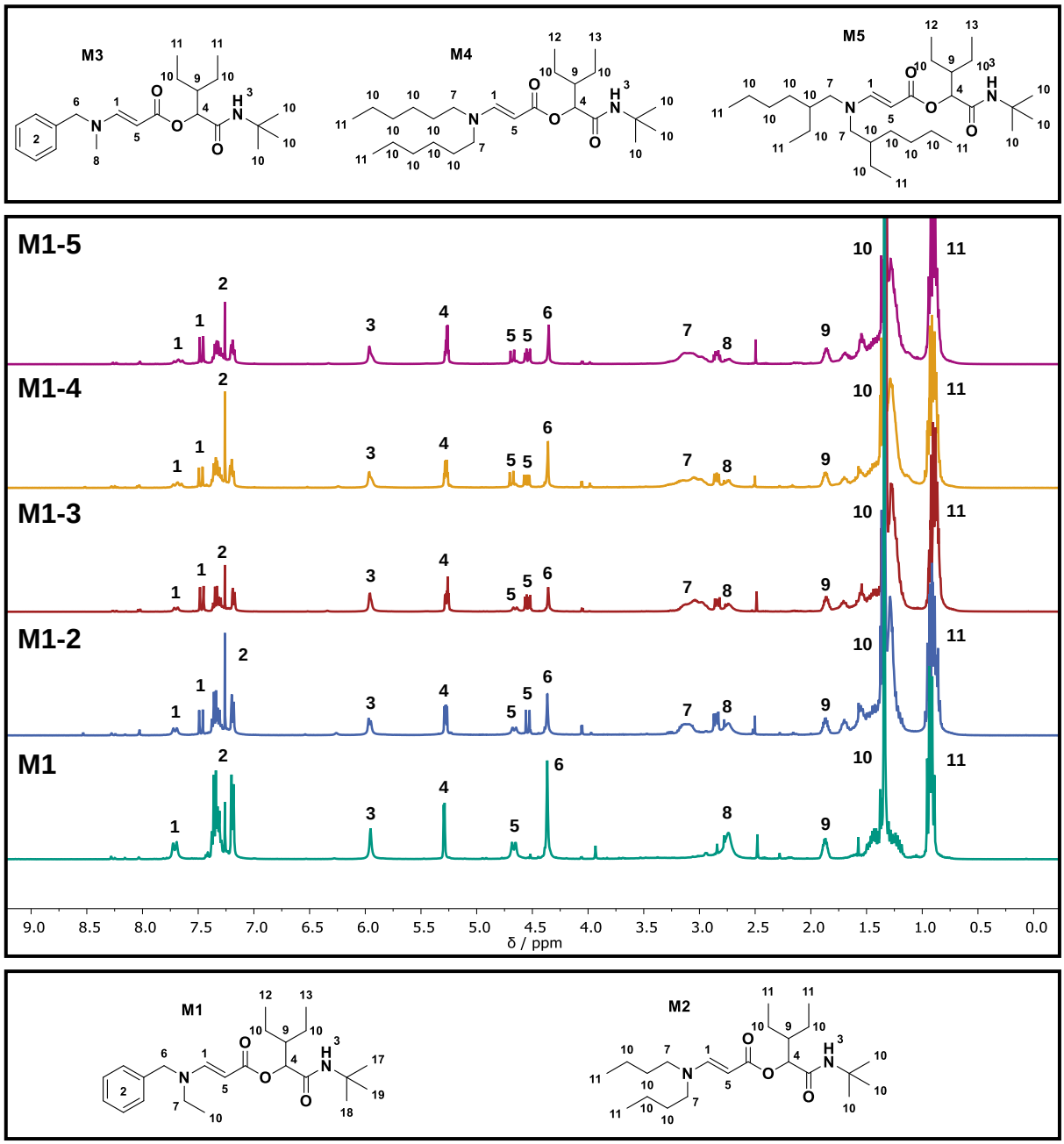

Figure 65: Comparison of the ^{1}H NMR spectra of reaction with one (green spectrum on bottom) to five (purple spectrum on top) secondary amines used for the amino-yne reaction.

To further increase the number of permutations and thus the storage capacity per molecule, the combination of the Ugi four-component reaction (U-4CR) instead of the P-3CR with a subsequent amino-yne reaction was tested. Since a primary amine is used for the U-4CR, which could also lead to side products, when reacting with the triple bond, the order of the addition of the components is crucial. *Vice versa*, if the secondary amine is added before the Ugi product is formed quantitively, it will also form the imine and result in a second side product. In the test reaction shown in Scheme 53, propiolic acid, benzaldehyde, *tert*-butyl isocyanide, and 4-bromoaniline

were used for the Ugi reaction. After full conversion was confirmed *via* GC analysis, diethyl amine was added for the subsequent amino-yne reaction to form the desired product **U1**. ^{1}H NMR analysis and the peak assignment of the crude product is shown in Figure 66, confirming a high purity and quantitative formation of the product.

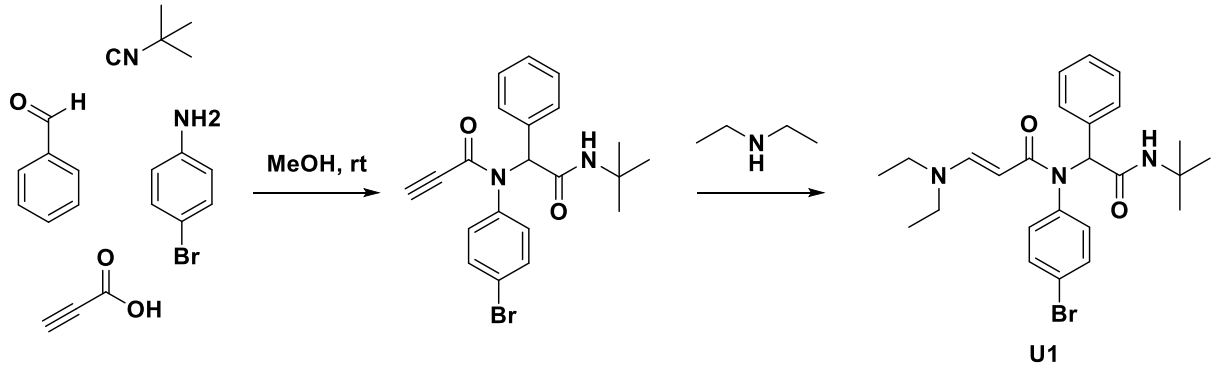

Scheme 53: Reaction scheme for the synthesis of product **U1** *via* a combination of the U-4CR and a subsequent amino-yne reaction.

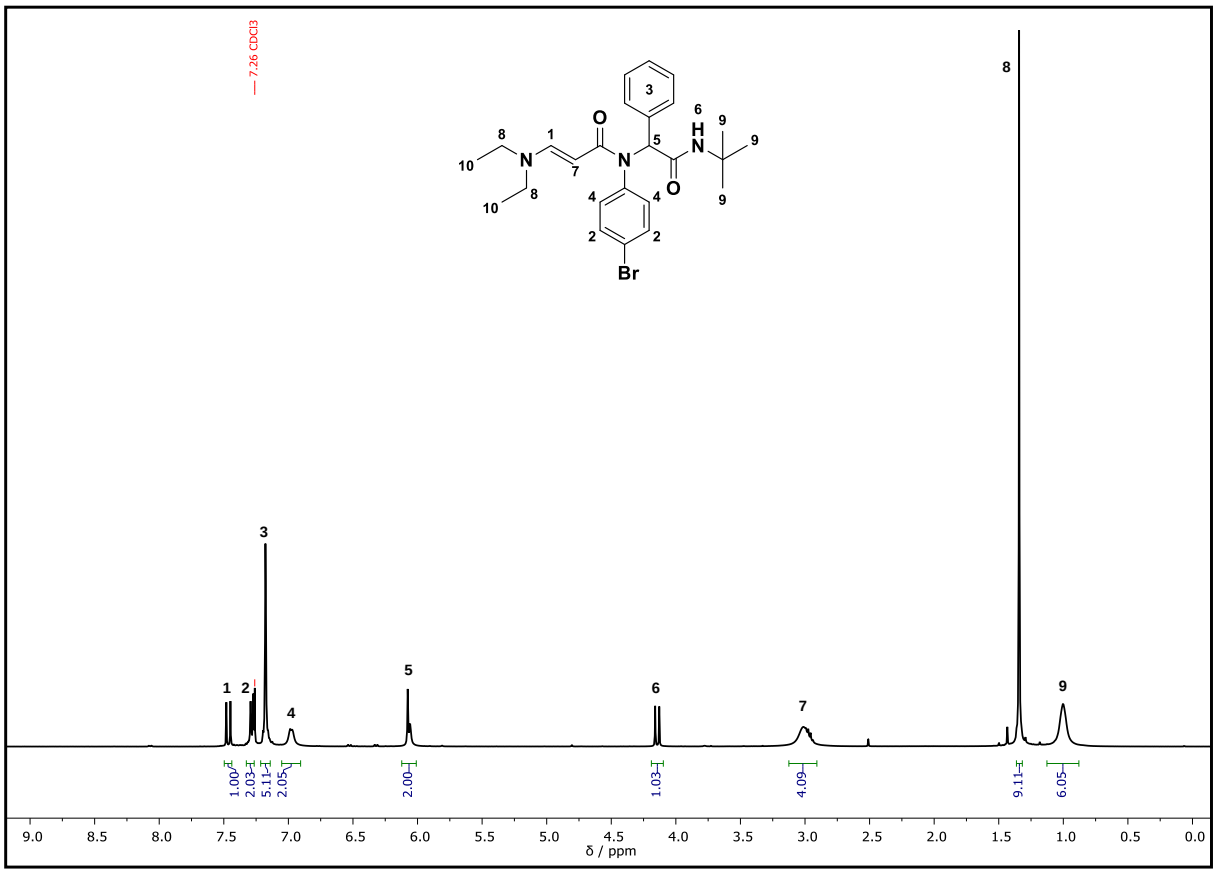

Figure 66: ^{1}H NMR and peak assignment of the crude product **U1**.

In summary, a new strategy, combining the Passerini reaction with a subsequent phenol-yne reaction to synthesize sequence-defined macromolecules for possible applications in the field of data storage gave unfavorable results, due to the low

reactivity of the aromatic aldehydes in the P-3CR. Nevertheless, a combinatorial approach for the synthesis of information-containing small molecules was introduced, which were used for the data storage on a glass slide. Therefore, a combination of the P-3CR and a subsequent Michael addition was used to write the information into molecules. MALDI-MS/MS was successfully applied for the read-out and identification of the molecule structure based on the fragmentation pattern. For the first test reactions, the products were obtained quantitatively after 10 min, providing a fast and highly efficient protocol for the storage of information in molecular structures. A more detailed kinetic study *via* ^{1}H NMR and online IR is currently under way. A comparable amount of data can be stored in a fraction of time, when compared to defined sequences, which need to be carefully purified after each reaction step. The amount of data was easily scalable by the parallel synthesis of up to 5 different products in a one-pot reaction and thus without additional synthetic effort as well as by using the U-4CR instead of the P-3CR. To further optimize the principle of a write once, read often data storage approach using small information-containing molecules on a surface, we are currently on the way to optimize the reaction conditions to transfer the synthesis step directly onto the surface.

However, in order to store data in molecules, it is not necessary to have knowledge about the exact structure or to determine the compound composition using expensive and complex fragmentation methods. Furthermore, even the separate synthesis can be avoided by using commercially available compounds. In the following chapter the data storage without any synthetic effort and the readout *via* other analysis methods than mass spectrometry is presented.

4.6.3. Data storage with zero synthetic effort

Parts of this chapter and the associated supplementary information have already been published:

Bohn, P., Weisel, M.P., Wolfs, J., Meier, M. A R. Molecular data storage with zero synthetic effort and simple read-out. *Sci Rep* **12**, 13878 (2022). https://doi.org/10.1038/s41598-022-18108-9.[494]

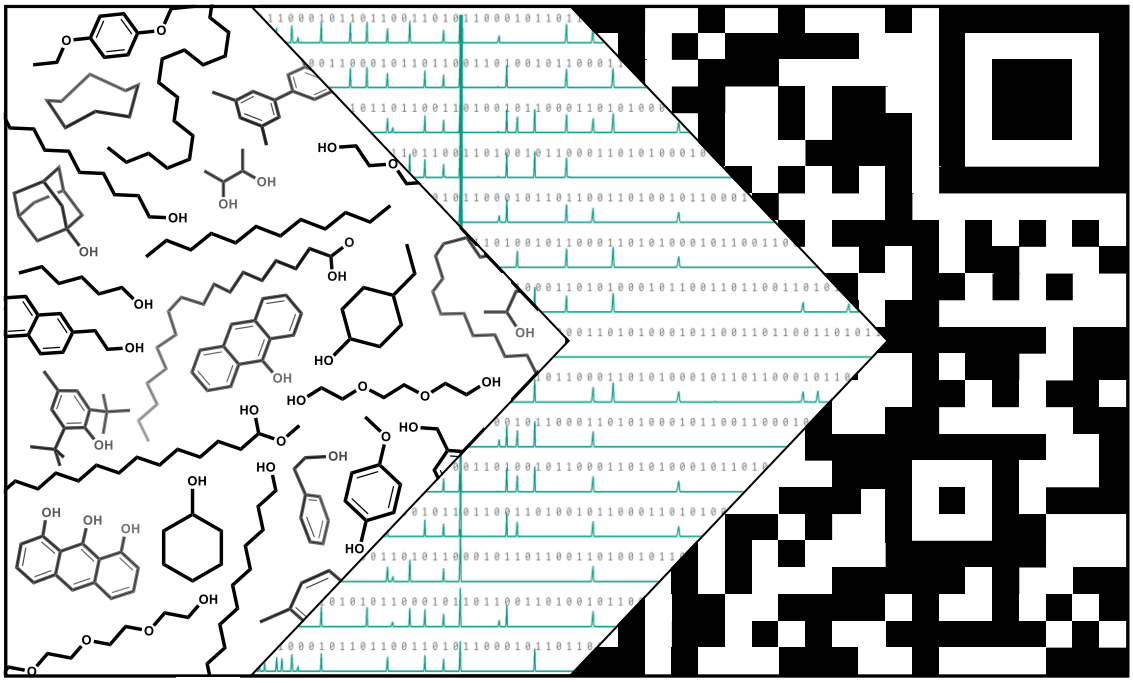

Compound mixtures represent an alternative, additional approach to DNA and synthetic sequence-defined macromolecules in the field of non-conventional molecular data storage, which may be useful depending on the target application. Here, we report a fast and efficient method for information storage in molecular mixtures by the direct use of commercially available chemicals and thus, zero synthetic steps need to be performed. As a proof of principle, a binary coding language is used for encoding words in ASCII or black and white pixels of a bitmap. This way, we stored a 25 × 25-pixel QR code (625 bits) and a picture of the same size. Decoding of the written information is achieved via spectroscopic (^{1}H NMR) or chromatographic (gas chromatography) analysis. In addition, for a faster and automated read-out of the data, we developed a decoding software, which also orders the data sets according to an internal "ordering" standard. Molecular keys or anticounterfeiting are possible areas of application for information-containing compound mixtures.

Molecular data storage using NMR spectroscopy. As a first and simple proof of concept, mixtures of up to nine different molecules, which each shows only one specific singlet ^{1}H NMR-signal, were mixed in an NMR tube (Supplementary Table 31: Chemical shifts of molecules used for data storage in NMR). Eight of them were used to encode an eight-bit (one byte) American Standard Code for Information Interchange (ASCII), whereas the last molecule (TMS) serves as a reference for the chemical shift. All of the information-containing chemicals are commercially available and standard solvents in a common laboratory. ASCII is a character encoding standard that allows 256 characters to be translated into a binary code. These include not only the alphabet, but also numbers, punctuations, and special characters. The reading direction was defined from left to right within the 1 H NMR spectrum, *i.e.*, from low field to high field. For the later read-out, a reference spectrum, a mixture that contained every of the eight information-containing compounds and thus the information of 11111111, was recorded (Figure 67). To encode a certain character, the required molecules were added to write a “1” or left out for a “0” in binary language. An example is the letter “F” (in ASCII 01000110), which translates to DCM, acetone, MeCN, which were mixed with $CDCl_3$ and the reference substance TMS to obtain the desired peak pattern (see Figure 67 and Supplementary Table 31 for solvents and their order). In order to write a word, the sequence of the letters is determined by the manual placement of the eight-bit NMR tubes into the instrument sample holder in the correct order. Afterwards, the reading process works *vice versa* and is based on an alignment principle. The reference spectrum is compared to the individual eight-bit spectrum to be evaluated. Depending on the compound mixture, the obtained peaks are slightly shifted towards higher or lower ppm. The average peak maximum as well as the largest chemical shifts for a certain signal were determined in all measurements (Supplementary Table 31) and remained unproblematic for the read-out. With the presence of a signal within the standard deviation of the respective chemical shift, the value “1” is defined, otherwise a “0” is defined in case of absence. Thus, the NMR peak pattern is retranslated into the ASCII code and the associated character. Using this method, the names “Felix␣Bloch” (Figure 67) and “Edward␣Mills␣Purcell” (Supplementary Figure 208) were successfully encoded into 31 molecular mixtures (in total 248 bits) and decoded manually *via* NMR spectroscopy. Both were awarded the 1952 Nobel Prize in physics “for their development of new methods for nuclear magnetic precision measurements and discoveries in connection therewith”.[648,649]

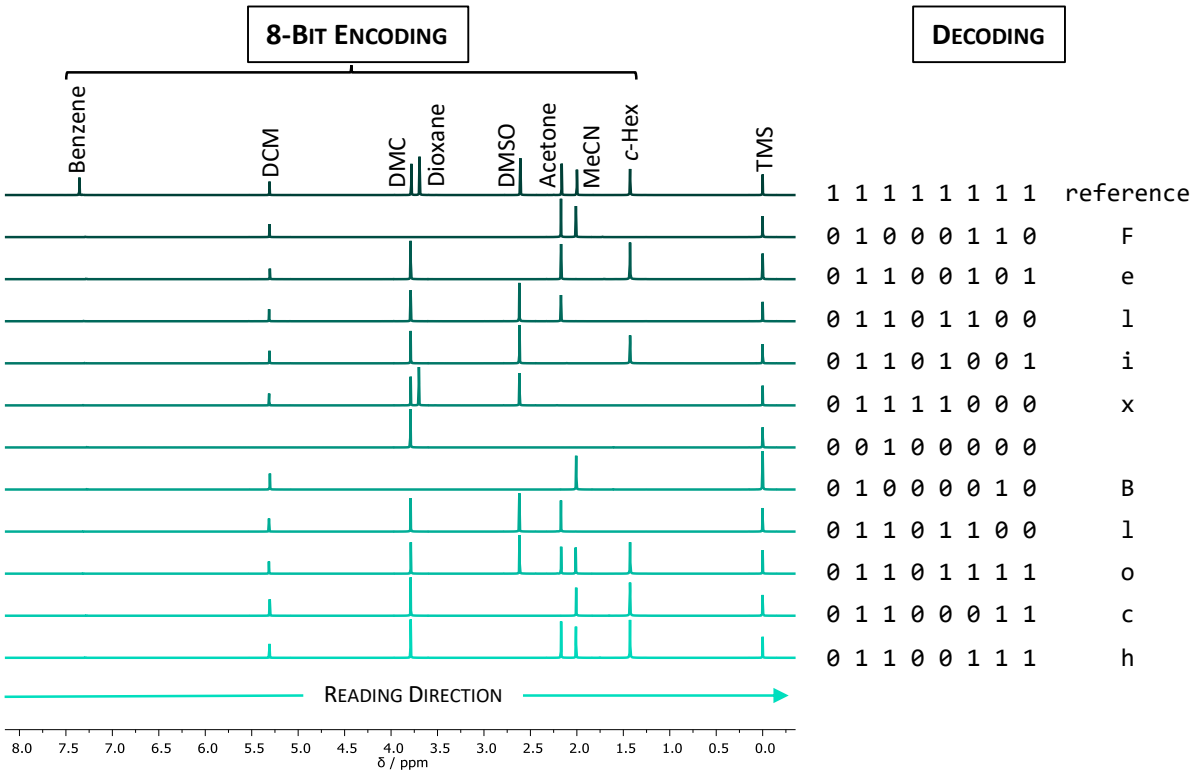

Figure 67: Encoding and decoding by ^{1}H NMR analysis. “Felix ␣ Bloch”, who was awarded the Nobel Prize together with Edward Mills Purcell (Supplementary Figure 208) in 1952,[648,649] was encoded and decoded in mixtures of up to eight information-containing compounds *via* an 8-bit ASCII code. The reading direction was specified from low to high field and the ordering *via* manual placement in the sample holder. The absence or presence of a compound signal in the spectra was retranslated to a sequence of “0”s and “1”s to reconstruct the binary code.

Molecular data storage using GC. To underline the simplicity and effciency of this strategy of data storage in molecular mixtures, the writing and reading process was easily transferred to a standard GC-FID system. Here, we increased the storage capacity per mixture to 24 bits (3 bytes) by using 24 commercially available molecules, each of them with a different retention time in the chromatogram (Supplementary Table 32 for the compound list and their order). Thus, in one mixture, three characters can be stored in a binary ASCII form (triads). *n*-Tetradecane was added to every mixture as the reference. Analogously to the NMR approach discussed above, a reference chromatogram of a mixture containing all molecules was recorded. By applying the from left-to-right reading (lower to higher retention time) and alignment strategy, the name of our university “Karlsruhe ␣ Institute ␣ of ␣ Technology” was successfully written and manually decoded using 11 mixtures (in total 264 bits, Supplementary Figure 209). The order of the triads is also determined by placing the samples into the GC autosampler in the predefined order.

The challenge of sorting the information-containing molecules, whether it is sequence-defined macromolecules or molecular mixtures, has been addressed by applying different approaches. Either by an “internal” position mass tag[149,155] or a short ordering sequence,[148] or by the “external” arrangement of the samples on *e.g.* a surface.[116,513,515] We have so far shown the external arrangement of the samples for the data storage *via* NMR and GC, but we would also like to present a simple way for the internal approach. The reference substance *n*-tetradecane was therefore varied in its concentration in increments of 1 mg per sample and termed as the “ordering” compound in this context. Using this approach, only one more compound had to be added to the system, acting as the internal standard (2,6-dimethylphenol) to circumvent signal intensity deviations caused by *e.g.*, variations of the injection volume or pipetting errors. Thus, the integral ratio of the ordering compound relative to the internal standard is calculated and the descending order of these values determines the sequence of the information pieces (Supplementary Figure 211). This way, an internal sorting is achieved, and the information-containing samples can be stored and analyzed in any order, achieving always the correct original data.

For an illustration of the sorting process, a part of the KIT logo, which symbolizes the fan-shape of the city Karlsruhe, was saved as an image in a 25 by 25 bitmap by using 25 mixtures, containing 25 bits of information each (Figure 68). If a black pixel is painted in the picture, the corresponding compound was added into the mixture to produce the required signal at that specific position in the data set. On the other hand, for a white pixel, the respective molecule was left out. The decoding process works *vice versa* again by comparison with a reference chromatogram. The presence of a compound and thus a signal stands for a black pixel and the absence of the molecule for a white one. In the schematic overview provided in Figure 68, the information-containing mixtures were prepared in the first step (a) and analyzed in a random order. The unsorted chromatograms are depicted in (b) and were translated into the corresponding bitmap (c). At this point of the decoding process, the original information is not readable due to the disordering, which underlines the importance of the internal “ordering” compound. After the sorting process of the information pieces, the correct image was obtained (d).

The used compounds are listed in Supplementary Table 32 and the 625 bitmap was manually written and decoded error-free. To optimize the read-out process in terms of reading speed and error-proneness, we next developed a decoding software, which is explained in detail in the following section.

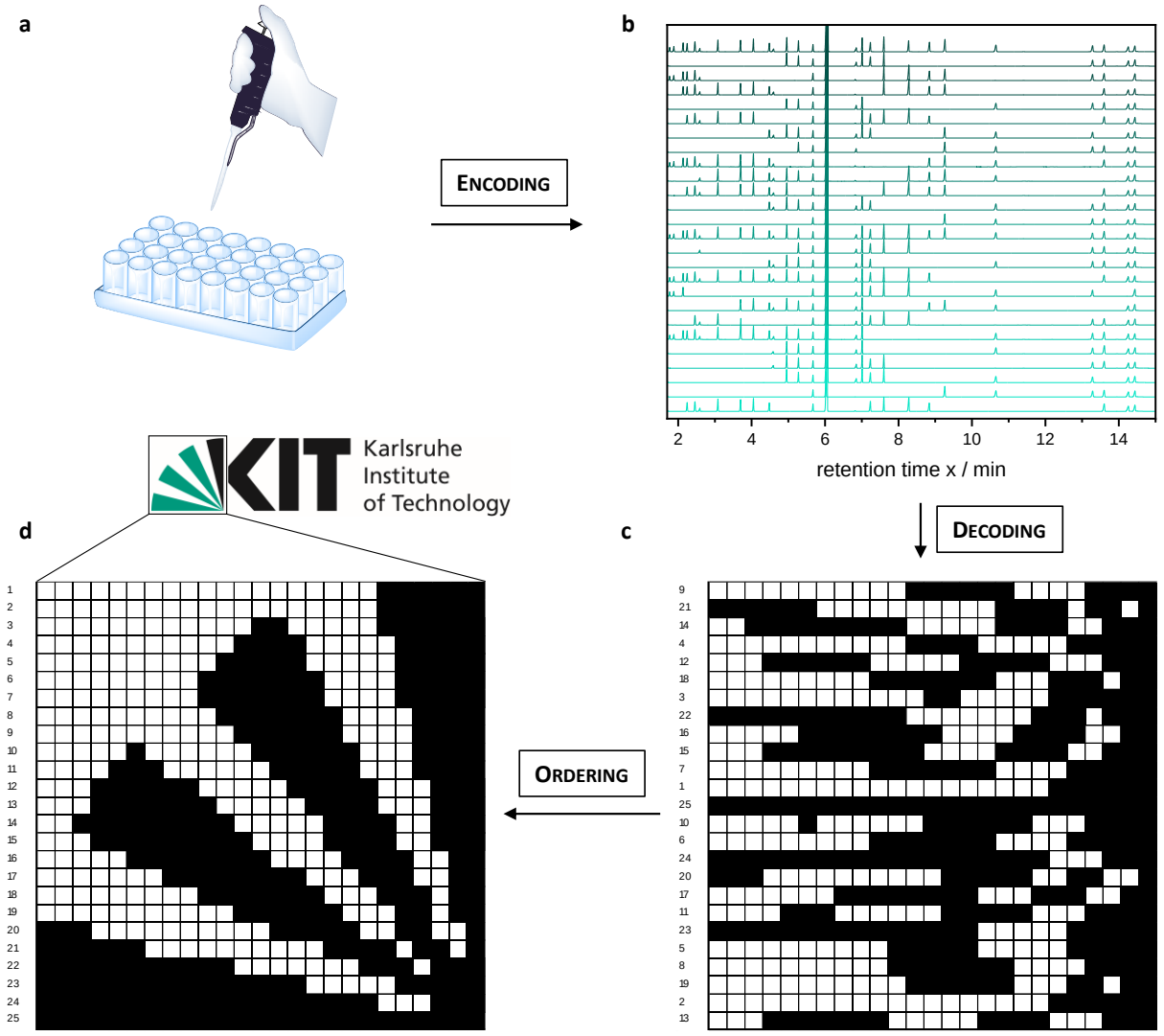

Figure 68: Schematic representation of bitmap coding. (a) Production of mixtures of up to 25 information-containing compounds per sample (25 bits) plus two reference molecules. (b) Randomly stacked, as obtained, GC chromatograms of information-containing samples plus reference chromatogram containing all compounds. (c) Translation of chromatograms into 25×25-pixel bitmap *via* alignment principle with the reference chromatogram. The absence of a signal is translated into a white pixel and the presence into a black pixel. The signals for the internal standard and the “ordering” compound were excluded from the translation process. (d) Ordering of the pixel lines according to the integral ratio of the two reference signals (Supplementary Figure 211) revealing a picture of a fan, which symbolizes the fan shape of the city Karlsruhe and is also part of the KIT logo. The KIT logo was copied and modified with permission of the KIT. © Karlsruhe Institute of Technology.

Computer assisted read-out of GC mixtures In order to establish a faster and more effcient read-out of the data, different research groups have developed custom-made decoding softwares.[121,149,155] Here, we present a software tool for automatically decoding the data sets obtained by gas chromatography. First, some calculations were necessary to adjust the settings of the software, as will be explained in detail. Small deviations in the retention time of a certain molecule in GC measurements cannot be avoided. These retention time offsets were calculated manually for each signal with the data sets corresponding to the QR code and summarized in Supplementary Table 32 and visualized in Supplementary Figure 210. The average retention time x_{Ref} of all used molecules was calculated *via* a three-fold determination of the reference sample measurement, and starting from this value, the distance to the maxima with the largest ±x-value shift over all 75 measurements (three-fold determination of each out of the 25 mixture) was determined. From these values, the width of the x-axis (ω) section was calculated, in which all maxima of the corresponding molecule are located. The largest deviation from the average retention time was observed for methyl stearate ($\Delta - x_{MAX} = 10.83 \times 10^{-3}$ min). In order to avoid errors in the decoding process, a higher value ($\Delta \pm x_{MAX} = 15.0 \times 10^{-3}$ min) was defined in the settings of the software to make it more robust against major deviations. Thus, a width of $\omega = 30.0 \times 10^{-3}$ min is set as x-range, in which it searches for a maximum in information-containing molecule mixtures. These small deviations did not influence a manual or automated read-out. Furthermore, a y-threshold of y = 50 mV was set to eliminate the baseline noise. The integration area for the ordering compound signal, *n*-tetradecane, was defined as [x_1 = 5.98 min; x_2 = 6.10 min] and for the internal standard, 2,6-dimethylphenol, as [x_3 = 5.63 min; x_4 = 5.70 min].

In the first step, the CSV (Comma-Separated Values) data files obtained from the GC instrument were imported into the script. For the ordering process, the reference signals were integrated using the trapezoidal rule. The values obtained for the *n*-tetradecane signal are divided by the ones for the internal standard (2,6-dimethylphenol). These ratios are then arranged in ascending order, defining the sequence of the information-containing molecule mixtures (Supplementary Figure 211). Ten, the software calculates the absolute maxima of each data set by comparing each y-value with its nearest neighbor in ±x direction and recognizes the reference sample based on the presence of the highest amount of found maxima. In the last step, the x-values of the maxima of the reference chromatogram are compared with those of the

individual mixtures within the specified tolerance of $\omega = 30.0 \times 10^{-3}$ min. The reference signals were excluded from this step, as they do not carry information, apart from the sample order already evaluated above. If a match and thus the presence of a compound is determined, a black pixel is displayed. On the other hand, if a maximum is not observed and thus the absence of a compound is determined, a white pixel is displayed. With help of this software, a QR code (Figure 69) referring to the homepage of the Karlsruhe Institute of Technology, could be decoded with 100% accordance. To confirm the errorless functioning of the software, the image of the "fan" was re-read automatically with the same precision. The individual steps of the entire encoding and decoding process is shown in the flowchart in Supplementary Figure 212.

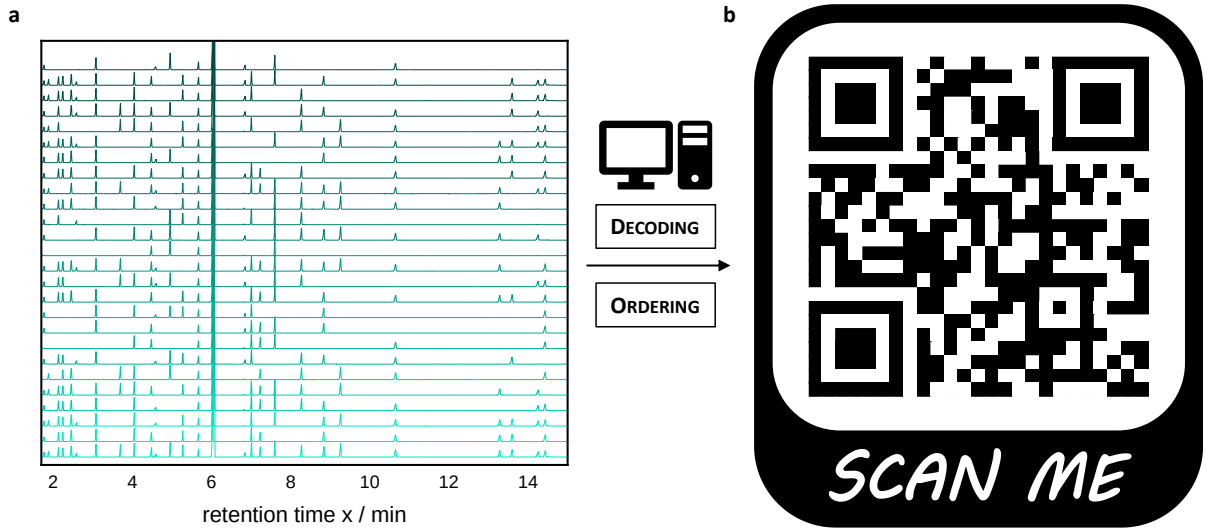

Figure 69: Schematic representation of QR coding. (a) Randomly ordered GC chromatograms of information-containing samples plus reference chromatogram containing all compounds. (b) Bitmap of a 25×25-pixel QR code containing 625 bits of information. Encoding was achieved *via* GC in 25 mixtures using 25 information compounds (25 bits) plus two reference molecules and a reference sample containing all molecules. Decoding was performed manually and using a new decoding software. The QR leads to the homepage of the KIT (https://www.kit.edu/index.php).

In summary, we presented a fast and efficient strategy for data storage using commercially available chemicals. Mixtures of up to 25 information-containing compounds were prepared manually and decoded *via* spectroscopic (^{1}H NMR) or chromatographic (GC) approaches. Thus, the writing and reading of binary ASCII codes and bitmaps was shown as well as an easy ordering approach. We developed a decoding software, which automatically put the data sets into correct order and guaranteed a faster read-out of the original information. Thus, we have introduced a simple strategy for molecular data storage that avoids complicated syntheses and

complex analytical methods by demonstrating encoding and automated decoding of QR codes. Especially the use of a standard GC-FID instrument for the read-out cheapens the analysis by more than one order of magnitude in terms of acquisition cost, if compared to the typically available NMR or MS equipment.

5. CONCLUSION AND OUTLOOK

Within the framework of this thesis, uniform and highly defined structures were investigated towards either their structure-property relationships or their application as potential data storage devices.

Uniform PEG-*b*-PCL BCPs were prepared *via* Steglich esterification of the corresponding uniform PEG and PCL homopolymers, which were synthesized using an IEG protocol. A PCL containing 64 repeating units was obtained in 20 steps in an overall yield of 33% according to the optimized reaction protocol of HAWKER *et al*.[240] TBDMS ether and benzyl ester were employed as orthogonal protecting groups. Consistently high yields for both the deprotection (>95%) and the coupling steps (>83%) were achieved (chapter 4.2).

For the synthesis of the uniform PEGs, a comparative study of literature-known procedures was carried out regarding practicality, selectivity, yield, and product purity. SEC analysis provided an important insight into the formation of side products, which were identified by SEC-ESI-MS. Time-consuming purification with loss in yield was necessary to achieve uniformity. THP and benzyl ether as protecting groups and KO^{t}Bu as base for the etherification showed the most promising results and a uniform mPEG$_{16}$ was obtained in 11 steps in an overall yield of 3% (chapter 4.1).

In connection to this, a study was carried out to determine the resolution limits of common analytical tools used for purity determination of uniform oligomers. A PEG$_8$ containing different amounts of PEG$_7$ was investigated by NMR, SEC, and ESI-MS (chapter 4.1.1.3). The highest sensitivity was observed for MS and SEC, detecting impurities of ≥1wt%, whereas NMR provided a resolution limit of ≤97%. This study demonstrated the importance of multidimensional analysis when determining the purity of substances.

Furthermore, the potential of a GaBr$_3$-catalyzed reduction of esters was shown to be a competitive synthesis protocol to previously reported approaches in order to prepare uniform PEGs (chapter 4.1.2). The reduction step was optimized with focus on full

conversion of the ester to the corresponding ether, while keeping the overreduction towards the alcohol at a minimum. TES as reductant showed the best results and the reduction was monitored quantitatively by NMR and IR spectroscopy. Due to the milder reaction conditions and an easier purification protocol, this method presents an alternative to conventional ether syntheses. So far, the addition of one monomer unit per chain elongation cycle was presented. The potential of increasing the degree of elongation per cycle was shown, to improve the efficiency of this strategy for the synthesis of high-molecular weight PEGs.

The coupling of the PEG and the PCL homopolymers *via* Steglich esterification resulted in three uniform PEG-*b*-PCL block copolymers ($Đ$ = 1.01), varying in the length of the PCL domain. Identical structures, similar in M_n with the uniform BCP, but exhibiting a slight molecular weight distribution ($Đ$ = 1.06) were prepared to investigate the influence of the dispersity on thermal properties and morphologies obtained *via* self-assembly through thermal and solvent-vapor annealing (chapter 4.3 and 4.4).

The thermal properties and the self-assembly behavior of the BCPs were investigated by DSC and SAXS, respectively (chapter 4.5). A clear constitution and dispersity dependent structure-property relationship based on the crystallization temperature T_c, and the difference in self-assembly of the smallest BCP as a function of dispersity was observed. Further investigations of the self-assembly behavior in bulk and in solution analyzed with TEM, AFM and DLS could give more insights and confirm the described results.

The high purity (>99%) and uniformity ($Đ$ = 1.00) of all synthesized homopolymers as well as the corresponding BCP were achieved by successive fractional silica column chromatography and confirmed by SEC, NMR spectroscopy, and MS.

It would be of high interest to use automated column chromatography and preparative SEC for the synthesis of the uniform homopolymers as well as the corresponding block copolymers. Furthermore, a semiautomated flow-chemistry approach, which was recently reported for the synthesis of uniform polyesters, could be easily transferred to the synthesis of uniform PCL, thus reducing the operating time by several magnitudes.[148] Another strategy based on the separation of narrowly distributed products *via* successive/ recycling chromatographic purification is also described in the literature[75,76] and would result in a library of uniform BCPs varying in their composition.

In this way, even more information about the structure-property relationship and the self-assembly behavior could possibly be achieved.

In the second part of this thesis, a combinatorial approach was developed for the synthesis of information-containing small molecules, which were used for data storage on a glass slide. As a synthesis protocol, a P-3CR in combination with a hetero-Michael addition was employed. The compounds were prepared in a straight-forward, one-pot reaction procedure by using propiolic acid as a linker component of both reactions. Consistently high conversions were observed in short reactions times for both reaction steps and no further purification was necessary for the application shown here, thus providing a fast and highly efficient protocol for the storage of information in molecular structures. Using a database of 708 commercially available components and considering all permutations, 2.63 M unique structures are accessible with the described approach. This number of permutations corresponds to a data storage capacity of 21 bits per molecule. The compound structures were exemplary identified by MALDI-MS/MS fragmentation with 100% accuracy (chapter 4.6.2). Thus, a similar data storage capacity as in sequence-defined macromolecules could be achieved. Furthermore, the scalability of this approach for the data storage in molecular structures was demonstrated by the parallel synthesis of up to five unique products in a one-pot reaction without additional synthetic effort. To further optimize the principle of a write once, read often data storage approach in terms of a faster writing rate, the reaction could be directly conducted on the surface. In principle, the presented molecules could also serve as molecular keys, *e.g.*, as anti-counterfeiting tags.

In the last part of this thesis, a fast and efficient strategy for the molecular data storage with zero synthetic effort and read-out *via* non-fragmenting analysis was demonstrated. Mixtures of up to 25 commercially available compounds were used and simple read-out was carried out *via* GC analysis (chapter 4.6.3). The writing and reading of binary ASCII codes and bitmaps of 625 bits were shown as well as an easy sorting approach of the obtained data sets. A decoding software to guarantee a faster and error-free read-out of the original information with 100% accuracy was custom made. Thus, a simple strategy for the molecular data storage by encoding and automated decoding of a QR code was described, while avoiding complicated syntheses and complex analytical methods.

6. EXPERIMENTAL SECTION

6.1. Materials

6.1.1. Materials used in connection with the synthesis of PEG-*b*-PCL BCPs in chapters 4.1 - 4.4.

1,1,3,3-Tetramethyldisiloxane (TMDS, 97%, Fisher Scientific), 1,5,7-triazabicyclo[4.4.0]dec-5-ene (TBD, >98.0%, TCI) (1,8-Diazabicyclo[5.4.0]undec-7-en (DBU, >98.0% (GC), TCI), 3,4-dihydro-2*H*-pyran (DHP, 99%, Acros Organics), acetone (99.5%, Bernd Kraft), acetonitrile (MeCN, HPLC Gradient grade, Fisher Chemical), acetic acid (96%, Carl Roth), ammonium chloride (technical grade, BASF), anhydrous *N*,*N*-Dimethylformamide (DMF, extra dry, 99.8%, stored over molecular sieve, AcroSeal, Fisher Scientific), benzyl bromide (98%, Sigma Aldrich), calcium chloride (94%, Carl Roth), Celite® 545 (particle size 0.02-0.1 mm, Merck), chloroform (Fisher Chemical, analytical reagent grade stabilized with amylene), chloroform-*d* ($CDCl_3$, 99.80 atom-% D stabilized with silver foils, Eurisotop®), citric acid (99%, Sigma Aldrich), copper(II) sulfate ($CuSO_4$, ≥99.8%, Sigma Aldrich), cyclohexane (HPLC grade, VWR), dichloromethane (DCM, ≥99.8%, HPLC grade, Fisher Chemical), dichloromethane (anhydrous, >99.8%, Sigma Aldrich), dicyclohexylcarbodiimide (DCC, 99% Sigma Aldrich), diethyl ether (technical grade, VWR), dimethyl sulfoxide-d_6 (DMSO-d_6, 99.80 atom-% D, Eurisotop®), ε-caprolactone (>99%, TCI), ethanol (HPLC grade, VWR), ethyl acetate (EA, HPLC grade, VWR), ethyl bromoacetate (EBA, reagent grade, 98%, Sigma Aldrich), ethyl hydroxy acetate (98%, Sigma Aldrich), gallium(III)-bromide (ultra-dry, 99.998%, Fisher Scientific), hydrochloric acid (HCl, 37 % solution in water, Acros Organics), hydrogen gas (99.999%, Alphagaz™ H_2, Air Liquide), 1*H*-imidazole (≥99%, Carl Roth), Lipase B *Candida antarctica* (CALB, immobilized on Immobead 150, recombinant from *Aspergillus oryzae*, ≥1800U/g), methanol (HPLC-Gradient grade, VWR Chemicals; anhydrous 99.8% Sigma Aldrich), mono methoxy polyethylene glycol ($mPEG_{750}$, M_n = 750, Sigma Aldrich), methyl iodide (contains copper as stabilizer, 99%, Sigma Aldrich), methyl *tert*-butyl ether (MTBE,

99%, ABCR), *N*,*N*-diisopropylethylamine (DIPEA, ≥99%, Sigma Aldrich), *N*,*N*-dimethylpyridin-4-amine (DMAP, ≥99%, Sigma Aldrich), palladium on activated carbon (10 wt% Pd basis, Sigma Aldrich), potassium *tert*-butoxide (KO*t*Bu, 98+%, pure, Acros Organics), *p*-toluenesulfonic acid monohydrate (99% extra pure, Acros Organics), *p*-toluenesulfonyl chloride (>99%, TCI), pyridine (analytical reagent grade, Fisher Chemical), ruthenium(III) chloride trihydrate (reagent plus, Sigma Aldrich), silica gel (technical grade, pore size 60 Å, 230-400 mesh particle size, 40-63 µm particle size), sodium carbonate (Na_2CO_3, food quality, Solvay), sodium chloride (NaCl, >99.5%, Fisher Scientific), sodium hydride (NaH, 60% dispersion in mineral oil, Sigma Aldrich), sodium hydrogencarbonate ($NaHCO_3$, laboratory reagent grade, Fisher Scientific), sodium hydroxid (NaOH, Bernd Kraft, for analysis), sodium iodide (NaI, ≥99.5%, Sigma Aldrich), sodium periodate ($NaIO_4$, ≥99%, Sigma Aldrich), sodium sulfate (Na_2SO_4, Bernd Kraft, pure), *tert*-butyldimethylsilyl chloride (TBDMS-Cl, 98% chemPUR), tetrabutylammonium fluoride (TBAF, 95%, Oxchem), tetra(ethylene glycol) (≥99.5%, Sigma Aldrich), tetra(ethylene glycol) monomethyl ether (≥98% (GC), TCI), tetrahydrofuran (THF, for HPLC, Sigma Aldrich; anhydrous ≥99.9%, inhibitor-free, Sigma Aldrich), thionyl chloride (≥99%, Sigma Aldrich), toluene (>99.7%, for synthesis, Bernd Kraft; extra dry, 99.8%, stored over molecular sieve, AcroSeal, Fisher Scientific), triethyl silane (TES, 99%, Fisher Scientific), triethylamine (TEA, 99.5%, Carl Roth), tri(ethylene glycol) (≥98%, for synthesis, Carl Roth), triphenylmethyl chloride (≥95.0% (HPLC), Fluka).

ε-caprolactone was stirred over night over CaH_2 and distilled at 105 °C at 10^{-2} mbar. Afterwards it was stored over activated molecular sieve (3 and 4 Å) and under argon atmosphere for not longer than two days. Mono methoxy polyethylene glycol ($mPEG_{750}$, M_n = 750) was dissolved in toluene and stirred for one week at 120 °C in a Dean-Stark apparatus. Right before usage, it was dried *via* azeotropic distillation of toluene (3 ×) at 70 °C and 100 to 8 mbar. The macroinitiator was stored under argon atmosphere. TBD was dried at room temperature at 10^{-2} mbar for 24 hours and stored under argon atmosphere. All ring opening polymerizations were performed in flame dried young flasks under inert conditions.

6.1.2. Materials used in connection with the molecular data storage in chapter 4.6.

1,2-Propanediol (Acros Organics, ACS reagent), 1,10-decanediol (Acros Organics, 99%), 1,12-dodecanediol (Sigma Aldrich, 99%), 1,4-diazabicyclo[2.2.2]octane (DABCO, ≥99, Sigma Aldrich), 1,4-diethoxybenzene (TCI, >98.0%), 1,5,7-triazabicyclo[4.4.0]dec-5-ene (TBD, >98.0%, TCI), 1,8,9-trihydroxyanthracene (Alfa Aesar, 97%), 1-adamantanol (Acros Organics, 99%), 1-butanol (99.9%, Sigma Aldrich), 1-decanthiol (99%, Sigma Aldich), 1-hexanol (Sigma Aldrich, 98%), 2-naphthyl isocyanide (95%, Sigma Aldrich), 2,3-butanediol (Sigma Aldrich, 98%), 2,6-dimethoxyphenol (Sigma Aldrich, 99%), 2,6-dimethylphenyl isocyanide (≥98.0% (GC), Sigma Aldrich), 2,6-di-*t*Bu-4-methylphenol (Sigma Aldrich, ≥99.0% (GC)), 2-ethylbutyraldehyde (>98.0% (GC), TCI), 2-naphthaleneethanol (Sigma Aldrich, 98%), 2-phenylethanol (Sigma Aldrich, ≥99.0% (GC)), DL-2-phenylpropionaldehyde (98%, Fisher Scientific), 3-(methylthio)propanal (98%, Fisher Scientific), 3,3'-iminodipropionitrile (technical grade, 90%, Sigma Aldrich), 3-hydroxypropanitrile (97%, Fisher Scientific), 3-mercapto-2-butanone (96%, stab. With 0.1% calcium carbonate, ABCR), 3,3',5,5'-tetramethylbiphenyl (Alfa Aesar, 97+%), 4-(3,3,4,4,5,5,6,6,7,7,8,8,8-tridecafluorooctylthio)-phenol (≥97%, Sigma Aldrich), 4-bromoaniline (97%, Sigma Aldrich), 4-ethylphenol (Sigma Aldrich, 99%), 4-hydroxy-3-methoxybenzencarbaldehyd (vanillin, 99%, Fisher Scientific), 4-hydroxybenzaldehyde (98%, Fisher Scientific), 4-methoxyphenol (Sigma Aldrich, 99%), 9-anthracenemethanol (Sigma Aldrich, 97%), acetaldehyde (ACS reagent, ≥99.5%, Sigma Aldrich), acetone (Honeywell, ≥99.8%, for HPLC), acetonitrile (MeCN, Fisher Scientific, HPLC Gradient grade), benzene (Sigma Aldrich, anhydrous, 99.8%), benzyl aldehyde (*ReagentPlus*®, ≥99%, Sigma Aldrich), benzyl isocyanide (98%, Fisher Scientific), benzyl alcohol (Honeywell, ≥99.0%), bis(2-ethylhexyl)amine (99%, Fisher Scientific), chloroform (Fisher Chemical, analytical reagent grade stabilized with amylene), chloroform-*d* ($CDCl_3$, Eurisotop®, 99.80 atom-% D, stabilized with silver foil), cyclohexane (VWR, HPLC grade), cyclohexanol (Sigma Aldrich, 99%), cyclohexyl isocyanide (99%, Fisher Scientific), cyclooctane (Fluka, ≥99.0% (GC)), diallyl amine (99% Sigma Aldrich), dichloromethane (DCM, Fisher Scientific, ≥99.8%, HPLC grade), diethyl isocyanomethylphosphonate (97%, Sigma Aldrich), diethylamine (≥99.5%, Sigma Aldrich), diethylene glycol (Sigma Aldrich, ≥99.0% (GC)), dimethyl carbonate

(DMC, Acros Organics, 99%), dimethyl sulfoxide (DMSO, Fisher Scientific, ≥99.9%), dioxane (Acros Organics, 99+%, extra pure, stabilized), diphenyl acetaldehyde (97%, Sigma Aldrich), dodecyl aldehyde (≥95%, VWR), ethyl acetate (VWR, HPLC grade), ethyl isocyanoacetate (95%, Sigma Aldrich), ethyl propiolate (99%, Sigma Aldrich), *n*-hexadecane (Alfa Aesar, 99%), methyl oleate (ABCR, 96%), methyl stearate (Acros Organics, mixtures of homologs), *tert*-butyl isocyanide (98%, Sigma Aldrich), *n*-tetradecane (Sigma Aldrich, ≥99.0% (GC)), tetraethylene glycol monomethyl ether (TCI, >98.0%), tetramethyl silane (TMS, ABCR, 99.9%, NMR grade), triethylene glycol (Sigma Aldrich, 99%).

6.2. General Methods and Instrumentation

6.2.1. Nuclear Magnetic Resonance (NMR) spectroscopy

NMR spectra were recorded using following spectrometer hardware.

Bruker AVANCE 300

^{1}H NMR (300 MHz), ^{13}C-NMR (75 MHz)

Bruker AVANCE 400

^{1}H NMR (400 MHz), ^{13}C-NMR (101 MHz)

Bruker AVANCE 500

^{1}H NMR (500 MHz), ^{13}C-NMR (126 MHz)

DMSO–d_6 and $CDCl_3$ were used as solvents and their respective resonance signal served as reference for the chemical shift δ in parts per million: ^{1}H: $CDCl_3$ = 7.26 ppm, DMSO-d_6 = 2.50 ppm; ^{13}C: $CDCl_3$ = 77.2 ppm, DMSO-d_6 = 39.5 ppm. The spin multiplicity and corresponding signal patterns were abbreviated as follows: s = singlet, d = doublet, t = triplet, q = quartet, quint. = quintet, m = multiplet. Coupling constants *J* were noted in Hz. Furthermore, 2D NMR methods (*e.g.*, heteronuclear single quantum coherence (HSQC), heteronuclear multiple bond correlation (HMBC) and correlated spectroscopy (COSY)) were carried out, if necessary, for signal assignment and structure elucidation. Diffusion-Ordered NMR Spectroscopy (DOSY) measurements were carried out for validation of the product purity.

6.2.2. Thin Layer Chromatography (TLC)

All thin layer chromatography (TLC) experiments were performed on silica-gel-coated aluminum foil (silica gel 60 F_{254}, layer thickness: 0.25 mm, Sigma-Aldrich). Compounds were visualized by irradiation with a UV lamp (λ = 254 and 365 nm), by staining with Seebach solution (mixture of 5.00 g phosphomolybdic acid hydrate, 2.00 g cerium(IV)-sulfate, 16.0 mL concentrated sulfuric acid and 200 mL water) or vanillin staining solution (mixture of 8.60 g vanillin and 2.50 mL concentrated sulfuric acid and 200 mL ethanol), or $KMnO_4$ staining solution (1.50 g $KMnO_4$, 10.0 g K_2CO_3, 1.25 mL 10% NaOH and 200 mL water).

6.2.3. Infrared (IR) spectroscopy

IR spectra were recorded on a Bruker alpha-p instrument in a frequency range of 3997.41 to 373.828 cm^{-1} applying KBr- and ATR-technology.

6.2.4. Size Exclusion Chromatography (SEC)

System I: The macrocyclic sulfites were characterized on a Varian 390-LC gel permeation chromatography (GPC) system equipped with a LC-290 pump (Varian), a refractive index detector (24 °C), a PL AS RT GPC-autosampler (Polymer laboratories) and a Varian Pro Star column oven Model 510, operating at 40 °C. For separation, two SDV 5 µm linear S columns (8 × 300 mm) and a guard column (8 × 50 mm) were used. Detection was performed using a differential refractive index (RI) detector operating in THF (anhydrous, contains 250 ppm butylated hydroxytoluene (BHT) as inhibitor, ≥99.9%, Sigma Aldrich, flow rate 1.0 mL min^{-1}). For calibration, linear poly(methyl methacrylate) standards (Agilent) ranging from 875 Da to 1677 kDa were used.

System II: Ethylene glycol oligomers were characterized on a Shimadzu Size Exclusion Chromatography (SEC) system equipped with a Shimadzu isocratic pump model LC-20AD, a Shimadzu refractive index detector (24 °C) model RID-20A, a Shimadzu autosampler model SIL-20A and a Varian column oven model 510 (50 °C). For separation, a three-column setup was used with one SDV 3 µm, 8 × 50 mm precolumn and two SDV 3 µm, 1000 Å, 3 × 300 mm columns supplied by PSS, Germany. Anhydrous tetrahydrofuran (THF) stabilized with 250 ppm butylated hydroxytoluene (BHT, ≥99.9%) supplied by Sigma Aldrich was used at a flow rate of 1.0 mL min^{-1}. For calibration, linear poly(methyl methacrylate) standards (Agilent) ranging from 875 Da

to 1677 kDa were used. The peak around 20.15 min. is a system peak and does not belong to any impurities. Dispersity *Đ* was determined by integration of the peak in LabSolution software. The program calculates M_w/M_n, which are obtained *via* the calibration.

System III: A PSS SECcurity^2 SEC system based on the Agilent infinity 1260 II hardware was used for the measurements. The system is equipped with a refractive index detector SECcurity² RI, a column oven "(Bio)SECcurity² column compartment TCC6500", a "standard SECcurity²" autosampler, isocratic pump "SECcurity² isocratic pump", and anhydrous tetrahydrofuran (THF) stabilized with 250 ppm butylated hydroxytoluene (BHT, ≥99.9%) supplied by Sigma Aldrich was used at a flow rate of 1.0 mL min^{-1} and at 30 °C as mobile phase. The analysis was performed on the following column system: Two columns PSS SDV analytical (3 µm, 300 × 8.0 mm^2, 1000 Å) with a PSS SDV analytical precolumn (3 µm, 50 × 8.0 mm^2). For the calibration, narrow linear poly(methyl methacrylate) standards (Polymer Standards Service, PPS, Germany) ranging from 102 to 62200 Da were used.

For the preparation of the samples, 1.5 mg of analyte was dissolved in 1.5 mL anhydrous tetrahydrofuran (THF) stabilized with 250 ppm butylated hydroxytoluene (BHT, ≥99.9%) supplied by Sigma Aldrich. All samples were filtered by syringe filter prior to use, to avoid plugging of the injection setup or the column.

6.2.5. Orbitrap Electrospray Ionization-Mass Spectrometry (ESI-MS)

Mass spectra were recorded on a Q Exactive (Orbitrap) mass spectrometer (Thermo Fisher Scientific, San José, CA, USA) equipped with an atmospheric pressure ionization source operating in the nebulizer assisted electrospray mode. The instrument was calibrated in the *m*/*z*-range 150-2000 using a standard containing caffeine, Met-Arg-Phe-Ala acetate (MRFA) and a mixture of fluorinated phosphazenes (Ultramark 1621, all from Sigma Aldrich). A constant spray voltage of 3.5 kV, a dimensionless sheath gas of 6, and a sweep gas flow rate of 2 were applied. The capillary voltage and the S-lens RF level were set to 68.0 V and 320 °C, respectively. For the interpretation of the spectra, molecular peaks $[M]^+$, peaks of pseudo molecules $[M+H]^+$, $[M+NH_4]^+$, $[M+Na]^+$ and $[M+K]^+$ characteristic fragment peaks are indicated with their mass to charge ratio (*m/z*) and their intensity in percent, relative to the most intense peak (100%). For the fragmentation of the compounds, the parent ion was

preselected in the quadrupole and fragmentated in the collision ion cell applying a collision energy (CE).

6.2.6. Size Exclusion Chromatography coupled to Electrospray Ionization-Mass Spectrometry (SEC-ESI-MS)

SEC-ESI-MS spectra were recorded on a Q Exactive (Orbitrap) mass spectrometer (Thermo Fisher Scientific, San Jose, CA, USA) equipped with a HESI II probe. The instrument was calibrated in the m/z range 74-1822 using premixed calibration solutions (Thermo Scientific). A constant spray voltage of 4.6 kV, a dimensionless gasflow rate of 8, and a dimensionless auxiliary gas flow rate of 2 were applied. The capillary temperature and the S-lens RF level were set to 320 °C and 62.0 V, respectively. The Q Exactive was coupled to an UltiMate 3000 UHPLC System (Dionex, Sunnyvale, CA, USA) consisting of a pump (LPG 3400SD), an autosampler (WPS 3000TSL), and a thermostatic column department (TCC 3000SD). Separation was performed on two mixed bed size exclusion chromatography columns (Polymer Laboratories, Mesopore 250 × 4.6 mm, particle diameter 3 µm) with precolumn (Mesopore 50 × 4.6 mm) operating at 30 °C. THF at a flow rate of 0.30 mL min^{-1} was used as eluent. The mass spectrometer was coupled to the column in parallel to a RI detector (RefractoMax520, ERC, Japan). 0.27 mL min^{-1} of the eluent were directed through the RI-detector and 30 µL min^{-1} infused into the electrospray source after postcolumn addition of a 100 µM solution of sodium iodide in methanol at 20 µL min^{-1} by a micro-flow HPLC syringe pump (Teledyne ISCO, Model 100DM). A 20 µL aliquot of a polymer solution with a concentration of 1 mg mL^{-1} was injected onto the HPLC system.

6.2.7. Gas Chromatography coupled to Mass Spectrometry (GC-MS)

GC-MS (electron impact (EI)) measurements were performed on a Varian 431 GC instrument with a capillary column FactorFour VF-5 ms (30 m × 0.25 mm × 0.25 mm) and a Varian 210 ion trap mass detector. Scans were performed from 40 to 650 *m*/*z* at a rate of 1.0 scans s^{-1}. The oven temperature program was: initial temperature 95 °C, hold for 1 min, ramp at 15 °C min^{-1} to 220 °C, hold for 4 min, ramp at 15 °C min^{-1} to 300 °C, hold for 2 min. The injector transfer line temperature was set to 250 °C. Measurements were performed in the split-split mode (split ratio 50:1) using helium as carrier gas (flow rate 1.0 mL min^{-1}).

6.2.8. Gas Chromatography – Flame Ionization Detector (GC-FID)

System I: GC chromatograms were recorded on a Bruker 430 GC instrument equipped with capillary column FactorFourTM VF-5 ms (30.0 m × 0.25 mm × 0.25 µm), using flame ionization detection (FID). The oven temperature program was: initial temperature 95 °C, hold for 1 min, ramp at 15 °C min^{-1} to 200 °C, hold for 4 min, ramp at 15°C min^{-1} to 300 °C, hold for 2 min. Measurements were performed in split-split mode using nitrogen as the carrier gas (flow rate 30 mL min^{-1}) and were recorded for 20 min in total.

System II: GC measurements were performed using an Agilent 8860 gas chromatograph with a HP-5 column (30 m × 0.32 mm × 0.25 µm) and a flame ionization detector (FID). The measurements were carried out using the following heating program of the oven: initial temperature 95 °C, hold for 1 min, ramp up to 200 °C with a rate of 15 °C min^{-1}, hold 200 °C for 4 min, ramp up to 300 °C with a rate of 15 °C min^{-1} and then holds 300 °C for 2 min. This system was used for the molecular data storage with zero synthetic effort described in chapter 4.6.3.

The samples for the molecular data storage (section 4.6.3.) were prepared as followed: Stock solutions with a concentration of c = 50 mg mL^{-1} were prepared in EA. For 1-adamantanol: c = 25 mg mL^{-1}, 1,10-decanediol and 9-anthracenemethanol: c = 12.5 mg mL^{-1}, 1,12-dodecanediol and 1,8,9-trihydroxyanthracene: c = 8.33 mg mL^{-1}, due to solubility issues. The respective volumes to achieve 1.5 mg of substance were added to the mixture. 900 µL of the internal standard (c = 1.5 mg mL^{-1} in EA) was added. The second reference, *n*-tetradecane, was added in 1 mg increments, starting from 1 mg for the first mixture and 26 mg for mixture number 26. All samples were filtered by syringe filter prior to use, to avoid plugging of the injection setup or the column. The injection volume was set to 1 µL and the injection temperature to 220 °C.

6.2.9. Differential Scanning Calorimetry (DSC)

The DSC experiments were caried out using a Mettler Toledo DSC stare system. The DSC experiments are carried out under nitrogen atmosphere using 40 µl aluminium crucibles and a sample mass of 5.5 or 6.5 mg. The BCP were analyzed with the following heating program with two cycles: first heating cycle: isotherm at 25 °C for 5 min; cooling: 25 °C to -15 °C

in -10 K min^{-1}, heating: -15 °C to 70 °C in 20 K min^{-1}; cooling: 70 °C to -15 °C in -10 K min^{-1}; second heating cycle: -15 °C to 70 °C in 20 K min^{-1}, cooling: 70 °C to -15 °C in -10 K min^{-1}.

6.2.10. Fast atom bombardment (FAB)

FAB mass spectra were recorded on a FINNIGAN MAT 95 instrument. The protonated molecule ion is expressed by the term: $[M+H]^+$.

6.2.11. Small-Angle X-ray Scattering (SAXS)

For the investigation of the BCP SA, the SAXS laboratory camera Xeuss 2.0 Q-Xoom (Xenocs SA, Grenoble, France) was used at the Institute of Mechanical Process Engineering and Mechanics at the Karlsruhe Institute of Technology (KIT, Karlsruhe, Germany). The camera is equipped with the X-ray micro focus source Genix3D Cu ULC (Ultra Low divergence) of Cu-k-alpha with an energy of 8.04 keV and a wavelength of 1.5406 Å. Prior the measurement, the samples were self-assembled directly on Kapton® foil *via* thermal or solvent vapor annealing. The sample-to-detector distance was set to 1000 mm and the exposure time to 30 min without a beam stop using the Pilatus3 R 300K detector (Dectris Ltd., Baden, Switzerland).

6.2.12. Liquid Dispenser

Molecules and matrix were printed on a 25 × 75 mm glass slide using a Certus Flex liquid dispenser (Fritz Gyger AG, Gwatt, Switzerland) at the Institute of Biological and Chemical Systems (IBCS-FMS) at the Karlsruhe Institute of Technology (KIT, Karlsruhe, Germany). The operating pressure was set to 0.3 bar. Spots in the size of 900 µm in distances of 225 µm were printed with analyte concentrations of 10, 50, and 100 pmol per spot. Stock solutions of the analyte were prepared in DMSO, and the matrices stock solutions were prepared as follows: HCCA: 0.1 M and 0.05 M in 70% MeCN/H_2O; DHB: 0.7 M and 1.4 M in 70% MeCN/H_2O; SA: 12.5 mM and 0.25 M in 70% MeCN/H_2O; DCTP 28.5 mM and 57 mM in 80% THF/H_2O. In total 18 × 64 (1152) spots can be printed on the respective glass slide.

6.2.13. Matrix-assisted Laser Desorption/ Ionization – tandem Mass Spectrometry (MALDI-MS/MS)

Full scan MS and MS/MS spectra were recorded on a timsTOFflex (Bruker Daltonics, Bremen, Germany) mass spectrometer to assist the molecular identification. Spectra

were acquired in qTOF mode of operation in positive ion mode within the m/z range 80 – 1000 Da. MALDI parameters were optimized to maximize intensity and resolution. The laser repetition rate was 10,000 Hz and 200 laser shots were accumulated per spectrum form 5 different raster positions within a sample spot.

6.2.14. Self-assembly of the uniform and non-uniform BCPs

Thermal annealing: 2 mg of the respective BCP was placed directly on Kapton® foil and the sample was heated to 70 °C under vacuum, kept at that temperature for three hours and subsequently cooled to room temperature overnight.

Solvent vapor annealing: 5 mg of the respective polymer was dissolved in 30 µL acetone, one drop was added onto the Kapton® foil and put into a chamber with acetone saturated atmosphere. The solvent was allowed to evaporate over four days.

6.2.15. Sample preparation for the purity study described in chapter 4.1.1.3

For the preparation of the samples containing the double protected PEG_8 (**P10**) and different quantities, ranging from 1 to 15wt%, of the double protected PEG_7 (**P9**), stock solutions with a concentration of 40 mg ml^{-1} for **P10** (200 mg analyte in 5 mL $CDCl_3$) and 8 mg mL^{-1} for **P9** (40 mg analyte in 5 mL $CDCl_3$) were prepared. Samples containing a total of 10 mg of the analytes were prepared as follows:

Impurity / wt%	V stock solution **P10** / µL	V stock solution **P9** / µL
1	247.5	12.5
2	245.0	25.0
3	242.5	37.5
4	240.0	50.0
5	237.5	62.5
7	232.5	87.5
9	227.5	112.5
11	222.5	137.5
13	217.5	162.5
15	212.5	187.5

The volume for each sample was filled to 500 µL and ^1H NMR was measured (triple determination). Subsequently, the solvent was removed under reduced pressure and 3.0 mg of the residue was dissolved in 1.5 mL THF (anhydrous, contains 250 ppm butylated hydroxytoluene (BHT) as inhibitor, ≥99.9%, Sigma Aldrich) and SEC was measured (triple determination). For the mass analysis *via* HR-ESI-MS, the samples were dissolved in HPLC MeOH in a concentration ranging from 0.05 – 0.01 mg mL^{-1}.

6.3. Experimental Procedures

6.3.1. Experimental procedures of chapters 4.1.1.1 - 4.1.1.6

Mono(tetrahydropyranyl) tri(ethylene glycol) - P1[I]

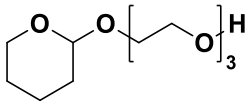

Chemical Formula: $C_{11}H_{22}O_5$
Exact Mass: 234.1467 Da
Molecular Weight: 234.2920 Da

The synthesis was performed according to a procedure of BAKER *et al*.[317] 3,4-Dihydro-2*H*-pyran (3.10 mL, 2.86 g, 34.0 mmol, 1.00 equiv.) was added dropwise to a mixture of tri(ethylene glycol) (22.8 mL, 25.6 g, 170 mmol, 5.00 equiv.) and *p*-toluenesulfonic acid monohydrate (112 mg, 0.59 mmol, 0.017 equiv.) dissolved in DCM (50 mL). The reaction mixture was stirred for 24 hours at room temperature. Half of the solvent was evaporated under reduced pressure and the mixture was washed with saturated aqueous NaCl solution (6 × 50 mL), dried over anhydrous sodium sulfate, filtered and the solvent was removed under reduced pressure. Purification of the crude product *via* column chromatography (EA) yielded the mono(tetrahydropyranyl) tri(ethylene glycol) **P1** as a colorless oil (4.85 g, 20.7 mmol, 60.9%). The product was dried under high vacuum before further use.

^{1}H NMR (400 MHz, DMSO-d_6): δ / ppm = 4.62 – 4.53 (m, 2H, CH^1 and OH^1), 3.80 – 3.35 (m, 14H, CH_2^2), 1.84 – 1.29 (m, 6H, CH_2^3).

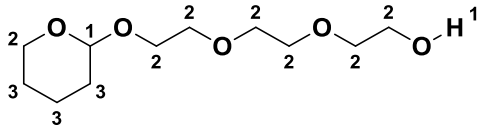

^{13}C NMR (101 MHz, DMSO-d_6): δ / ppm = 98.07 (CH^1), 72.37 (CH_2^2), 69.87 (CH_2^2), 69.78 (CH_2^2), 69.75 (CH_2^2), 66.08 (CH_2^2), 61.26 (CH_2^2), 60.23 (CH_2^2), 30.23 (CH_2^3), 25.03 (CH_2^3), 19.14 (CH_2^3).

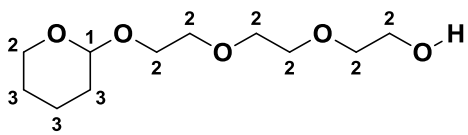

[I] The synthesis was carried out by B. Sc. PETER GÖDTEL under the lab-supervision of PHILIPP BOHN.

HRMS (ESI) of $C_{11}H_{22}O_5$ $[M+H]^+$ *m/z* calc. 235.1541, found 235.1535; $[M+NH_4]^+$ *m/z* calc. 252.1806, found 252.1800.

IR (ATR platinum diamond) ν / cm^{-1} = 3445.2, 2938.4, 2868.8, 1644.6, 1454.5, 1350.2, 1323.2, 1259.0, 1201.4, 1183.8, 1119.9, 1070.2, 1031.9, 985.6, 929.7, 906.4, 871.2, 812.8, 522.1, 428.4.

R_f = 0.11 (EA)

Đ (System II) = 1.00

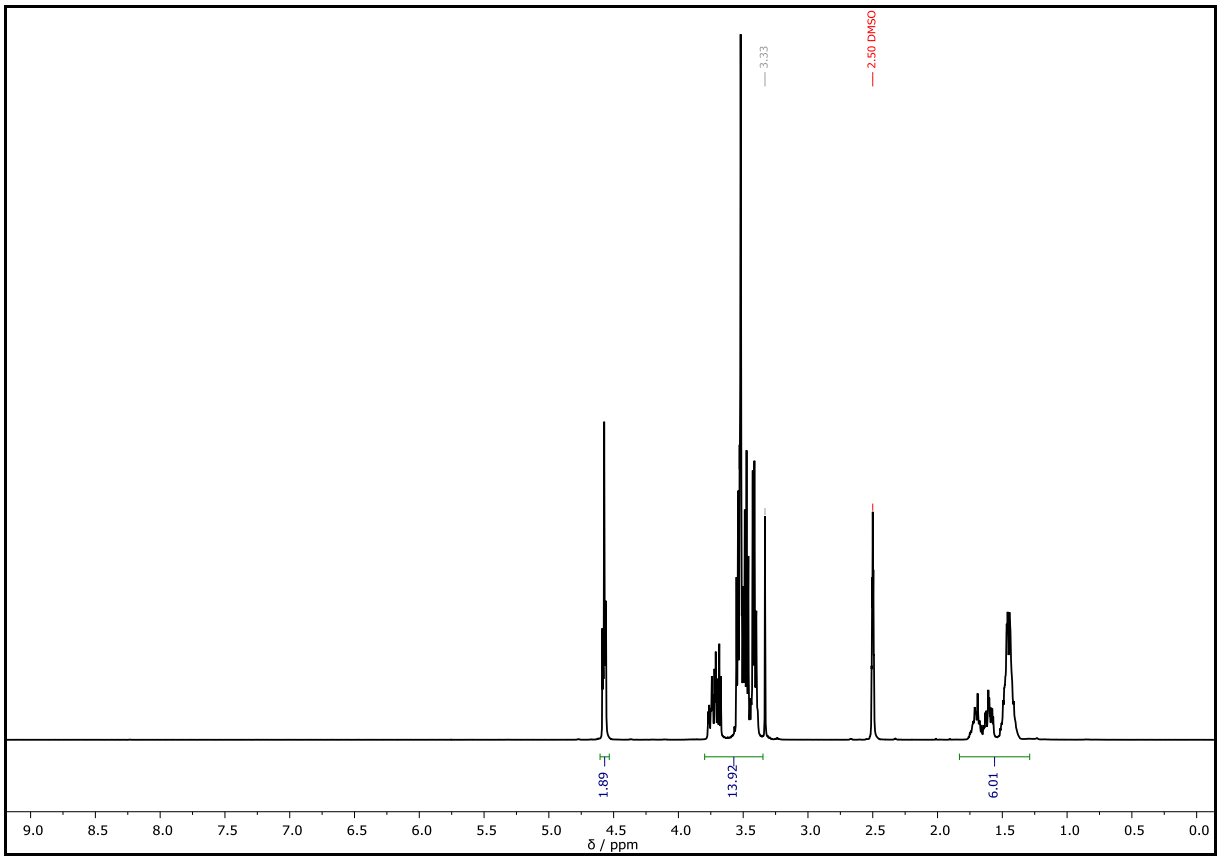

Supplementary Figure 1: ^{1}H NMR spectrum of **P1** recorded at 400 MHz in DMSO-d_6.

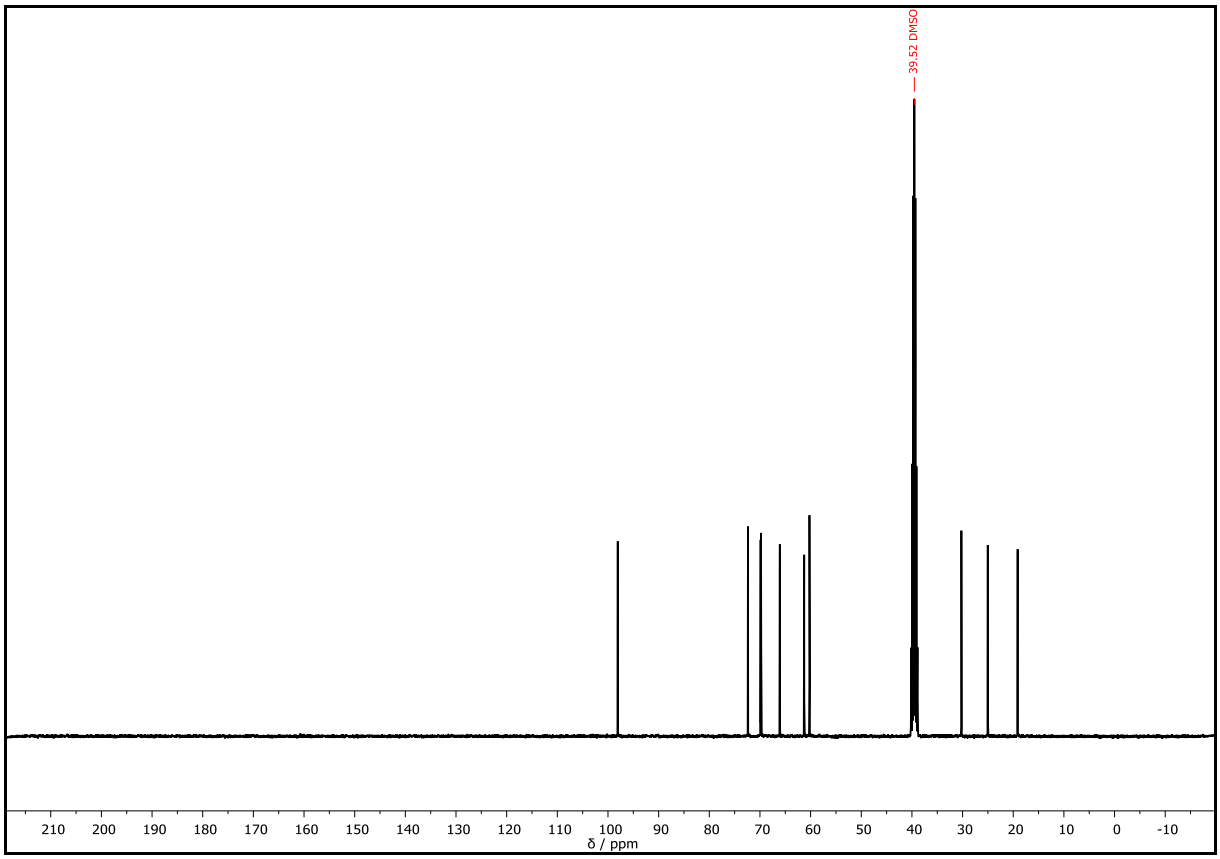

Supplementary Figure 2: ^{13}C NMR spectrum of **P1** recorded at 101 MHz in DMSO-d_6.

Mono(tetrahydropyranyl) tetra(ethylene glycol) – P2

Procedure according to BAKER *et al.*[317] – P2a

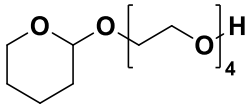

Chemical Formula: $C_{13}H_{26}O_6$
Exact Mass: 278.1729 Da
Molecular Weight: 278.3450 Da

3,4-Dihydro-2*H*-pyran (1.00 mL, 930 mg, 11.1 mmol, 1.00 equiv.) was added dropwise to a mixture of tetra(ethylene glycol) (8.30 mL, 9.34 g, 48.1 mmol, 4.35 equiv.) and *p*-toluenesulfonic acid monohydrate (27.4 mg, 0.14 mmol, 0.013 equiv.) dissolved in dry DCM (17 mL). The reaction mixture was stirred for 24 hours at room temperature. Half of the solvent was evaporated under reduced pressure. Here the mixture was washed with water (1 × 18 mL) and aqueous NaCl solution (6 × 10 mL) and dried over anhydrous sodium sulfate. The solvent was removed under reduced pressure, yielding the crude product as a colorless oil (2.30 g, 74.4%) which was further dried under high vacuum and used without additional purification. ^{1}H NMR analysis indicated a

contamination with 12% of the doubly protected product. Therefore, a complete analysis was not performed. A full characterization is given in the following for the pure product **P2b**.

Procedure according to TANAKA *et al*.[108] – P2b

Tetra(ethylene glycol) (1.72 mL, 1.94 g, 9.99 mmol, 5.00 equiv.) and 3,4-dihydro-2*H*-pyran (176 µL, 164 mg, 2.00 mmol, 1.00 equiv.) were dissolved in dry DCM (50 mL). While stirring at room temperature, *p*-toluenesulfonic acid monohydrate (38.0 mg, 0.20 mmol, 0.10 equiv.) was added and the reaction mixture was stirred for further 30 minutes. Subsequently, water (50 mL) was added, and the phases were separated. The organic layer was washed with water (1 × 50 mL), dried over anhydrous sodium sulfate, filtered, and concentrated *in vacuo*. Purification of the crude product (362 mg, 1.30 mmol, 65.0%) *via* column chromatography (cyhex:EA = 1:2 → EA:MeOH = 9:1) yielded the mono(tetrahydropyranyl) tetra(ethylene glycol) **P2b** as a colorless oil (283 mg, 1.02 mmol, 51.0%). The product was dried under high vacuum before further use.

^{1}H NMR (400 MHz, DMSO-d_6): δ / ppm = 4.63 – 4.51 (m, 2H, CH^{1} and OH^{1}), 3.80 – 3.37 (m, 18H, CH_2^{2}), 1.79 – 1.35 (m, 6H, CH_2^{3}).

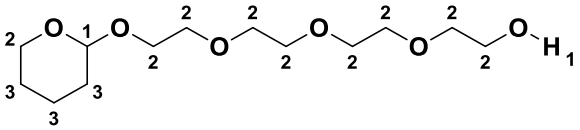

^{13}C NMR (101 MHz, DMSO-d_6): δ / ppm = 98.07 (CH^{1}), 72.37 (CH_2^{2}), 69.85 (CH_2^{2}), 69.81 (CH_2^{2}), 69.74 (CH_2^{2}), 66.08 (CH_2^{2}), 61.25 (CH_2^{2}), 60.22 (CH_2^{2}), 30.23 (CH_2^{3}), 25.03 (CH_2^{3}), 19.14 (CH_2^{3}).

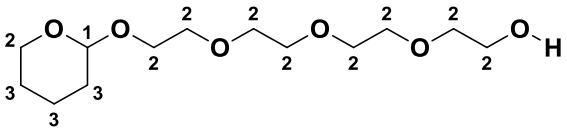

HRMS (ESI) of $C_{13}H_{26}O_6$ $[M+H]^+$ *m/z* calc. 279.1803, found 279.1798; $[M+Na]^+$ *m/z* calc. 301.1623, found 301.1616; $[M+NH_4]^+$ *m/z* calc. 296.2068, found 296.2063; $[M+K]^+$ *m/z* calc. 317.1356, found 317.1356.

The mass of the tetra(ethylene glycol) was also found. $C_8H_{18}O_5$ $[M+H]^+$ *m/z* calc. 195.1211, found 195.1225.

IR (ATR platinum diamond) $\tilde{\nu}$ / cm^{-1} = 3429.8, 2868.8, 1643.6, 1454.5, 1349.0, 1323.5, 1284.8, 1258.4, 1201.5, 1120.1, 1071.1, 1031.9, 985.7, 930.0, 906.9, 871.5, 812.7, 521.1, 428.9.

R_f = 0.17 (EA)

Đ (System II) = 1.00

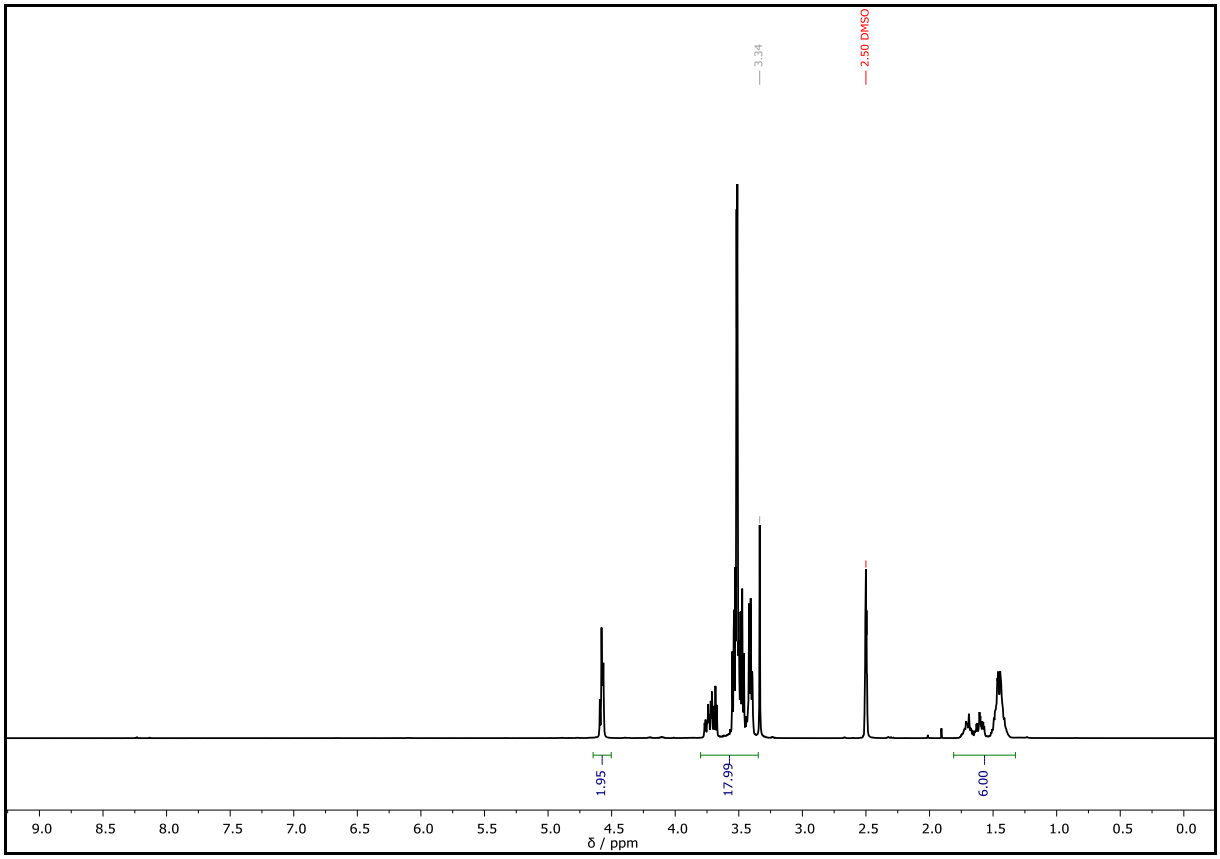

Supplementary Figure 3: ^{1}H NMR spectrum of **P2b** recorded at 400 MHz in DMSO-d_6.

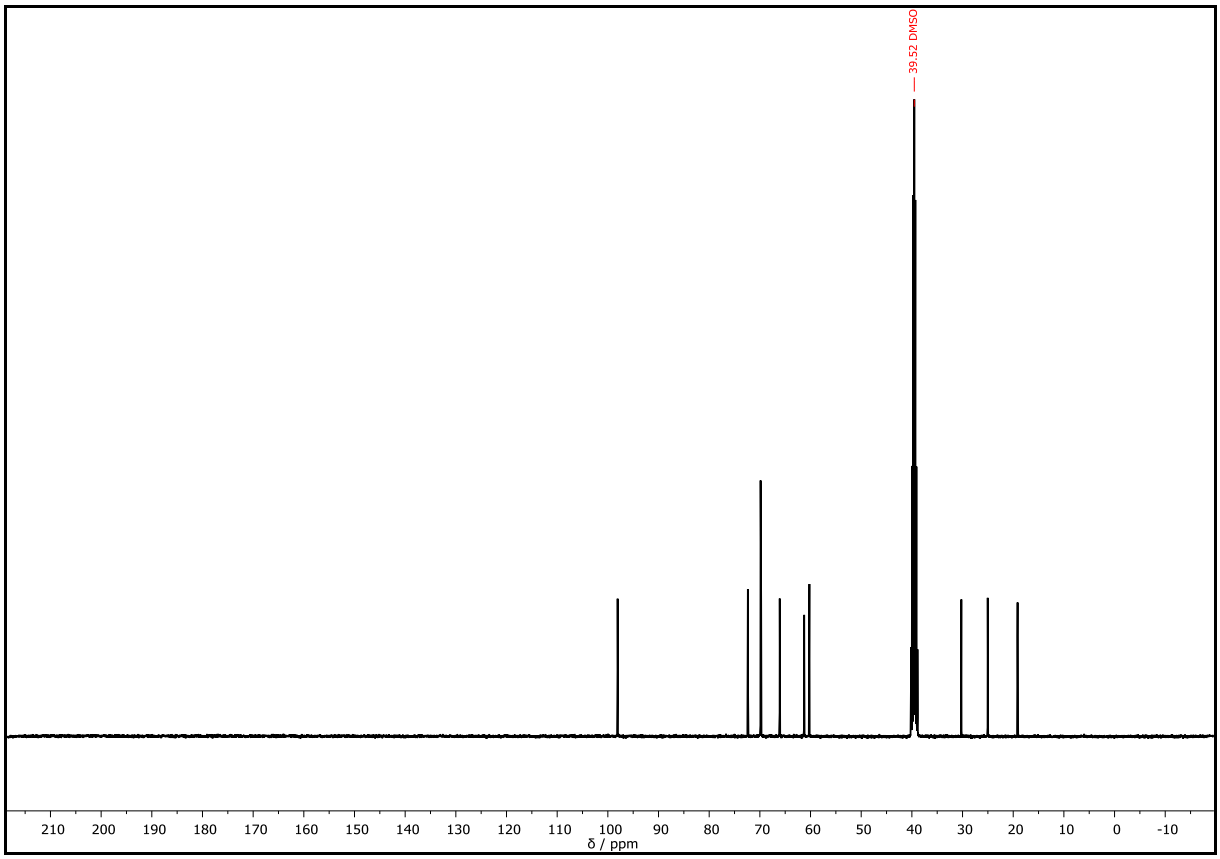

Supplementary Figure 4: ^{13}C NMR spectrum of **P2b** recorded at 101 MHz in DMSO-d_6.

Monotrityl tetra(ethylene glycol) - P3

Procedure according to JIANG *et al.*[318] – P3a

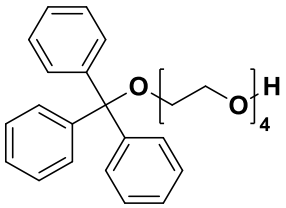

Chemical Formula: $C_{27}H_{32}O_5$
Exact Mass: 436.2250
Molecular Weight: 436.5480

Tetra(ethylene glycol) (5.17 mL, 5.82 g, 30.0 mmol, 3.00 equiv.), triethylamine (2.78 mL, 2.03 g, 20.0 mmol, 2.00 equiv.) and DMAP (122 mg, 0.10 µmol, 0.1 equiv.) were dissolved in DCM (67 mL). The mixture was heated to 40 °C and a solution of triphenylmethyl chloride (2.79 g, 10.0 mmol, 1.00 equiv.) in DCM (11 mL) was added dropwise. After refluxing for six hours, the reaction was quenched with brine (35 mL). The phases were separated, and the aqueous layer was extracted with DCM (2 × 35 mL). The combined organic layers were dried over anhydrous sodium sulfate, filtered and the solvent was evaporated under reduced pressure. Purification of the

crude product *via* column chromatography (cyhex:EA = 1:1 → 1:10) yielded the monotrityl-protected tetra(ethylene glycol) **P3a** (2.82 g, 6.46 mmol, 64.6%) as a colorless, viscous oil. The product was dried under high vacuum before further use.

^{1}H NMR (400 MHz, DMSO-d_6): δ / ppm = 7.44-7.38 (m, 6H, $H_{Ar,ortho}^{1}$), 7.38-7.29 (m, 6H, $H_{Ar,meta}^{2}$), 7.30 – 7.22 (m, 3H, $H_{Ar,para}^{3}$), 4.60 (t, J = 5.5 Hz, 1H, OH^{4}), 3.63 – 3.50 (m, 10H, CH_2^{5}), 3.48 (t, J = 5.3 Hz, 2H, CH_2^{6}), 3.42 (t, J = 4.9 Hz, 2H, CH_2^{7}), 3.07 (t, J = 4.9 Hz, 2H, CH_2^{8}).

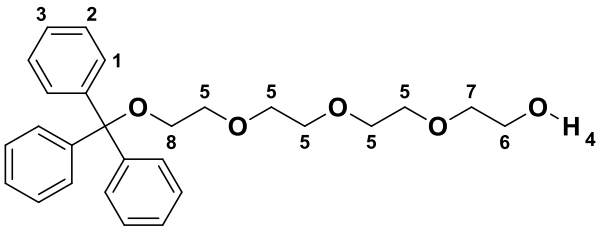

^{13}C NMR (101 MHz, DMSO-d_6): δ / ppm = 143.84 (C_q^{1}), 128.27 ($C_{Ar,ortho}^{2}$), 127.88 ($C_{Ar,meta}^{3}$), 126.99 ($C_{Ar,para}^{4}$), 85.91 (C_q^{5}), 72.38 (CH_2^{6}), 70.11 (CH_2^{7}), 69.94 (CH_2^{7}), 69.87 (CH_2^{7}), 69.83 (CH_2^{7}), 69.68 (CH_2^{7}), 63.08 (CH_2^{8}), 60.24 (CH_2^{9}).

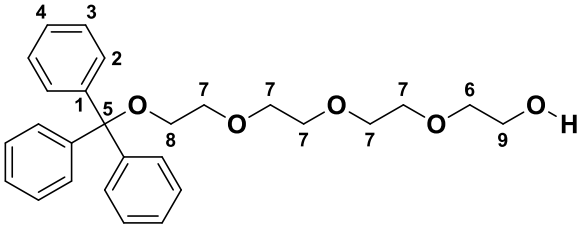

HRMS (ESI) of $C_{27}H_{32}O_5$ $[M+NH_4]^+$ *m/z* calc. 454.2590, found 454.2582; $[M+Na]^+$ *m/z* calc. 459.2144, found 459.2135; $[M+K]^+$ *m/z* calc. 475.1878, found 475.1876.

IR (ATR platinum diamond) $\tilde{\nu}$ / cm^{-1} = 3452.9, 3057.2, 2869.4, 1596.5, 1489.6, 1448.0, 1349.7, 1288.7, 1219.7, 1075.4, 1032.7, 1009.4, 934.0, 899.8, 774.1, 762.9, 747.0, 705.3, 697.3, 649.4, 631.9, 509.0 cm^{-1}.

R_f = 0.17 (cyhex: EA = 2:1)

Đ (System II) = 1.00

Procedure according to KINBARA *et al*.[319] – P3b

Tetra(ethylene glycol) (49.8 mL, 56.0 g, 288 mmol, 6.43 equiv.) was dried *via* azeotropic evaporation under reduced pressure with toluene (3 × 50 mL). Then, triethylamine (8.00 mL, 5.84 g, 57.7 mmol, 1.29 equiv.) was added under argon atmosphere. Then, triphenylmethyl chloride (12.5 g, 44.8 mmol, 1.00 equiv.) was added in small portions over five minutes. After stirring for three hours at room temperature, the reaction mixture was diluted with EA (50 mL). The present solid was filtered and rinsed with EA (2 × 15 mL). The filtrate was washed with water (2 × 75 mL, 3 × 25 mL), saturated aqueous ammonium chloride solution (2 × 25 mL), brine (3 × 25 mL) and 50% aqueous solution of sodium chloride (1 × 25 mL) and the solvent was evaporated under reduced pressure. The mixture was further dried under high vacuum while stirring to afford the crude product as a yellow high viscous oil (18.8 g), which was used without further purification in the next synthesis. SEC analysis showed a contamination with 8% of symmetric tetra(ethylene glycol) bis-trityl ether and 17.3 g (39.6 mmol, 88.4%) of pure monotrityl-protected tetra(ethylene glycol)) **P3b**.

The analytical data is consistent with the one for **P3a**.

Procedure according to DAVIS *et al*.[237] – P3c

A round bottomed flask was charged with tetra(ethylene glycol) (17.3 mL, 19.4 g, 100 mmol, 10.0 equiv.), pyridine (1.21 mL, 1.19 g, 15 mmol, 1.50 equiv.) and triphenylmethyl chloride (2.79 g, 10.0 mmol, 1.00 equiv.). The reaction mixture was stirred over night at 45 °C. Subsequently, water (30 mL) was added to the reaction and phases were separated. The aqueous layer was extracted with toluene (2 × 50 mL). The combined organic layers were dried over anhydrous sodium sulfate, filtered, and concentrated *in vacuo*. Purification of the crude product *via* column chromatography (cyhex:EA = 1:1 → 1:10) yielded the monotrityl-protected tetra(ethylene glycol) **P3c** (4.07 g, 9.32 mmol, 93.2%) as a colorless, viscous oil. The product was dried under high vacuum before further use.

The analytical data is consistent with the one of **P3a**.

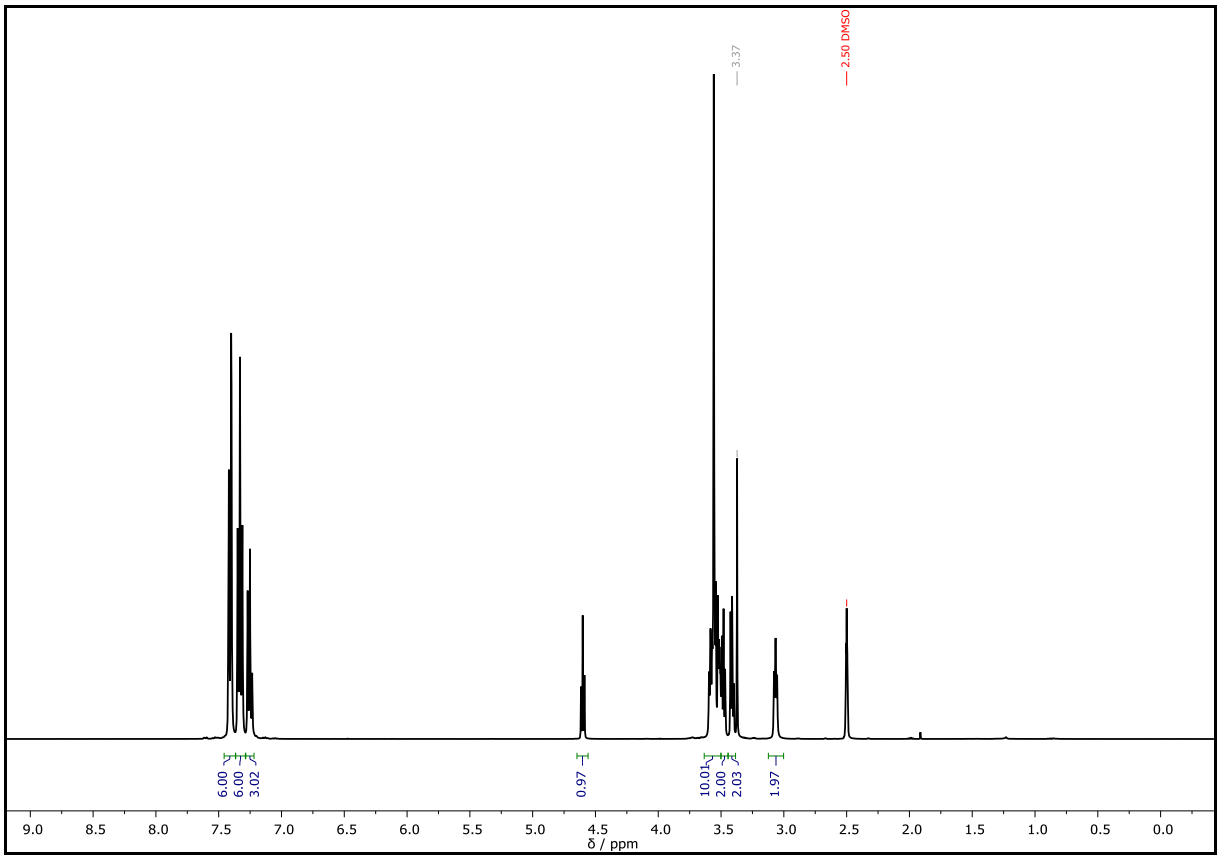

Supplementary Figure 5: ^{1}H NMR spectrum of **P3a** recorded at 400 MHz in DMSO-d_6.

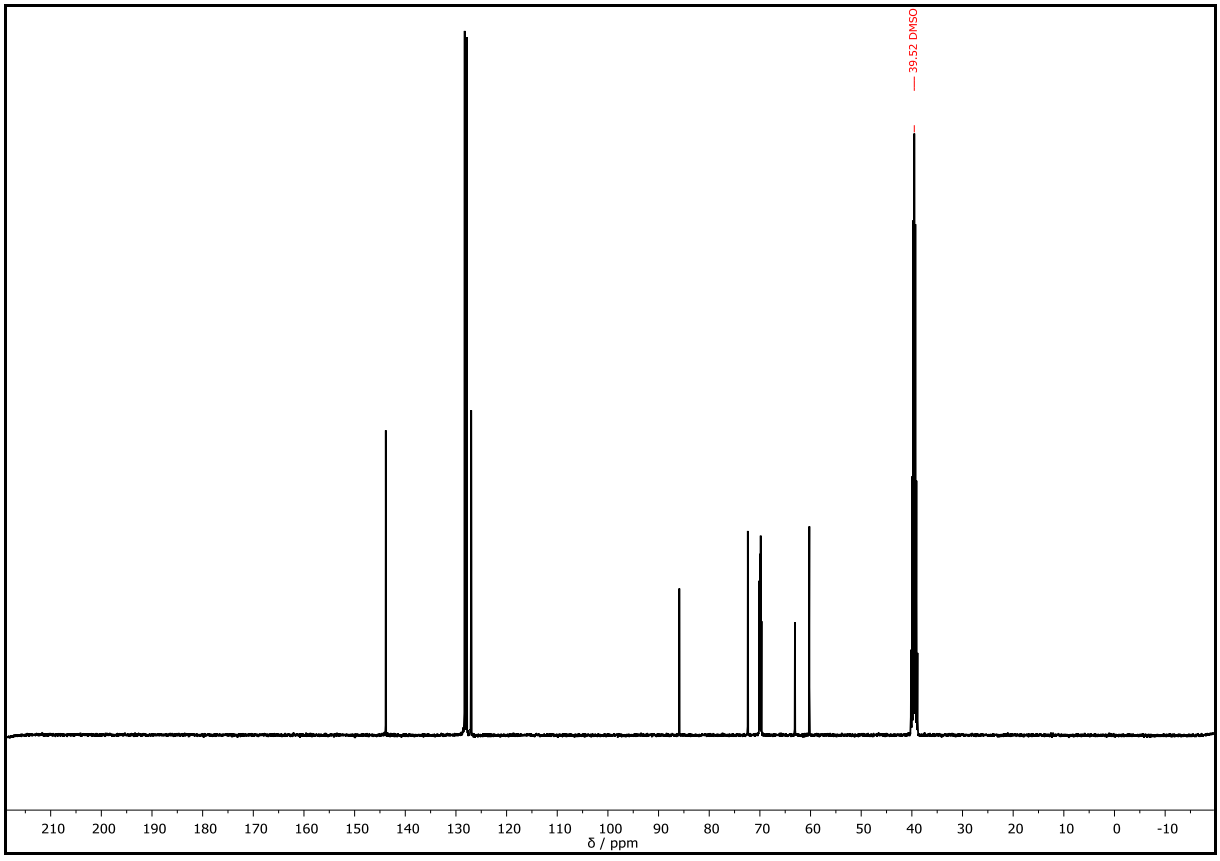

Supplementary Figure 6: ^{13}C NMR spectrum of **P3a** recorded at 101 MHz in DMSO-d_6.

Monobenzyl tri(ethylene glycol) – P4[I]

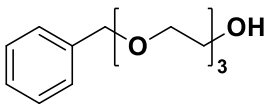

Chemical Formula: $C_{13}H_{20}O_4$
Exact Mass: 240.1362 Da
Molecular Weight: 240.2990 Da

The monobenzylated tetra(ethylene glycol) **P4a** was prepared according to the procedure of DAVIS *et al*.[237] Benzyl bromide (14.3 mL, 20.5 g, 0.12 mmol, 1.00 equiv.) was added dropwise over 40 minutes to a mixture of tri(ethylene glycol) (111 mL, 125 g, 0.83 mmol, 6.92 equiv.) and 50% aqueous NaOH (5.3 g solid in 10.6 mL H_2O, 1.10 equiv.). The reaction mixture was allowed to cool after stirring for 20 hours at 100 °C. Subsequently, 175 mL of water was added, and the remaining base was neutralized with 1 M HCl. The solution was extracted with diethyl ether (7 × 100 mL). The combined organic layers were dried over anhydrous sodium sulfate, filtered, and concentrated under reduced pressure. SEC analysis indicated a contamination with 5% of symmetric tri(ethylene glycol) bis-benzyl ether. 5.00 g of the crude product (24.6 g) were purified *via* column chromatography (cyhex:EA = 1:2) yielding the monobenzylated tri(ethylene glycol) **P4a** (4.27 g, 17.8 mmol, 72.9%) as a colorless oil. The product was dried under high vacuum before further use.

^{1}H NMR (400 MHz, DMSO-d_6): δ / ppm = 7.38 – 7.25 (m, 5H, H_{Ar}^1), 4.59 (t, J = 5.5 Hz, 1H, OH^2), 4.48 (s, 2H, CH_2^3), 3.59 – 3.50 (m, 8H, CH_2^4), 3.48 (t, J = 5.2 Hz, 2H, CH_2^5), 3.42 (t, J = 5.3 Hz, 2H, CH_2^6).

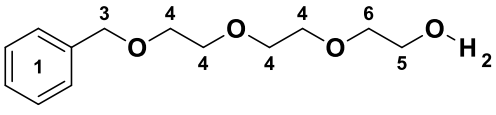

^{13}C NMR (101 MHz, DMSO-d_6): δ / ppm = 138.49 (C_q^1), 128.24 (C_{Ar}^2), 127.52 (C_{Ar}^2), 127.39 (C_{Ar}^2), 72.39 (CH_2^3), 72.04 (CH_2^3), 69.89 (CH_2^3), 69.81 (CH_2^3), 69.79 (CH_2^3), 69.16 (CH_2^3), 60.24 (CH_2^3), 39.52(CH_2^4).

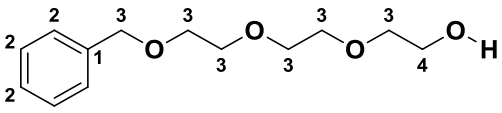

[I] The synthesis was carried out by B. Sc. PETER GÖDTEL under the lab-supervision of PHILIPP BOHN.

HRMS (ESI) of $C_{13}H_{20}O_4$ $[M+H]^+$ *m/z* calc. 241.1436, found 241.1432.

IR (ATR platinum diamond) ν / cm^{-1} = 3435.4, 3030.6, 2865.1, 1495.8, 1453.5, 1350.3, 1248.5, 1091.9, 933.6, 886.0, 849.4, 737.3, 697.8, 612.1, 464.0.

R_f = 0.24 (cyhex:EA = 1:2)

Đ (System II)= 1.00

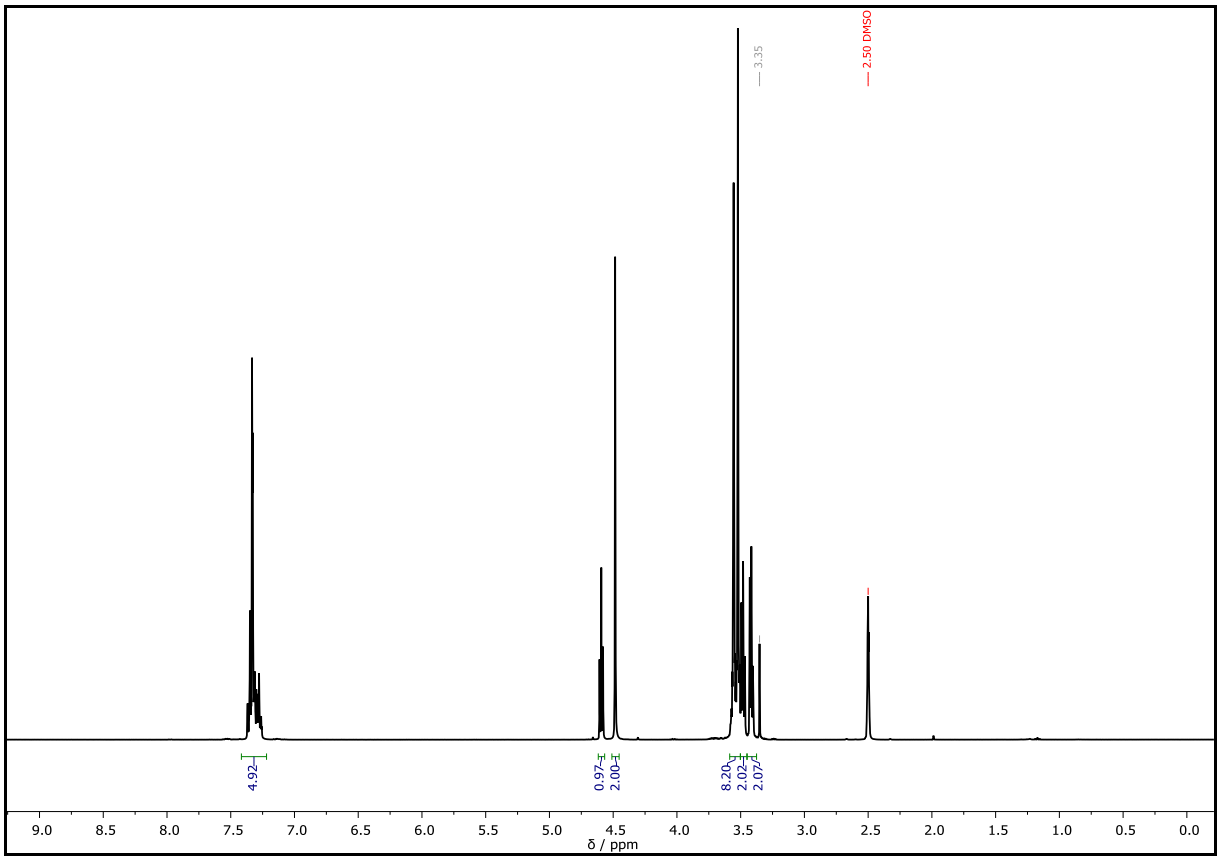

Supplementary Figure 7: ^{1}H NMR spectrum of **P4** recorded at 400 MHz in DMSO-d_6.

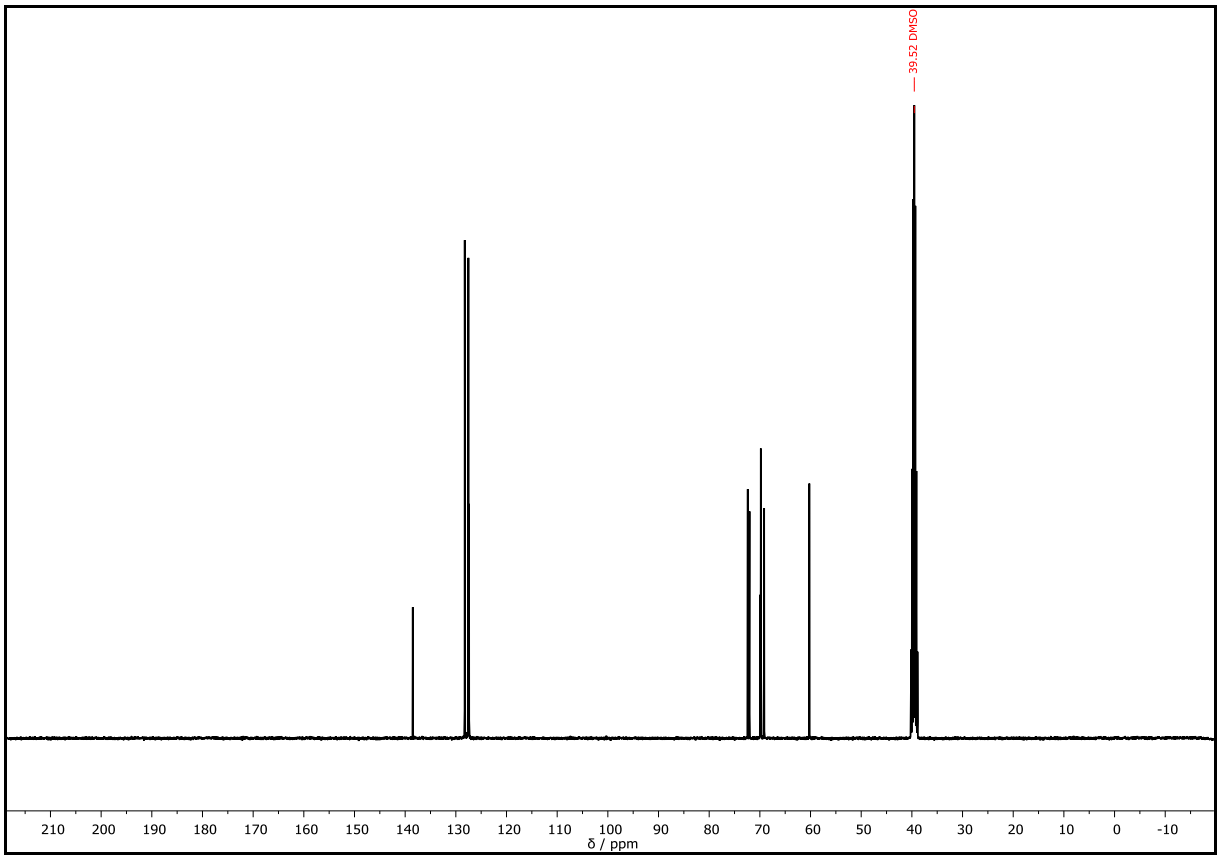

Supplementary Figure 8: ^{13}C NMR spectrum of **P4** recorded at 101 MHz in DMSO-d_6.

Monobenzyl tetra(ethylene glycol) – P5

Procedure according to DAVIS *et al*.[237] – P5a

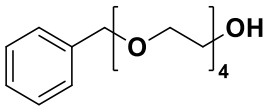

Chemical Formula: $C_{15}H_{24}O_5$
Exact Mass: 284.1624 Da
Molecular Weight: 284.3520 Da

Benzyl bromide (1.39 mL, 2.00 g, 11.7 mmol, 1.00 equiv.), tetra(ethylene glycol) (20.2 mL, 22.7 g, 117 mmol, 10.0 equiv.), 50% aqueous NaOH (516 mg solid in 1.00 mL H_2O, 1.10 equiv.) were used. SEC analysis indicated a contamination with 7% of symmetric tetra(ethylene glycol) bis-benzyl ether. Purification of the crude product *via* column chromatography (cyhex:EA = 1:2) yielded the monobenzylated tetra(ethylene glycol) **P5a** (2.56 g, 9.00 mmol, 76.9%) as a colorless oil. The product was dried under high vacuum before further use.

^{1}H NMR (400 MHz, DMSO-d_6): δ / ppm = 7.48 – 7.16 (m, 5H, H_{Ar}^{1}), 4.58 (t, J = 5.4 Hz, 1H, OH^{2}), 4.48 (s, 2H, CH_2^{3}), 3.59 – 3.37 (m, 12H, CH_2^{4}), 3.48 (t, J = 5.3 Hz, 2H, CH_2^{5}), 3.41 (t, J = 5.4 Hz, 2H, CH_2^{6}).

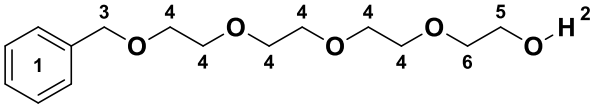

^{13}C NMR (101 MHz, DMSO-d_6): δ / ppm = 138.50 (C_q^{1}), 128.24 (C_{Ar}^{2}), 127.51 (C_{Ar}^{2}), 127.39 (C_{Ar}^{2}), 72.37 (CH_2^{3}), 72.04 (CH_2^{3}), 69.87 (CH_2^{3}), 69.86 (CH_2^{3}), 69.83 (CH_2^{3}), 69.80 (CH_2^{3}), 69.79 (CH_2^{3}), 69.15 (CH_2^{3}), 60.23 (CH_2^{4}).

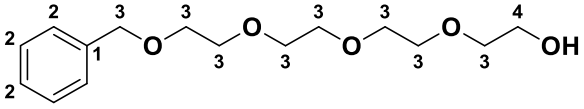

HRMS (ESI) of $C_{15}H_{24}O_5$ $[M+H]^+$ *m/z* calc. 285.1698, found 285.1692; $[M+NH_4]^+$ *m/z* calc. 302.1963, found 302.1957; $[M+Na]^+$ *m/z* calc. 307.1517, found 307.1510; $[M+K]^+$ *m/z* calc. 323.1251, found 323.1249.

IR (ATR platinum diamond) $\tilde{\nu}$ / cm^{-1} = 3435.0, 2865.9, 1718.7, 1641.8, 1453.5, 1350.3, 1276.8, 1249.4, 1092.7, 940.4, 885.0, 846.5, 738.6, 698.4, 606.1, 526.9.

R_f = 0.25 (EA)

Đ (System II) = 1.00

Procedure according to BRUCE *et al.*[273] – P5b

Tetra(ethylene glycol) (69.1 mL, 77.7 g, 400 mmol, 4.00 equiv.) was added to a suspension of sodium hydride (60% dispersion in mineral oil, 16.0 g, 400 mmol, 4.00 equiv.) in dry THF (500 mL). The mixture was refluxed at 80 °C and a solution of benzyl bromide (11.9 mL, 17.1 g, 100 mmol, 1.00 equiv.) in dry THF (80 mL) was added dropwise. The reaction mixture was refluxed for another three hours. After cooling, methanol was slowly added to decompose the remaining excess of sodium hydride. The solvent was evaporated under reduced pressure and the obtained residue was redissolved in 5 wt% aqueous hydrochloric acid (200 mL). The product was extracted with chloroform (8 × 200 mL) and washed with water (1 × 100 mL). The combined organic layers were dried over anhydrous sodium sulfate, filtered, and concentrated *in vacuo*. Purification of the crude product *via* column chromatography (EA) yielded the monobenzylated tetra(ethylene glycol) **P5b** (23.7 g, 83.4 mmol, 83.4%) as a colorless oil. The product was dried under high vacuum before further use.

The analytical data is consistent with the one of **P5a**.

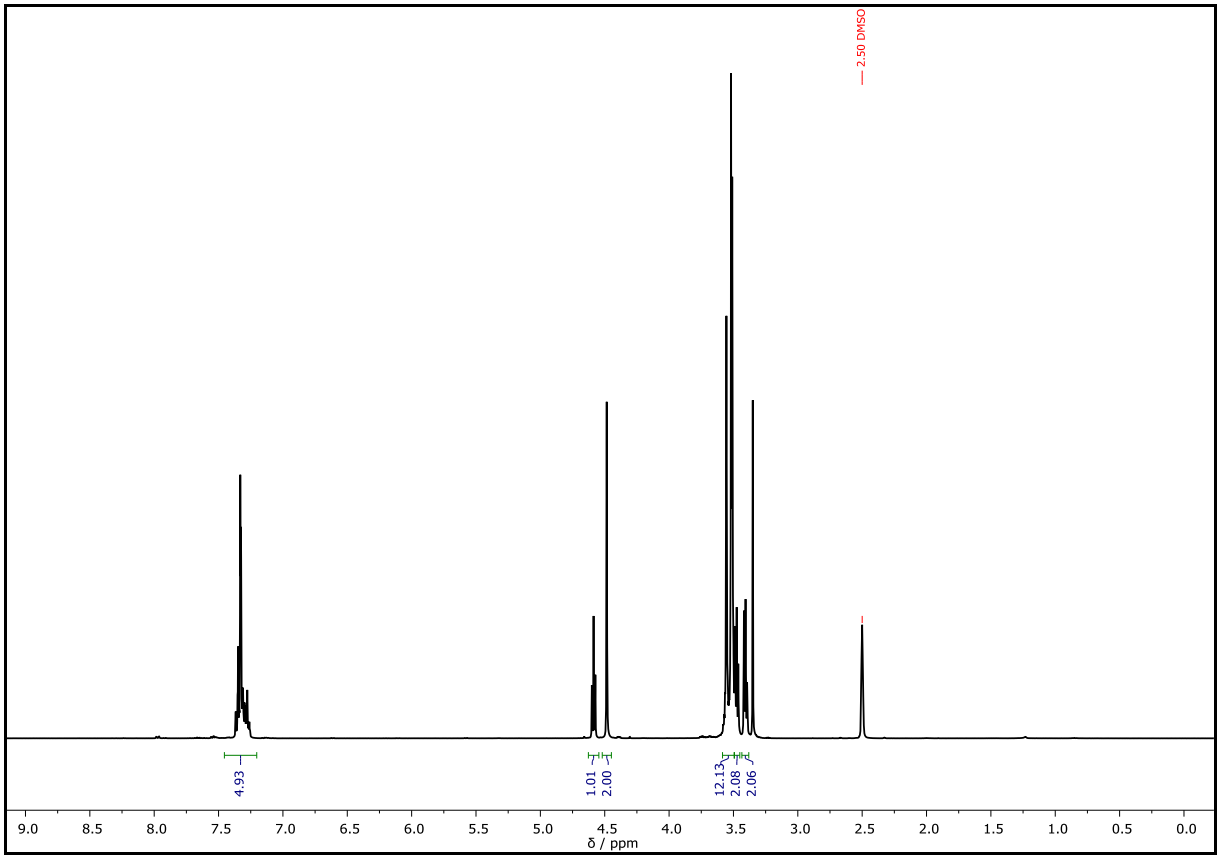

Supplementary Figure 9: ^{1}H NMR spectrum of **P5a** recorded at 400 MHz in DMSO-d_6.

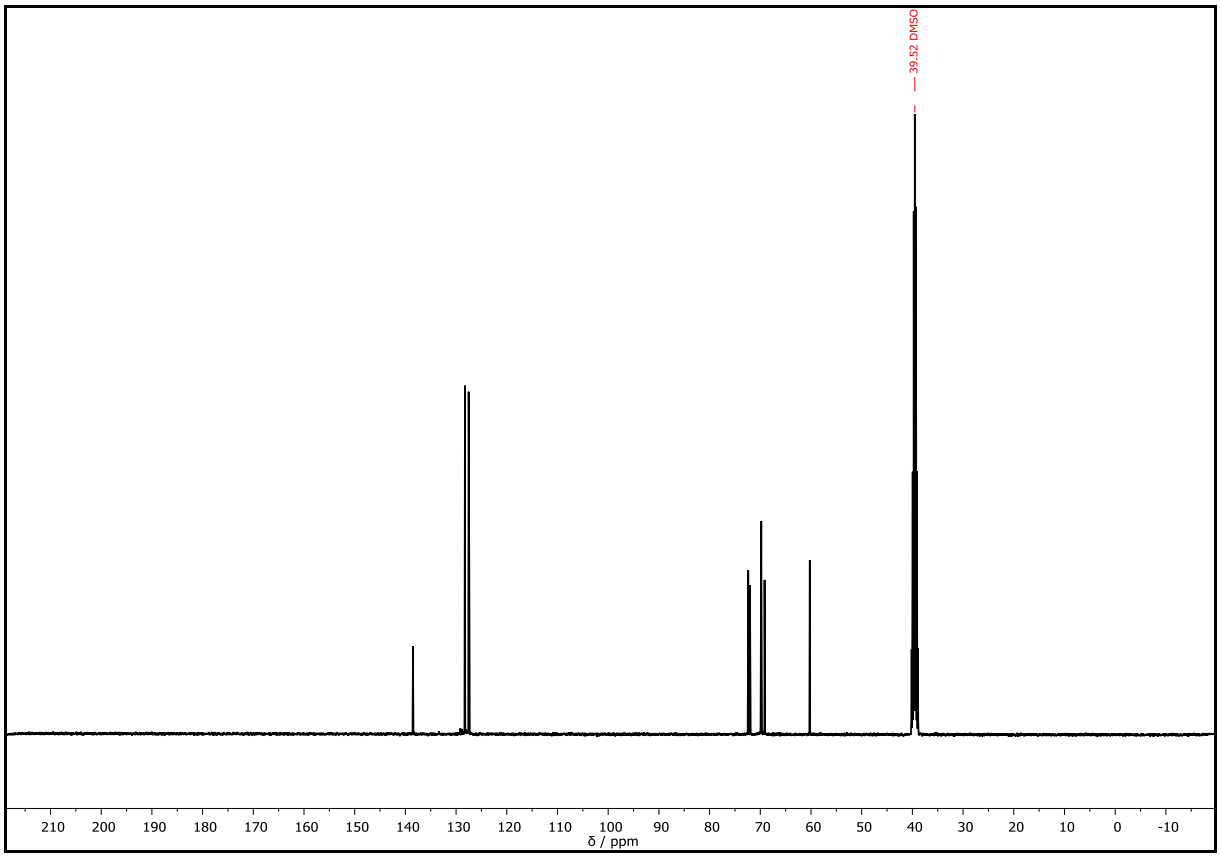

Supplementary Figure 10: ^{13}C NMR spectrum of **P5a** recorded at 101 MHz in DMSO-d_6.

Monobenzyl tri(ethylene glycol) tosylate – P6[l]

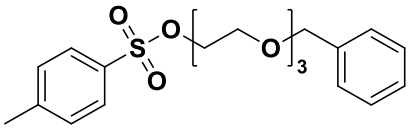

Chemical Formula: $C_{20}H_{26}O_6S$
Exact Mass: 394.1450 Da
Molecular Weight: 394.4820 Da

The synthesis was performed according to a procedure of Bruce *et al*.[273] Monobenzyl tri(ethylene glycol) **P4** (14.6 g, 60.8 mmol, 1.00 equiv.) was dissolved in THF (36.4 mL) and added dropwise to a solution of sodium hydroxide (8.47 g, 212 mmol, 3.53 equiv.) in water (42.5 mL) at 0 °C. Then, a solution of *p*-toluenesulfonyl chloride (13.8 g, 72.4 mmol, 1.19 equiv.) dissolved in THF (41.5 mL) was added dropwise, after which the reaction mixture was allowed to warm to room temperature and stirred for 15 hours. Subsequently, 1M HCl was slowly added to neutralize the excess of NaOH while cooling in an ice bath. The solvent was evaporated under reduced pressure and the product was extracted with DCM (3 × 75 mL). The combined organic layers were

[l] The synthesis was carried out by B. Sc. PETER GÖDTEL under the lab-supervision of PHILIPP BOHN.

washed with 10% aqueous Na_2CO_3 (2 × 60 mL) and water (4 × 60 mL), dried over anhydrous sodium sulfate, filtered, and concentrated *in vacuo*. Purification of the crude product *via* column chromatography (cyhex:EA = 1:1) yielded the monobenzyl tri(ethylene glycol) tosylate **P6** (13.3 g, 33.7 mmol, 55.7%) as a colorless oil. The product was dried under high vacuum, stored under argon atmosphere, and shielded from light until further use.

^{1}H NMR (500 MHz, DMSO-*d*$_6$): δ / ppm = 7.78 (d, *J* = 8.2 Hz, 2H, CH_{Ar}^1), 7.46 (d, *J* = 8.0 Hz, 2H, CH_{Ar}^2), 7.38 – 7.25 (m, 5H, H_{Ar}^3), 4.48 (s, 2H, CH_2^4), 4.13 – 4.08 (m, 2H, CH_2^5), 3.60 – 3.55 (m, 2H, CH_2^6), 3.53 (s, 4H, CH_2^7), 3.46 (s, 4H, CH_2^8), 2.40 (s, 3H, CH_3^9).

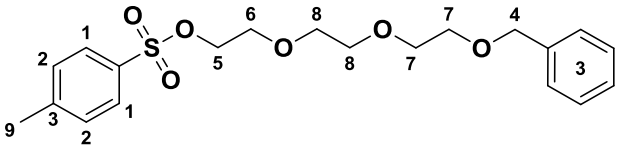

^{13}C NMR (126 MHz, DMSO-*d*$_6$): δ / ppm = 144.86 (C_q^1), 138.45 (C_q^2), 132.38 (C_q^3), 130.10 (CH_{Ar}^4), 128.19 (CH_{Ar}^5), 127.60 (CH_{Ar}^5), 127.46 (CH_{Ar}^6), 127.34 (CH_{Ar}^5), 72.00 (CH_2^7), 69.96 (CH_2^8), 69.75 (CH_2^9), 69.71 (CH_2^9), 69.70 (CH_2^9), 69.09 (CH_2^9), 67.88 (CH_2^{10}), 21.07 (CH_3^{11}).

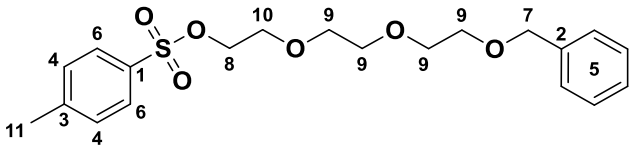

HRMS (ESI) of $C_{20}H_{26}O_6S$ $[M+H]^+$ *m/z* calc. 395.1517, found 395.1518; $[M+NH_4]^+$ *m/z* calc. 412.1782, found 412.1783; $[M+Na]^+$ *m/z* calc. 417.1336, found 417.1335.

IR (ATR platinum diamond) *v* / cm^{-1} = 3435.0, 2865.9, 1718.7, 1641.8, 1453.5, 1350.3, 1276.8, 1249.4, 1092.7, 940.4, 885.0, 846.5, 738.6, 698.4, 606.1, 526.9.

R_f = 0.57 (cyhex:EA = 1:1).

Đ (System II)= 1.00

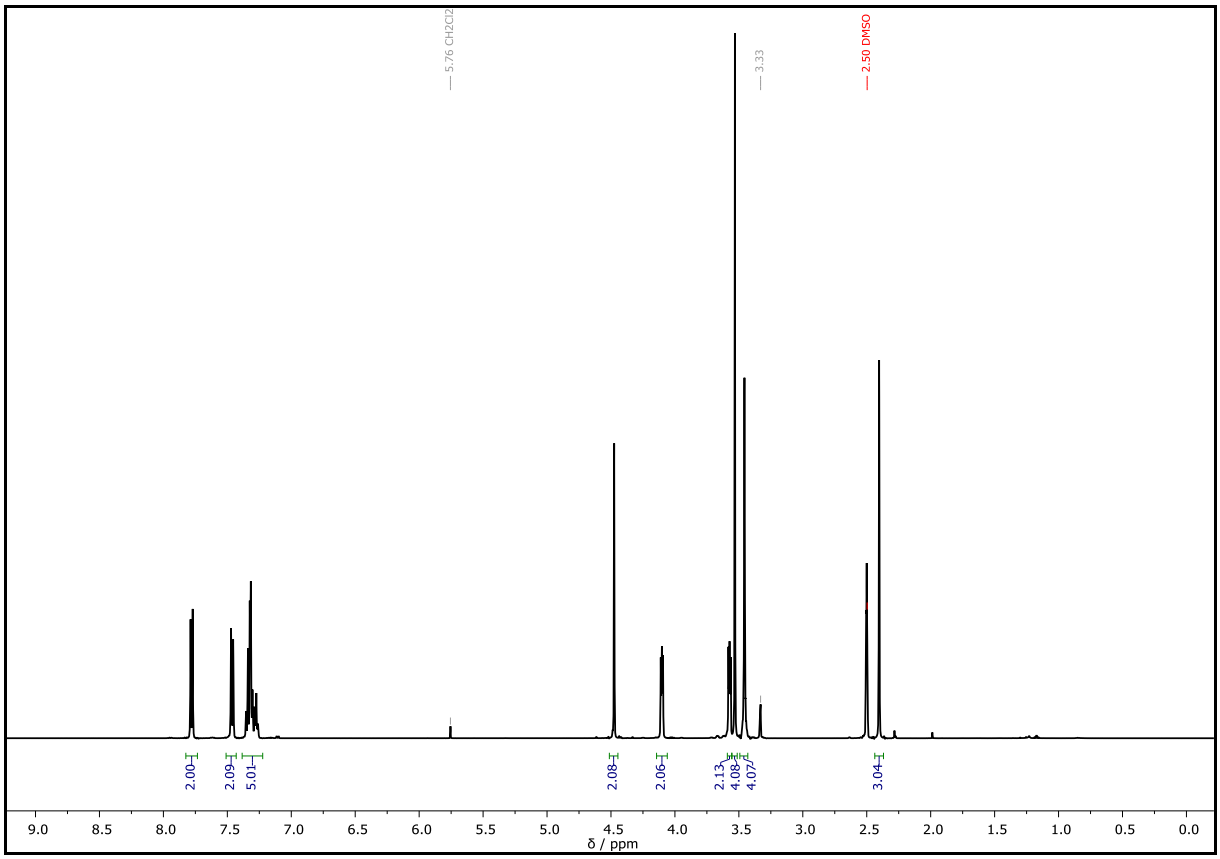

Supplementary Figure 11: ^{1}H NMR spectrum of **P6** recorded at 500 MHz in DMSO-d_6.

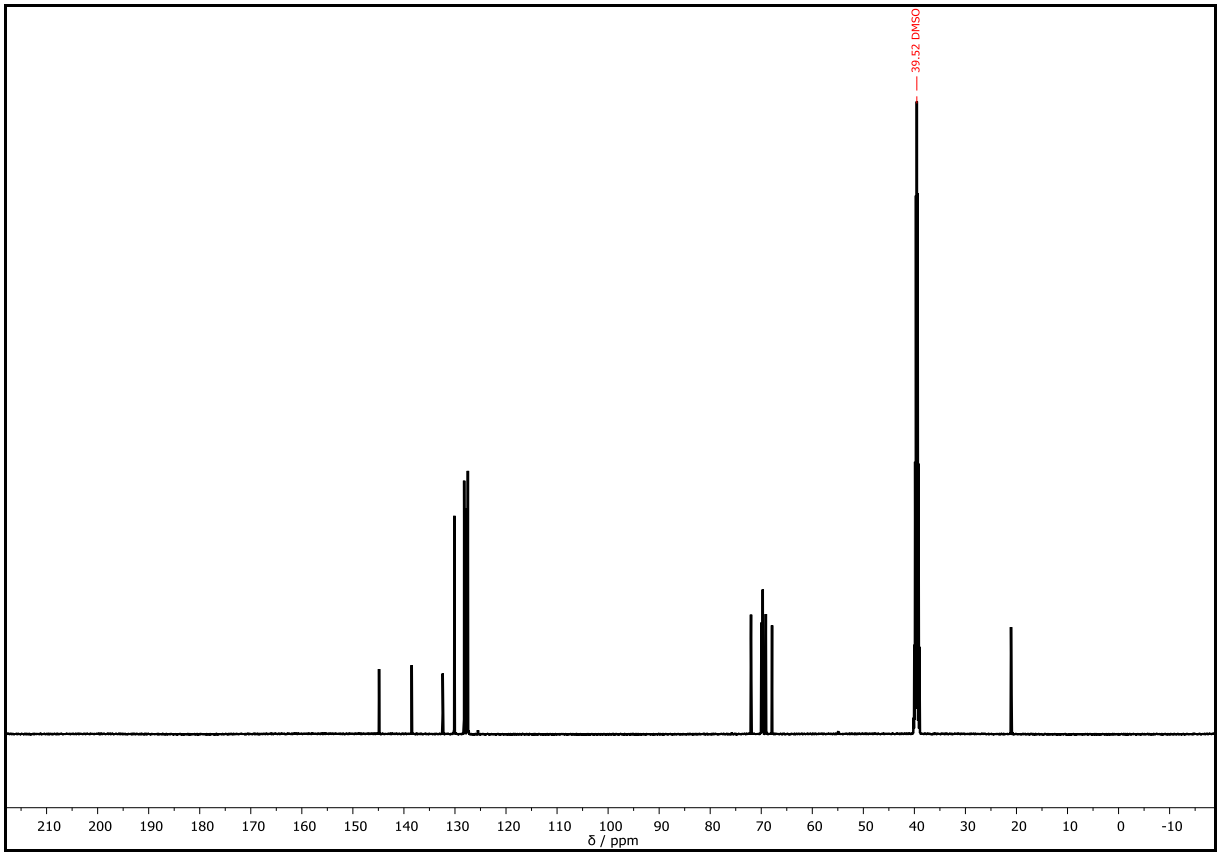

Supplementary Figure 12: ^{13}C NMR spectrum of **P6** recorded at 126 MHz in DMSO-d_6.

Monobenzyl tetra(ethylene glycol) tosylate P7

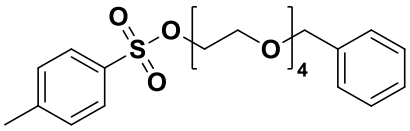

Chemical Formula: $C_{22}H_{30}O_7S$
Exact Mass: 438.1712 Da
Molecular Weight: 438.5350 Da

The monobenzyl tetra(ethylene glycol) tosylate **P7** was prepared according to the procedure of BRUCE *et al*.[273] Monobenzyl tetra(ethylene glycol) **P5** (2.00 g, 7.03 mmol, 1.00 equiv.), sodium hydroxide (984 mg, 24.6 mmol, 3.50 equiv.), *p*-toluenesulfonyl chloride (1.61 g, 8.44 mmol, 1.20 equiv.) were used. Purification of the crude product *via* column chromatography (cyhex:EA = 1:1) yielded the monobenzyl tetra(ethylene glycol) tosylate **P7** (2.96 g, 6.75 mmol, 96.2%) as a colorless oil. The product was dried under high vacuum, stored under argon atmosphere, and shielded from light until further use.

^{1}H NMR (300 MHz, DMSO-*d*$_6$): δ / ppm = 7.83 – 7.71 (m, 2H, CH_{Ar}^1), 7.53 – 7.42 (m, 2H, CH_{Ar}^2), 7.40 – 7.23 (m, 5H, H_{Ar}^3), 4.47 (s, 2H, CH_2^4), 4.16 – 4.03 (m, 2H, CH_2^5), 3.62 – 3.40 (m, 14H, CH_2O^6), 2.41 (s, 3H, CH_3^7).

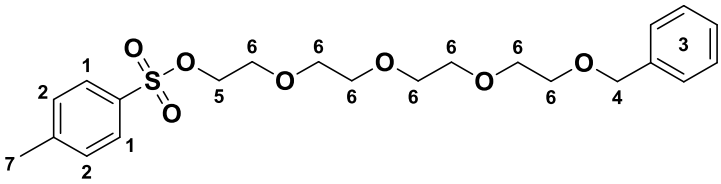

^{13}C NMR (101 MHz, DMSO-*d*$_6$): δ / ppm = 144.84 (C_q^1), 138.42 (C_q^2), 132.33 (C_q^3), 130.08 (CH_{Ar}^4), 128.21 (CH_{Ar}^5), 127.99 (CH_{Ar}^5), 127.58 (CH_{Ar}^6), 127.47 (CH_{Ar}^5), 71.97 (CH_2^7), 69.94 (CH_2^8), 69.76 (CH_2^9), 69.74 (CH_2^9), 69.71 (CH_2^9), 69.68 (CH_2^9), 69.65 (CH_2^9), 69.61 (CH_2^9), 69.08 (CH_2^{10}), 21.05 (CH_3^{10}).

Please note: the product partially degraded in the time between the ^{1}H and the ^{13}C NMR measurement. The impurities are marked in the ^{13}C NMR spectrum (Supplementary Figure 14)

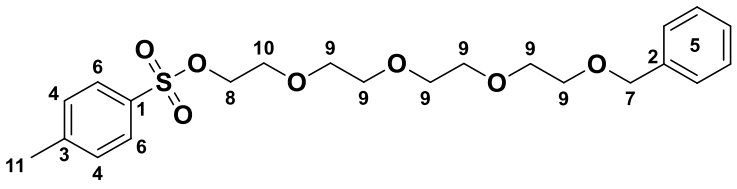

HRMS (ESI) of $C_{22}H_{30}O_7S$ $[M+H]^+$ *m/z* calc. 439.1780, found 439.1762.

IR (ATR platinum diamond) $\tilde{\nu}$ / cm^{-1} = 2865.6, 1597.8, 1495.4, 1453.2, 1353.2, 1292.0, 1248.8, 1188.7, 1175.0, 1094.6, 1016.3, 916.8, 815.3, 774.0, 740.4, 698.6, 662.0, 582.3, 552.9, 465.4.

R_f = 0.45 (cyhex:EA = 1:1).

Đ (System II) = 1.00

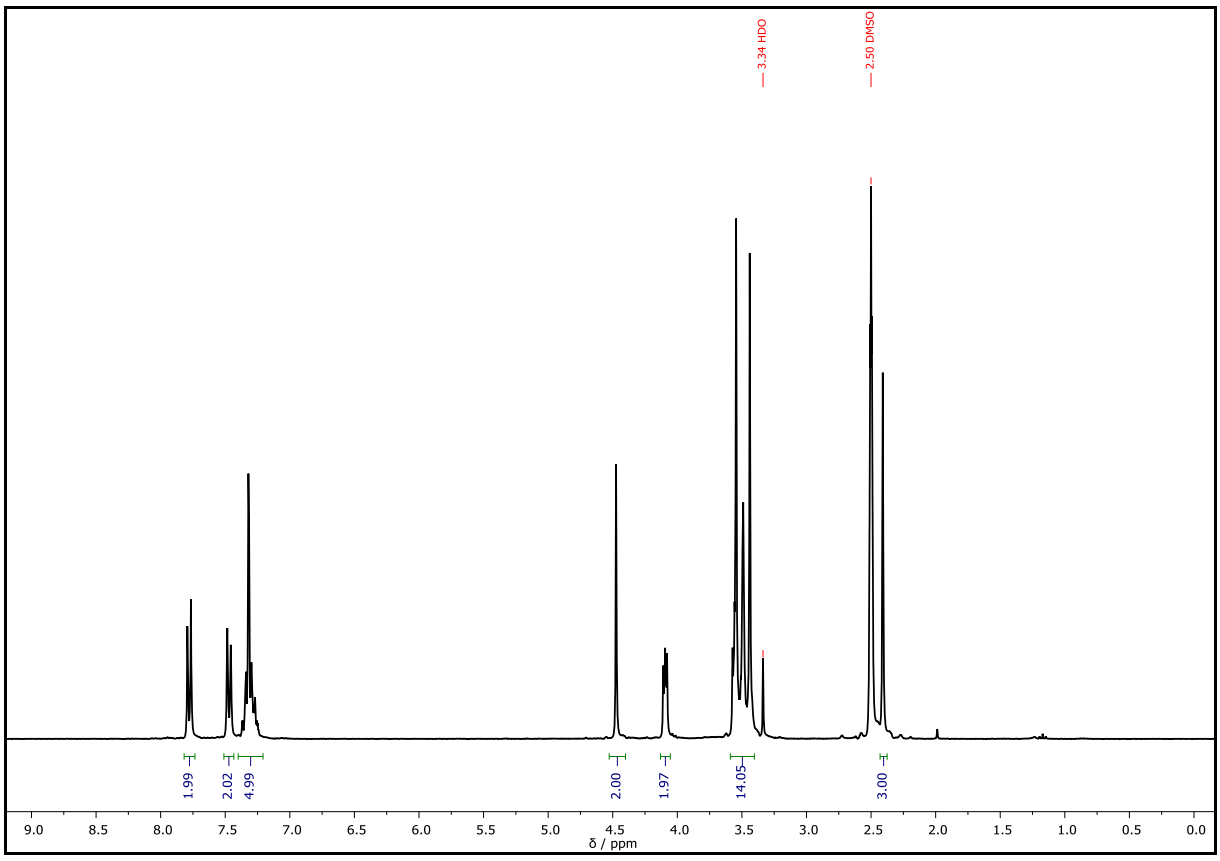

Supplementary Figure 13: ^{1}H NMR spectrum of **P7** recorded at 300 MHz in DMSO-d_6.

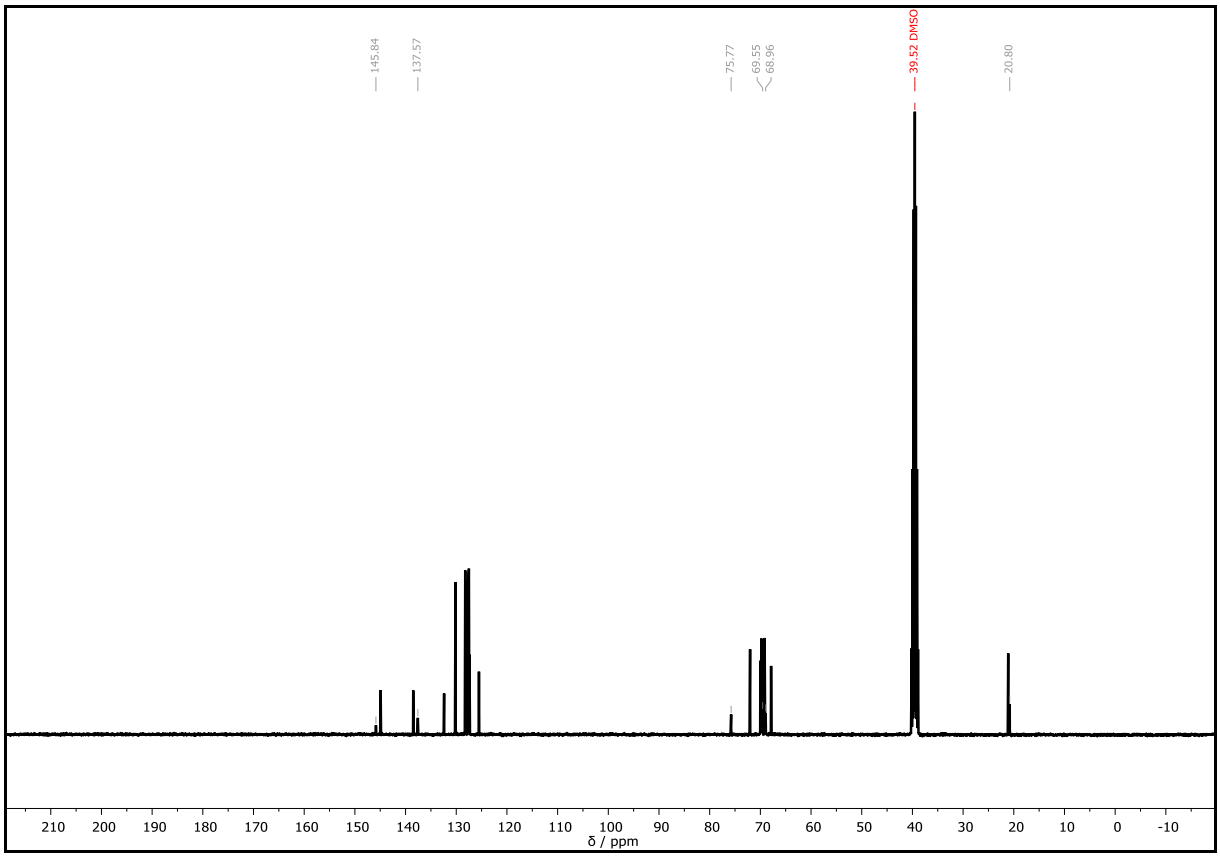

Supplementary Figure 14: ^{13}H NMR spectrum of **P7** recorded at 101 MHz in DMSO-d_6.

Bis-dibenzyl dodeca(ethylene glycol) – P8

Procedure according to BAKER *et al.*[317] – P8a[l]

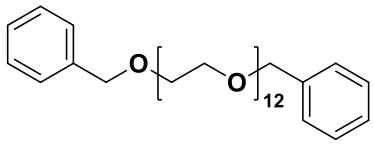

Chemical Formula: $C_{38}H_{62}O_{13}$
Exact Mass: 726.4190 Da
Molecular Weight: 726.9010 Da

Tetra(ethylene glycol) (444 µL, 500 mg, 2.57 mmol, 1.00 equiv.) dissolved in dry THF (1.4 mL) was added to sodium hydride (60% dispersion in mineral oil, 246.7 mg, 6.17 mmol, 1.20 equiv.) and sodium iodide (38.5 mg, 0.26 mmol, 0.10 equiv.) in dry THF (10.5 mL). The reaction mixture was cooled to 0°C with an ice bath and a solution of monobenzyl tetra(ethylene glycol) tosylate **P7** (1.24 g, 2.83 mmol, 1.10 equiv.) in dry THF (2.1 mL) was added dropwise over one hour. Subsequently, the reaction mixture was stirred for 12 hours under reflux. The solid was filtered off using celite and

[l] The synthesis was carried out by B. Sc. MAXIMILIAN KNAB under the lab-supervision of PHILIPP BOHN.

the filtrate was concentrated under reduced pressure. The obtained residue was redissolved in dichloromethane (30 mL) and washed with aqueous NaCl/NaOH solution (2 × 15 mL). The organic phase was dried over anhydrous sodium sulfate, filtered and the solvent was removed under reduced pressure. Purification of the crude product *via* column chromatography (cyhex:EA = 1:1 → DCM:acetone = 3:2) yielded the bis-dibenzyl dodeca(ethylene glycol) **P8a** (235 mg, 0.32 mmol, 12.6%) as a yellowish oil. SEC analysis indicated a contamination with 2% of a side product, which could not be separated *via* column chromatography.

^{1}H NMR (500 MHz, DMSO-d_6): δ / ppm = 7.45 – 7.22 (m, 10H, H_{Ar}^{1}), 4.48 (s, 4H, CH_2^{2}), 3.59 – 3.45 (m, 48H, CH_2O^{3}).

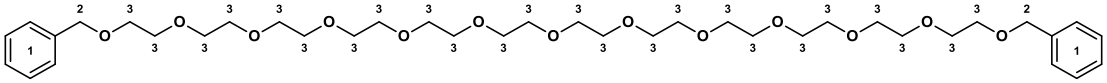

^{13}C NMR (126 MHz, DMSO-d_6): δ / ppm = 138.48 (C_q^{1}), 128.20 (CH_{Ar}^{2}), 127.47 (CH_{Ar}^{2}), 127.35 (CH_{Ar}^{2}), 72.01 (CH_2^{3}), 69.84 (CH_2^{4}), 69.79 (CH_2^{4}), 69.77 (CH_2^{4}), 69.13 (CH_2^{4}).

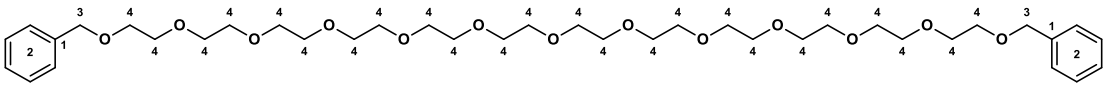

HRMS (ESI) of $C_{38}H_{62}O_{13}$ $[M+H]^+$ *m/z* calc. 727.4250, found 427.4266; $[M+NH_4]^+$ *m/z* calc. 744.4509, found 744.4531; $[M+Na]^+$ *m/z* calc. 749.4059, found 749.4086; $[M+K]^+$ *m/z* calc. 765.3788, found 765.3762.

IR (ATR platinum diamond) *v* / cm^{-1} = 3519.9, 2864.3, 1642.8, 1453.6, 1349.5, 1296.0, 1249.0, 1092.0, 946.7, 848.2, 739.0, 698.9, 524.3.

R_f = 0.06 (EA).

Đ (System II) = 1.00

Procedure according to BRUCE *et al*.[273] – P8b

Tetra(ethylene glycol) (444 µL, 500 mg, 2.57 mmol, 1.00 equiv.) dissolved in dry THF (3.00 mL) was added over 30 minutes to a solution of KO*t*Bu (808 mg, 7.20 mmol, 2.80 equiv.) in dry THF (7.20 mL) at 0 °C. Then, monobenzyl tetra(ethylene glycol) tosylate **P7** (2.93 g, 6.68 mmol, 2.60 equiv.) dissolved in THF (9.00 mL) was added over three hours at the same temperature. The reaction mixture was gradually warmed up to room temperature and left stirring for 20 hours. The mixture was cooled again to

0 °C with an ice bath and the solution was neutralized with cold 1M aqueous HCl. The solvent was evaporated, and water (50 mL) was added to the residue. The product was extracted with DCM (4 × 150 mL). The combined organic layers were washed with water (3 × 75 mL), dried over anhydrous sodium sulfate, filtered, and evaporated under reduced pressure. Purification of the crude product *via* column chromatography (cyhex:EA = 1:1 → DCM:acetone = 3:2) yielded the bis-dibenzyl dodeca(ethylene glycol) **P8b** as a colorless oil (683 mg, 0.94 mmol, 36.6%). SEC analysis indicated a contamination with 1% of a side product, which could not be separated *via* column chromatography.

The analytical data is consistent with the one of **P8b**.

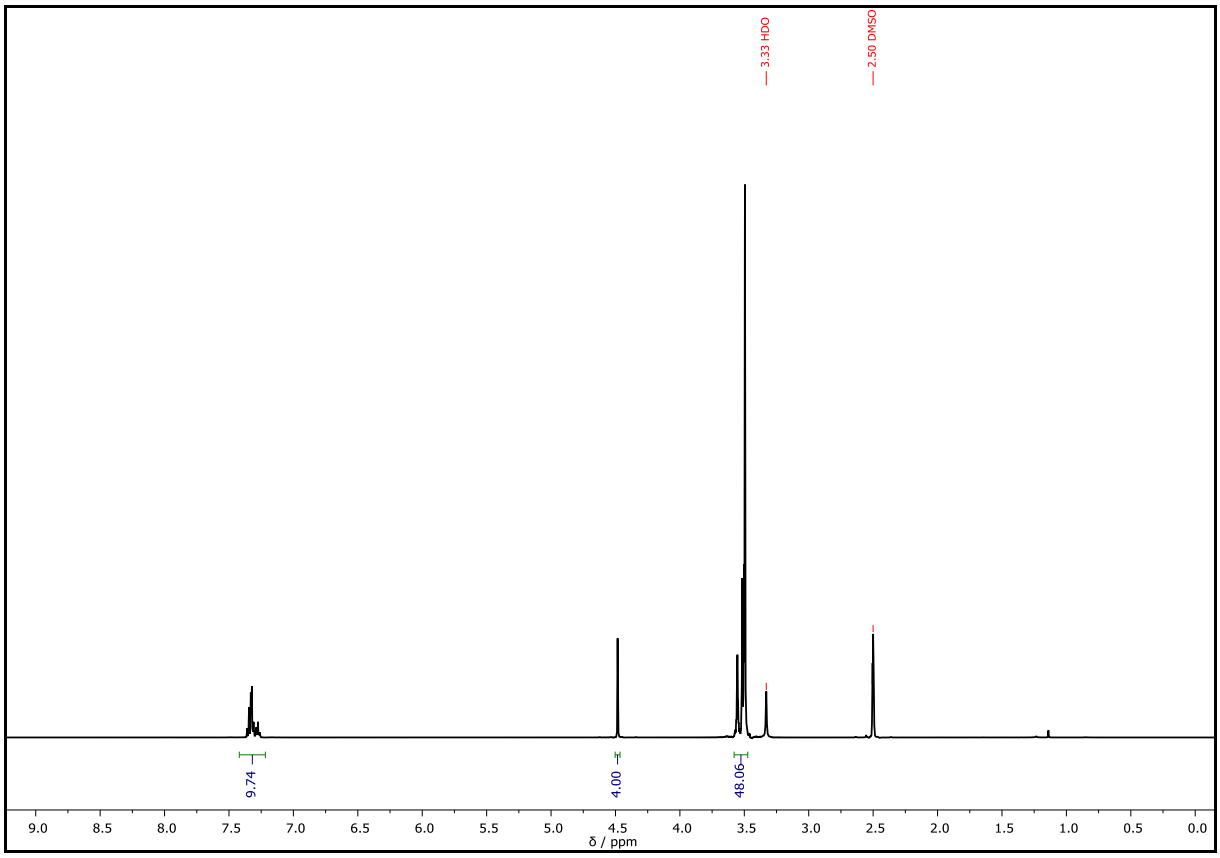

Supplementary Figure 15: ^{1}H NMR spectrum of **P8a** recorded at 500 MHz in DMSO-d_6.

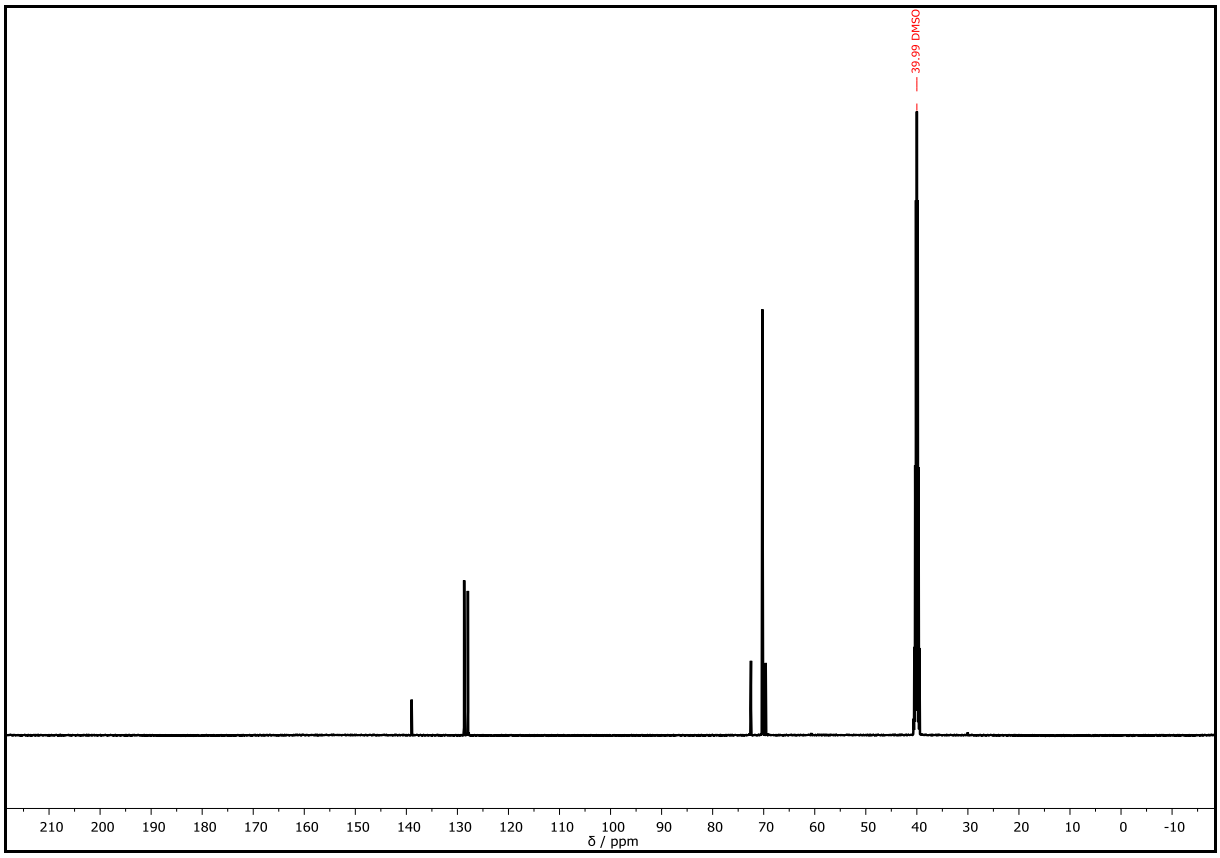

Supplementary Figure 16: ^{13}C NMR spectrum of **P8a** recorded at 126 MHz in DMSO-d_6.

Supplementary Table 1 SEC-ESI-MS results of **P8b**		
Formular	M calc. / Da[1]	M found / Da
$[Bn(EG)_{20}Bn+Na]^+$	1101.6159	1101.6155
$[Bn(EG)_{16}Bn+Na]^+$	925.5076	925.5103
$[Bn(EG)_{16}OH+Na]^+$	835.4664	835.4635
$[Bn(EG)_{16}OH+H]^+$	813.4845	813.4817
$[Bn(EG)_{12}Bn+Na]^+$	749.4086	749.4061
$[Bn(EG)_{12}Bn+H]^+$	727.4266	727.4247
$[Bn(EG)_{12}OH+Na]^+$	659.3616	659.3596
$[Bn(EG)_{12}OH+H]^+$	637.3796	637.3777
$[Bn(EG)_8Bn+Na]^+$	573.3037	573.3024
$[Bn(EG)_8Bn+H]^+$	551.3217	551.3200
$[Bn(EG)_8OH+Na]^+$	483.2566	483.2555
$[Bn(EG)_8OH+H]^+$	461.2747	461.2735
$[Bn(EG)_3CHCH2+Na]^+$	289.1412	289.1404
[1] mMass Version 5.5.0 was used for the mass calculations		

α-Benzyl-ω-tetrahydropyranyl hepta(ethylene glycol) – P9

Procedure according to BAKER *et al*.[317] – P9a[I]

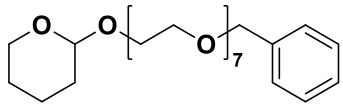

Chemical Formula: $C_{26}H_{44}O_9$
Exact Mass: 500.2985 Da
Molecular Weight: 500.6290 Da

Mono(tetrahydropyranyl) tri(ethylene glycol) **P1** (500 mg, 2.13 mmol, 1.00 equiv.) dissolved in dry THF (1.50 mL) was added dropwise over two hours to a mixture of NaH (60% dispersion in mineral oil, 170 mg, 4.26 mmol, 2.00 equiv.) and NaI (16.5 mg, 0.11 mmol, 0.05 equiv.) in 12.4 mL of dry THF at 0 °C. Subsequently, a solution of monobenzyl tetra(ethylene glycol) tosylate **P7** (1.13 g, 2.34 mmol, 1.10 equiv.) in 2.78 mL of dry THF was added dropwise over one hour at the same temperature. After stirring under reflux for 12 hours, the reaction mixture was filtered through a pad of celite to remove the solids. The filtrate was concentrated under reduced pressure and the residue was redissolved in DCM (30 mL). The organic phase was washed with aqueous NaCl/NaOH solution (2 × 30 mL), dried over anhydrous sodium sulfate, filtered and the solvent was evaporated *in vacuo*. Purification of the crude product *via* column chromatography (EA) yielded the α-benzyl-ω-tetrahydropyranyl hepta(ethylene glycol) **P9a** (368 mg, 0.74 mmol, 34.5%) as a colorless oil.

^{1}H NMR (400 MHz, DMSO-d_6): δ / ppm = 7.46 – 7.18 (m, 5H, H_{Ar}^{1}), 4.57 (t, J = 3.6 Hz, 1H, CH^{2}), 4.48 (s, 2H, CH_2^{3}), 3.84 – 3.61 (m, 2H, CH_2^{4}), 3.61 – 3.37 (m, 28H, CH_2^{5}), 1.79 – 1.35 (m, 6H, CH_2^{6}).

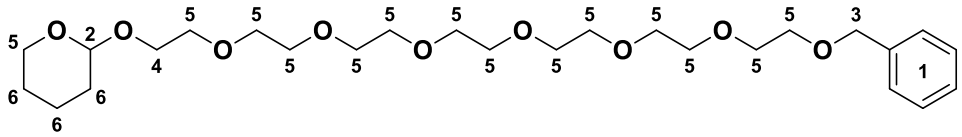

^{13}C NMR (101 MHz, DMSO-d_6): δ / ppm = 138.49 (C_q^{1}), 128.22 (CH_{Ar}^{2}), 127.49 (CH_{Ar}^{2}), 127.38 (CH_{Ar}^{2}), 99.55 (CH^{3}), 98.05 (CH^{3}), 72.02 (CH_2^{4}), 69.85 (CH_2^{5}), 69.80 (CH_2^{5}), 69.73 (CH_2^{5}), 69.14 (CH_2^{5}), 66.07 ($CH_2^{5,6}$), 61.23 ($CH_2^{5,6}$), 30.23 (CH_2^{7}), 25.03 (CH_2^{7}), 19.13 (CH_2^{7}).

[I] The synthesis was carried out by REBECCA SEIM under the lab-supervision of PHILIPP BOHN.

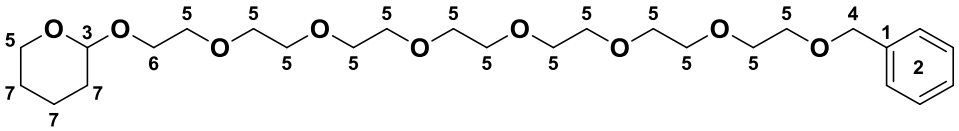

HRMS (ESI) of $C_{26}H_{44}O_9$ $[M+NH_4]^+$ *m/z* calc. 518.3326, found 518.3327; $[M+Na]^+$ *m/z* calc. 523.2880, found 523.2882; $[M+K]^+$ *m/z* calc. 539.2614, found 539.2615.

The mass of the α-benzyl-ω-tetrahydropyranyl octa(ethylene glycol) was also found. $C_{28}H_{48}O_{10}$ $[M+NH_4]^+$ *m/z* calc. 562.3588, found 562.3583.

The mass of the bis-benzyl octa(ethylene glycol) was also found. $C_{30}H_{46}O_9$ $[M+H]^+$ *m/z* calc. 573.3037, found 573.3032.

IR (ATR platinum diamond) ν / cm^{-1} = 2865.5, 1453.8, 1349.6, 1285.1, 1251.0, 1201.4, 1098.8, 1075.4, 1032.7, 986.9, 871.5, 813.6, 738.7, 698.7, 537.7, 428.5.

R_f = 0.21 (EA)

Đ (System II) = 1.00

Procedure according to Bruce *et al*.[273] – P9b

Mono(tetrahydropyranyl) tri(ethylene glycol) **P1** (206 mg, 0.88 mmol, 1.00 eq) dissolved in dry THF (1.50 mL) was added over 30 minutes to a solution of KO*t*Bu (138 mg, 1.23 mmol, 1.40 equiv.) in dry THF (1.24 mL) at 0 °C. Then, monobenzyl tetra(ethylene glycol) tosylate **P7** (500 mg, 1.14 mmol, 1.30 equiv.) dissolved in THF (1.24 mL) was added over three hours at the same temperature. The reaction mixture was gradually warmed up to room temperature and left stirring for 20 hours. The mixture was cooled again to 0 °C with an ice bath and the solution was neutralized with cold 1M aqueous HCl. The solvent was evaporated, and water (50 mL) was added to the residue. The product was extracted with DCM (4 × 150 mL). The combined organic layers were washed with water (3 × 75 mL), dried over anhydrous sodium sulfate, filtered, and evaporated under reduced pressure. Purification of the crude product *via* column chromatography (EA) yielded the the α-benzyl-ω-tetrahydropyranyl hepta(ethylene glycol) **P9b** (314 mg, 0.63 mmol, 71.3%) as a yellowish oil.

The analytical data is consistent with the one of **P9a**.

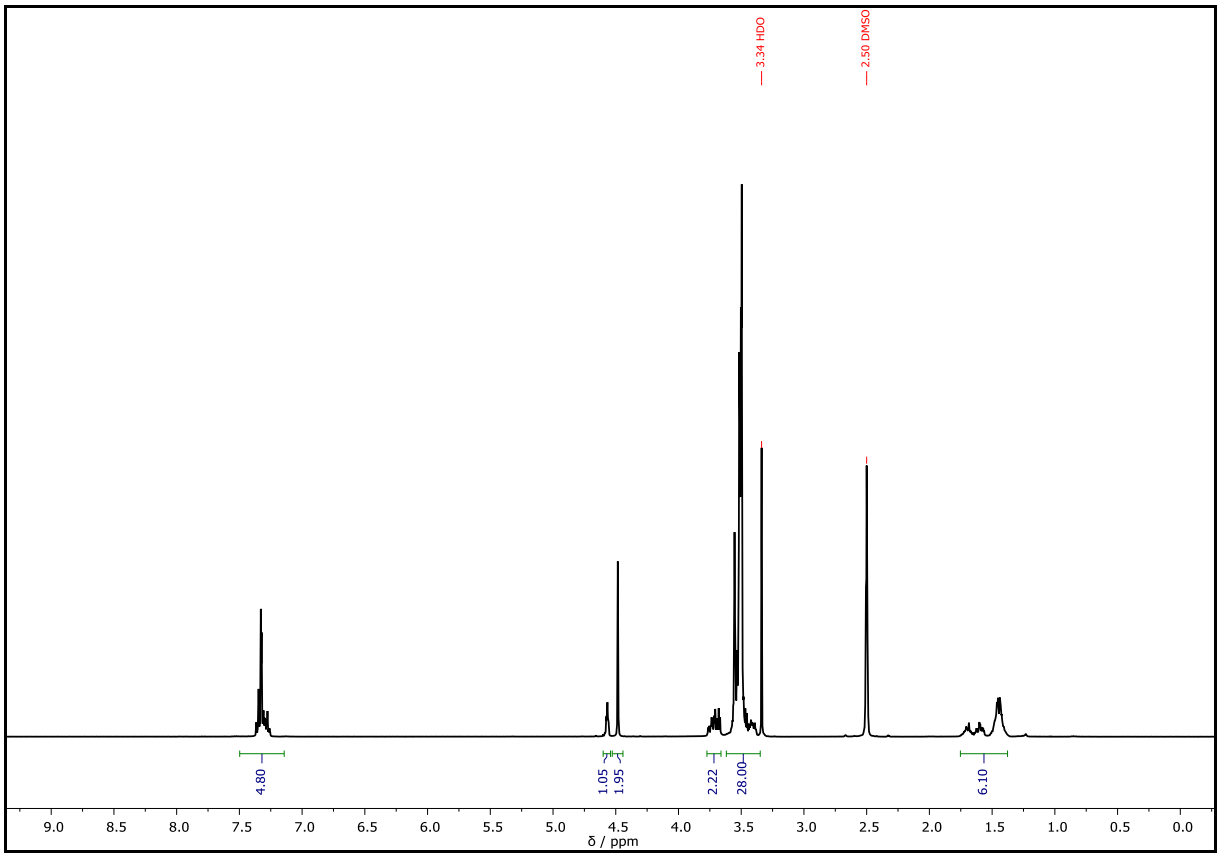

Supplementary Figure 17: ^{1}H NMR spectrum of **P9a** recorded at 400 MHz in DMSO-d_6.

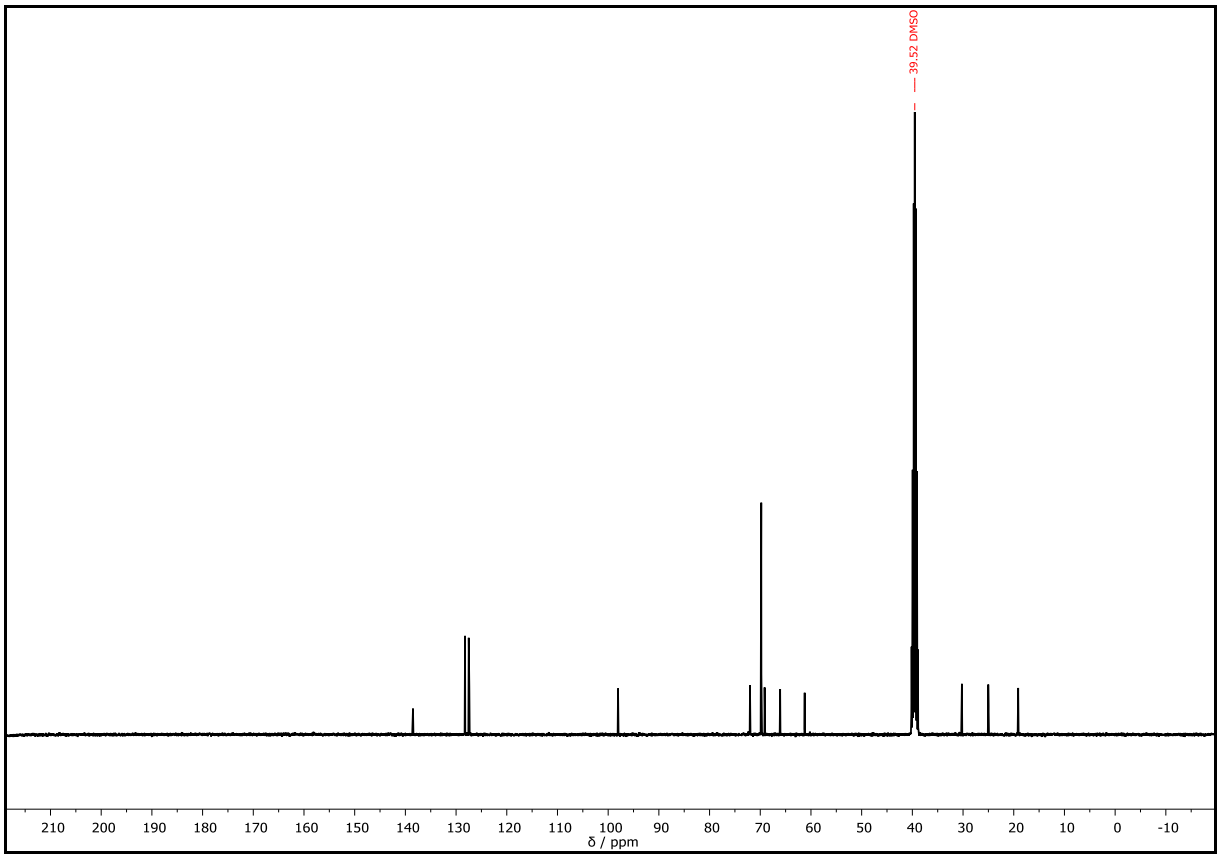

Supplementary Figure 18: ^{13}C NMR spectrum of **P9a** recorded at 101 MHz in DMSO-d_6.

The synthesis of **P9b** was repeated on a 20.1 g scale and the purification *via* column chromatography is reported in the following.

Supplementary Table 2: SEC results of the first purification of P9b.

cc 1	*m* / g	M_n / Da	M_w / Da	M_z / Da	*Đ*	purity / %
F1	10.1	*n.a.*	*n.a.*	*n.a.*	*n.a.*	*n.a.*
F2	1.96	650	650	650	1.00	>99
F3	4.00	650	650	650	1.00	>99
F4	1.56	650	650	650	1.00	>99
F5	549×10^{-3}	650	650	650	1.00	>99
F6	196×10^{-3}	650	650	650	1.00	>99

eluent: DCM:Acetone = 5:1 → 4:1; yellow: product containing fractions with insufficient purity.

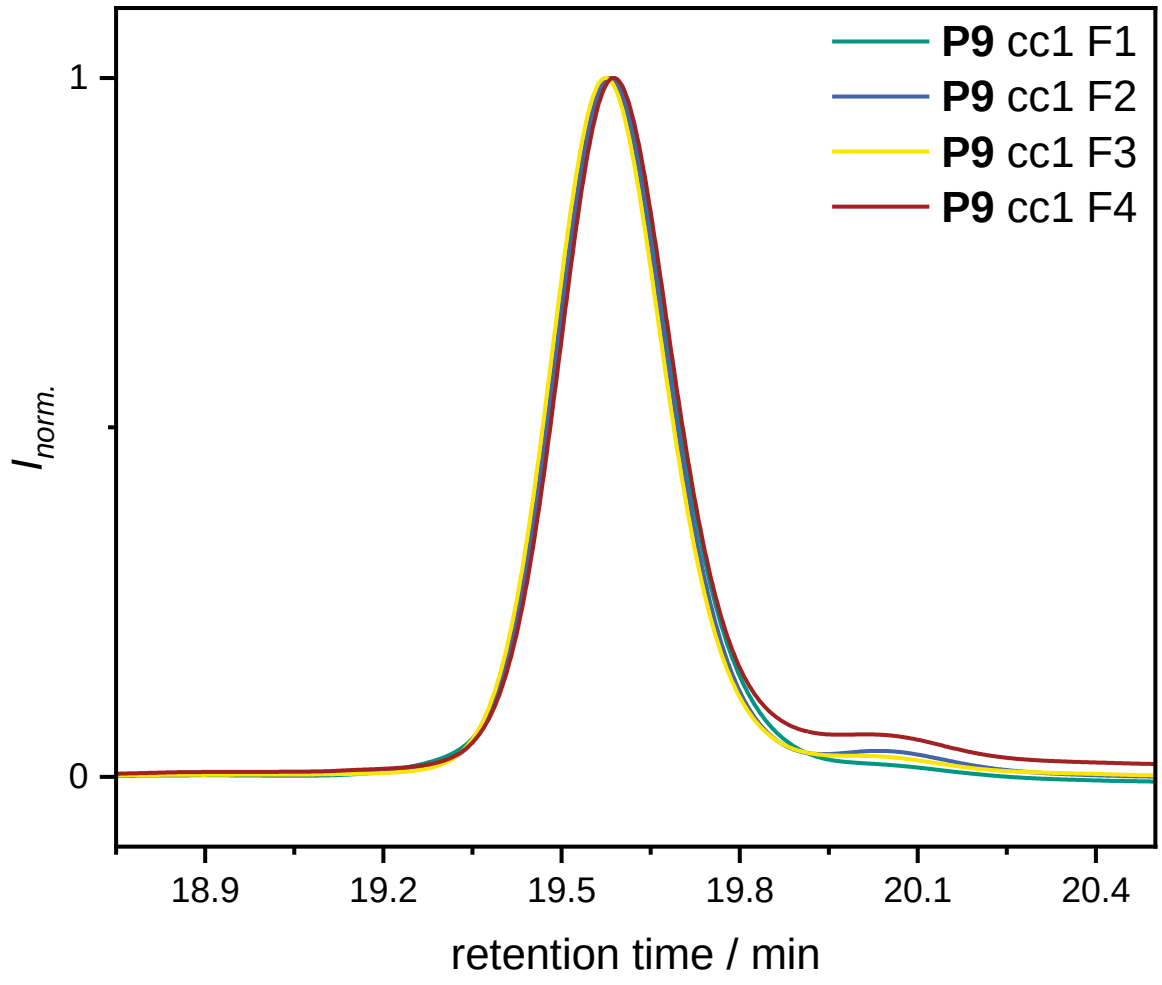

Supplementary Figure 19: SEC traces of the individual fractions obtained from the purification *via* column chromatography (cc1) of **P9b**.

Supplementary Table 3: SEC results of the second purification of P9b.						
cc 2	*m* / mg	M_n / Da	M_w / Da	M_z / Da	*Đ*	purity / %
F1	768	*n.a.*	*n.a.*	*n.a.*	*n.a.*	*n.a.*
F2	1160	*n.a.*	*n.a.*	*n.a.*	*n.a.*	*n.a.*
F3	956	600	650	650	1.00	5
F4	896	650	650	650	1.00	93
F5	981	650	650	650	1.00	>99
F6	782	650	650	650	1.00	>99
F7	707	650	650	650	1.00	>99
F8	719	650	650	650	1.00	>99
F9	558	650	650	650	1.00	>99
F10	590	650	650	650	1.00	>99
F11	570	650	650	650	1.00	>99
F12	485	650	650	650	1.00	>99
F13	366	650	650	650	1.00	>99
F14	342	650	650	650	1.00	>99
F15	336	650	650	650	1.00	>99
F16	326	650	650	650	1.00	>99
F17	291	650	650	650	1.00	>99
F18	289	650	650	650	1.00	>99
F19	376	650	650	650	1.00	>99
F20	308	650	650	650	1.00	>99
F21	312	650	650	650	1.00	>99
F22	337	650	650	650	1.00	>99
F23	476	650	650	650	1.00	>99
F24	334	650	650	650	1.00	>99
F25	348	650	650	650	1.00	>99
F26	299	650	650	650	1.00	>99

eluent: DCM:Acetone = 8:1 → 7:1; Red: fractions containing only impurities; yellow: product containing fractions with insufficient purity; green: fractions containing only product P9.

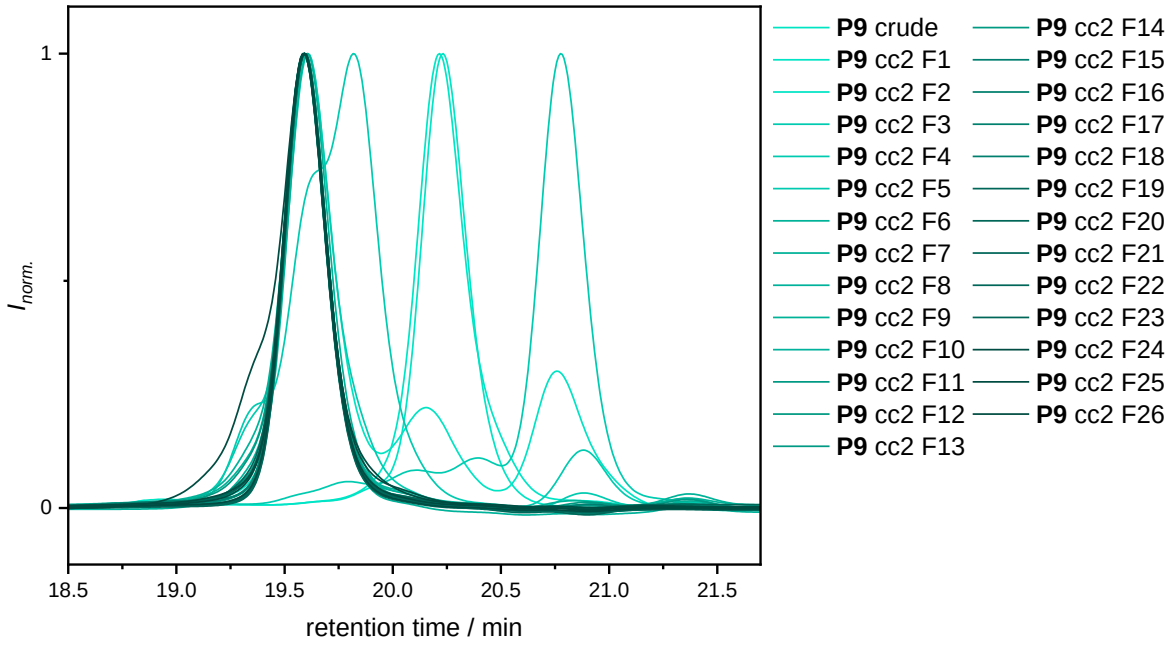

Supplementary Figure 20: SEC traces of the individual fractions obtained from the purification *via* column chromatography (cc2) of **P9b**.

α-Benzyl-ω-tetrahydropyranyl octa(ethylene glycol) – P10

Procedure according to BAKER *et al.*[317] – P10a

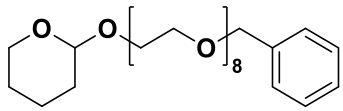

Chemical Formula: $C_{28}H_{48}O_{10}$
Exact Mass: 544.3247 Da
Molecular Weight: 544.6820 Da

Mono(tetrahydropyranyl) tetra(ethylene glycol) **P2** (500 mg, 1.80 mmol, 1.00 equiv.), sodium hydride (60% dispersion in mineral oil, 144 mg, 3.60 mmol, 2.00 equiv.), sodium iodide (14.0 mg, 94.4 µmol, 0.05 equiv.), monobenzyl tetra(ethylene glycol) monotosylate **P7** (868 mg, 1.98 mmol, 1.10 equiv.) were used. Purification of the crude product *via* column chromatography (DCM:MeOH = 40:1) afforded the α-benzyl-ω-tetrahydropyranyl octa(ethylene glycol) **P10a** as a colorless oil (671 mg, 1.23 mmol, 68.4%). The product was dried under high vacuum until further use.

^{1}H NMR (400 MHz, DMSO-d_6): δ / ppm = 7.43 – 7.21 (m, 5H, H_{Ar}^1), 4.57 (d, J = 3.7 Hz, 1H, CH^2), 4.49 (d, J = 2.3 Hz, 2H, CH_2^3), 3.79 – 3.64 (m, 2H, CH_2^4), 3.63 – 3.35 (m, 32H, CH_2O^5), 1.78 – 1.35 (m, 6H, CH_2^6).

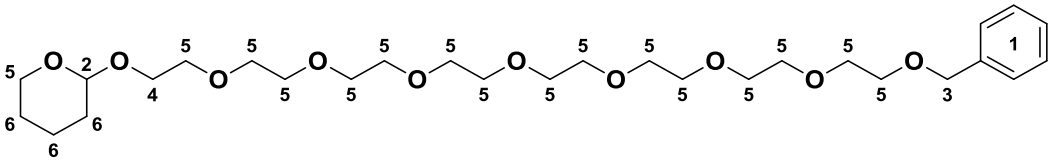

^{13}C NMR (101 MHz, DMSO-d_6): δ / ppm = 138.49 (C_q^1), 128.21 (CH_{Ar}^2), 127.48 (CH_{Ar}^2), 127.36 (CH_{Ar}^2), 98.04 (CH^3), 72.02 (CH_2^4), 69.85 (CH_2^5), 69.81 (CH_2^5), 69.79 (CH_2^5), 69.73 (CH_2^5), 69.14 (CH_2^5), 66.07 ($CH_2^{5,6}$), 61.23 ($CH_2^{5,6}$), 30.22 (CH_2^7), 25.03 (CH_2^7), 19.12 (CH_2^7).

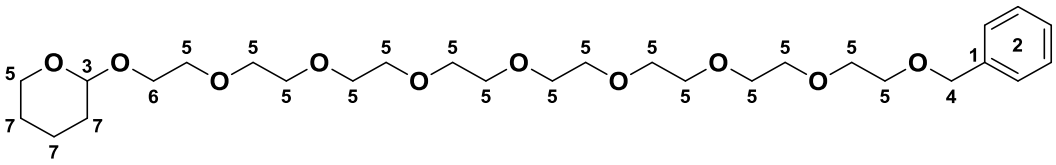

HRMS (ESI) of $C_{28}H_{48}O_{10}$ $[M+Na]^+$ *m/z* calc. 567.3142, found 567.3126; $[M+K]^+$ *m/z* calc. 583.2876, found 583.2864.

The mass of the α-benzyl-ω-tetrahydropyranyl hepta(ethylene glycol) **P9** was also found. $[M+Na]^+$ *m/z* calc. 523.2880, found 523.2866; $[M+K]^+$ *m/z* calc. 539.2614, found 539.2606.

IR (ATR platinum diamond) $\tilde{\nu}$ / cm^{-1} = 2865.7, 1453.9, 1349.5, 1287.0, 1250.0, 1201.5, 1098.1, 1032.7, 987.0, 871.5, 813.8, 739.0, 698.9, 536.8, 428.9.

R_f = 0.18 (EA)

Đ (System II) = 1.00

Procedure according to Bruce *et al*.[273] – P10b

Mono(tetrahydropyranyl) tetra(ethylene glycol) **P2** (261 mg, 0.94 mmol, 1.00 equiv.), KO*t*Bu (145 mg, 1.29 mmol, 1.37 equiv.), monobenzyl tetra(ethylene glycol) monotosylate **P7** (530 mg, 1.21 mmol, 1.29 equiv.) were used. Here, water instead of 1M aqueous HCl was added to quench the reaction. Purification of the crude product *via* column chromatography (EA:methanol = 1:0 → 9:1) yielded the α-benzyl-ω-tetrahydropyranyl octa(ethylene glycol) **P10b** (243 mg, 0.45 mmol, 47.6%) as a yellowish oil. The product was dried under high vacuum before further use.

The analytical data is consistent with the one of **P10a**.

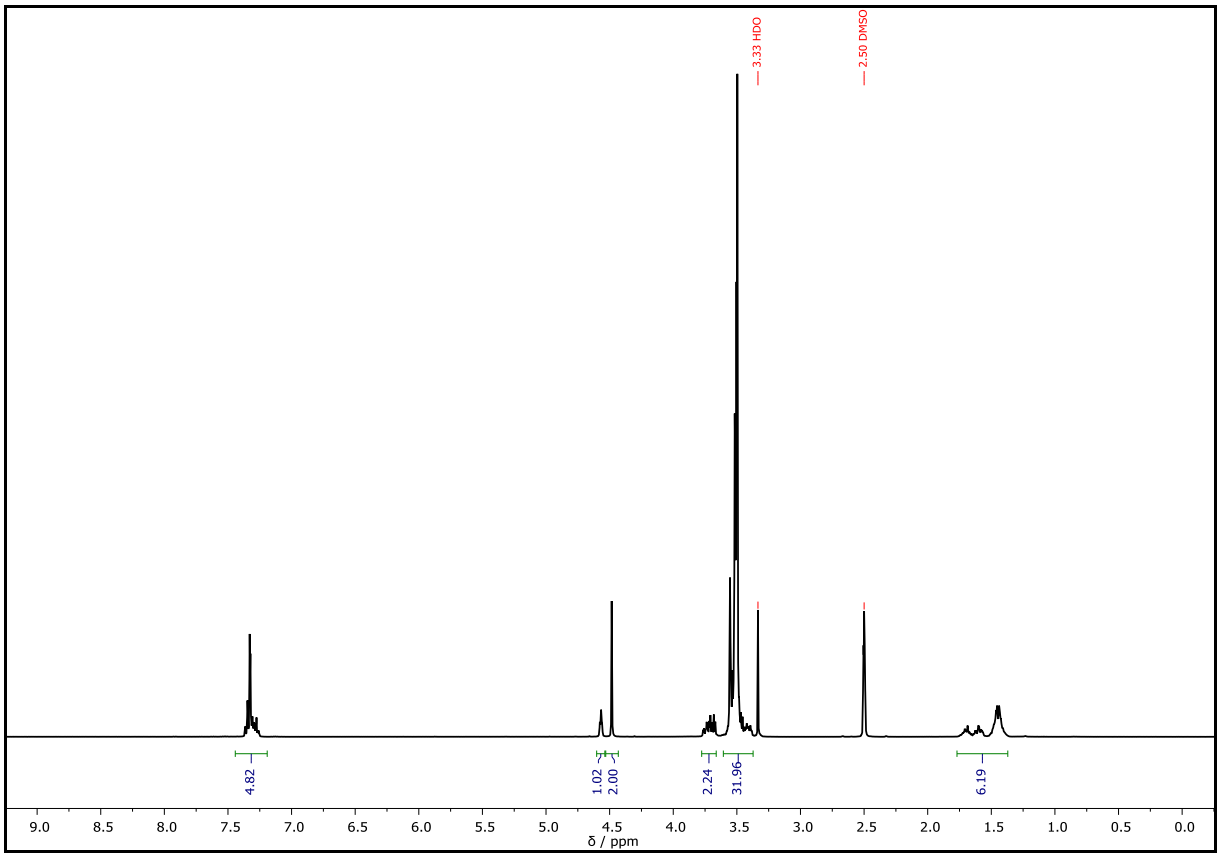

Supplementary Figure 21: ^{1}H NMR spectrum of **P10a** recorded at 400 MHz in DMSO-d_6.

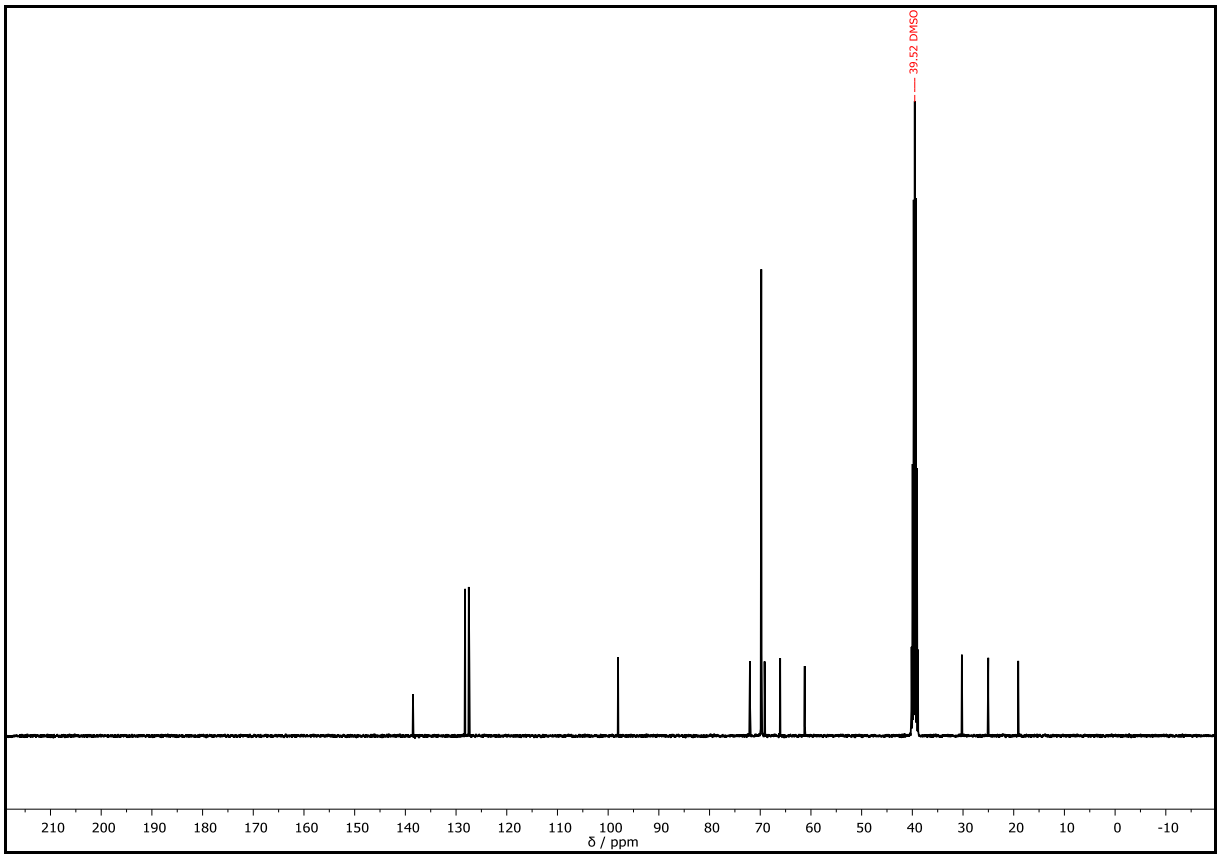

Supplementary Figure 22: ^{13}C NMR spectrum of **P10a** recorded at 101 MHz in DMSO-d_6.

Supplementary Table 4: SEC-ESI-MS results of **P10b**		
Formular	M calc. / Da[1]	M found / Da
$[Bn(EG)_{16}OH+H]^+$	813.4845	813.4807
$[THP(EG)_{16}OH+H]^+$	807.4951	807.4912
$[Bn(EG)_{12}Bn+Na]^+$	749.4086	749.4064
$[THP(EG)_{12}Bn+Na]^+$	743.4191	743.4171
$[THP(EG)_{12}THP+Na]^+$	737.4297	737.4277
$[Bn(EG)_{12}OH+H]^+$	637.3796	637.3781
$[THP(EG)_{12}OH+H]^+$	631.3902	631.3831
$[THP(EG)_8Bn+Na]^+$	567.3142	567.3127
$[Bn(EG)_8OH+H]^+$	461.2747	461.2737
$[Bn(EG)_4Ts+Na]^+$	461.1599	461.1594
$[Bn(EG)_4Ts+H]^+$	439.1780	439.1775
[1] mMass Version 5.5.0 was used for the mass calculations		

The synthesis of **P10b** was repeated on a 58.7 g scale and the purification *via* column chromatography is reported in the following.

Supplementary Table 5: SEC results of the first purification of P10b.

cc	*m* / g	M_n / Da	M_w / Da	M_z / Da	*Đ*	purity / %
F1	14.6	650	650	650	1.00	98
F2	6.67	700	700	700	1.00	97
F3	5.11	700	700	700	1.00	97
F4	4.36	700	700	700	1.00	98
F5	3.63	700	700	700	1.00	98
F6	2.84	700	700	700	1.00	98
F7	2.10	700	700	700	1.00	>99
F8	1.68	700	700	700	1.00	>99
F9	1.05	700	700	700	1.00	>99
F10	0.89	700	700	700	1.00	>99
F11	0.57	700	700	700	1.00	>99
F12	0.85	700	700	700	1.00	>99
F13	0.55	700	700	700	1.00	>99
F14	0.58	700	700	700	1.00	>99
F15	0.49	700	700	700	1.00	>99

eluent: DCM:Acetone = 4:1 → EA:MeOH = 9:1; Yellow: product containing fractions with insufficient purity; green: fractions containing only product P10.

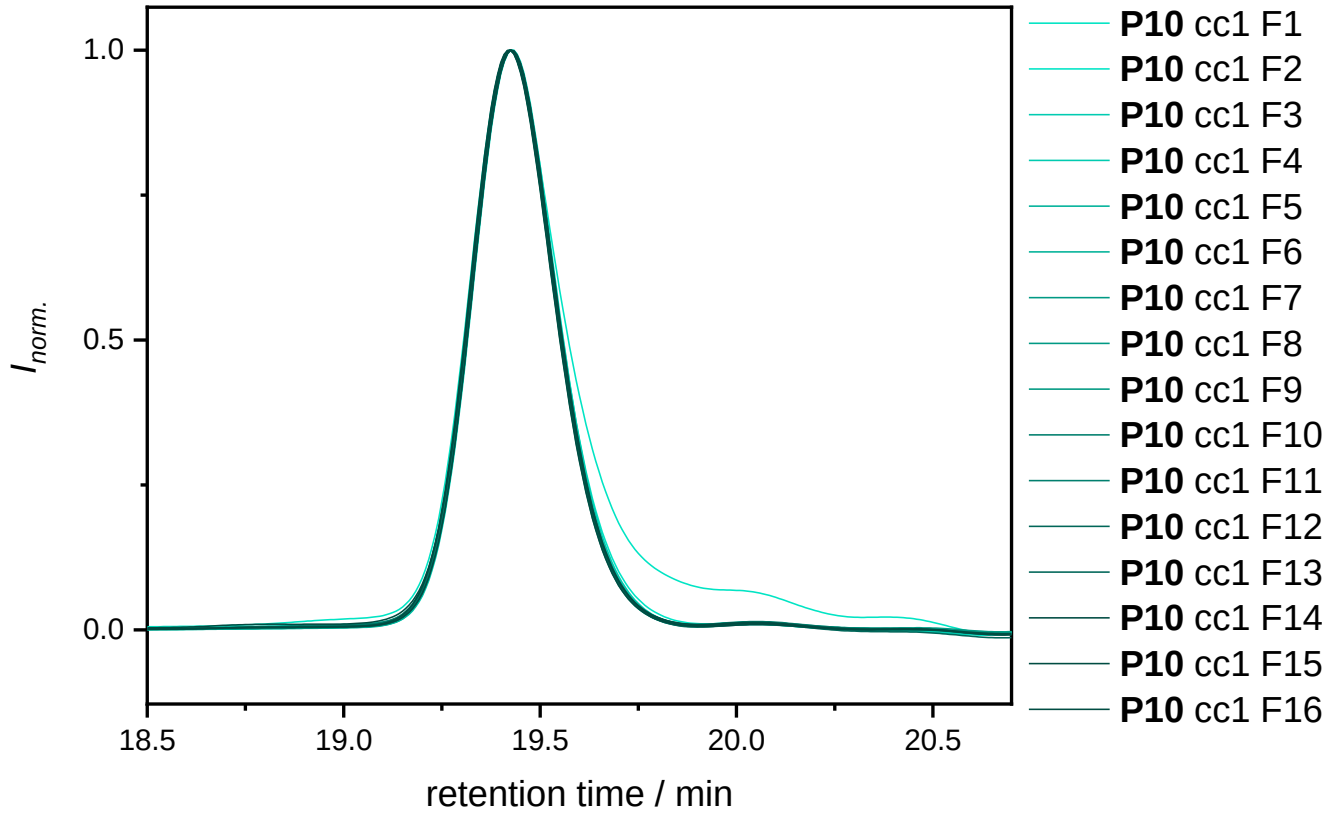

Supplementary Figure 23: SEC traces of the individual fractions obtained from the purification *via* column chromatography (cc1) of **P10b**.

The fractions **P10** cc1 F1-F6 were purified further *via* column chromatography.

Supplementary Table 6: SEC results of the second purification of P10b						
cc 2	*m* / g	M_n / Da	M_w / Da	M_z / Da	*Đ*	purity / %
F1	5.62	650	650	672	1.00	>99[a]
F2	5.43	650	650	671	1.00	>99[a]
F3	1.23	700	700	679	1.00	95
F4	1.40	700	700	679	1.00	99
F5	0.95	700	700	679	1.00	98
F6	0.68	700	700	678	1.00	98
F7	0.73	700	700	678	1.00	98
F8	0.69	700	700	678	1.00	98
F9	0.77	700	700	677	1.00	96
F10	0.69	700	700	678	1.00	96
F11	0.56	700	700	678	1.00	95
F12	0.51	700	700	678	1.00	97
F13	0.49	650	700	676	1.00	97
F14	0.40	700	700	677	1.00	94
F15	0.51	700	700	677	1.00	96
F16	0.49	700	700	678	1.00	96
F17	0.31	700	700	676	1.00	94
F18	0.27	650	700	676	1.00	95
F19	0.27	650	650	675	1.00	94
F20	0.47	650	650	675	1.00	93
F21	0.48	650	650	675	1.00	94

eluent: DCM:Acetone = 4:1 → EA:MeOH = 9:1; Red: fractions containing only impurities; yellow: product containing fractions with insufficient purity; green: fractions containing only product P10.

[a]The purity is erroneously >99% because only the broad peak was considered for the evaluation.

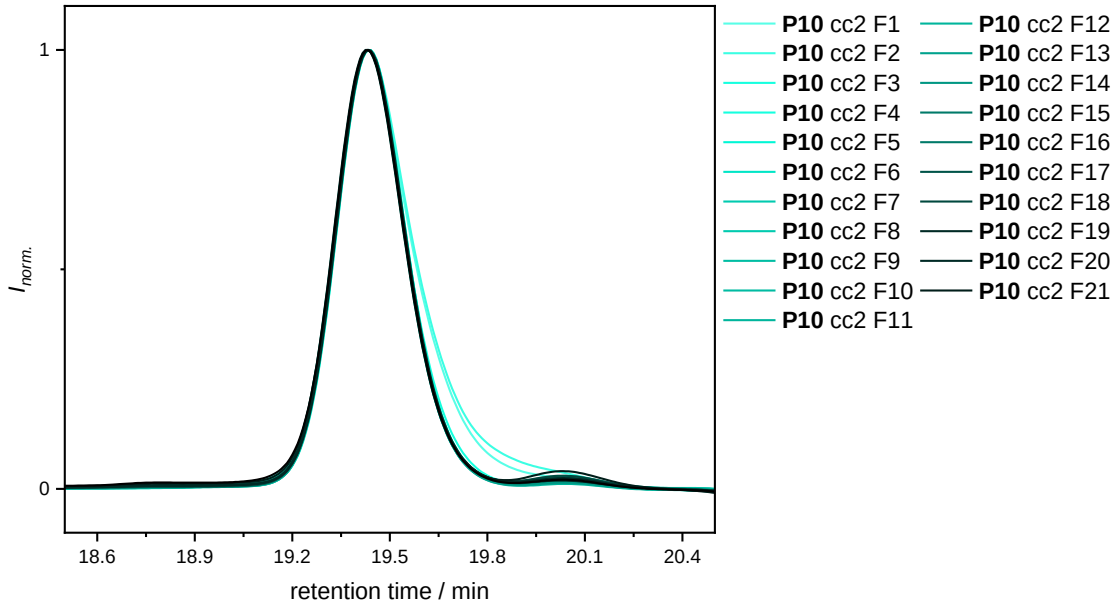

Supplementary Figure 24: SEC traces of the individual fractions obtained from the purification *via* column chromatography (cc2) of **P10b**.

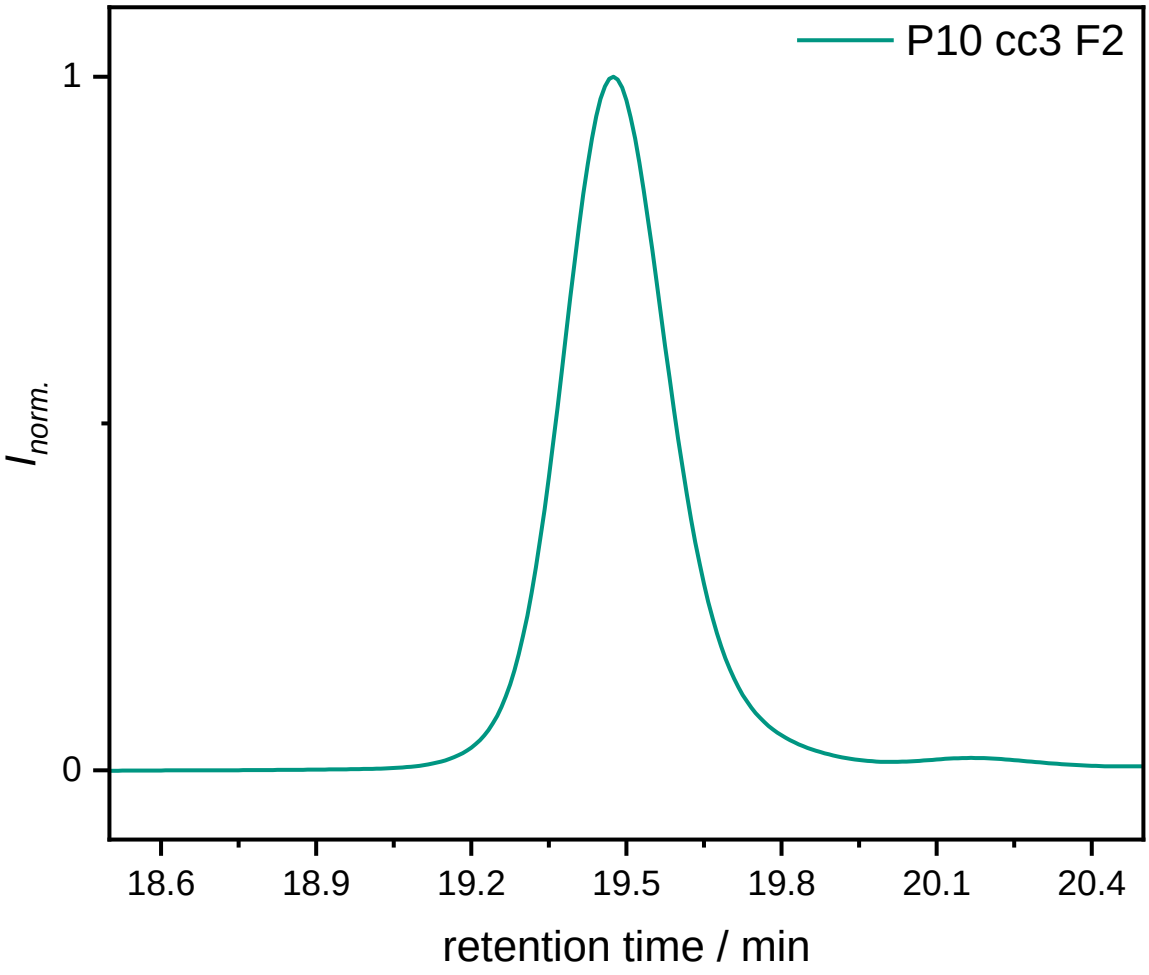

Supplementary Figure 25: SEC traces of the individual fractions obtained from the purification of **P10 cc2 F4** *via* column chromatography (cc3) of **P10b**.

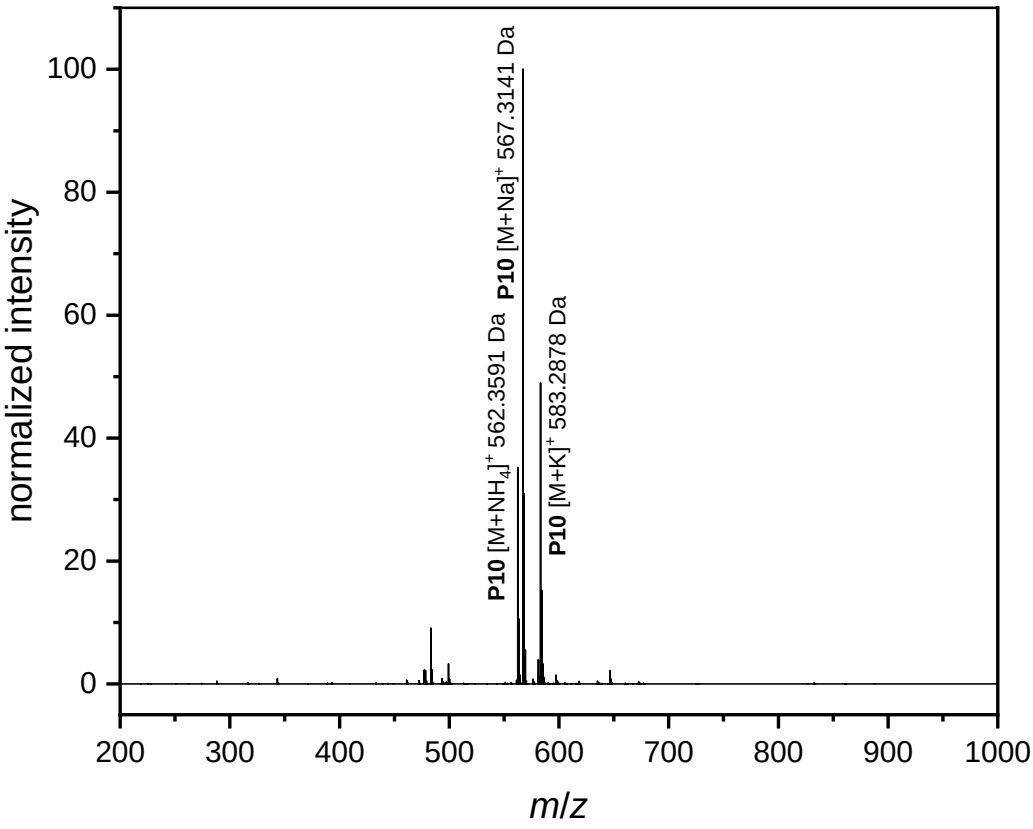

Supplementary Figure 26: ESI-MS spectrum of **P10**.

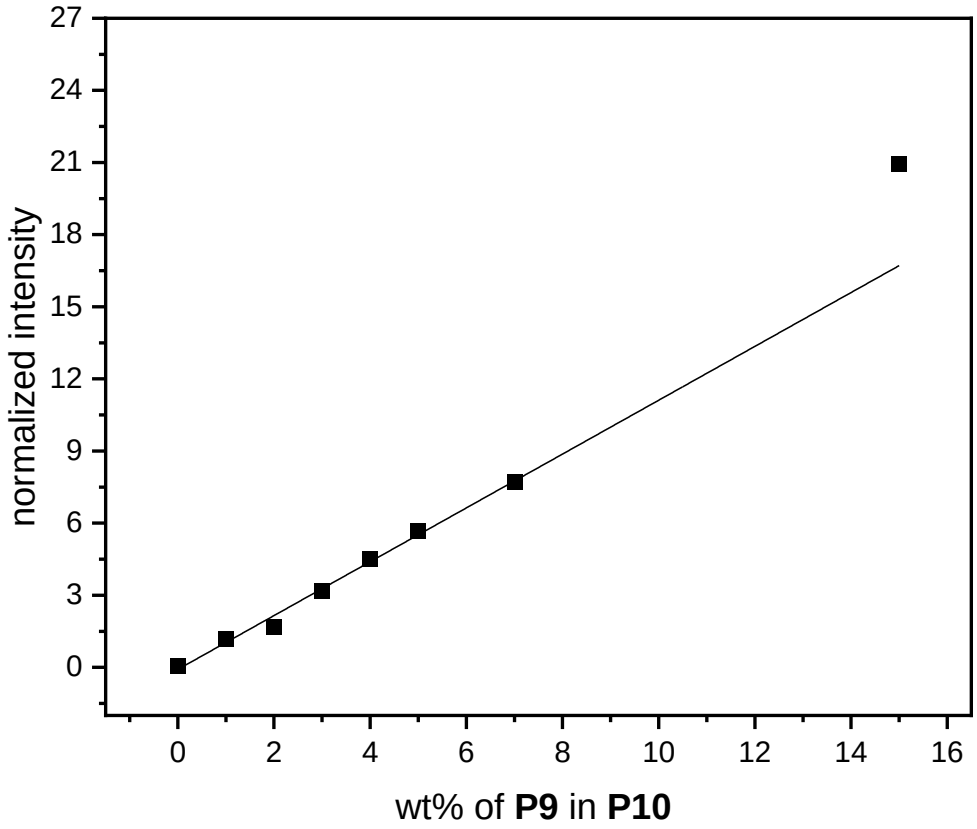

Supplementary Figure 27: Increase of the signal intensity of the sodium adduct of the doubly protected heptamer **P9** ([M+Na]$^+$: m/z = 523.2882) relative to the sodium adduct of the doubly protected octamer **P10** ([M+Na]$^+$: m/z = 567.3141 depending on the quantity in wt% of the heptamer in the sample.

α-Benzyl-ω-trityl octa(ethylene glycol) – P11[I]

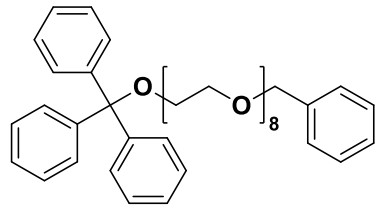

Chemical Formula: $C_{42}H_{54}O_9$
Exact Mass: 702.3768 Da
Molecular Weight: 702.8850 Da

The α-benzyl-ω-trityl octa(ethylene glycol) **P11** was prepared according to the procedure of BRUCE *et al.*[273] Monotrityl tetra(ethylene glycol) **P3** (400 mg, 0.93 mmol, 1.00 equiv.), KO*t*Bu (145 mg, 1.29 mmol, 1.39 equiv.), monobenzyl tetra(ethylene glycol) monotosylate **P7** (526 mg, 1.20 mmol, 1.29 equiv.) were used. Here, water instead of 1M aqueous HCl was added to quench the reaction. Purification of the crude product *via* column chromatography (cyhex:EA = 1:2) yielded the α-benzyl-ω-trityl octa(ethylene glycol) **P11** (325 mg, 463 µmol, 49.6%) as a yellowish oil.

^{1}H NMR (500 MHz, DMSO-d_6): δ / ppm = 7.46 – 7.21 (m, 20H, H_{Ar}^1), 4.48 (s, 2H, CH_2^2), 3.58 (dd, J = 5.6, 4.3 Hz, 2H, CH_2^3), 3.56 – 3.45 (m, 28H, CH_2^4), 3.06 (dd, J = 5.8, 4.1 Hz, 2H, CH_2^5).

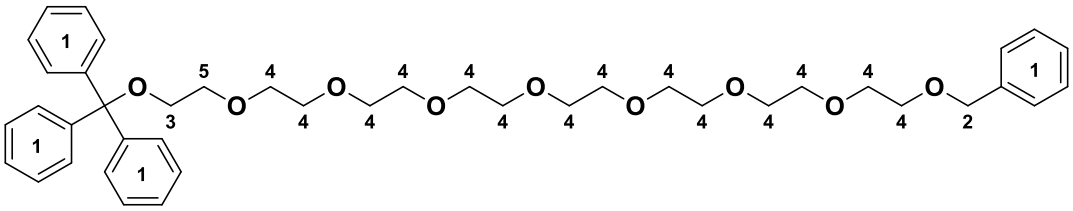

^{13}C NMR (126 MHz, DMSO-d_6): δ / ppm = 143.82 (C_q^1), 138.47 (C_q^2), 128.24 (CH_{Ar}^3), 128.20 (CH_{Ar}^3), 127.87 (CH_{Ar}^3), 127.47 (CH_{Ar}^3), 127.35 (CH_{Ar}^3), 126.98 (CH_{Ar}^3), 85.88 (C_q^4), 72.01 (CH_2^5), 70.07 (CH_2^6), 69.88 (CH_2^6), 69.84 (CH_2^6), 69.82 (CH_2^6), 69.79 (CH_2^6), 69.77 (CH_2^6), 69.64 (CH_2^6), 69.12 (CH_2^6), 63.06 (CH_2^7).

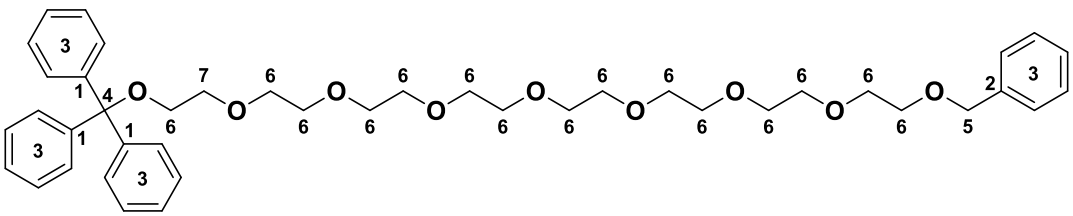

[I] The synthesis was carried out by B. Sc. MAXIMILIAN KNAB under the lab-supervision of PHILIPP BOHN.

HRMS (ESI) of $C_{42}H_{54}O_9$ $[M+NH_4]^+$ *m/z* calc. 720.4109, found 720.4081; $[M+Na]^+$ *m/z* calc. 725.3663, found 725.3625.

IR (ATR platinum diamond) $\tilde{\nu}$ / cm^{-1} = 3058.4, 2865.4, 1596.9, 1490.0, 1448.8, 1349.6, 1294.8, 1247.6, 1091.7, 1032.0, 1010.1, 951.2, 848.0, 762.5, 746.3, 697.3, 649.8, 632.4, 506.2.

R_f = 0.28 (DCM:acetone = 18:1).

Đ (System II) = 1.00

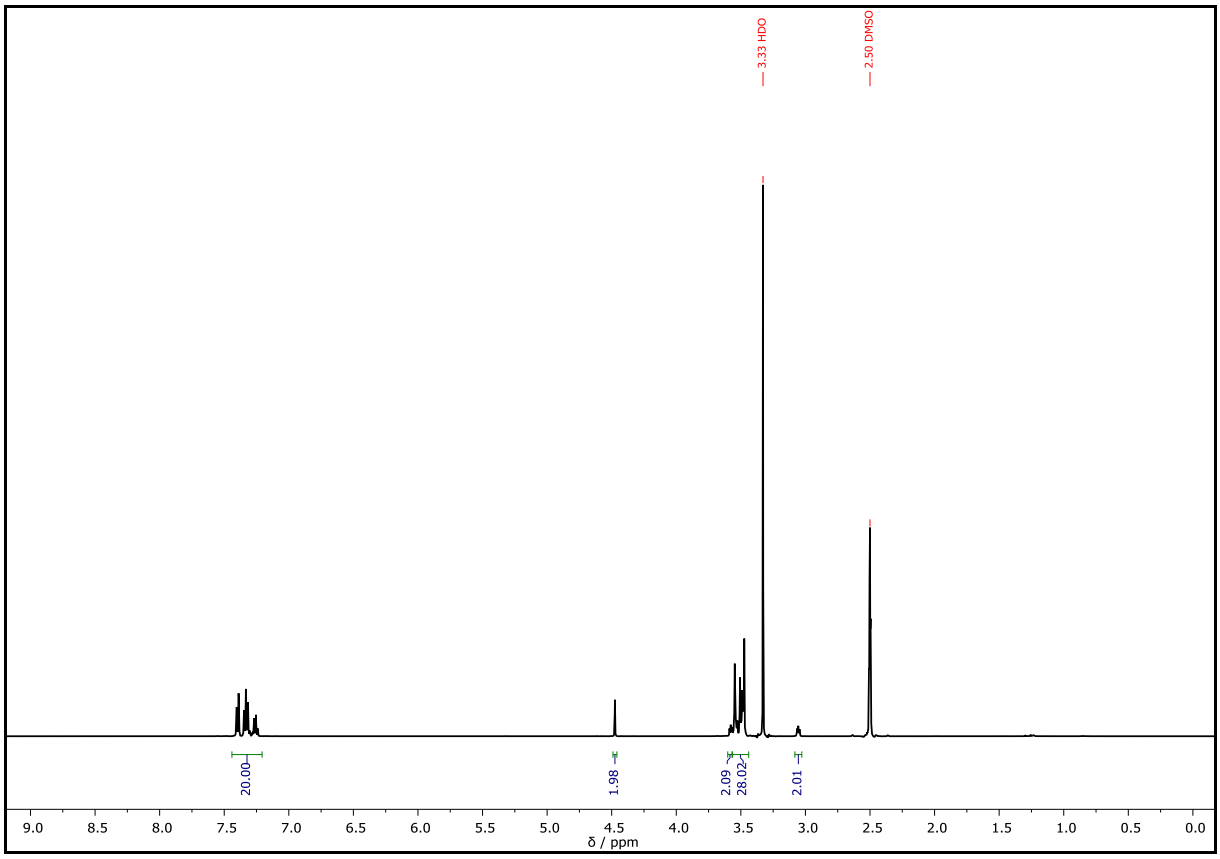

Supplementary Figure 28: ^{1}H NMR spectrum of **P11** recorded at 500 MHz in DMSO-d_6.

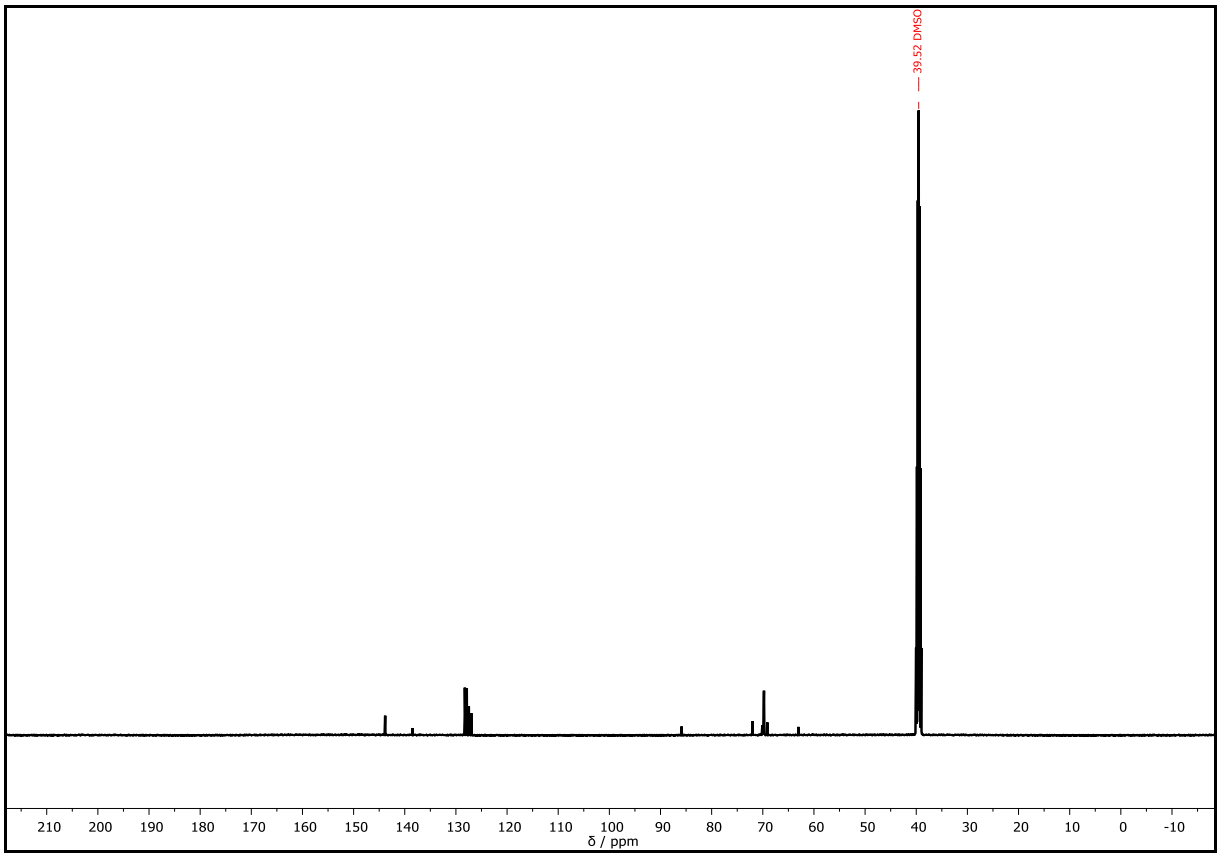

Supplementary Figure 29: ^{13}C NMR spectrum of **P11** recorded at 126 MHz in DMSO-d_6.

Monotrityl tetra(ethylene glycol) tosylate – P12

Procedure according to KINBARA *et al.*[319] – P12a

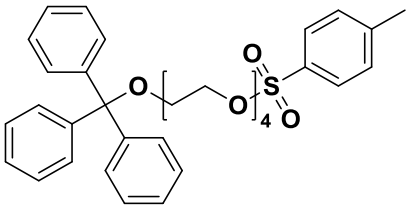

Chemical Formula: $C_{34}H_{38}O_7S$
Exact Mass: 590.2338 Da
Molecular Weight: 590.7310 Da

Monotrityl tetra(ethylene glycol) **P3** (18.8 g, contaminated with 8% of symmetric tetra(ethylene glycol) bis trityl ether, 17.3 g, 39.6 mmol of pure Trt(EG)$_4$OH, since **P3** was not further purified) was dissolved in 62 mL dry THF and cooled to 0 °C with an ice bath. Then, an aqueous solution of sodium hydroxide (6.43 g, 161 mmol, 4.07 equiv. in 20.6 mL H_2O) was added in one portion. Subsequently, a solution of *p*-toluenesulfonyl chloride (9.06 g, 47.5 mmol, 1.20 equiv.) in 20.6 mL dry THF was added dropwise over 15 min. The reaction mixture was stirred for five hours at 0 °C and was monitored *via* TLC. After full consumption of Trt(EG)$_4$OH **P3**, the ice bath was

removed and the reaction was stirred at room temperature for additional 16 hours. Water (30 mL) and methyl *t*-butyl ether (100 mL) were added. The phases were separated, and the organic layer was washed with water (50 mL) and brine (2 × 50 mL), dried over anhydrous sodium sulfate, filtered and the solvent was removed under reduced pressure. The product was further dried under high vacuum while stirring, affording **P12a** as a yellowish highly viscous oil (26.6 g, quant. yield), which was used without further purification in the next synthesis. SEC analysis showed a contamination with 8% of symmetric tetra(ethylene glycol) bis-trityl ether. A full characterization is given in the following for the pure monotrityl tetra(ethylene glycol) tosylate **P12b**.The product was stored under argon atmosphere and shielded from light before further use.

Procedure according to BRUCE *et al*.[273] – P12b

Monotrityl tetra(ethylene glycol) **P3** (500 mg, 1.15 mmol, 1.00 equiv.), sodium hydroxide (161 mg, 4.03 mmol, 3.50 equiv.), *p*-toluenesulfonyl chloride (263 mg, 1.38 mmol, 1.20 equiv.) were used. Purification of the crude product *via* column chromatography (cyhex:EA = 7:3) yielded the monotrityl tetra(ethylene glycol) tosylate **P12b** (567 mg, 0.96 mmol, 83.5%) as a yellowish oil. The product was dried under high vacuum, stored under argon atmosphere, and shielded from light before further use.

^{1}H NMR (500 MHz, DMSO-d_6): δ / ppm = 7.77 (d, J = 8.3 Hz, 2H, CH_{Ar}^{1}), 7.45 (d, J = 8.1 Hz, 2H, CH_{Ar}^{2}), 7.42 – 7.39 (m, 6H, $H_{Ar,Trt,ortho}^{3}$), 7.35 – 7.29 (m, 6H, $H_{Ar,Trt,meta}^{4}$), 7.28 – 7.22 (m, 3H, $H_{Ar,Trt,para}^{5}$), 4.10 – 4.07 (m, 2H, CH_2^{6}), 3.60 – 3.41 (m, 12H, CH_2O^{7}), 3.06 (t, J = 5.0 Hz, 2H, CH_2O^{8}), 2.39 (s, 3H, CH_3^{9}).

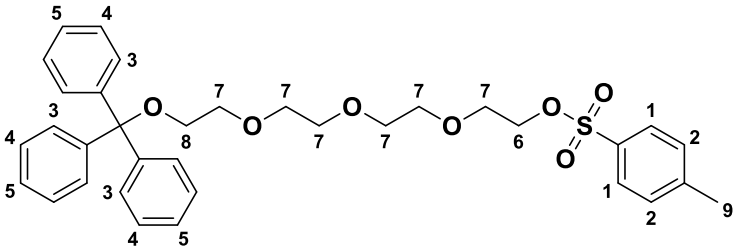

^{13}C NMR (126 MHz, DMSO-d_6): δ / ppm = 144.84 (C_q^{1}), 143.82 (C_q^{2}), 132.39 (C_q^{3}), 130.10 (CH_{Ar}^{4}), 128.24 (CH_{Ar}^{4}), 127.85 (CH_{Ar}^{4}), 127.61 (CH_{Ar}^{4}), 126.97 (CH_{Ar}^{4}), 85.89 (C_q^{5}), 70.06 (CH_2^{6}), 69.95 (CH_2^{6}), 69.84 (CH_2^{6}), 69.77 (CH_2^{6}), 69.75 (CH_2^{6}), 69.66 (CH_2^{6}), 67.89 (CH_2^{6}), 63.06 (CH_2^{7}), 21.08 (CH_2^{8}).

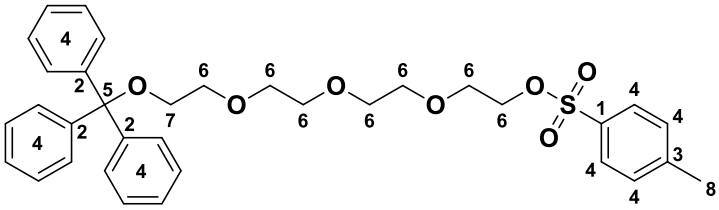

HRMS (ESI) of $C_{34}H_{38}O_7S$ $[M+NH_4]^+$ *m/z* calc. 608.2673, found 608.2667; $[M+Na]^+$ *m/z* calc. 613.2227, found 613.2218; $[M+K]^+$ *m/z* calc. 629.1905, found 629.1955.

IR (ATR platinum diamond) $\tilde{\nu}$ / cm^{-1} = 3057.6, 2870.1, 1597.3, 1490.4, 1447.9, 1354.6, 1292.0, 1247.2, 1213.3, 1188.6, 1175.2, 1094.4, 1010.8, 916.5, 815.1, 761.8, 748.2, 698.8, 662.2, 632.6, 582.5, 553.1.

R_f = 0.34 (cyhex:EA).

Đ (System II) = 1.00

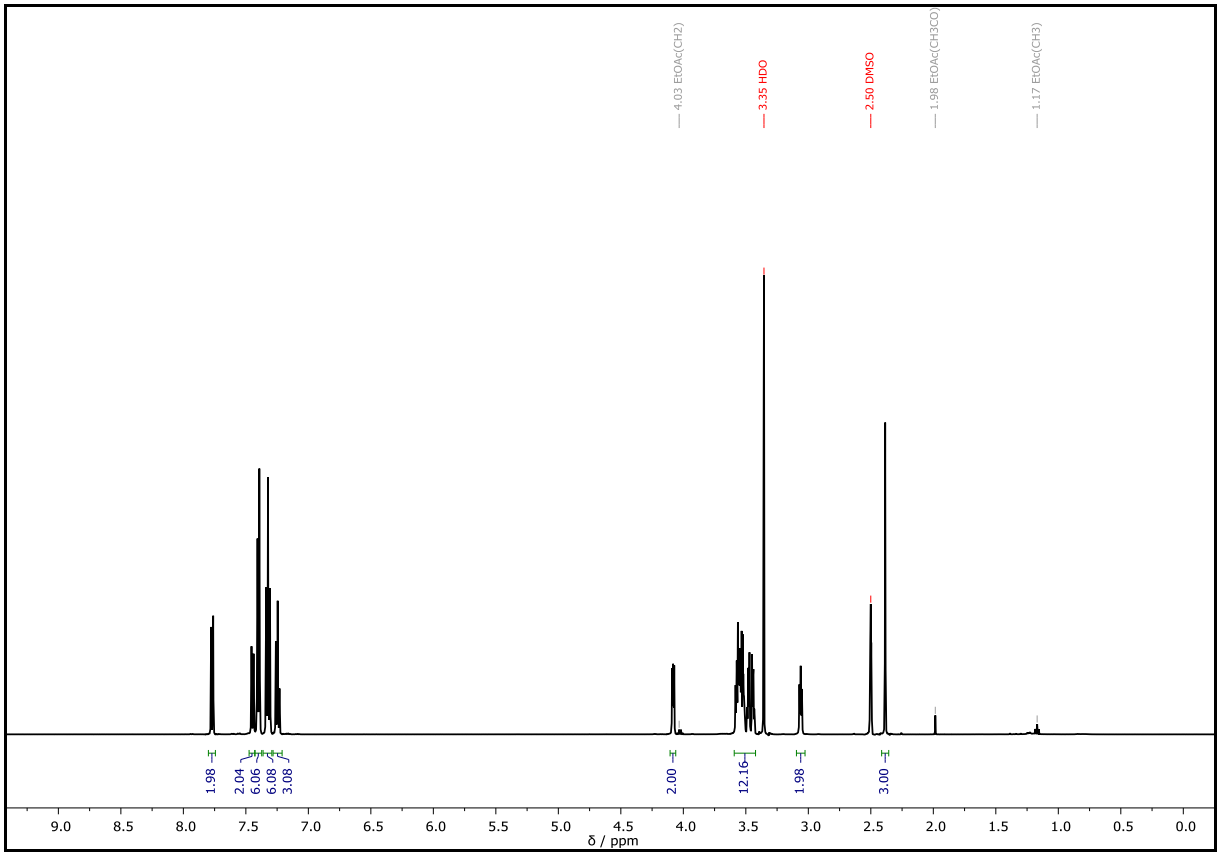

Supplementary Figure 30: ^{1}H NMR spectrum of **P12b** recorded at 500 MHz in DMSO-d_6.

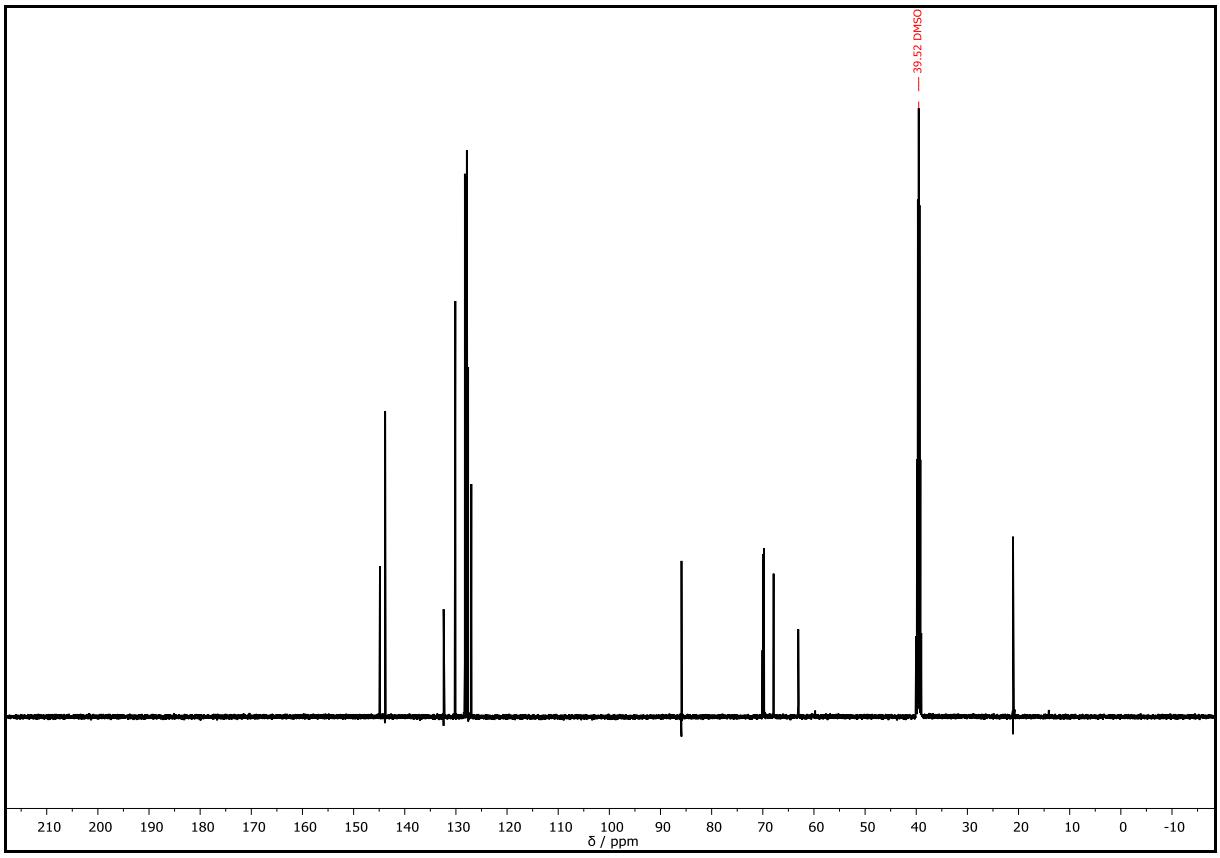

Supplementary Figure 31: ^{13}C NMR spectrum of **P12b** recorded at 126 MHz in DMSO-d_6.

Monotrityl octa(ethylene glycol) – P13[l]

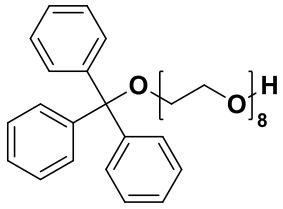

Chemical Formula: $C_{35}H_{48}O_9$
Exact Mass: 612.3298 Da
Molecular Weight: 612.7600 Da

The synthesis was performed according to a procedure of KINBARA *et al*.[319] A three-necked flask was charged with sodium hydride (60% dispersion in mineral oil, 2.40 g, 60.0 mmol, 1.52 equiv.) and dry THF (50 mL) under argon atmosphere und cooled to 0 °C with an ice bath. Tetra(ethylene glycol) (50.0 mL, 56.3 g, 290 mmol, 7.32 equiv.) in dry THF (20 mL) was dried *via* azeotropic distillation with toluene and added dropwise to the suspension. Subsequently, the monotrityl tetra(ethylene glycol) tosylate **P12** (26.6 g, containing 39.6 mmol of pure 9b, 1.00 equiv.), dissolved in dry THF (20 mL), was added to the reaction mixture over five minutes. The ice bath was

[l] The synthesis was carried out by B. Sc. MAXIMILIAN KNAB under the lab-supervision of PHILIPP BOHN.

removed, and the reaction mixture was refluxed for six hours. TLC indicated the completeness of the reaction, and the solution was cooled down to room temperature. The organic phase was washed with a brine-water mixture (1:1, 3 × 100 mL) and brine (1 × 50 mL). The phases were separated, and the organic layer was dried over anhydrous sodium sulfate, filtered, and the solvent was evaporated under reduced pressure. The crude product was dried under high vacuum, while stirring, affording **P13** (24.7 g, containing 36.3 mmol of pure **P13**, 99.2%) as a yellowish, highly viscous oil. SEC analysis showed a contamination with 8% of symmetric tetra(ethylene glycol) bis-trityl ether and 2% of dodeca(ethylene glycol) bis-trityl ether. 2.84 g of the crude product were purified by column chromatography (EA) yielding monotrityl octa(ethylene glycol) **P13** as a yellowish oil (1.36 g, 2.22 mmol, 48.2%).

^{1}H NMR (400 MHz, DMSO-d_6): δ / ppm = 7.44-7.37 (m, 6H, $H_{Ar,ortho}^{1}$), 7.38 – 7.29 (m, 6H, $H_{Ar,meta}^{2}$), 7.29 – 7.22 (m, 3H, $H_{Ar,para}^{3}$), 4.59 (t, J = 5.5 Hz, 1H, OH^{4}), 3.63 – 3.37 (m, 30H, CH_2^{5}), 3.06 (t, J = 4.9 Hz, 2H, CH_2OTrt)

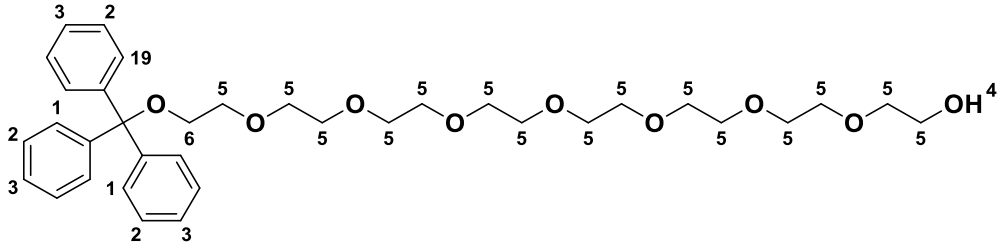

^{13}C NMR (101 MHz, DMSO-d_6): δ / ppm = 143.84 (C_q^{1}), 128.26 (CH_{Ar}^{2}), 127.89 (CH_{Ar}^{2}), 127.00 (CH_{Ar}^{2}), 85.89 (C_q^{3}), 72.36 (CH_2^{4}), 70.09 (CH_2^{4}), 69.90 (CH_2^{4}), 69.86 (CH_2^{4}), 69.83 (CH_2^{4}), 69.78 (CH_2^{4}), 69.66 (CH_2^{4}), 63.07 (CH_2^{5}), 60.21 (CH_2^{4}), 54.95 (CH_2^{4}).

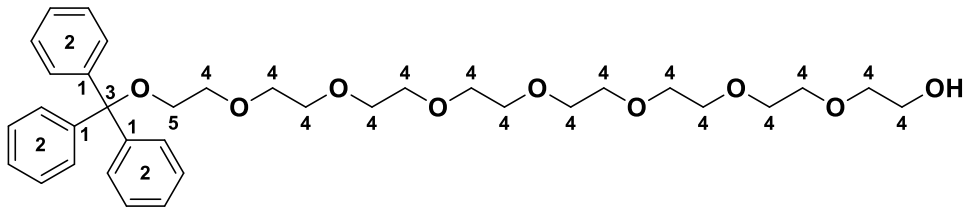

HRMS (ESI) of $C_{35}H_{48}O_9$ $[M+NH_4]^+$ *m/z* calc. 630.3639, found 630.3613; $[M+Na]^+$ *m/z* calc. 635.3193, found 635.3157, $[M+K]^+$ *m/z* calc. 651.2870, found 651.2918.

IR (ATR platinum diamond) ν / cm^{-1} = 3480.4, 3057.8, 2867.8, 1596.8, 1489.5, 1448.5, 1349.1, 1295.0, 1247.4, 1090.5, 1033.1, 1010.0, 950.6, 845.9, 762.7, 747.8, 706.2, 649.6, 632.3, 509.7.

R_f = 0.04 (EA).

Đ (System II) = 1.00

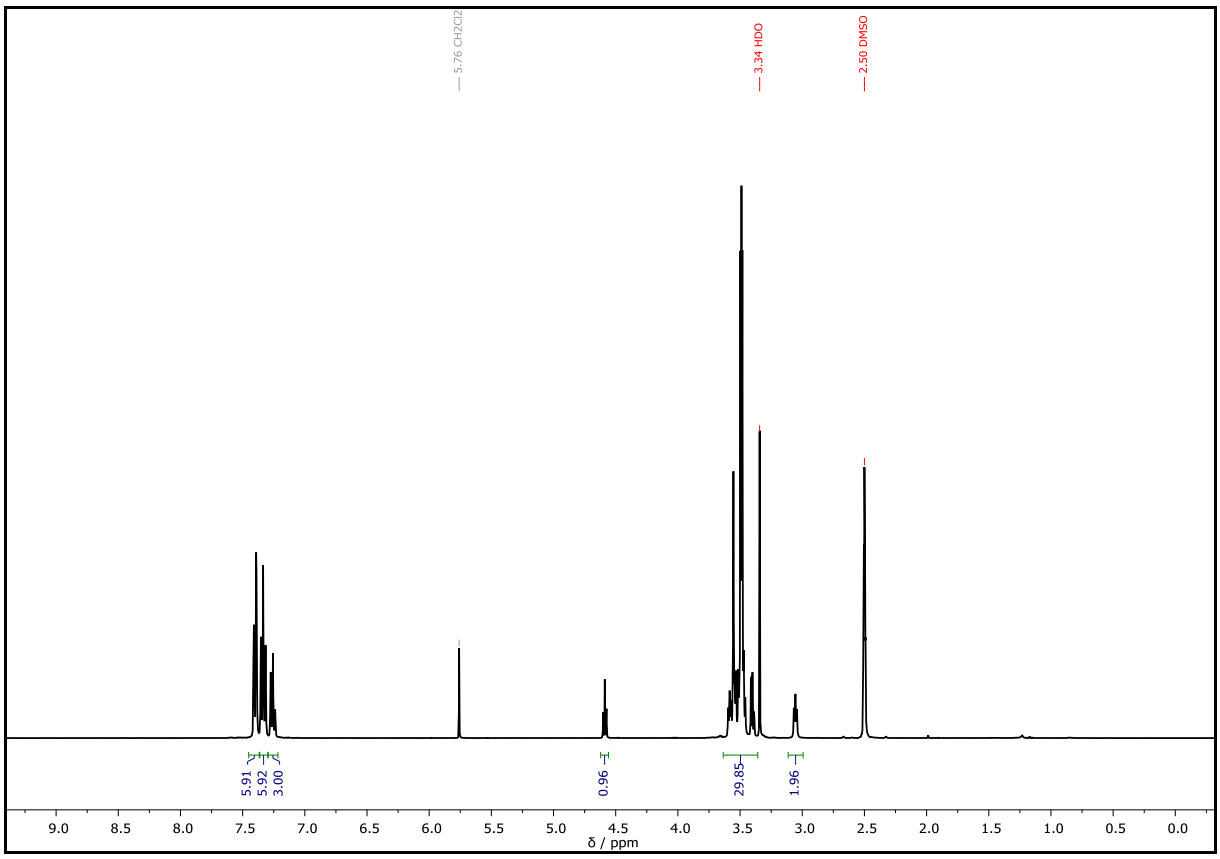

Supplementary Figure 32: ^{1}H NMR spectrum of **P13** recorded at 400 MHz in DMSO-d_6.

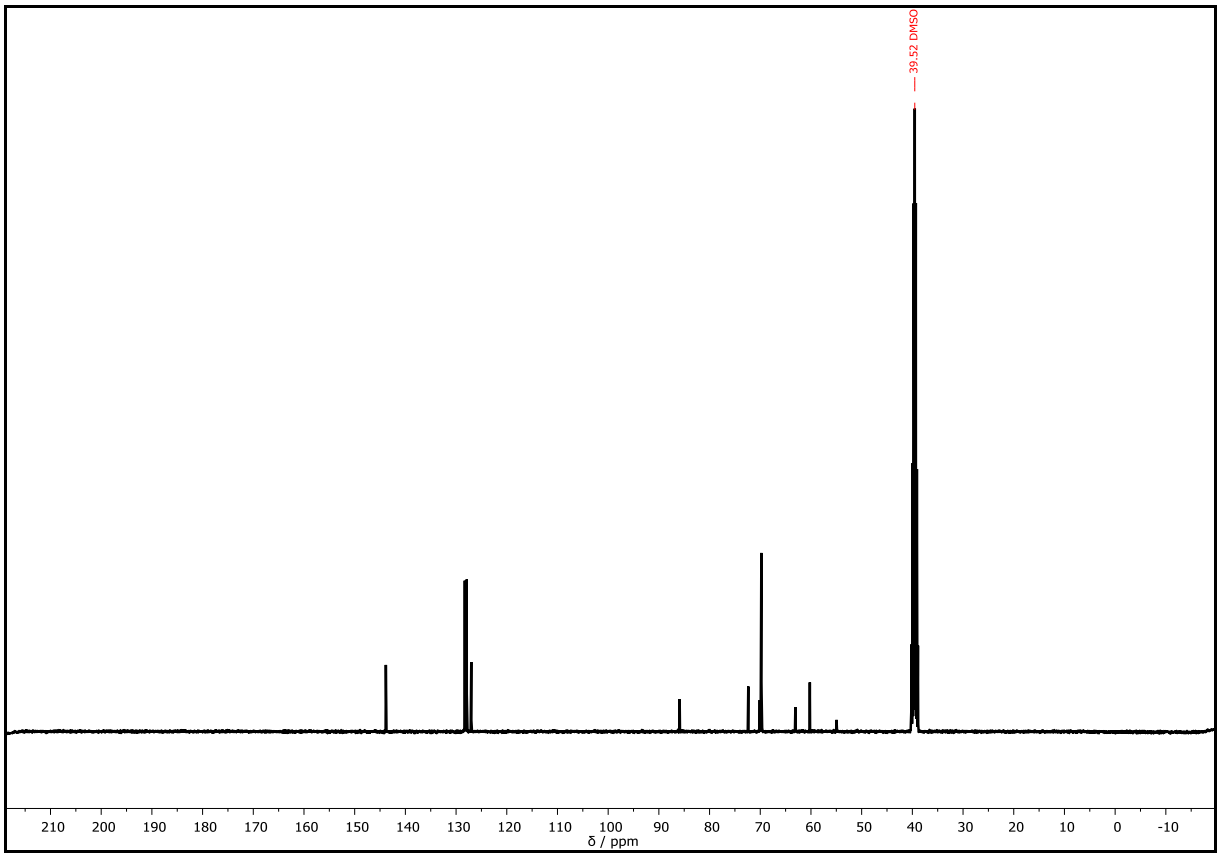

Supplementary Figure 33 ^{13}C NMR spectrum of **P13** recorded at 101 MHz in DMSO-d_6.

Monotrityl octa(ethylene glycol) tosylate – P14

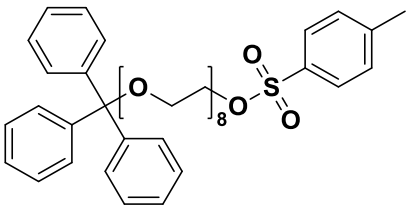

Chemical Formula: $C_{42}H_{54}O_{11}S$
Exact Mass: 766.3387 Da
Molecular Weight: 766.9430 Da

The synthesis was performed according to a procedure of KINBARA *et al*.[319] Monotrityl octa(ethylene glycol) **P13** (21.6 g, containing 31.7 mmol of pure **P13**, 1.00 equiv.) was dissolved in THF (70 mL) and cooled to 0°C on an ice bath. A solution of sodium hydroxide (6.34 g, 158 mmol, 4.98 equiv.) in water (20 mL) was added and the mixture was stirred for 30 minutes at 0 °C. Subsequently, *p*-toluenesulfonyl chloride (8.72 g, 45.8 mmol, 1.44 mmol) dissolved in THF (20 mL) was added dropwise over 15 minutes. After stirring the reaction mixture for five hours at 0 °C and additional 16 hours at room temperature, water (30 mL) and methyl *t*-butyl ether (100 mL) was added. The phases were separated, the organic layer was washed with water (50 mL)

and brine (2 × 50 mL), dried over anhydrous sodium sulfate and the solvent was removed under reduced pressure. The crude product was dried under high vacuum while stirring, affording **P14** as a yellowish highly viscous oil (25.9 g, containing 30.4 mmol of pure **P14**, 95.9%), stored under argon atmosphere, shielded from light, and was used without further purification in the next synthesis. SEC analysis showed a contamination with 8% of symmetric tetra(ethylene glycol) bis-trityl ether and 2% of dodeca(ethylene glycol) bis trityl ether. 1.88 g of the crude product was purified *via* column chromatography (cyhex:EA = 3:7) yielding the monotrityl octa(ethylene glycol) tosylate **P14** as a yellowish highly viscous oil (837 mg, 1.09 mmol, 49.5%).

^{1}H NMR (300 MHz, DMSO-d_6): δ / ppm = 7.78 (d, J = 8.3 Hz, 2H, CH_{Ar}^{1}), 7.47 (d, J = 8.1 Hz, 2H, CH_{Ar}^{2}), 7.44 – 7.38 (m, 6H, $H_{Ar,Trt,ortho}^{3}$), 7.37 – 7.29 (m, 6H, $H_{Ar,Trt,meta}^{4}$), 7.29 – 7.21 (m, 3H, $H_{Ar,Trt,para}^{5}$), 4.15 – 4.07 (m, 2H, CH_2^{6}), 3.66 – 3.39 (m, 28H, CH_2^{7}), 3.06 (t, J = 4.9 Hz, 2H, CH_2^{8}), 2.39 (s, 3H, CH_3^{9}).

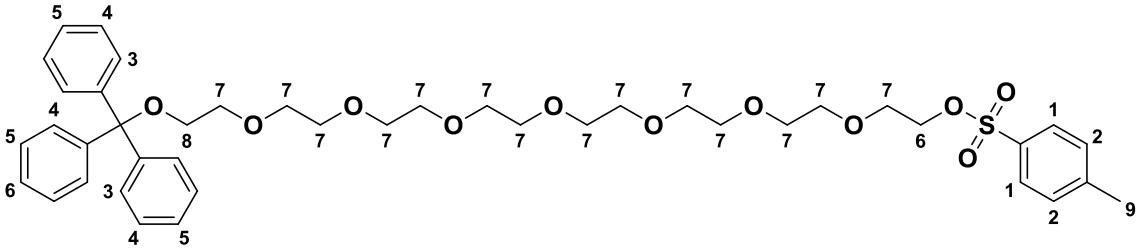

^{13}C NMR (126 MHz, DMSO-d_6): δ / ppm = 144.83 (C_q^{1}), 143.81 (C_q^{2}), 130.09 (C_q^{3}), 128.23 (CH_{Ar}^{4}), 127.83 (CH_{Ar}^{4}), 127.73 (CH_{Ar}^{4}), 127.60 (CH_{Ar}^{4}), 126.95 (CH_{Ar}^{4}), 85.87 (CH_q^{5}), 70.08 (CH_2^{6}), 69.95 (CH_2^{6}), 69.89 (CH_2^{6}), 69.85 (CH_2^{6}), 69.82 (CH_2^{6}), 69.77 (CH_2^{6}), 69.75 (CH_2^{6}), 69.70 (CH_2^{6}), 69.65 (CH_2^{6}), 67.87 (CH_2^{6}), 63.05 (CH_2^{7}), 21.06 (CH_2^{7}).

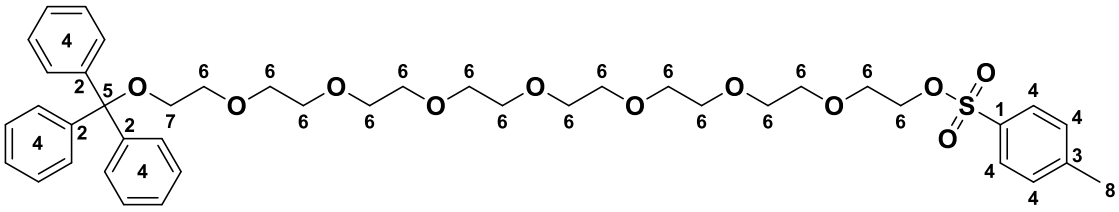

HRMS (ESI) of $C_{42}H_{54}O_{11}S$ $[M+NH_4]^+$ *m/z* calc. 784.3671, found 784.3708; $[M+Na]^+$ *m/z* calc. 789.3225, found 789.3260, $[M+K]^+$ *m/z* calc. 805.2962, found 805.2997.

IR (ATR platinum diamond) $\tilde{\nu}$ / cm^{-1} = 2920.7, 2854.3, 1738.5, 1597.4, 1490.1, 1449.2, 1355.6, 1292.6, 245.2, 1188.7, 1176.1, 1094.1, 1033.2, 1010.6, 917.1, 816.0, 762.7, 748.1, 706.6, 662.8, 632.4, 581.6, 553.6.

R_f = 0.53 (EA).

Đ (System II) = 1.00

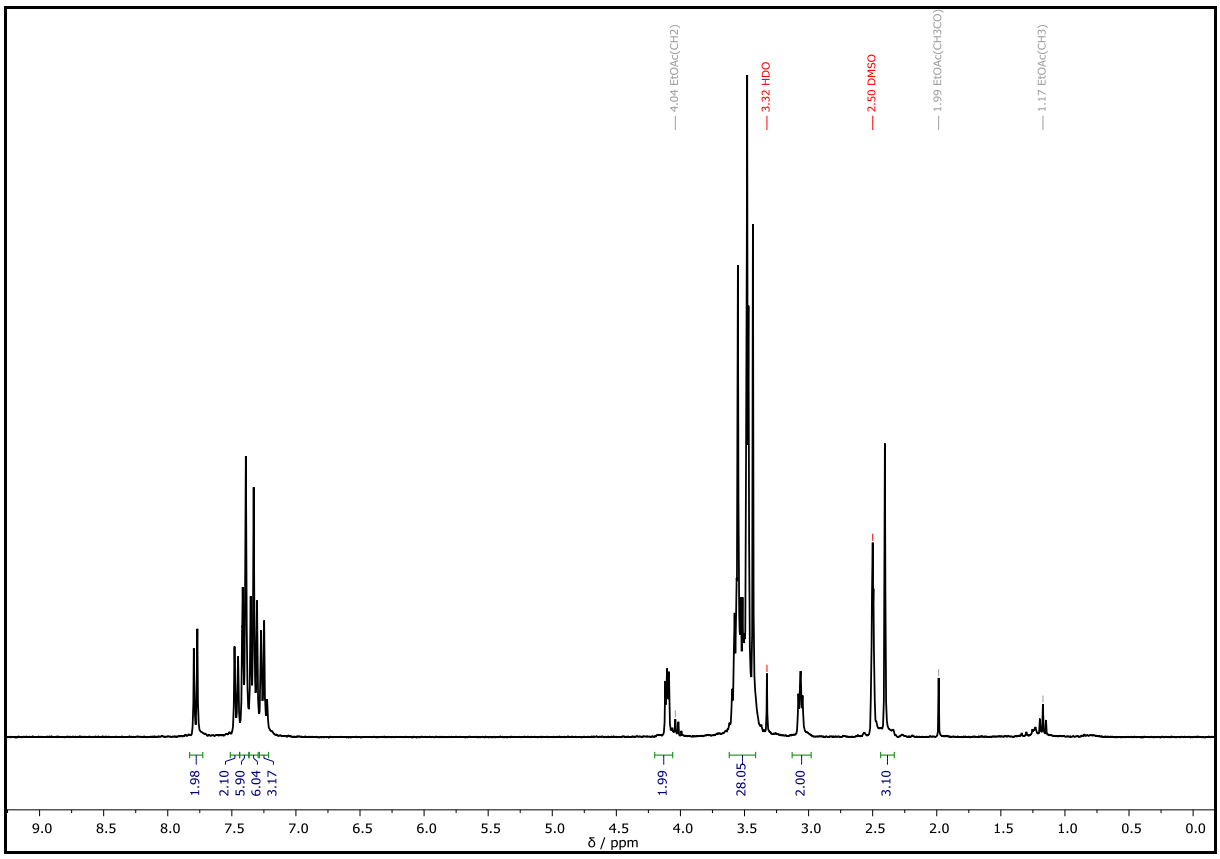

Supplementary Figure 34: ^{1}H NMR spectrum of **P14** recorded at 300 MHz in DMSO-d_6.

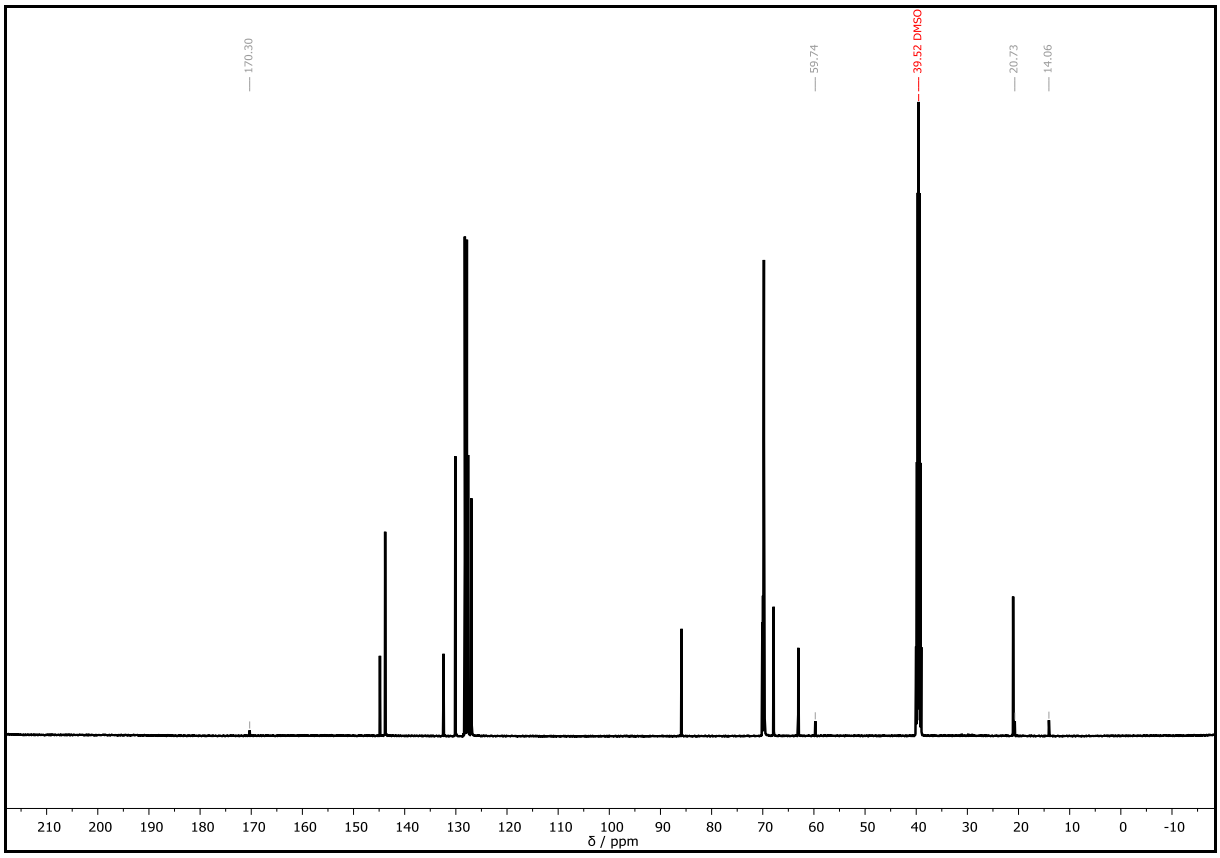

Supplementary Figure 35: ^{13}C NMR spectrum of **P14** recorded at 126 MHz in DMSO-d_6.

Octa(ethylene glycol) tosylate – P15

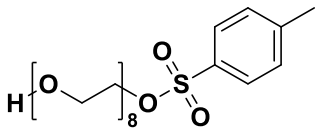

Chemical Formula: $C_{23}H_{40}O_{11}S$
Exact Mass: 524.2291 Da
Molecular Weight: 524.6220 Da

The synthesis was performed according to a procedure of KINBARA *et al*.[319] Monotrityl octa(ethylene glycol) tosylate **P14** (24.0 g, containing 28.2 mmol, 1.00 equiv.) was dissolved in methanol (75 mL). Then, *p*-toluenesulfonic acid monohydrate (200 mg, 1.16 mmol, 0.04 equiv.) was added and the reaction mixture was stirred for three hours at room temperature. Crushed ice was added (15 g) until a white solid precipitated and water (75 mL) was slowly added over five minutes. The mixture was cooled below 10 °C on an ice bath, filtered, and the white solid was rinsed with water (3 × 15 mL). Methanol was evaporated under reduced pressure and brine (50 mL) was added to the residue. The aqueous layer was extracted with EA (5 × 75 mL). The combined organic phases were washed with a brine-water mixture (1:1 v/v, 2 × 50 mL), saturated aqueous solution of sodium hydrogen carbonate (25 mL), brine (2 × 50 mL), dried over

anhydrous sodium sulfate, filtered, and the solvent was removed under reduce pressure. The crude product was dried under high vacuum, while stirring, affording **P15** as a colorless oil (13.3 g, containing 22.3 mmol of pure 10d, 78.8%), stored under argon atmosphere and shielded from light. SEC analysis showed impurities of 12%. Purification *via* column chromatography (EA:MeOH = 9:1) afforded octa(ethylene glycol) tosylate **P15** as a colorless oil (11.2 g, 21.4 mmol, 75.9%).

^{1}H NMR (400 MHz, DMSO-d_6): δ (ppm) = 7.79 (d, J = 8.3 Hz, 2H, CH_{Ar}^{1}), 7.48 (d, J = 8.1 Hz, 2H, CH_{Ar}^{2}), 4.56 (t, J = 5.4 Hz, 1H, OH^{3}), 4.15 – 4.06 (m, 2H, CH_2^{4}), 3.62 – 3.53 (m, 2H, CH_2^{5}) 3.51 – 3.37 (m, 28H, CH_2^{6}), 2.42 (s, 3H, CH_3).

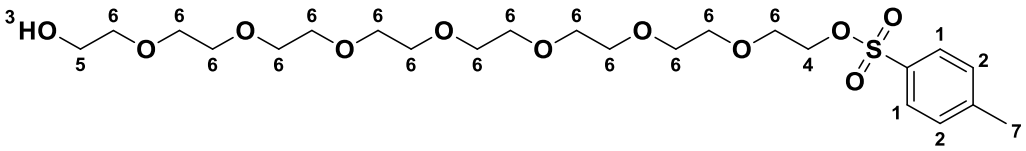

^{13}C NMR (126 MHz, DMSO-d_6): δ / ppm = 144.88 (C_q^1), 132.39 (C_q^2), 130.13 (CH_{Ar}^3), 127.62 (CH_{Ar}^4), 72.34 (CH_2^5), 69.99 (CH_2^5), 69.77 (CH_2^5), 69.69 (CH_2^5), 69.64 (CH_2^5), 67.87 (CH_2^5), 60.20 (CH_2^5), 21.09 (CH_2^6).

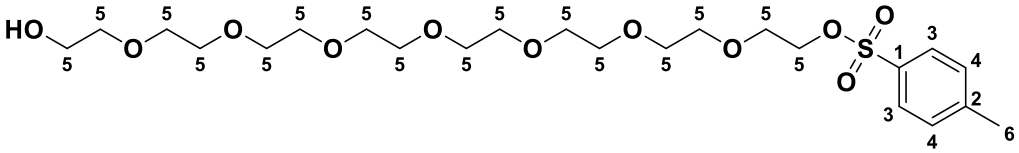

HRMS (ESI) of $C_{23}H_{40}O_{11}S$ $[M+H]^+$ *m/z* calc. 525.2367, found 525.2358; $[M+NH_4]^+$ *m/z* calc. 542.2632, found 542.2623; $[M+Na]^+$ *m/z* calc. 547.2186, found 547.2175, $[M+K]^+$ *m/z* calc. 563.1865, found 563.1912.

IR (ATR platinum diamond) *v* / cm^{-1} = 3465.6, 2867.5, 1735.5, 1597.7, 1452.9, 1351.9, 1292.6, 1246.4, 1188.7, 1175.6, 1094.6, 1016.7, 918.1, 816.6, 774.5, 705.9, 662.8, 582.4, 553.4.

R_f = 0.32 (EA:MeOH = 9:1).

Đ (System II) = 1.00

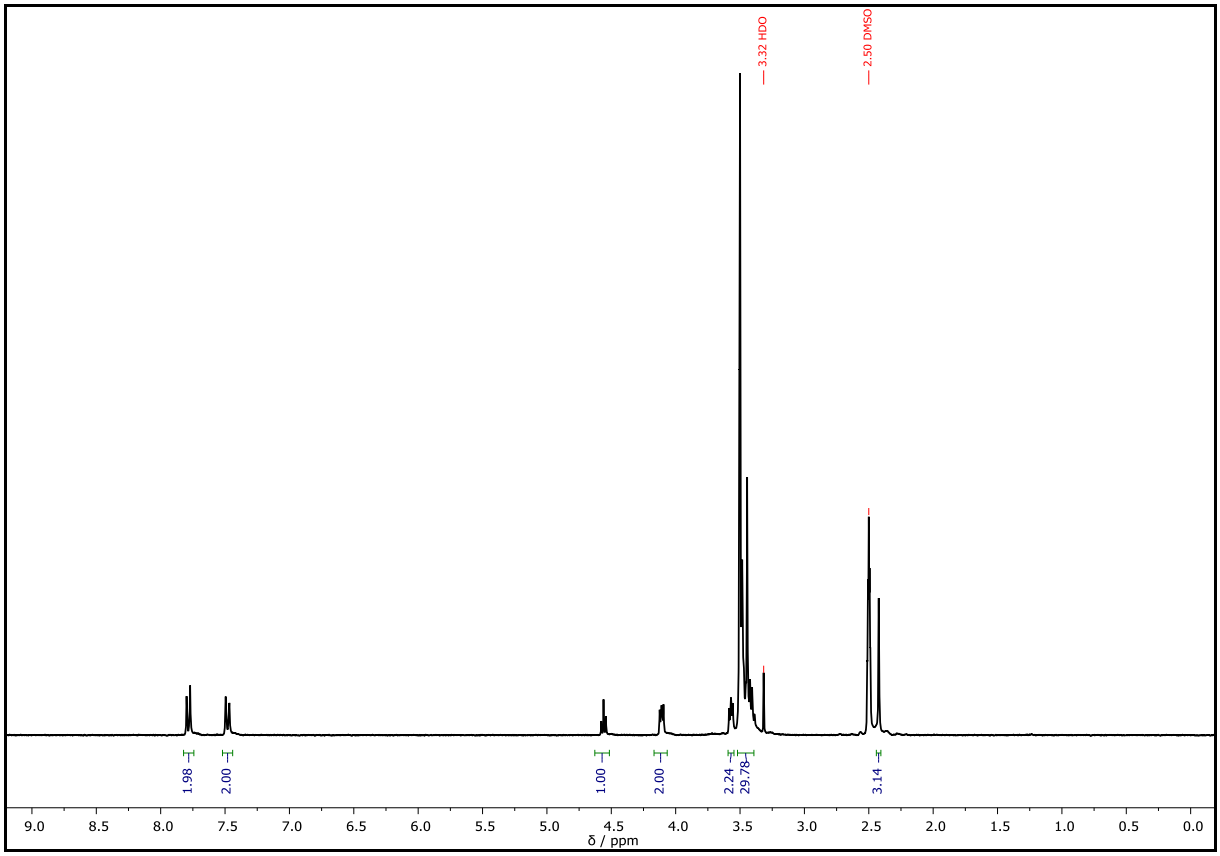

Supplementary Figure 36: ^{1}H NMR spectrum of **P15** recorded at 400 MHz in DMSO-d_6.

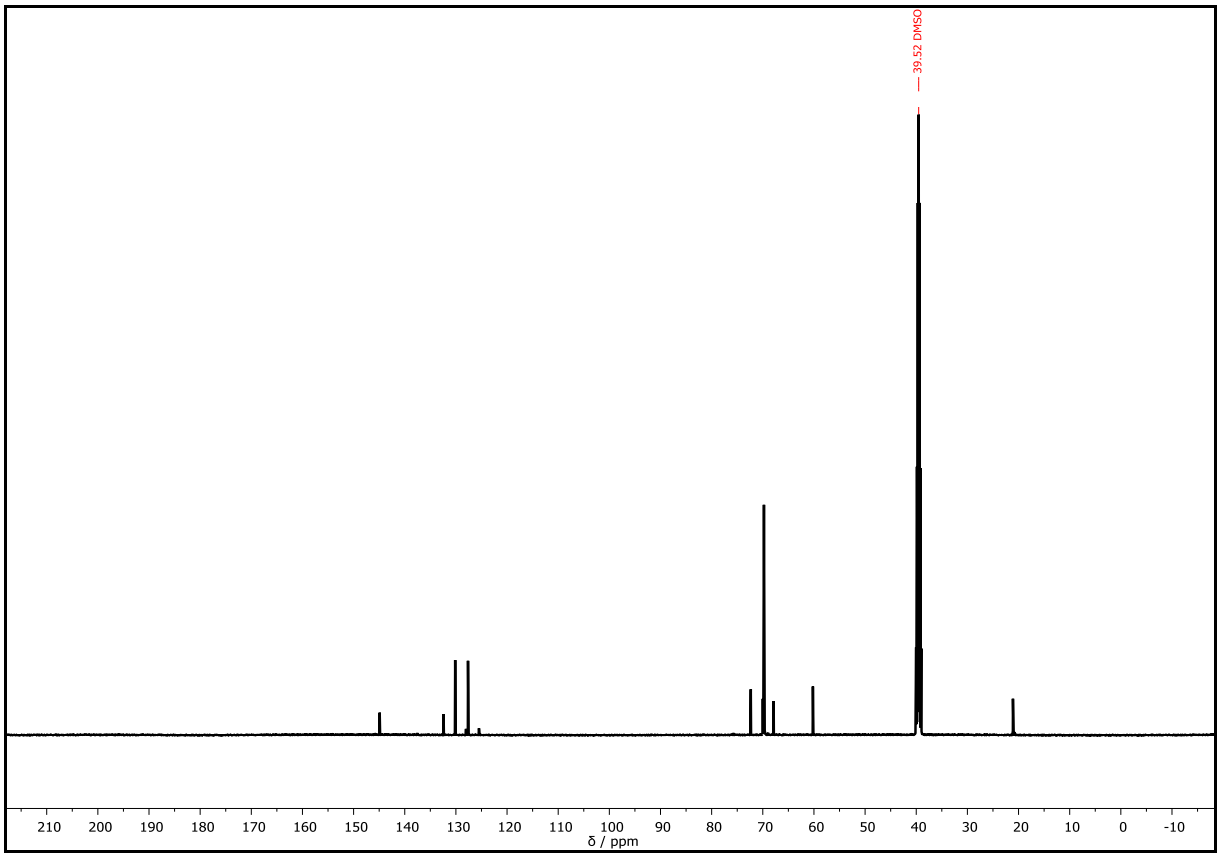

Supplementary Figure 37: ^{13}C NMR spectrum of **P15** recorded at 126 MHz in DMSO-d_6.

Monobenzyl octa(ethylene glycol) – P16

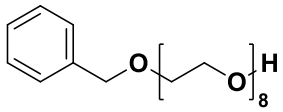

Chemical Formula: $C_{23}H_{40}O_9$
Exact Mass: 460.2672 Da
Molecular Weight: 460.5640 Da

The synthesis was performed according to a procedure of BAKER *et al*.[317] α-Benzyl-ω-tetrahydropyranyl octa(ethylene glycol) **P10** (4.00 g, 7.34 mmol, 1.00 eq) was added to a solution of *p*-toluenesulfonic acid monohydrate (12.6 mg, 73.2 µmol, 0.01 equiv.) in anhydrous methanol (7 mL). After stirring the reaction mixture for 36 hours at room temperature, the solvent was evaporated under reduced pressure. The residue was dissolved in DCM (50 mL) and washed with aqueous NaCl/HCl solution (50 mL). The phases were separated, and the organic layer was dried over anhydrous sodium sulfate, filtered and concentrated *in vacuo* to afford the monobenzyl octa(ethylene glycol) **P16** as a colorless oil (3.30 g, 7.17 mmol, 97.7%).

^{1}H NMR (300 MHz, DMSO-d_6): δ / ppm = 7.46 – 7.19 (m, 5H, H_{Ar}^{1}), 4.58 (t, J = 5.4 Hz, 1H, OH^{2}), 4.49 (s, 2H, CH_2^{3}), 3.69 – 3.36 (m, 32H, CH_2^{4}).

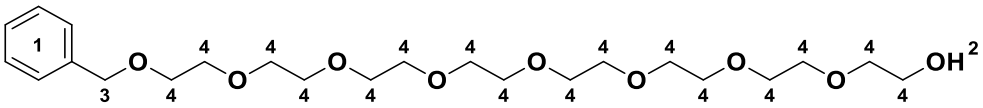

^{13}C NMR (101 MHz, DMSO-d_6): δ / ppm = 138.49 (C_q^{1}), 128.23 (CH_{Ar}^{2}), 127.50 (CH_{Ar}^{2}), 127.39 (CH_{Ar}^{2}), 72.36 (CH_2^{3}), 72.03 (CH_2^{4}), 69.85 (CH_2^{3}), 69.80 (CH_2^{3}), 69.14 (CH_2^{3}), 60.22 (CH_2^{3}).

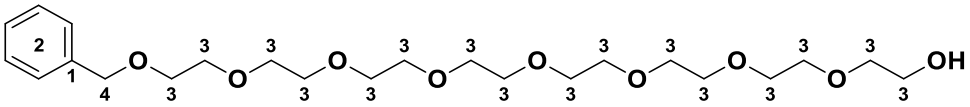

HRMS (ESI) of $C_{23}H_{40}O_9$ $[M+H]^+$ *m/z* calc. 461.2747, found 461.2746; $[M+NH_4]^+$ *m/z* calc. 478.3012, found 478.3013; $[M+Na]^+$ *m/z* calc. 483.2566, found 438.2565; $[M+K]^+$ *m/z* calc. 499.2301, found 499.2303.

The mass of the α-benzyl-ω-tetrahydropyranyl octa(ethylene glycol) **P10** was also found. $C_{28}H_{48}O_{10}$ $[M+NH_4]^+$ *m/z* calc. 562.3588, found 562.3583; $[M+Na]^+$ *m/z* calc. 567.3142, found 567.3139.

The mass of the bis-benzyl octa(ethylene glycol) was also found. $C_{30}H_{46}O_9$ $[M+H]^+$ *m/z* calc. 573.3037, found 573.3032.

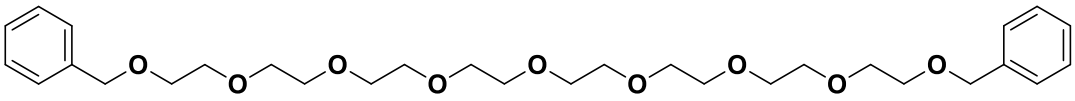

Chemical Formula: $C_{30}H_{46}O_9$
Exact Mass: 550.3142 Da

The mass of the octa(ethylene glycol) was also found. $C_{16}H_{34}O_9$ $[M+H]^+$ *m/z* calc. 371.2277, found 371.2275.

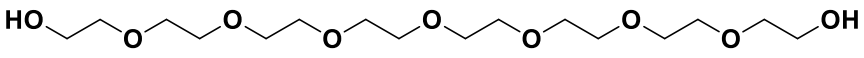

Chemical Formula: $C_{16}H_{34}O_9$
Exact Mass: 370.2203 Da

IR (ATR platinum diamond) $\tilde{\nu}$ / cm^{-1} = 3475.1, 2865.4, 1719.4, 1453.6, 1349.6, 1276.0, 1250.5, 1094.0, 944.6, 848.3, 740.0, 716.8, 699.3, 527.3.

R_f = 0.11 (EA).

Đ (System II) = 1.00

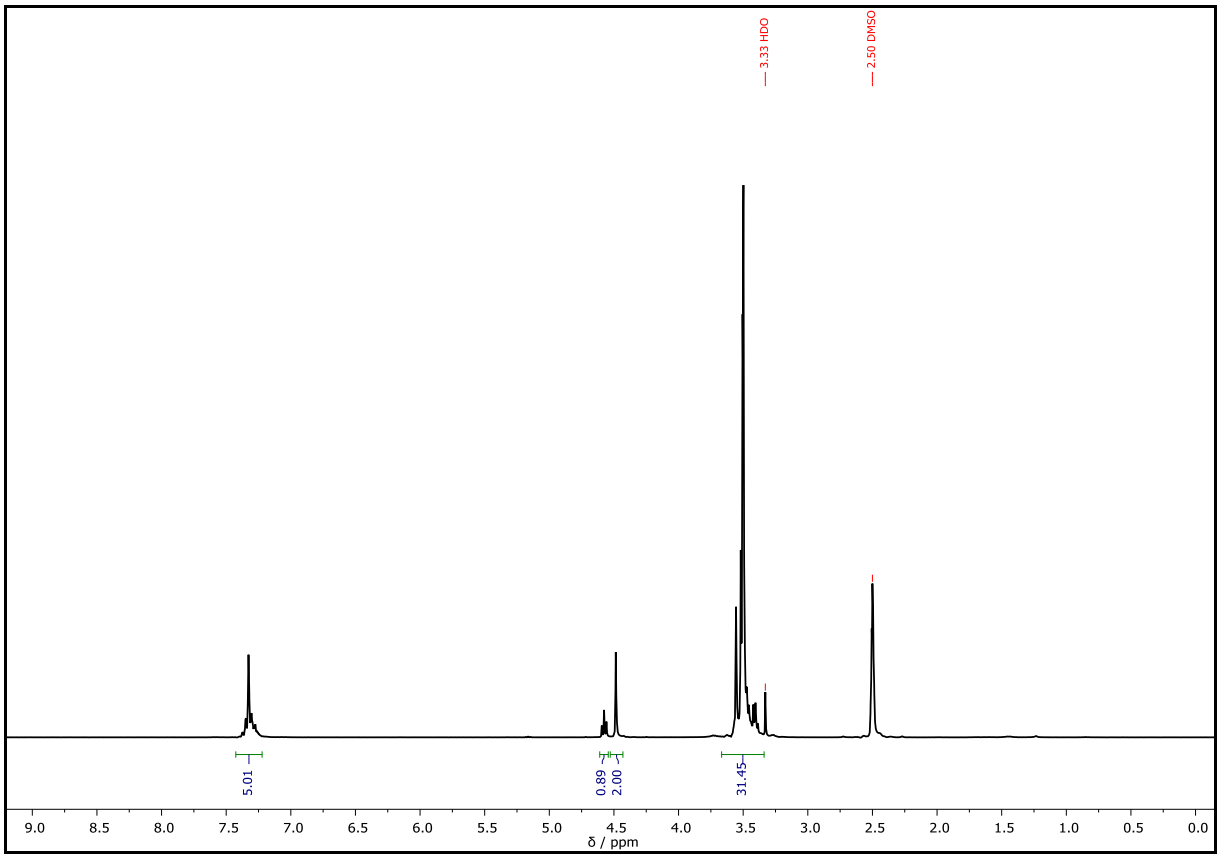

Supplementary Figure 38 ^{1}H NMR spectrum of **P16** recorded at 300 MHz in DMSO-d_6.

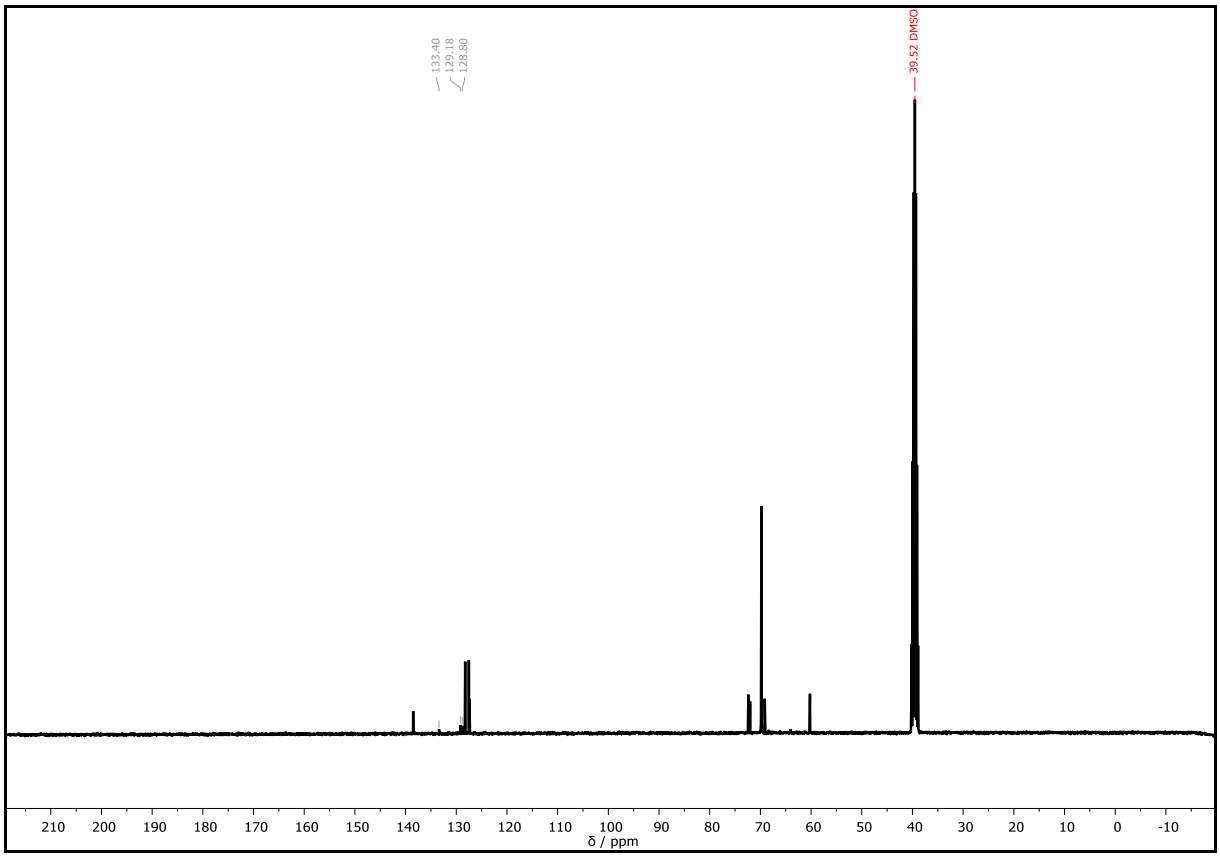

Supplementary Figure 39 ^{13}C NMR spectrum of **P16** recorded at 101 MHz in DMSO-d_6.

Mono(tetrahydropyranyl) octa(ethylene glycol) – P17

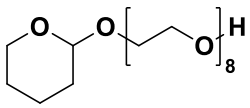

Chemical Formula: $C_{21}H_{42}O_{10}$
Exact Mass: 454.2778 Da
Molecular Weight: 454.5570 Da

Palladium on carbon (400 mg, 10 wt%) was added to a solution of α-benzyl-ω-tetrahydropyranyl octa(ethylene glycol) **P10** (4.00 g, 7.34 mmol, 1.00 eq) dissolved in EA (35 mL). The reaction mixture was stirred overnight at reflux under hydrogen atmosphere (balloon). After cooling to room temperature, the mixture was filtered through a pad of celite to remove the Pd/C. The organic phase was dried over anhydrous sodium sulfate and the solvent was removed under reduced pressure affording the product **P17** as a colorless oil (3.30 g, 7.26 mmol, 98.9%).

^{1}H NMR (300 MHz, DMSO-d_6): δ / ppm = 4.64 – 4.51 (m, 2H, OH^1 and CH^1), 3.86 – 3.64 (m, 2H, CH$_2^2$), 3.64 – 3.35 (m, 32H, CH$_2^3$), 1.83 – 1.34 (m, 6H, CH$_2^4$).

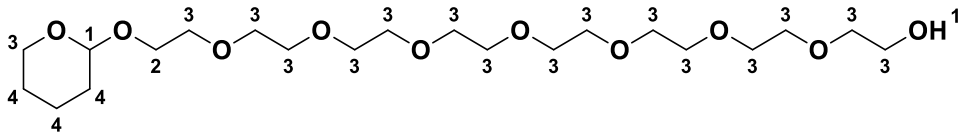

^{13}C NMR (101 MHz, DMSO-d_6): δ / ppm = 98.06 (CH^1), 72.36 (CH_2^2), 69.83 (CH_2^2), 69.80 (CH_2^2), 69.74 (CH_2^2), 66.08 (CH_2^2), 61.25 (CH_2^2), 60.22 (CH_2^2), 30.23 (CH_2^3), 25.04 (CH_2^3), 19.14 (CH_2^3).

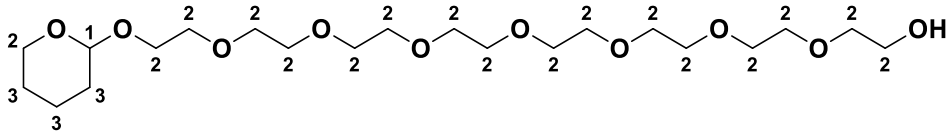

HRMS (ESI) of $C_{21}H_{42}O_{10}$ $[M+H]^+$ *m/z* calc. 455.2852, found 455.2851; $[M+NH_4]^+$ *m/z* calc. 472.3117, found 472.3119; $[M+Na]^+$ *m/z* calc. 477.2671, found 477.2670; $[M+K]^+$ *m/z* calc. 493.2406, found 493.2408.

The mass of the octa(ethylene glycol) was also found. $C_{16}H_{34}O_9$ $[M+H]^+$ *m/z* calc. 371.2277, found 371.2275; $[M+Na]^+$ *m/z* calc. 393.2096, found 393.2092.

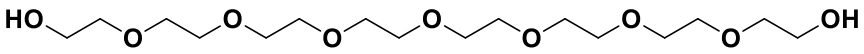

Chemical Formula: $C_{16}H_{34}O_9$
Exact Mass: 370.2203 Da

The mass of the bis-tetrahydropyranyl octa(ethylene glycol) was also found. $C_{26}H_{50}O_{11}$ $[M+Na]^+$ *m/z* calc. 561.3247, found 561.3243.

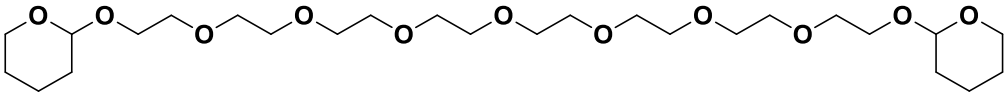

Chemical Formula: $C_{26}H_{50}O_{11}$
Exact Mass: 538.3353 Da

IR (ATR platinum diamond) $\tilde{\nu}$ / cm^{-1} = 3439.5, 2868.5, 1731.0, 1454.3, 1349.5, 1248.5, 1201.4, 1096.9, 1033.0, 988.2, 942.2, 871.3, 524.2.

R_f = 0.03 (EA)

Đ (System II) = 1.00

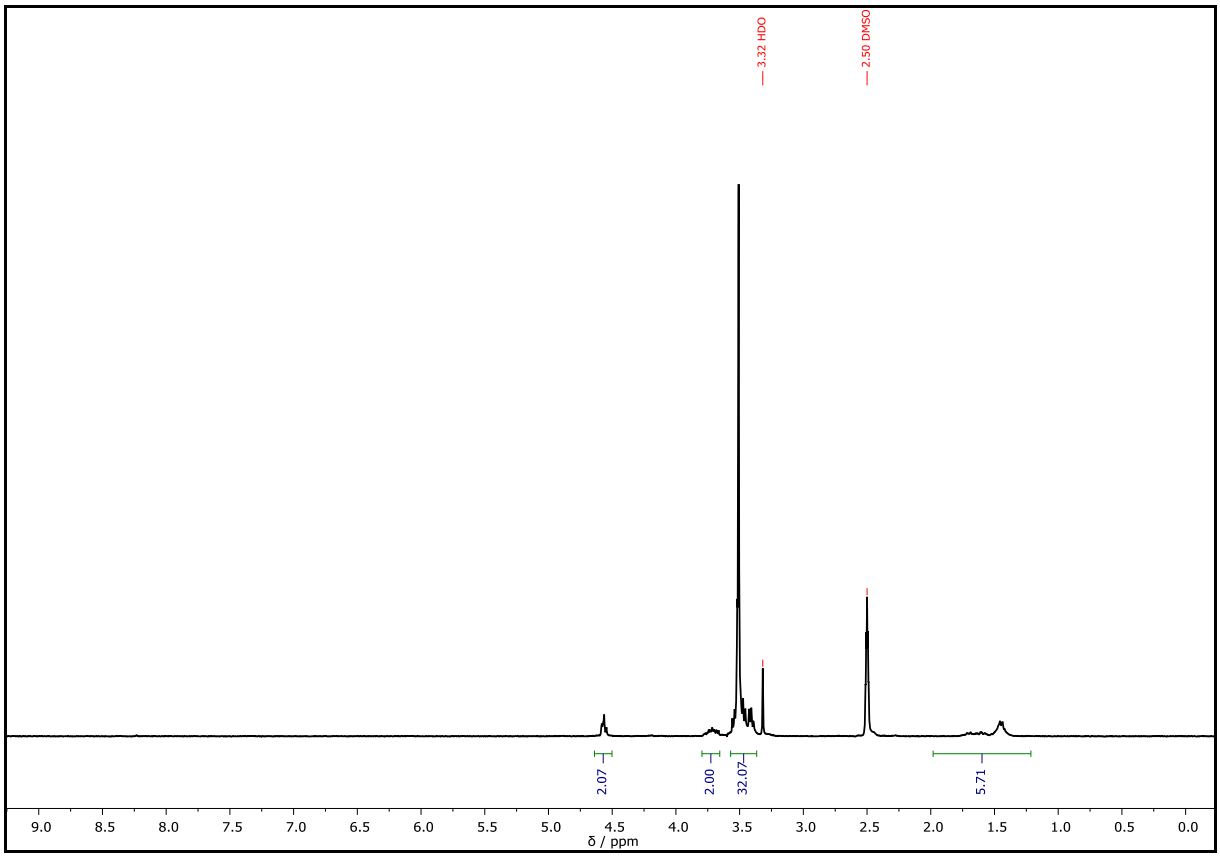

Supplementary Figure 40: ^{1}H NMR spectrum of **P17** recorded at 300 MHz in DMSO-d_6.

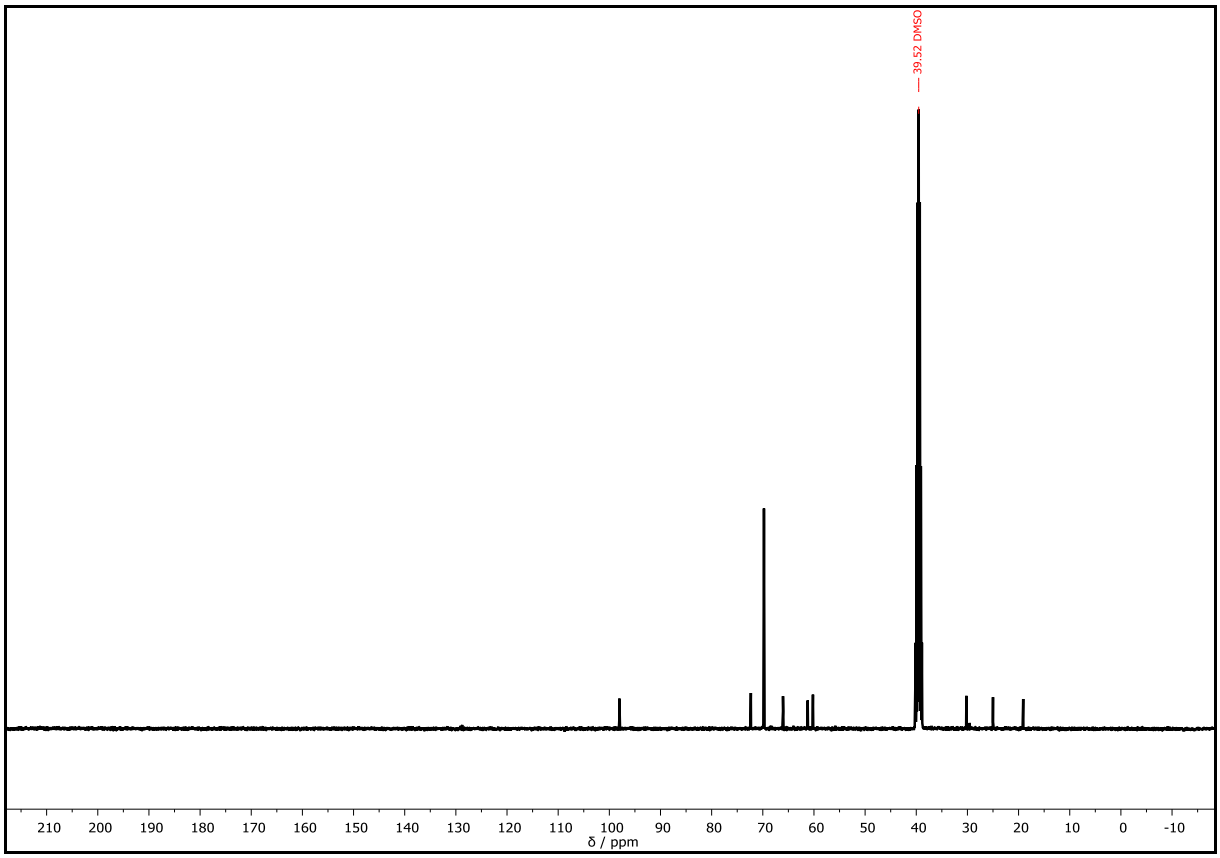

Supplementary Figure 41: ^{13}C NMR spectrum of **P17** recorded at 101 MHz in DMSO-d_6.

Macrocyclic sulfate – P18[l]

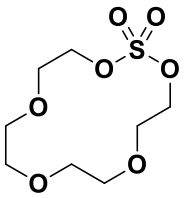

Chemical Formula: $C_8H_{16}O_7S$
Exact Mass: 256.0617 Da
Molecular Weight: 256.2690 Da

The synthesis was performed according to a procedure of JIANG *et al*.[318] Thionyl chloride (375 mL, 306 mg, 5.15 mmol, 1.98 eq) was dissolved in DCM (25 mL) and added over one hour at 0 °C to a solution of tetra(ethylene glycol) (448 µL, 504 mg, 2.59 mmol, 1.00 equiv.), DIPEA (2.16 mL, 1.56 g, 12.4 mmol, 4.77 equiv.) and DMAP (15.6 mg, 125 µmol, 0.05 equiv.) in DCM (100 mL) under argon atmosphere. After stirring for an additional hour at the same temperature, cold brine (100 mL) was added to quench the reaction, after full conversion, as indicated by GC-MS analysis (Supplementary Figure 43). The organic layer was dried over anhydrous sodium sulfate, filtered, the solvent was removed under reduced pressure and the macrocyclic sulfite **P18-1** was obtained in 1.03 g. SEC-ESI-MS analysis indicated the formation of macrocyclic oligomers up to the cyclic pentamer (Supplementary Table 7). Macrocyclic sulfite **P18-1** (191 mg, 0.80 mmol, 1.00 equiv.) was dissolved in a mixture of acetonitrile (8.00 mL), dichloromethane (8.00 mL) and water (12.0 mL) at 0°C. Subsequently, sodium periodate (200 mg, 0.94 mmol, 1.18 equiv.) and ruthenium trichloride ($RuCl_3$*xH_2O) (1.09 mg, 0.005 mmol, 0.006 equiv.) were added and the reaction mixture was stirred for one hour at 0 °C. The phases were separated, and the aqueous layer was extracted with dichloromethane (2 × 20 mL) after full conversion, indicated by GC-MS analysis (Supplementary Figure 43). The combined organic layers were dried over anhydrous sodium sulfate, filtered through a pad of celite and the solvent was removed under reduced pressure. Purification of the crude product *via* column chromatography (cyhex:EA = 1:1) yielded the macrocyclic sulfate **P18** (196 mg, 0.76 mmol, 95.6%) as a brownish solid.

^{1}H NMR (300 MHz, $CDCl_3$): δ / ppm = 4.45 (t, *J* = 5.0 Hz, 4H, CH_2OS), 3.82 (t, *J* = 5.0 Hz, 4H, CH_2CH_2OS), 3.70 – 3.60 (m, 8H, CH_2O).

[l] This molecule was synthesized by PHILIPP BOHN during the Master thesis.[618].

^{13}C NMR (126 MHz, $CDCl_3$): δ / ppm = 72.27, 70.79, 70.73, 69.51.

HRMS (ESI) of $C_8H_{16}O_7S$ $[M+Na]^+$ *m/z* calc. 279.0501, found 279.0511.

The masses up to the cyclic pentamer were also observed with SEC-ESI-MS analysis (Supplementary Table 7 and Supplementary Table 8).

IR (ATR platinum diamond) $\tilde{\nu}$ / cm^{-1} = 2867.0, 1451.7, 1388.2, 1294.1, 1249.2, 1190.1, 1113.8, 1009.2, 975.2, 917.0, 873.5, 841.2, 812.1, 735.0, 601.9, 539.5, 468.1.

R_f = 0.22 (cyhex:EA = 1:1).

Đ (System II) = 1.00

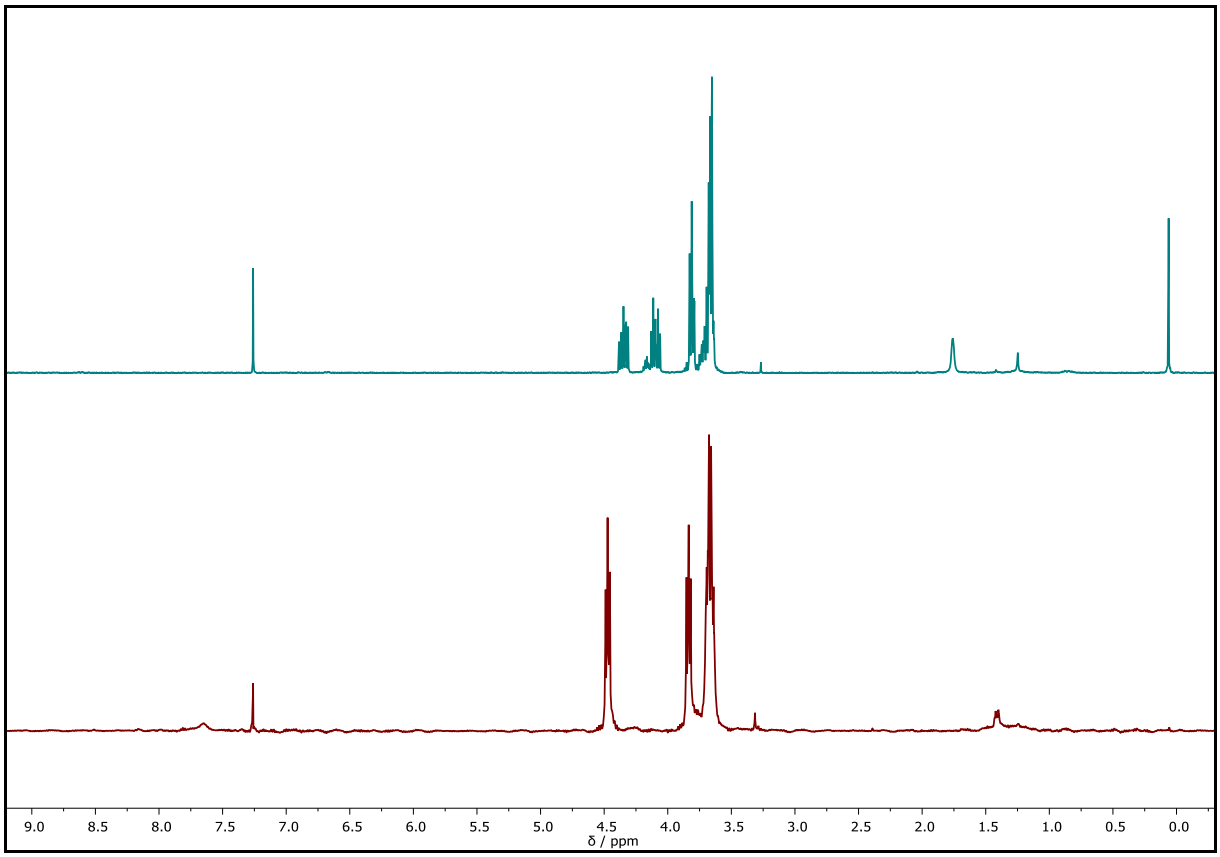

Supplementary Figure 42: Stacked ^{1}H NMR spectra of **P18-1** and **P18** recorded at 300 MHz in $CDCl_3$.

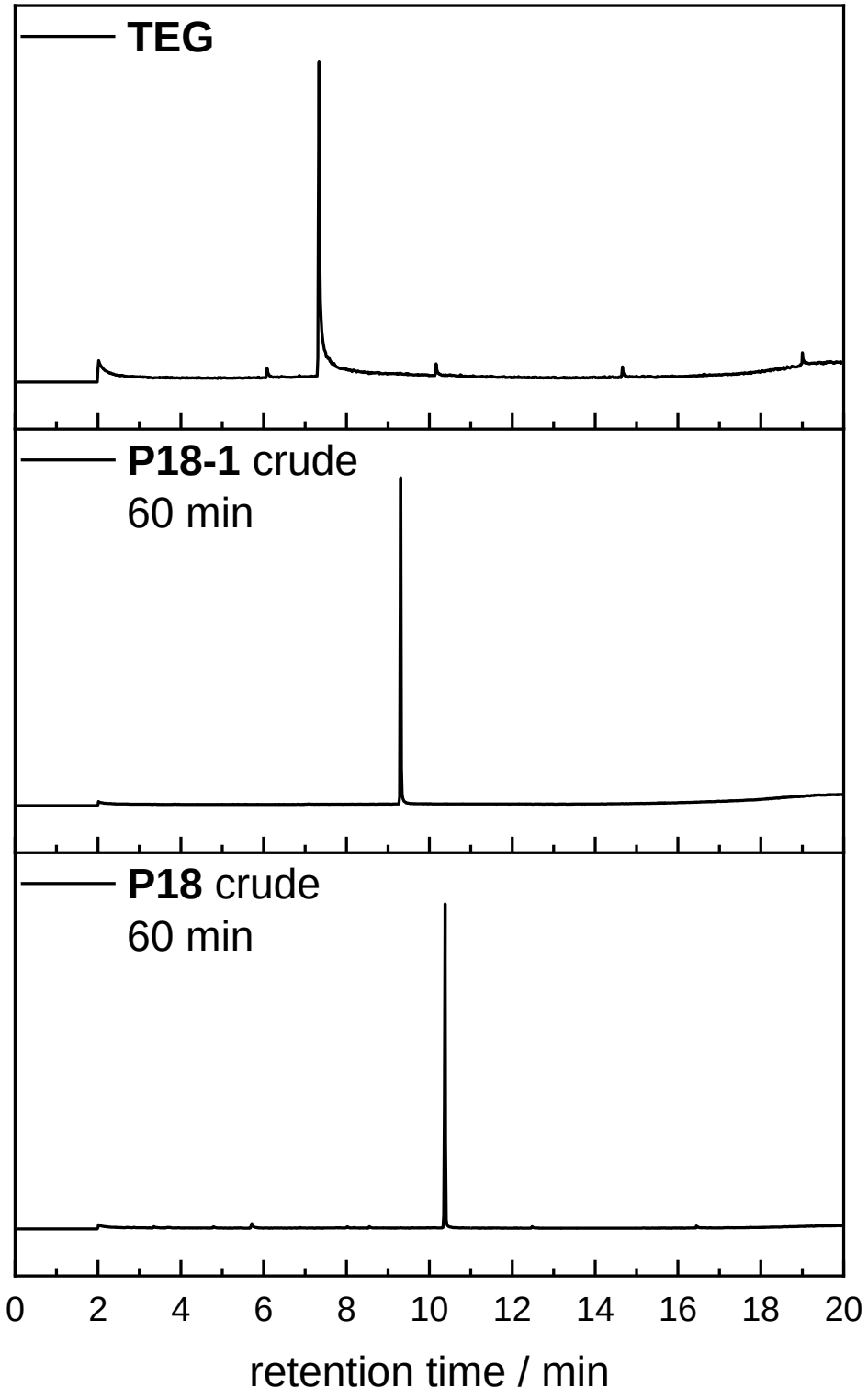

Supplementary Figure 43: GC-MS monitoring of the macrocyclization of TEG and the oxidation of **P18-1** affording the macrocyclic sulfate **P18**.

Supplementary Table 7: SEC-ESI-MS results of the macrocyclic sulfite **P18-1**		
Formular	M calc. / Da[1]	M found / Da
$[C_{40}H_{80}O_{30}S_5+Na]^+$	1223.3154	1223.3242
$[C_{32}H_{64}O_{24}S_4+Na]^+$	983.2495	983.2565
$[C_{24}H_{48}O_{18}S_3+Na]^+$	743.1828	743.1892
$[C_{16}H_{32}O_{12}S_2+Na]^+$	503.1161	503.1232
$[C_8H_{16}O_6S+Na]^+$	263.0552	263.0562
[1] mMass Version 5.5.0 was used for the mass calculations		

Supplementary Table 8: SEC-ESI-MS results of the MCS **P18**		
Formular	M calc. / Da[1]	M found / Da
$[C_{40}H_{80}O_{35}S_5+Na]^+$	1303.2900	1303.3005
$[C_{32}H_{64}O_{28}S_4+Na]^+$	1047.2326	1047.2367
$[C_{24}H_{48}O_{21}S_3+Na]^+$	791.1676	791.1750
$[C_{16}H_{32}O_{14}S_2+Na]^+$	535.1060	535.1133
$[C_8H_{16}O_7S+Na]+$	279.0501	279.0511
[1] mMass Version 5.5.0 was used for the mass calculations		

Supplementary Table 9: ESI-MS results of the nucleophilic ring opening of MCS **P18** with **P5**		
Formular	M calc. / Da[1]	M found / Da
$[Bn(EG)_8OH+K]^+$	499.2300	499.2289
$[Bn(EG)_8OH+Na]^+$	483.2566	483.2550
$[Bn(EG)_8OH+NH4]^+$	478.3012	478.3000
$[Bn(EG)_8OH+H]^+$	461.2747	461.2733
[1] mMass Version 5.5.0 was used for the mass calculations		

6.3.2. Experimental procedures of chapter 4.1.1.7

α-Benzyl-ω-tosyl octa(ethylene glycol) – P19

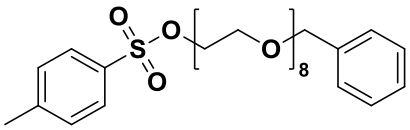

Chemical Formula: $C_{30}H_{46}O_{11}S$
Exact Mass: 614.2761 Da
Molecular Weight: 614.7470 Da

The monobenzyl octa(ethylene glycol) tosylate **P19** was prepared according to the procedure of BRUCE *et al*.[273] Monobenzyl octa(ethylene glycol) (2.75 g, 5.97 mmol, 1.00 equiv.), sodium hydroxide (836 mg, 20.9 mmol, 3.50 equiv.), *p*-toluenesulfonyl chloride (1.37 g, 7.16 mmol, 1.20 equiv.) were used. Purification of the crude product *via* column chromatography (EA) yielded the monobenzyl octa(ethylene glycol) tosylate **P19** (1.87 g, 3.04 mmol, 50.9%) as a colorless, oil. The product was dried under high vacuum, stored under argon atmosphere, and shielded from light until further use.

^{1}H NMR (400 MHz, DMSO-d_6): δ / ppm = 7.78 (d, J = 8.3 Hz, 2H, CH_{Ar}^1), 7.48 (d, J = 8.1 Hz, 1H, CH_{Ar}^2), 7.38 – 7.24 (m, 5H, CH_{Ar}^3), 4.48 (s, 2H, CH_2^4), 4.13 – 4.06 (m, 2H, CH_2^5), 3.59 – 3.42 (m, 30H, CH_2^6), 2.42 (s, 3H, CH_3^7).

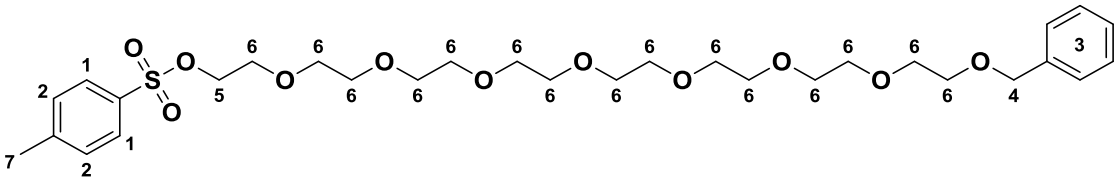

^{13}C NMR (101 MHz, DMSO-d_6): δ / ppm = 144.87 (C_q^1), 138.48 (C_q^2), 132.41 (C_q^3), 130.12 (CH^4), 128.19 (CH^5), 127.61 (CH^5), 127.46 (CH^5), 127.34 (CH^5), 72.01 (CH_2^6), 69.97 (CH_2^7), 69.83 (CH_2^8), 69.76 (CH_2^8), 69.69 (CH_2^8), 69.64 (CH_2^8), 69.12 (CH_2^8), 67.87 (CH_2^8), 21.07 (CH_3^9).

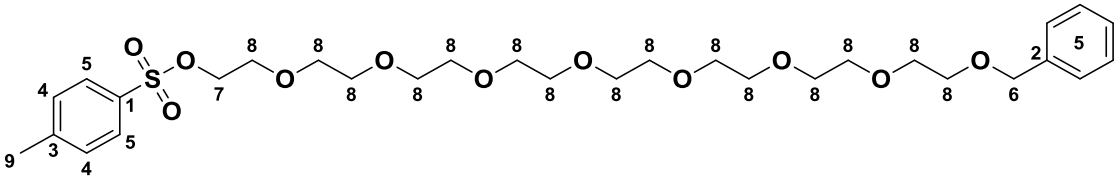

HRMS (FAB) of $C_{30}H_{47}O_{11}S_1$ $[M+H]^+$ calcd. 615.2839, found 615.2841.

IR (ATR platinum diamond) v / cm^{-1} = 2864.8, 1597.3, 1452.6, 1352.3, 1292.0, 1248.4, 1175.9, 1095.9, 1017.7, 920.2, 816.8, 747.5, 699.4, 663.4, 554.7.

R_f = 0.31 (EA).

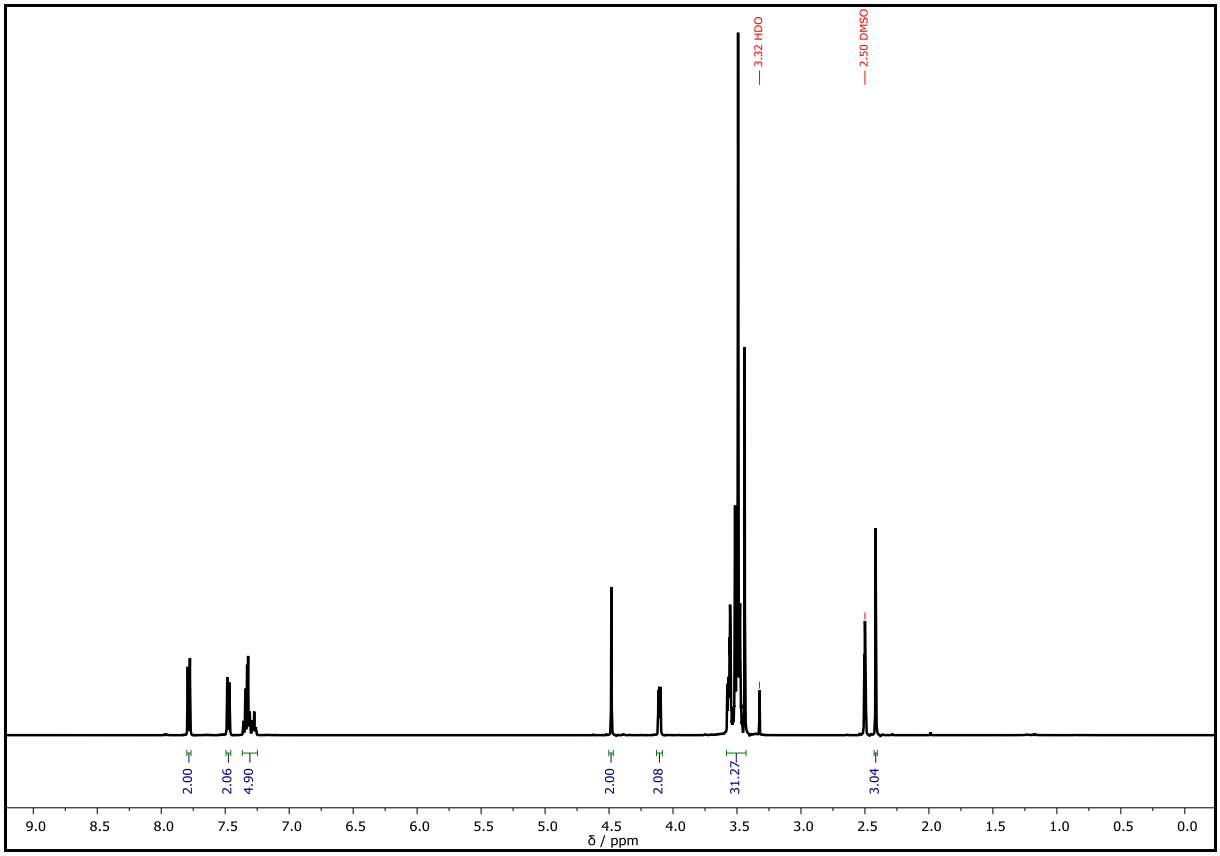

Supplementary Figure 44: ^{1}H NMR spectrum of **P19** recorded at 400 MHz in DMSO-d_6.

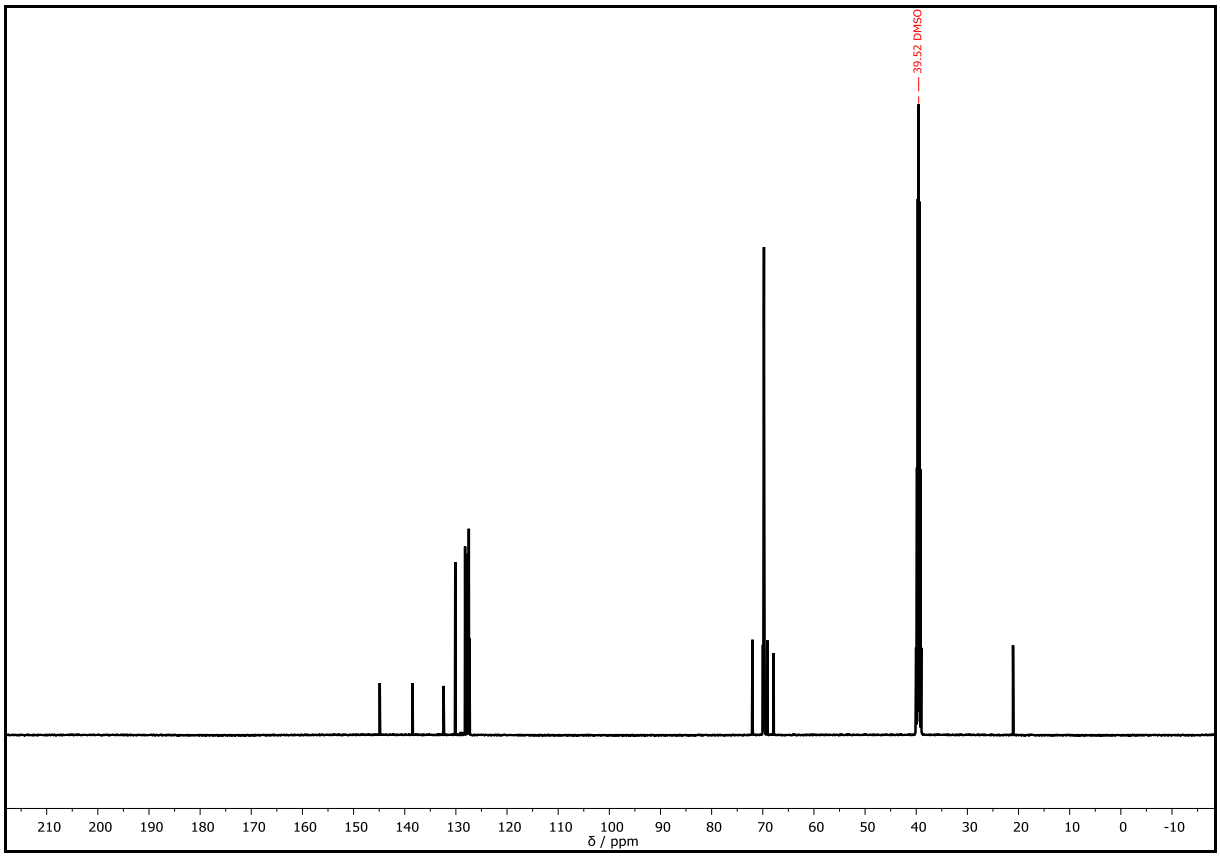

Supplementary Figure 45 ^{13}C NMR spectrum of **P19** recorded at 101 MHz in DMSO-d_6.

α-Benzyl-ω-tetrahydropyranyl hexadeca(ethylene glycol) – P20

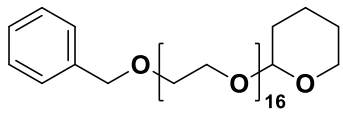

Chemical Formula: $C_{44}H_{80}O_{18}$
Exact Mass: 896.5345 Da
Molecular Weight: 897.1060 Da

The doubly protected hexadeca(ethylene glycol) **P20** was prepared using the procedure described above for the synthesis of the doubly protected octa(ethylene glycol) **P10**.[273] The reaction was performed in a 15.6 mmol scale using the monobenzyl octa(ethylene glycol) tosylate **P7** and the mono(tetrahydropyranyl) octa(ethylene glycol) **P17**. Purification of the crude product *via* column chromatography (DCM:acetone = 6:1 → 1:1) yielded the product **P20** as a yellowish solid (6.01 g, 6.70 mmol, 43.0%).

^{1}H NMR (400 MHz, DMSO-d_6): δ / ppm = 7.39 – 7.22 (m, 5H, CH_{Ar}^1), 4.57 (t, J = 3.8 Hz, 1H, CH^2), 4.49 (s, 2H, CH_2^3), 3.79 – 3.66 (m, 2H, CH_2^4), 3.60 – 3.38 (m, 64H, CH_2^5), 1.77 – 1.39 (m, 6H, CH_2^6).

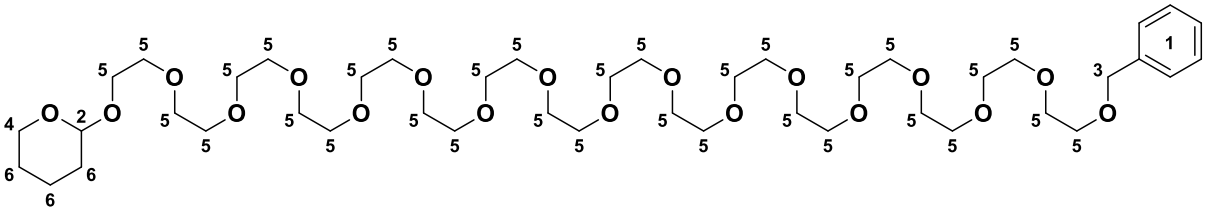

^{13}C NMR (101 MHz, DMSO-d_6): δ / ppm = 138.48 (C_q^1), 128.19 (CH_{Ar}^2), 127.45 (CH_{Ar}^2), 127.34 (CH_{Ar}^3), 98.03 (CH^4), 72.00 (CH_2^5), 69.83 (CH_2^6), 69.77 (CH_2^6), 69.71 (CH_2^6), 69.12 (CH_2^6), 66.05 (CH_2^7), 61.21 (CH_2^7), 30.20 (CH_2^8), 25.00 (CH_2^8), 19.09 (CH_2^8).

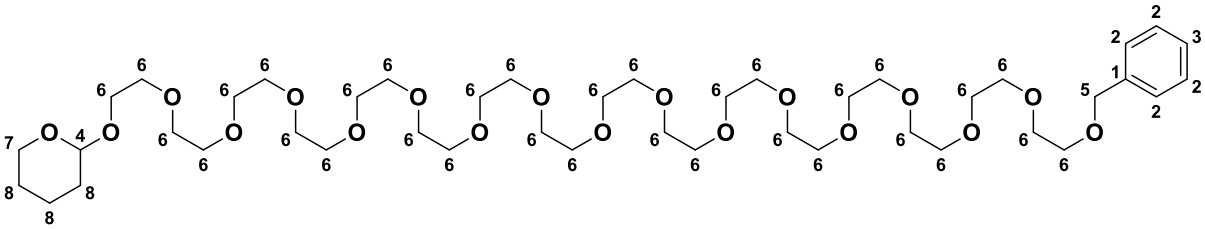

HRMS (ESI) of $C_{44}H_{80}O_{18}$ $[M+NH_4]^+$ *m/z* calc. 914.5683, found 914.5454; $[M+Na]^+$ *m/z* calc. 919.5208, found 919.5237; $[M+K]^+$ *m/z* calc. 935.4976, found 935.4952.

The mass of the α-benzyl-ω-hydroxy hexadeca(ethylene glycol) was found as most intensive signal. $C_{39}H_{72}O_{17}$ $[M+H]^+$ *m/z* calc. 813.4842, found 913.4815.

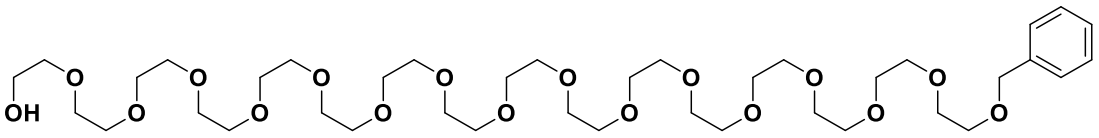

Chemical Formula: $C_{39}H_{72}O_{17}$
Exact Mass: 812.4770 Da

IR (ATR platinum diamond) $\tilde{\nu}$ / cm^{-1} = 2864.7, 1720.4, 1454.0, 1349.0, 1293.7, 1250.0, 1201.4, 1095.5, 1032.9, 987.8, 945.8, 870.5, 814.0, 741.2, 699.7, 520.0.

R_f = 0.29 (EA:MeOH = 9:1).

Đ (System II) = 1.00

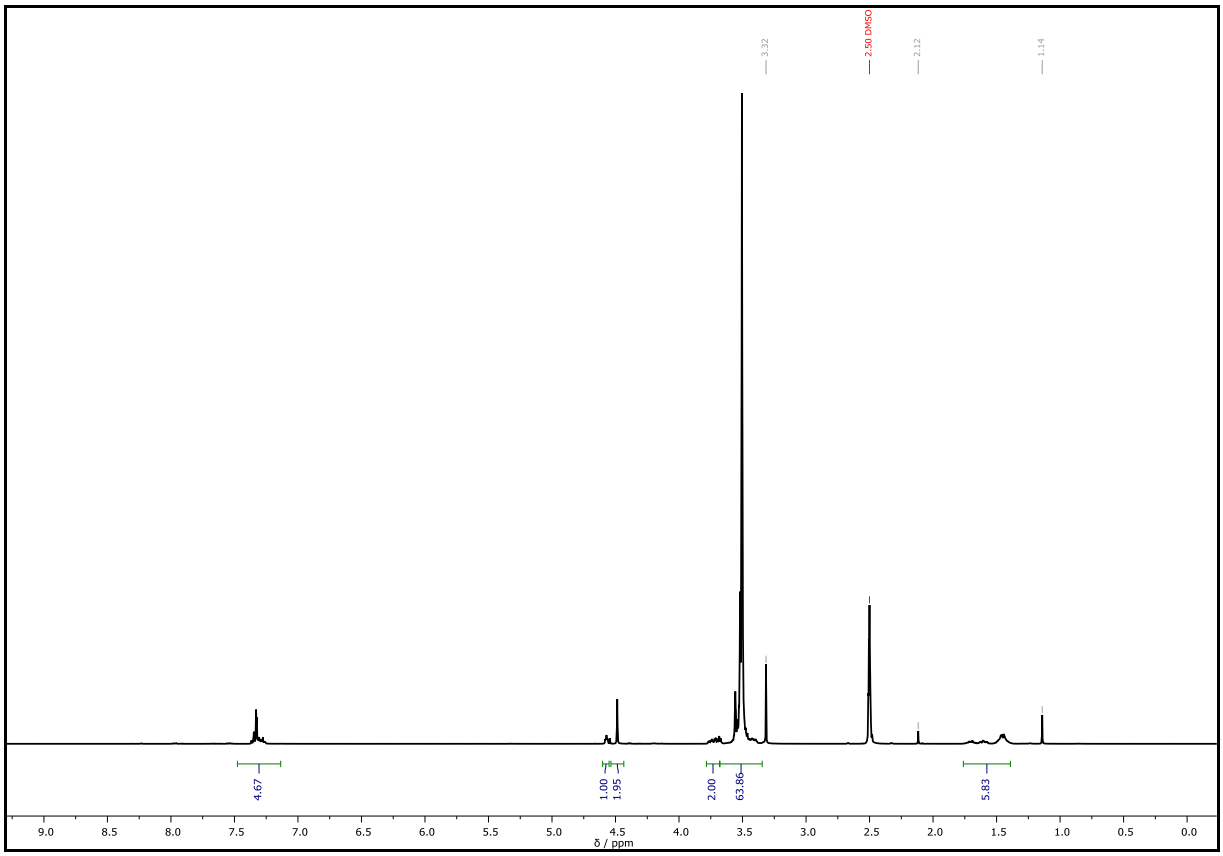

Supplementary Figure 46: ^{1}H NMR spectrum of **P20** recorded at 400 MHz in DMSO-d_6.

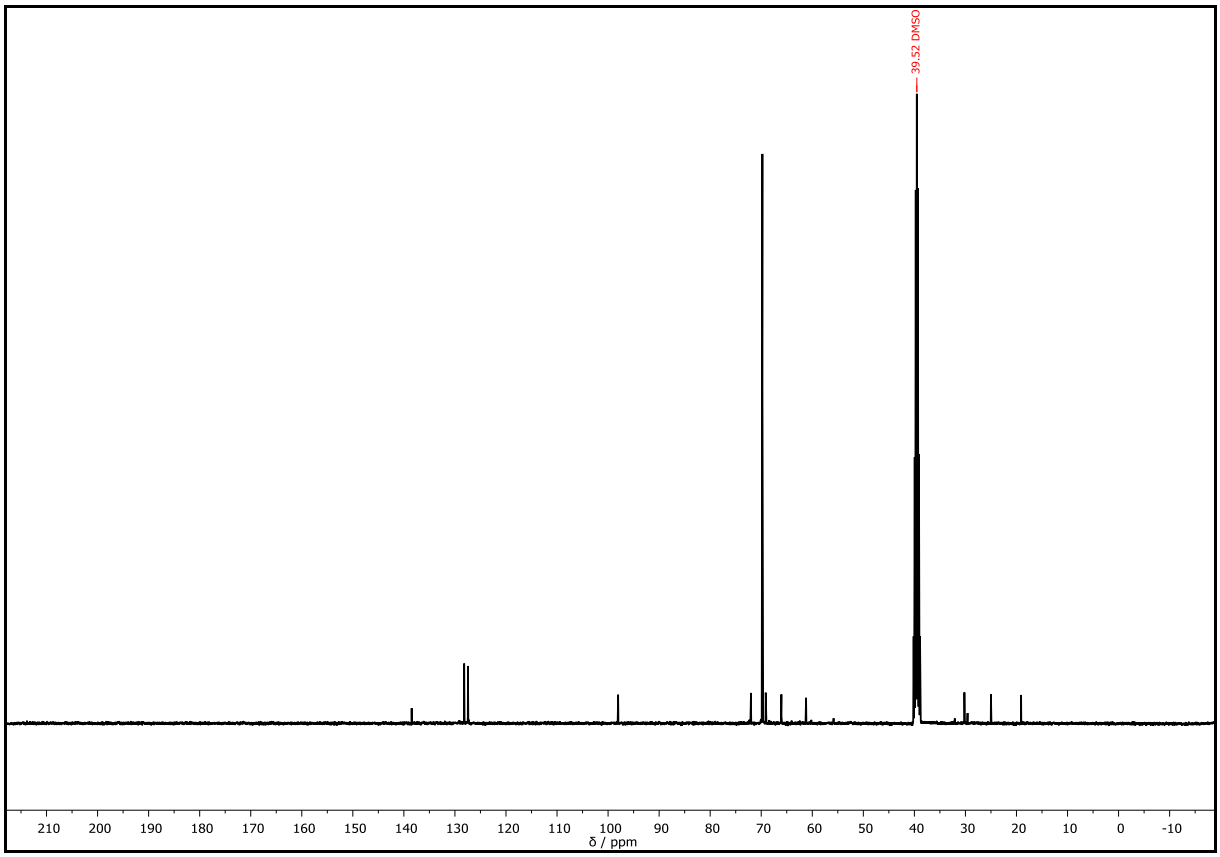

Supplementary Figure 47: ^{13}C NMR spectrum of **P20** recorded at 101 MHz in DMSO-d_6.

The synthesis of **P20** was repeated on a 14 g scale and the purification *via* column chromatography is provided in the following.

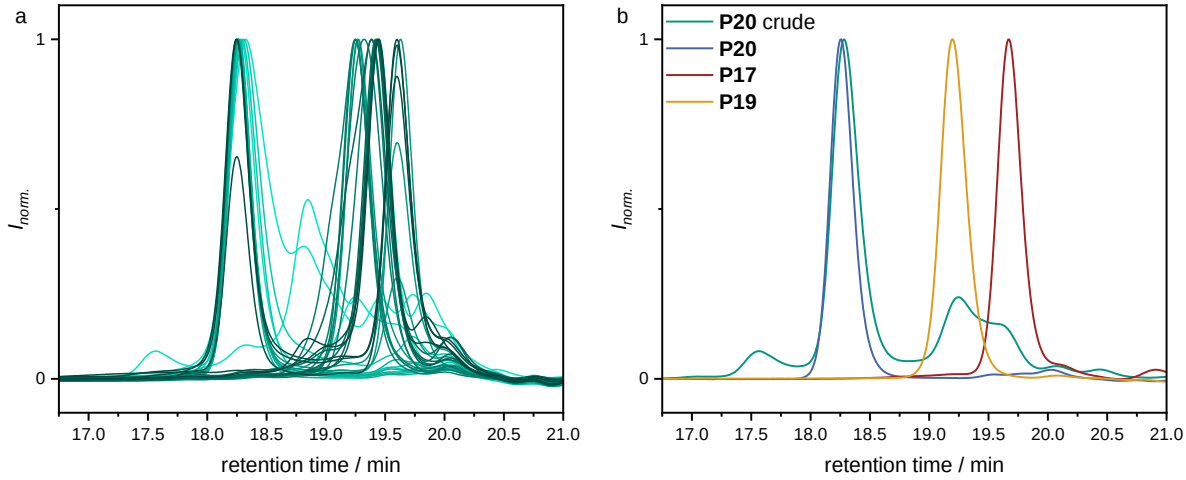

Supplementary Figure 48: **a** SEC of individual fractions obtained from the purification process of **P20** *via* column chromatography; **b** comparison of the SEC traces of **P20** before (green trace) and after purification (blue trace) and the starting materials **P17** (red trace) and **P19** (yellow trace).

Supplementary Table 10 SEC data of P20

cc 1	*m* / mg	M_n / Da	M_w / Da	M_z / Da	*Đ*	purity / %
F1	652	*n.a.*	*n.a.*	*n.a.*	*n.a.*	*n.a.*
F2	64.0	*n.a.*	*n.a.*	*n.a.*	*n.a.*	*n.a.*
F3	90.5	*n.a.*	*n.a.*	*n.a.*	*n.a.*	*n.a.*
F4	111	*n.a.*	*n.a.*	*n.a.*	*n.a.*	*n.a.*
F5	189	*n.a.*	*n.a.*	*n.a.*	*n.a.*	*n.a.*
F6	87.0	*n.a.*	*n.a.*	*n.a.*	*n.a.*	*n.a.*
F7	70.9	*n.a.*	*n.a.*	*n.a.*	*n.a.*	*n.a.*
F8	64.4	*n.a.*	*n.a.*	*n.a.*	*n.a.*	*n.a.*
F9	58.6	*n.a.*	*n.a.*	*n.a.*	*n.a.*	*n.a.*
F10	80.0	*n.a.*	*n.a.*	*n.a.*	*n.a.*	*n.a.*
F11	57.6	*n.a.*	*n.a.*	*n.a.*	*n.a.*	*n.a.*
F12	41.2	*n.a.*	*n.a.*	*n.a.*	*n.a.*	*n.a.*
F13	36.8	*n.a.*	*n.a.*	*n.a.*	*n.a.*	*n.a.*
F14	80.3	*n.a.*	*n.a.*	*n.a.*	*n.a.*	*n.a.*
F15	39.6	n.a.	n.a.	n.a.	n.a.	n.a.
F16	48.1	1200	1200	1200	1.01	5.4

Supplementary Table 11 SEC data of P20						
cc 1	*m* / mg	M_n / Da	M_w / Da	M_z / Da	*Đ*	purity / %
F17	150	1100	1100	1100	1.01	56.2
F18	231	1100	1100	1100	1.01	71.8
F19	433	1100	1100	1100	1.01	83.3
F20	1581	1100	1100	1150	1.01	87.6
F21	1613	1150	1150	1150	1.00	>99
F22	1272	1150	1150	1150	1.00	>99
F23	1445	1150	1150	1150	1.00	>99
F24	978	1150	1150	1150	1.00	>99
F25	704	1150	1150	1150	1.00	>99
F26	459	1150	1150	1150	1.00	91.3
F27	590	1150	1150	1150	1.00	75.4
F28	232	1150	1150	1150	1.01	53.7
F29	160	1150	1150	1150	1.01	48.4
F30	133	1150	1150	1150	1.01	47.2
F31	317	1150	1150	1150	1.01	36.5

Chromatograms were recorded on SEC system II. Red: fractions containing only impurities; yellow: product containing fractions with insufficient purity; green: fractions containing only product P20.

Monobenzyl hexadeca(ethylene glycol) – P21

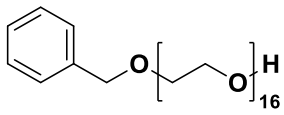

Chemical Formula: $C_{39}H_{72}O_{17}$
Exact Mass: 812.4770 Da
Molecular Weight: 812.9880 Da

The monobenzyl protected hexadeca(ethylene glycol) **P21** was prepared using the procedure described above for the synthesis of the monobenzyl protected octa(ethylene glycol) **P16**.

P20	4.00 g, 4.46 mmol, 1.00 equiv.
TsOH	8.48 mg, 44.6 µmol, 0.01 equiv.
MeOH	5.00 mL
Yield	3.61 g, 4.44 mmol, 99.7%, yellowish solid
R_f	0.26 (EA/MeOH = 4:1).
Đ (system II)	1.00

^{1}H NMR (400 MHz, DMSO-d_6): δ / ppm = 7.43 – 7.18 (m, 5H, CH_{Ar}^1), 4.56 (t, J = 5.5 Hz, 1H, OH^2), 4.49 (s, 2H, CH_2^3), 3.63 – 3.38 (m, 64H, CH_2^4).

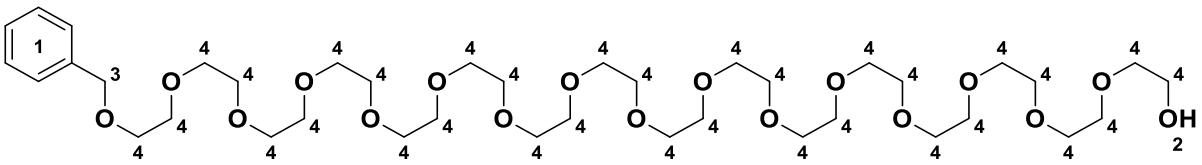

^{13}C NMR (101 MHz, DMSO-d_6): δ / ppm = 138.48 (C_q^1), 128.19 (CH_{Ar}^2), 127.45 (CH_{Ar}^2), 127.34 (CH_{Ar}^3), 72.33 (CH_2^4), 72.00 (CH_2^5), 69.83 (CH_2^4), 69.77 (CH_2^4), 69.12 (CH_2^4), 60.20 (CH_2^4).

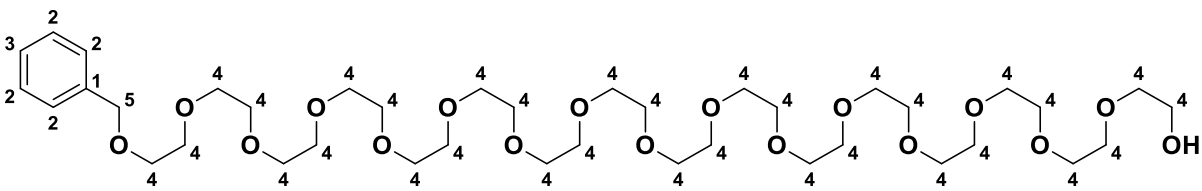

HRMS (ESI) of $C_{39}H_{72}O_{17}$ $[M+NH_4]^+$ *m/z* calc. 830.5108, found 830.5112; $[M+Na]^+$ *m/z* calc. 835.4662, found 835.4664; $[M+K]^+$ *m/z* calc. 851.4401, found 851.4398.

IR (ATR platinum diamond) ν / cm^{-1} = 3474.3, 2863.9, 1719.7, 1638.1, 1453.2, 1348.7, 1294.3, 1246.2, 1095.7, 946.6, 847.0, 741.8, 699.9, 535.9.

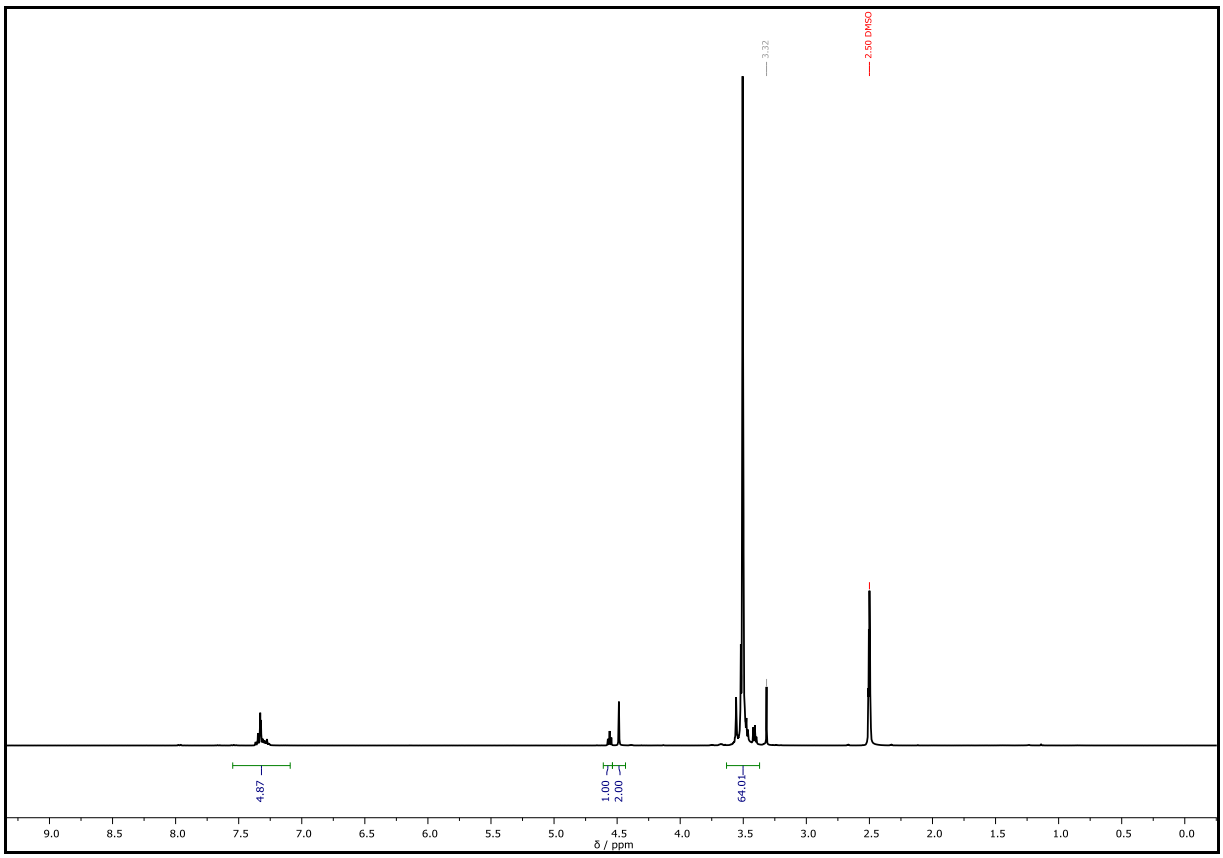

Supplementary Figure 49: ^{1}H NMR spectrum of **P21** recorded at 400 MHz in DMSO-d_6.

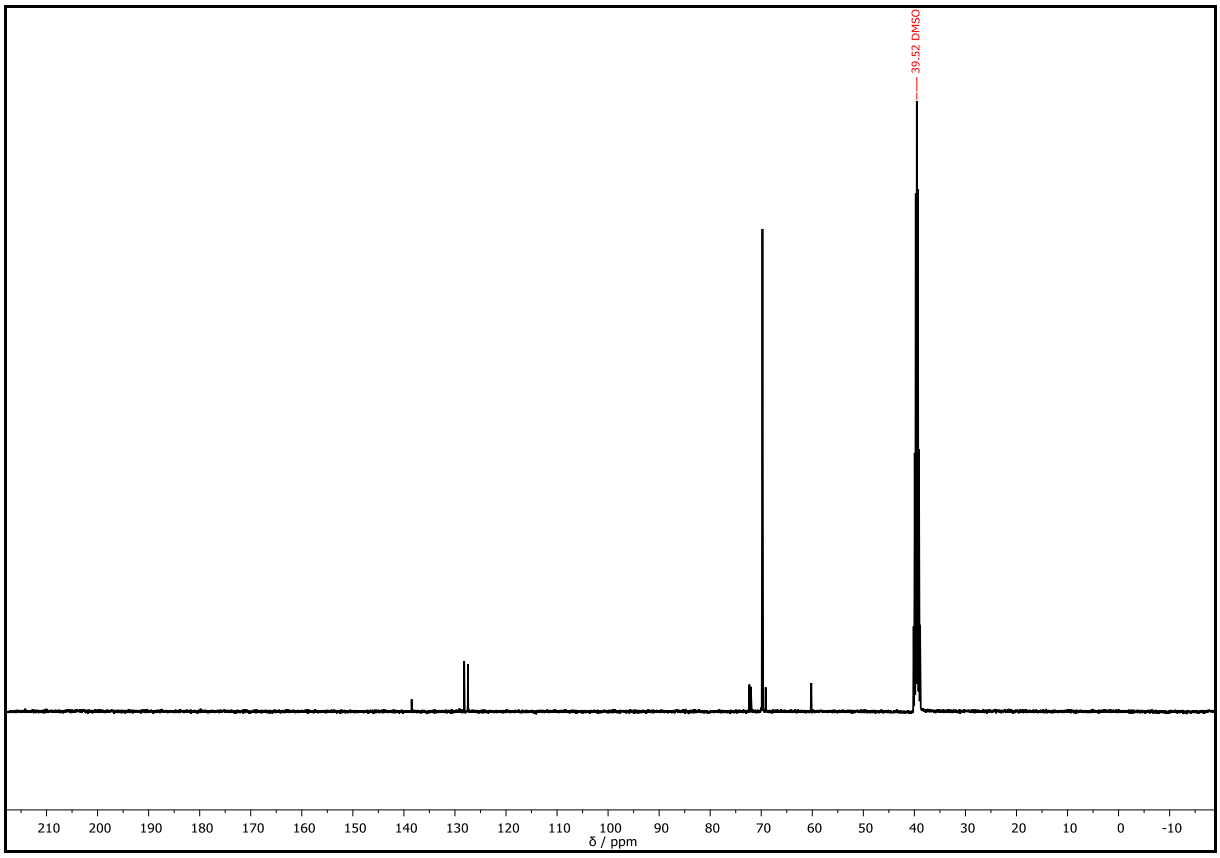

Supplementary Figure 50: ^{13}C NMR spectrum of **P21** recorded at 101 MHz in DMSO-d_6.

α-Benzyl-ω-methyl hexadeca(ethylene glycol) – P22

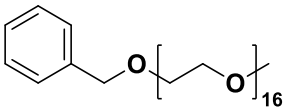

Chemical Formula: $C_{40}H_{74}O_{17}$
Exact Mass: 826.4926 Da
Molecular Weight: 827.0150 Da

NaH (177 mg, 4.43 mmol, 1.20 equiv., dispersed in 60% mineral oil) was added to monobenzyl hexadeca(ethylene glycol) **P21** (2.30 mL, 3.00 g, 3.69 mmol, 1.00 equiv.) dissolved in anhydrous THF (38 mL) at 0 °C under argon-atmosphere. Methyl iodide (5.24 g, 36.9 mmol, 10.0 equiv.) was added dropwise and the reaction mixture was stirred over night at room temperature. The solution was cooled to 0 °C and water (38 mL) was added to quench the excess of NaH. Subsequently, the mixture was extracted with EA, and the aqueous phase was further extracted with DCM (3 × 20 mL). The combined organic layers were dried over anhydrous sodium sulfate, filtered, and concentrated under reduced pressure. Purification of the crude product *via* column chromatography (EA:MeOH = 9:1) yielded the α-benzyl-ω-methyl hexadeca(ethylene glycol) **P22** as a yellowish solid in 29.7% (908 mg, 1.10 mmol).

^{1}H NMR (400 MHz, $CDCl_3$): δ / ppm = ^{1}7.36 – 7.27 (m, 5H, CH_{Ar}^{1}), 4.57 (s, 2H, CH_2^{2}), 3.78 – 3.58 (m, 62H, CH_2^{3}), 3.57 – 3.53 (m, 2H, CH_2^{4}), 3.38 (s, 3H, CH_3^{5}).

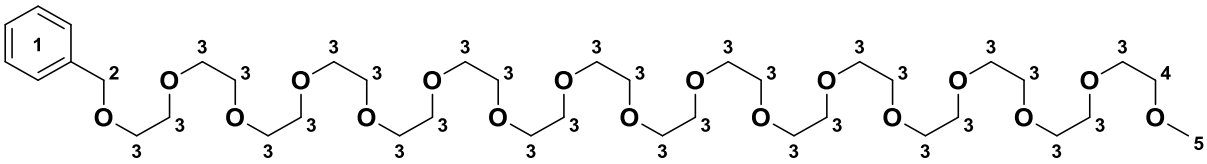

^{13}C NMR (101 MHz, $CDCl_3$): δ / ppm = 128.50 (CH_{Ar}^{2}), 127.89 (CH_{Ar}^{2}), 127.73 (CH_{Ar}^{3}), 73.39 (CH_2^{4}), 72.09 (CH_2^{5}), 70.76 (CH_2^{6}), 70.72 (CH_2^{6}), 69.59 (CH_2^{6}), 59.18 (CH_3^{7}).

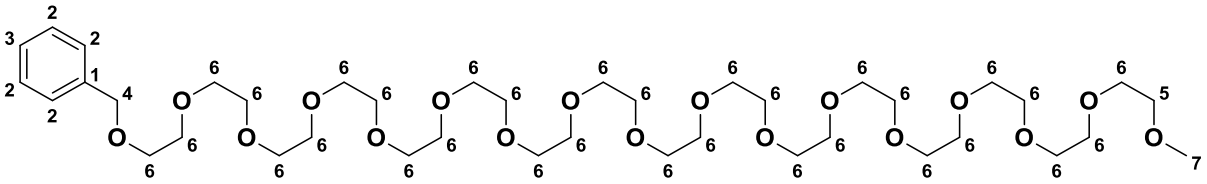

Note that C_q^{1} is not visible in the ^{13}C spectra due to low sample concentration.

HRMS (ESI) of $C_{40}H_{74}O_{17}$ $[M+H]^+$ *m/z* calc. 827.4999, found 827.4978; $[M+NH_4]^+$ *m/z* calc. 844.5264, found 844.5231; $[M+K]^+$ *m/z* calc. 865.4558, found 865.4519.

R_f = 0.16 (EA:MeOH = 9:1).

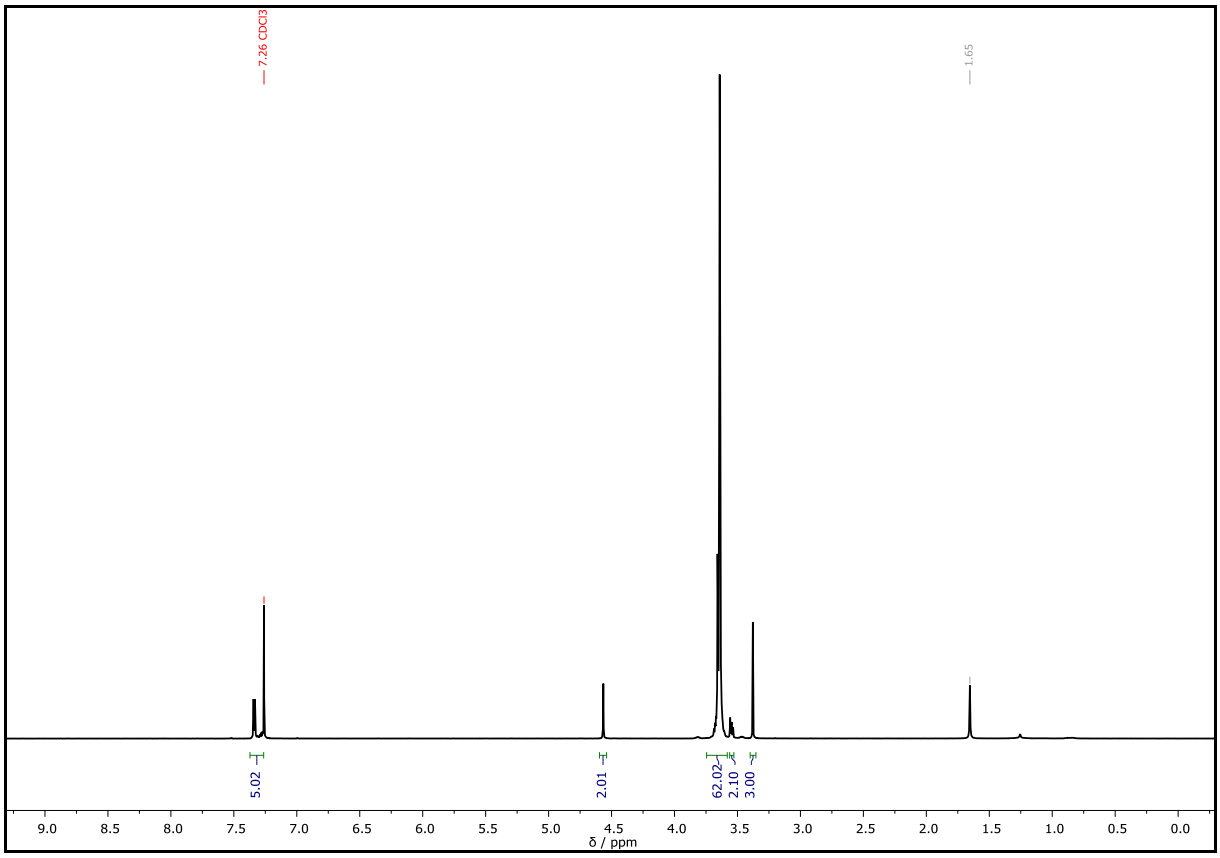

Supplementary Figure 51: ^{1}H NMR spectrum of **P22** recorded at 400 MHz in $CDCl_3$.

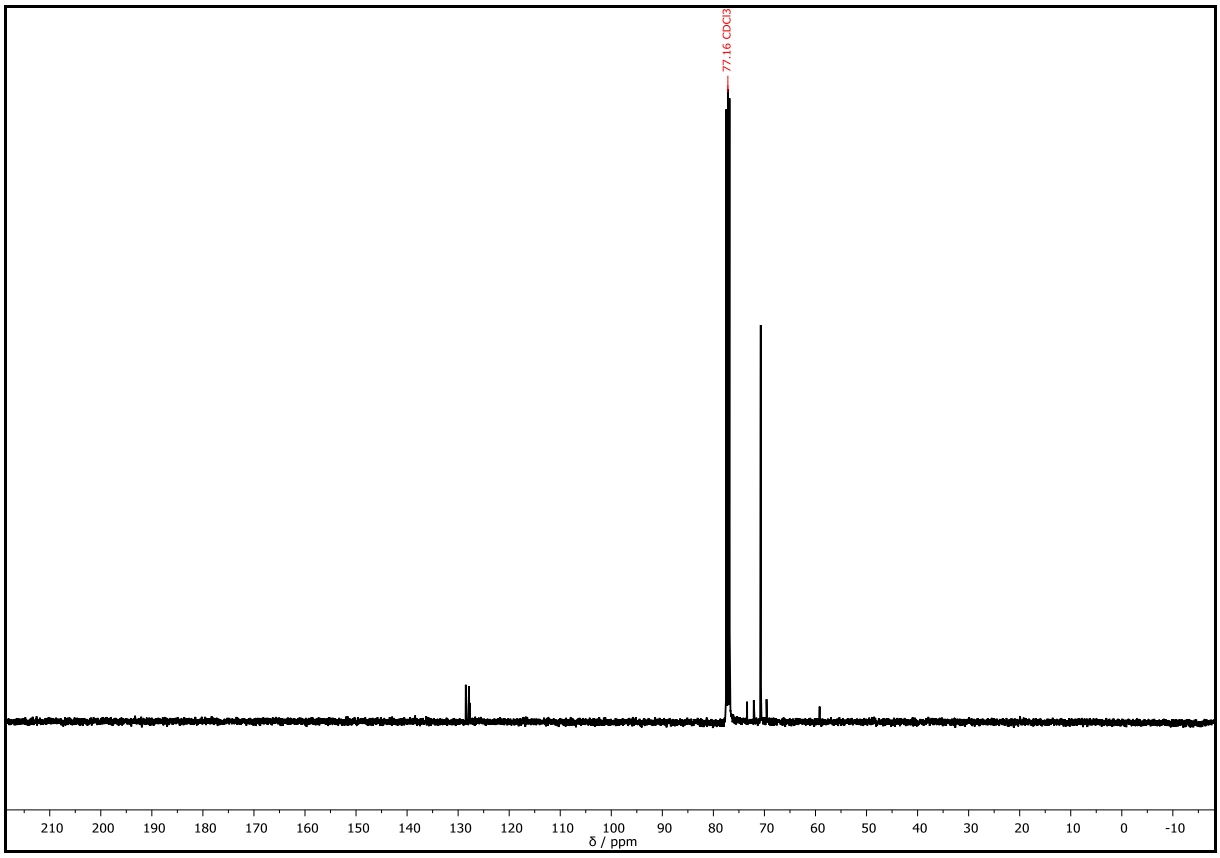

Supplementary Figure 52: ^{13}C NMR spectrum of **P22** recorded at 101 MHz in $CDCl_3$.

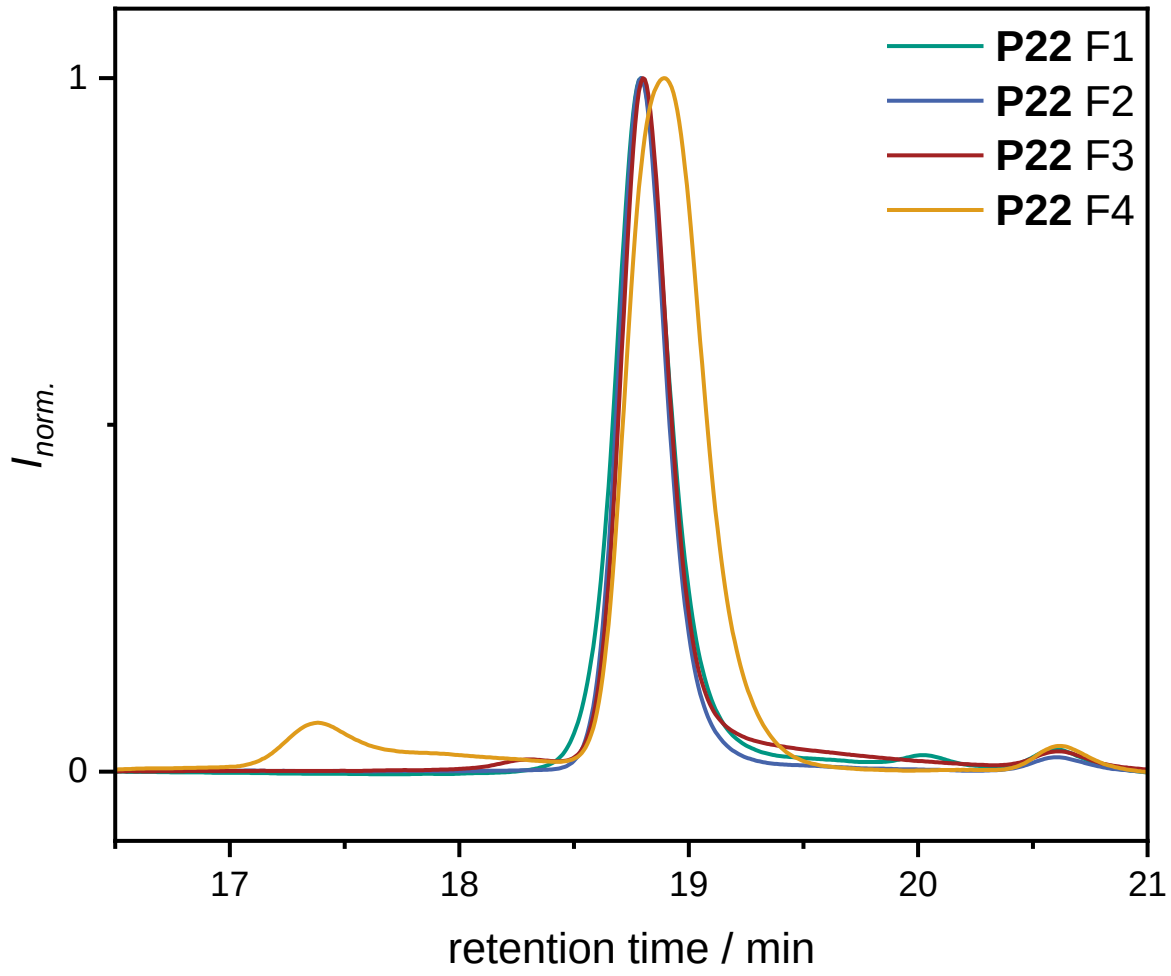

Supplementary Figure 53: SEC traces of **P22** after column chromatography. F2 showed the narrowest peak and was used for further synthesis. Compared to F1, F2 shows a broadening towards higher and lower retention times and a second peak around 20 min. The chromatogram for F3 exhibits an impurity signal towards lower and a tailing towards higher retention times. A broad impurity signal is observed in F4. Furthermore, the signal shows a higher distribution and is shifted towards higher retention times.

Monomethyl hexadeca(ethylene glycol) – P23

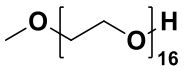

Chemical Formula: $C_{33}H_{68}O_{17}$
Exact Mass: 736.4457 Da
Molecular Weight: 736.8900 Da

α-Benzyl-ω-methyl hexadeca(ethylene glycol) **P22** (908 mg, 1.10 mmol, 1.00 equiv.) was dissolved in ethanol (20 mL) and palladium on carbon (90.8 mg, 10 wt%) was added. The reaction mixture was flushed with hydrogen (balloon) and stirred under hydrogen-atmosphere over night at room temperature. Afterwards, the mixture was filtered through a pad of Celite® to remove the heterogeneous catalyst and the filter cake was washed with methanol. The solvent was evaporated under reduced pressure yielding the monomethyl hexadeca(ethylene glycol) **P23** as a yellowish solid (789 mg, 954 µmol, 97.6%).

^{1}H NMR (400 MHz, $CDCl_3$): δ / ppm = 3.73 – 3.69 (m, 2H, CH_2^1), 3.67 – 3.61 (m, 58H, CH_2^2), 3.61 – 3.58 (m, 2H, CH_2^3), 3.55 – 3.51 (m, 2H, CH_2^4), 3.36 (s, 3H, CH_3^5).

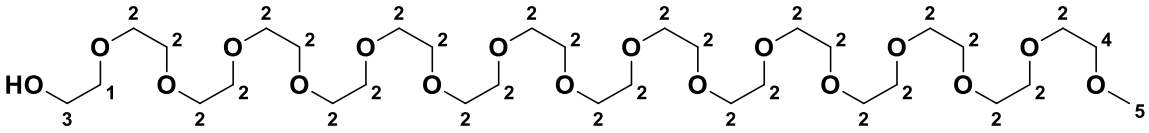

^{13}C NMR (101 MHz, $CDCl_3$): δ / ppm = 72.65 (CH_2^1), 72.06 (CH_2^2), 70.73 (CH_2^3), 70.69 (CH_2^3), 70.67 (CH_2^3), 70.64 (CH_2^3), 70.44 (CH_2^4), 61.82 (CH_2^5), 59.15 (CH_3^6).

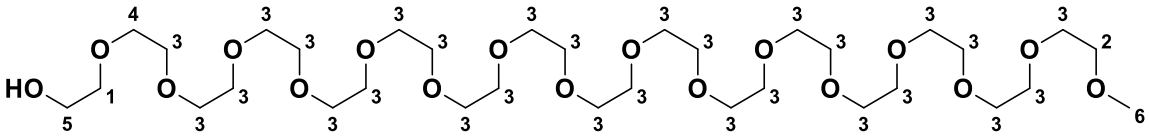

HRMS (ESI) of $C_{33}H_{68}O_{17}$ $[M+Na]^+$ *m/z* calc. 759.4349, found 759.4337; $[M+K]^+$ *m/z* calc. 775.4088, found 775.4073.

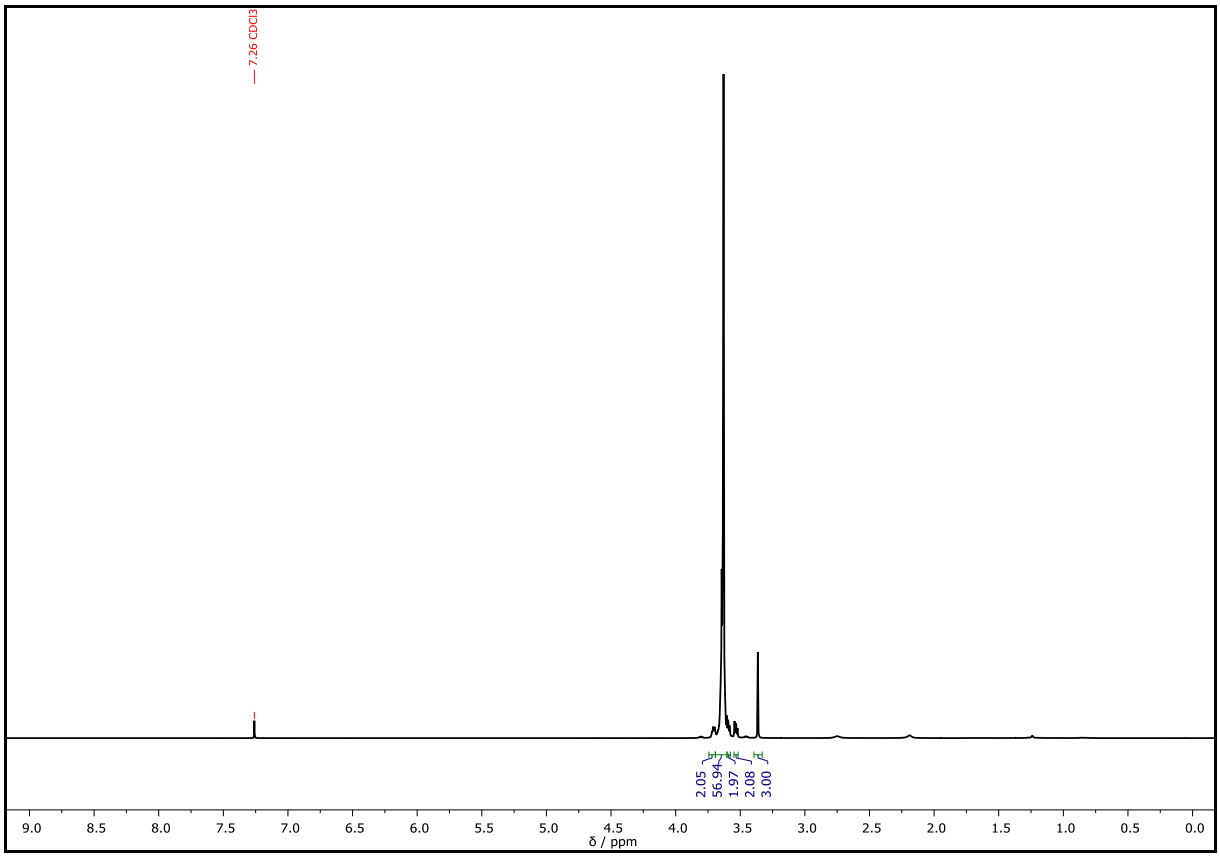

Supplementary Figure 54: ^{1}H NMR spectrum of **P23** recorded at 400 MHz in $CDCl_3$.

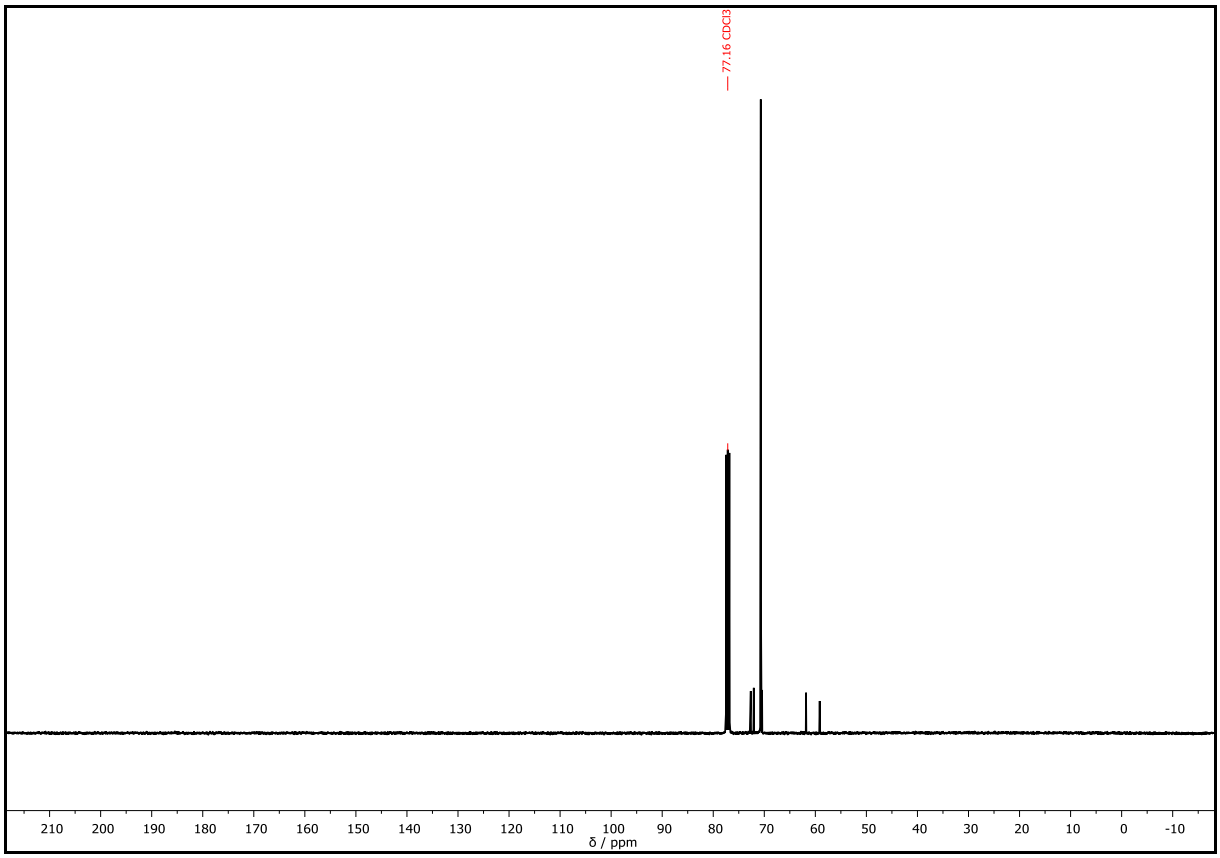

Supplementary Figure 55: ^{13}C NMR spectrum of **P23** recorded at 101 MHz in $CDCl_3$.

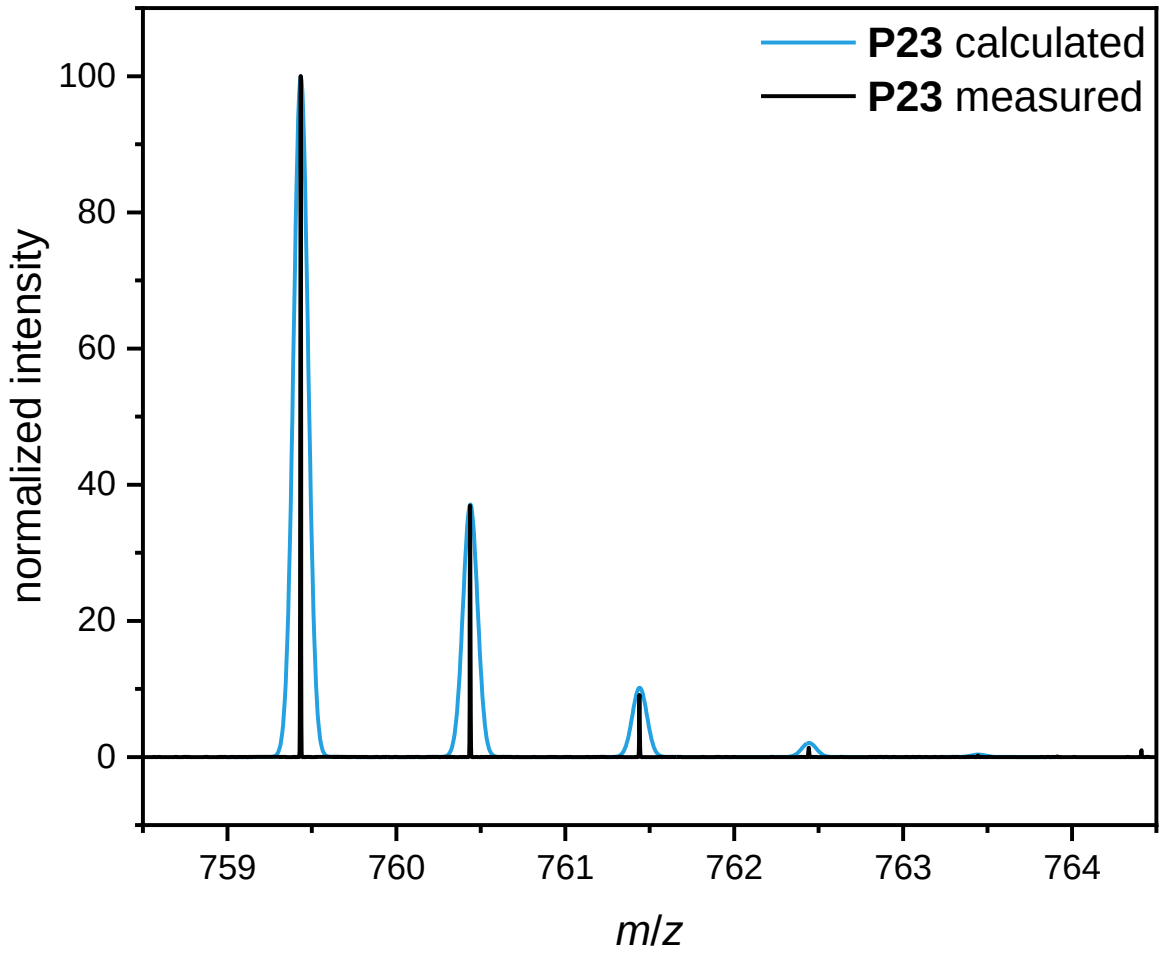

Supplementary Figure 56: Comparison of the calculated and measured isotopic pattern of the sodium adduct of **P23** ($[M+Na]^+$ *m/z* calc. 759.4349, found 759.4337).

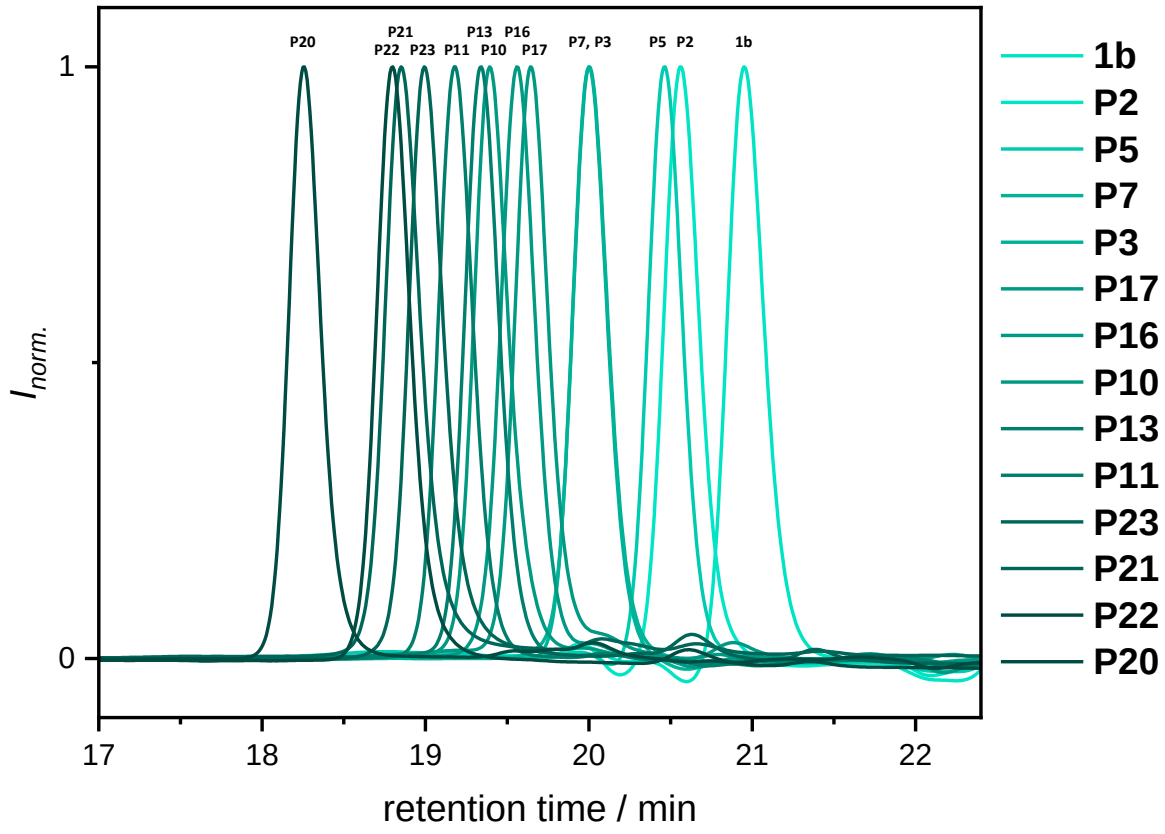

Supplementary Figure 57: SEC overview of the synthesized PEGs. The SEC traces range from the starting material tetra(ethylene glycol) at a retention time of 21.0 min in light green to the doubly protected hexadeca(ethylene glycol) **P20** at 18.3 min in dark green.

6.3.3. Experimental procedures of chapter 4.1.2

Ethyl 2-(benzyloxy)acetate – P24[I]

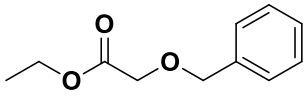

Chemical Formula: $C_{11}H_{14}O_3$
Exact Mass: 194.0943 Da
Molecular Weight: 194.2300 Da

Ethyl hydroxyacetate (ethyl glycolate) (454 µL, 500 mg, 4.80 mmol, 1.00 equiv.) was added dropwise to a suspension of NaH (60% dispersion in mineral oil, 211 mg, 5.28 mmol, 1.10 equiv.) in THF (6.00 mL) and the mixture was refluxed for half an hour. Afterwards, a solution of benzyl bromide (628 µL, 904 mg, 5.28 mmol, 1.10 equiv.) in THF (4.50 mL) was added dropwise to the mixture and the reaction was stirred for another three hours. After cooling, ethanol was added to decompose the excess of sodium hydride. The solvent was evaporated, and the obtained residue was poured into 5wt% aqueous hydrochloric acid. The product was extracted with chloroform (3 × 10 mL) and the combined organic layers were washed with water (2 × 10 mL). The organic phase was dried over anhydrous sodium sulfate, filtered, and the solvent was removed under reduced pressure. Purification of the crude product *via* column chromatography (EA:cyhex = 1:2) yielded the product **P24** as a yellowish oil (876 mg, 4.51 mmol, 94%).

^{1}H NMR (400 MHz, $CDCl_3$): δ / ppm = 7.43 – 7.27 (m, 5H, CH_{Ar}^1), 4.64 (s, 2H, CH_2^2), 4.23 (q, *J* = 7.1 Hz, 2H, CH_2^3), 4.09 (s, 2H, CH_2^4), 1.29 (t, *J* = 7.1 Hz, 3H, CH_3^5).

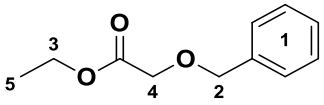

^{13}C NMR (101 MHz, $CDCl_3$): δ / ppm = 170.45 (C_q^1), 137.24 (C_q^2), 128.59 (CH_{Ar}^3), 128.18 (CH_{Ar}^3), 128.11 (CH_{Ar}^4), 73.44 (CH_2^5), 67.35 (CH_2^6), 60.97 (CH_2^7), 14.31 (CH_3^8).

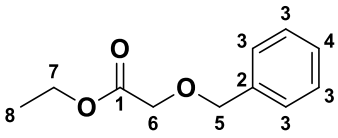

[I] The synthesis was carried out by B. Sc. QIANYU CAI under the lab-supervision of PHILIPP BOHN.

HRMS (ESI) of $C_{11}H_{14}O_3$ $[M+H]^+$ *m/z* calc. 195.1016, found 195.1016.

IR (ATR platinum diamond) ν / cm^{-1} = 3031, 2953, 1753, 1497, 1454, 1437, 1393, 1281, 1205, 1116, 1028, 1001, 950, 907, 845, 737, 697, 605, 547, 464.

R_f = 0.20 (cyhex:EA = 2:1).

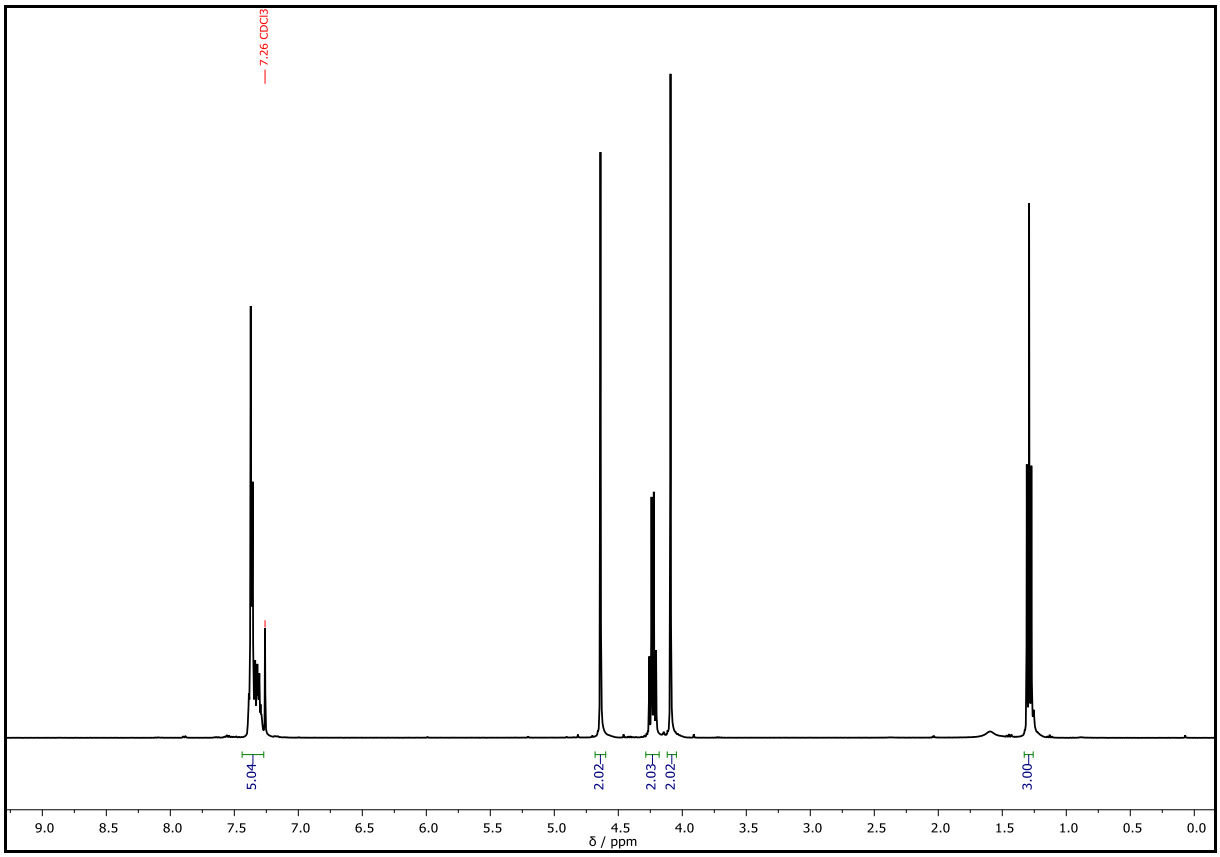

Supplementary Figure 58: ^{1}H NMR spectrum of **P24**, recorded at 400 MHz in $CDCl_3$.

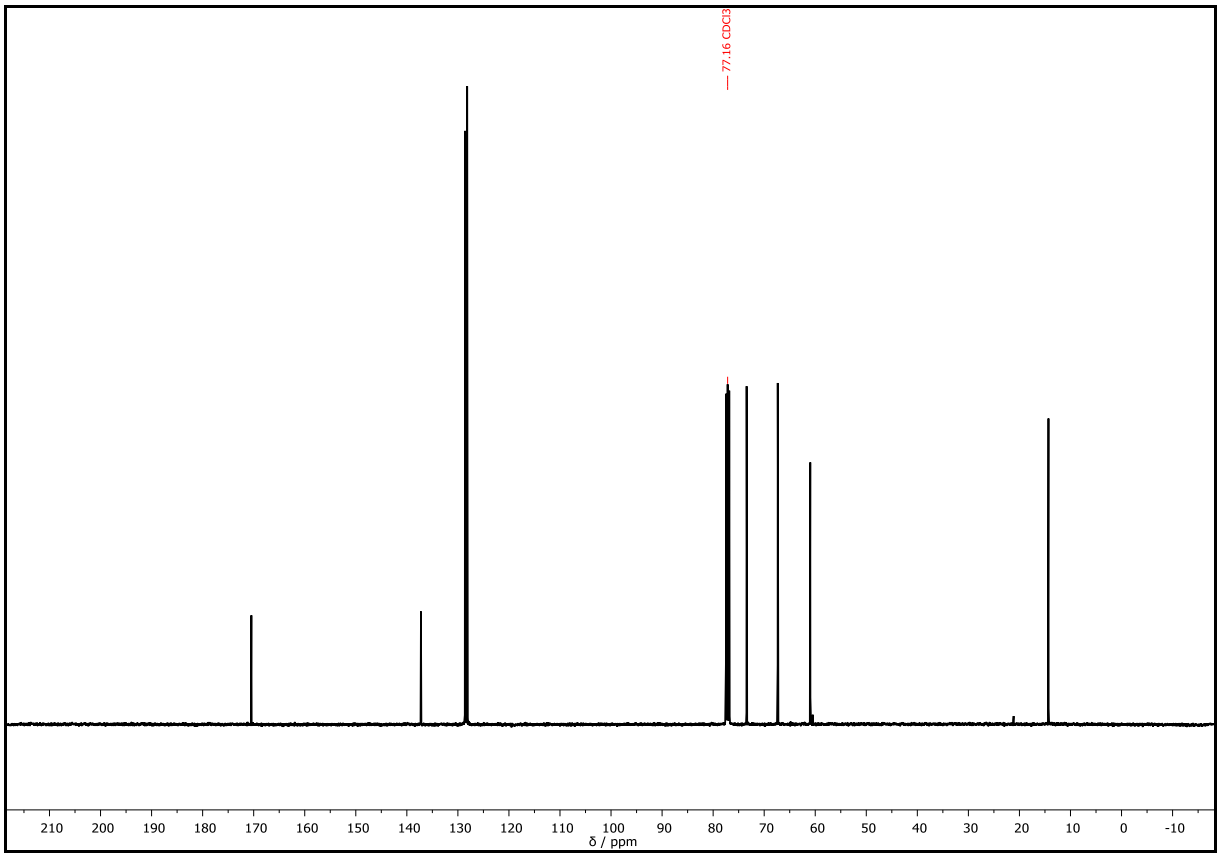

Supplementary Figure 59: ^{13}C NMR spectrum of **P24**, recorded at 101 MHz in $CDCl_3$.

2,5,8,11-Tetraoxatridecan-13-yl 2-(benzyloxy)acetate – P25[l]

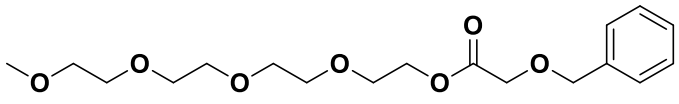

Chemical Formula: $C_{18}H_{28}O_7$
Exact Mass: 356.1835 Da
Molecular Weight: 356.4150 Da

The synthesis of product **P25** was performed according to the procedure of PUSKAS *et al*.[631] Tetra(ethylene glycol) monomethyl ether (6.25 g, 30.0 mmol, 1.00 equiv.) was reacted with ethyl 2-(benzyloxy)acetate **P24** (5.83 g, 30.0 mmol, 1.00 equiv.) in the presence of CALB (494 mg resin at 20 wt% enzyme) in bulk at 65 °C under vacuum (8 mbar) for 3 h. Purification of the crude product *via* column chromatography (cyhex:EA = 1:1 → 1:3) yielded the desired product **P25** as a colorless oil (8.47 g, 23.8 mmol, 79%). The product was dried *via* azeotropic distillation with toluene (3 × 50 mL), dried under high vacuum and stored under argon atmosphere prior to further usage.

[l] The synthesis was carried out by B. Sc. QIANYU CAI under the lab-supervision of PHILIPP BOHN.

^{1}H NMR (400 MHz, $CDCl_3$): δ / ppm = 7.40 – 7.28 (m, 5H, CH_{Ar}^{1}), 4.64 (s, 2H, CH_2^{2}), 4.37 – 4.29 (m, 2H, CH_2^{3}), 4.13 (s, 2H, CH_2^{4}), 3.75 – 3.69 (m, 2H, CH_2^{5}), 3.67 – 3.61 (m, 10H, CH_2^{6}), 3.56 – 3.51 (m, 2H, CH_2^{7}), 3.37 (s, 3H, CH_3^{8}).

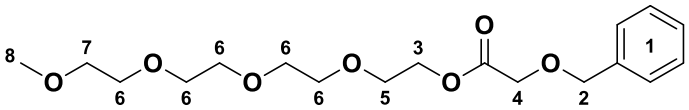

^{13}C NMR (101 MHz, $CDCl_3$): δ / ppm = 170.49 (C_q^{1}), 137.25 (C_q^{2}), 128.63 (CH_{Ar}^{3}), 128.24 (CH_{Ar}^{3}), 128.15 (CH_{Ar}^{4} and CH_{Ar}^{5}), 73.48 (CH_2^{6}), 72.08 (CH_2^{7}), 70.76 (CH_2^{8}), 70.72 (CH_2^{8}), 70.67 (CH_2^{8}), 69.11 (CH_2^{9}), 67.23 (CH_2^{10}), 64.00 (CH_2^{11}), 59.17 (CH_3^{12}).

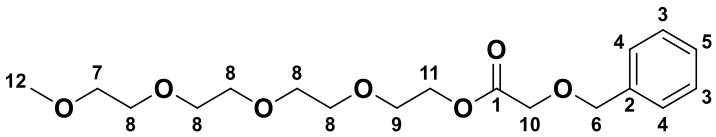

HRMS (ESI) of $C_{18}H_{28}O_7$ $[M+H]^+$ *m/z* calc. 357.1908, found 357.1900; $[M+Na]^+$ *m/z* calc. 379.1727, found 379.1721.

IR (ATR platinum diamond) $\tilde{\nu}$ / cm^{-1} = 2871, 1752, 1736, 1454, 1395, 1351, 1281, 1249, 1197, 1103, 1041, 1028, 991, 948, 913, 852, 740, 699, 607, 578.

R_f = 0.30 (cyhex:EA = 2:1).

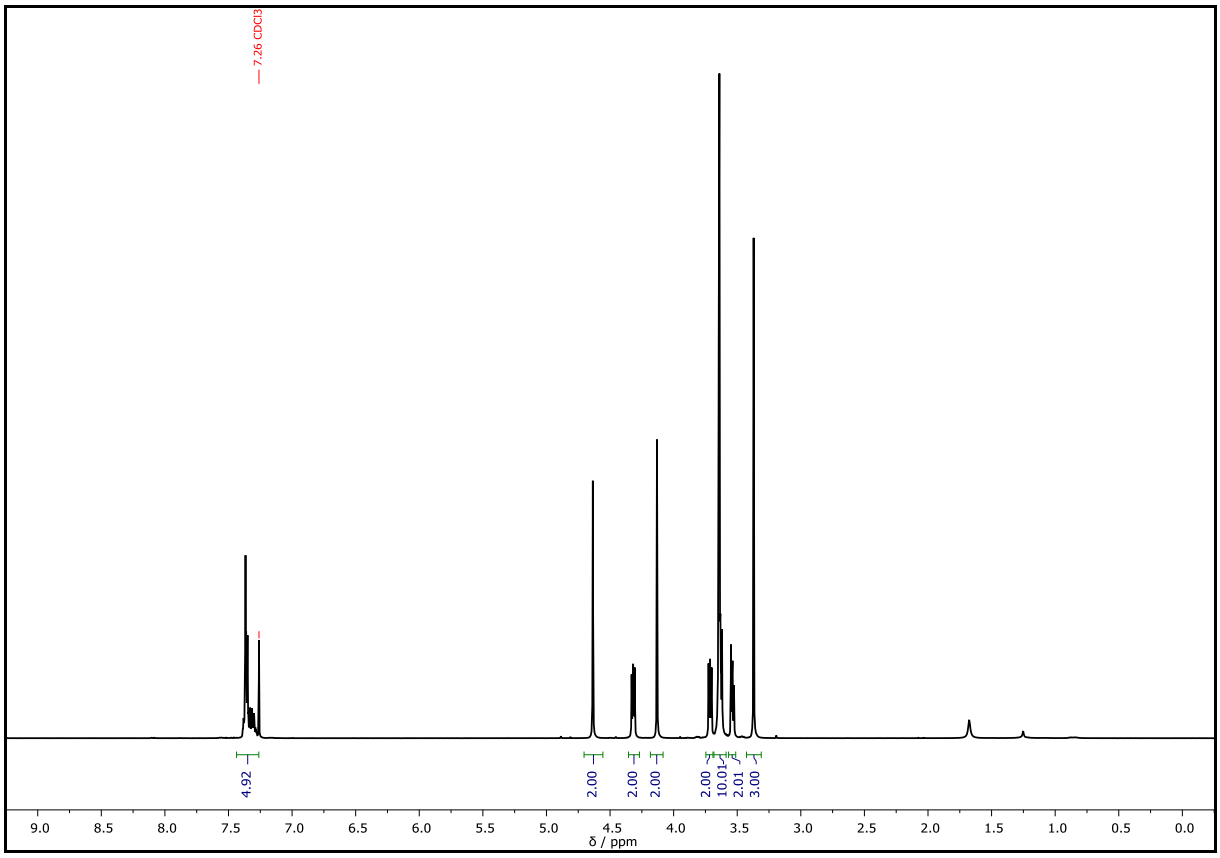

Supplementary Figure 60: ^{1}H NMR spectrum of **P25**, recorded at 400 MHz in $CDCl_3$.

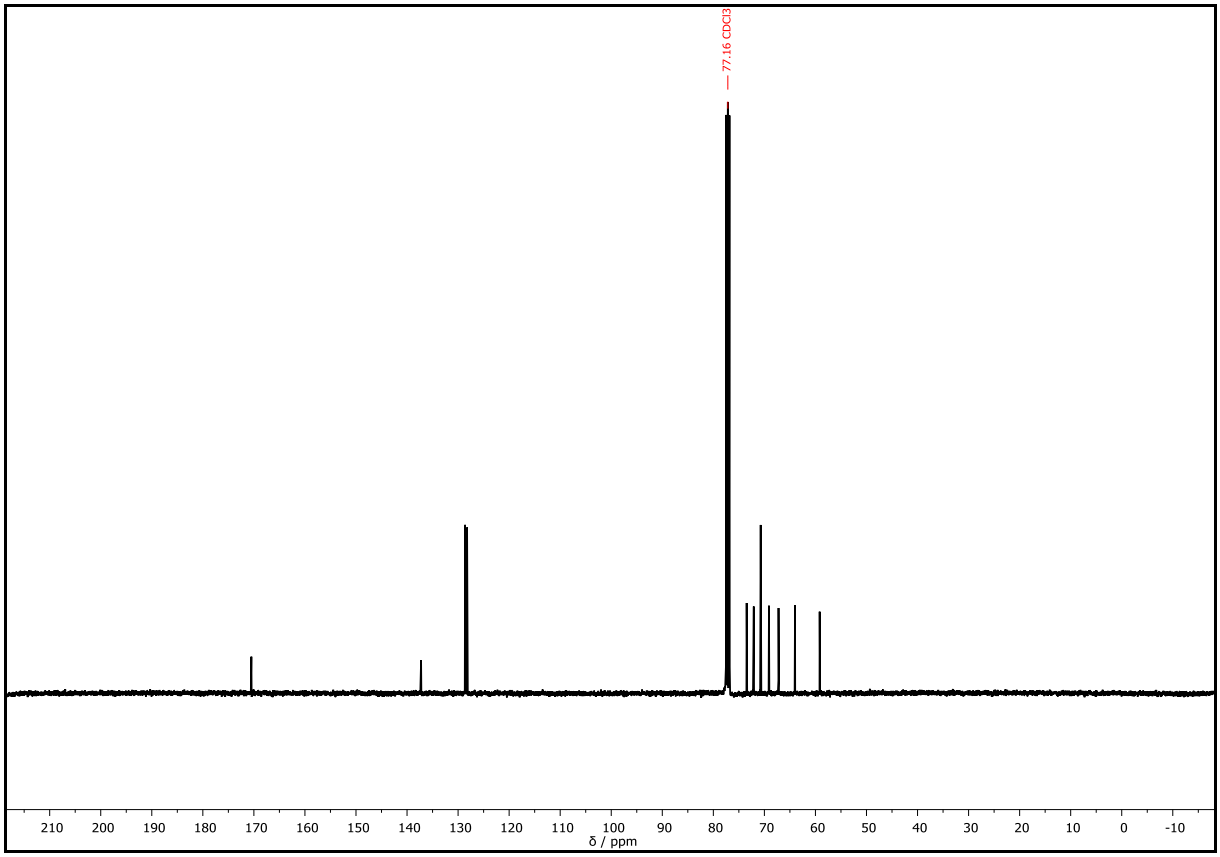

Supplementary Figure 61: ^{13}C NMR spectrum of **P25**, recorded at 101 MHz in $CDCl_3$.

α-Benzyl-ω-methyl penta(ethylene glycol) – P26[I]

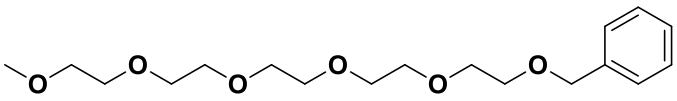

Chemical Formula: $C_{18}H_{30}O_6$
Exact Mass: 342.2042 Da
Molecular Weight: 342.4320 Da

The different approaches for the reduction of ester **P25** as well as the corresponding quantities of used reagents are summarized in Supplementary Table 12.

The ester **P25** (1.00 g, 2.81 mmol, 1.00 equiv.) was dissolved in dry DCM (600 µL) in a flame dried Schlenk flask. After 10 min of stirring, a solution of $GaBr_3$ (1 - 5mol%) in dry DCM (2.20 mL) was added. The respective quantity of reducing agent was added over three hours *via* a syringe pump. The reaction was stirred under Ar-atmosphere at room temperature and the reduction of the carbonyl function was monitored with ^{1}H NMR and IR spectroscopy. After full conversion, the approaches using 5 mol% $GaBr_3$ and 4.40 or 6.60 equiv. TES, respectively (Supplementary Table 12), were combined and water was added to the reaction mixture to quench the reaction process. The aqueous phase was extracted with DCM (5 × 10 mL). The combined organic phases were dried over anhydrous sodium sulfate, filtered, and the solvent was removed under reduce pressure. The residue was redissolved in MeOH (20 mL) and water (1 mL) and washed with petroleum ether (5 × 10 mL). The combined organic phases were dried over anhydrous sodium sulfate, filtered, and the solvent was removed under reduced pressure. Purification of the crude product *via* column chromatography (cyhex:EA = 1:3 → 0:1) resulted the product **P26** as a colorless oil in a yield of 39% (756 mg, 2.21 mmol).

Note: The purification protocol was not optimized. Further, since several samples were taken out of the reaction mixture for the monitoring *via* 1H NMR and IR spectroscopy, the yield is significantly decreased and is lower than the observed conversion.

^{1}H NMR (400 MHz, DMSO-d_6): δ / ppm = 7.43 – 7.21 (m, 5H, CH_{Ar}^1), 4.49 (s, 2H, CH_2^2), 3.56 (s, 4H, CH_2^3), 3.54 – 3.47 (m, 14H, CH_2^4), 3.42 (dd, J = 5.8, 3.4 Hz, 2H, CH_2^5), 3.23 (s, 3H, CH_3^6).

[I] All reduction steps were performed by B. Sc. PETER CONEN under the lab-supervision of PHILIPP BOHN.

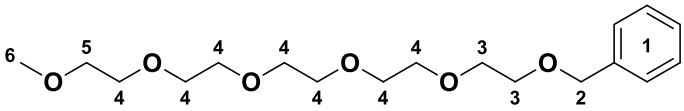

^{13}C NMR (101 MHz, DMSO-d_6): δ / ppm = 138.49 ($C_{q,Ar}$[1]), 128.19 (CH_{Ar}[2]), 127.46 (CH_{Ar}[3]), 127.35 (CH_{Ar}[4]), 72.01 (CH_2[5]), 71.26 (CH_2[6]), 69.83 (CH_2[7]), 69.79 (CH_2[7]), 69.57 (CH_2[7]), 69.12 (CH_2[8]), 58.03 (CH_3[9]).

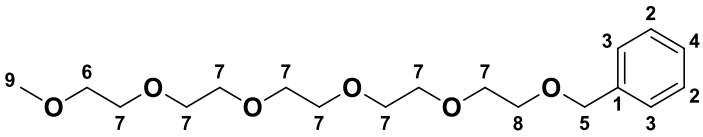

HRMS (ESI) of $C_{18}H_{30}O_6$ $[M+H]^+$ *m/z* calc. 343.2115, found 343.2110; $[M+Na]^+$ *m/z* calc. 365.1935, found 365.1930; $[M+K]^+$ *m/z* calc. 381.1674, found 381.1668.

The mass of the α-benzyl-ω-methyl tetra(ethylene glycol) was also found. $[M+H]^+$ *m/z* calc. 299.1853, found 299.1849.

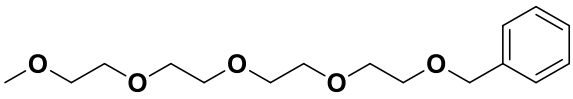

Chemical Formula: $C_{16}H_{26}O_5$
Exact Mass: 298.1780 Da

The mass of the monomethyl penta(ethylene glycol) was also found. $[M+H]^+$ *m/z* calc. 253.1646, found 253.1642.

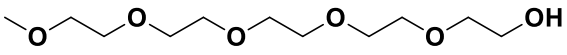

Chemical Formula: $C_{11}H_{24}O_6$
Exact Mass: 252.1573 Da

The mass of the monomethyl tetra(ethylene glycol) was also found. $[M+H]^+$ *m/z* calc. 209.1384, found 209.1381.

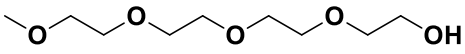

Chemical Formula: $C_9H_{20}O_5$
Exact Mass: 208.1311 Da

IR (ATR platinum diamond) $\tilde{\nu}$ / cm^{-1} = 2871, 1454, 1351, 1281, 1249, 1197, 1103, 1041, 1028, 991, 948, 913, 852, 740, 699, 607, 578.

R_f = 0.18 (cyhex:EA = 1:3).

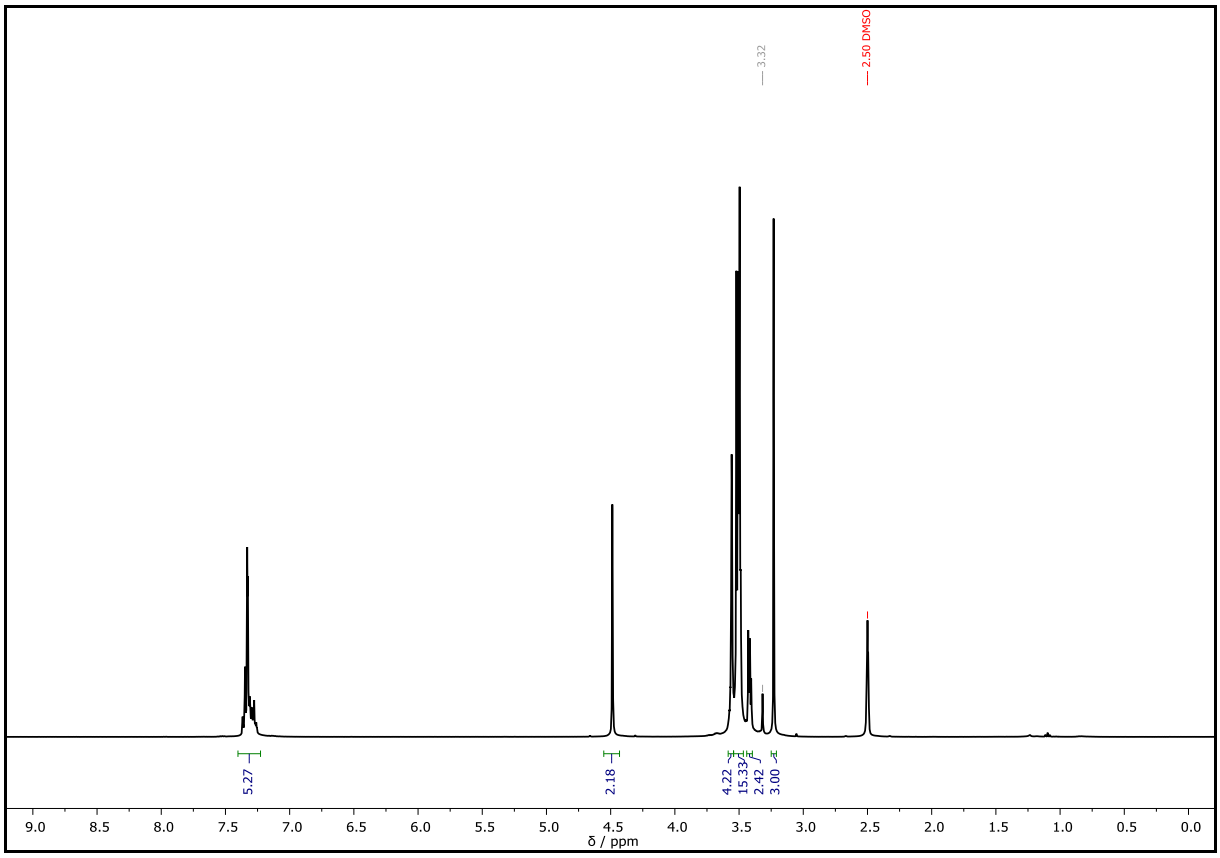

Supplementary Figure 62: ^{1}H NMR spectrum of **P26**, recorded at 400 MHz in DMSO-d_6.

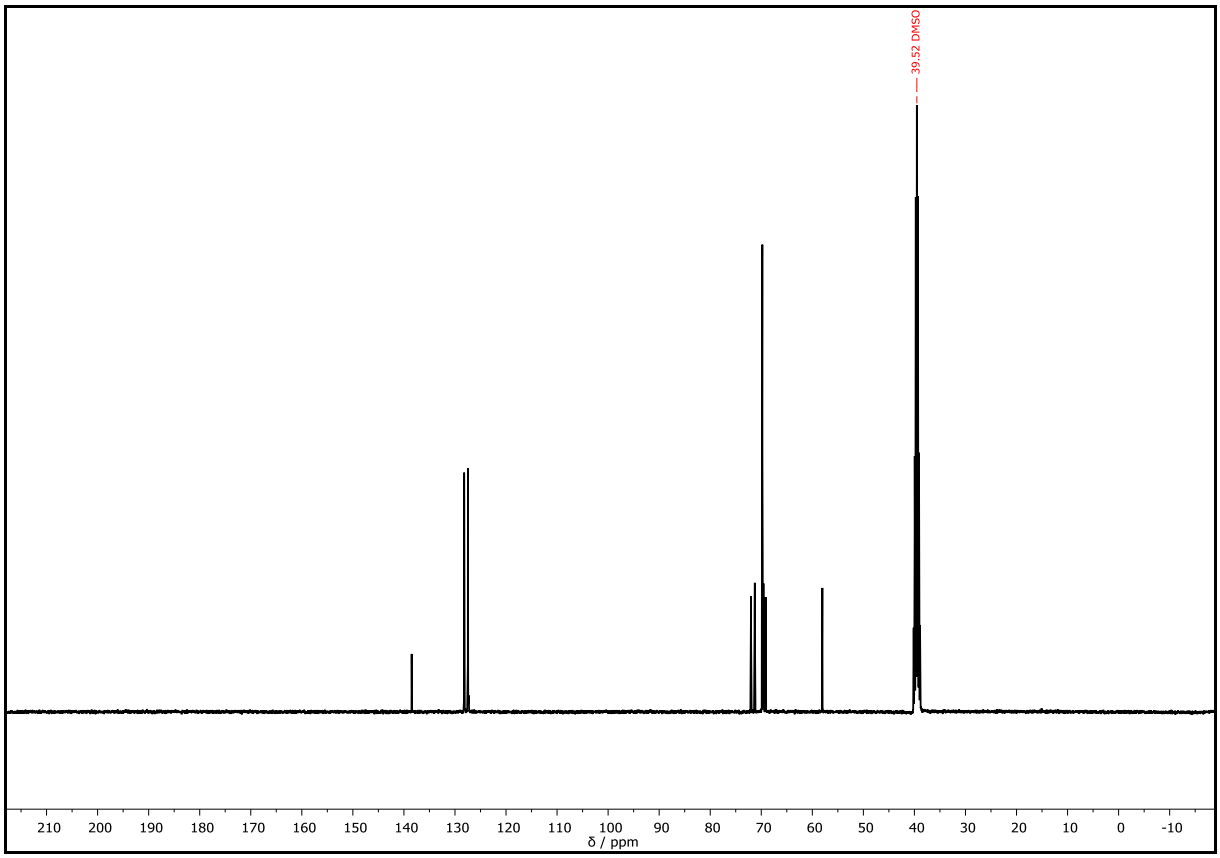

Supplementary Figure 63: ^{13}C NMR spectrum of **P26**, recorded at 101 MHz in DMSO-d_6.

Supplementary Table 12: Conversion of the individual reduction approaches (**P26**) determined by ^{1}H NMR and IR spectroscopy.														
$GaBr_3$ / mol%	1.00	1.00	1.00	2.00	2.00	2.00	2.00	2.00	2.00	3.00	3.00	5.00	5.00	5.00
TMDS / equiv.	1.10	2.20	3.30	1.10	2.20	3.30	-	-	-	-	1.10	-	-	-
TES / equiv.	-	-	-	-	-	-	2.20	4.40	6.60	2.20	-	2.20	4.40	6.60
t / min	conversion / % (first value by 1H NMR, second value by IR spectroscopy)													
3	3 / 1	6 / 8	40 / 41	30 / 31	47 / 50	63 / 62	24 / 28	28 / 33	28 / 32	40	30	47 / 52	59 / 64	68 / 75
17	-	-	-	67 / 70	91 / 92	-	-	-	-	-	-	-	-	-
18	8 / 1	4 / 7	-	-	-	-	-	-	-	69 / 75	64 / 66	-	-	-
19	-	-	-	-	-	-	-	-	-	-	-	82 / 84	87 / 89	94 / 96
20	-	-	86 / 89	-	-	>99 / >99	-	-	-	-	-	-	-	-
21	-	-	-	-	-	-	55 / 56	55 / 58	50 / 51	-	-	-	-	-
24	-	-	-	72 / 76	96 / 97	-	-	-	-	-	-	-	-	-
42	-	-	-	78 / 81	>99 / >99	-	-	-	-	-	-	-	-	-
44	-	-	-	-	-	-	-	-	-	-	-	91 / 94	96 / 99	98 / >99
46	-	-	>99 / 96	-	-	>99 / >99	-	-	-	-	-	-	-	-
66	8 / 3	9 / 7	-	-	-	-	-	-	-	-	-	-	-	-
67	-	-	-	82 / 83	>99 / >99	-	-	-	-	-	-	94 / 97	>99 / >99	-
68	-	-	-	-	-	-	69 / 75	76 / 76	70 / 71	-	-	-	-	-
73	-	-	-	-	-	-	-	-	-	86 / 89	86 / 87	-	-	-
93	-	-	>99 / 99	-	-	>99 / >99	77 / 80	83 / 87	76 / 82	-	-	-	-	-
116	-	-	-	82 / 83	-	>99 / >99	-	-	-	-	-	-	-	-
140	14 / 4	-	-	82 / 84	-	-	-	-	-	-	-	-	-	-
144	-	-	-	-	-	-	83 / 87	94 / 96	85 / 90	-	-	96	-	-
168		-	-	-	-	-	-	-	-	88	-	-	-	-
190		-	-	82 / 86	-	-	-	-	-	-	-	-	-	-

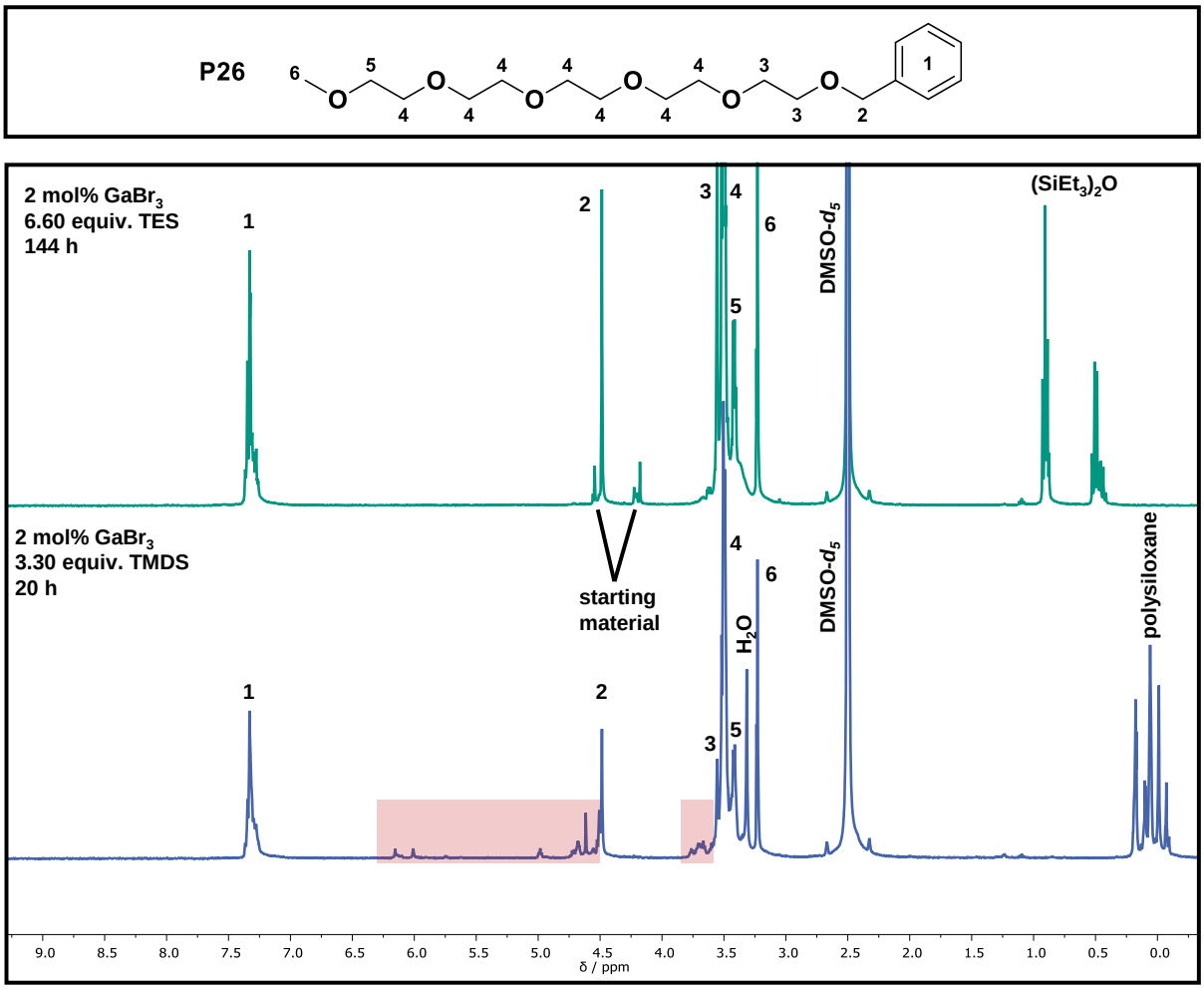

Supplementary Figure 64: Investigation of the side product formation *via* ^{1}H NMR spectroscopy by a comparison of the reducing agents TES (green spectrum, top) and TMDS (blue spectrum, bottom) in the reduction reaction (**P26**). Impurity signals, highlighted in red, could not be characterized so far.

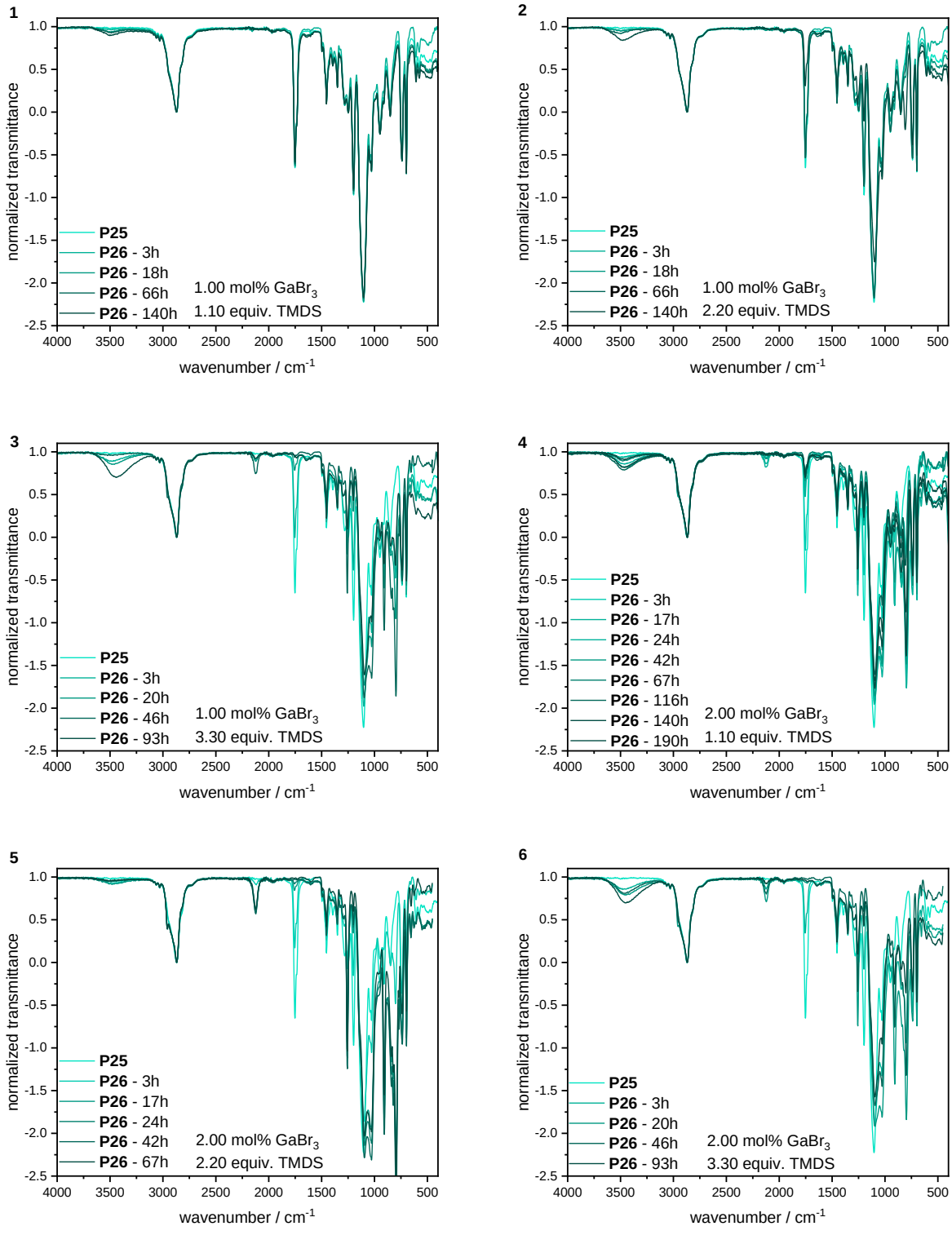

Supplementary Figure 65: IR spectroscopy monitoring of the reduction reaction of **P25**.

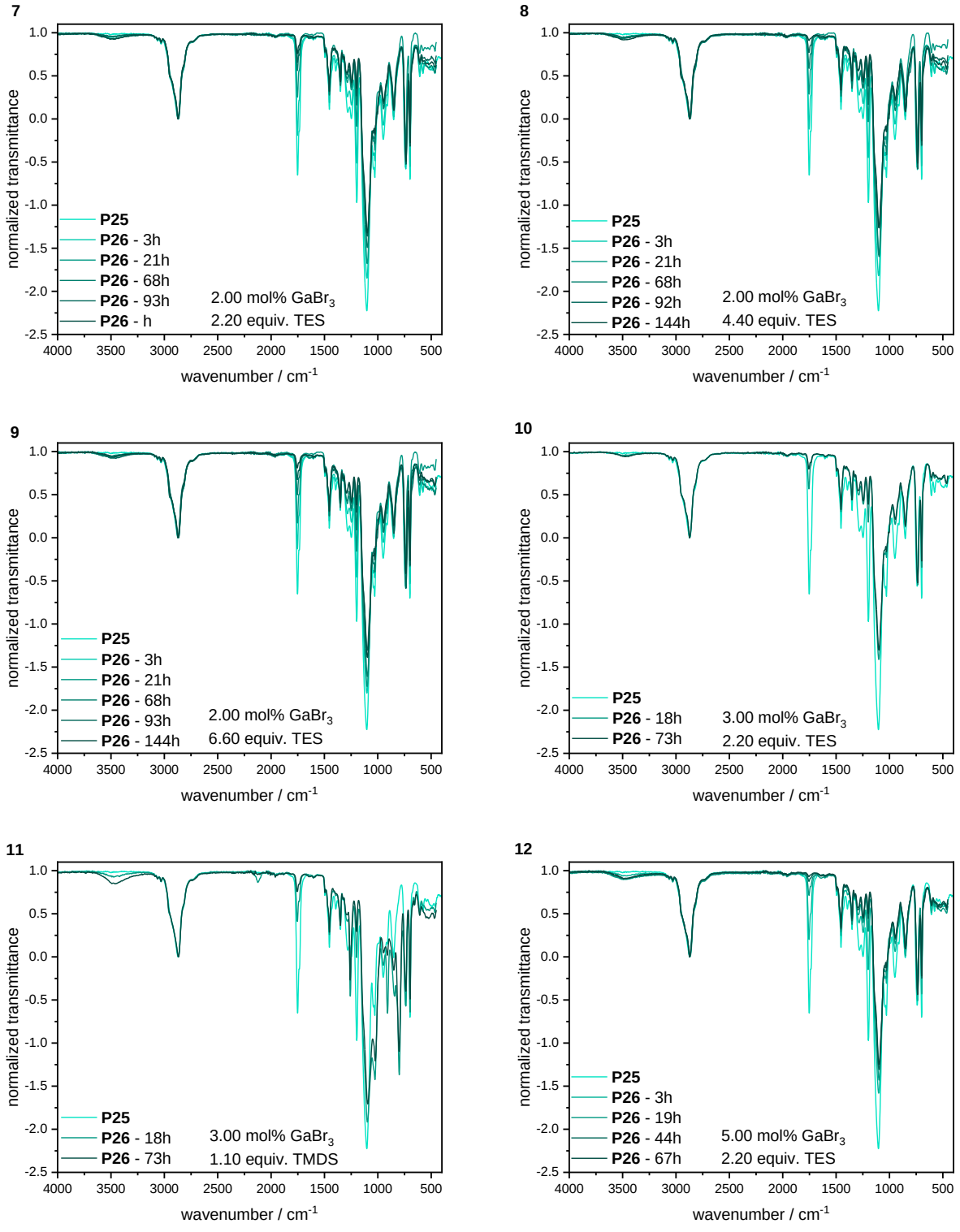

Supplementary Figure 66: IR spectroscopy monitoring of the reduction reaction of **P25**.

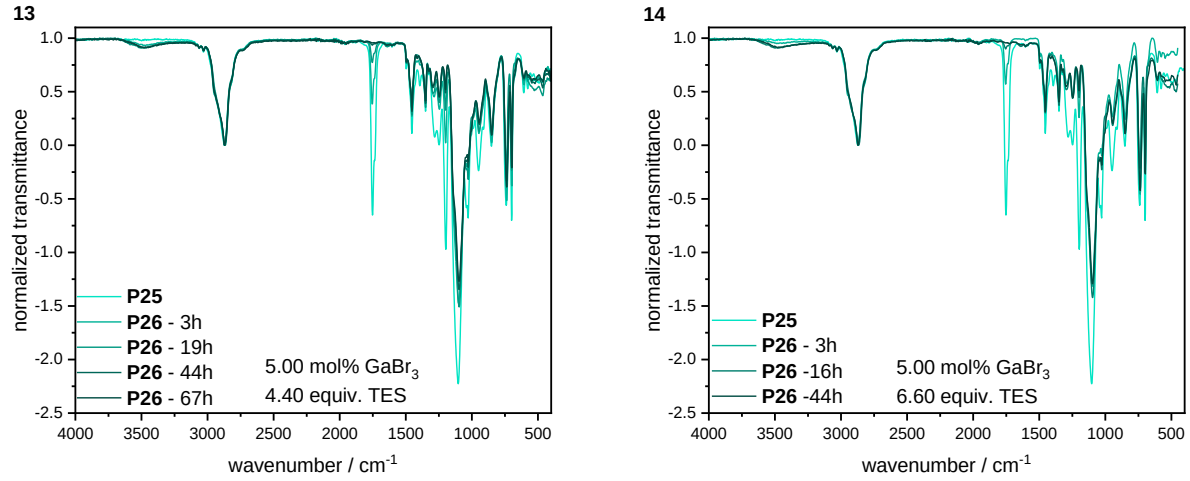

Supplementary Figure 67: IR spectroscopy monitoring of the reduction reaction of **P25**.

Monomethyl penta(ethylene glycol) – P27

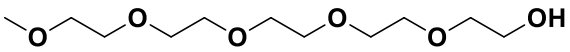

Chemical Formula: $C_{11}H_{24}O_6$
Exact Mass: 252.1573 Da
Molecular Weight: 252.3070 Da

Monomethyl penta(ethylene glycol) **P27** was prepared using the procedure described above for the synthesis of the reductive hydrogenation of **P22**.

P26	733 mg, 2.14 mmol, 1.00 equiv.
Pd/C	73.3 mg, 10 wt%
EtOH	30 mL
yield	539 g, 2.14 mmol, quant. yield, colorless oil

^{1}H NMR (400 MHz, DMSO-d_6): δ / ppm = 4.58 (t, J = 5.5 Hz, 1H, OH^1), 3.50 (s, 14H, CH_2^2), 3.49 - 3.46 (m, 2H, CH_2^3), 3.44 – 3.39 (m, 4H, CH_2^4), 3.24 (s, 3H, CH_3^5).

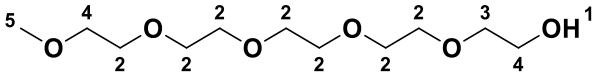

^{13}C NMR (101 MHz, DMSO-d_6): δ / ppm = 72.36 (CH_2^1), 71.29 (CH_2^2), 69.83 (CH_2^3), 69.81 (CH_2^3), 69.79 (CH_2^3), 69.59 (CH_2^4), 60.22 (CH_2^5), 58.06 (CH_3^6).

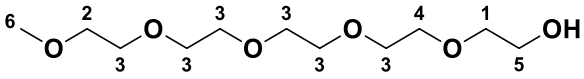

HRMS (ESI) of $C_{11}H_{24}O_6$ $[M+H]^+$ *m/z* calc. 253.1646, found 253.1644; $[M+NH_4]^+$ *m/z* calc. 270.1911, found 270.1910; $[M+Na]^+$ *m/z* calc. 275.1465, found 275.1461; $[M+K]^+$ *m/z* calc. 291.1204, found 291.1200.

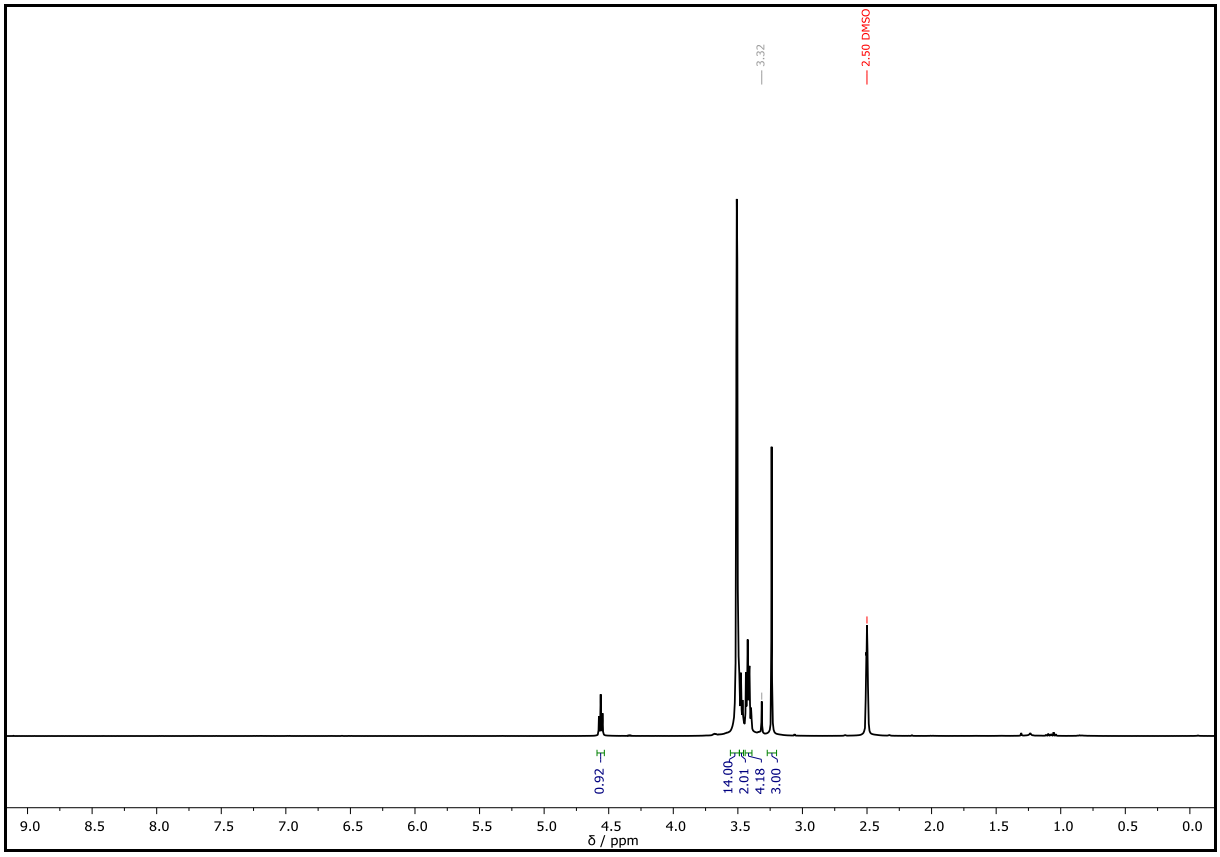

Supplementary Figure 68: ^{1}H NMR spectrum of **P27**, recorded at 400 MHz in DMSO-d_6.

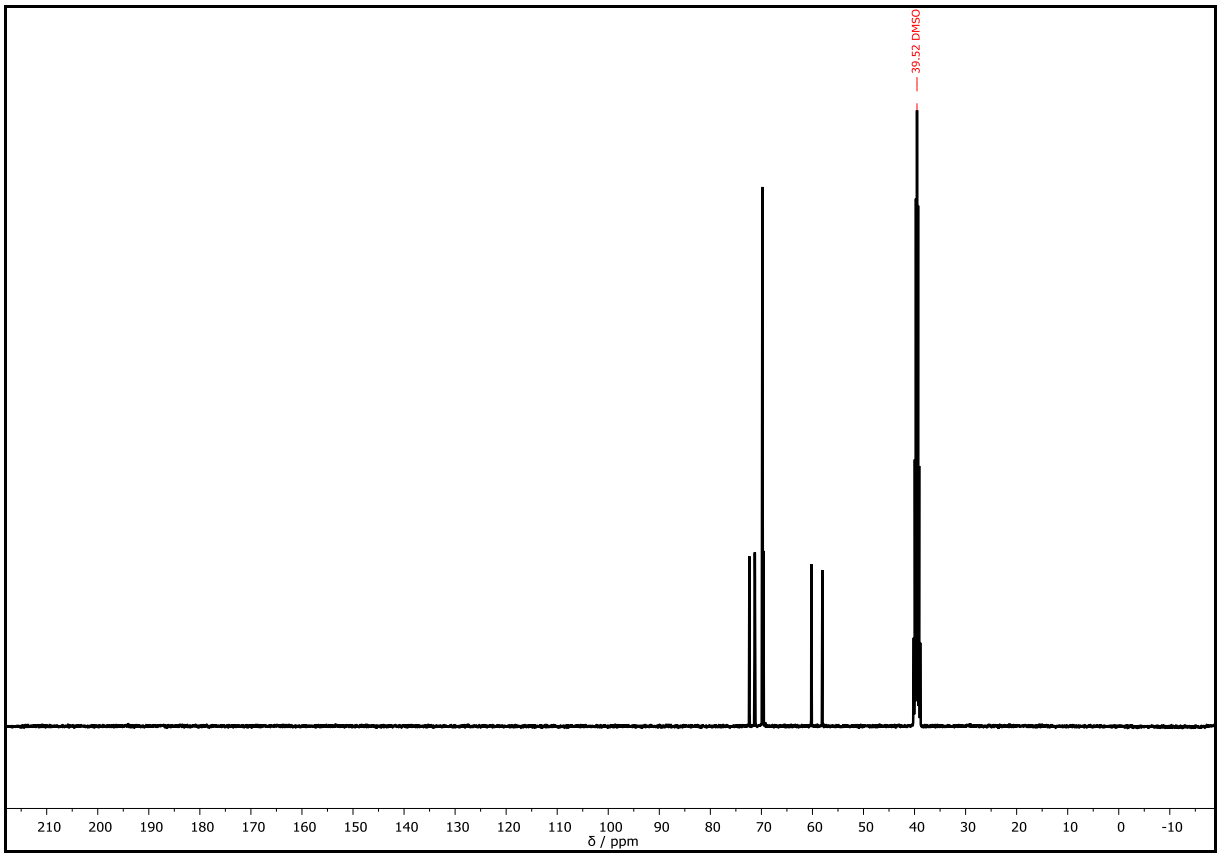

Supplementary Figure 69: ^{13}C NMR spectrum of **P27**, recorded at 101 MHz in DMSO-d_6.

Ethyl 1-phenyl-2,5,8,11,14-pentaoxahexadecan-16-oate – P28[I]

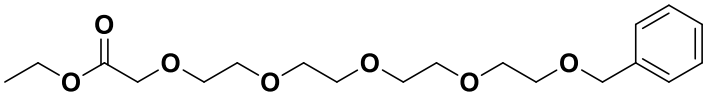

Chemical Formula: $C_{19}H_{30}O_7$
Exact Mass: 370.1992 Da
Molecular Weight: 370.4420 Da

Tetra(ethylene glycol) monobenzyl ether **P5** (12.0 mL, 12.5 g, 44.0 mmol, 1.00 equiv.) was dissolved in dry DMF (105 mL) and stirred under argon atmosphere. NaH (60% dispersion in mineral oil, 1.76 g, 44.0 mmol, 1.00 equiv.) was added and the reaction mixture was stirred for 6 h at 0 °C. The mixture was warmed to room temperature and ethyl bromoacetate (8.32 mL, 12.5 g, 74.7 mmol, 1.70 mmol) was added and the mixture was stirred for another 15 h. Ethanol (20 mL) was added to decompose the excess of NaH and the solvent was removed under reduced pressure. The crude product was purified *via* column chromatography (cyhex:EA = 1:6) and the desired product **P28** was obtained as a colorless oil in a yield of 77.8% (12.7 g, 34.2 mmol).

^{1}H NMR (400 MHz, $CDCl_3$): δ / ppm = 7.36 – 7.27 (m, 5H, CH_{Ar}^1), 4.56 (s, 2H, CH_2^2), 4.21 (q, *J* = 7.1 Hz, 2H, CH_2^3), 4.14 (s, 2H, CH_2^4), 3.77 – 3.58 (m, 16H, CH_2^5), 1.28 (t, *J* = 7.1 Hz, 3H, CH_3^6).

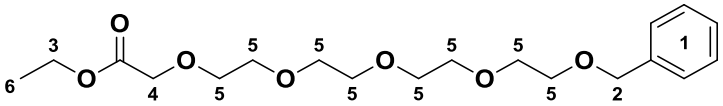

^{13}C NMR (101 MHz, $CDCl_3$): δ / ppm = 170.48 (C_q^1), 138.31 ($C_{q,Ar}^2$), 128.36 ($CH_{Ar,meta}^3$), 127.75 ($CH_{Ar,ortho}^4$), 127.59 ($CH_{Ar,para}^5$), 73.25 (CH_2^6), 70.91 (CH_2^7), 70.67 (CH_2^8), 70.65 (CH_2^8), 70.64 (CH_2^8), 70.60 (CH_2^8), 69.46 (CH_2^9), 68.75 (CH_2^{10}), 60.80 (CH_2^{11}), 14.22 (CH_3^{12}).

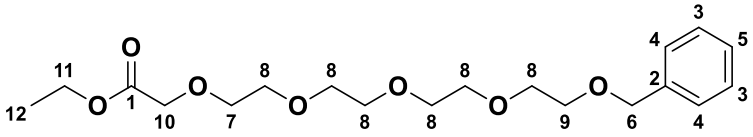

HRMS (ESI) of $C_{19}H_{30}O_7$ $[M+H]^+$ *m/z* calc. 371.2064, found 371.2061; $[M+NH_4]^+$ *m/z* calc. 388.2330, found 388.2327; $[M+Na]^+$ *m/z* calc. 393.1884, found 393.1879; $[M+K]^+$ *m/z* calc. 409.1623, found 409.1620.

[I] The synthesis was carried out by B. Sc. MAYA EYLEEN LUDWIG under the lab-supervision of PHILIPP BOHN.

R_f = 0.50 (cyhex:EA = 1:9).

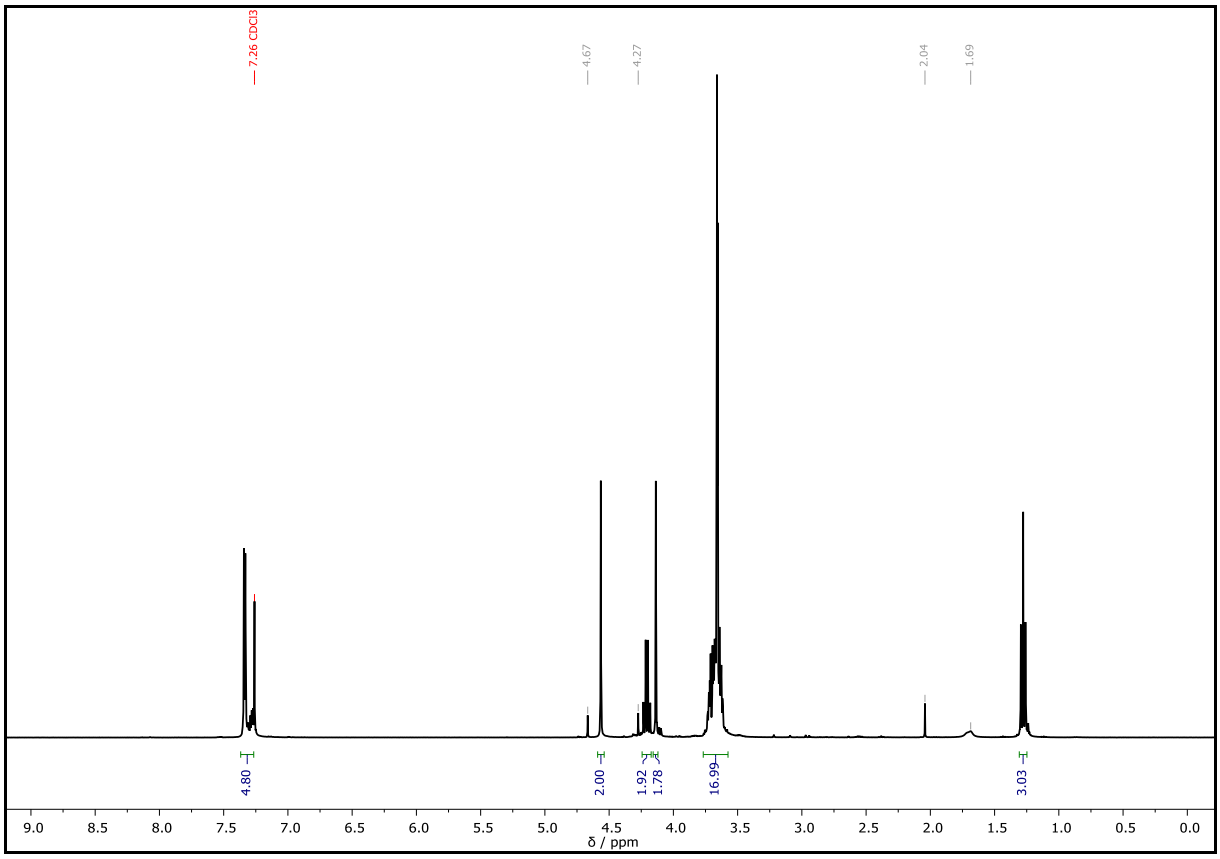

Supplementary Figure 70: ^{1}H NMR spectrum of **P28**, recorded at 400 MHz in $CDCl_3$.

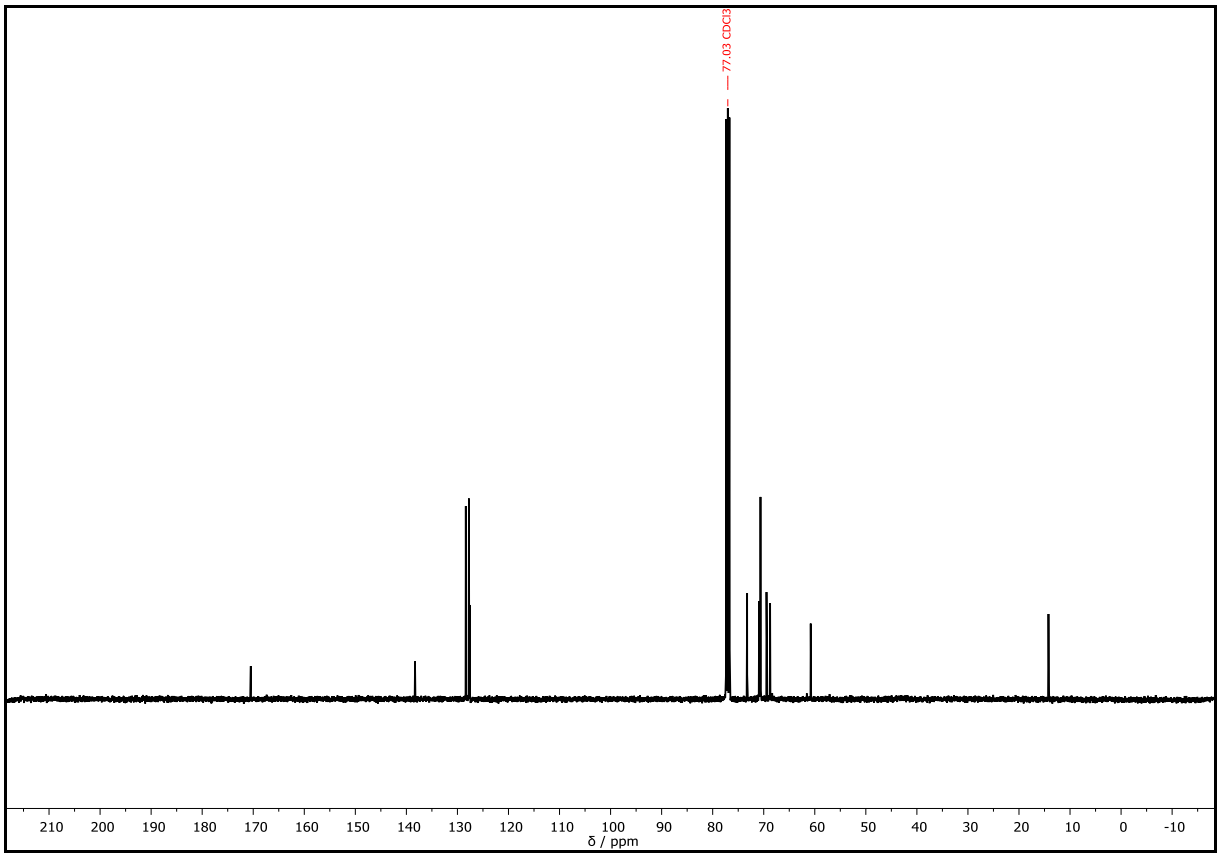

Supplementary Figure 71: ^{13}C NMR spectrum of **P29**, recorded at 101 MHz in $CDCl_3$.

2,5,8,11-Tetraoxatridecan-13-yl 1-phenyl-2,5,8,11,14-pentaoxahexadecan-16-oate – P29[l]

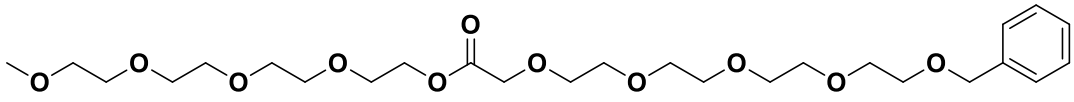

Chemical Formula: $C_{26}H_{44}O_{11}$
Exact Mass: 532.2884 Da
Molecular Weight: 532.6270 Da

The synthesis of product **P29** was performed according to the procedure of PUSKAS *et al*.[631] See **P25**.

mTEG	1.41 g, 6.77 mmol, 1.00 equiv.
P28	2.50 mg, 6.77 mmol, 1.00 equiv.
CALB	111 mg resin at 20 wt% enzyme
reaction conditions	7 h, 65 °C, 8 mbar
yield	2.33 g, 4.37 mmol, 64.5%, yellowish oil

[l] The synthesis was carried out by KIARA MAURER under the lab-supervision of PHILIPP BOHN.

^{1}H NMR (400 MHz $CDCl_3$): δ / ppm = 7.37 – 7.27 (m, 5H, CH_{Ar}^{1}), 4.56 (d, *J* = 1.6 Hz, 2H, CH_2^{2}), 4.34 – 4.26 (m, 2H, CH_2^{3}), 4.17 (d, *J* = 1.6 Hz, 2H, CH_2^{4}), 3.76 – 3.60 (m, 28H, CH_2^{5}), 3.58 – 3.51 (m, 2H, CH_2^{6}), 3.37 (d, *J* = 1.7 Hz, 3H, CH_3^{7}).

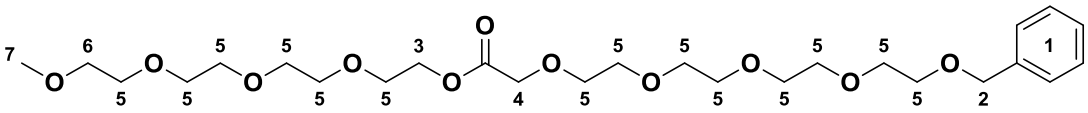

^{13}C NMR (101 MHz $CDCl_3$): δ / ppm = 170.57 (C_q^{1}), 138.41 ($C_{q,Ar}^{2}$), 128.47 (CH_{Ar}^{3}), 127.86 (CH_{Ar}^{3}), 127.70 (CH_{Ar}^{4}), 73.36 (CH_2^{5}), 72.06 (CH_2^{6}), 71.03 (CH_2^{7}), 70.77 (CH_2^{7}), 70.73 (CH_2^{7}), 70.70 (CH_2^{7}), 70.68 (CH_2^{7}), 70.65 (CH_2^{7}), 69.56 (CH_2^{7}), 69.09 (CH_2^{7}), 68.65 (CH_2^{8}), 63.89 (CH_2^{9}), 59.15 (CH_3^{10}).

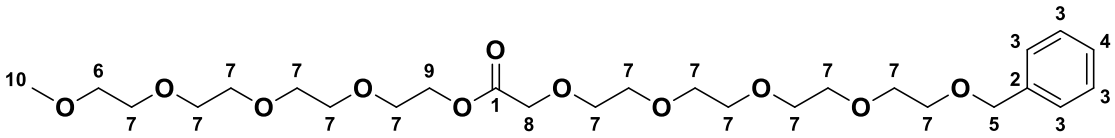

HRMS (ESI) of $C_{26}H_{44}O_{11}$ $[M+H]^+$ *m/z* calc. 533.2956, found 533.2957; $[M+NH_4]^+$ *m/z* calc. 550.3222, found 550.3222; $[M+Na]^+$ *m/z* calc. 555.2776, found 555.2774; $[M+K]^+$ *m/z* calc. 571.2515, found 571.2512.

IR (ATR platinum diamond) *v* / cm^{-1} = 2867, 1752, 1454, 1351, 1325, 1281, 1249, 1199, 1096, 1039, 1028, 946, 850, 740, 718, 699.

R_f = 0.44 (EA:MeOH = 19:1).

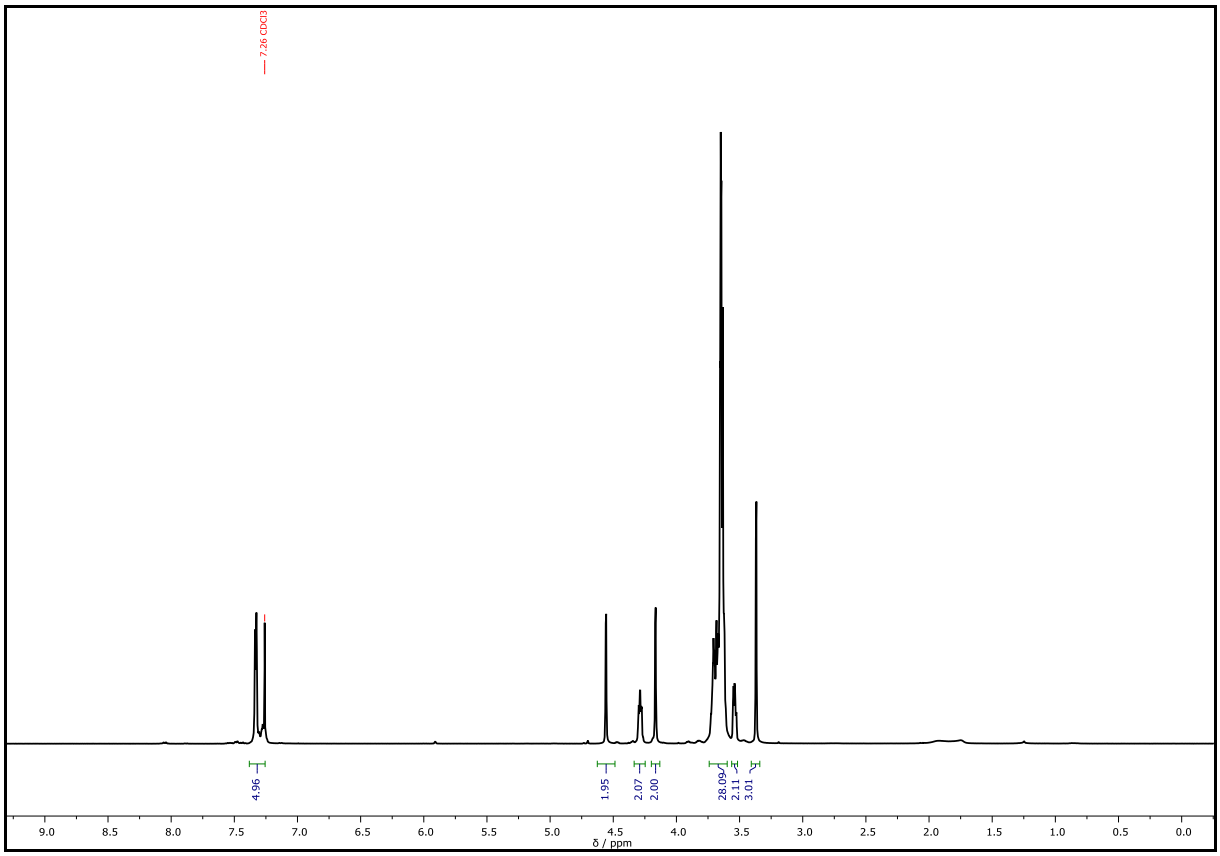

Supplementary Figure 72: ^{1}H NMR spectrum of **P29**, recorded at 400 MHz in $CDCl_3$.

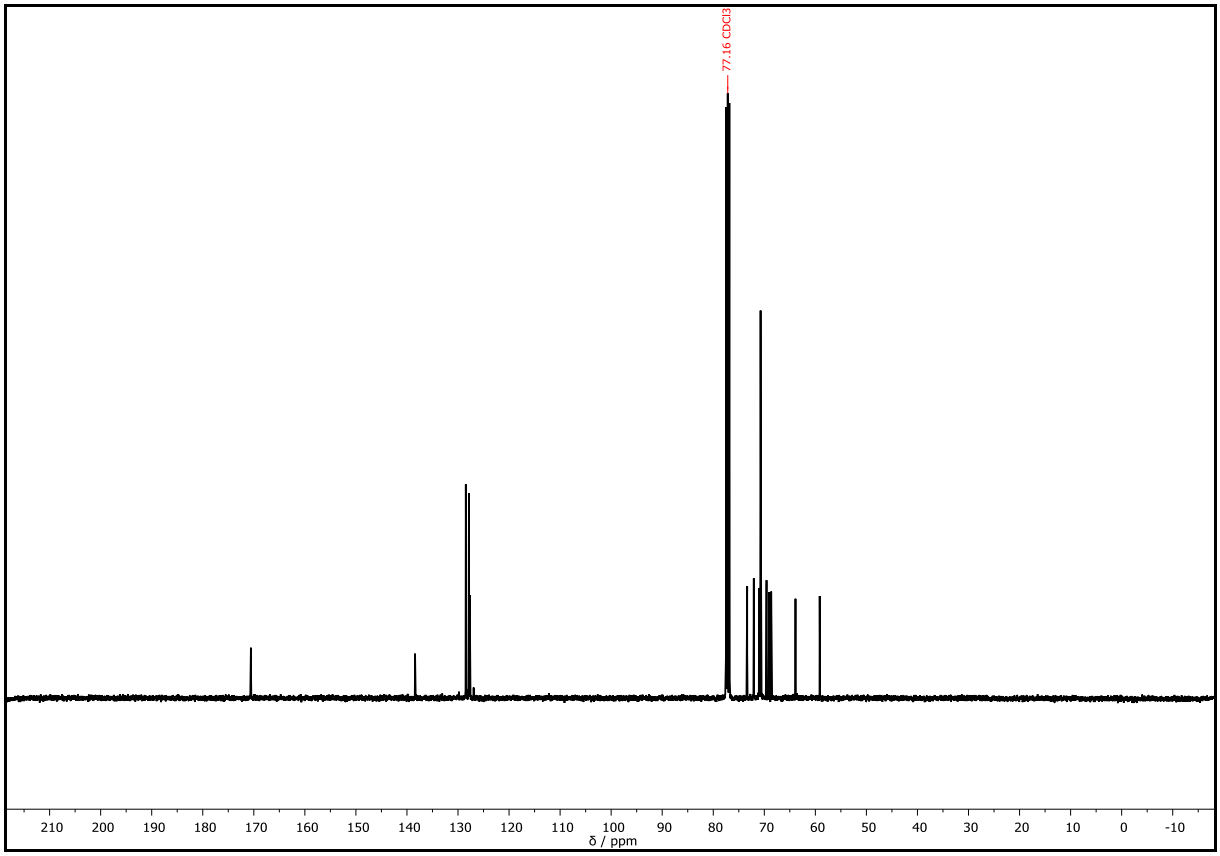

Supplementary Figure 73: ^{13}C NMR spectrum of **P29**, recorded at 101 MHz in $CDCl_3$.

6.3.4. Experimental procedures of chapter 4.2

6-Hydroxyhexanoic acid – C1[I]

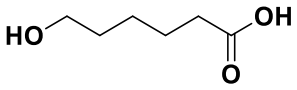

Chemical Formula: $C_6H_{12}O_3$
Exact Mass: 132.0786 Da
Molecular Weight: 132.1590 Da

NaOH (21.0 g, 525 mmol, 2.00 equiv.) and *ε*-caprolactone (27.8 mL, 30.0 g, 263 mmol, 1.00 equiv.) were added in a round bottom flask, charged with 800 mL water. The mixture was stirred overnight at room temperature. Subsequently, the pH was adjusted to 2 using 3 M hydrochloride solution and the reaction mixture was extracted with 1500 mL diethyl ether by applying a liquid/liquid continuous extractor. The organic layers were dried over anhydrous sodium sulfate, filtered, and concentrated under reduced pressure to give product **C1** (32.8 g, 248 mmol, 94.3%) as a white solid.

^{1}H NMR (DMSO-d_6, 400 MHz): δ / ppm = 11.96 (s, 1 H, CO_2H^1), 4.34 (t, J = 5.0 Hz, 1 H, OH^2), 3.26–3.43 (m, 2 H, CH_2^3), 2.18 (t, J = 7.3 Hz, 2 H, CH_2^4), 1.49 (dt, J = 14.8, 7.3 Hz, 2 H, CH_2^5), 1.39 (dd, J = 13.3, 6.5 Hz, 2 H, CH_2^6), 1.20–1.34 (m, 2 H, CH_2^7).

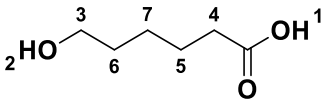

^{13}C NMR (DMSO-d_6, 101 MHz): δ / ppm = 174.46 (C_q^1), 60.54 (CH_2^2), 24.38 (CH_2^3), 33.66 (CH_2^4), 32.16 (CH_2^5), 25.07 (CH_2^6).

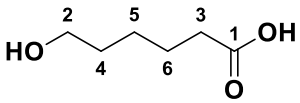

FAB of $C_6H_{12}O_3$ ($M+H^+$ = 133.1); HRMS (FAB) of $C_6H_{12}O_3$ $[M+H]^+$ calcd. 133.0865, found 133.0865.

IR (ATR platinum diamond) ν / cm^{-1} = 3246.1, 2938.0, 2859.2, 2525.8, 1911.3, 1681.8, 1464.4, 1412.6, 1292.5, 1266.1, 1235.3, 1159.9, 1111.6, 1081.1, 1045.4, 984.1, 899.5, 841.9, 730.7, 675.6, 488.6.

[I] The analytical data were adapted from the Master thesis of the author.[618]

R_f = 0.10 (cyhex/EA = 1:1).

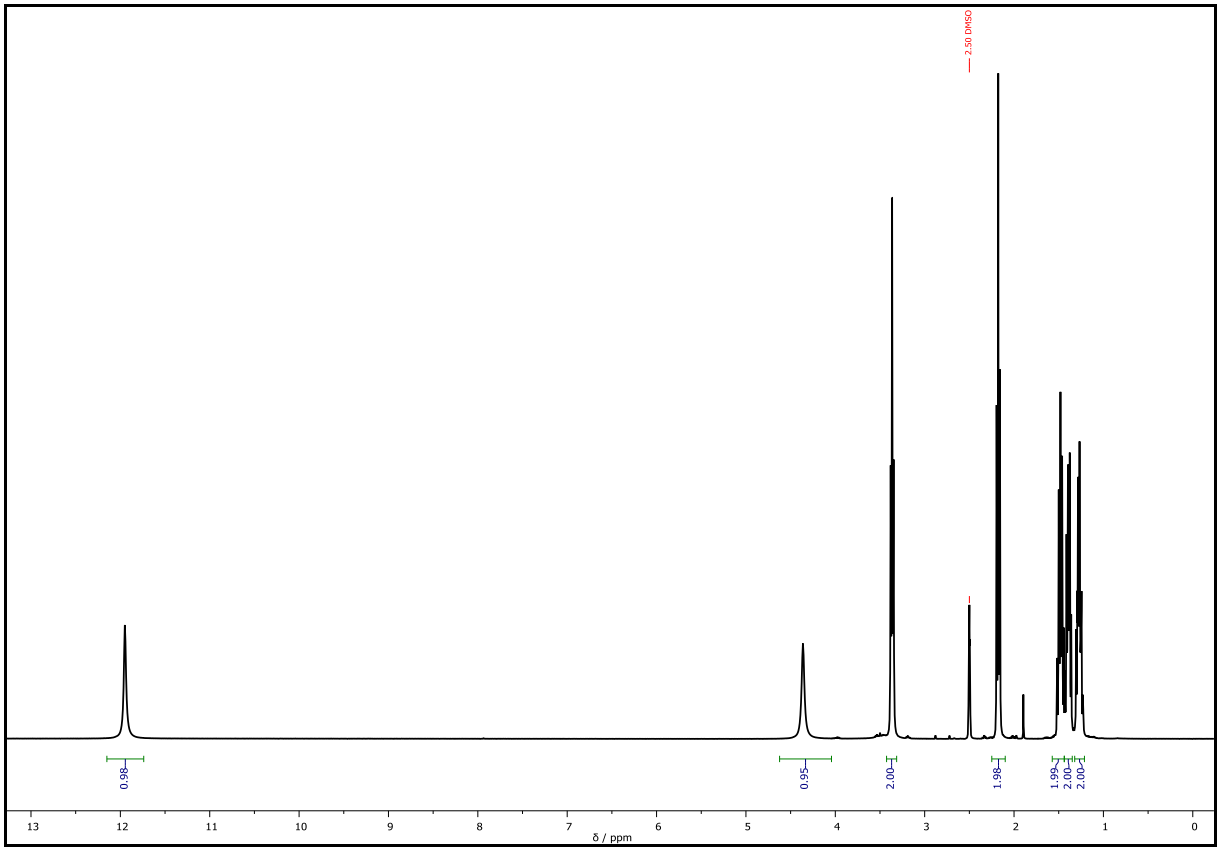

Supplementary Figure 74: ^{1}H NMR spectrum of **C1**, recorded at 400 MHz in DMSO-d_6.

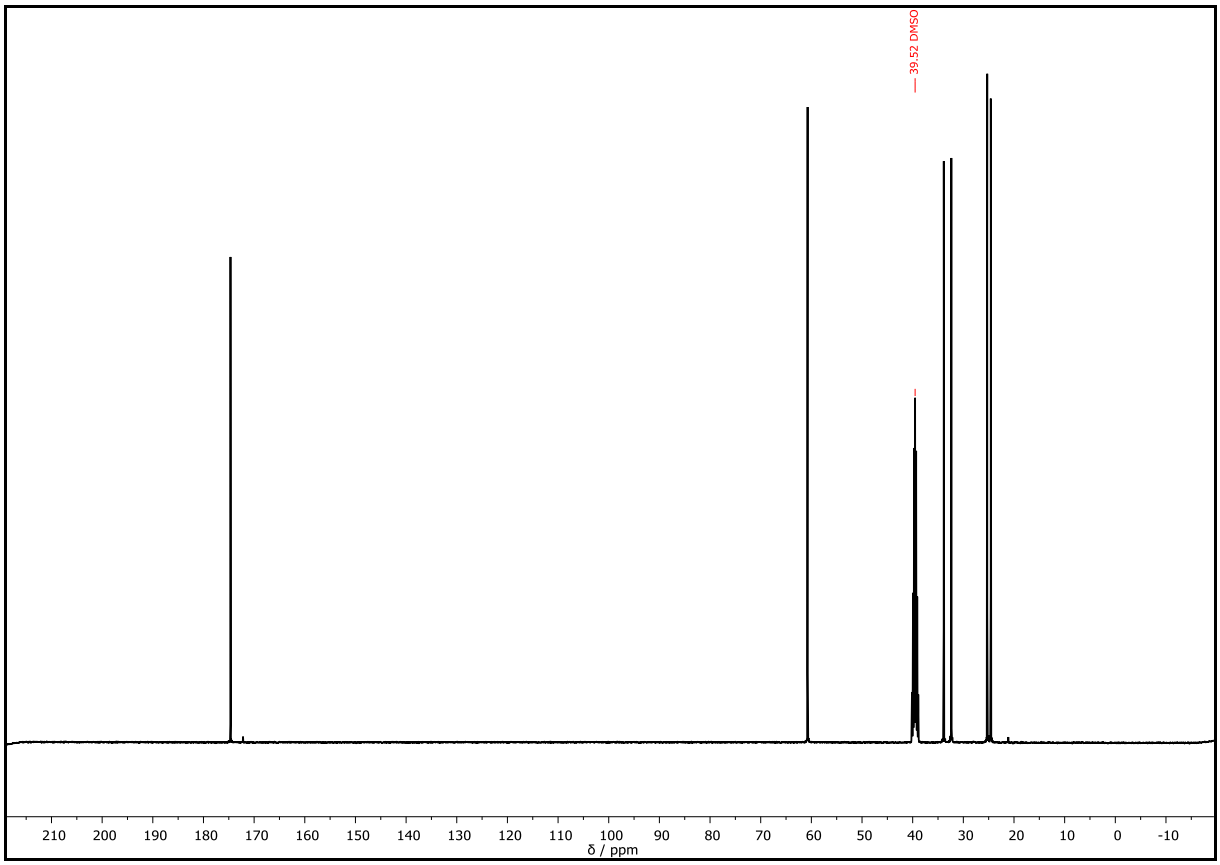

Supplementary Figure 75: ^{13}C NMR spectrum of **C1**, recorded at 101 MHz in DMSO-d_6.

6-(*tert*-Butyldimethyl)siloxyhexanoic acid – C2[l]

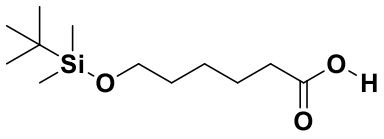

Chemical Formula: $C_{12}H_{26}O_3Si$
Exact Mass: 246.1651 Da
Molecular Weight: 246.4220 Da

6-Hydroxyhexanoic acid **C1** (16.5 g, 125 mmol, 1.00 equiv.) and imidazole (20.4 g, 300 mmol, 2.40 equiv.) were dissolved in 108 mL dry DMF. After stirring for 10 minutes at room temperature, *tert*-butyldimethylsilylchloride (24.5 g, 162 mmol, 1.30 equiv.) was added and the reaction mixture was stirred overnight at 50 °C under argon atmosphere. Subsequently, the solution was poured into a separation funnel, containing 250 mL of brine. The organic layer was separated, and the aqueous phase was extracted with diethyl ether (4 × 250 mL). The combined organic layers were dried over anhydrous sodium sulfate, filtered, and concentrated under reduced pressure.

[l] The analytical data were adapted from the Master thesis of the author.[618]

Purification of the crude product by column chromatography (cyhex/EA 1:1 → 1:3) yielded the product **C2** (26.2 g, 106 mmol, 85.3%) as a yellowish oil.

^{1}H NMR (DMSO-*d*$_6$, 400 MHz): δ / ppm = 11.96 (s, 1 H, CO_2H^1), 3.56 (t, *J* = 6.3, 2 H, CH_2^2), 2.18 (t, *J* = 7.3 Hz, 2 H, CH_2^3), 1.38-1.56 (m, 4 H, CH_2^4), 1.25–1.35 (m, 2 H, CH_2^5), 0.85 (s, 9 H, CH_3^6), 0.01 (s, 6 H, CH_3^7).

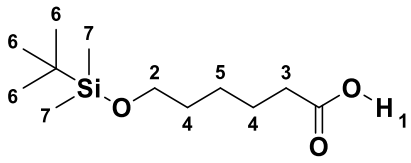

^{13}C NMR (DMSO-*d*$_6$, 101 MHz): δ / ppm = 174.39 (C_q^1), 62.37 (CH_2^2), 33.72 (CH_2^3), 32.06 (CH_2^4), 25.82 (CH_3^5), 24.97 (CH_2^6), 24.33 (CH_2^7), 17.95 (C_q^8), 5.35 (CH_3^9).

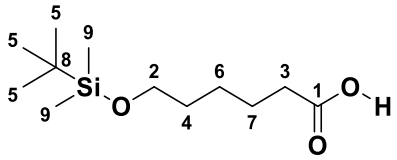

FAB of $C_{12}H_{26}O_3Si$ ($M+H^+$ = 247.2); HRMS (FAB) of $C_{12}H_{26}O_3Si$ $[M+H]^+$ calcd. 247.1729, found 247.1731.

IR (ATR platinum diamond) *v* / cm^{-1} = 2929.2, 2857.2, 1708.3, 1462.4, 1411.6, 1388.5, 1360.9, 1282.3, 1251.7, 1096.8, 1005.4, 982.6, 937.4, 832.3, 773.3, 661.0, 469.6, 403.0.

R_f = 0.52 (cyclohexane/EA = 5:1).

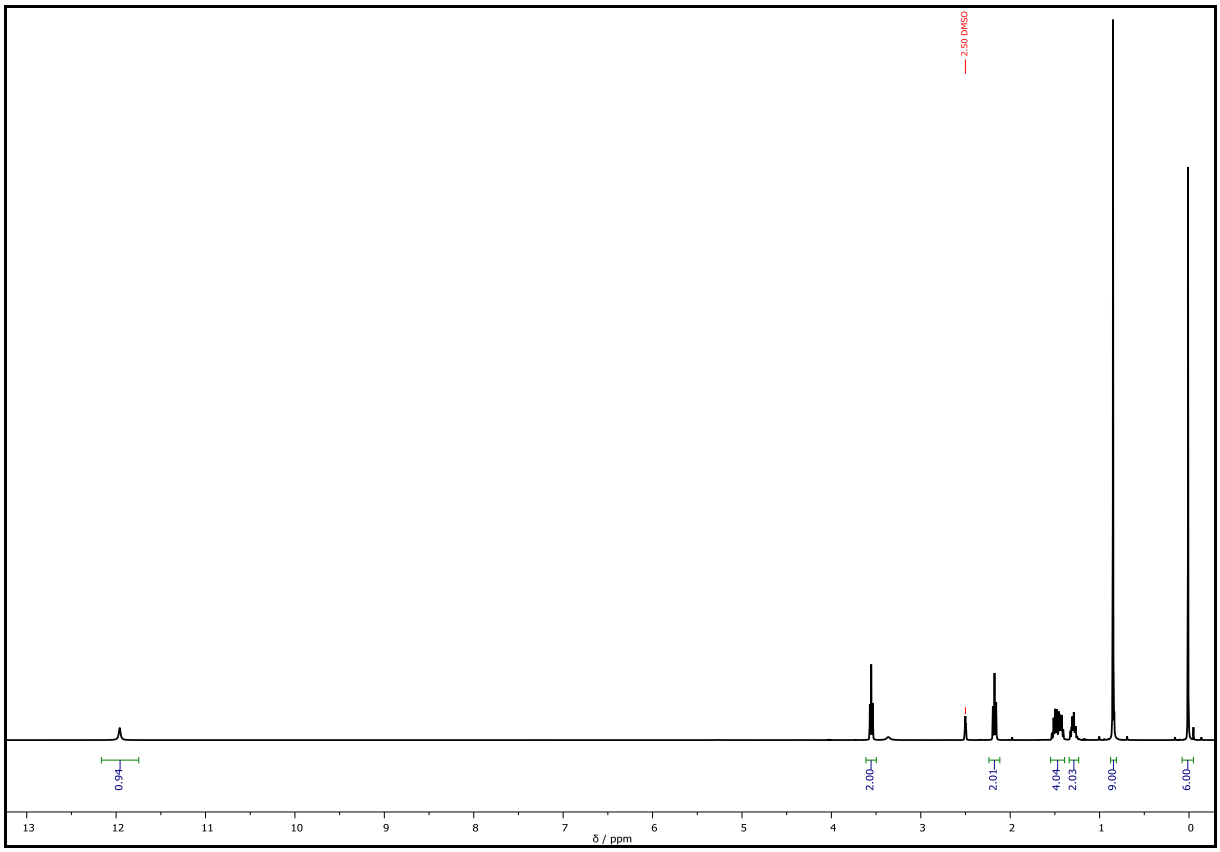

Supplementary Figure 76: ^{1}H NMR spectrum of **C2**, recorded at 400 MHz in DMSO-d_6.

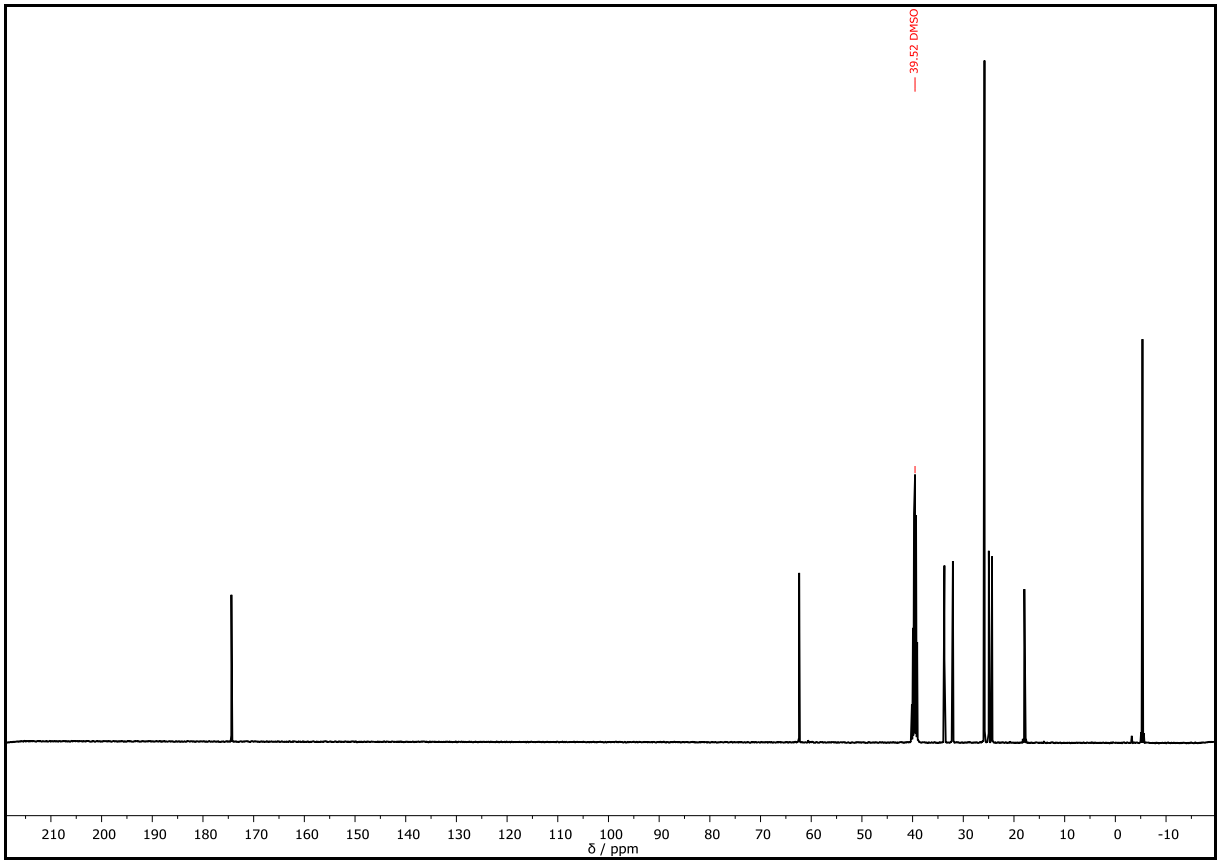

Supplementary Figure 77: ^{13}C NMR spectrum of **C2**, recorded at 101 MHz in DMSO-d_6.

Benzyl 6-hydroxyhexanoate – C3[I]

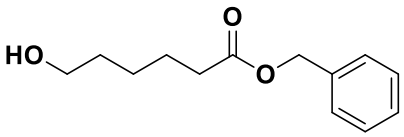

Chemical Formula: $C_{13}H_{18}O_3$
Exact Mass: 222.1256 Da
Molecular Weight: 222.2840 Da

6-Hydroxyhexanoic acid **C1** (16.8 g, 127 mmol, 1.00 equiv.) and DBU (19.3 g, 127 mmol, 1.00 equiv.) were dissolved in dichloromethane (76 mL). Benzyl bromide (18.1 mL, 26.1 g, 152 mmol, 1.20 equiv.) in dichloromethane (51 mL) was added dropwise to the solution. The reaction mixture was stirred overnight at room temperature. Subsequently, the mixture was washed with water (100 mL) and extracted with dichloromethane (2 × 100 mL). The combined organic layers were dried over anhydrous sodium sulfate, filtered, and the solvent was removed under reduced pressure. Purification of the crude product *via* column chromatography (cyhex/EA 5:1 → 1:3) yielded the benzyl-6-hydroxyhexanoate **C3** (24.8 g, 112 mmol, 87.9%) as a yellowish oil.

^{1}H NMR (DMSO-*d*$_6$, 400 MHz): δ / ppm = 7.29-7.42 (m, 5H, CH_{Ar}[1]), 5.08 (s, 2H, CH_2[2]), 4.35 (t, *J* =5.2 Hz, 1H, OH[3]), 3.31-3.41 (m, 2H, CH_2[4]), 2.34 (t, *J* = 7.4 Hz, 2H, CH_2[5]), 1.48-1.60 (m, 2H, CH_2[6]), 1.34-1.46 (m, 2H, CH_2[7]), 1.24-1.34 (m, 2H, CH_2[8]).

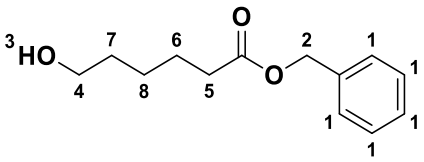

^{13}C NMR (DMSO-*d*$_6$, 101 MHz): δ / ppm = 172.79 (C_q[1]), 136.33 ($C_{q,Ar}$[2]), 128.42 ($CH_{Ar,ortho}$[3]), 127.69 ($CH_{Ar,para}$[4]), 127.92 ($CH_{Ar,meta}$[5]), 65.31 (CH_2[6]), 60.59 (CH_2[7]), 33.57 (CH_2[8]), 32.18 (CH_2[9]), 25.08 (CH_2[10]), 24.43 (CH_2[11]).

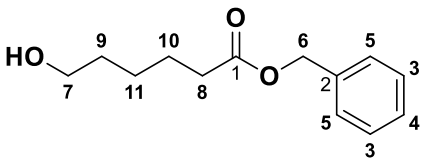

[I] The analytical data were adapted from the Master thesis of the author.[618]

FAB of $C_{13}H_{18}O_3$ ($M+H^+$ = 222.2); HRMS (FAB) of $C_{13}H_{18}O_3$ $[M+H]^+$ calcd. 222.1256, found 222.1255.

IR (ATR platinum diamond) ν / cm^{-1} = 3400.0, 3033.3, 2934.5, 2862.0, 1730.6, 1497.2, 1455.0, 1382.2, 1351.1, 1150.0, 1073.5, 1051.9, 1026.4, 736.3, 696.9, 578.2, 502.4.

R_f = 0.62 (cyhex/EA = 1:1).

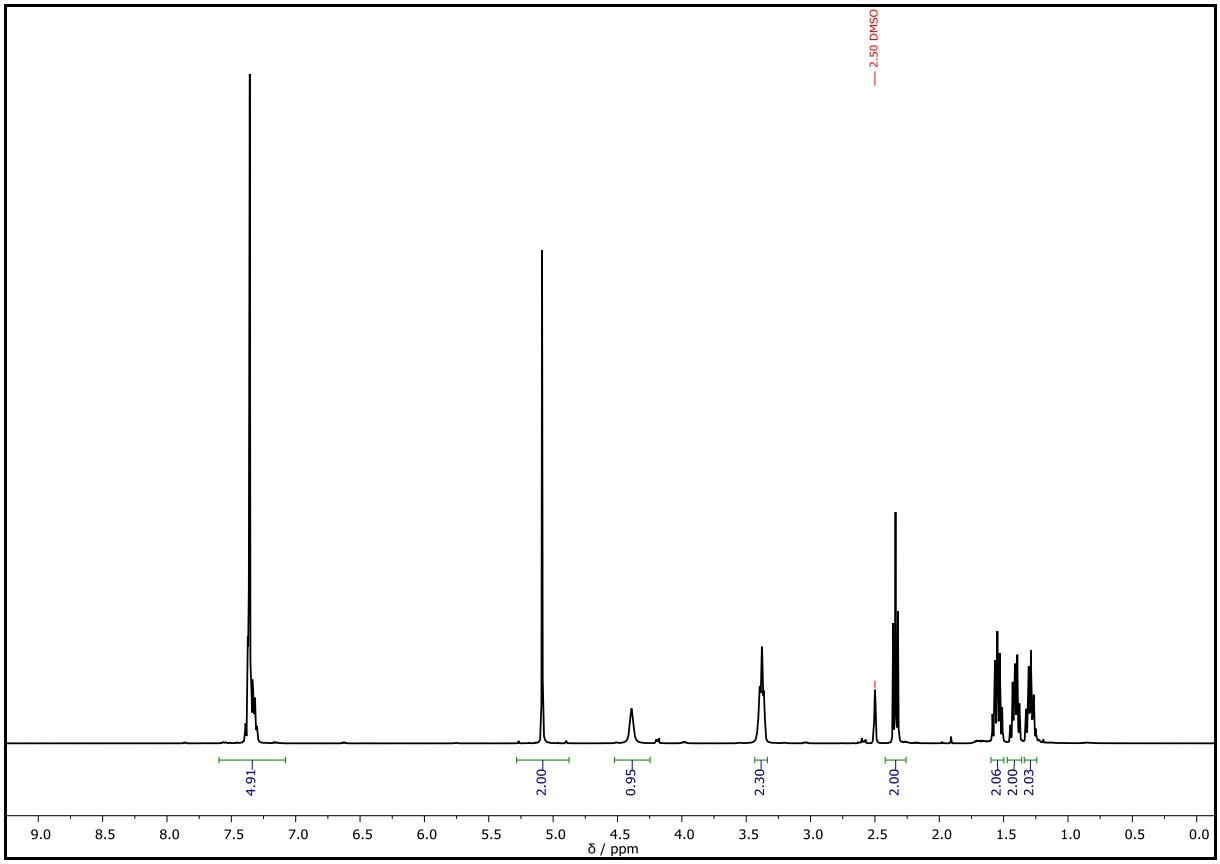

Supplementary Figure 78: ^{1}H NMR spectrum of **C3**, recorded at 400 MHz in DMSO-d_6.

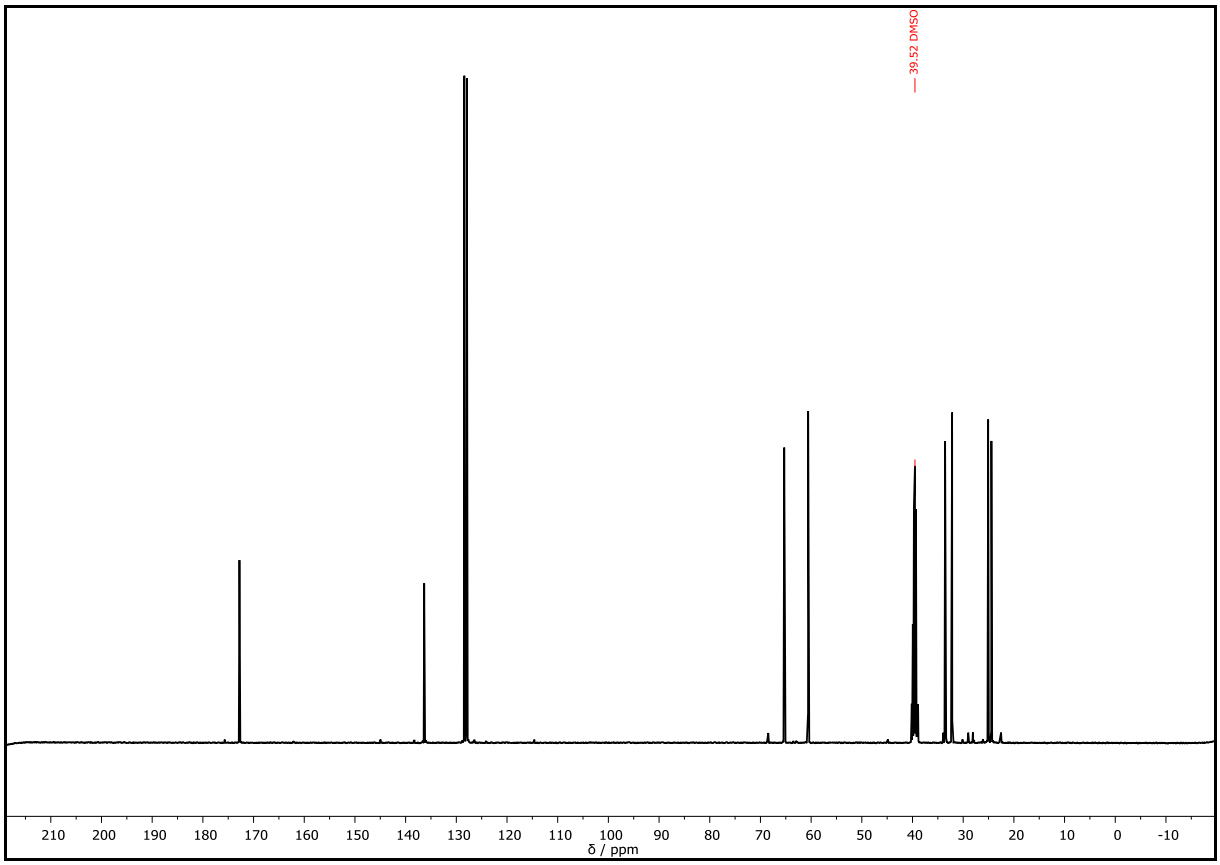

Supplementary Figure 79: ^{13}C NMR spectrum of **C3**, recorded at 101 MHz in DMSO-d_6.

Doubly protected dimer – C4[l]

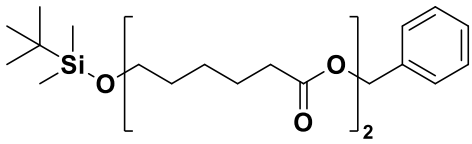

Chemical Formula: $C_{25}H_{42}O_5Si$
Exact Mass: 450.2802 Da
Molecular Weight: 450.6910 Da

6-(*tert*-Butyldimethyl)siloxyhexanoic acid **C2** (11.1 g, 45.1 mmol, 1.00 equiv.), benzyl-6-hydroxyhexanoate **C3** (10.0 g, 45.1 mmol, 1.00 equiv.), 1,3-dicyclohexylcarbodiimide (DCC) (11.2 g, 54.1 mmol, 1.10 equiv.) and 4-(dimethylamino)pyridine (DMAP) (6.60 g, 54.1 mmol, 1.10 equiv.) were dissolved in 108 mL dichloromethane. The solution was stirred overnight at room temperature until complete conversion of the starting materials was indicated by GC analysis. Subsequently, the reaction mixture was washed with 100 mL saturated $CuSO_4$-solution and twice with 100 mL of water. The organic layer was separated, dried over anhydrous sodium sulfate, filtered, and concentrated under reduced

[l] The analytical data were adapted from the Master thesis of the author.[618]

pressure. Purification of the crude product *via* column chromatography (cyhex/EA 20:1 → 8:1) yielded the doubly protected dimer **C4** (17.9 g, 39.8 mmol, 88.3%) as a colorless oil.

^{1}H NMR ($CDCl_3$, 400 MHz): δ / ppm = 7.35 (s, 5H, CH_{Ar}^{11}), 5.12 (s, 2H, CH_2^{10}), 4.04 (t, *J* = 6.6 Hz, 2H, CH_2^{9}), 3.60 (t, *J* = 6.4 Hz, 2H, CH_2^{8}), 2.36 (t, *J* = 7.5 Hz, 2H, CH_2^{7}), 2.28 (t, *J* = 7.6 Hz, 2H, CH_2^{6}), 1.58-1.71 (m, 6H, CH_2^{5}), 1.47-1.56 (m, 2H, CH_2^{4}), 1.28-1.45 (m, 4H CH_2^{3}), 0.89 (s, 9H, CH_3^{2}), 0.04 (s, 6H, CH_3^{1}).

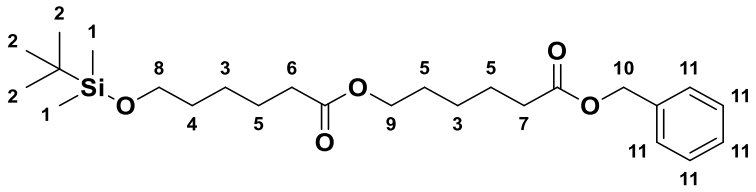

^{13}C NMR ($CDCl_3$, 101 MHz): δ / ppm = 173.80 (C_q^{1}), 173.33 (C_q^{1}), 136.12 ($C_{q,Ar}^{2}$), 128.61 (CH_{Ar}^{3}), 128.24 (CH_{Ar}^{3}), 66.19 (CH_2^{4}), 64.07 (CH_2^{5}), 63.01 (CH_2^{6}), 34.38 (CH_2^{7}), 34.18 (CH_2^{7}), 32.53 (CH_2^{8}), 28.40 (CH_2^{9}), 26.03 (CH_3^{10}), 25.58 (CH_2^{11}), 25.51 (CH_2^{11}), 24.87 (CH_2^{11}), 24.62 (CH_2^{11}), 18.40 (C_q^{12}), -5.22 (CH_3^{13}).

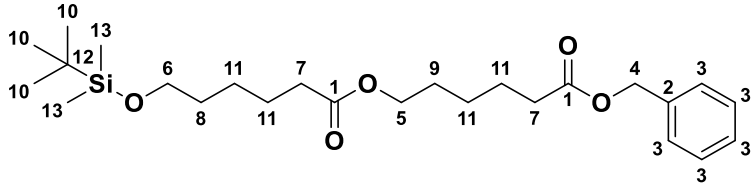

FAB of $C_{25}H_{42}O_5Si$ ($M+H^+$ = 451.3); HRMS (FAB) of $C_{25}H_{42}O_5Si$ $[M+H]^+$ calcd. 451.2880, found 451.279.

IR (ATR platinum diamond) *v* / cm^{-1} = 2930.2, 2857.2, 1733.5, 1461.5, 1386.4, 1359.6, 1253.1, 1155.7, 1094.7, 1005.0, 833.5, 774.4, 735.2, 696.8, 661.3, 577.3, 497.1, 400.2.

R_f = 0.50 (cyhex/EA = 5:1).

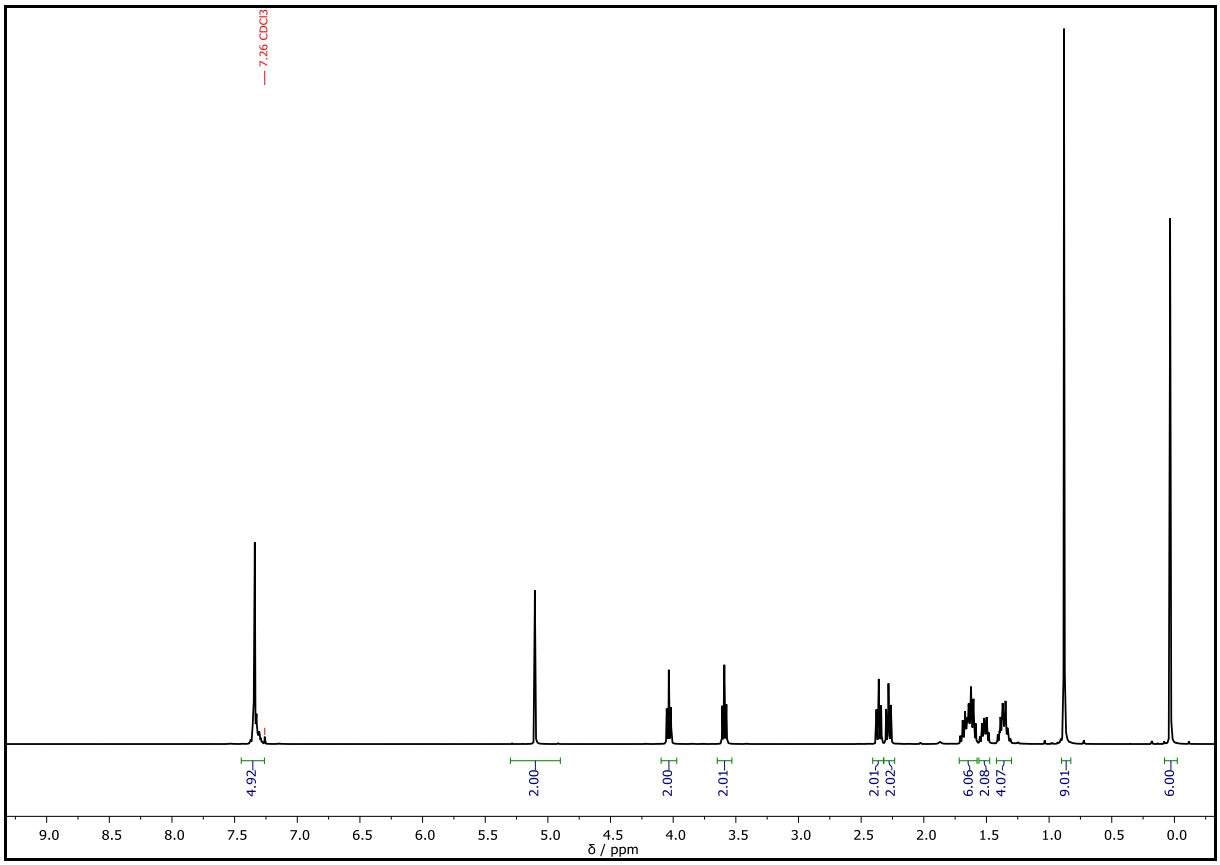

Supplementary Figure 80: ^{1}H NMR spectrum of **C4**, recorded at 400 MHz in $CDCl_3$.

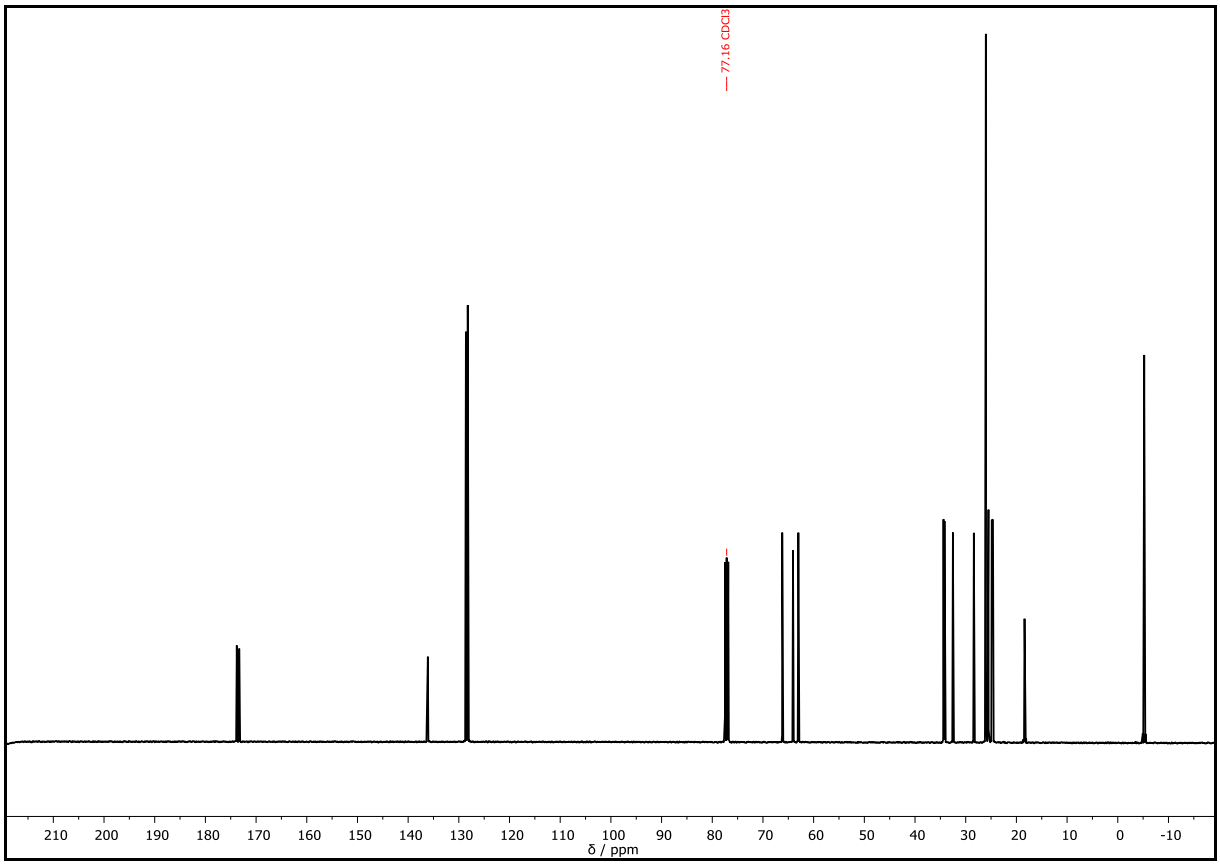

Supplementary Figure 81: ^{13}C NMR spectrum of **C4**, recorded at 101 MHz in $CDCl_3$.

Carboxyl–terminated Dimer – C5[I]

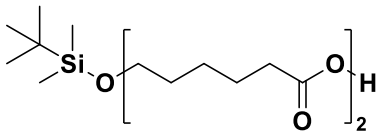

Chemical Formula: $C_{18}H_{36}O_5Si$
Exact Mass: 360.2332 Da
Molecular Weight: 360.5660 Da

Doubly protected dimer **C4** (5.00 g, 11.1 mmol, 1.00 equiv.) was dissolved in 60 mL EA under argon atmosphere. Subsequently, palladium on activated carbon (10 wt%, 500 mg) was added to the solution and the reaction mixture was stirred for 45 min under hydrogen atmosphere using a balloon. After TLC indicated complete deprotection of the starting material, the mixture was filtered through a pad of celite. The residue was washed with EA (3 × 30 mL) and the combined filtrate was concentrated under reduced pressure yielding the carboxyl terminated dimer **C5** (3.96 g, 11.0 mmol, 99.0%) as a clear colorless oil.

^{1}H NMR (DMSO-*d*$_6$, 300 MHz): δ / ppm = 12.00 (s, 1H, CO_2H^1), 3.98 (t, *J* = 6.6 Hz, 2H, CH_2^2), 3.55 (t, *J* = 6.2 Hz, 2H, CH_2^3), 2.27 (t, *J* = 7.3 Hz, 2H, CH_2^4), 2.19 (t, *J* = 7.3 Hz, 2H, CH_2^5), 1.37–1.62 (m, 8H, CH_2^6), 1.21–1.37 (m, 4H CH_2^7), 0.85 (s, 9H, CH_3^8), 0.01 (s, 6H, CH_3^9).

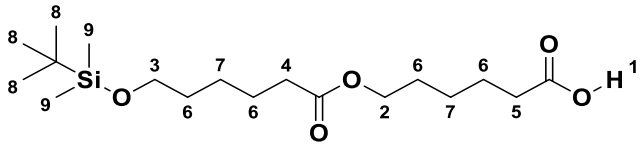

^{13}C NMR (DMSO-*d*$_6$, 101 MHz): δ / ppm = 174.36 (C_q^1), 172.78 (C_q^2), 63.50 (CH_2^3), 62.33 (CH_2^4), 33.58 (CH_2^5), 31.95 (CH_2^6), 27.94 (CH_2^7), 25.78 (CH_3^8), 25.03 (CH_2^9), 24.90 (CH_2^9), 24.33 (CH_2^9), 24.16 (CH_2^9), 17.92 (C_q^{10}), -5.39 (CH_3^{11}).

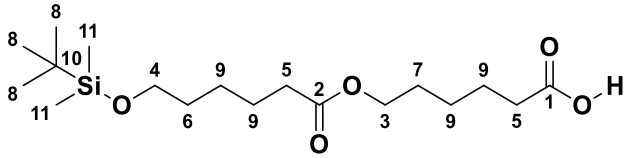

FAB of $C_{18}H_{36}O_5Si$ ($M+H^+$ = 361.3); HRMS (FAB) of $C_{18}H_{36}O_5Si$ $[M+H]^+$ calcd. 361.2410, found 361.2409.

[I] The analytical data were adapted from the Master thesis of the author.[618]

IR (ATR platinum diamond) ν / cm^{-1} = 2935.7, 2862.7, 1707.4, 1460.0, 1393.0, 1163.4, 1050.0, 835.4, 775.7, 732.2, 585.0.

R_f = 0.36 (cyhex/EA = 4:1).

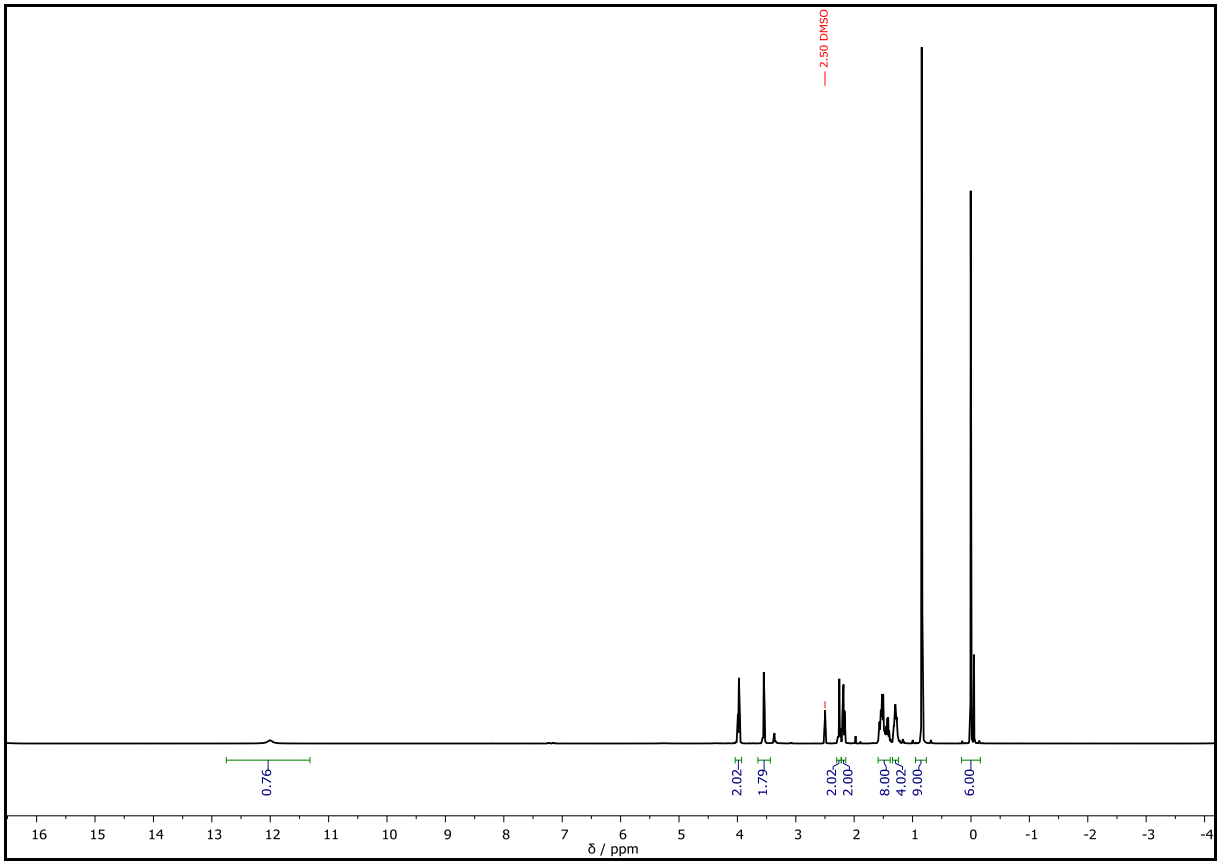

Supplementary Figure 82: ^{1}H NMR spectrum of **C5**, recorded at 300 MHz in DMSO-d_6.

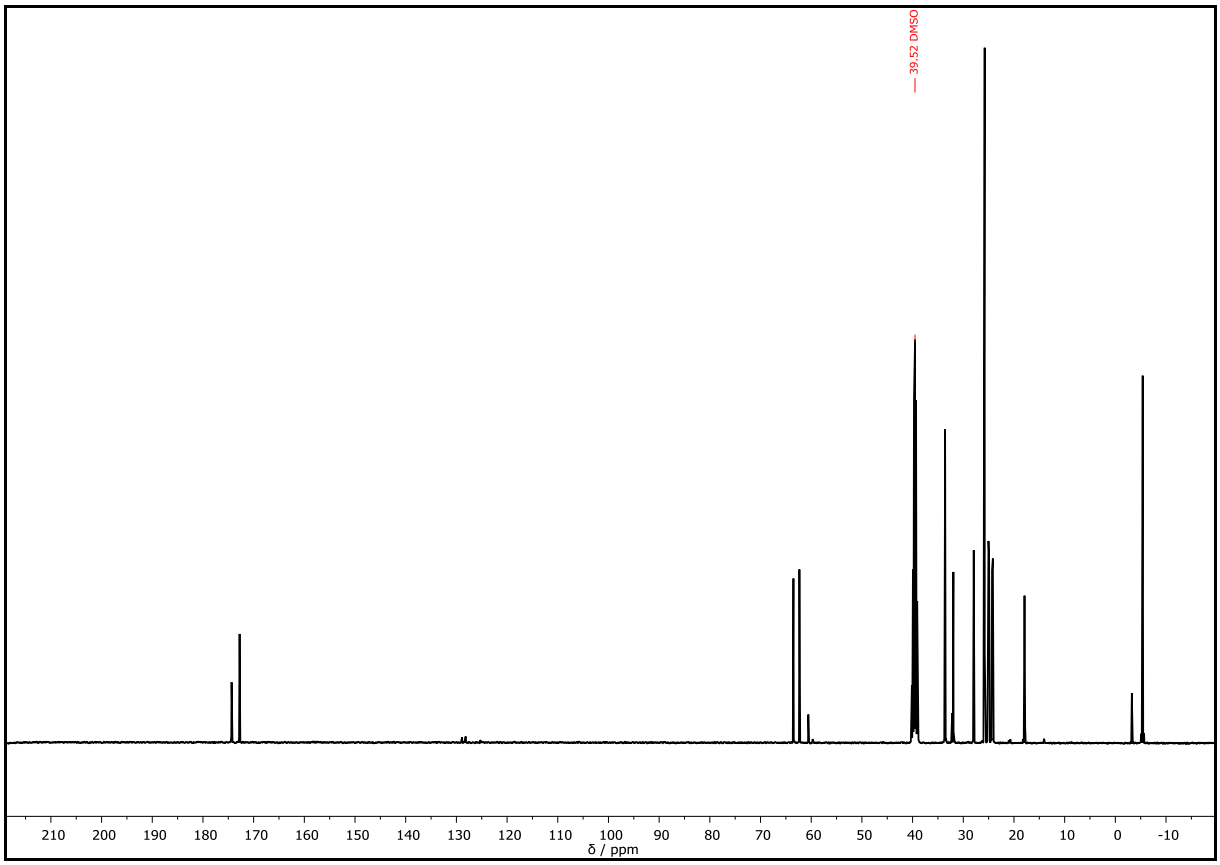

Supplementary Figure 83: ^{1}H NMR spectrum of **C5**, recorded at 101 MHz in DMSO-d_6.

Hydroxyl–terminated dimer – C6[l]

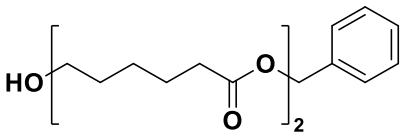

Chemical Formula: $C_{19}H_{28}O_5$
Exact Mass: 336.1937 Da
Molecular Weight: 336.4280 Da

Tetrabutylammonium fluoride (TBAF) (17.5 g, 55.5 mmol, 2.00 equiv.) and glacial acetic acid (3.18 mL, 3.33 mg, 55.5 mmol, 2.00 equiv.) were dissolved in 56 mL THF and added to a solution of doubly protected dimer **C4** (12.5 g, 27.7 mmol, 1.00 equiv.) in THF (57 mL). The reaction mixture was stirred overnight at 50 °C and monitored *via* TLC until complete conversion of the starting material. Subsequently, the mixture was poured into a separation funnel containing dichloromethane (300 mL) and water (300 mL). The organic phase was separated and washed with saturated $NaHCO_3$ (2 × 200 mL), 5 wt% citric acid (2 × 200 mL) and water (1 × 200 mL). The combined organic layers were dried over anhydrous sodium sulfate, filtered, and concentrated

[l] The analytical data were adapted from the Master thesis of the author.[618]

under reduced pressure. Purification of the crude product *via* column chromatography (cyhex/EA = 1:1) yielded the hydroxyl-terminated dimer **C6** (9.23 g, 27.4 mmol, 98.9%) as a colorless oil.

^{1}H NMR (DMSO-d_6, 300 MHz): δ / ppm = 7.27–7.39 (m, 5H, CH_{Ar}^{1}), 5.09 (s, 2H, CH_2^{2}), 4.37 (t, J =5.1 Hz, 1H, OH^{3}), 3.98 (t, J = 6.6, 2H, CH_2^{4}), 3.38 (t, J = 6.4 Hz, 2H, CH_2^{5}), 2.35 (t, J = 7.4, 2H, CH_2^{6}), 2.25 (t, J = 7.4, 2H, CH_2^{7}), 1.46-1.62 (m, 6H, CH_2^{8}), 1.35-1.46 (m, 2H, CH_2^{9}), 1.22-1.35 (m, 4H, CH_2^{10}).

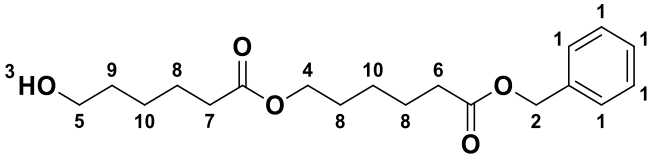

^{13}C NMR (DMSO-d_6, 101 MHz): δ / ppm = 172.89 (C_q^{1}), 172.66 (C_q^{1}), 136.30 ($C_{q,Ar}^{2}$), 128.40 ($CH_{Ar,meta}^{3}$), 127.96 ($CH_{Ar,para}^{4}$), 127.91 ($CH_{Ar,ortho}^{5}$), 65.33 (CH_2^{6}), 63.48 (CH_2^{7}), 60.58 (CH_2^{8}), 33.36 (CH_2^{9}), 33.34 (CH_2^{9}), 32.19 (CH_2^{10}), 27.83 (CH_2^{11}), 25.08 (CH_2^{12}), 24.91 (CH_2^{12}), 24.45 (CH_2^{13}), 24.10 (CH_2^{13}).

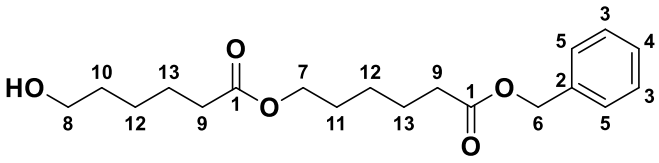

FAB of $C_{19}H_{28}O_5$ ($M+H^+$ = 337.2); HRMS (FAB) of $C_{19}H_{28}O_5$ $[M+H]^+$ calcd. 337.2015, found 337.2014.

IR (ATR platinum diamond) $\tilde{\nu}$ / cm^{-1} = 3431.4, 2936.2, 2863.1, 1729.3, 1497.7, 1455.5, 1385.1, 1353.3, 1154.6, 1080.1, 736.3, 697.5, 579.8, 498.1.

R_f = 0.63 (cyhex/EA = 1:1).

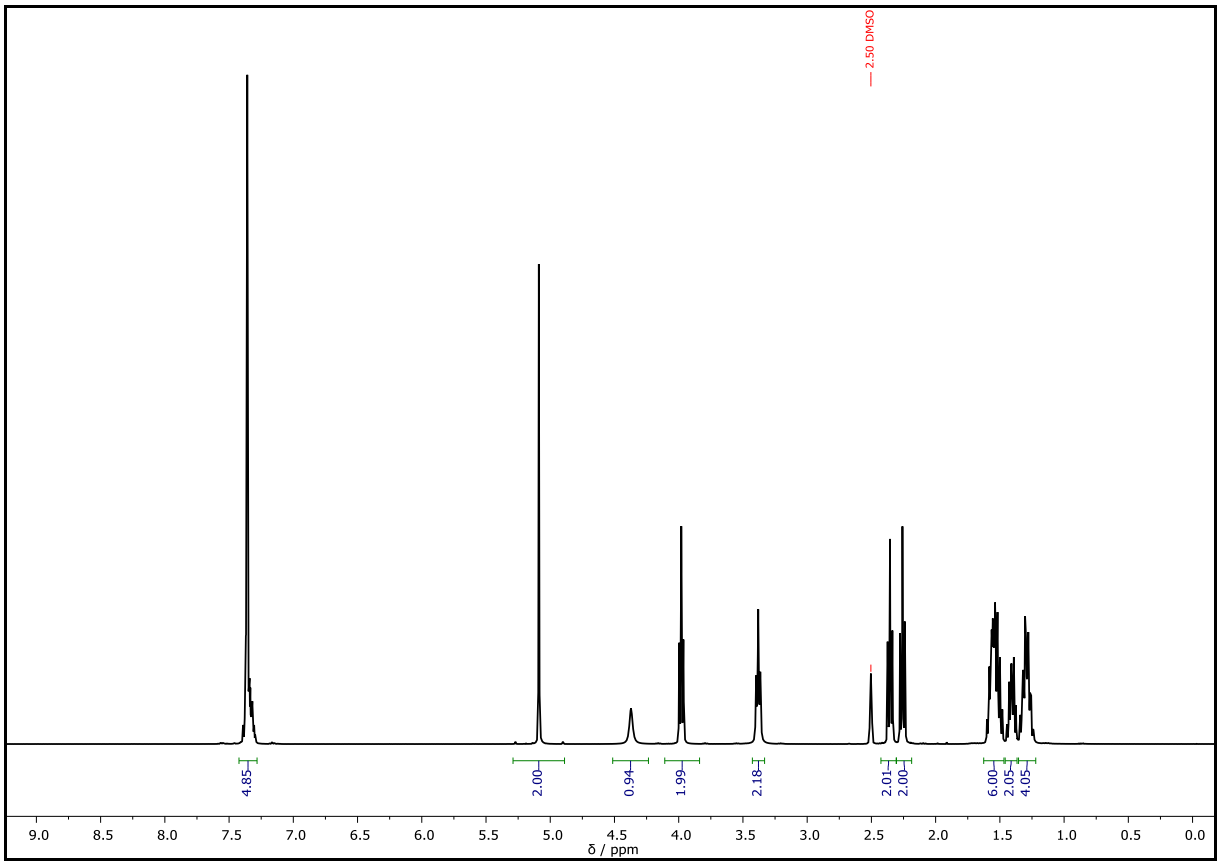

Supplementary Figure 84: ^{1}H NMR spectrum of **C6**, recorded at 300 MHz in DMSO-d_6.

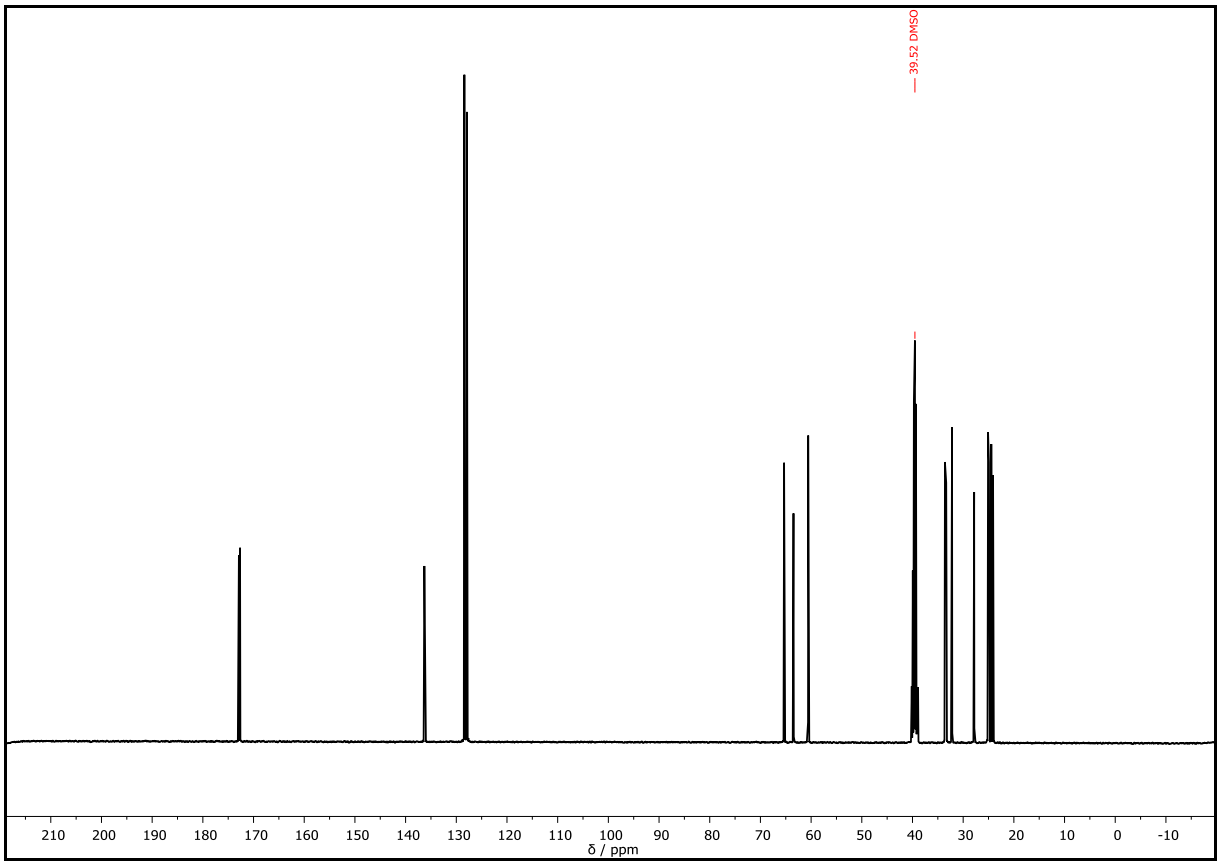

Supplementary Figure 85: ^{1}H NMR spectrum of **C6**, recorded at 101 MHz in DMSO-d_6.

Doubly protected tetramer – C7[I]

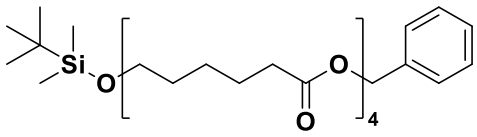

Chemical Formula: $C_{37}H_{62}O_9Si$
Exact Mass: 678.4163 Da
Molecular Weight: 678.9790 Da

The doubly protected tetramer **C7** was prepared using the procedure described above for the synthesis of the doubly protected dimer **C4**. The reaction was performed in two batches, which were combined and purified in one batch *via* column chromatography. Quantities of the starting materials and the yield are the sum of both reactions.

C5	31.0 g, 86.3 mmol, 1.00 equiv.
C6	29.0 g, 86.3 mmol, 1.00 equiv.
DCC	19.6 g, 94.9 mmol, 1.10 equiv.
DMAP	11.6 g, 94.9 mmol, 1.10 equiv.
DCM	208 mL
eluent	cyhex/EA = 5:1
yield	51.5 g, 75.9 mmol, 87.9%, colorless oil
R_f	0.32 (cyhex/EA = 6:1).
Đ (system II)	1.00

^{1}H NMR ($CDCl_3$, 300 MHz): δ / ppm = 7.34 (s, 5H, CH_{Ar}^1), 5.10 (s, 2H, CH_2^2), 4.04 (t, J = 6.6 Hz, 6H, CH_2^3), 3.59 (t, J = 6.4 Hz, 2H, CH_2^4), 2.35 (t, J = 7.5 Hz, 2H, CH_2^5), 2.28 (t, J = 7.6 Hz, 6H, CH_2^6), 1.55-1.73 (m, 14H, CH_2^7), 1.45-1.55 (m, 2H, CH_2^8), 1.28-1.43 (m, 8H CH_2^9), 0.87 (s, 9H, CH_3^{10}), 0.03 (s, 6H, CH_3^{11}).

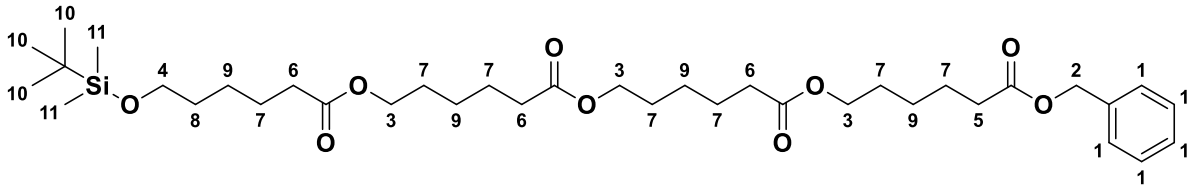

[I] The analytical data were adapted from the Master thesis of the author.[618]

^{13}C NMR ($CDCl_3$, 101 MHz): δ / ppm = 173.92 (C_q^1), 173.66 (C_q^1), 173.43 (C_q^1), 136.14 ($C_{q,Ar}^2$), 128.68 ($CH_{Ar,meta}^3$), 128.34 ($CH_{Ar,para}^4$), 128.31 ($CH_{Ar,ortho}^5$), 66.28 (CH_2^6), 64.24 (CH_2^7), 64.17 (CH_2^7), 63.09 (CH_2^8), 34.45 (CH_2^9), 34.24 (CH_2^{10}), 32.59 (CH_2^{11}), 28.46 (CH_2^{12}), 28.44 (CH_2^{12}), 26.08 (CH_3^{13}), 25.65 (CH_2^{14}), 25.57 (CH_2^{14}), 24.93 (CH_2^{15}), 24.70 (CH_2^{15}), 24.67 (CH_2^{15}), 18.46 (C_q^{16}), -5.16 (CH_3^{17}).

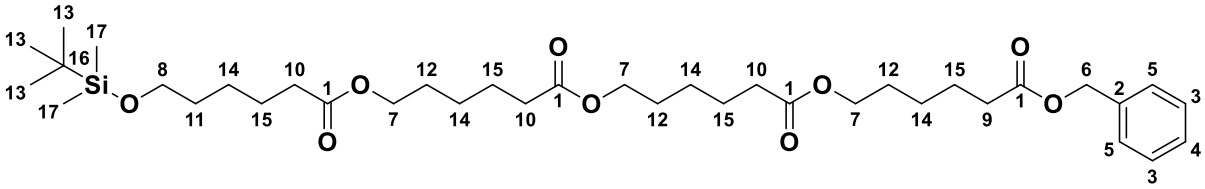

FAB of $C_{37}H_{62}O_9Si$ ($M+H^+$ = 679.4); HRMS (FAB) of $C_{37}H_{62}O_9Si$ $[M+H]^+$ calcd. 679.4241, found 679.4242.

IR (ATR platinum diamond) $\tilde{\nu}$ / cm^{-1} = 2932.4, 2858.3, 1732.6, 1459.2, 1387.4, 1358.8, 1232.4, 1157.2, 1094.2, 833.8, 774.9, 736.3, 697.0, 500.8, 445.0.

R_f = 0.32 (cyhex/EA = 6:1).

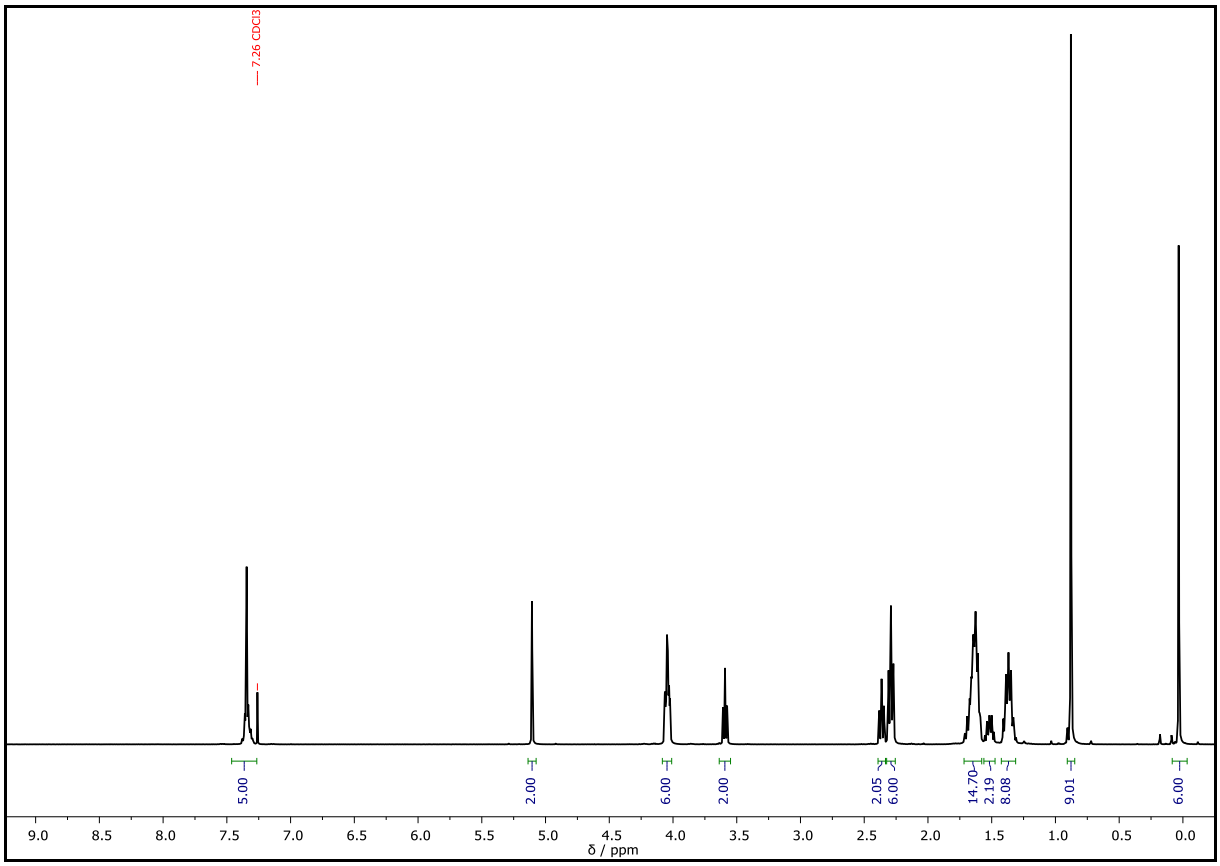

Supplementary Figure 86: ^{1}H NMR spectrum of **C7**, recorded at 300 MHz in $CDCl_3$.

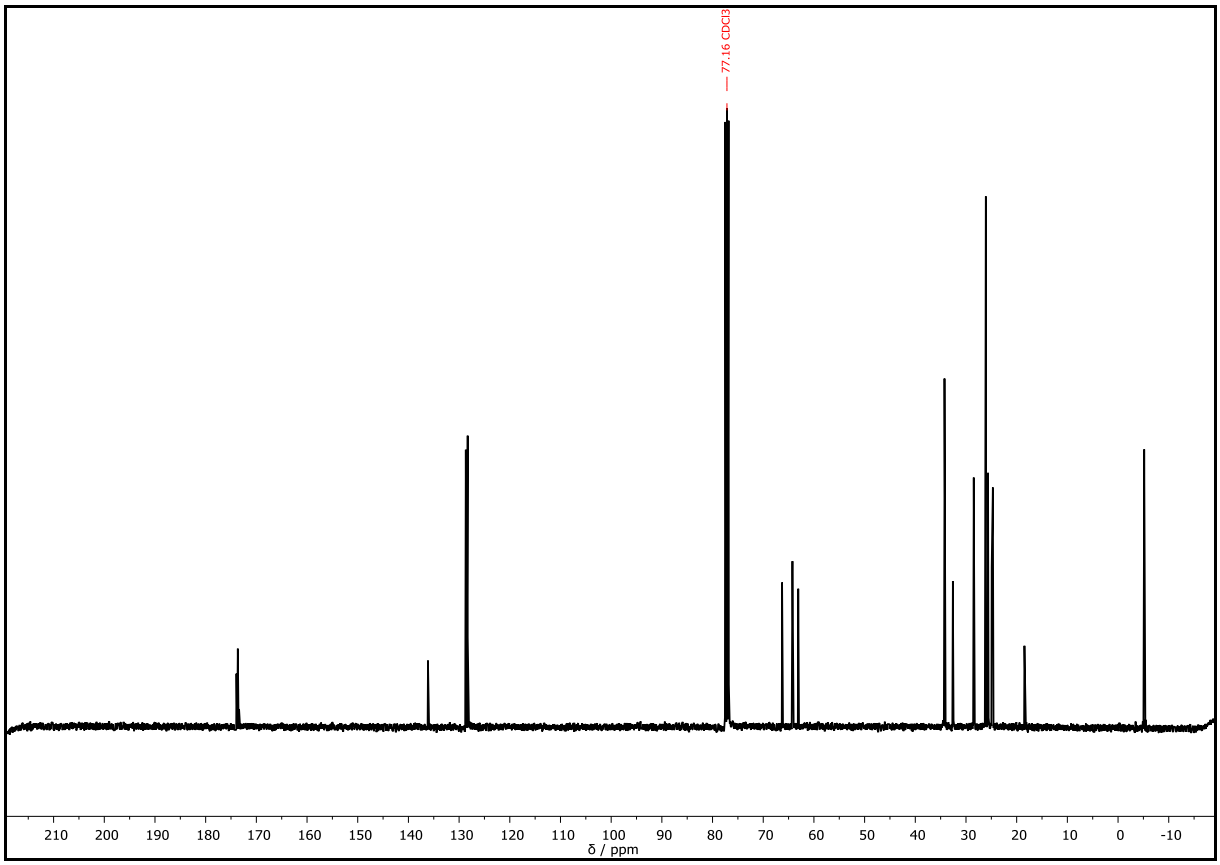

Supplementary Figure 87: ^{13}C NMR spectrum of **C7**, recorded at 101 MHz in $CDCl_3$.

Carboxyl–terminated tetramer – C8[l]

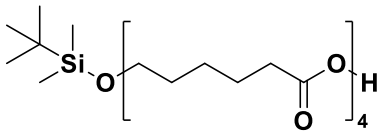

Chemical Formula: $C_{30}H_{56}O_9Si$
Exact Mass: 588.3694 Da
Molecular Weight: 588.8540 Da

The carboxyl-terminated tetramer **C8** was prepared using the procedure described above for the synthesis of the carboxyl-terminated dimer **C5**.

C7	10.0 g, 14.7 mmol, 1.00 equiv.
Pd/C	1.00 g, 10 wt%
EA	120 mL
yield	8.59 g, 14.6 mmol, 99.1%, colorless oil
Đ (system II)	1.00

[l] The analytical data were adapted from the Master thesis of the author.[618]

^{1}H NMR (DMSO-d_6, 400 MHz): δ / ppm = 12.00 (s, 1H, CO_2H^1), 3.98 (t, J = 6.5 Hz, 6H, CH_2^2), 3.55 (t, J = 6.2 Hz, 2H, CH_2^3), 2.27 (td, J = 7.3, 3.8 Hz, 6H, CH_2^4), 2.19 (t, J = 7.3 Hz, 2H, CH_2^5), 1.46-1.62 (m, 14H, CH_2^6), 1.38–1.46 (m, 2H, CH_2^7), 1.22–1.36 (m, 8H CH_2^8), 0.85 (s, 9H, CH_3^9), 0.01 (s, 6H, CH_3^{10}).

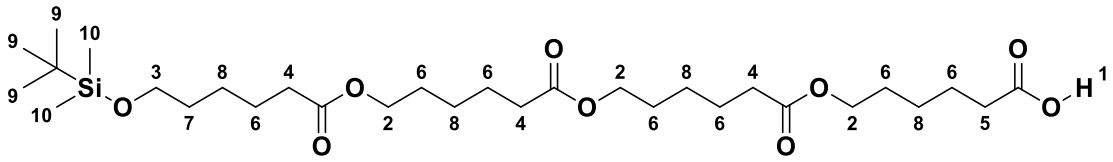

^{13}C NMR (DMSO-d_6, 101 MHz): δ / ppm = 174.35 (C_q^1), 172.83 (C_q^2), 172.77 (C_q^2), 172.76 (C_q^2), 63.50 (CH_2^3), 62.30 (CH_2^4), 33.57 (CH_2^5), 33.52 (CH_2^5), 33.37 (CH_2^5), 31.90 (CH_2^6), 27.88 (CH_2^7), 27.81 (CH_2^7), 25.80 (CH_3^8), 24.98 (CH_2^9), 24.90 (CH_2^9), 24.86 (CH_2^9), 24.30 (CH_2^{10}), 24.09 (CH_2^{10}), 17.92 (C_q^{11}), -5.35 (CH_3^{12}).

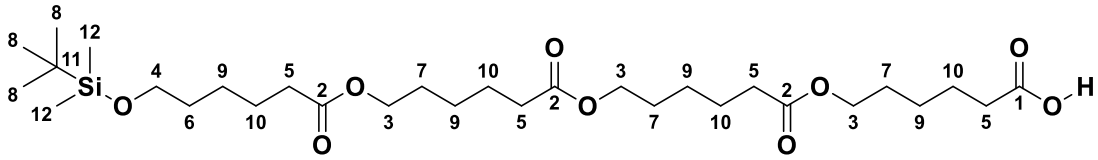

FAB of $C_{30}H_{56}O_9Si$ ($M+H^+$ = 589.4); HRMS (FAB) of $C_{30}H_{56}O_9Si$ $[M+H]^+$ calcd. 589.3772, found 589.3773.

IR (ATR platinum diamond) ν / cm^{-1} = 2931.5, 2858.3, 1732.2, 1708.8, 1461.8, 1389.6, 1359.8, 1232.9, 1159.0, 1094.1, 1006.0, 833.9, 774.9, 661.5, 398.2.

R_f = 0.26 (cyhex/EA = 2:1).

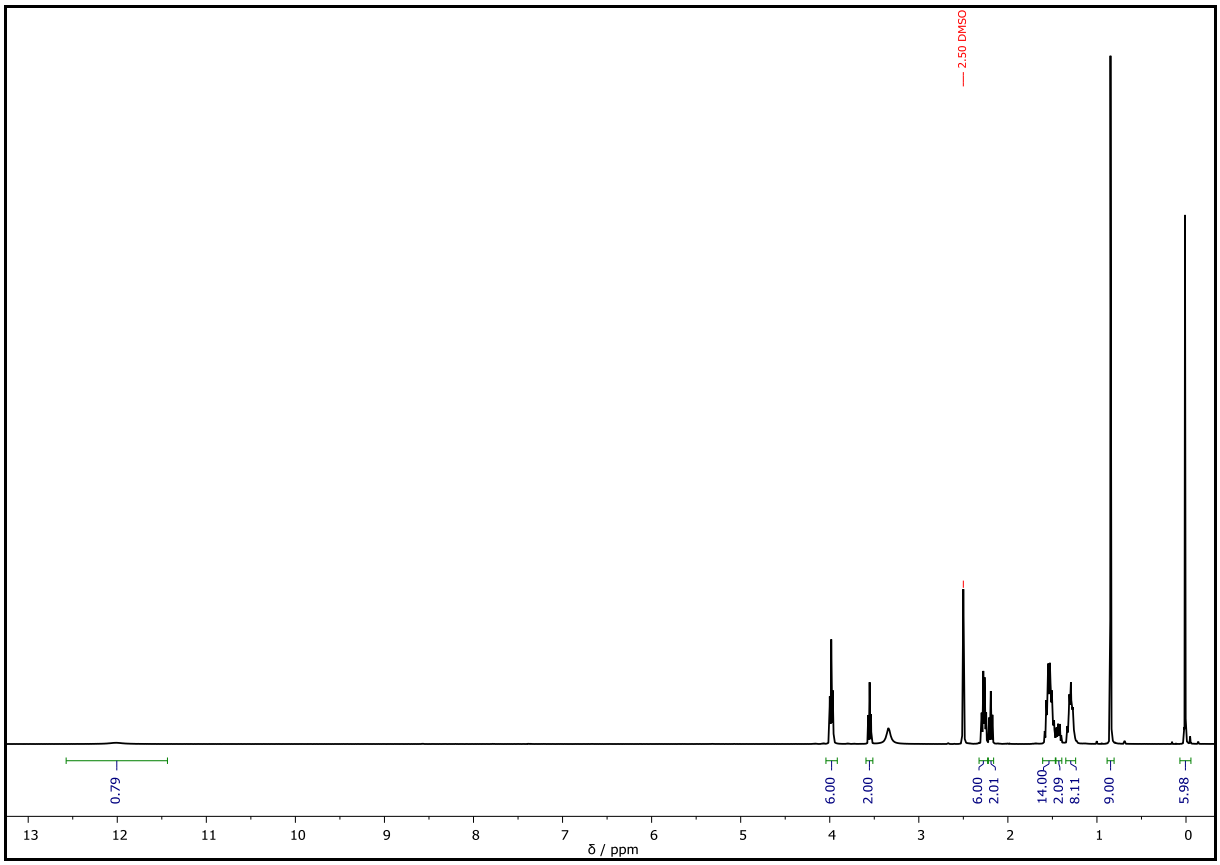

Supplementary Figure 88: ^{1}H NMR spectrum of **C8**, recorded at 400 MHz in DMSO-d_6.

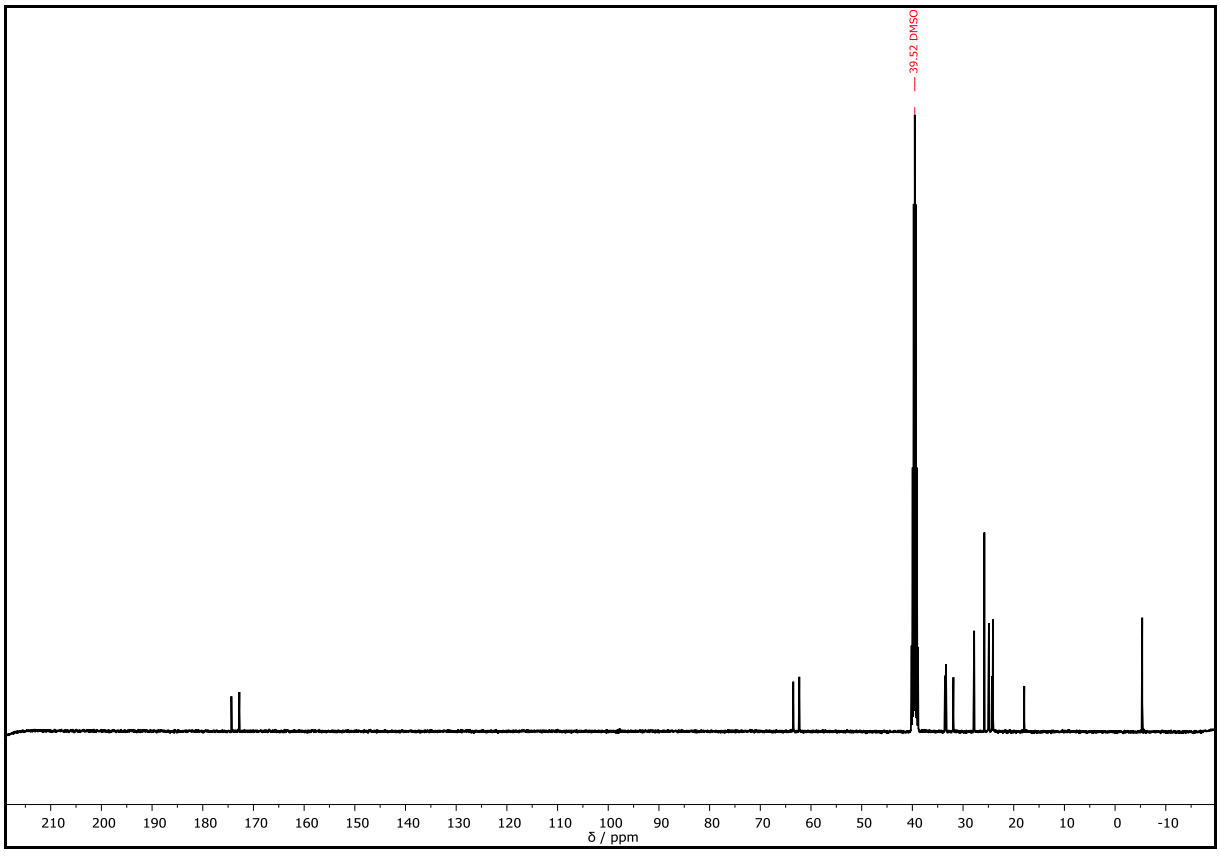

Supplementary Figure 89: ^{13}C NMR spectrum of **C8**, recorded at 101 MHz in DMSO-d_6.

Hydroxyl–terminated tetramer – C9[I]

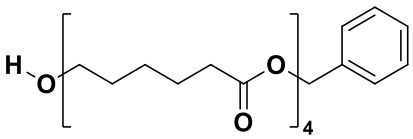

Chemical Formula: $C_{31}H_{48}O_9$
Exact Mass: 564.3298 Da
Molecular Weight: 564.7160 Da

The hydroxyl-terminated tetramer **C9** was prepared according to the procedure described above for the synthesis of the hydroxyl-terminated dimer **C6**.

C7	6.00 g, 8.84 mmol, 1.00 equiv.
TBAF	16.0 g, 17.7 mmol, 2.00 equiv.
glacial acetic acid	1.01 mL, 1.06 g, 17.7 mmol, 2.00 equiv.
total THF	35.0 mL
eluent	cyclohexane/EA = 1:1
yield	4.98 g, 8.82 mmol, 99.8%, colorless oil
R_f	0.42 (cyhex/EA = 1:1).
Đ (system II)	1.00

^{1}H NMR (DMSO-d_6, 300 MHz): δ / ppm = 7.26–7.42 (m, 5H, CH_{Ar}^1), 5.08 (s, 2H, CH_2^2), 4.37 (s, 1H, OH^3), 3.98 (t, J = 6.5, 6H, CH_2^4), 3.35 (t, J = 6.4 Hz, 2H, CH_2^5), 2.36 (t, J = 7.3 Hz, 2H, CH_2^6), 2.26 (m, 6H, CH_2^7), 1.46-1.62 (m, 14H, CH_2^8), 1.36-1.45 (m, 2H, CH_2^9), 1.20-1.36 (m, 8H, CH_2^{10}).

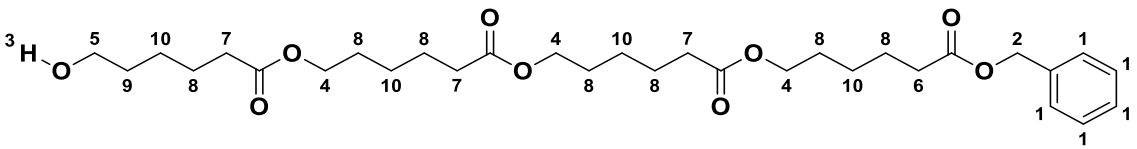

[I] The analytical data were adapted from the Master thesis of the author.[618]

^{13}C NMR (DMSO-d_6, 101 MHz): δ / ppm = 172.90 (C_q^1), 172.80 (C_q^1), 172.67 (C_q^1), 136.28 ($C_{q,Ar}^2$), 128.41 ($CH_{Ar,meta}^3$), 127.97 ($CH_{Ar,para}^4$), 127.91 ($CH_{Ar,ortho}^5$), 65.31 (CH_2^6), 63.50 (CH_2^7), 63.46 (CH_2^7), 60.53 (CH_2^8), 33.58 (CH_2^9), 33.37 (CH_2^9), 33.32 (CH_2^9), 32.16 (CH_2^{10}), 27.80 (CH_2^{11}), 25.05 (CH_2^{12}), 24.89 (CH_2^{12}), 24.42 (CH_2^{13}), 24.09 (CH_2^{13}), 24.07 (CH_2^{13}).

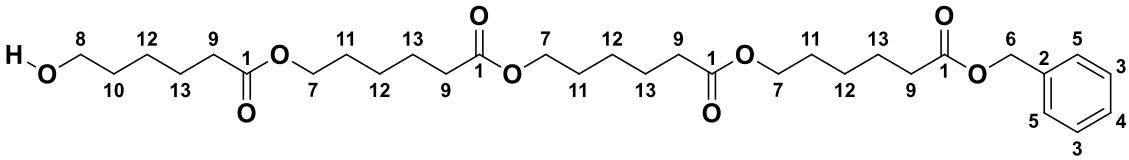

FAB of $C_{31}H_{48}O_9$ ($M+H^+$ = 565.3); HRMS (FAB) of $C_{31}H_{48}O_9$ $[M+H]^+$ calcd. 565.3377, found 565.3375.

IR (ATR platinum diamond) $\tilde{\nu}$ / cm^{-1} = 3528.8, 2936.8, 2863.0, 1730.0, 1455.7, 1388.0, 1354.3, 1158.8, 1090.7, 738.0, 698.3, 580.7, 387.8.

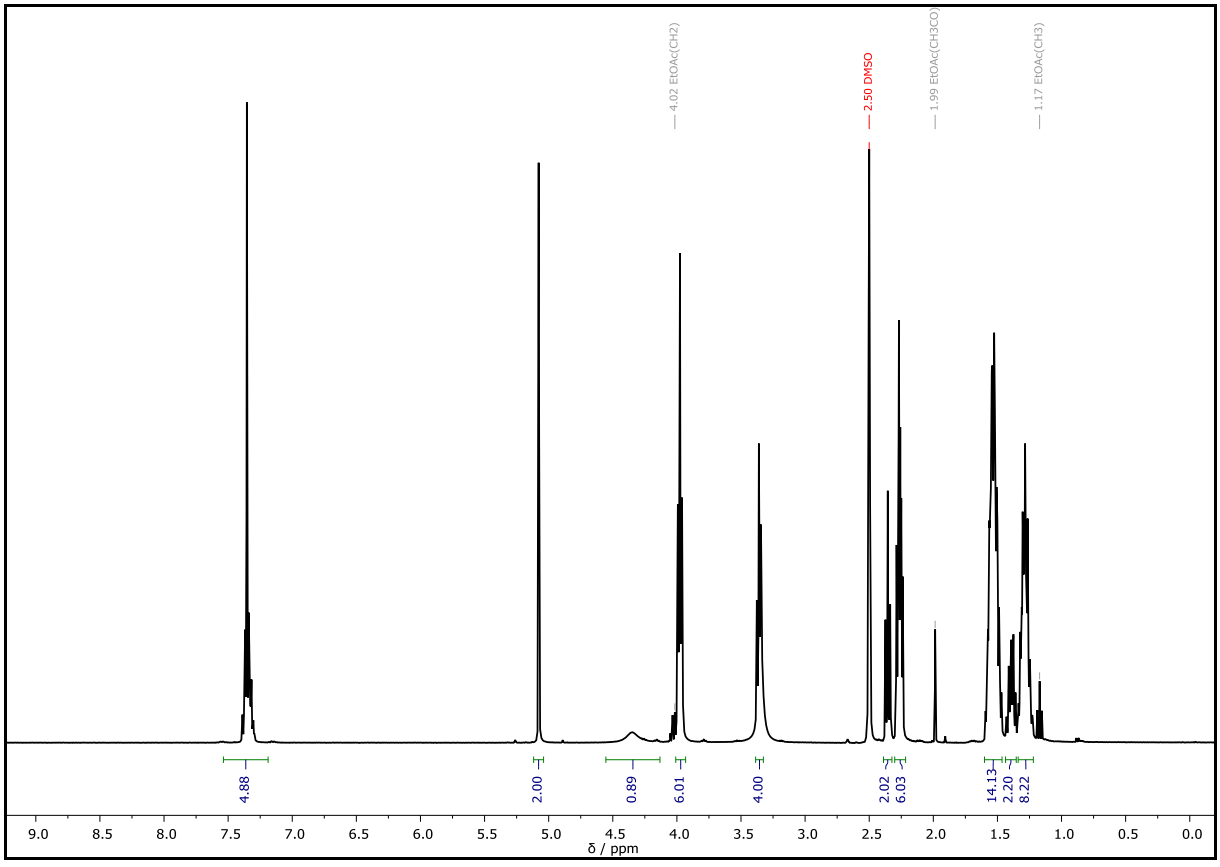

Supplementary Figure 90: ^{1}H NMR spectrum of **C9**, recorded at 300 MHz in DMSO-d_6.

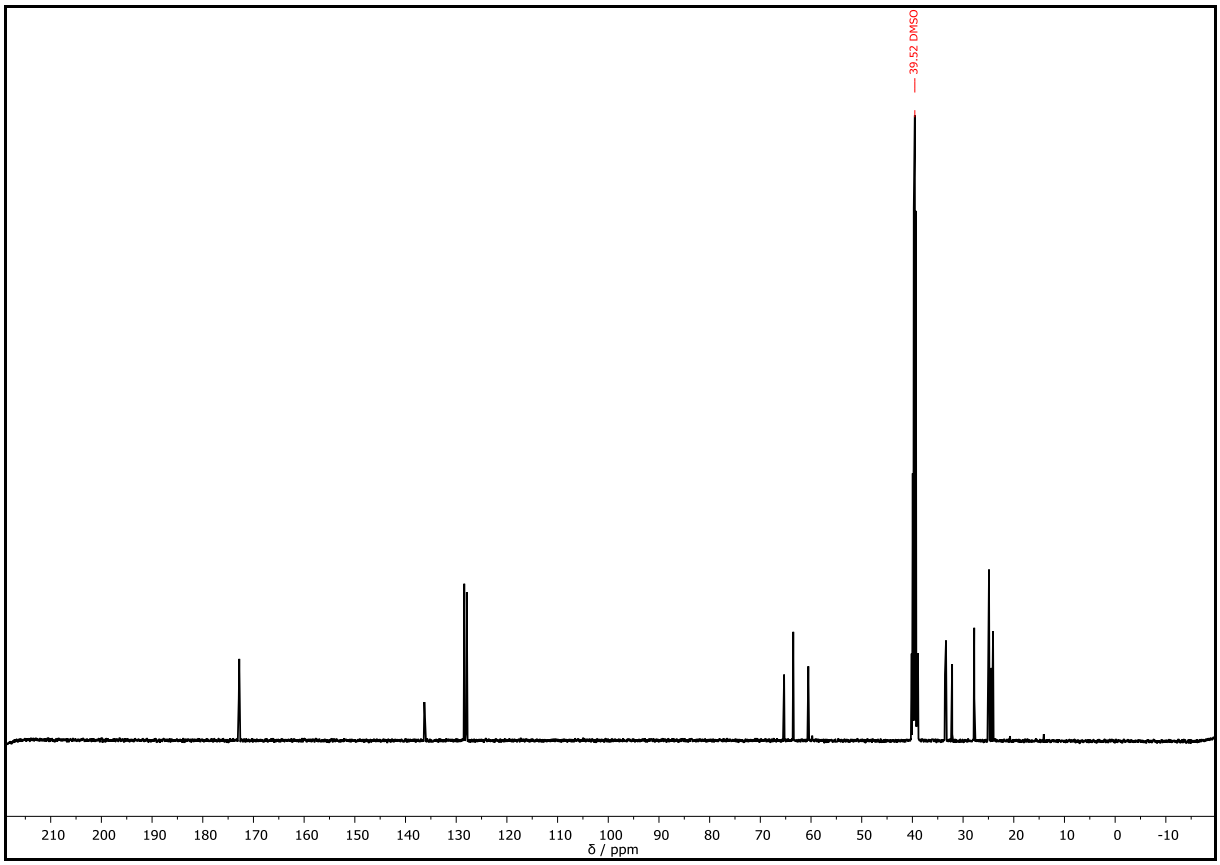

Supplementary Figure 91: ^{13}C NMR spectrum of **C9**, recorded at 101 MHz in DMSO-d_6.

Doubly protected octamer – C10

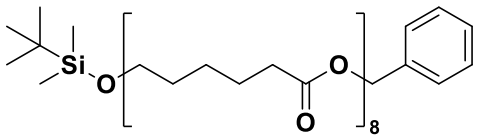

Chemical Formula: $C_{61}H_{102}O_{17}Si$
Exact Mass: 1134.6886 Da
Molecular Weight: 1135.5550 Da

The doubly protected octamer **C10** was prepared using the procedure described above for the synthesis of the doubly protected dimer **C4**. 0.20 equiv. DPTS was used instead of 1.10 equiv. DMAP.

C8	24.5 g, 41.5 mmol, 1.00 equiv.
C9	23.5 g, 41.5 mmol, 1.00 equiv.
DCC	9.43 g, 45.7 mmol, 1.10 equiv.
DPTS	2.45 g, 8.31 mmol, 0.20 equiv.
DCM	100 mL
eluent	cyhex/EA = 3:1
yield	44.5 g, 39.2 mmol, 94.4%, white solid
R_f	0.50 (cyhex/EA = 2:1).
Đ (system II)	1.00

^{1}H NMR (DMSO-d_6, 400 MHz): δ / ppm = 7.41 – 7.30 (m, 5H, CH_{Ar}^1), 5.08 (s, 2H, CH_2^2), 3.98 (t, J = 6.4 Hz, 14H, CH_2^3), 3.55 (t, J = 6.2 Hz, 2H, CH_2^4), 2.35 (t, J = 7.3 Hz, 2H, CH_2^5), 2.26 (t, J = 7.4 Hz, 14H, CH_2^6), 1.64 – 1.45 (m, 30H, CH_2^7), 1.41 (t, J = 6.9 Hz, 2H, CH_2^8), 1.36 – 1.22 (m, 16H, CH_2^9), 0.85 (s, 9H, CH_3^{10}), 0.01 (s, 6H, CH_3^{11}).

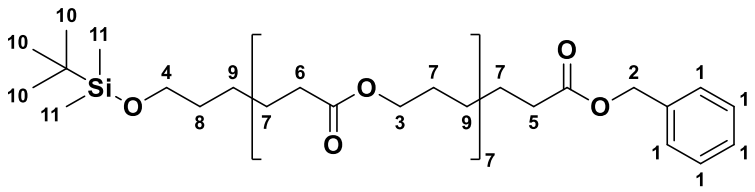

^{13}C NMR (DMSO-d_6, 101 MHz): δ / ppm = 172.79(C_q^1), 172.73 (C_q^1), 172.62 (C_q^1), 136.26 ($C_{q,Ar}^2$), 128.38 ($CH_{Ar,meta}^3$), 127.94 ($CH_{Ar,para}^4$), 127.87 ($CH_{Ar,ortho}^5$), 65.28 (CH_2^6), 63.47 (CH_2^7), 63.43 (CH_2^7), 62.28 (CH_2^8), 33.54 (CH_2^9), 33.35 (CH_2^9), 33.30 (CH_2^9), 31.87 (CH_2^{10}), 27.78 (CH_2^{11}), 25.77 (CH_3^{12}), 24.87 (CH_2^{13}), 24.83 (CH_2^{13}), 24.27 (CH_2^{14}), 24.07 (CH_2^{14}), 24.05 (CH_2^{14}), 17.89 (C_q^{15}), -5.38 (CH_3^{16}).

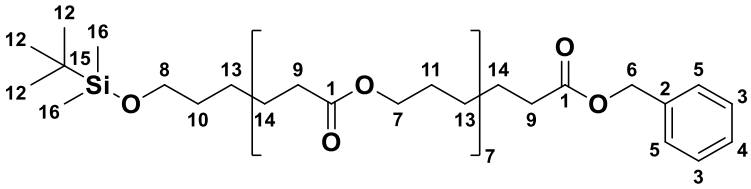

HRMS (ESI) of $C_{61}H_{102}O_{17}Si$ $[M+H]^+$ calcd. 1135.6959, found 1135.6947; $[M+Na]^+$ calcd. 1157.6778, found 1157.6758; $[M+K]^+$ calcd. 1173.6518, found 1173.6498.

IR (ATR platinum diamond) $\tilde{\nu}$ / cm^{-1} = 2934.0, 2859.1, 1730.5, 1458.3, 1358.0, 1157.6, 1094.6, 835.2, 776.0, 737.0, 698.3.

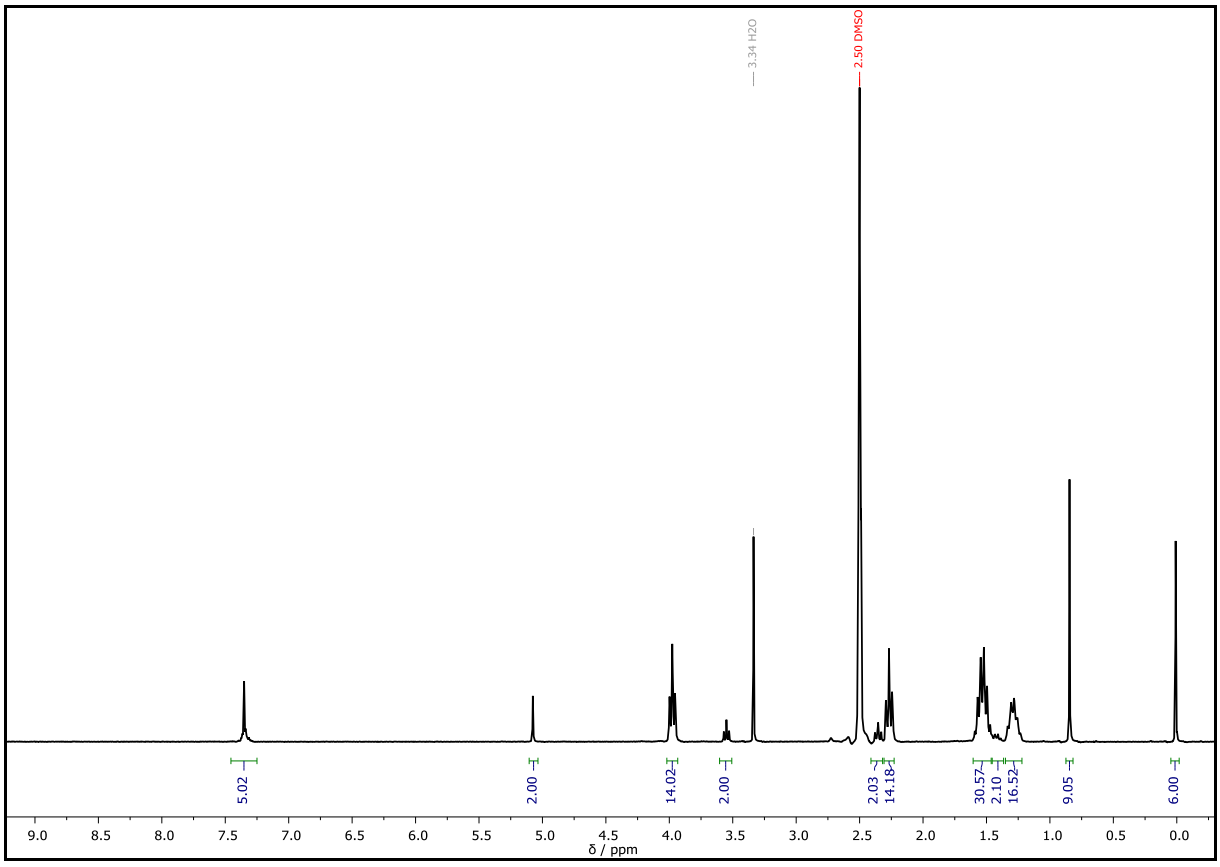

Supplementary Figure 92: ^{1}H NMR spectrum of **C10**, recorded at 400 MHz in DMSO-d_6.

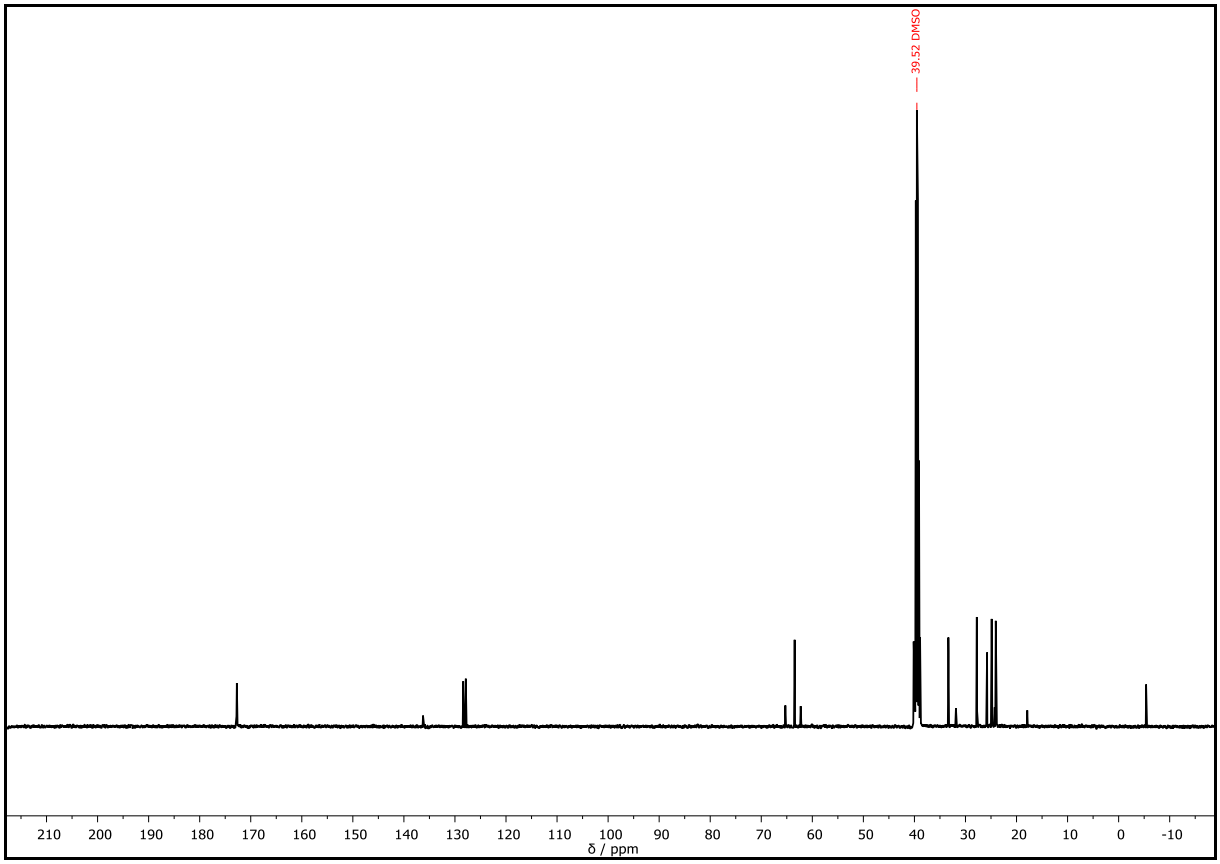

Supplementary Figure 93: ^{13}C NMR spectrum of **C10**, recorded at 101 MHz in DMSO-d_6.

Carboxyl–terminated octamer – C11

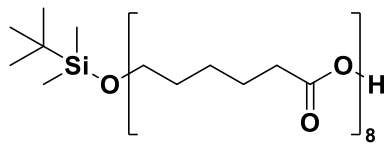

Chemical Formula: $C_{54}H_{96}O_{17}Si$
Exact Mass: 1044.6417 Da
Molecular Weight: 1045.4300 Da

The carboxyl-terminated octamer **C11** was prepared using the procedure described above for the synthesis of the carboxyl-terminated dimer **C5**.

C10	3.00 g, 2.64 mmol, 1.00 equiv.
Pd/C	300 mg, 10 wt%
EA	42 mL
yield	2.76 g, 2.64 mmol, quant. yield, white solid
Đ (system II)	1.00

^{1}H NMR (DMSO-d_6, 400 MHz): δ / ppm = 12.05 (br, 1H, CO_2H^1), 3.98 (t, J = 6.7 Hz, 14H, CH_2^2), 3.55 (t, J = 6.3 Hz, 2H, CH_2^3), 2.32 – 2.23 (m, 14H, CH_2^4), 2.19 (t, J = 7.3 Hz, 2H, CH_2^5), 1.60 – 1.46 (m, 30H, CH_2^6), 1.46 – 1.39 (m, 2H, CH_2^7), 1.35 – 1.24 (m, 16H, CH_2^8), 0.84 (s, 9H, CH_3^9), 0.01 (s, 6H, CH_3^{10}).

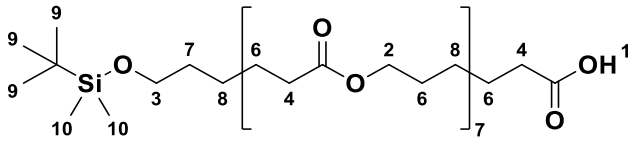

^{13}C NMR ($CDCl_3$, 101 MHz): δ / ppm = 174.35 (C_q^1), 172.77 (C_q^2), 172.74 (C_q^2), 172.71 (C_q^2), 63.50 (CH_2^3), 63.45 (CH_2^3), 63.41 (CH_2^3), 62.25 (CH_2^4), 33.50 (CH_2^5), 33.31 (CH_2^5), 31.85 (CH_2^6), 27.84 (CH_2^7), 27.76 (CH_2^7), 25.74 (CH_3^8), 24.94 (CH_2^9), 24.85 (CH_2^9), 24.81 (CH_2^9), 24.25 (CH_2^{10}), 24.08 (CH_2^{10}), 24.05 (CH_2^{10}), 17.87 (C_q^{11}), -5.42 (CH_3^{12}).

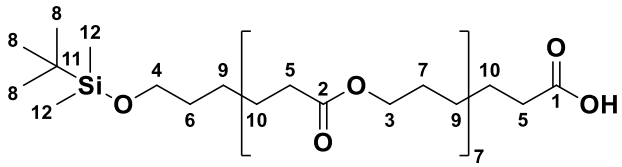

HRMS (ESI) of $C_{54}H_{96}O_{17}Si$ $[M+H]^+$ calcd. 1045.6490, found 1045.6477; $[M+NH_4]^+$ calcd. 1062.6755, found 1062.6742.

IR (ATR platinum diamond) ν / cm^{-1} = 2935.2, 2860.3, 1730.3, 1461.4, 1390.2, 1359.3, 1157.9, 1094.1, 834.9, 776.0, 736.9.

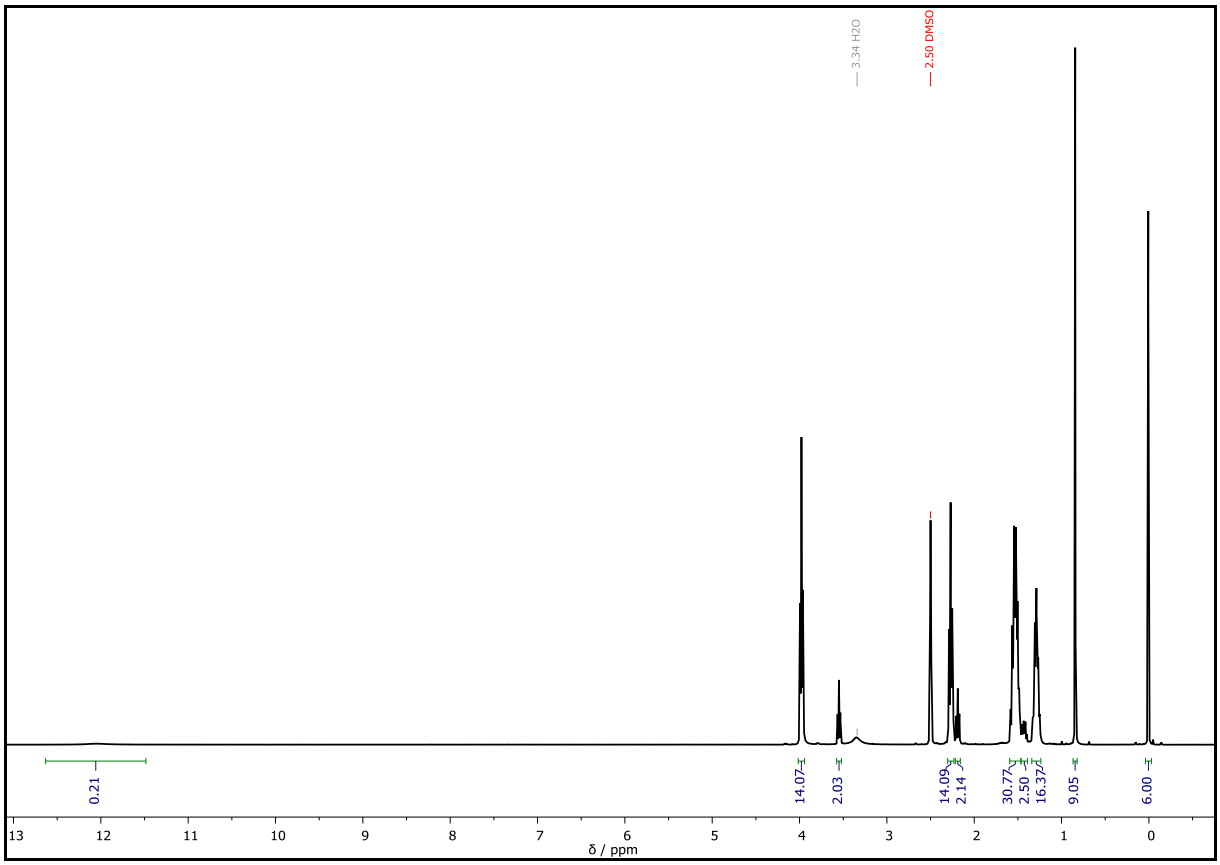

Supplementary Figure 94: ^{1}H NMR spectrum of **C11**, recorded at 400 MHz in DMSO-d_6.

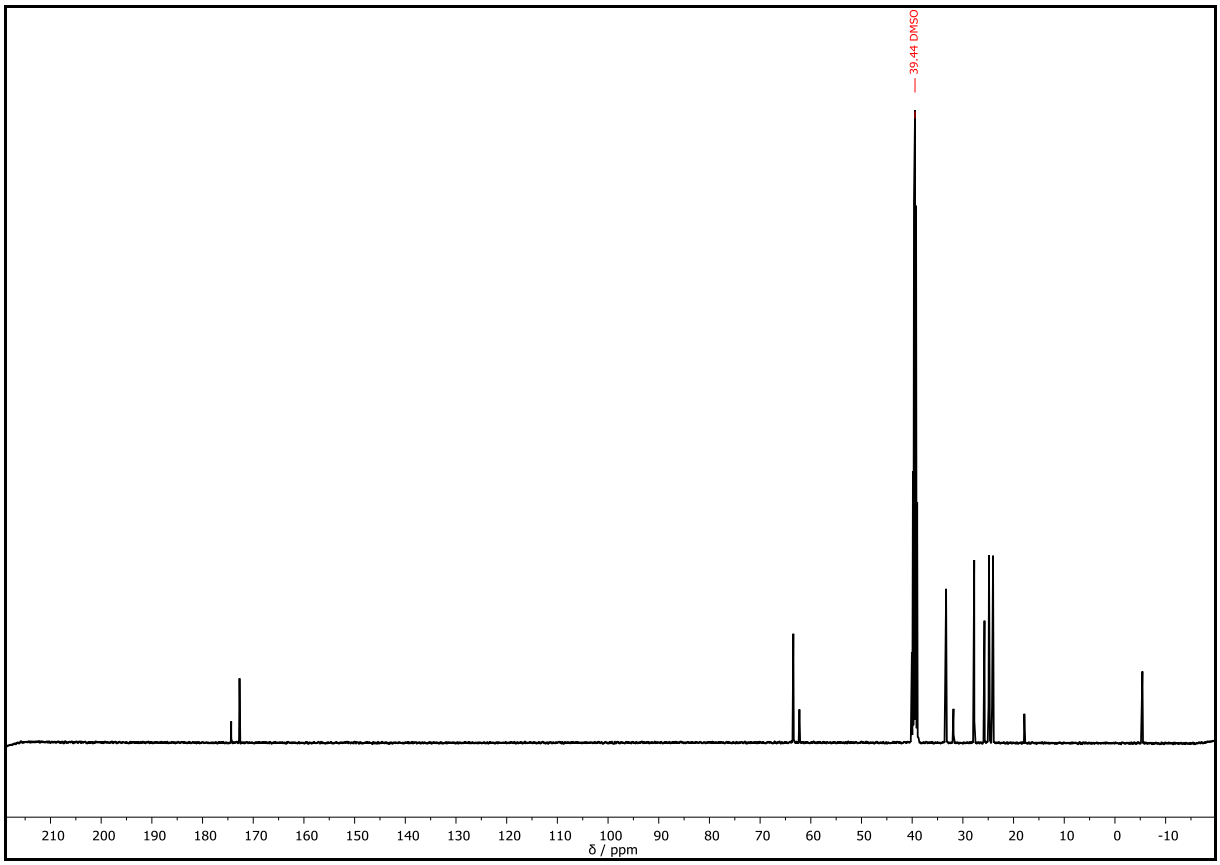

Supplementary Figure 95: ^{13}C NMR spectrum of **C11**, recorded at 101 MHz in DMSO-d_6.

Hydroxyl–terminated octamer – C12

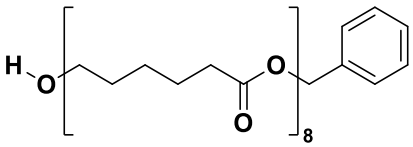

Chemical Formula: $C_{55}H_{88}O_{17}$
Exact Mass: 1020.6022 Da
Molecular Weight: 1021.2920 Da

The hydroxyl-terminated tetramer **C12** was prepared according to the procedure described above for the synthesis of the hydroxyl-terminated dimer **C6**.

C10	3.00 g, 2.64 mmol, 1.00 equiv.
TBAF	1.67 g, 6.39 mmol, 2.42 equiv.
glacial acetic acid	305 µL, 320 mg, 5.33 mmol, 2.02 equiv.
total THF	10.6 mL
eluent	cyhex/EA = 1:1
yield	2.62 g, 2.57 mmol, 97.3%, white solid
R_f	0.53 (cyhex/EA = 1:1).
Đ (system II)	1.00

^{1}H NMR (DMSO-d_6, 400 MHz): δ / ppm = 7.40 – 7.28 (m, 5H, $CH_{Ar}{}^1$), 5.07 (s, 2H, $CH_2{}^2$), 4.36 (t, *J* = 5.1 Hz, 1H, OH^3), 3.97 (t, *J* = 6.5 Hz, 14H, $CH_2{}^4$), 3.36 (t, *J* = 6.5 Hz, 2H, $CH_2{}^5$), 2.35 (t, *J* = 7.4 Hz, 2H, $CH_2{}^6$), 2.30 – 2.21 (m, 14H, $CH_2{}^7$), 1.61-1.46 (m, 30H, $CH_2{}^8$), 1.44 – 1.35 (m, 2H, $CH_2{}^9$), 1.35 – 1.22 (m, 16H, $CH_2{}^{10}$).

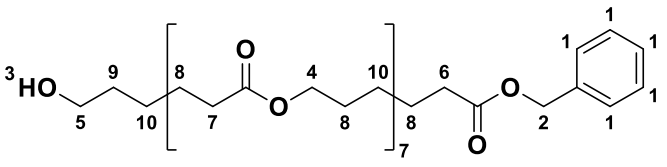

^{13}C NMR (DMSO-*d*$_6$, 101 MHz): δ / ppm = 172.92 (C_q^1), 172.81 (C_q^1), 172.69 (C_q^1), 136.29 ($C_{q,Ar}^2$), 128.43 ($CH_{Ar,meta}^3$), 128.00 ($CH_{Ar,para}^4$), 127.94 ($CH_{Ar,ortho}^5$), 65.33 (CH_2^6), 63.52 (CH_2^7), 60.55 (CH_2^8), 33.59 (CH_2^9), 33.38 (CH_2^9), 32.19 (CH_2^{10}), 27.83 (CH_2^{11}), 25.08 (CH_2^{12}), 24.92 (CH_2^{12}), 24.45 (CH_2^{13}), 24.12 (CH_2^{13}).

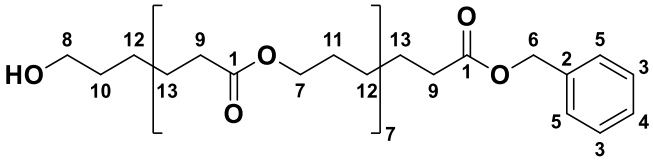

HRMS (ESI) of $C_{55}H_{88}O_{17}$ $[M+H]^+$ calcd. 1021.6094, found 1021.6075; $[M+NH_4]^+$ calcd. 1038.6360, found 1038.6328.

IR (ATR platinum diamond) *v* / cm^{-1} = 2943.5, 2864.6, 1719.0, 1470.7, 1417.8, 1397.3, 1364.8, 1292.2, 1238.0, 1177.1, 1107.4, 1043.4, 959.5, 933.5, 840.1, 730.6, 697.4, 580.8, 453.0.

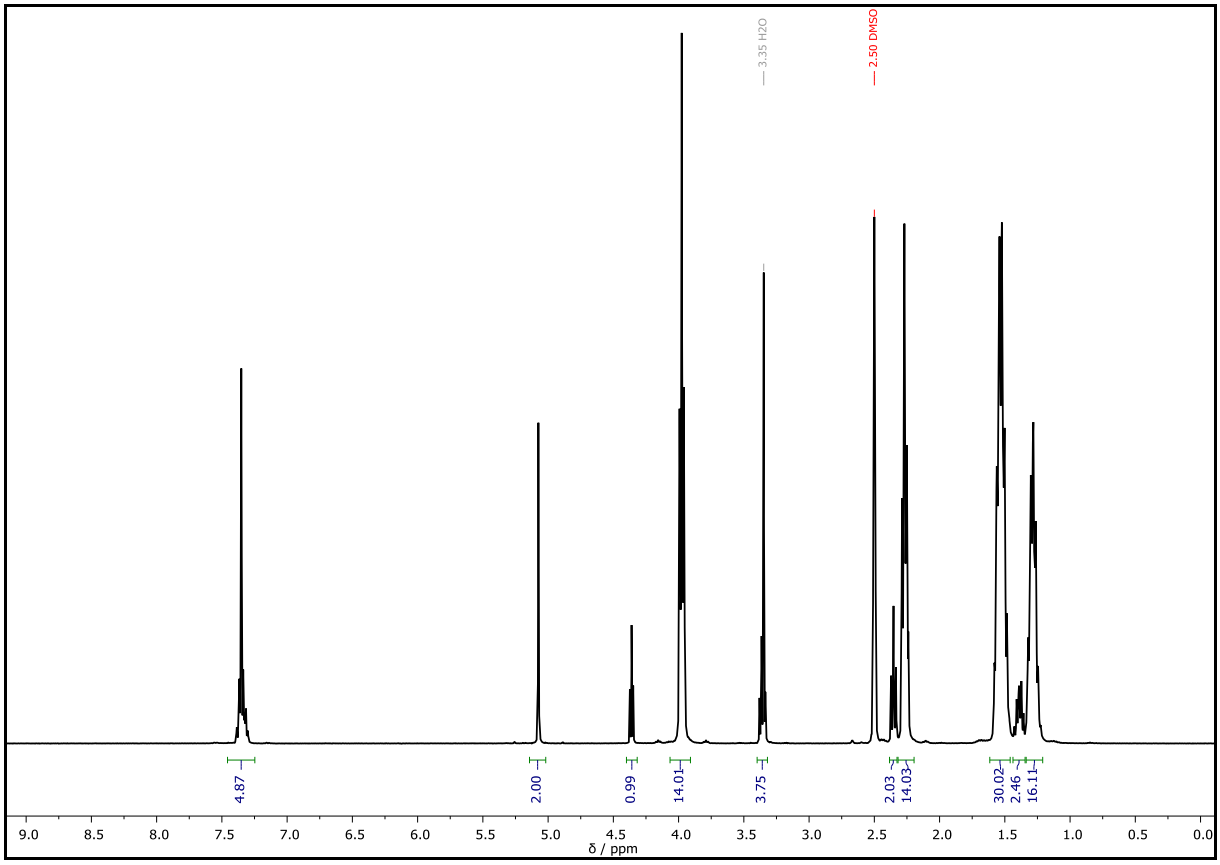

Supplementary Figure 96: ^{1}H NMR spectrum of **C12**, recorded at 400 MHz in DMSO-*d*$_6$.

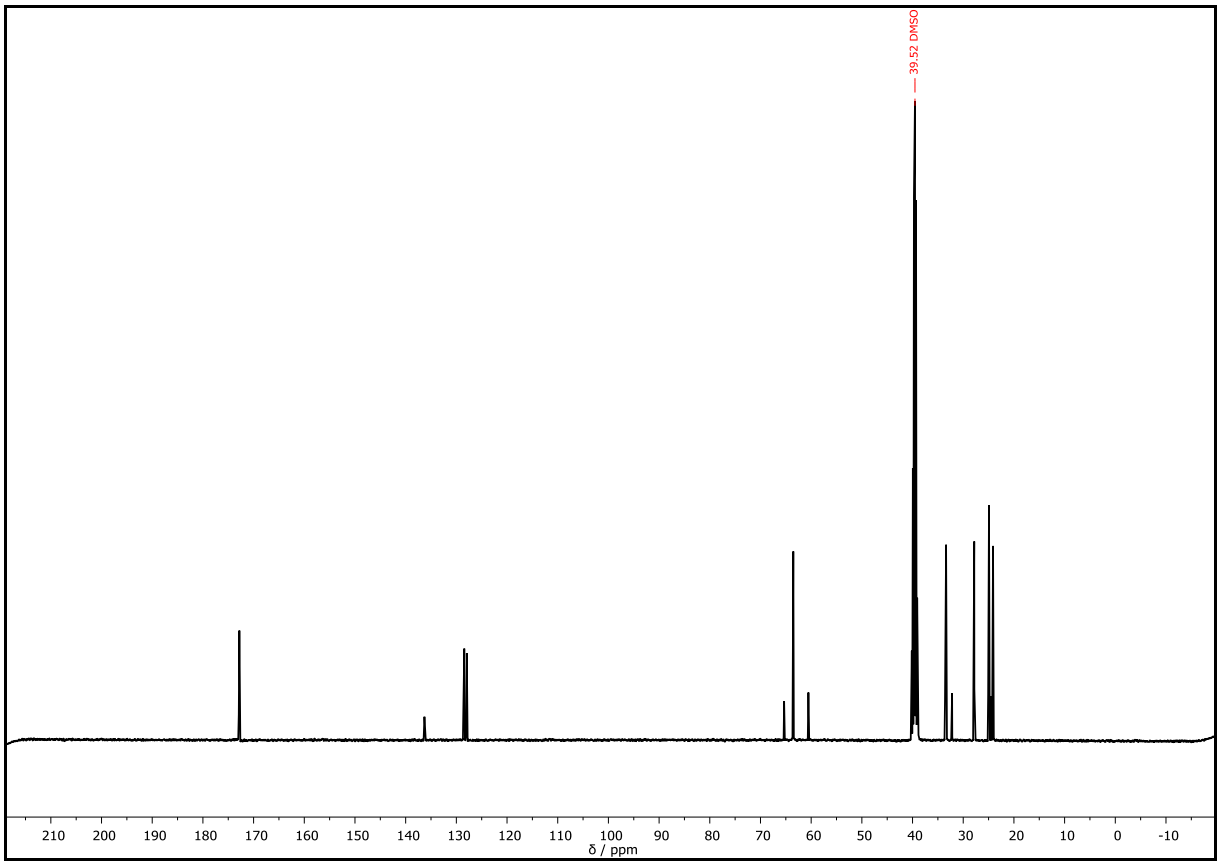

Supplementary Figure 97: ^{13}C NMR spectrum of **C12**, recorded at 101 MHz in DMSO-d_6.

Doubly protected hexadecamer – C13

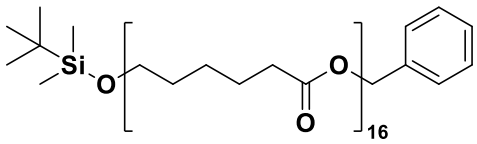

Chemical Formula: $C_{109}H_{182}O_{33}Si$
Exact Mass: 2047.2333 Da
Molecular Weight: 2048.7070 Da

The doubly protected hexadecamer **C13** was prepared using the procedure described above for the synthesis of the doubly protected dimer **C4**. The reaction was performed in two batches, which were combined and purified *via* column chromatography. Quantities of the starting materials and the yield are the sum of both reactions. 0.20 equiv. DPTS was used instead of 1.10 equiv. DMAP.

C11	2.00 g, 1.92 mmol, 1.00 equiv.
C12	1.95 g, 1.92 mmol, 1.00 equiv.
DCC	434 mg, 2.10 mmol, 1.10 equiv.
DPTS	112 mg, 380 µmol, 0.20 equiv.
DCM	10.0 mL
eluent	cyhex/EA = 2:1
yield	3.82 g, 1.86 mmol, 97.1%, white solid
R_f	0.49 (cyhex/EA = 3:1).
Đ (system II)	1.00

^{1}H NMR ($CDCl_3$, 400 MHz): δ / ppm = 7.41 – 7.30 (m, 5H, CH_{Ar}^1), 5.11 (s, 2H, CH_2^2), 4.05 (t, *J* = 6.7 Hz, 30H, CH_2^3), 3.59 (t, *J* = 6.4 Hz, 2H, CH_2^4), 2.49 – 2.21 (m, 32H, CH_2^5, CH_2^6), 1.77 – 1.25 (m, 96H, CH_2^7, CH_2^8 and CH_2^9), 0.88 (s, 9H, CH_3^{10}), 0.03 (s, 6H, CH_3^{11}).

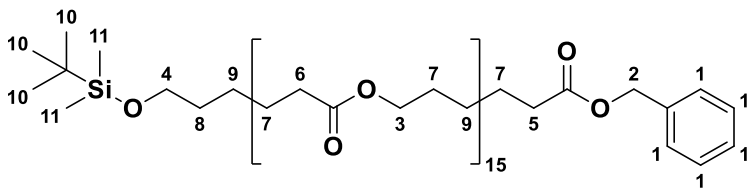

^{13}C NMR ($CDCl_3$, 101 MHz): δ / ppm = 173.94 (C_q^1), 173.68 (C_q^1), 173.44 (C_q^1), 136.13 ($C_{q,Ar}^2$), 128.68 ($CH_{Ar,meta}^3$), 128.34 ($CH_{Ar,para}^4$), 128.31 ($CH_{Ar,ortho}^5$), 66.28 (CH_2^6), 64.26 (CH_2^7), 63.09 (CH_2^8), 34.45 (CH_2^9), 34.23 (CH_2^9), 32.59 (CH_2^{10}), 28.46 (CH_2^{11}), 26.08 (CH_3^{12}), 25.65 (CH_2^{13}), 24.93 (CH_2^{14}), 24.69 (CH_2^{14}), 18.47 (C_q^{15}), -5.16 (CH_3^{16}).

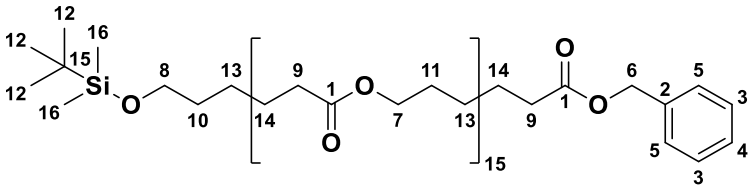

HRMS (ESI) of $C_{109}H_{182}O_{33}Si$ $[M+H]^+$ calcd. 2048.2405, found 2048.2424.

IR (ATR platinum diamond) $\tilde{\nu}$ / cm^{-1} = 3323.7, 2928.7, 2851.3, 1721.6, 1624.8, 1569.1, 1470.8, 1419.3, 1364.6, 1293.4, 1239.9, 1160.5, 1087.7, 1044.2, 960.4, 891.7, 836.3, 775.9, 731.5, 614.6, 453.2, 416.9.

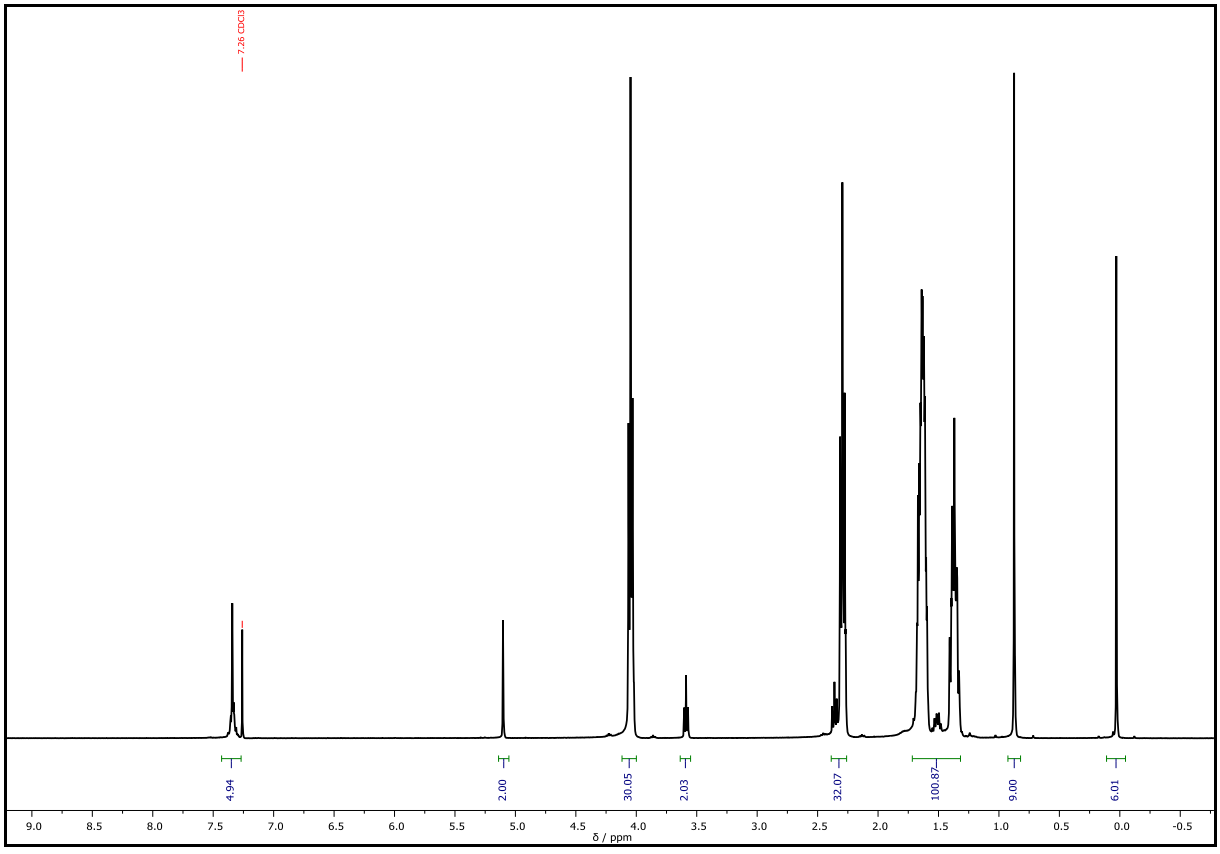

Supplementary Figure 98: ^{1}H NMR spectrum of **C13**, recorded at 400 MHz in $CDCl_3$.

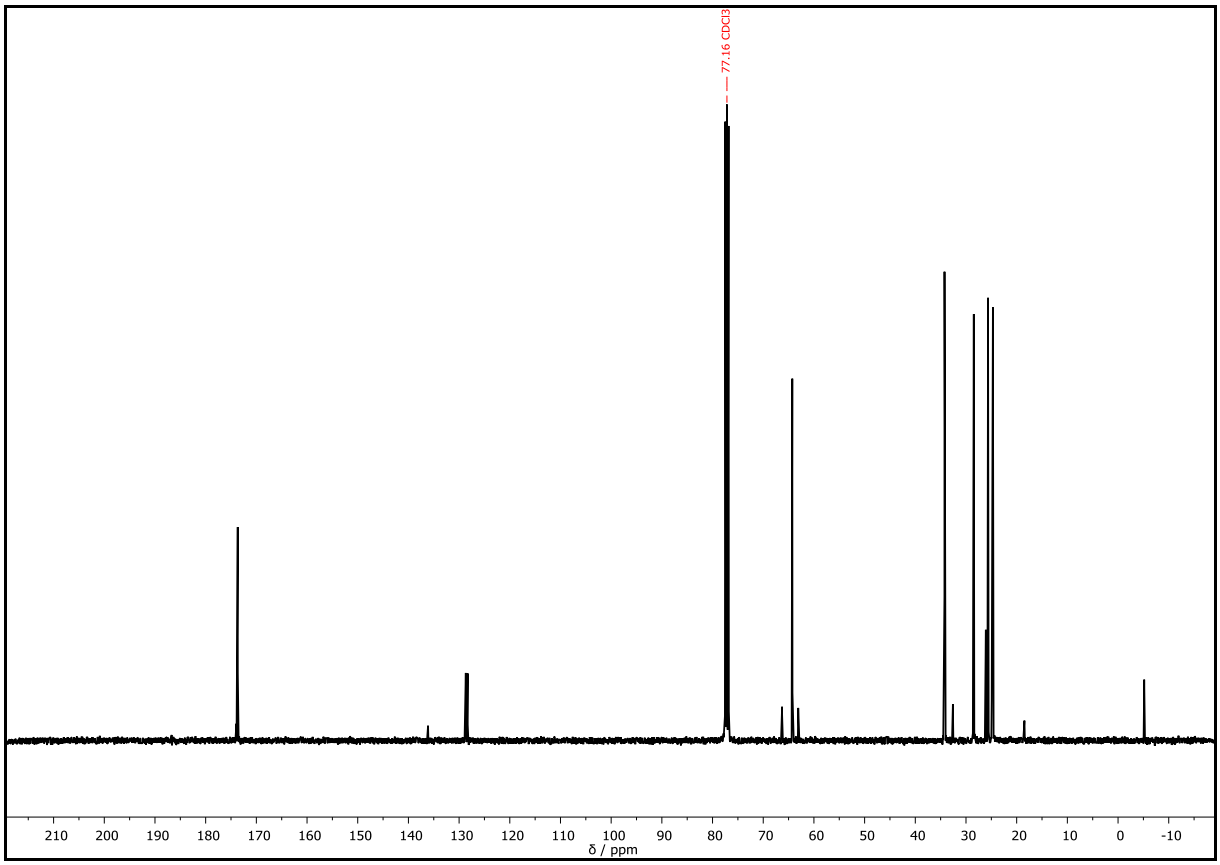

Supplementary Figure 99: ^{13}C NMR spectrum of **C13**, recorded at 101 MHz in $CDCl_3$.

In a second approach, the reaction was performed in a 15.5 mmol scale. The crude product (38.8 g) was purified *via* column chromatography for four times. In total 46 fractions were collected. The respective amounts, the analysis *via* GPC (system II) and the chromatograms are given in the following. The ones highlighted in green were used for further synthesis. The ones in yellow were purified *via* another column chromatography and the ones marked in red were discarded.

Supplementary Table 13: SEC results of the first purification of C13.

cc 1	*m* / g	M_n / Da	M_w / Da	M_z / Da	*Đ*	purity / %
F1	29.8	3800	3850	3850	1.00	98.5
F2	1.54	3800	3800	3850	1.00	>99
F3	0.32	3850	3900	3900	1.00	98.4
eluent: cyhex:EA = 2:1 → 1:1; in total 31.7 g of product with a purity of 98.6%.						

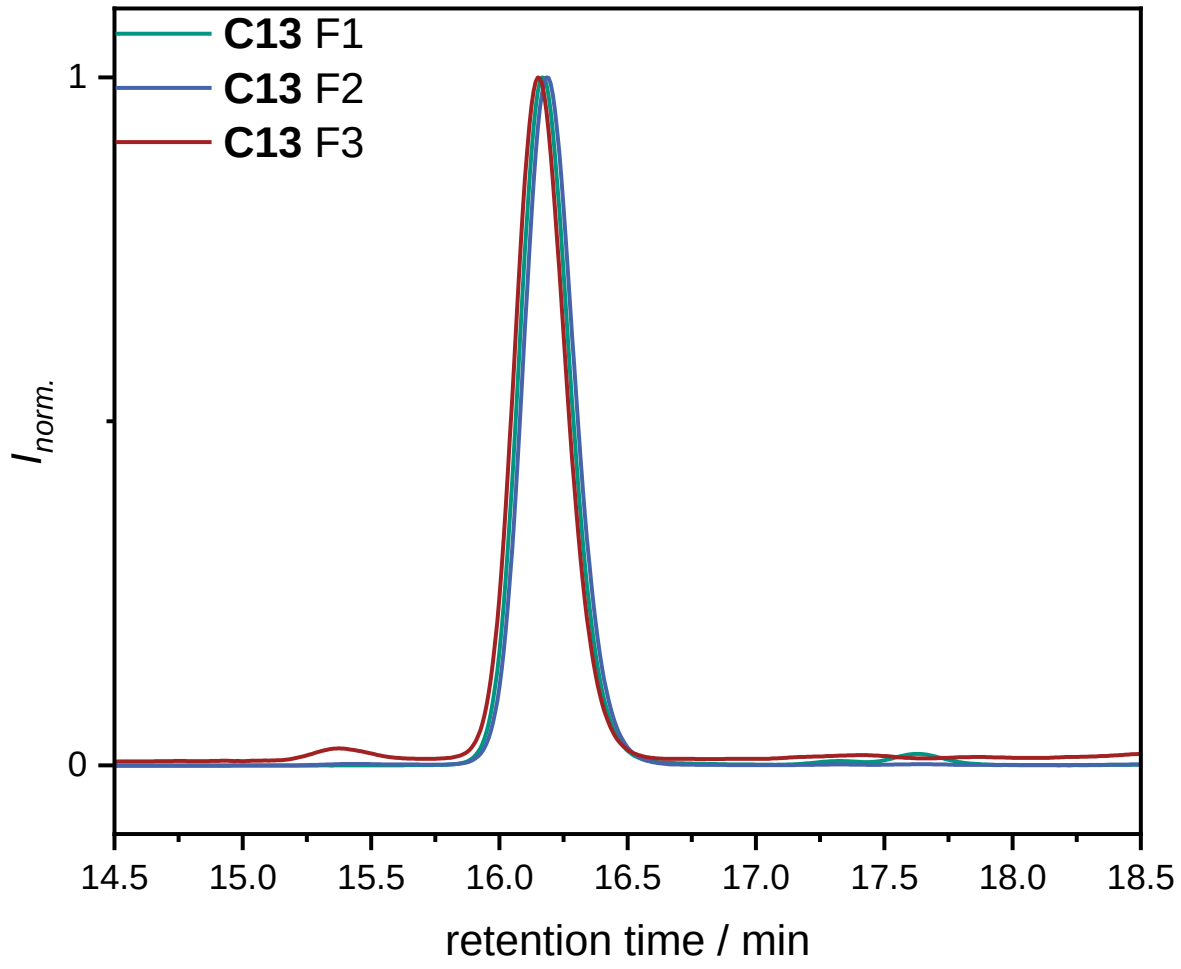

Supplementary Figure 100: SEC traces of the individual fractions obtained from the first purification *via* column chromatography of **C13**.

The fractions **C13** cc1 F1-2 were further purified *via* column chromatography.

Supplementary Table 14: SEC results of the second purification of C13.

cc 2	*m* / g	M_n / Da	M_w / Da	M_z / Da	*Đ*	purity / %
F1	0.61	3900	3900	3950	1.00	81.0
F2	0.12	3900	3900	3900	1.00	82.2
F3	0.49	3900	3900	3900	1.00	91.6
F4	0.84	3900	3900	3950	1.00	97.2
F5	7.64	3900	3900	3900	1.00	98.8
F6	5.83	3900	3900	3950	1.00	99.4
F7	6.02	3900	3900	3950	1.00	>99
F8	3.87	3900	3900	3950	1.00	>99
F9	2.48	3850	3900	3900	1.00	>99
F10	1.09	3900	3900	3900	1.00	>99
F11	1.81	3900	3900	3900	1.00	>99
F12	1.15	3900	3900	3900	1.00	>99
F13	0.80	3900	3900	3900	1.00	>99
F14	0.48	3900	3900	3900	1.00	>99
F15	0.09	3900	3900	3950	1.00	92.5
F16	0.03	4000	4050	4050	1.01	53.2

eluent: cyhex:EA = 3:1 → 2:1 → 1:1 → 0:1

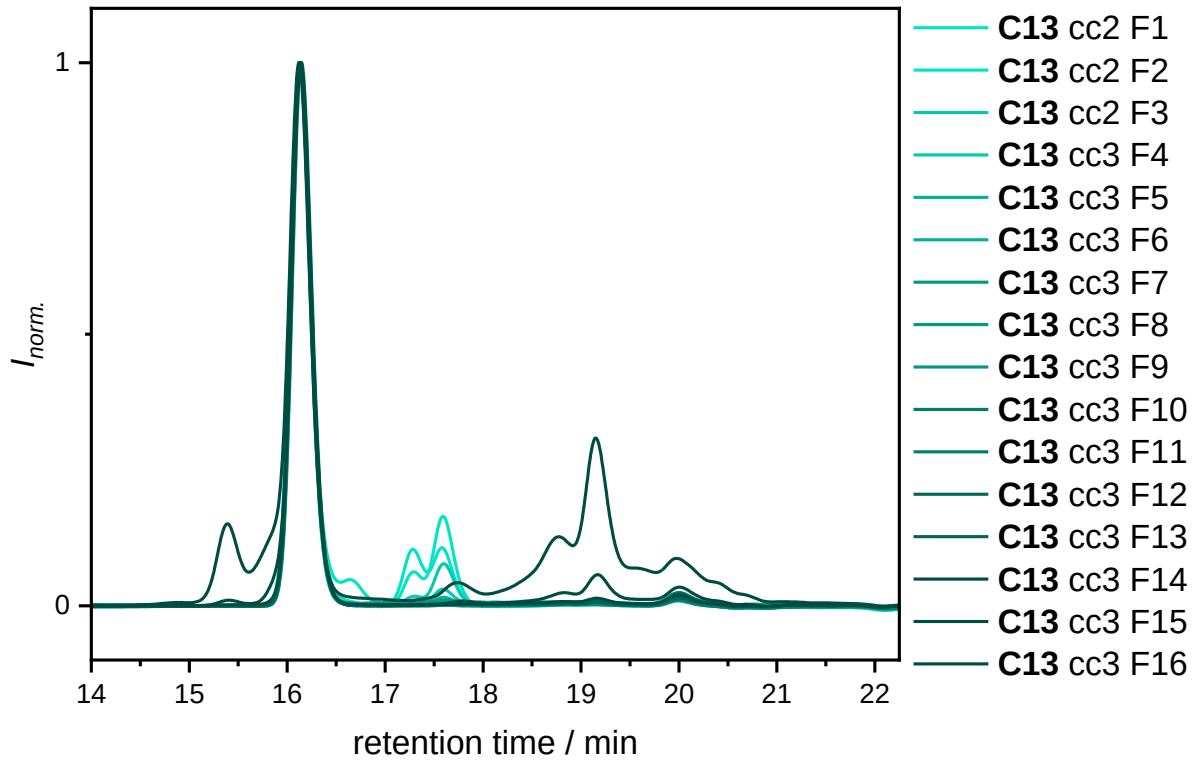

Supplementary Figure 101: SEC traces of the individual fractions obtained from the second purification *via* column chromatography of **C13**.

The fractions **C13** cc2 F2-6 were further purified *via* column chromatography.

Supplementary Table 15: SEC results of the third purification of C13.

cc 3	*m* / mg	M_n / Da	M_w / Da	M_z / Da	$Đ$	purity / %
F1	246	*n.a.*[1]	*n.a.*[1]	*n.a.*[1]	*n.a.*[1]	*n.a.*[1]
F2	512	3850	3900	3900	1.00	50.2
F3	353	3900	3900	3900	1.00	92.8
F4	5590	3900	3900	3900	1.00	>99
F5	2400	3900	3900	3900	1.00	99.5
F6	3330	3900	3900	3900	1.00	>99
F7	1710	3900	3900	3900	1.00	>99
F8	762	3900	3900	3900	1.00	>99
F9	273	3900	3900	3900	1.00	>99
F10	87.1	3850	3850	3900	1.00	99.4
F11	39.4	3850	3900	3900	1.00	99.4
F12	44.0	3900	3900	3900	1.00	99.4
F13	18.0	3900	3900	3950	1.00	97.1

eluent: cyhex:EA = 3:1 → 2:1 → 1:1 → 0:1; [1]This fraction did not contain any product.

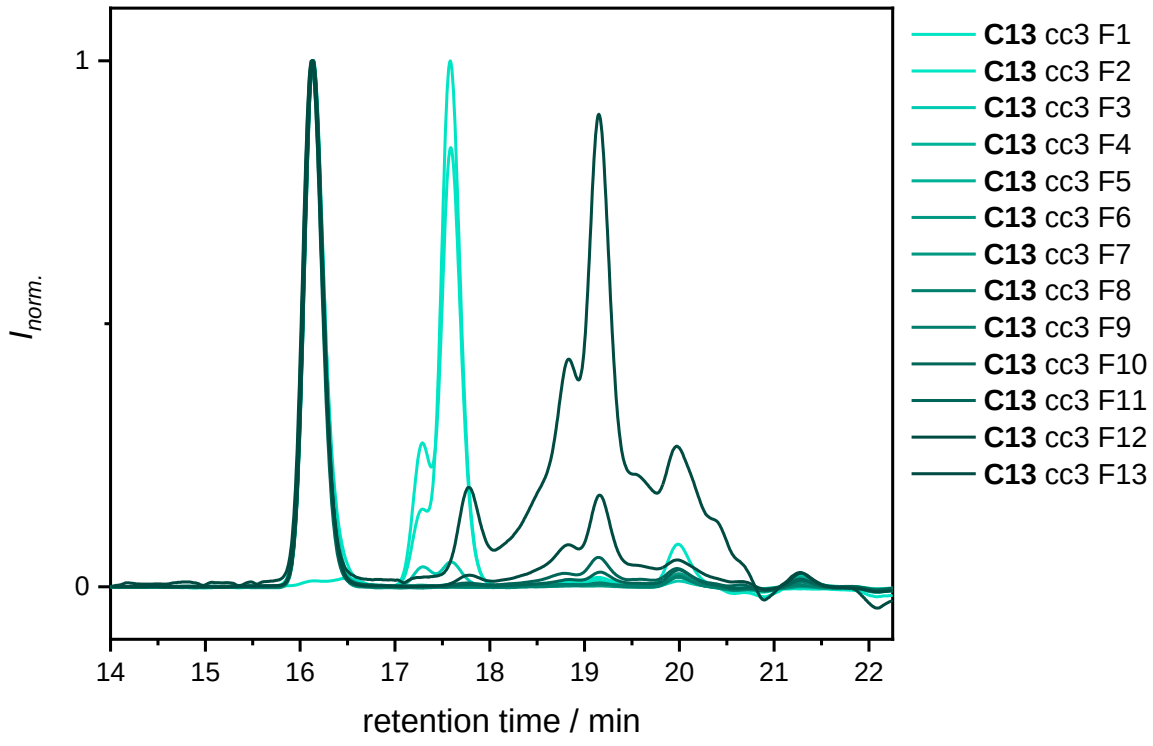

Supplementary Figure 102: SEC traces of the individual fractions obtained from the third purification *via* column chromatography of **C13**.

Supplementary Table 16: SEC results of the fourth purification of C13.

cc 4	*m* / mg	M_n / Da	M_w / Da	M_z / Da	*Đ*	purity / %
F1	7.3	*n.a.*[1]	*n.a.*[1]	*n.a.*[1]	*n.a.*[1]	*n.a.*[1]
F2	7.8	*n.a.*[1]	*n.a.*[1]	*n.a.*[1]	*n.a.*[1]	*n.a.*[1]
F3	42.3	*n.a.*[1]	*n.a.*[1]	*n.a.*[1]	*n.a.*[1]	*n.a.*[1]
F4	99.5	*n.a.*[1]	*n.a.*[1]	*n.a.*[1]	*n.a.*[1]	*n.a.*[1]
F5	89.7	*n.a.*[1]	*n.a.*[1]	*n.a.*[1]	*n.a.*[1]	*n.a.*[1]
F6	55.6	*n.a.*[1]	*n.a.*[1]	*n.a.*[1]	*n.a.*[1]	*n.a.*[1]
F7	15.4	*n.a.*[1]	*n.a.*[1]	*n.a.*[1]	*n.a.*[1]	*n.a.*[1]
F8	248	3800	3800	3850	1.00	93.4
F9	1190	3850	3900	3900	1.00	>99
F10	1150	3850	3850	3900	1.00	>99
F11	711	3850	3900	3900	1.00	>99
F12	389	3900	3900	3900	1.00	99.4
F13	321	3900	3900	3950	1.00	97.1
F14	87.0	3850	3900	3900	1.00	96.8

eluent: cyhex:EA = 3:1 → 2:1 → 1:1 → 0:1; [1]This fraction did not contain any product.

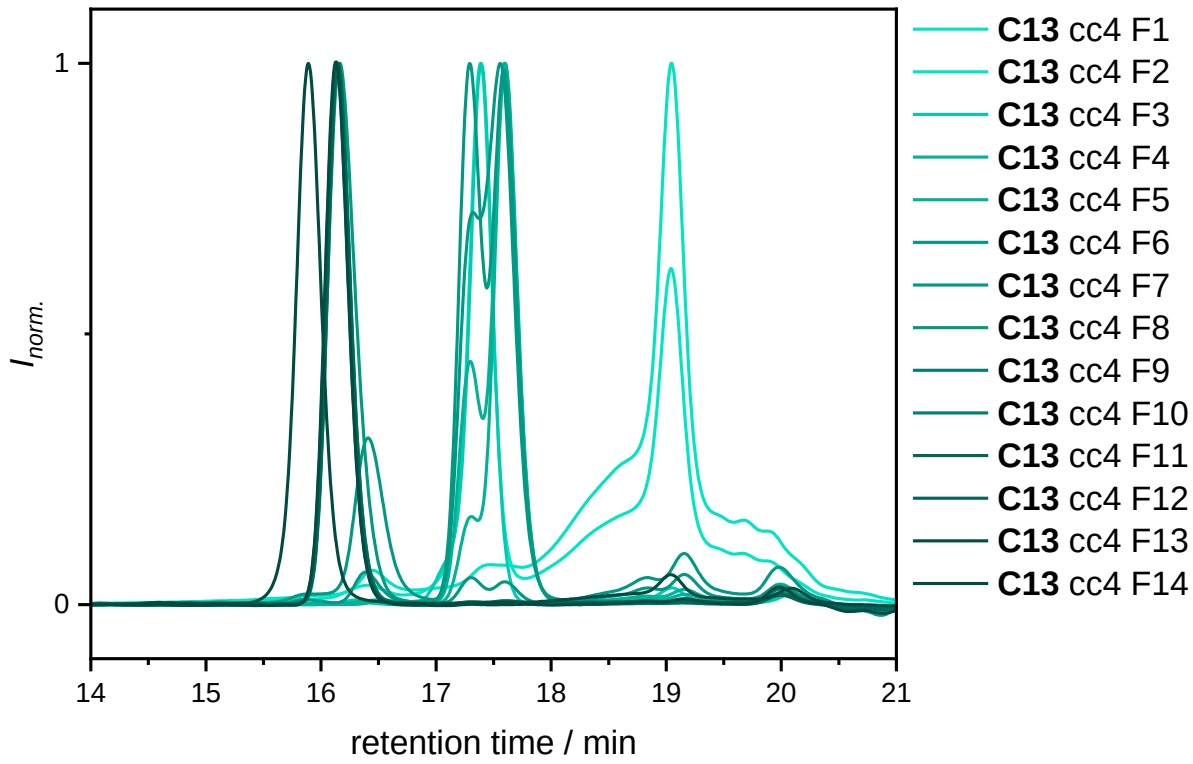

Supplementary Figure 103: SEC traces of the individual fractions obtained from the fourth purification *via* column chromatography of **C13**.

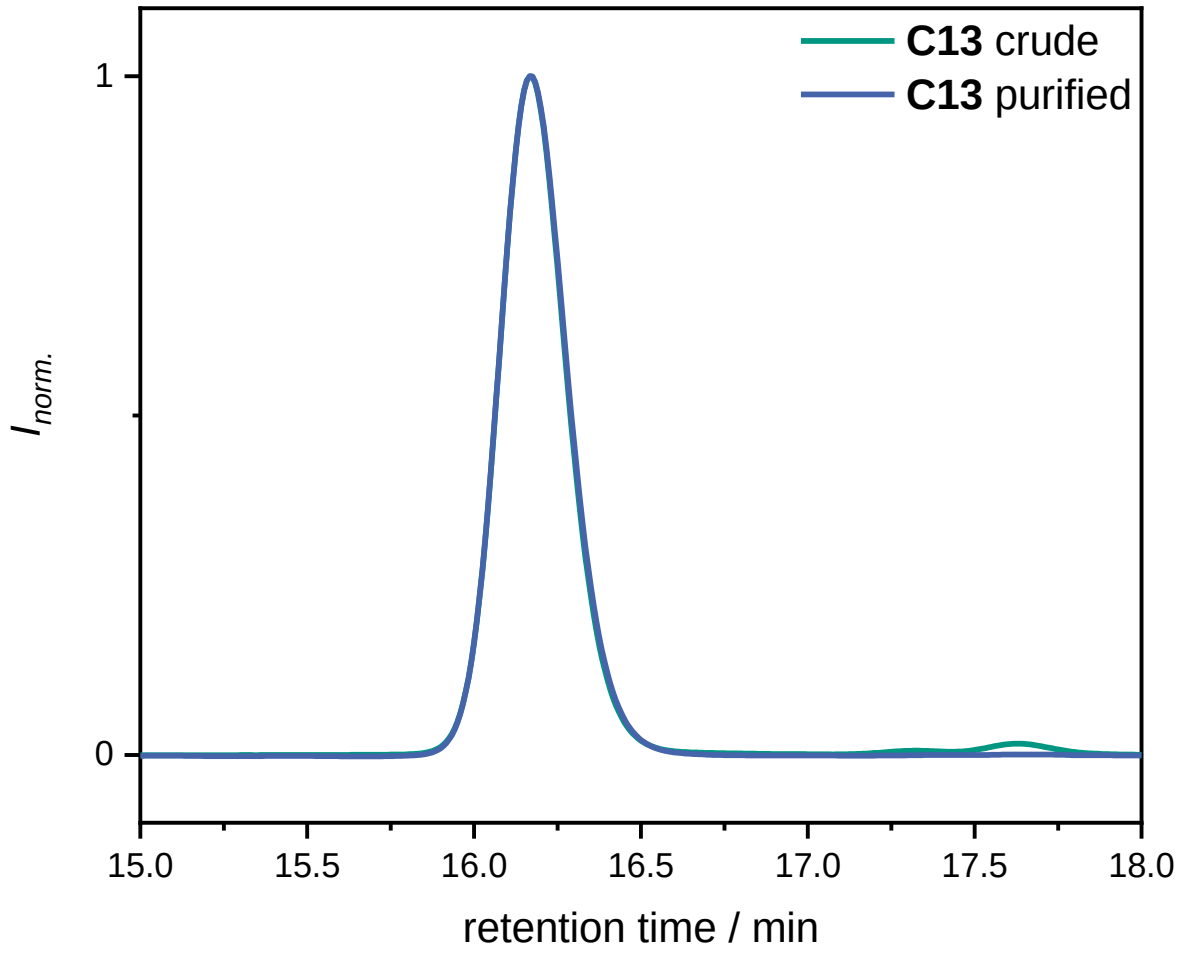

Supplementary Figure 104: SEC traces of product **C13** before and after four column chromatographic purification steps.

Carboxyl–terminated hexadecamer – C14

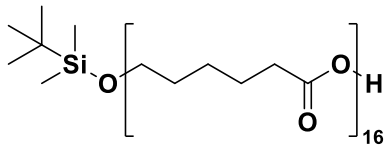

Chemical Formula: $C_{102}H_{176}O_{33}Si$
Exact Mass: 1957.1863 Da
Molecular Weight: 1958.5820 Da

The carboxyl-terminated hexadecamer **C14** was prepared using the procedure described above for the synthesis of the carboxyl-terminated dimer **C5**.

C13	14.9 g, 7.29 mmol, 1.00 equiv.
Pd/C	1.49 g, 10 wt%
EA	180 mL
yield	14.3 g, 7.29 mmol, quant. yield, white solid
Đ (system II)	1.00

^{1}H NMR ($CDCl_3$, 400 MHz): δ / ppm = 4.05 (t, *J* = 6.7 Hz, 30H, CH_2^1), 3.59 (t, *J* = 6.5 Hz, 2H, CH_2^2), 2.50 – 2.19 (m, 32H. CH_2^3, CH_2^4), 1.84 – 1.27 (m, 96H, CH_2^5, CH_2^6 and CH_2^7), 0.87 (s, 9H, CH_3^8), 0.03 (s, 6H, CH_3^9).

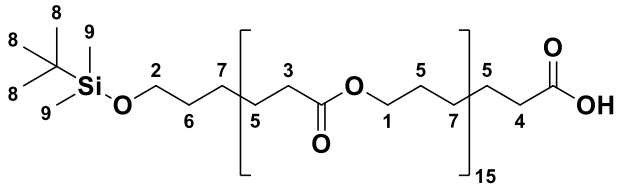

^{13}C NMR ($CDCl_3$, 101 MHz): δ / ppm = 173.96 (C_q^1), 173.84 (C_q^2), 173.70 (C_q^2), 64.32 (CH_2^3), 64.28 (CH_2^3), 64.21 (CH_2^3), 64.19 (CH_2^3), 63.10 (CH_2^4), 34.45 (CH_2^5), 34.29 (CH_2^5), 34.24 (CH_2^5), 33.65 (CH_2^6), 32.58 (CH_2^7), 28.46 (CH_2^8), 28.43 (CH_2^8), 26.08 (CH_3^9), 25.64 (CH_2^{10}), 25.56 (CH_2^{10}), 24.93 (CH_2^{11}), 24.69 (CH_2^{11}), 24.46 (CH_2^{11}), 18.47 (C_q^{12}), -5.16 (CH_3^{13}).

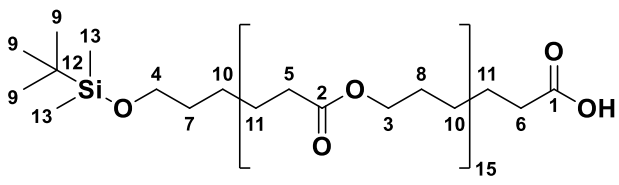

HRMS (ESI) of $C_{102}H_{176}O_{33}Si$ $[M+H]^+$ calcd. 1958.1936, found 1958.1937; $[M+NH_4]^+$ calcd. 1975.2201, found 1975.2194.

IR (ATR platinum diamond) ν / cm^{-1} = 2944.0, 2864.0, 1720.5, 1470.8, 1418.6, 1396.9, 1365.0, 1292.8, 1238.6, 1176.0, 1106.2, 1065.2, 1044.0, 960.1, 933.5, 836.4, 775.5, 730.9, 584.5, 453.0.

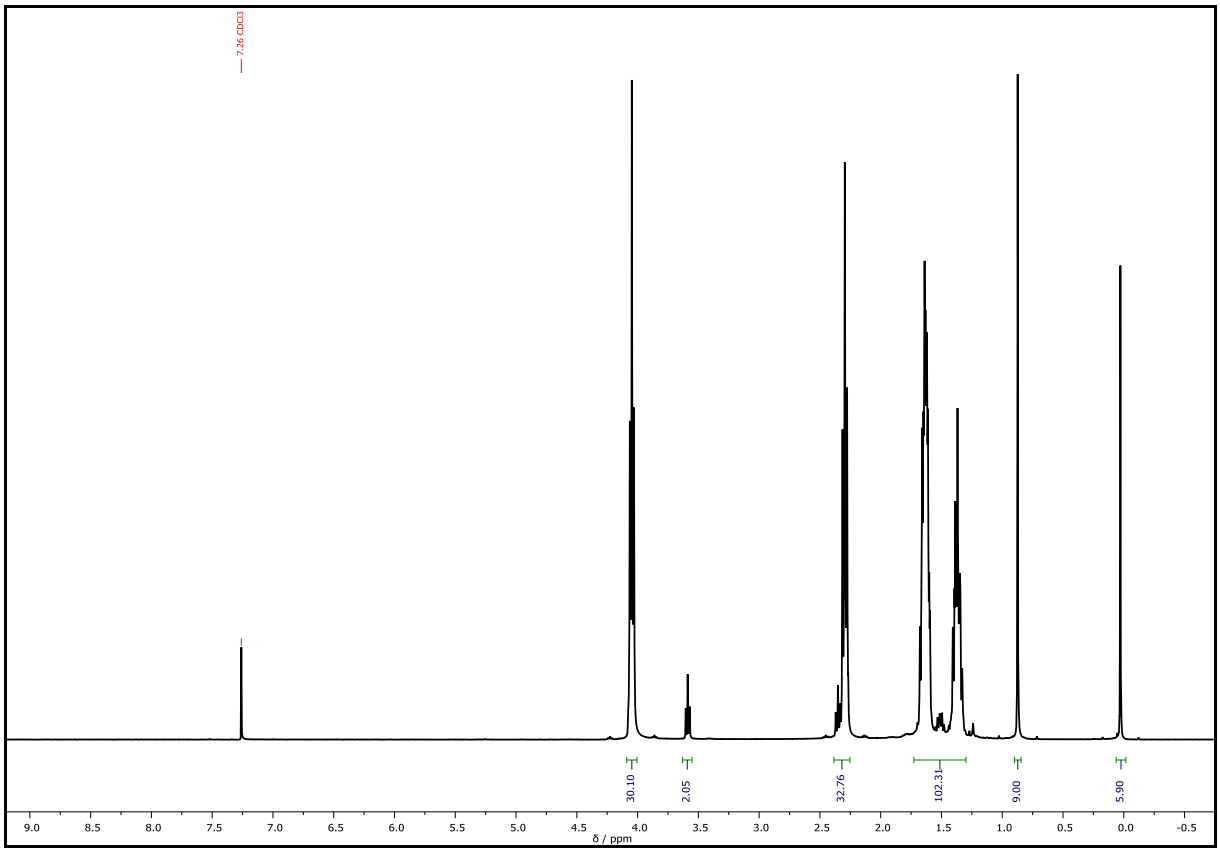

Supplementary Figure 105: ^{1}H NMR spectrum of **C14**, recorded at 400 MHz in $CDCl_3$.

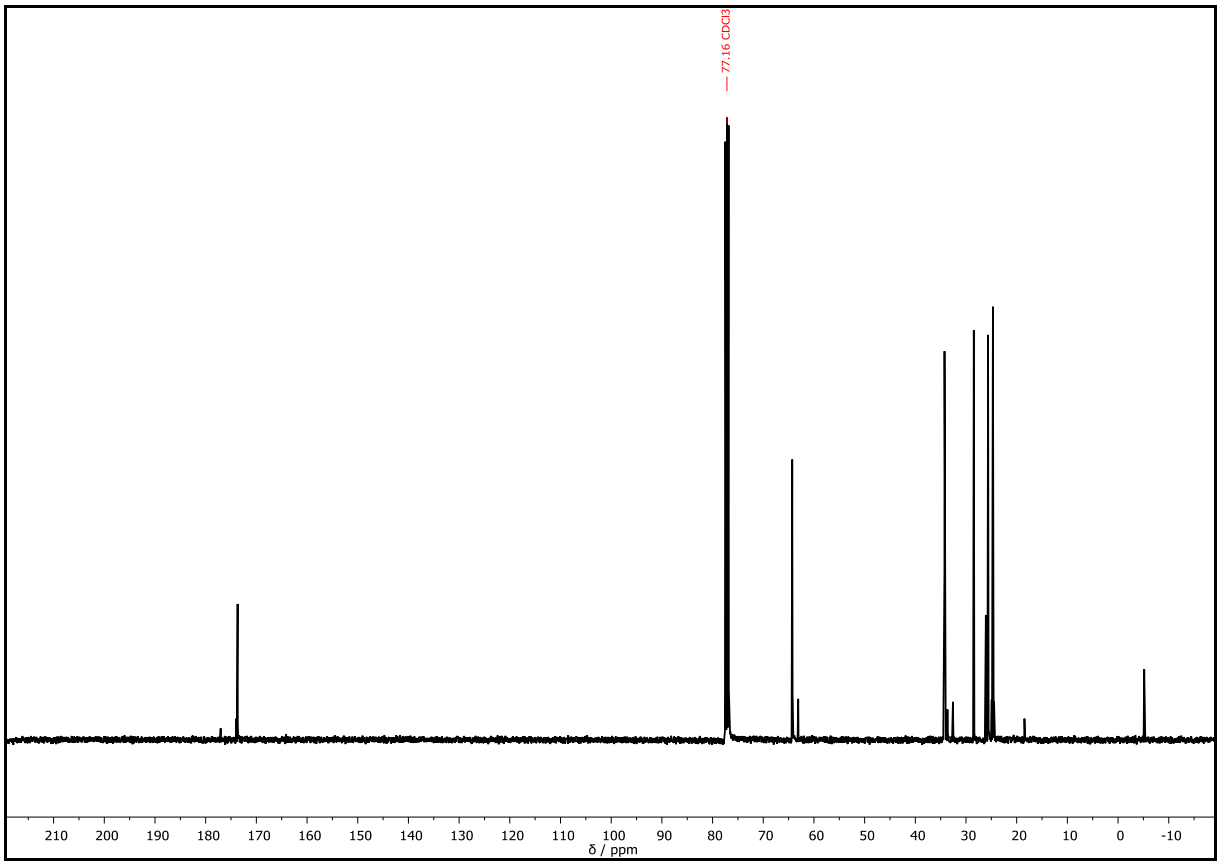

Supplementary Figure 106: ^{13}C NMR spectrum of **C14**, recorded at 101 MHz in $CDCl_3$.

Hydroxyl–terminated hexadecamer – C15

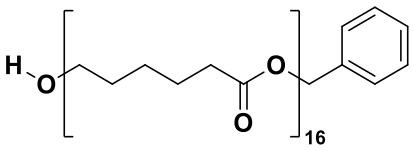

Chemical Formula: $C_{103}H_{168}O_{33}$
Exact Mass: 1933.1468 Da
Molecular Weight: 1934.4440 Da

The hydroxyl-terminated tetramer **C15** was prepared according to the procedure described above for the synthesis of the hydroxyl-terminated dimer **C6**.

C13	15.0 g, 7.32 mmol, 1.00 equiv.
TBAF	4.62 g, 14.6 mmol, 2.00 equiv.
glacial acetic acid	838 µL, 879 mg, 14.6 mmol, 2.00 equiv.
total THF	35.0 mL
eluent	cyhex/EA = 1:2
yield	13.9 g, 7.16 mmol, 98.1%, white solid
R_f	0.42 (cyhex/EA = 1:1).
Đ (system II)	1.00

^{1}H NMR ($CDCl_3$, 400 MHz): δ / ppm = 7.39 – 7.29 (m, 5H, $CH_{Ar}{}^1$), 5.10 (s, 2H, $CH_2{}^2$), 4.05 (t, *J* = 6.7 Hz, 30H, $CH_2{}^3$), 3.63 (q, *J* = 6.0 Hz, 2H, $CH_2{}^4$), 2.36 (t, *J* = 7.5 Hz, 32H, $CH_2{}^5$, $CH_2{}^6$), 1.72 – 1.30 (m, 96H, $CH_2{}^7$, $CH_2{}^8$ and $CH_2{}^9$).

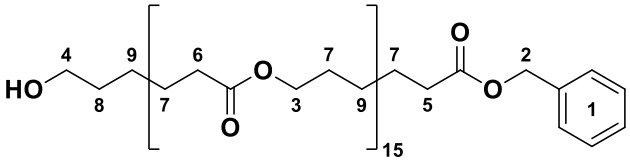

^{13}C NMR ($CDCl_3$, 101 MHz): δ / ppm = 173.86 (C_q^1), 173.73 (C_q^1), 173.67 (C_q^1), 173.43 (C_q^1), 136.13 ($C_{q,Ar}^2$), 128.68 ($CH_{Ar,meta}^3$), 128.34 ($CH_{Ar,para}^4$), 128.31 ($CH_{Ar,ortho}^5$), 66.28 (CH_2^6), 64.26 (CH_2^7), 64.23 (CH_2^7), 62.73 (CH_2^8), 34.34 (CH_2^9), 34.23 (CH_2^9), 32.45 (CH_2^{10}), 28.46 (CH_2^{11}), 25.64 (CH_2^{12}), 25.41 (CH_2^{12}), 24.80 (CH_2^{13}), 24.69 (CH_2^{13}).

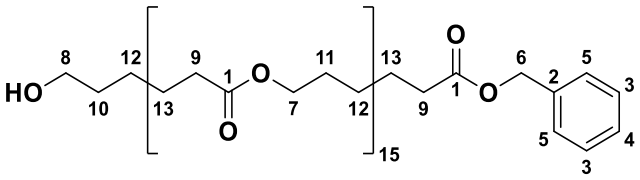

HRMS (ESI) of $C_{103}H_{168}O_{33}$ $[M+H]^+$ calcd. 1934.1541, found 1934.43; $[M+NH_4]^+$ calcd. 1951.1806, found 1951.1812; $[M+2H]^{2+}$ calcd. 967.5807, found 967.5786; $[M+3H]^{3+}$ calcd. 645.3895, found 645.3878.

IR (ATR platinum diamond) ν / cm^{-1} = 2943.6, 2864.8, 1720.2, 1470.6, 1364.9, 1292.6, 1238.0, 1171.9, 1107.2, 1043.6, 959.8, 731.1, 452.9.

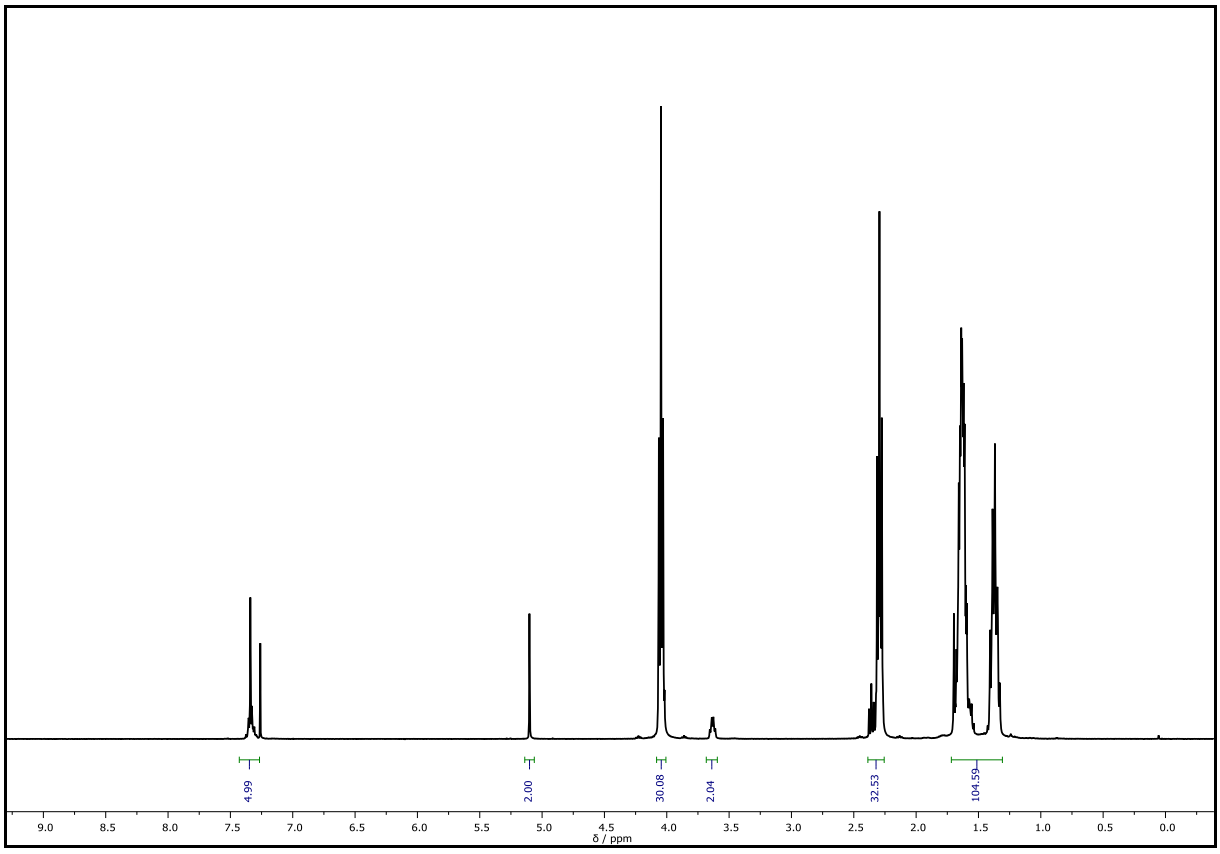

Supplementary Figure 107: ^{1}H NMR spectrum of **C15**, recorded at 400 MHz in $CDCl_3$.

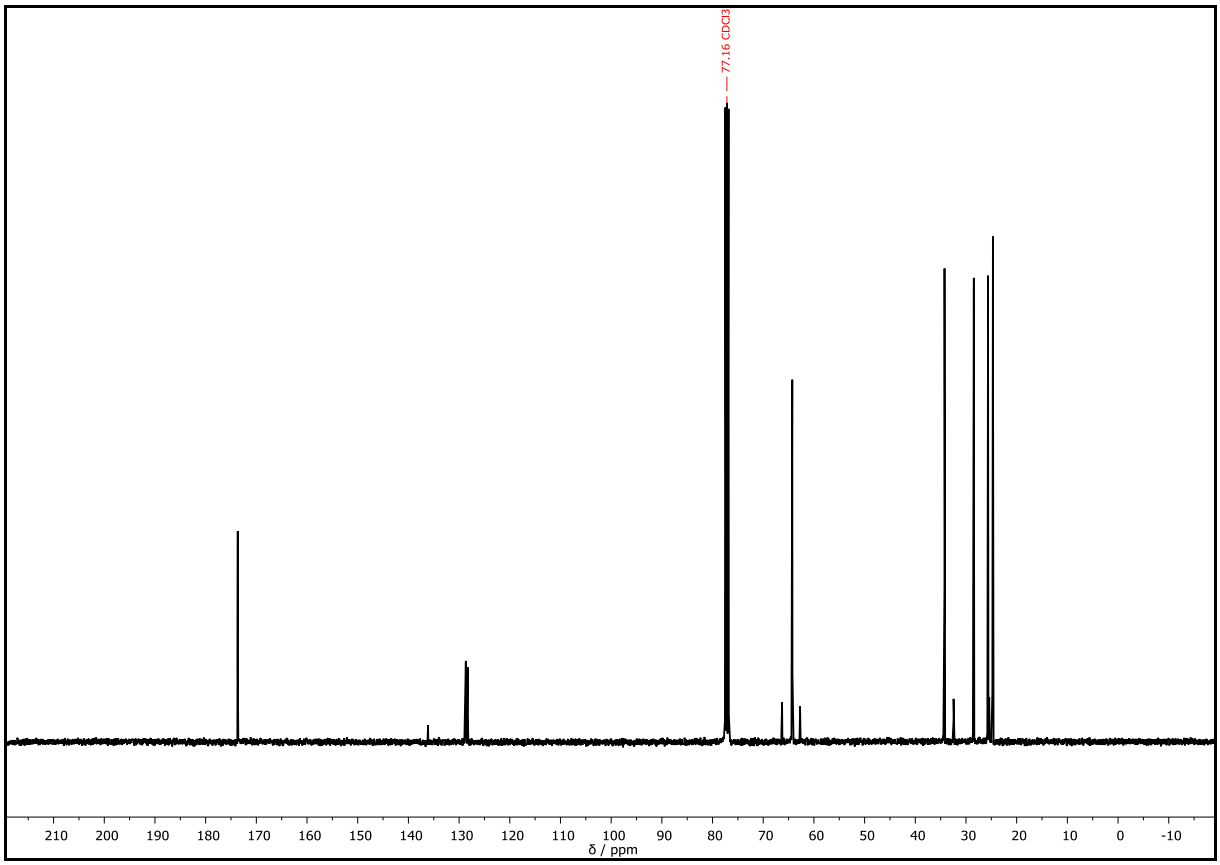

Supplementary Figure 108: ^{13}C NMR spectrum of **C15**, recorded at 101 MHz in $CDCl_3$.

Doubly protected 32-mer – C16

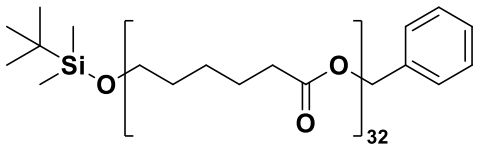

Chemical Formula: $C_{205}H_{342}O_{65}Si$
Exact Mass: 3872.3225 Da
Molecular Weight: 3875.0110 Da

The doubly protected 32-mer **C16** was prepared using the procedure described above for the synthesis of the doubly protected dimer **C4**. 0.20 equiv. DPTS was used instead of 1.10 equiv. DMAP.

C14	10.5 g, 5.37 mmol, 1.00 equiv.
C15	10.4 g, 5.37 mmol, 1.00 equiv.
DCC	1.22 g, 5.91 mmol, 1.10 equiv.
DPTS	316 mg, 1.07 mmol, 0.20 equiv.
DCM	100 mL
eluent	1st cc: cyhex/EA = 3:2 → 1:1,
	2nd cc: cyhex/EA = 3:2 → 5:4
yield	17.2 g, 4.44 mmol, 82.8%, white solid
R_f	0.88 (cyhex/EA = 1:2).
Đ (system II)	1.00

^{1}H NMR (400 MHz, $CDCl_3$) δ / ppm = 7.38 – 7.30 (m, 5H, CH_{Ar}^1), 5.10 (s, 2H, CH_2^2), 4.04 (t, *J* = 6.7 Hz, 62H, CH_2^3), 3.58 (t, *J* = 6.5 Hz, 2H, CH_2^4), 2.36 (t, *J* = 7.5 Hz, 2H, CH_2^5), 2.29 (t, *J* = 7.5 Hz, 62H, CH_2^6), 1.69 – 1.58 (m, 126H, CH_2^7), 1.55 – 1.47 (m, 2H, CH_2^8), 1.42 – 1.33 (m, 64H, CH_2^9), 0.87 (s, 9H, CH_3^{10}), 0.02 (s, 6H, CH_3^{11}).

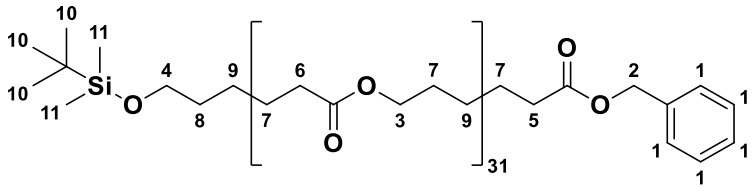

^{13}C NMR ($CDCl_3$, 101 MHz): δ / ppm = 173.91 (C_q^1), 173.65 (C_q^1), 173.41 (C_q^1), 136.13 ($C_{q,Ar}^2$), 128.67 ($CH_{Ar,meta}^3$), 128.33 ($CH_{Ar,para}^4$), 128.30 ($CH_{Ar,ortho}^5$), 66.27 (CH_2^6), 64.25 (CH_2^7), 63.08 (CH_2^8), 34.44 (CH_2^9), 34.22 (CH_2^9), 32.57 (CH_2^{10}), 28.46 (CH_2^{11}), 26.07 (CH_3^{12}), 25.64 (CH_2^{13}), 24.92 (CH_2^{14}), 24.68 (CH_2^{14}), 18.45 (C_q^{15}), -5.17 (CH_3^{16}).

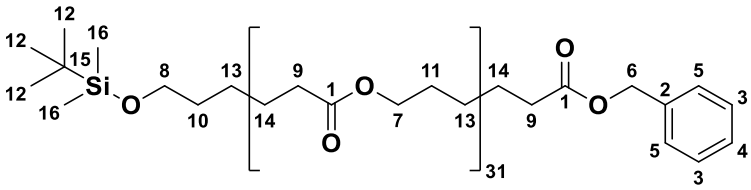

HRMS (ESI) of $C_{205}H_{342}O_{65}Si$ $[M+H]^+$ calcd. 3873.3298, found 3873.3579; $[M+2H]^{2+}$ calcd. 1937.1685, found 1937.16687.

IR (ATR platinum diamond) $\tilde{\nu}$ / cm^{-1} = 2943.7, 2864.3, 1720.9, 1470.6, 1364.4, 1292.6, 1237.9, 1161.6, 1106.0, 1043.0, 959.8, 837.6, 731.2, 452.9.

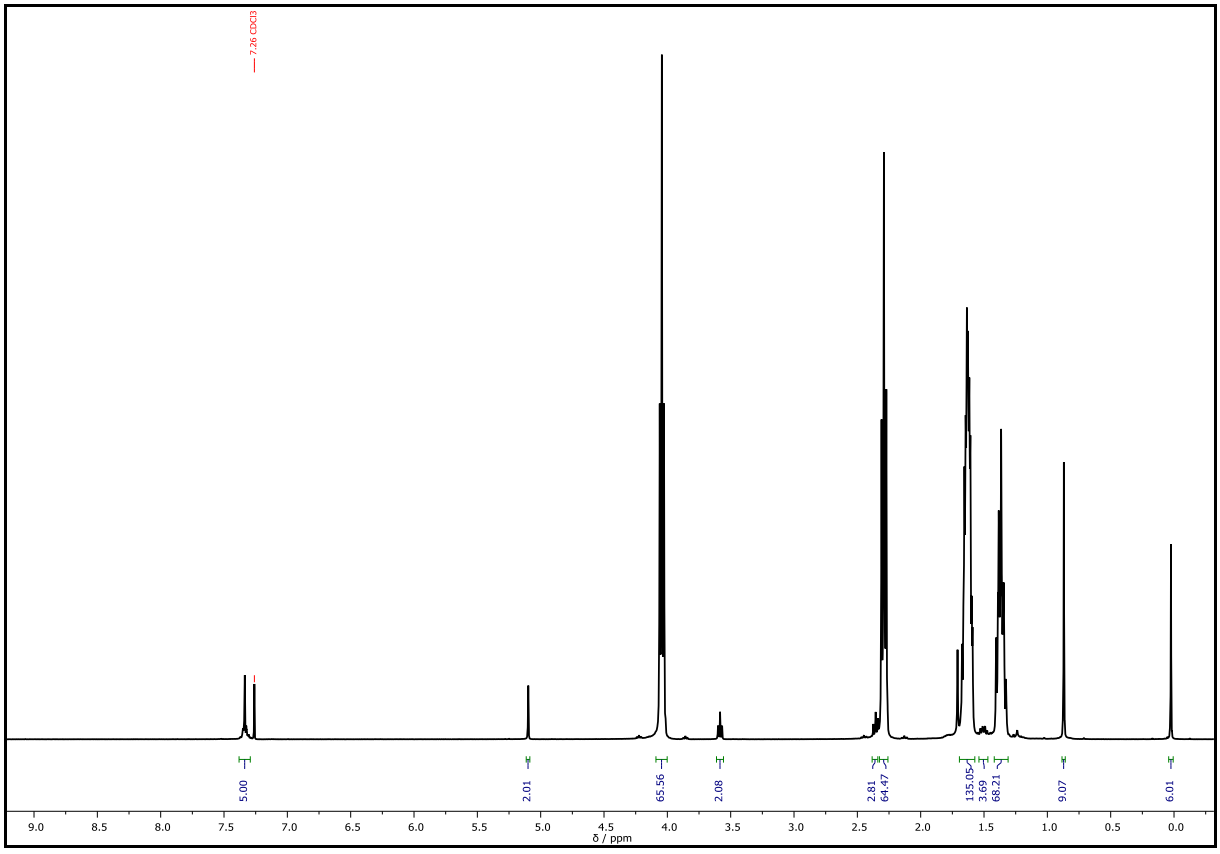

Supplementary Figure 109: ^{1}H NMR spectrum of **C16**, recorded at 400 MHz in $CDCl_3$.

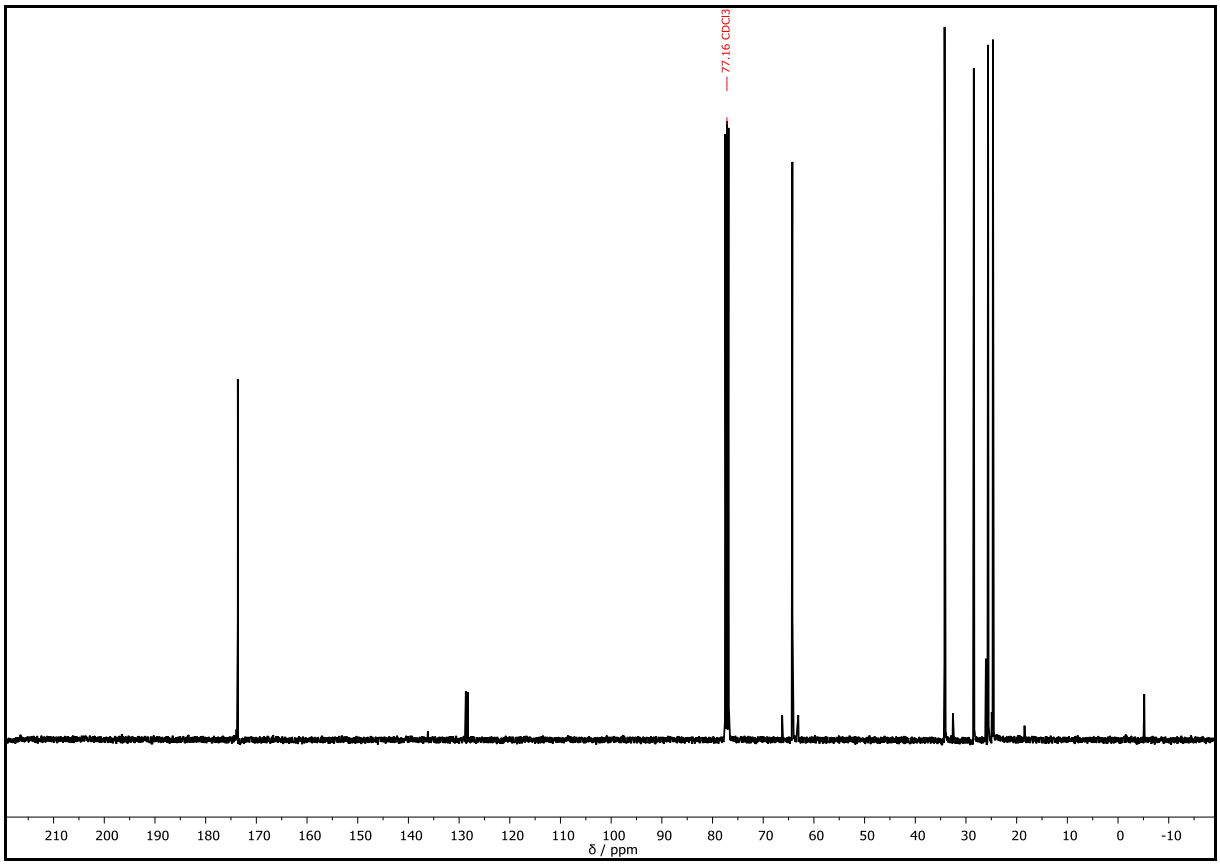

Supplementary Figure 110: ^{13}C NMR spectrum of **C16**, recorded at 101 MHz in $CDCl_3$.

The crude product of **C16** was purified *via* column chromatography for two times. In total 39 fractions were collected. The respective amounts, the analysis *via* GPC (system II) and the chromatograms are given in the following. The ones highlighted in green were used for further synthesis. The ones in yellow were purified once again *via* column chromatography and the fractions marked in red were discarded.

Supplementary Table 17 SEC results of the first purification of C16.						
cc 1	*m* / g	M_n / Da	M_w / Da	M_z / Da	*Đ*	purity / %
F1	117E-3	*n.a.*[1]	*n.a.*[1]	*n.a.*[1]	*n.a.*[1]	*n.a.*[1]
F2	56.1E-3	*n.a.*[1]	*n.a.*[1]	*n.a.*[1]	*n.a.*[1]	*n.a.*[1]
F3	74.2E-3	8200	8250	8300	1.01	10.6
F4	2.20	8100	8100	8150	1.00	92.1
F5	2.68	8100	8100	8150	1.00	98.8
F6	2.09	8050	8100	8100	1.00	>99
F7	1.78	8100	8100	8150	1.00	>99
F8	1.62	8100	8150	8150	1.00	>99
F9	2.09	8050	8100	8100	1.00	>99
F10	2.81	8050	8100	8100	1.00	>99
F11	4.16	8050	8100	8100	1.00	>99
F12	1.48	8050	8100	8100	1.00	98.5
F13	271E-3	8050	8100	8100	1.00	981

eluent: cyhex:EA = 3:2 → 1:1. [1]This fraction did not contain any product.

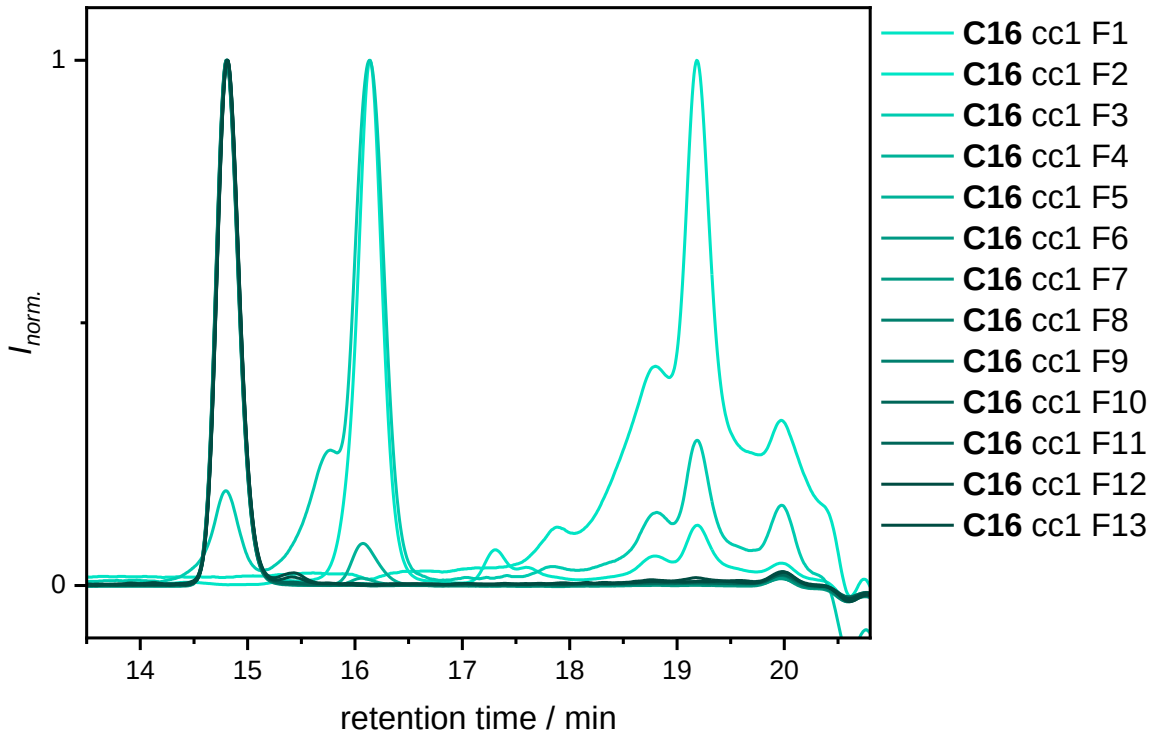

Supplementary Figure 111: SEC traces of the individual fractions obtained from the first purification *via* column chromatography of **C16**.

The fractions **C16** cc1 F4+5, 12+13 were further purified *via* column chromatography.

Supplementary Table 18: SEC results of the second purification of C16.

cc 2	*m* / mg	M_n / Da	M_w / Da	M_z / Da	*Đ*	purity / %
F1	26.4	*n.a.*[1]	*n.a.*[1]	*n.a.*[1]	*n.a.*[1]	*n.a.*[1]
F2	33.6	*n.a.*[1]	*n.a.*[1]	*n.a.*[1]	*n.a.*[1]	*n.a.*[1]
F3	26.1	*n.a.*[1]	*n.a.*[1]	*n.a.*[1]	*n.a.*[1]	*n.a.*[1]
F4	33.7	*n.a.*[1]	*n.a.*[1]	*n.a.*[1]	*n.a.*[1]	*n.a.*[1]
F5	55.5	*n.a.*[1]	*n.a.*[1]	*n.a.*[1]	*n.a.*[1]	*n.a.*[1]
F6	62.1	*n.a.*[1]	*n.a.*[1]	*n.a.*[1]	*n.a.*[1]	*n.a.*[1]
F7	47.4	*n.a.*[1]	*n.a.*[1]	*n.a.*[1]	*n.a.*[1]	*n.a.*[1]
F8	31.1	8200	8300	8300	1.00	11.9
F9	96.1	7950	8000	8050	1.01	89.7
F10	272	8050	8050	8100	1.00	98.2
F11	426	8050	8100	8100	1.00	99.3
F12	566	8050	8100	8100	1.00	>99
F13	655	8100	8100	8150	1.00	>99
F14	659	8100	8150	8150	1.00	>99
F15	579	8050	8100	8100	1.00	>99
F16	812	8050	8050	8100	1.00	>99
F17	939	8050	8100	8100	1.00	99.6
F18	550	8050	8050	8100	1.00	99.1
F19	326	8050	8100	8100	1.00	98.6
F20	194	8100	8100	8150	1.00	98.3
F21	104	8100	8100	8150	1.00	98.2
F22	93.2	8100	8150	8150	1.00	98.3
F23		8050	8100	8100	1.00	76.6

eluent: cyhex:EA = 3:2 → 5:4. [1]This fraction did not contain any product.

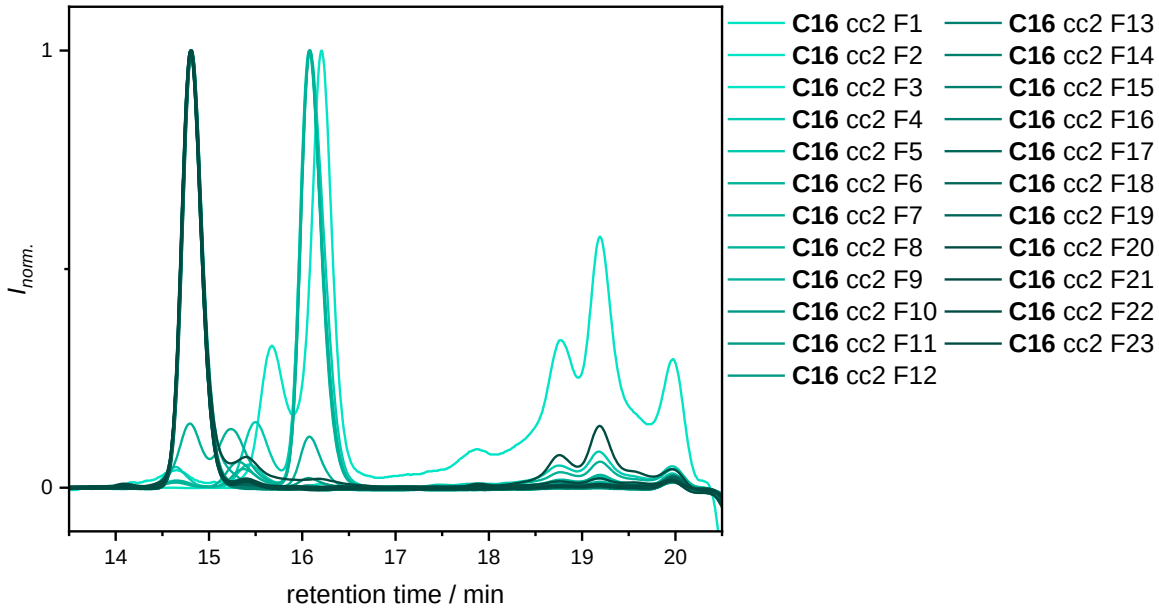

Supplementary Figure 112: SEC traces of the individual fractions obtained from the second purification *via* column chromatography of **C16**.

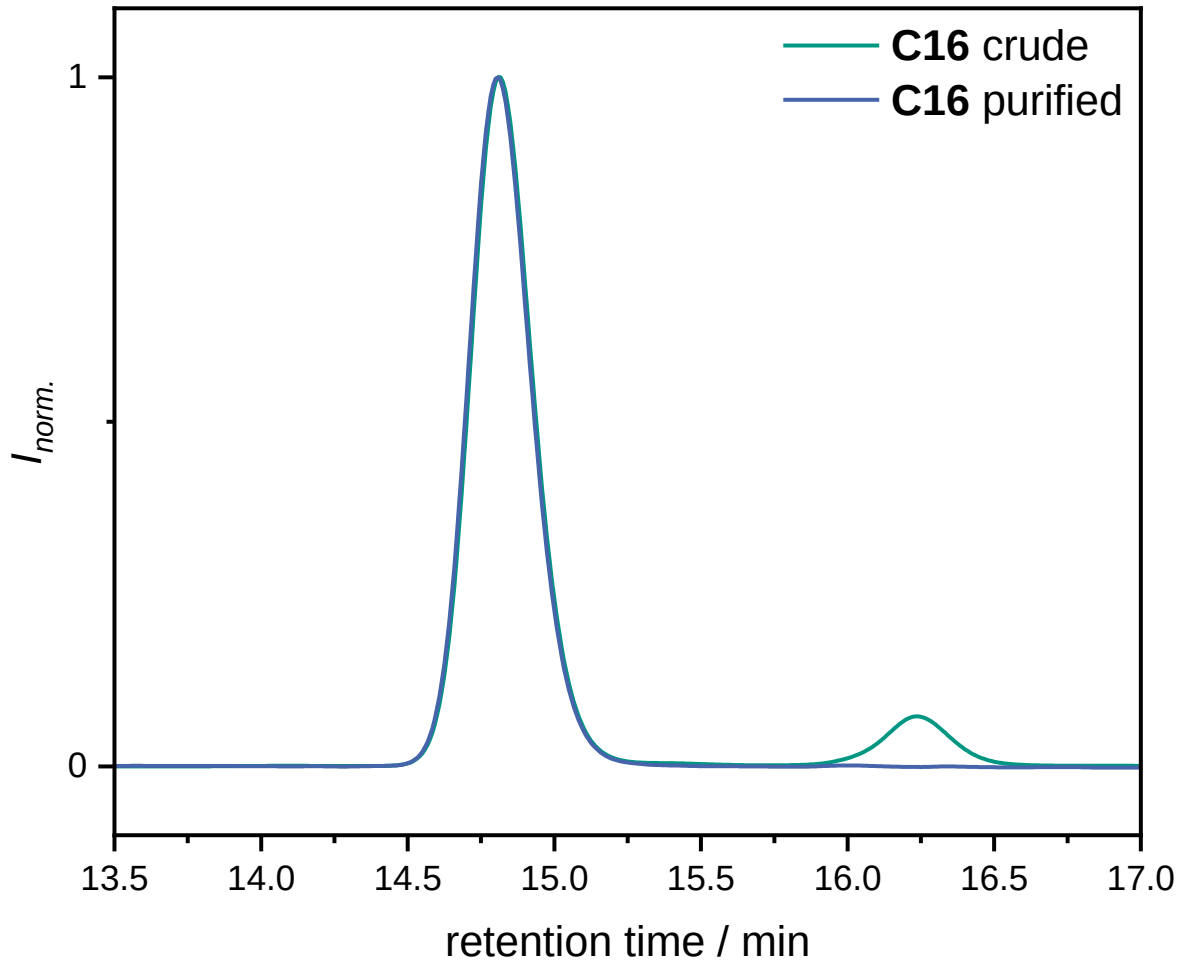

Supplementary Figure 113: SEC traces of product **C16** before and after two column chromatographic purification steps.

Carboxyl–terminated 32-mer – C17

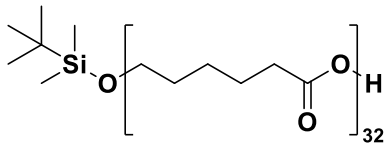

Chemical Formula: $C_{198}H_{336}O_{65}Si$
Exact Mass: 3782.2756 Da
Molecular Weight: 3784.8860 Da

The carboxyl-terminated 32-mer **C17** was prepared using the procedure described above for the synthesis of the carboxyl-terminated dimer **C5**.

C16	7.00 g, 1.81 mmol, 1.00 equiv.
Pd/C	700 mg, 10 wt%
EA	45.0 mL
Yield	6.39 g, 1.69 mmol, 93.4%, white solid
R_f	0.47 (cyhex/EA = 1:2).
Đ (system II)	1.00

^{1}H NMR ($CDCl_3$, 400 MHz): δ / ppm = 4.05 (t, *J* = 6.7 Hz, 62H, CH_2^1), 3.59 (t, *J* = 6.5 Hz, 2H, CH_2^2), 2.35 (t, *J* = 7.3 Hz, 2H, CH_2^3), 2.29 (t, *J* = 7.5 Hz, 64H, CH_2^4), 1.71 – 1.57 (m, 126H, CH_2^5), 1.55 – 1.47 (m, 2H, CH_2^6), 1.42 – 1.32 (m, 64H, CH_2^7), 0.87 (s, 9H, CH_3^8), 0.03 (s, 6H, CH_3^9).

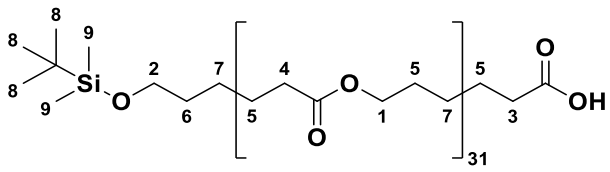

^{13}C NMR ($CDCl_3$, 101 MHz): δ / ppm = 173.92 (C_q^1), 173.82 (C_q^2), 173.65 (C_q^2), 64.31 (CH_2^3), 64.26 (CH_2^3), 64.17 (CH_2^3), 63.09 (CH_2^4), 34.45 (CH_2^5), 34.29 (CH_2^5), 34.23 (CH_2^5), 33.58 (CH_2^6), 32.58 (CH_2^7), 28.46 (CH_2^8), 28.42 (CH_2^8), 26.08 (CH_3^9), 25.64 (CH_2^{10}), 25.61 (CH_2^{10}), 25.56 (CH_2^{10}), 24.92 (CH_2^{11}), 24.69 (CH_2^{11}), 24.49 (CH_2^{11}), 18.45 (C_q^{12}), -5.17 (CH_3^{13}).

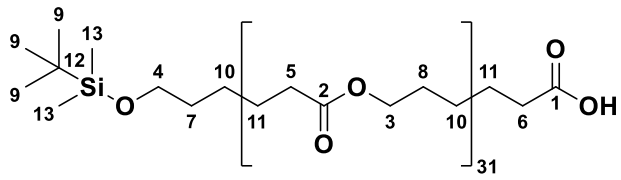

Note: The molecule was not detectable by ESI-MS analysis.

IR (ATR platinum diamond) $\tilde{\nu}$ / cm^{-1} = 2943.7, 2864.3, 1720.6, 1470.5, 1418.8, 1396.9, 1364.5, 1292.6, 1238.0, 1163.6, 1106.3, 1065.0, 1043.3, 959.8, 933.9, 837.9, 776.1, 731.1, 585.2, 524.1, 453.1.

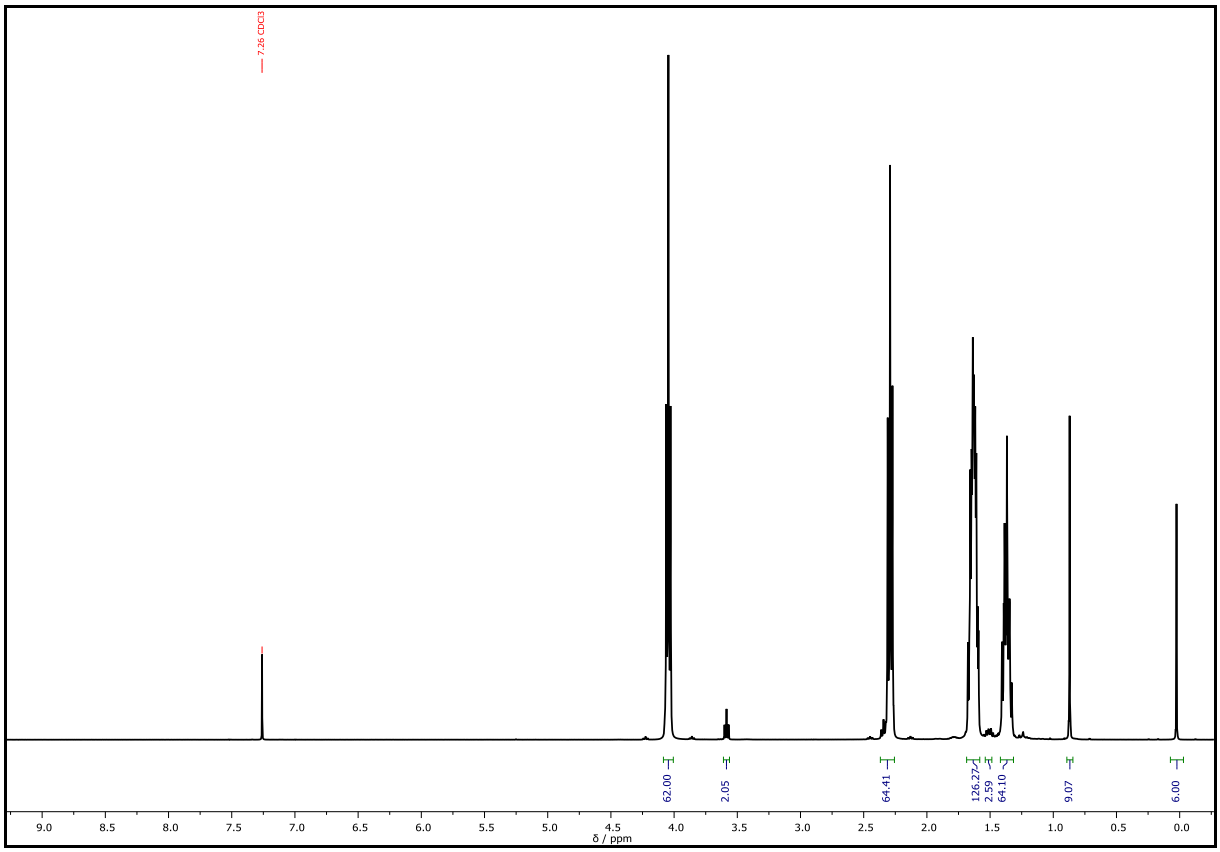

Supplementary Figure 114: ^{1}H NMR spectrum of **C17**, recorded at 400 MHz in $CDCl_3$.

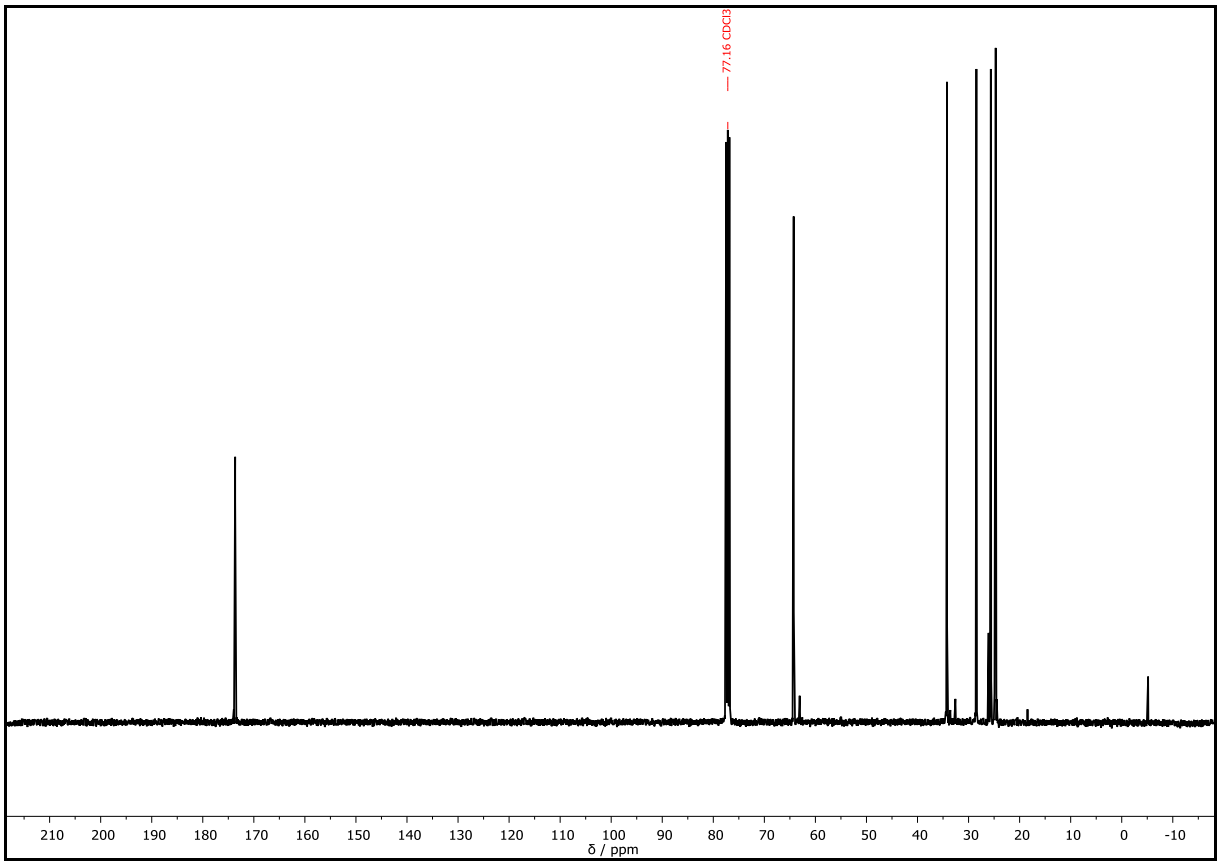

Supplementary Figure 115: ^{13}C NMR spectrum of **C17**, recorded at 101 MHz in $CDCl_3$.

Hydroxyl–terminated 32-mer – C18

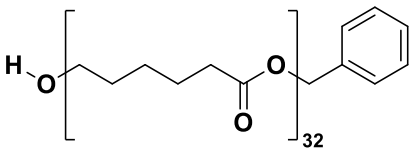

Chemical Formula: $C_{199}H_{328}O_{65}$
Exact Mass: 3758.2361 Da
Molecular Weight: 3760.7480 Da

The hydroxyl-terminated tetramer **C18** was prepared according to the procedure described above for the synthesis of the hydroxyl-terminated dimer **C6**.

C16	7.00 g, 1.81 mmol, 1.00 equiv.
TBAF	1.14 g, 3.61 mmol, 2.00 equiv.
glacial acetic acid	207 µL, 217 mg, 3.61 mmol, 2.00 equiv.
total THF	7.20 mL
eluent	cyhex/EA = 1:1 → 1:2
yield	6.55 g, 1.74 mmol, 96.5%, white solid
R_f	0.63 (cyhex/EA = 1:2).
Đ (system II)	1.00

^{1}H NMR ($CDCl_3$, 400 MHz): δ / ppm = 7.39 – 7.29 (m, 5H, $CH_{Ar}{}^1$), 5.10 (s, 2H, $CH_2{}^2$), 4.05 (t, *J* = 6.7 Hz, 62H, $CH_2{}^3$), 3.64 (t, *J* = 6.5 Hz, 2H, $CH_2{}^4$), 2.36 (t, *J* = 7.5 Hz, 2H, $CH_2{}^5$), 2.30 (t, *J* = 7.5 Hz, 62H, $CH_2{}^6$), 1.72 – 1.55 (m, 128H, $CH_2{}^7$ and $CH_2{}^8$), 1.43 – 1.31 (m, 64H, $CH_2{}^9$).

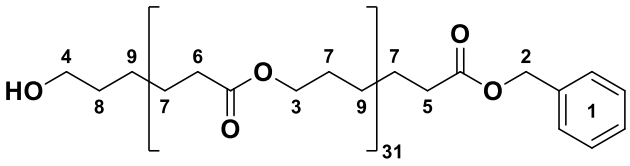

^{13}C NMR ($CDCl_3$, 101 MHz): δ / ppm = 173.85 (C_q^1), 173.66 (C_q^1), 173.42 (C_q^1), 128.69 ($CH_{Ar,meta}^3$), 128.34 ($CH_{Ar,para}^4$), 128.31 ($CH_{Ar,ortho}^5$), 66.28 (CH_2^6), 64.27 (CH_2^7), 62.75 (CH_2^8), 34.36 (CH_2^9), 34.25 (CH_2^9), 32.47 (CH_2^{10}), 28.48 (CH_2^{11}), 25.66 (CH_2^{12}), 25.43 (CH_2^{12}), 24.81 (CH_2^{13}), 24.71 (CH_2^{13}).

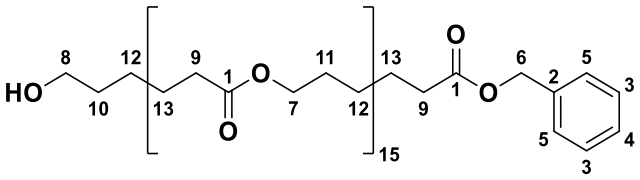

Note: $C_{q,Ar}^2$ at around 136 ppm was not visible in the ^{13}C spectrum.

Note: The molecule was not detectable by ESI-MS analysis.

IR (ATR platinum diamond) $\tilde{\nu}$ / cm^{-1} = 2943.8, 2865.2, 1720.7, 1470.7, 1418.2, 1396.9, 1364.6, 1292.6, 1237.9, 1164.1, 1106.9, 1043.6, 959.7, 840.3, 731.5, 584.0, 452.6.

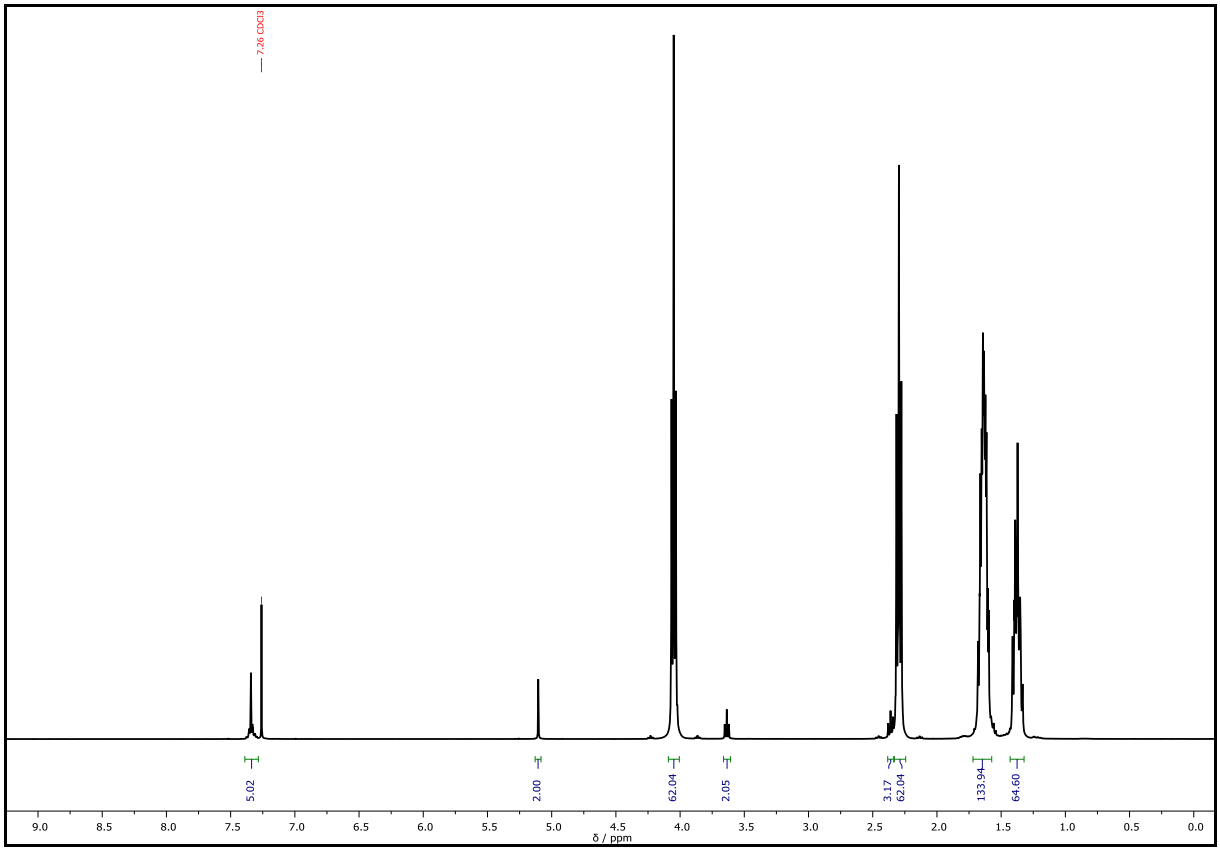

Supplementary Figure 116: ^{1}H NMR spectrum of **C18**, recorded at 400 MHz in $CDCl_3$.

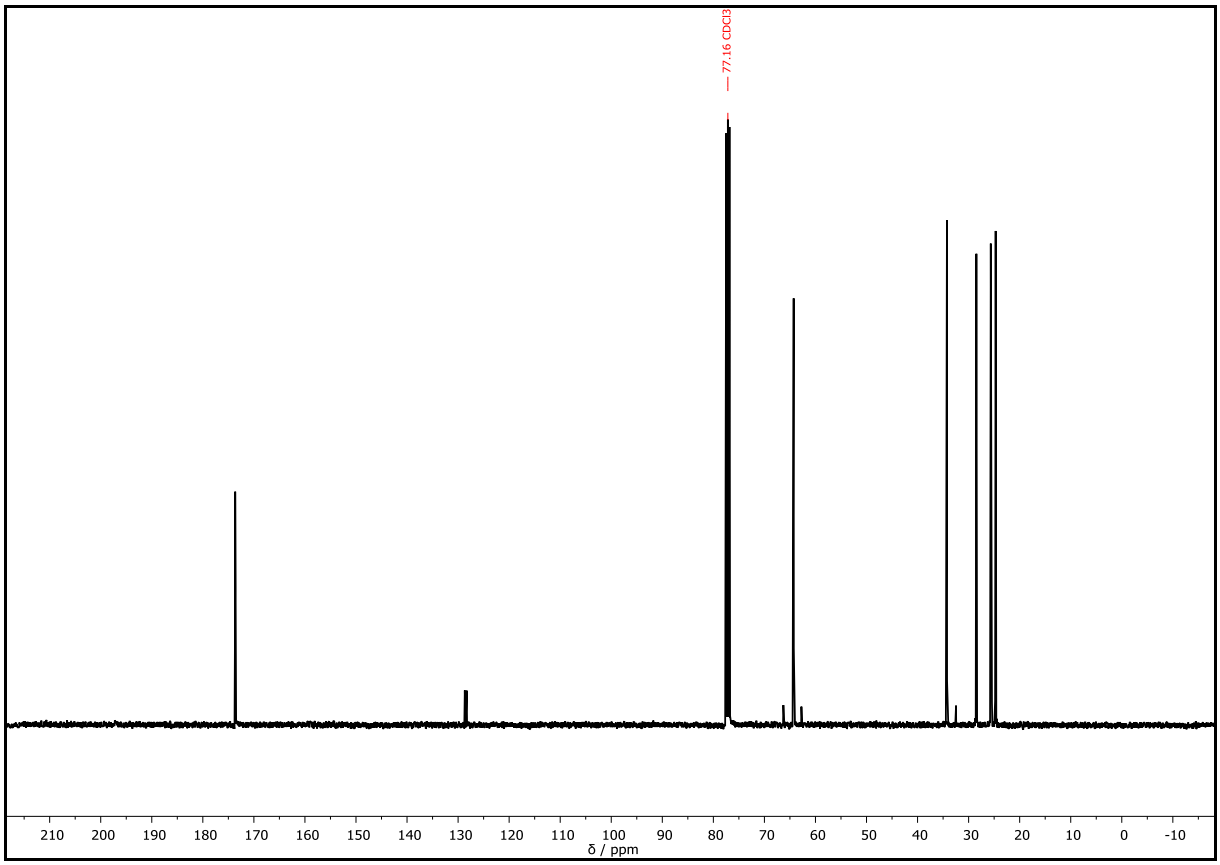

Supplementary Figure 117: ^{13}C NMR spectrum of **C18**, recorded at 101 MHz in $CDCl_3$.

Doubly protected 64-mer – C19

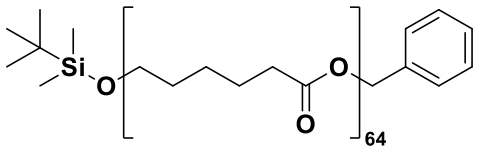

Chemical Formula: $C_{397}H_{662}O_{129}Si$
Exact Mass: 7522.5011 Da
Molecular Weight: 7527.6190 Da

The doubly protected 64-mer **C19** was prepared using the procedure described above for the synthesis of the doubly protected dimer **C4**. 0.20 equiv. DPTS was used instead of 1.10 equiv. DMAP.

C17	4.36 g, 1.16 mmol, 1.00 equiv.
C18	4.39 g, 1.16 mmol, 1.00 equiv.
DCC	263 mg, 1.28 mmol, 1.10 equiv.
DPTS	68.3 mg, 232 µmol, 0.20 equiv.
DCM	30 mL
eluent	cyhex/EA = 1:1
yield	7.34 g, 975 µmol, 84.1%, white solid
R_f	0.14 (cyhex/EA = 1:1).
Đ (system II)	1.00

^{1}H NMR (400 MHz, $CDCl_3$) δ / ppm = 7.39 – 7.30 (m, 5H, CH_{Ar}^1), 5.11 (s, 2H, CH_2^2), 4.06 (t, *J* = 6.7 Hz, 126H, CH_2^3), 3.60 (t, *J* = 6.5 Hz, 2H, CH_2^4), 2.37 (t, *J* = 7.5 Hz, 2H, CH_2^5), 2.30 (t, *J* = 7.5 Hz, 126H, CH_2^6), 1.64 (m, 254H, CH_2^7), 1.54 – 1.49 (m, 2H, CH_2^8), 1.43 – 1.33 (m, 128H, CH_2^9), 0.88 (s, 9H, CH_3^{10}), 0.04 (s, 6H, CH_3^{11}).

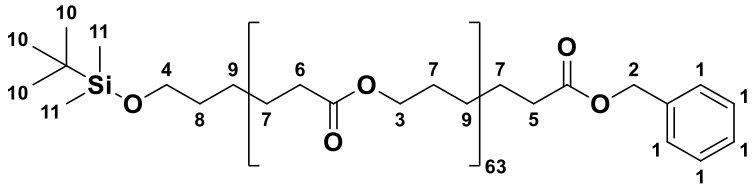

^{13}C NMR ($CDCl_3$, 101 MHz): δ / ppm = 173.68 (C_q^1), 128.71 (CH_{Ar}^3), 128.33 (CH_{Ar}^3), 66.31 (CH_2^4), 64.29 (CH_2^5), 63.12 (CH_2^6), 34.49 (CH_2^7), 34.27 (CH_2^7), 32.61 (CH_2^8), 28.50 (CH_2^9), 26.11 (CH_2^{10}), 25.68 (CH_2^{11}), 24.73 (CH_2^{12}), -5.12 (CH_3^{14}).

Note: C^2 and C^{13} are not visible in the ^{13}C NMR spectrum.

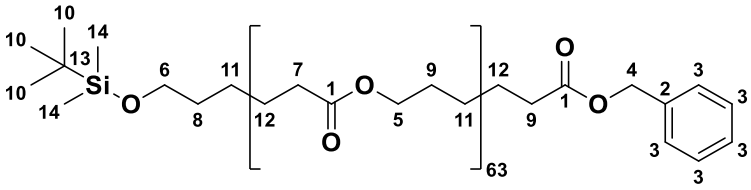

Note: The molecule was not detectable by ESI-MS analysis.

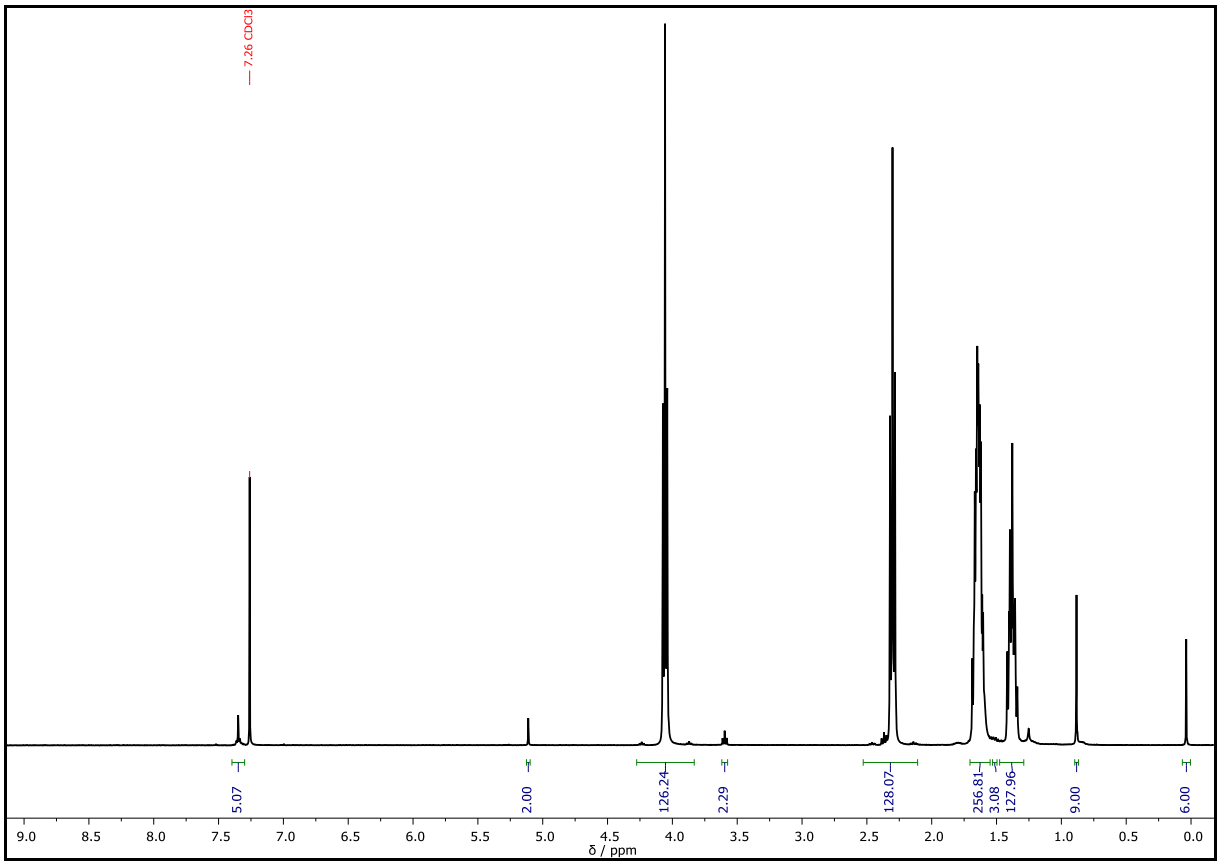

Supplementary Figure 118: ^{1}H NMR spectrum of **C19**, recorded at 400 MHz in $CDCl_3$.

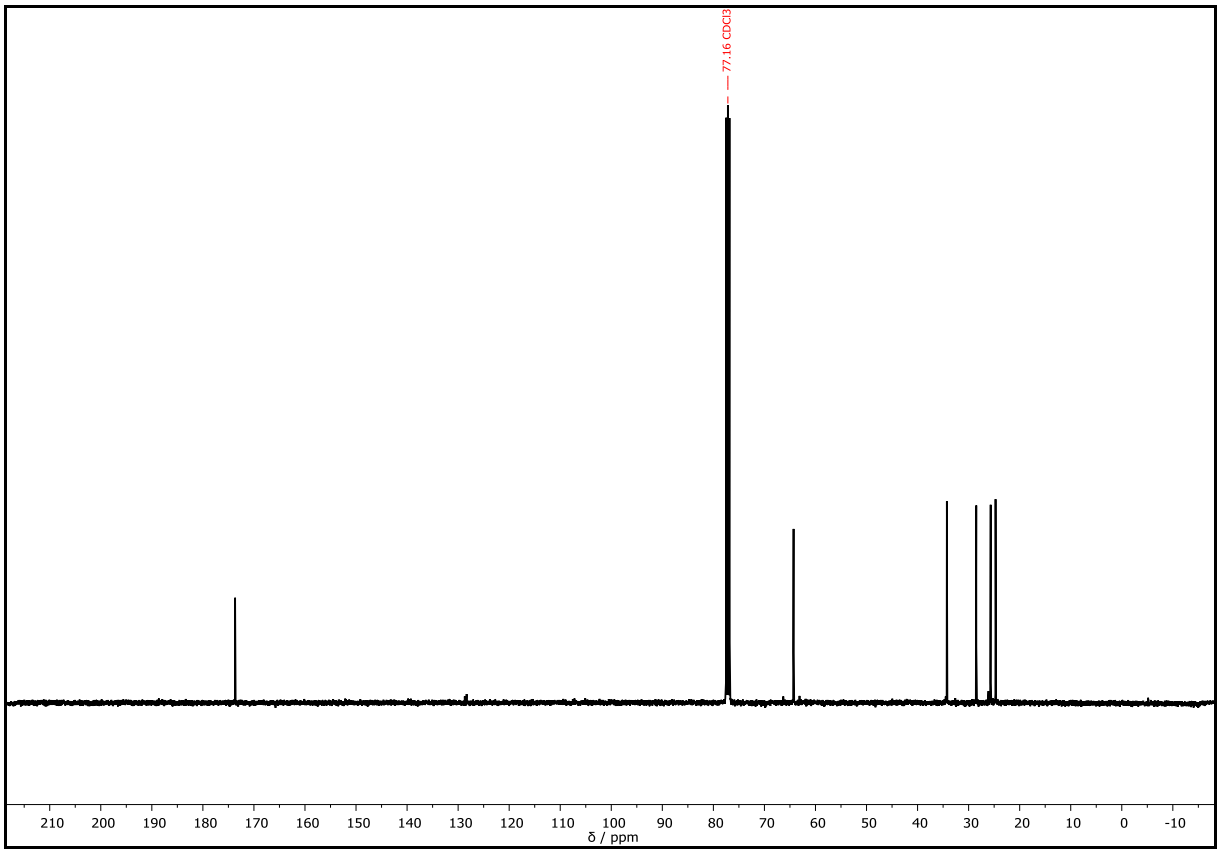

Supplementary Figure 119: ^{13}C NMR spectrum of **C19**, recorded at 101 MHz in $CDCl_3$.

Supplementary Table 19: SEC results of the purification of C19.						
cc 1	*m* / g	M_n / Da	M_w / Da	M_z / Da	*Đ*	purity / %
F1	3.28	16050	16150	16350	1.01	90.0
F2	2.44	16050	16100	16150	1.00	>99
F3	609×10^{-3}	15950	16050	16100	1.00	>99
F4	213×10^{-3}	16000	16100	16200	1.01	>99
F5	1.86	16150	16250	16350	1.01	61.7
F6	137×10^{-3}	15900	16000	16100	1.01	23.1

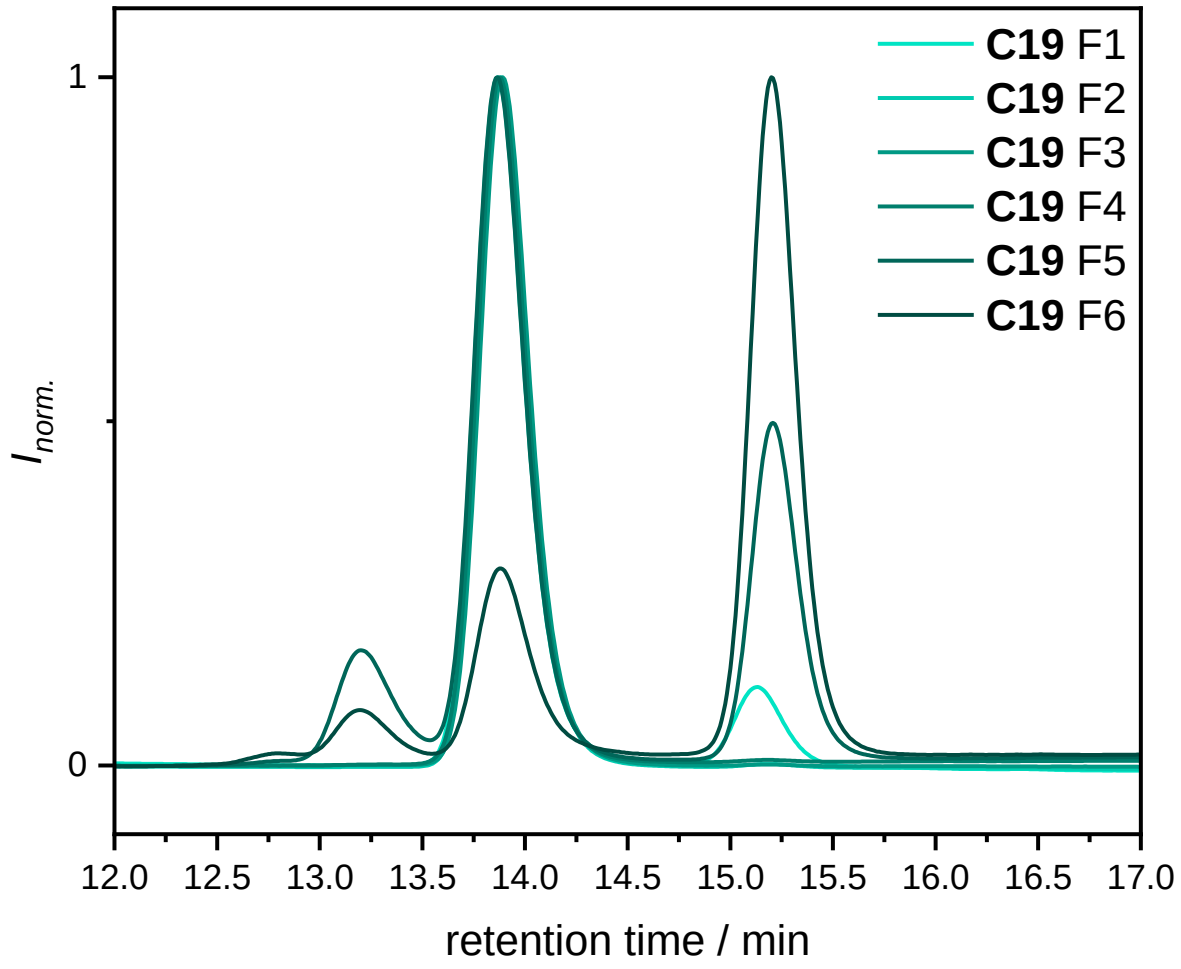

Supplementary Figure 120: SEC traces of the individual fractions obtained from the purification *via* column chromatography of **C19**.

Carboxyl–terminated 64-mer – C20

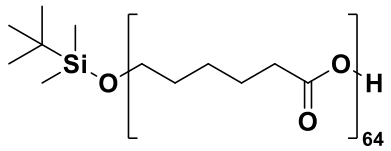

Chemical Formula: $C_{390}H_{656}O_{129}Si$
Exact Mass: 7432.4541 Da
Molecular Weight: 7437.4940 Da

The carboxyl-terminated 64-mer **C20** was prepared according to the procedure described above for the synthesis of the carboxyl-terminated dimer **C5**.

C19	3.00 g, 403 µmol, 1.00 equiv.
Pd/C	300 mg, 10 wt%
EA	35 mL
yield	2.85 g, 383 µmol, 95.0%
Đ (system II)	1.00

^{1}H NMR ($CDCl_3$, 500 MHz): δ / ppm = 4.06 (t, *J* = 6.7 Hz, 126H, CH_2^1), 3.60 (t, *J* = 6.5 Hz, 2H, CH_2^2), 2.30 (t, *J* = 7.5 Hz, 128H, CH_2^3 and CH_2^4), 1.63 (m, 254H, CH_2^5), 1.55 – 1.46 (m, 2H, CH_2^6), 1.42 (m, 128H, CH_2^7), 0.88 (s, 9H, CH_3^8), 0.04 (s, 6H, CH_3^9).

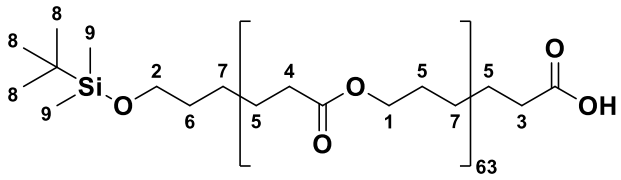

^{13}C NMR ($CDCl_3$, 126 MHz): δ / ppm = 173.63 (C_q^2), 64.38 (CH_2^3), 64.28 (CH_2^3), 64.23 (CH_2^3), 64.14 (CH_2^3), 63.06 (CH_2^4), 34.42 (CH_2^5), 34.32 (CH_2^5), 34.26 (CH_2^5), 34.20 (CH_2^5), 34.07 (CH_2^5), 33.96 (CH_2^5), 32.55 (CH_2^7), 28.57 (CH_2^8), 28.43 (CH_2^8), 28.29 (CH_2^8), 28.27 (CH_2^8), 26.05 (CH_3^9), 25.74 (CH_2^{10}), 25.61 (CH_2^{10}), 25.57 (CH_2^{10}), 25.53 (CH_2^{10}), 25.49 (CH_2^{10}), 25.39 (CH_2^{10}), 25.00 (CH_2^{11}), 24.89 (CH_2^{11}), 24.77 (CH_2^{11}), 24.66 (CH_2^{11}), 24.51 (CH_2^{11}), 18.43 (C_q^{12}), -5.20 (CH_3^{13}).

Note: C_q^1 and CH_2^6 are not visible in the ^{13}C spectrum

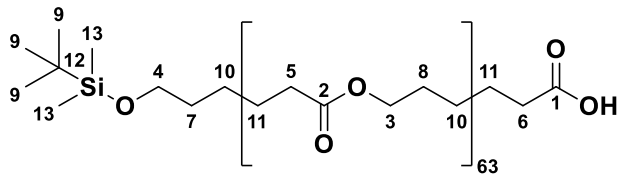

Note: The molecule was not detectable by ESI-MS analysis.

IR (ATR platinum diamond) $\tilde{\nu}$ / cm^{-1} = 2943, 2896, 2865, 1722, 1471, 1419, 1397, 1366, 1294, 1238, 1170, 1107, 1065, 1045, 991, 961, 934, 839, 775, 732, 710, 584, 453.

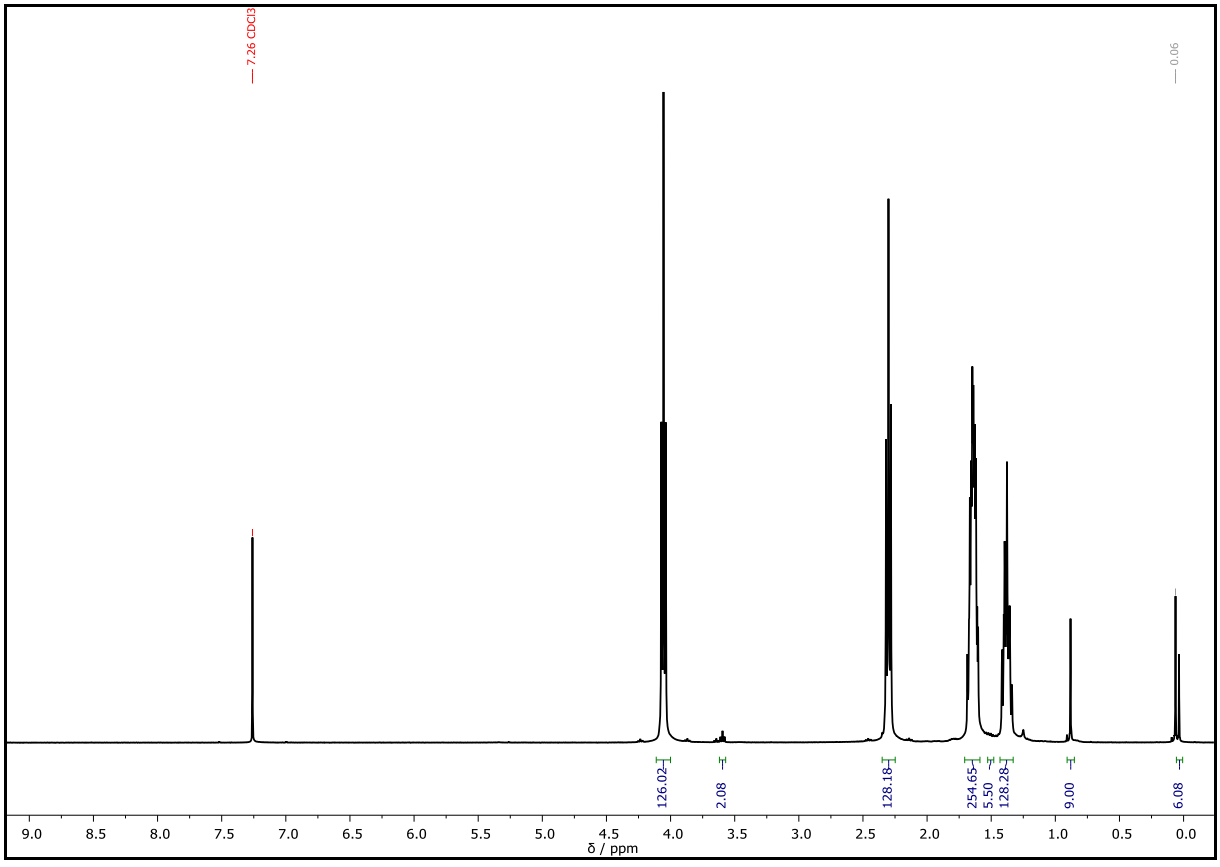

Supplementary Figure 121: ^{1}H NMR spectrum of **C19**, recorded at 500 MHz in $CDCl_3$.

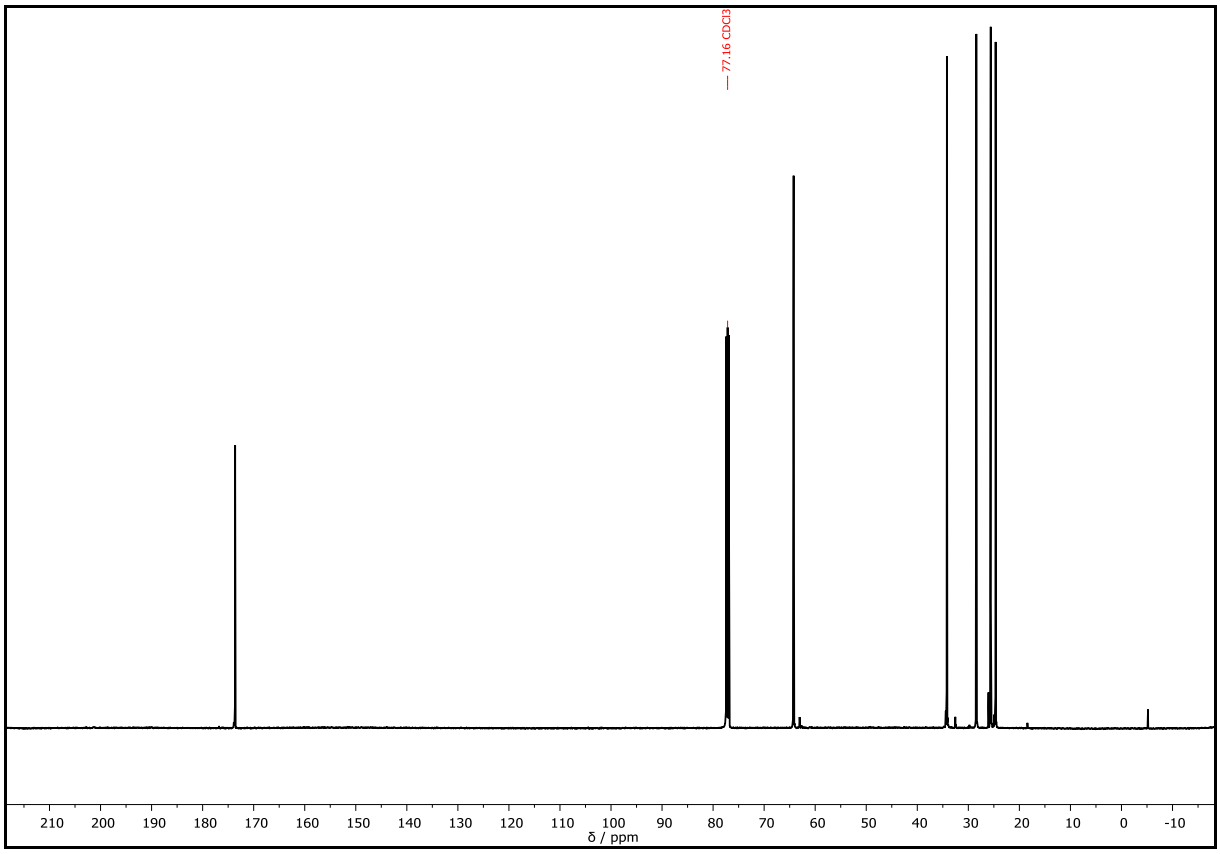

Supplementary Figure 122: ^{13}C NMR spectrum of **C19**, recorded at 126 MHz in $CDCl_3$.

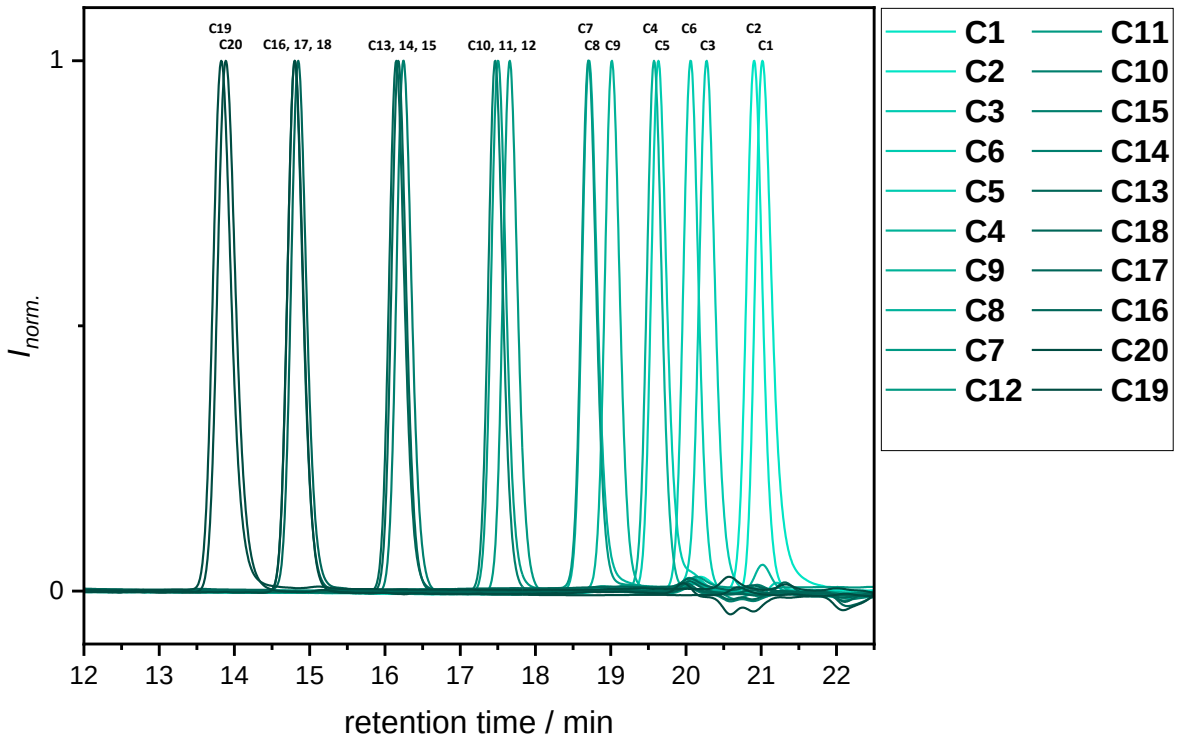

Supplementary Figure 123: SEC overview of the synthesized PCLs. The SEC traces range from the monomer, 6-hydroxyhexanoic acid **C1** at a retention time of 21.0 min in light green to the doubly protected PCL_{64} **C19** at 13.8 min in dark green.

6.3.5. Experimental procedures of chapter 4.3

mPEG$_{16}$-*b*-PCL$_{16}$-TBDMS (uBCP-1)

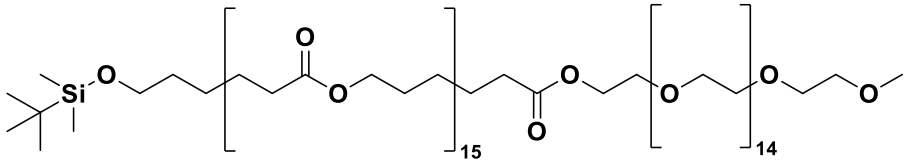

Chemical Formula: $C_{135}H_{242}O_{49}Si$
Exact Mass: 2675.6214 Da
Molecular Weight: 2677.4570 Da

The block copolymer **uBCP-1** was prepared according to the procedure described above for the synthesis of the doubly protected dimer **C4**.

C14	319 mg, 163 µmol, 1.00 equiv.
P23	120 mg, 163 µmol, 1.00 equiv.
DCC	202 mg, 977 µmol, 6.00 equiv.
DPTS	48.0 mg, 163 µmol, 1.00 equiv.
DCM	4.00 mL
Eluent	1st column chromatography (cc): EA → EA:MeOH = 99:1 → 9:1 → acetone; 2nd cc: EA → acetone
yield	161 mg, 60.1 µmol, 36.9%, white solid
R_f	0.21 (EA:MeOH = 9:1)
Đ (system III)	1.01

^{1}H NMR (500 MHz, $CDCl_3$): δ / ppm = 4.24 – 4.20 (m, 2H, CH_2^{1}), 4.05 (t, *J* = 6.7 Hz, 30H, CH_2^{2}), 3.70 – 3.68 (m, 2H, CH_2^{3}), 3.66 – 3.63 (m, 58H, CH_2^{4}), 3.61 – 3.58 (m, 2H, CH_2^{5}), 3.56 – 3.53 (m, 2H, CH_2^{6}), 3.37 (s, 3H, CH_3^{7}), 2.34 (t, *J* = 7.6 Hz, 2H, CH_2^{8}), 2.30 (t, *J* = 7.5 Hz, 30H, CH_2^{9}), 1.69 – 1.60 (m, 62H, CH_2^{10}), 1.54 – 1.49 (m, 2H, CH_2^{11}), 1.42 – 1.33 (m, 32H, CH_2^{12}), 0.88 (s, 9H, CH_3^{13}), 0.03 (s, 6H, CH_3^{14}).

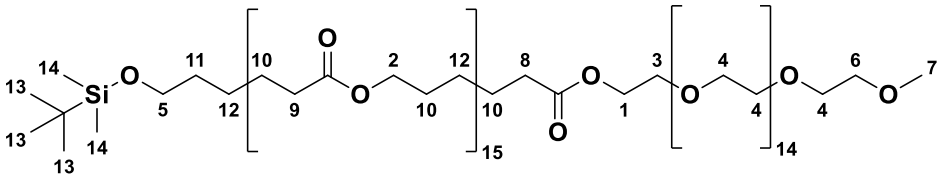

^{13}C NMR (126 MHz, $CDCl_3$): δ / ppm = 173.94 (C_q^{1}), 173.67 (C_q^{1}), 173.59 (C_q^{1}), 72.07 (CH_2^{2}), 70.74 (CH_2^{3}), 70.70 (CH_2^{3}), 69.31 (CH_2^{4}), 64.27 (CH_2^{5}), 64.19 (CH_2^{5}), 63.58 (CH_2^{6}), 63.10 (CH_2^{7}), 59.18 (CH_3^{8}), 34.47 (CH_2^{9}), 34.25 (CH_2^{9}), 34.11 (CH_2^{9}), 32.60 (CH_2^{10}), 28.48 (CH_2^{11}), 26.10 (CH_3^{12}), 25.66 (CH_2^{13}), 25.58 (CH_2^{13}), 24.94 (CH_2^{14}), 24.71 (CH_2^{14}), 24.63 (CH_2^{14}), 18.48 (C_q^{15}), -5.15 (CH_3^{16}).

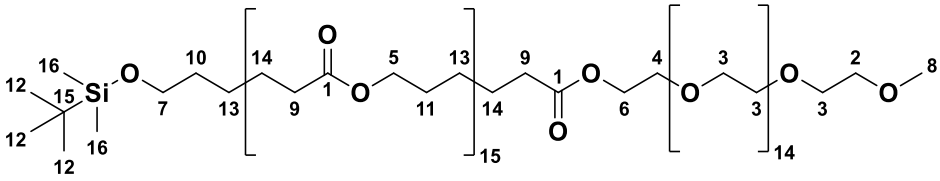

HRMS (ESI) of $C_{135}H_{242}O_{49}Si$ $[M+NH_4]^+$ *m/z* calc. 2693.6552, found 2693.6589; $[M+Na]^+$ *m/z* calc. 2698.6106, found 2698.6143; $[M+K]^+$ *m/z* calc. 2714.5846, found 2714.5945. $[M+2Na]^{2+}$ *m/z* calc. 1360.7999, found 1360.7990; $[M+Na+K]^{2+}$ *m/z* calc. 1368.7869, found 1368.7859.

IR (ATR platinum diamond) *v* / cm^{-1} = 2943, 2894, 2865, 1722, 1471, 1419, 1397, 1366, 1294, 1242, 1189, 1105, 1065, 1045, 961, 934, 837, 815, 775, 732, 710, 453.

R_f = 0.21 (EA:methanol = 9:1).

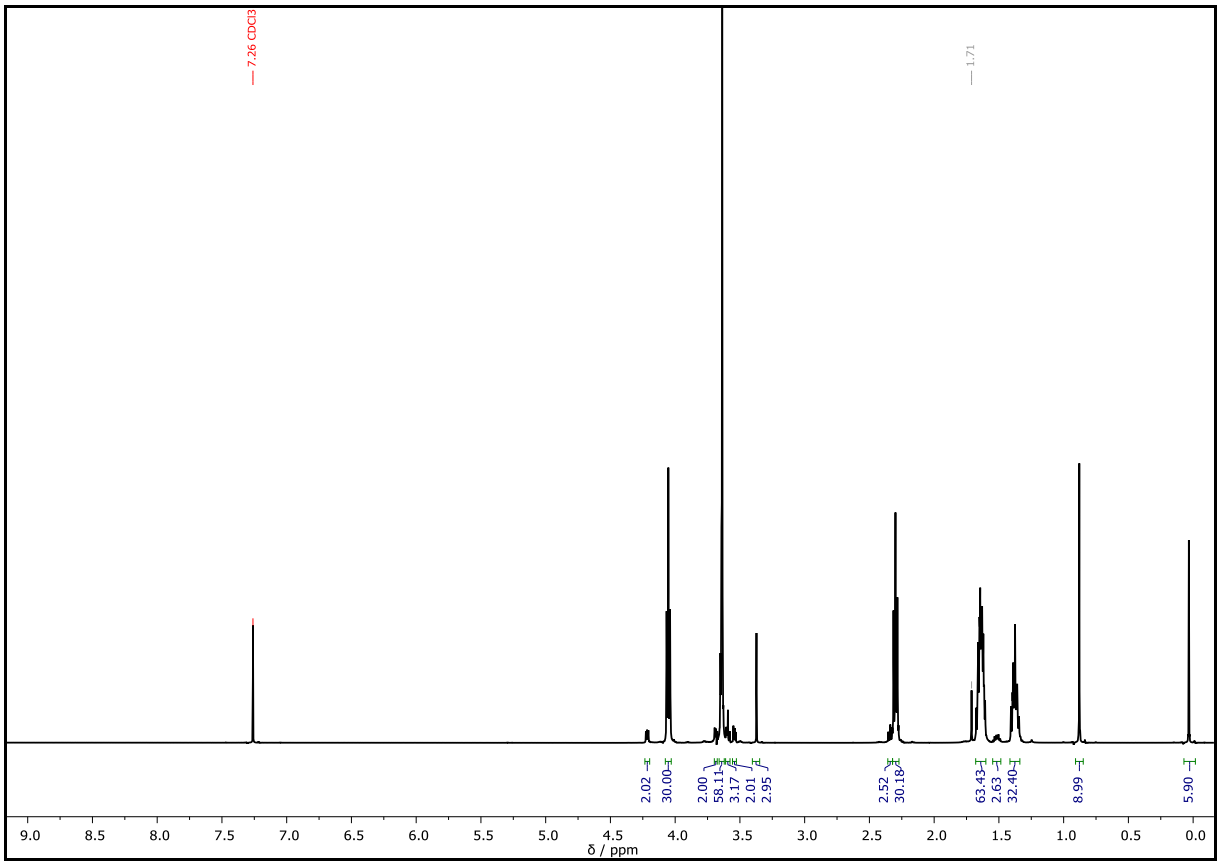

Supplementary Figure 124: ^{1}H NMR spectrum of **uBCP-1** recorded at 500 MHz in $CDCl_3$.

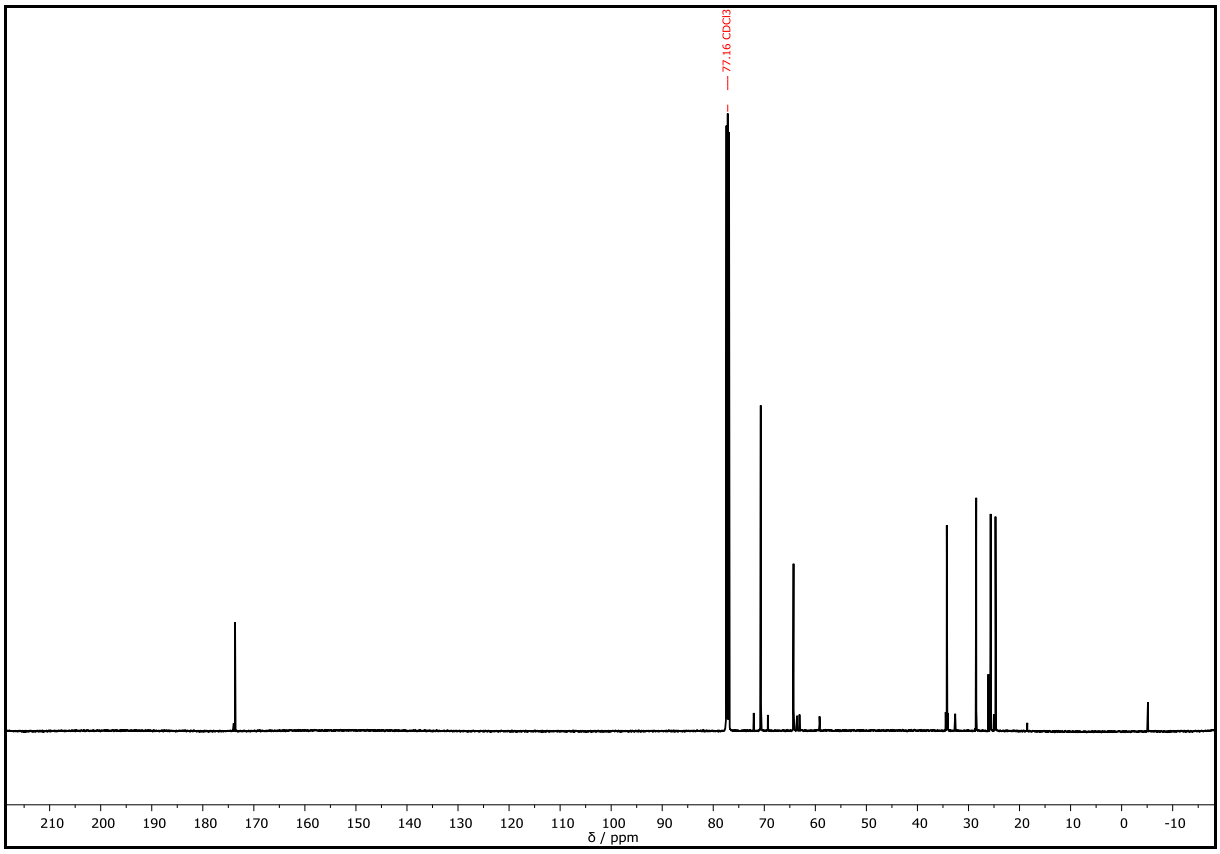

Supplementary Figure 125: ^{13}C NMR spectrum of **uBCP-1** recorded at 126 MHz in $CDCl_3$.

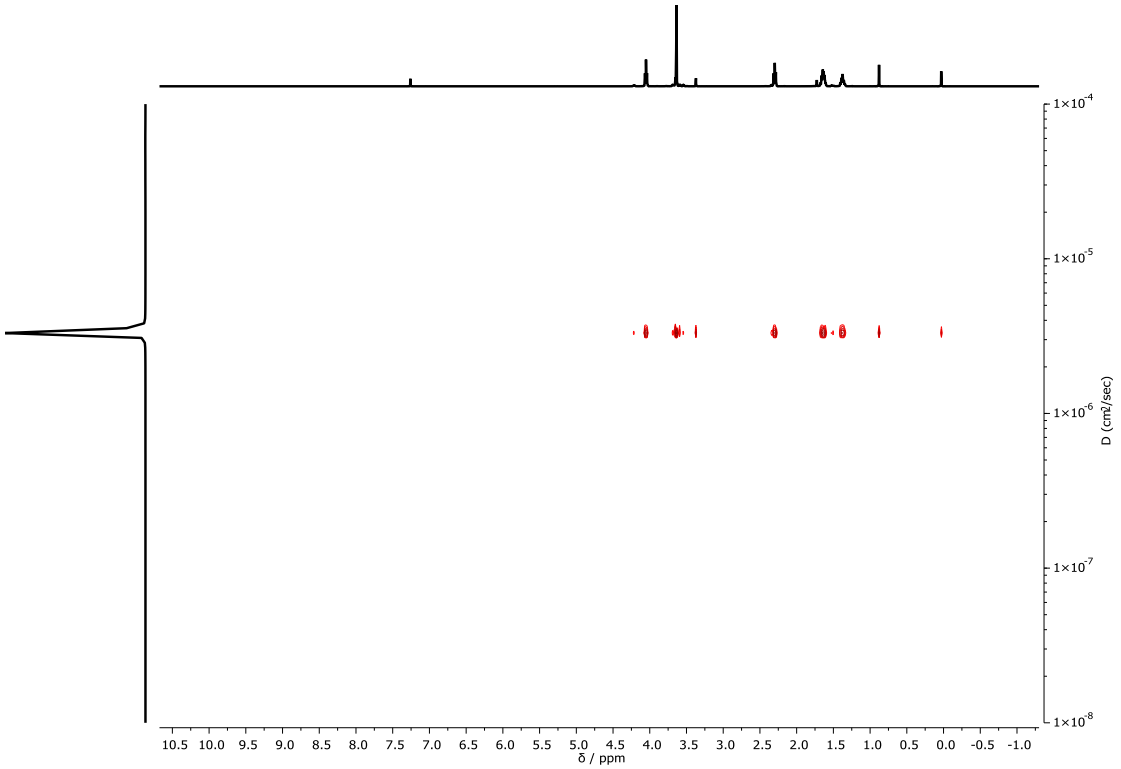

Supplementary Figure 126: DOSY NMR spectrum of **uBCP-1** recorded at 500 MHz in $CDCl_3$.

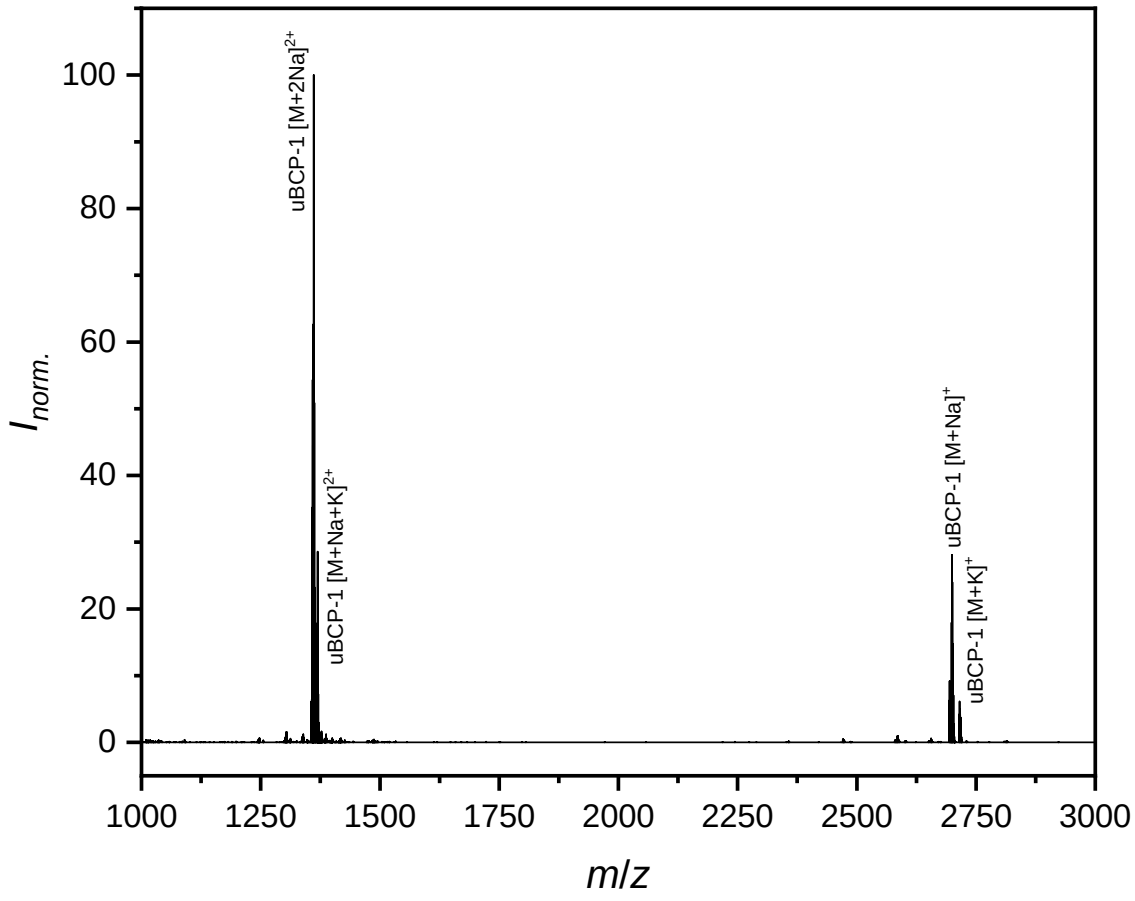

Supplementary Figure 127: ESI-MS spectrum of **uBCP-1**.

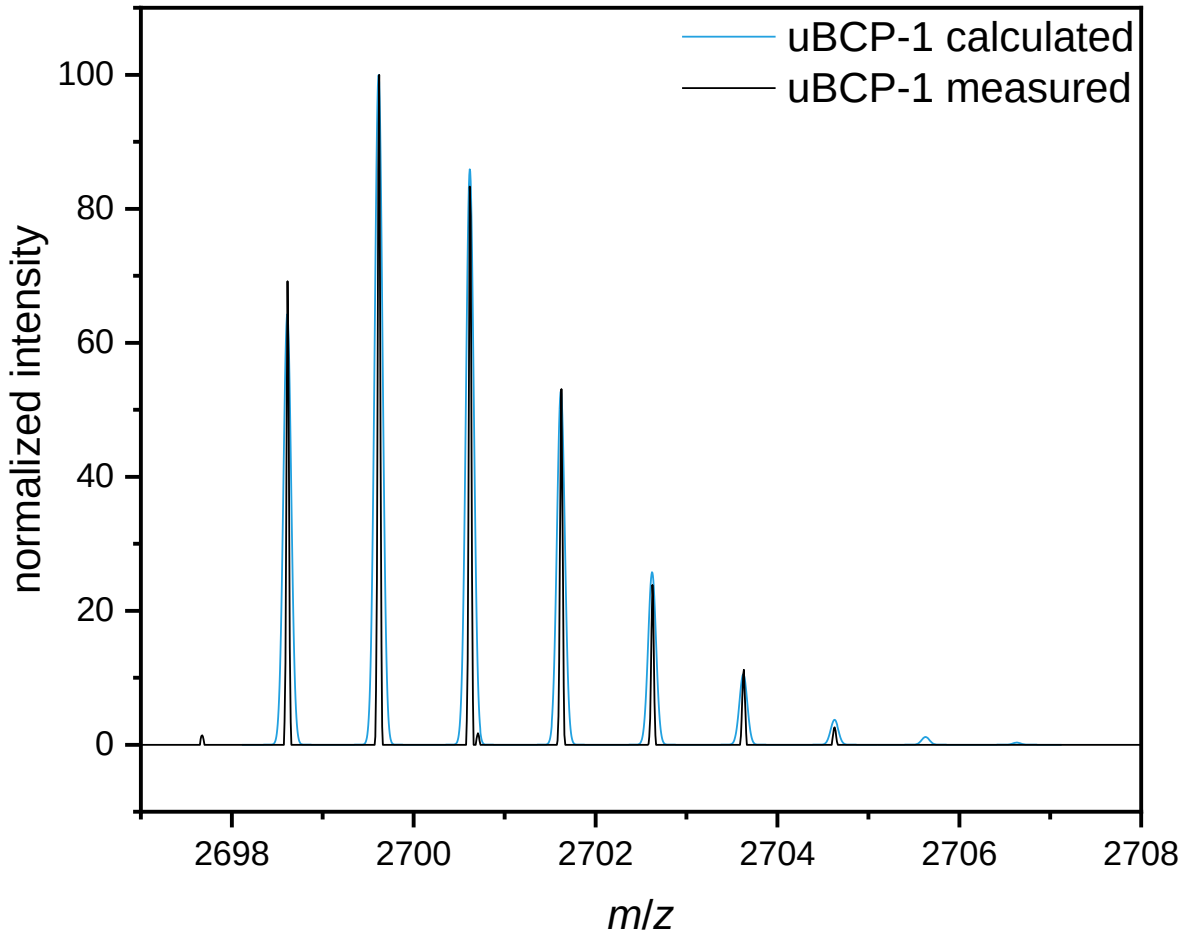

Supplementary Figure 128: Comparison of the calculated and experimental isotopic pattern (ESI-MS) of the sodium adduct of **uBCP-1**.

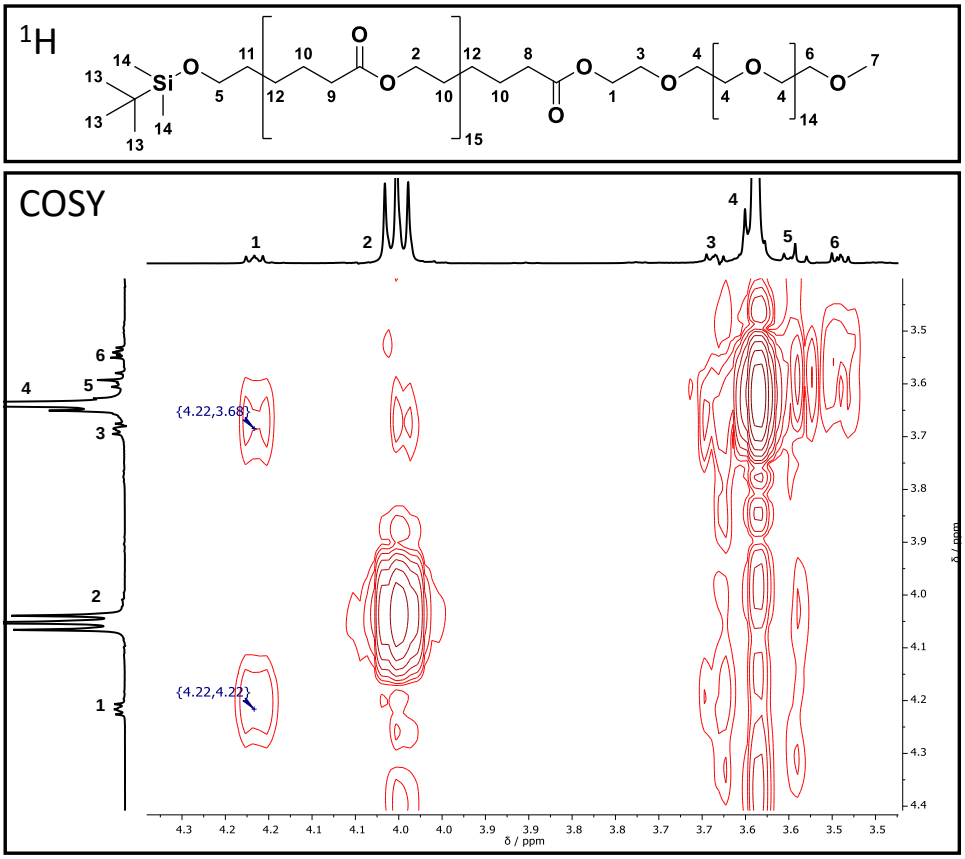

Supplementary Figure 129: COSY NMR spectrum of **uBCP-1**.

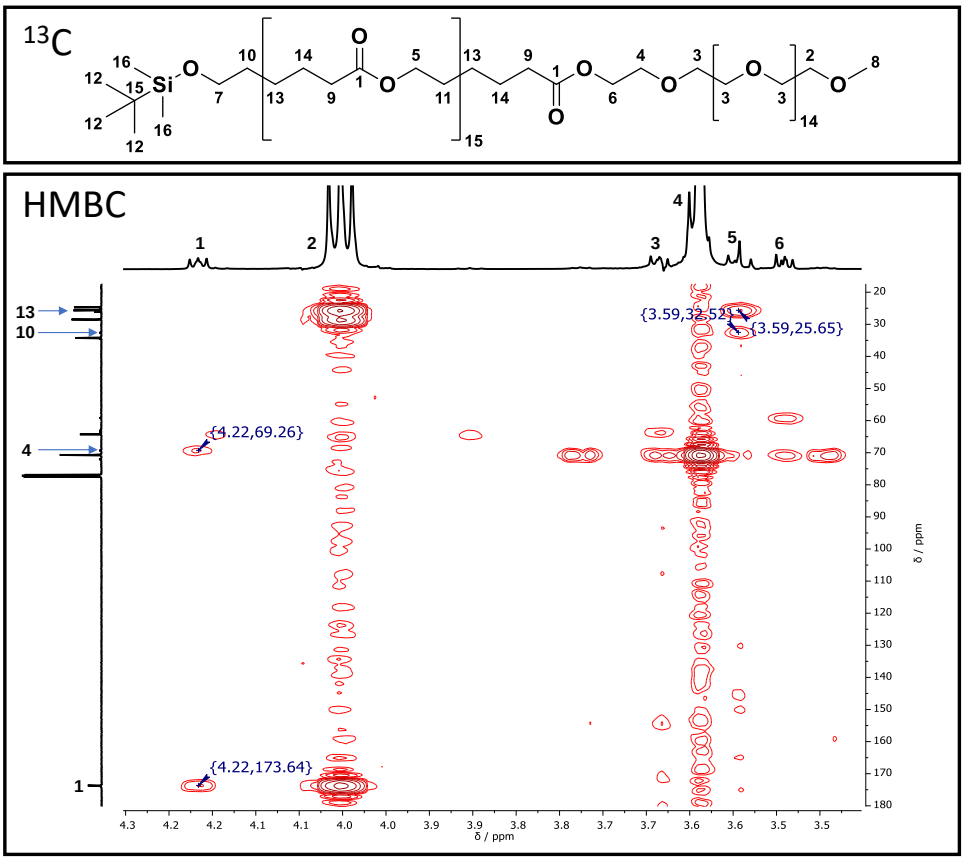

Supplementary Figure 130: HMBC NMR spectrum of **uBCP-1**.

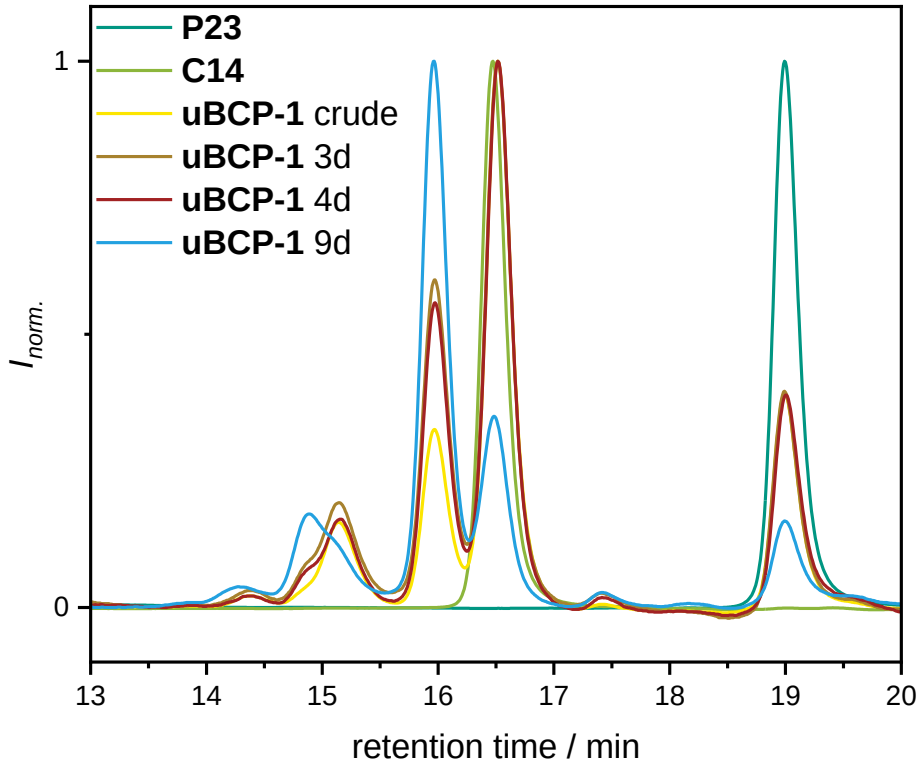

Supplementary Figure 131: Reaction monitoring for the synthesis of **uBCP-1** *via* SEC and comparison to the starting materials **C14** and **P23**.

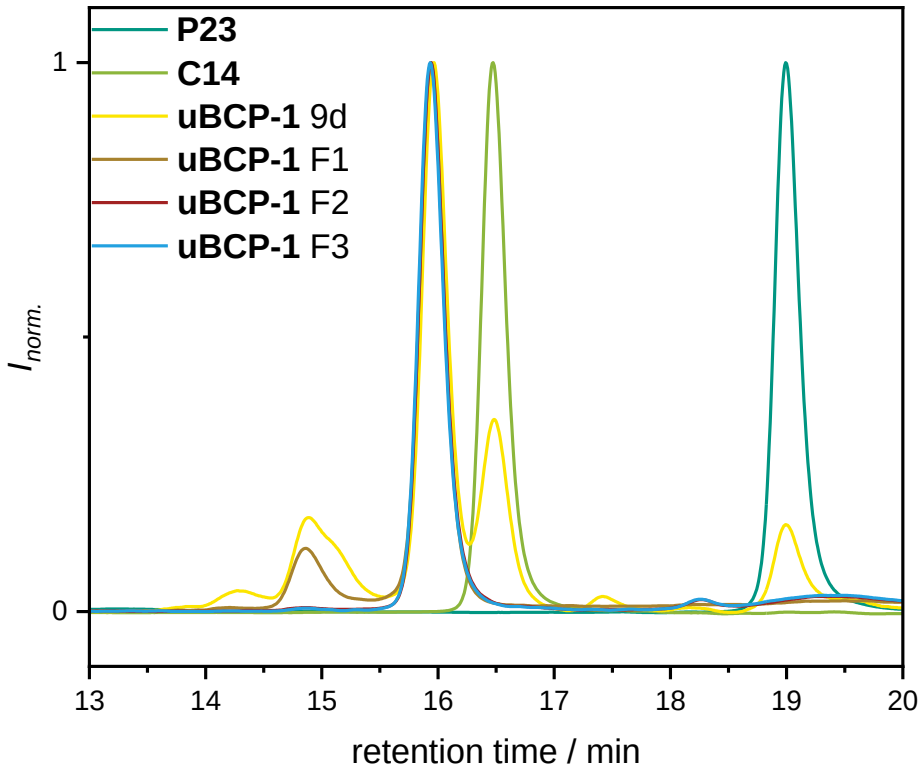

Supplementary Figure 132 SEC results of the first purification step of **uBCP-1** *via* column chromatography compared to the starting materials **C14** and **P23**.

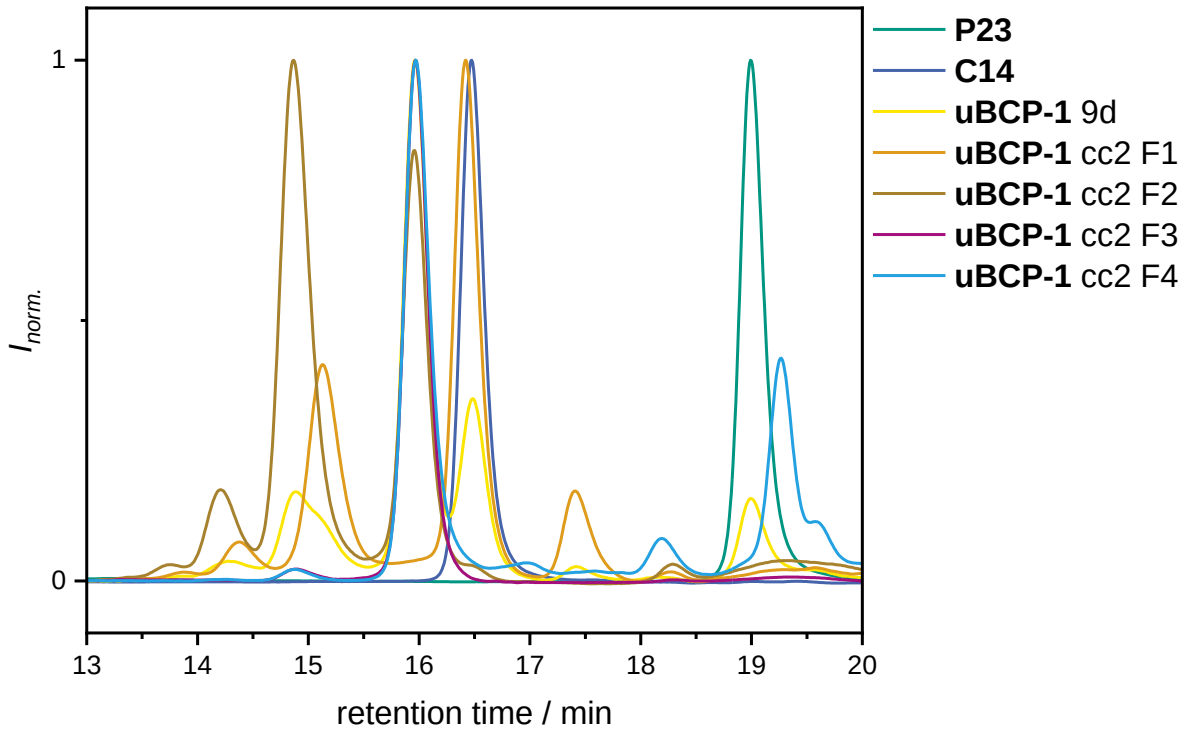

Supplementary Figure 133: SEC results of the second purification step of **uBCP-1** *via* column chromatography compared to the starting materials **C14** and **P23**.

mPEG$_{16}$-*b*-PCL$_{32}$TBDMS (uBCP-2)

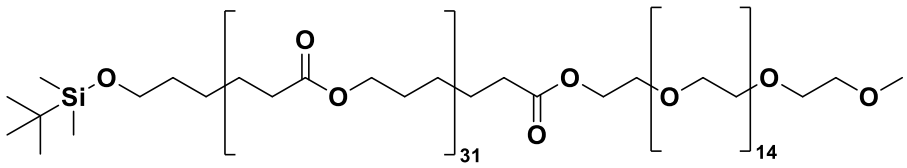

Chemical Formula: $C_{231}H_{402}O_{81}Si$
Exact Mass: 4500.7107 Da
Molecular Weight: 4503.7610 Da

The block copolymer **uBCP-2** was prepared according to the procedure described above for the synthesis of the doubly protected dimer **C4**.

C17	257 mg, 67.9 µmol, 1.00 equiv.
P23	50.0 mg, 67.9 µmol, 1.00 equiv.
DCC	84.0 mg, 407 µmol, 6.00 equiv.
DPTS	20.0 mg, 67.9 µmol, 1.00 equiv.
DCM	6.00 mL
eluent	1st cc: cyhex:EA = 1:2 → EA → EA:MeOH = 19:1 → 9:1 → acetone; 2nd cc: EA → EA:MeOH = 99:1 → 9:1 → acetone; 3rd cc: EA → EA:MeOH = 99:1 → 9:1 → acetone; 4th cc: EA → acetone
yield	132 mg, 29.3 µmol, 43.2%, white solid
R_f	0.18 (EA:MeOH = 9:1)
Đ (system III)	1.01

^{1}H NMR (500 MHz, $CDCl_3$): δ / ppm = 4.24 – 4.20 (m, 2H, CH_2^1), 4.05 (t, *J* = 6.7 Hz, 62H, CH_2^2), 3.71 – 3.67 (m, 2H, CH_2^3), 3.66 – 3.63 (m, 58H, CH_2^4), 3.61 – 3.58 (m, 2H, CH_2^5), 3.56 – 3.53 (m, 2H, CH_2^6), 3.37 (s, 3H, CH_3^7), 2.35 (t, *J* = 7.5 Hz, 2H, CH_2^8), 2.30 (t, *J* = 7.5 Hz, 62H, CH_2^9), 1.71 – 1.60 (m, 126H, CH_2^{10}), 1.55 – 1.49 (m, 2H, CH_2^{11}), 1.43 – 1.32 (m, 64H, CH_2^{12}), 0.88 (s, 9H, CH_3^{13}), 0.03 (s, 6H, CH_3^{14}).

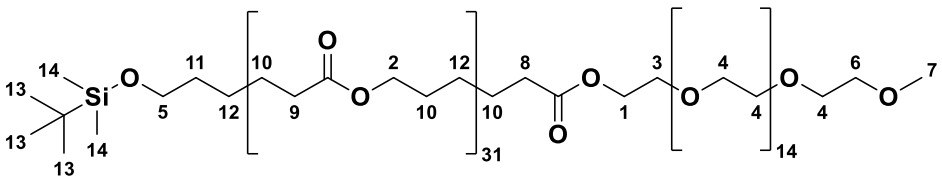

^{13}C NMR (126 MHz, $CDCl_3$): δ / ppm = 173.94 (C_q^1), 173.67 (C_q^1), 173.60 (C_q^1), 72.07 (CH_2^2), 70.70 (CH_2^3), 69.31 (CH_2^4), 64.28 (CH_2^5), 64.19 (CH_2^5), 63.58 (CH_2^6), 63.11 (CH_2^7), 59.18 (CH_3^8), 34.47 (CH_2^9), 34.25 (CH_2^9), 34.11 (CH_2^9), 32.60 (CH_2^{10}), 28.48 (CH_2^{11}), 26.10 (CH_3^{12}), 25.66 (CH_2^{13}), 24.95 (CH_2^{14}), 24.71 (CH_2^{14}), 18.48 (C_q^{15}), -5.15 (CH_3^{16}).

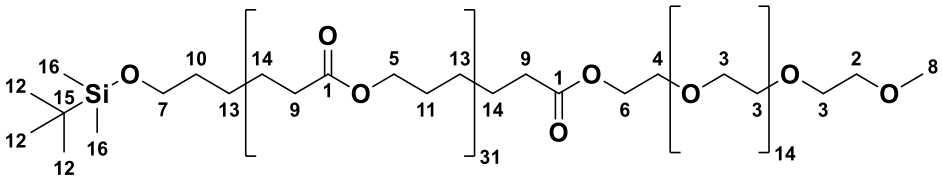

HRMS (ESI) of $C_{231}H_{402}O_{81}Si$ $[M+Na]^{1+}$ *m/z* calc. 4523.6999, found 4523.6934; $[M+2Na]^{2+}$ *m/z* calc. 2273.3446, found 2273.3415; $[M+Na+K]^{2+}$ *m/z* calc. 2281.3315, found 2281.3361; $[M+2K]^{2+}$ *m/z* calc. 2289.3185, found 2289.3427; $[M+3Na]^{3+}$ *m/z* calc. 1523.2261, found 1523.2236; $[M+2Na+K]^{3+}$ *m/z* calc. 1528.5508, found 1528.5493; $[M+Na+2K]^{3+}$ *m/z* calc. 1533.8754, found 1533.8869; $[M+4Na]^{4+}$ *m/z* calc. 1148.1669, found 1148.1660.

The mass of $mPEG_{16}$-*b*-PCL_{31}-TBDMS was found as well. HRMS (ESI) of $C_{225}H_{392}O_{79}Si$ $[M+2Na]^{2+}$ *m/z* calc. 2216.3105, found 2216.2996; $[M+Na+K]^{2+}$ *m/z* calc. 2224.2975, found 2224.2905; $[M+2K]^{2+}$ *m/z* calc. 2232.2845, found 2232.3013; $[M+3Na]^{3+}$ *m/z* calc. 1485.2034, found 1485.2162; $[M+2Na+K]^{3+}$ *m/z* calc. 1490.5281, found 1490.5225; $[M+Na+2K]^{3+}$ *m/z* calc. 1495.8527, found 1495.8470.

IR (ATR platinum diamond) $\tilde{\nu}$ / cm^{-1} = 2943, 2894, 2865, 1722, 1471, 1438, 1419, 1397, 1366, 1323, 1294, 1238, 1174, 1105, 1065, 1043, 961, 934, 839, 775, 732, 710, 584, 537, 522, 502, 492, 483, 453, 424, 411.

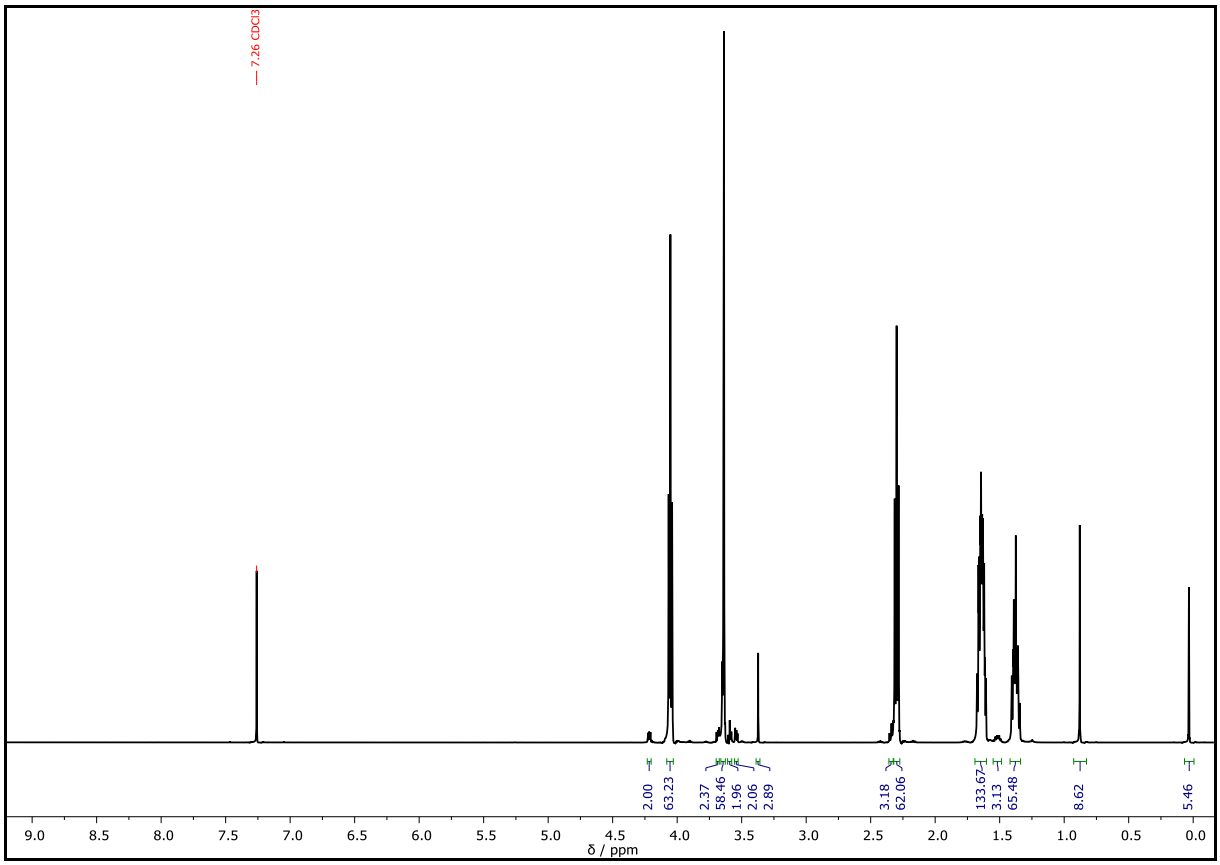

Supplementary Figure 134: ^{1}H NMR spectrum of **uBCP-2** recorded at 500 MHz in $CDCl_3$.

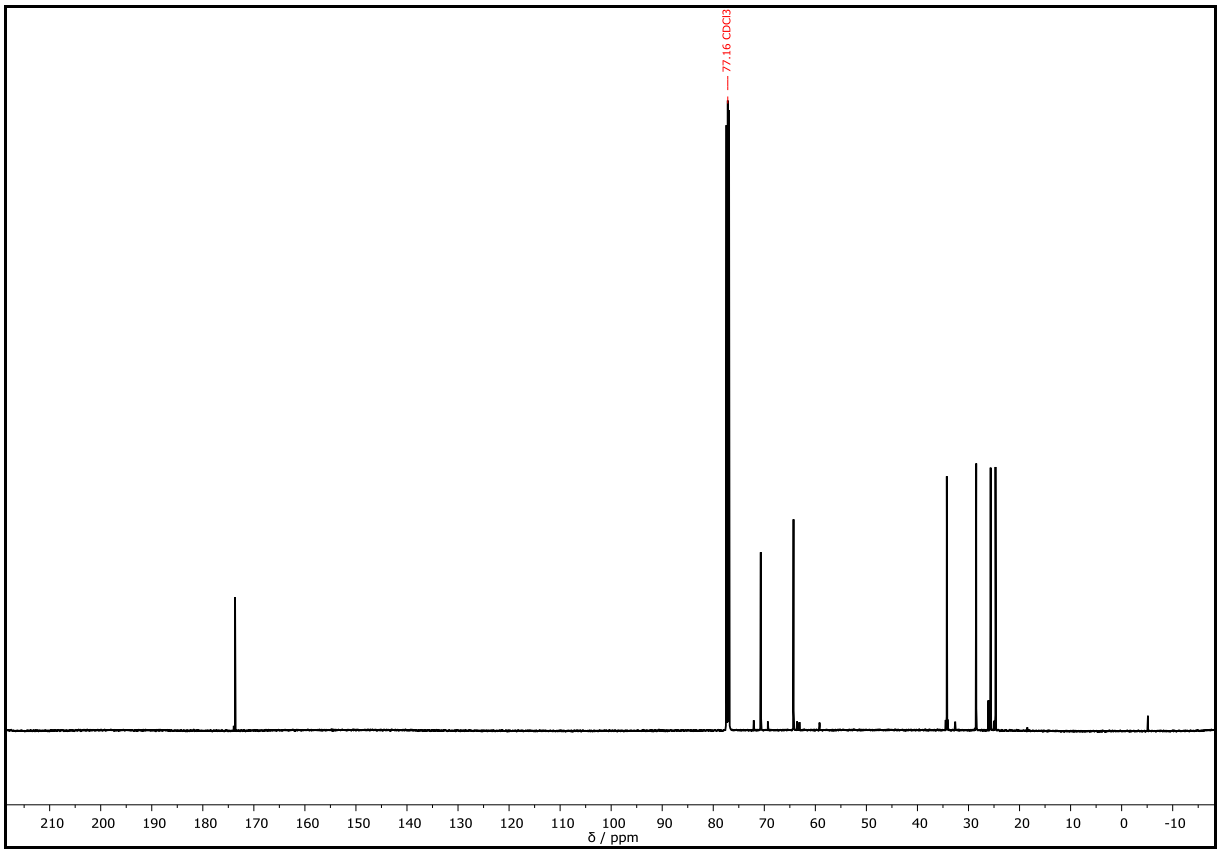

Supplementary Figure 135: ^{13}C NMR spectrum of **uBCP-2** recorded at 126 MHz in $CDCl_3$.

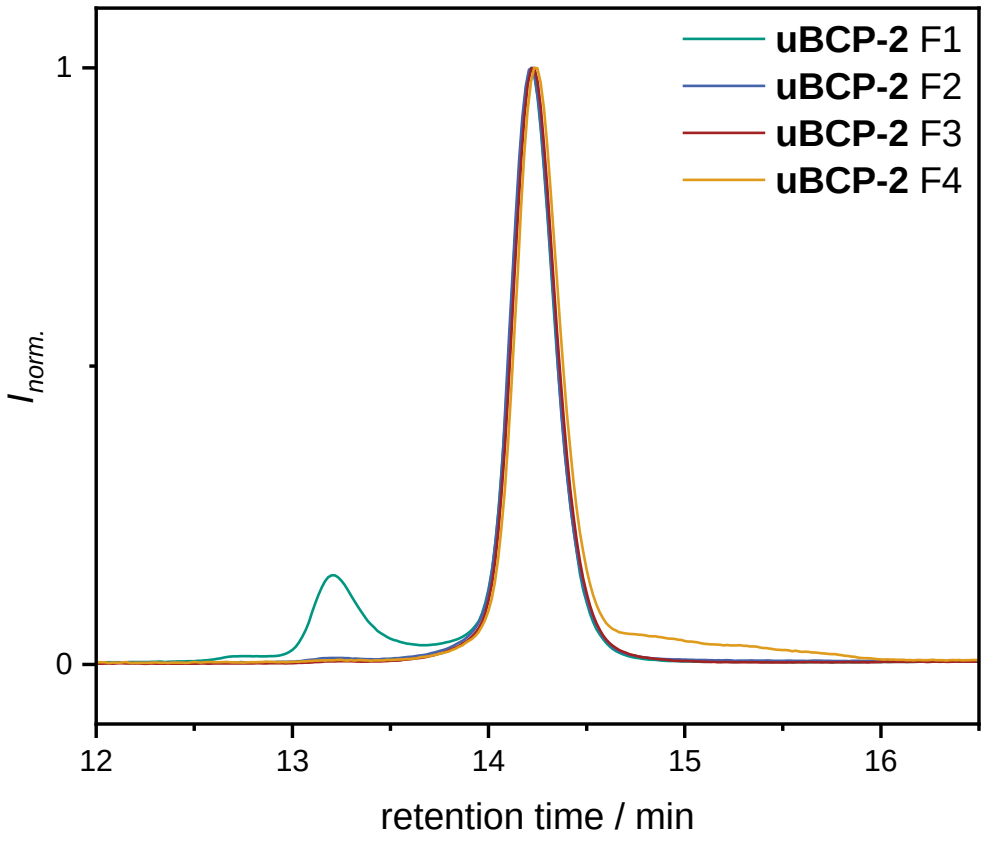

Supplementary Figure 136: SEC results of the purification step of **uBCP-2** *via* column chromatography.

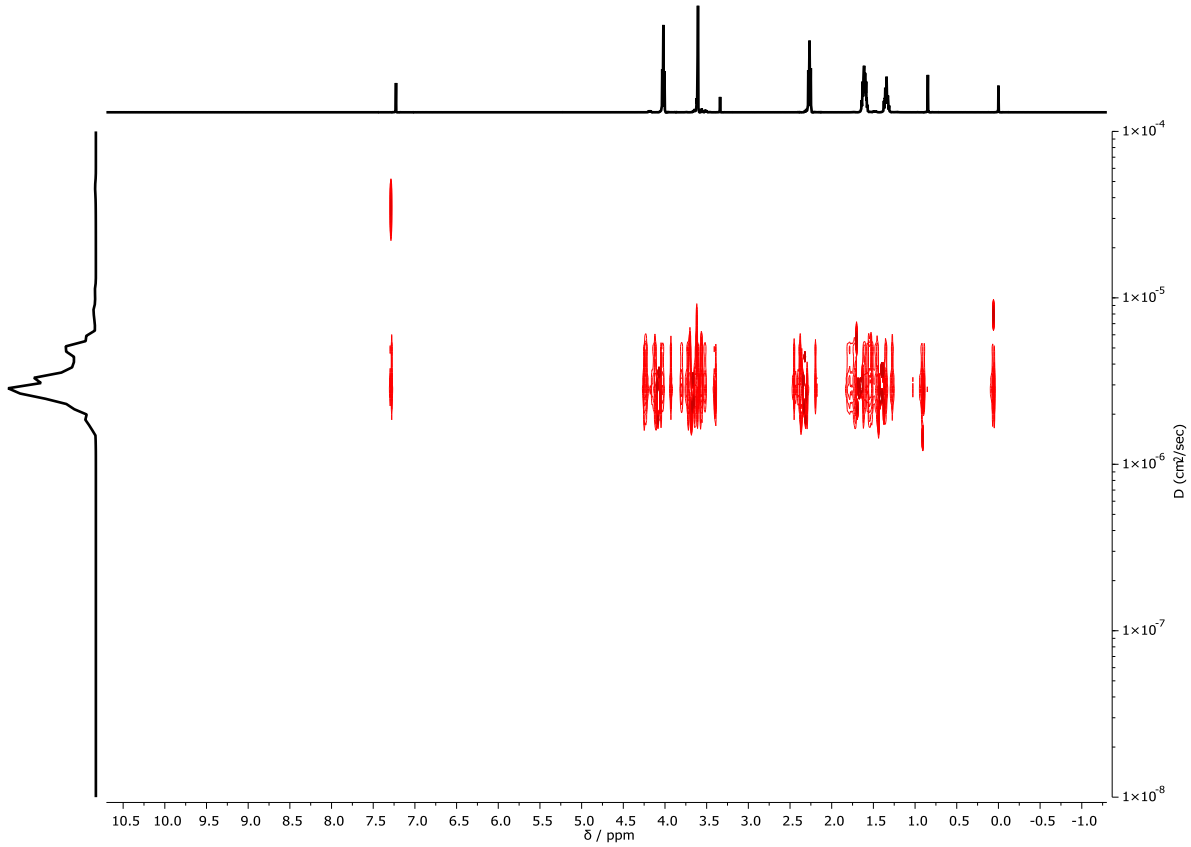

Supplementary Figure 137: DOSY NMR spectrum of **uBCP-2** recorded at 500 MHz in $CDCl_3$.

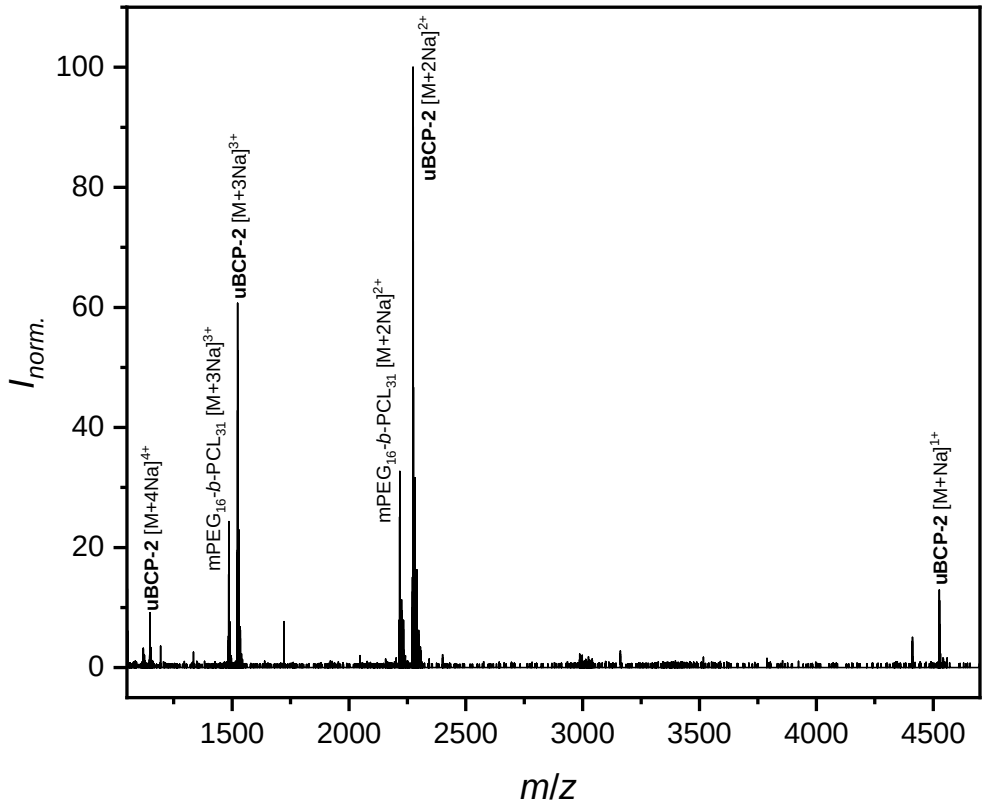

Supplementary Figure 138: ESI-MS spectrum of **uBCP-2**.

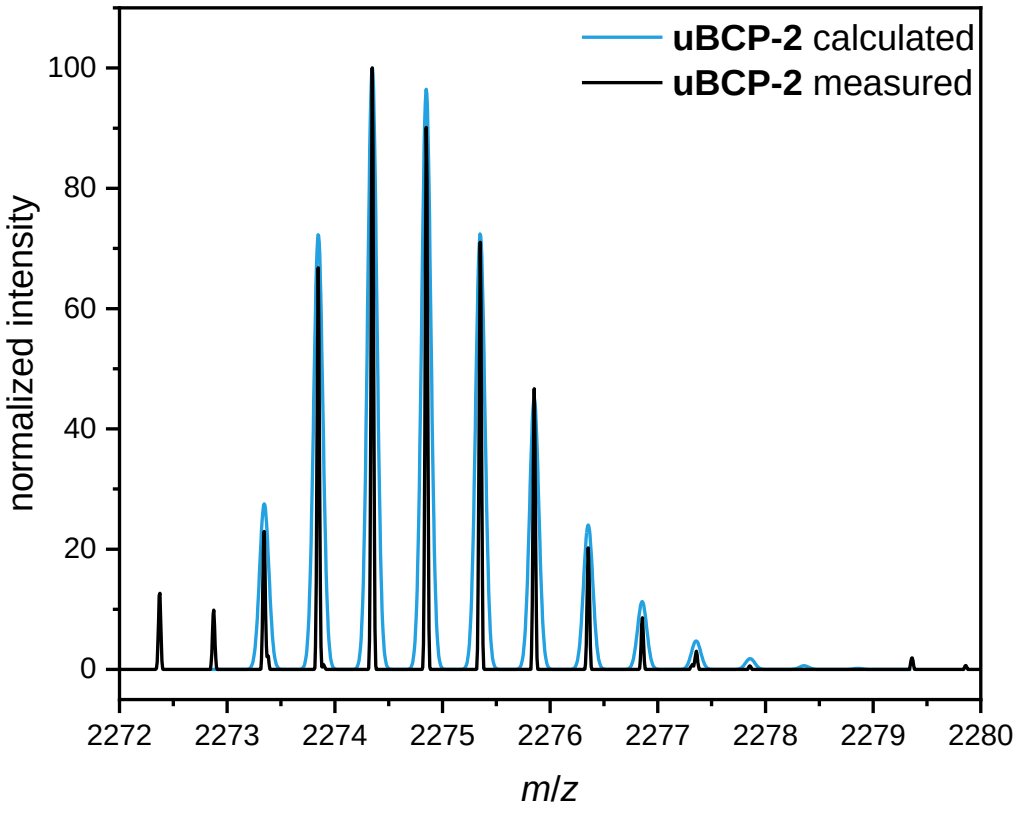

Supplementary Figure 139: Comparison of the calculated and experimental isotopic pattern (ESI-MS) of the sodium adduct of **uBCP-**2.

mPEG$_{16}$-*b*-PCL$_{64}$TBDMS (uBCP-3)

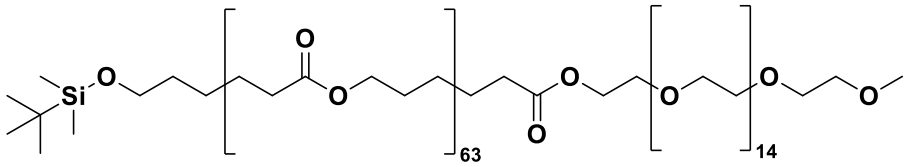

Chemical Formula: $C_{423}H_{722}O_{145}Si$
Exact Mass: 8150.8892 Da
Molecular Weight: 8156.3690 Da

C20	505 mg, 67.9 µmol, 1.00 equiv.
P23	50.0 mg, 67.9 µmol, 1.00 equiv.
DCC	84.0 mg, 407 µmol, 6.00 equiv.
DPTS	20.0 mg, 67.9 µmol, 1.00 equiv.
DCM	6.00 mL
eluent	1st cc: cyhex:EA = 1:2 → EA → EA:MeOH = 99:1 → 4:1 → acetone 2nd cc: EA → EA:MeOH = 99:1 → 9:1 → acetone; acetone; 3rd cc: EA → acetone
yield	102 mg, 12.5 µmol, 18.4%, white solid
R_f	0.68 (EA:MeOH = 4:1)
Đ (system III)	1.01

^{1}H NMR (500 MHz, $CDCl_3$): δ / ppm = 4.24 – 4.20 (m, 2H, CH_2^1), 4.05 (t, *J* = 6.7 Hz, 126H, CH_2^2), 3.70 – 3.67 (m, 2H, CH_2^3), 3.66 – 3.62 (m, 58H, CH_2^4), 3.59 (t, *J* = 6.5 Hz, 2H, CH_2^5), 3.56 – 3.53 (m, 2H, CH_3^6), 3.37 (s, 3H, CH_2^7), 2.35 (t, *J* = 7.4 Hz, 2H, CH_2^8), 2.30 (t, *J* = 7.5 Hz, 126H, CH_2^9), 1.69 – 1.60 (m, 254H, CH_2^{10}), 1.55 – 1.48 (m, 2H, CH_2^{11}), 1.42 – 1.34 (m, 128H, CH_2^{12}), 0.88 (s, 9H, CH_3^{13}), 0.03 (s, 6H, CH_3^{14}).

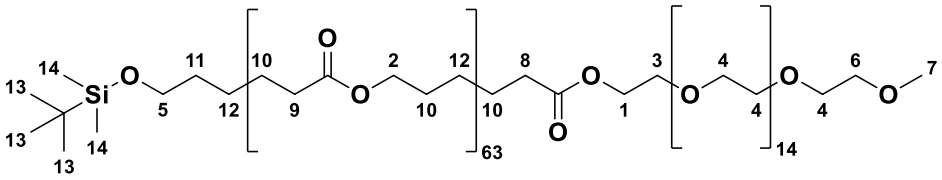

^{13}C NMR (126 MHz, $CDCl_3$): δ / ppm = 173.68 (C_q^1), 72.07 (CH_2^2), 70.70 (CH_2^3), 69.31 (CH_2^4), 64.28 (CH_2^5), 63.58 (CH_2^6), 63.11 (CH_2^7), 59.18 (CH_3^8), 34.47 (CH_2^9), 34.25 (CH_2^9), 32.61 (CH_2^{10}), 28.49 (CH_2^{11}), 26.10 (CH_3^{12}), 25.67 (CH_2^{13}), 24.71 (CH_2^{14}), 18.48 (C_q^{15}), -5.14 (CH_3^{16}).

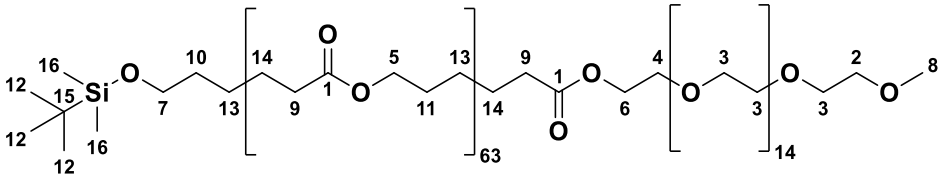

HRMS (ESI) of $C_{423}H_{722}O_{145}Si$ $[M+2Na]^{2+}$ *m/z* calc. 4100.9427, found 4100.9558 (most intense peak of isotopic pattern); $[M+3Na]^{3+}$ *m/z* calc. 2739.9523, found 2739.9696; $[M+2Na+K]^{3+}$ *m/z* calc. 2746.9478, found 2746.9524 (most intense peak of isotopic pattern); $[M+Na+2K]^{3+}$ *m/z* calc. 2752.2725, found 2752.2813 (most intense peak of isotopic pattern); $[M+4Na]^{4+}$ *m/z* calc. 2060.7225, found 2060.7280; $[M+3Na+K]^{4+}$ *m/z* calc. 2064.7050, found 2064.7099; $[M+2Na+2K]^{4+}$ *m/z* calc. 2068.6985, found 2068.7167; $[M+Na+3K]^{4+}$ *m/z* calc. 2072.6920, found 2072.6946; $[M+5Na]^{5+}$ *m/z* calc. 1653.1671, found 1653.1743; $[M+4Na+K]^{5+}$ *m/z* calc. 1656.3619, found 1656.3705; $[M+3Na+2K]^{5+}$ *m/z* calc. 1659.5566, found 1659.5607; $[M+6Na]^{6+}$ *m/z* calc. 1381.4708, found 1381.4686; $[M+5Na+K]^{6+}$ *m/z* calc. 1384.1331, found 1384.1423; $[M+4Na+2K]^{6+}$ *m/z* calc. 1386.7954, found 1386.7979.

The mass of $mPEG_{16}$-*b*-PCL_{63}-TBDMS was found as well. HRMS (ESI) of $C_{417}H_{712}O_{143}Si$ $[M+3Na]^{3+}$ *m/z* calc. 2701.9296, found 2701.9394; $[M+4Na]^{4+}$ *m/z* calc. 2032.1945, found 2032.2086; $[M+3Na+K]^{4+}$ *m/z* calc. 2036.1880, found 2036.2043; $[M+5Na]^{5+}$ *m/z* calc. 1630.3534, found 1630.3623; $[M+4Na+K]^{5+}$ *m/z* calc. 1633.5482, found 1633.5529.

IR (ATR platinum diamond) $\tilde{\nu}$ / cm^{-1} = 2943, 2894, 2865, 1722, 1471, 1419, 1397, 1366, 1294, 1238, 1172, 1107, 1065, 1045, 961, 934, 868, 839, 775, 732, 710, 586, 453.

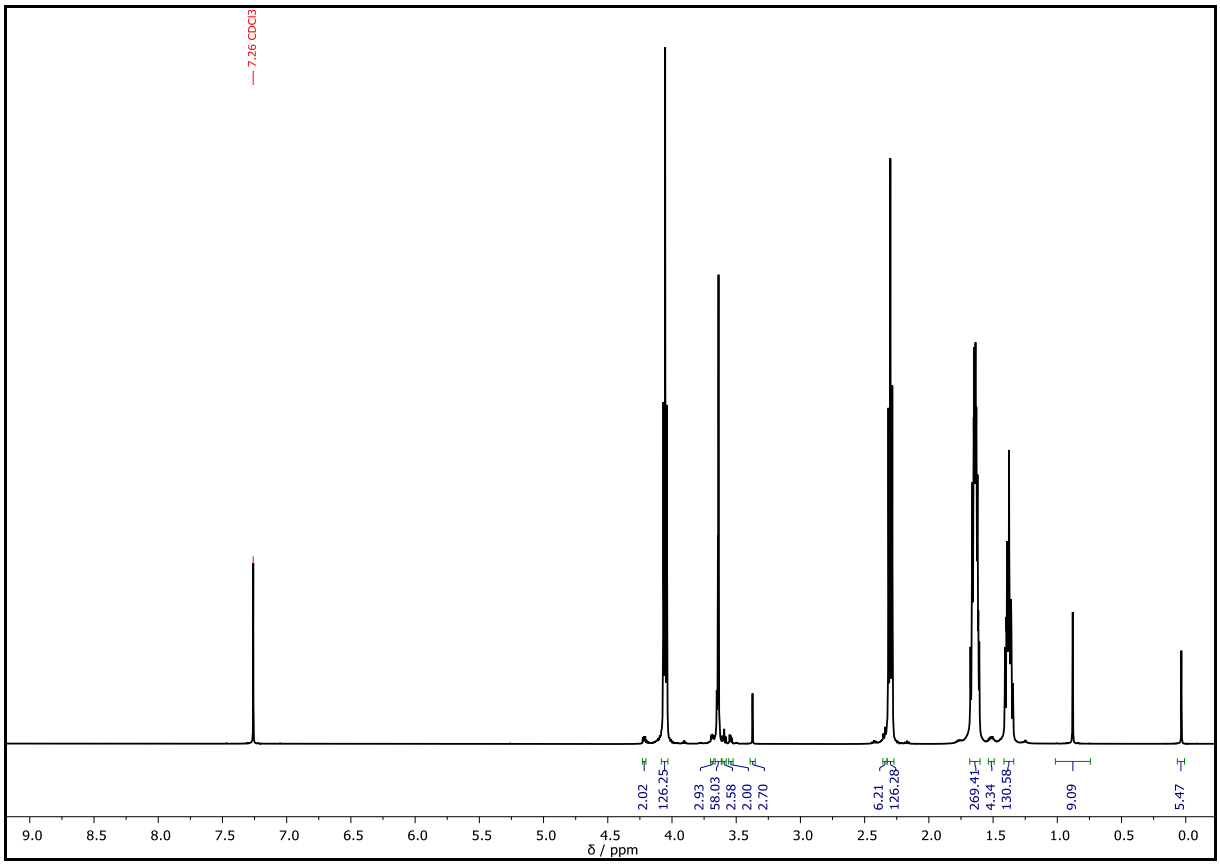

Supplementary Figure 140: ^{1}H NMR spectrum of **uBCP-3** recorded at 500 MHz in $CDCl_3$.

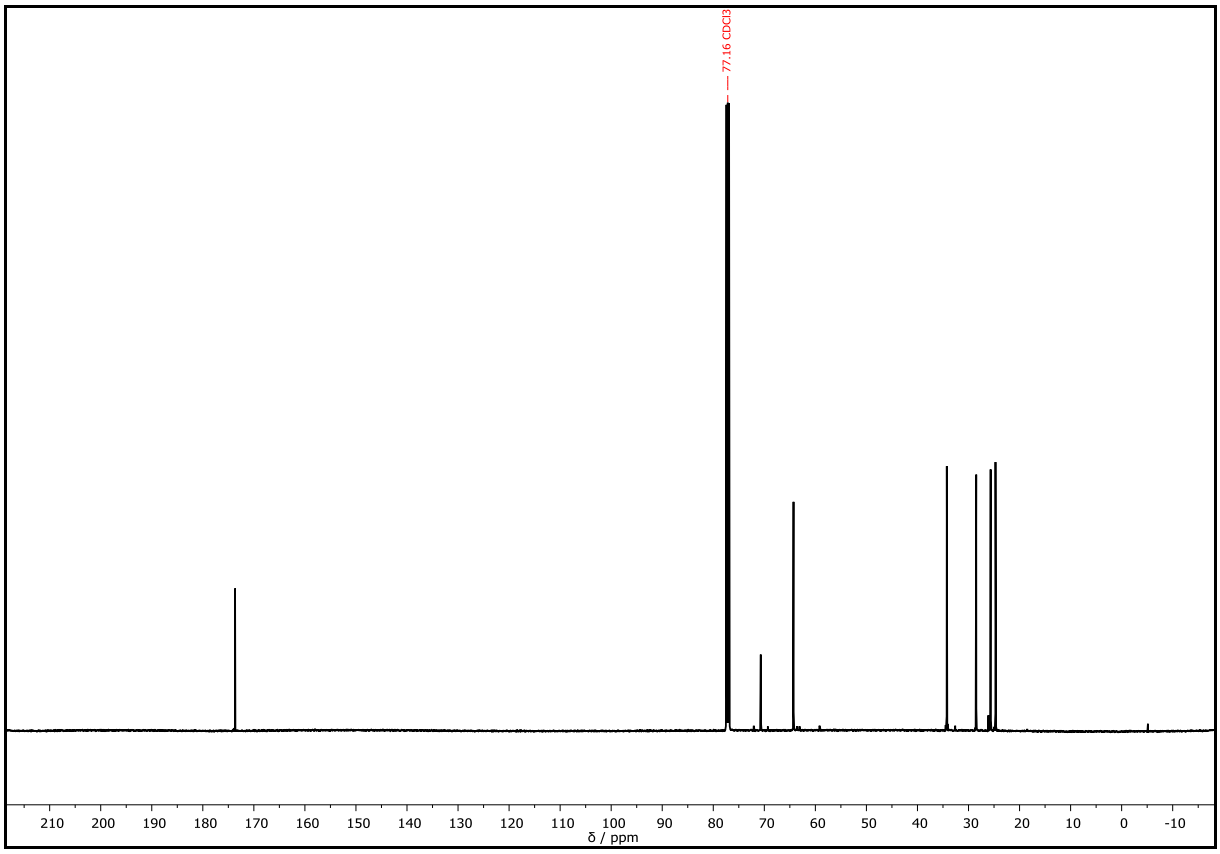

Supplementary Figure 141: ^{13}C NMR spectrum of **uBCP-3** recorded at 126 MHz in $CDCl_3$.

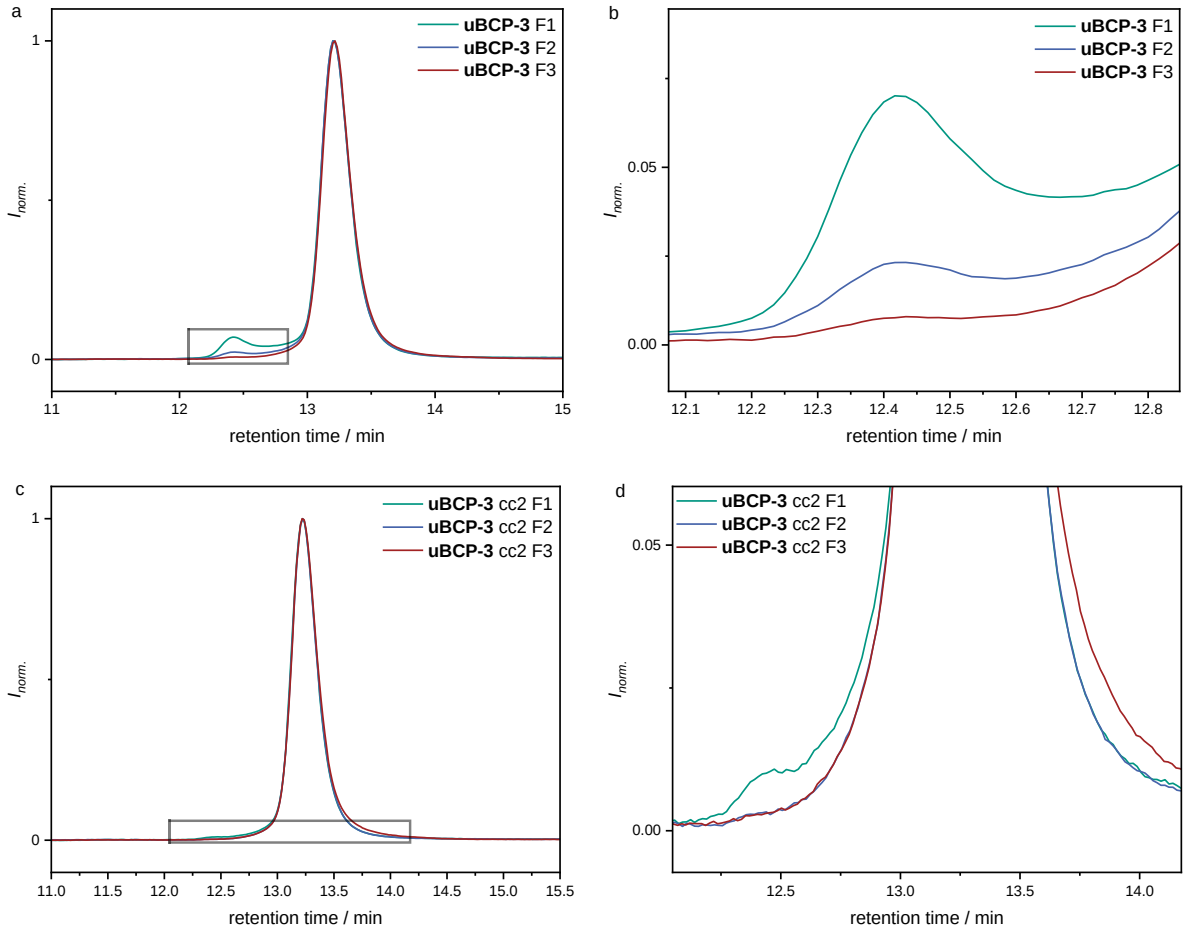

Supplementary Figure 142: **a** SEC traces of the individual fractions obtained after the first column chromatographic purification of the crude product **uBCP-3**; **b** Detailed section of the high molecular weight shoulder; **c** SEC traces of the individual fractions obtained after the second column chromatographic purification of **uBCP-3** F3; **d** Detailed section of the high molecular weight shoulder and tailing towards higher retention times.

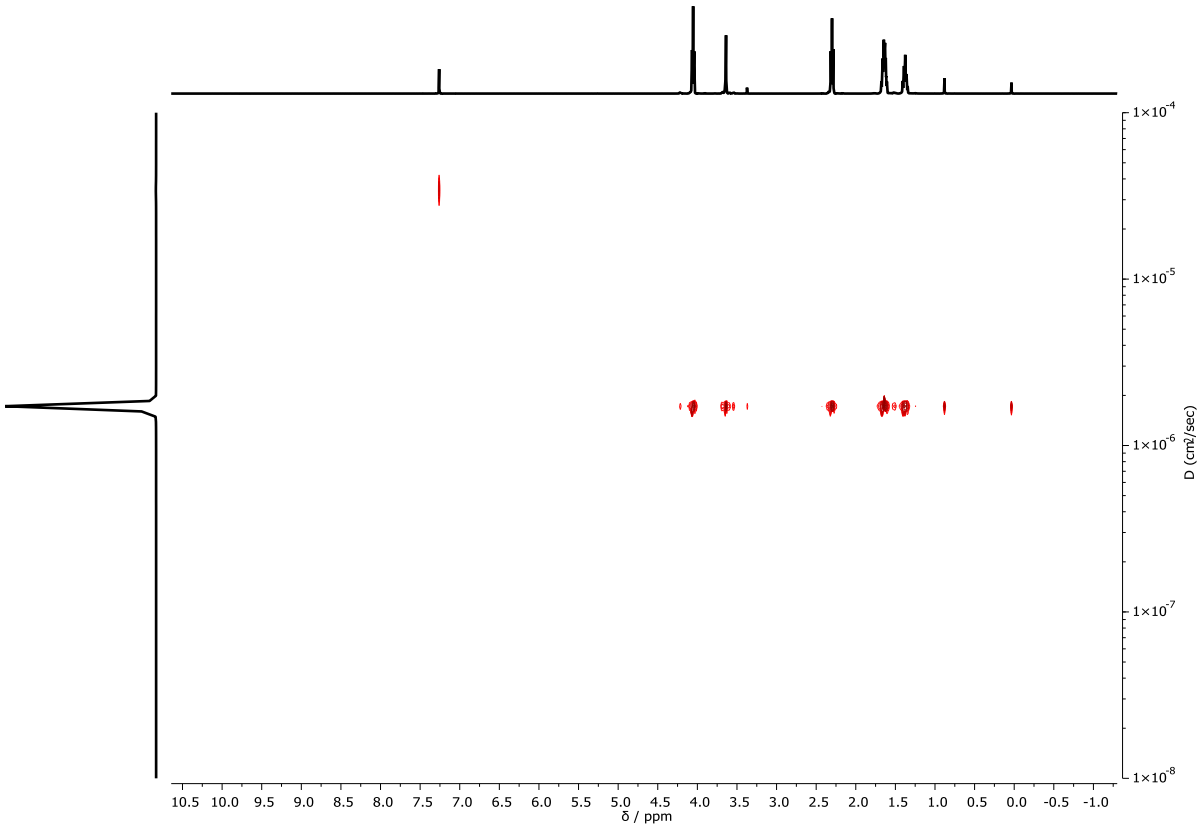

Supplementary Figure 143: DOSY NMR spectrum of **uBCP-3** recorded at 500 MHz in $CDCl_3$.

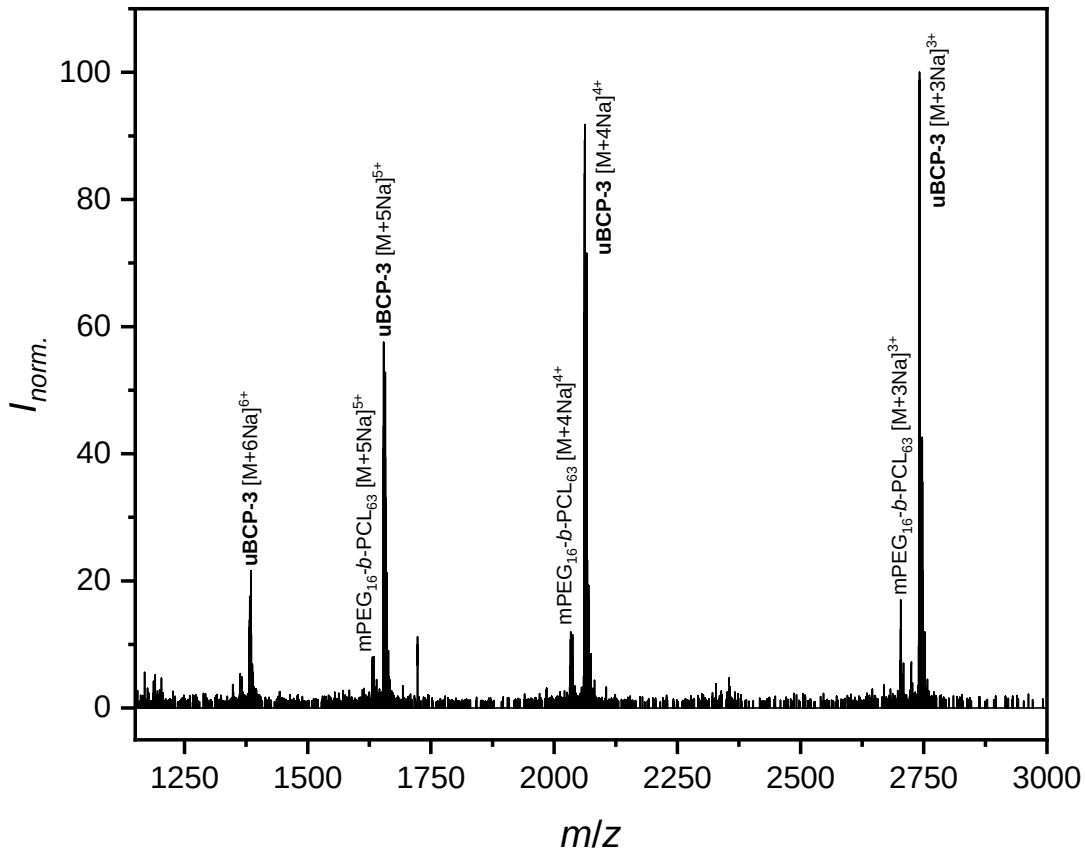

Supplementary Figure 144: ESI-MS spectrum of **uBCP-3**.

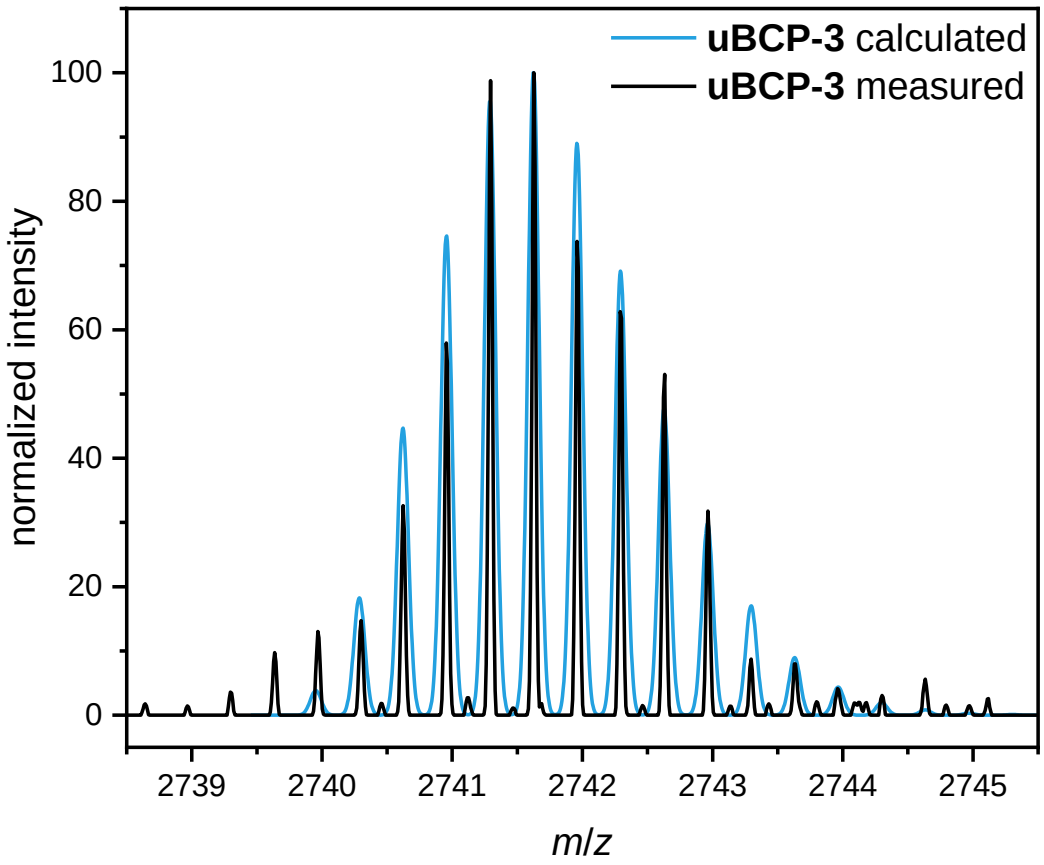

Supplementary Figure 145: Comparison of the calculated and experimental isotopic pattern (ESI-MS) of the sodium adduct of **uBCP-3**.

6.3.6. Experimental procedures of chapter 4.4

General procedure for the ring opening polymerization of ε-caprolactone with mPEG (M_n = 750 Da)

The reaction procedure was adopted from Lohmeijer *et. al*.[408] A stock solution of $mPEG_{750}$ (M_n = 750 Da) and TBD in extra dry toluene was prepared in a flame dried young flask. Hereby, the concentration of the mPEG (M_n = 750 Da) varied according to the striven DP values. Subsequently, the catalyst and initiator solution were added to another flame dried young flask filled with extra dry toluene. ε-Caprolactone was added to the reaction fast with a syringe, while stirring vigorously under argon atmosphere. After the respective reaction time for the three different polymers, the reaction process was quenched by the fast addition of benzoic acid. Afterwards, the solvent was removed under reduced pressure and the residue was precipitated twice out of cold *n*-hexane. Further individual purification steps for the obtained block copolymers by column chromatography as well as the quantities of the starting materials are mentioned in the corresponding sections.

SEC reaction monitoring of the ROP of ε-caprolactone

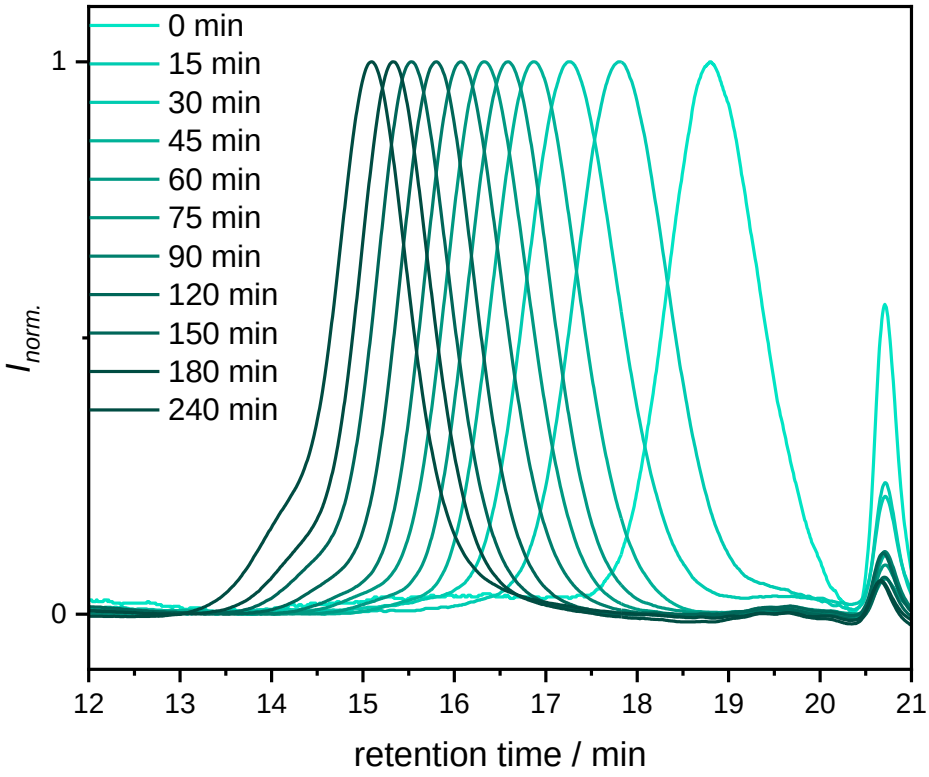

Supplementary Figure 146: SEC reaction monitoring of the ROP of ε-caprolactone with mPEG (M_n = 750 Da). Ratio of the monomer ε-caprolactone (M) to macroinitiator mPEG (I, M_n = 750 Da); M/I = 40.

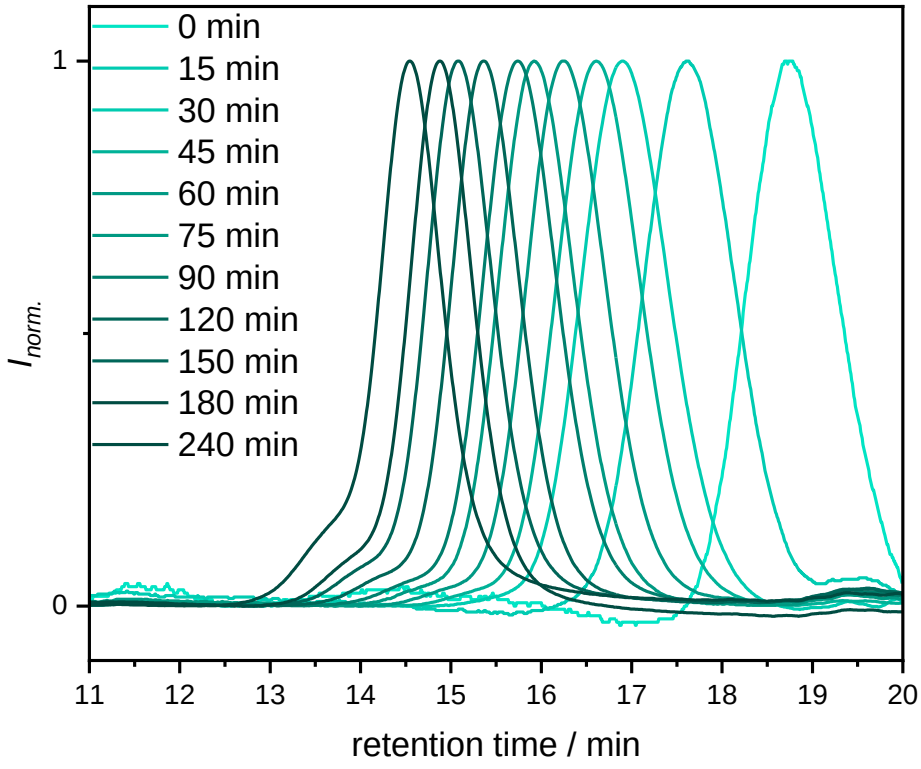

Supplementary Figure 147: SEC reaction monitoring of the ROP of ε-caprolactone with mPEG (M_n = 750 Da). Ratio of the monomer ε-caprolactone (M) to macroinitiator mPEG (I, M_n = 750 Da); M/I = 80.

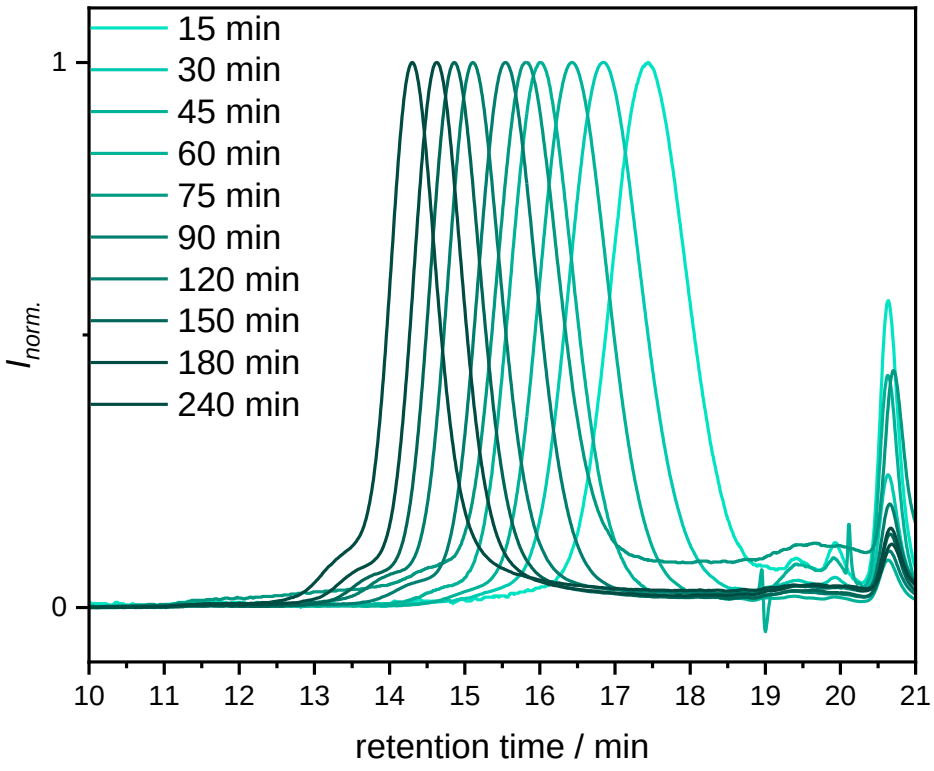

Supplementary Figure 148: SEC reaction monitoring of the ROP of ε-caprolactone with mPEG (M_n = 750 Da). Ratio of the monomer ε-caprolactone (M) to macroinitiator mPEG (I, M_n = 750); M/I = 167.

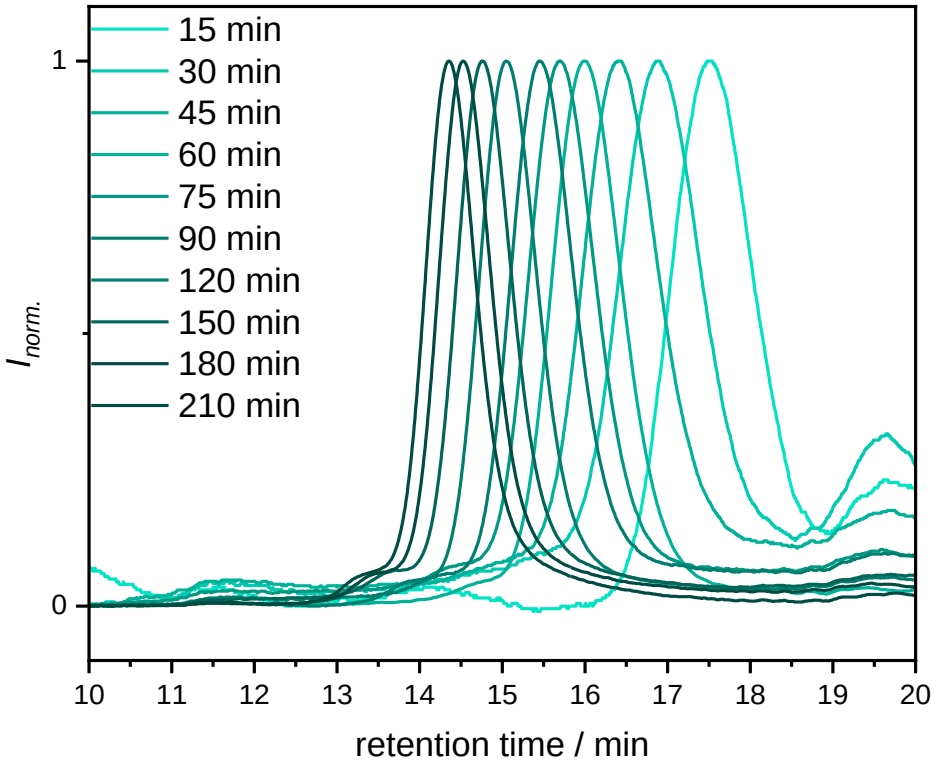

Supplementary Figure 149: SEC reaction monitoring of ROP of ε-caprolactone with mPEG (M_n = 750 Da). Ratio of the monomer ε-caprolactone (M) to macroinitiator mPEG (I, M_n = 750 Da); M/I = 335.

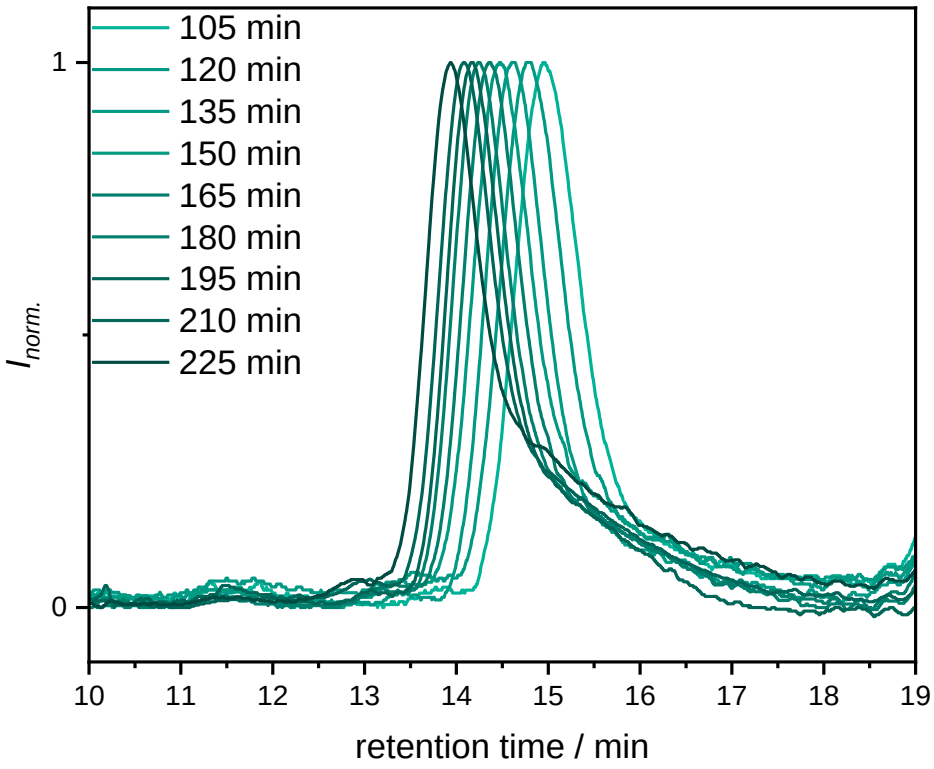

Supplementary Figure 150: SEC reaction monitoring of the ROP of ε-caprolactone with mPEG (M_n = 750 Da). Ratio of the monomer ε-caprolactone (M) to macroinitiator mPEG (I, M_n = 750 Da); M/I = 1226.

Supplementary Table 20: SEC data of the monitoring of the ROP of ε-caprolactone using mPEG as initiator.

	M/I = 40		M/I = 80		M/I = 167		M/I = 335		M/I = 1226	
t / min	M_n / Da	*Đ*	M_n / Da	*Đ*	M_n / Da	*Đ*	M_n / Da	*Đ*	M_n / Da	*Đ*
15	1800	1.05	2000	1.05	2150	1.05	2100	1.04	-	-
30	2300	1.05	2800	1.06	2850	1.06	2850	1.05	3100	1.04
45	3850	1.06	3300	1.06	3600	1.06	3650	1.05	4100	1.05
60	3350	1.07	4000	1.07	4600	1.07	4550	1.05	5200	1.04
75	3850	1.07	4800	1.06	5050	1.05	5450	1.04	6350	1.04
90	4400	1.08	5300	1.08	5950	1.07	6250	1.04	7050	1.04
105	-	-	-	-	-	-	-	-	8400	1.03
120	5250	1.08	6700	1.07	7650	1.08	7900	1.04	9500	1.03
135	-	-	-	-	-	-	-	-	10400	1.03
150	6100	1.08	7850	1.08	9000	1.06	9350	1.04	11400	1.03
165	-	-	-	-	-	-	-	-	12300	1.03
180	6850	1.08	8950	1.07	10300	1.06	10750	1.04	12900	1.03
195	-	-	-	-	-	-	-	-	13750	1.03
210	-	-	-	-	-	-	11950	1.04	14400	1.03
225	-	-	-	-	-	-	-	-	15800	1.03
240	7850	1.13	1100	1.10	12350	1.08	-	-	-	-

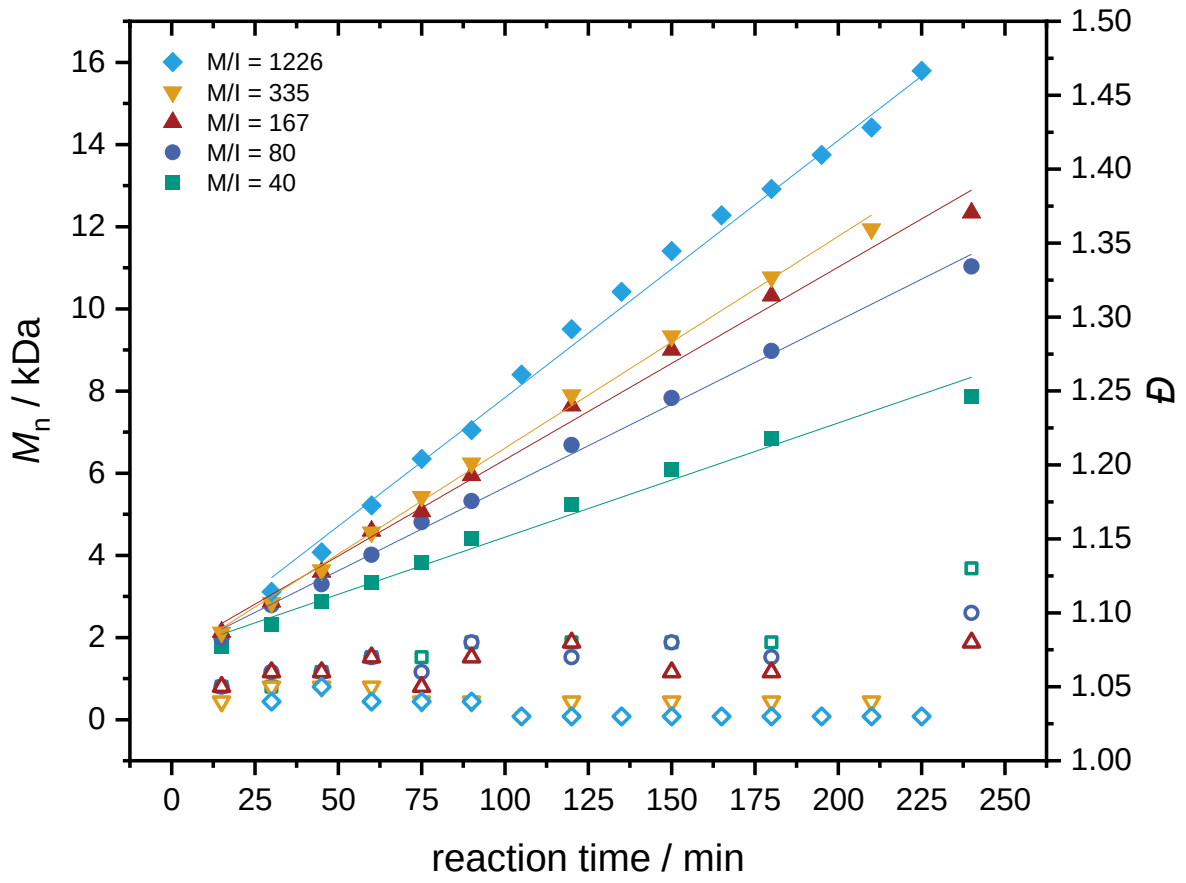

Supplementary Figure 151: ROP of ε-caprolactone (M) with the macroinitiator mPEG (I, M_n = 750 Da) and TBD as organocatalyst. The molecular weight M_n in kDa of the resulting dBCP is plotted against the reaction time in minutes, depended on the different M/I ratios. The open symbols represent the corresponding dispersity *Đ*.

Disperse mPEG$_{16}$-*b*-PCL$_{16}$-OH – dBCP-1

ε-Caprolactone	20.0 mL, 21.6 g, 189 mmol (167 equiv.)
mPEG (M_n = 750 Da)	848 mg, 1.13 mmol, (1.00 equiv.)
TBD	127 mg, 912 µmol (0.81 equiv.)
toluene (total amount)	90 mL
reaction time	52 min
yield	5.15 g

^{1}H NMR (500 MHz, $CDCl_3$): δ / ppm = 4.23 – 4.19 (m, CH_2^1), 4.04 (t, *J* = 6.6 Hz, CH_2^2), 3.69 – 3.67 (m, CH_2^3), 3.66 – 3.61 (m, CH_2^4 and CH_2^5), 3.55 – 3.52 (m, CH_2^6), 3.36 (s, CH_3^7), 2.29 (t, *J* = 7.6 Hz, CH_2^8 and CH_2^9), 1.69 – 1.31 (m, CH_2^{10}, CH_2^{11} and CH_2^{12}).

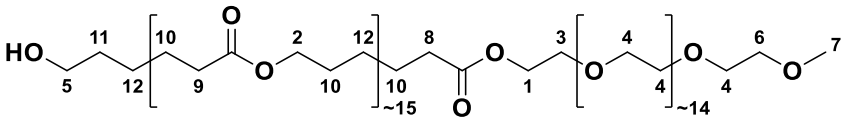

^{13}C NMR (126 MHz, $CDCl_3$): δ / ppm = 173.76 (C_q^1), 173.62 (C_q^1), 173.59 (C_q^1), 173.57 (C_q^1), 173.48 (C_q^1), 71.94 (CH_2^2), 70.61 (CH_2^3), 70.57 (CH_2^3), 70.51 (CH_2^3), 69.18 (CH_2^4), 64.16 (CH_2^5), 64.12 (CH_2^5), 63.45 (CH_2^6), 62.62 (CH_2^7), 59.05 (CH_3^8), 34.24 (CH_2^9), 34.19 (CH_2^9), 34.15 (CH_2^9), 34.12 (CH_2^9), 33.98 (CH_2^9), 32.33 (CH_2^{10}), 28.35 (CH_2^{11}), 25.57 (CH_2^{12}), 25.54 (CH_2^{12}), 25.50 (CH_2^{12}), 24.69 (CH_2^{13}), 24.58 (CH_2^{13}), 24.50 (CH_2^{13}).

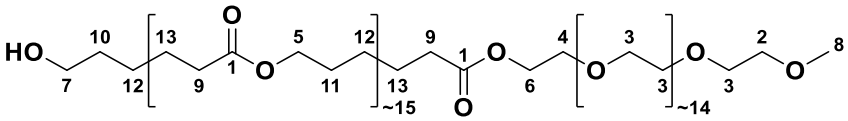

IR (ATR platinum diamond) $\tilde{\nu}$ / cm^{-1} = 3493, 2943, 2894, 2865, 1722, 1652, 1471, 1440, 1419, 1397, 1366, 1323, 1294, 1240, 1187, 1177, 1105, 1065, 1043, 961, 934, 860, 841, 815, 796, 788, 730, 716, 675, 654, 617, 584, 574, 562, 520, 514, 490, 479, 469, 453, 422, 411, 401.

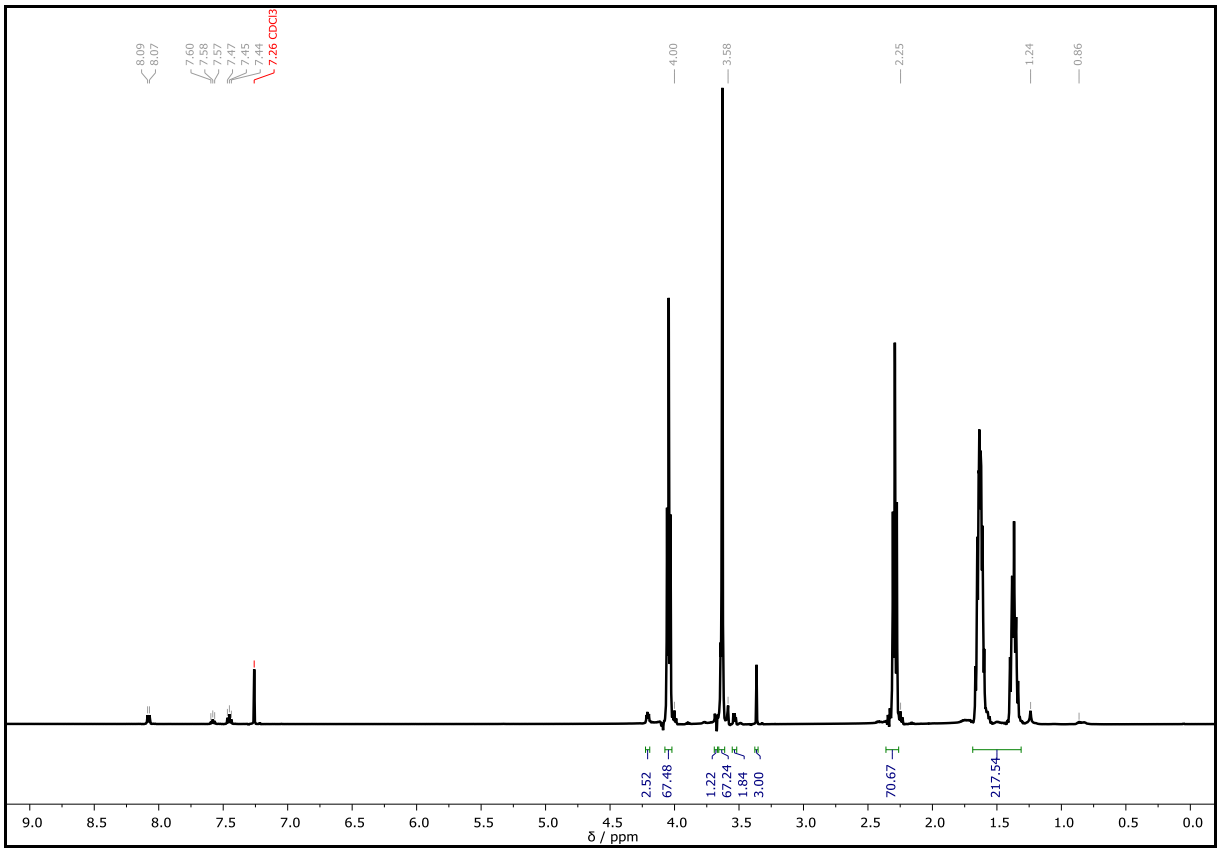

Supplementary Figure 152: ^{1}H NMR spectrum of **dBCP-1** recorded at 500 MHz in $CDCl_3$. Impurities are marked in grey.

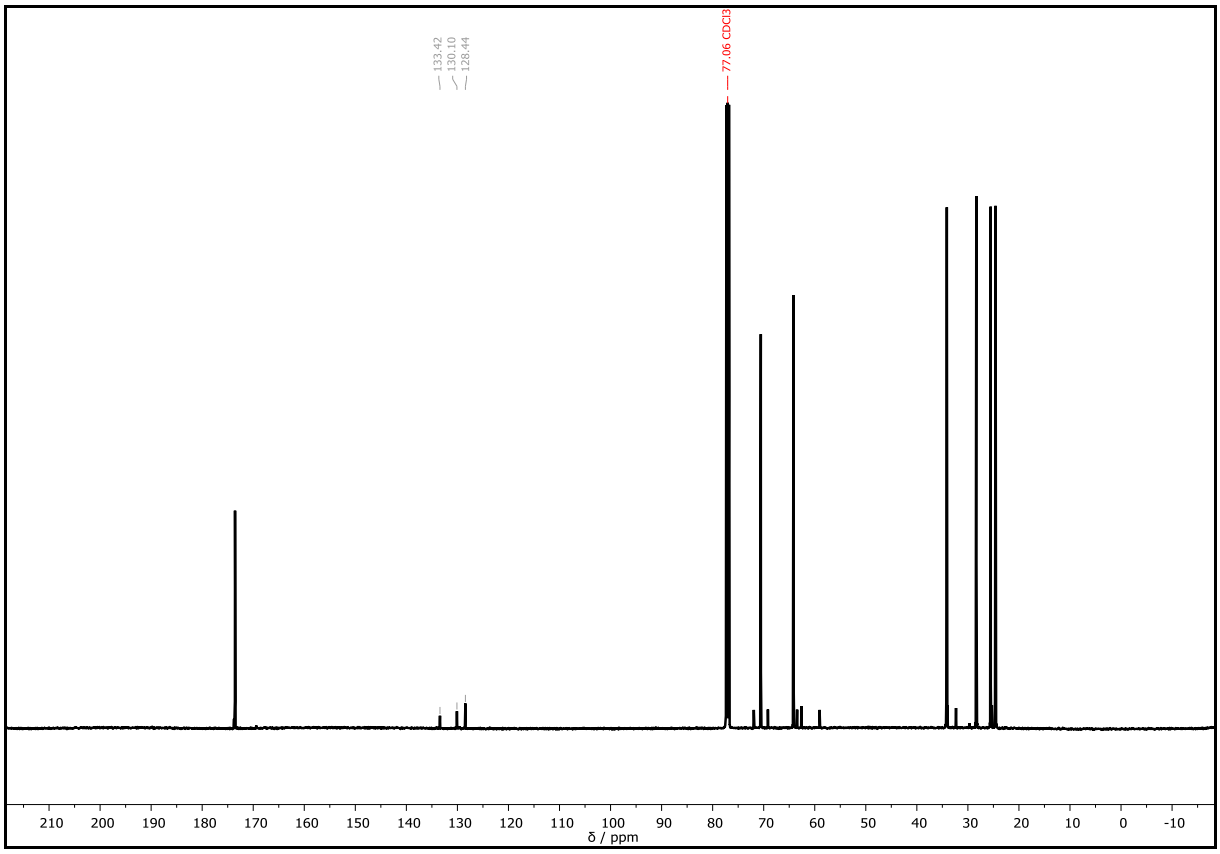

Supplementary Figure 153 ^{13}C NMR spectrum of **dBCP-1** recorded at 126 MHz in $CDCl_3$. Impurities are marked in grey.

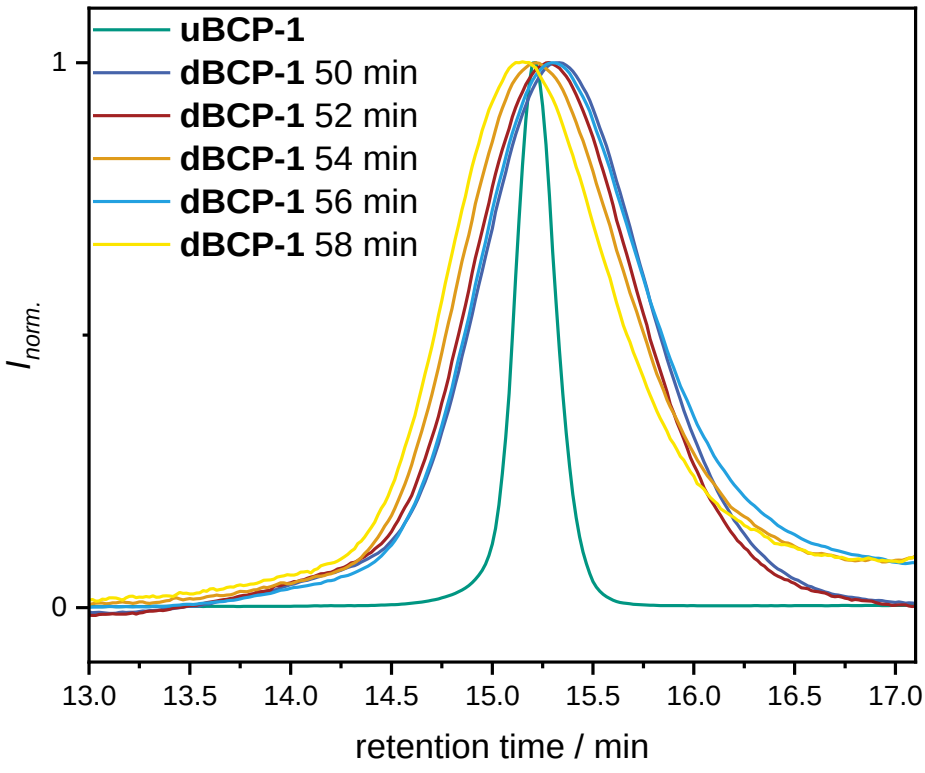

Supplementary Figure 154. SEC traces of the ring-opening polymerization of ε-caprolactone (M/I = 167) after the respective reaction time in comparison to **uBCP-1**.

Disperse mPEG$_{16}$-*b*-PCL$_{32}$-OH – dBCP-2

ε-Caprolactone	20.0 mL, 21.6 g, 189 mmol (335 equiv.)
mPEG (M_n = 750 Da)	424 mg, 565 µmol, (1.00 equiv.)
TBD	127 mg, 912 µmol (1.61 equiv.)
toluene (total amount)	90 mL
reaction time	109 min
yield	6.35 g
eluent	EA → EA:MeOH = 9:1 → acetone
R_f	0.41 (EA:MeOH = 9:1)

^{1}H NMR (500 MHz, $CDCl_3$): δ / ppm = 4.23 – 4.17 (m, CH_2^1), 4.03 (t, J = 6.7 Hz, CH_2^2), 3.66 (dd, J = 5.7, 4.1 Hz, CH_2^3), 3.65 (s, CH_2^4 and CH_2^5), 3.52 (dd, J = 5.8, 3.6 Hz, CH_2^6), 3.35 (s, CH_3^7), 2.28 (t, J = 7.5 Hz, CH_2^8 and CH_2^9), 1.69 – 1.30 (m, CH_2^{10}, CH_2^{11} and CH_2^{12}).

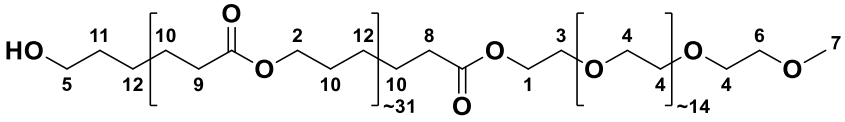

^{13}C NMR (126 MHz, $CDCl_3$): δ / ppm = 173.83 (C_q^1), 173.69 (C_q^1), 173.66 (C_q^1), 173.63 (C_q^1), 173.55 (C_q^1), 72.00 (CH_2^2), 70.68 (CH_2^3), 70.67 (CH_2^3), 70.63 (CH_2^3), 70.57 (CH_2^3), 69.24 (CH_2^4), 64.22 (CH_2^5), 64.18 (CH_2^5), 63.52 (CH_2^6), 62.65 (CH_2^7), 59.11 (CH_3^8), 34.30 (CH_2^9), 34.23 (CH_2^9), 34.19 (CH_2^9), 34.05 (CH_2^9), 32.39 (CH_2^{10}), 28.42 (CH_2^{11}), 25.63 (CH_2^{12}), 25.60 (CH_2^{12}), 25.57 (CH_2^{12}), 24.76 (CH_2^{13}), 24.65 (CH_2^{13}), 24.57 (CH_2^{13}).

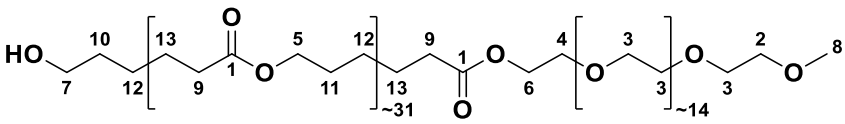

IR (ATR platinum diamond) ν / cm^{-1} = 3507, 2943, 2894, 2865, 1722, 1471, 1438, 1419, 1397, 1366, 1294, 1238, 1174, 1105, 1065, 1043, 961, 934, 841, 810, 775, 732, 714, 648, 584, 555, 525, 512, 502, 485, 453, 436, 428, 413.

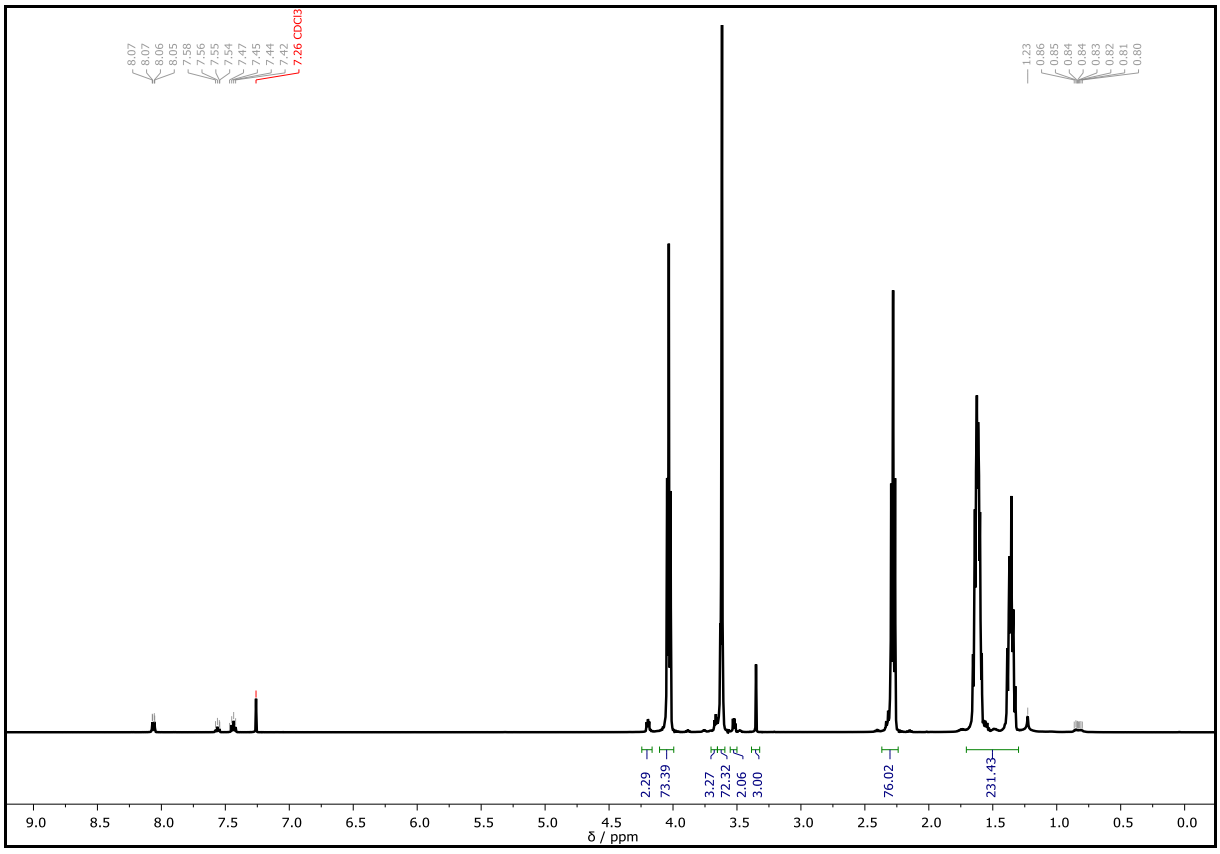

Supplementary Figure 155: ^{1}H NMR spectrum of **dBCP-2** recorded at 500 MHz in $CDCl_3$. Impurities are marked in grey.

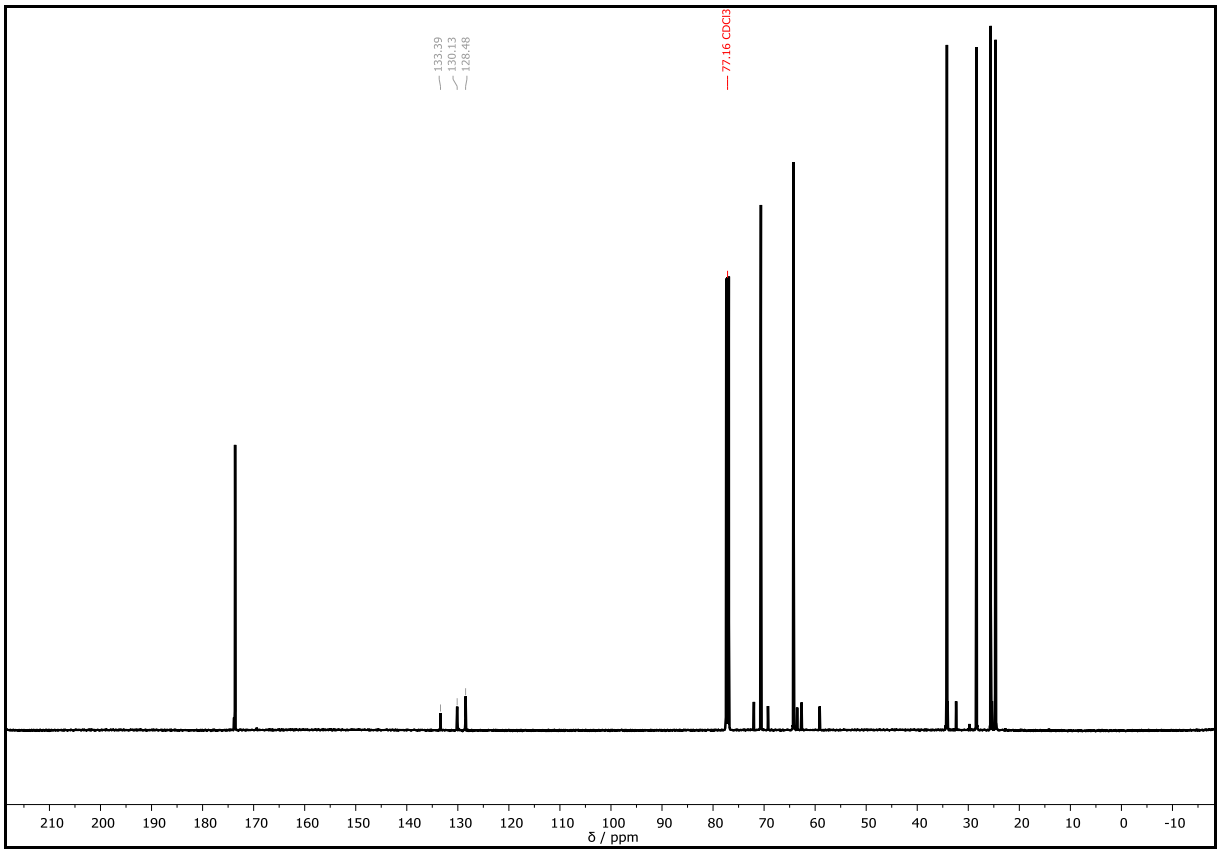

Supplementary Figure 156 ^{13}C NMR spectrum of **dBCP-2** recorded at 126 MHz in $CDCl_3$. Impurities are marked in grey.

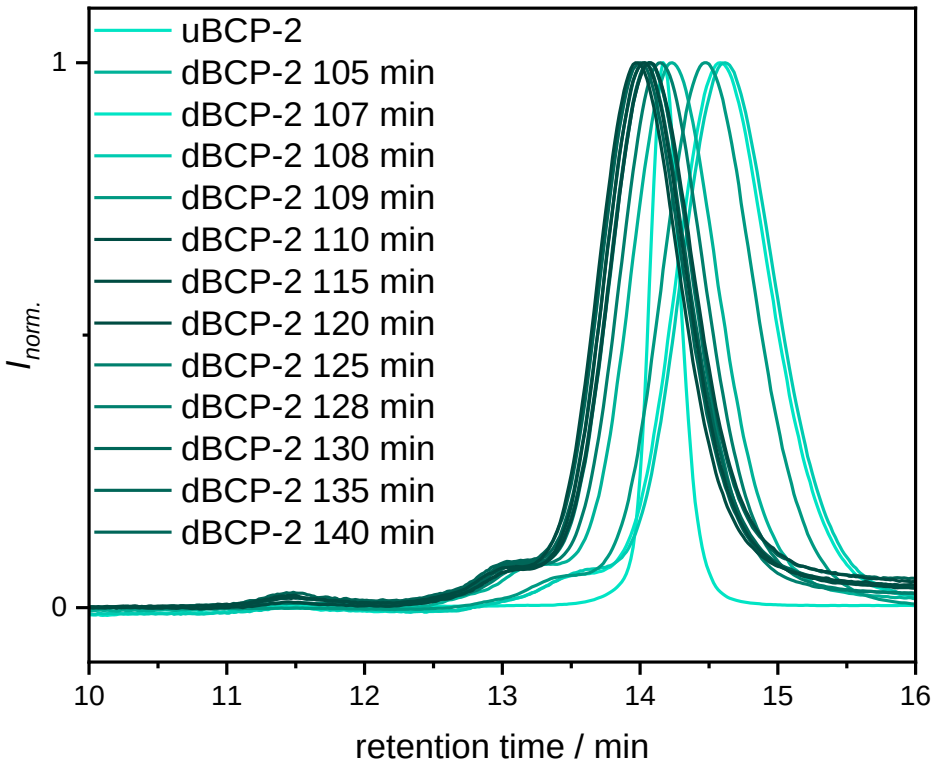

Supplementary Figure 157: SEC traces of the ROP of ε-caprolactone (M/I = 335) after the respective reaction time in comparison to **uBCP-2**.

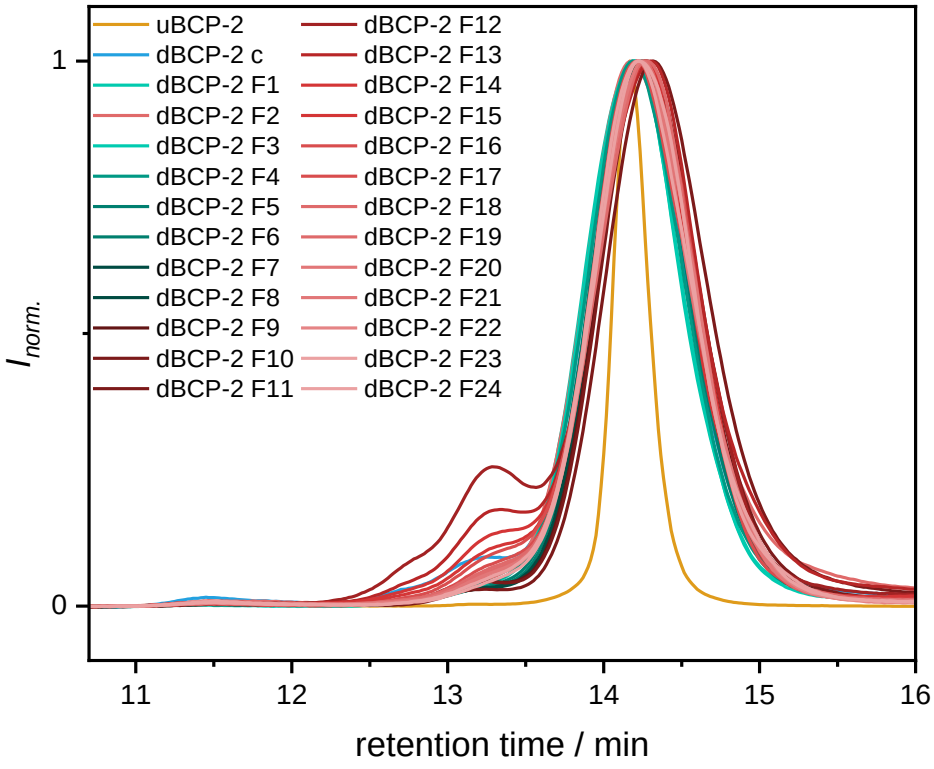

Supplementary Figure 158: SEC traces of the individual fractions of the column chromatographic purification of **dBCP-2** (109 min.) in comparison to the crude product (blue trace) and **uBCP-2** (yellow trace). The fractions in green were combined and employed in the subsequent protection step. The fractions in red were discarded.

Disperse mPEG$_{16}$-*b*-PCL$_{64}$-OH – dBCP-3

ε-Caprolactone	10.0 mL, 10.3 g, 90.2 mmol (1226 equiv.)
mPEG (M_n = 750 Da)	55.2 mg, 73.6 µmol (1.00 equiv.)
TBD	67.0 mg, 481 µmol (6.54 equiv.)
toluene (total amount)	45 mL
reaction time	225 min
yield	350 mg
eluent	EE → EE:MeOH = 9:1 → acetone
R_f	0.61 (EE:MeOH = 9:1)
Đ (system III)	1.05 (1.18 before purification)

^{1}H NMR (500 MHz, $CDCl_3$): δ / ppm = 4.24 – 4.18 (m, CH_2^1), 4.05 (t, *J* = 6.7 Hz, CH_2^3), 3.70 – 3.61 (m, CH_2^3, CH_2^4 and CH_2^5), 3.54 (dd, *J* = 5.8, 3.6 Hz, CH_2^6), 3.37 (s, CH_3^7), 2.39 – 2.27 (m, CH_2^8 and CH_2^9), 1.72 – 1.33 (m, CH_2^{10}, CH_2^{11} and CH_2^{12}).

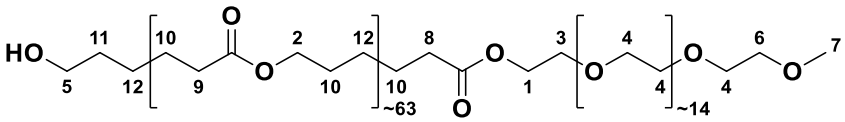

^{13}C NMR (126 MHz, $CDCl_3$): δ / ppm = 173.91 (C_q^1), 173.70 (C_q^1), 173.61 (C_q^1), 72.05 (CH_2^2), 70.72 (CH_2^3), 70.68 (CH_2^3), 70.63 (CH_2^3), 69.29 (CH_2^4), 64.28 (CH_2^5), 64.13 (CH_2^5), 63.58 (CH_2^6), 62.81 (CH_2^7), 59.16 (CH_3^8), 34.40 (CH_2^9), 34.35 (CH_2^9), 34.29 (CH_2^9), 34.24 (CH_2^9), 34.10 (CH_2^9), 32.43 (CH_2^{10}), 32.39 (CH_2^{10}), 32.34 (CH_2^{10}), 28.47 (CH_2^{11}), 25.65 (CH_2^{12}), 25.60 (CH_2^{12}), 25.54 (CH_2^{12}), 24.80 (CH_2^{13}), 24.70 (CH_2^{13}), 24.62 (CH_2^{13}).

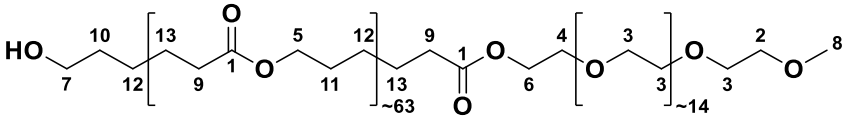

IR (ATR platinum diamond) $\tilde{\nu}$ / cm^{-1} = 3449, 2941, 2896, 2865, 1722, 1471, 1419, 1397, 1366, 1294, 1240, 1185, 1177, 1107, 1065, 1045, 961, 934, 887, 866, 841, 732, 714, 582, 453.

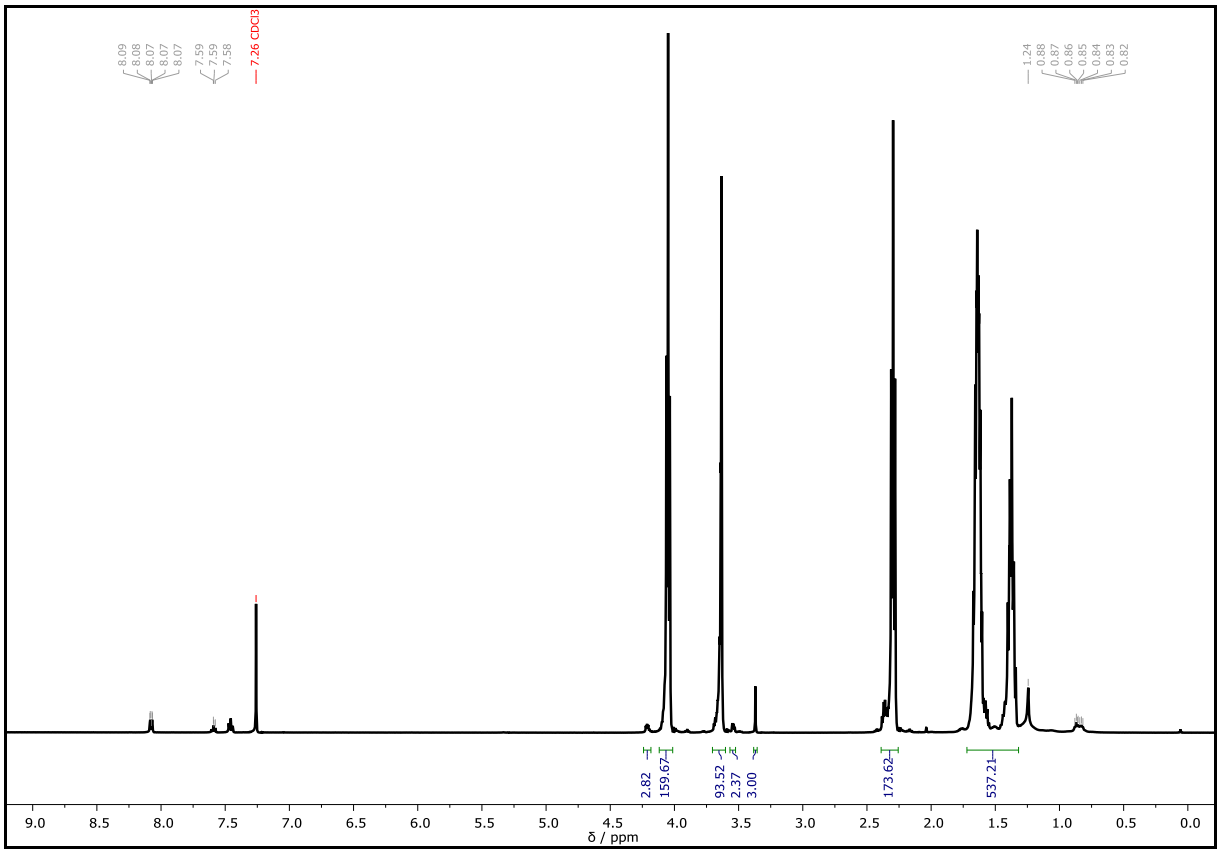

Supplementary Figure 159: ^{1}H NMR spectrum of **dBCP-3** recorded at 500 MHz in $CDCl_3$. Impurities are marked in grey.

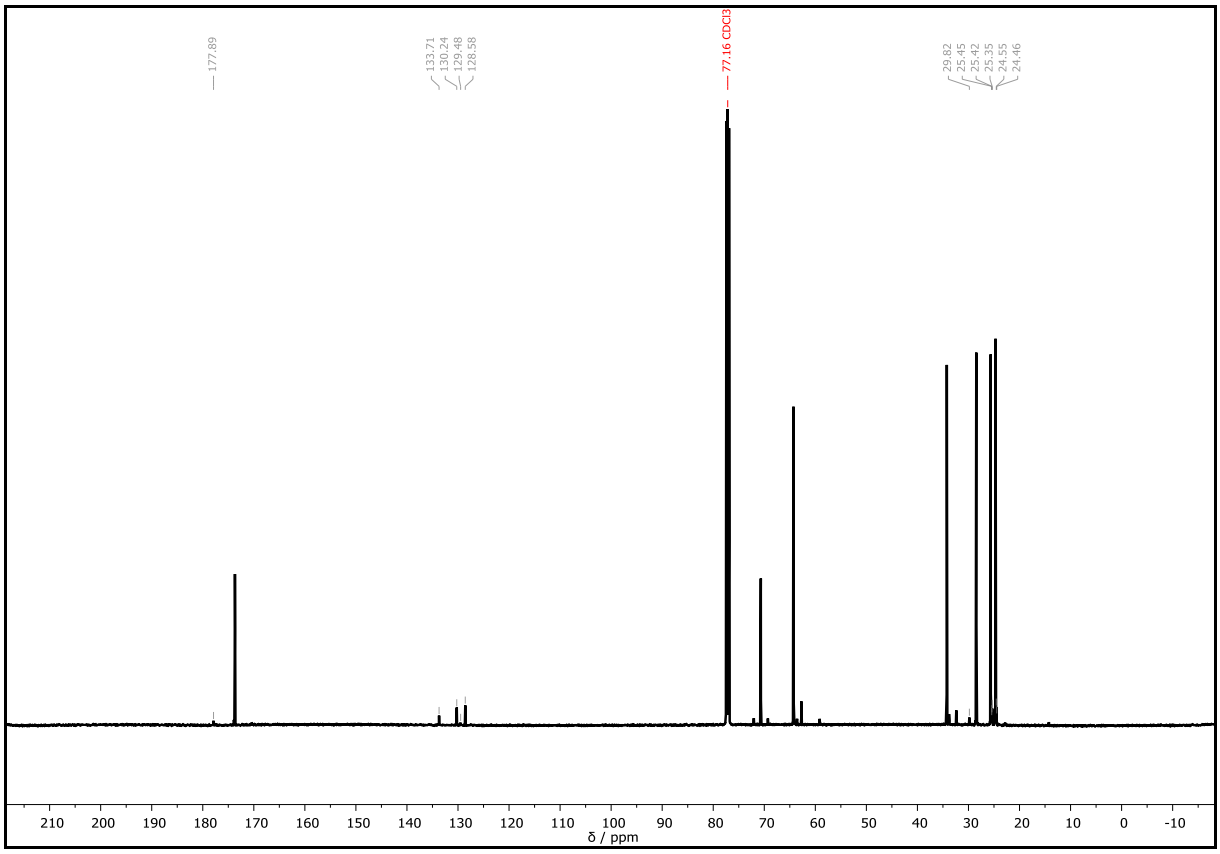

Supplementary Figure 160: ^{1}H NMR spectrum of **dBCP-3** recorded at 126 MHz in $CDCl_3$. Impurities are marked in grey.

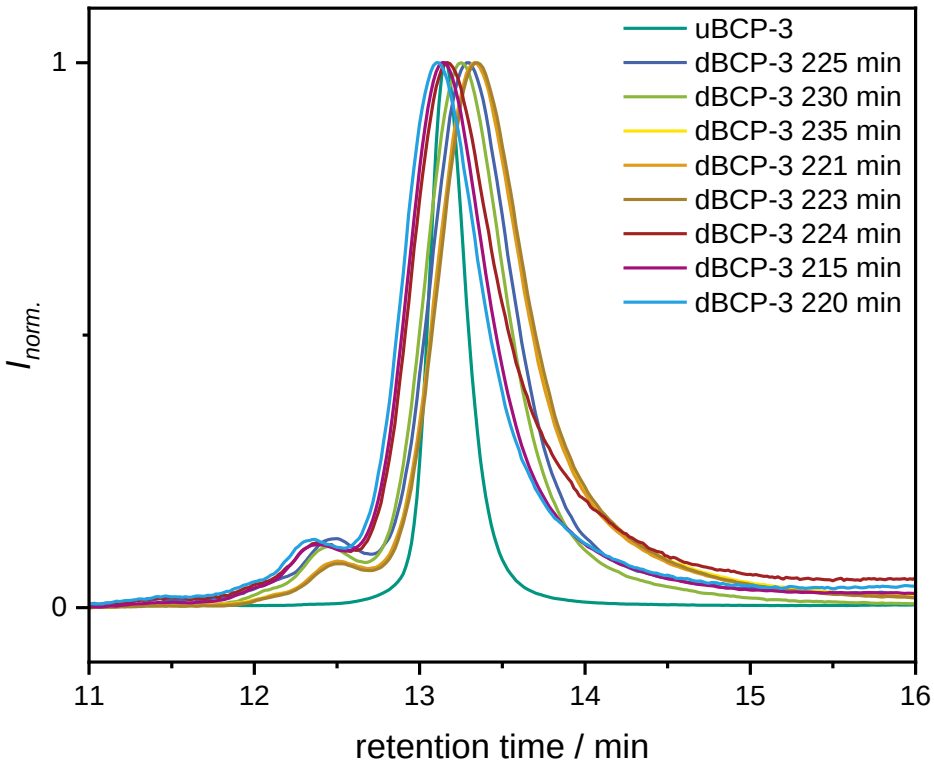

Supplementary Figure 161: SEC traces of the ROP of ε-caprolactone (M/I = 1226) after the respective reaction time in comparison to **uBCP-3**.

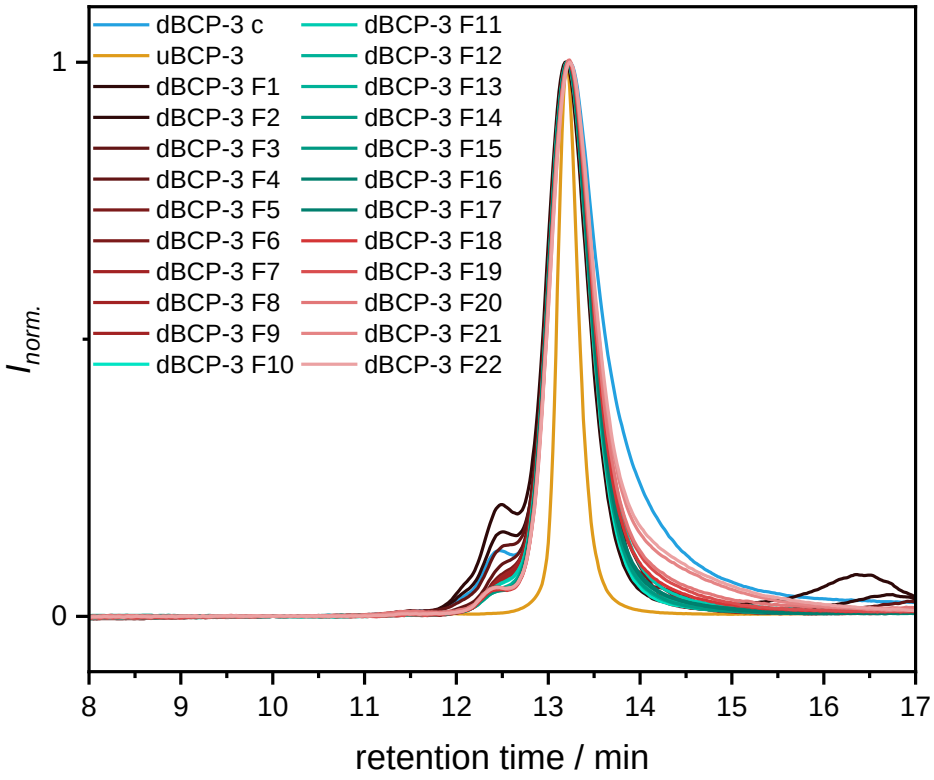

Supplementary Figure 162: SEC traces of the individual fractions of the column chromatographic purification of **dBCP-3** (225 min.) in comparison to the crude product (blue trace) and **uBCP-3** (yellow trace). The fractions in green were combined and employed in the subsequent protection step. The fractions in red were discarded.

General procedure for the protection of the BCP alcohol with TBDMS-Cl

1*H*-Imidazole (30.0 equiv.) was added to a solution of the BCP alcohol (1.00 equiv.) in dry DMF. The reaction was stirred for 10 min at room temperature and TBDMS-Cl (30.0 equiv.) was added. The mixture was stirred at 50 °C under argon atmosphere overnight. The product was precipitated in cold *n*-hexane. The precipitate was dissolved in DCM, washed with water (2 ×) and brine (2 ×), filtered and the solvent was removed under reduced pressure. The crude product was purified *via* column chromatography (1st column chromatography: EA → EA:MeOH = 99:1 → 9:1 → acetone; 2nd column chromatography: EA → acetone). The quantities of the starting materials are mentioned in the corresponding sections.

Disperse mPEG$_{16}$-*b*-PCL$_{16}$-TBDMS – dBCP-4

1*H*-imidazole	573 mg, 8.41 mmol, 30.0 equiv.
dBCP-1	750 mg, 280 µmol, 1.00 equiv.
TBDMS-Cl	1.27 g, 8.41 mmol, 30.0 equiv.
dry DMF	7.50 mL
yield	122 mg
R_f(product)	0.18 (EA:MeOH = 9:1)
Đ (system III)	1.06

^{1}H NMR (400 MHz, $CDCl_3$): δ / ppm = 4.25 – 4.18 (m, 2H, CH_2^1), 4.05 (t, *J* = 6.7 Hz, 32H, CH_2^2), 3.70 – 3.67 (m, 2H, CH_2^3), 3.65 – 3.62 (m, 54H, CH_2^4), 3.59 (t, *J* = 6.5 Hz, 2H, CH_2^5), 3.56 – 3.52 (m, 2H, CH_2^6), 3.37 (s, 3H, CH_3^7), 2.35 (t, *J* = 7.5 Hz, 2H, CH_2^8), 2.30 (t, *J* = 7.5 Hz, 32H, CH_2^9), 1.69 – 1.59 (m, 66H, CH_2^{10}), 1.54 – 1.49 (m, 2H, CH_2^{11}), 1.42 – 1.33 (m, 34H, CH_2^{12}), 0.88 (s, 9H, CH_3^{13}), 0.03 (s, 6H, CH_3^{14}).

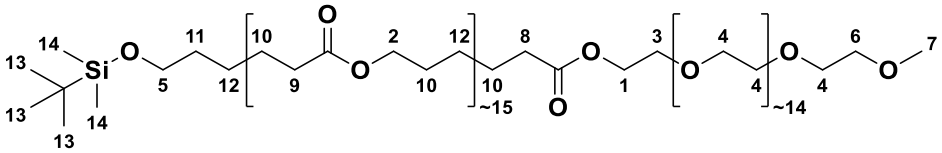

^{13}C NMR (101 MHz, $CDCl_3$): δ / ppm = 173.93 (C_q^1), 173.66 (C_q^1), 173.59 (C_q^1), 72.07 (CH_2^2), 70.70 (CH_2^3), 69.31 (CH_2^4), 64.27 (CH_2^5), 64.18 (CH_2^5), 63.58 (CH_2^6), 63.10 (CH_2^7), 59.17 (CH_3^8), 34.47 (CH_2^9), 34.25 (CH_2^9), 34.11 (CH_2^9), 32.60 (CH_2^{10}), 28.49 (CH_2^{11}), 26.10 (CH_3^{12}), 25.67 (CH_2^{13}), 25.58 (CH_2^{13}), 24.94 (CH_2^{14}), 24.71 (CH_2^{14}), 24.63 (CH_2^{14}), 18.48 (C_q^{15}), -5.15 (CH_3^{16}).

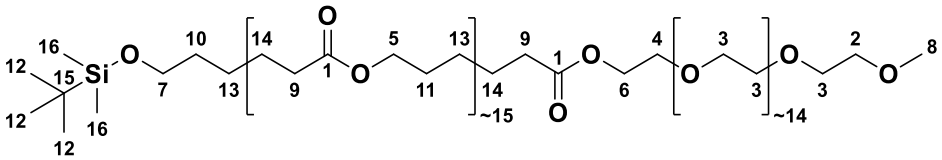

IR (ATR platinum diamond) $\tilde{\nu}$ / cm^{-1} = 2943, 2894, 2865, 1722, 1471, 1438, 1419, 1397, 1366, 1323, 1294, 1240, 1187, 1105, 1065, 1045, 961, 934, 837, 775, 732, 710, 582, 578, 557, 533, 522, 502, 485, 467, 453, 418, 409.

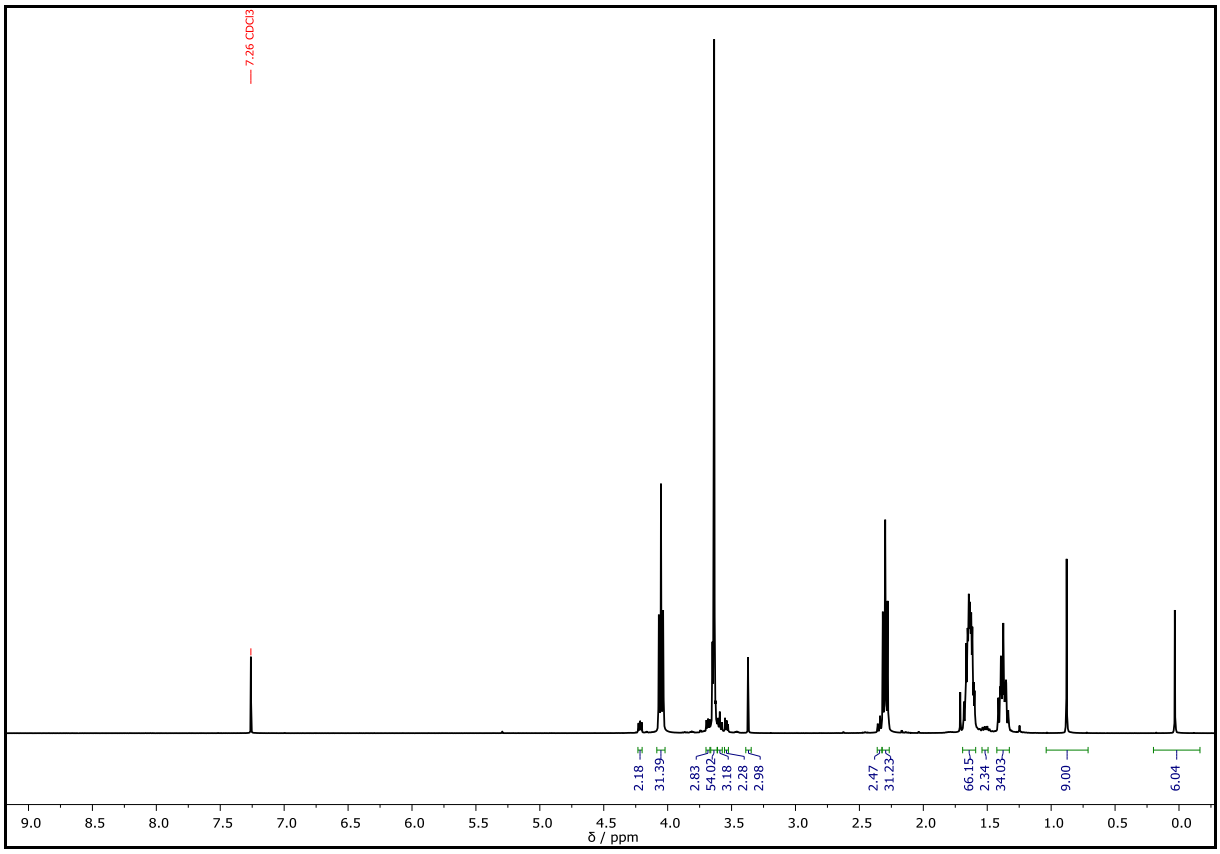

Supplementary Figure 163: ^{1}H NMR spectrum of **dBCP-4** recorded at 500 MHz in $CDCl_3$.

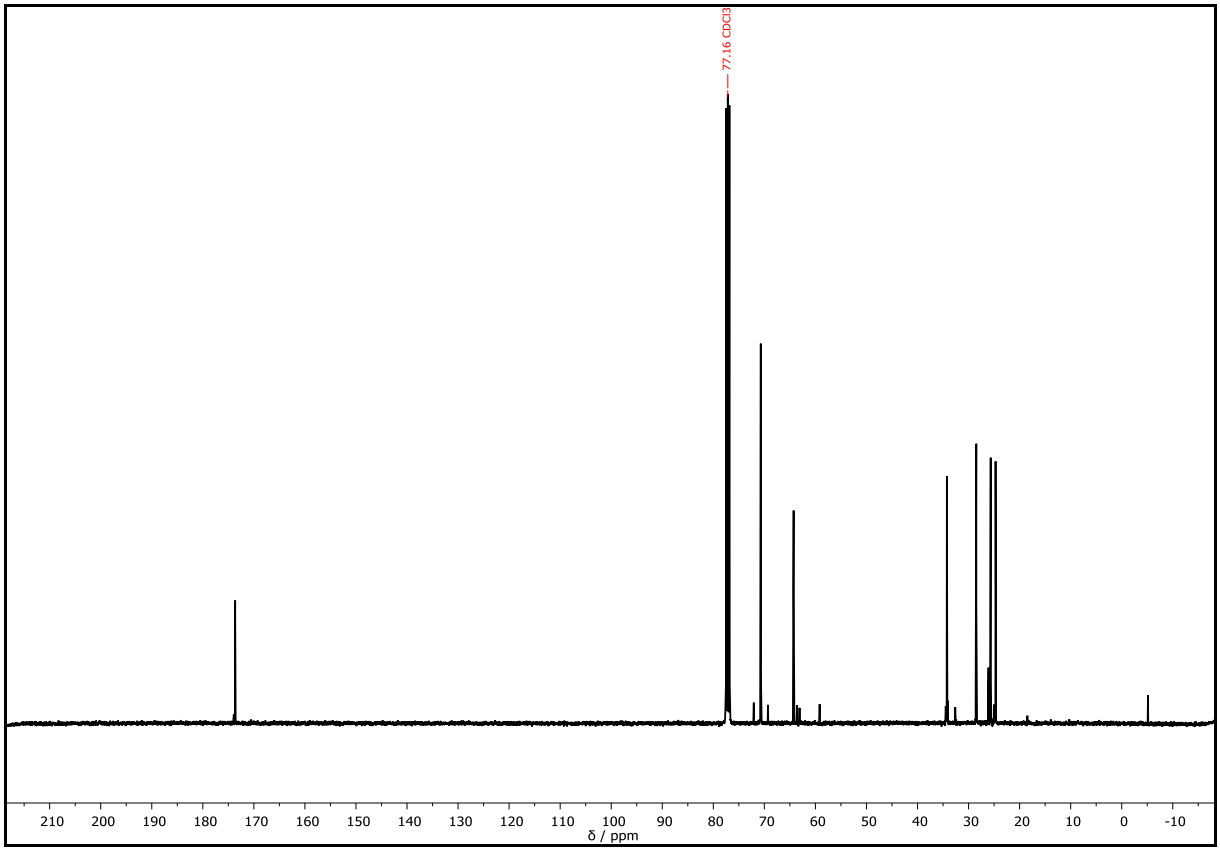

Supplementary Figure 164: ^{13}C NMR spectrum of **dBCP-4** recorded at 126 MHz in $CDCl_3$.

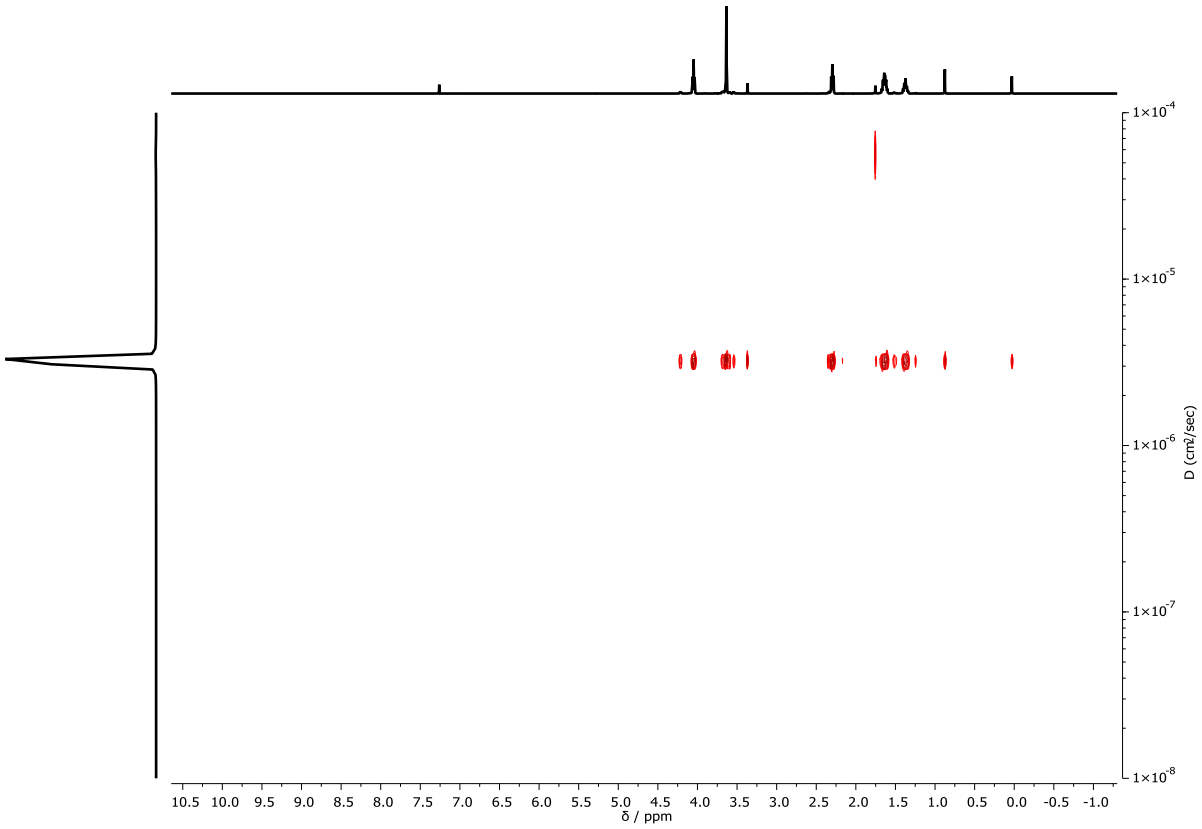

Supplementary Figure 165: DOSY NMR spectrum of **dBCP-4** recorded at 500 MHz in $CDCl_3$.

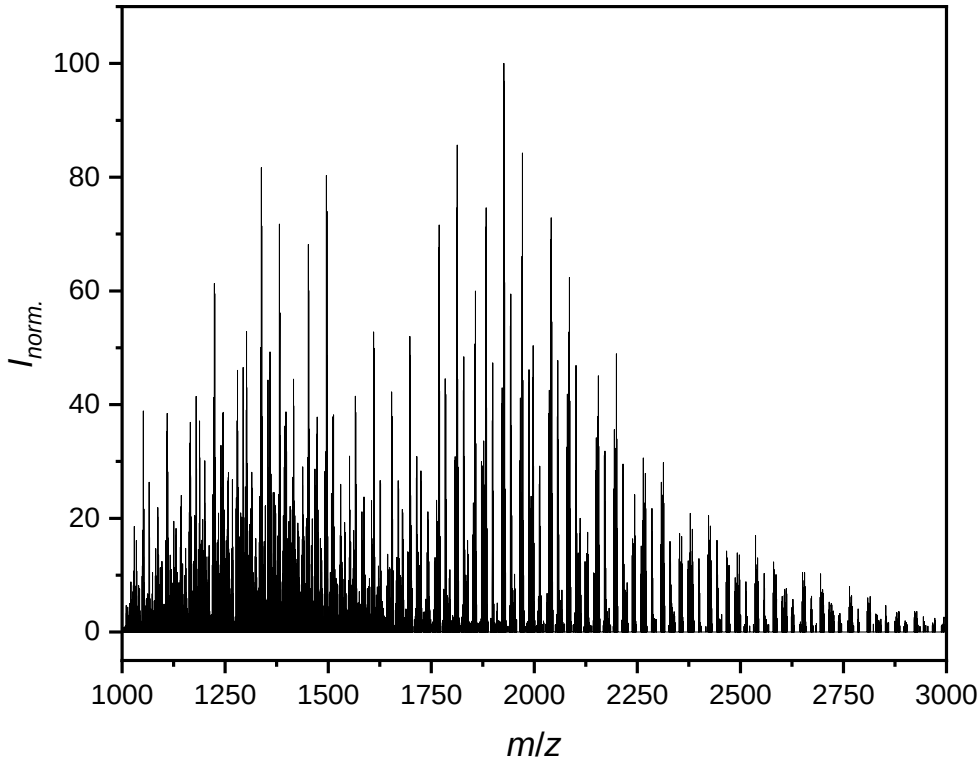

Supplementary Figure 166 ESI-MS spectrum of **dBCP-4**.

Disperse mPEG$_{16}$-*b*-PCL$_{32}$-TBDMS – dBCP-5

1*H*-imidazole	227 mg, 3.33 mmol, 30.0 equiv.
dBCP-2	500 mg, 111 µmol, 1.00 equiv.
TBDMS-Cl	502 mg, 3.33 mmol, 30.0 equiv.
dry DMF	5.00 mL
yield	160 mg
R_f(product)	0.19 (EA:MeOH = 9:1)
Đ (system III)	1.06

^{1}H NMR (500 MHz, $CDCl_3$): δ / ppm = 4.23 – 4.20 (m, 2H, CH_2^1), 4.05 (t, *J* = 6.7 Hz, 66H, CH_2^2), 3.70 – 3.67 (m, 2H, CH_2^3), 3.65 – 3.62 (m, 64H, CH_2^4), 3.59 (t, *J* = 6.5 Hz, 2H, CH_2^5), 3.55 – 3.53 (m, 2H, CH_2^6), 3.37 (s, 3H, CH_3^7), 2.34 (t, *J* = 7.8 Hz, 2H, CH_2^8), 2.30 (t, *J* = 7.5 Hz, 66H, CH_2^9), 1.69 – 1.59 (m, 134H, CH_2^{10}), 1.53 – 1.49 (m, 2H, CH_2^{11}), 1.42 – 1.34 (m, 68H, CH_2^{12}), 0.88 (s, 9H, CH_3^{13}), 0.03 (s, 6H, CH_3^{14}).

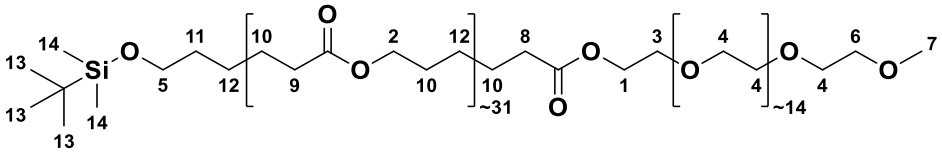

^{13}C NMR (126 MHz, $CDCl_3$): δ / ppm = 173.67 (C_q^1), 72.09 (CH_2^2), 70.72 (CH_2^3), 69.32 (CH_2^4), 64.28 (CH_2^5), 64.19 (CH_2^5), 63.59 (CH_2^6), 63.11 (CH_2^7), 59.19 (CH_3^8), 34.26 (CH_2^9), 32.61 (CH_2^{10}), 34.12 (CH_2^9), 28.50 (CH_2^{11}), 26.10 (CH_3^{12}), 25.67 (CH_2^{13}), 25.59 (CH_2^{13}), 24.95 (CH_2^{14}), 24.72 (CH_2^{14}), -5.14 (CH_3^{16}).

Note: C_q^{15} is not visible in the ^{13}C NMR spectrum.

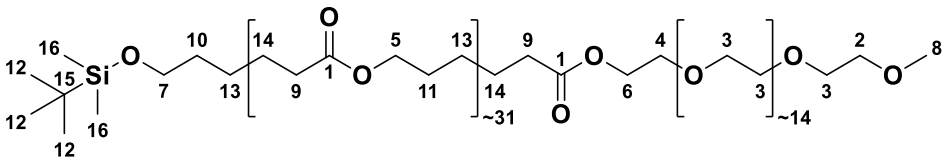

IR (ATR platinum diamond) $\tilde{\nu}$ / cm^{-1} = 2943, 2894, 2865, 1722, 1471, 1438, 1419, 1397, 1366, 1323, 1294, 1238, 1177, 1105, 1065, 1043, 961, 934, 839, 817, 775, 732, 710, 584, 541, 522, 453, 436, 424, 401.

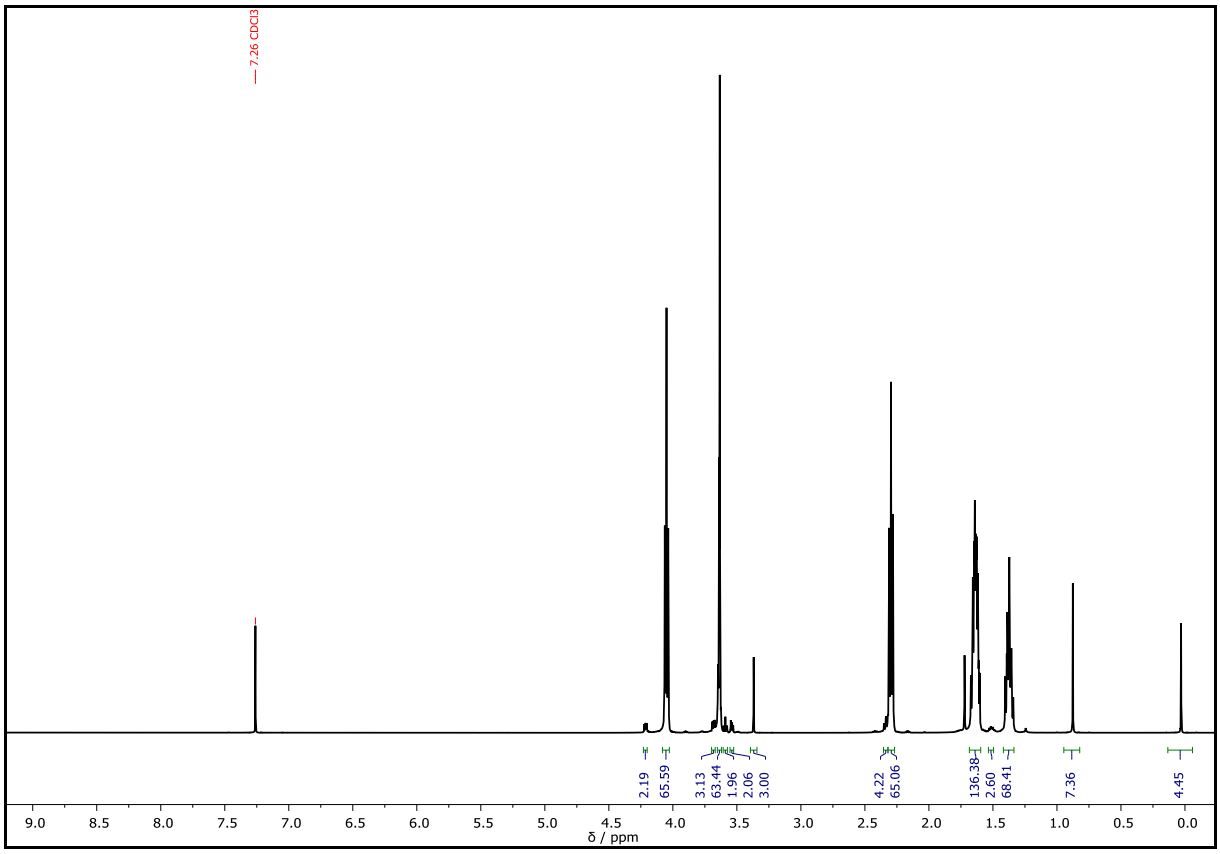

Supplementary Figure 167: ^{1}H NMR spectrum of **dBCP-5** recorded at 500 MHz in $CDCl_3$.

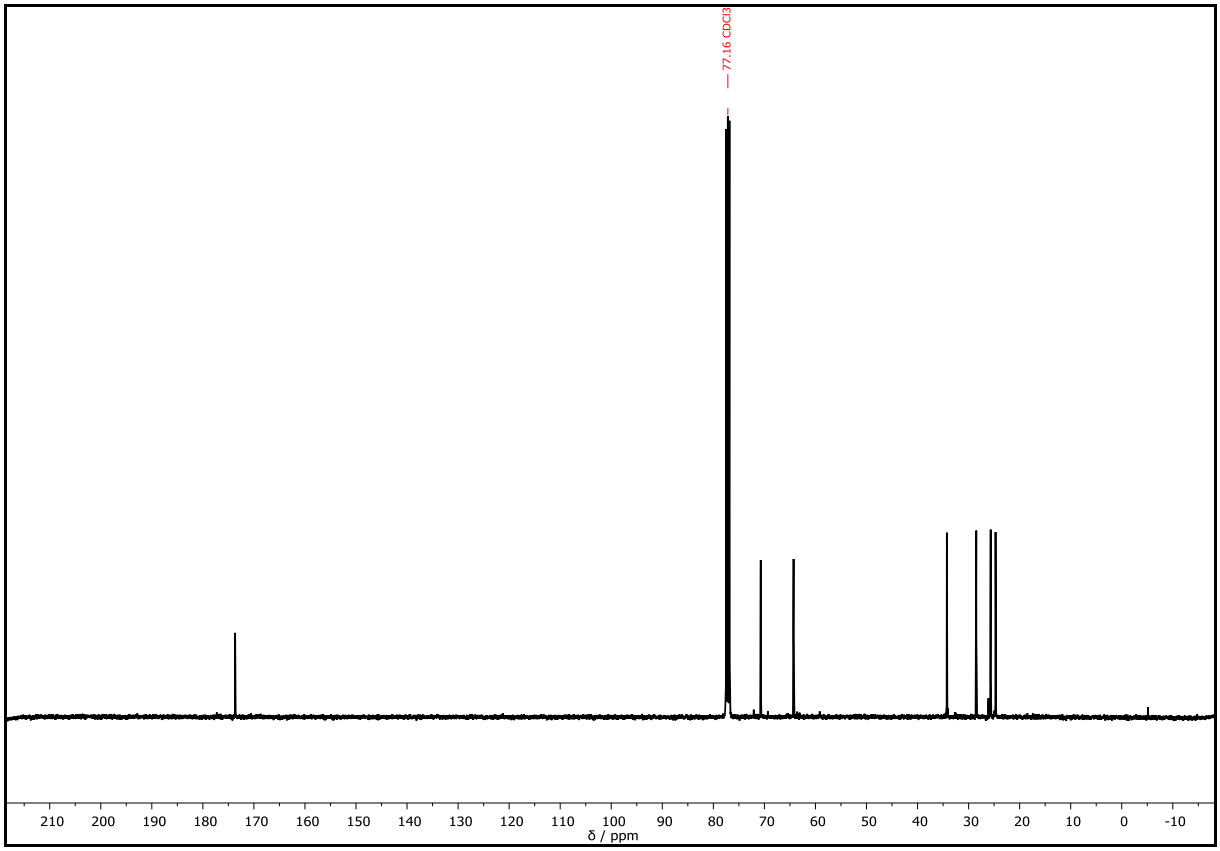

Supplementary Figure 168: ^{13}C NMR spectrum of **dBCP-5** recorded at 126 MHz in $CDCl_3$.

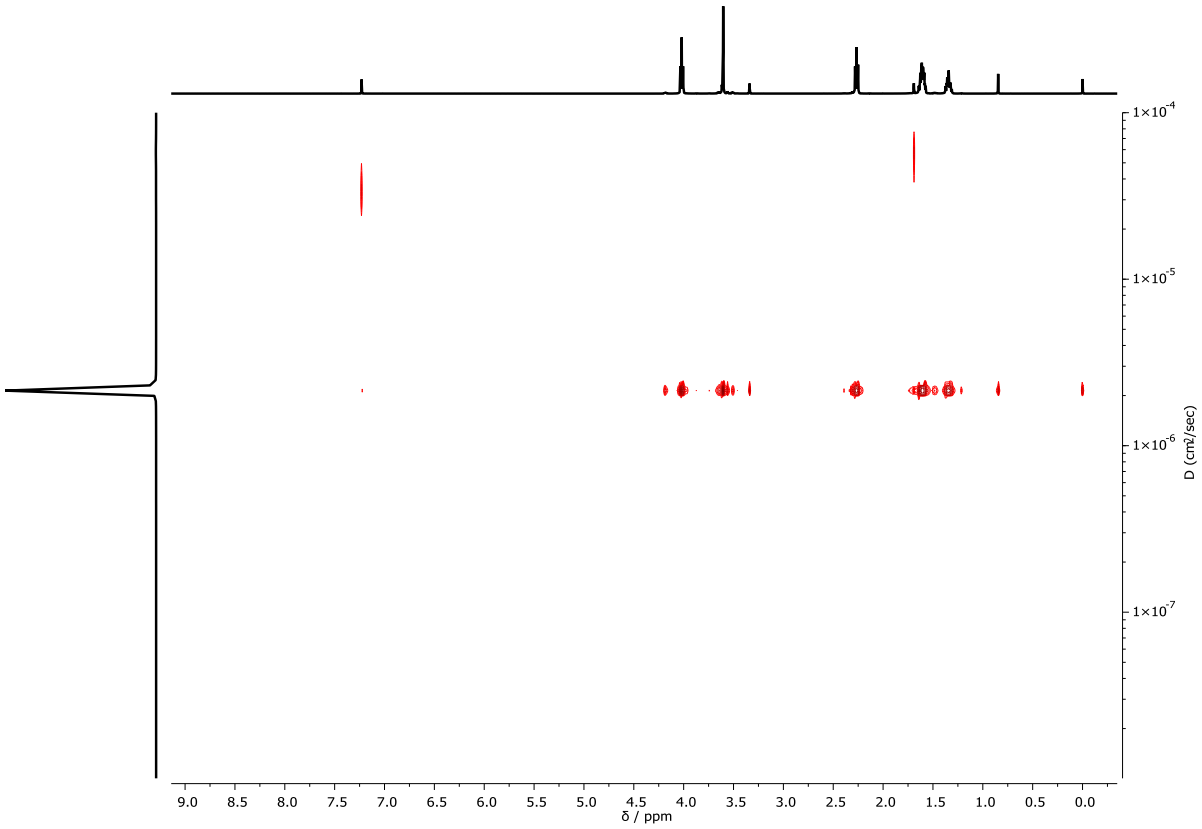

Supplementary Figure 169: DOSY NMR spectrum of **dBCP-5** recorded at 500 MHz in $CDCl_3$.

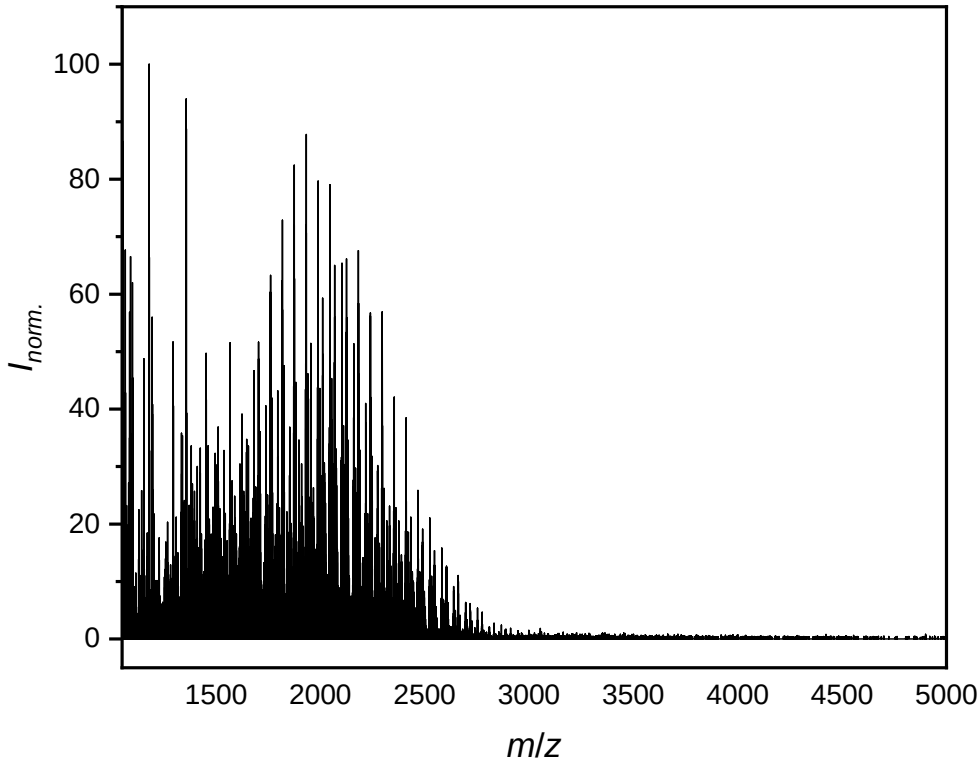

Supplementary Figure 170: ESI-MS spectrum of **dBCP-5**.

Disperse mPEG$_{16}$-*b*-PCL$_{64}$-TBDMS – dBCP-6

1*H*-imidazole	70.9 mg, 1.04 mmol, 30.0 equiv.
dBCP-3	283 mg, 34.7 µmol, 1.00 equiv.
TBDMS-Cl	157 mg, 1.04 mmol, 30.0 equiv.
dry DMF	5.00 mL
yield	91.5 mg
R_f(product)	0.26 (EA:MeOH = 9:1)
Đ (system III)	1.06

^{1}H NMR (500, MHz, $CDCl_3$): δ / ppm = 4.24 – 4.21 (m, 1H, CH_2^1), 4.05 (t, *J* = 6.7 Hz, CH_2^2), 3.70 – 3.67 (m, CH_2^3), 3.67 – 3.62 (m, CH_2^4), 3.61 – 3.58 (m, CH_2^5), 3.56 – 3.53 (m, CH_2^6), 3.37 (s, CH_3^7), 2.36 – 2.32 (m, CH_2^8), 2.30 (t, *J* = 7.5 Hz, CH_2^9), 1.69 – 1.59 (m, CH_2^{10}), 1.54 – 1.48 (m, CH_2^{11}), 1.44 – 1.33 (m, CH_2^{12}), 0.88 (s, CH_3^{13}), 0.03 (s, CH_3^{14}).

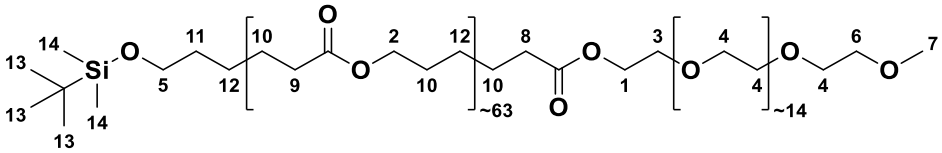

^{13}C NMR (126, MHz, $CDCl_3$): δ / ppm = 173.67 (C_q^1), 72.08 (CH_2^2), 70.70 (CH_2^3), 69.32 (CH_2^4), 64.28 (CH_2^5), 63.59 (CH_2^6), 63.11 (CH_2^7), 59.18 (CH_3^8), 34.26 (CH_2^9), 28.49 (CH_2^{11}), 26.10 (CH_3^{12}), 25.67 (CH_2^{13}), 24.72 (CH_2^{14}), -5.14 (CH_3^{13}).

Note: CH_2^{10} and C_q^{15} are not visible in the ^{13}C NMR spectrum.

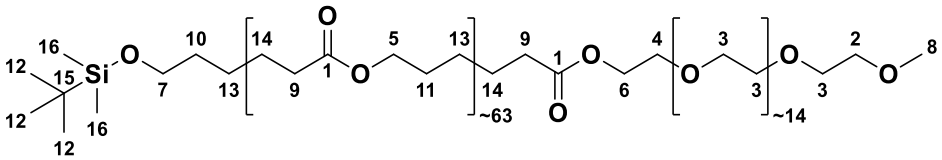

IR (ATR platinum diamond) $\tilde{\nu}$ / cm^{-1} = 2943, 2896, 2865, 1722, 1471, 1438, 1419, 1397, 1366, 1323, 1294, 1240, 1174, 1107, 1065, 1045, 961, 934, 839, 817, 775, 732, 710, 584, 453.

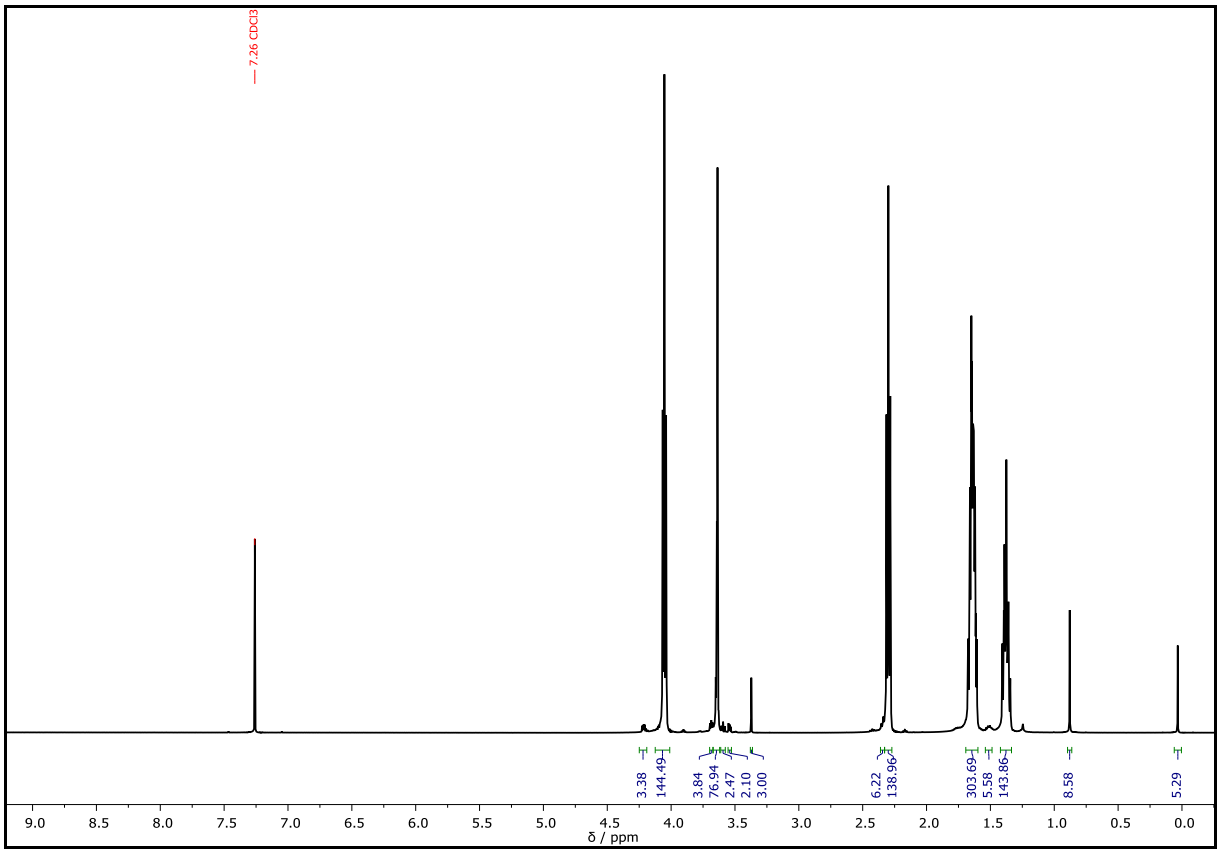

Supplementary Figure 171 ^{1}H NMR spectrum of **dBCP-6** recorded at 500 MHz in $CDCl_3$.

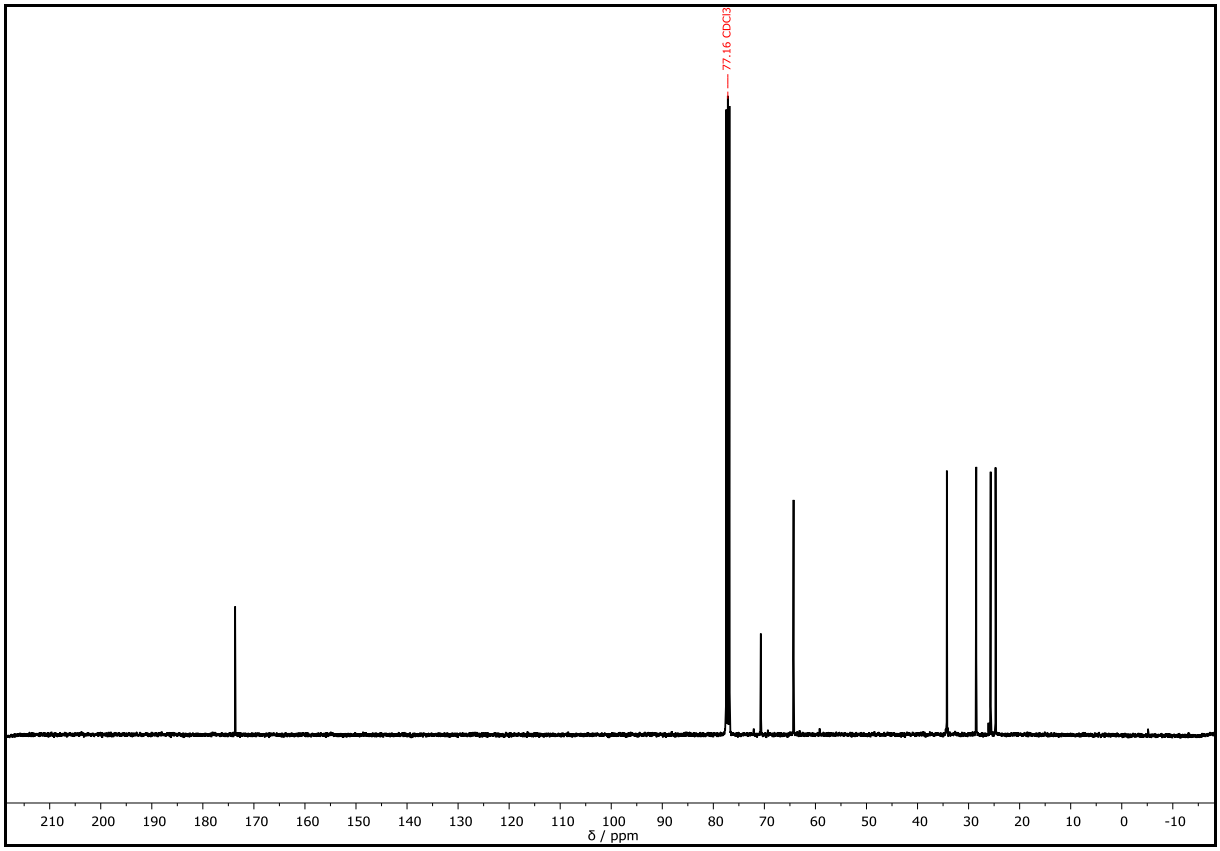

Supplementary Figure 172 ^{13}C NMR spectrum of **dBCP-6** recorded at 126 MHz in $CDCl_3$.

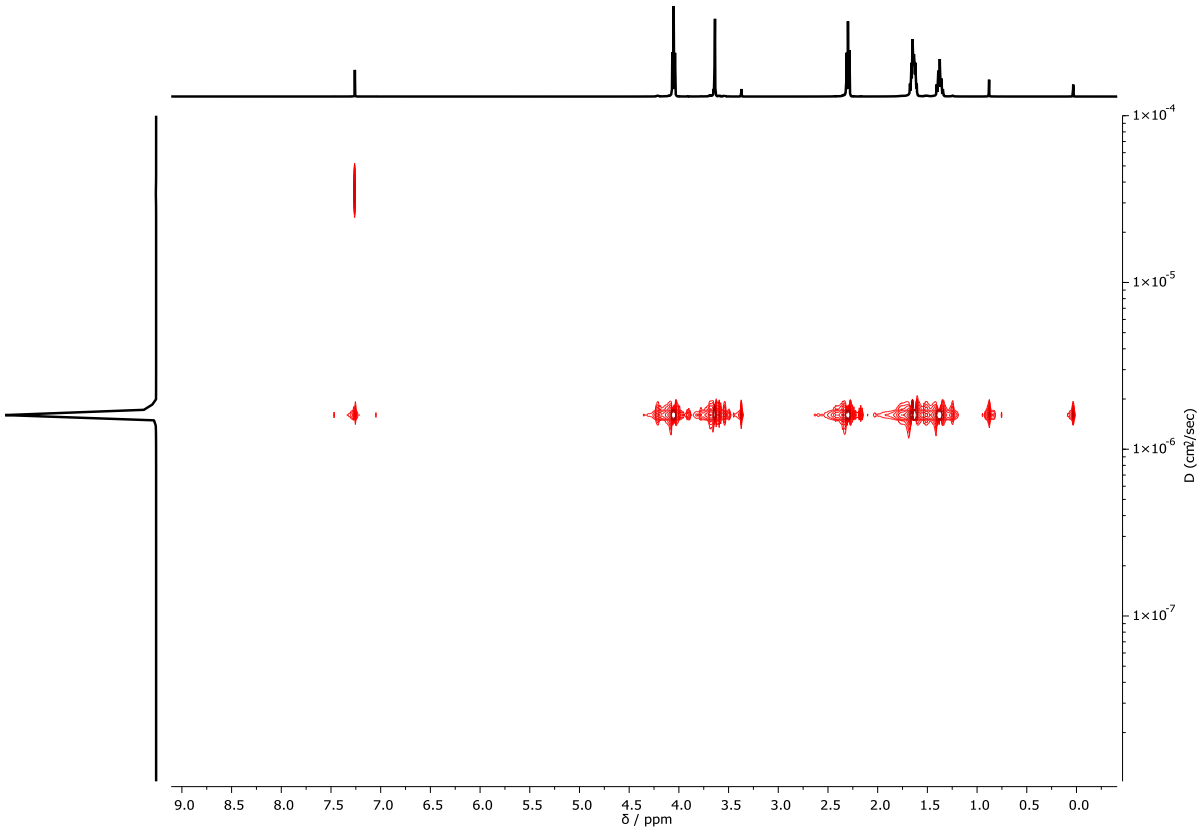

Supplementary Figure 173 DOSY NMR spectrum of **dBCP-6** recorded at 500 MHz in $CDCl_3$.

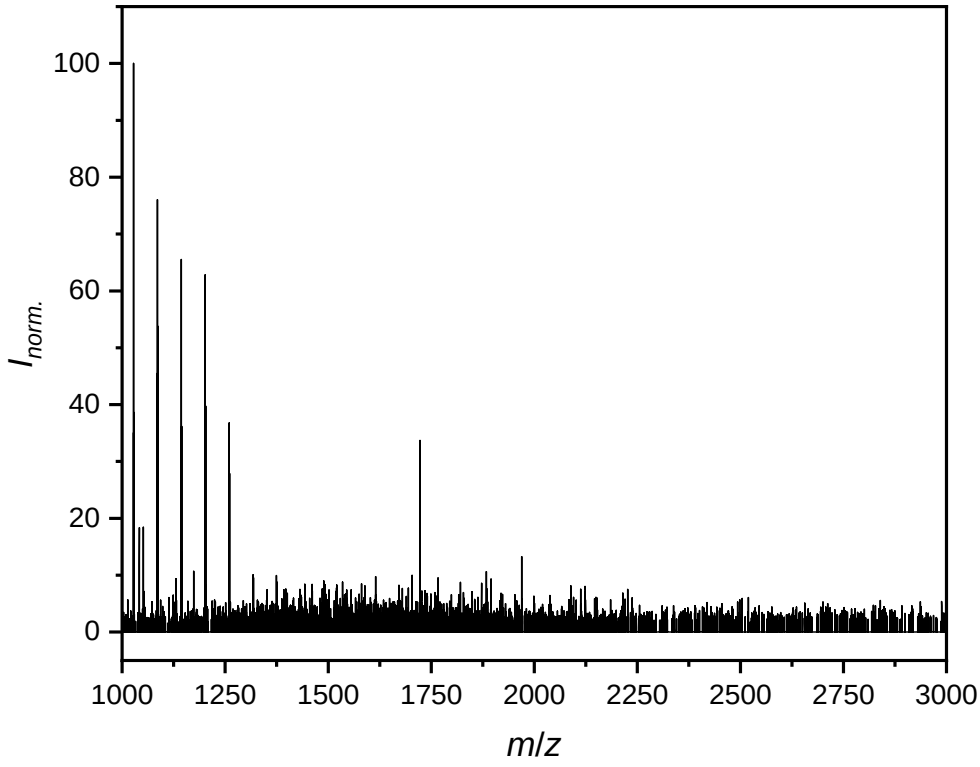

Supplementary Figure 174 ESI-MS spectrum of **dBCP-6**.

6.3.7. Experimental procedures of chapter 4.6.1

Linear sequence-defined oligomer *via* P3CR and oxa-Michael Addition one-pot reaction

Ethyl (*E*)-3-butoxyacrylate – S1 (test reaction)

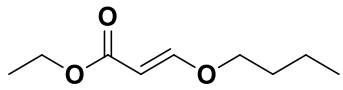

Chemical Formula: $C_9H_{16}O_3$
Exact Mass: 172.1099 Da
Molecular Weight: 172.2240 Da

Ethyl propiolate (101 µL, 98.1 mg, 1.00 mmol, 1.00 equiv.) was dissolved in DCM (1.00 mL). Subsequently, 1-butanol (91.5 µL, 74.1 mg, 1.00 mmol, 1.00 equiv.) and DABCO (11.2 mg, 100 µmol, 0.10 equiv.) was added and the reaction mixture was stirred overnight at room temperature. The product **S1** was obtained in quantitative yield after evaporation of the solvent after reduced pressure.

^{1}H NMR (400 MHz $CDCl_3$): δ / ppm = 7.59 (d, *J* = 12.6 Hz, 1H, CH^1), 5.18 (d, *J* = 12.6 Hz, 1H, CH^2), 4.16 (q, *J* = 7.1 Hz, 2H, CH_2^3), 3.84 (t, *J* = 6.5 Hz, 2H, CH_2^4), 1.74 – 1.60 (m, 2H, CH_2^5), 1.47 – 1.34 (m, 2H, CH_2^6), 1.27 (t, *J* = 7.1 Hz, 3H, CH_3^7), 0.94 (t, *J* = 7.4 Hz, 3H, CH_3^8).

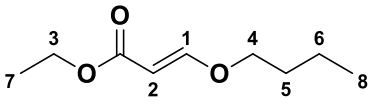

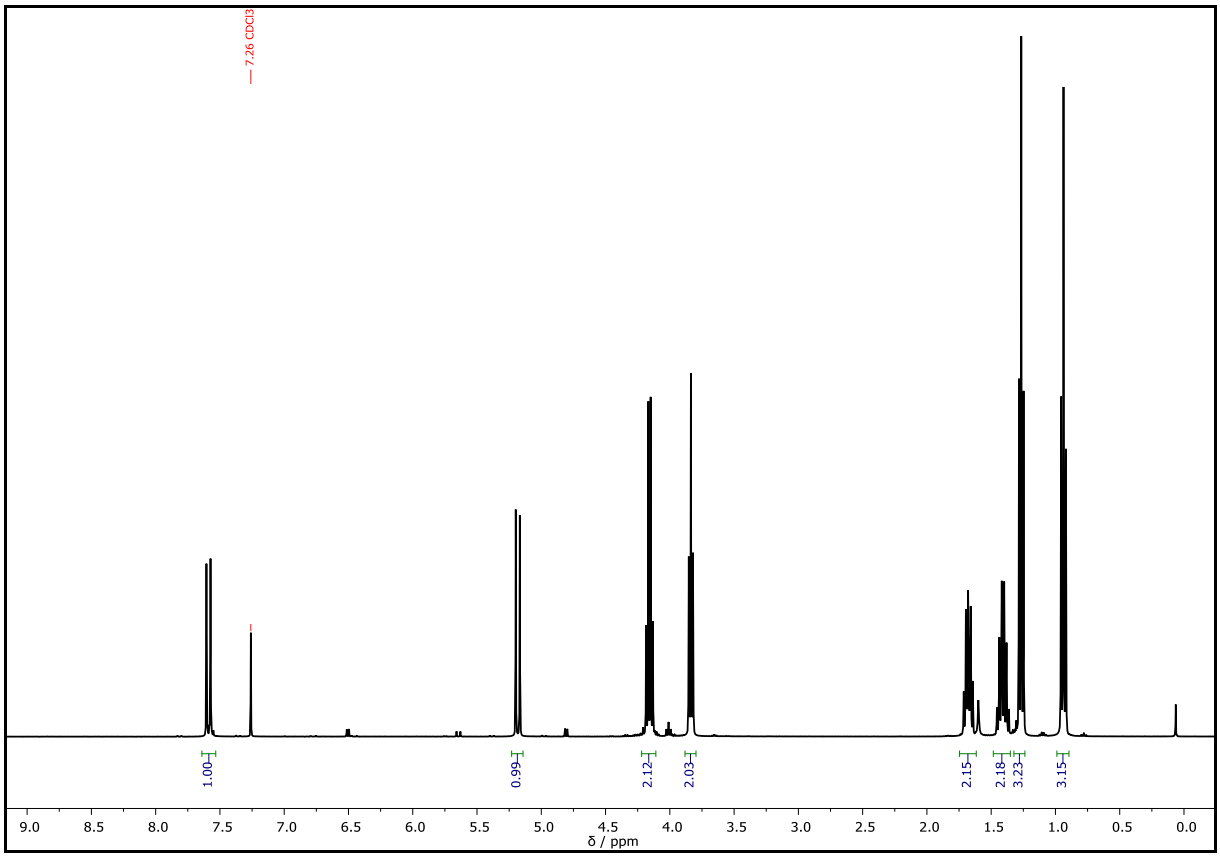

Supplementary Figure 175: ^{1}H NMR spectrum of **S1** recorded at 400 MHz in $CDCl_3$.

1-(*tert*-Butylamino)-3-ethyl-1-oxopentan-2-yl propiolate – S2[I]

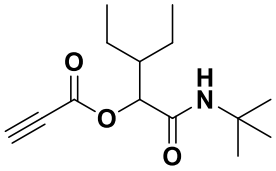

Chemical Formula: $C_{14}H_{23}NO_3$
Exact Mass: 253.1678 Da
Molecular Weight: 253.3420 Da

Propiolic acid (62.0 µL, 70.1 mg, 1.00 mmol, 1.00 equiv.) and 2-ethylbutyraldehyde (123 µL, 100 mg, 1.00 mmol, 1.00 eq.) were dissolved in DCM (1.00 mL). Subsequently, *tert*-butyl isocyanide (113 µL, 83.1 mg, 1.00 mmol, 1.00 eq.) was added dropwise and the reaction mixture was stirred overnight at room temperature. Purification of the crude product *via* column chromatography (cyhex:EA = 9:1 → 7:1) yielded **S2** as a white solid (207 mg, 81.8 µmol, 81.8%). SEC analysis indicated a product purity of 98% and GC analysis 90%.

[I] The synthesis was carried out by REBECCA SEIM under the lab-supervision of PHILIPP BOHN, who evaluated the obtained results.

^{1}H NMR (400 MHz $CDCl_3$): δ / ppm = 5.77 (s, 1H, NH^{1}), 5.27 (d, *J* = 3.7 Hz, 1H, CH^{2}), 3.00 (s, 1H, CH^{3}), 1.91 – 1.79 (m, 1H, CH^{4}), 1.53 – 1.38 (m, 2H, CH_2^{5}), 1.36 (s, 9H, CH_3^{6}), 1.33 – 1.18 (m, 3H, CH_2^{5}), 0.93 (td, *J* = 7.5, 3.7 Hz, 6H, CH_3^{7}).

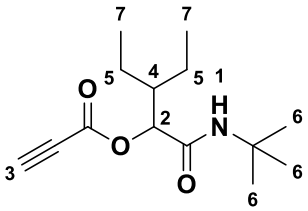

^{13}C NMR (101 MHz $CDCl_3$): δ / ppm = 167.79 (C^{1}), 151.52 (C^{2}), 77.28 (C^{3}), 76.43 (C^{4}), 74.16 (C^{5}), 51.67 (C^{6}), 43.81 (C^{7}), 28.78 (C^{8}), 22.27 (C^{9}), 21.94 (C^{9}), 11.74 (C^{10}), 11.69 (C^{10}).

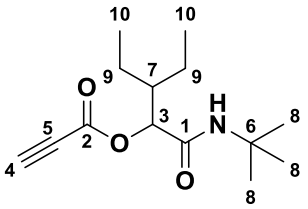

HRMS (ESI) of $C_{14}H_{23}NO_3$ $[M+H]^+$ *m/z* calc. 254.1751, found 254.1754.

R_f = 0.30 (cyhex:EA = 5:1)

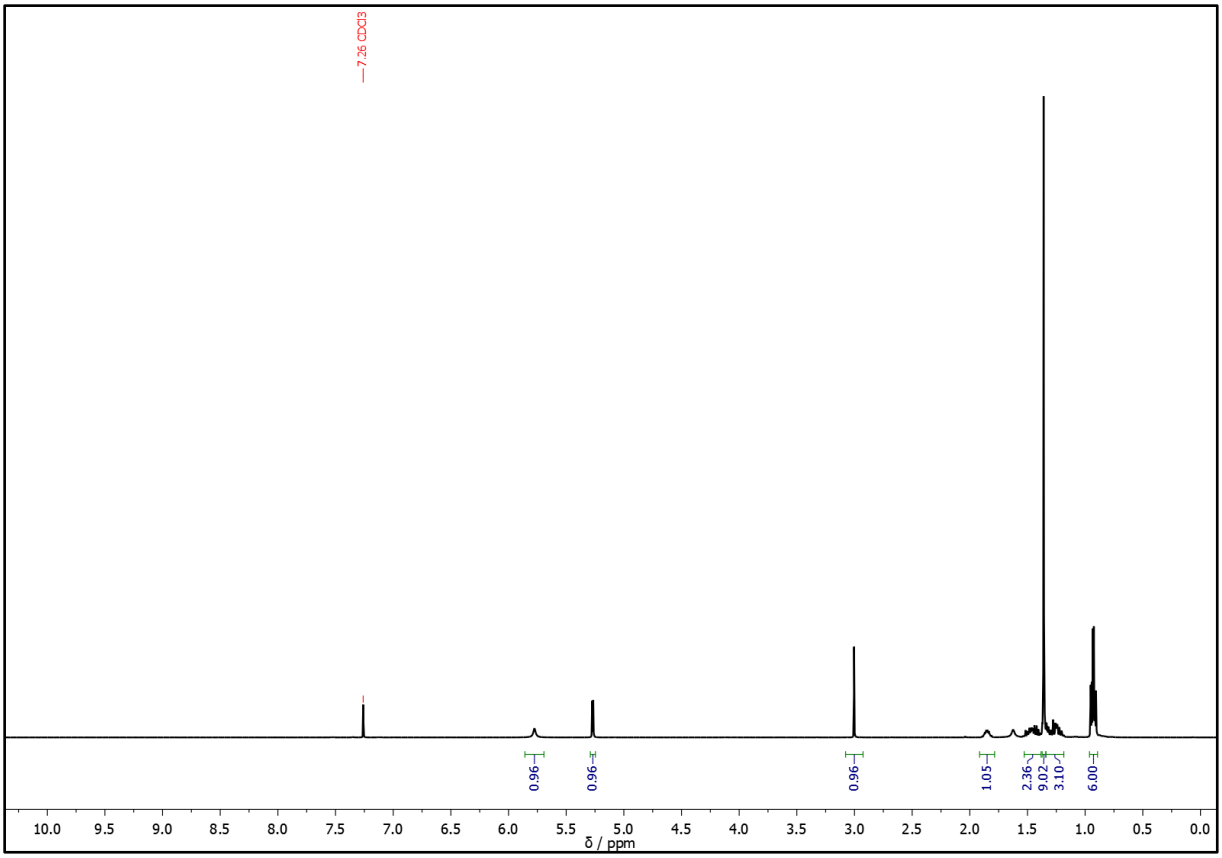

Supplementary Figure 176: ^{1}H NMR spectrum of **S2** recorded at 400 MHz in $CDCl_3$.

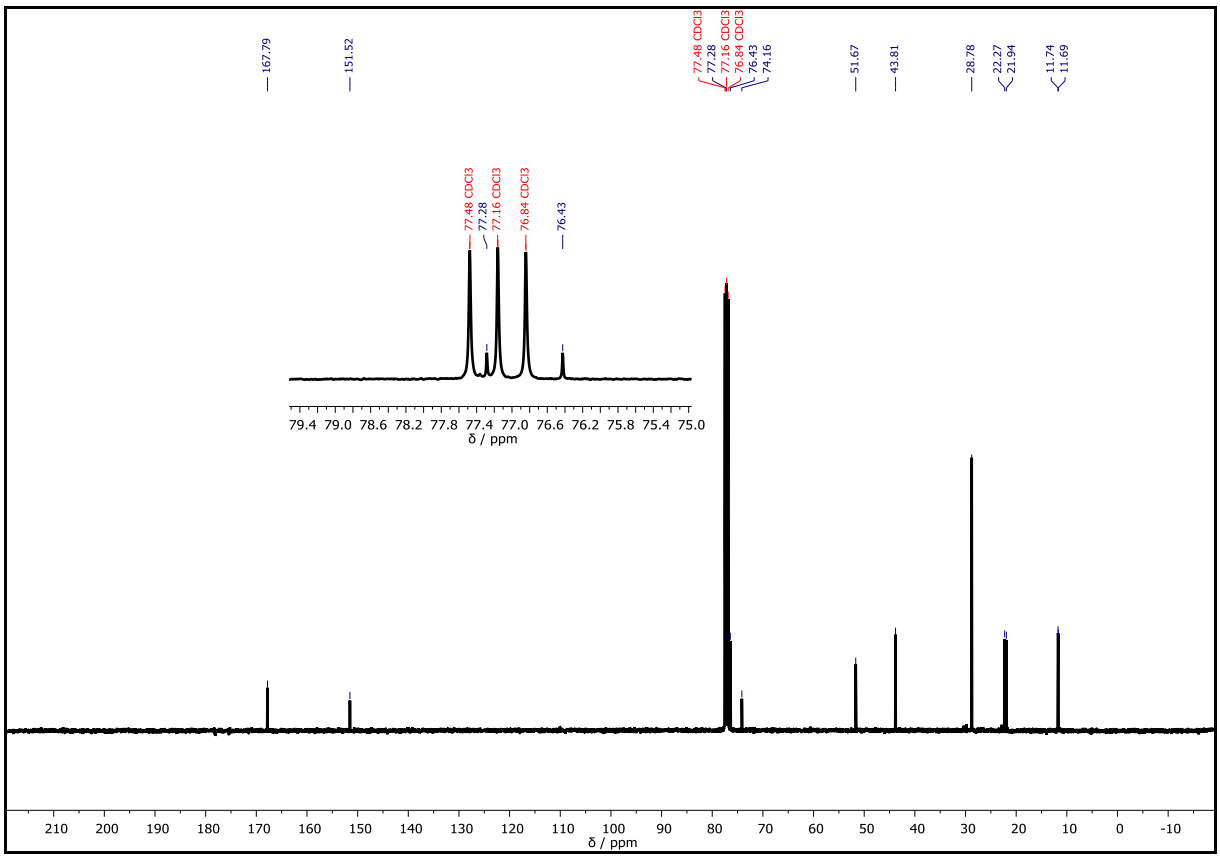

Supplementary Figure 177: ^{13}C NMR spectrum of **S2** recorded at 400 MHz in $CDCl_3$.

1-(*tert*-Butylamino)-3-ethyl-1-oxopentan-2-yl (*E*)-3-(4-formylphenoxy)acrylate – S3[I]

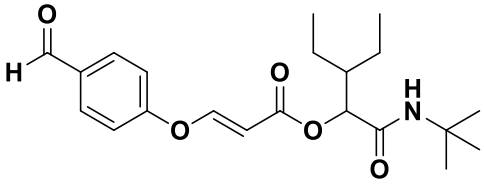

Chemical Formula: $C_{21}H_{29}NO_5$
Exact Mass: 375.2046 Da
Molecular Weight: 375.4650 Da

Propiolic acid (744 µL, 841 mg, 12.0 mmol, 1.00 equiv.) and 2-ethylbutyraldehyde (1.48 mL, 1.20 g, 12.0 mmol, 1.00 eq.) were dissolved in DCM (12.0 mL). Subsequently, *tert*-butyl isocyanide (1.36 mL, 998 mg, 12.0 mmol, 1.00 eq.) was added dropwise and the reaction mixture was stirred overnight at room temperature. After full conversion indicated by GC-FID, 4-hydroxybenzaldehyde (1.46 g, 12.0 mmol, 1.00 equiv.) and DABCO (135 mg, 1.20 mmol, 0.10 equiv.) were added at 0 °C. The reaction mixture was stirred overnight at room temperature. The mixture was washed with water (2 × 10 mL), the phases were separated, and the organic layer was dried over anhydrous sodium sulfate, filtered, and the solvent was removed under reduced pressure. Purification of the crude product *via* column chromatography (cyhex:EA = 4:1) yielded product **S3** as a yellowish liquid (2.93 g, 7.80 mmol, 65%).

^{1}H NMR (400 MHz $CDCl_3$): δ / ppm = 9.98 (s, 1H, CHO^1), 7.97 – 7.93 (m, 2H, $CH_{Ar}{}^2$), 7.91 (d, *J* = 12.1 Hz, 1H, CH^3), 7.25 – 7.20 (m, 2H, $CH_{Ar}{}^4$), 5.78 (d, *J* = 12.1 Hz, 1H, CH^5), 5.75 (s, 1H, NH^6), 5.25 (d, *J* = 3.9 Hz, 1H, CH^7), 1.94 – 1.83 (m, 1H, CH^8), 1.53 – 1.40 (m, 2H, $CH_2{}^9$), 1.35 (s, 9H, $CH_3{}^{10}$), 1.30 – 1.19 (m, 2H, $CH_2{}^9$), 0.93 (q, *J* = 7.4 Hz, 6H, $CH_3{}^{11}$).

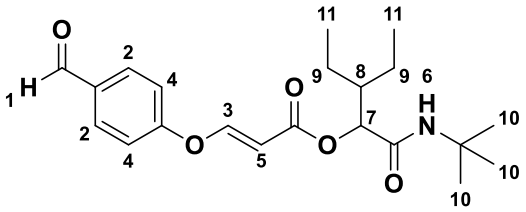

[I] The synthesis was carried out by REBECCA SEIM under the lab-supervision of PHILIPP BOHN, who evaluated the obtained results.

^{13}C NMR (101 MHz $CDCl_3$): δ / ppm = 190.57 (C_q^1), 168.92 (C_q^2), 165.75 (C_q^3), 160.14 ($C_{q,Ar}^4$), 158.00 (CH^5), 133.45 ($C_{q,Ar}^6$), 132.18 (CH_{Ar}^7), 118.02 (CH_{Ar}^8), 103.38 (CH^9), 75.38 (CH^{10}), 51.47 (C_q^{11}), 43.65 (CH^{12}), 28.83 (CH_3^{13}), 22.40 (CH_2^{13}), 22.05 (CH_2^{13}), 11.75 (CH_3^{14}).

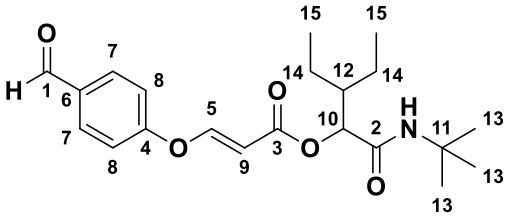

HRMS (ESI) of $C_{21}H_{29}NO_5$ $[M+H]^+$ *m/z* calc. 376.2118, found 376.2114.

IR (ATR platinum diamond) *v* / cm^{-1} = 3336.0, 2963.8, 2876.0, 1697.1, 1651.1, 1593.0, 1503.1, 1454.9, 1391.8, 1364.2, 1298.1, 1209.9, 1157.6, 1099.3, 1047.9, 1012.0, 947.6, 833.2, 713.3, 646.0, 615.3, 517.4.

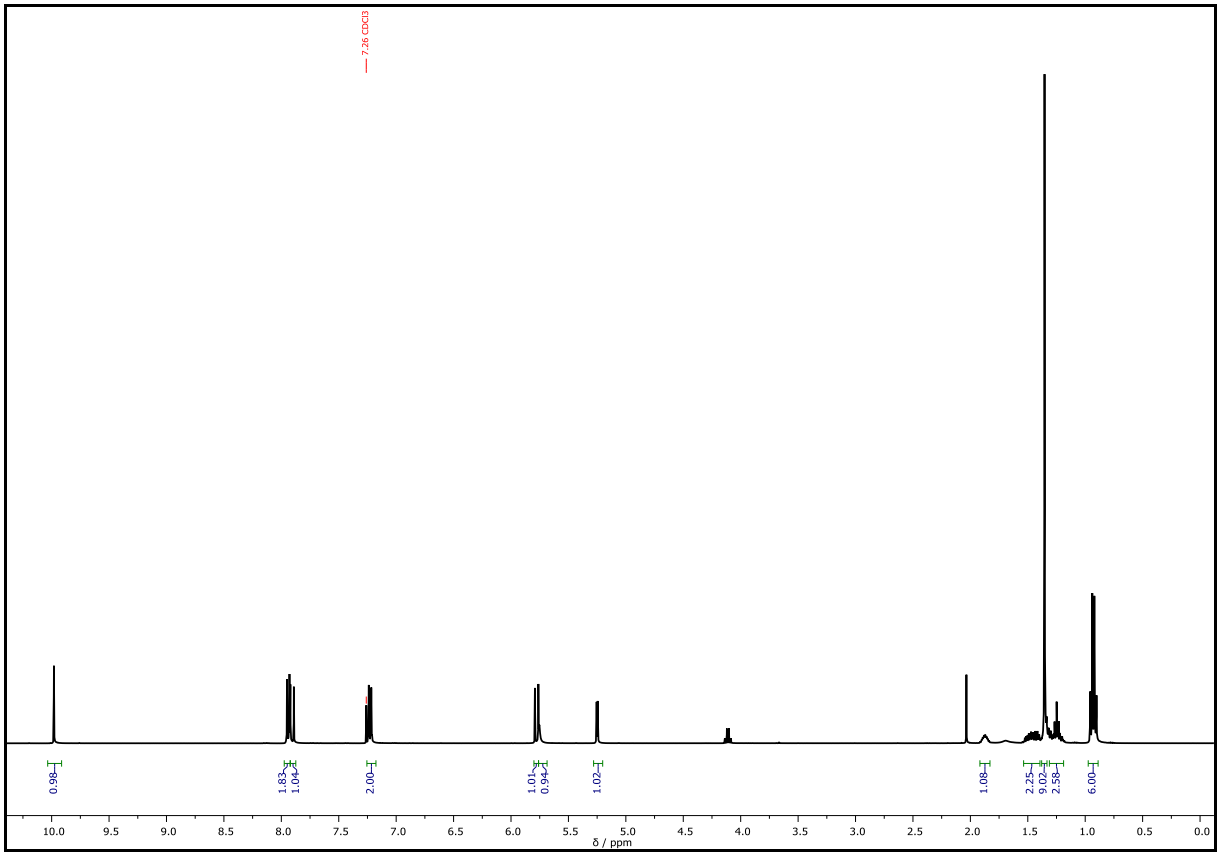

Supplementary Figure 178: ^{1}H NMR spectrum of **S3** recorded at 400 MHz in $CDCl_3$.

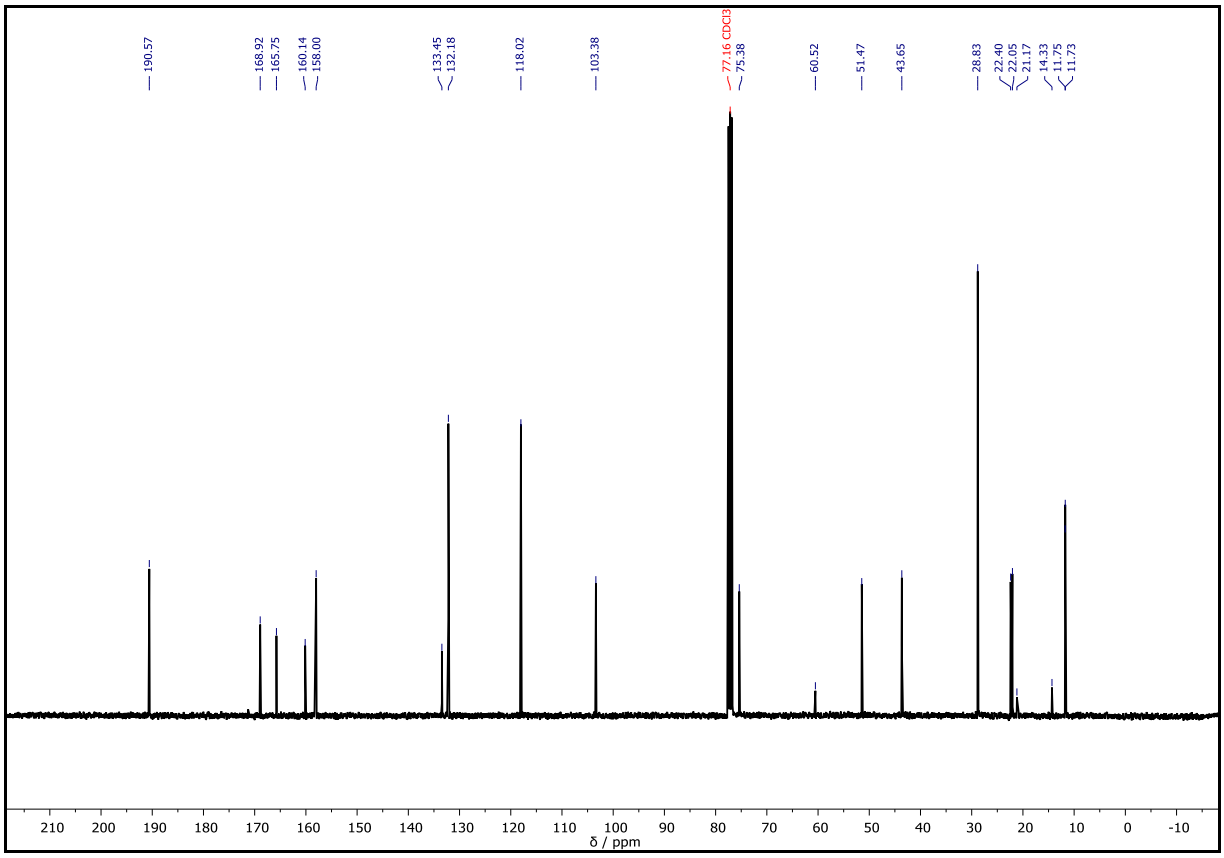

Supplementary Figure 179: ^{13}C NMR spectrum of **S3** recorded at 400 MHz in $CDCl_3$.

1-(*tert*-Butylamino)-3-ethyl-1-oxopentan-2-yl (E)-3-(4-(2-(cyclohexylamino)-2-oxo-1-(propioloyloxy)ethyl)phenoxy)acrylate – S4[l]

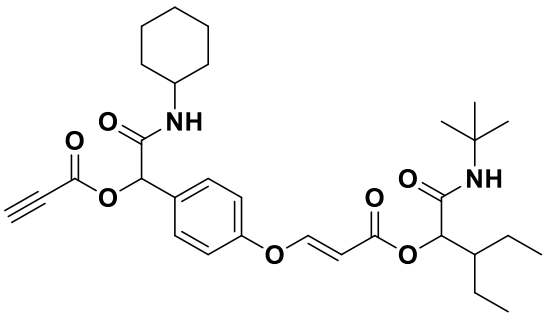

Chemical Formula: $C_{31}H_{42}N_2O_7$
Exact Mass: 554.2992 Da
Molecular Weight: 554.6840 Da

Propiolic acid (250 µL, 283 mg, 4.04 mmol, 1.00 equiv.) and aldehyde **S3** (2.24 g, 4.04 mmol, 1.00 equiv.) were dissolved in DCM (4.00 mL). Subsequently, cyclohexyl isocyanide (502 µL, 441 mg, 4.04 mmol, 1.00 equiv.) was added dropwise and the solution was stirred at room temperature overnight. Purification of the crude product

[l] The synthesis was carried out by REBECCA SEIM under the lab-supervision of PHILIPP BOHN, who evaluated the obtained results.

via column chromatography (cyhex:EA = 1:0 → 9:1 → 4:1 → 7:3) yielded the product as a yellowish viscous liquid (357 mg, 644 µmol, 16%).

Note: further 0.2 equiv. of propiolic acid and cyclohexyl isocyanide were added, but only 72% conversion was achieved.

^{1}H NMR (400 MHz $CDCl_3$): δ / ppm = 7.83 (d, *J* = 12.1 Hz, 1H, CH^{1}), 7.47 (d, *J* = 8.6 Hz, 2H, $CH_{Ar}{}^{2}$), 7.09 (d, *J* = 8.7 Hz, 2H, $CH_{Ar}{}^{3}$), 6.10 (d, *J* = 3.1 Hz, 2H, CH^{4} and NH^{4}), 5.76 (s, 1H, NH^{5}), 5.64 (d, *J* = 12.2 Hz, 1H, CH^{6}), 5.26 (d, *J* = 3.7 Hz, 1H, CH^{7}), 3.90 – 3.73 (m, 1H, CH^{8}), 3.03 (s, 1H, CH^{9}), 1.97 – 1.60 (m, 7H, $CH_2{}^{10}$, CH^{10}), 1.52 – 1.40 (m, 3H, $CH_2{}^{10}$, CH^{10}), 1.35 (s, 9H, $CH_3{}^{11}$), 1.29 – 1.15 (m, 6H, $CH_2{}^{10}$, CH^{10}), 0.93 (2 × t, *J* = 7.3 Hz, 6H, $CH_3{}^{12}$).

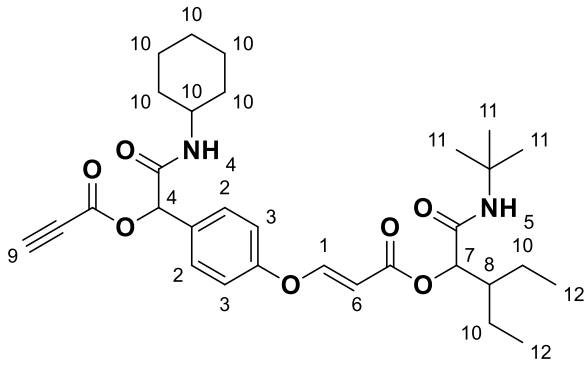

^{13}C NMR (101 MHz $CDCl_3$): δ / ppm = 169.12, 165.98, 159.66, 156.34, 150.67, 132.05, 129.68, 118.47, 101.81, 76.22, 75.14, 73.97, 51.43, 48.63, 43.72, 33.12, 33.02, 28.85, 25.55, 24.89, 22.46, 22.11, 11.82, 11.79.

HRMS (ESI) of $C_{14}H_{23}NO_3$ $[M+H]^+$ *m/z* calc. 555.3065, found 555.3066.

R_f = 0.25 (cyhex:EA = 7:3)

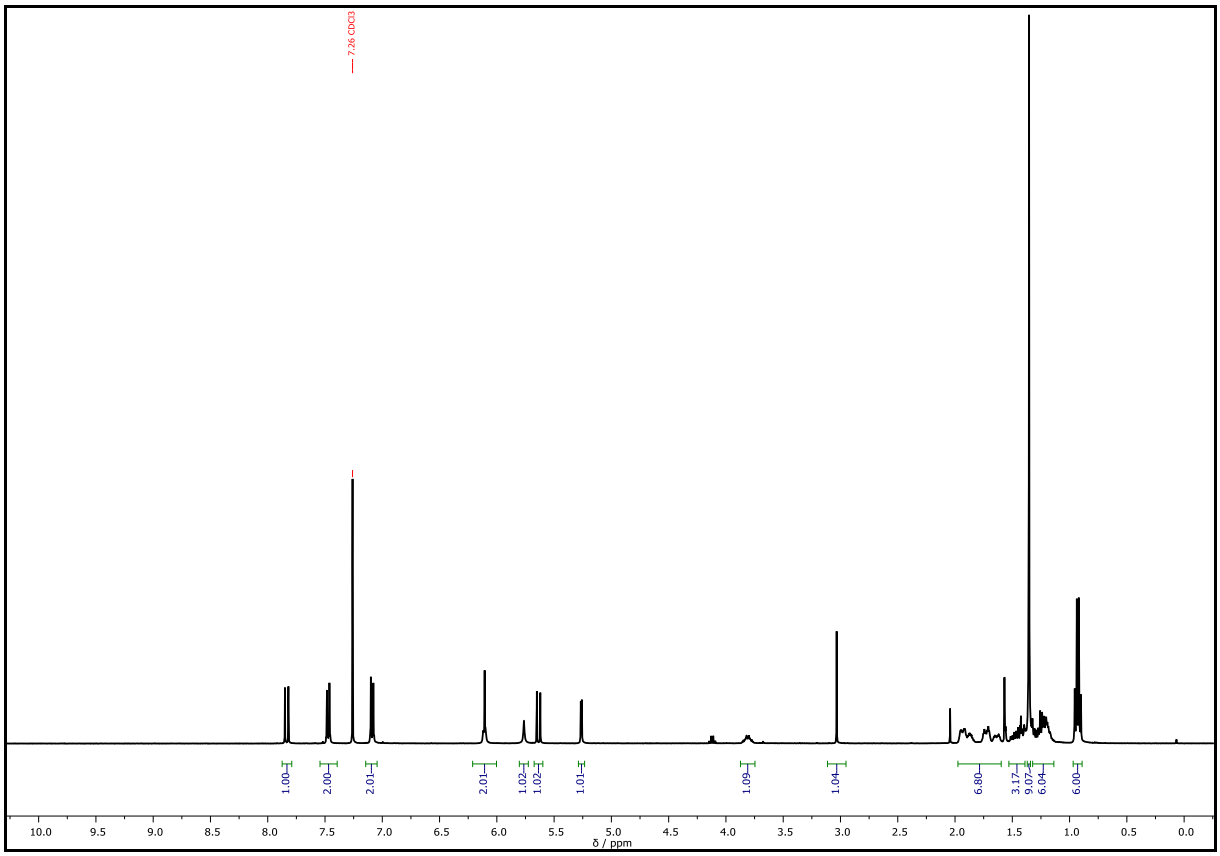

Supplementary Figure 180: ^{1}H NMR spectrum of **S4** recorded at 400 MHz in $CDCl_3$.

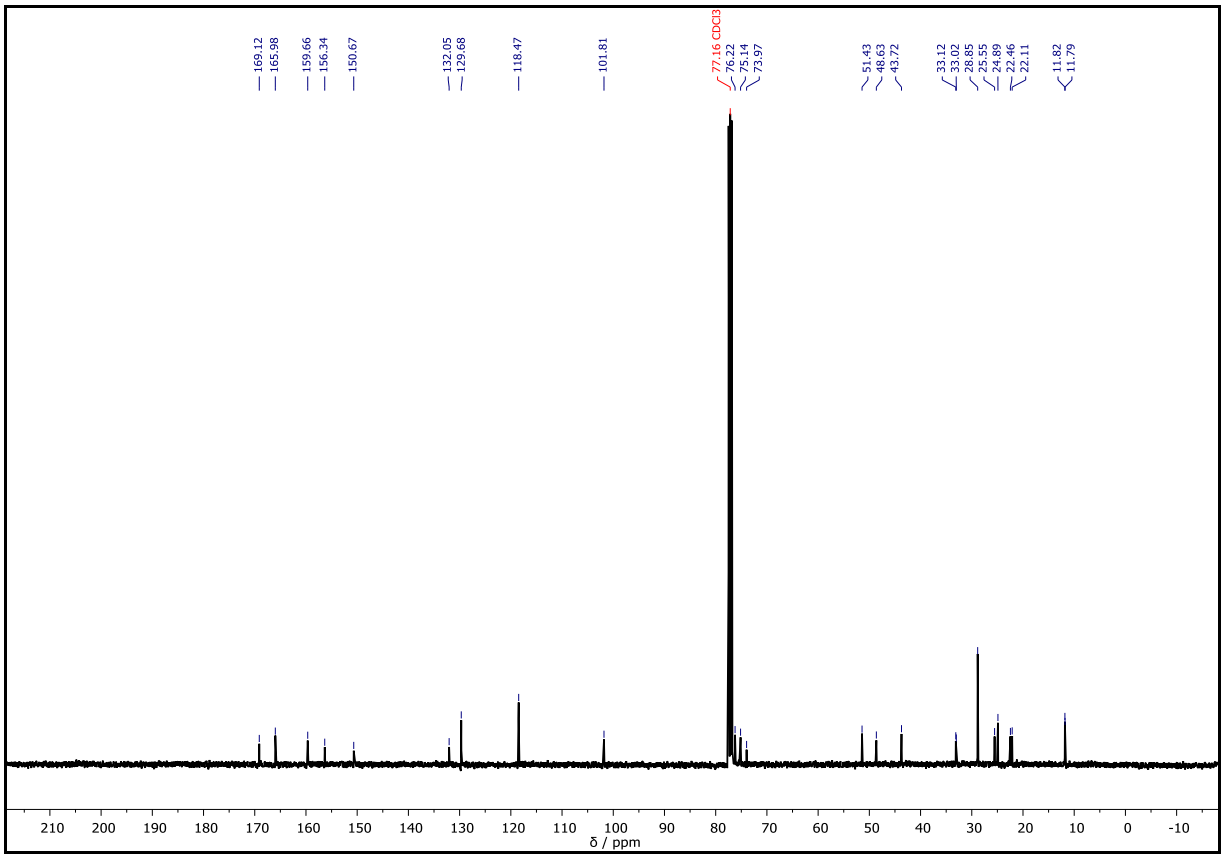

Supplementary Figure 181: ^{13}C NMR spectrum of **S4** recorded at 400 MHz in $CDCl_3$.

1-(*tert*-Butylamino)-3-ethyl-1-oxopentan-2-yl (*E*)-3-(4-(2-(cyclohexylamino)-1-(((*E*)-3-(4-formyl-2-methoxyphenoxy)acryloyl)oxy)-2-oxoethyl)phenoxy)acrylate – S5[I]

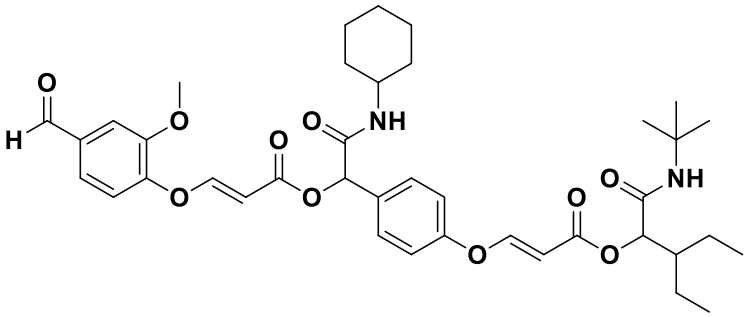

Chemical Formula: $C_{39}H_{50}N_2O_{10}$
Exact Mass: 706.3465 Da
Molecular Weight: 706.8330 Da

Vanillin (75.2 mg, 494 µmol, 1.00 equiv.) and DABCO (5.50 mg, 49.4 mmol, 0.10 equiv.) were added to a stirring solution of product **S4** (274 mg, 494 µmol, 1.00 equiv.) in DCM (500 µL). The reaction mixture was stirred at room temperature overnight and SEC indicated full conversion. DCM (5 mL) as added, and the solution was washed with water (2 × 5 mL). The phases were separated, the organic layer was dried over anhydrous sodium sulfate, filtered, and the solvent was removed under reduced pressure. Purification of the crude product *via* column chromatography (cyhex:EA = 5:1 → 4:1 → 2:1) yielded product **S5** as a yellowish viscous liquid (349 mg, 403 µmol, 82%).

^{1}H NMR (400 MHz $CDCl_3$): δ / ppm = 9.95 (s, 1H, CHO^1), 7.83 (2 × d, *J* = 12.2 Hz, 2H, CH2 and CH^3), 7.54 – 7.44 (m, 4H, CH_{Ar}^{4} and CH_{Ar}^{5}), 7.22 (d, *J* = 8.0 Hz, 1H, CH_{Ar}^{6}), 7.10 – 7.04 (m, 2H, CH_{Ar}^{7}), 6.13 (s, 1H, CH^8), 6.04 (d, *J* = 8.3 Hz, 1H, NH^9), 5.76 (s, 1H, NH^{10}), 5.68 (d, *J* = 12.2 Hz, 1H, CH^{11}), 5.62 (d, *J* = 12.2 Hz, 1H, CH^{12}), 5.26 (d, *J* = 3.7 Hz, 1H, CH^{13}), 3.94 (s, 3H, CH_3^{14}), 3.86 – 3.75 (m, 1H, CH^{15}), 1.97 – 1.60 (m, 6H, CH_2^{16} and CH_2^{16}), 1.52 – 1.38 (m, 3H, CH_2^{16} and CH_2^{16}), 1.35 (s, 9H, CH_3^{17}), 1.32 – 1.10 (m, 6H, CH_2^{16} and CH_2^{16}), 0.93 (2 × t, *J* = 7.3 Hz, 6H).

[I] The synthesis was carried out by REBECCA SEIM under the lab-supervision of PHILIPP BOHN, who evaluated the obtained results.

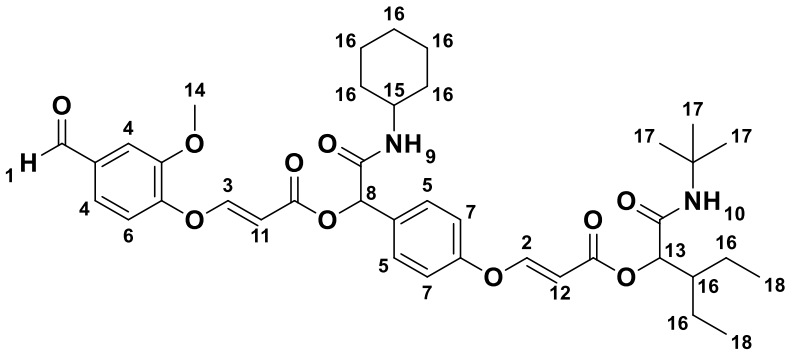

HRMS (ESI) of $C_{14}H_{23}NO_3$ $[M+H]^+$ *m/z* calc. 707.3538, found 707.3530.

R_f = 0.60 (cyhex:EA = 2:1)

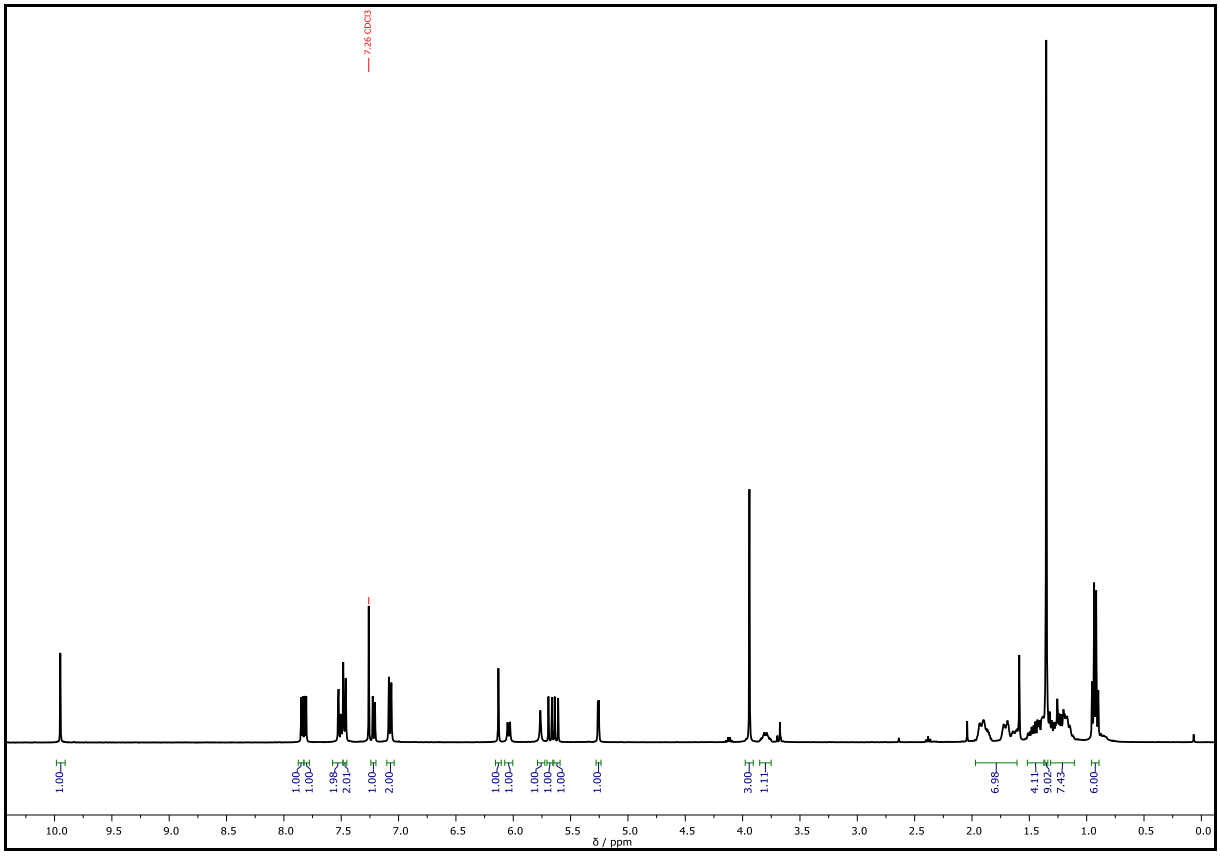

Supplementary Figure 182: ^{1}H NMR spectrum of **S5** recorded at 400 MHz in $CDCl_3$.

6.3.8. Experimental procedures of chapter 4.6.2

Synthesis of compound library *via* P-3CR and subsequent hetero Michael addition

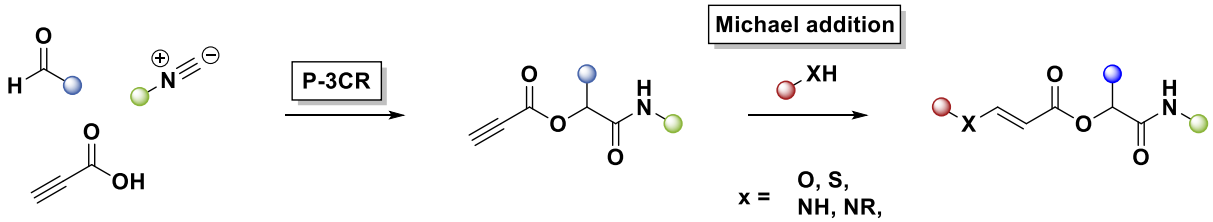

Supplementary Scheme 1: General reaction scheme for the P-3CR and subsequent hetero-Michael addition, using primary and secondary amines, alcohols, and thiols as nucleophiles.

Prior the synthesis, a Design of Experiments (DoE) based on the logP value per connolly molecular area (CMA)[I] was conducted. In case of the reaction approach depicted in Supplementary Scheme 1, the logP value per CMA of the three variable components (aldehyde, isocyanide, and nucleophile) are the adjustable parameters. A list of the logP per CMA ratios of the complete compound libraries is provided as supplementary information on the CD. Using a database of commercially available components (160 aldehydes, 32 isocyanides, 229 primary and secondary amines, 54 thiols, and 231 alcohols) and considering all permutations, 2.63 M unique structures are accessible with the described approach. 25 different P-3CR products were synthesized and reacted with an unpolar and a polar nucleophile, respectively. Thus, in total 150 different molecules were prepared and analyzed *via* ESI-MS. For individual compounds also the characterization *via* NMR spectroscopy is demonstrated (please note: within the framework of this project, the focus was on the identification of the molecular structure *via* tandem MS). The compound combinations dependent on their logP value per Connolly Molecular Area (CMA) are depicted as colored spheres for the alcohols in Supplementary Figure 183, for the thiols in Supplementary Figure 184 and for the amines in Figure 62. In case of using amines as nucleophiles, also the reaction for the component combinations in the middle of the cube was conducted.

[I] The contact surface created when a spherical probe is rolled over the molecular model.

For demonstration purposes, only the analysis of the corner combinations of the DoEs and their corresponding Passerini precursors are shown here in detail (if NMR analysis was performed). The calculated and found masses (*via* ESI-MS) of all compounds are summarized in Supplementary Table 23 - Supplementary Table 29. Further evaluated NMR analyses of individual combinations are provided as supplementary information on the CD.

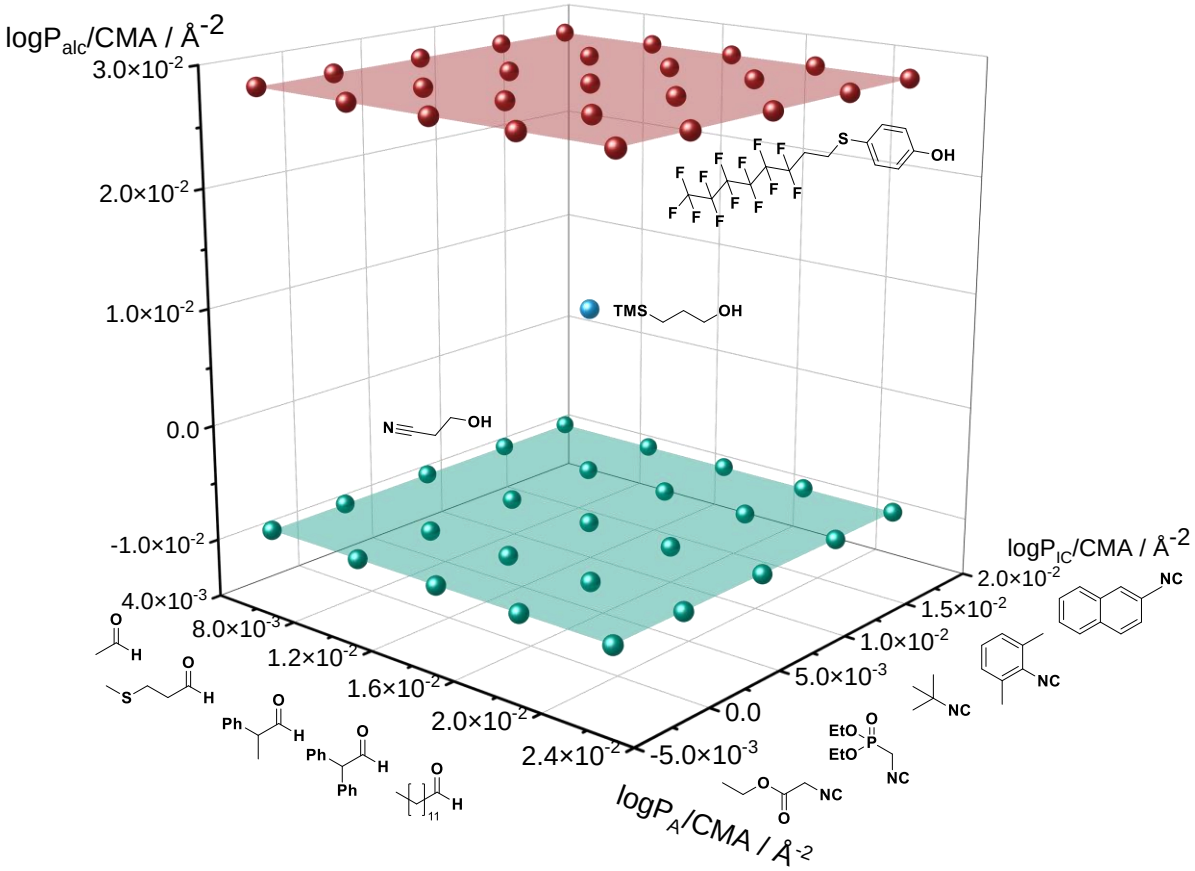

Supplementary Figure 183: DoE based on the logP/CMA ratio of the components used for a Passerini reaction and subsequent hydroxy-yne Michael addition shown in Supplementary Scheme 1.

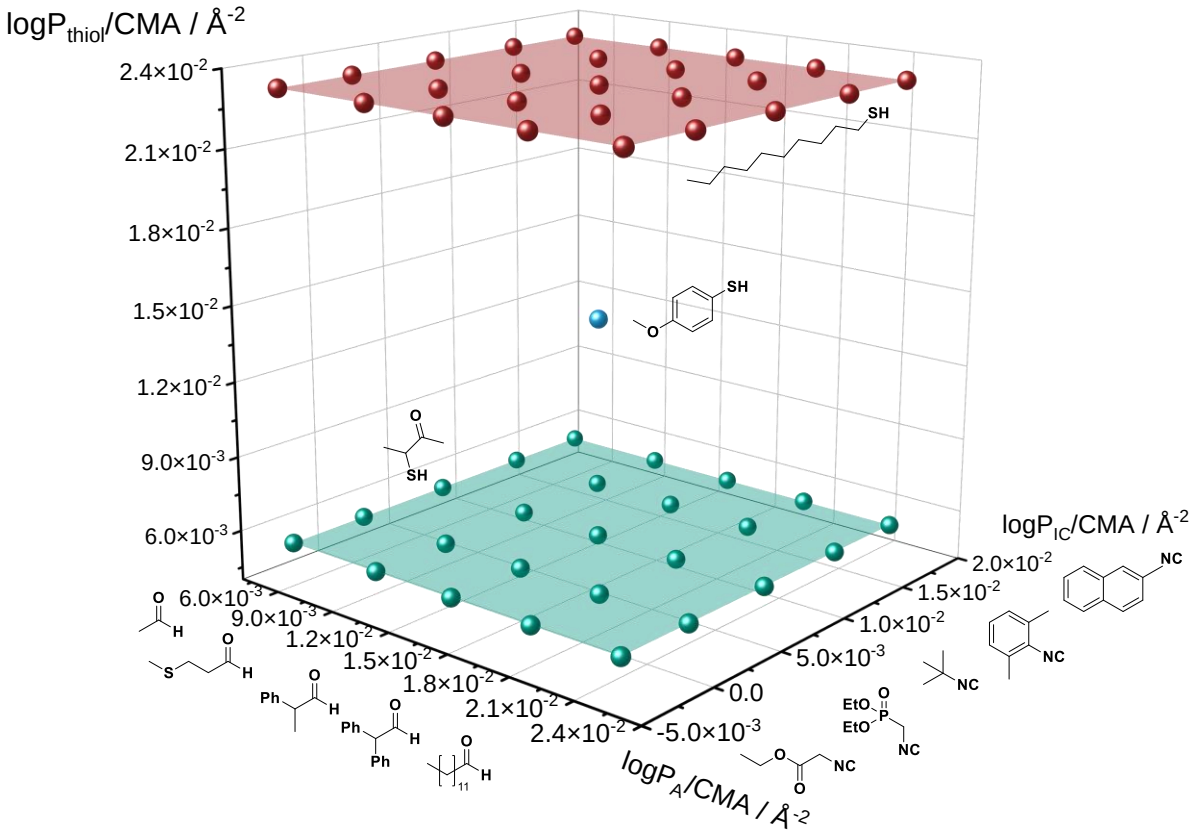

Supplementary Figure 184: DoE based on the logP/CMA ratio of the components used for a Passerini reaction and subsequent thiol-yne Michael addition shown in Supplementary Scheme 1.

General procedure

Propiolic acid (1.00 equiv.) and the respective aldehyde **I**-**V** (1.00 equiv.) were dissolved in DCM (250 µL) and the corresponding isocyanide **α**-**ε** (1.00 equiv.) was added slowly to the solution. The reaction mixture was stirred overnight at room temperature and the respective nucleophile (1.00 equiv.) and if required a catalyst (0.1 equiv.) were added. After stirring the mixture another 12 hours at room temperature, the solvent was removed under reduced pressure. Purification of the crude product *via* column chromatography yielded the product.

All reactions were performed on a 250 µmol scale. The quantities of the starting materials are listed in Supplementary Table 21.

Supplementary Table 21: Quantities of starting materials for the P-3CR and subsequent hetero-Michael addition.

Carboxylic acid	V / µL	m / mg
Propiolic acid	15.5	17.5
Aldehydes		
I Acetaldehyde (3.00 equiv.)	42.2	33.1
II 3-(Methylthio)propanal	25.0	26.0
III DL-2-Phenylpropionaldehyde	33.5	33.5
IV Diphenyl acetaldehyde	44.4	49.06
V Dodecyl aldehyde	55.5	46.1
Isocyanides		
α Ethyl isocyanoacetate	27.3	28.3
β Diethyl isocyanomethylphosphonate	40.4	44.3
χ *tert*-Butyl isocyanide	28.3	20.8
δ 2,6-Dimethylphenyl isocyanide	-	32.8
ε 2-Naphthyl isocyanide	-	38.3
Amines		
a1 3,3'-Iminodipropionitrile	30.2	30.8
a2 Bis(2-ethylhexyl)amine	75.0	60.4
a3 Diallyl amine	30.7	24.3
Alcohols		
b1 3-Hydroxypropannitrile	16.8	17.8
b2 4-(3,3,4,4,5,5,6,6,7,7,8,8,8)-Tridecafluorooctylthiol)-phenol	-	118
Thiols		
c1 3-Mercapto-2-butanone	25.2	26.0
c2 1-Decanthiol	51.9	43.6

Supplementary Table 22: Molecular nomenclature.

	α	β	χ	δ	ε
I	**D1xy**	**D6xy**	**D11xy**	**D16xy**	**D21xy**
II	**D2xy**	**D7xy**	**D12xy**	**D17xy**	**D22xy**
III	**D3xy**	**D8xy**	**D13xy**	**D18xy**	**D23xy**
IV	**D4xy**	**D9xy**	**D14xy**	**D19xy**	**D24xy**
V	**D5xy**	**D10xy**	**D15xy**	**D20xy**	**D25xy**
x = class of nucleophile (a for amines, b for alcohols, and c for thiols); y = polarity of nucleophile (1 = polar; 2 = unpolar; 3 = center point); I-V = type of aldehyde; α-ε = type of isocyanide.					

Supplementary Table 23: Summary of the masses of the Passerini precursor molecules **D1**-**D25** calculated and found for the respective proton adducts $[M+H]^+$ *via* ESI-MS.

compound	formular	*m*/*z* calculated / Da	*m*/*z* found / Da
D1	$C_{10}H_{13}NO_5$	228.0866	228.0864
D2	$C_{12}H_{17}NO_5S$	288.0900	288.0897
D3	$C_{17}H_{19}NO_5$	318.1336	318.1333
D4	$C_{22}H_{21}NO_5$	380.1492	*n.a.*
D5	$C_{20}H_{33}NO_5$	368.2431	368.2429
D6	$C_{11}H_{18}NO_6P$	292.0945	292.0941
D7	$C_{13}H_{22}NO_6PS$	352.0978	352.0975
D8	$C_{18}H_{24}NO_6P$	382.1414	382.1411
D9	$C_{23}H_{26}NO_6P$	444.1571	*n.a.*
D10	$C_{21}H_{38}NO_6P$	432.2510	432.2507
D11	$C_{10}H_{15}NO_3$	198.1125	198.1124
D12	$C_{12}H_{19}NO_3S$	258.1158	258.1157
D13	$C_{17}H_{21}NO_3$	288.1594	*n.a.*
D14	$C_{22}H_{23}NO_3$	350.1751	*n.a.*
D15	$C_{20}H_{35}NO_3$	338.2690	338.2685
D16	$C_{14}H_{15}NO_3$	246.1125	246.1123
D17	$C_{16}H_{19}NO_3S$	306.1158	306.1155
D18	$C_{21}H_{21}NO_3$	336.1594	336.1590
D19	$C_{26}H_{23}NO_3$	398.1751	*n.a.*
D20	$C_{24}H_{35}NO_3$	386.2687	386.2687
D21	$C_{16}H_{13}NO_3$	268.0968	268.0966
D22	$C_{18}H_{17}NO_3S$	328.1002	*n.a.*
D23	$C_{23}H_{19}NO_3$	358.1438	358.1434
D24	$C_{28}H_{21}NO_3$	420.1594	*n.a.*
D25	$C_{26}H_{33}NO_3$	408.2533	*n.a.*

Supplementary Table 24: Summary of the molecule masses of **D1a1**-**D25a1** calculated and found for the respective proton adducts $[M+H]^+$ *via* ESI-MS.

compound	formular	*m*/*z* calculated / Da	*m*/*z* found / Da
D1a1	$C_{16}H_{22}N_4O_5$	351.1663	351.1661
D2a1	$C_{18}H_{26}N_4O_5S$	411.1697	411.1693
D3a1	$C_{23}H_{28}N_4O_5$	441.2132	441.2132
D4a1	$C_{28}H_{30}N_4O_5$	503.2289	503.2286
D5a1	$C_{26}H_{42}N_4O_5$	491.3228	491.3227
D6a1	$C_{17}H_{27}N_4O_6P$	415.1741	415.1740
D7a1	$C_{19}H_{31}N_4O_6PS$	475.1775	475.1774
D8a1	$C_{24}H_{33}N_4O_6P$	505.2210	505.2210
D9a1	$C_{29}H_{35}N_4O_6P$	567.2367	567.2366
D10a1	$C_{27}H_{47}N_4O_6P$	555.3306	555.3306
D11a1	$C_{16}H_{24}N_4O_3$	321.1921	321.1920
D12a1	$C_{18}H_{28}N_4O_3S$	381.1955	381.1951
D13a1	$C_{23}H_{30}N_4O_3$	411.2391	411.2388
D14a1	$C_{28}H_{32}N_4O_3$	473.2547	473.2547
D15a1	$C_{26}H_{44}N_4O_3$	461.3486	461.3486
D16a1	$C_{20}H_{24}N_4O_3$	369.1921	369.1918
D17a1	$C_{22}H_{28}N_4O_3S$	429.1955	429.1953
D18a1	$C_{27}H_{30}N_4O_3$	459.2391	459.2388
D19a1	$C_{32}H_{32}N_4O_3$	521.2547	521.2540
D20a1	$C_{30}H_{44}N_4O_3$	509.3486	509.3486
D21a1	$C_{22}H_{22}N_4O_3$	391.1765	391.1764
D22a1	$C_{24}H_{26}N_4O_3S$	451.1798	451.1797
D23a1	$C_{29}H_{28}N_4O_3$	481.2234	481.2232
D24a1	$C_{34}H_{30}N_4O_3$	543.2391	543.2390
D25a1	$C_{32}H_{42}N_4O_3$	531.3330	*n.a.*

Supplementary Table 25: Summary of the molecule masses of **D1a2**-**D25a2** calculated and found for the respective proton adducts $[M+H]^+$ *via* ESI-MS.

compound	formular	*m*/*z* calculated / Da	*m*/*z* found / Da
D1a2	$C_{26}H_{48}N_2O_5$	469.3636	469.3632
D2a2	$C_{28}H_{52}N_2O_5S$	529.3670	*n.a.*
D3a2	$C_{33}H_{54}N_2O_5$	559.4105	559.4100
D4a2	$C_{38}H_{56}N_2O_5$	621.4262	621.4255
D5a2	$C_{26}H_{42}N_4O_5$	609.5201	609.5187
D6a2	$C_{27}H_{53}N_2O_6P$	533.3714	533.3708
D7a2	$C_{29}H_{57}N_2O_6PS$	593.3748	593.3741
D8a2	$C_{34}H_{59}N_2O_6P$	623.4184	623.4175
D9a2	$C_{39}H_{61}N_2O_6P$	685.4340	685.4330
D10a2	$C_{37}H_{73}N_2O_6P$	673.5279	673.5263
D11a2	$C_{26}H_{50}N_2O_3$	439.3894	439.3891
D12a2	$C_{28}H_{54}N_2O_3S$	499.3928	499.3927
D13a2	$C_{33}H_{56}N_2O_3$	529.4364	529.4361
D14a2	$C_{38}H_{58}N_2O_3$	591.4520	591.4521
D15a2	$C_{36}H_{70}N_2O_3$	579.5459	579.5458
D16a2	$C_{30}H_{50}N_2O_3$	487.3894	487.3892
D17a2	$C_{32}H_{54}N_2O_3S$	547.3928	547.3928
D18a2	$C_{37}H_{56}N_2O_3$	577.4364	577.4362
D19a2	$C_{42}H_{58}N_2O_3$	639.4520	639.4515
D20a2	$C_{40}H_{70}N_2O_3$	627.5458	627.5459
D21a2	$C_{32}H_{48}N_2O_3$	509.3738	*n.a.*
D22a2	$C_{34}H_{52}N_2O_3S$	569.3771	569.3773
D23a2	$C_{39}H_{54}N_2O_3$	599.4207	599.4209
D24a2	$C_{44}H_{56}N_2O_3$	611.4364	611.4362
D25a2	$C_{42}H_{68}N_2O_3$	649.5303	649.5301

Supplementary Table 26: Summary of the molecule masses of **D1b1**-**D25b1** calculated and found for the respective proton adducts $[M+H]^+$ *via* ESI-MS.

compound	formular	*m*/*z* calculated / Da	*m*/*z* found / Da
D1b1	$C_{13}H_{18}N_2O_6$	299.1238	299.1233
D2b1	$C_{15}H_{22}N_2O_6S$	359.1271	359.1266
D3b1	$C_{20}H_{24}N_2O_6$	389.1707	389.1702
D4b1	$C_{25}H_{26}N_2O_6$	451.1864	451.1860
D5b1	$C_{23}H_{38}N_2O_6$	439.2803	439.2802
D6b1	$C_{14}H_{23}N_2O_7P$	363.1316	363.1311
D7b1	$C_{16}H_{27}N_2O_7PS$	423.1349	423.1347
D8b1	$C_{21}H_{29}N_2O_7P$	453.1785	453.1780
D9b1	$C_{26}H_{31}N_2O_7P$	515.1942	515.1938
D10b1	$C_{24}H_{43}N_2O_7P$	503.2881	503.2878
D11b1	$C_{13}H_{20}N_2O_4$	269.1496	269.1494
D12b1	$C_{15}H_{24}N_2O_4S$	329.1530	329.1527
D13b1	$C_{20}H_{26}N_2O_4$	359.1965	359.1963
D14b1	$C_{25}H_{28}N_2O_4$	421.2122	421.2121
D15b1	$C_{23}H_{40}N_2O_4$	409.3061	409.3058
D16b1	$C_{17}H_{20}N_2O_4$	317.1496	317.1494
D17b1	$C_{19}H_{24}N_2O_4S$	377.1530	377.1528
D18b1	$C_{24}H_{26}N_2O_4$	407.1965	407.1963
D19b1	$C_{29}H_{28}N_2O_4$	469.2122	469.2120
D20b1	$C_{27}H_{40}N_2O_4$	457.3061	457.3058
D21b1	$C_{19}H_{18}N_2O_4$	339.1339	339.1333
D22b1	$C_{21}H_{22}N_2O_4S$	399.1373	339.1366
D23b1	$C_{26}H_{24}N_2O_4$	429.1809	429.1802
D24b1	$C_{31}H_{26}N_2O_4$	491.1965	*n.a.*
D25b1	$C_{29}H_{38}N_2O_4$	479.2904	479.2898

Supplementary Table 27: Summary of the molecule masses of **D1b2**-**D25b2** calculated and found for the respective proton adducts $[M+H]^+$ *via* ESI-MS.

compound	formular	*m*/*z* calculated / Da	*m*/*z* found / Da
D1b2	$C_{24}H_{22}F_{13}NO_6S$	700.1033	700.1030
D2b2	$C_{26}H_{26}F_{13}NO_6S_2$	760.1067	760.1064
D3b2	$C_{31}H_{28}F_{13}NO_6S$	790.1503	790.1492
D4b2	$C_{36}H_{30}F_{13}NO_6S$	851.1659	851.1661
D5b2	$C_{34}H_{42}F_{13}NO_6S$	840.2598	840.2586
D6b2	$C_{25}H_{27}F_{13}NO_7PS$	764.1111	764.1103
D7b2	$C_{27}H_{31}F_{13}NO_7PS_2$	824.1145	824.1142
D8b2	$C_{32}H_{33}F_{13}NO_7PS$	854.1581	854.1577
D9b2	$C_{37}H_{35}F_{13}NO_7PS$	916.1737	916.1727
D10b2	$C_{35}H_{47}F_{13}NO_7PS$	904.2676	904.2673
D11b2	$C_{24}H_{24}F_{13}NO_4S$	670.1291	670.1288
D12b2	$C_{26}H_{28}F_{13}NO_4S_2$	730.1325	*n.a.*
D13b2	$C_{31}H_{30}F_{13}NO_4S$	760.1761	760.1758
D14b2	$C_{36}H_{32}F_{13}NO_4S$	822.1917	822.1912
D15b2	$C_{34}H_{44}F_{13}NO_4S$	810.2856	810.2852
D16b2	$C_{28}H_{24}F_{13}NO_4S$	718.1291	718.1287
D17b2	$C_{30}H_{28}F_{13}NO_4S_2$	778.1325	778.1318
D18b2	$C_{35}H_{30}F_{13}NO_4S$	808.1761	808.1763
D19b2	$C_{40}H_{32}F_{13}NO_4S$	870.1917	870.1916
D20b2	$C_{38}H_{44}F_{13}NO_4S$	858.2856	858.2854
D21b2	$C_{30}H_{22}F_{13}NO_4S$	740.1135	740.1133
D22b2	$C_{32}H_{26}F_{13}NO_4S_2$	800.1168	800.1158
D23b2	$C_{37}H_{28}F_{13}NO_4S$	830.1604	830.1597
D24b2	$C_{42}H_{30}F_{13}NO_4S$	892.1761	892.1757
D25b2	$C_{40}H_{42}F_{13}NO_4S$	880.2700	880.2693

Supplementary Table 28: Summary of the molecule masses of **D1c1**-**D25c1** calculated and found for the respective proton adducts $[M+H]^+$ *via* ESI-MS.

compound	formular	*m*/*z* calculated / Da	*m*/*z* found / Da
D1c1	$C_{14}H_{21}NO_6S$	332.1162	332.1161
D2c1	$C_{16}H_{25}NO_6S_2$	392.1196	392.1194
D3c1	$C_{21}H_{27}NO_6S$	422.1632	422.1630
D4c1	$C_{26}H_{29}NO_6S$	484.1788	484.1788
D5c1	$C_{24}H_{41}NO_6S$	472.2727	472.2728
D6c1	$C_{15}H_{26}NO_7PS$	396.1240	396.1237
D7c1	$C_{17}H_{30}NO_7PS_2$	456.1274	456.1273
D8c1 [M+Na]$^+$	$C_{22}H_{32}NO_7PS$	508.1529	508.1526
D9c1	$C_{27}H_{34}NO_7PS$	548.1866	548.1865
D10c1	$C_{25}H_{46}NO_7PS$	536.2805	*n.a.*
D11c1	$C_{14}H_{23}NO_4S$	302.1421	302.1419
D12c1	$C_{16}H_{27}NO_4S_2$	362.1454	362.1451
D13c1	$C_{21}H_{29}NO_4S$	392.1890	392.1886
D14c1	$C_{26}H_{31}NO_4S$	454.2047	454.2043
D15c1	$C_{24}H_{43}NO_4S$	442.2986	442.2983
D16c1	$C_{18}H_{23}NO_4S$	350.1421	350.1416
D17c1	$C_{20}H_{27}NO_4S_2$	410.1454	410.1449
D18c1	$C_{25}H_{29}NO_4S$	440.1890	*n.a.*
D19c1	$C_{30}H_{31}NO_4S$	502.2047	502.2045
D20c1	$C_{28}H_{43}NO_4S$	490.2986	490.2985
D21c1	$C_{20}H_{21}NO_4S$	372.1264	372.1260
D22c1	$C_{22}H_{25}NO_4S_2$	432.1298	432.1294
D23c1	$C_{27}H_{27}NO_4S$	462.1734	462.1729
D24c1	$C_{32}H_{29}NO_4S$	524.1890	524.1891
D25c1	$C_{30}H_{41}NO_4S$	512.2829	512.2829

Supplementary Table 29: Summary of the molecule masses of **D1c2**-**D25c2** calculated and found for the respective proton adducts $[M+H]^+$ *via* ESI-MS.

compound	formular	*m*/*z* calculated / Da	*m*/*z* found / Da
D1c2	$C_{20}H_{35}NO_5S$	402.2309	402.2302
D2c2	$C_{22}H_{39}NO_5S_2$	462.2342	462.2334
D3c2	$C_{27}H_{41}NO_5S$	492.2778	492.2769
D4c2	$C_{32}H_{43}NO_5S$	554.2935	554.2927
D5c2	$C_{30}H_{55}NO_5S$	542.3874	542.3868
D6c2	$C_{21}H_{40}NO_6PS$	466.2387	466.2388
D7c2	$C_{23}H_{44}NO_6PS_2$	526.2420	526.2420
D8c2	$C_{28}H_{46}NO_6PS$	556.2856	556.2849
D9c2	$C_{33}H_{48}NO_6PS$	618.3013	618.2999
D10c2	$C_{31}H_{60}NO_6PS$	606.3952	606.3951
D11c2	$C_{20}H_{37}NO_3S$	372.2567	372.2563
D12c2	$C_{22}H_{41}NO_3S_2$	432.2601	432.2594
D13c2	$C_{27}H_{43}NO_3S$	462.3036	462.3032
D14c2	$C_{32}H_{45}NO_3S$	524.3193	524.3190
D15c2	$C_{30}H_{57}NO_3S$	512.4123	512.4130
D16c2	$C_{24}H_{37}NO_3S$	420.2567	420.2558
D17c2	$C_{26}H_{41}NO_3S_2$	480.2601	480.2593
D18c2	$C_{31}H_{43}NO_3S$	510.3036	510.3029
D19c2	$C_{36}H_{45}NO_3S$	572.3193	572.3187
D20c2	$C_{34}H_{57}NO_3S$	560.4132	560.4121
D21c2	$C_{26}H_{35}NO_3S$	442.2410	442.2403
D22c2	$C_{28}H_{39}NO_3S_2$	502.2444	502.2437
D23c2	$C_{33}H_{41}NO_3S$	532.2880	532.2873
D24c2	$C_{38}H_{43}NO_3S$	594.3036	594.3030
D25c2	$C_{36}H_{55}NO_3S$	582.3975	582.3965

1-((2-Ethoxy-2-oxoethyl)amino)-1-oxopropan-2-yl propiolate – D1

^{1}H NMR (400 MHz $CDCl_3$): δ / ppm = 6.67 (s, 1H, NH^{1}), 5.33 (q, *J* = 6.8 Hz, 1H, CH^{2}), 4.24 (q, *J* = 7.1 Hz, 2H, CH_2^{3}), 4.14 – 3.98 (m, 2H, CH_2^{4}), 3.00 (s, 1H, CH^{5}), 1.56 (d, *J* = 6.9 Hz, 3H, CH_3^{6}), 1.30 (t, *J* = 7.2 Hz, 3H, CH_3^{7}).

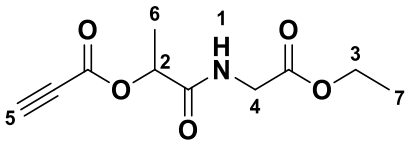

Chemical Formula: $C_{10}H_{13}NO_5$
Exact Mass: 227.0794 Da
Molecular Weight: 227.2160 Da

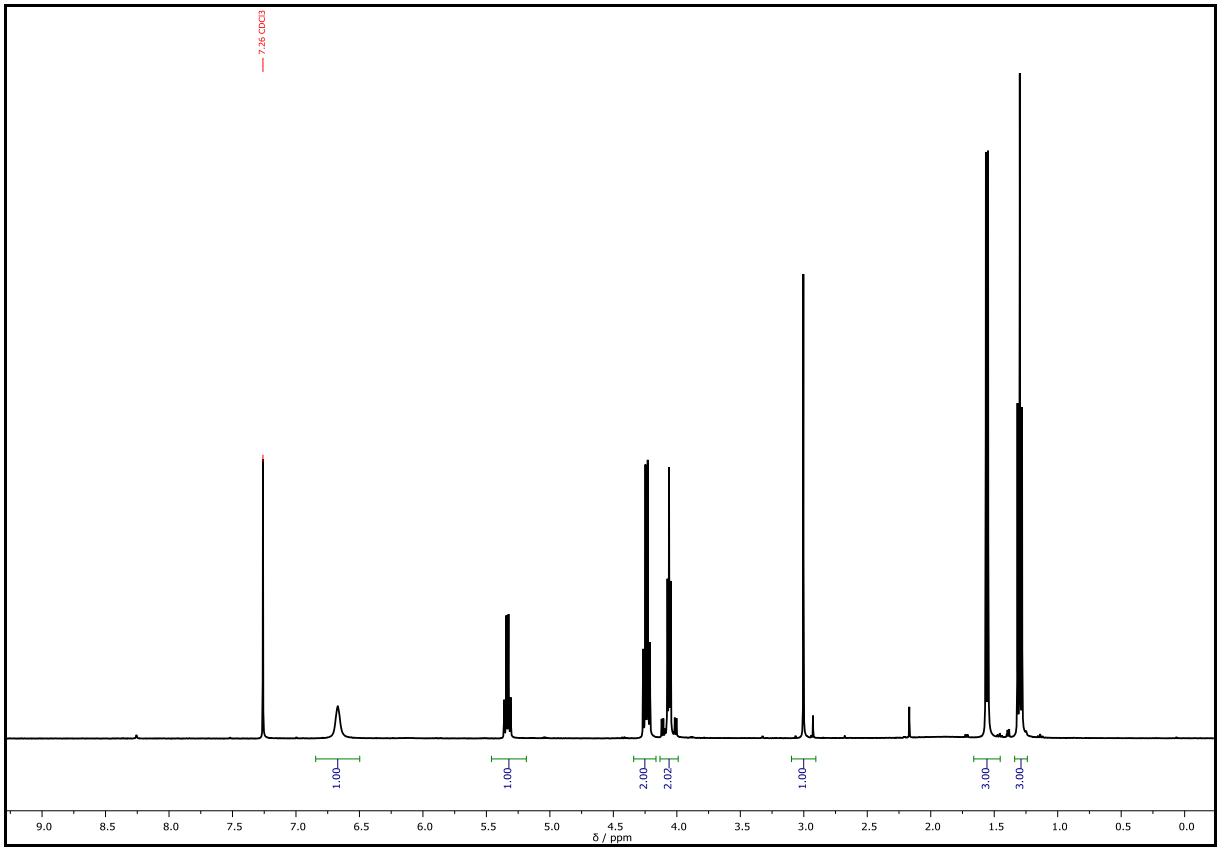

Supplementary Figure 185: ^{1}H NMR spectrum of **D1** recorded at 400 MHz in $CDCl_3$.

1-((2-Ethoxy-2-oxoethyl)amino)-1-oxopropan-2-yl (*E*)-3-(bis(2-cyanoethyl)amino)acrylate – D1a1

^{1}H NMR (400 MHz $CDCl_3$): δ / ppm = 7.49 (d, *J* = 13.5 Hz, 1H, CH^{1}), 6.74 (s, 1H, NH^{2}), 5.31 (q, *J* = 6.8 Hz, 1H, CH^{3}), 4.75 (d, *J* = 13.4 Hz, 1H, CH^{4}), 4.22 (q, *J* = 7.1 Hz, 2H, CH_2^{5}), 4.16 – 3.93 (m, 2H, CH_2^{6}), 3.64 (t, *J* = 6.4 Hz, 4H, CH_2^{7}), 2.69 (t, *J* = 6.4 Hz, 4H, CH_2^{8}), 1.49 (d, *J* = 6.9 Hz, 3H, CH_3^{9}), 1.29 (t, *J* = 7.2 Hz, 3H, CH_3^{10}).

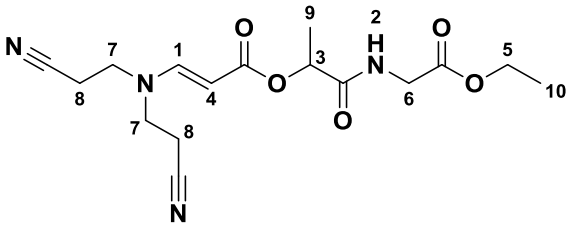

Chemical Formula: $C_{16}H_{22}N_4O_5$
Exact Mass: 350.1590 Da
Molecular Weight: 350.3750 Da

^{13}C NMR (101 MHz, $CDCl_3$) δ / ppm = 171.49 (C_q^{1}), 170.00 (C_q^{2}), 166.73 (C_q^{3}), 150.17 (CH^{4}), 117.29 (C_q^{5}), 88.38 (CH^{6}), 69.66 (CH^{7}), 61.79 (CH_2^{8}), 48.33 (CH_2^{9}), 41.16 (CH_2^{10}), 18.10 (CH_3^{11}), 17.01 (CH_2^{12}) 14.27 (CH_3^{13}).

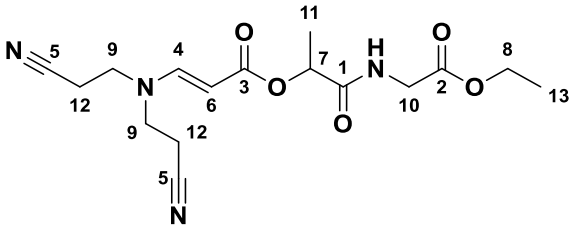

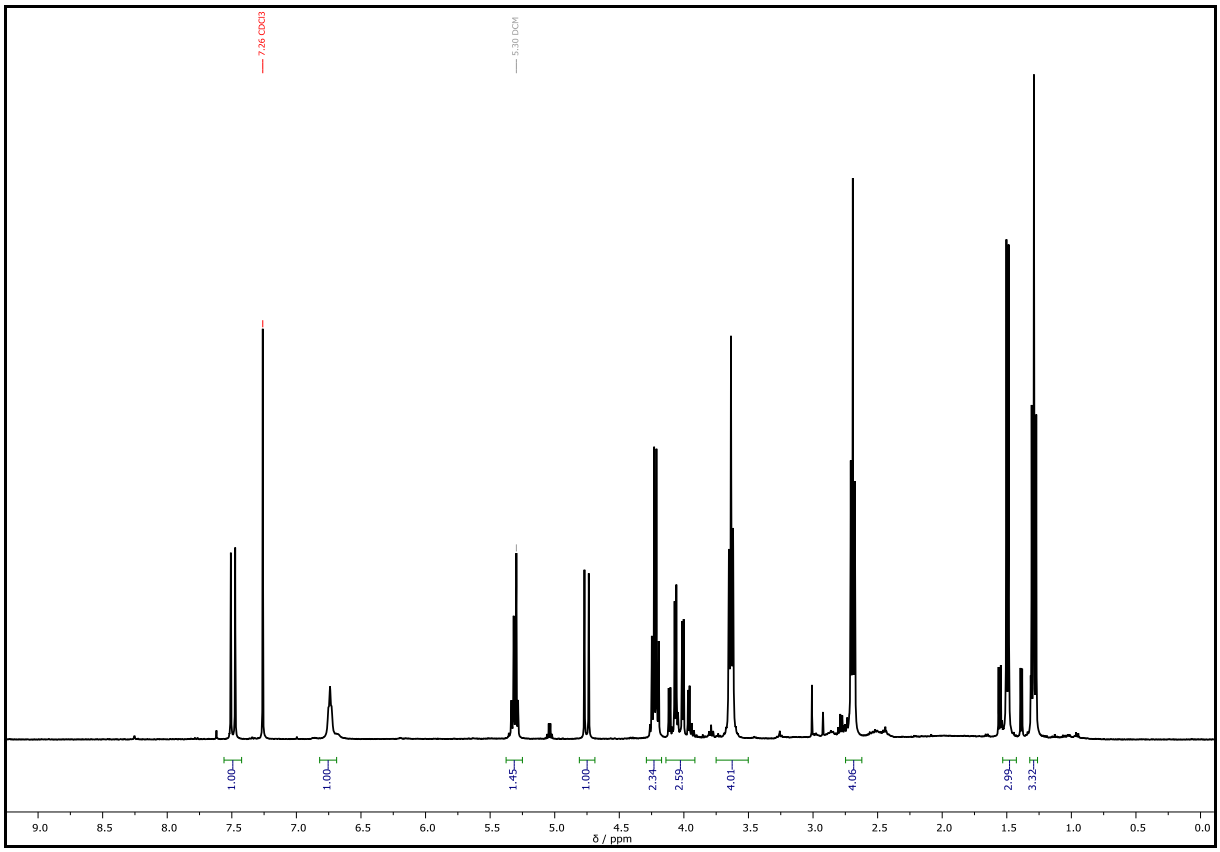

Supplementary Figure 186: ^{1}H NMR spectrum of **D1a1** recorded at 400 MHz in $CDCl_3$.

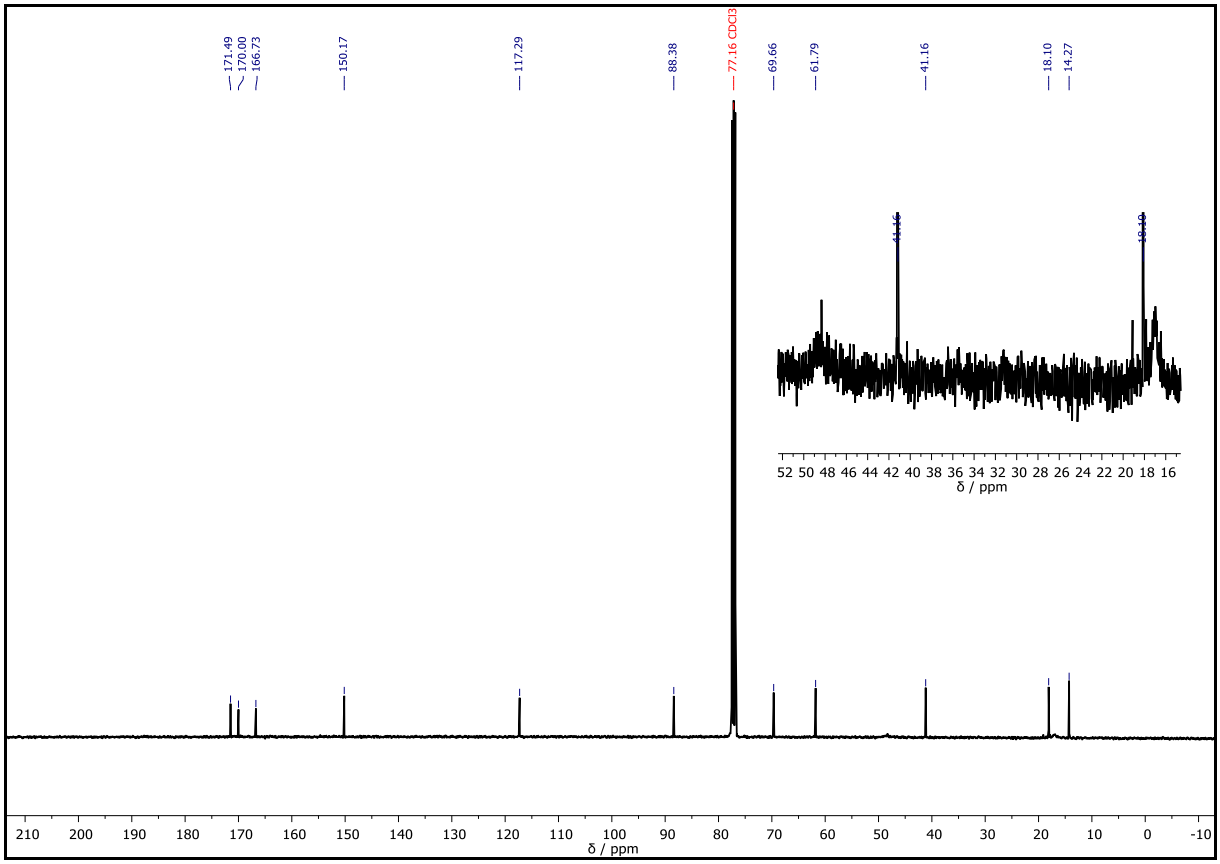

Supplementary Figure 187: ^{13}C NMR spectrum of **D1a1** recorded at 400 MHz in $CDCl_3$.

1-((2-Ethoxy-2-oxoethyl)amino)-1-oxopropan-2-yl (*E*)-3-(bis(2-ethylhexyl)amino)acrylate – D1a2

^{1}H NMR (400 MHz $CDCl_3$): δ / ppm = 7.49 (d, *J* = 13.0 Hz, 1H, CH^{1}), 6.79 (t, *J* = 5.3 Hz, 1H, NH^{2}), 5.33 (q, *J* = 6.9 Hz, 1H, CH^{3}), 4.58 (d, *J* = 13.0 Hz, 1H, CH^{4}), 4.21 (q, *J* = 7.1 Hz, 2H, CH_2^{5}), 4.16 – 3.92 (m, 2H, CH_2^{6}), 3.02 (d, *J* = 30.7 Hz, 4H, CH_2^{7}), 1.72 (m, 2H, CH^{8}), 1.47 (d, *J* = 6.9 Hz, 3H, CH_3^{9}), 1.36 – 1.18 (m, 19H, CH_2^{10} and CH_3^{10}), 0.98 – 0.80 (m, 12H, CH_3^{11}).

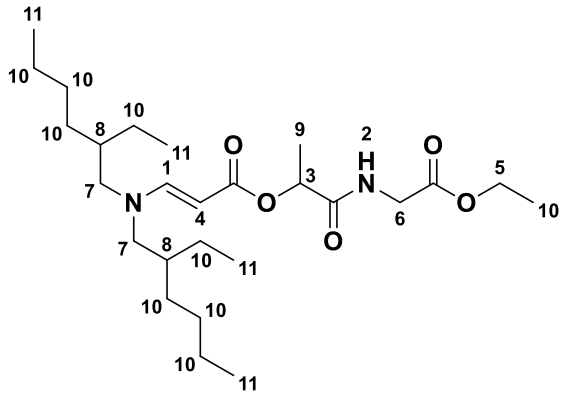

Chemical Formula: $C_{26}H_{48}N_2O_5$
Exact Mass: 468.3563 Da
Molecular Weight: 468.6790 Da

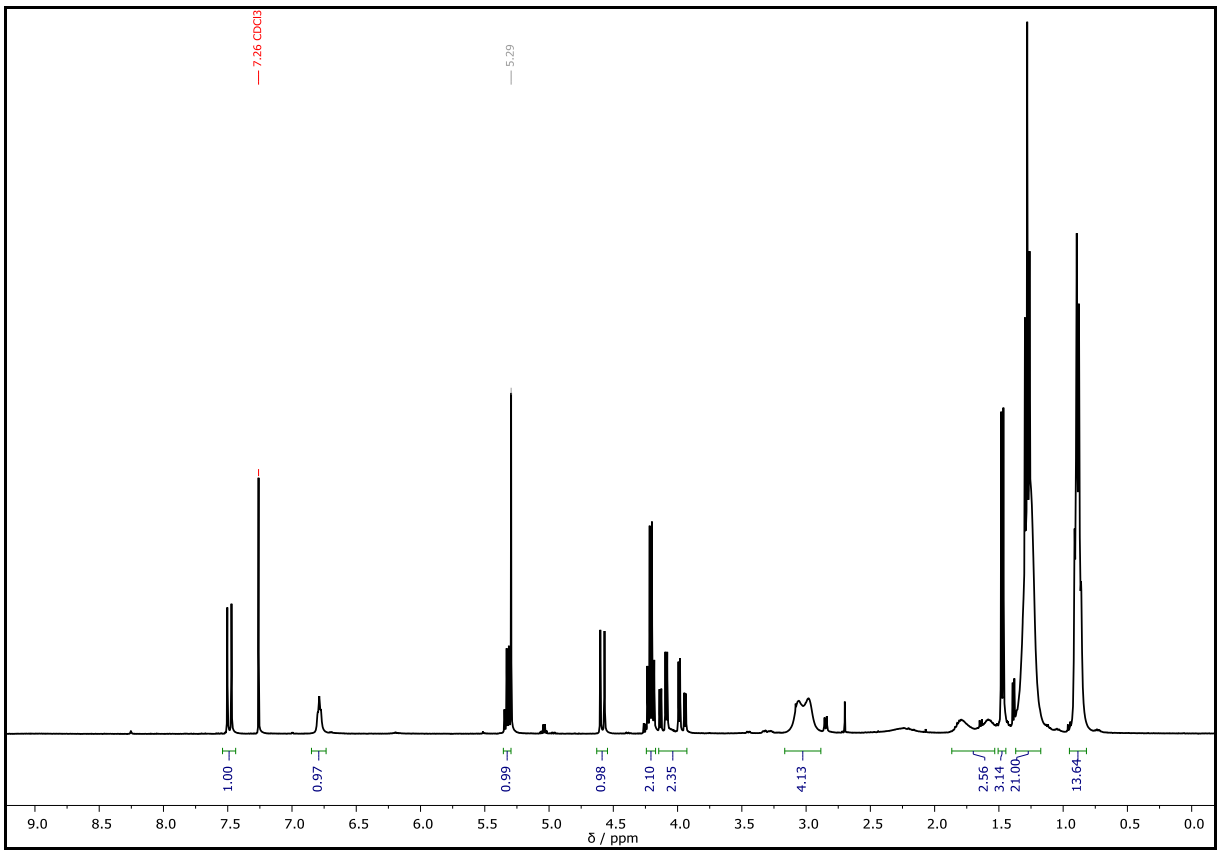

Supplementary Figure 188: ^{1}H NMR spectrum of **D1a2** recorded at 400 MHz in $CDCl_3$.

1-((2-Ethoxy-2-oxoethyl)amino)-1-oxotridecan-2-yl (*E*)-3-(bis(2-ethylhexyl)amino)acrylate – D5a2

^{1}H NMR (400 MHz $CDCl_3$): δ / ppm = 7.48 (d, *J* = 13.0 Hz, 1H, CH^1), 6.71 (t, *J* = 5.3 Hz, 1H, NH^2), 5.26 (dd, *J* = 7.6, 4.4 Hz, 1H, CH^3), 4.59 (d, *J* = 13.0 Hz, 1H, CH^4), 4.25 – 4.14 (m, 2H, CH_2^5), 4.12 – 3.89 (m, 2H, CH_2^6), 3.13 – 2.93 (m, 4H, CH_2^7), 1.95 – 1.71 (m, 3H, CH_2^8 and CH^9), 1.68 – 1.53 (m, 1H, CH^9), 1.48 – 1.18 (m, 37H, CH_2^{10} and CH_3^{10}), 0.94 – 0.83 (m, 15H, CH_3^{11}).

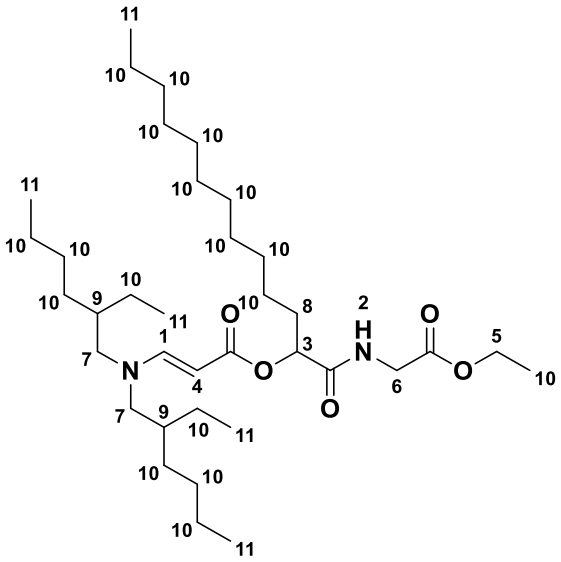

Chemical Formula: $C_{36}H_{68}N_2O_5$
Exact Mass: 608.5128 Da
Molecular Weight: 608.9490 Da

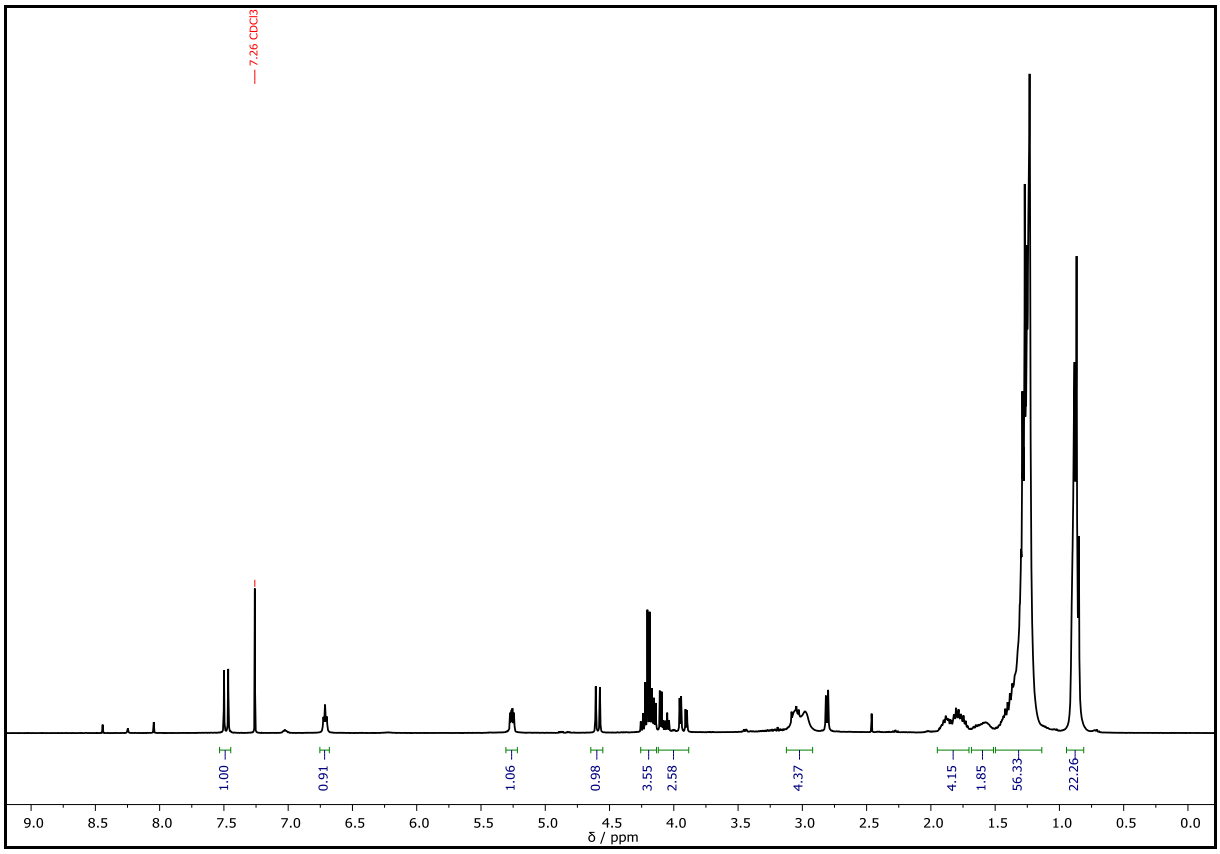

Supplementary Figure 189: ^{1}H NMR spectrum of **D5a2** recorded at 400 MHz in $CDCl_3$.

1-(Naphthalen-2-ylamino)-1-oxopropan-2-yl propiolate – D21

^{1}H NMR (400 MHz $CDCl_3$): δ / ppm = 8.23 (d, *J* = 2.3 Hz, 1H, CH_{Ar}^{1}), 8.02 (s, 1H, NH^{2}), 7.92 – 7.39 (m, 6H, CH_{Ar}^{3}), 5.48 (q, *J* = 6.8 Hz, 1H, CH^{4}), 5.05 (q, *J* = 5.1 Hz, 1H, CH^{4}), 3.08 (s, 1H, CH^{5}), 2.94 (s, 1H, CH^{5}), 1.67 (d, *J* = 6.8 Hz, 3H, CH_3^{6}), 1.39 (d, *J* = 5.1 Hz, 3H, CH_3^{6}).

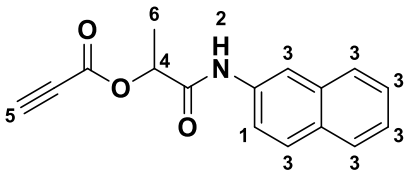

Chemical Formula: $C_{16}H_{13}NO_3$
Exact Mass: 267.0895 Da
Molecular Weight: 267.2840 Da

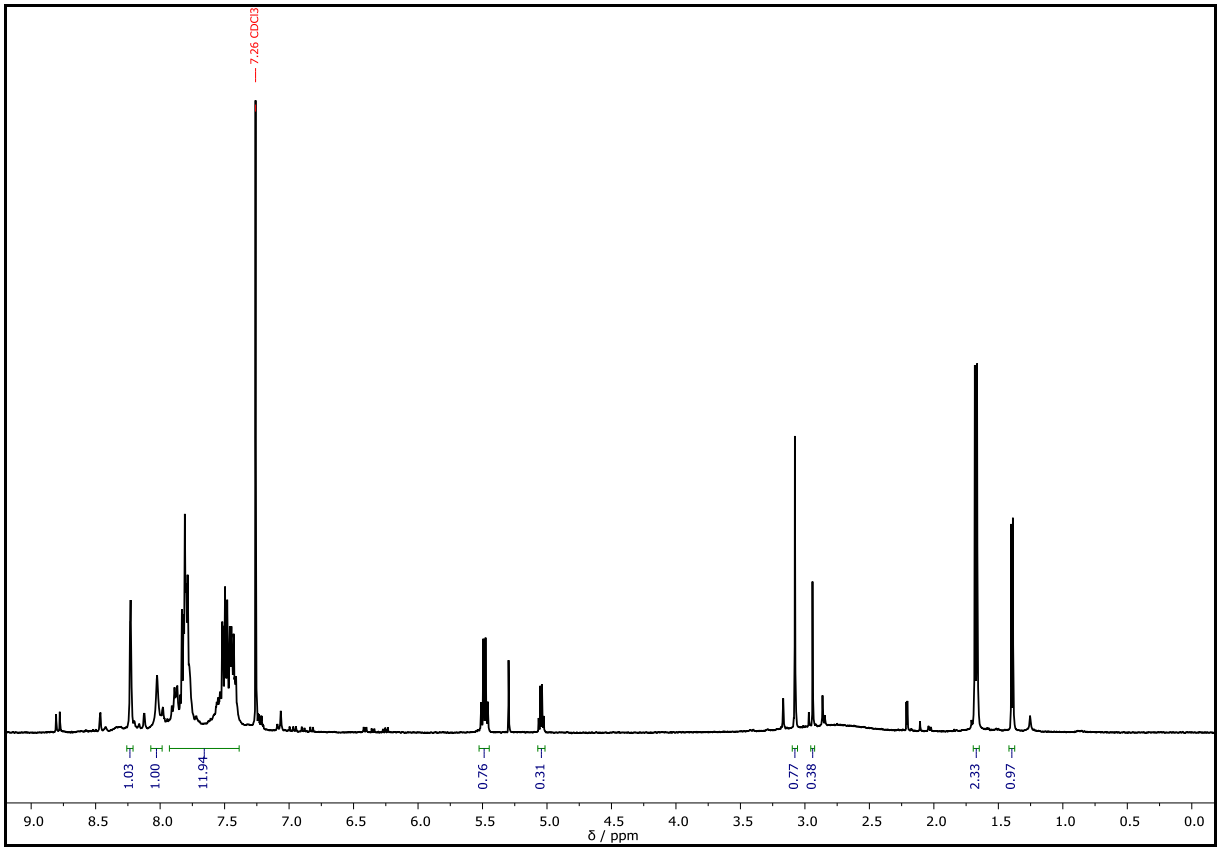

Supplementary Figure 190: ^{1}H NMR spectrum of **D21** recorded at 400 MHz in $CDCl_3$.

1-(Naphthalen-2-ylamino)-1-oxotridecan-2-yl propiolate – D25

^{1}H NMR (400 MHz $CDCl_3$): δ / ppm = 8.16 (d, *J* = 2.2 Hz, 1H, CH_{Ar}^{1}), 7.84 (s, 1H, NH^{2}), 7.79 – 7.69 (m, 3H, CH_{Ar}^{3}), 7.49 – 7.32 (m, 3H, CH_{Ar}^{3}), 5.38 (dd, *J* = 6.6, 5.2 Hz, 1H, CH^{4}), 3.01 (s, 1H, CH^{5}), 2.03 – 1.88 (m, 2H, CH_2^{6}), 1.49 – 1.32 (m, 2H, CH_2^{7}), 1.31 – 1.14 (m, 16H, CH_2^{8}), 0.80 (t, *J* = 6.8 Hz, 3H, CH_3^{9}).

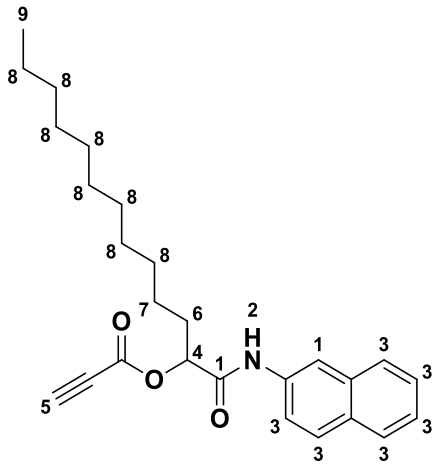

Chemical Formula: $C_{26}H_{33}NO_3$
Exact Mass: 407.2460 Da
Molecular Weight: 407.5540 Da

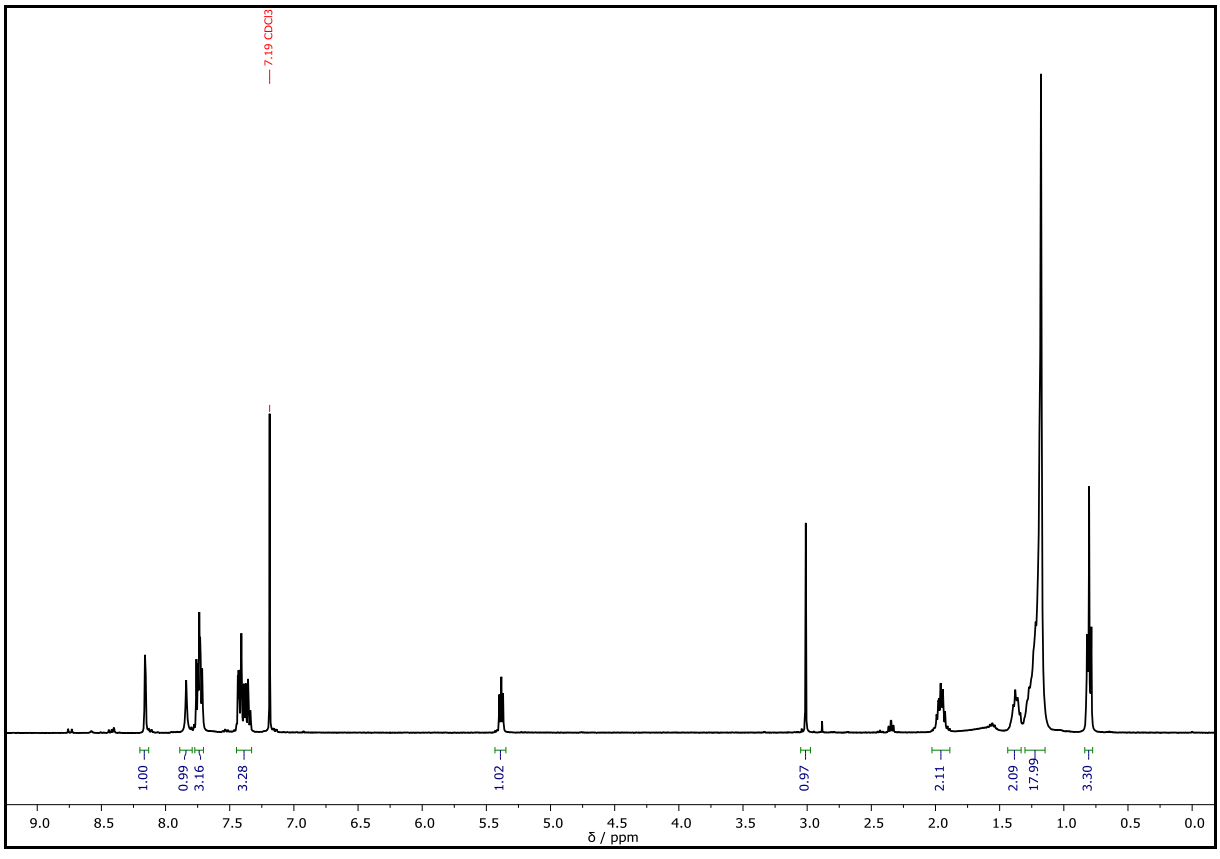

Supplementary Figure 191: ^{1}H NMR spectrum of **D25** recorded at 400 MHz in $CDCl_3$.

1-(Naphthalen-2-ylamino)-1-oxotridecan-2-yl (*E*)-3-(bis(2-cyanoethyl)amino)acrylate – D25a1

^{1}H NMR (500 MHz $CDCl_3$): δ / ppm = 8.23 (d, *J* = 2.2 Hz, 1H, CH_{Ar}^{1}), 8.04 (s, 1H, NH^{2}), 7.83 – 7.76 (m, 3H, CH_{Ar}^{3}), 7.53 – 7.37 (m, 4H, CH^{4} and CH_{Ar}^{3}), 5.37 (dd, *J* = 7.6, 4.8 Hz, 1H, CH^{5}), 4.83 (d, *J* = 13.4 Hz, 1H, CH^{6}), 3.63 (t, *J* = 6.5 Hz, 4H, CH_2^{7}), 2.68 (t, *J* = 6.4 Hz, 4H, CH_2^{8}), 2.07 – 1.88 (m, 2H, CH_2^{9}), 1.47 – 1.40 (m, 2H, CH_2^{10}), 1.25 (s, 16H, CH_2^{11}), 0.87 (t, *J* = 6.9 Hz, 3H, CH_3^{12}).

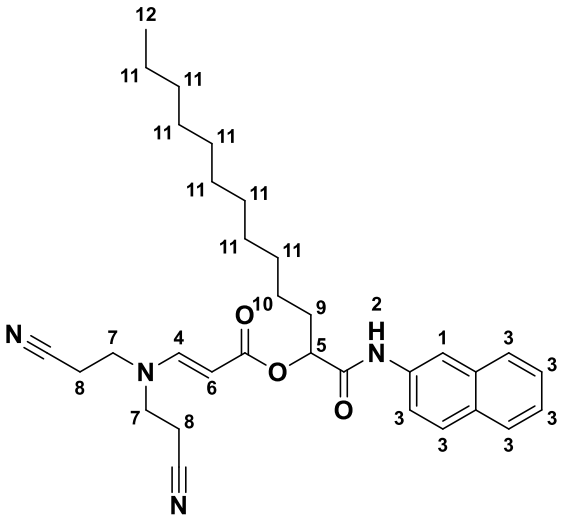

Chemical Formula: $C_{32}H_{42}N_4O_3$
Exact Mass: 530.3257 Da
Molecular Weight: 530.7130 Da

^{13}C NMR (126 MHz $CDCl_3$): δ / ppm = 169.10 (C_q^1), 167.39 (C_q^2), 150.58 (CH^3), 134.74 (C_q^3), 133.91 (C_q^3), 130.92 (C_q^3), 128.89 (CH_{Ar}^4), 127.83 (CH_{Ar}^4), 127.69 (CH_{Ar}^4), 126.70 (CH_{Ar}^4), 125.30 (CH_{Ar}^4), 120.12 (CH_{Ar}^4), 117.20 (CH_{Ar}^4 and C_q^5), 117.12 (CH_{Ar}^4 and C_q^5), 88.04 (CH^6), 73.74 (CH^7), 32.16 (CH_2^8), 32.05 (CH_2^8), 29.78 (CH_2^8), 29.76 (CH_2^8), 29.73 (CH_2^8), 29.61 (CH_2^8), 29.53 (CH_2^8), 29.49 (CH_2^8), 25.21 (CH_2^8), 22.83 (CH_2^8), 14.26 (CH_3^9).

Note: C^{10} and C^{11} are not visible in the ^{13}C NMR spectra.

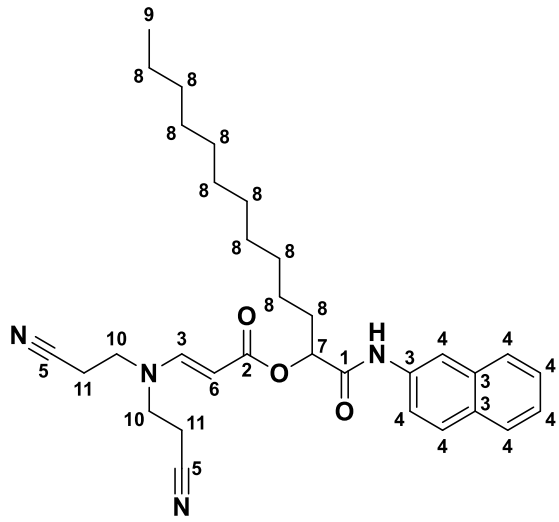

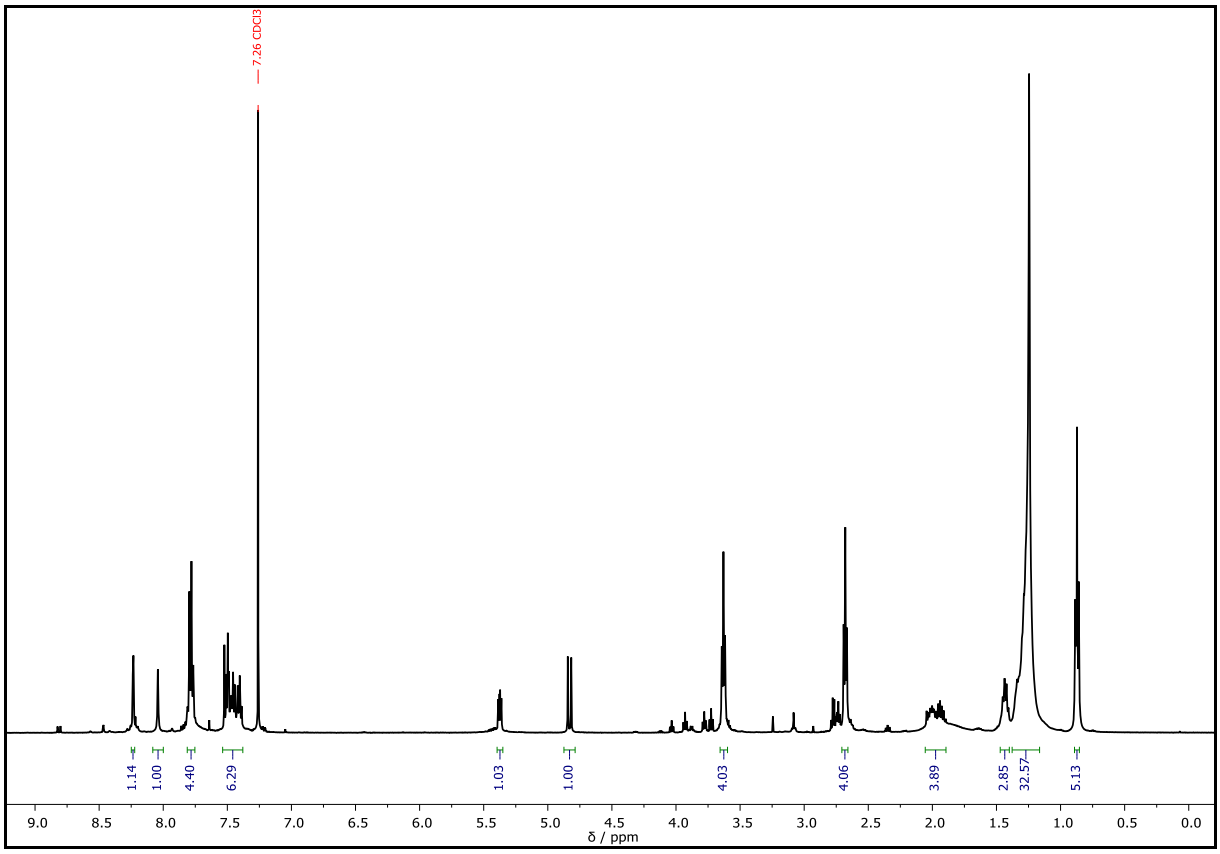

Supplementary Figure 192: ^{1}H NMR spectrum of **D25a1** recorded at 400 MHz in $CDCl_3$.

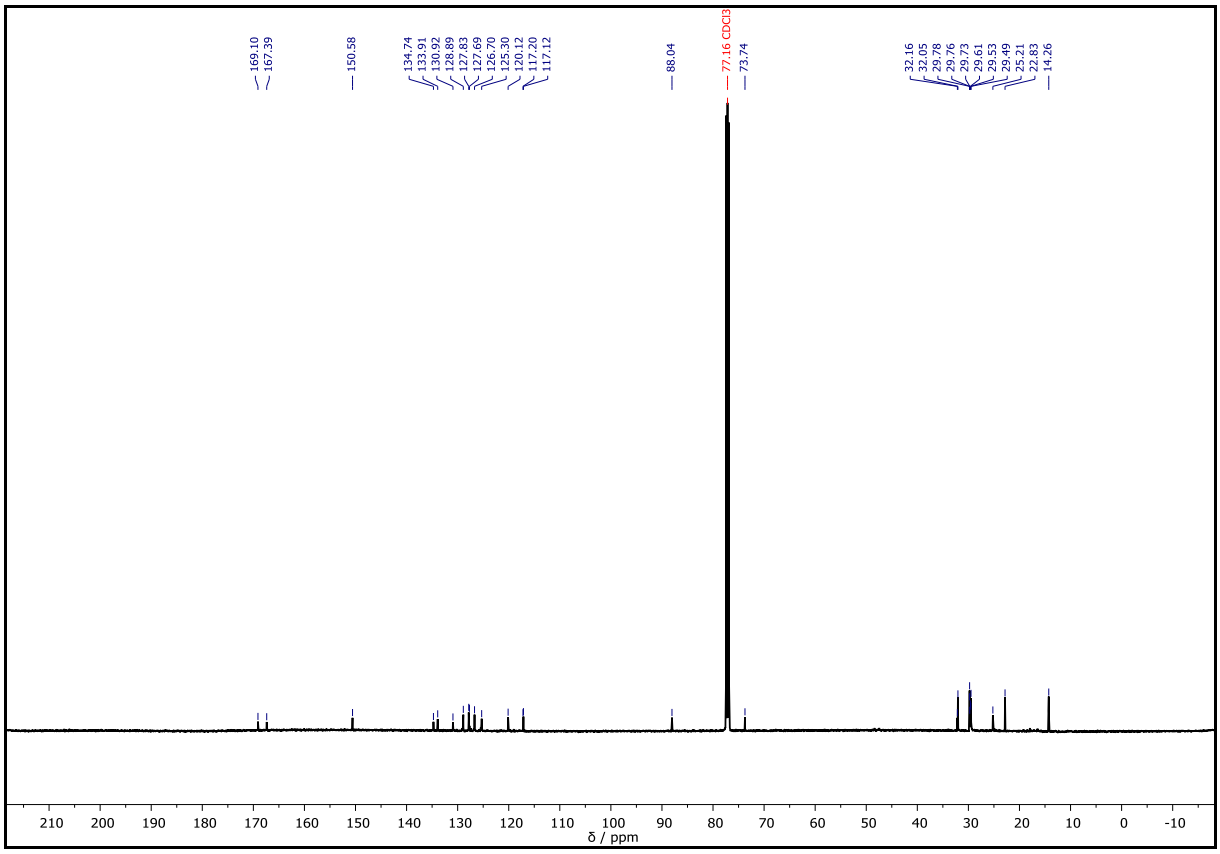

Supplementary Figure 193: ^{13}C NMR spectrum of **D25a1** recorded at 400 MHz in $CDCl_3$.

1-(Naphthalen-2-ylamino)-1-oxotridecan-2-yl (*E*)-3-(bis(2-ethylhexyl)amino)acrylate – D25a2

^{1}H NMR (400 MHz $CDCl_3$): δ / ppm = 8.28 (s, 1H, NH^{1}), 8.25 (d, *J* = 2.1 Hz, 1H, $CH_{Ar}{}^{2}$), 7.80 – 7.75 (m, 3H, $CH_{Ar}{}^{3}$), 7.55 (d, *J* = 13.0 Hz, 1H, CH^{4}), 7.51 – 7.36 (m, 3H, $CH_{Ar}{}^{3}$), 5.40 (dd, *J* = 7.6, 4.7 Hz, 1H, CH^{5}), 4.67 (d, *J* = 12.9 Hz, 1H, CH^{6}), 3.14 – 2.98 (m, 4H, $CH_2{}^{7}$), 2.07 – 1.89 (m, 2H, CH^{8}), 1.86 – 1.79 (m, 1H, CH^{9}), 1.65 – 1.57 (m, 1H, CH^{9}), 1.50 – 1.16 (m, 34H, $CH_2{}^{10}$), 0.98 – 0.82 (m, 15H, $CH_3{}^{11}$).

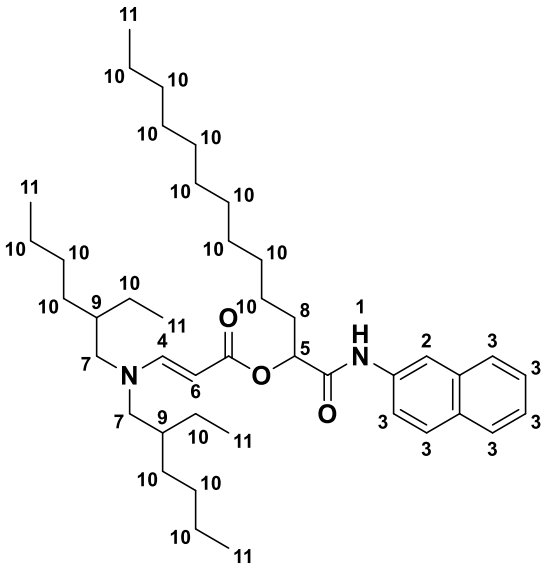

Chemical Formula: $C_{42}H_{68}N_2O_3$
Exact Mass: 648.5230 Da
Molecular Weight: 649.0170 Da

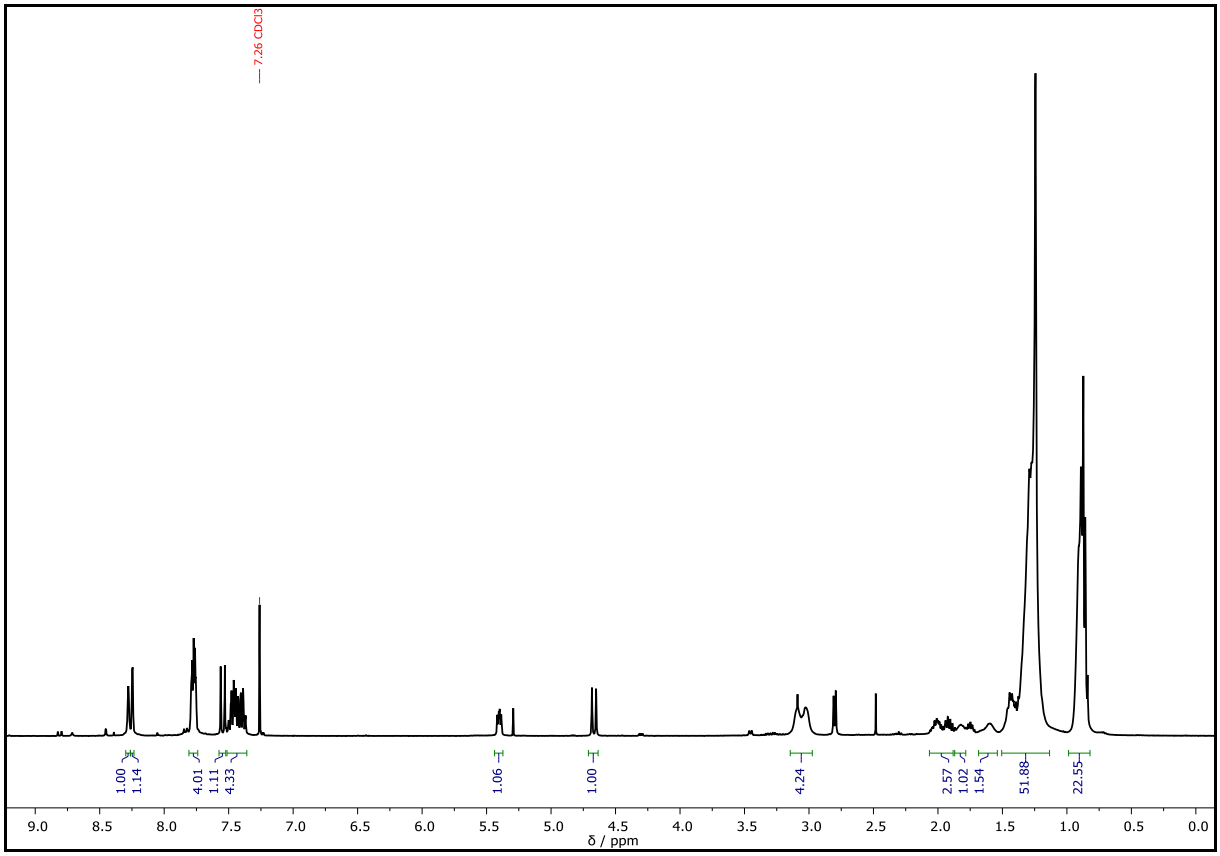

Supplementary Figure 194: ^{1}H NMR spectrum of **D25a2** recorded at 400 MHz in $CDCl_3$.

1-(tert-butylamino)-1-oxo-3-phenylbutan-2-yl (E)-3-(diallylamino)acrylate – D13a3

^{1}H NMR (400 MHz $CDCl_3$): δ / ppm = 7.50 (dd, *J* = 13.0, 10.4 Hz, 1H, CH^{1}), 7.34 – 7.12 (m, 5H, $CH_{Ar}{}^{2}$), 5.84 – 5.70 (m, 2H, CH^{3}), 5.55 (2 × s, 1H, NH^{4}), 5.35 – 5.29 (m, 1H, CH^{5}), 5.27 – 5.16 (m, 4H, $CH_2{}^{6}$), 4.67 (dd, *J* = 13.0, 5.3 Hz, 1H, CH^{7}), 3.79 – 3.74 (m, 4H, $CH_2{}^{8}$), 3.57 – 3.40 (m, 1H, CH^{9}), 1.40 – 1.32 (m, 3H, $CH_3{}^{10}$), 1.23 (s, 5H, $CH_3{}^{11}$), 1.13 (s, 4H, $CH_3{}^{11}$).

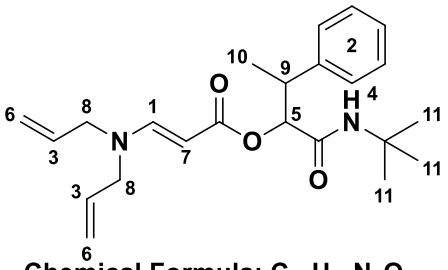

Chemical Formula: $C_{23}H_{32}N_2O_3$
Exact Mass: 384.2413 Da
Molecular Weight: 384.5200 Da

^{13}C NMR (101 MHz, $CDCl_3$) δ / ppm = ^{13}C NMR (101 MHz, $CDCl_3$) δ 169.08 (C_q^1), 168.98 (C_q^1), 168.46 (C_q^2), 168.35 (C_q^2), 152.82 (CH^3), 152.74 (CH^3), 142.73 (C_q^4), 141.78 (C_q^4), 133.11 (CH^5, weak), 130.79 (CH^5, weak), 128.79 (CH_{Ar}^6), 128.31 (CH_{Ar}^6), 128.21 (CH_{Ar}^6), 127.98 (CH_{Ar}^6), 126.74 (CH_{Ar}^6), 126.66 (CH_{Ar}^6), 118.44 (CH_2^7, weak), 84.17 (CH^8), 83.97 (CH^8), 76.57 (CH^9), 76.06 (CH^9), 57.93 (CH_2^{10}, weak), 51.02 (C_q^{11}), 50.76 (C_q^{11}), 50.61 (CH_2^{10}, weak), 41.61 (CH^{12}), 41.54 (CH^{12}), 28.63 (CH_3^{13}), 28.55 (CH_3^{13}), 17.79 (CH_3^{14}), 15.69 (CH_3^{14}).

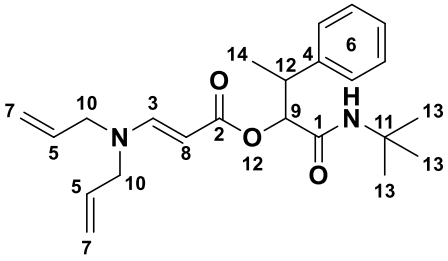

HRMS (ESI) of $C_{23}H_{32}N_2O_3$ $[M+H]^+$ *m/z* calc: 385.2486, found 385.2480.

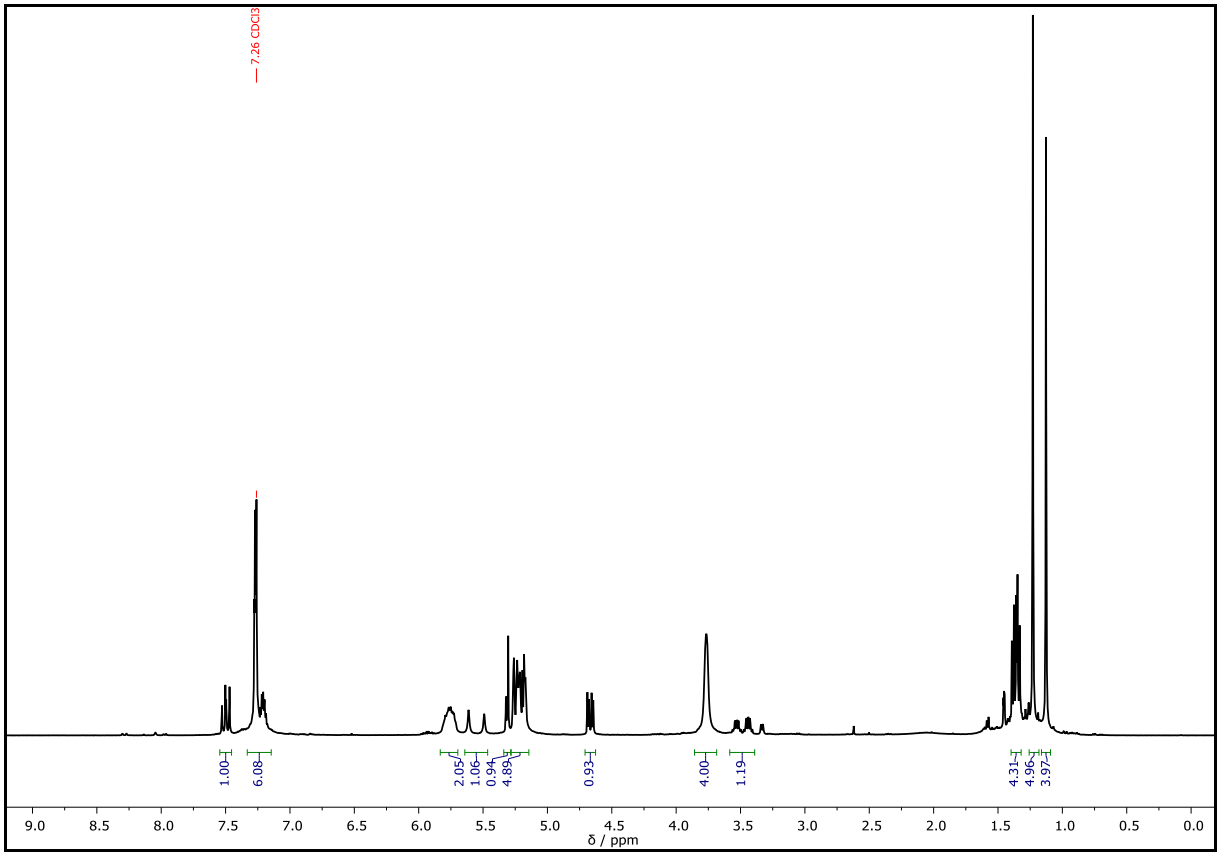

Supplementary Figure 195: ^{1}H NMR spectrum of **D13a3** recorded at 400 MHz in $CDCl_3$.

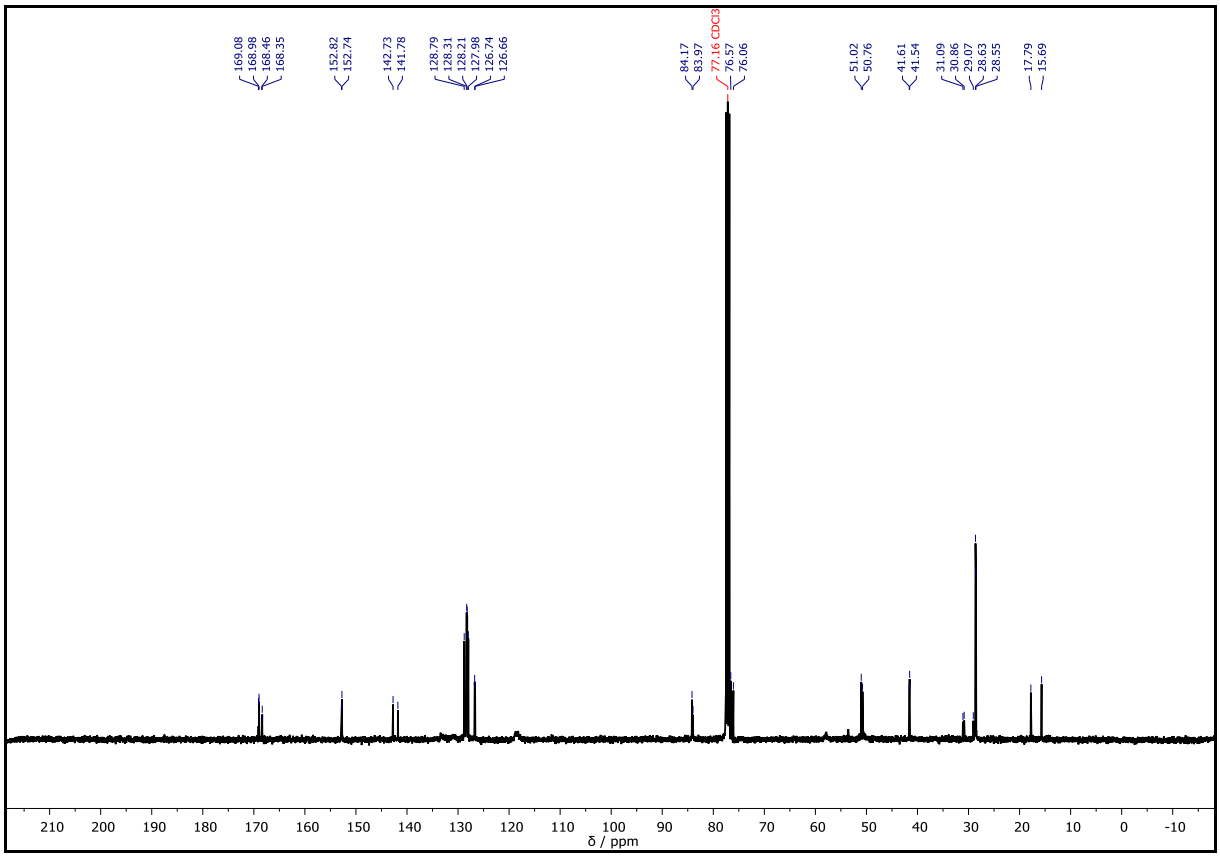

Supplementary Figure 196: ^{13}C NMR spectrum of **D13a3** recorded at 101 MHz in $CDCl_3$.

1-((2-Ethoxy-2-oxoethyl)amino)-1-oxotridecan-2-yl (*E*)-3-(4-((3,3,4,4,5,5,6,6,7,7,8,8,8-tridecafluorooctyl)thio)phenoxy)acrylate – D5b2

^{1}H NMR (400 MHz $CDCl_3$): δ / ppm = 7.85 (d, *J* = 12.2 Hz, 1H, CH^{1}), 7.44 – 7.35 (m, 2H, $CH_{Ar}{}^{2}$), 7.10 – 7.04 (m, 2H, $CH_{Ar}{}^{3}$), 6.60 (t, *J* = 5.2 Hz, 1H, NH^{4}), 5.66 (d, *J* = 12.2 Hz, 1H, CH^{5}), 5.32 – 5.25 (m, 1H, CH^{6}), 4.22 (q, *J* = 7.2 Hz, 2H, $CH_2{}^{7}$), 4.12 – 3.95 (m, 2H, $CH_2{}^{8}$), 3.13 – 3.06 (m, 2H, $CH_2{}^{9}$), 2.46 – 2.27 (m, 2H, $CH_2{}^{10}$), 1.98 – 1.78 (m, 2H, $CH_2{}^{11}$), 1.47 – 1.15 (m, 21H, $CH_3{}^{12}$, $CH_2{}^{13}$), 0.87 (t, *J* = 6.8 Hz, 3H, $CH_3{}^{14}$).

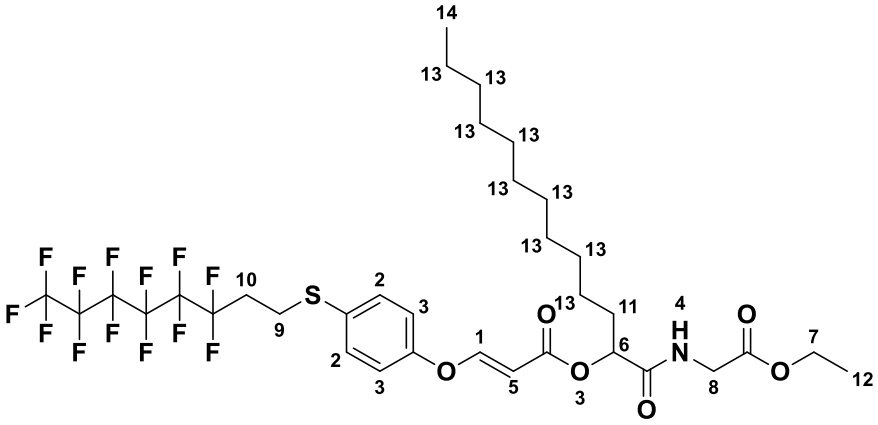

Chemical Formula: $C_{34}H_{42}F_{13}NO_6S$
Exact Mass: 839.2525 Da
Molecular Weight: 839.7502 Da

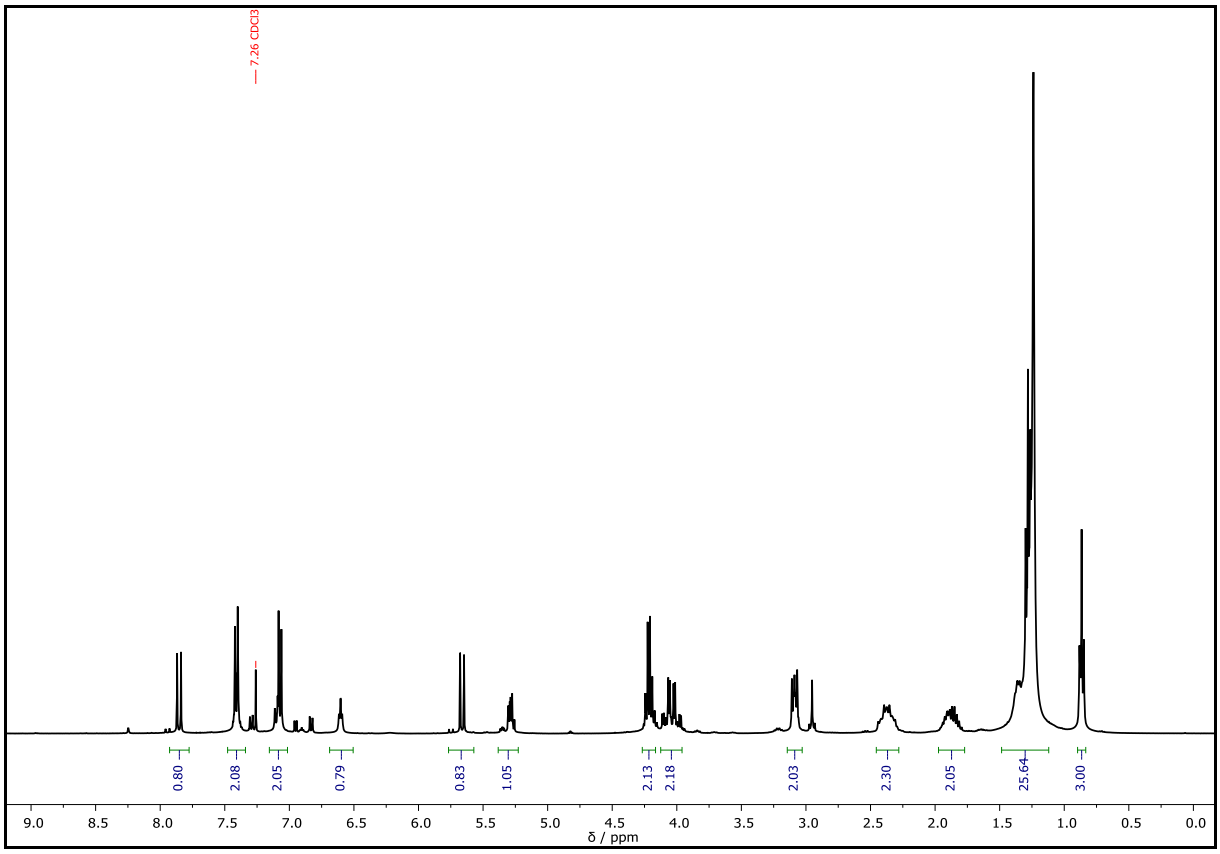

Supplementary Figure 197: ^{1}H NMR spectrum of **D5b2** recorded at 400 MHz in $CDCl_3$.

1-((2-Ethoxy-2-oxoethyl)amino)-1-oxopropan-2-yl (*E*)-3-((3-oxobutan-2-yl)thio)acrylate – D1c1

^{1}H NMR (400 MHz $CDCl_3$): δ / ppm = 7.66 (d, *J* = 15.3 Hz, 1H, CH^{1E}), 7.13 (d, *J* = 10.2, 1H, CH^{1Z}), 6.75 (s, 1H, NH^{2}), 6.68 (s, 1H, NH^{2}), 6.01 – 5.90 (m, 1H, CH^{3}), 5.38 – 5.24 (m, 1H, CH^{4}), 4.26 – 4.16 (m, 2H, CH_2^{5}), 4.07 – 4.00 (m, 2H, CH_2^{6}), 3.76 (q, *J* = 7.2 Hz, 1H, CH^{7}), 3.63 (q, *J* = 7.1 Hz, 1H, CH^{7}), 2.29 (d, *J* = 3.2 Hz, 3H, CH_3^{8}), 1.55 – 1.46 (m, 6H, CH_3^{9}), 1.32 – 1.22 (m, 3H, CH_3^{10}).

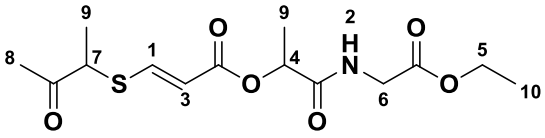

Chemical Formula: $C_{14}H_{21}NO_6S$
Exact Mass: 331.1090 Da
Molecular Weight: 331.3830 Da

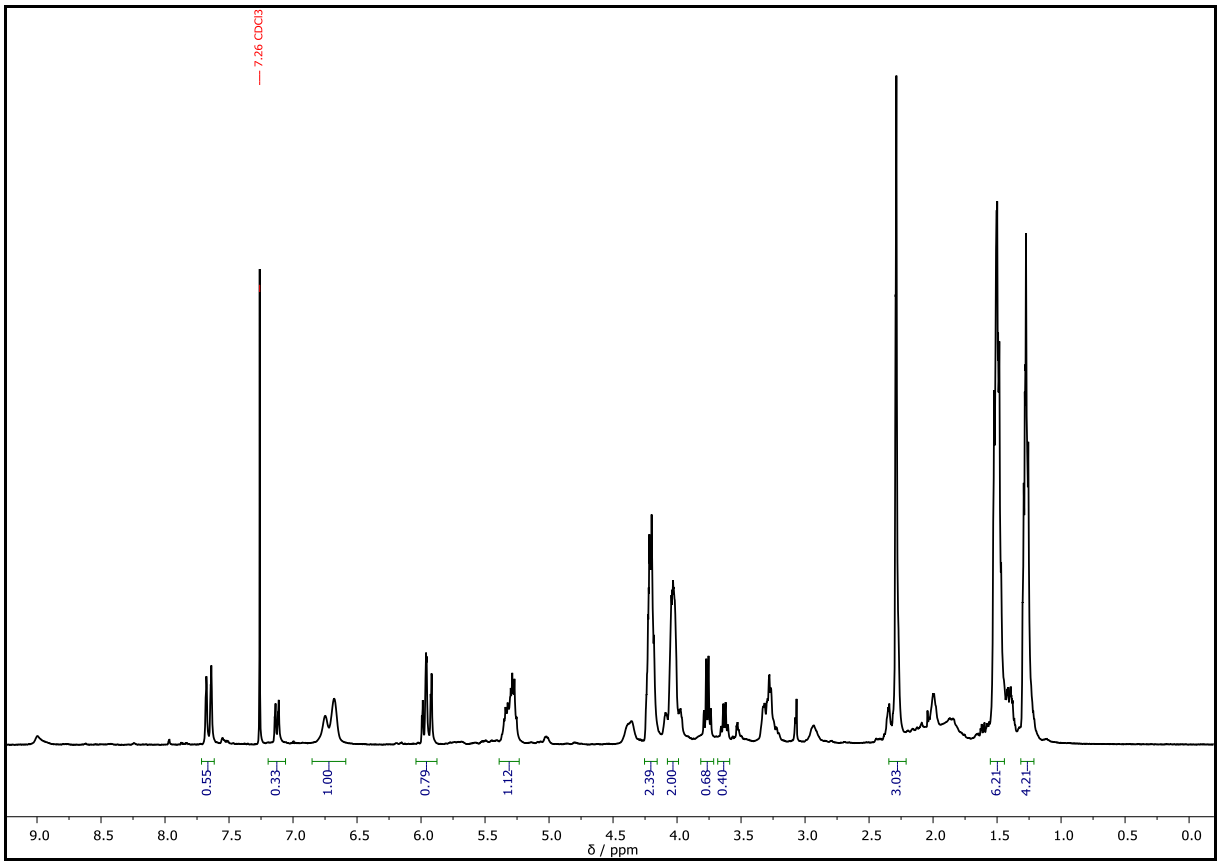

Supplementary Figure 198: ^{1}H NMR spectrum of **D1c1** recorded at 400 MHz in $CDCl_3$.

1-((2-Ethoxy-2-oxoethyl)amino)-1-oxotridecan-2-yl (*E*)-3-((3-oxobutan-2-yl)thio)acrylate – D5c1

^{1}H NMR (400 MHz $CDCl_3$): δ / ppm = 7.67 (d, *J* = 15.3 Hz, 1H, CH^{1E}), 7.13 (dd, *J* = 10.3, 1.0 Hz, 1H, CH^{1Z}), 6.65 (t, *J* = 5.1 Hz, 1H, NH^2), 6.58 (q, *J* = 4.9 Hz, 1H, NH^2), 5.99 (d, *J* = 10.3 Hz, 1H, CH^{3Z}), 5.96 (d, *J* = 15.4 Hz, 1H, CH^{3E}), 5.30 (dd, *J* = 7.0, 4.9 Hz, 1H, CH^4), 5.24 (dd, *J* = 7.3, 4.8 Hz, 1H, CH^4), 4.30 – 4.14 (m, 2H, CH_2^5), 4.13 – 3.92 (m, 2H, CH_2^6), 3.77 (q, *J* = 7.2 Hz, 1H, CH^7), 3.63 (q, *J* = 7.1 Hz, 1H, CH^7), 2.29 (s, 3H, CH_3^8), 1.95 – 1.78 (m, 2H, CH_2^9), 1.52 (dd, *J* = 7.2, 1.5 Hz, 3H, CH_3^{10}), 1.48 (dd, *J* = 7.1, 1.4 Hz, 3H, CH_3^{10}), 1.37 – 1.17 (m, 21H, CH_2^{11} and CH_3^{11}), 0.86 (t, *J* = 6.8 Hz, 3H, CH_3^{12}).

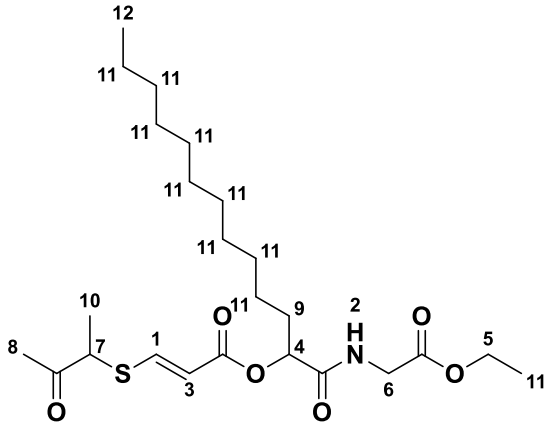

Chemical Formula: $C_{24}H_{41}NO_6S$
Exact Mass: 471.2655 Da
Molecular Weight: 471.6530 Da

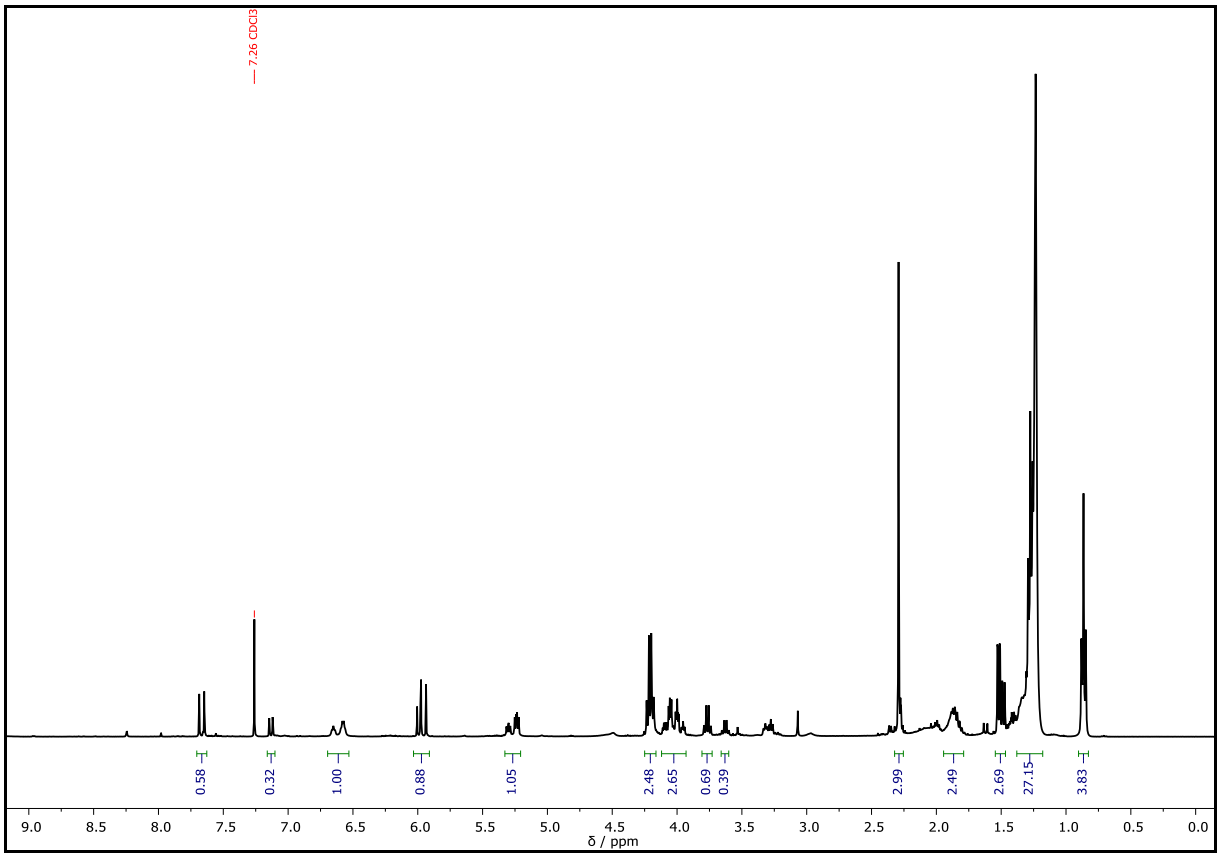

Supplementary Figure 199: ^{1}H NMR spectrum of **D5c1** recorded at 400 MHz in $CDCl_3$.

1-(((Diethoxyphosphoryl)methyl)amino)-1-oxo-3-phenylbutan-2-yl (*E*)-3-((3-oxobutan-2-yl)thio)acrylate – D8c1

^{1}H NMR (400 MHz $CDCl_3$): δ / ppm = 7.57 (dd, *J* = 15.4, 4.8 Hz, 1H, CH^{1E}), 7.32 – 7.17 (m, 5H, $CH_{Ar}{}^{2}$), 7.10 (dd, *J* = 10.3, 6.4 Hz, 1H, CH^{1Z}), 6.33 (s, 0.5H, NH^{3a}), 6.18 (s, 0.5H, NH^{3b}), 5.97 – 5.93 (m, 1H, CH^{4Z}), 5.93 – 5.84 (m, 1H, CH^{4E}), 5.45 – 5.31 (m, 1H, CH^{5}), 4.20 – 3.93 (m, 4H, $CH_2{}^{6}$), 3.79 – 3.55 (m, 2H, $CH_2{}^{7}$ and CH^{8}), 3.52 – 3.35 (m, 2H, $CH_2{}^{7}$ and CH^{9}), 2.28 (d, *J* = 4.8 Hz, 3H, $CH_3{}^{10}$), 1.54 – 1.43 (m, 3H, $CH_3{}^{11}$), 1.38 – 1.31 (m, 3H, $CH_3{}^{12}$), 1.31 – 1.23 (m, 6H, $CH_3{}^{13}$).

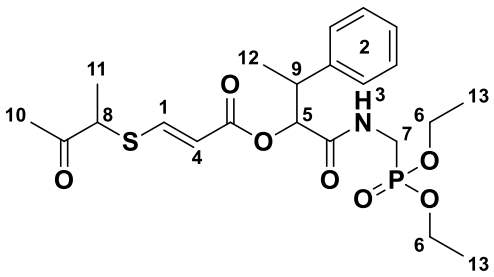

Chemical Formula: $C_{22}H_{32}NO_7PS$
Exact Mass: 485.1637 Da
Molecular Weight: 485.5318 Da

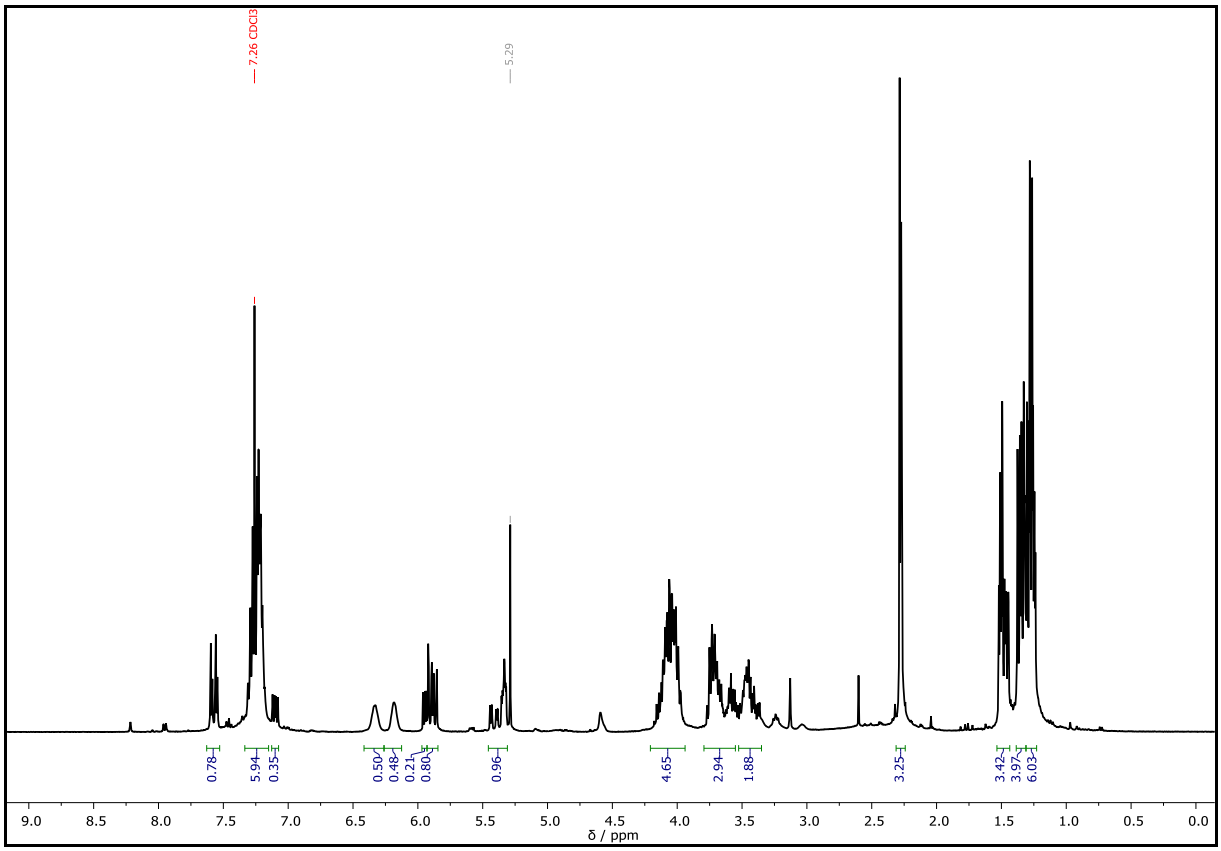

Supplementary Figure 200: ^{1}H NMR spectrum of **D8c1** recorded at 400 MHz in $CDCl_3$.

1-((2-Ethoxy-2-oxoethyl)amino)-1-oxopropan-2-yl (*E*)-3-(decylthio)acrylate – D1c2

^{1}H NMR (400 MHz $CDCl_3$): δ / ppm = 7.81 (d, *J* = 15.1 Hz, 1H, $CH^{1,E}$), 7.21 (d, *J* = 10.3 Hz, 1H, $CH^{1,Z}$), 6.68 (t, *J* = 5.3 Hz, 1H, NH^{2}), 5.90 (d, *J* = 10.3 Hz, 1H, $CH^{3,Z}$), 5.79 (d, *J* = 15.1 Hz, 1H, $CH^{3,E}$), 5.31 (q, *J* = 6.9 Hz, 1H, CH^{4}), 4.21 (q, *J* = 7.1 Hz, 2H, CH_2^{5}), 4.03 (qd, *J* = 18.4, 5.2 Hz, 2H, CH_2^{6}), 2.81 (t, *J* = 7.4 Hz, 2H, CH_2^{7}), 1.68 (p, *J* = 7.4 Hz, 3H, CH_3^{8}), 1.50 (d, *J* = 6.8 Hz, 2H, CH_2^{9}), 1.45 – 1.35 (m, 2H, CH_2^{10}), 1.34 – 1.21 (m, 15H, CH_2^{11} and CH_3^{11}), 0.87 (t, *J* = 6.8 Hz, 3H, CH_3^{12}).

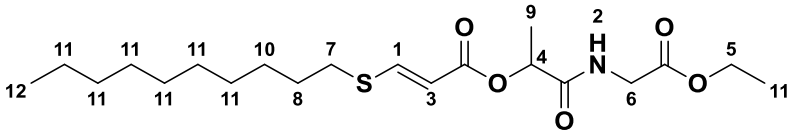

Chemical Formula: $C_{20}H_{35}NO_5S$
Exact Mass: 401.2236 Da
Molecular Weight: 401.5620 Da

^{13}C NMR (101 MHz, $CDCl_3$) δ / ppm = 170.99 (C_q^1), 169.75 (C_q^2), 163.96 (C_q^3), 152.80 ($CH^{4,Z}$), 149.75 ($CH^{4,E}$), 112.27 ($CH^{5,E}$), 111.92 ($CH^{5,Z}$), 70.20 (CH^6), 61.76 (CH_2^7), 41.19 (CH_2^8), 32.32 (CH_2^9), 31.98 (CH_2^{10}), 29.61 (CH_2^{10}), 29.55 (CH_2^{10}), 29.38 (CH_2^{10}), 29.19 (CH_2^{10}), 28.88 (CH_2^{11}), 28.64 (CH_2^{12}), 22.77 (CH_2^{10}), 17.97 (CH_3^{13}), 14.23 (CH_3^{14}), 14.21 (CH_3^{14}).

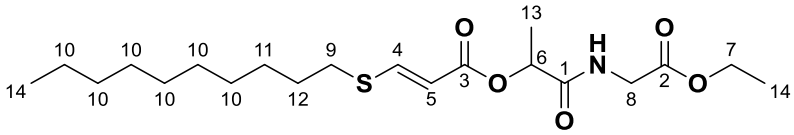

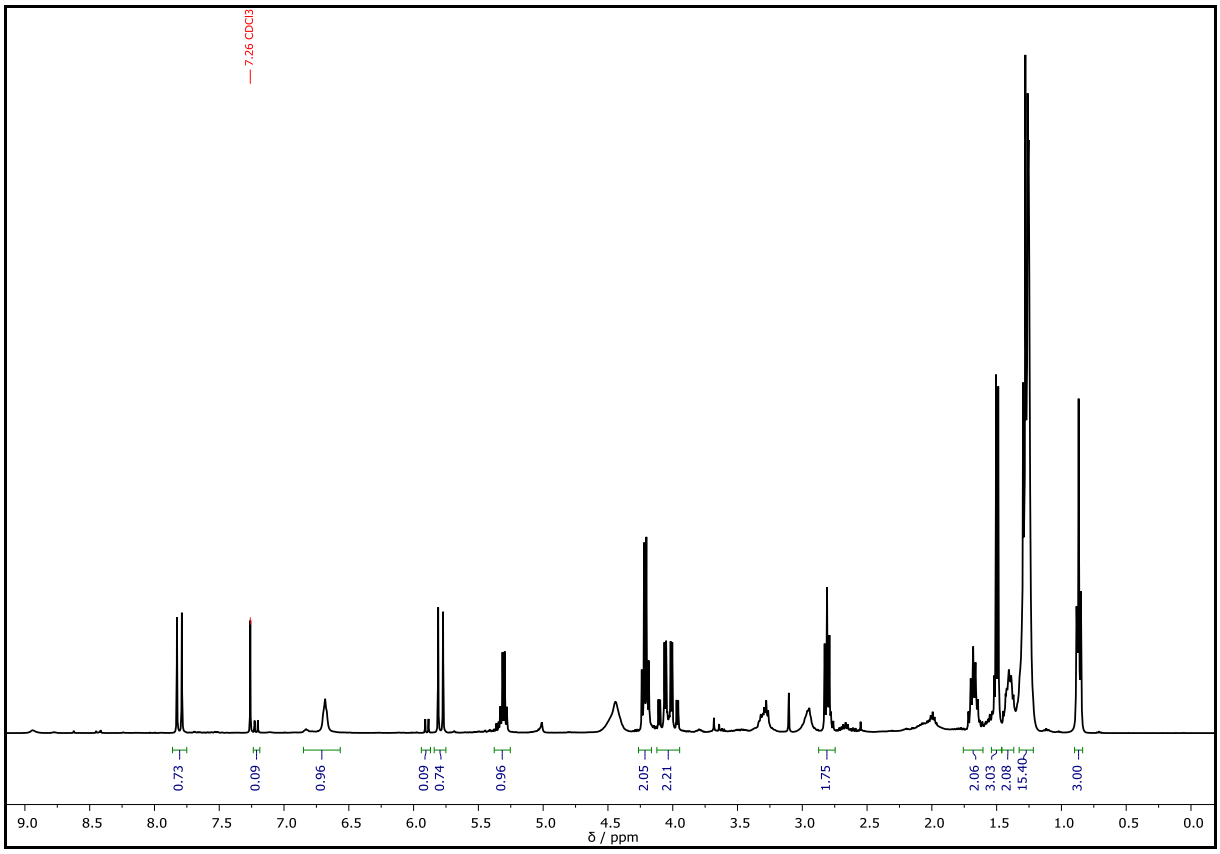

Supplementary Figure 201: ^{1}H NMR spectrum of **D1c2** recorded at 400 MHz in $CDCl_3$.

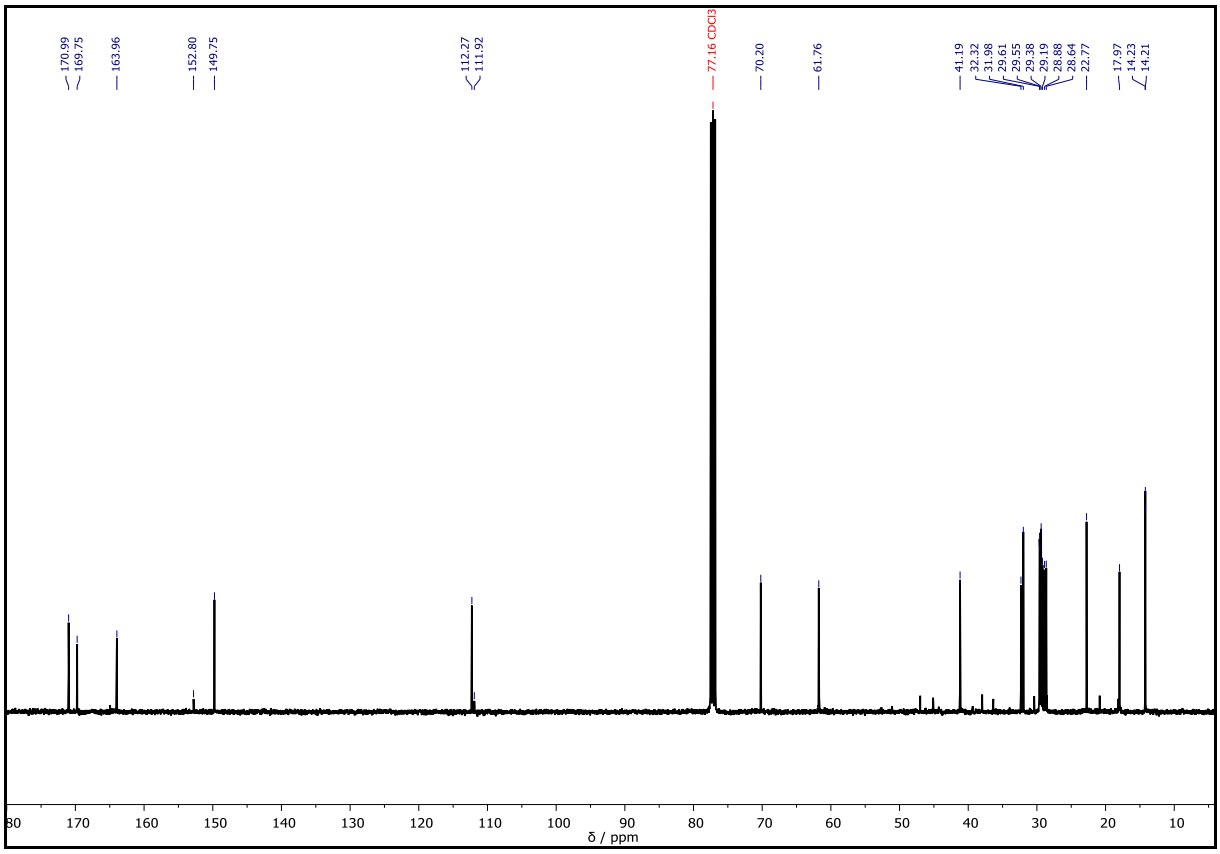

Supplementary Figure 202: ^{13}C NMR spectrum of **D1c2** recorded at 400 MHz in $CDCl_3$.

1-((2-Ethoxy-2-oxoethyl)amino)-1-oxotridecan-2-yl (*E*)-3-(decylthio)acrylate – D5c2

^{1}H NMR (400 MHz $CDCl_3$): δ / ppm = 7.81 (d, *J* = 15.1 Hz, 1H, $CH^{1,E}$), 7.22 (d, *J* = 10.3 Hz, 1H, $CH^{1,Z}$), 6.59 (t, *J* = 5.2 Hz, 1H, NH^{2}), 5.91 (d, *J* = 10.3 Hz, 1H, $CH^{3,Z}$), 5.81 (d, *J* = 15.1 Hz, 1H, $CH^{3,E}$), 5.42 – 5.19 (m, 1H, CH^{4}), 4.21 (q, *J* = 7.2 Hz, 2H, CH_2^{5}), 4.13 – 3.93 (m, 2H, CH_2^{6}), 2.82 (t, *J* = 7.4 Hz, 2H, CH_2^{7}), 1.97 – 1.76 (m, 2H, CH_2^{8}), 1.69 (p, *J* = 7.4 Hz, 2H, CH_2^{9}), 1.27 (dd, *J* = 15.7, 7.8 Hz, 35H, CH_2^{10}, CH_3^{11}, CH_2^{12}), 0.97 – 0.82 (m, 6H, CH_3^{13}).

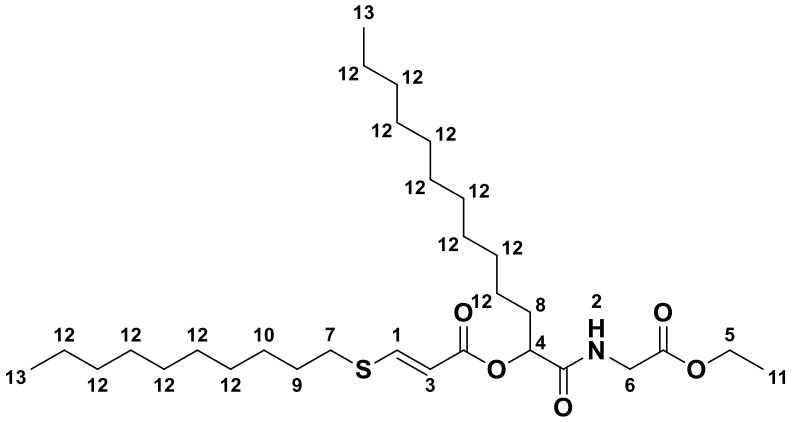

Chemical Formula: $C_{30}H_{55}NO_5S$
Exact Mass: 541.3801 Da
Molecular Weight: 541.8320 Da

^{13}C NMR (101 MHz, $CDCl_3$) δ / ppm = 170.59 (C_q^{1}), 169.76 (C_q^{2}), 164.19 (C_q^{3}), 149.75 (CH^{4}), 112.25 (CH^{5}), 73.74 (CH^{6}), 61.75 (CH_2^{7}), 41.17 (CH_2^{8}), 32.34 (CH_2^{9}), 32.09 ($CH_2^{10\text{ or }11}$), 32.04 ($CH_2^{10\text{ or }11}$), 32.00 ($CH_2^{10\text{ or }11}$), 29.74 (CH_2^{11}), 29.67 (CH_2^{11}), 29.63 (CH_2^{11}), 29.58 (CH_2^{11}), 29.52 (CH_2^{11}), 29.46 (CH_2^{11}), 29.40 (CH_2^{11}), 29.38 (CH_2^{11}), 29.21 (CH_2^{11}), 28.91 (CH_2^{12}), 28.65 (CH_2^{13}), 24.93 (CH_2^{11}), 22.81 (CH_2^{11}), 22.79 (CH_2^{11}), 14.24 (CH_3^{14}), 14.23 (CH_3^{14}).

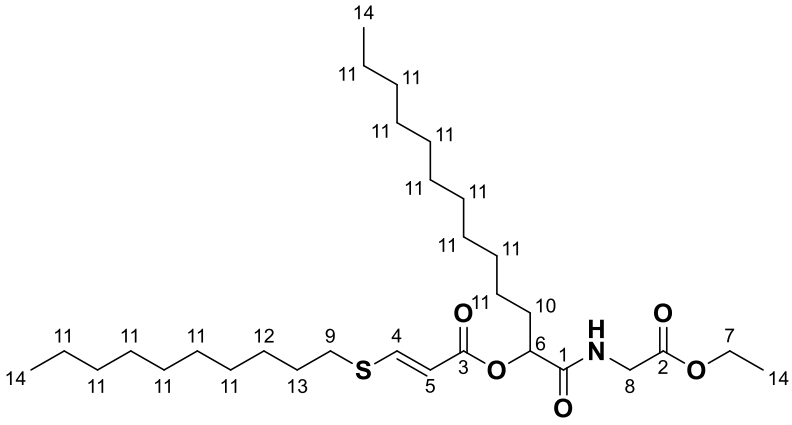

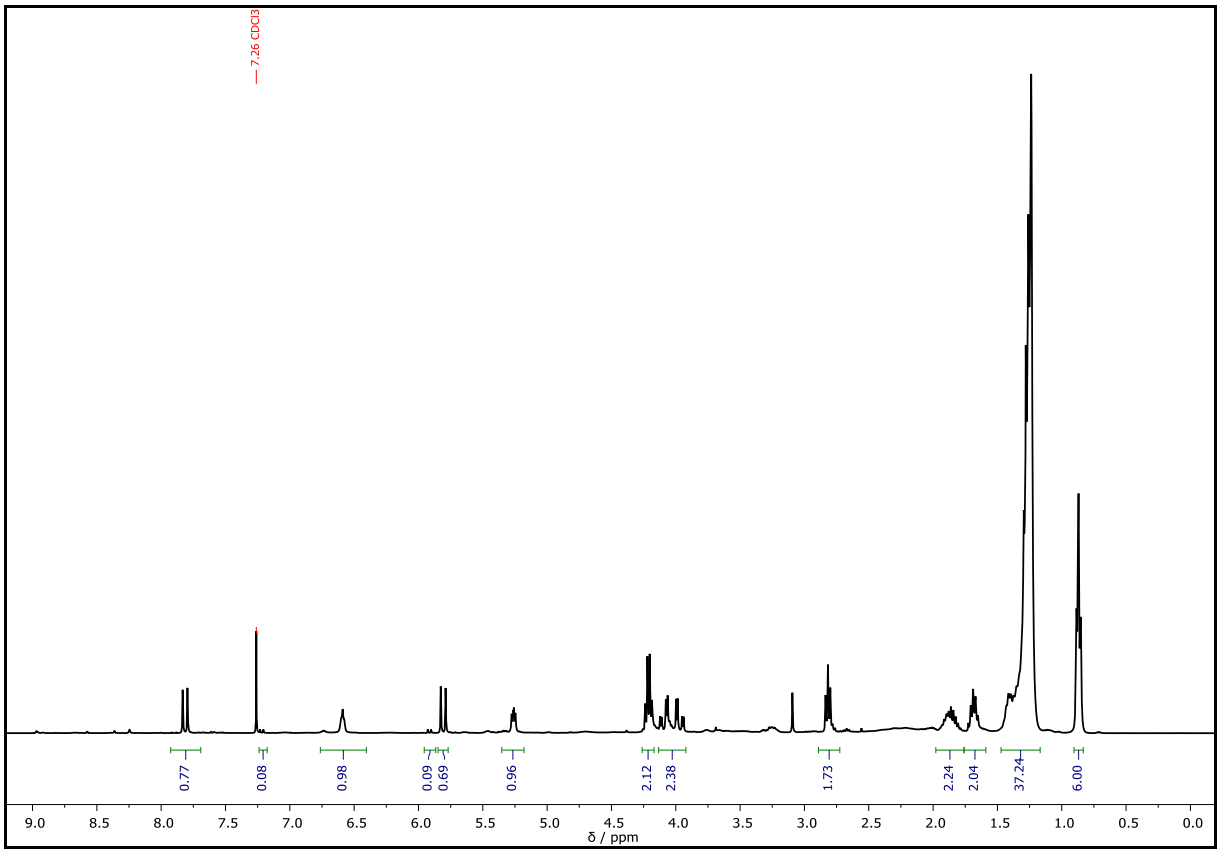

Supplementary Figure 203: ^{1}H NMR spectrum of **D5c2** recorded at 400 MHz in $CDCl_3$.

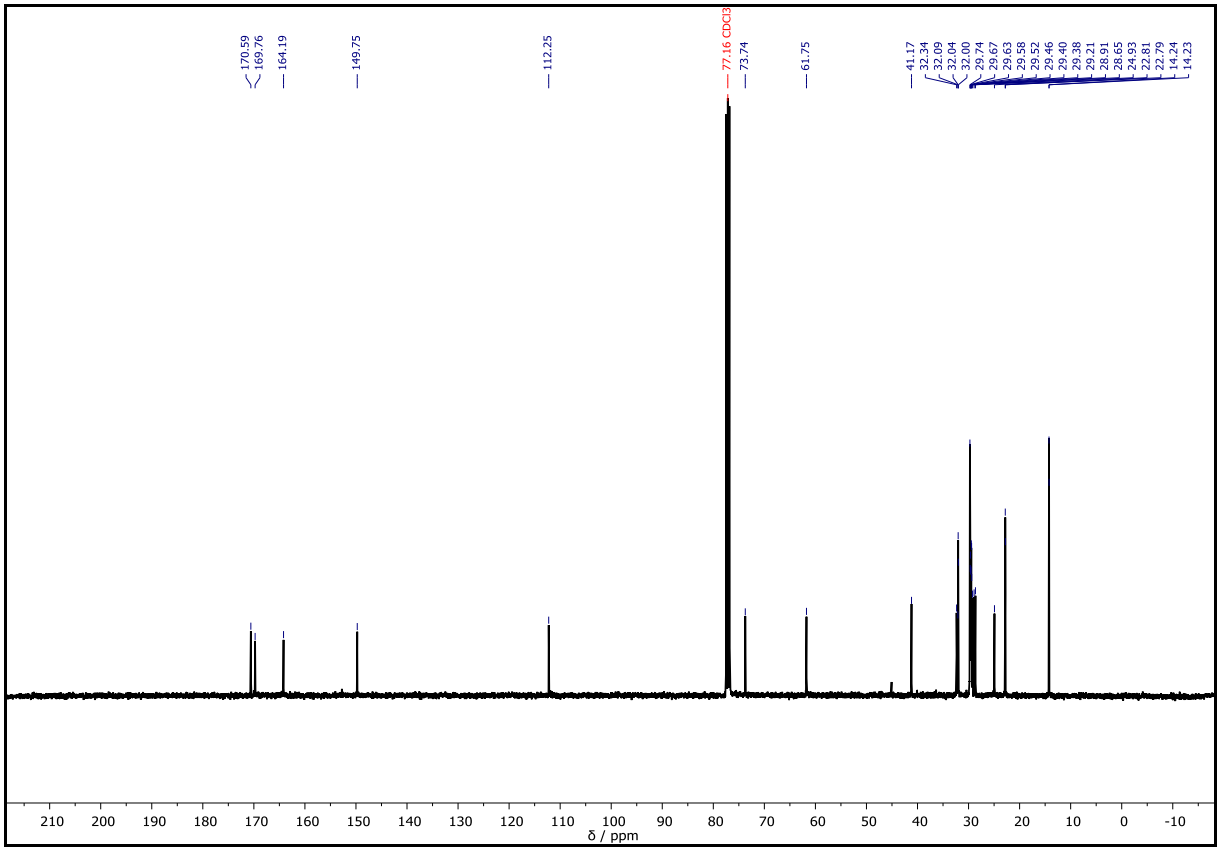

Supplementary Figure 204: ^{13}C NMR spectrum of **D5c2** recorded at 400 MHz in $CDCl_3$.

1-(Naphthalen-2-ylamino)-1-oxotridecan-2-yl (*E*)-3-(decylthio)acrylate – D25c2

^{1}H NMR (400 MHz $CDCl_3$): δ / ppm = 8.23 (s, 1H, CH_{Ar}^{1}), 8.08 (s, 1H, NH^{2}), 7.89 (d, *J* = 15.1 Hz, 1H, CH^{3}), 7.82 – 7.75 (m, 3H, CH_{Ar}^{4}), 7.53 – 7.37 (m, 3H, CH_{Ar}^{4}), 5.88 (d, *J* = 15.1 Hz, 1H, CH^{5}), 5.40 (dd, *J* = 7.3, 4.9 Hz, 1H, CH^{6}), 2.85 (t, *J* = 7.4 Hz, 2H, CH_2^{7}), 2.09 – 1.90 (m, 2H, CH_2^{8}), 1.71 (p, *J* = 7.3 Hz, 2H, CH_2^{9}), 1.50 – 1.19 (m, 32H, CH_2^{10}), 0.87 (dt, *J* = 7.0, 3.3 Hz, 6H, CH_3^{11}).

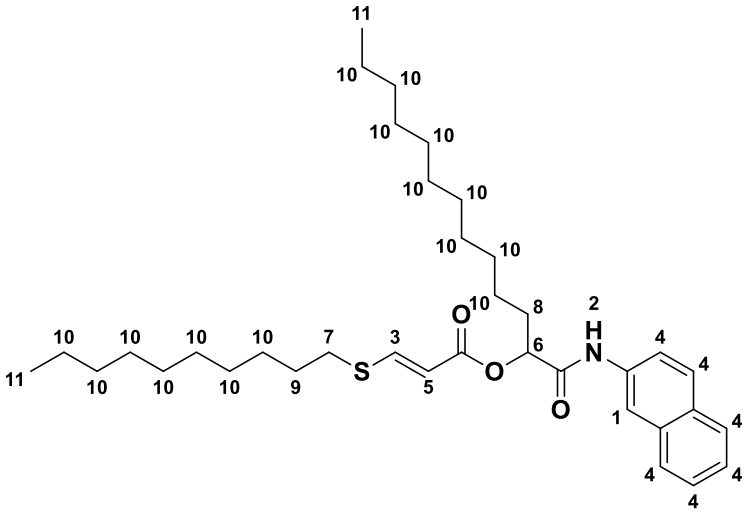

Chemical Formula: $C_{36}H_{55}NO_3S$
Exact Mass: 581.3903 Da
Molecular Weight: 581.9000 Da

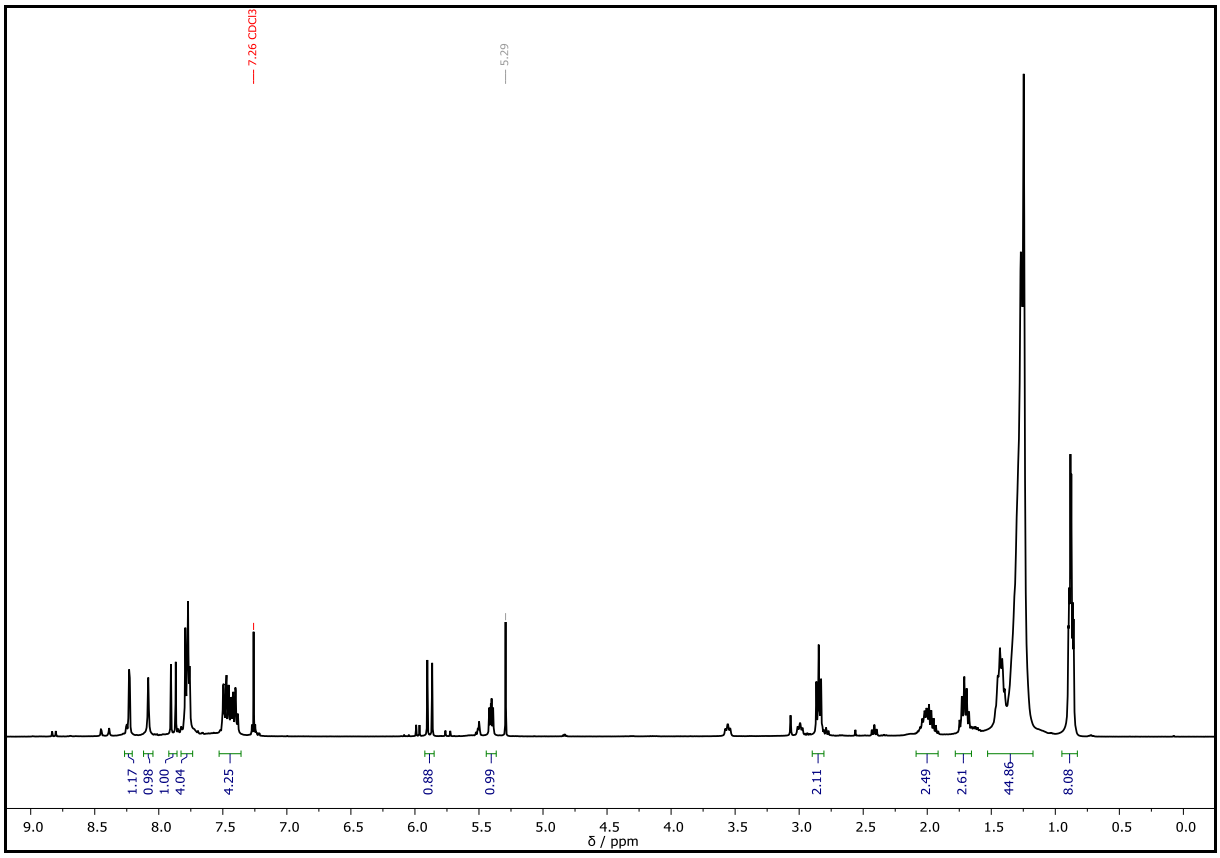

Supplementary Figure 205: ^{1}H NMR spectrum of **D25c2** recorded at 400 MHz in $CDCl_3$.

Supplementary Table 30: ESI-MS data for the P-3CR and subsequent amino-yne reaction using 5 different amines in a one-pot manner. Calculated and measured data of the proton adducts $[M+H]^+$.

compound	formular	*m*/*z* calculated / Da	*m*/*z* found / Da
M1	$C_{22}H_{34}N_2O_3$	375.2642	375.2643
M2	$C_{22}H_{42}N_2O_3$	383.3268	383.3268
M3	$C_{23}H_{36}N_2O_3$	389.2799	389.2798
M4	$C_{26}H_{50}N_2O_3$	439.3894	439.3897
M5	$C_{30}H_{58}N_2O_3$	495.4520	495.4520

(*E*)-*N*-(4-Bromophenyl)-*N*-(2-(*tert*-butylamino)-2-oxo-1-phenylethyl)-3-(diethylamino)acrylamide – U1

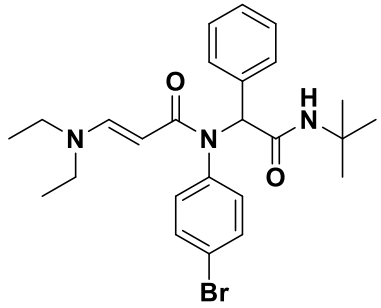

Chemical Formula: $C_{25}H_{32}BrN_3O_2$
Exact Mass: 485.1678 Da
Molecular Weight: 486.4540 Da

Benzyl aldehyde (102 µL, 106 mg, 1.00 mmol, 1.00 equiv.) was dissolved in MeOH and 4-bromoaniline (172 mg, 1.00 mmol, 1.00 equiv.) was added, and the mixture was stirred for one hour at room temperature. Propiolic acid (62.0 µL, 70.1 mg, 1.00 mmol, 1.00 equiv.) was added and stirring was continued for 15 min, followed by the dropwise addition of *tert*-butyl isocyanide (113 µL, 83 mg, 1.00 mmol, 1.00 equiv.). The reaction mixture was stirred at room temperature for another three hours. After full conversion indicated by GC, diethylamine (103 µL, 73.1 mg, 1.00 mmol, 1.00 equiv.) was added slowly. The solvent was removed under reduced pressure after one hour of stirring and the product **U1** was obtained in a yield of 96% (466 mg, 0.96 mmol).

^{1}H NMR (400 MHz $CDCl_3$): δ / ppm = 7.46 (d, *J* = 12.7 Hz, 1H, CH^1), 7.30 – 7.27 (m, 2H, $CH_{Ar}{}^2$), 7.21 – 7.14 (m, 5H, $CH_{Ar}{}^3$), 7.02 – 6.93 (m, 2H, $CH_{Ar}{}^4$), 6.08 (s, 1H, CH^5), 6.06 (s, 1H, NH^6), 4.14 (d, *J* = 12.7 Hz, 1H, CH^7), 3.06 – 2.94 (m, 4H, $CH_2{}^8$), 1.34 (s, 9H, $CH_3{}^9$), 1.00 (s, 6H, $CH_3{}^{10}$).

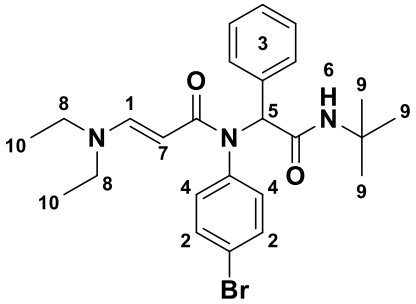

^{13}C NMR (101 MHz $CDCl_3$): δ / ppm = 169.94 (C_q^1), 169.66 (C_q^2), 150.14 (CH^3), 140.72 (C_q^4), 136.06 (C_q^5), 132.75 (CH_{Ar}^6), 131.66 (CH_{Ar}^7), 130.14 (CH_{Ar}^8), 128.31 (CH_{Ar}^8), 127.97 (CH_{Ar}^8), 121.13 (C_q^9), 85.41 (CH^{10}), 65.10 (CH^{11}), 51.45 (C_q^{12}), 42.34 (CH_2^{13}), 28.85 (CH_3^{14}), 11.45 (CH_3^{15}).

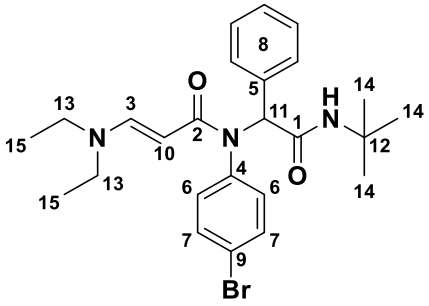

HRMS (FAB) of $C_{25}H_{32}BrN_3O_2$ $[M+H]^+$ *m/z* calc. 486.1751, found 486.1757.

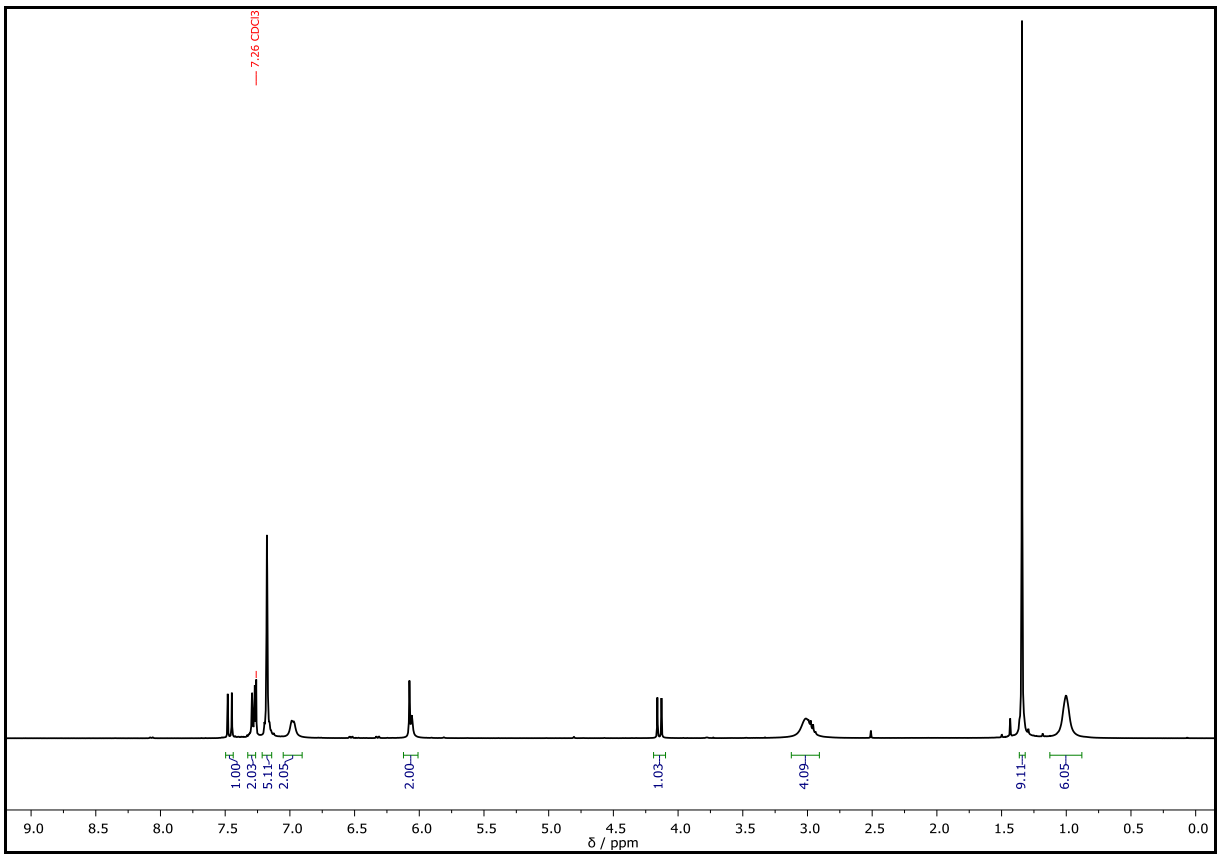

Supplementary Figure 206: ^{1}H NMR spectrum of **U1** recorded at 400 MHz in $CDCl_3$.

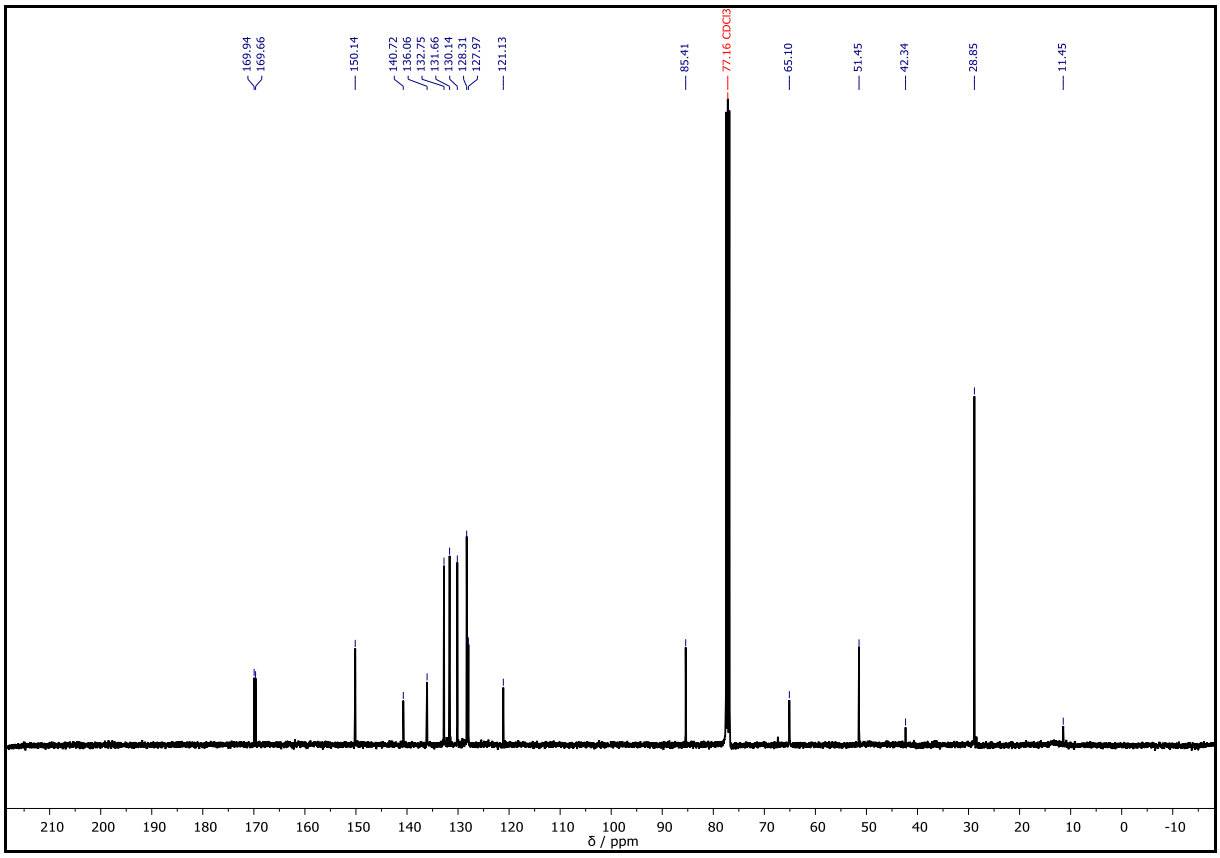

Supplementary Figure 207: ^{13}C NMR spectrum of **U1** recorded at 400 MHz in $CDCl_3$.

6.3.9. Supplementary information of chapter 4.6.3

Supplementary Table 31: Chemical shifts of molecules used for data storage in NMR

compound	Average chemical shift and maximal deviation δ / ppm
Benzene	7.3546
DCM	5.3084 ± 0.0092
DMC	3.7861 ± 0.0044
Dioxane	3.6972 ± 0.0038
DMSO	2.6137 ± 0.0055
Acetone	2.1666 ± 0.0038
MeCN	2.0052 ± 0.0060
Cyclohexane	1.4278 ± 0.0007
TMS	0.0000 ± 0.0000

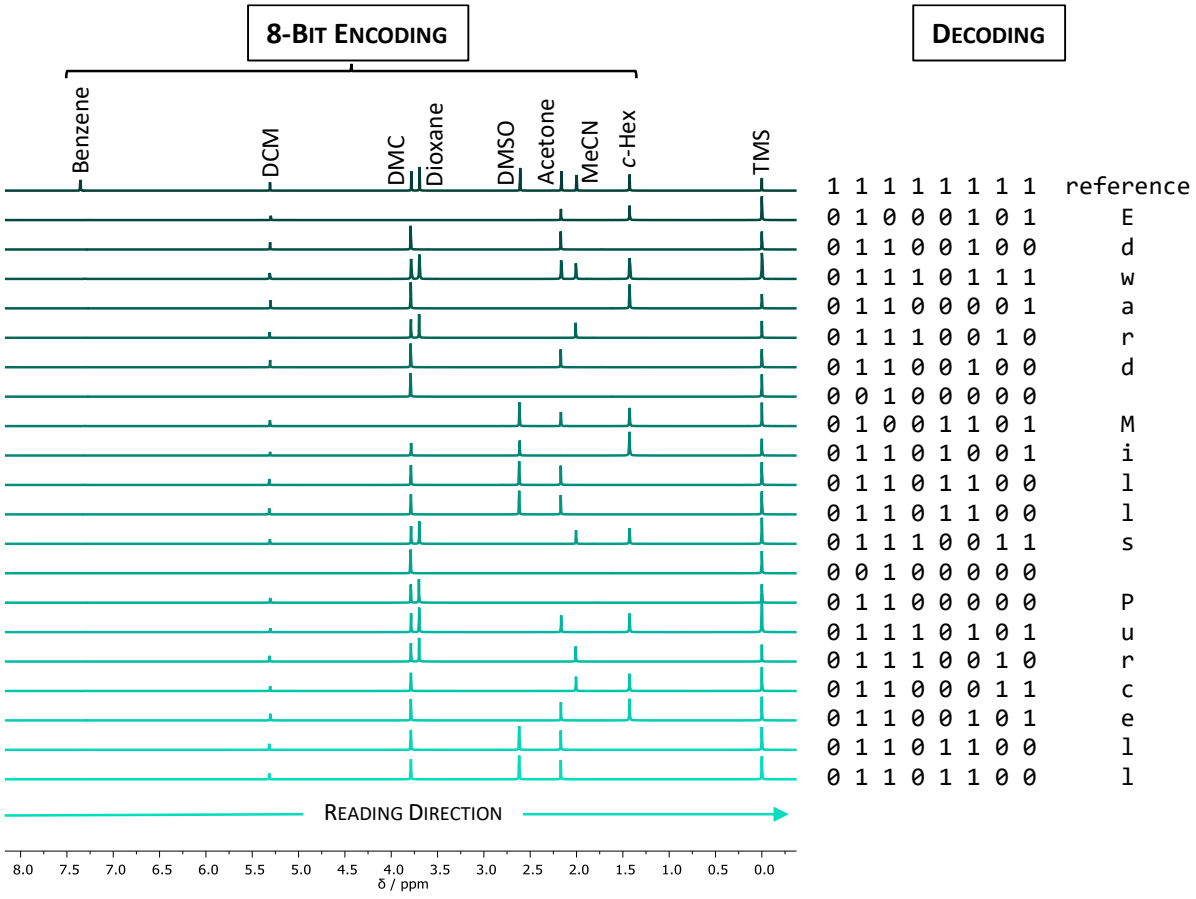

Supplementary Figure 208: Encoding and decoding with ^{1}H NMR analysis. “Edward␣Mills␣Purcell”, who was awarded the Nobel Prize together with Felix Bloch in 1952,[648,649] was encoded and decoded in mixtures of up to eight compounds *via* an 8-bit ASCII code. The reading direction was specified from low to high field and the ordering *via* manual placement in the sample holder. The absence or presence of a compound signal in the spectra was retranslated in the binary code into “0” and “1”.

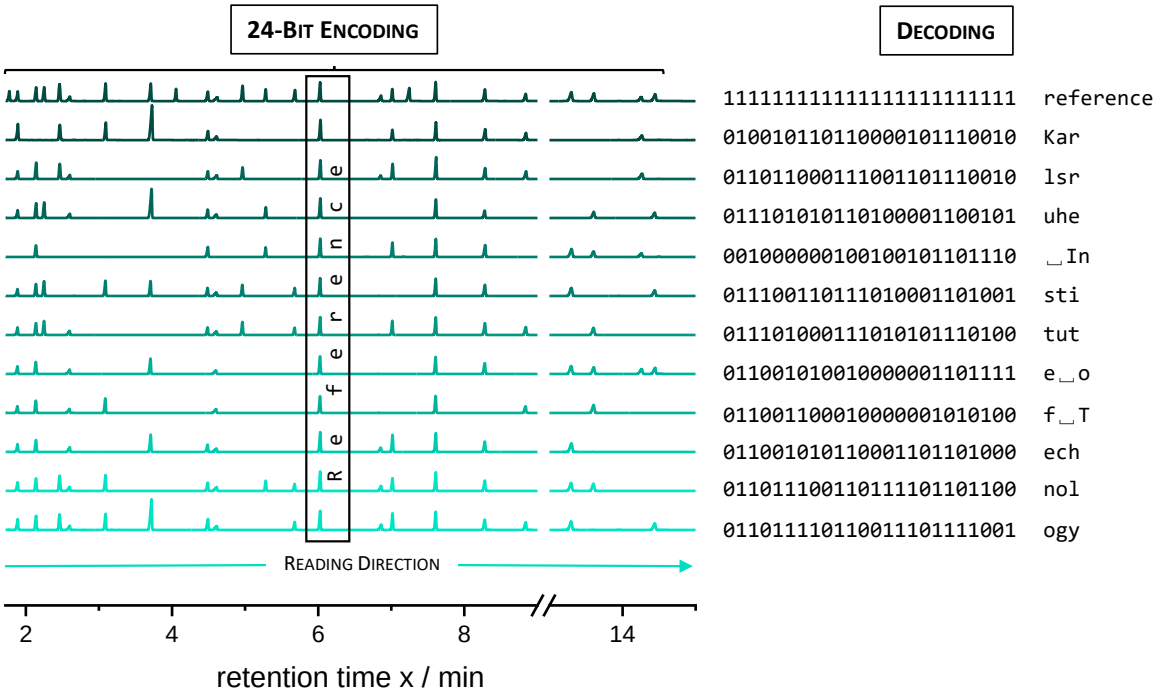

Supplementary Figure 209: Encoding and decoding with GC analysis. “Karlsruhe␣Institute␣of␣Technology” was encoded and decoded in mixtures of up to 24 compounds *via* an 8-bit ASCII code (3 byte per mixture). The reading direction was specified from lower to higher retention time and the ordering *via* manual placement in the sample holder. The absence or presence of a compound signal in the chromatogram was retranslated in the binary code into “0” and “1”.

Supplementary Table 32: Retention time and processed data of molecules used for data storage in GC

Compound	x_{Refa} **/min**	Δ-x_{MAX} × 10^{-3} [b]	Δ+x_{MAX} × 10^{-3} [c]	ω × 10^{-3} [d]
1,2-Propandiol	1.768	2.920	1.250	4.170
2,3-Butandiol	1.882	2.505	0.835	3.340
1-Hexanol	2.135	3.335	0.835	4.170
Cyclohexanol	2.245	2.505	0.835	3.340
Cyclooctane	2.456	1.665	2.505	4.170
Diethylenglycol	2.590	2.920	1.250	4.170
Benzyl alcohol	3.077	2.230	2.160	4.390
2-Phenylethanol	3.698	2.495	2.505	5.000
4-Ethylphenol	4.049	3.330	1.670	5.000
4-Methoxyphenol	4.483	4.165	1.665	5.830
Triethylenglycol	4.599	10.00	1.670	11.670
1-Adamantanol	4.958	6.250	1.250	7.500
1,4-Diethoxybenzene	5.273	2.923	1.835	4.758
2,6-Dimethylphenol	5.672	2.920	2.080	5.000
TEGMeO	6.850	4.580	2.920	7.500
2,6-Di-^{t}Bu-4-methylphenol	7.012	4.995	1.665	6.660
1,10-Decandiol	7.234	4.170	5.000	9.170
n-Hexadecane	7.601	2.910	2.090	5.000
2-Naphthaleneethanol	8.275	2.080	1.250	3.330
1,12-Dodecandiol	8.844	8.750	1.250	10.000
3,3',5,5'-Tetramethylbiphenyl[e]	9.265	6.665	1.665	8.330
Methyl palmitate[e]	10.653	5.420	2.920	5.712
Methyl oleate	13.284	1.670	5.000	6.670
Methyl Stearate	13.599	10.830	2.500	13.330
1,8,9-Trihydroxyanthracene	14.248	3.330	4.170	7.500
9-Anthracenemethanol	14.437	5.830	3.330	9.160

Values were determined from the data sets measured for the encoding of the QR code; [a] averaged x-values (x_{Ref}) of the respective peak maxima (retention time) of the associated compound calculated from the reference spectra (three-fold determination); [b] distance to the maxima over all measurements with the largest Δx-value in the direction of lower (Δ-x_{MAX}) and [c] higher (Δ+x_{MAX}) retention times; [d] range in which all maxima of the respective compound are located ($\omega = \Delta+x_{MAX} + \Delta-x_{MAX}$); [e] compound was not used for the data storage shown in Supplementary Figure 209.

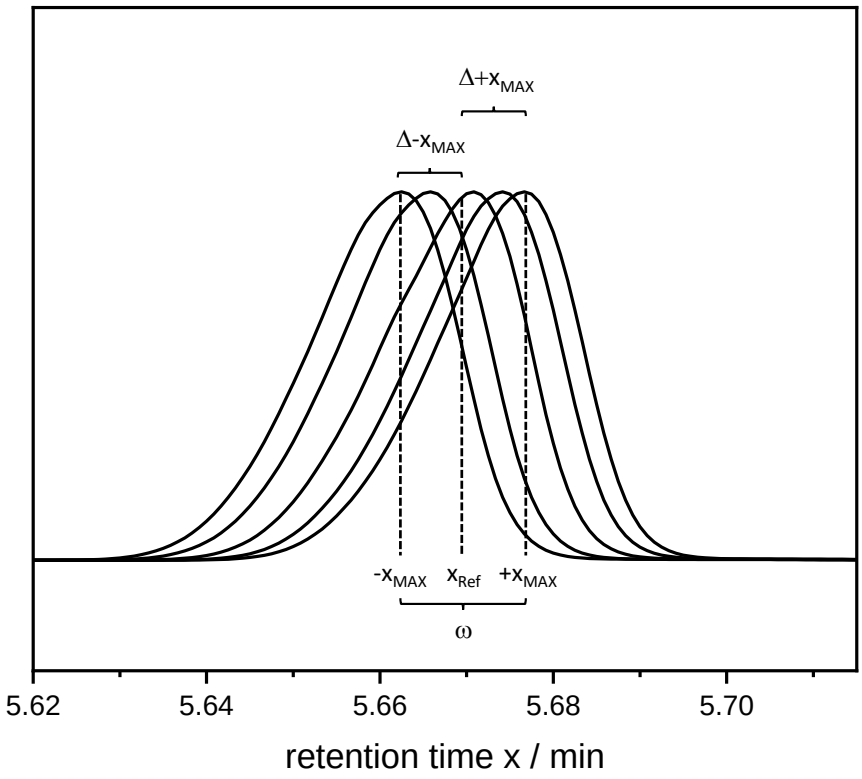

Supplementary Figure 210: Schematic representation of the calculated values in Supplementary Table 32.

$x_{Ref} = (-X_{MAX}) + (+X_{MAX})/2; \Delta - x_{MAX} = x_{Ref} - (-x_{MAX}); \Delta + x_{MAX} = (+x_{MAX}) - x_{Ref};$

$\omega = (-X_{MAX}) + (+X_{MAX})$

Note that the + and – sign directly before X_{MAX} is no arithmetic operator.

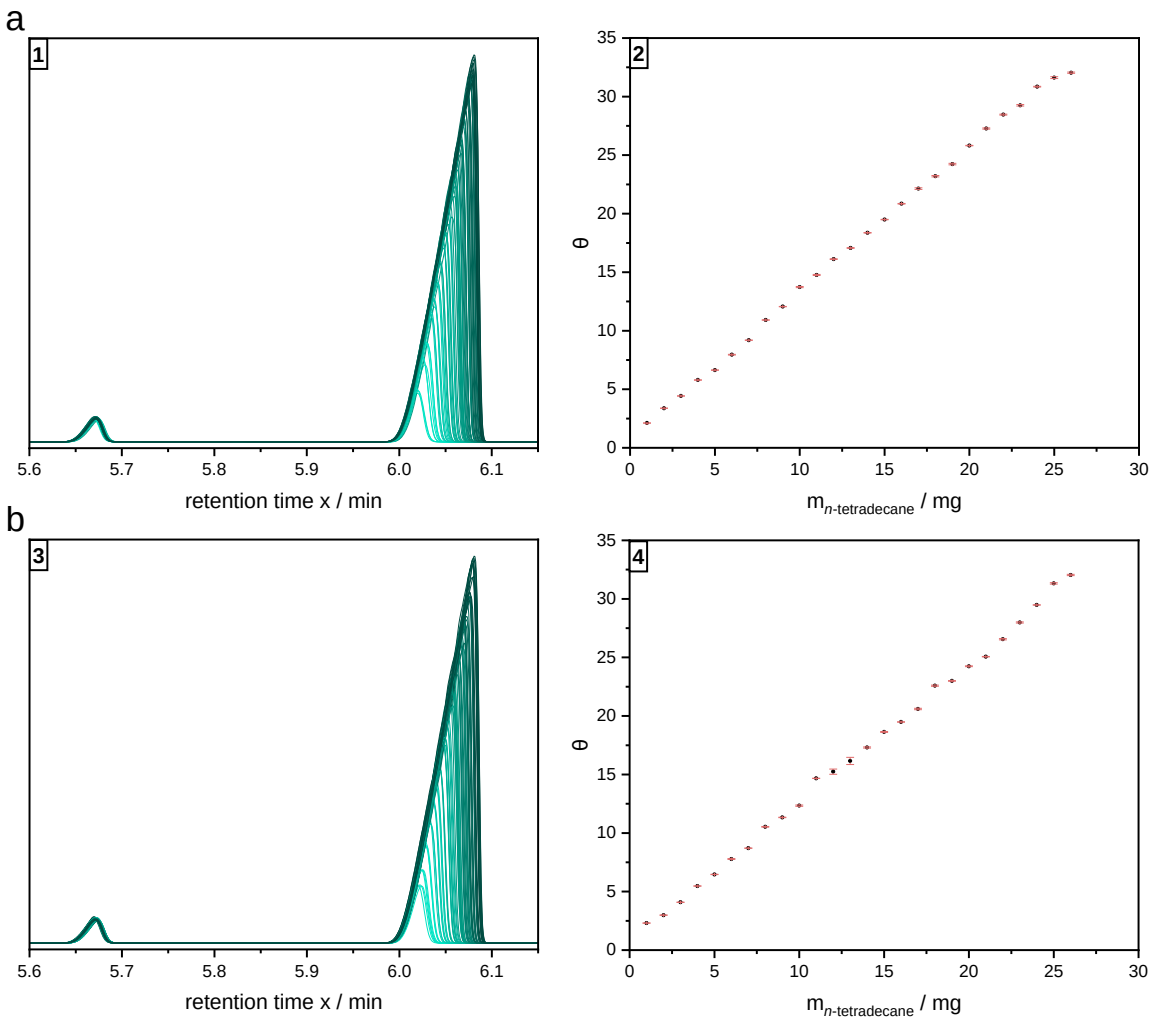

Supplementary Figure 211: Calibration curve and chromatograms of the reference. Ordering of data sets dependent on the integral ratio of the two reference signals of *n*-tetradecane $[x_1 = 5.98;\ x_2 = 6.10]$ and 2,6-dimethylphenol $[x_3 = 5.63;\ x_4 = 5.70]$ calculated by a three-fold determination $(f(x), g(x), h(x))$. **a** represent the data set for the "fan" bit map and **b** for the QR code. **1** and **3** Cutout of GC chromatograms focusing on the two reference peaks. Left signal: 2,6-dimethylphenol with same concentration in each mixture. Right signal: *n*-tetradecane with varying concentration. **2** and **4** Plot of the averaged integral ratio θ against the amount of *n*-tetradecane added to the respective mixture with $\theta = \bar{\mathrm{x}}\left[\int_{x_1}^{x_2} f(x); \int_{x_1}^{x_2} g(x); \int_{x_1}^{x_2} h(x)\right] \times \bar{\mathrm{x}}\left[\int_{x_3}^{x_4} f(x); \int_{x_3}^{x_4} g(x); \int_{x_3}^{x_4} h(x)\right]^{-1}$.

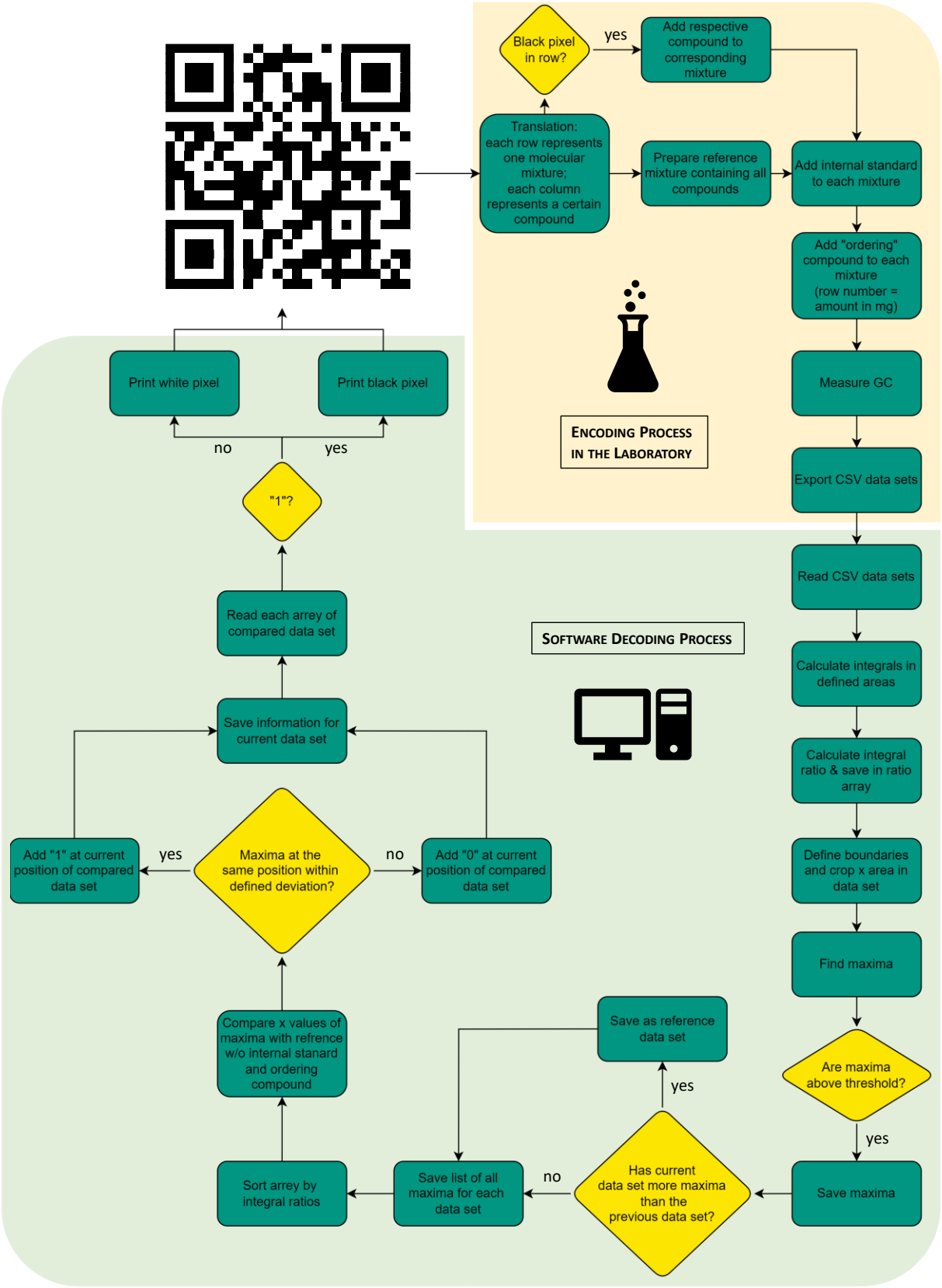

Supplementary Figure 212: Flowchart describing the encoding and decoding process for the QR code. The individual steps for the encoding process in the laboratory are highlighted in light yellow and for the decoding process *via* the software in light green. The processing steps are represented in green rectangles and the decision points in yellow rhombi. The QR leads to the homepage of the KIT (https://www.kit.edu/index.php). For detailed information about the code, refer to the provided files (README.txt and the read.py).

7. APPENDIX

7.1. List of Abbreviation

µm	Micromole
χ	Flory-Huggins interaction parameter
Φ	Volume fraction
ABS	Acrylonitrile butadiene styrene
ADMET	Acyclic diene metathesis
AFM	Atomic force microscopy
Ar	Argon
aROP	Anionic ring-opening polymerization
ASCII	American Standard Coder for Information Interchange
ATRP	Atomic transfer radical polymerization
BCP	Block copolymer
CALB	*Candida antarctica* Lipase B
CAN	Covalent adaptable networks
CID	Collision-induced dissociation
CMA	Connolly Molecular Area
Conv.	Conversion
COSY	Correlation spectroscopy
CuAAC	Copper-catalyzed azide/alkyne cycloaddition
$Đ$	Dispersity
Da	Dalton
DABCO	1,4-Diazabicyclo[2.2.2]octan
DBU	1,8-Diazabicyclo[5.4.0]undec-7-en
DCC	*N*,*N*‘-Dicyclohexylcarbodiimide
DCM	Dichloromethane

DCTB	2-[(2E)-3-(4-*tert*-Butylphenyl)-2-methylprop-2-enylidene]malonitrile
DCU	Dicyclohexylurea
DEDG	Double exponential dendrimer growth
DFT	Density functional theory
DHB	2,5-Dihydroxybenzoic acid
DHMP	3,4-Dihydropyrimidin-2(1*H*)-one
DHP	1,4-dihydropyridines
DIEPA	Diisopropylethylamine
DLS	Dynamic light scattering
DMAP	*N*,*N*-(Dimethylamino)pyridine
DMC	Dimethyl carbonate
DMF	*N,N*-Dimethylformamide
DMPA	2,2-Dimethoxy-1,2-diphenylethan-1-one
DMS-*b*-LA	oligo(dimethylsiloxane)-*block*-oligo(lactic acid)
DMS-*b*-MMA	Dimethylsiloxane-*block*-methyl methacrylate
DMSO	Dimethyl sulfoxide
DMSO-d_6	Deuturated dimethyl sulfoxide
DMT	dimethoxytrityl
DNA	Deoxyribonucleic acid
dNbipy	4,4’-Dinonyl-2-2’-dipyridyl
DoE	Design of Experiments
DOSY	Diffusion ordered spectroscopy
DPTS	4-(Dimethylamino)pyridinium *p*-toluenesulfonate
DSC	Differential scanning calorimetry
EA	Ethyl acetate
EBA	Ethyl bromoacetate
EDC	1-Ethyl-3-(3-dimethylaminopropyl)carbodiimid
EG	Ethylene glycol
Equiv.	Equivalents
ESI	Electrospray ionization

ESI-MS	Electrospray ionization - mass spectrometry
ESI-MS/MS	Electrospray ionization tandem mass spectrometry
eV	electronvolt
EWG	Electron withdrawing group
Fmoc	Fluorenylmethoxycarbonyl
FSPE	Fluorous solid-phase extraction
GC	Gas chromatography
GC-FID	Gas chromatography – flame ionization detector
GPC	Gel permeation chromatography
GPE	Glycidyl propargyl ether
HC	Hexagonal cylinder
HCCA	α-Cyano-4-hydroxy-cinnamic acid
HF	Hydrofluoric acid
HFIP	1,1,1,3,3,3-Hexafluoropropan-2-ol
HMBC	Heteronuclear multiple bond correlation
HOBt	1*H*-1,2,3-Benzotriazol-1-ol
HSAB	“hard and soft (Lewis) acids and bases”
HSQC	Heteronuclear single quantum coherence spectroscopy
IBX	1-Hydroxy-1λ^5,2-benziodoxol-3(1*H*)-one 1-oxide
IEG	Iterative exponential growth
IMCR	Isocyanide-based multicomponent reaction
$I_{norm.}$	Normalized intensity
IR	Infrared
IrAAC	Iridium-catalyzed azide/alkyne cycloaddition
ISG	Iterative sequential growth
IUPAC	International Union of Pure and Applied Chemistry
L_0	Long-range-order distance
LC-MS	Liquid chromatography – mass spectrometry
LC-MS/MS	Liquid chromatography – tandem mass spectrometry
logP	Octanol-water partition coefficient

m	Mass
M	Molar mass
M/I	Monomer-to-initiator ratio
m/*z*	Mass-to-charge ratio
MALDI	Matrix assisted laser desorption ionization
MALDI-MS	matrix assisted laser desorption ionization – mass spectrometry
MALDI-MS/MS	matrix assisted laser desorption ionization – tandem mass spectrometry
MALDI-TOF-MS	matrix assisted laser desorption ionization – time of flight – mass spectrometry
MALDI-TOF-MS/MS	matrix assisted laser desorption ionization – time of flight – tandem mass spectrometry
mbar	Millibar
MCR	Multicomponent reaction
MCS	Macrocyclic sulfate
Me_6TREN	Tris[2-(dimethylamino)ethyl]amine
MEM	2-Methoxyethoxymethyl
mg	Milligram
MIDI	Musical Instrumental Digital Interface
min	Minute
M_n	Number of average molar mass
mPEG	Monomethoxy poly(ethylene glycol)
mPEG-b-PCL	Monomethoxy poly(ethylene glycol)-*block*-poly(ε-caprolactone)
MPS	Microphase separation
MS	Mass spectrometry
MTBD	1-Methyl-2,3,4,6,7,8-hexahydro-1*H*-pyrimido[1,2-a]pyrimidine
mTEG	Tetra(ethylene glycol) monomethyl ether
M_w	Mass average molar mass
NHC	*N*-Heterocyclic carbene
nm	Nanometer

NMP	Nitroxide-mediated radical polymerization
NMR	Nuclear magnetic resonance
oBL	Oligo(γ-butyrolactone)
oCLBL	Oligo(ε-caprolactone-*co*-γ-butyrolactone)
oDMS-*b*-oLA	Oligo(dimethylsiloxane)-*block*-oligo(lactic acid)
ODT	Order-disorder phase transition
OEG	Oligo(ethylene glycol)
oGA	Oligo(glycolide acid)
OHB	Oligo((*R*)-3-hydroxybutanoic acid)
oLA	Oligo(lactic acid)
OLED	Organic light-emitting diode
oPDO	Oligo(*p*-diocanone)
OPE	oligo(phenylene ethynylene)
OPV	Organic photovoltaics
P-3CR	Passerini-three-component reaction
P-3KR	Passerini Dreikomponentenreaktion
PAA	Poly(acrylic acid)
PCL	Poly(ε-caprolactone)
PEG	Poly(ethylene glycol)
PEG-*b*-PCL	Poly(ethylene glycol)-*block*-poly(ε-caprolactone)
PISA	Polymerization-induced self-assembly
PLA	Poly(lactic acid)
PLA-b-PPL	Poly(lactic acid)-*block*-poly(phenyllactic acid)
PLGA	Poly(lactic-*co*-glycolic acid)
PMB	*p*-Methoxybenzyl
PMDETA	N^1-[2-(Dimethylamino)ethyl]-N^1,N^3,N^3-trimethylethane-1,2-diamine
pmol	Picomole
PPL	Poly(phenyllactic acid)
ppm	Parts per million
PS-b-PAA	Polystyrene-*block*-poly(acrylic acid)

PVC	Polyvinyl chloride
PyBOP	(Benzotriazol-1-yloxy)tripyrrolidinophosphonium hexafluorophosphate
QR code	Quick response code
RAFT	Reversible-addition-fragmentation chain-transfer
RDRP	Reversible-deactivation radical polymerization
RNA	Ribonucleic acid
ROMP	Ring-opening metathesis polymerization
ROP	Ring-opening polymerization
rt	Room temperature
SA	Self-assembly
SAN	Styrene-acrylonitrile
SAXS	Small-angle X-ray scattering
SCMFT	self-consistent mean field theory
SDC	Sample displacement chromatography
SEC	Size exclusion chromatography
SEC-ESI-MS	Size exclusion chromatography - electrospray ionization - mass spectrometry
SEM	Scanning electron microscope
SPE	Solid-phase extraction
SPPS	Solid phase peptide synthesis
SVA	Solvent vapor annealing
TAD	1,2,4-Triazoline-3,5-diones
TBAF	*N*,*N*,*N*-Tributylbutan-1-aminium fluoride
TBD	1,5,7-Triazabicyclo[4.4.0]dec-5-en
TBDMSCl	*tert*-Butyl(chloro)di(methyl)silane
TBDPS	*tert*-Butyldiphenylsilyl
T_c	Crystallization temperature
TCA	Trichloroacetic acid
TEA	Triethylamine
TEG-SH	tri(ethylene glycol) monomethyl ether
TEM	Transmission electron microscope

TEMPO	(2,2,6,6-Tetramethylpiperidin-1-yl)oxyl
TES	Triethyl silane
TFA	Trifluoroacetic acid
TGA	Thermogravimetric analysis
TG-SH	thioglycerol
THF	Tetrahydrofuran
THP	Tetrahydropyran
TIPSCl	Triisopropyl(chloro)silane
TLC	Thin-layer chromatography
TMDS	1,1,3,3-Tetramethyldisiloxane
T_{ODT}	Order-to-disorder phase transition temperature
TPB	1-(4-Hydroxy-4′-biphenylyl)-2-(4-hydroxyphenyl)butane
TS	Transition state
U-4CR	Ugi-four-component reaction
UV	Ultraviolet
WAXS	Wide-angle X-ray scattering
wt%	Weight percent
ZB	Zettabyte

7.2. List of Figures

7.3. List of Schemes

7.4. List of Tables

7.5. Publications

1. *"Uniform poly(ethylene glycol): a comparative study",* P. Bohn, M. A. R. Meier, *Polym. J*. **2020**, *52*, 165-178. (https://doi.org/10.1038/s41428-019-0277-1)

2. *"Molecular data storage with zero synthetic effort and simple read out."* P. Bohn, M. P. Weisel, J. Wolfs, M. A. R. Meier, *Sci. Rep*. **2022**, *12*, 13878. (https://doi.org/10.1038/s41598-022-18108-9)

7.6. Conference Contributions

Participation at the ACS Spring 2021, April 4 – 16, **2021**, San Diego, USA (Online Conference).

"Uniform PCL-b-PEG Block Copolymers: Synthesis and Characterization"
Poster at the #RSCPoster Twitter Conference **2021** (Online Conference).

Participation at the "Makromolekulares Kolloquium Freiburg 2021", February 9th, **2021**, Freiburg, Germany (Online Conference).

"Monodisperse PCL-b-PEG Block Copolymers: Synthesis and Characterization"
Poster at the Polydays Conference, September 11 – 13, **2019**, Berlin, Germany.

"Synthesis and Characterization of Monodisperse PCL-b-PEG Block Copolymers"
Poster at the European Polymer Federation (EPF) Conference, June 9 – 14, **2019**, Heraklion (Crete), Greece.

Participation at the 10th Workshop on Fats and Oils as Renewable Feedstock for the Chemical Industry, March 17 – 19, **2019**, Karlsruhe, Germany.

"Preparation and Characterization of Monodisperse Macromolecules"
Poster at the Meeting of the GDCh-Division together with SFB 1176, September 24 – 27, **2018**, Karlsruhe, Germany.

8. Bibliography

[1] R. Mülhaupt, *Angew. Chem. Int. Ed.* **2004**, *43*, 1054.

[2] H. Staudinger, *Chem. Ber.* **1920**, *53*, 1073.

[3] W. H. Carothers, *Chem. Rev.* **1931**, *8*, 353.

[4] M. Szwarc, *Nature* **1956**, *178*, 1168.

[5] M. Kato, T. Ito, Y. Aoyama, K. Sawa, T. Kaneko, N. Kawase, H. Jinnai, *J. Polym. Sci. B Polym. Phys.* **2007**, *45*, 677.

[6] H. Fischer, *J. Am. Chem. Soc.* **1986**, *108*, 3925.

[7] H. Fischer, *Chem. Rev.* **2001**, *101*, 3581.

[8] H. Fischer, *J. Polym. Sci. A Polym. Chem.* **1999**, *37*, 1885.

[9] S. N. Khanna, M. Levy, M. Szwarc, *Trans. Faraday Soc.* **1962**, *58*, 747.

[10] H. W. Melville, M. G. Evans, W. C. Price, R. P. Bell, J. H. Schulman, *Annu. Rep. Prog. Chem.* **1939**, *36*, 33.

[11] P. J. Flory, *J. Am. Chem. Soc.* **1940**, *62*, 1561.

[12] K. Ziegler, *Angew. Chem. Int. Ed.* **1936**, *49*, 455.

[13] S. Z. Perry, H. Hibbert, *Can. J. Res.* **1936**, *14B*.

[14] M. Kato, M. Kamigaito, M. Sawamoto, T. Higashimura, *Macromolecules* **1995**, *28*, 1721.

[15] J.-S. Wang, K. Matyjaszewski, *J. Am. Chem. Soc.* **1995**, *117*, 5614.

[16] K. Matyjaszewski, *Macromolecules* **2012**, *45*, 4015.

[17] T. Otsu, M. Yoshida, *Macromol. Rapid Commun.* **1982**, *3*, 127.

[18] T. Otsu, M. Yoshida, T. Tazaki, *Macromol. Rapid Commun.* **1982**, *3*, 133.

[19] M. R. Hill, R. N. Carmean, B. S. Sumerlin, *Macromolecules* **2015**, *48*, 5459.

[20] G. Moad, E. Rizzardo, D. H. Solomon, *Macromolecules* **1982**, *15*, 909.

[21] D. H. Solomon, E. Rizzardo, P. Cacioli, *Polymerization process and polymers produced thereby*. US4581429, **1986**.

[22] D. H. Solomon, *J. Polym. Sci. A Polym. Chem.* **2005**, *43*, 5748.

[23] M. K. Georges, R. P. N. Veregin, P. M. Kazmaier, G. K. Hamer, *Macromolecules* **1993**, *26*, 2987.

[24] C. J. Hawker, *J. Am. Chem. Soc.* **1994**, *116*, 11185.

[25] C. J. Hawker, *Acc. Chem. Res.* **1997**, *30*, 373.

[26] S. M. Kharasch, H. Engelmann, F. R. Mayo, *J. Org. Chem.* **1937**, *02*, 288.

[27] T. Ouhadi, C. Stevens, P. Teyssié, *Makromol. Chem.* **1975**, *1*, 191.

[28] S. Slomkowski, S. Penczek, *Macromolecules* **1976**, *9*, 367.

[29] A. Deffieux, S. Boileau, *Macromolecules* **1976**, *9*, 369.

[30] T. J. Katz, S. J. Lee, N. Acton, *Tetrahedron Lett.* **1976**, *17*, 4247.

[31] F. N. Tebbe, G. W. Parshall, G. S. Reddy, *J. Am. Chem. Soc.* **1978**, *100*, 3611.

[32] F. A. Bovey, *NMR of polymers*, Academic Press, San Diego, **1996**.

[33] G. Montaudo, R. P. Lattimer, *Mass spectrometry of polymers*, CRC Press, Boca Raton, Fla., **2002**.

[34] J. C. Moore, *J. Polym. Sci. A Gen. Pap.* **1964**, *2*, 835.

[35] W. A. Braunecker, K. Matyjaszewski, *Prog. Polym. Sci.* **2007**, *32*, 93.

[36] K. Parkatzidis, H. S. Wang, N. P. Truong, A. Anastasaki, *Chem* **2020**, *6*, 1575.

[37] A. Hirao, R. Goseki, T. Ishizone, *Macromolecules* **2014**, *47*, 1883.

[38] A. H. E. Müller, K. Matyjaszewski (Eds.) *Controlled and living polymerizations*. *Methods and materials*, Wiley-VCH, Weinheim, **2009**.

[39] J.-F. Lutz, M. Ouchi, D. R. Liu, M. Sawamoto, *Science* **2013**, *341*, 1238149.

[40] J.-F. Lutz, *Macromol. Rapid Commun.* **2017**, *38*.

[41] C. Qu, J. He, *Sci. China Chem.* **2015**, *58*, 1651.

[42] N. Badi, J.-F. Lutz, *Chem. Soc. Rev.* **2009**, *38*, 3383.

[43] J.-F. Lutz, *Polym. Chem.* **2010**, *1*, 55.

[44] J.-F. Lutz in *ACS symposium series*, *Vol. 1170* (Ed.: J.-F. Lutz), American Chemical Society, Washington, DC, **2014**, pp. 1–11.

[45] J.-F. Lutz (Ed.) *ACS symposium series*, *Vol. 1170*, American Chemical Society, Washington, DC, **2014**.

[46] C. Yang, K. B. Wu, Y. Deng, J. Yuan, J. Niu, *ACS Macro. Lett.* **2021**, *10*, 243.

[47] Y. Mai, A. Eisenberg, *Chem. Soc. Rev.* **2012**, *41*, 5969.

[48] S. B. Darling, *Prog. Polym. Sci.* **2007**, *32*, 1152.

[49] P. Alexandridis, B. Lindman, *Amphiphilic block copolymers*. *Self-assembly and applications*, Elsevier, Amsterdam, **2000**.

[50] A. Blanazs, S. P. Armes, A. J. Ryan, *Macromol. Rapid Commun.* **2009**, *30*, 267.

[51] A. Rösler, G. W. Vandermeulen, H.-A. Klok, *Adv. Drug. Deliv. Rev.* **2012**, *64*, 270.

[52] R. A. Segalman, B. McCulloch, S. Kirmayer, J. J. Urban, *Macromolecules* **2009**, *42*, 9205.

[53] H.-A. Klok, S. Lecommandoux, *Adv. Mater.* **2001**, *13*, 1217.

[54] M. L. Huggins, *J. Chem. Phys.* **1941**, *9*, 440.

[55] P. J. Flory, *J. Chem. Phys.* **1942**, *10*, 51.

[56] L. Leibler, *Macromolecules* **1980**, *13*, 1602.

[57] P. Alexandridis, B. Lindman, *Amphiphilic block copolymers*. *Self-assembly and applications*, Elsevier, Amsterdam, **2000**.

[58] F. S. Bates, G. H. Fredrickson, *Phys. Today* **1999**, *52*, 32.

[59] S. Förster, T. Plantenberg, *Angew. Chem. Int. Ed.* **2002**, *41*, 688.

[60] J. K. Kim, S. Y. Yang, Y. Lee, Y. Kim, *Prog. Polym. Sci.* **2010**, *35*, 1325.

[61] M. C. Orilall, U. Wiesner, *Chem. Soc. Rev.* **2011**, *40*, 520.

[62] J. C. van Hest, D. A. Delnoye, M. W. Baars, M. H. van Genderen, E. W. Meijer, *Science* **1995**, *268*, 1592.

[63] L. Zhang, A. Eisenberg, *Science* **1995**, *268*, 1728.

[64] Zhang, Yu, Eisenberg, *Science* **1996**, *272*, 1777.

[65] N. A. Lynd, M. A. Hillmyer, *Macromolecules* **2005**, *38*, 8803.

[66] K. E. B. Doncom, L. D. Blackman, D. B. Wright, M. I. Gibson, R. K. O'Reilly, *Chem. Soc. Rev.* **2017**, *46*, 4119.

[67] O. Terreau, L. Luo, A. Eisenberg, *Langmuir* **2003**, *19*, 5601.

[68] S. R. George, R. Champagne-Hartley, G. A. Deeter, J. D. Campbell, B. Reck, D. Urban, M. F. Cunningham, *Macromolecules* **2017**, *50*, 315.

[69] Y. Hirai, T. Terashima, M. Takenaka, M. Sawamoto, *Macromolecules* **2016**, *49*, 5084.

[70] A. Buckinx, M. Rubens, N. R. Cameron, C. Bakkali-Hassani, A. Sokolova, T. Junkers, *Polym. Chem.* **2022**.

[71] E. Konishcheva, D. Häussinger, S. Lörcher, W. Meier, *Eur. Polym. J.* **2016**, *83*, 300.

[72] B. van Genabeek, B. F. M. de Waal, B. Ligt, A. R. A. Palmans, E. W. Meijer, *ACS Macro. Lett.* **2017**, *6*, 674.

[73] Y. Jiang, M. R. Golder, H. V.-T. Nguyen, Y. Wang, M. Zhong, J. C. Barnes, D. J. C. Ehrlich, J. A. Johnson, *J. Am. Chem. Soc.* **2016**, *138*, 9369.

[74] M. R. Golder, Y. Jiang, P. E. Teichen, H. V.-T. Nguyen, W. Wang, N. Milos, S. A. Freedman, A. P. Willard, J. A. Johnson, *J. Am. Chem. Soc.* **2018**, *140*, 1596.

[75] C. Zhang, M. W. Bates, Z. Geng, A. E. Levi, D. Vigil, S. M. Barbon, T. Loman, K. T. Delaney, G. H. Fredrickson, C. M. Bates et al., *J. Am. Chem. Soc.* **2020**, *142*, 9843.

[76] B. Oschmann, J. Lawrence, M. W. Schulze, J. M. Ren, A. Anastasaki, Y. Luo, M. D. Nothling, C. W. Pester, K. T. Delaney, L. A. Connal et al., *ACS Macro. Lett.* **2017**, *6*, 668.

[77] D. T. Gentekos, J. Jia, E. S. Tirado, K. P. Barteau, D.-M. Smilgies, R. A. DiStasio, B. P. Fors, *J. Am. Chem. Soc.* **2018**, *140*, 4639.

[78] D. T. Gentekos, B. P. Fors, *ACS Macro. Lett.* **2018**, *7*, 677.

[79] D. T. Gentekos, R. J. Sifri, B. P. Fors, *Nat. Rev. Mater.* **2019**, *4*, 761.

[80] V. Gold in *The IUPAC Compendium of Chemical Terminology* (Ed.: V. Gold), International Union of Pure and Applied Chemistry (IUPAC), Research Triangle Park, NC, **2019**.

[81] Watson, J. D., Crick, F. H., *Nature* **1953**, 737.

[82] P. Nanjan, M. Porel, *Polym. Chem.* **2019**, *10*, 5406.

[83] S. C. Solleder, R. V. Schneider, K. S. Wetzel, A. C. Boukis, M. A. R. Meier, *Macromol. Rapid Commun.* **2017**, *38*.

[84] M. A. R. Meier, C. Barner-Kowollik, *Adv. Mater.* **2019**, *31*, e1806027.

[85] S. A. Hill, C. Gerke, L. Hartmann, *Chem. Asian. J.* **2018**, *13*, 3611.

[86] R. Aksakal, C. Mertens, M. Soete, N. Badi, F. Du Prez, *Adv. Sci.* **2021**, *8*, 2004038.

[87] A. S. Knight, E. Y. Zhou, M. B. Francis, R. N. Zuckermann, *Adv. Mater.* **2015**, *27*, 5665.

[88] Z. Deng, Q. Shi, J. Tan, J. Hu, S. Liu, *ACS Mater. Lett* **2021**, *3*, 1339.

[89] R. B. Merrifield, *J. Am. Chem. Soc.* **1963**, *85*.

[90] R. B. Merrifield, *Angew. Chem. Int. Ed.* **1985**, *24*, 799.

[91] R. J. Simon, R. S. Kania, R. N. Zuckermann, V. D. Huebner, D. A. Jewell, S. Banville, S. Ng, L. Wang, S. Rosenberg, C. K. Marlowe, *Proc. Natl. Acad. Sci. U.S.A.* **1992**, *89*, 9367.

[92] H. Herzner, T. Reipen, M. Schultz, H. Kunz, *Chem. Rev.* **2000**, *100*, 4495.

[93] S. L. Beaucage, R. P. Iyer, *Tetrahedron* **1992**, *48*, 2223.

[94] S. L. Beaucage, M. H. Caruthers, *Tetrahedron Lett.* **1981**, *22*, 1859.

[95] B. Genabeek, B. A. G. Lamers, C. J. Hawker, E. W. Meijer, W. R. Gutekunst, B. V. K. J. Schmidt, *J. Polym. Sci.* **2021**, *59*, 373.

[96] J. W. Grate, K.-F. Mo, M. D. Daily, *Angew. Chem. Int. Ed.* **2016**, *128*, 3993.

[97] A. Al Ouahabi, M. Kotera, L. Charles, J.-F. Lutz, *ACS Macro. Lett.* **2015**, *4*, 1077.

[98] S. Martens, J. van den Begin, A. Madder, F. E. Du Prez, P. Espeel, *J. Am. Chem. Soc.* **2016**, *138*, 14182.

[99] W. Konrad, C. Fengler, S. Putwa, C. Barner-Kowollik, *Angew. Chem. Int. Ed.* **2019**, *58*, 7133.

[100] J. C. Barnes, D. J. C. Ehrlich, A. X. Gao, F. A. Leibfarth, Y. Jiang, E. Zhou, T. F. Jamison, J. A. Johnson, *Nat. Chem.* **2015**, *7*, 810.

[101] X. Tong, B. Guo, Y. Huang, *ChemComm* **2011**, *47*, 1455.

[102] J. J. Haven, J. A. de Neve, T. Junkers, *ACS Macro. Lett.* **2017**, *6*, 743.

[103] S. Ida, T. Terashima, M. Ouchi, M. Sawamoto, *J. Am. Chem. Soc.* **2009**, *131*, 10808.

[104] S. Ida, M. Ouchi, M. Sawamoto, *Macromol. Rapid Commun.* **2011**, *32*, 209.

[105] O. I. Paynter, D. J. Simmonds, M. C. Whiting, *J. Chem. Soc., Chem. Commun.* **1982**, 1165.

[106] G. M. Brooke, S. Burnett, S. Mohammed, D. Proctor, M. C. Whiting, *J. Chem. Soc., Perkin Trans. 1* **1996**, *0*, 1635.

[107] E. M. D. Keegstra, J. W. Zwikker, M. R. Roest, L. W. Jenneskens, *J. Org. Chem.* **1992**, *57*.

[108] S. A. Ahmed, M. Tanaka, *J. Org. Chem.* **2006**, *71*.

[109] W. Konrad, F. R. Bloesser, K. S. Wetzel, A. C. Boukis, M. A. R. Meier, C. Barner-Kowollik, *Chem. Eur. J.* **2018**, *24*, 3413.

[110] N. Zydziak, W. Konrad, F. Feist, S. Afonin, S. Weidner, C. Barner-Kowollik, *Nat. Commun.* **2016**, *7*, 13672.

[111] Statista Research Department, "Total data volume worldwide 2010-2025. Access: 23.03.2022, 6:05 am", can be found under https://www.statista.com/statistics/871513/worldwide-data-created/, **2022**.

[112] F. Sanger, *Nature* **1948**, *162*, 491.

[113] M. F. Perutz, *Nature* **1962**, *194*, 914.

[114] J. C. Venter, M. D. Adams, E. W. Myers, P. W. Li, R. J. Mural, G. G. Sutton, H. O. Smith, M. Yandell, C. A. Evans, R. A. Holt et al., *Science* **2001**, *291*, 1304.

[115] M. G. T. A. Rutten, F. W. Vaandrager, J. A. A. W. Elemans, R. J. M. Nolte, *Nat. Rev. Chem.* **2018**, *2*, 365.

[116] J.-A. Amalian, T. Mondal, E. Konishcheva, G. Cavallo, B. E. Petit, J.-F. Lutz, L. Charles, *Adv. Mater. Technol.* **2021**, *6*, 2001088.

[117] J.-F. Lutz, *Macromolecules* **2015**, *48*, 4759.

[118] L. Charles, G. Cavallo, V. Monnier, L. Oswald, R. Szweda, J.-F. Lutz, *J. Am. Soc. Mass. Spectrom.* **2017**, *28*, 1149.

[119] A. Al Ouahabi, J.-A. Amalian, L. Charles, J.-F. Lutz, *Nat. Commun.* **2017**, *8*, 967.

[120] E. Laurent, J.-A. Amalian, T. Schutz, K. Launay, J.-L. Clément, D. Gigmes, A. Burel, C. Carapito, L. Charles, M.-A. Delsuc et al., *Comptes Rendus. Chimie* **2021**, *24*, 69.

[121] A. Burel, C. Carapito, J.-F. Lutz, L. Charles, *Macromolecules* **2017**, *50*, 8290.

[122] L. Charles, J.-F. Lutz, *Acc. Chem. Res.* **2021**, *54*, 1791.

[123] E. Laurent, J.-A. Amalian, M. Parmentier, L. Oswald, A. Al Ouahabi, F. Dufour, K. Launay, J.-L. Clément, D. Gigmes, M.-A. Delsuc et al., *Macromolecules* **2020**, *53*, 4022.

[124] N. F. König, A. Al Ouahabi, L. Oswald, R. Szweda, L. Charles, J.-F. Lutz, *Nat. Commun.* **2019**, *10*, 3774.

[125] J.-A. Amalian, A. Al Ouahabi, G. Cavallo, N. F. König, S. Poyer, J.-F. Lutz, L. Charles, *J. Mass Spectrom.* **2017**, *52*, 788.

[126] N. F. König, A. Al Ouahabi, S. Poyer, L. Charles, J.-F. Lutz, *Angew. Chem. Int. Ed.* **2017**, *56*, 7297.

[127] L. Charles, T. Mondal, V. Greff, M. Razzini, V. Monnier, A. Burel, C. Carapito, J.-F. Lutz, *Rapid. Commun. Mass Spectrom.* **2020**, *34*, e8815.

[128] T. Mondal, L. Charles, J.-F. Lutz, *Angew. Chem. Int. Ed.* **2020**, *59*, 20390.

[129] S. Poyer, B. E. Petit, S. Telitel, D. Karamessini, J.-F. Lutz, L. Charles, *Int. J. Mass Spectrom.* **2020**, *448*, 116271.

[130] T. Mondal, V. Greff, B. É. Petit, L. Charles, J.-F. Lutz, *ACS Macro. Lett.* **2019**, *8*, 1002.

[131] S. Poyer, T. Fouquet, H. Sato, J.-F. Lutz, L. Charles, *Macromol. Chem. Phys.* **2018**, *219*, 1800173.

[132] J.-A. Amalian, S. Poyer, B. E. Petit, S. Telitel, V. Monnier, D. Karamessini, D. Gigmes, J.-F. Lutz, L. Charles, *J. Mass Spectrom.* **2017**, *421*, 271.

[133] D. Karamessini, S. Poyer, L. Charles, J.-F. Lutz, *Macromol. Rapid Commun.* **2017**, *38*.

[134] U. S. Gunay, B. E. Petit, D. Karamessini, A. Al Ouahabi, J.-A. Amalian, C. Chendo, M. Bouquey, D. Gigmes, L. Charles, J.-F. Lutz, *Chem* **2016**, *1*, 114.

[135] K. Launay, J.-A. Amalian, E. Laurent, L. Oswald, A. Al Ouahabi, A. Burel, F. Dufour, C. Carapito, J.-L. Clément, J.-F. Lutz et al., *Angew. Chem. Int. Ed.* **2021**, *60*, 917.

[136] J.-A. Amalian, G. Cavallo, A. Al Ouahabi, J.-F. Lutz, L. Charles, *Anal. Chem.* **2019**, *91*, 7266.

[137] G. Cavallo, A. Al Ouahabi, L. Oswald, L. Charles, J.-F. Lutz, *J. Am. Chem. Soc.* **2016**, *138*, 9417.

[138] G. Cavallo, S. Poyer, J.-A. Amalian, F. Dufour, A. Burel, C. Carapito, L. Charles, J.-F. Lutz, *Angew. Chem. Int. Ed.* **2018**, *57*, 6266.

[139] S. Poyer, C. Chendo, C. Laure, J.-F. Lutz, D. Siri, L. Charles, *Int. J. Mass Spectrom.* **2019**, *438*, 29.

[140] L. Charles, C. Laure, J.-F. Lutz, R. K. Roy, *Rapid. Commun. Mass Spectrom.* **2016**, *30*, 22.

[141] C. Laure, D. Karamessini, O. Milenkovic, L. Charles, J.-F. Lutz, *Angew. Chem. Int. Ed.* **2016**, *55*, 10722.

[142] L. Charles, C. Laure, J.-F. Lutz, R. K. Roy, *Macromolecules* **2015**, *48*, 4319.

[143] R. K. Roy, C. Laure, D. Fischer-Krauser, L. Charles, J.-F. Lutz, *ChemComm* **2015**, *51*, 15677.

[144] R. K. Roy, A. Meszynska, C. Laure, L. Charles, C. Verchin, J.-F. Lutz, *Nat. Commun.* **2015**, *6*, 7237.

[145] J.-A. Amalian, T. T. Trinh, J.-F. Lutz, L. Charles, *Anal. Chem.* **2016**, *88*, 3715.

[146] T. T. Trinh, L. Oswald, D. Chan-Seng, L. Charles, J.-F. Lutz, *Chem. Eur. J.* **2015**, *21*, 11961.

[147] H. Mutlu, J.-F. Lutz, *Angew. Chem. Int. Ed.* **2014**, *53*, 13010.

[148] J. M. Lee, J. Kwon, S. J. Lee, H. Jang, D. Kim, J. Song, K. T. Kim, *Sci. Adv.* **2022**, *8*, eabl8614.

[149] M. Frölich, D. Hofheinz, M. A. R. Meier, *Commun. Chem.* **2020**, *3*.

[150] K. S. Wetzel, M. Frölich, S. C. Solleder, R. Nickisch, P. Treu, M. A. R. Meier, *Commun. Chem.* **2020**, *3*.

[151] A. C. Boukis, M. A. Meier, *European Polymer Journal* **2018**, *104*, 32.

[152] M. Soete, C. Mertens, R. Aksakal, N. Badi, F. Du Prez, *ACS Macro. Lett.* **2021**, *10*, 616.

[153] J. O. Holloway, F. van Lijsebetten, N. Badi, H. A. Houck, F. E. Du Prez, *Adv. Sci.* **2020**, *7*, 1903698.

[154] J. Steinkoenig, R. Aksakal, F. Du Prez, *European Polymer Journal* **2019**, *120*, 109260.

[155] S. Martens, A. Landuyt, P. Espeel, B. Devreese, P. Dawyndt, F. Du Prez, *Nat. Commun.* **2018**, *9*, 4451.

[156] S. D. Dahlhauser, S. R. Moor, M. S. Vera, J. T. York, P. Ngo, A. J. Boley, J. N. Coronado, Z. B. Simpson, E. V. Anslyn, *Cell Reports Physical Science* **2021**, *2*, 100393.

[157] B. Liu, Q. Shi, L. Hu, Z. Huang, X. Zhu, Z. Zhang, *Polym. Chem.* **2020**, *11*, 1702.

[158] K. Ding, Y. Zhang, Z. Huang, B. Liu, Q. Shi, L. Hu, N. Zhou, Z. Zhang, X. Zhu, *European Polymer Journal* **2019**, *119*, 421.

[159] Z. Huang, J. Zhao, Z. Wang, F. Meng, K. Ding, X. Pan, N. Zhou, X. Li, Z. Zhang, X. Zhu, *Angew. Chem. Int. Ed.* **2017**, *56*, 13612.

[160] X. Wang, X. Zhang, Y. Sun, S. Ding, *Macromolecules* **2021**, *54*, 9437.

[161] X. Wang, X. Zhang, Y. Wang, S. Ding, *Polym. Chem.* **2021**, *12*, 3825.

[162] X. Zhang, F. Gou, X. Wang, Y. Wang, S. Ding, *ACS Macro. Lett.* **2021**, *10*, 551.

[163] B. Song, D. Lu, A. Qin, B. Z. Tang, *J. Am. Chem. Soc.* **2022**, *144*, 1672.

[164] M. Passerini, *Gazz. Chem. Ital.* **1921**, *51*, 126.

[165] I. Ugi, R. Meyr, U. Fetzer, *Angew. Chem. Int. Ed.* **1959**, *71*, 386.

[166] S. C. Solleder, M. A. R. Meier, *Angew. Chem. Int. Ed.* **2014**, *53*, 711.

[167] S. C. Solleder, K. S. Wetzel, M. A. R. Meier, *Polym. Chem.* **2015**, *6*, 3201.

[168] S. C. Solleder, D. Zengel, K. S. Wetzel, M. A. R. Meier, *Angew. Chem. Int. Ed.* **2016**, *55*, 1204.

[169] S. C. Solleder, S. Martens, P. Espeel, F. Du Prez, M. A. R. Meier, *Chem. Eur. J.* **2017**, *23*, 13906.

[170] S. Wang, Y. Tao, J. Wang, Y. Tao, X. Wang, *Chem. Sci.* **2019**, *10*, 1531.

[171] J. H. Futrell, C. D. Miller, *Rev. Sci. Instrum.* **1966**, *37*, 1521.

[172] M. Dole, L. L. Mack, R. L. Hines, R. C. Mobley, L. D. Ferguson, M. B. Alice, *J. Chem. Phys.* **1968**, *49*, 2240.

[173] M. Yamashita, J. B. Fenn, *J. Phys. Chem.* **1984**, *88*, 4451.

[174] M. Karas, D. Bachmann, F. Hillenkamp, *Anal. Chem.* **1985**, *57*, 2935.

[175] M. Karas, D. Bachmann, U. Bahr, F. Hillenkamp, *International Journal of Mass Spectrometry and Ion Processes* **1987**, *78*, 53.

[176] F. Crick, *J. Mol. Biol.* **1968**, *38*, 367.

[177] S. Nurk, S. Koren, A. Rhie, M. Rautiainen, A. V. Bzikadze, A. Mikheenko, M. R. Vollger, N. Altemose, L. Uralsky, A. Gershman et al., *Science* **2022**, *376*, 44.

[178] A. Ambrogelly, S. Palioura, D. Söll, *Nat. Chem. Biol.* **2007**, *3*, 29.

[179] J. D. Watson, F. H. Crick, *Cold. Spring. Harb. Symp. Quant. Biol.* **1953**, *18*, 123.

[180] R. R. Sinden, *DNA Structure and Function*, Elsevier Science, San Diego, **1994**.

[181] J.-F. Lutz, *ACS Macro. Lett.* **2014**, *3*, 1020.

[182] P. J. Flory, *J. Am. Chem. Soc.* **1940**, *62*, 1561.

[183] K. Matyjaszewski, A. H. Müller, *Prog. Polym. Sci.* **2006**, *31*, 1039.

[184] J.-S. Wang, K. Matyjaszewski, *J. Am. Chem. Soc.* **1995**, *117*, 5614.

[185] R. B. Grubbs, R. H. Grubbs, *Macromolecules* **2017**, *50*, 6979.

[186] M. Szwarc, M. Levy, R. Milkovich, *J. Am. Chem. Soc.* **1956**, *78*.

[187] R. Kakuchi, M. Zamfir, J.-F. Lutz, P. Theato, *Macromol. Rapid Commun.* **2012**, *33*, 54.

[188] D. Chan-Seng, M. Zamfir, J.-F. Lutz, *Angew. Chem. Int. Ed.* **2012**, *51*, 12254.

[189] U. T. Bornscheuer, G. W. Huisman, R. J. Kazlauskas, S. Lutz, J. C. Moore, K. Robins, *Nature* **2012**, *485*, 185.

[190] C. K. McLaughlin, G. D. Hamblin, H. F. Sleiman, *Chem. Soc. Rev.* **2011**, *40*, 5647.

[191] P. Dervan, *Bioorg. Med. Chem.* **2001**, *9*, 2215.

[192] H. Jian, J. M. Tour, *J. Org. Chem.* **2005**, *70*, 3396.

[193] M. Porel, C. A. Alabi, *J. Am. Chem. Soc.* **2014**, *136*, 13162.

[194] R. L. Kanasty, A. J. Vegas, L. M. Ceo, M. Maier, K. Charisse, J. K. Nair, R. Langer, D. G. Anderson, *Angew. Chem. Int. Ed.* **2016**, *55*, 9529.

[195] Y. Li, Q. Guo, X.-. F. Li, H. Zhang, F.-. H. Yu, W.-. J. Yu, G.-. Q. Xia, M.-. Y. Fu, Z.-. G. Yang, Z.-. X. Jiang, *Tetrahedron Lett.* **2014**, *55*.

[196] T. T. Trinh, L. Oswald, D. Chan-Seng, L. Charles, J.-F. Lutz, *Chem. Eur. J.* **2015**, *21*, 11961.

[197] M. Landa, M. Kotera, J.-S. Remy, N. Badi, *European Polymer Journal* **2016**, *84*, 338.

[198] G. Székely, M. Schaepertoens, R. R. J. Gaffney, A. G. Livingston, *Polym. Chem.* **2014**, *5*.

[199] M. Amblard, J.-A. Fehrentz, J. Martinez, G. Subra, *Mol. Biotechnol.* **2006**, *33*, 239.

[200] M. Amblard, J.-A- Fehrentz, J. Martinez, G. Subra, *Mol. Biotechnol.* **2006**, *33*, 239.

[201] R. B. Merrifield, J. M. Stewart, N. Jernberg, *Anal. Chem.* **1966**, *38*, 1905.

[202] B. Marglin, R. B. Merrifield, *J. Am. Chem. Soc.* **1966**, *88*, 5051.

[203] B. Gutte, R. B. Merrifield, *J. Biol. Chem.* **1971**, *246*, 1922.

[204] R. L. Letsinger, V. Mahadevan, *J. Am. Chem. Soc.* **1965**, *87*, 3526.

[205] R. N. Zuckermann, J. M. Kerr, S. B. H. Kent, W. H. Moos, *J. Am. Chem. Soc.* **1992**, *114*, 10646.

[206] N. Usman, K. K. Ogilvie, M.-Y. Jiang, R. J. Cedergren, *J. Am. Chem. Soc.* **1987**, *109*, 7845.

[207] N. Cankařová, E. Schütznerová, V. Krchňák, *Chem. Rev.* **2019**, *119*, 12089.

[208] P. Espeel, L. L. G. Carrette, K. Bury, S. Capenberghs, J. C. Martins, F. E. Du Prez, A. Madder, *Angew. Chem. Int. Ed.* **2013**, *52*, 13261.

[209] J. O. Holloway, C. Mertens, F. E. Du Prez, N. Badi, *Macromol. Rapid Commun.* **2019**, *40*, e1800685.

[210] J. O. Holloway, S. Aksakal, F. E. Du Prez, C. R. Becer, *Macromol. Rapid Commun.* **2017**, *38*.

[211] C. Mertens, R. Aksakal, N. Badi, F. E. Du Prez, *Polym. Chem.* **2021**, *12*, 4193.

[212] C. Mertens, M. Soete, M. L. Ślęczkowski, A. R. A. Palmans, E. W. Meijer, N. Badi, F. E. Du Prez, *Polym. Chem.* **2020**, *11*, 4271.

[213] S. Celasun, F. E. Du Prez, H. G. Börner, *Macromol. Rapid Commun.* **2017**, *38*.

[214] M. Frölich, *Increasing the data storage capacity of sequence-defined macromolecules*, Karlsruher Institut für Technologie (KIT), **2021**.

[215] K. S. Wetzel, M. A. R. Meier, *Polym. Chem.* **2019**, *10*, 2716.

[216] J. O. Holloway, K. S. Wetzel, S. Martens, F. E. Du Prez, M. A. R. Meier, *Polym. Chem.* **2019**, *10*, 3859.

[217] W. Konrad, F. R. Bloesser, K. S. Wetzel, A. C. Boukis, M. A. R. Meier, C. Barner-Kowollik, *Chem. Eur. J.* **2018**, *24*, 3413.

[218] C. Li, L. Han, X. Chen, X. Bao, Q. Sun, H. Ma, Y. Li, *Polym. Chem.* **2021**, *12*, 3510.

[219] P. Nanjan, A. Jose, L. Thurakkal, M. Porel, *Macromolecules* **2020**, *53*, 11019.

[220] B. Zhao, Z. Gao, Y. Zheng, C. Gao, *J. Am. Chem. Soc.* **2019**, *141*, 4541.

[221] R. V. Schneider, K. A. Waibel, A. P. Arndt, M. Lang, R. Seim, D. Busko, S. Bräse, U. Lemmer, M. A. R. Meier, *Sci. Rep.* **2018**, *8*, 17483.

[222] R. V. Schneider, *Synthesis and Characterization of Sequence-Defined Stiff Oligomers Using the Sonogashira Reaction*, Karlsruhe, **2018**.

[223] D. Hahn, *Improved Strategies towards Conjugated Oligo Phenylene Ethynylenes*, Karlsruher Institut für Technologie (KIT), **2022**.

[224] D. Hahn, R. V. Schneider, E. Foitzik, M. A. R. Meier, *Macromol. Rapid Commun.* **2021**, *42*, e2000735.

[225] S. Zhang, N. E. Bauer, I. Y. Kanal, W. You, G. R. Hutchison, T. Y. Meyer, *Macromolecules* **2017**, *50*, 151.

[226] S. Zhang, G. R. Hutchison, T. Y. Meyer, *Macromol. Rapid Commun.* **2016**, *37*, 882.

[227] B. N. Norris, S. Zhang, C. M. Campbell, J. T. Auletta, P. Calvo-Marzal, G. R. Hutchison, T. Y. Meyer, *Macromolecules* **2013**, *46*, 1384.

[228] B. N. Norris, T. Pan, T. Y. Meyer, *Org. Lett.* **2010**, *12*, 5514.

[229] M. Jørgensen, F. C. Krebs, *J. Org. Chem.* **2005**, *70*, 6004.

[230] M. Jørgensen, F. C. Krebs, *J. Org. Chem.* **2004**, *69*, 6688.

[231] R. Szweda, C. Chendo, L. Charles, P. N. W. Baxter, J.-F. Lutz, *ChemComm* **2017**, *53*, 8312.

[232] S. Huang, J. M. Tour, *Tetrahedron Lett.* **1999**, *40*, 3447.

[233] J.-J. Hwang, J. M. Tour, *Tetrahedron* **2002**, *58*, 10387.

[234] J. C. Barnes, D. J. C. Ehrlich, A. X. Gao, F. A. Leibfarth, Y. Jiang, E. Zhou, T. F. Jamison, J. A. Johnson, *Nat. Chem.* **2015**, *7*, 810.

[235] V. Percec, A. D. Asandei, *Macromolecules* **1997**, *30*, 7701.

[236] F. A. Loiseau, K. K. Hii, A. M. Hill, *J. Org. Chem.* **2004**, *69*.

[237] A. C. French, A. L. Thompson, B. G. Davis, *Angew. Chem. Int. Ed.* **2009**, *48*.

[238] C. J. Burns, L. D. Field, K. Hashimoto, B. J. Petteys, D. D. Ridley, Sandanayake, K. R. A. S., *Synth. Commun.* **1999**, *29*.

[239] M. B. Koo, S. W. Lee, J. M. Lee, K. T. Kim, *J. Am. Chem. Soc.* **2020**, *142*, 14028.

[240] K. Takizawa, C. Tang, C. J. Hawker, *J. Am. Chem. Soc.* **2008**, *130*, 1718.

[241] K. Takizawa, H. Nulwala, J. Hu, K. Yoshinaga, C. J. Hawker, *J. Polym. Sci. A Polym. Chem.* **2008**, *46*, 5977.

[242] B. Huang, M. E. Hermes, *J. Polym. Sci. A Polym. Chem.* **1995**, *33*, 1419.

[243] J. B. Williams, T. M. Chapman, D. M. Hercules, *Macromolecules* **2003**, *36*, 3898.

[244] N. Franz, L. Menin, H.-A. Klok, *Eur. J. Org. Chem.* **2009**, *2009*, 5390.

[245] J. M. Lee, M. B. Koo, S. W. Lee, H. Lee, J. Kwon, Y. H. Shim, S. Y. Kim, K. T. Kim, *Nat. Commun.* **2020**, *11*, 56.

[246] J. S. Schumm, D. L. Pearson, J. M. Tour, *Angew. Chem. Int. Ed.* **1994**, *33*, 1360.

[247] J. Zhang, J. S. Moore, Z. Xu, R. A. Aguirre, *J. Am. Chem. Soc.* **1992**, *114*, 2273.

[248] J. S. Schumm, D. L. Pearson, J. M. Tour, *Angew. Chem. Int. Ed.* **1994**, *33*, 1360.

[249] D. L. Pearson, J. S. Schumm, J. M. Tour, *Macromolecules* **1994**, *27*, 2348.

[250] C. Cai, A. Vasella, *Helv. Chim. Acta* **1996**, *79*, 255.

[251] U. D. Lengweiler, M. G. Fritz, D. Seebach, *Helv. Chim. Acta* **1996**, *79*, 670.

[252] G. Li, X. Wang, F. Wang, *Tetrahedron Lett.* **2005**, *46*, 8971.

[253] G. Li, X. Wang, J. Li, X. Zhao, F. Wang, *Synth. Commun.* **2005**, *35*, 115.

[254] P. Liess, V. Hensel, A.-D. Schlüter, *Liebigs Ann.* **1996**, *1996*, 1037.

[255] J. P. Sadighi, R. A. Singer, S. L. Buchwald, *J. Am. Chem. Soc.* **1998**, *120*, 4960.

[256] J. Louie, J. F. Hartwig, *Macromolecules* **1998**, *31*, 6737.

[257] R. E. Martin, F. Diederich, *Angew. Chem. Int. Ed.* **1999**, *38*, 1350.

[258] C.-Z. Zhou, T. Liu, J.-M. Xu, Z.-K. Chen, *Macromolecules* **2003**, *36*, 1457.

[259] S. Binauld, C. J. Hawker, E. Fleury, E. Drockenmuller, *Angew. Chem. Int. Ed.* **2009**, *48*, 6654.

[260] F. P. V. Koch, P. Smith, M. Heeney, *J. Am. Chem. Soc.* **2013**, *135*, 13695.

[261] F. A. Leibfarth, J. A. Johnson, T. F. Jamison, *Proc. Natl. Acad. Sci. U.S.A.* **2015**, *112*, 10617.

[262] A. C. Wicker, F. A. Leibfarth, T. F. Jamison, *Polym. Chem.* **2017**, *8*, 5786.

[263] W. Zhang, D. P. Curran, *Tetrahedron* **2006**, *62*, 11837.

[264] M. Van De Walle, K. De Bruycker, T. Junkers, J. P. Blinco, C. Barner-Kowollik, *ChemPhotoChem* **2019**, *3*, 225.

[265] F. Wojcik, A. G. O'Brien, S. Götze, P. H. Seeberger, L. Hartmann, *Chem. Eur. J.* **2013**, *19*, 3090.

[266] J. Lawrence, S.-H. Lee, A. Abdilla, M. D. Nothling, J. M. Ren, A. S. Knight, C. Fleischmann, Y. Li, A. S. Abrams, B. V. K. J. Schmidt et al., *J. Am. Chem. Soc.* **2016**, *138*, 6306.

[267] J. Lawrence, E. Goto, J. M. Ren, B. McDearmon, D. S. Kim, Y. Ochiai, P. G. Clark, D. Laitar, T. Higashihara, C. J. Hawker, *J. Am. Chem. Soc.* **2017**, *139*, 13735.

[268] C. Zhang, D. S. Kim, J. Lawrence, C. J. Hawker, A. K. Whittaker, *ACS Macro. Lett.* **2018**, *7*, 921.

[269] J. M. Ren, J. Lawrence, A. S. Knight, A. Abdilla, R. B. Zerdan, A. E. Levi, B. Oschmann, W. R. Gutekunst, S.-H. Lee, Y. Li et al., *J. Am. Chem. Soc.* **2018**, *140*, 1945.

[270] S. Park, K. Kwon, D. Cho, B. Lee, M. Ree, T. Chang, *Macromolecules* **2003**, *36*, 4662.

[271] S. Park, D. Cho, J. Ryu, K. Kwon, W. Lee, T. Chang, *Macromolecules* **2002**, *35*, 5974.

[272] B. Chung, S. Park, T. Chang, *Macromolecules* **2005**, *38*, 6122.

[273] K. Maranski, Y. G. Andreev, P. G. Bruce, *Angew. Chem. Int. Ed.* **2014**, *53*.

[274] P. Bohn, M. A. R. Meier, *Polym. J.* **2020**, *52*, 165.

[275] F. E. Bailey, J. V. Koleske, *Alkylene oxides and their polymers*, Dekker, New York, NY, **1991**.

[276] S. Penczek, J. Pretula, S. Slomkowski, *Chemistry Teacher International* **2021**, *3*, 33.

[277] Webster Owen W., *Science* **1991**, *251*, 887.

[278] A. A. D'souza, R. Shegokar, *Expert Opin. Drug Deliv.* **2016**, *13*, 1257.

[279] I. Strehin, Z. Nahas, K. Arora, T. Nguyen, J. Elisseeff, *Biomaterials* **2010**, *31*, 2788.

[280] C. B. Smith, C. L. Raston, A. N. Sobolev, *Green Chem.* **2005**, *7*, 650.

[281] C.-C. Lin, K. S. Anseth, *Pharm.* **2009**, *26*, 631.

[282] K. B. Bjugstad, D. E. Redmond, K. J. Lampe, D. S. Kern, J. R. Sladek, M. J. Mahoney, *Cell Transplant* **2008**, *17*, 409.

[283] R. K. Sharma, P. Ganesan, V. V. Tyagi, T. Mahlia, *Sol. Energy Mater. Sol. Cells* **2016**, *147*, 235.

[284] A. K. Ansu, R. K. Sharma, V. V. Tyagi, A. Sarı, P. Ganesan, D. Tripathi, *Int. J. Energy Res.* **2020**, *44*, 2183.

[285] B. Zhang, Z. Wu, J. Liang, L. Yu, X. Xi, H. Lei, G. Du, *Eur. J. Wood Wood Prod.* **2022**.

[286] K. Abe, K. Higashi, K. Watabe, A. Kobayashi, W. Limwikrant, K. Yamamoto, K. Moribe, *Colloids Surf.* **2015**, *474*, 63.

[287] A. Anne, J. Moiroux, *Macromolecules* **1999**, *32*, 5829.

[288] G. Liu, Y. Li, L. Yang, Y. Wei, X. Wang, Z. Wang, L. Tao, *RSC Adv.* **2017**, *7*, 18252.

[289] G. Pasut, A. Panisello, E. Folch-Puy, A. Lopez, C. Castro-Benítez, M. Calvo, T. Carbonell, A. García-Gil, R. Adam, J. Roselló-Catafau, *World J. Gastroenterol.* **2016**, *22*, 6501.

[290] C. Özdemir, A. Güner, *European Polymer Journal* **2007**, *43*, 3068.

[291] *J Whelan, C Pan. (Bayer Pharmaceuticals Corporation, USA), PCT Application WO. 2005-US20469, 2005*.

[292] J. Wang, T. Deng, Y. Liu, K. Chen, Z. Yang, Z.-X. Jiang, *Biomacromolecules* **2020**, *21*, 3134.

[293] X. Wang, Y. Li, T. Wu, Z. Yang, X. Zheng, S. Chen, X. Zhou, Z.-X. Jiang, *Biomacromolecules* **2020**, *21*, 725.

[294] A. Mero, B. Spolaore, F. M. Veronese, A. Fontana, *Bioconj. Chem.* **2009**, *20*, 384.

[295] F. M. Veronese, A. Mero, *BioDrugs* **2008**, *22*, 315.

[296] F. M. Veronese, G. Pasut, *Drug Discov. Today* **2005**, *10*, 1451.

[297] J. M. Harris, R. B. Chess, *Nat. Rev. Drug Discov.* **2003**, *2*, 214.

[298] J. M. Harris, N. E. Martin, M. Modi, *Clin. Pharmacokinet.* **2001**, *40*, 539.

[299] F. M. Veronese, *Biomaterials* **2001**, *22*, 405.

[300] S. Brocchini, A. Godwin, S. Balan, J.-. W. Choi, M. Zloh, S. Shaunak, *Adv. Drug. Deliv. Rev.* **2008**, *60*.

[301] R. Haag, F. Kratz, *Angew. Chem. Int. Ed.* **2006**, *118*.

[302] S. Zalipsky, *Adv. Drug. Deliv. Rev.* **1995**, *16*.

[303] R. B. Greenwald, Y. H. Choe, J. McGuire, C. D. Conover, *Adv. Drug. Deliv. Rev.* **2003**, *55*.

[304] M. J. Roberts, M. D. Bentley, J. M. Harris, *Adv. Drug. Deliv. Rev.* **2012**, *64*.

[305] P. Caliceti, F. M. Veronese, *Adv. Drug. Deliv. Rev.* **2003**, *55*.

[306] J. M. Harris, R. B. Chess, *Nat. Rev. Drug Discov.* **2003**, *2*.

[307] F. M. Veronese, G. Pasut, *Drug Discov. Today* **2005**, *10*.

[308] C. S. Fishburn, *J. Pharm. Sci.* **2008**, *97*.

[309] K. Knop, R. Hoogenboom, D. Fischer, U. S. Schubert, *Angew. Chem. Int. Ed.* **2010**, *49*.

[310] H. Furusho, K. Kitano, S. Hamaguchi, Y. Nagasaki, *Chem. Mater.* **2009**, *21*.

[311] Ganapatibhotla, L. V. N. R., J. Zheng, D. Roy, S. Krishnan, *Chem. Mater.* **2010**, *22*.

[312] S. A. S. Shah, M. Nag, T. Kalagara, S. Singh, S. V. Manorama, *Chem. Mater.* **2008**, *20*.

[313] H. Elimelech, D. Avnir, *Chem. Mater.* **2008**, *20*.

[314] "Octaethylenglycol ≥95% (oligomer purity) | Sigma-Aldrich. Access: 01.04.2022, 9:22 pm.", can be found under https://www.sigmaaldrich.com/DE/de/product/aldrich/15879, **2022**.

[315] A. Harada, J. Li, M. Kamachi, *J. Am. Chem. Soc.* **1994**, *116*.

[316] D. Niculescu-Duvaz, J. Getaz, C. J. Springer, *Bioconj. Chem.* **2008**, *19*.

[317] Q. Zhang, H. Ren, G. L. Baker, *Tetrahedron Lett.* **2014**, *55*.

[318] H. Zhang, X. Li, Q. Shi, Y. Li, G. Xia, L. Chen, Z. Yang, Z.-. X. Jiang, *Angew. Chem. Int. Ed.* **2015**, *54*.

[319] A. M. Wawro, T. Muraoka, M. Kato, K. Kinbara, *Org. Chem. Front.* **2016**, *3*.

[320] A. Khanal, S. Fang, *Chem. Eur. J.* **2017**, *23*.

[321] R. Fordyce, E. L. Lovell, H. Hibbert, *J. Am. Chem. Soc.* **1939**, *61*.

[322] G. Székely, M. Schaepertoens, P. R. J. Gaffney, A. G. Livingston, *Chem. Eur. J.* **2014**, *20*.

[323] A. Williamson, *Philos. Mag.* **1850**, *37*.

[324] N. Boden, R. J. Bushby, S. Clarkson, S. D. Evans, P. F. Knowles, A. Marsh, *Tetrahedron* **1997**, *53*.

[325] R. Dong, R. Liu, P. R. J. Gaffney, M. Schaepertoens, P. Marchetti, C. M. Williams, R. Chen, A. G. Livingston, *Nat. Chem.* **2019**, *11*, 136.

[326] C. Malanga, N. Spassky, R. Menicagli, E. Chiellini, *Polym. Bull.* **1983**, *9*, 328.

[327] E. C. Knuf, J.-K. Jiang, M. S. Gin, *J. Org. Chem.* **2003**, *68*, 9166.

[328] K. C. K. Swamy, N. N. B. Kumar, E. Balaraman, Kumar, K. V. P. Pavan, *Chem. Rev.* **2009**, *109*, 2551.

[329] G. Evano, N. Blanchard, M. Toumi, *Chem. Rev.* **2008**, *108*, 3054.

[330] F. Monnier, M. Taillefer, *Angew. Chem. Int. Ed.* **2009**, *48*, 6954.

[331] C. Sambiagio, S. P. Marsden, A. J. Blacker, P. C. McGowan, *Chem. Soc. Rev.* **2014**, *43*, 3525.

[332] J. Qiao, P. Lam, *Synthesis* **2011**, *2011*, 829.

[333] K. Sanjeeva Rao, T.-S. Wu, *Tetrahedron* **2012**, *68*, 7735.

[334] J. F. Hartwig, *Acc. Chem. Res.* **1998**, *31*, 852.

[335] C. H. Burgos, T. E. Barder, X. Huang, S. L. Buchwald, *Angew. Chem. Int. Ed.* **2006**, *45*, 4321.

[336] M. Sutter, E. Da Silva, N. Duguet, Y. Raoul, E. Métay, M. Lemaire, *Chem. Rev.* **2015**, *115*, 8609.

[337] J. E. Rorrer, A. T. Bell, F. D. Toste, *ChemSusChem* **2019**, *12*, 2835.

[338] T. A. Natsir, S. Shimazu, *Fuel Process. Technol.* **2020**, *200*, 106308.

[339] *P. Wothers*, **2001**.

[340] F. Alonso, I. P. Beletskaya, M. Yus, *Chem. Rev.* **2004**, *104*, 3079.

[341] A. Corma, A. Leyva-Pérez, M. J. Sabater, *Chem. Rev.* **2011**, *111*, 1657.

[342] V. Rodriguez-Ruiz, R. Carlino, S. Bezzenine-Lafollée, R. Gil, D. Prim, E. Schulz, J. Hannedouche, *Dalton Trans.* **2015**, *44*, 12029.

[343] W.-B. Xie, Z. Li, *Synthesis* **2020**, *52*, 2127.

[344] C. Lluna-Galán, L. Izquierdo-Aranda, R. Adam, J. R. Cabrero-Antonino, *ChemSusChem* **2021**, *14*, 3744.

[345] N. Sakai, T. Moriya, T. Konakahara, *J. Org. Chem.* **2007**, *72*, 5920.

[346] U. Biermann, J. O. Metzger, *ChemSusChem* **2014**, *7*, 644.

[347] U. Biermann, J. O. Metzger, *Eur. J. Lipid Sci. Technol.* **2014**, *116*, 74.

[348] P.-K. Dannecker, U. Biermann, M. von Czapiewski, J. O. Metzger, M. A. R. Meier, *Angew. Chem. Int. Ed.* **2018**, *57*, 8775.

[349] P.-K. Dannecker, U. Biermann, A. Sink, F. R. Bloesser, J. O. Metzger, M. A. R. Meier, *Macromol. Chem. Phys.* **2019**, *220*, 1800440.

[350] P.-Q. Huang, Q.-W. Lang, Y.-R. Wang, *J. Org. Chem.* **2016**, *81*, 4235.

[351] R. C. Chadwick, V. Kardelis, P. Lim, A. Adronov, *J. Org. Chem.* **2014**, *79*, 7728.

[352] E. Blondiaux, T. Cantat, *ChemComm* **2014**, *50*, 9349.

[353] H. Nagashima, *Synlett* **2015**, *26*, 866.

[354] Carothers Wallace Hume, *Trans. Faraday Soc.* **1936**, *1936*, 39.

[355] F. J. Natta, J. W. Hill. W. H. Carothers, *J. Am. Chem. Soc.* **1934**, *56*, 455.

[356] M. Labet, W. Thielemans, *Chem. Soc. Rev.* **2009**, *38*, 3484.

[357] L. Malinová, J. Brožek, *Polym. Bull.* **2014**, *71*, 111.

[358] W. Limwanich, P. Meepowpan, K. Nalampang, N. Kungwan, R. Molloy, W. Punyodom, *J Therm Anal Calorim* **2015**, *119*, 567.

[359] S. Agarwal, *Polym. Chem.* **2010**, *1*, 953.

[360] R. F. Storey, J. W. Sherman, *Macromolecules* **2002**, *35*, 1504.

[361] H. R. Kricheldorf, M. Berl, N. Scharnagl, *Macromolecules* **1988**, *21*, 286.

[362] *James E. Mark*, **1999**.

[363] V. R. Sinha, K. Bansal, R. Kaushik, R. Kumria, A. Trehan, *Int. J. Pharm.* **2004**, *278*, 1.

[364] M. Bartnikowski, T. R. Dargaville, S. Ivanovski, D. W. Hutmacher, *Prog. Polym. Sci.* **2019**, *96*, 1.

[365] T. T. Ruckh, K. Kumar, M. J. Kipper, K. C. Popat, *Actra Biomater.* **2010**, *6*, 2949.

[366] Y. Ikada, H. Tsuji, *Macromol. Rapid Commun.* **2000**, *21*, 117.

[367] M. Thakur, I. Majid, S. Hussain, V. Nanda, *Packag. Technol. Sci.* **2021**, *34*, 449.

[368] X. Luo, K. E. Lauber, P. T. Mather, *Polymer* **2010**, *51*, 1169.

[369] P. Joshi, G. Madras, *Polym. Degrad. Stab.* **2008**, *93*, 1901.

[370] J. L. Hedrick, T. Magbitang, E. F. Connor, T. Glauser, W. Volksen, C. J. Hawker, V. Y. Lee, R. D. Miller, *Chem. Eur. J.* **2002**, *8*, 3308.

[371] C. X. F. Lam, S. H. Teoh, D. W. Hutmacher, *Polym. Int.* **2007**, *56*, 718.

[372] M. J. Jenkins, K. L. Harrison, M. Silva, M. J. Whitaker, K. M. Shakesheff, S. M. Howdle, *European Polymer Journal* **2006**, *42*, 3145.

[373] J. Peña, T. Corrales, I. Izquierdo-Barba, A. L. Doadrio, M. Vallet-Regí, *Polym. Degrad. Stab.* **2006**, *91*, 1424.

[374] D. W. Hutmacher, T. Schantz, I. Zein, K. W. Ng, S. H. Teoh, K. C. Tan, *J. Biomed. Mater. Res.* **2001**, *55*, 203.

[375] M. Abedalwafa, F. Wang, L. Wang, *Rev. Adv. Mater. Sci.* **2013**, *34*, 123.

[376] M. Janmohammadi, M. S. Nourbakhsh, *Int. J. Polym. Mater. Polym. Biomater.* **2019**, *68*, 527.

[377] D. Mondal, M. Griffith, S. S. Venkatraman, *Int. J. Polym. Mater. Polym. Biomater.* **2016**, *65*, 255.

[378] V. R. Sinha, K. Bansal, R. Kaushik, R. Kumria, A. Trehan, *Int. J. Pharm.* **2004**, *278*, 1.

[379] D. Chen, J. Bei, S. Wang, *Polym. Degrad. Stab.* **2000**, *67*, 455.

[380] U. D. Lengweiler, M. G. Fritz, D. Seebach, *Helv. Chim. Acta* **1996**, *79*, 670.

[381] D. Seebach, M. G. Fritz, *Int. J. Biol. Macromol.* **1999**, *25*, 217.

[382] M. G. Fritz, D. Seebach, *Helv. Chim. Acta* **1998**, *81*, 2414.

[383] S. Duan, X. Yang, Z. Yang, Y. Liu, Q. Shi, Z. Yang, H. Wu, Y. Han, Y. Wang, H. Shen et al., *Macromolecules* **2021**, *54*, 10830.

[384] K. Yokota, *Prog. Polym. Sci.* **1999**, *24*, 517.

[385] K. Matyjaszewski, M. J. Ziegler, S. V. Arehart, D. Greszta, T. Pakula, *J. Phys. Org. Chem.* **2000**, *13*, 775.

[386] J. Huang, S. R. Turner, *Polymer* **2017**, *116*, 572.

[387] H. Feng, X. Lu, W. Wang, N.-G. Kang, J. W. Mays, *Polymers* **2017**, *9*.

[388] I. Mita, A. D. Jenkins, N. M. Bikales, *Pure Appl. Chem.* **1427**, 1427.

[389] J.-S. Wang, K. Matyjaszewski, *Macromolecules* **1995**, *28*, 7572.

[390] J. Chiefari, Y. K. Chong, F. Ercole, J. Krstina, J. Jeffery, T. P. T. Le, *Macromolecules* **1998**, *31*, 5559.

[391] J. Nicolas, Y. Guillaneuf, C. Lefay, D. Bertin, D. Gigmes, B. Charleux, *Prog. Polym. Sci.* **2013**, *38*, 63.

[392] K. Hong, D. Uhrig, J. W. Mays, *Curr. Opin. Solid State Mater. Sci.* **1999**, *4*, 531.

[393] H. Zhang, K. Hong, J. W. Mays, *Macromolecules* **2002**, *35*, 5738.

[394] D. Uhrig, J. W. Mays, *J. Polym. Sci. A Polym. Chem.* **2005**, *43*, 6179.

[395] N. Hadjichristidis, H. Iatrou, M. Pitsikalis, J. Mays, *Prog. Polym. Sci.* **2006**, *31*, 1068.

[396] A. F. Halasa, *Rubber Chem. Technol.* **1981**, *54*, 627.

[397] G. Gody, P. B. Zetterlund, S. Perrier, S. Harrisson, *Nat. Commun.* **2016**, *7*, 10514.

[398] Y. Matsuo, R. Konno, T. Ishizone, R. Goseki, A. Hirao, *Polymers* **2013**, *5*, 1012.

[399] N. Hadjichristidis, M. Pitsikalis, S. Pispas, H. Iatrou, *Chem. Rev.* **2001**, *101*, 3747.

[400] G. Gaucher, M.-H. Dufresne, V. P. Sant, N. Kang, D. Maysinger, J.-C. Leroux, *J. Control. Release* **2005**, *109*, 169.

[401] C. Park, J. Yoon, E. L. Thomas, *Polymer* **2003**, *44*, 6725.

[402] R. J. Spontak, N. P. Patel, *Curr. Opin. Colloid Interface Sci.* **2000**, *5*, 333.

[403] H.-C. Kim, S.-M. Park, W. D. Hinsberg, *Chem. Rev.* **2010**, *110*, 146.

[404] K. M. Stridsberg, M. Ryner and A.-C. Albertsson, *Adv. Polym. Sci.*, *2002*, 41.

[405] A. Khanna, Y. S. Sudha, S. Pillai, S. S. Rath, *J. Mol. Model.* **2008**, *14*, 367.

[406] P. Dubois, O. Coulembier, J.-M. Raquez, *Handbook of ring-opening polymerization*, Wiley-VCH, Weinheim, **2009**.

[407] M. S. Kim, K. S. Seo, G. Khang, H. B. Lee, *Macromol. Rapid Commun.* **2005**, *26*, 643.

[408] B. G. G. Lohmeijer, R. C. Pratt, F. Leibfarth, J. W. Logan, D. A. Long, A. P. Dove, F. Nederberg, J. Choi, C. Wade, R. M. Waymouth et al., *Macromolecules* **2006**, *39*, 8574.

[409] K. M. Stridsberg, M. Ryner, A.-C. Albertsson in *Advances in Polymer Science*, *Vol. 157* (Ed.: A.-C. Albertsson), Springer, Berlin, Heidelberg, **2002**, pp. 41–65.

[410] M. Martina, D. W. Hutmacher, *Polym. Int.* **2007**, *56*, 145.

[411] R. Duncan, *Nat. Rev. Drug Discov.* **2003**, *2*, 347.

[412] A.-C. Albertsson, I. K. Varma, *Biomacromolecules* **2003**, *4*, 1466.

[413] A. P. Dove, *ChemComm* **2008**, 6446.

[414] K. Hashimoto, *Prog. Polym. Sci.* **2000**, *25*, 1411.

[415] O. Dechy-Cabaret, B. Martin-Vaca, D. Bourissou, *Chem. Rev.* **2004**, *104*, 6147.

[416] M. A. Hillmyer in *Block Copolymers II*, Springer, Berlin, Heidelberg, pp. 137–181.

[417] G. Riess, *Prog. Polym. Sci.* **2003**, *28*, 1107.

[418] Y. Mai, A. Eisenberg, *Chem. Soc. Rev.* **2012**, *41*, 5969.

[419] M. W. Bates, S. M. Barbon, A. E. Levi, R. M. Lewis, H. K. Beech, K. M. Vonk, C. Zhang, G. H. Fredrickson, C. J. Hawker, C. M. Bates, *ACS Macro. Lett.* **2020**, *9*, 396.

[420] L.-Y. Shi, Y. Zhou, X.-H. Fan, Z. Shen, *Macromolecules* **2013**, *46*, 5308.

[421] E. M. Lennon, K. Katsov, G. H. Fredrickson, *Phys. Rev. Lett.* **2008**, *101*, 138302.

[422] M. W. Matsen, F. S. Bates, *Macromolecules* **1996**, *29*, 7641.

[423] J. E. Poelma, K. Ono, D. Miyajima, T. Aida, K. Satoh, C. J. Hawker, *ACS Nano* **2012**, *6*, 10845.

[424] F. S. Bates, G. H. Fredrickson, *Annu. Rev. Phys. Chem.* **1990**, *41*, 525.

[425] C. M. Bates, F. S. Bates, *Macromolecules* **2017**, *50*, 3.

[426] F. S. Bates, M. A. Hillmyer, T. P. Lodge, C. M. Bates, K. T. Delaney, G. H. Fredrickson, *Science* **2012**, *336*, 434.

[427] H.-C. Kim, S.-M. Park, W. D. Hinsberg, *Chem. Rev.* **2010**, *110*, 146.

[428] J. M. Widin, A. K. Schmitt, A. L. Schmitt, K. Im, M. K. Mahanthappa, *J. Am. Chem. Soc.* **2012**, *134*, 3834.

[429] M. W. Matsen, F. S. Bates, *J. Chem. Phys.* **1997**, *106*, 2436.

[430] M. W. Matsen, F. S. Bates, *Macromolecules* **1996**, *29*, 1091.

[431] I. Botiz, S. B. Darling, *Mater. Today* **2010**, *13*, 42.

[432] H. Feng, M. Changez, K. Hong, J. W. Mays, N.-G. Kang, *Macromolecules* **2017**, *50*, 54.

[433] I. W. Hamley, *Nanotechnology* **2003**, *14*, R39-R54.

[434] I. A. Nyrkova, A. N. Semenov, *Faraday Discuss.* **2005**, *128*, 113.

[435] J. N. Israelachvili, D. J. Mitchell, B. W. Ninham, *J. Chem. Soc., Faraday Trans. 2* **1976**, *72*, 1525.

[436] L. Zhang, A. Eisenberg, *J. Am. Chem. Soc.* **1996**, *118*, 3168.

[437] H. Shen, L. Zhang, A. Eisenberg, *J. Phys. Chem. B* **1997**, *101*, 4697.

[438] L. Zhang, H. Shen, A. Eisenberg, *Macromolecules* **1997**, *30*, 1001.

[439] K. Yu, A. Eisenberg, *Macromolecules* **1998**, *31*, 3509.

[440] F. Liu, A. Eisenberg, *J. Am. Chem. Soc.* **2003**, *125*, 15059.

[441] P. Lim Soo, A. Eisenberg, *J. Polym. Sci. B Polym. Phys.* **2004**, *42*, 923.

[442] N. J. Warren, S. P. Armes, *J. Am. Chem. Soc.* **2014**, *136*, 10174.

[443] S. L. Canning, G. N. Smith, S. P. Armes, *Macromolecules* **2016**, *49*, 1985.

[444] M. J. Derry, L. A. Fielding, S. P. Armes, *Prog. Polym. Sci.* **2016**, *52*, 1.

[445] J. Rieger, *Macromol. Rapid Commun.* **2015**, *36*, 1458.

[446] Y. Pei, A. B. Lowe, P. J. Roth, *Macromol. Rapid Commun.* **2017**, *38*, 1600528.

[447] A. B. Lowe, *Polymer* **2016**, *106*, 161.

[448] J. Yeow, C. Boyer, *Adv. Sci.* **2017**, *4*, 1700137.

[449] B. Charleux, G. Delaittre, J. Rieger, F. D'Agosto, *Macromolecules* **2012**, *45*, 6753.

[450] J. C. Foster, S. Varlas, B. Couturaud, Z. Coe, R. K. O'Reilly, *J. Am. Chem. Soc.* **2019**, *141*, 2742.

[451] S. P. Armes, S. Perrier, P. B. Zetterlund, *Polym. Chem.* **2021**, *12*, 8.

[452] E. J. Cornel, J. Jiang, S. Chen, J. Du, *CCS Chem.* **2021**, *3*, 2104.

[453] N. J. W. Penfold, J. Yeow, C. Boyer, S. P. Armes, *ACS Macro. Lett.* **2019**, *8*, 1029.

[454] T. Hashimoto, K. Nagatoshi, A. Todo, H. Hasegawa, H. Kawai, *Macromolecules* **1974**, *7*, 364.

[455] T. Hashimoto, M. Shibayama, H. Kawai, *Macromolecules* **1980**, *13*, 1237.

[456] Y.-Y. Won, A. K. Brannan, H. T. Davis, F. S. Bates, *J. Phys. Chem. B* **2002**, *106*, 3354.

[457] P. Leclère, R. Lazzaroni, J. L. Brédas, J. M. Yu, P. Dubois, R. Jérôme, *Langmuir* **1996**, *12*, 4317.

[458] *Small angle x-ray scattering*. *Edited by O. Glatter and O. Kratky*, Academic Press, London, New York, **1983**.

[459] S. Klingelhöfer, W. Heitz, A. Greiner, S. Oestreich, S. Förster, M. Antonietti, *J. Am. Chem. Soc.* **1997**, *119*, 10116.

[460] K. Kataoka, A. Harada, Y. Nagasaki, *Adv. Drug Deliv. Rev.* **2012**, *64*, 37.

[461] R. A. Segalman, *Mater. Sci. Eng. R Rep.* **2005**, *48*, 191.

[462] M. Park, C. Harrison, P. M. Chaikin, R. A. Register, D. H. Adamson, *Science* **1997**, *276*, 1401.

[463] S. B. Darling, *Energy Environ. Sci.* **2009**, *2*, 1266.

[464] D. Bendejacq, V. Ponsinet, M. Joanicot, Y.-L. Loo, R. A. Register, *Macromolecules* **2002**, *35*, 6645.

[465] Y. Matsushita, A. Noro, M. Iinuma, J. Suzuki, H. Ohtani, A. Takano, *Macromolecules* **2003**, *36*, 8074.

[466] J. N. K.M. Hong, *Polym. Commun.* **1984**, 265-268.

[467] L. Leibler, H. Benoit, *Polymer* **1981**, *22*, 195.

[468] G. H. Fredrickson, E. Helfand, *J. Chem. Phys.* **1987**, *87*, 697.

[469] D. M. Cooke, A.-C. Shi, *Macromolecules* **2006**, *39*, 6661.

[470] A. B. Kutikov, J. Song, *ACS Biomater Sci Eng* **2015**, *1*, 463.

[471] P. Grossen, D. Witzigmann, S. Sieber, J. Huwyler, *J. Control. Release* **2017**, *260*, 46.

[472] F. Ahmed, D. E. Discher, *J. Control. Release* **2004**, *96*, 37.

[473] J. C. de La Vega, P. Elischer, T. Schneider, U. O. Häfeli, *Nanomedicine* **2013**, *8*, 265.

[474] Y. Xu, Y. He, J. Wei, Z. Fan, S. Li, *Macromol. Chem. Phys.* **2008**, *209*, 1836.

[475] C. He, J. Sun, J. Ma, X. Chen, X. Jing, *Biomacromolecules* **2006**, *7*, 3482.

[476] C. He, J. Sun, C. Deng, T. Zhao, M. Deng, X. Chen, X. Jing, *Biomacromolecules* **2004**, *5*, 2042.

[477] M. S. Sadeghi, M. R. Moghbeli, W. A. Goddard, *J. Polym. Sci.* **2021**, *59*, 614.

[478] A. Ianiro, J. Patterson, Á. González García, M. M. J. van Rijt, M. M. R. M. Hendrix, N. A. J. M. Sommerdijk, I. K. Voets, A. C. C. Esteves, R. Tuinier, *J. Polym. Sci. B Polym. Phys.* **2018**, *56*, 330.

[479] W. Qi, P. P. Ghoroghchian, G. Li, D. A. Hammer, M. J. Therien, *Nanoscale* **2013**, *5*, 10908.

[480] Z.-X. Du, J.-T. Xu, Z.-Q. Fan, *Macromolecules* **2007**, *40*, 7633.

[481] P. P. Ghoroghchian, G. Li, D. H. Levine, K. P. Davis, F. S. Bates, D. A. Hammer, M. J. Therien, *Macromolecules* **2006**, *39*, 1673.

[482] K. Rajagopal, A. Mahmud, D. A. Christian, J. D. Pajerowski, A. E. X. Brown, S. M. Loverde, D. E. Discher, *Macromolecules* **2010**, *43*, 9736.

[483] D. J. Adams, C. Kitchen, S. Adams, S. Furzeland, D. Atkins, P. Schuetz, C. M. Fernyhough, N. Tzokova, A. J. Ryan, M. F. Butler, *Soft Matter* **2009**, *5*, 3086.

[484] M. Dionzou, A. Morère, C. Roux, B. Lonetti, J.-D. Marty, C. Mingotaud, P. Joseph, D. Goudounèche, B. Payré, M. Léonetti et al., *Soft Matter* **2016**, *12*, 2166.

[485] P. Schuetz, M. J. Greenall, J. Bent, S. Furzeland, D. Atkins, M. F. Butler, T. C. B. McLeish, D. M. A. Buzza, *Soft Matter* **2011**, *7*, 749.

[486] S. George, R. Champagne-Hartley, G. Deeter, D. Campbell, B. Reck, D. Urban, M. Cunningham, *Macromolecules* **2015**, *48*, 8913.

[487] J. Sun, A. A. Teran, X. Liao, N. P. Balsara, R. N. Zuckermann, *J. Am. Chem. Soc.* **2013**, *135*, 14119.

[488] J. Sun, X. Jiang, R. Lund, K. H. Downing, N. P. Balsara, R. N. Zuckermann, *Proc. Natl. Acad. Sci. U.S.A.* **2016**, *113*, 3954.

[489] J. Sun, A. A. Teran, X. Liao, N. P. Balsara, R. N. Zuckermann, *J. Am. Chem. Soc.* **2014**, *136*, 2070.

[490] R. H. Zha, B. F. M. de Waal, M. Lutz, A. J. P. Teunissen, E. W. Meijer, *J. Am. Chem. Soc.* **2016**, *138*, 5693.

[491] B. van Genabeek, B. F. M. de Waal, M. M. J. Gosens, L. M. Pitet, A. R. A. Palmans, E. W. Meijer, *J. Am. Chem. Soc.* **2016**, *138*, 4210.

[492] W. He, S. Wang, M. Li, X. Wang, Y. Tao, *Angew. Chem. Int. Ed.* **2022**, *61*, e202112439.

[493] S. Honda, T. Yamamoto, Y. Tezuka, *J. Am. Chem. Soc.* **2010**, *132*, 10251.

[494] P. Bohn, M. P. Weisel, J. Wolfs, M. A. R. Meier, *Sci. Rep.* **2022**, *12*, 13878.

[495] G. M. Church, Y. Gao, S. Kosuri, *Science* **2012**, *337*, 1628.

[496] V. Zhirnov, R. M. Zadegan, G. S. Sandhu, G. M. Church, W. L. Hughes, *Nat. Mater.* **2016**, *15*, 366.

[497] N. Goldman, P. Bertone, S. Chen, C. Dessimoz, E. M. LeProust, B. Sipos, E. Birney, *Nature* **2013**, *494*, 77.

[498] L. Ceze, J. Nivala, K. Strauss, *Nat. Rev. Genet.* **2019**, *20*, 456.

[499] Erlich Yaniv, Zielinski Dina, *Science* **2017**, *355*, 950.

[500] J. Shendure, S. Balasubramanian, G. M. Church, W. Gilbert, J. Rogers, J. A. Schloss, R. H. Waterston, *Nature* **2017**, *550*, 345.

[501] R. N. Grass, R. Heckel, M. Puddu, D. Paunescu, W. J. Stark, *Angew. Chem. Int. Ed.* **2015**, *54*, 2552.

[502] Y. Jiang, M. R. Golder, H. V.-T. Nguyen, Y. Wang, M. Zhong, J. C. Barnes, D. J. C. Ehrlich, J. A. Johnson, *J. Am. Chem. Soc.* **2016**, *138*, 9369.

[503] J. Niu, R. Hili, D. R. Liu, *Nat. Chem.* **2013**, *5*, 282.

[504] A. Al Ouahabi, L. Charles, J.-F. Lutz, *J. Am. Chem. Soc.* **2015**, *137*, 5629.

[505] T. T. Trinh, L. Oswald, D. Chan-Seng, J.-F. Lutz, *Macromol. Rapid Commun.* **2014**, *35*, 141.

[506] S. Telitel, B. É. Petit, S. Poyer, L. Charles, J.-F. Lutz, *Polym. Chem.* **2017**, *8*, 4988.

[507] E. M. LeProust, B. J. Peck, K. Spirin, H. B. McCuen, B. Moore, E. Namsaraev, M. H. Caruthers, *Nucleic Acids Res.* **2010**, *38*, 2522.

[508] G. Audran, S. R. A. Marque, P. Mellet, *Acc. Chem. Res.* **2020**, *53*, 2828.

[509] L. Oswald, A. Al Ouahabi, C. Laure, J.-A. Amalian, L. Charles, J.-F. Lutz, *J. Polym. Sci. Part A: Polym. Chem.* **2019**, *57*, 403.

[510] L. Nagy, Á. Kuki, T. Nagy, B. Vadkerti, Z. Erdélyi, L. Kárpáti, M. Zsuga, S. Kéki, *Int. J. Mol. Sci.* **2020**, *21*.

[511] C. C. A. Ng, W. M. Tam, H. Yin, Q. Wu, P.-K. So, M. Y.-M. Wong, F. C. M. Lau, Z.-P. Yao, *Nat. Commun.* **2021**, *12*, 4242.

[512] T. Gruendling, K. K. Oehlenschlaeger, E. Frick, M. Glassner, C. Schmid, C. Barner-Kowollik, *Macromol. Rapid Commun.* **2011**, *32*, 807.

[513] C. E. Arcadia, E. Kennedy, J. Geiser, A. Dombroski, K. Oakley, S.-L. Chen, L. Sprague, M. Ozmen, J. Sello, P. M. Weber et al., *Nat. Commun.* **2020**, *11*, 691.

[514] A. C. Boukis, K. Reiter, M. Frölich, D. Hofheinz, M. A. R. Meier, *Nat. Commun.* **2018**, *9*, 1439.

[515] B. J. Cafferty, A. S. Ten, M. J. Fink, S. Morey, D. J. Preston, M. Mrksich, G. M. Whitesides, *ACS Cent. Sci.* **2019**, *5*, 911.

[516] J. K. Rosenstein, C. Rose, S. Reda, P. M. Weber, E. Kim, J. Sello, J. Geiser, E. Kennedy, C. Arcadia, A. Dombroski et al., *IEEE Trans. Nanobioscience* **2020**, *19*, 378.

[517] A. A. Nagarkar, S. E. Root, M. J. Fink, A. S. Ten, B. J. Cafferty, D. S. Richardson, M. Mrksich, G. M. Whitesides, *ACS Cent. Sci.* **2021**.

[518] Y. Tang, C. He, X. Zheng, X. Chen, T. Gao, *Chem. Sci.* **2020**, *11*, 3096.

[519] T. Sarkar, K. Selvakumar, L. Motiei, D. Margulies, *Nat. Commun.* **2016**, *7*, 11374.

[520] T. Ratner, O. Reany, E. Keinan, *ChemPhysChem* **2009**, *10*, 3303.

[521] B. M. Fung, V. L. Ermakov, *J. Magn. Reson.* **2004**, *166*, 147.

[522] A. Strecker, *Liebigs Ann. Chem.* **1850**, *75*, 27.

[523] T. Zarganes-Tzitzikas, A. L. Chandgude, A. Dömling, *Chem. Rec.* **2015**, *15*, 981.

[524] W. Cao, F. Dai, R. Hu, B. Z. Tang, *J. Am. Chem. Soc.* **2020**, *142*, 978.

[525] B. T. Tuten, L. de Keer, S. Wiedbrauk, P. H. M. van Steenberge, D. R. D'hooge, C. Barner-Kowollik, *Angew. Chem. Int. Ed.* **2019**, *58*, 5672.

[526] A. Llevot, A. C. Boukis, S. Oelmann, K. Wetzel, M. A. R. Meier in *Polymer Synthesis Based on Triple-bond Building Blocks* (Eds.: B. Z. Tang, R. Hu), Springer International Publishing, Cham, **2018**, pp. 127–155.

[527] X. Jiang, C. Feng, G. Lu, X. Huang, *Sci. China Chem.* **2015**, *58*, 1695.

[528] A. Sehlinger, M. A. R. Meier in *Multi-Component and Sequential Reactions in Polymer Synthesis* (Ed.: P. Theato), Springer International Publishing, Cham, **2015**, pp. 61–86.

[529] R. Kakuchi, *Angew. Chem. Int. Ed.* **2014**, *53*, 46.

[530] S. Wang, C. Fu, Y. Wei, L. Tao, *Macromol. Chem. Phys.* **2014**, *215*, 486.

[531] J. G. Rudick, *J. Polym. Sci. A Polym. Chem.* **2013**, *51*, 3985.

[532] O. Kreye, T. Tóth, M. A. R. Meier, *J. Am. Chem. Soc.* **2011**, *133*, 1790.

[533] R. Afshari, A. Shaabani, *ACS Comb. Sci.* **2018**, *20*, 499.

[534] A. Dömling, *Chem. Rev.* **2006**, *106*, 17.

[535] A. Dömling, *Comb. Chem. High Throughput Screen.* **1998**, *1*, 1.

[536] K. Oertel, G. Zech, H. Kunz, *Angew. Chem. Int. Ed.* **2000**, *39*, 1431.

[537] O. Pando, S. Stark, A. Denkert, A. Porzel, R. Preusentanz, L. A. Wessjohann, *J. Am. Chem. Soc.* **2011**, *133*, 7692.

[538] I. Akritopoulou-Zanze, *Curr. Opin. Chem. Biol.* **2008**, *12*, 324.

[539] B. Yang, Y. Zhao, Y. Wei, C. Fu, L. Tao, *Polym. Chem.* **2015**, *6*, 8233.

[540] D. L. Wright, S. T. Handy, P. A. Wender, *ChemInform* **1998**, *29*, no-no.

[541] I. Ugi, *J. prakt. Chem.* **339**, *1997*, 499.

[542] H. L. Le Chatelier, *CR Hebd. Seances Acas. Sci.* **1884**, *99*, 786.

[543] Z.-K. Liu, J. Ågren, M. Hillert, *Fluid Ph. Equilibria* **1996**, *121*, 167.

[544] A. Hantzsch, *Justus Liebigs Ann. Chem.* **1882**, *215*, 1.

[545] M. Filipan-Litvić, M. Litvić, I. Cepanec, V. Vinković, *Molecules* **2007**, *12*, 2546.

[546] F. Bossert, H. Meyer, E. Wehinger, *Angew. Chem. Int. Ed.* **1981**, *20*, 762.

[547] A. Hantzsch, *Ber. Dtsch. Chem. Ges.* **1890**, *23*, 1474.

[548] C. Oliver Kappe, *Tetrahedron* **1993**, *49*, 6937.

[549] W. K. C. Mannich, *Arch. Pharm.* **1912**, *250*, 647.

[550] H. T. Bucherer, H. T: Fischbeck, *J. prakt. Chem.* **1934**, 69.

[551] J. J. Li in *Springer eBook Collection* (Ed.: J. J. Li), Springer Berlin Heidelberg, Berlin, Heidelberg, s.l., **2002**, p. 53.

[552] Y. Zhang, Y. Zhao, B. Yang, C. Zhu, Y. Wei, L. Tao, *Polym. Chem.* **2014**, *5*, 1857.

[553] *ACS Macro Lett., 2013, 2, 419;(b) R. Kakuchi and P. Theato*, **2014**.

[554] N. Wagner, L. Schneider, M. Michelswirth, K. Küpper, P. Theato, *Macromol. Chem. Phys.* **2015**, *216*, 783.

[555] I. Ugi, A. Dömling, W. Hörl, *Endeavour* **1994**, *18*, 115.

[556] F. Asinger, *Angew. Chem. Int. Ed.* **1956**, *68*, 376.

[557] C. Boy, W. A. Herrmann, M. Rasch, *Angew, Chem. Int. Ed.* **1994**, *33*, 2144.

[558] W. Reppe, *Neue Entwicklungen Auf Dem Gebiete der Chemie des Acetylens und Kohlenoxyds*, Springer Berlin / Heidelberg, Berlin, Heidelberg, **1949**.

[559] I. U.Khand, G. R. Knox, P. L. Pauson, W. E. Watts, *ChemComm* **1971**, *36a*, 36.

[560] J. G. Rudick, S. Shaabani, A. Dömling, *Front. Chem.* **2020**, *7*, 918.

[561] W. Lieke, *Justus Liebigs Ann. Chem.* **1859**, *112*, 316.

[562] A. Gautier, *Liebigs Ann. Chem.* **1869**, *146*, 119.

[563] N. Kornblum, R. A. Smiley, H. E. Ungnade, A. M. White, B. Taub, S. A. Herbert, *J. Am. Chem. Soc.* **1955**, *77*, 5528.

[564] N. Kornblum, R. A. Smiley, R. K. Blackwood, D. C. Iffland, *J. Am. Chem. Soc.* **77**, *1955*, 6269.

[565] A. W. Hofmann, *Justus Liebigs Ann. Chem.* **1867**, *144*, 114.

[566] I. Ugi, R. Meyr, *Angew. Chem. Int. Ed.* **1958**, *70*, 702.

[567] I. Ugi, R. Meyr, *Chem. Ber.* **1960**, *93*, 239.

[568] K. A. Waibel, R. Nickisch, N. Möhl, R. Seim, M. A. R. Meier, *Green Chem.* **2020**, *22*, 933.

[569] S. M. Creedon, H. K. Crowley, D. G. McCarthy, *J. Chem. Soc., Perkin Trans. 1* **1998**, *0*, 1015.

[570] A. Dömling, I. Ugi, *Angew. Chem. Int. Ed.* **2000**, *39*, 3168.

[571] P. Patil, M. Ahmadian-Moghaddam, A. Dömling, *Green Chem.* **2020**, *22*, 6902.

[572] C. G. Neochoritis, T. Zarganes-Tzitzikas, S. Stotani, A. Dömling, E. Herdtweck, K. Khoury, A. Dömling, *ACS Comb. Sci.* **2015**, *17*, 493.

[573] I. Ugi, B. Werner, A. Dömling, *Molecules* **2003**, *8*, 53.

[574] I. Ugi, C. Steinbrückner, *Chem. Ber.* **1961**, *94*, 2802.

[575] R. H. Baker, D. Stanonis, *J. Am. Chem. Soc.* **1951**, *73*, 699.

[576] I. Hagedorn, U. Eholzer, *Chem. Ber.* **1965**, *98*, 936.

[577] M. C. Pirrung, K. D. Sarma, *J. Am. Chem. Soc.* **2004**, *126*, 444.

[578] I. Ugi, *Angew. Chem. Int. Ed.* **1962**, *1*, 8.

[579] S. Maeda, S. Komagawa, M. Uchiyama, K. Morokuma, *Angew. Chem. Int. Ed.* **2011**, *50*, 644.

[580] R. Ramozzi, K. Morokuma, *J. Org. Chem.* **2015**, *80*, 5652.

[581] K. N. Onwukamike, S. Grelier, E. Grau, H. Cramail, M. A. R. Meier, *RSC Adv.* **2018**, *8*, 31490.

[582] L. El Kaim, M. Gizolme, L. Grimaud, *Org. Lett.* **2006**, *8*, 5021.

[583] L. El Kaïm, M. Gizolme, L. Grimaud, J. Oble, *J. Org. Chem.* **2007**, *72*, 4169.

[584] R. M. I. Ugi, *Chem. Ber.* **1961**, *94*, 2229.

[585] C. H. T. nixey, *Tetrahedron Lett.* **2002**, *43*, 6833.

[586] A. L. Chandgude, A. Dömling, *Green Chem.* **2016**, *18*, 3718.

[587] U. E. I. Hagedorn, *Chem. Ber.* **1965**, *98*, 444.

[588] J. M. Saya, R. Berabez, P. Broersen, I. Schuringa, A. Kruithof, R. V. A. Orru, E. Ruijter, *Org. Lett.* **2018**, *20*, 3988.

[589] T. Ngouansavanh, J. Zhu, *Angew. Chem. Int. Ed.* **2006**, *45*, 3495.

[590] R. Neidlein, *Zeitschrift für Naturforschung B* **1964**, *19*, 1159.

[591] K. R. I. Ugi, *Chem. Ber.* **1961**, *94*, 2233.

[592] Kevin Andreas Waibel.

[593] Y.-Z. Wang, J.-C. Wang, Y.-H. Wu, C.-X. Shi, F.-S. Du, Z.-C. Li, *Polym. J.* **2020**, *52*, 133.

[594] B. T. Tuten, A. H. Bui, S. Wiedbrauk, V. X. Truong, C. L. Raston, C. Barner-Kowollik, *ChemComm* **2021**, *57*, 8328.

[595] B. T. Tuten, L. de Keer, S. Wiedbrauk, P. H. M. van Steenberge, D. R. D'hooge, C. Barner-Kowollik, *Angew. Chem. Int. Ed.* **2019**, *58*, 5672.

[596] I. Ugi, F. K. Rosendahl, F. Bodesheim, *Justus Liebigs Ann. Chem.* **1963**, *666*, 54.

[597] C. S. I. Ugi, *Angew, Chem.* **1960**, *72*, 267.

[598] M. A. Fouad, H. Abdel-Hamid, M. S. Ayoup, *RSC Adv.* **2020**, *10*, 42644.

[599] A. Dömling, S. Achatz, B. Beck, *Bioorganic Med. Chem. Lett.* **2007**, *17*, 5483.

[600] A. C. Boukis, *Moleküle als potentielle Datenspeichersysteme: Multikomponentenreaktionen sind der Schlüssel*, KIT, **2018**.

[601] L. El Kaim, L. Grimaud, *Tetrahedron* **2009**, *65*, 2153.

[602] L. E. Kaïm, M. Gizolme, L. Grimaud, J. Oble, *J. Org. Chem.* **2007**, *72*, 4169.

[603] L. El Kaïm, L. Grimaud, J. Oble, *Angew. Chem. Int. Ed.* **2005**, *117*, 8175.

[604] T. A. Keating, R. W. Armstrong, *J. Org. Chem.* **1998**, *63*, 867.

[605] I. Ugi, C. Steinbrückner, *Chem. Ber.* **1961**, *94*, 2802.

[606] M. Mohammadi-Khanaposhtani, N. Jalalimanesh, M. Saeedi, B. Larijani, M. Mahdavi, *Mol. Divers.* **2020**, *24*, 855.

[607] S. Balalaie, P. Shakeri, *Targets Heterocycl. Syst.* **2018**, *22*, 468.

[608] A. Michael, *Am. Chem. J.* **1887**, *9*, 115.

[609] B. D. Mather, K. Viswanathan, K. M. Miller, T. E. Long, *Prog. Polym. Sci.* **2006**, *31*, 487.

[610] J. C. Worch, C. J. Stubbs, M. J. Price, A. P. Dove, *Chem. Rev.* **2021**, *121*, 6744.

[611] B. He, H. Su, T. Bai, Y. Wu, S. Li, M. Gao, R. Hu, Z. Zhao, A. Qin, J. Ling et al., *J. Am. Chem. Soc.* **2017**, *139*, 5437.

[612] M. Bararjanian, S. Balalaie, B. Movassagh, H. R. Bijanzadeh, *Tetrahedron Lett.* **2010**, *51*, 3277.

[613] M. Bararjanian, S. Balalaie, F. Rominger, B. Movassagh, H. R. Bijanzadeh, *Mol. Divers.* **2011**, *15*, 583.

[614] H. C. Kolb, M. G. Finn, K. B. Sharpless, *Angew. Chem. Int. Ed.* **2001**, *40*, 2004.

[615] S. Balalaie, M. Z. Kassaee, H. R. Bijanzadeh, F. Darvish, M. Bararjanian, F. Jalaiyan, *J. Iran. Chem. Soc.* **2014**, *11*, 1483.

[616] C. F. Nising, S. Bräse, *Chem. Soc. Rev.* **2008**, *37*, 1218.

[617] N. van Herck, D. Maes, K. Unal, M. Guerre, J. M. Winne, F. E. Du Prez, *Angew. Chem. Int. Ed.* **2020**, *59*, 3609.

[618] Philipp Bohn, Master Thesis at Karlsruhe Institute of Technology (KIT) **2017**.

[619] N. N. Reed, K. D. Janda, *J. Org. Chem.* **2000**, *65*.

[620] J. Zhang, Y.-. J. Zhao, Z.-. G. Su, G.-. H. Ma, *J. Appl. Polym. Sci.* **2007**, *105*.

[621] A. Bouzide, G. Sauvé, *Org. Lett.* **2002**, *4*.

[622] G. Coudert, M. Mpassi, G. Guillaumet, C. Selve, *Synth. Commun.* **1986**, *16*.

[623] A. M. Wawro, T. Muraoka, K. Kinbara, *Polym. Chem.* **2016**, *7*.

[624] Z. Wan, Y. Li, S. Bo, M. Gao, X. Wang, K. Zeng, X. Tao, X. Li, Z. Yang, Z.-. X. Jiang, *Org. Biomol. Chem.* **2016**, *14*.

[625] G. Xia, Y. Li, Z. Yang, Z.-. X. Jiang, *Org. Process Res. Dev.* **2015**, *197*.

[626] Y. Li, B. Thapa, H. Zhang, X. Li, F. Yu, E.-. K. Jeong, Z. Yang, Z.-. X. Jiang, *Tetrahedron* **2013**, *69*.

[627] M. Shan, A. Bujotzek, F. Abendroth, A. Wellner, R. Gust, O. Seitz, M. Weber, R. Haag, *ChemBioChem* **2011**, *12*, 2587.

[628] Exactmer, "Synthesis of defined structures based on Nanostar Sieving Technology, based in London, England (GB). Access: 26.03.2022, 5:42 am.", can be found under https://exactmer.com/, **2022**.

[629] Polypure, "Uniform PEGs via Sample Displacement Chromatography (SDC), based in Oslo, Norway. Access: 26.03.2022, 6:48 am.", can be found under https://polypure.com/, **2022**.

[630] Qianyu Cai, *Synthesis of uniform PEGs via GaBr3-catalyzed Reduction, KIT.*, **2021**.

[631] M. Castano, K. S. Seo, E. H. Kim, M. L. Becker, J. E. Puskas, *Macromol. Rapid Commun.* **2013**, *34*, 1375.

[632] Y. Cao, Y. Li, X.-Y. Hu, X. Zou, S. Xiong, C. Lin, L. Wang, *Chem. Mater.* **2015**, *27*, 1110.

[633] C. J. Hawker, J. M. J. Fréchet, *J. Chem. Soc., Perkin Trans. 1* **1992**, 2459.

[634] J. S. Moore, S. I. Stupp, *Macromolecules* **1990**, *23*, 65.

[635] X. Guo, K. S. Wetzel, S. C. Solleder, S. Spann, M. A. R. Meier, M. Wilhelm, B. Luy, G. Guthausen, *Macromol. Chem. Phys.* **2019**, *220*, 1900155.

[636] M.-J. Fan, G.-Q. Li, Y.-M. Liang, *Tetrahedron* **2006**, *62*, 6782.

[637] Y. Shi, T. Bai, W. Bai, Z. Wang, M. Chen, B. Yao, J. Z. Sun, A. Qin, J. Ling, B. Z. Tang, *Chem. Eur. J.* **2017**, *23*, 10725.

[638] Stefano Flavio Sechi, *Digital Monomers via the Passerini-Amino-yne Cascade One-Pot-Reaction, KIT.*, **2020**.

[639] Tamara Meyer, *Data Storage in Small Molecules, KIT.*, **2021**.

[640] J. Zhang, Z. Zhang, J. Wang, Q. Zang, J. Z. Sun, B. Z. Tang, *Polym. Chem.* **2021**, *12*, 2978.

[641] M. E. Jung, K. R. Buszek, *J. Org. Chem.* **1985**, *50*, 5440.

[642] N. van Herck, D. Maes, K. Unal, M. Guerre, J. M. Winne, F. E. Du Prez, *Angew. Chem. Int. Ed.* **2020**, *132*, 3637.

[643] L. Sobenina, A. P. Demenev, A. I. Mikhaleva, V. N. Elokhina, A. G. Mal'kina, O. A. Tarasova, I. Ushakov, B. A. Trofimov, *Synthesis* **2001**, *2001*, 293.

[644] L. Dong, W. Fu, P. Liu, J. Shi, B. Tong, Z. Cai, J. Zhi, Y. Dong, *Macromolecules* **2020**, *53*, 1054.

[645] I. Yavari, S. Z. Sayyed-Alangi, M. Sabbaghan, R. Hajinasiri, N. Iravani, *Monatsh. Chem.* **2008**, *139*, 1025.

[646] M. J. Soth, K. Le, M. E. Di Francesco, M. M. Hamilton, G. Liu, J. P. Burke, C. L. Carroll, J. J. Kovacs, J. P. Bardenhagen, C. A. Bristow et al., *J. Med. Chem.* **2020**, *63*, 12957.

[647] C. Wiles, P. Watts, S. J. Haswell, E. Pombo-Villar, *Lab Chip* **2002**, *2*, 62.

[648] E. M. Purcell, H. C. Torrey, R. V. Pound, *Phys. Rev.* **1946**, *69*, 37.

[649] F. Bloch, *Phys. Rev.* **1946**, *70*, 460.